RELACION DE PROFESORES DEL CURSO DISEÑO Y CONSTRUCCION DE ESTRUCTURAS ESPACIALES Y DE CASCARON.

Dr. Isaías García Terrazas
Inst. Mex. del Petróleo
Depto.de Transferencia de Calor
Sub. Director de Ing. de Proyectos
Av. de los 100 Mts. No. 500
México 14, D.F.

Dr. Javier Salazar Resines
Jefe de la Div. de Estudios Superiores
Facultad de Ing.
U. N. A. M.

Arq. Enrique de la Mora y Palomar
Despacho Particular
Av. Progreso 158-3
Coyoacan México 21, D.F.

Arq. Jorge Molina Montes
Molina y Núñez Asesores S.A.
Plateros No. 7
Despacho 106
México, D.F.

Ing. Guillermo Gargollo Rivas
Bradley 52-Despacho 307
Col. Nva. Anzures
México, D.F.

Ing.Francisco Castaño Hernández
Triodetic de México, S.A. Gte. Gral.
Cerrada de Malaga No. 43 Nte.
Col. Mixcoac
México, D.F.

PROFESORES DEL CURSO DISEÑO Y CONSTRUCCION DE ESTRUCTURAS ESPACIALES Y DE CASCARON

Dr. Porfirio Ballesteros Barocio
Div. de Estudios Superiores
Secc. de Estructuras
U. N. A. M.

Ing. Miguel Angel Velazco Ruiz
Div. de Estudios Superiores
Secc. de Estructuras
U. N. A. M.

Ing. Alejandro Fierro Manly
Gerente de Diseño y Supervisión
D I R A C
Empresa 136-4°Piso
México, D.F.

Ing. José Flavio Madrigal Rodríguez
Despacho Particular
Saragoza No. 640
San Luis Potosí, S.L.P.

Ing. Ignacio Canals

DIRECTORIO DE ASISTENTES AL CURSO DE DISEÑO Y CONSTRUCCION DE ESTRUCTURAS ESPACIALES Y DE CASCARON (DEL 2 DE OCTUBRE AL 17 DE NOVIEMBRE DE 1972)

NOMBRE Y DIRECCION	EMPRESA Y DIRECCION
1. ING. JAIME CASTILLO VAZQUEZ Amatista No. 55 Col. Estrella México, D. F.	COMPAÑIA DE LUZ Y FUERZA DEL CENTRO,S.A Melchor Ocampo No. 177 México, D. F.
2. ING. JOSE LUIS CERVANTES ELIAS Norte 85 No. 517 Col. Libertad México 16, D. F.	COMPAÑIA DE LUZ Y FUERZA DEL CENTRO,S.A Melchor Ocampo No. 177 México, D. F.
3. SR. BALFRE DOMINGUEZ GUTIERREZ Brillante No. 80 Col. Estrella México 14, D. F.	BUFETE INDUSTRIAL DISEÑOS Y PROYECTOS, S. A. Tolstoi No. 22 Col. Anzures México 5, D. F.
4. ING. EDUARDO ESCALANTE ROBLEDA México, D. F.	SECRETARIA DE OBRAS PUBLICAS Av. Fernando No. 268 México, D. F.
5. ING. PEDRO ESPARZA SANDOVAL Extremadura No. 189-5 Insurgentes Mixcoac México 19, D. F.	BUFETE INDUSTRIAL DISEÑOS Y PROYECTOS, S. A. Tolstoi No. 22 Col. Anzures México 5, D. F.
6. ARQ. JUSTINO HUERTA GONZALEZ Xola No. 1562-8 Col. Narvarte México 12, D. F.	COMISION CONSTRUCTORA E I.S. DE S.S.A. Cordoba No. 49-3er. Piso Col. Roma México 7, D. F.
7. SR. PABLO LE ROAL LEAL Av. Cuauhtémoc No. 1103-1 Col. del Valle México 12, D. F.	INSTITUTO MEXICANO DEL SEGURO SOCIAL Reforma No. 506-17o. Piso México, D. F.
8. ARQ. GUILLERMO LUYANDO BUENO Epigmenio Ibarra No. 11 Col. Romero de Terreros México 21, D. F.	

DIRECTORIO DE ASISTENTES AL CURSO DE DISEÑO Y CONSTRUCCION DE ESTRUCTURAS ESPACIALES Y DE CASCARON (DEL 2 DE OCTUBRE AL 17 DE NOVIEMBRE DE 1972)

NOMBRE Y DIRECCION	EMPRESA Y DIRECCION
9. ING. ALEJANDRO MUÑOZ DIAZ Playa Miramar No. 568 México, D. F.	SECRETARIA DE OBRAS PUBLICAS Av. Fernando No. 268 México, D. F.
10. ING. RUBEN QUESADAS MARTINEZ Cerrada de Allende No. 36 México, D. F.	COMISION FEDERAL DE ELECTRICIDAD Ródano No. 14 México 5, D. F.
11. ING. ALBERTO RESENDIZ MOLINA Nicolas Campa Nte. 1-Bis Queretaro, Qro.	ARQ. EDUARDO RUIZ POSADA ING. ALBERTO RESENDIZ M. Ocampo Sur No. 2-D Queretaro, Qro.
12. ING. ENRIQUE SALDAÑA TOULET Calle Convento de San Lorenzo 8 Col. Jardines de Sta. Mónica Tlalnepantla, Edo. de México	BUFETE INDUSTRIAL DISEÑOS Y PROYECTOS, S. A. Tolstoi No. 22 Col. Anzures México 5, D. F.
13. SR. DAVID SANCHEZ MARTINEZ Xochicalco No. 94-4 México 12, D. F.	I.A.E.S.A. Baja California No. 284-702 México 11, D. F.
14. ING. ROBERTO ELEAZAR SUAREZ REYES Av. Madero Ote. No. 691 Morelia, Mich.	FACULTAD DE INGENIERIA UNIVERSIDAD MICHOACANA Morelia, Mich.
15. ING. PEDRO URZUA RODRIGUEZ Playa Copacabana No. 127 Col. Marte México 13, D. F.	SECRETARIA DE OBRAS PUBLICAS Av. Fernando No. 268 México, D. F.

centro de educación contínua
facultad de ingeniería, unam

DISEÑO Y CONSTRUCCION DE ESTRUCTURAS ESPACIALES Y DE CASCARON

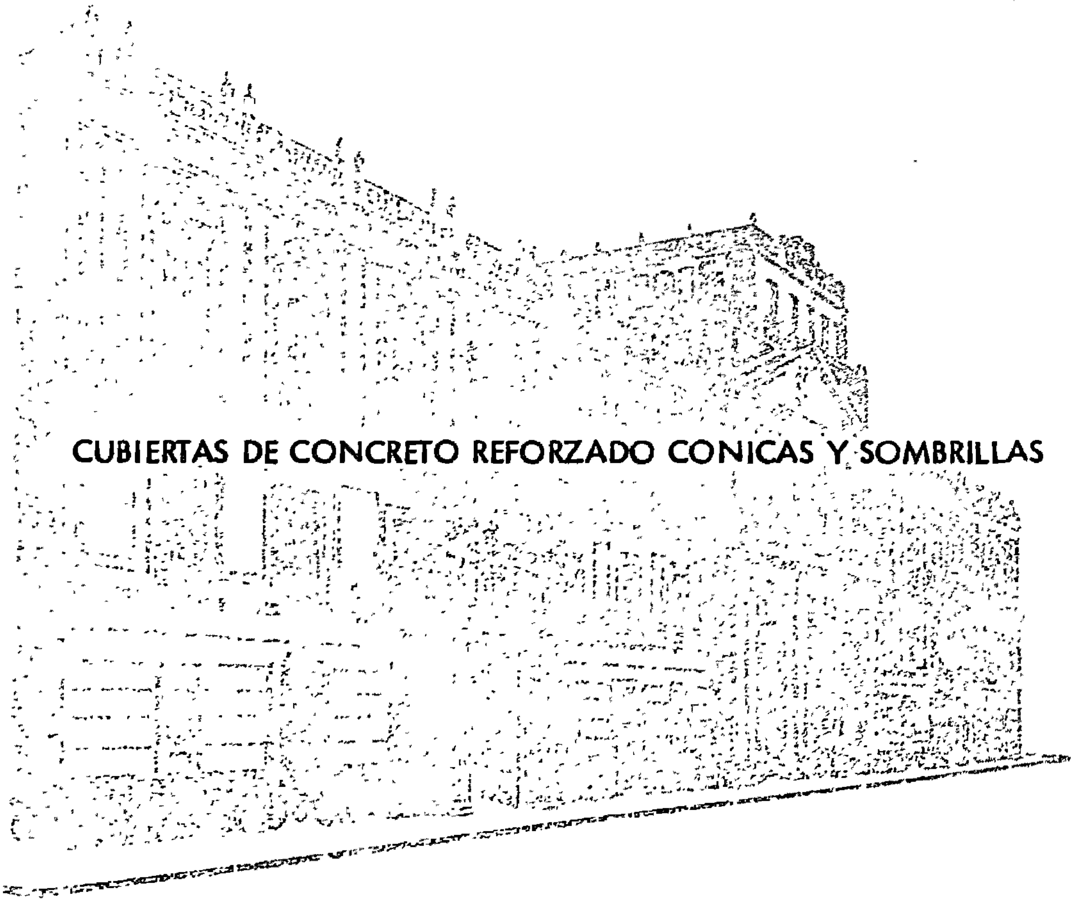

CUBIERTAS DE CONCRETO REFORZADO CONICAS Y SOMBRILLAS

Arq. Jorge Molina Montes

1972

Tacuba 5, primer piso. México 1, D.F.
Teléfonos: 521-30-95 y 513-27-95

CALCULO SIMPLIFICADO DE LOS ESFUERZOS DE MEMBRANA EN UNA CUBIERTA DE CONCRETO TIPO "CASCARON" EN FORMA DE CONO

ARQ. JORGE MOLINA MONTES

Las exigencias de un proyecto arquitectónico en el cual as cubiertas de la bomba de una estación de servicio de --- EMEX, estaban resueltas con unos conos invertidos descansando sobre una columna central, hizo posible la búsqueda de los esfuerzos de membrana en una superficie cónica. Nos dimos --- cuenta que el proceso se podía simplificar partiendo unicamente de ecuaciones de equilibrio dadas por el sendido común. --- En este artículo presentamos dichas ecuaciones y las comparamos con la teoría de la membrana posteriormente.

En la Fig. 1 se muestran las condiciones arquitectónicas de la cubierta y también las constantes geometricas que la definen.

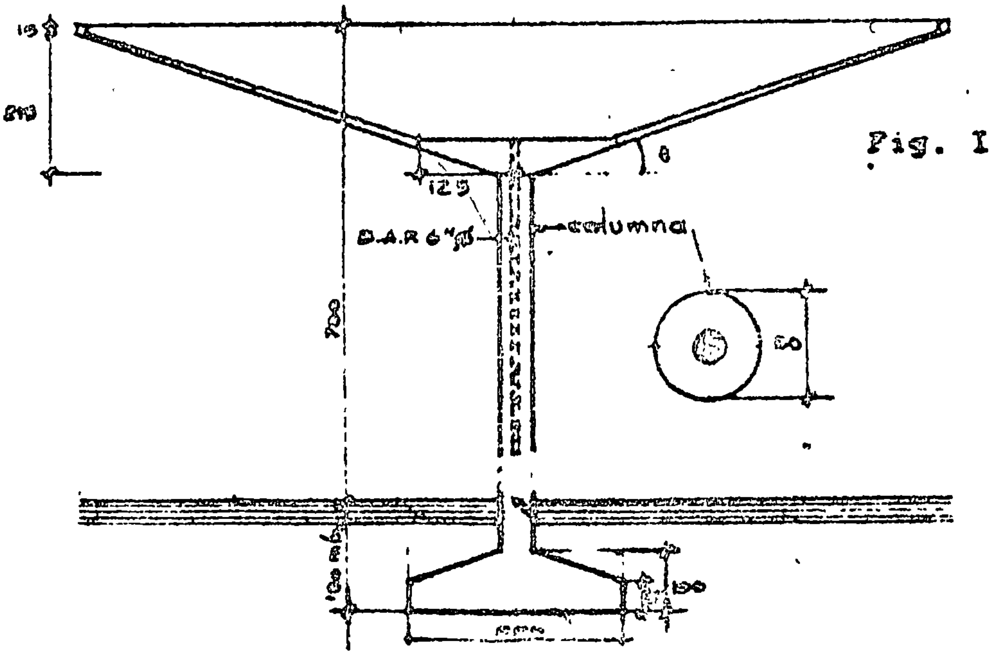

Fig. 1

I.- Ecuaciones de equilibrio según el método simplificado

Las premisas sobre las cuales descansa este método son las que se describen a continuación:

1.- Las fuerzas extensionales que actuan sobre la membrana se dividieron en una radial, llamada S_I dada en unidad de peso entre unidad de longitud, y otra siguiendo la dirección de la tangente al círculo de corte llamada S_{II} .Estos esfuerzos de membrana se representan en la Fig. 2. Sus proyecciones sobre un plano horizontal las llamamos G_I y G_{II} respectivamente.

Estas fuerzas son principales, estos es no existen fuerzas cortantes paralelas a ellas.

2.- La carga exterior, denominada g es unacarga vertical dada en Kg/m2 que actua sobre la superficie media.

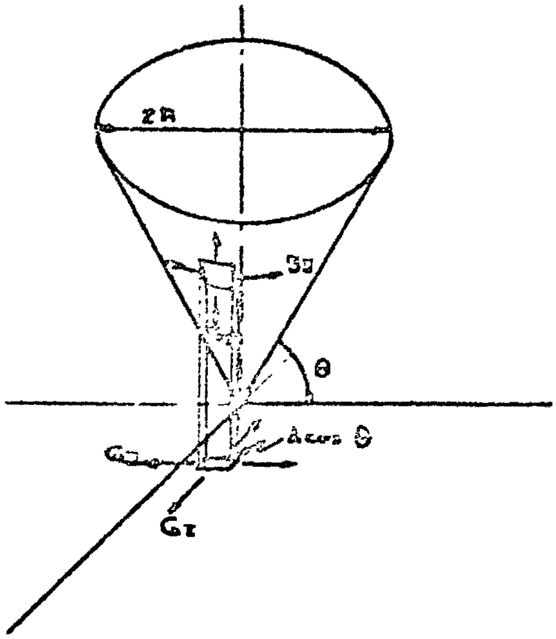

Fig. 2

Cálculo de S_I

Elegimos un corte cualquiera por un plano horizontal (π) llamado r al radio del círculo en el corte. El area arriba del corte será la semisuma de los perimetros del circulo superior, o de frontera, de radio R y del círculo inferior de radio r, multiplicada por la distancia, sobre el cono, entre los dos círculos. Si esta superficie la multiplicamos por la carga por unidad de area g, obtendremos la carga total del plano de corte. π

$$\text{Area} = \frac{\pi\,(R^2 - r^2)}{\cos\theta}$$

$$\text{Carga} = \frac{g\pi\,(R^2 - r^2)}{\cos\theta}$$

Esta carga por unidad de longitud será:

$$p = \frac{g\,(R^2 - r^2)}{2\cos\theta\, r}$$

En virtud de que se han supuesto solamente como fuerzas actuando en el corte a S_I y a S_{II}, la proyección vertial de S_I será igual a la carga total por unidad de longitud en el corte citado.

Por tanto:

$$\boxed{S_I = \frac{g\,(R^2 - r^2)}{r\ \text{sen}\ 2\theta}} \quad (1)$$

Cumpliendo así con el equilibrio vertical.

Cálculo de S_{II}

Para el cálculo del esfuerzo S_{II} a lo largo de la dirección de la tangente, es necesario hacer un corte unitario de la superficie, como se representa en la Fig. 3

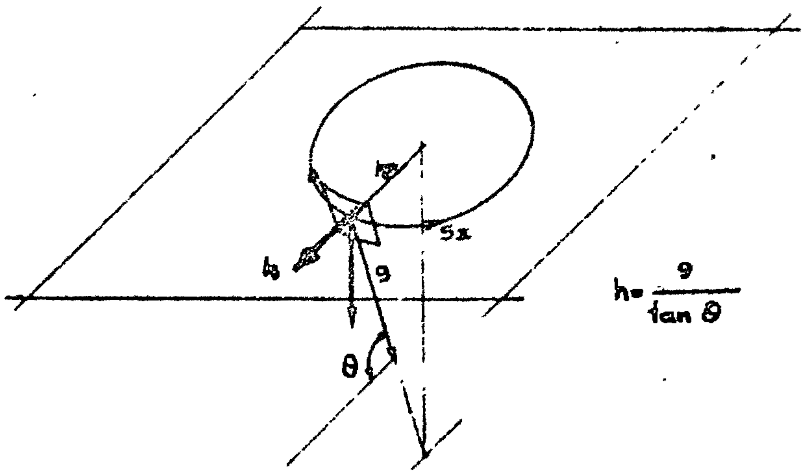

$$h = \frac{g}{\tan\theta}$$

El esfuerzo tangencial inducido por la -- presión h en un anillo es:

$$S_{II} = hr$$

Por tanto:

$$\boxed{S_{II} = \frac{gr}{\tan\theta}} \quad (2)$$

Las expresiones (1) y (2) nos darán en cualquier punto de la superficie los esfuerzos extensionales deseados.

En la expresión (1) cuando r = 0, S_I esta indeterminado. Esto es, en la cercanía de la columna, el - valor de S_I es muy grande. Para evitar esta dificultad - se aumenta, en un radio r tal que el esfuerzo S_I sea elpermisible, el espesor formado una placa que se diseña a flexo-compresión, por no cumplirse la llamada teoría de la membrana en ese tipo de placas donde no puede despreciarse el espesor.

La comparación de este método se presenta a continuación partiendo de las ecuaciones de equilibrio de membrana para superficies de revolución obtenidas por Adolf Pücher.

II.- Ecuaciones de equilibrio en coordenadas cilíndricas.

En la figura (4) se muestra el estado de equilibrio de un elemento de una superficie cualquiera z=f(r) de revolución.

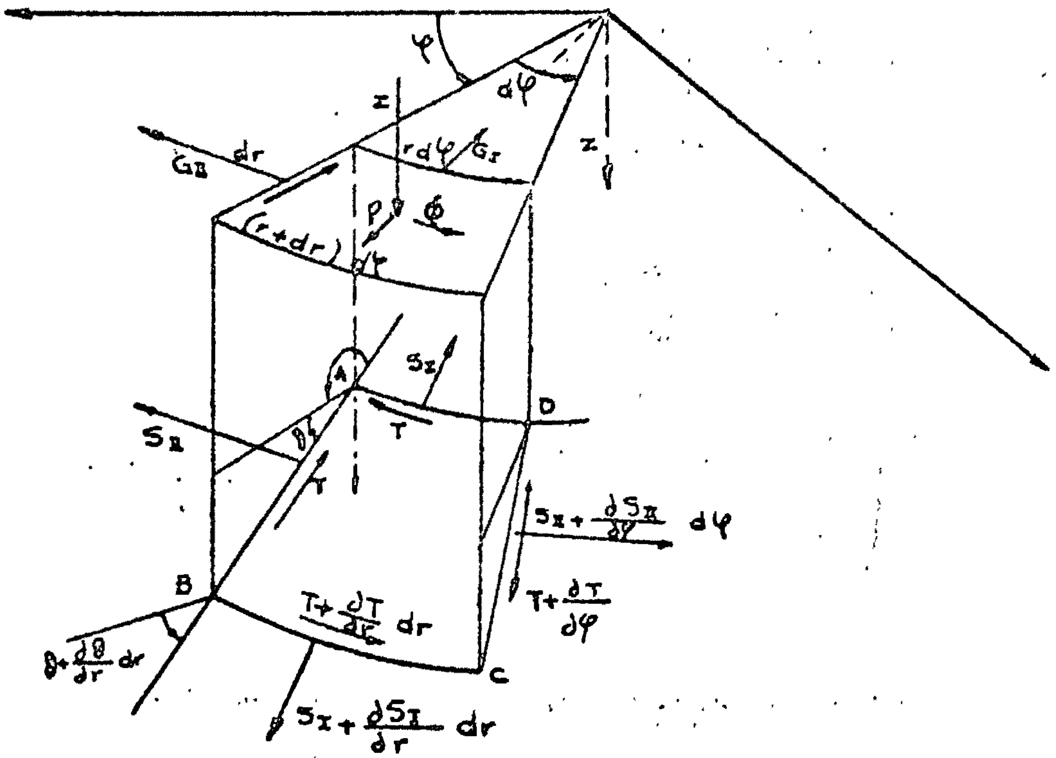

Z, P, y Ø son la carga actuando sobre la superficie proyectada

$$\tan\theta = \frac{\partial z}{\partial r} \qquad\qquad G_I = S_I \cos\theta$$

$$\overline{AD} = r\, d\varphi \qquad\qquad G_{II} = S_{II}\,\frac{1}{\cos\theta}$$

$$\overline{AB} = \frac{dr}{\cos\theta} \qquad\qquad \tau = T$$

Las ecuaciones de equilibrio según la dirección - radial, la dirección de la tangente y en la dirección- del eje z son:

$$(a)\begin{cases} \dfrac{\partial G_I}{\partial r} + \dfrac{G_I - G_{II}}{r} + \dfrac{1}{r}\dfrac{\partial \tau}{\partial \varphi} + P = 0 & (I) \\[2ex] \dfrac{1}{r}\dfrac{\partial G_{II}}{\partial \varphi} + \dfrac{2\tau}{r} + \dfrac{\partial \tau}{\partial r} + \phi = 0 & (II) \\[2ex] \dfrac{\partial (G_I \tan\theta)}{\partial r} + \dfrac{1}{r} G_I \tan\theta + \dfrac{1}{r}\dfrac{\partial (T\tan\theta)}{\partial \varphi} + Z = 0 & (III) \end{cases}$$

Para obtener la función de fuerzas elásticas, observemos que:

$$(b)\begin{cases} G_I = \dfrac{1}{r^2}\dfrac{\partial^2 F}{\partial \varphi^2} + \dfrac{1}{r}\dfrac{\partial F}{\partial r} + A \\[2ex] G_{II} = \dfrac{\partial^2 F}{\partial r^2} + B \\[2ex] \tau = \dfrac{1}{r^2}\dfrac{\partial F}{\partial \varphi} - \dfrac{1}{r}\dfrac{\partial^2 F}{\partial r\,\partial \varphi} = -\dfrac{\partial\left(\frac{1}{r}\frac{\partial F}{\partial \varphi}\right)}{\partial r} \end{cases}$$

Derivando parcialmente las ecuaciones (b) y sustituyendo en las ecuaciones (a) quedan:

$$\frac{dA}{dr} + \frac{A}{r} - B + P = 0 \quad \therefore \quad Ar = \int_{r_1}^{r_2}\left(P + \int_{\varphi_1}^{\varphi_2} \phi\, r\, d\varphi\right) dr$$

$$\frac{1}{r}\frac{\partial B}{\partial \varphi} + \phi = 0 \quad \therefore \quad B = -\int_{\varphi_1}^{\varphi_2} \phi\, r\, d\varphi$$

$$\frac{1}{r}\frac{\partial^2 z}{\partial r^2}\frac{\partial^2 F}{\partial \varphi^2} + \frac{1}{r}\frac{\partial^2 z}{\partial r^2}\frac{\partial F}{\partial r} + \frac{1}{r}\frac{\partial z}{\partial r}\frac{\partial^2 F}{\partial r^2} = -\left[Z + \frac{\partial}{\partial r}\left(A\frac{\partial z}{\partial r}\right) + \frac{A}{r}\frac{\partial z}{\partial r}\right]$$

Aplicando a nuestro caso particular la ecuaciones - obtenidas para el caso general anteriormente: en primer- lugar la carga Z es la carga g obrando sobre la proyección de la superficie ver Fig. 5

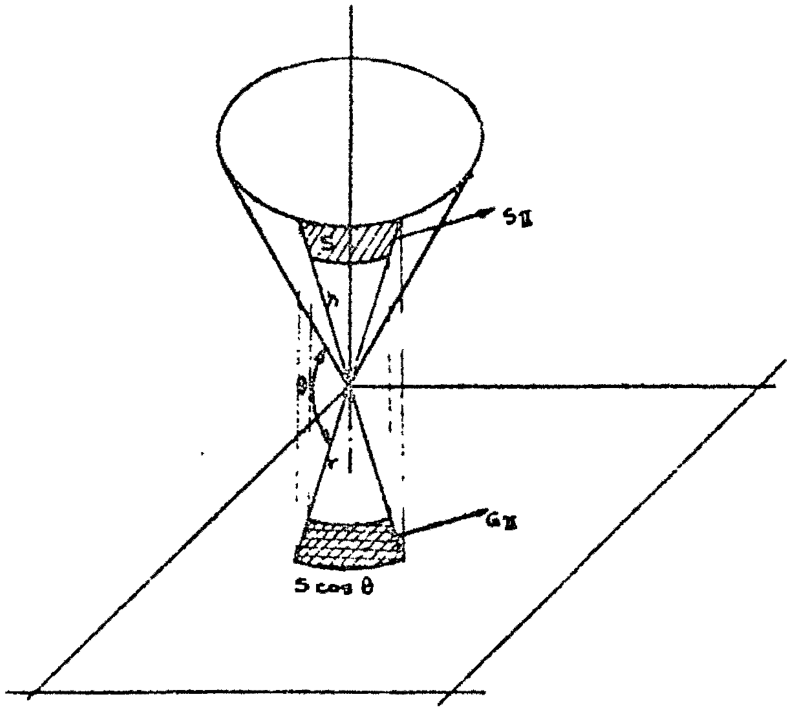

$r = h \cos\theta$

$g = z \cos\theta$

$Z = \dfrac{g}{\cos\theta}$

$$\frac{\partial z}{\partial r} = -\tan\theta$$

$$\frac{\partial^2 z}{\partial r^2} = 0$$

La ecuación de una generatriz recta del cono es -- igual a $z = -r \tan\theta$. $z = f(r)$ por ser un circulo completo.

A y B dependen de P y ϕ que en nuestro caso son nulas y $\dfrac{\partial F}{\partial \varphi} = 0$ por las condiciones de carga y por la simetría.

Entonces de la solucuón de (b)

$$\frac{1}{r}\frac{\partial z}{\partial r}\frac{\partial^2 F}{\partial r^2} = -Z$$

$$\frac{1}{r}\tan\theta\frac{\partial^2 F}{\partial r^2} = Z$$

Si hacemos:

$$\frac{Z}{\tan\theta} = A$$

Por tanto: $\dfrac{\delta^2 F}{\delta r^2} = A r$

Intengrando: $\dfrac{\delta F}{\delta r} = \dfrac{A r^2}{2} + C_1$ (c)

$$F = \frac{A r^3}{6} + C_1 + C_2 \qquad (d)$$

Pero de (c)

$$\frac{\delta^2 F}{\delta r \delta \varphi} = \frac{\delta C_1}{\delta \varphi} = 0$$

y de (d) $\dfrac{\delta F}{\delta \varphi} = r \dfrac{\delta C_1}{\delta \varphi} + \dfrac{\delta C_2}{\delta \varphi} = 0$

Lo cual implica que: $\dfrac{\delta C_2}{\delta \varphi} = 0$

Aplicando la condición de borde para r=R, s_r = 0, - entonces de la la. ecuación de (b)

$$\frac{1}{R^2}\frac{\delta^2 F}{\delta \varphi^2} + \frac{1}{R}\left(\frac{A R^2}{2} + C_1\right) = 0 \qquad (e)$$

Por tanto c_1 $= - a \dfrac{A R^2}{2}$ (f)

Intruduciendo este valor de la ecuación (f) en (d)

$$F = \frac{A r^3}{\delta} - \frac{A R^2}{2} r \qquad \frac{\delta F}{\delta r} = \frac{A r^2}{2} - \frac{A R^2}{2} \qquad (g)$$

$$\frac{\delta F}{\delta r^2} = A r$$

En la la. ecuación de (b)

$$G_I = \frac{A}{2r}(r^2 - R^2)$$

$$G_{II} = Ar$$

$$\tau = 0$$

Las ecuaciones anteriores dan las proyecciones de los esfuerzos de membranas en cualquier punto de la superficie. Cambiando Z por $\frac{g}{\cos\theta}$ y a G_I y G_{II} por s_I y s_{II} resulta:

$$S_I = \frac{G_I}{\cos\theta}\ ;\quad S_{II} = G_{II}\cos\theta \quad y \quad A = \frac{Z}{\tan\theta}$$

$$S_I = \frac{g\ (r^2 - R^2)}{2r\ \mathrm{sen}\,\theta\ \cos\theta}$$

$$\boxed{\begin{aligned} S_I &= \frac{g}{r\ \mathrm{sen}\,2\theta}(r^2 - R^2) \\ S_{II} &= \frac{gr}{\tan\theta} \end{aligned}}$$

Que son las mismas ecuaciones obtenidas anteriormente.

III.- Solución de caso practico.

En el caso practico que se resolvio donde g=200 kg/m²
r= 7.00 mt y $\theta = 16^\circ$ $s_{II} = \frac{200 \times 7 \times 7.50}{2.15} = 4555$ kg/m.l.

Que si espaciamos las barras de refuerzos 20 cms., nos daria una fuerza de 911 kls., que puede ser tomada ampliamente por barra de 3/8".

El esfuerzo s_I max. se encontró a la orilla del plato y su valor fue de:

$$s_I = \frac{200 \quad (49 - 2.25)}{1.50 \quad X \quad 0.53}$$ 11,765 kg/ m.l. por unidad de espeso .

De donde:

$$fc = \frac{11765}{500} = 28.82 \text{ kg/cm}^2$$

Ponencia Nº 21

FORMULAS GENERALES PARA EL CALCULO DE ESFUERZOS EN CASCARONES PARABOLOIDES-HIPERBOLICOS

por el Sr. Arquitecto Don Félix Candela

Datos sobre el Autor:

El Sr. Arquitecto don Félix Candela nació en Madrid, España en 1910, y en 1935 recibió el título de Arquitecto de la Escuela Superior de Arquitectura de Madrid. Radica en México desde 1939, y en 1941 obtuvo la ciudadanía mexicana. Después de varios años de practicar la Arquitectura en México, fundó en 1950, junto con su hermano Antonio, la Empresa "Cubiertas Ala, S. A.", especialista en el diseño y construcción de estructuras de cascarones de concreto armado. Como Presidente de esta firma ha diseñado y construido tan sólo en la Ciudad de México más de 300 estructuras de cascarón. Además ha actuado como Consultor en varios proyectos de cascarones en Sud, y Centro América, y también en los Estados Unidos. Desde 1953 tiene a su cargo una Cátedra de Proyectos en la Escuela de Arquitectura de la Universidad Nacional de México.

A partir de 1955, cuando en un estudio previo del mismo autor, publicado por el Instituto Americano del Concreto,* apareció la designación "HYPAR",** ésta ha sido aceptada con beneplácito, tanto por los Ingenieros cuanto por los Arquitectos, y es ahora ampliamente usada en todo el mundo.

Poco después de publicado dicho estudio observó el autor varios errores en el texto que obscurecían la exposición, y un cambio de variables que motivaba que las fórmulas finales se hiciesen innecesariamente complicadas.

En lugar de limitarnos sólo estrictamente a corregir el texto original, hemos considerado más conveniente, en vista del empleo cada vez mayor de las cubiertas constituidas por este tipo de cascarones de concreto armado, publicar un conjunto de fórmulas más generales. Estas son las que permiten calcular los esfuerzos en un hypar cargado con su propio peso, pero colocado en el espacio en una posición arbitraria, es decir, con carga que presenta componentes a lo largo de los tres ejes del hypar. Las fórmulas mejor conocidas para el hypar con su eje z en posición vertical pueden deducirse como casos particulares a partir de la serie de ecuaciones de carácter más general que son las que presentamos.

* "Aplicaciones estructurales de los cascarones paraboloides hiperbólicos", por Félix Candela, Revista del Instituto Americano del Concreto, Vol. 26, No. 5, Enero-1955.

** Con objeto de simplificar, se ha sugerido abreviar el nombre de paraboloide hiperbólico empleando la designación "HYPAR" que se utilizará de aquí en adelante.

Las anotaciones y figuras son las mismas que empleamos en el estudio antes citado, excepto en aquellos casos cuando se indique cosa en contrario.

Definición de la superficie

Supongamos dos rectas no paralelas en el espacio, las cuales no se cortan: HOD y ABC (Fig. 1) y a las cuales provisionalmente llamaremos *directrices*. Las líneas rectas h_n que interceptan ambas directrices, y que al mismo tiempo

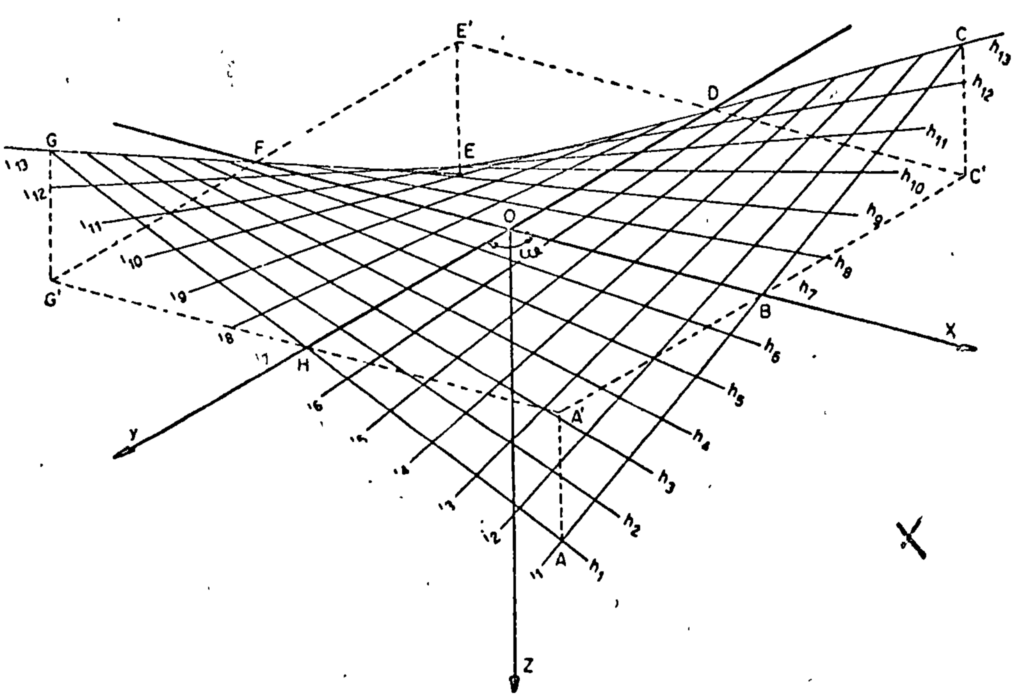

Definición de la Superficie

FIG 1

son paralelas al plano xOz que llamaremos *plano director* son las que definen la superficie. Estas últimas rectas las designaremos como el *primer sistema de generatrices*.

Las dos directrices precitadas determinan a su vez un segundo plano director yOz, paralelo a ellas. La superficie puede considerarse como generada por un *segundo sistema de generatrices* i_n, paralelo a este plano y que intercepta cualquier generatriz h_n del primer sistema.

El hypar está constituido, por lo tanto, por dos sistemas de líneas rectas h_n e i_n, cada sistema paralelo a un plano director, formando ambos planos un ángulo arbitrario ω. Cada punto de la superficie está determinado por la intersección de dos líneas rectas, que quedan dentro de la superficie.

Tomando como ejes de coordenadas a las dos generatrices que pasan por la corona del hypar, y el eje del hypar o sea la intersección de ambos planos

directores, la ecuación de la superficie, en estas coordenadas birectangulares, será:

$$z = kxy \tag{1}$$

siendo k una constante que representa la *pendiente unitaria* o el *alabeo* del hypar (en la Fig. 1, $k = AA'/[OB \,.\, OH]$); $xOy = \omega$ puede ser cualquier ángulo; xOz e yOz son ángulos rectos.

Esta es la *ecuación más sencilla posible* de segundo grado que liga simultáneamente las tres coordenadas de cada punto. Cuando los planos directores forman un ángulo recto ($\omega = 90°$) el hypar es equilátero o rectangular. Cuando ω es cualquier otro ángulo, el hypar es oblicuo. Las secciones planas paralelas a los planos bisectores del ángulo diedro director xOy son parabólicas. Se les designa como *parábolas principales*, y su curvatura es, respectivamente, hacia arriba (GOC), y hacia abajo (AOE); de aquí que la superficie sea anticlástica o de doble curvatura inversa. Todas las demás secciones planas y sus proyecciones sobre el plano xy son hipérbolas o su degradación en dos líneas rectas, excepto aquellas paralelas al eje z las cuales son parábolas, y por supuesto, los cortes paralelos a los planos directores, los cuales son generatrices rectas.

Como una superficie de traslación (Fig. 2), el hypar puede considerarse como generado por una parábola principal ABC que se mueve paralela a sí

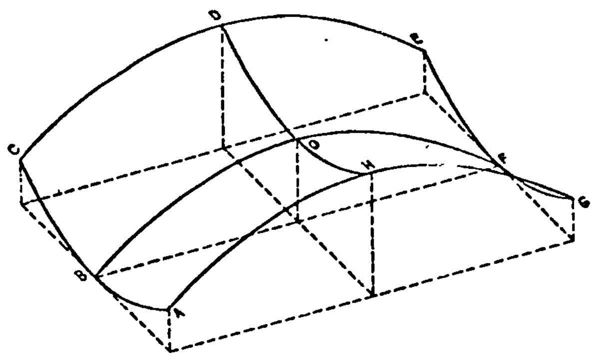

La superficie del Hypar presenta dos sistemas de generatrices parabólicas

FIG. 2

misma a lo largo de la parábola principal inversa BOF. Por lo tanto, la superficie presenta dos sistemas de generatrices parabólicas. Cada sistema está constituido por parábolas idénticas situadas en planos paralelos.

Ecuaciones para el cálculo de esfuerzos en ejes birectangulares

Las ecuaciones para el cálculo de esfuerzos de membrana,* en una superficie representada por $z = f(xy)$, en un sistema de coordenadas en el cual el ángulo xOy puede presentar cualquier valor ω y tanto xOz, cuanto yOz son

* Debe considerarse que en el presente estudio, los esfuerzos referidos, son, hablando estrictamente, esfuerzos unitarios multiplicados por el espesor del cascarón.

ángulos rectos, se obtienen,[6] expresando el equilibrio a lo largo de x, y, y z de las fuerzas que actúan sobre el elemento superficial, mostrado en la Fig. 3, y en la inteligencia que se desprecian las diferenciales de segundo orden. Se tiene así:

$$\frac{\partial v_x}{\partial x} + \frac{\partial \tau}{\partial y} = -X \operatorname{sen} \omega \tag{2a}$$

$$\frac{\partial \tau}{\partial x} + \frac{\partial v_y}{\partial y} = -Y \operatorname{sen} \omega \tag{2b}$$

$$r v_x + t v_y + 2 s \tau = (pX + qY - Z) \operatorname{sen} \omega \tag{2c}$$

donde, de acuerdo con la notación de Monge

$$p = \frac{\partial z}{\partial x}; \quad q = \frac{\partial z}{\partial y}; \quad r = \frac{\partial^2 z}{\partial x^2}; \quad s = \frac{\partial^2 z}{\partial x \partial y}; \quad t = \frac{\partial^2 z}{\partial y^2} \tag{3}$$

−ky sen ω   −kx sen ω

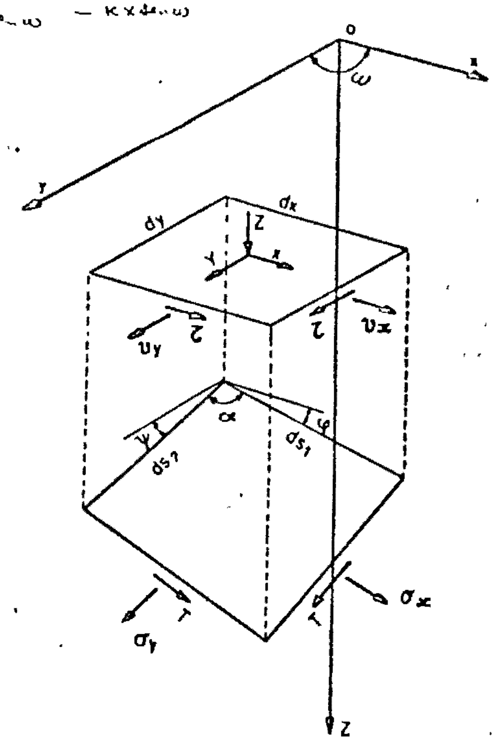

El ángulo α está formado por la intersección de dos generatrices

FIG 3

además v_x, v_t y τ son las proyecciones de los esfuerzos reales sobre el plano xy (Fig. 3).

$$v_x = \sigma_x \sqrt{\frac{1+q^2}{1+p^2}}\,; \quad v_y = \sigma_y \sqrt{\frac{1+p^2}{1+q^2}}\,; \quad \tau = T \tag{4}$$

X, Y, y Z son las coordenadas de los componentes de las fuerzas externas medidas por unidad de superficie proyectada sobre el plano xy.

Todas las fuerzas, esfuerzos, y direcciones de los ejes de coordenadas representados en la Fig. 3, se consideran como positivos.

Ya que el hypar está representado por la ecuación (1):

$$p = ky \quad q = kx \quad r = t = 0 \quad s = k\,, \tag{5}$$

la ecuación (2c) se convierte en:

$$2k\tau = (kyX + kxY - Z) \operatorname{sen} \omega \tag{6}$$

Diferenciando la ecuación (6) con respecto a x, e y, substituyendo en la ecuación (2a) y (2b), e integrando las expresiones resultantes, se obtienen las soluciones generales para v_x y v_y, que contienen funciones arbitrarias respectivamente ya sea de y o de x las cuales deben determinarse para las condiciones de borde. La ecuación (4) da los valores finales de los esfuerzos reales σ_x, σ_y, y τ.

Debe observarse que σ_x y σ_y son componentes oblicuos de los esfuerzos, ya que son paralelos a los lados ds_1 y ds_2 del elemento de superficie. Por consiguiente, el diagrama común de Mohr o círculo diádico no puede usarse para obtener los esfuerzos en otras secciones, excepto en forma sólo aproximada en hypares rectangulares muy planos.

El ángulo α (Fig. 3) formado por dos generatrices que se intersectan se obtiene mediante:

$$\cos \alpha = \frac{pq + \cos \omega}{\sqrt{(1+p^2)\,(1+q^2)}} \tag{7}$$

En forma análoga, el ángulo β formado por cualquier sección contenida en el primer cuadrante, y la porción positiva de la generatriz x que pasa por un punto (Fig. 4) se obtiene mediante:

$$\cos \beta = \frac{pq_\beta + \cos \omega_\beta}{\sqrt{(1+p^2)\,(1+q^2_\beta)}} \tag{8}$$

En el cual ω_β es la proyección del ángulo β sobre el plano xy y q_β es la tangente trigonométrica del ángulo formado por la linea recta que representa la sección con el plano xy. Con objeto de evitar errores, es indispensable apegarse estrictamente al empleo de los signos convenidos. El signo del producto pq_β será positivo cuando ambos lados del ángulo ω_β son ascendentes o descendentes a partir del vértice. Será negativo cuando un lado va hacia arriba y el otro hacia abajo en relación con el propio vértice.

Los esfuerzos normal y tangencial σ_β y τ_β en cualquier sección como la indicada se obtienen considerando el equilibrio en las direcciones σ_β y τ_β, respectivamente (Fig. 4).

$$\sigma_\beta = \sigma_x \frac{\operatorname{sen}^2 \beta}{\operatorname{sen} \alpha} + 2\tau \frac{\operatorname{sen} \beta \operatorname{sen}(\beta - \alpha)}{\operatorname{sen} \alpha} + \sigma_y \frac{\operatorname{sen}^2 (\beta - \alpha)}{\operatorname{sen} \alpha} \tag{9a}$$

$$\tau_\beta = -\sigma_x \frac{\operatorname{sen} \beta \cos \beta}{\operatorname{sen} \alpha} - \tau \frac{\operatorname{sen}(2\beta - \alpha)}{\operatorname{sen} \alpha} - \sigma_y \frac{\operatorname{sen}(\beta - \alpha) \cos(\beta - \alpha)}{\operatorname{sen} \alpha} \tag{9b}$$

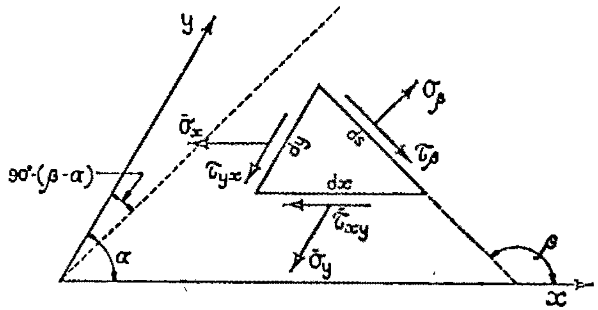

Condiciones de Equilibrio

FIG 4

Se determinan las direcciones de los esfuerzos principales igualando τ_β con cero en la ecuación (9b)

$$tg2\,\theta = \frac{2\tau \operatorname{sen} \alpha + \sigma_y \operatorname{sen} 2\alpha}{\sigma_x + 2\tau \cos \alpha + \sigma_y \cos 2\alpha} \qquad (10)$$

θ y $(90° - \theta)$ son los ángulos de los esfuerzos principales con la parte positiva de la generatriz x que pasa por el punto considerado. Los valores de los esfuerzos principales son:

$$\sigma_I = \sigma_x \frac{\operatorname{sen}^2 \theta}{\operatorname{sen} \alpha} + 2\tau \frac{\operatorname{sen} \theta \operatorname{sen} (\theta - \alpha)}{\operatorname{sen} \alpha} + \sigma_y \frac{\operatorname{sen}^2 (\theta - \alpha)}{\operatorname{sen} \alpha} \qquad (11a)$$

$$\sigma_{II} = \sigma_x \frac{\cos^2 \theta}{\operatorname{sen} \alpha} + 2\tau \frac{\cos \theta \cos (\theta - \alpha)}{\operatorname{sen} \alpha} + \sigma_y \frac{\cos^2 (\theta - \alpha)}{\operatorname{sen} \alpha} \qquad (11b)$$

Hypar con carga uniformemente distribuida en su superficie (carga muerta)

Supondremos en este análisis que el eje z del hypar tiene una posición arbitraria en el espacio. En consecuencia, la carga tendrá 3 componentes X_1, Y_1 y Z_1, a lo largo de los 3 ejes del hypar. Estos componentes están relacionados a las fuerzas X, Y y Z (tal como aparecen en las ecuaciones: 2a, 2b, 2c), por la relación entre el área real del elemento de superficie, y el área de su proyección sobre el plano xy.

$$X\, dx\, dy \operatorname{sen} \omega = X_1\, ds_1\, ds_2 \operatorname{sen} \alpha \qquad (12)$$

De la ecuación (7) obtenemos:

$$\operatorname{sen}^2 \alpha = \frac{1 + p^2 + q^2 + p^2q^2 - p^2q^2 - \cos^2 \omega - 2pq \cos \omega}{(1 + p^2)\,(1 + q^2)} \qquad (13)$$

$$\operatorname{sen} \alpha = \frac{\sqrt{\operatorname{sen}^2 \omega + p^2 + q^2 - 2pq \cos \omega}}{\sqrt{(1 + p^2)(1 + q^2)}}$$

además (Fig. 3)

$$\frac{ds_1}{dx} = \sec \varphi = \sqrt{1 + p^2}; \quad \frac{ds_2}{dy} = \sec \psi = \sqrt{1 + q^2}; \qquad (14a\text{, }14b)$$

Substituyendo las ecuaciones (13, 14a, 14b), en la ecuación (12), se tiene:

$$X \operatorname{sen} \omega = X_1 \sqrt{\operatorname{sen}^2 \omega + p^2 + q^2 - 2pq \cos \omega} = X_1 \sqrt{\phi} \qquad (15a)$$

siendo

$$\phi = \operatorname{sen}^2 \omega + p^2 + q^2 - 2pq \cos \omega = \operatorname{sen}^2 \omega + k^2y^2 + k^2x^2 - 2k^2xy \cos \omega \qquad (16)$$

Análogamente

$$Y \operatorname{sen} \omega = Y_1 \sqrt{\phi} \qquad (15b)$$

$$Z \operatorname{sen} \omega = Z_1 \sqrt{\phi} \qquad (15c)$$

y finalmente las ecuaciones 2a, 2b, y 2c, se transforman en:

$$\frac{\partial \nu_x}{\partial x} + \frac{\partial \tau}{\partial y} = -X_1 \sqrt{\phi} \qquad (17a)$$

$$\frac{\partial \tau}{\partial x} + \frac{\partial \nu_y}{\partial y} = -Y_1 \sqrt{\phi} \qquad (17b)$$

$$\tau = \left(\frac{y}{2} X_1 + \frac{x}{2} Y_1 - \frac{Z_1}{2k} \right) \sqrt{\phi} \qquad (17c)$$

La ecuación (17c) es una expresión algebraica la cual inequivocamente proporciona el valor de τ en cada punto. Diferenciando (17c) con respecto a x, e y, sustituyendo estas diferenciales en las ecuaciones (17a, 17b), e integrando las ecuaciones resultantes con respecto a y y x, se obtienen las ecuaciones para ν_x y ν_y.

$$\frac{\partial \tau}{\partial y} = \frac{1}{2} X_1 \sqrt{\phi} + k^2X_1 \frac{y(y - x \cos \omega)}{2\sqrt{\phi}} + $$

$$+ k^2Y_1 \frac{x(y - x \cos \omega)}{2\sqrt{\phi}} - kZ_1 \frac{y - x \cos \omega}{2\sqrt{\phi}}$$

Sustituyendo en la ecuación (17a)

$$\nu_x = -\frac{1}{2} \int \left[3X_1 \sqrt{\phi} + \frac{k^2X_1\, y^2 - k\, Z_1 y}{\sqrt{\phi}} + \right.$$

$$\left. + \frac{(k^2Y_1\, y - k^2 \cos \omega\, X_1\, y + k \cos \omega Z_1)\, x}{\sqrt{\phi}} - k^2 \cos \omega\, Y_1 \frac{x^2}{\sqrt{\phi}} \right] dx$$

Resolviendo la integral anterior se tiene

$$\nu_x = \left[\frac{1}{4} (\cos \omega\, Y_1 - 3X_1)\, x + \left(\frac{5}{4} \cos \omega\, X_1 - \frac{1}{2} Y_1 + \frac{3}{4} \ldots^2 \omega\, Y_1 \right) y - \right.$$

$$-\frac{1}{2k}\cos\omega\, Z_1\Big]\sqrt{\phi}+\Big[\Big(-\frac{5}{4}k\,\mathrm{sen}^2\omega\, X_1-\frac{3}{4}k\cos\omega\,\mathrm{sen}^2\omega\, Y_1\Big)y^2+$$

$$+\Big(\frac{1}{2}Z_1\,\mathrm{sen}^2\omega\Big)y-\frac{1}{4k}\mathrm{sen}^2\omega(3X_1+\cos\omega\, Y_1)\Big]\cdot$$

$$\cdot\,\mathrm{Log}_n\frac{kx-ky\cos\omega+\sqrt{\phi}}{\mathrm{sen}\,\omega\sqrt{1+k^2y^2}}+f_1(y)$$

o en forma abreviada

$$\nu_x=(A_1x+A_2y+A_3)\sqrt{\phi}+(A_4y^2+A_5y+A_0)\mathrm{Log}_n\,[X_7]+f_1(y) \qquad (18a)$$

en la cual

$$A_1=\frac{1}{4}(\cos\omega\, Y_1-3X_1)$$

$$A_2=\frac{5}{4}\cos\omega\, X_1-\frac{1}{2}Y_1+\frac{3}{4}\cos^2\omega\, Y_1$$

$$A_3=-\frac{1}{2k}\cos\omega\, Z_1$$

$$A_4=-\frac{5}{4}k\,\mathrm{sen}^2\omega\, X_1-\frac{3}{4}k\cos\omega\,\mathrm{sen}^2\omega\, Y_1$$

$$A_5=\frac{1}{2}\mathrm{sen}^2\omega\, Z_1$$

$$A_0=-\frac{1}{4k}\mathrm{sen}^2\omega\,(3X_1+\cos\omega\, Y_1)$$

$$X_7=\frac{kx-ky\cos\omega+\sqrt{\phi}}{\mathrm{sen}\,\omega\sqrt{1+k^2y^2}}$$

Análogamente

$$\nu_y=(B_1y+B_2x+B_3)\sqrt{\phi}+(B_4x^2+B_5x+B_6)\mathrm{Log}_n\,[Y_7]+f_2(x) \qquad (18b)$$

donde,

$$B_1=\frac{1}{4}(\cos\omega\, X_1-3Y_1)$$

$$B_2=\frac{5}{4}\cos\omega\, Y_1-\frac{1}{2}X_1+\frac{3}{4}\cos^2\omega\, X_1$$

$$B_3=-\frac{1}{2k}\cos\omega\, Z_1=A_3$$

$$B_4=-\frac{5}{4}k\,\mathrm{sen}^2\omega\, Y_1-\frac{3}{4}k\cos\omega\,\mathrm{sen}^2\omega\, X_1$$

$$B_5=\frac{1}{2}\mathrm{sen}^2\omega\, Z_1=A_5$$

$$B_6=-\frac{1}{4k}\mathrm{sen}^2\omega\,(3Y_1+\cos\omega\, X_1)$$

$$Y_7=\frac{ky-kx\cos\omega+\sqrt{\phi}}{\mathrm{sen}\,\omega\sqrt{1+k^2x^2}}$$

$f_1(y)$ y $f_2(x)$ en las ecuaciones (18a) y (18b) son funciones arbitrarias de integración, las cuales nos permiten satisfacer determinadas condiciones de borde.

Casos particulares

Las simplificaciones de las ecuaciones (17c, 18a, 18b), para otras inclinaciones de los ejes en relación con la vertical o para hypares rectangulares se obtienen fácilmente mediante la cancelación de los valores correspondientes en las ecuaciones generales. Las simplificaciones más comunes son:

a) $\omega=90°$ (Hypar rectangular)

$$\mathrm{sen}\,\omega=1\,,\ \cos\omega=0 \quad A_3=B_3=0$$

$$\sqrt{\phi}=\sqrt{1+k^2y^2+k^2x^2}$$

$$\tau=\Big(\frac{1}{2}X_1y+\frac{1}{2}Y_1x-\frac{1}{2k}Z_1\Big)\sqrt{\phi} \qquad (19a)$$

$$\nu_x=\Big(-\frac{3}{4}X_1x-\frac{1}{2}Y_1y\Big)\sqrt{\phi}+\Big(-\frac{5}{4}kX_1y^2+\frac{1}{2}Z_1y-\frac{3}{4k}X_1\Big)\cdot$$

$$\cdot\,\mathrm{Log}_n\frac{kx+\sqrt{\phi}}{\sqrt{1+k^2y^2}}+f_1(y) \qquad (19b)$$

$$\nu_y=\Big(-\frac{3}{4}Y_1y-\frac{1}{2}X_1x\Big)\sqrt{\phi}+\Big(-\frac{5}{4}kY_1x^2+\frac{1}{2}Z_1x-\frac{3}{4k}Y_1\Big)\cdot$$

$$\cdot\,\mathrm{Log}_n\frac{ky+\sqrt{\phi}}{\sqrt{1+k^2x^2}}+f_2(x) \qquad (19c)$$

b) $X_1=0$; $Y_1=0$ (Hypar con el eje z vertical) (Fig. 5)

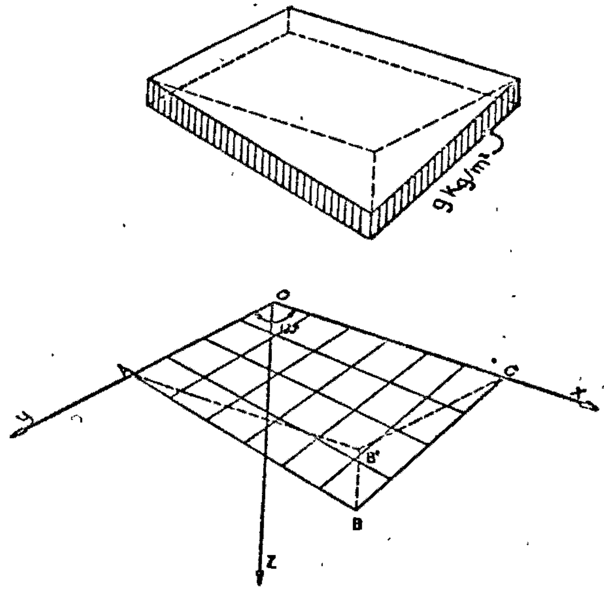

Carga uniformemente repartida sobre la superficie, y actuando en la dirección de Z

FIG 5

$$\tau = -\frac{1}{2k} Z_1 \sqrt{\phi} \tag{20a}$$

$$v_x = -\frac{1}{2k} Z_1 \cos\omega \sqrt{\phi} + \frac{1}{2} \operatorname{sen}^2\omega\, Z_1 y \operatorname{Log}_n \frac{kx - ky\cos\omega + \sqrt{\phi}}{\operatorname{sen}\omega \sqrt{1 + k^2y^2}} + f_1(y) \tag{20b}$$

$$v_y = -\frac{1}{2k} Z_1 \cos\omega \sqrt{\phi} + \frac{1}{2} \operatorname{sen}^2\omega\, Z_1 x \operatorname{Log}_n \frac{ky - kx\cos\omega + \sqrt{\phi}}{\operatorname{sen}\omega \sqrt{1 + k^2x^2}} + f_2(x) \tag{20c}$$

c) $X_1 = 0$, $Y_1 = 0$, $\omega = 90°$ (Hypar rectangular con el eje z vertical)

$$\tau = -\frac{1}{2k} Z_1 \sqrt{\phi} \tag{21a}$$

$$v_x = \frac{1}{2} Z_1 y \operatorname{Log}_n \frac{kx + \sqrt{\phi}}{\sqrt{1 + k^2y^2}} + f_1(y) \tag{21b}$$

$$v_y = \frac{1}{2} Z_1 x \operatorname{Log}_n \frac{ky + \sqrt{\phi}}{\sqrt{1 + k^2x^2}} + f_2(x) \qquad (21$$

d) $X_1 = 0$, $Y_1 = 0$, $Z_1 = Z = g =$ constante (Fig. 6) (carga uniformemente repartida sobre la proyección horizontal, siendo vertical el eje z).

$$\tau = -\frac{g \operatorname{sen}\omega}{2k} = \text{constante} \tag{22a}$$

$$v_x = f_1(y) \tag{22b}$$

$$v_y = f_2(x) \tag{22c}$$

$f_1(y)$, y $f_2(x)$ son funciones arbitrarias de integración y pueden tener cualquier valor, inclusive 0, lo cual da $v_x = 0$, $v_y = 0$. En este caso $\theta \simeq \omega/2$ y ambos esfuerzos principales tienen el mismo valor absoluto de τ y su dirección es aproximadamente la que se tiene a lo largo de las líneas bisectrices del ángulo ω.

$$\sigma_I = -\sigma_{II} = |\tau| \tag{23}$$

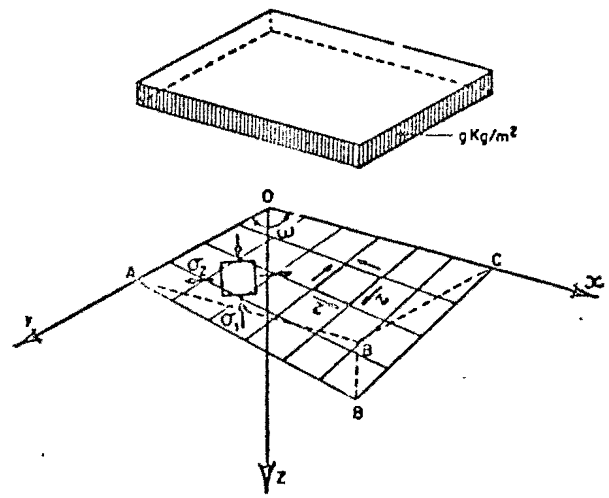

Carga uniformemente repartida sobre la proyección horizontal

FIG. 6

Este caso, muy particular, es el más comúnmente conocido, pero debemos recordar que tratándose de una simplificación aproximada de la fórmula general, que supone a g prácticamente constante y α casi igual a ω en cualquier punto de la superficie, sólo puede aplicarse en un número muy limitado de casos, cuando el eje z es vertical y la superficie es suficientemente plana para permitirnos considerar la carga efectiva, como uniformemente repartida sobre el plano xy. Si la elevación se incrementa sustancialmente, o el eje z deja de ser vertical, se deberán emplear las fórmulas más generales.

Debe observarse que en todos los casos el valor de τ se define en forma fija, mediante la ecuación (17c); pero los valores v_x, v_y y σ_x, y σ_y pueden ser variables que dependen de los valores seleccionados para las funciones arbitrarias de integración $f_1(y)$ y $f_2(x)$ que aparecen en las ecuaciones (18a, 18b). Esto significa que los esfuerzos oblicuos en una superficie no limit son estáticamente indeterminados, o hiperestáticos. Para poder determinarlos necesitamos fijar las condiciones de borde o arista. Esta propiedad nos da alguna libertad para seleccionar los dispositivos de borde o de soporte.

Condiciones de borde

a) *Hypar limitado por generatrices rectas*

Dando los valores convenientes a las funciones arbitrarias de integración, es posible dejar dos lados contiguos de cualquier cuadrángulo alabeado exentos de esfuerzos oblicuos. Pero por supuesto los esfuerzos en los dos lados

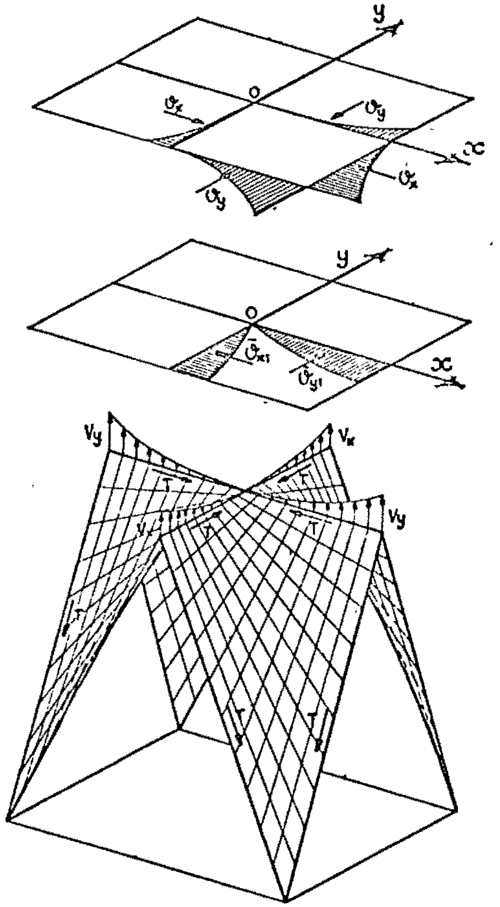

Formas estructurales obtenidas por asociación de cuadrángulos alabeados

FIG. 7

opuestos tomarán un valor fijo y determinado, y estas aristas estarán sujetas a fuerzas oblicuas que deben soportarse proveyendo un apoyo continuo a lo largo de ellas. Esto significa que en la práctica será suficiente encontrar el valor numérico, que debe sumarse a los esfuerzos a lo largo de cada generatriz (dentro del entramado de ellas que queramos considerar) para poder satisfacer las

condiciones de apoyo en determinado borde. Podemos por ejemplo, suprimir el componente oblicuo del esfuerzo a lo largo de un borde, introduciendo como Δv_x o Δv_y, un grupo de esfuerzos iguales y opuestos a los resultantes en el propio borde según las ecuaciones (18a) o (18b), pero esto involucra la introducción de los mismos esfuerzos adicionales en el borde opuesto, como si cada generatriz fuese un tirante o un puntal, y producirá por consiguiente, alteraciones en el estado de esfuerzos en los puntos interiores de la superficie.

De estas consideraciones resulta que un cuadrángulo alabeado sencillo sometido a este tipo de carga, no puede estar en equilibrio, a menos que siquiera dos lados contiguos estén provistos de miembros de borde o elementos de apoyo capaces de resistir cargas en cualquier dirección. Consideraciones de simetría en la asociación de varios cuadrángulos alabeados pueden motivar simplificaciones de las condiciones de apoyo necesarias; pero existirán siempre componentes de esfuerzo no equilibrados a lo largo de determinadas aristas (Figura 7).

Dado que los esfuerzos cortantes a lo largo de las generatrices se han considerado como fijos, es imposible que cualquier borde recto quede exento de esfuerzo cortante. Las fuerzas tangenciales resultantes de la adición de esfuerzos cortantes a lo largo del borde deben ser soportados por el propio borde trabajando en tensión o en compresión.

b) *Hypar con bordes de curvatura arbitraria*

Puesto que en las fórmulas (9a y 9b), que dan los esfuerzos normales y tangenciales sobre cualquier sección no paralela a las generatrices, σ_x y σ_y, pueden tener cualquier valor arbitrario, es decir, son variables, es posible en el caso de un borde curvo dar a σ_β y τ_β, cualquier valor optativo, inclusive cero. Cuando se anulan σ_β y τ_β a lo largo de dicho borde, es claro que estando este borde exento de esfuerzos, no requiere ningún elemento auxiliar de rigidez. Esto puede dar como resultado un borde de líneas extremadamente gráciles. Los valores de σ_x y σ_y requeridos para anular σ_β y τ_β, se obtienen haciendo las ecuaciones (9a, y 9b), iguales a cero.

$$\overline{\sigma}_x = -\tau \frac{\operatorname{sen}(\beta-\alpha)}{\operatorname{sen}\beta} \tag{24a}$$

$$\overline{\sigma}_y = -\tau \frac{\operatorname{sen}\beta}{\operatorname{sen}(\beta-\alpha)} \tag{24b}$$

Si por otra parte, fijamos de antemano los valores de σ_β y τ_β correspondientes a cada punto del borde, los valores de σ_x y σ_y necesarios para equilibrar dichos esfuerzos se obtienen mediante:

$$\overline{\sigma}_x = \sigma_\beta \frac{\cos(\beta-\alpha)}{\operatorname{sen}\beta} - (\tau_\beta+\tau)\frac{\operatorname{sen}(\beta-\alpha)}{\operatorname{sen}\beta} \tag{25a}$$

$$\overline{\sigma}_y = (\tau_\beta-\tau)\frac{\operatorname{sen}\beta}{\operatorname{sen}(\beta-\alpha)} - \sigma_\beta\frac{\cos\beta}{\operatorname{sen}(\beta-\alpha)} \tag{25b}$$

Una vez que los valores $\overline{\sigma}_x$ y $\overline{\sigma}_y$ en los puntos de borde han sido determinados, los propios valores a lo largo de las generatrices que interceptan dicho orde se consideran con un valor ya no indeterminado sino fijo. Cuando estas eneratrices interceptan otro borde, los esfuerzos de borde resultantes σ_β, y τ_β ›btenidos mediante las ecuaciones (9a) y (9b) se deberán soportar mediante ın apoyo integro, es decir, un apoyo que pueda resistir fuerzas en cualquier lirección. La distribución simétrica de varios hypares puede conducir a simılificar las condiciones necesarias de apoyo. Por ejemplo, en las aristas de cualquier bóveda con aristas simétricas, sólo permanecerán fuerzas en el plano

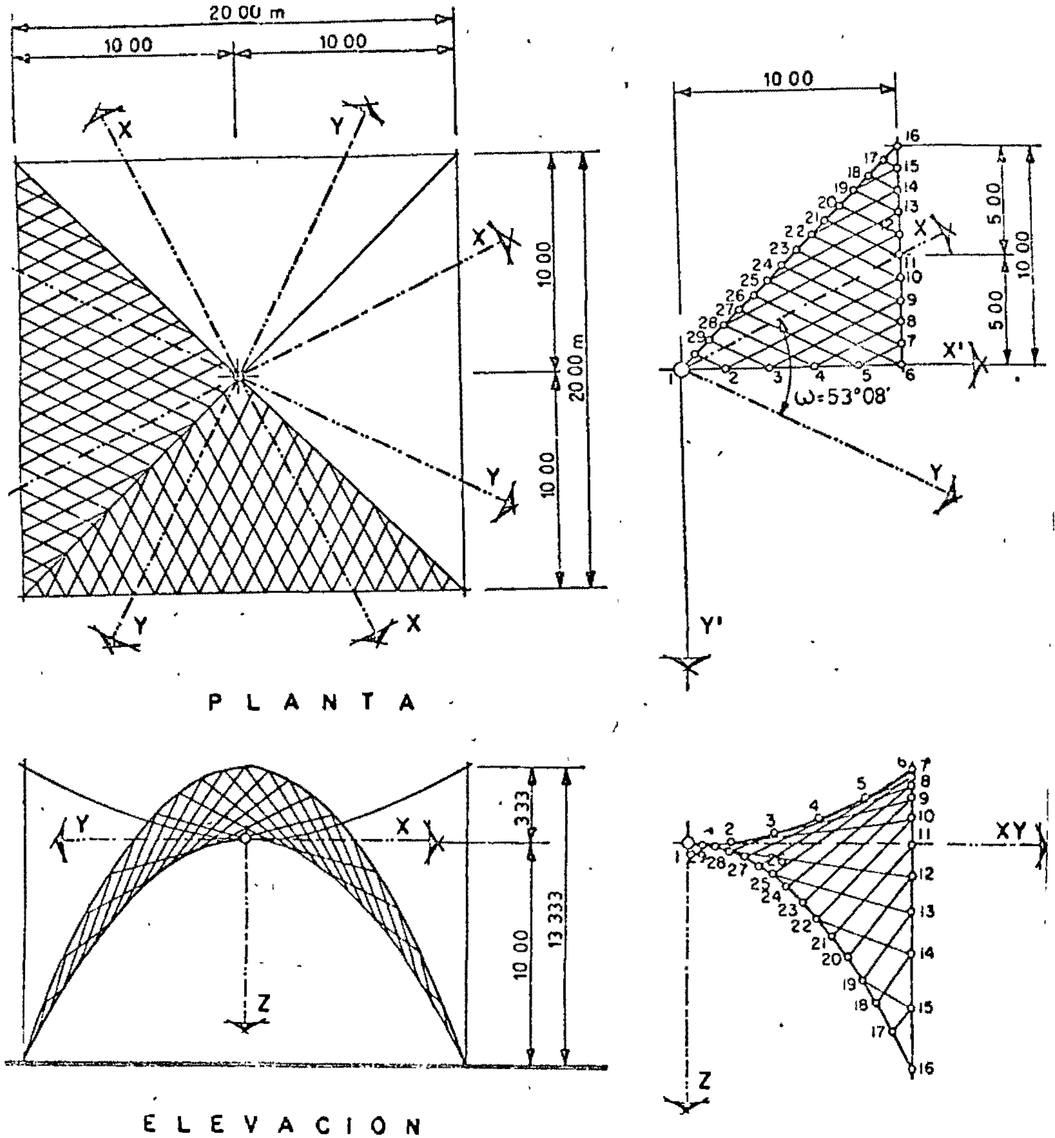

Fig. 8.
Boveda por aris' bre planta cuadrada L = 20 m, h = 10 m; $\omega/2$ = 26° 34', espesor = 4 cm

de la arista, puesto que las fuerzas normales a este plano se anulan una a otra con aquellas que provienen de superficies contiguas.

Hay algunas consideraciones importantes respecto al análisis práctico. Debemos tener presente, por ejemplo que cuando investigamos los puntos de cualquier entramado formado por generatrices, estamos empleando un método de diferencias finitas, en el cual la longitud real de cada intervalo cambia con su posición, pero los esfuerzos que actúan sobre cada punto de intersección, son esfuerzos unitarios o esfuerzos por unidad de longitud. Cuando los esfuerzos se transmiten de uno a otro extremo de una generatriz, la diferencia de longitud del intervalo sobre el cual estos esfuerzos están actuando en cada extremo se deberá tomar en cuenta.

Por otra parte, si empleamos las proyecciones de los esfuerzos ν_x, y ν_y, y las proyecciones de los intervalos sobre el plano xy, los estamos distribuyendo de acuerdo con una repartición uniforme, en la cual los intervalos son constantes. Para transmitir los esfuerzos debemos primero encontrar ν_x a partir de σ_x en un extremo, trasladar ν_x al otro extremo, y entonces encontrar σ_x a partir de ν_x sobre este último extremo.

En la Fig. 8, puede verse el caso de una bóveda por arista sobre una planta en cuadro: $L = 20$ m; $h = 10$ m; $\omega/2 = 26° 34'$; espesor = 4 cm

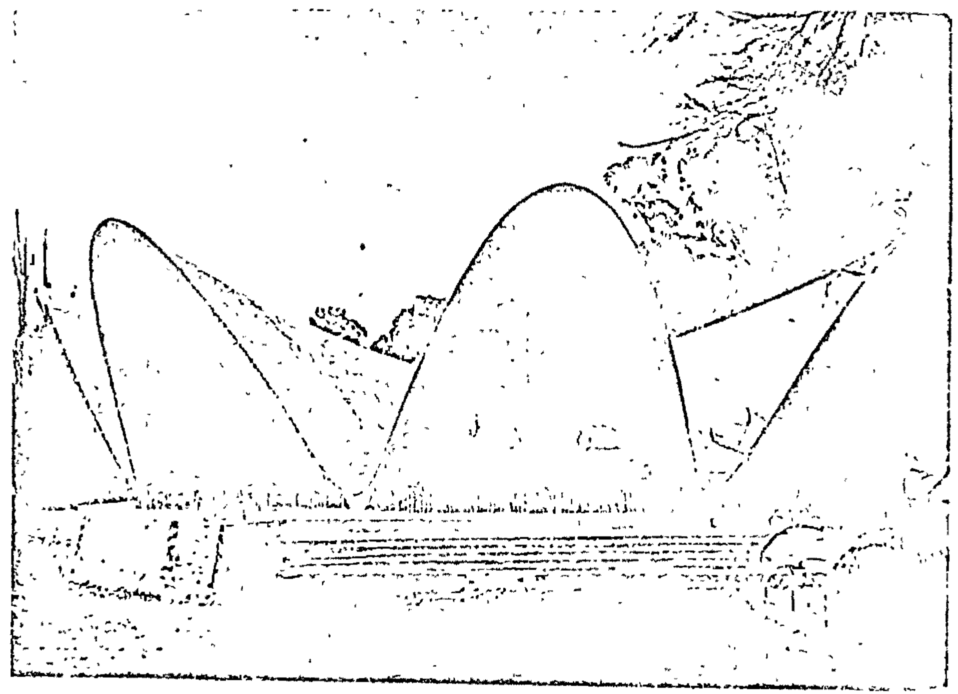

CUBIERTA CONSTITUIDA POR HYPARES, 8 GAJOS
Restaurante en Xochimilco, México, D F
Arq Joaquín Alvarez Ordoñez

Fig. 9

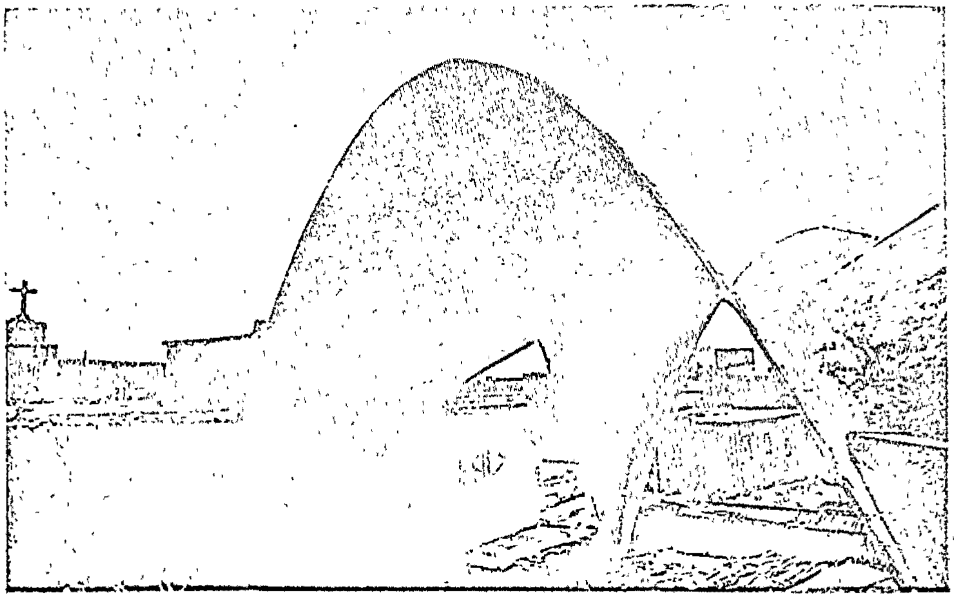

CUBIERTA CONSTITUIDA POR HYPARES
Iglesia de San Antonio de las Huertas, México, D F
Arq Enrique de la Mora

Fig 10

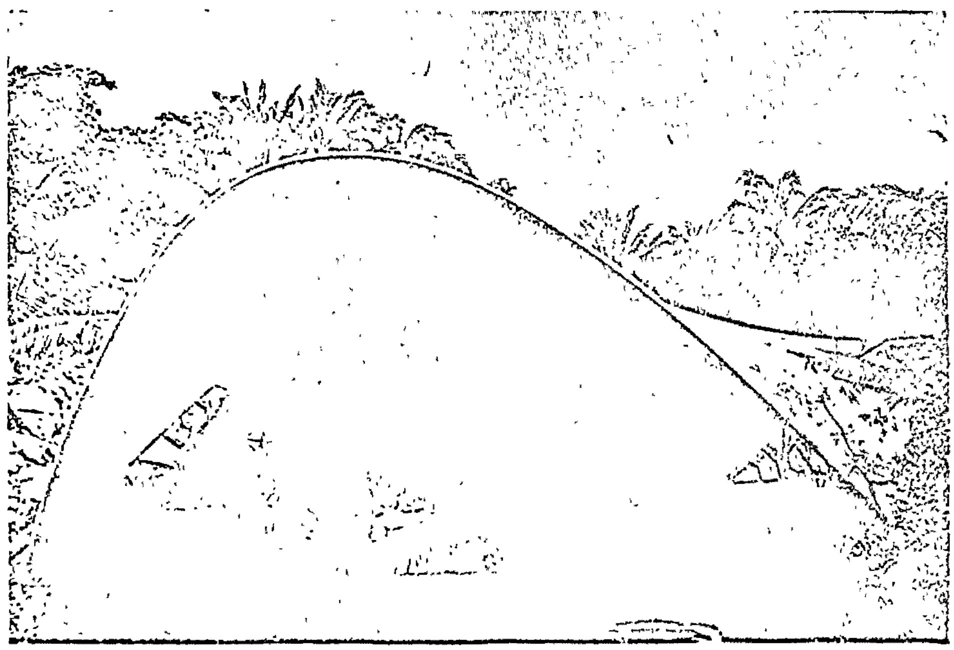

CUBIERTA CONSTITUIDA POR HYPARES, 3 GAJOS
Centro nocturno la Jacaranda, en Acapulco
Arq. Juan Sordo Madaleno

Fig 11

centro de educación contínua
facultad de ingeniería, unam

DISEÑO Y CONSTRUCCION DE ESTRUCTURAS ESPACIALES Y DE CASCARON

CASCARONES DE DOBLE CURVATURA

Dr. Porfirio Ballesteros

1972

Tacuba 5, primer piso. México 1, D.F.
Teléfonos: 521-30-95 y 513-27-95

Porfirio Ballesteros

CASCARONES DE DOBLE CURVATURA

AMERICAN SOCIETY OF CIVIL ENGINEERS

Founded November 5, 1852

TRANSACTIONS

Paper No. 2951

SHELLS OF DOUBLE CURVATURE

By Alfred L. Parme,[1] A. M. ASCE

With Discussion by Messrs. Tung Au; W. Watters Pagon; Santi P. Banerjee; Mario G. Salvadori; and Alfred L. Parme

Synopsis

A comprehensive derivation of formulas for the evaluation of the membrane forces acting in any doubly curved shell is presented. For the specific case of an elliptical paraboloid shell, numerical tables are given, thus simplifying the determination of the stresses. The applicability of these tabular values to other doubly curved shells is shown together with illustrative examples.

Introduction

The great strength of doubly curved concrete shells with edges stiffened by arches or ribs is due to their ability to support any continuous load principally by direct stresses—that is, by axial compression or tension. Moreover, the stresses for these shells, including those that are extremely thin, are relatively small compared with the compressive strength of concrete. The shell is free of flexural forces except for localized bending, which may occur near the edges of a doubly curved shell, due to the effect on the shell of the displacement of the edge members. This behavior is not restricted solely to surfaces of revolution that are suitably restrained horizontally and vertically at the base, but is typical of most doubly curved shells with edge beams. As will be described subsequently, it is not necessary that the edge members be capable of resisting lateral forces.

The direct forces acting in a doubly curved shell are obtained directly from a considera . . of statics only. There are innumerable coordinate systems that can be used to express the interrelationship between the internal forces acting in a shell. It has been found, however, that for the general case the Cartesian system leads to the simplest expressions.

Note.—Published, essentially as printed here, in September, 1956, in the Journal of the Structural Division, as *Proceedings Paper 1057*. Positions and titles given are those in effect when the paper or discussion was approved for publication in *Transactions*.

[1] Mgr., Structural & Railways Bureau, Portland Cement Assn., Chicago, Ill.

Adopting this coordinate system for convenience, a representative small element of a shell of double curvature is formed, as shown in Fig. 1, by two radial planes whose horizontal lines are parallel to the y-axis and by two other radial planes in which the horizontal lines are parallel to the x-axis. The direct forces, T_x and T_y, measured in pounds per unit length, are considered positive when they create tension. The shearing force, S, also measured in pounds per unit length, is positive when it creates tension in the diagonal direction of increasing values of x and y. The surface load, w, is considered positive when acting downward. The forces acting on the element are resolved into components that are parallel to the coordinate system but have their direction tangential to the surface. Thus, force T_x is parallel to the (zx)-plane but is inclined by the angle, ϕ, to the (xy)-plane.

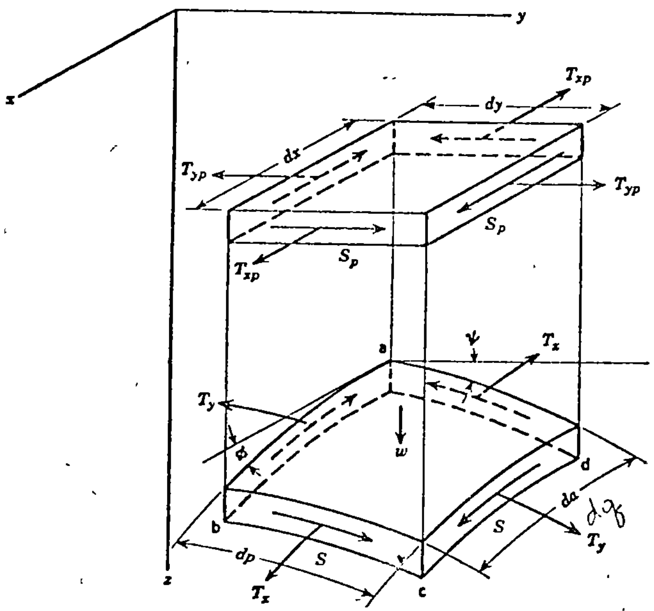

FIG. 1 —ELEMENT OF A SHELL OF DOUBLE CURVATURE

A considerable simplification[2] in the expressions for the equilibrium of forces parallel to the various axes results if the actual forces are transformed into fictitious forces acting on the projected area of the lower element in Fig. 1. From geometry it is evident that

$$dp \cos\psi = dy \qquad \text{(1a)}$$

and

$$dq \cos\phi = dx \qquad \text{(1b)}$$

The horizontal component of the normal force, T_x, acting on face ad is $T_x \cos\phi\, dp$

[2] "Stress Conditions in Shells Neglecting Bending," by K. W. Johansen, *Bygningsstatiske Meddelelser*, Dansk Selskab for Bygningsstatik, Copenhagen, 1938, pp. 61–84.

which, by introducing the notation of Eq. 1a, becomes $T_x(\cos\phi/\cos\psi)\,dy$. If the projected element is to have the same total force acting on it as the actual element,

$$T_{xp}\,dy = T_x \frac{\cos\phi}{\cos\psi}\,dy \qquad \text{(2a)}$$

or

$$T_{xp} = T_x \frac{\cos\phi}{\cos\psi} \qquad \text{(2b)}$$

Similarly,

$$T_{yp} = T_y \frac{\cos\psi}{\cos\phi} \qquad \text{(3)}$$

Equating the horizontal component of the shear acting on face ad to the shear on the projected element,

$$S\,dp \cos\psi = S_p\,dy \qquad \text{(4a)}$$

Substituting for the value of dp its value from Eq. 1a results in

$$S = S_p \qquad \text{(4b)}$$

Assuming that only a vertical load acts on the shell and recognizing that the forces acting on the element vary from the near face to the far face, the equilibrium of forces in the x-direction expressed in terms of T_{xp}, T_{yp}, and S_p (horizontal components of the actual forces) yields

$$\frac{\partial T_{xp}}{\partial x} + \frac{\partial S_p}{\partial y} = 0 \qquad \text{(5)}$$

Equilibrium of the forces in the y-direction results in

$$\frac{\partial T_{yp}}{\partial y} + \frac{\partial S_p}{\partial x} = 0 \qquad \text{(6)}$$

In order to establish the equations of equilibrium of forces in the z-direction, it is necessary first to obtain their vertical components. The vertical component of the normal force, T_x, acting on face ad is $T_x \sin\phi\,dp$. Substituting for T_x and dp their values as given by Eqs. 2b and 1a yields

$$T_{xp}\frac{\sin\phi}{\cos\psi}\,dy = T_{xp}\tan\phi\,dy = T_{xp}\frac{\partial z}{\partial x}\,dy \qquad \text{(7)}$$

Tx

The vertical component acting per unit of length along the y-axis is, therefore,

$T_{xp}\,(\partial z/\partial x)$. Similarly, the vertical component of T_y per unit of length along the x-axis is $T_{yp}\,(\partial z/\partial y)$. The vertical component of the shear force on face ad is $S\,dp\sin\psi$, which equals $S_p\,(\partial z/\partial y)\,dy$ which, per unit of length along the y-axis, equals $S_p\,(\partial z/\partial y)$. Similarly, the vertical component of shear acting on face ab is $S_p\,(\partial z/\partial x)$. Taking into account the variation in the magnitude of forces from one face to the other, the summation of forces in the z-direction yields

$$\frac{\partial}{\partial x}\left(T_{xp}\frac{\partial z}{\partial x}\right) + \frac{\partial}{\partial y}\left(T_{yp}\frac{\partial z}{\partial y}\right) + \frac{\partial}{\partial x}\left(S_p\frac{\partial z}{\partial y}\right) + \frac{\partial}{\partial y}\left(S_p\frac{\partial z}{\partial x}\right) + w_z = 0 \ldots\ldots (8a)$$

in which w_z is the load per unit of projected area. Eq. 8a reduces to

$$T_{xp}\frac{\partial^2 z}{\partial x^2} + T_{yp}\frac{\partial^2 z}{\partial y^2} + 2\,S_p\frac{\partial^2 z}{\partial x\,\partial y}$$

$$+ \frac{\partial z}{\partial x}\left(\frac{\partial T_{xp}}{\partial x} + \frac{\partial S_p}{\partial y}\right) + \frac{\partial z}{\partial y}\left(\frac{\partial T_{yp}}{\partial y} + \frac{\partial S_p}{\partial x}\right) = -\,w_z \ldots\ldots (8b)$$

$- X$ $- X$

By Eqs. 5 and 6, the terms in the parentheses equal zero. Hence, Eq. 8b reduces to

$$T_{xp}\frac{\partial^2 z}{\partial x^2} + T_{yp}\frac{\partial^2 z}{\partial y^2} + 2\,S_p\frac{\partial^2 z}{\partial x\,\partial y} = -\,w_z \ldots\ldots\ldots\ldots\ldots (8c)$$

Eqs. 5, 6, and 8a can be reduced to a single equation with one unknown by introducing the function, F, so that

$$\frac{\partial^2 F}{\partial y^2} = T_{xp} \ldots\ldots\ldots\ldots\ldots\ldots\ldots\ldots (9a)$$

$$\frac{\partial^2 F}{\partial x^2} = T_{yp} \ldots\ldots\ldots\ldots\ldots\ldots\ldots\ldots (9b)$$

and

$$-\frac{\partial^2 F}{\partial x\,\partial y} = S_p \ldots\ldots\ldots\ldots\ldots\ldots\ldots\ldots (9c)$$

These values satisfy the requirements of Eqs. 5 and 6 and reduce Eq. 8c to

$$\frac{\partial^2 F}{\partial y^2}\frac{\partial^2 z}{\partial x^2} + \frac{\partial^2 F}{\partial x^2}\frac{\partial^2 z}{\partial y^2} - 2\,\frac{\partial^2 F}{\partial x\,\partial y}\frac{\partial^2 z}{\partial x\,\partial y} = -\,w_z \ldots\ldots\ldots\ldots (10)$$

Except for a few special cases, the algebraic solution of differential Eq. 10 is difficult, and a numerical procedure such as finite differences must be used.

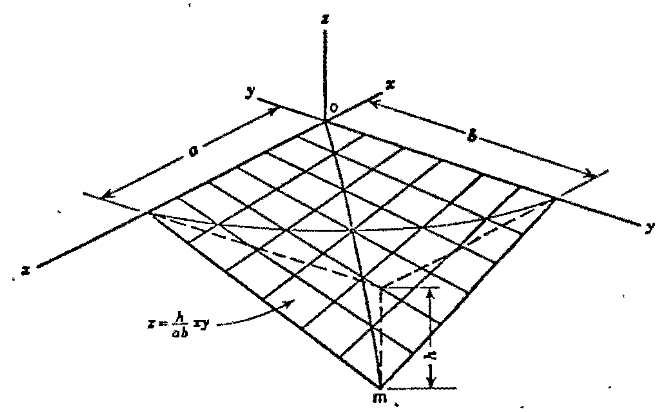

FIG. 2.—SECTIONS OF A HYPERBOLIC PARABOLOID SURFACE TAKEN AT 45° TO THE COORDINATE AXIS

One of the simpler cases to solve is the hyperbolic paraboloid shell subject to a uniform load. The surface of a hyperbolic paraboloid shell (Fig. 2) is formed by a series of straight lines parallel to the (zx)-plane and (zy)-plane and, hence, is defined by

$$z = \frac{h}{a\,b}\,x\,y \ldots\ldots\ldots\ldots\ldots\ldots\ldots\ldots (11)$$

The second differential of Eq. 11 equals zero. Therefore, for a hyperbolic paraboloid shell, Eq. 10 becomes

$$-\,2\,\frac{\partial^2 F}{\partial x\,\partial y}\,\frac{h}{a\,b} = w \ldots\ldots\ldots\ldots\ldots\ldots\ldots (12)$$

which simplifies by means of Eq. 9c to

$$S_p = \frac{a\,b}{2\,h}\,w \ldots\ldots\ldots\ldots\ldots\ldots\ldots\ldots (13)$$

Because the differential of S_p with respect to y and x is zero, when the direct forces normal to the edge are zero, it is seen from the relationships in Eqs. 5 and 6 that

$$T_{xp} = T_{yp} = 0 \ldots\ldots\ldots\ldots\ldots\ldots\ldots\ldots (14)$$

Eq. 14 indicates that the entire shell is subject solely to pure shear of constant intensity when uniformly loaded. Along the edges this uniform shear must be resisted by the edge member.

[illegible] be [illegible]

This state of pure shear, which actually resolves into principal stresses of equal and opposite magnitude acting on sections at 45° to shear plane, can be deduced from purely physical considerations without recourse to differential equations. As shown in Fig. 2, sections of a hyperbolic paraboloid surface taken at 45° to the coordinate axes form identical parabolic arches. In other words, the surface shown in Fig. 2 can be obtained by translating (moving) a parabolic curve along curve om. The parabolas parallel to om curve downward, whereas those at right angles to these parabolas curve in the opposite direction.

Assuming that the load is equally divided between the two sets of perpendicular parabolas, it is evident that at the edge the parabolas parallel to curve om exert an outward thrust, whereas those perpendicular to this curve exert an inward pull. Although opposite in character, the magnitude of these forces

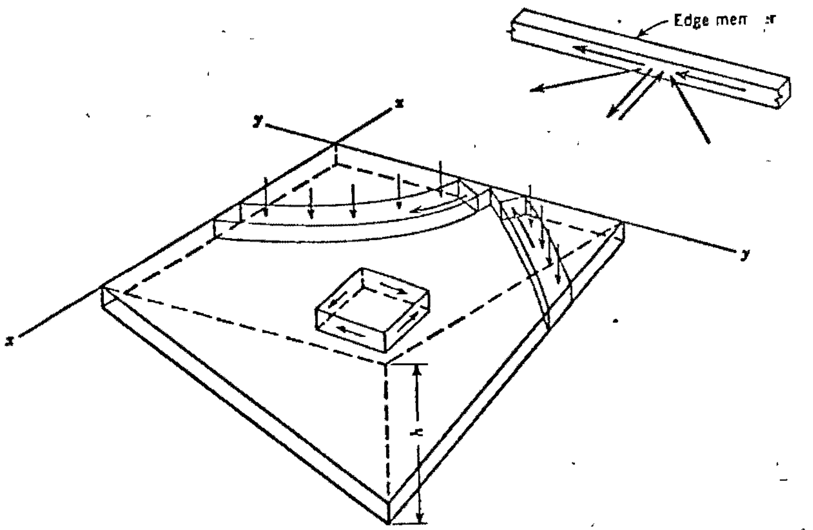

FIG. 3.—FORCES ACTING ON EDGE MEMBERS OF PARABOLIC ARCHES

intersecting at any point on the boundary of the surface is equal because the intersecting parabolas are identical. The net effect, as shown in Fig. 3, is that the outward force acting on the edge is cancelled and only pure shear acts along the edge. This shear must be resisted by a rigid edge member. Because horizontal reactions are supplied to the ends of the parabolas by the interaction of one on the other, it is valid to assume that the load is carried by a series of parabolas.

For most hyperbolic paraboloid shells of moderate rise, it is satisfactory to consider the load as being uniform. However, when the rise is great the dead load can no longer be considered as acting uniformly on the projected area. For this condition the dead load of the shell is

$$w_s = \frac{w}{\cos\phi\cos\psi} \quad \text{(15a)}$$

which, by trigonometry, can be shown to equal

$$w_s = w\sqrt{\left[1 + \left(\frac{h\,x}{a\,b}\right)^2\right]\left[1 + \left(\frac{h\,y}{a\,b}\right)^2\right]} \quad \text{(15b)}$$

Neglecting

$$\left(\frac{h\,x}{a\,b}\right)^2\left(\frac{h\,y}{a\,b}\right)^2$$

because it is small, Eq. 15b reduces to

$$w_s = w\sqrt{1 + \left(\frac{h\,x}{a\,b}\right)^2 + \left(\frac{h\,y}{a\,b}\right)^2} \quad \text{(15c)}$$

From Eqs. 10 and 13,

$$-\frac{\partial^2 F}{\partial x\,\partial y}\frac{2\,h}{a\,b} = S_p\frac{2\,h}{a\,b} = w\sqrt{1 + \left(\frac{h\,x}{a\,b}\right)^2 + \left(\frac{h\,y}{a\,b}\right)^2} \quad \text{(16)}$$

Differentiating Eq. 16 and integrating according to Eqs. 5 and 6 yields

$$T_{xp} = -w\frac{y}{2}\log\left[\frac{h\,x}{a\,b} + \sqrt{1 + \left(\frac{h\,x}{a\,b}\right)^2 + \left(\frac{h\,y}{a\,b}\right)^2}\right] + f(y) \quad \text{(17)}$$

$$T_{yp} = -w\frac{x}{2}\log\left[\frac{h\,y}{a\,b} + \sqrt{1 + \left(\frac{h\,x}{a\,b}\right)^2 + \left(\frac{h\,y}{a\,b}\right)^2}\right] + f(x) \quad \text{(18)}$$

in which $f(y)$ and $f(x)$ are constants of integration. With only one constant of integration available for each normal force and with two edges for each force—that is, at $x = 0$ and $x = a$ for T_{xp}, or at $y = 0$ and $y = b$ for T_{yp}—it is evident that, for pure membrane or direct-force action, normal reactions are required. If normal reactions are not provided along at least one of the two parallel edges, the surface is subject to bending moments.

The elliptical paraboloid is another surface that is amenable to algebraic solution, although it is slightly more involved than the solution for the hyperbolic paraboloid surface. This surface is generated by moving a parabolic curve along another parabola, as shown in Fig. 4(a). The equation of this surface is

$$z = \frac{h_y\,y^2}{b^2} + \frac{h_x\,x^2}{a^2} \quad \text{(19)}$$

The second differentials of the foregoing expression with respect to x and y are

$$\frac{\partial^2 z}{\partial x^2} = \frac{2\,h_x}{a^2} \quad \text{(20a)}$$

$$\frac{\partial^2 z}{\partial y^2} = \frac{2\,h_y}{b^2} \quad \text{(20b)}$$

and

$$\frac{\partial^2 z}{\partial x\,\partial y} = 0 \quad \text{(20c)}$$

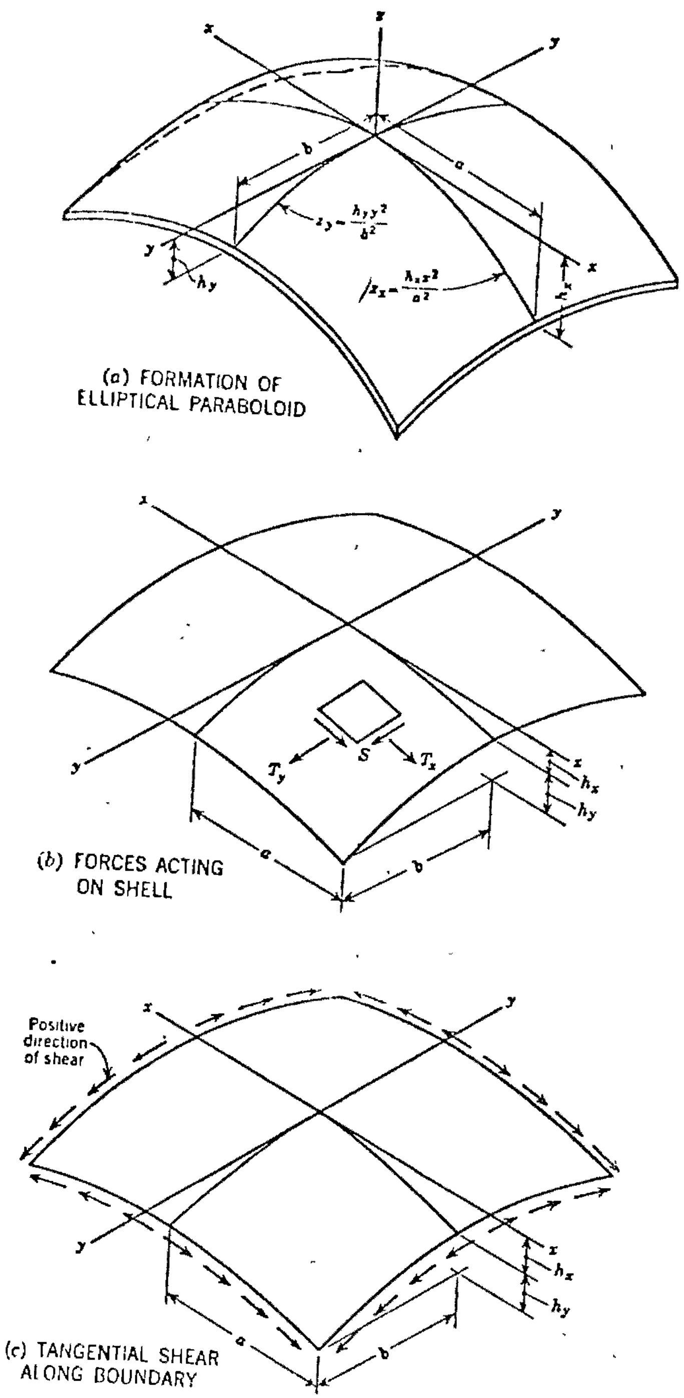

FIG. 4 —ELLIPTICAL PARABOLOID SHELL

Substituting these expressions in Eq. 10, for a uniform load, $w_z = w$,

$$\frac{\partial^2 F}{\partial y^2} + \frac{h_y a^2}{h_x b^2} \frac{\partial^2 F}{\partial x^2} = - \frac{a^2}{2 h_x} w \qquad (21)$$

Differential Eq. 21 is satisfied if

$$F = - \left[\sum_{n=1,3\ldots}^{\infty} A_n (\cosh \beta x) (\cos \lambda y) \right] - \frac{a^2 y^2 w}{4 h_x} \qquad (22)$$

in which

$$\beta = \sqrt{\frac{h_x}{h_y}} \frac{n \pi}{2 a} \qquad (23a)$$

and

$$\lambda = \frac{n \pi}{2 b} \qquad (23b)$$

In the foregoing expressions, the values of n considered are the odd integers. This can be checked by differentiating Eq. 22 and substituting the resulting values in Eq. 21. If the value of F is used in accordance with Eqs. 9, the expressions for the forces are

$$T_{xp} = \left[\sum_{n=1,3\ldots}^{\infty} A_n \lambda^2 (\cosh \beta x) (\cos \lambda y) \right] - \frac{a^2 w}{2 h_x} \qquad (24a)$$

$$T_{yp} = - \sum_{n=1,3\ldots}^{\infty} A_n \beta^2 (\cosh \beta x) \cos \lambda y \qquad (24b)$$

and

$$S_p = - \sum_{n=1,3\ldots}^{\infty} A_n \beta \lambda (\sinh \beta x) \sin \lambda y \qquad (24c)$$

At the boundary, $y = \pm b$, $T_{yp} = 0$ because $\cos \lambda b = 0$ for all values of n. In order to satisfy the condition that $T_{xp} = 0$ at $x = \pm a$, it is necessary that $\frac{a^2 w}{2 h_x}$ be expressed as a Fourier series. The general expression of the trigonometric series for a constant is

$$1 = \sum_{n=1,3\ldots}^{\infty} \frac{4 (-1)^{(n-1)/2} \cos \lambda y}{n \pi} \qquad (25)$$

Therefore, at $x = \pm a$, Eq. 24a becomes

$$T_{xp} = 0 = \sum_{n=1,3\ldots} \left\{ A_n \lambda^2 \cosh \beta a - \left[\frac{4 (-1)^{(n-1)/2}}{n \pi} \frac{a^2 w}{2 h_x} \right] \right\} \cos \lambda y \qquad (26)$$

This expression can equal only zero for all values of y if

$$A_n = \frac{2 a^2 w (-1)^{(n-1)/2}}{n \pi h_x \lambda^2 \cosh \beta a} \qquad (27)$$

Substituting A_n in Eqs. 24 and cancelling the common terms results in

$$T_{xp} = \frac{w\,a^2}{h_x}\left[\frac{2}{\pi}\sum_{n=1,3\ldots}^{\infty}\frac{(-1)^{(n-1)/2}\cosh\beta x}{n\cosh\beta a}\cos\lambda y - \tfrac{1}{2}\right]\ldots\ldots(28a)$$

$$T_{yp} = -\frac{w\,b^2}{h_y}\left[\frac{2}{\pi}\sum_{n=1,3\ldots}^{\infty}\frac{(-1)^{(n-1)/2}\cosh\beta x}{n\cosh\beta a}\cos\lambda y\right]\ldots\ldots\ldots(28b)$$

and

$$S_p = -\frac{w\,a\,b}{\sqrt{h_x h_y}}\left[\frac{2}{\pi}\sum_{n=1,3\ldots}^{\infty}\frac{(-1)^{(n-1)/2}\sinh\beta x}{n\cosh\beta a}\sin\lambda y\right]\ldots\ldots\ldots(28c)$$

By means of Eq. 28 and Eqs. 2b, 3, and 4b, the actual internal forces can be computed as the sum of a series. If h_x/h_y is greater than unity, rapid convergence of the series is obtained for most values, and, therefore, only the first three or four terms ($n = 1,3,5,$ and 7) are required to obtain sufficient accuracy. However, at the boundary $x = \pm a$ the expression for shear converges very slowly. In this case one can restate Eq. 28c at the boundary $x = a$ as

$$S_p = -\frac{w\,a\,b}{\sqrt{h_x h_y}}\left\{\frac{2}{\pi}\sum_{n=1,3\ldots}^{\infty}\left[\left(\frac{\sinh\beta a}{\cosh\beta a}-1\right)+1\right]\frac{(-1)^{(n-1)/2}}{n}\right\}\sin\lambda y\,..(29)$$

However,

$$\sum_{n=1,3\ldots}^{\infty}\frac{(-1)^{(n-1)/2}}{n}\sin\lambda y = \tfrac{1}{4}\log\left(\sec\frac{\pi y}{2b}+\tan\frac{\pi y}{2b}\right)^2\ldots\ldots\ldots(30)$$

Therefore, Eq. 29 reduces to

$$S_p = -\frac{w\,a\,b}{\sqrt{h_x h_y}}\left[\frac{1}{2\pi}\log\left(\sec\frac{\pi y}{2b}+\tan\frac{\pi y}{2b}\right)^2 - \frac{2}{\pi}\sum_{n=1,3\ldots}^{\infty}(1-\tanh\beta a)\frac{(-1)^{(n-1)/2}}{n}\sin\lambda y\right]..(31)$$

For values of h_x/h_y greater than 1, for practical purposes, $\tanh\beta a$ is equal to 1. Therefore, the second term in Eq. 31 can be ignored; thus, the expression for shear converges rapidly.

At $y = \pm b$, sec $(\pi y/2b)$ and tan $(\pi y/2b)$ are infinite. Therefore, the log of these values is also infinite. Consequently, Eq. 31 indicates that the shear at the corner is infinite. This would be true if the corner were completely free of normal forces and if the shell had no bending resistance. However, because of the integral action of the supporting ribs and shell, normal forces do exist at the corner. These normal forces alter the resistance to the extent that the shear does not need to be infinite to satisfy statics. Moreover, at the corner some of the load can be, and is, resisted by flexural resistance. From studies made of cylindrical shells, it has been found that this flexural action is confined to a distance of approximately $0.4\sqrt{r\,t}$ from the rib, in which r is the radius of the shell and t is the shell thickness. Therefore, it is felt that Eqs. 28c and 31 do not apply within the distance $0.4\sqrt{r\,t}$ from the corner. Shear can be considered maximum at the point $y = b - 0.4\sqrt{r\,t}$.

The symbols, T_x, T_y, and S, represent forces per unit of length. In order to obtain stresses, these values must be divided by the thickness of the shell.

The trigonometric functions involved in Eqs. 2b, 3, and 4b can be readily expressed as functions of x and y. Differentiating Eq. 19 with respect to x yields

$$\frac{\partial z}{\partial x} = \frac{2\,h_x}{a}\frac{x}{a} = \tan\phi\ldots\ldots\ldots\ldots\ldots\ldots(32)$$

By utilizing

$$\tan^2\phi = \frac{1}{\cos^2\phi} - 1\ldots\ldots\ldots\ldots\ldots\ldots(33)$$

Eq. 2b reduces to

$$\left(\frac{2\,h_x}{a}\frac{x}{a}\right)^2 + 1 = \frac{1}{\cos^2\phi}\ldots\ldots\ldots\ldots\ldots\ldots(34)$$

or

$$\cos\phi = \frac{1}{\sqrt{1+\left(\frac{2\,h_x}{a}\frac{x}{a}\right)^2}}\ldots\ldots\ldots\ldots\ldots\ldots(35a)$$

Similarly,

$$\cos\psi = \frac{1}{\sqrt{1+\left(\frac{2\,h_y}{b}\frac{y}{b}\right)^2}}\ldots\ldots\ldots\ldots\ldots\ldots(35b)$$

and, therefore,

$$\frac{\cos\phi}{\cos\psi} = \sqrt{\frac{1+\left(\frac{2\,h_y}{b}\frac{y}{b}\right)^2}{1+\left(\frac{2\,h_x}{a}\frac{x}{a}\right)^2}}\ldots\ldots\ldots\ldots\ldots\ldots(35c)$$

In order to avoid mathematical complications, the value of w_z was assumed to be constant in establishing Eq. 21. However, although the algebraic computations become extensive and rather formidable, the procedure outlined for the uniform load can also be applied to the case of any symmetrical loading, such as the dead weight of the shell. In this case the load is expressed in terms of the double Fourier series,

$$w_z = \sum_{m=1,3\ldots}^{\infty}\sum_{n=1,3\ldots}^{\infty}\beta_{mn}\cos\gamma x\cos\lambda y\ldots\ldots\ldots\ldots(36)$$

in which $\gamma = m\,\pi/2\,a$.

The resulting expressions for T_{xp} and T_{yp}, obtained by expressing w_z in this manner, indicate that any symmetrical loading can be resisted by direct forces without the necessity for lateral or normal forces at the boundaries. The behavior of the elliptical paraboloid shell under dead load therefore differs from that of the hyperbolic paraboloid shell, for which the dead load induces some bending if no lateral restraint is provided.

TABLE 1.—COEFFICIENTS FOR COMPUTING FORCE COMPONENTS OF ELLIPTICAL PARABOLOID SHELL

VALUE OF y/b

(a) $h_x/h_y = 1.0$

x/a	Force component	0	0.25	0.50	0.75	1.0
0.00	T_y	0.250	0.233	0.182	0.101	0
	T_x	0.250	0.207	0.318	0.399	0.500
	S	0	0	0	0	0
0.25	T_y	0.267	0.250	0.199	0.111	0
	T_x	0.233	0.250	0.301	0.389	0.500
	S	0	0.029	0.068	0.096	0.108
0.50	T_y	0.318	0.301	0.250	0.150	0
	T_x	0.182	0.199	0.250	0.350	0.500
	S	0	0.068	0.140	0.210	0.244
0.75	T_y	0.399	0.389	0.350	0.250	0
	T_x	0.101	0.111	0.150	0.250	0.500
	S	0	0.096	0.210	0.356	0.465
1.0	T_y	0.500	0.500	0.500	0.500	0
	T_x	0	0	0	0	0
	S	0	0.108	0.243	0.465	∞

(d) $h_x/h_y = 0.8$

x/a	Force component	0	0.25	0.50	0.75	1.0
0.00	T_y	0.289	0.270	0.213	0.119	0
	T_x	0.211	0.230	0.287	0.381	0.500
	S	0	0	0	0	0
0.25	T_y	0.301	0.285	0.228	0.130	0
	T_x	0.196	0.215	0.272	0.370	0.500
	S	0	0.034	0.069	0.100	0.114
0.50	T_y	0.347	0.331	0.277	0.169	0
	T_x	0.153	0.169	0.223	0.331	0.500
	S	0	0.065	0.139	0.215	0.255
0.75	T_y	0.416	0.406	0.369	0.270	0
	T_x	0.084	0.094	0.131	0.230	0.500
	S	0	0.091	0.201	0.353	0.480
1.0	T_y	0.500	0.500	0.500	0.500	0
	T_x	0	0	0	0	0
	S	0	0.101	0.229	0.443	∞

(b) $h_x/h_y = 0.6$

x/a	Force component	0	0.25	0.50	0.75	1.0
0.00	T_y	0.336	0.316	0.252	0.143	0
	T_x	0.164	0.184	0.248	0.357	0.500
	S	0	0	0	0	0
0.25	T_y	0.348	0.329	0.267	0.155	0
	T_x	0.152	0.171	0.233	0.345	0.500
	S	0	0.031	0.067	0.103	0.120
0.50	T_y	0.383	0.367	0.312	0.197	0
	T_x	0.117	0.133	0.188	0.304	0.500
	S	0	0.060	0.132	0.216	0.265
0.75	T_y	0.436	0.426	0.392	0.296	0
	T_x	0.064	0.074	0.108	0.204	0.500
	S	0	0.081	0.185	0.342	0.494
1.00	T_y	0.500	0.500	0.500	0.500	0
	T_x	0	0	0	0	0
	S	0	0.089	0.208	0.413	∞

(e) $h_x/h_y = 0.4$

x/a	Force component	0	0.25	0.50	0.75	1.0
0.00	T_y	0.395	0.374	0.307	0.180	0
	T_x	0.105	0.126	0.193	0.320	0.500
	S	0	0	0	0	0
0.25	T_y	0.403	0.383	0.319	0.192	0
	T_x	0.097	0.117	0.181	0.308	0.500
	S	0	0.026	0.060	0.101	0.125
0.50	T_y	0.425	0.410	0.357	0.235	0
	T_x	0.075	0.090	0.143	0.265	0.500
	S	0	0.049	0.115	0.208	0.274
0.75	T_y	0.459	0.451	0.419	0.331	0
	T_x	0.041	0.049	0.081	0.169	0.500
	S	0	0.065	0.156	0.316	0.506
1.00	T_y	0.500	0.500	0.500	0.500	0
	T_x	0	0	0	0	0
	S	0	0.070	0.173	0.363	∞

(c) $h_x/h_y = 0.2$

x/a	Force component	0	0.25	0.50	0.75	1.0
0.00	T_y	0.462	0.446	0.388	0.248	0
	T_x	0.038	0.054	0.112	0.252	0.500
	S	0	0	0	0	0
0.25	T_y	0.465	0.451	0.396	0.261	0
	T_x	0.035	0.049	0.104	0.239	0.500
	S	0	0.014	0.010	0.038	0.128
0.50	T_y	0.473	0.462	0.414	0.303	0
	T_x	0.027	0.038	0.086	0.197	0.500
	S	0	0.027	0.074	0.174	0.280
0.75	T_y	0.485	0.480	0.456	0.383	0
	T_x	0.015	0.020	0.044	0.117	0.500
	S	0	0.034	0.098	0.246	0.510
1.00	T_y	0.500	0.500	0.500	0.500	0
	T_x	0	0	0	0	0
	S	0	0.038	0.108	0.262	∞

In order to expedite the analysis of the elliptical paraboloid shells and to obtain a better understanding of their load-carrying characteristics, Table 1 has been compiled on the basis of Eqs. 28 and Fig. 4(b). The expressions inside the parentheses in Eqs. 28 contain only the parameter, h_x/h_y. Therefore, the behavior of this doubly curved shell can be expressed as a function of this single parameter.

Coefficients are given for computing the three force components, T_x, T_y, and S, at the eighth points of a dome. The forces determined by multiplying the coefficients by constants are

$$T_y = -\frac{w\,b^2}{k\,h_y}\,(\text{coefficient}) \qquad (37a)$$

$$T_x = -\frac{w\,a^2\,k}{h_x}\,(\text{coefficient}) \qquad (37b)$$

$$S = -\frac{w\,a\,b}{\sqrt{h_x\,h_y}}\,(\text{coefficient}) \qquad (37c)$$

and

$$k = \sqrt{\frac{1 + [(2\,h_x/a)(x/a)]^2}{1 + [(2\,h_y/b)(y/b)]^2}} \qquad (37d)$$

These constants are dependent only on the selected dimensions of the shell and on the load. In this connection for the sake of completeness, the factor k has been included. In practice the additional accuracy secured by the inclusion of this term is unwarranted because the stresses due to T_x and T_y are never critical. Except in the zone near the corners in which the principal stress due to the combination of the three force components is tensile, the stresses are so low in compression for spans being considered that an investigation of the stresses in a dome is of academic interest only. Therefore, the real reason and need for computing stresses in a shell with a fair degree of accuracy are to obtain a reliable determination of the tangential load which must be carried by the supporting arches.

For this purpose the tangential shear existing along the boundaries (Fig. 4(c)) at the tenth intervals of half the chord are shown in Table 2. Table 2 also permits a better evaluation of the tension near the corner because the principal stresses are primarily related to S.

A graphical presentation of the values in Table 1 for T_{yp} at midspan is shown in Fig. 5 for various values of h_x/h_y. The values of T_{yp} for h_x/h_y from 1.0 to 5.0 are obtained from the values of T_{xp} by symmetry. For example, the value of T_{yp} at $y = 0$ for $h_x/h_y = 5$ is the same as the value of T_{xp} at $x = 0$ for $h_x/h_y = 0.2$. At $x = \pm a$, for all values of h_x/h_y,

$$T_{yp} = -\frac{0.5\,w\,b^2}{h_y} = -\frac{0.125\,w\,L^2}{h_y} \qquad (38)$$

The last term in Eq. 38 is the thrust in a parabolic arch subject to the uniform load, w. This identity is not surprising because at the boundary the force normal to the edge was made equal to zero. Consequently, the imposed condition of restraint compels the entire load in the immediate vicinity of the edge to be carried by arch action in the y-direction. Furthermore, $0.5\,b^2/h_y$ equals the radius of the parabola at its crown. Therefore, the value T_{yp} at $x = a$ and $y = 0$ represents merely the thrust induced in a ring with the appropriate radius due to a radial load, w.

Near the crown, marked variations in the value of T_{yp} occur as h_x/h_y varies. When the rise in the x-direction is small compared with the rise in the y-direction—for example, when $h_x/h_y = 0.2$—the curves in Fig. 5 are almost horizontal, indicating that a large proportion of the load is being resisted in the y-direction. This can be anticipated from the geometry of the shell. As the

TABLE 2.—SHEAR ALONG THE EDGES OF ELLIPTICAL PARABOLOID SHELL

y/b	h_x/h_y				
	1.0	0.8	0.6	0.4	0.2
	At $x = \pm a$				
0.0	0.0000	0.0000	0.0000	0.0000	0.0000
0.1	0.0119	0.0389	0.0342	0.0307	0.0137
0.2	0.0854	0.0793	0.0701	0.0550	0.0286
0.3	0.1319	0.1231	0.1096	0.0872	0.0481
0.4	0.1836	0.1721	0.1516	0.1254	0.0731
0.5	0.2432	0.2294	0.2081	0.1728	0.1075
0.6	0.3204	0.3066	0.2859	0.2493	0.1818
0.7	0.4071	0.3897	0.3627	0.3173	0.2296
0.8	0.5363	0.5178	0.4887	0.4400	0.3443
0.85	0.6279	0.6090	0.5791	0.5292	0.4306
0.9	0.7570	0.7378	0.7074	0.6667	0.5659
0.95	0.9777	0.9582	0.9276	0.8763	0.7741
1.0	∞	∞	∞	∞	∞
x/a	At $y = \pm b$				
0.0	0.0000	0.0000	0.0000	0.0000	0.0000
0.1	0.0419	0.0444	0.0468	0.0488	0.0500
0.2	0.0854	0.0903	0.0950	0.0990	0.1014
0.3	0.1319	0.1391	0.1460	0.1519	0.1553
0.4	0.1836	0.1930	0.2019	0.2095	0.2140
0.5	0.2432	0.2545	0.2652	0.2743	0.2798
0.6	0.3204	0.3317	0.3425	0.3516	0.3571
0.7	0.4071	0.4213	0.4348	0.4463	0.4532
0.8	0.5363	0.5515	0.5659	0.5782	0.5855
0.85	0.6279	0.6434	0.6582	0.6707	0.6782
0.9	0.7570	0.7728	0.7878	0.8005	0.8081
0.95	0.9777	0.9935	1.0087	1.0215	1.0290
1.0	∞	∞	∞	∞	∞

curvature in one direction is flattened, thereby approaching a horizontal plane as a limit, it is natural that the load is transmitted in the other direction.

With no normal forces along the edges, it follows that the increase in the proportion of load carried in the y-direction as h_x/h_y decreases must be accompanied by an increase in the tangential shears along the edges, $x = \pm a$. Such an increase is confirmed by the coefficients listed in Table 2. Although these coefficients diminish at $x = \pm a$ as h_x/h_y decreases, they do not diminish as rapidly as $\sqrt{h_x/h_y}$.

For large values of h_x/h_y, the values of T_{yp} become appreciably smaller as the crown is approached, and, therefore, for such shells only the exterior

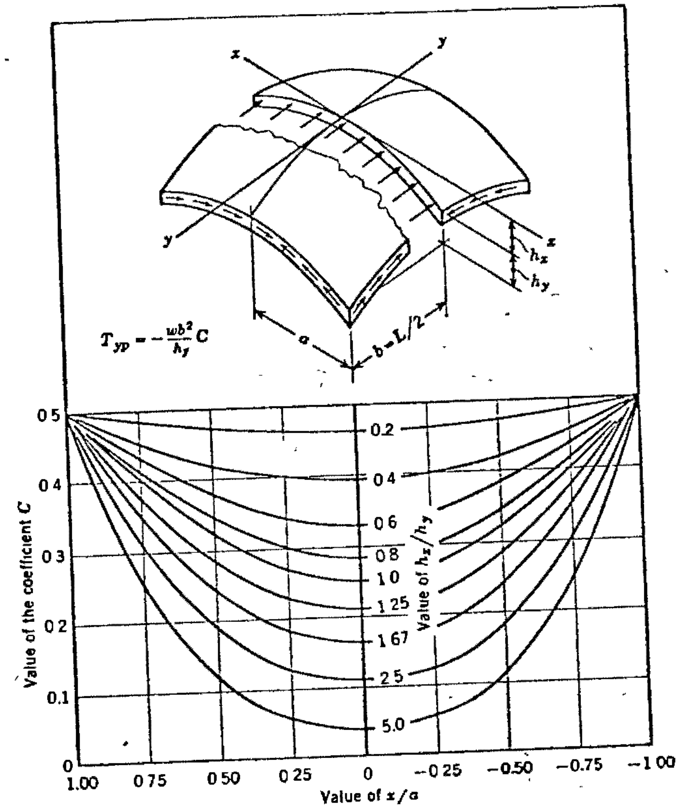

FIG. 5.—COEFFICIENT VALUES FOR VARIOUS VALUES OF h_x/h_y

portion of the shell is resisting load in the y-direction. At the crown the curve for $h_x/h_y = 1.0$ shows that half of the load is carried in one direction and the remaining half is carried in the other direction, which is natural from the condition of equal rise in the two directions.

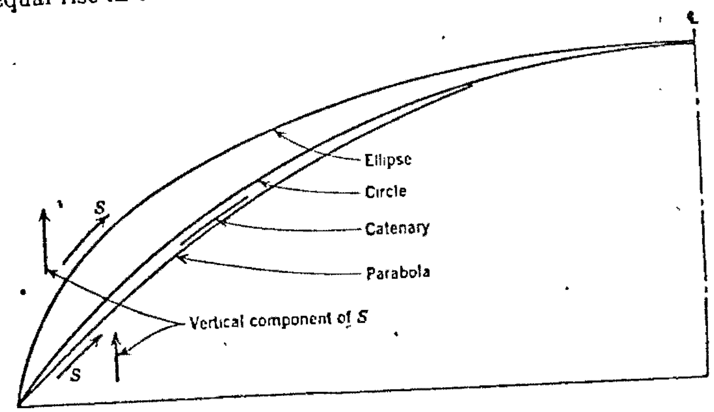

FIG. 6.—SLOPE COMPARISON FOR VARIOUS CURVES

An interesting question is whether or not the coefficients in Tables 1 and 2 can be applied to domes of other shapes with an equal rise and span. As cited previously, the critical stresses are a function of the shear near the corners. However, the summation of the vertical components of the shear along an edge must equal the load on the shell. If the same variation of shear along an edge is assumed for all shapes, it is apparent that, to satisfy the foregoing condition of equilibrium, the intensity of the tangential shear is dependent on the steepness of the slope near the corner. This is particularly true because the maximum shear occurs at the corner.

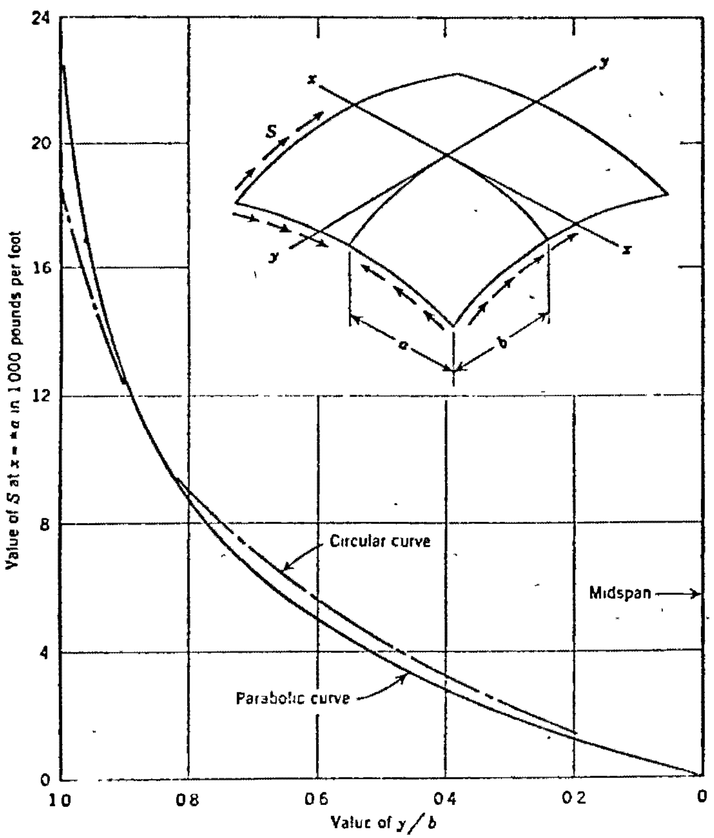

FIG. 7.—COMPARISON OF TANGENTIAL SHEAR

The slope near the corner of most of the commonly used shells of other curvature generally will be steeper than the slope of the elliptical paraboloid, as shown in Fig. 6. Consequently, the shear at the edge should be less for the shells of other curvature than for an elliptical paraboloid of the same dimensions. The magnitude of the reduction is dependent on the relative dimensions. The magnitude of the reduction is dependent on the relative slopes near the corners of the surfaces being compared. For domes whose edges are elliptical, the magnitude of the shear should be considerably less than that for domes with other shapes. If the edge of the dome is circular, the tangential shear should approximately the same as for an elliptical paraboloid.

To confirm this hypothesis, Fig. 7 compares the tangential shear computed[3] for domes at a factory in Brynmawr, England, and that obtained for an elliptical paraboloid of the same dimensions. The shape used for the Brynmawr domes was a surface of translation generated by moving one vertical circle on another. Fig. 7 shows good agreement between the two curves except in the immediate vicinity of the corner, in which a finite value is given for the circular curve in contrast to the infinite value implied for the parabolic curve. The reason for this apparent discrepancy is that, due to mathematical difficulties, a numerical procedure based on finite-differences equations was used to determine the forces for the Brynmawr dome. Because this procedure is based on the average value between the chosen interval, a finite value results at the corner. If a rigorous mathematical solution had been used, an infinite value for the circular curve would have resulted.

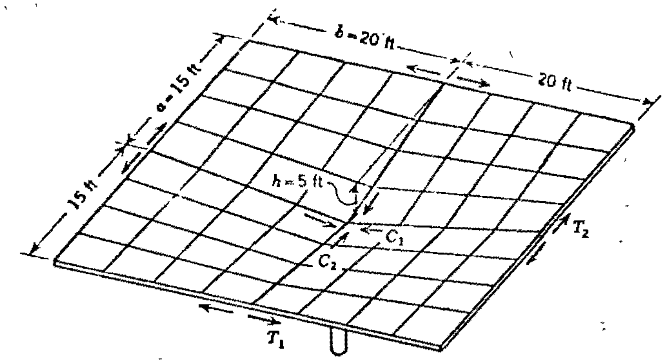

FIG. 8.—ROOF DESIGNED IN EXAMPLE 1

At $y = b - 0.4\sqrt{r\,t}$, the point previously recommended as the breakoff place for shear evaluation, the shear computed for the parabolic curve is approximately 7% higher than that for the circular curve. Whether this difference is real or merely due to dissimilarity in methods of computation is not known. However, the difference is in the proper direction.

Example 1.—A hyperbolic paraboloid shell with a column at the center is designed. The roof shown in Fig. 8 is obtained by joining four identical sections in a manner similar to the method used in Fig. 2. Many other arrangements can be used,[4] all of which are designed in the same manner by considering each quadrant of a rectangular unit individually.

Assuming $w = 60$ lb per sq ft, the internal forces at the critical points of the shell roof shown in Fig. 8 are

$$S = \frac{w\,a\,b}{2\,h} = \frac{60 \times 15 \times 20}{2 \times 5} = 1{,}800 \text{ lb-ft}$$

$$T_1 = -C_1\ 1{,}800 \times 20 = 36{,}000 \text{ lb}$$

[3] "The Design of a Reinforced Concrete Factory at Brynmawr, South Wales," by Ove Nyquist Arup and Ronald Jenkins, Pt. III, *Proceedings*, Inst. C. E., London, December, 1953, pp. 315-397.

[4] "Structural Applications of Hyperbolic Paraboloidal Shells," by Felix Candela, *Journal*, A C I, Vol. 26, No. 5, [illegible], pp. 397-415.

and

$$T_2 = -C_2\ 1{,}800 \times 15 = 27{,}000 \text{ lb}$$

Because the shell is subject to pure shear, the principal tensile force will also be 1,800 lb per ft. An allowable steel stress of 20,000 lb per sq in. results in a required area of steel of 0.09 sq in. per ft. Therefore, No. 2 bars, 6 in. on centers, are sufficient. This reinforcement should be placed diagonally, extending from one free edge to the other.

The shell exerts a constant shear on the edge members, which have been omitted in Fig. 8. The total thrust or pull exerted by this shear is equal to the product of the length of the edge member affected and the magnitude of the shear. In this example this equals 36,000 lb. Because there is no external reaction acting on the edge beams, either at the corners or along the edge, it is evident that the maximum tension or compression in the edge members

TABLE 3.—INTERNAL FORCES IN AN ELLIPTICAL PARABOLOID SHELL FOR EXAMPLE No. 2

x/a	Force	Value of y/b: 0	0.25	0.50	0.75	1 00
0	$T_y k$	−4,300	−4,100	−3,200	−1,800	0
	T_x/k	−1,900	−2,100	−2,600	−3,500	−4,600
	S	0	0	0	0	0
0.25	$T_y k$	−4,600	−4,300	−3,400	−2,000	0
	T_x/k	−1,800	−2,000	−2,500	−3,400	−4,600
	S	0	− 400	− 800	−1,200	−1,300
0.50	$T_y k$	−5,200	−5,000	−4,200	−2,500	0
	T_x/k	−1,400	−1,600	−2,100	−3,000	−4,600
	S	0	− 800	−1,600	−2,500	−3,000
0.75	$T_y k$	−6,200	−6,100	−5,500	−4,100	0
	T_x/k	− 800	− 900	−1,200	−2,100	−4,600
	S	0	−1,100	−2,400	−4,100	−5,600
1.00	$T_y k$	−7,500	−7,500	−7,500	−7,500	0
	T_x/k	0	0	0	0	0
	S	0	−1,200	−2,700	−5,200	∞

occurs at the midspan. The tension and compression in the edge member diminish along the length to zero at the ends.

To determine the type of force (compression or tension) present in the edge members, it is recommended that free body diagrams be drawn of the member being considered rather than relying merely on a sign convention. Thus, the possibility of making serious errors in complicated layouts will be minimized. For this case the layout is so simple that the type of force present can be ascertained by inspection. Because the shear is positive and the coordinate of each quadrant occurs at the corner, the shear is outward along the four horizontal edges and inward along the four sloping edges. Hence, the edge beams at the exterior edges are in tension, whereas those extending out from the column are in compression.

Example 2.—An elliptical paraboloid shell is designed. Table 3 shows the internal forces divided by k or $1/k$ acting in an elliptical paraboloid subject to a uniform load of 60 lb per sq ft and spanning 100 ft in one direction and 70 ft in the other with a total rise of 18 ft. These values are obtained by multiplying the coefficients for $h_x/h_y = 0.8$ shown in Table 1 by one of the following values:

For T_y—

$$\frac{w\,b^2}{h_y} = \frac{60\ (50)^2}{10} = 15{,}000 \text{ lb per ft}$$

For T_x—

$$\frac{w\,a^2}{h_x} = \frac{60\ (35)^2}{8} = 9{,}200 \text{ lb per ft}$$

For S—

$$\frac{w\,a\,b}{\sqrt{h_x\,h_y}} = \frac{60\ (50)\ (35)}{\sqrt{8\ (10)}} = 11{,}700 \text{ lb per ft}$$

Because the stresses are small the effect of k is ignored. The maximum compression due to an assumed load of 60 lb per sq ft on the shell is 7,500 lb

TABLE 4.—SHEAR S AND PRINCIPAL STRESS S' ALONG EDGE

$x = a$						
y/b	0	0.1	0.2	0.3	0 4	0.5
S	0	− 460	− 930	−1,440	−2,010	−2,680
S'	0	30	110	270	500	860
y/b	0 6	0 7	0 8	0 85	0 9	0 95
S	−3,590	−4,560	−6,060	−7,130	−8,630	−11,200
S'	1,440	2,150	3,380	4,300	4,880	8,060
$y = b$						
x/a	0	0 1	0.2	0.3	0.4	0 5
S	0	− 520	−1,060	−1,630	−2,260	−2,980
S'	0	60	230	520	920	1,460
x/a	0 6	0.7	0 8	0 85	0 9	0 95
S	−3,850	−4,930	−6,450	−7,530	−9,040	−11,600
S'	2,210	3,140	4,550	5,570	7,030	9,500

per ft. If the thickness of the shell is assumed as 3 in., the maximum compressive stress is only

$$f_c = \frac{7{,}500}{3 \times 12} = 208 \text{ lb per sq in.}$$

which is considerably lower than the allowable stress of concrete.

To obtain knowledge of the tensile forces existing in the shell, the minimum principal stresses have been evaluated along the edges in Table 4. The value of the shear, S, is computed by using Table 2, with the multiplier in this case being 11,700 lb per ft taken from Table 3. The principal stress, S', is computed as described in most standard mechanics textbooks. The direct force at $y = b$ is 4,000 lb per ft, and the direct force at $x = a$ is 7,500 lb per ft. In most of the cases these principal values along the shell represent the maximum value in their zone.

At the corner the radius of curvature in the x-direction can be computed from

$$R_x = \frac{\left[1 + \left(\frac{\partial z}{\partial x}\right)^2\right]^{3/2}}{\frac{\partial^2 z}{\partial x^2}} \qquad (39)$$

in which

$$z = \frac{8\,x^2}{35^2} + \frac{10\,y^2}{50^2}$$

and

$$\frac{\partial z}{\partial x} = \frac{16\,x}{35^2}$$

$$\frac{\partial^2 z}{\partial x^2} = \frac{16}{35^2}$$

At the corner $x = 35$, Eq. 39 yields

$$R_x = \frac{35^2\,[1 + (16/35)^2]^{3/2}}{16} = 102 \text{ ft}$$

and, similarly,

$$R_y = 156 \text{ ft}$$

The maximum shear can therefore be expected to be at

$$\frac{x}{a} = \frac{35 - 0.4\sqrt{101 \times \frac{1}{4}}}{35} = 0.94$$

and at

$$\frac{y}{b} = \frac{50 - 0.4\sqrt{156 \times \frac{1}{4}}}{50} = 0.95$$

Therefore, from Table 4 the largest minimum principal stress along the edges is 9,500 lb per ft. Several points in the interior should be investigated also to determine the extent of the tensile area. Using the internal forces shown in Table 3, the principal stress at $y/b = x/a = 0.75$ and at $y/b = x/a = 0.5$ is

$$S' = -\left(\frac{4\quad - 2{,}100}{2} - \sqrt{\frac{2{,}000^2}{4} + 4{,}100^2}\right) = 1{,}100 \text{ lb per ft}$$

and

$$S' = -\left(\frac{4{,}200 + 2{,}100}{2} - \sqrt{\frac{2{,}100^2}{4} - 1{,}600^2}\right) = -1{,}200 \text{ lb per ft}$$

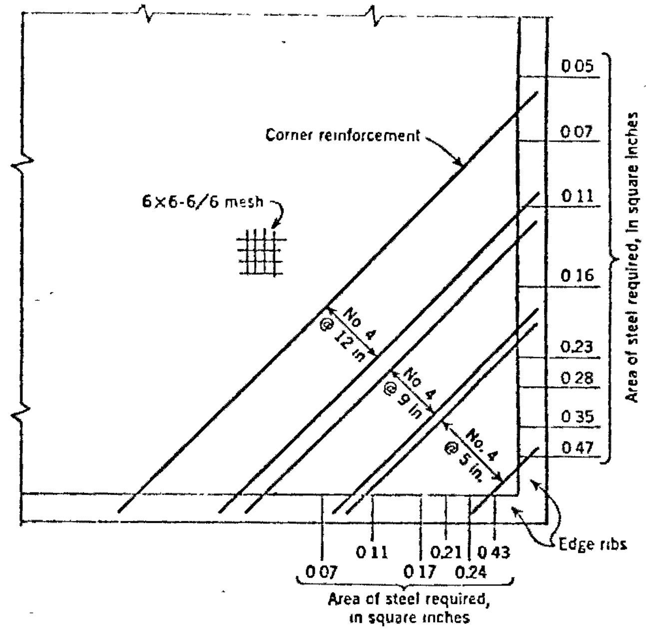

FIG. 9.—REQUIRED STEEL FOR ELLIPTICAL PARABOLOID SHELL

Assuming a linear variation in principal stress between these points, zero tension would occur at $x/a = y/b = \frac{5}{8}$.

From a theoretical point of view, the reinforcement should follow the lines of principal stress. However, this is not practical, and, therefore, it is customary to place the reinforcement in the corners along diagonal lines, as shown in Fig. 9. For this particular example and probably for all instances, the controlling tension for any group of bars occurs at the edge. The amount of reinforcement, with $f_s = 20{,}000$ lb per sq in., computed from the principal stresses shown in Table 4 is shown along the edge ribs of one corner.

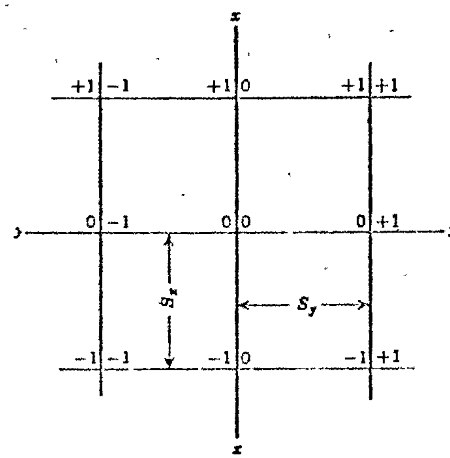

FIG. 10.—FINITE-DIFFERENCES EQUATIONS NOTATION

For most of the shells of double curvature, even for such a simple case as a translational shell formed by moving one circular curve on the other, an algebraic solution becomes extremely involved. In such cases the conversion of the various differential equations into finite-differences equation[5] is

[5] "Solution of Difficult Structural Problems by Finite Differences," by Alfred Parme, Journal, A.C.I., Vol. 22, November, 1950, pp. 237-255

more practical. This numerical procedure consists of substituting for the surface a grid of evenly spaced lines that simulate the behavior of the surface. For each intersection, a finite-differences equation is established that expresses the relationship between the stresses or functions of the stresses at this point, and at neighboring points and the load at the intersection.

Using the notation in Fig. 10, the general finite-differences equation equivalent to differential Eq. 10 is

$$F_{0,1} - 2\,F_{0,0} + F_{0,-1} + k_1\,(F_{1,0} - 2\,F_{0,0} + F_{-1,0})$$
$$- 0.5\,k_2\,(F_{1,1} - F_{-1,1} - F_{1,-1} + F_{-1,-1}) = - \frac{w_z\,S_y^2}{\partial^2 z/\partial x^2} \quad \text{(40)}$$

in which

$$k_1 = \frac{\partial^2 z/\partial y^2}{\partial^2 z/\partial x^2}\,\frac{S_y^2}{S_x^2} \quad \text{(41a)}$$

and

$$k_2 = \frac{\partial^2 z/\partial x\,\partial y}{\partial^2 z/\partial x^2}\,\frac{S_y^2}{S_x\,S_y} \quad \text{(41b)}$$

The finite-differences equations for Eqs. 9a and 9b are, respectively,

$$T_{xp} = \frac{F_{0,-1} - 2\,F_{0,0} + F_{0,1}}{S_y^2} \quad \text{(42)}$$

and

$$T_{yp} = \frac{F_{1,0} - 2\,F_{0,0} + F_{-1,0}}{S_x^2} \quad \text{(43)}$$

Because of the quantity of equations which result even with a coarse grid, a direct solution of the simultaneous equations obtained from Eq. 40 is not feasible. Generally, an iteration process called the relaxation method[6] is used.

Eqs. 42 and 43 have a disadvantage in that a value for F must be determined quite accurately to obtain reliable stress values. With the stress equal to the second differences in F (Eqs. 9), minor errors in F greatly affect the value of the stresses. In addition it is somewhat difficult to estimate the initial values to commence the iteration process. For this reason finite-differences equations based on the internal forces are preferable. For the general case these equations become cumbersome. However, for the case of translational shells, the resulting equations are no more complicated than Eq. 40.

To express the relationship in terms of the internal forces, first express T_{xp} in terms of T_{yp} by differentiating Eqs. 5 and 6 with respect to x and y, respectively, which yields

$$\frac{\partial^2 T_x}{\partial x^2} - \frac{\partial^2 T_{yp}}{\partial y^2} = 0 \quad \text{(44)}$$

Because $\partial^2 z/\partial x\,\partial y = 0$, Eq. 8c can be rewritten as

$$T_{xp} + T_{yp}\,\frac{\partial^2 z/\partial y^2}{\partial^2 z/\partial x^2} = - \frac{w_z}{\partial^2 z/\partial x^2} \quad \text{(45)}$$

[6] "Some Improvements in the Use of Relaxation Methods for the Solution of Ordinary and Partial Differential Equations," *Proceedings*, Royal Soc. of London, Series A-190, 1947.

Differentiating Eq. 45 twice with respect to x and subtracting Eq. 44 from the result yields

$$\frac{\partial^2 T_{yp}}{\partial y^2} + k_1\,\frac{\partial^2 T_{yp}}{\partial x^2} + 2\,k_2\,\frac{\partial T_{yp}}{\partial x} + k_3\,T_{yp} = - k_4 \quad \text{(46)}$$

in which

$$\left.\begin{aligned} k_1 &= \frac{\partial^2 z/\partial y^2}{\partial^2 z/\partial x^2} \\ k_2 &= \frac{\partial}{\partial x}\left(\frac{\partial^2 z/\partial y^2}{\partial^2 z/\partial x^2}\right) \\ k_3 &= \frac{\partial^2}{\partial x^2}\left(\frac{\partial^2 z/\partial y^2}{\partial^2 z/\partial x^2}\right) \\ k_4 &= \frac{\partial^2}{\partial x}\left(\frac{w_z}{\partial^2 z/\partial x^2}\right) \end{aligned}\right\} \quad \text{(47)}$$

Allowing T to equal T_{yp}, the finite-differences equation corresponding to differential Eq. 46 is

$$T_{0,1} - 2\,T_{0,0} + T_{0,-1} + \left(\frac{S_y}{S_x}\right)^2 k_1\,(T_{1,0} - 2\,T_{0,0} + T_{-1,0})$$
$$+ \frac{k_2\,S_y^2}{S_x}\,(T_{1,0} - T_{-1,0}) + k_3\,T_{0,0} = - k_4\,S_y^2 \quad \text{(48)}$$

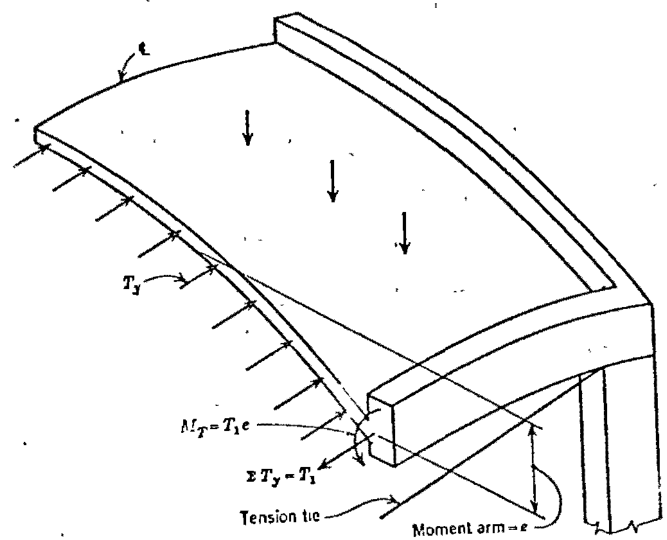

Fig. 11.—Bending Moment in Shells of Double Curvature

The ribs supporting the arches must be designed to carry the tangential shear load imparted to them by the shell. Because this problem involves only a routine analysis of an arch, this subject will not be examined herein except to note that the analysis of the arch can be made by dealing only with the tangential shear obtained from the coefficients in Table 2, or by using directly the surface loads on the shell.[7]

If the vertical loads are used directly for shells of double curvature, consideration must be given to the bending moment created by the rise of the shell in the direction normal to the arch. This moment, as shown in Fig. 11, equals the product of the summation of the T_{xp}-forces or T_{yp}-forces from the midspan to the edge and the lever arm between the centroid of the internal forces in the shell and the centroidal axis of the arch. The tensile force, T_1, must be superimposed on the thrust due to the end reactions in order to obtain the net thrust in the arch.

APPENDIX. BIBLIOGRAPHY

"Some Aspects of the Theory of Thin Elastic Shells," by Eric Reissner, *Proceedings*, Conference on Thin Concrete Shells, Massachusetts Inst. of Technology, Cambridge, June, 1954, p. 81.

"Hyperbolic Paraboloids," by Felix Candela, *ibid.*, p. 91.

"Skew Shell Utilized in Unusual Roof," by Felix Candela, *Proceedings*, A.C.I., 1953, Vol. 49, pp. 657–664.

"Deformation of Hyperbolic Paraboloid Shells," by Shisuo Ban, *Publications*, International Assn. for Bridge and Structural Eng., Zurich, Vol. 13, 1953, p. 1.

"Simple Concrete Shell Structures," by Felix Candela, *Proceedings*, A.C.I., Vol. 48, 1952, p. 321.

"Theory of New Forms of S[illegible]," by R. S. Jenkins, *Paper No. 7*, Symposium on Concrete Shell Roof [illegible]truction, Cement and Concrete Assn., London, July 2–4, 1952.

"Hyperbolic Paraboloid Conc[illegible]te Roofs in Czechoslovakia," by K. Hruban, *Concrete and Constructional Engineering*, London, Vol. 44, No. 8, 1949, pp. 247–252.

"Hyperbolic Paraboloid Shells," by I. Fytos, *Technika Chronika*, Athens, Vol. 26, Nos. 295–296, 1949, pp. 35–44.

"Analysis of Hyperbolic Tanks in Reinforced Concrete," by A. Favini, *Giornale del Genio Civile*, Rome, Vol. 87, 1949, pp. 515–533.

"Doubly Curved Thin Slab Structures," by M. P. Borkowski, *Translation No. 31*, Cement and Concrete Assn., London, 1951.

"Calculations for Shells of Double Curvature Using Differential Equations," by A. Pucher, *Bauingenieur*, Vol. 18, 1937, p. 118.

[7] "Design of Cylindrical Concrete Shell Roofs," *Manual of Engineering Practice No. 31*, ASCE, 1952, p. 90.

"Treatise on Statics of Parabolic Hyperboloidal Shells Not Stiff in Bending," by F. Aimond, *Publications*, International Assn. for Bridge and Structural Eng., Zurich, Vol. 4, 1936, p. 1.

"Calculation of Thin Shells in Reinforced Concrete," by L. Issenmann Pirlaski, Dunod, Paris, 1935, Chapter 7.

"General Investigation Concerning Skew Surface Shells," by B. Laffaille, *Publications*, International Assn. for Bridge and Structural Eng., Zurich, Vol. 3, 1935, p. 295.

"Thin Shells in the Shape of Hyperbolic Paraboloids," by B. Laffaille, *Le Genie Civile*, Paris, Vol. 104, 1934, pp. 409–410.

14

DISCUSSION

TUNG AU,[8] A.M. ASCE.—The general equations for shells of double curvature based on the membrane theory have been presented in a systematic and logical order, with special applications to hyperbolic paraboloids and elliptical paraboloids. Although only a limited number of loading conditions are amenable to an algebraic solution, the author has included the cases of practical importance. Thus, the solutions are obtained with mathematical rigor, and the structural behavior of these shells is also clearly explained.

The use of difference equations and the relaxation method are suggested for the solution of other shells of double curvature for which the classical solutions are either extremely complicated or unavailable. Therefore, it may be desirable to indicate also that such techniques can be adapted to hyperbolic and elliptical paraboloids with loadings other than uniform vertical load and with different boundary conditions. By considering w_x and w_y as components of force in the direction of the x-axis and the y-axis, respectively, acting at the center of the element in Fig. 1, Eqs. 5, 6, 8, 9, and 10 can be generalized as follows:

$$\frac{\partial T_{xp}}{\partial x} + \frac{\partial S_p}{\partial y} + w_x = 0 \qquad (49)$$

$$\frac{\partial T_{yp}}{\partial y} + \frac{\partial S_p}{\partial x} + w_y = 0 \qquad (50)$$

Eqs. 8 remain unchanged. Then the stress function, F, can be introduced so that

$$T_{xp} = \frac{\partial^2 F}{\partial y^2} - \int_{x_0}^{x} w_x \, dx \qquad (51a)$$

$$T_{yp} = \frac{\partial^2 F}{\partial x^2} - \int_{y_0}^{y} w_y \, dy \qquad (51b)$$

and

$$S_p = -\frac{\partial^2 F}{\partial x \, \partial y} \qquad (51c)$$

These values satisfy Eqs. 5 and 6 and reduce Eq. 8c to

$$\frac{\partial^2 F}{\partial y^2}\frac{\partial^2 z}{\partial x^2} + \frac{\partial^2 F}{\partial x^2}\frac{\partial^2 z}{\partial y^2} - 2\frac{\partial^2 F}{\partial x \, \partial y}\frac{\partial^2 z}{\partial x \, \partial y}$$
$$= -w_z + w_x \frac{\partial z}{\partial x} + w_y \frac{\partial z}{\partial y} + \frac{\partial^2 z}{\partial x^2}\int_{x_0}^{x} w_x \, dx + \frac{\partial^2 z}{\partial y^2}\int_{y_0}^{y} w_y \, dy \qquad (52)$$

Solutions of these equations, either by algebraic or numerical methods, for hyperbolic paraboloids subjected to several types of lateral loads are well known in European literature.[9] However, they have been considered elsewhere[10] as being only of academic significance because the distribution of lateral forces is generally simplified and assumed in a mathematically convenient manner. Even though the assumption of the distribution of wind pressure in these solutions may not meet the requirements of building codes in the United States, the effect of an earthquake can be simulated by a distributed horizontal force. This latter problem is probably not academic, and a similar approach has been used to compute earthquake stresses in spherical domes and in cones.[11]

There is a minor point in the paper, which is perhaps not pertinent in practical applications but which nevertheless should be clarified. In the derivation of Eq. 14 for hyperbolic paraboloids with a moderate rise, it is stated that "because the differential of S_p with respect to y and x is zero, it is seen from the relationships in Eqs. 5 and 6 that $T_{xp} = T_{yp} = 0$." Actually, from the derivation the following equations are obtained:

$$T_{xp} = f(y) \qquad (53)$$

and

$$T_{yp} = f(x) \qquad (54)$$

The functions, $f(y)$ and $f(x)$, become zero only if the boundary conditions indicate that no normal forces are acting on the edges. Hence, it is the boundary conditions of the free edges that prescribe the constants of integration, and Eq. 14 represents only one of the many possible edge conditions. Mr. Parme has not neglected this point for hyperbolic paraboloids with a great rise because the terms, $f(y)$ and $f(x)$, are included in Eqs. 17 and 18, respectively.

W. WATTERS PAGON,[12] M. ASCE.—Many engineers and architects have recently become interested in the use of the hyperbolic paraboloid as a structure. The author's authoritative presentation of this subject is of great value to the profession.

However, a review of the deflections of shells of double curvature has not been included. In addition, although the hyperbolic paraboloid is considered to be rigid because of the opposing parabolic elements, no statement concerning its limiting flatness has been presented.

For roof structures, dead load and snow are usually the essential loadings because a wind load seldom will have a marked influence on domes. However, there are three other load conditions that are not included—earthquake loading, uniform radial pressure,[11] and a radial uniform pressure or suction. In 1956 the writer designed a building to house a jet-engine test facility. One of the design conditions was a large unit load per square foot with either inside pressure or inside suction. This caused large stresses and large structural members that could have been avoided had a domed structure been used.

[8] Visiting Associate Prof., Dept. of Civ. Eng., Carnegie Inst. of Technology, Pittsburgh, Pa.

[9] "Beitrag zur Berechnung der hyperbolischen Paraboloidschale," by K. G. Tester, *Ingenieur-Archiv*, Vol. 16, 1947, pp. 39-44.

[10] "Structural Applications of Hyperbolic Paraboloidical Shell," by F. Candela, *Journal*, A.C.I., Vol. 26, No. 5, January, 1955, pp. 379-415.

[11] "Earthquake Stresses in Spherical Domes and in Cones," by E. P. Popov, *Proceedings Paper 974*, ASCE, May, 1956.

[12] Cons. Engr., Baltimore, Md.

Mr. Parme has examined only a square or rectangular roof slab. Could not the hyperbolic paraboloid be used to house a cylindrical structure, or structures of hexagonal or octagonal shape?

SANTI P. BANERJEE,[13] A. M. ASCE.—The formulation of the equations and the method adopted for their solution have been presented.

The dead load, w_s, of a hyperbolic paraboloid shell with a reasonably great rise has been represented by Eq. 15*a*, in which w is the constant weight of shell membrane per unit area. Eq. 15*a* is also applicable to doubly curved shells of other shapes. The writer finds that, as the elements in the shell away from the origin form oblique angles, ω, between their adjacent sides, the relationship between the variable load, w_s, on the projected area and the unit weight, w, should be shown as

$$w_s = \frac{w}{\cos\phi\cos\psi}\sin\omega \qquad (55)$$

instead of Eq. 15*a*. The subsequent related equations presented in the paper also require modification.

With regard to the solution of Eqs. 5, 6, and 8*c* for the three unknowns, it is customary, as has been shown, to reduce them to a single equation with one unknown by suitably introducing a stress function, F. The mathematical solution of such an equation becomes extremely involved, and, therefore, relaxation or another similar iterative method is applied for a practical solution of F. However, these procedures also require a great amount of time because an estimate of the initial values is required to begin the iteration process.

However, the writer has found it more convenient to solve the three equations simultaneously after representing them through algebraic expressions obtained from the geometry of the shell form. A solution by this method is more direct.

To illustrate the procedure a hyperbolic paraboloid may be considered. The fundamental equations are Eqs. 5, 6, and 8*c*. The representative equation of shell form is given by Eq. 11 as

$$z = \left(\frac{h}{a\,b}\right) x\,y = C\,x\,y \qquad (56)$$

Thus,

$$\left.\begin{aligned} \frac{\partial z}{\partial x} &= C\,y & \frac{\partial z}{\partial y} &= C\,x \\ \frac{\partial^2 z}{\partial x^2} &= \frac{\partial^2 z}{\partial y^2} = 0 & \frac{\partial^2 z}{\partial x\,\partial y} &= C \end{aligned}\right\} \qquad (57)$$

Also,

$$\tan\phi = \left(\frac{h}{b}\,y\right)\frac{1}{a} = C\,y \qquad (58)$$

and

$$\tan\psi = \left(\frac{h}{a}\,x\right)\frac{1}{b} = C\,x \qquad (59)$$

[13] Cons. Engr., Calcutta, India.

Thus,

$$\left.\begin{aligned} \phi &= \tan^{-1} C\,y \\ \psi &= \tan^{-1} C\,x \\ \omega &= \cos^{-1}(\sin\phi\sin\psi) \end{aligned}\right\} \qquad (60)$$

From Eq. 8*c*, after substitution of values,

$$2\,S_p\,C = -\,w_s \qquad (61a)$$

Therefore,

$$S_p = -\frac{w_s}{2\,C} \qquad (61b)$$

When w_s varies, due to the constant weight, w, of the shell slab, then

$$w_s = w\left(\frac{\sin\omega}{\cos\phi\cos\psi}\right) = w\,m \qquad (62)$$

and Eq. 61*b* becomes

$$S_p = -\,w\left(\frac{m}{2\,C}\right) = -\,w\,r \qquad (63)$$

From Eq. 5 of the paper,

$$T_{xp} = -\int \frac{\partial S_p}{\partial y}\,dx + f(y) \qquad (64a)$$

and

$$T_{xp} = w\int \frac{\partial r}{\partial y}\,dx + f(y) \qquad (64b)$$

The conditions at the boundaries require that, at $x = a$, $T_{xp} = 0$. Therefore,

$$\left.\begin{aligned} f(y) &= -\,w\int_0^a \frac{\partial r}{\partial y}\,dx \\ f(y) &= -\,w\,\delta x \sum_0^a \frac{\partial r}{\partial y} \\ f(y) &= -\,w\,\delta x\,K_x \end{aligned}\right\} \qquad (65)$$

in which

$$K_x = \sum_0^a \frac{\partial r}{\partial y} \qquad (66)$$

Therefore,

$$T_{xp} = w\,\delta x\left(\sum_0^x \frac{\partial r}{\partial y} - K_x\right) \qquad (67)$$

Similarly, from Eq. 6,

$$T_{yp} = w\,\delta y\left(\sum_0^y \frac{\partial r}{\partial x} - K_y\right) \qquad (68)$$

in which $K_y = \sum_0^b \frac{\partial r}{\partial x}$.

Eqs. 63, 67, and 68 replace Eqs. 16, 17, and 18 of the paper, and, for purposes of solution, are suitable for representation in finite-differences forms.

The numerical values of r at each nodal point of the working grid on the (xy)-plane are known from the geometry of the shell form (Eqs. 60, 62, and 63). Therefore, the values of $\partial r/\partial x$ and $\partial r/\partial y$ and those of the unknowns, S_p, T_{xp}, and T_{yp} are easily obtained.

Equations similar to those derived in the foregoing can also be formed for doubly curved shells of other shapes.

centro de educación contínua
facultad de ingeniería, unam

DISEÑO Y CONSTRUCCION DE ESTRUCTURAS ESPACIALES Y DE CASCARON

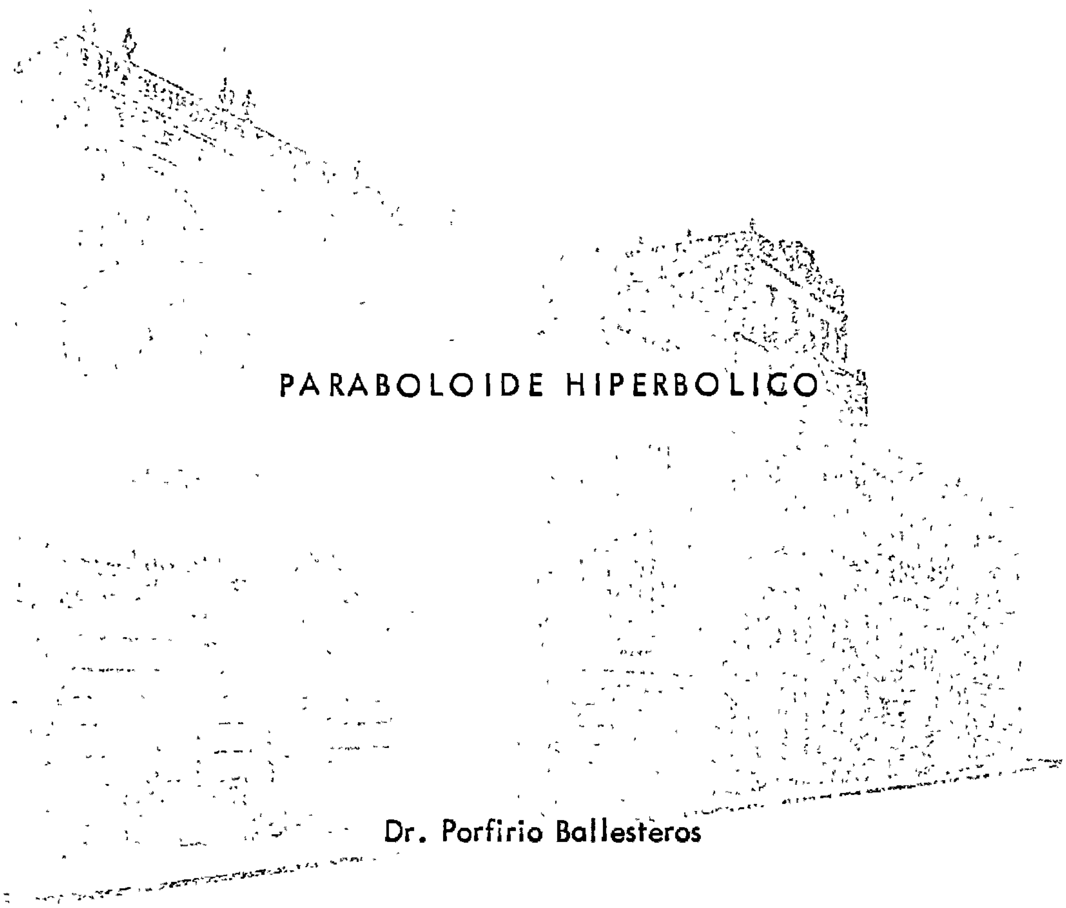

PARABOLOIDE HIPERBOLICO

Dr. Porfirio Ballesteros

1972

Tacuba 5, primer piso. México 1, D.F.
Teléfonos: 521-30-95 y 513-27-95

The continuing development of design and construction techniques of shell structures is resulting in an increasing fund of information of practical interest to Architects, Engineers and Contractors. The aim of furthering all branches of this progress has inspired the formation of the **international association for shell and spatial structures**, whose purpose is to organise meetings and congresses for the interchange of ideas and their dissemination by means of periodical publications.

Everyone interested in the various branches of shell techniques and their architectonic possibilities or realizations is invited to join this International Association.

the advisory board

A. L. L. Baker (Gt. Britain)
N. Esquillan (France)
R. S. Jenkins (Gt. Britain)
K. W Johansen (Denmark)
F. Levi (Italy)
W. Olszak (Poland)

the executive council

Honorary President:
A. M. Haas (The Netherlands)

President:
A. Paduart (Belgium)

Vice presidents:
A L. Parme (U. S. A.)
F. del Pozo (Spain)
H. Rühle (German D. R.)

Treasurer:
G. Lacombe (France)

Secretary:
R. López Palanco (Spain)

Members of the Executive Council:
A. Aas-Jackobsen (Norway)
P. Ballesteros (Mexico)
T. Brøndum - Nielsen (Denmark)
L. Finzi (Italy)
K. A. Glukhovskoi (U. S. S. R.)
G. K. Khaidukov (U. S. S. R.)
J Kozak (Czechoslovakia)
R. Krapfenbauer (Austria)
J. Munro (Gt. Britain)
E. P. Popov (U. S. A.)
G. S. Ramaswamy (India)
K. Szmodits (Hungary)
Y. Tsuboi (Japan)
W. Zerna (German F. R.)

To become a member or to obtain more detailed information, please write to the Secretariat of the International Association for Shell and Spatial Structures, Alfonso XII, 3, Madrid (7). Spain.

Porfirio Ballesteros

Hyperbolic Paraboloid Shells

The following discussion is a brief resume of a talk given at the Thin Shell Seminar in Chicago in March 1955. This is not intended to be a complete treatise on the analysis of hyperbolic paraboloid shells but has been prepared to give a physical picture of the structural action involved. Results obtained agree with the exact solution presented by F. Candela in the January 1955 issue of the ACI Journal as far as uniform loads are concerned.

Figure 1:

Consider the horizontal plane A'C'E'G'. This surface contains the generatrices i_n parallel to the y axis and h_n parallel to the x axis. A warping of this surface is achieved by vertically depressing the corners A' and E' to new positions A and E respectively. During this action the i_n generatrices pivot about the fixed axis FOB while the h_n generatrices pivot about HOD. The resulting warped surface is the hyperbolic paraboloid and contains two systems of straight lines h_n and i_n, these systems being parallel to the planes XOZ and YOZ respectively which form an arbitrary angle ω. Every point on this surface may be considered the intersection of two straight lines contained in the surface.

Figure 2:

The portion of the hyperbolic paraboloid with which we are concerned is the square ABOH, representing a portion of the roof structure in Figure 8. Figure 2, illustrating this section, shows that any point on the surface may be defined in terms of x, y and z where z equals a constant multiplied by the X and Y coordinates.

Figure 3:

For convenience, the axes OX and OY shown in Figure 2 are rotated through an angle ϕ of 45°, so that the axis OY' now lies in a vertical plane with OA. Figure 3 gives the standard formulas for transformation of coordinates by rotation. These formulas are modified for application here by introduction of the angle $\phi = 45^\circ$.

Figure 4:

Figure 4 shows the transformed coordinates OX' and OY' in position above ABOH. At the top of Figure 4 the equation defining the surface of the hyperbolic paraboloid in terms of x, y and z is transformed to the new coordinate system by means of expressions given with Figure 3. When x' is given a constant value in the transformed equation the result is the equation of a parabola lying either in or parallel to the Y'Z plane. The vertex of the parabola defined by setting $x' = 0$ intersects the X' axis at the origin of the X', Y' and Z axes, but for any other value of x' the vertex falls ~~below~~ above the X'Y' plane. In any case the principal axes of all these parabolas are parallel to the Z axis and lie in the X'Z plane.

In a similar manner, for any given value of y' the general expression becomes the equation of a parabola lying either in or parallel to the X'Z plane. If $y' = 0$ the equation is for a parabola having a vertex which intersects the Y' axis at the origin. Any other value of y' defines a parabola having its vertex below the X'Y' plane but with its principal axis parallel to the Z axis and lying in the Y'Z plane.

It is important to note that for any given warped surface either x' or y' may be varied without affecting the term "0.5k" in the parabolic equation. As a result, all parabolas in both directions have the same shape. In addition it can be seen that one of the expressions is positive while the other is negative. This difference in sign indicates that parabolas parallel to the X'Z plane are concave upward while those parallel to the Y'Z plane are concave downward.

If z is given a constant value in the general expression the warped surface is cut by a horizontal plane, the elevation of which depends on the particular value given to z. This cutting plane forms a hyperbola.

Figure 5:

Figure 5 illustrates the advantage resulting from the fact that the hyperbolic paraboloid is made up entirely of two sets of parabolic arches, one set normal to the other and all of the same shape.

Assume that the total load w is divided equally in two directions so that any given arch carries a load of intensity $\frac{w}{2}$. The midspan simple beam bending moment due to this uniform load is $\frac{w}{2} \cdot \frac{\ell^2}{8}$. The only other force acting on any of the arches is the horizontal thrust H which, when multiplied by the arm b, also produces a midspan moment equal to $\frac{w}{2} \cdot \frac{\ell^2}{8}$ but opposite in direction to the uniform load moment. To prove that H produces the same midspan moment as the uniform load consider the parabolic arch shown below.

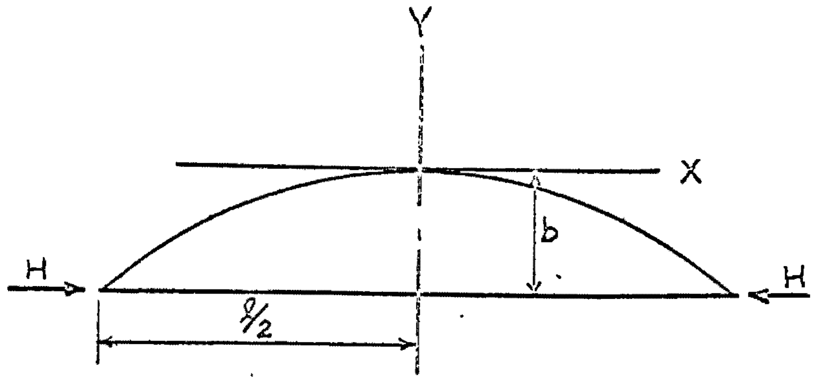

The general equation for this parabola is $y = px^2$. The parameter p may be evaluated from the fact that y=b, when $x = \frac{\ell}{2}$; therefore, $p = \frac{4b}{\ell^2}$.

The general equation may then be written:

$$y = \frac{4b}{\ell^2} x^2$$

The general expression for simple beam bending moment in an arch is:

$$M_s = \frac{\frac{W}{2}\ell^2}{8} - \frac{\frac{W}{2}x^2}{2} = \frac{\frac{W}{2}\ell^2}{8}\left[1-4\left(\frac{x}{\ell}\right)^2\right] \qquad (1)$$

while the general expression for moment due to thrust H is:

$$M_t = H\,(b-y) = H\left(b-\frac{4b}{\ell^2}x^2\right) = Hb\left[1-4\left(\frac{x}{\ell}\right)^2\right] \qquad (2)$$

For the two-hinged arch carrying uniform load:

$$\Delta H = 0 = \int_0^{\frac{L}{2}} \frac{Myds}{EI} = \int (M_t + M_s)\,\frac{yds}{EI} \qquad (3a)$$

$$0 = Hb\int\left[1-4\left(\frac{x}{\ell}\right)^2\right]\frac{ydx}{EI} + \frac{\frac{W}{2}\ell^2}{8}\int\left[1-4\left(\frac{x}{\ell}\right)^2\right]\frac{ydx}{EI} \qquad (3b)$$

from which:

$$Hb = -\frac{W}{2}\cdot\frac{\ell^2}{8} \qquad (4)$$

Substituting (4) in (2) reveals that M_t and M_s are equal and opposite and as a result under uniform load there is zero moment throughout the arch. Horizontal thrust H may be expressed as $\frac{w}{2k}$ as shown.

Figure 6:

Figure 6 shows the theoretical parabolic arches of the roof in plan. It is evident that at any point along the edge of the roof where two perpendicular arches intersect the components (normal to the edge) of horizontal thrust H are equal in magnitude but opposite in direction. As a result there is no force normal to the edge. Components parallel to the edge all act in the same direction and, as shown in Figure 6, produce a constant shearing stress along the edge equal to $\frac{w}{2k}$. This shear combines with the vertical component of arch thrust to put pure compression in the edge beam. The accumulated horizontal compression at the intersection of edge beam and column then equals $\frac{wb}{h} \cdot \frac{a^2}{2}$ as shown on Figure 7.

Figure 7:

Compression at the column may be checked by statics by referring to the figure below which represents an elevation view of the roof section ABOH cantilevered from the central post.

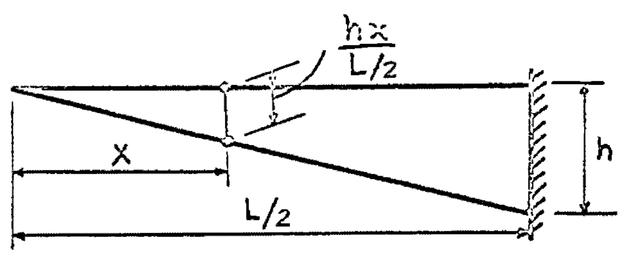

Moment at any section due to a uniform load w is $\frac{wx^2}{2}$. Dividing this moment by the depth of the roof at that point gives the magnitude of horizontal compression at the bottom fiber equal to

$\frac{wx^2}{2} \cdot \frac{L}{2hx} = \frac{wx}{2h} \cdot \frac{L}{2}$. Therefore, thrust at the support, considering the load w applied to an area ab where $x = \frac{L}{2} = a$ is

$$\frac{wa^2}{2h} \cdot b = \frac{wb}{h} \cdot \frac{a^2}{2}$$

Summary:

This material agrees with the derivations for warped surfaces given on pages 402-404 of the January 1955 issue of the ACI Journal.

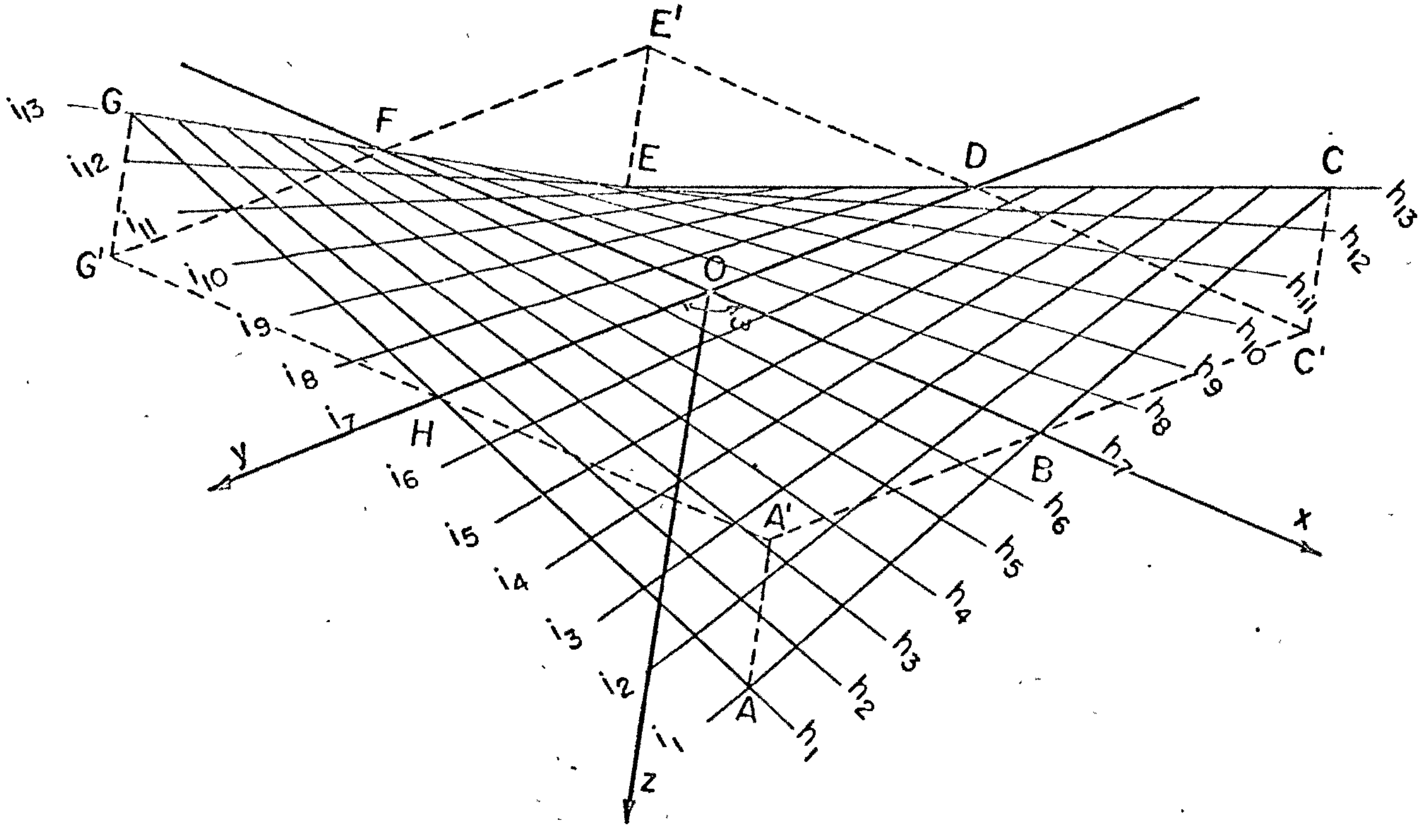

SURFACE DEFINITIONS
Fig. 1

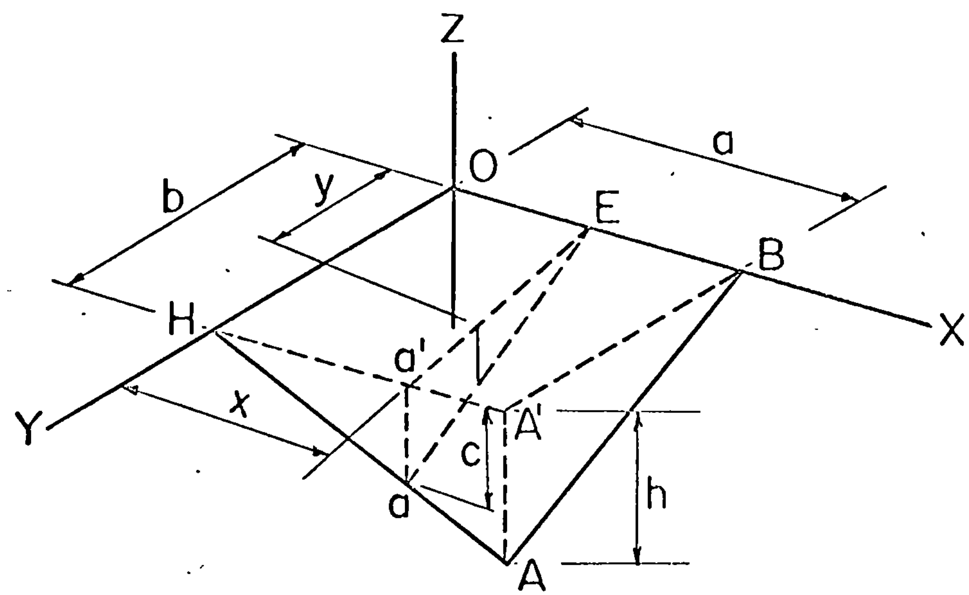

In $\Delta HA'A$

$$\frac{c}{h} = \frac{x}{a} \quad \text{or} \quad c = \frac{xh}{a}$$

In $\Delta Ea'a$

$$\frac{z}{c} = \frac{y}{b}$$

$$z = \frac{yc}{b} = \frac{y}{b} \cdot \frac{xh}{a} = xy \cdot \frac{h}{ab}$$

letting $k = \dfrac{h}{ab}$

$$z = kxy$$

Fi 2

6

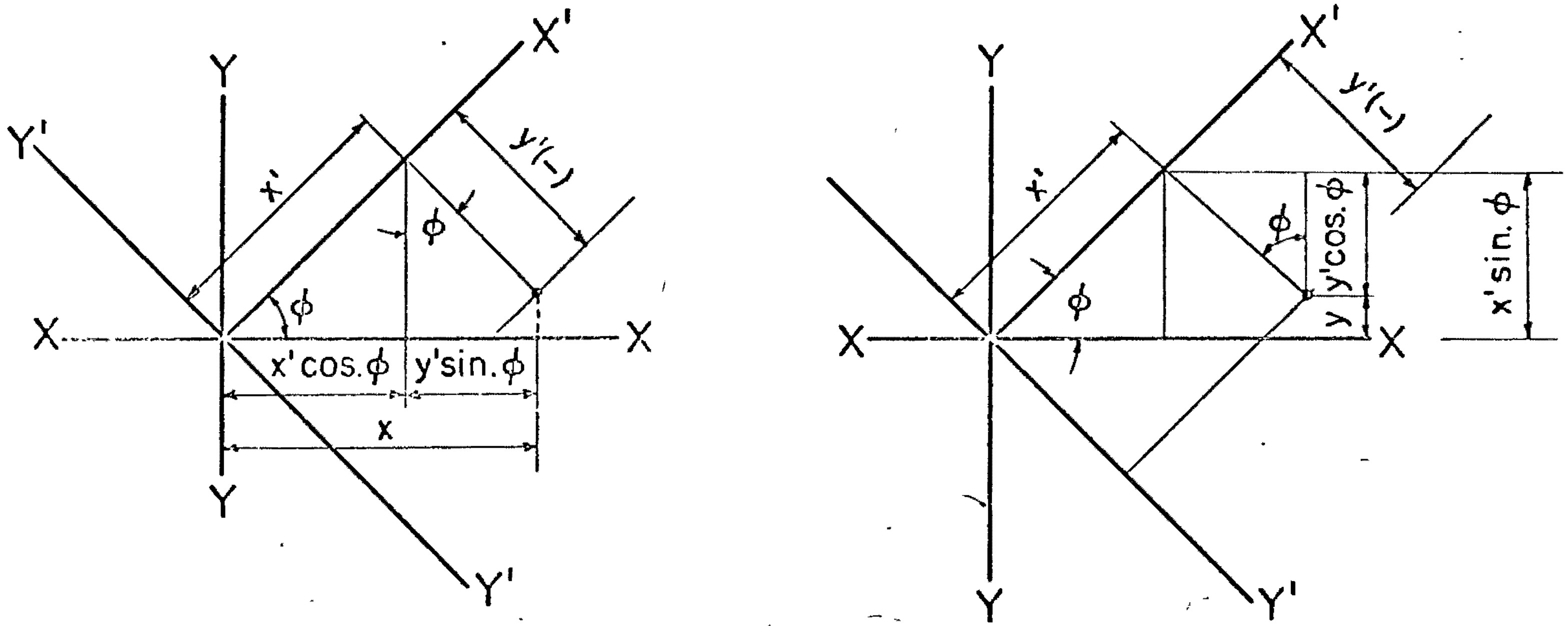

$$x = x' \cos.\phi - y' \sin.\phi = .707\,(x' - y')$$

$$y = y' \cos.\phi + x' \sin.\phi = .707\,(x' + y')$$

Fig. 3

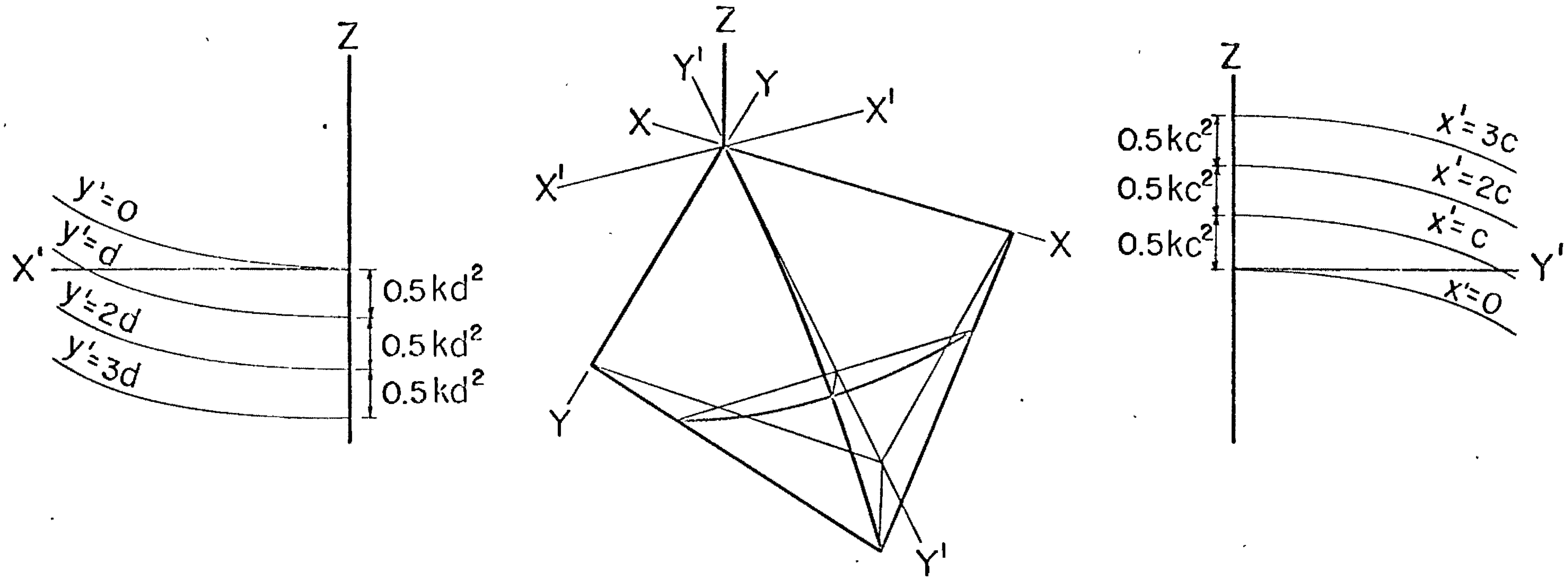

$$z = kxy = 0.5k\,(x'+y')(x'-y') = 0.5k\left[(x')^2-(y')^2\right]$$

when x' is constant

$$z-k_1 = z' = 0.5k\,(-)\,(y')^2$$

when y' is constant

$$z-k_2 = z' = 0.5k\,(x')^2$$

when z is constant

$$1 = k_3\left[(x')^2-(y')^2\right]$$

Fig. 4

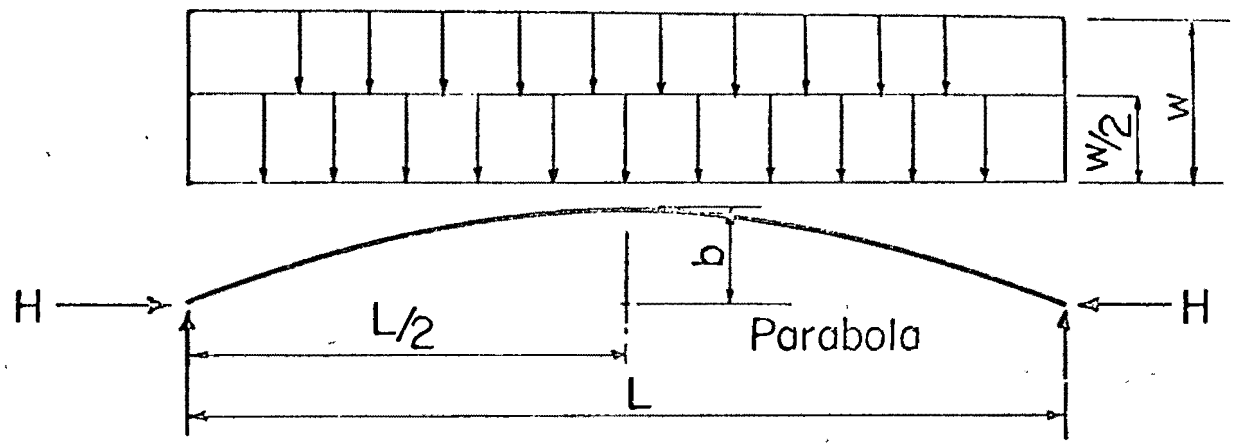

Simple Beam Bending Moment $= \frac{w}{2} \cdot \frac{L^2}{8}$

$$Hb = \frac{w}{2} \cdot \frac{L^2}{8} \quad \text{or} \quad H = \frac{wL^2}{16b} = \frac{w}{4} \cdot \frac{L^2}{4b}$$

Equation of Parabola

$$y = px^2 \quad \text{when} \quad y = b \quad x = \frac{L}{2}$$

Therefore

$$b = p\frac{L^2}{4} \quad \text{or} \quad \frac{L^2}{4b} = \frac{1}{p}$$

Hence

$$H = \frac{w}{4} \cdot \frac{1}{p} = \frac{w}{4} \cdot \frac{1}{0.5k} = \frac{w}{2k}$$

Fig. 5

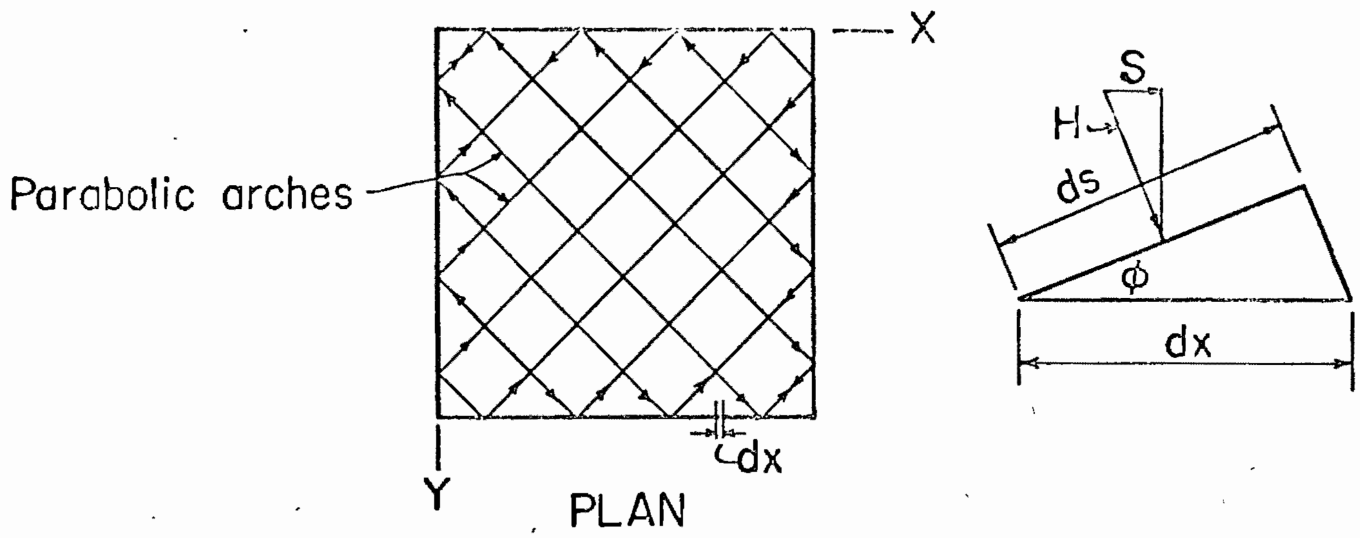

Total Force = $S = H ds \sin\phi$

Unit Force = $s = \dfrac{S}{dx} = \dfrac{H ds \sin\phi}{dx} = H \sin\phi \cos\phi$

With $\phi = 45^\circ$ and $H = \dfrac{w}{2k}$

Combing effect of both arches

$$v = 2\left(\frac{0.5\,w}{2k}\right) = \frac{w}{2k}$$

Fig. 6

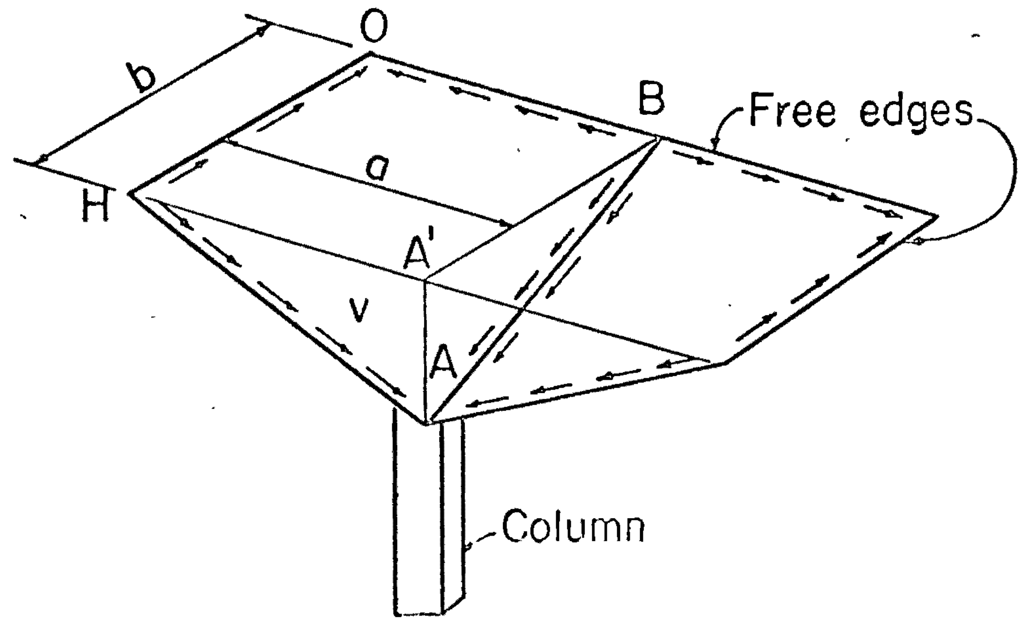

$$C = \Sigma s = \frac{wa}{2k}$$

Since $k = \dfrac{h}{ab}$

$$C = \frac{wa}{2} \cdot \frac{ab}{h} = \frac{wb}{h} \cdot \frac{a^2}{2}$$

From Statics

$$C = \frac{wba^2}{2h}$$

Fig. 7

13

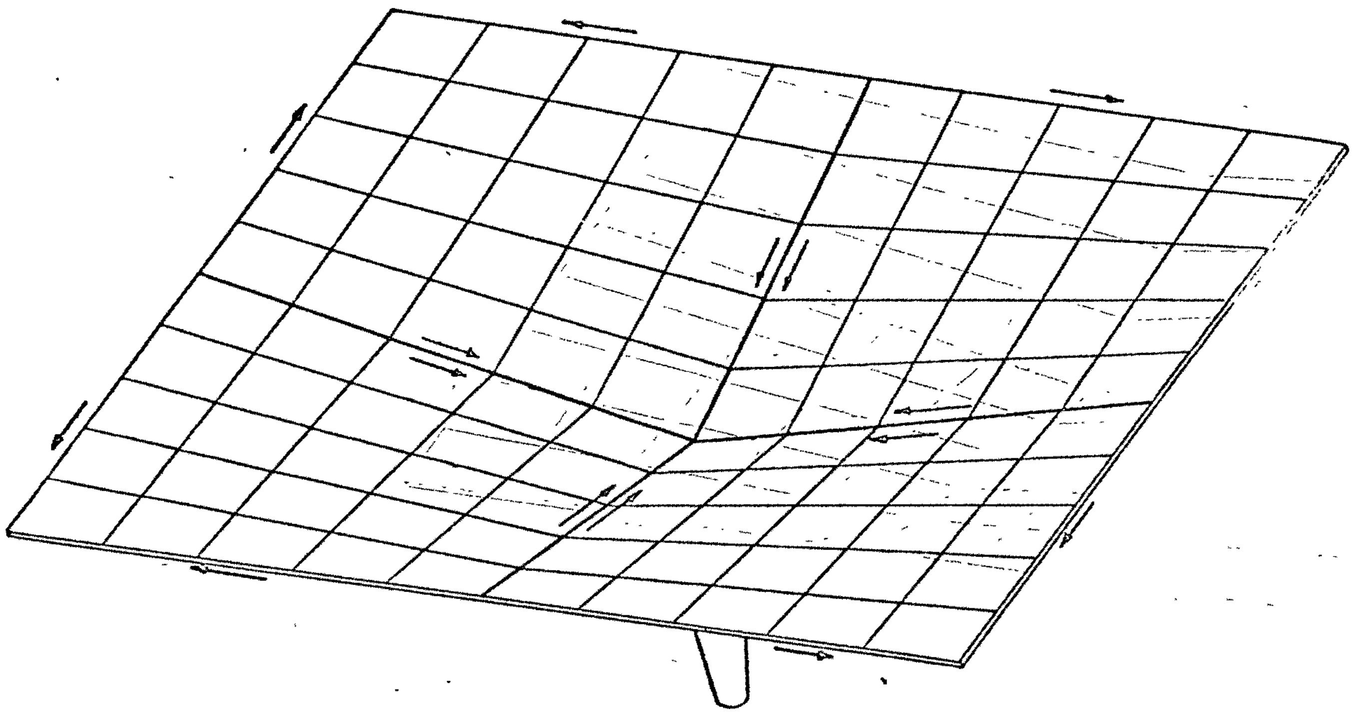

STRUCTURAL SHAPES OBTAINED BY
JOINING WARPED PARALLELOGRAMS

Fig. 8

14

Porfirio Ballesteros

Elementary Analysis of Hyperbolic Paraboloid Shells

Introduction

The rapid growth of interest in one of the newest forms of shell roof construction—the hyperbolic paraboloid—is due largely to its economical use of construction materials, the simplicity of its structural action and to its inherent beauty.

The hyperbolic paraboloid is one of the types of construction that make efficient use of materials by relying on form or shape for strength rather than on mass. Double curvature enables loads to be transferred to supports entirely by direct forces so that all material in the cross-section of the shell is uniformly stressed.

Although intricacies of mathematics obscured the analysis of hyperbolic paraboloids for many years, it will be shown that the underlying static principles are not difficult to understand or to apply and that the design can be handled as easily as the design of many other types of structures.

Economy in the construction and design of hyperbolic paraboloids allows the architect to depart from the conventional practice of forcing all structures to conform to networks of linear members confined to three perpendicular planes and to make imaginative use of the many graceful shapes that may be developed.

Surface Definition

The doubly curved surface of the hyperbolic paraboloid may be defined in two ways, either as a surface of translation or as a warped parallelogram. In the first case the surface can be defined by translating or moving a vertical parabola having upward curvature over another parabola with downward curvature, the parabola of translation lying in a plane perpendicular to the first but moving parallel to it. This is shown graphically in Fig. 1 where the saddle-shaped surface is formed by moving parabola *ABC* over parabola *BOF*.

Fig. 1

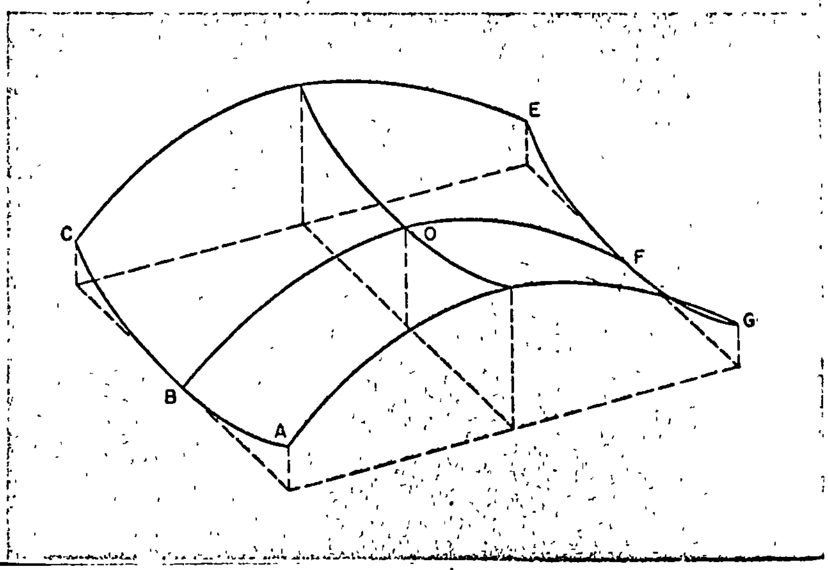

The hyperbolic paraboloid surface may also be generated as shown in Fig. 2 by moving along the Y axis a straight line that remains parallel to the XZ plane at all times but pivots while sliding along the straight line ABC. The resulting surface is represented in Fig. 2 by the grid of straight lines h_n and i_n, and every point on it may be considered to be the intersection of two such lines contained in the surface. This surface can be visualized by considering the horizontal plane $A'C'E'G'$ to be warped by vertically depressing corners A' and E' to new positions A and E. Straight lines h_n and i_n are, of course, longer in the warped surface than in the projected horizontal surface in order that an intersection such as A may remain directly under A'.

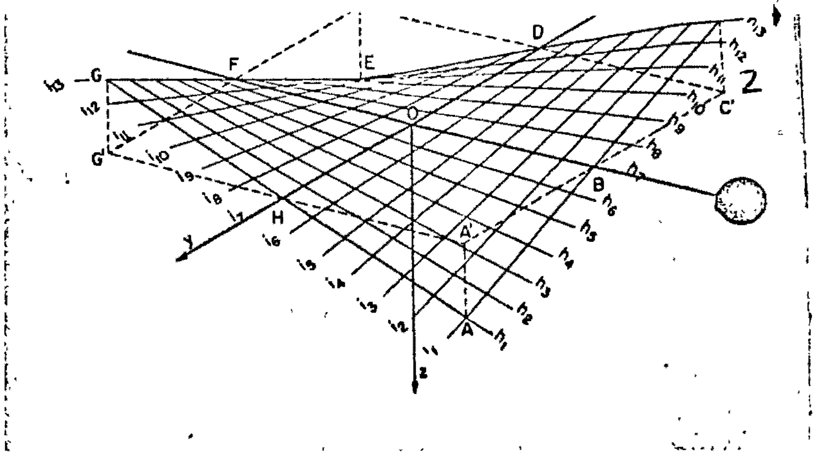

Fig. 2. Surface definitions.

Structural Shapes

A variety of roof forms may be developed either by use of the entire warped surface or by combining parts of it in various ways. A few of these are illustrated in Fig. 3.

The surface in Fig. 3a has been used successfully to give a striking appearance to such diverse structures as churches, banks and restaurants. This is the complete warped surface identical to that shown in Fig. 2.

Surfaces in Figs. 3b, 3c and 3d are formed by combining in various ways one quadrant of the surface in Fig. 2. For example, consider quadrant $ABOH$ in which lines BO and OH are horizontal, coincident with the axes OX and OY. In Fig. 3b four of these quadrants are joined, with the horizontal edges of each quadrant at the exterior of the roof and all depressed corners A at the single center column. This shape is commonly known as the inverted umbrella.

In Fig. 3c, edges HO and OB of the near quadrant are horizontal, while the depressed corner A is at the column. A corresponding arrangement of the other three sections of the roof results in one horizontal ridge line and two horizontal exterior edges. In contrast to Fig. 3c, both ridge lines in Fig. 3d are horizontal, the roof dropping to each of the corner columns. Roof types in Figs. 3b, 3c and 3d are well suited for covering the large rectangular areas common to industrial plants.

Fig. 3. (Edge beams and ties not shown)

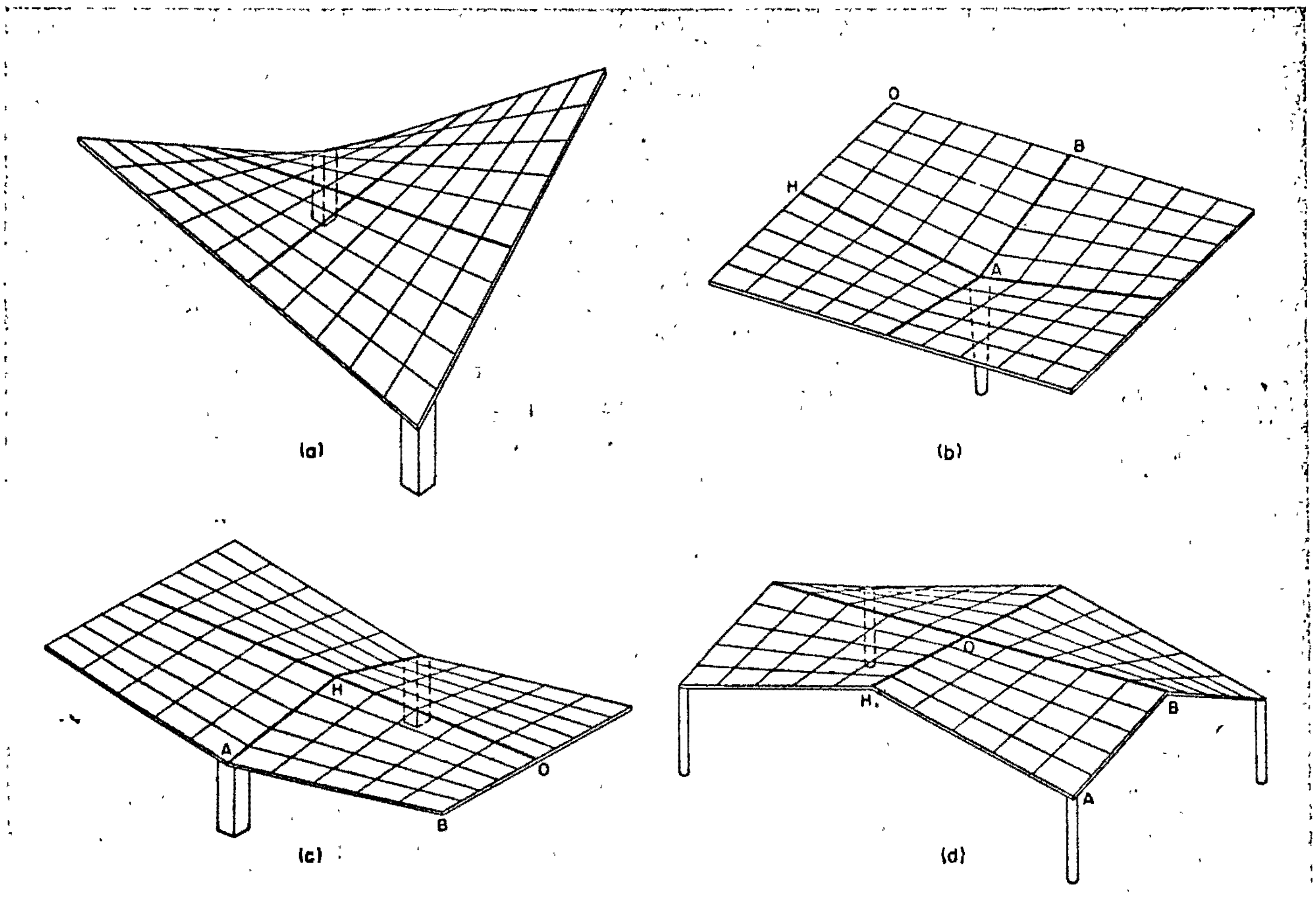

Construction

One of the principal economies of the hyperbolic paraboloid is that its forming is simple, even though the doubly curved surface has the appearance of posing a complicated forming problem. Because the surface is defined by two intersecting systems of straight lines, the formwork requires only straight wood joist generators. The smooth, warped surface may be secured merely by covering these joists with flexible plywood sheathing.

Stresses in the hyperbolic paraboloid roof are low and require only a minimum thickness of concrete. In fact, the roof of the Cosmic Ray Pavilion at the University of Mexico has a thickness of only ⅝ in. Generally, however, shell thickness depends upon the concrete cover required for the reinforcement, with 3 in. being an average figure.

Geometry

The study of the hyperbolic paraboloid may be confined to the basic quadrant *ABOH* of the surface shown in Fig. 2. Referring to Fig. 4, any point on the surface may be defined in terms of x, y and z, where z equals the product of the x and y coordinates and a constant h/ab. For example, in triangle $HA'A$, by similar triangles,

$$\frac{c}{h} = \frac{x}{a} \text{ or } c = \frac{xh}{a}$$

Similarly in triangle $Ed'd$,

$$\frac{z}{c} = \frac{y}{b}$$

from which

$$z = \frac{yc}{b} = \left(\frac{y}{b}\right)\left(\frac{xh}{a}\right) = xy\left(\frac{h}{ab}\right)$$

Letting $k = \dfrac{h}{ab}$

$$z = kxy \qquad (1)$$

For convenience in analysis, axes OX and OY shown in Fig. 4 are rotated through an angle $\phi = 45°$ so that the axis OY' lies in a vertical plane with OA. Using the standard formulas for transformation of coordinates by rotation and letting $\phi = 45°$ in Fig. 5, gives

$$x = x' \cos\phi - y' \sin\phi = 0.707\,(x' - y') \qquad (2a)$$

and

$$y = y' \cos\phi + x' \sin\phi = 0.707\,(x' + y') \qquad (2b)$$

Substituting equations (2a) and (2b) into equation (1) gives

$$\boxed{\begin{aligned} z = kxy &= 0.5k\,(x' + y')\,(x' - y') \\ &= 0.5k\left[(x')^2 - (y')^2\right] \end{aligned}} \qquad (3)$$

which defines the surface of the hyperbolic paraboloid in terms of the new coordinate system. The rotated position of the coordinates above the quadrant *ABOH* is shown in Fig. 6.

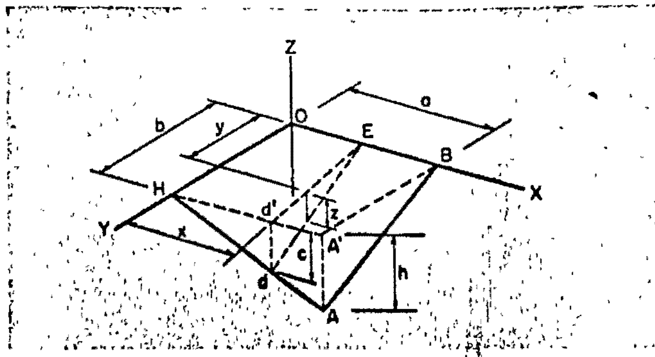

Fig. 4

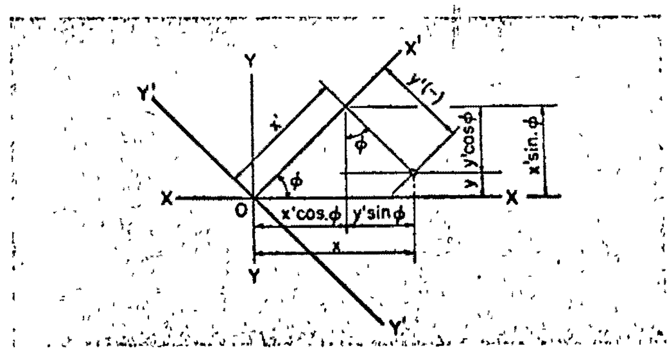

Fig. 5

Fig. 6

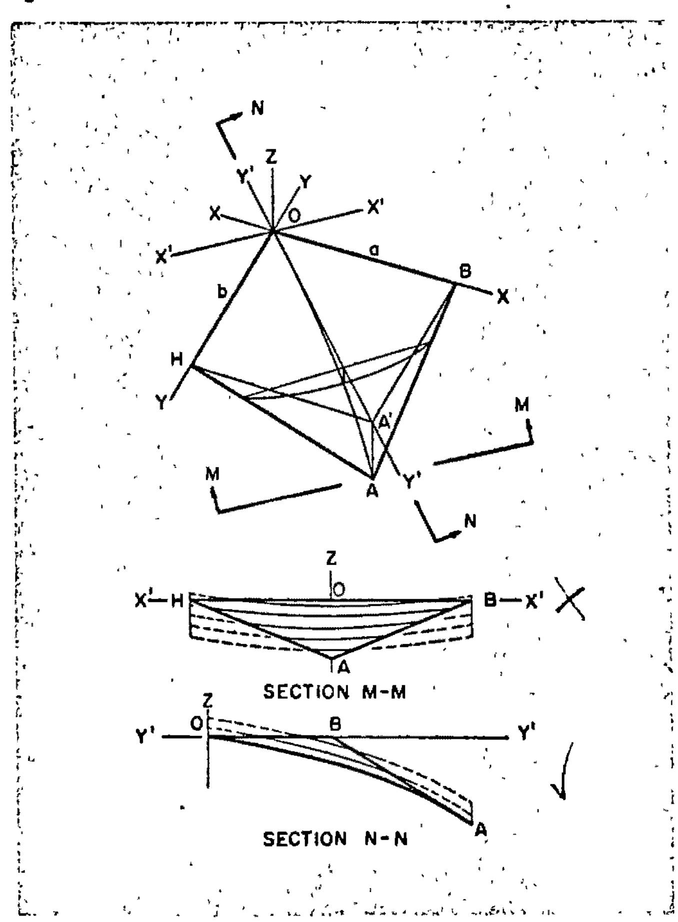

A study of physical properties of the surface is possible by introducing specific values of x', y' and z into equation (3). When x' is constant,

$$z - 0.5k\,(x')^2 = z - k_1 = z' = -0.5k\,(y')^2 \qquad (4)$$

which is the equation of a parabola lying either in or parallel to the $Y'Z$ plane. The vertex of the parabola defined by setting $x'=0$ intersects the X' axis at the origin of the X', Y' and Z axes, but for any other value of x' the vertex is above the $X'Y'$ plane. In any case the principal axes of all these parabolas are parallel to the Z axis and lie in the $X'Z$ plane.

In a similar manner, if y' is constant,

$$z + 0.5k\,(y')^2 = z + k_2 = z' = 0.5k\,(x')^2 \qquad (5)$$

Equation (5) is the general expression for a parabola lying either in or parallel to the $X'Z$ plane. If $y'=0$ the equation represents a parabola having a vertex which intersects the Y' axis at the origin. Any other value of y' defines a parabola having its vertex below the $X'Y'$ plane but with its principal axis parallel to the Z axis and lying in the $Y'Z$ plane.

It is important to note in equations (4) and (5) that for any given warped surface the value of either x' or y' may be varied without affecting the term "$0.5k$" in the equation for the parabola. As a result, all parabolas in both directions have the same shape. Also note that one of the expressions is positive while the other is negative. This difference in sign indicates that parabolas parallel to the $X'Z$ plane are concave upward, while those parallel to the $Y'Z$ plane are concave downward.

If z is given a constant value in equation (3),

$$1 = k_3\left[(x')^2 - (y')^2\right] \qquad (6)$$

This is the equation of a horizontal plane cutting the warped surface, the elevation of which depends on the particular value given to z. This cutting plane forms a hyperbola, thereby indicating the reason for the designation hyperbolic paraboloid for the surface.

Design

In Fig. 7, a typical parabolic arch is shown representing a strip cut parallel to the $Y'Z$ plane. Since the surface is made up entirely of two sets of parabolic arches, one set normal to the other and all having the same shape, it can be assumed that the total load w is divided equally in two directions. Any given arch will, therefore, carry a load of intensity $w/2$.

The internal moment in any two-hinged arch is equal to the simple beam bending moment minus the moment due to the horizontal reaction H. Midspan simple beam bending moment due to uniform load is $\left(\frac{w}{2}\right)\left(\frac{L^2}{8}\right)$. The bending moment throughout a parabolic arch supporting only a uniform load equals zero. Hence moment produced by horizontal thrust must be equal and opposite to the simple beam bending moment. Therefore, thrust moment Hh_{xy} at midspan is

$$H(-h_{xy}) = \frac{w}{2}\,\frac{L^2}{8} \qquad (7a)$$

$$\text{or } H = -\frac{w}{4}\,\frac{L^2}{4h_{xy}} \qquad (7b)$$

But the expression for all arches in this direction has been shown in equation (4) to be:

$$z' = -0.5k(y')^2$$

Letting $z' = h_{xy}$ and $y' = \frac{L}{2}$:

$$h_{xy} = -0.5k\left(\frac{L^2}{4}\right)$$

$$\text{or } \frac{L^2}{4h_{xy}} = -\frac{1}{0.5k}$$

Substituting this in equation (7b) gives

$$H = -\frac{w}{4}\left[-\frac{1}{0.5k}\right] = \frac{w}{2k} = \frac{wab}{2h} \qquad (8)$$

Equation (8) gives the tensile or compressive thrust, induced in the shell by a uniform load. The shell must be reinforced only for this force. Actually, since the slope of the surface steepens near the column, the load is not strictly uniform; but the departure from uniform loading is insignificant.

Proof of Analysis

In the foregoing it has been assumed that the arches are properly supported at their ends. The validity of this assumption will be demonstrated.

Fig. 8a shows theoretical positions of typical parabolic arches and indicates their action on edge members of the roof. Each arch exerts both a vertical and horizontal force at its ends. It is seen in Fig. 8b that where two perpendicular arches intersect an edge, the normal components H_N of H are equal in magnitude but opposite in direction. As a result both components cancel each other and there is no force normal to any edge.

The other components of the horizontal forces H, called S_p in Fig. 8b, act in the same direction for both

Fig. 7

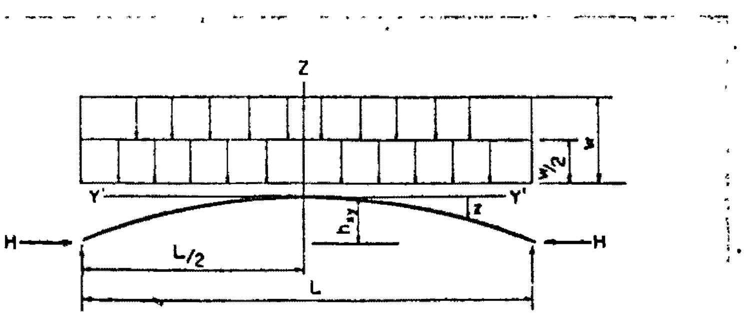

sets of arches and, therefore, are additive. When applied to the surface of length ds, each force equals $S_p ds$ or $H \sin\phi\, ds$. To determine the intensity of shear S per unit of length along the edge beam, an equation of equilibrium is written for forces parallel to the edge acting on the small triangular wedge:

$$2H \sin\phi\, ds = S\, dx$$

from which

$$S = 2H \sin\phi \frac{ds}{dx} = 2H \sin\phi \cos\phi$$

With $\phi = 45°$ and $H = \dfrac{w}{2k}$

$$S = 2\left[\frac{0.5w}{2k}\right] = \frac{w}{2k} = \frac{wab}{2h} \tag{9}$$

The effect of vertical components V along horizontal edges OB and OH is different from that at the sloped edges AB and AH. In either case, because the thrust line in a parabolic arch supporting a uniform load follows the centroidal axis, the combined vertical component at any point due to the thrust in the two arches is

$$V = \Sigma H \tan\Theta = H\frac{dz}{dy'} + H\frac{dz}{dx'} \tag{10}$$

where the angle Θ lies in a vertical plane between the arch thrust line and its horizontal projection as shown in Fig. 8c. From equation (3), slopes of the arches are

$$\frac{dz}{dy'} = (-0.5k)(2y') = -ky' \tag{11a}$$

and

$$\frac{dz}{dx'} = (0.5k)(2x') = +kx' \tag{11b}$$

At any point on the horizontal edge OH, $x'=y'$ as evident in Fig. 6. Therefore by equations (11) the slope of two arches must be equal but of different sign. Vertical components, therefore, cancel because they are equal in magnitude and opposite in direction. Vertical components along edge OB also nullify each other.

Along sloping edges, coordinates x' and y' are not equal at any point. With edge OB in Fig. 6 equal to a and OH equal to b, the equation of line AB is from the general expression $y=mx+b$:

$$y' = x' - a\sqrt{2} \tag{12}$$

Substituting this value in equations (11), slopes of arches at edge AB are

$$\frac{dz}{dy'} = -k\left(x' - a\sqrt{2}\right) \tag{13a}$$

and

$$\frac{dz}{dx'} = kx' \tag{13b}$$

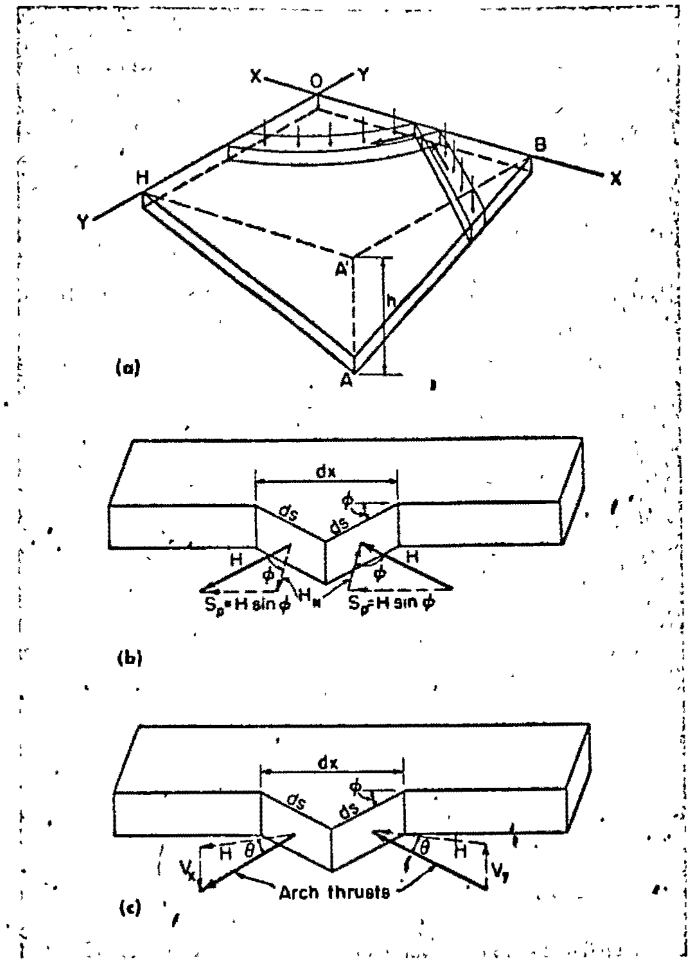

Fig. 8

Substituting in equation (10), net vertical component of arch thrusts at the edge is

$$V = H\left[-k\left(x' - a\sqrt{2}\right)\right] + H\left(kx'\right) = Hka\sqrt{2} \tag{14}$$

With $k = \dfrac{h}{ab}$ equation (14) may be written

$$V = H\frac{h}{ab}a\sqrt{2} = \frac{Hh\sqrt{2}}{b} \tag{15}$$

The force V is applied on the surface having the length ds in Fig. 8c. To determine intensity V' per unit length of the edge beam,

$$V'dx = Vds = \frac{Hh\sqrt{2}}{b}ds$$

$$V' = V\frac{ds}{dx} = V\cos\phi = \frac{V}{\sqrt{2}}$$

Therefore, from equation (15)

$$V' = \frac{Hh\sqrt{2}}{b}\left(\frac{1}{\sqrt{2}}\right) = \frac{Hh}{b} \tag{16a}$$

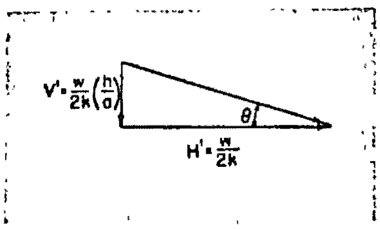

Fig. 9

In a similar manner it can be shown that the vertical force exerted by the shell along edge HA is

$$V' = \frac{Hh}{a} \tag{16b}$$

If there were no other force present along the inclined edges, the shell would require vertical supports. However, as shown previously the arches simultaneously exert a horizontal force in the plane of the edge. The two forces, horizontal and vertical, combine as shown in Fig. 9 to produce a resultant force parallel to the edge.

In summary, the net result of the interaction of the two systems of arch elements is that they exert merely shearing forces parallel to the edges. Therefore, the assumption that the ends of the arches are adequately supported is justified, proper support being provided by the presence of members parallel to the edges only, as shown in Fig. 10.

Statical Check

The horizontal thrust given by equation (8) may be checked by comparing it with the thrust determined statically using the total shell as a free body. In the elevation view of Fig. 11, assume the structure left of section PP to be a cantilever beam carrying the uniform load w. Moment at section PP equals $2wba\frac{a}{2}$. Dividing this by the height h gives thrust

$$\frac{2wba^2}{2}\left(\frac{1}{h}\right) = \frac{wba^2}{h} \tag{17}$$

The force expressed by equation (17) may be thought of as the force which occurs in the top and bottom flanges of an I-beam, with the flanges represented here by edge beams. In the lower or sloping edge beam this thrust is the horizontal component of the axial force in the beam. The corresponding vertical component is

$$\frac{wba^2}{h}\left(\frac{h}{a}\right) = wba \tag{18}$$

This indicates that of the total vertical roof load $2wba$ applied left of section PP, an amount wba is carried down beam HA and that the remainder, or $2wba - wba = wba$, must be carried down beams AB and AB' as shown in plan, Fig. 11. Shears acting on the shell adjacent to these beams are shown in section PP, and vertical components of these shears must add up to the load wba. Calling S_s the shear intensity per unit length in the

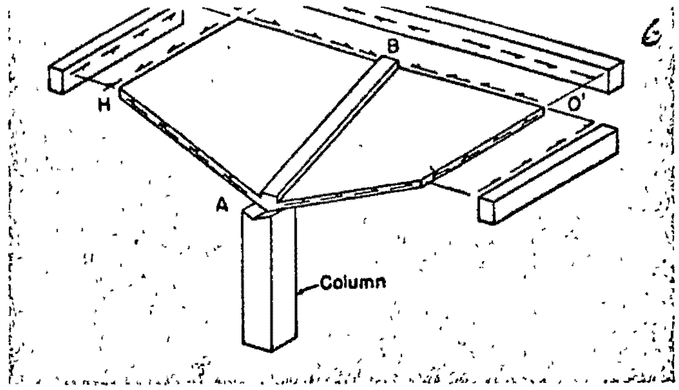

Fig. 10

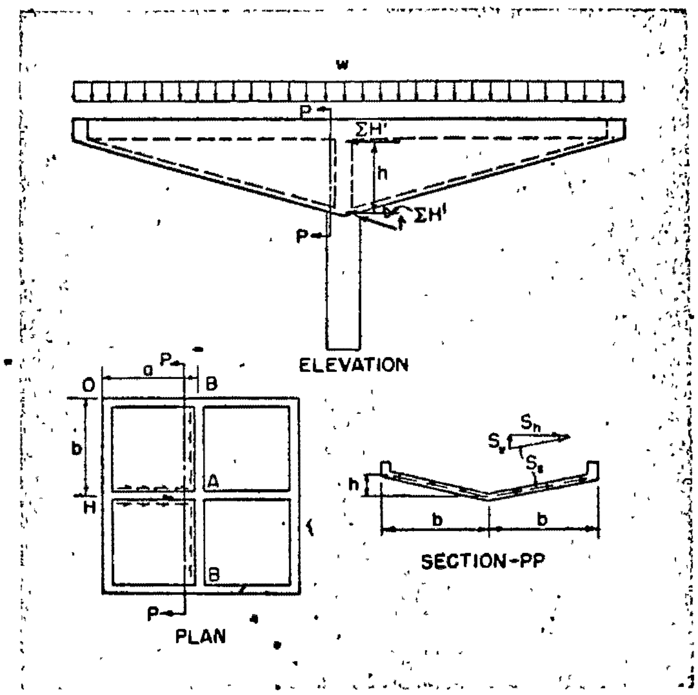

Fig. 11

sloped direction and assuming it uniformly distributed along the shell, total shear in the sloped direction is found by multiplying S_s by the total sloped length, or

$$S_s\left(2\sqrt{h^2 + b^2}\right)$$

The total vertical component then is expressed as

$$S_s\left(2\sqrt{h^2 + b^2}\right)\left(\frac{h}{\sqrt{h^2 + b^2}}\right) = wba$$

from which

$$S_s = \frac{wba}{2h} = \frac{w}{2k} \tag{19}$$

which agrees with equation (9).

It should be noted that S_v in section PP, Fig. 11, is not a vertical shear, but is the vertical component of the thrust in the shell. The presence of any radial shear would necessitate bending in the shell, a condition which does not exist under uniform loads.

Skewed Hyperbolic Paraboloids

The preceding discussion concerns hyperbolic paraboloids that are rectangular in plan. However, the same basic approach may be applied to the more general case of roofs skewed in plan as shown in Fig. 12. In this case the surface is defined by the equation

$$z = \frac{h}{ab} uv \tag{20}$$

in which u and v represent skewed coordinates. In this system the location of any point is designated by a distance u measured parallel to the U axis and a distance v measured parallel to the V axis. Hence the surface still contains two systems of straight lines parallel to the coordinate axes, U and V.

As with the rectangular surface, it is necessary first to determine the directions of the load-carrying parabolic arches. The procedure for determining this direction is developed in the Appendix. Briefly it consists of rotating the axes U and V (Fig. 12), skewed at the angle ω, through the angle ϕ to new positions U' and V'. The angle of rotation ϕ which defines the positions of the parabolas is given by the expression

$$\sin \phi = \frac{\sin \omega}{\sqrt{2}} \tag{21}$$

Note that the parabolas as well as the axes intersect at the angle ω instead of being perpendicular to each other as in the rectangular roof.

As shown in the derivation in the Appendix, arch thrusts in the skewed shell are

$$H_{V'} = \left(\frac{wab}{4h}\right) \frac{\sqrt{2} \sin \omega}{\sin (\omega - \phi)} \tag{22a}$$

$$\text{and } H_{U'} = \left(\frac{wab}{4h}\right) \frac{\sqrt{2} \sin \omega}{\sin (\omega + \phi)} \tag{22b}$$

equations (22) correspond to equation (8) and give thrusts induced in the V' and U' directions. Shear at the boundaries is equal to

$$S = \frac{wab}{2h} \sin \omega \tag{23}$$

Fig. 12

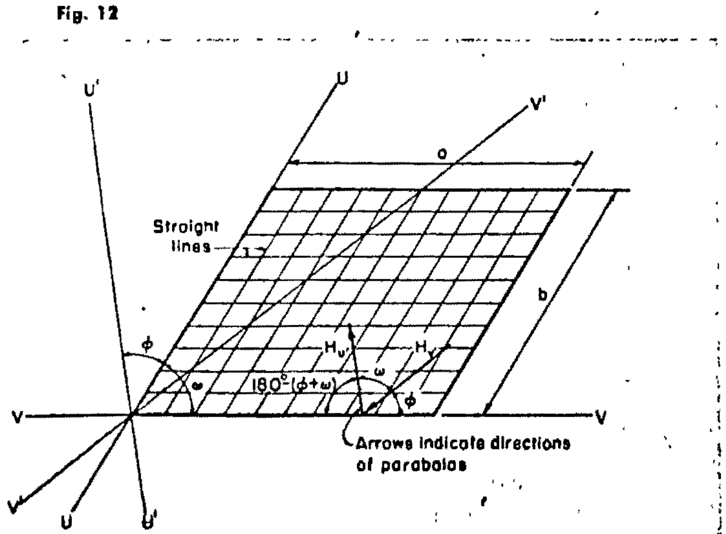

The derivation in the Appendix also shows that the horizontal components of the thrusts of any two arches intersecting at the edge of the surface combine so that no force is exerted normal to the edge. Only shears parallel to the edge exist, and these can be resisted effectively by an edge member.

Sloping Hyperbolic Paraboloids

In the previous derivations it was assumed that each hyperbolic paraboloid shell has two horizontal intersecting edge beams. However, this is not a necessary condition. The method is equally suitable for a sloping hyperbolic paraboloid shown in Fig. 13. For example, each quadrant of the structure in Fig. 13 is composed of hyperbolic paraboloids with one horizontal and three sloping edge beams. The magnitude of the forces acting in the arches can be determined by extending the shell in quandrant $BCDO$ so that two edges BC' and $C'D'$ are horizontal, and substituting the dimensions of $BC'D'O$ in equation (9). Since, in previous derivations, it was shown that components of the arch thrust perpendicular to sections parallel to the axis nullify each other, the force obtained for quadrant $BC'D'O$ applies equally well to quadrant $BCDO$ even though edge CD is free. If the preceding operation is performed in general terms the resulting equation reduces to

$$H = \pm \frac{wab}{2h} \tag{24}$$

Fig. 13

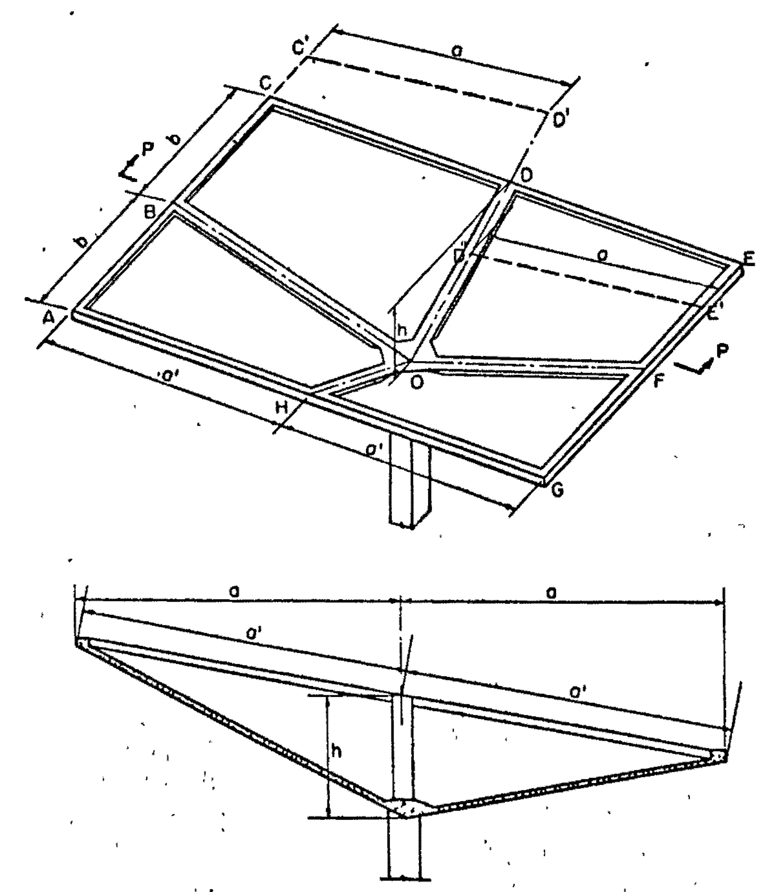

Equation (24) is the same as equation (9). It should be noted that dimension a is the projected length rather than the true length of the edge beam. The same expression may be derived by considering quadrant $DEFO$. The horizontal edges in this case are $E'F$ and $E'D''$ or EE' and $E'D''$, and the dimensions of $D''E'FO$ or $D''E'ED$ may be used to substitute in equation (9). As previously, total force in any edge beam equals the sum of the shear forces acting along its length. For example,

$$T = \frac{wab}{2h} a' \text{ etc.} \tag{25}$$

Design Example

The following example illustrates the design of a typical hyperbolic paraboloid shell roof.

Consider a roof unit of the shape shown in Fig. 3b having exterior edges horizontal. A unit 40x40 ft. in plan is selected as being typical of the unobstructed floor area generally required for industrial buildings. Because compressive stresses in the concrete are quite low, shell thickness is controlled only by requirements of adequate coverage for reinforcement, and in this case a thickness of 3 in. is selected. Vertical rise h of the shell from column to exterior edge beam is chosen to be 5½ ft. A live load of 30 psf plus 5 psf to account for the weight of the edge beams is added to the 37.5 psf for weight of the shell to give a uniform load w of 72.5 psf.

Horizontal thrusts created in the parabolic arches by this load are, by equation (8),

$$H = \pm \frac{wab}{2h} = \pm \frac{72.5 \times 20 \times 20}{2 \times 5.5}$$
$$= \pm 2{,}640 \text{ lb. per ft.}$$

Reinforcement required for negative thrust is

$$A_s = \frac{2{,}640}{20{,}000} = 0.132 \text{ sq.in. per ft.}$$

Compressive stress in the concrete is

$$f_c = \frac{2{,}640}{3 \times 12} = 74 \text{ psi}$$

Although no reinforcement is indicated in the direction of the parabolic arches under compression, a nominal amount should be used to take care of shrinkage stresses. In Fig. 14, reinforcement is shown placed diagonally, but if due account is taken of the direction of the stress it can be placed parallel to the edges.

Total force in any edge beam equals the sum of the shear forces acting along its length. In the horizontal edge members of this example, tension at the roof corner is zero and increases to a maximum value at the center. Therefore, the maximum force equals the sum of shear forces acting over only one-half the length of the edge beam.

Tension in the horizontal edge beams is

$$H_a = 2{,}640 \times 20 = 52{,}800 \text{ lb.}$$

from which

8

$$A_s = \frac{52{,}800}{20{,}000} = 2.64 \text{ sq.in.}$$

The steel should be detailed so that its centroid coincides with the line of application of the shear forces, otherwise due account should be taken of the eccentricity. In this connection, the effect of secondary bending moments induced near the corners and discussed under the heading of Secondary Stresses should also be included in the design of the edge members.

Compression in the sloped edge members is

$$2Ha\frac{20.75}{20} = 2 \times 52{,}800 \times \frac{20.75}{20} = 109{,}560 \text{ lb.}$$

Note that the shearing force at both sides of a sloped member contributes to its total axial force.

There is some question regarding the allowable stress and method of analysis to be used in determining the area of the compression member in the valley of the shell. Because this member is only subject to an axial thrust with small eccentricity, the use of column formulas is indicated. But since the member also acts as the flange of an I-beam having the shell as a web, the use of the allowable compressive stress permitted in flexure is justified. For average spans the section area obtained from column formulas is small and a design is not penalized by this conservative interpretation. Furthermore, it is desirable to reduce strains in edge members as much as possible to minimize bending moments caused by the interaction of shell and edge beam. Although analysis of the shell does not include effect of no strains parallel to the edge beam, strains occurring in the edge beam are

Fig. 14

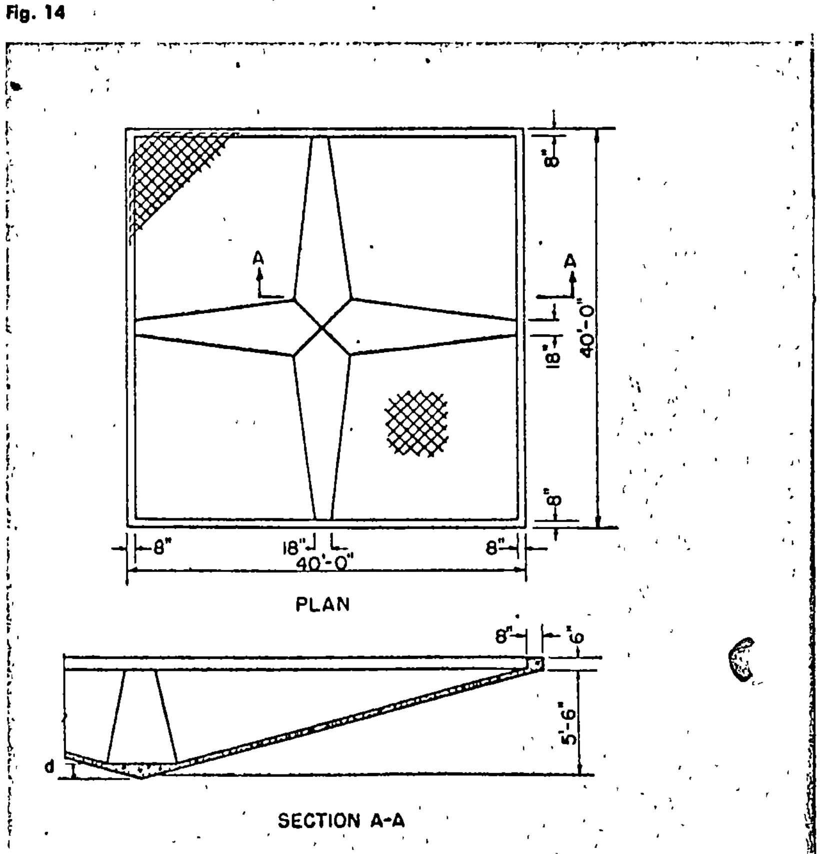

reflected into the shell because the two are joined integrally. This effect is reduced when beams are slightly larger than required.

Using the standard formula for tied columns with a percentage of steel $p_g = 0.01$, the gross area required at the valley for the sloped beam is

$$A_g = \frac{P}{0.8(0.225f'_c + f_s p_g)}$$

$$= \frac{100{,}560}{540 + 16{,}000 \times 0.01} = 157 \text{ sq.in.}$$

With a rise of 5½ ft. in 20 ft., the depth d shown in section AA of Fig. 14 is

$$d = \sqrt{\frac{157 \times 5.5}{20}} = 7 \text{ in.}$$

A depth of 9 in. will be used at this point to provide sufficient strength in bending for unsymmetrical loading conditions.

Groined Vaults

The approach just outlined—examining a shell in terms of the behavior of individual arches—can also be employed in considering other shells. One of these is the groined vault made by the hyperbolic paraboloid surface as shown in Fig. 15. Although for clarity only the rectangular plan is shown, intersecting barrels can also be adapted in many ways to triangular or polygonal plans.

The chief difference between previously discussed shells and the groined vault is that in the former case the free edges were placed along the straight lines, but in this case the free edges occur as shown in Fig. 15, parallel to the arches. For one particular segment as previously derived, the equation of the surface is

$$z = kuv = \frac{h_x}{a'b'} uv \tag{26}$$

This expression can be altered to the form

$$z = -h_x\left(\frac{x}{a}\right)^2 + h_y\left(\frac{y}{b}\right)^2 \tag{27}$$

which may be more suitable in preparing a layout and studying the general arrangement.

In the case of the groined vault it is advantageous to consider arches that are parallel and perpendicular to the free edges. It is apparent that the arches normal to the free edge, being unrestrained at that edge, can offer little resistance to the load. Hence, loads are carried mainly by the arches acting parallel to the free edges.

In the case of a uniform load, these arches are completely free of bending, and thus the load is transmitted directly to the intersection of the barrels as pure axial thrust. The horizontal component of this thrust is merely equal to $wa^2/2h_y$ or $wb^2/2h_y$, depending on the barrel that is being considered. However, for this type of hyperbolic paraboloid the dead load of structure cannot be assumed as uniform, since the weight per square foot of projected area is considerably more at the support than at the crown.

For this loading condition, if the shell is considered as a series of independent arches parallel to the free edges, each arch would be subject to bending as well as axial load.

Fig. 15

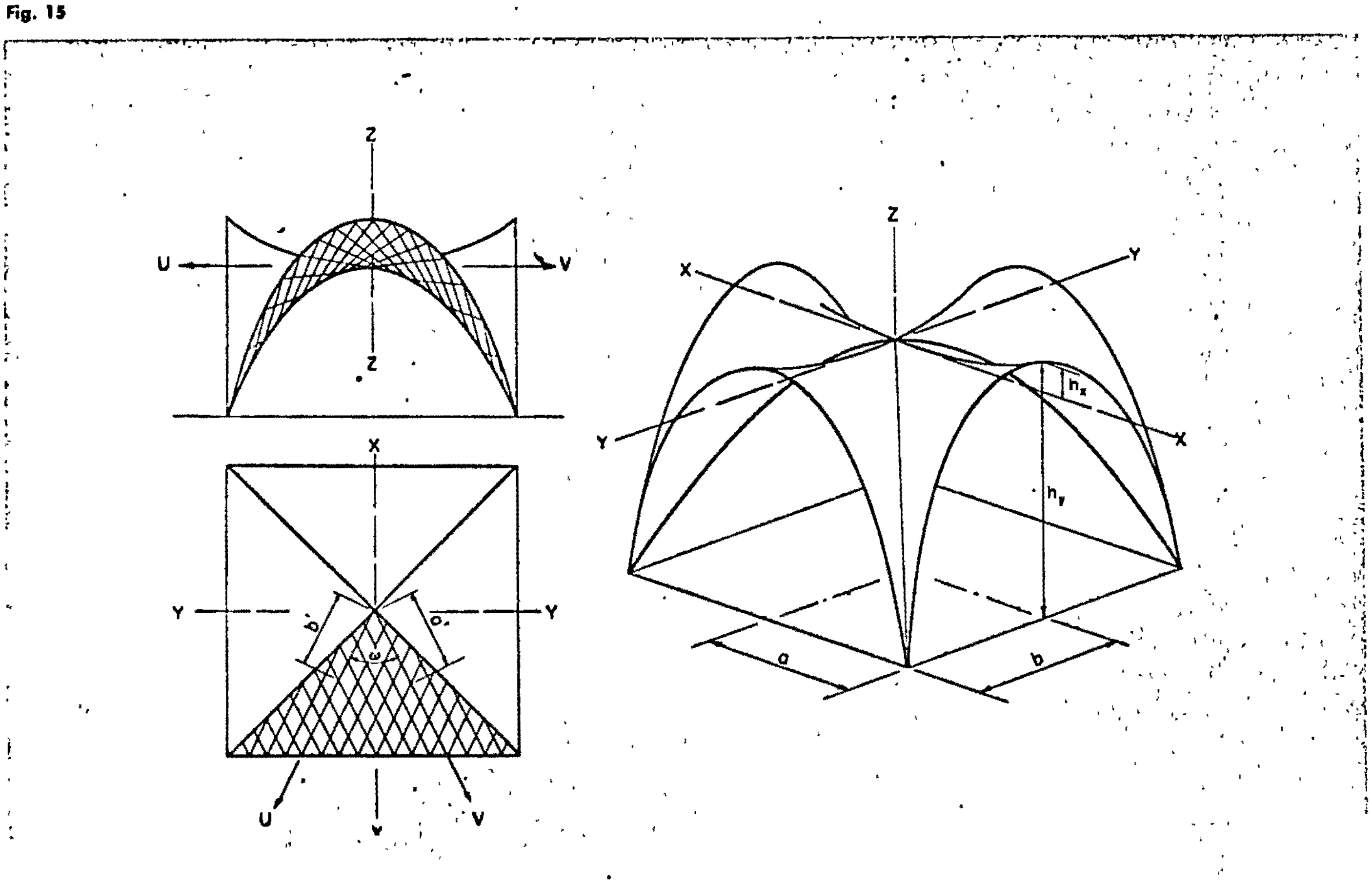

Although the calculated bending moments in the arches would be relatively small, such moments do not exist in the shell. Hence, a modification of the general arch treatment is necessary.

If the arches are to be completely free of bending, the thrust line must follow the axis of the arch. The dead load cannot by itself satisfy the requirement. However, as an arch tends to deflect, it creates a difference in shear between itself and the neighboring arch. This difference in shear between the various elements can be regarded as an external load on the arch. The magnitude and distribution of this shear must be such that the thrust line produced by the shear and dead load lies on the axis of the arch. Since the edge of the shell is completely free of shear, one could commence from this plane and by trial and error determine the shear required at various sections to maintain the arches free of bending. Such a procedure is, however, very lengthy and involved. To simplify the task, Table 1 gives force coefficients to permit rapid calculation of internal forces throughout a shell.

To obtain a generalized solution it was found more advantageous to solve the differential equations expressing the behavior of the shell, rather than a lengthy arch analysis. Further simplification was achieved by assuming that the dead weight varied as

$$w = w_c \left[k_1 + k_2 \cos \frac{\pi y}{2b} \right] \tag{28}$$

In Table 1, T_x, T_y and S represent the internal forces acting tangent to the surface in pounds per foot occurring in the shell at various points designated as y/b in the first column and as $(1 - x/a)\sqrt{h_x/h_y}$ in the top row.

As noted in Table 1 the formulas and coefficients are applicable only to shells where $h_x \neq 0$. If the dimension h_x becomes zero, the groined vault is no longer composed of hyperbolic paraboloids. The component units are sections of parabolic cylinders. The formulas for the limiting condition $h_x = 0$ are transformed to

$$T_x = \frac{k_2 a^2}{16 h_y} w_c k \left[\pi^2 \left(1 - \frac{x}{a}\right)^2 \cos \frac{\pi y}{2b} \right] \tag{29a}$$

$$T_y = - \frac{k_1 b^2}{2 h_y} \frac{w_c}{k} \left[\frac{k_2}{k_1} \cos \frac{\pi y}{2b} + 1 \right] \tag{29b}$$

$$S = \frac{k_2 a b}{4 h_y} w_c \left[\pi \left(1 - \frac{x}{a}\right) \sin \frac{\pi y}{2b} \right] \tag{29c}$$

The definition of the various symbols is the same as in the table.

The foregoing analysis has been predicated on the basis that the shell is rigidly supported along the intersections or groins. Since this is not the case, the groin must be designed to transmit the reaction from the shell to the support. Depending on the type of support, the groin can be considered either as a fixed or two-hinged arch. For small spans (because of the small stiffness occurring at the crown) it is possible to consider the groin as three-hinged.

To determine the moments and stresses produced in the arch, it is necessary to estimate what portion of the shell acts as the arch. For a very conservative estimate, it could be assumed that half the width of the arch is equal to eight times the thickness of the shell. For a more realistic figure, it could be assumed that the effective width acting as an arch equals $1.52\sqrt{rt}$, in which r is the average radius at the intersection. Even when a constant effective width is assumed, the moment of inertia will vary because the cross-section of the arch rib depends on the slope at which the two adjacent shells intersect, the angle or V being most acute near the corner.

The analysis for an arch consists of solving for the unknown horizontal reaction by means of the moments produced by the external loads and the elastic properties of the arch. Two methods can be used to determine the loading which the arch is subjected to. The first and most natural one is to compute the internal forces acting in the shell along the intersection. These forces are then resolved into vertical and horizontal forces in the plane of the arch, and used as external loads on the arch. This method has the disadvantage that the determination of the angle at the intersections and the components of the forces parallel to the arch is complicated.

The second method, shown in Fig. 16, consists of treating an entire section of the shell as a free body. In such a free body, the moment parallel to the direction of the arch axis produced by the external loads and the internal forces can be obtained quite readily. For example, the moment at C equals the algebraic sum of the moments of the load w and the reaction V as in an ordinary arch, and the moments of the internal forces T_y and S. The internal forces are computed from Table 1. For these forces, only the component of the moment acting parallel to the arch axis is used. It will be necessary to find the slope of the

Fig. 16

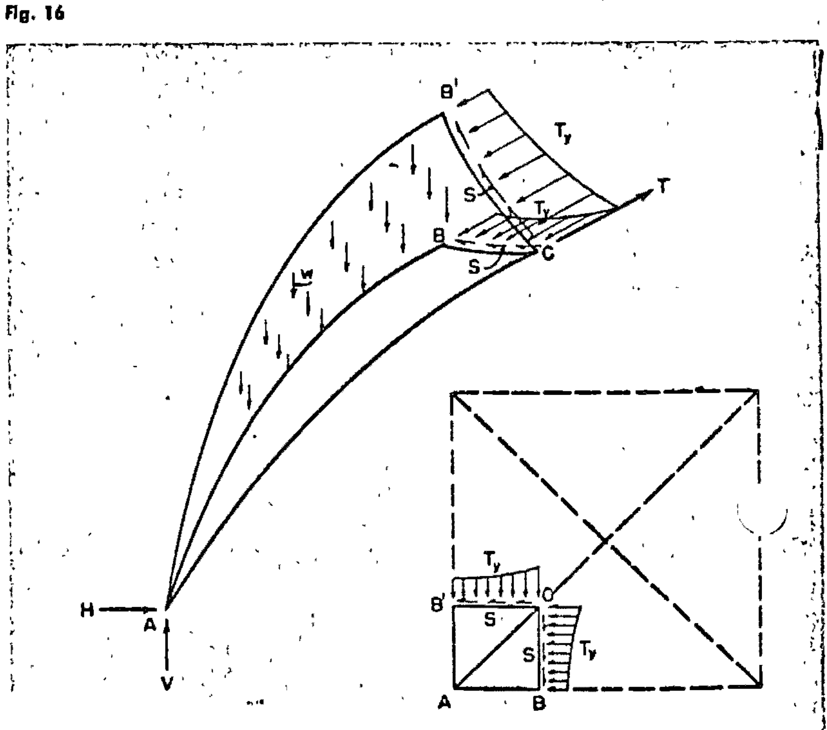

Table 1—Internal Forces in Groined Vaults for Dead Loads

w_c = intensity of distributed load at the crown, (lb. per sq.ft.)

$$k = \sqrt{\frac{1+\left[(2h_x/a)(x/a)\right]^2}{1+\left[(2h_y/b)(y/b)\right]^2}}$$

$$k_1 = \sqrt{1+(2h_y/b)^2}$$

$$k_2 = 1 - k_1$$

NOTE: $h_x \neq 0$

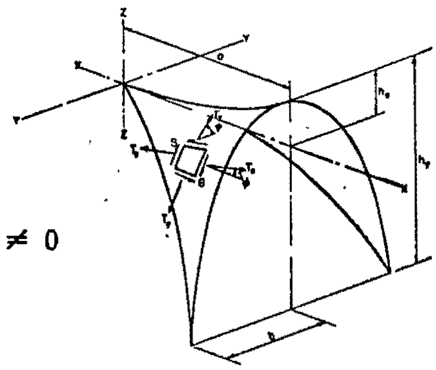

$$\left(1-\frac{x}{a}\right)\sqrt{h_x/h_y}$$

$$T_x = \frac{k_2\,a^2}{2h_x}\,w_c\,k \text{ (coefficient)}$$

Force	y/b	0	0.04	0.08	0.12	0.16	0.20	0.24	0.28	0.32	0.36	0.40	0.45	0.50	0.55	0.60	0.65	0.70	0.75
T_x	0	.0000	.0020	.0079	.0177	.0314	.0489	.0702	.0952	.1237	.1557	.1910	.2396	.2929	.3506	.4122	.4775	.5460	.6173
	0.10	.0000	.0019	.0078	.0175	.0310	.0483	.0694	.0940	.1222	.1538	.1886	.2366	.2893	.3462	.4071	.4716	.5393	.6097
	0.20	.0000	.0019	.0075	.0168	.0299	.0465	.0668	.0905	.1176	.1481	.1816	.2279	.2786	.3334	.3920	.4541	.5193	.5871
	0.30	.0000	.0018	.0070	.0158	.0280	.0436	.0626	.0848	.1102	.1387	.1702	.2135	.2610	.3123	.3673	.4255	.4865	.5500
	0.40	.0000	.0016	.0064	.0143	.0254	.0396	.0568	.0770	.1001	.1259	.1545	.1938	.2370	.2836	.3335	.3863	.4417	.4994
	0.50	.0000	.0014	.0056	.0125	.0222	.0346	.0497	.0673	.0875	.1101	.1350	.1694	.2071	.2479	.2915	.3376	.3861	.4365
	0.60	.0000	.0012	.0046	.0104	.0185	.0288	.0413	.0559	.0727	.0915	.1123	.1408	.1722	.2060	.2423	.2807	.3209	.3628
	0.70	.0000	.0009	.0036	.0080	.0143	.0222	.0319	.0432	.0562	.0707	.0867	.1088	.1330	.1591	.1871	.2168	.2479	.2803
	0.80	.0000	.0006	.0024	.0055	.0097	.0151	.0217	.0294	.0382	.0481	.0590	.0740	.0905	.1083	.1274	.1476	.1687	.1908
	0.90	.0000	.0003	.0012	.0028	.0049	.0077	.0110	.0149	.0193	.0244	.0299	.0375	.0458	.0548	.0645	.0747	.0854	.0966
	1.00	.0000	.0000	.0000	.0000	.0000	.0000	.0000	.0000	.0000	.0000	.0000	.0000	.0000	.0000	.0000	.0000	.0000	.0000

$$T_y = -\frac{k_1\,b^2}{2h_y}\,\frac{w_c}{k}\left[1+\frac{k_2}{k_1}\text{ (coefficient)}\right]$$

Force	y/b	0	0.04	0.08	0.12	0.16	0.20	0.24	0.28	0.32	0.36	0.40	0.45	0.50	0.55	0.60	0.65	0.70	0.75
T_y	0	1.0000	.9980	.9921	.9823	.9686	.9511	.9298	.9048	.8763	.8443	.8090	.7604	.7071	.6494	.5878	.5225	.4540	.3827
	0.10	.9877	.9857	.9799	.9702	.9567	.9393	.9183	.8937	.8655	.8339	.7991	.7510	.6984	.6415	.5805	.5161	.4484	.3780
	0.20	.9511	.9492	.9436	.9342	.9212	.9045	.8843	.8605	.8334	.8030	.7694	.7232	.6725	.6177	.5590	.4969	.4318	.3640
	0.30	.8910	.8892	.8840	.8752	.8630	.8474	.8284	.8062	.7808	.7523	.7208	.6775	.6300	.5787	.5237	.4655	.4045	.3410
	0.40	.8090	.8074	.8026	.7947	.7836	.7694	.7522	.7320	.7089	.6831	.6545	.6152	.5721	.5254	.4755	.4227	.3673	.3096
	0.50	.7071	.7057	.7015	.6946	.6849	.6725	.6574	.6398	.6196	.5970	.5721	.5377	.5000	.4592	.4156	.3695	.3210	.2706
	0.60	.5878	.5866	.5831	.5774	.5693	.5590	.5465	.5318	.5151	.4963	.4755	.4470	.4156	.3817	.3455	.3071	.2668	.2249
	0.70	.4540	.4531	.4504	.4459	.4397	.4318	.4221	.4108	.3978	.3833	.3673	.3452	.3210	.2948	.2668	.2372	.2061	.1737
	0.80	.3090	.3084	.3066	.3035	.2993	.2939	.2873	.2796	.2708	.2609	.2500	.2350	.2185	.2007	.1816	.1615	.1403	.1183
	0.90	.1564	.1561	.1552	.1537	.1515	.1488	.1454	.1415	.1371	.1321	.1266	.1190	.1106	.1016	.0919	.0817	.0710	.0599
	1.00	.0000	.0000	.0000	.0000	.0000	.0000	.0000	.0000	.0000	.0000	.0000	.0000	.0000	.0000	.0000	.0000	.0000	.0000

$$S = \frac{k_1\,ab}{2\sqrt{h_x h_y}}\,w_c \text{ (coefficient)}$$

Force	y/b	0	0.04	0.08	0.12	0.16	0.20	0.24	0.28	0.32	0.36	0.40	0.45	0.50	0.55	0.60	0.65	0.70	0.75
S	0	.0000	.0000	.0000	.0000	.0000	.0000	.0000	.0000	.0000	.0000	.0000	.0000	.0000	.0000	.0000	.0000	.0000	.0000
	0.10	.0000	.0098	.0196	.0293	.0389	.0483	.0576	.0666	.0754	.0838	.0920	.1016	.1106	.1190	.1266	.1334	.1394	.1445
	0.20	.0000	.0194	0387	.0579	.0768	.0955	.1138	.1316	.1489	.1656	.1816	.2007	.2185	.2350	.2500	.2635	.2753	.2855
	0.30	.0000	.0285	.0569	.0851	.1129	.1403	.1671	.1933	.2187	.2433	.2669	.2948	.3210	.3452	.3673	.3871	.4045	.4194
	0.40	.0000	.0369	.0737	.1101	.1462	.1816	.2164	.2503	.2832	.3150	.3455	.3817	.4156	.4470	.4755	.5012	.5237	.5430
	0.50	.0000	.0444	.0886	.1325	.1759	.2185	.2603	.3011	.3407	.3789	.4156	.4592	.5000	.5377	.5721	.6029	.6300	.6533
	0.60	.0000	.0508	.1014	.1516	.2012	.2500	.2978	.3445	.3897	.4335	.4755	.5254	.5721	.6152	.6545	.6898	.7208	.7474
	0.70	.0000	.0559	.1117	.1670	.2216	.2753	.3280	.3794	.4292	.4774	.5237	.5787	.6300	.6775	.7208	.7597	.7939	.8232
	0.80	.0000	.0597	.1192	.1782	.2365	.2939	.3501	.4049	.4582	.5096	.5590	.6177	.6725	.7232	.7694	.8109	.8474	.8787
	0.90	.0000	.0620	.1238	.1851	.2456	.3052	.3636	.4205	.4758	.5292	.5806	.6415	.6984	.7510	.7991	.8421	.8800	.9125
	1.00	.0000	.0628	.1253	.1874	.2487	.3090	.3681	.4258	.4818	.5358	.5878	.6494	.7071	.7604	.8090	.8526	.8910	.9239

forces T_y and S before proceeding with the summation of moments. The angle ψ which T_y makes with the horizontal is obtained from the relationship that

$$\tan \psi = \frac{2h_y y}{b^2} \qquad (30a)$$

and angle ϕ between force S and the horizontal can be calculated from the relationship that

$$\tan \phi = \frac{2h_x x}{a^2} \qquad (30b)$$

Design Example

The following example illustrates the design of a typical groined vault using Table 1.

Consider the unit shown in Fig. 17. The roof is 100x 100 ft. in plan with a maximum height h_y=37.5 ft. The rise of the central arch h_x=6.0 ft. and the shell thickness is 4 in. The dead load of the shell, roofing, etc. is w_c=60 psf, with a uniform live load equal to 30 psf.

Before the calculation of internal forces the quantities k_1 and k_2 must be computed from the expressions shown in Table 1.

$$k_1 = \sqrt{1 + (2h_y/b)^2} = \sqrt{1 + (2 \times 37.5/50)^2} = 1.8$$

$$k_2 = 1 - k_1 = 1 - 1.8 = -0.80$$

and

$$\frac{k_2}{k_1} = \frac{-0.8}{1.8} = -0.444$$

The internal forces will be obtained for $\frac{x}{a}$ and $\frac{y}{b}$ varying at intervals of 0.2, therefore coefficient k must also be evaluated for the same points from the equation for k shown in Table 1. For example at point $\frac{x}{a} = 0.6, \frac{y}{b} = 0.4$.

$$k = \sqrt{\frac{1 + [(2h_x/a)(x/a)]^2}{1 + [(2h_y/b)(y/b)]^2}}$$

$$= \sqrt{\frac{1 + [(2 \times 6/50)(0.6)]^2}{1 + [(2 \times 37.5/50)(0.4)]^2}} = 0.866$$

The values of the coefficient k for the remaining points on the shell are shown in the first section of Table 2.

All the constants required to determine internal forces are now available. The procedure will be illustrated by calculating forces at the same point $\frac{x}{a} = 0.6, \frac{y}{b} = 0.4$.

Fig. 17

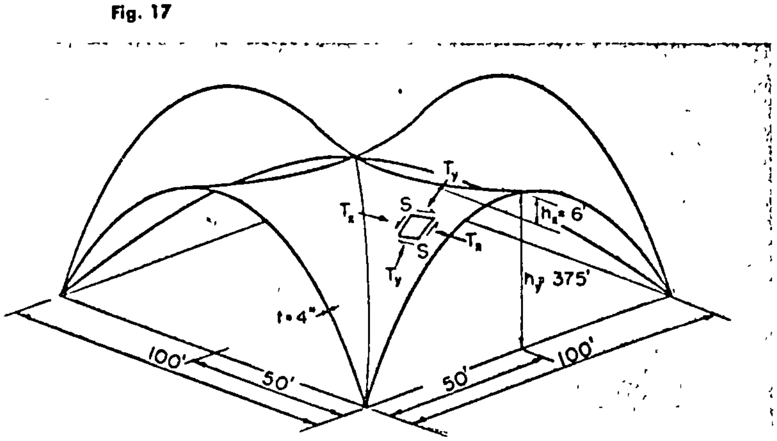

From Table 1, for $\frac{y}{b}$ =0.4 and

$$\left(1 - \frac{x}{a}\right)\sqrt{h_x/h_y} = (1 - 0.6)\sqrt{6/37.5} = 0.16$$

the coefficients for T_x, T_y and S are 0.0254, 0.7836 and 0.1462 respectively. Using the equations shown in Table 1,

$$T_x = \frac{k_2 a^2}{2h_x} w_c k \text{ (coefficient)}$$

$$= \frac{-0.8 \times 50^2}{2 \times 6} \times 60 \times 0.866 \times 0.0254$$

$$= -220 \text{ lb. per ft.}$$

$$T_y = -\frac{k_1 b^2}{2h_y}\left(\frac{w_c}{k}\right)\left[1 + \frac{k_2}{k_1}\text{(coefficient)}\right]$$

$$= -\frac{1.8 \times 50^2}{2 \times 37.5} \times \frac{60}{0.866}\left[1 - 0.444 \times 0.7836\right]$$

$$= - 2{,}709 \text{ lb. per ft.}$$

$$S = \frac{k_2 ab}{2\sqrt{h_x h_y}} w_c \text{ (coefficient)}$$

$$= \frac{-0.8 \times 50 \times 50}{2\sqrt{6 \times 37.5}} \times 60 \times 0.1462$$

$$= -585 \text{ lb. per ft.}$$

The internal forces due to dead load for the entire shell are shown in Table 2. It should be noted that values below the horizontal broken line in the tables were omitted be cause these points lie below the groin. Calculations of constants beyond the boundary of the shell are only needed when it is necessary to obtain values at the groin by interpolation.

As mentioned previously, uniform load such as live load is transmitted to the support by pure axial thrust; therefore only forces T_y exist for this loading condition. The horizontal component T_y^H of this thrust with a live load of 30 psf for all points on the shell is

$$T_y^H = \frac{wa^2}{2h_y} = \frac{30 \times 50^2}{2 \times 37.5} = 1{,}000 \text{ lb. per ft.}$$

The axial thrust is obtained from

$$T_y = \frac{T_y^H}{\cos \psi}$$

where angle ψ is evaluated from equation (30a):

$$\tan \psi = \frac{2h_y y}{b^2}$$

For all points along the line $\frac{y}{b}$ =0.4,

$$\tan \psi = \frac{2 \times 37.5}{50} \times 0.4 = 0.6$$

and therefore

$$\cos \psi = 0.857$$

$$\text{Therefore } T_y = -\frac{1{,}000}{0.857} = -1{,}166 \text{ lb. per ft.}$$

and the final dead plus live load force is

$$T_y = -(2{,}709 + 1{,}166) = -3{,}875 \text{ lb. per ft.}$$

Internal forces T_x and S are a function of dead load only, and are not increased by the live load.

Examination of Table 2 shows that the forces are compressive throughout the shell. Furthermore, their magnitude is very small. The maximum compressive force T_y occurs at $\frac{x}{a} = 1.0$, $\frac{y}{b} = 1.0$. The live load force at this point is $-1{,}803$ lb. per ft. and the dead load force from Table 2 is $-6{,}316$ lb. per ft. Thus the maximum compressive stress is

$$f_c = -\frac{1{,}803 + 6{,}316}{4 \times 12} = -169 \text{ psi}$$

Compressive stresses due to T_x are considerably smaller. The maximum shear stress shown in Table 2 is

$$v = \frac{866}{4 \times 12} = 18 \text{ psi}$$

By inspection of Table 2 it is evident that the combined stresses are small; therefore it will not be necessary to compute them. Although the above stresses do not require any reinforcing, it is advisable to provide at least the minimum steel specified by the ACI Code to accommodate unsymmetrical loads and stresses due to volumetric changes.

The last step is the analysis and design of the groin arch by either one of the two procedures already described. The forces computed in Table 2 should be used in determining the loading to which the arch is subjected.

Unsymmetrical Loads

In the preceding discussion it was assumed that all of the quadrants were equally and uniformly loaded. In certain cases, however, such as the inverted umbrella shown in Fig. 3b, it may be desirable to investigate the effect of unsymmetrical loading or the effect of lateral loads.

To visualize readily the behavior of a shell under unsymmetrical loading, it is preferable to consider the action of the shell and the edge beams separately. Furthermore, in the initial stage the edge beams must be considered restrained in a manner similar to the fictitious clamping assumed in the moment distribution technique.

From the physical relationship just discussed, it should be apparent that a uniform load on any one quadrant will create internal forces in the shell of that quadrant in accordance to formulas previously derived. For example, a uniform load on the two quadrants in Fig. 18 is resisted by parabolic arches which require only shearing forces at their ends for stability. These shearing forces are computed by equation (8). Thus even though only part of the structure is loaded, the shell proper is in equilibrium with the stresses readily determinable.

Table 2—Coefficient k and Internal Forces for Dead Loads in Example Groined Vault

	y/b	x/a = 0	0.2	0.4	0.6	0.8	1.0
		$[1-(x/a)]\sqrt{h_x/h_y}$ = 0.40	0.32	0.24	0.16	0.08	0
k	0	1.000	1.001	1.005	1.010	1.018	1.028
	0.2		0.959	0.962	0.968	0.975	0.985
	0.4			0.861	0.866	0.873	0.882
	0.6				0.751	0.757	0.764
	0.8					0.652	0.658
	1.0						0.570
T_x	0	−1910	−1238	− 706	− 317	− 80	0
	0.2		−1128	− 643	− 289	− 73	0
	0.4			− 489	− 220	− 56	0
	0.6				− 139	− 35	0
	0.8					− 16	0
	1.0						0
T_y	0	−2305	−2195	−2101	−2030	−1977	−1945
	0.2		−2363	−2272	−2196	−2143	−2110
	0.4			−2783	−2709	−2652	−2614
	0.6				−3581	−3523	−3481
	0.8					−4769	−4720
	1.0						−6316
S	0	0	0	0	0	0	0
	0.2		− 596	− 455	− 307	− 155	0
	0.4			− 866	− 585	− 295	0
	0.6				− 805	− 406	0
	0.8					− 477	0
	1.0						0

Note: Coefficient k is dimensionless. Forces T_x, T_y and S are in lb. per ft.

Fig. 18

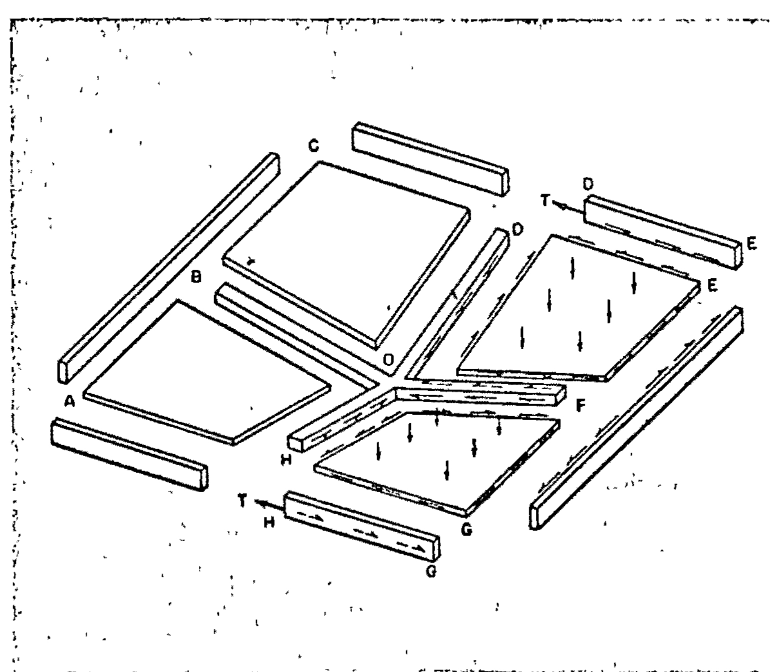

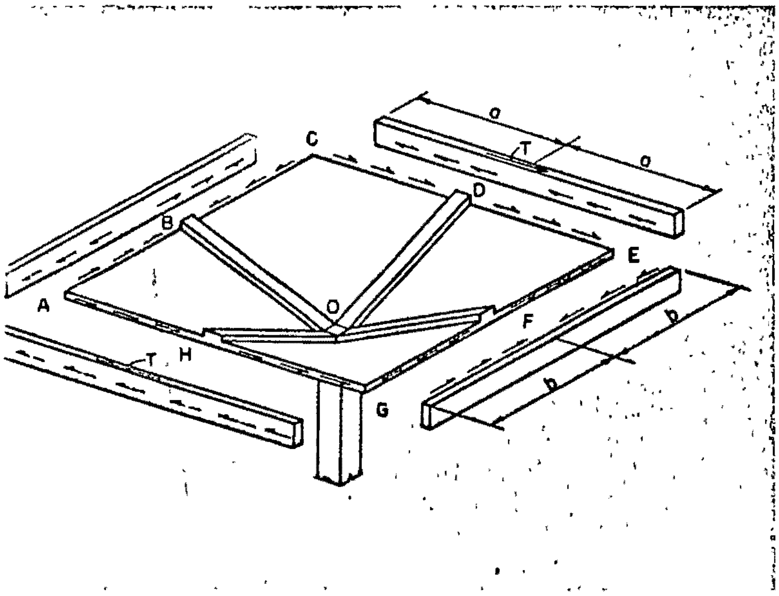

Fig. 19

Tensile and compressive forces in the edge beams can be determined from these. Assuming the column capable of resisting horizontal forces, all edge beams are in equilibrium except beams *AHG* and *CDE*. For these beams, the shear acts in only one direction. To maintain equilibrium, a concentrated force *T* is needed at *D* and *H*. If it is assumed that restraint exists at *D* and *H*, then the force *T* can be considered as an external load.

This is contrary to the actual boundary conditions. Hence, a concentrated load equal and opposite to *T* must be applied at *D* and *H*. In this case, the entire roof is considered to act as a unit (see Fig. 19). Determination of the exact distribution of stresses created by this horizontal load involves lengthy and complex arithmetical calculations. Fortunately, as in the case of flat plate floors, such refinement is not necessary. The effect of this concentrated load can be bracketed within narrow ranges.

Since the concentrated load acts parallel to the edge beam, it is reasonable to assume that resistance to the load will be provided by nonuniform tangential shears acting at the junction of the shell and edge beam with the maximum intensity at center. Hence, the shell proper is subject to a shearing force parallel to the exterior edges. If there was no warping of the shell surface, the shearing forces would penetrate to the interior edge with only a slight change in their distribution. However, because of warping, the direction of the tangential shear at any section or at the interior edges is different than that at the exterior. For equilibrium of forces of a section of the shell as a free body, shears normal to the surface as well as tangential shears must be created. These normal shearing forces, generally termed radial shears, are naturally concentrated in that area near the valley at which the change in elevation is most pronounced.

ASCE Manual No. 31, *Design of Cylindrical Concrete Shell Roofs*, indicates that the bending moment produced by tangential shears in a shell is very small. On this basis, most of the shell is relatively free of bending, with bending moments concentrated only in that area near the column support at which radial shears are developed. However, in this area, since the edge beams stiffen the shell, it is probable that only slight bending is developed. Consequently for average spans, the bending moments produced in the shell are not usually critical.

But the presence of radial shears near the column produces bending of the two interior sloping edge beams parallel to the direction of *T*, and torsion of the edge beams perpendicular to the force *T*. Considering only the concentrated load *T*, because it is antisymmetrical, the moment resisted by the two interior edge beams must be equal and opposite as shown in Fig. 20. In this figure, the concentrated load is shown as *T* because the effect at the two edges, the near and the far, are considered. A force of $T/2$ is considered acting respectively on *AH* and *CD*.

If it were not for the presence of the torsional resisting moment M_t provided by members *HO* and *OD*, the moments M_b acting at the junction of the members and the column, could be determined exactly, and would be equal to *Th*. Since it is difficult to ascertain how much help the torsional resistance contributes, a conservative approach is to design the area near edge beams *BO* and *OF* at the columns for a moment *Th*. From a consideration of the geometry of Fig. 20 and strain relationship, the magnitude of the moment along the valley reduces to zero at *B* and *F*. A conservative assumption is that the moment varies linearly from *O* to *B* and *O* to *F*.

The minimum depth of the resisting moment arm at the junction of the edge beam and column can be taken as the depth of the beam. At this and other sections some

Fig. 20

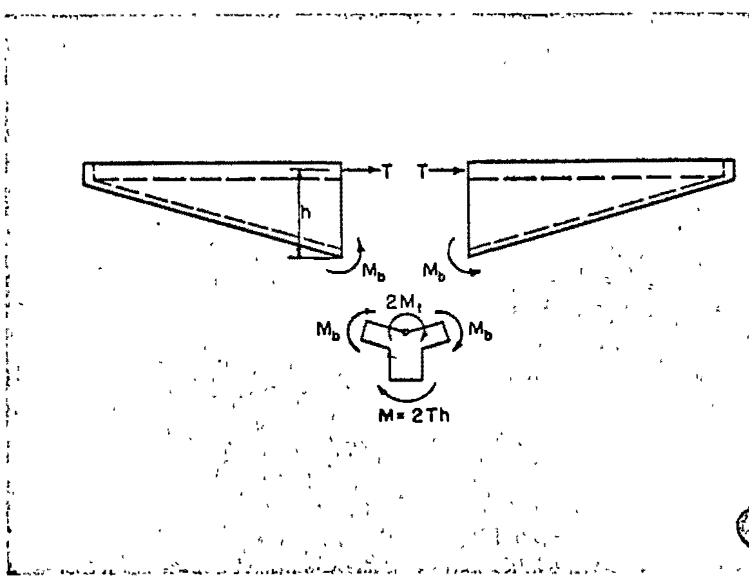

of the shell will act together with the edge beam, forming a V-section. From a practical point of view the effective width can be considered as that defined by lines radiating at 45 deg. from the edges of the columns.

Test

To substantiate the capacity of hyperbolic paraboloid shells to carry a variety of loads, a series of tests was carried out by the Structural Development Section of the Research and Development Division of the Portland Cement Association. The shell tested was of the type shown in Fig. 3b. It covered an area of 24x24 ft. with a 1½-in. shell thickness and a 2-ft. 10-in. rise. The reinforcing in the shells consisted of No. 3 bars at 12 in. each way. All edge beams projected above the shells. The perimeter edge beams were 4x6 in. and were reinforced with No. 4 bars. The dimensions of the interior edge beams varied from 15x5 in. at the columns to 9x1½ in. (the shell thickness) at the perimeter. They were reinforced with 3 No. 4 bars. The structure was supported on a 15x15-in. square tied column reinforced with 12 No. 8 bars and a 4-ft. 6-in. square footing which was anchored at four corners. A uniform load on the shell was simulated by simultaneously applying equal concentrated loads on a 3x3-ft. grid.

The test program included three different loading conditions on the same structure. Therefore, only the last test was carried to destruction.

In the first test a uniform load was applied and increased to a maximum 48.5 psf. The sum of dead load and maximum applied load produced a calculated thrust in the arches of 95 psi and a tensile stress in the perimeter beam reinforcing of 25,755 psi. No distress was observed under this load.

The loading in the second test consisted of two equal concentrated loads applied on the shell, near the center of two adjacent quadrants. The contact area between the load and the shell was a single 3x4-in. washer, or 12 sq.in. Some minor radial and circumferential cracking appeared at the points of loading when the concentrated loads reached 4,510 lb. each, at which point the second test was concluded. A concentrated load of 4,510 lb. will produce a local bending moment of 1.0 kip-ft./ft. at the point of application of the load* and a punching shear of 322 psi.

Regarding the problem of concentrated loads, a point loading P on a flat plate whose thickness-to-span ratio is more than 0.033 will cause a positive moment under the load whose maximum value is $0.42P$ irrespective of the support condition. For a spherical dome with a thickness-to-radius ratio of 0.04 or more, the moment created by a radial concentrated load with small bearing area has been shown to be equal to $0.26P$. For design purposes, an average value of $0.34P$ appears justified. Where the moment is critical, advantage should be taken of the thrust produced in curved shells.

The third loading condition consisted of a uniform load applied to two adjacent quadrants. This unsymmetrical load was gradually increased to 58 psf. No distress was observed over the major portion of the shell even as the ultimate capacity was approached. Cracking occurred at the interior edge beams and in the shell in the vicinity of the column. Cracks in the unloaded side of the structure occurred at the underside of the interior edge beam almost adjacent to the column. In the loaded side the cracks started at the top of the interior edge beam. Torsional cracks appeared in the other two interior edge beams. The 58 psf load applied over half of the structure produced a bending moment of 100 kip-ft., considerably more than the capacity of the two 15x5-in. interior beams. It is, therefore, evident that the participation of the 1½-in. shell acting as a deep V-shaped beam, and to a minor extent the torsion in the other two beams, were instrumental in carrying the unsymmetrical load. Hence, the recommendation that the unbalanced moment is resisted by two edge beams is extremely conservative.

This test demonstrated that hyperbolic paraboloids, even with a shell thickness of only 1½ in., can resist large concentrated loads as well as unsymmetrical loads.

Secondary Stresses

One question that arises about these shells is the degree of flatness that can be used without invalidating the membrane analysis. This depends to a large extent on the magnitude of the secondary bending moments caused by axial strain. The analysis presented is based on a satisfaction solely of the equilibrium of forces, and no attention is given to the compatibility between strains and stresses. For the usual rise, $h/a=1/5$ or $h/b=1/5$, the effect of axial strains is unimportant and can be ignored safely. However, when the ratio h/a decreases, the effect of axial strains begins to exert a dominant influence on the behavior of the shell. The departure in behavior from that indicated by the simple membrane analysis in a flat shell is analogous to that occurring in a two-hinged parabolic arch subject to uniform load as the ratio of rise to span decreases. For very flat parabolic arches, it can be shown that if the rib-shortening effect (axial deformations) is included in the analysis, the horizontal component of the reaction for a given span decreases as the ratio of rise to span decreases. With no rise the horizontal component decreases to zero, and, thus, the secondary bending due to axial strains approaches the simple-beam bending moment as a limiting value.

*The moment calculation is based on material presented by Eric Reissner, in Appendix I of "Thin-Shelled Domes Loaded Eccentrically" by Voss, Peabody, Staley and Dietz, *Transactions of the American Society of Civil Engineers*, Vol. 113, 1948, pages 312-314.

The structural action of a hyperbolic paraboloid shell is due to the fact that its curved surface resists the load by two sets of parabolic arches perpendicular to each other, as shown in Fig. 8a. Therefore, some insight into the effect of curvature can be obtained by examining a strip parallel to the arches as a free body. If the shearing forces and normal forces on the two opposite faces are ignored, and if it is assumed that the ends of the arches are not free to move, then the secondary bending moments due to lack of curvature can be determined as for an arch. The result of such a study is presented in Fig. 21 for various ratios of $\frac{ht}{ab}$.

The secondary bending moment at various distances from the corner, designated by the dimensionless quantity x/t, is expressed in terms of the simple-beam bending moments occurring in a strip of length L. Fig. 21 indicates that because the ratio of rise to span approaches zero at the corner, the load is carried entirely by beam action, which is contrary to what can be expected from membrane theory. For strips farther away from the corner, the secondary moment decreases. The rate of the decrease is a function of $\frac{ht}{ab}$. The larger the ratio of $\frac{ht}{ab}$, the more rapid the decrease in the magnitude of the secondary moments. The usual value of $\frac{ht}{ab}$ for the umbrella type of hyperbolic paraboloid is approximately 0.004. Assuming that the thickness is 3 in., the secondary moment becomes unimportant at a distance of approximately 5 ft. from the corner.

Fig. 21 shows another important characteristic observed on some of the shells that have been built. At the corner the load is carried mainly by ordinary beam action. Hence, the load is transmitted to the edge beams principally by radial shears. The edge beams near the corner are thus loaded vertically and act as cantilevers for a small part of their length. Consequently, the edge beams in this vicinity should not only be designed for the tension computed by membrane theory, but should also be deepened to prevent excessive deflection and should be reinforced for negative moment. This is especially desirable when the edge beam is upturned.

Because the value of L increases linearly in proportion to the distance from the corner, it is more expedient to show the effect of axial strains in terms of the secondary flexural stresses that are created. Such values are plotted in Fig. 22, which brings into sharper relief the importance of curvature on the magnitude of the secondary stresses. For an umbrella type of hyperbolic paraboloid subjected to a load of 72 psf and with a ratio of $\frac{ht}{ab} = 0.004$, the maximum secondary stresses occur at $x/t = 20$ and are

$$f_c = \frac{145 \times 72}{144} = 72 \text{ psi.}$$

Fig. 21

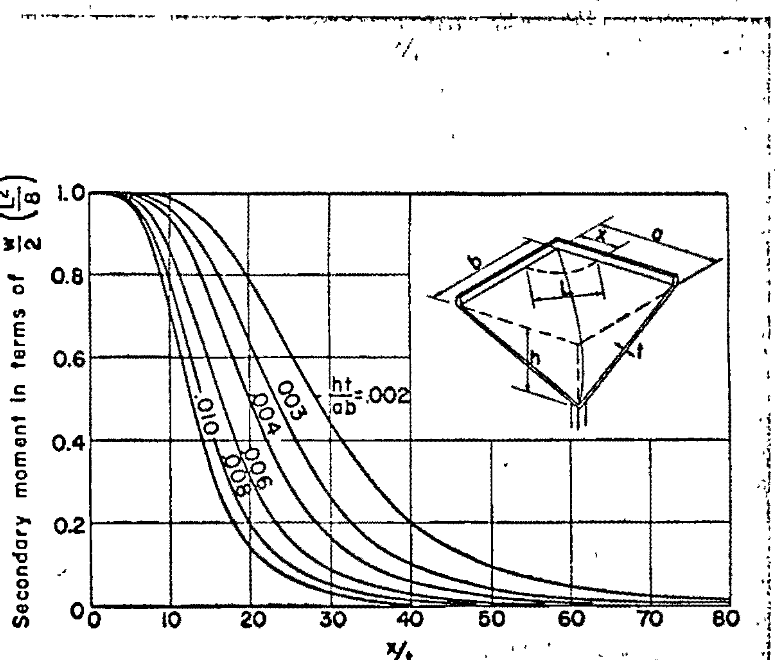

Fig. 22

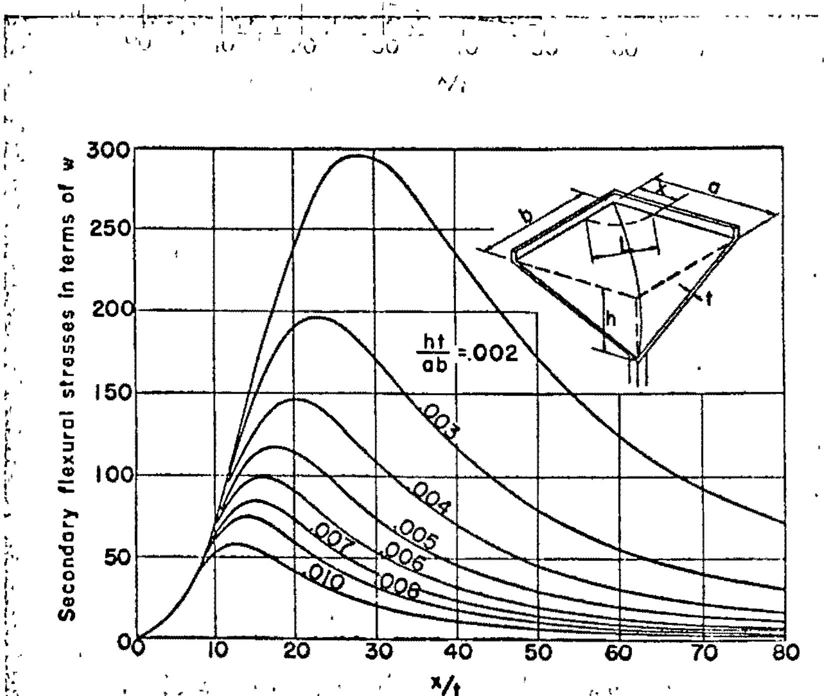

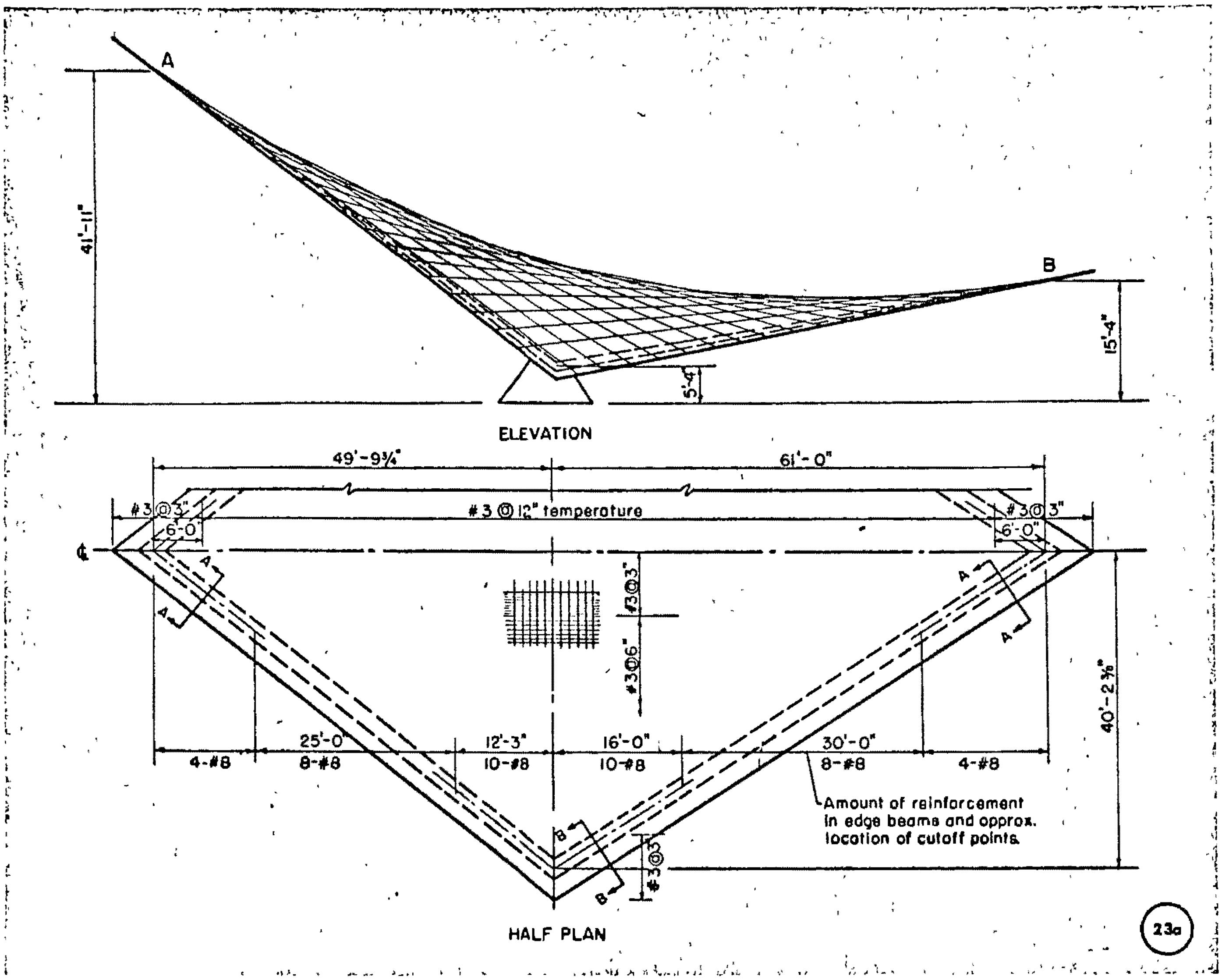

Examples

The previous discussion on secondary stresses pointed out the importance of providing sufficient curvature in a hyperbolic paraboloid surface. Since there has not yet been developed any exact method of determining the minimum rise-to-span ratio which can be tolerated, salient features of three shells selected from the large number already built are presented merely as a guide. The dimensions do not represent limits of applicability. These typical shells have been built in accordance with theory presented previously and are behaving satisfactorily.

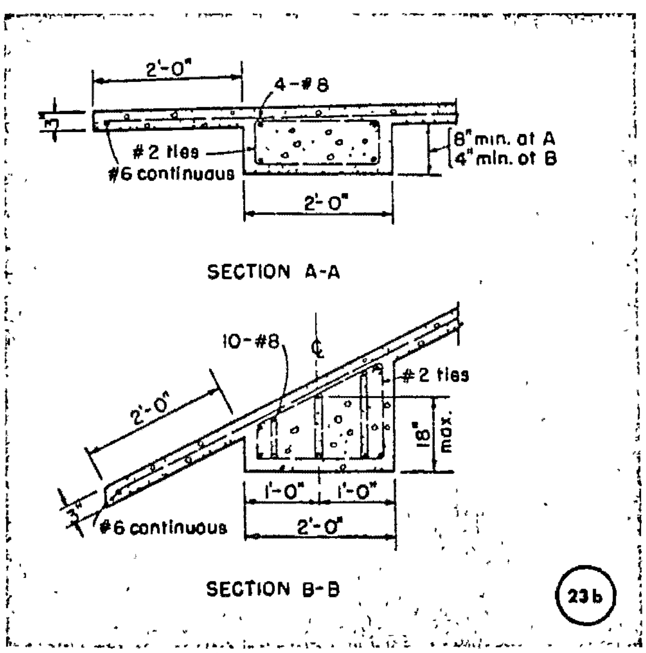

Figs. 23 a, b. The roof of St. Edmund's Episcopal Church, Elm Grove, Wis., features a 3-in. thick hyperbolic paraboloid shell supported on two narrow concrete buttresses. The tilt of the saddle shape gives the effect of spaciousness in the sanctuary. Architect was Wm. P. Wenzler of Milwaukee, Wis. General contractor was Gebhard-Borghammer, Inc., of Milwaukee.

Figs. 24 a, b. Ralph's Supermarket in Wichita, Kan., has nine adjacent hyperbolic paraboloid shells, each 40 ft. square, covering the store, work rooms and outside walks. For a live load of 30 psf, each shell has an average thickness of 4.5 in. and 2.4 lb. of reinforcement per square foot. A roof drain is located at the low point of each shell, with the drain line carried down through the column core. Architects were Vanlandingham and Haney. Structural engineers were G. Hartwell and Co. of Wichita. General contractor was H. F. Sell Construction Co. of Wichita.

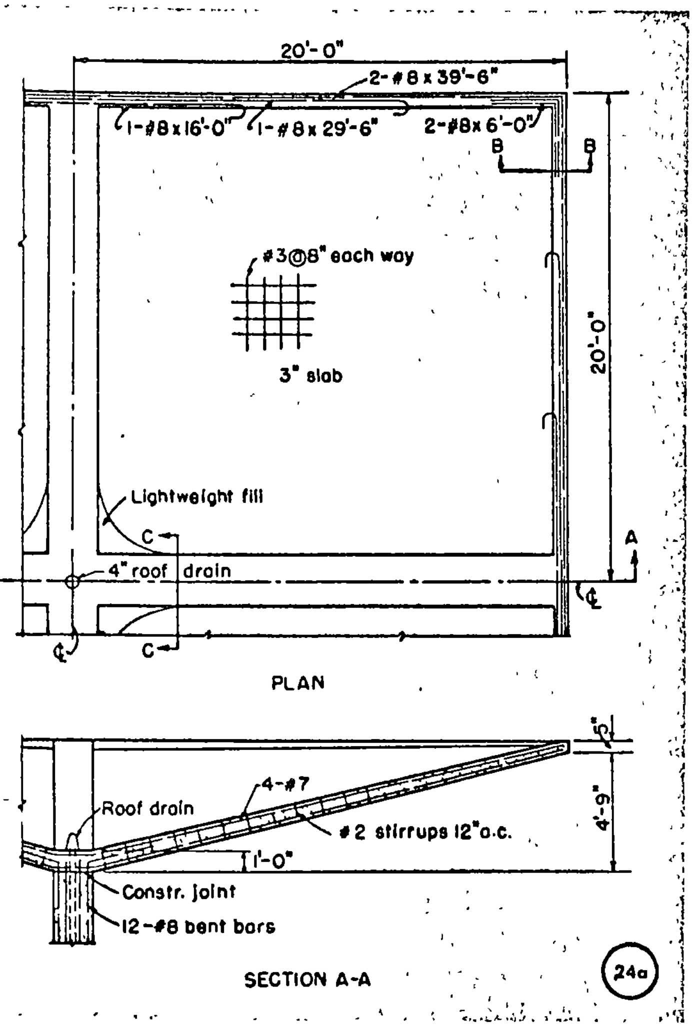

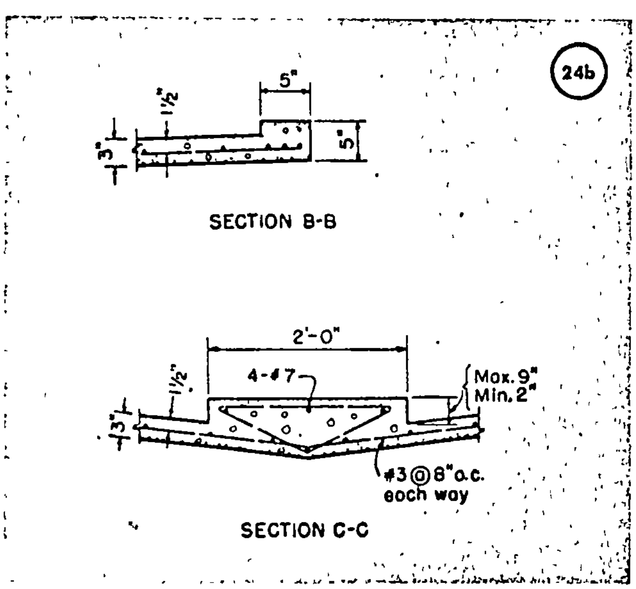

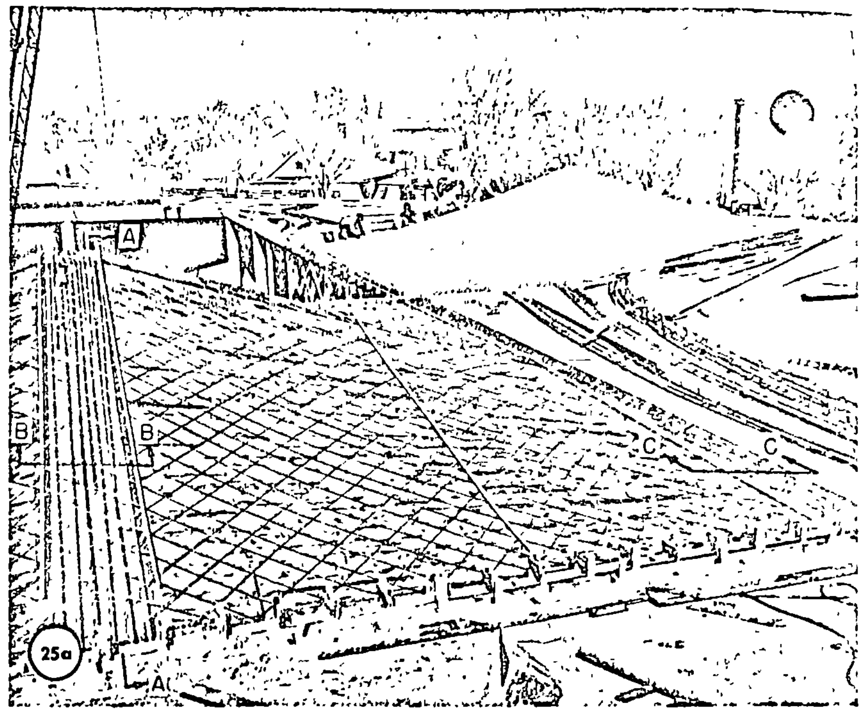

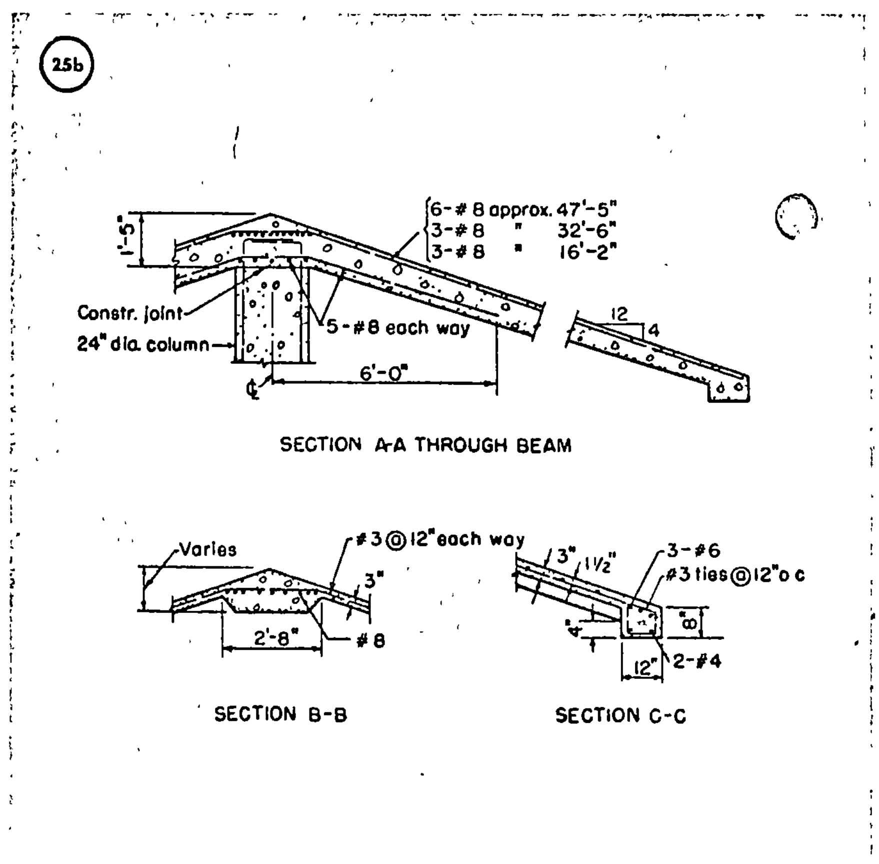

Figs. 25 a, b. Fifty-two hyperbolic paraboloid concrete shells form new roof for Argentine reservoir in Kansas City, Kan. Measuring 45 ft. 6 in. square with a rise of 7 ft. 8 in., the 3-in. thick shells were built with movable forms constructed in two sections that match on centerline of the shell. Design live load was 30 psf. An average thickness of 4.8 in. and 2.7 lb. of reinforcement per square foot were required for each shell. Design was by Burns and McDonnell Engineering Co. of Kansas City, Mo., for the Board of Public Utilities, Kansas City, Kan. General contractor was Eastmount Construction Co. of Kansas City, Mo.

Appendix

Derivation of Formulas for Skewed Hyperbolic Paraboloid Shells

The derivation of formulas for analyzing hyperbolic paraboloid surfaces is somewhat similar to the derivation for those rectangular in plan.

With reference to Fig. 26, in accordance with the law of sines,

$$BC = \frac{v' \sin(\omega - \phi)}{\sin(180^\circ - \omega)} = \frac{v' \sin(\omega - \phi)}{\sin \omega}$$

and

$$AB = \frac{-u' \sin \phi}{\sin \omega}$$

Fig. 26

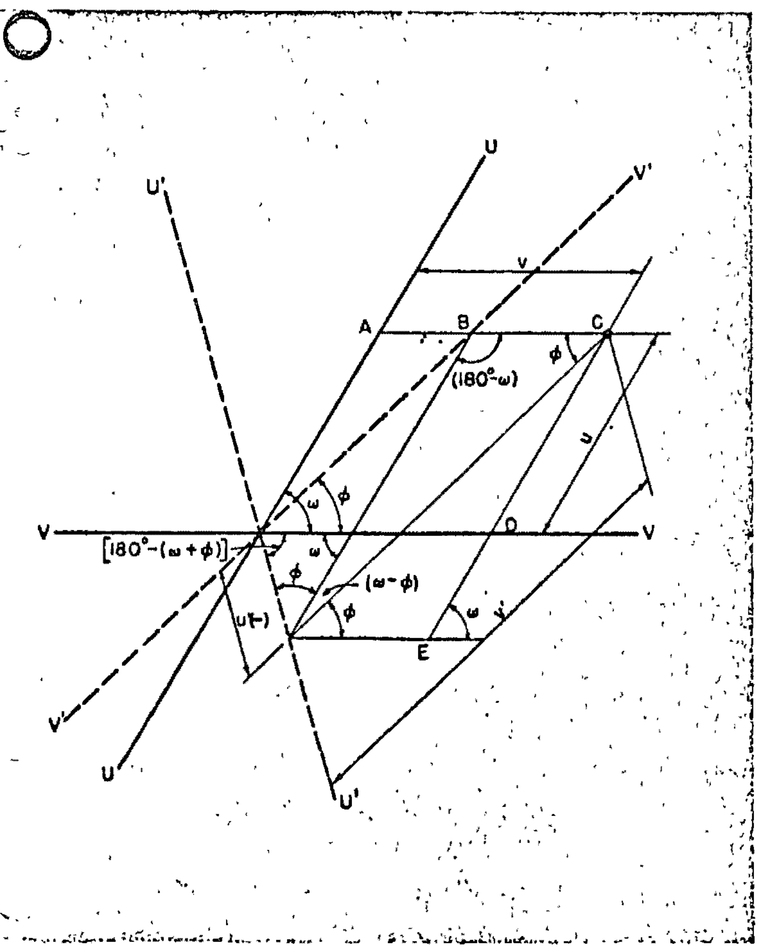

Therefore, since $v = AB+BC$,

$$v = \frac{1}{\sin \omega}\Big[v' \sin(\omega - \phi) - u' \sin \phi \Big] \tag{31}$$

Also,

$$CE = \frac{v' \sin \phi}{\sin \omega}$$

and

$$DE = \frac{-u'}{\sin \omega} \sin\Big[180^\circ - (\omega + \phi)\Big] = \frac{-u' \sin(\omega + \phi)}{\sin \omega}$$

hence

$$u = CE - DE = \frac{1}{\sin \omega}\Big[v' \sin \phi + u' \sin(\omega + \phi)\Big] \tag{32}$$

Substituting equations (31) and (32) into equation (20) gives

$$z = \frac{h}{ab}\, uv = \frac{h}{ab \sin^2 \omega}\Big\{\Big[v' \sin(\omega - \phi) - u' \sin \phi\Big]\Big[v' \sin \phi + u' \sin(\omega + \phi)\Big]\Big\}$$

Expanding this expression and substituting the trigonometric identity $\sin^2\omega - \sin^2\phi$ for $\sin(\omega-\phi)\sin(\omega+\phi)$, gives

$$z = \frac{h}{ab \sin^2 \omega}\Big\{\sin \phi\Big[(v')^2 \sin(\omega - \phi) - (u')^2 \sin(\omega + \phi)\Big] + v'u'\Big[\sin^2 \omega - 2 \sin^2 \phi\Big]\Big\} \tag{33}$$

The coefficient of $v'u'$ becomes zero where the value of ϕ is chosen so that

$$\sin \phi = \frac{\sin \omega}{\sqrt{2}} \tag{34}$$

Designating the particular value which will satisfy this condition as ϕ_c, equation (33) reduces to

$$z = \frac{h}{ab \sin^2 \omega} \sin \phi_c \Big[(v')^2 \sin(\omega - \phi_c) - (u')^2 \sin(\omega + \phi_c) \Big] \quad (35)$$

It should be noted that equation (35) is of the same form as equation (3) because ω and ϕ_c are constants for a particular angle of skew ω. Therefore, the oblique surface $z = \frac{huv}{ab}$ can also be formed by translating one parabola along another. In this general case, however, the parabolas are not perpendicular to each other as in the specific rectangular case, but are skewed at the angle ω.

At the edge of the skewed surface horizontal arch thrusts H_U' and H_V' of the two systems of arches are determined in a manner similar to that illustrated in equations (7) and (8). For example, thrust H_V' may be expressed

$$H_V' = \frac{w}{4}\left(\frac{L^2}{4h_{xy}}\right) \quad (36)$$

If the term involving u'^2 in equation (35) is constant, the expression for parabolas parallel to the V' axis is

$$z' = \frac{h \sin \phi_c}{ab \sin^2 \omega}\left[v'^2 \sin(\omega - \phi_c) \right] \quad (37)$$

Letting $z' = h_{xy}$ at $v' = L/2$ gives

$$\frac{L^2}{4h_{xy}} = \frac{ab}{h}\left[\frac{\sin^2 \omega}{\sin \phi_c \sin(\omega - \phi_c)}\right] \quad (38)$$

Substituting equation (38) into equation (36) gives

$$H_V' = \frac{w}{4}\left(\frac{ab}{4}\right)\frac{\sin^2 \omega}{\sin \phi_c \sin(\omega - \phi_c)}$$

But from equation (34) $\sin \phi = \frac{\sin \omega}{\sqrt{2}}$; therefore

$$H_V' = \frac{wab}{4h}\left[\frac{\sqrt{2} \sin \omega}{\sin(\omega - \phi_c)}\right] \quad (39)$$

In a similar manner it may be shown that

$$H_U' = \frac{wab}{4h}\left[\frac{\sqrt{2} \sin \omega}{\sin(\omega + \phi_c)}\right] \quad (40)$$

To prove that components of the horizontal thrust acting normal to the edge of the surface nullify each other, the combined normal components of both H_U' and H_V' are expressed

$$H_N = H_V' \sin^2 \phi_c - H_U' \sin^2(\omega + \phi_c) \quad (41)$$

Substituting equations (39) and (40) in equation (41),

$$H_N = \frac{wab\sqrt{2} \sin \omega}{4h}\left[\frac{\sin^2 \phi_c}{\sin(\omega - \phi_c)} - \sin(\omega + \phi_c)\right] \quad (42)$$

or

$$H_N = \frac{wab\sqrt{2} \sin \omega}{4h}\left[\frac{2 \sin^2 \phi_c - \sin^2 \omega}{\sin(\omega - \phi_c)}\right] \quad (43)$$

However, the numerator of the term inside the bracket was previously made equal to zero. Therefore, equation (43) equals zero, indicating that the combined thrusts exerted by intersecting arches produce no force normal to the edge.

Shear exerted along the edge of the skewed surface is obtained by adding algebraically the components of the horizontal thrusts H_U' and H_V' parallel to the edge:

$$S = H_V' \sin \phi_c \cos \phi_c - H_U' \sin(\omega + \phi_c) \cos(\omega + \phi_c)$$

Substituting for H_V' and H_U', their values given by equations (39) and (40),

$$S = \frac{wab \sin \omega}{2\sqrt{2}\, h}\left[\frac{\sin \phi_c \cos \phi_c}{\sin(\omega - \phi_c)} - \cos(\omega + \phi_c)\right] \quad (44)$$

Utilizing the identity that $\sin \omega \cos \omega - \sin \phi \cos \phi = \cos(\omega+\phi) \sin(\omega-\phi)$, equation (44) reduces to

$$S = \frac{wab \sin \omega}{2\sqrt{2}\, h}\left[\frac{\sin \phi_c \cos \phi_c - \sin \omega \cos \omega + \sin \phi_c \cos \phi_c}{\sin \omega \cos \phi_c - \cos \omega \sin \phi_c}\right]$$

Substituting for $\sin \phi_c$ its value given by equation (34), then

$$S = \frac{wab \sin \omega}{2\sqrt{2}\, h}\left[\frac{\sqrt{2} \sin \omega \cos \phi_c - \sin \omega \cos \omega}{\sin \omega \cos \phi_c - \frac{\cos \omega \sin \omega}{\sqrt{2}}}\right]$$

$$= \frac{wab \sin \omega}{2h} \quad (45)$$

Corte lateral de 1
una concha de 15m x 15m
(octubre 10-1960)

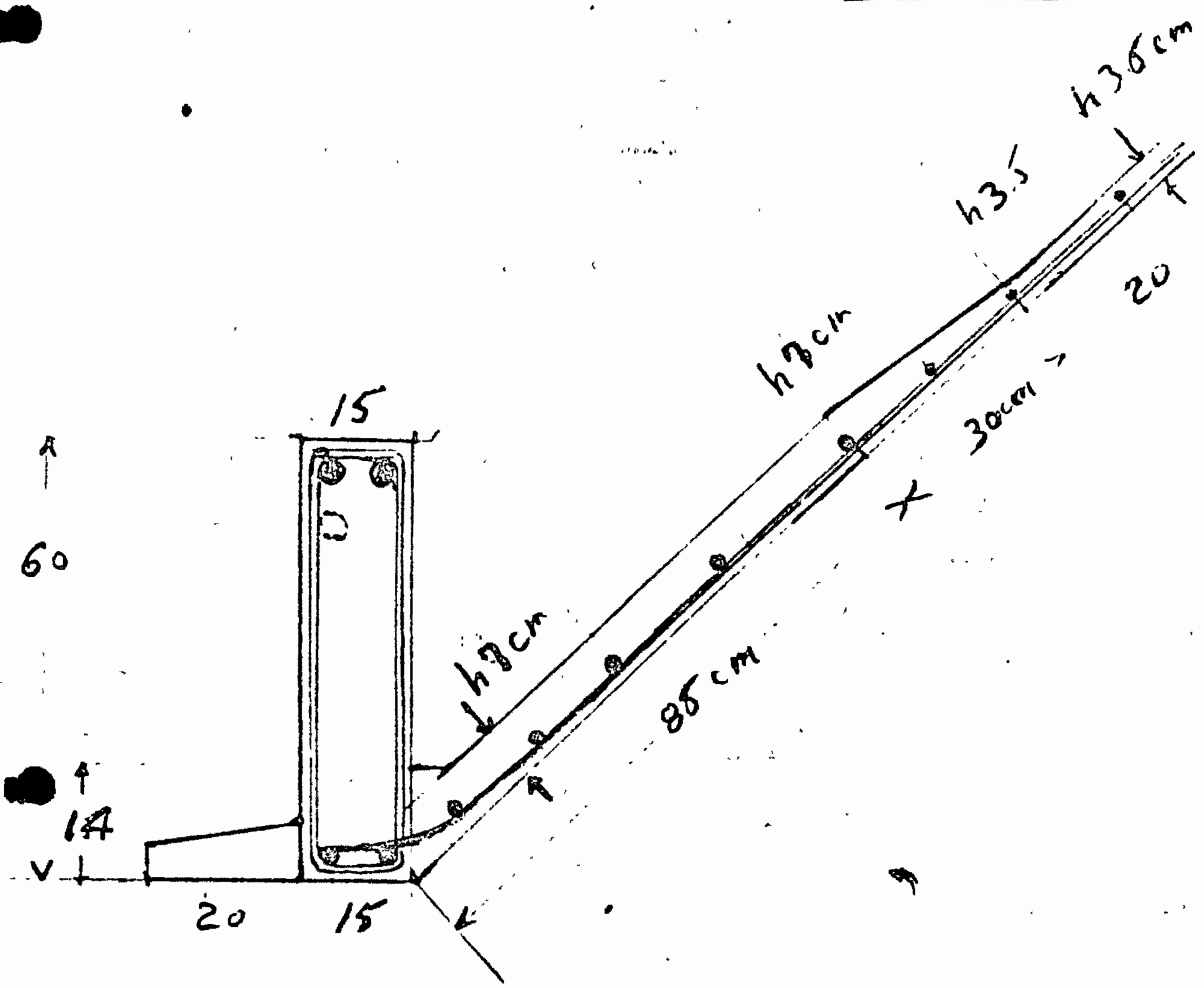

Volado	20 x 6.5	130	
Trabe	15 x 60	900	
losa 7cm	7 x 81.5	570	.1795 x 60m = 10.8 m³
chaflan	5 x 6/2	15	250m² - 70m²
transicion	30 x 6	180	180m² x 3.5 6.3
Concha 3.5cm	20 x 3.5	70	17.1 m³
		.1865	

7 7 mas pesada
que la de 16 m³
de Horimera

2

Espesores de una concha de 15m x 15 m

Concha 14.75 x 14.85 = 218.3 m²

Lados $\frown$ 2 0.83 x 15 x 4 x 2/3 — 83.2

251.5 m²

		m²	m³
3.5 cm		188.1	6.[illegible]
(7+3.5)/2	5.25 cm 4x3.15 x2	25.2	1.3
	7 cm 4x8x.85	27.2	1.9
(7+14)/2	10.5 4x1.9x1.2	9.2	.[illegible]
	14 cm 2x0.8²	1.3	.1
		251.5	10.[illegible]

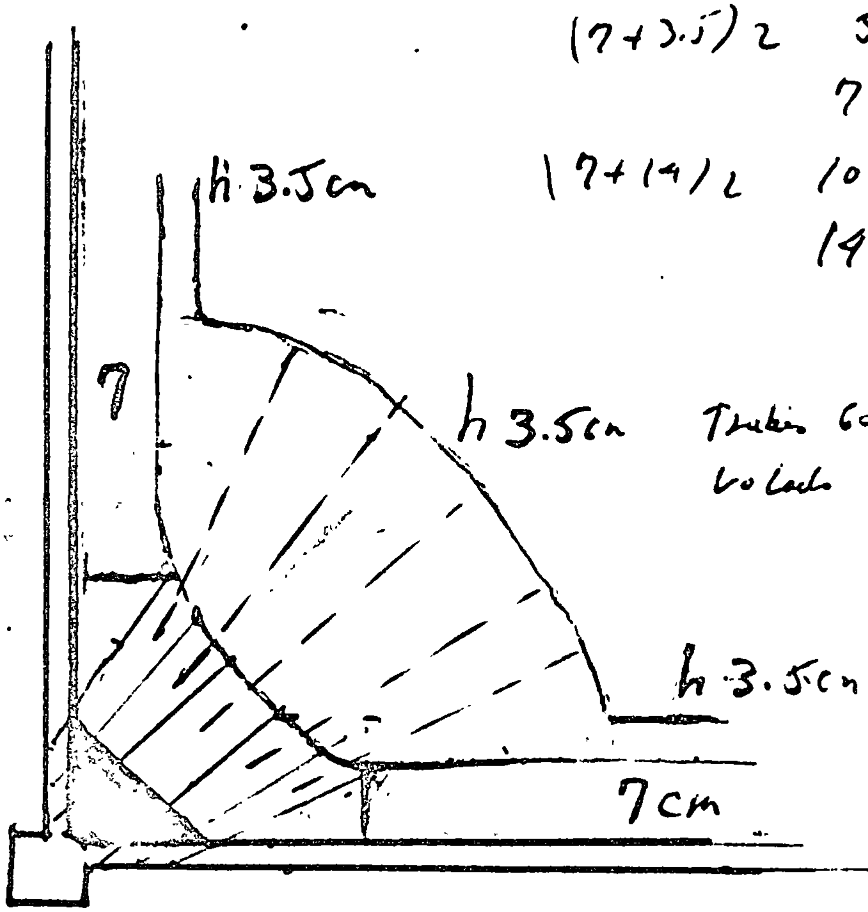

Tubos 60x15x10 — 5 4.[illegible]

Volado .013x15 — 0 2.[illegible]

16.57

16.57 m³

(h media 7.4 cm)

Planta horizontal

Escala 1/50

>>~

Armado de una
Concha de 15m x 15m

Trabe de 15 x 60
con 2 altas de 1" Tor una de 3.60m Cac
una de 2.40m Cac

al centro para armar 2 ø 3/8 normal

2 ø bajos de 3/8 normal

e 3/8 a 5 - 15 - 25 - 35 - 50 - 65 - 80 - 95 - 115
135 160 185 210 normal

e 1/4 a cada 25 cm

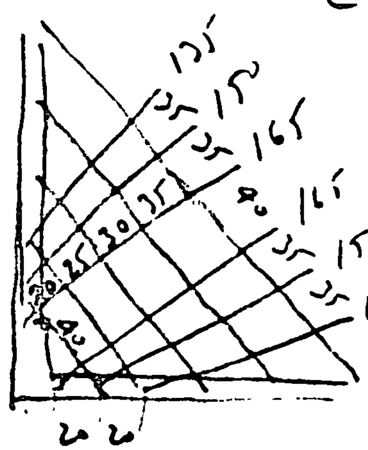

Abanico de 6 ø 3/4 Tor
2 de 1.35
2 de 1.50
2 de 1.65

amarrados con 5 ø 3/8 normal
diagonales a 0-20-45-75 y 110
5 ø 3/8 en abanico de 2.40 normal

traslapados 40 cm y al eje de los de 3/4

Tensor de 8 ø 1/4 tensado a 26 Tons

Marco de ø 3/8 a 10 25 40 60 85 (normal)
Marco de 1/4 a 100 115 135 160 190 220 @ 40
domo con ø 1/4 en cuadros de 40 x 40

Columna en concha de 15m x 15m

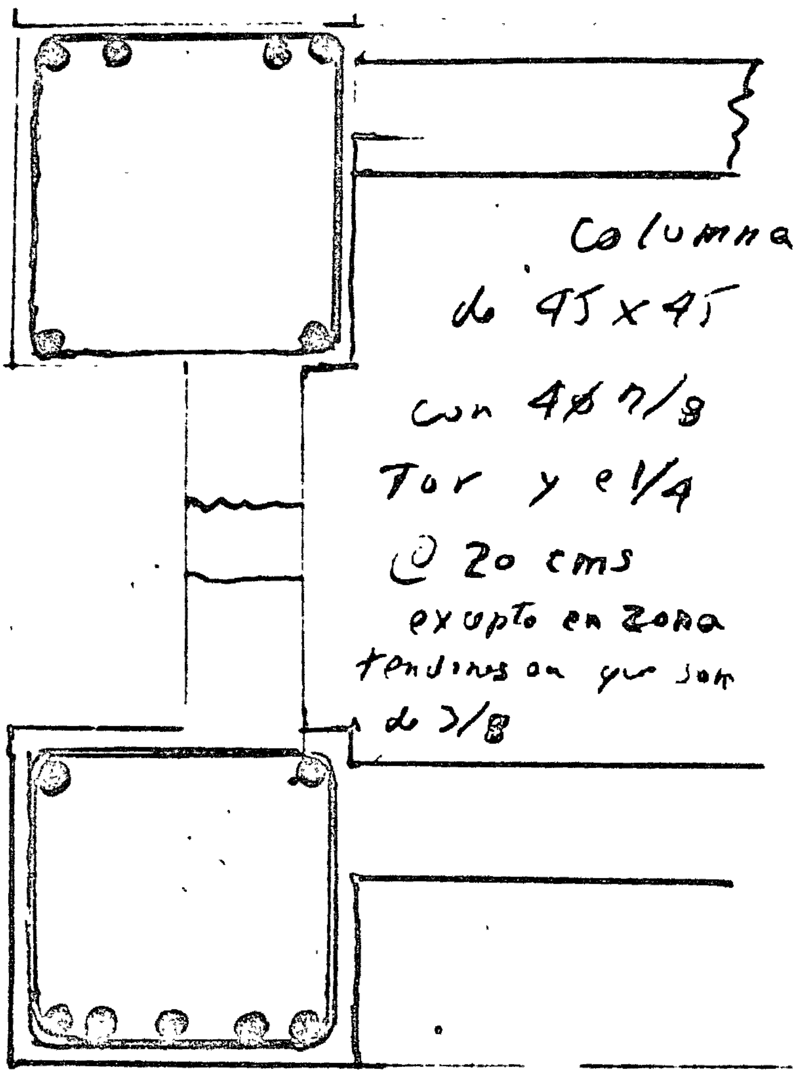

Planta escala 1/10

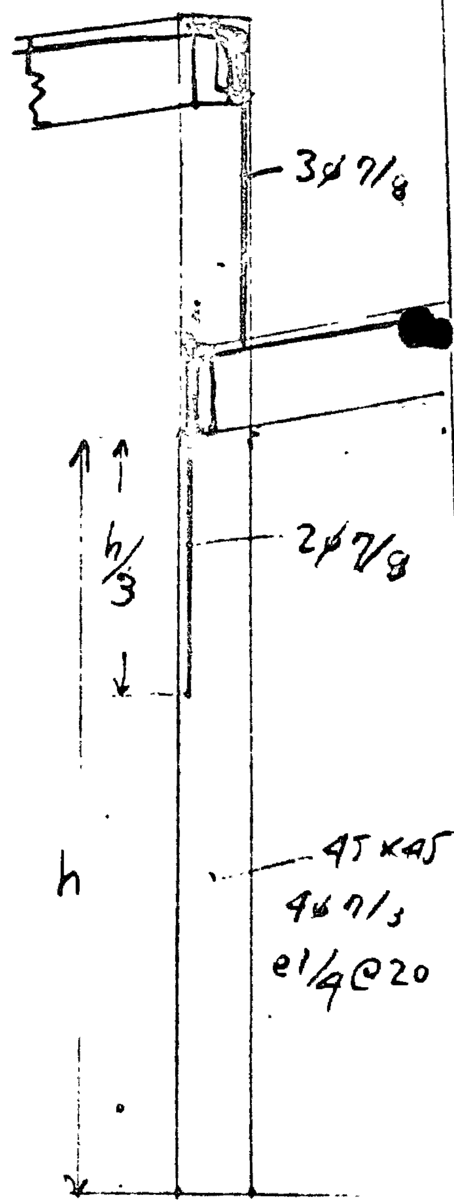

Corte escala 1/50

En col de esquina
dos bastones que
van en la
esquina
exterior

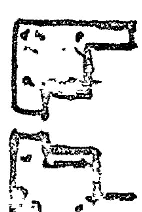

Concha de 15m x 15m en la bodega

Aumenta el peso 10% — concha $13.2^3 \times 2.4 = 43.8$
enladrillado $2500 \times 7 = 17.5$
61.3T

Columnas 50x50 con ⌀ 1" (en vez de 7/8)

Abanico 7/8 en vez de 3/4

Trabe de borde de 18 x 60

~~Trabe central 1? x 60 de 2m para adelante~~

~~Trabe orilla 21 x 60 de 1.80m para cat~~

3 A de 1" — 1 interior de 2m
1 ext de 2.40 m
1 ext de 3.60 m

e 3/8 — 7-12-21-30-40-50-60-70-82 95 110
1.27 - 1.47 - 1.70 - 195 220 y 2.45
e 1/4 @ 25 cm

Tensor de 10 ⌀ 1/4 tensado a 35 tons

Concha 15.50 x 15.50 casi igual
excepto ① trabes de 65 en vez de 60
② Tensor de 38.5 tons en vez de 30
③ 9cm en vez de 7cm y 18cm en vez de 14cm

Resumen de las conchas

flecha	Obra	Medidas ventana	largo	Materiales por m² horizontal concreto	fierro
2.10	Gonzalo Rio	10.00m	x 12.60m	8.1cm/m²	8.4 Kgr/m²
2.40	San Pedro	10.00m	x 15.00m	8.9cm/m²	7.2 Kgr/m²
2.00	Abousmrad	10.60m	x 12.60m	9.3cm/m²	7.8 Kgr/m²
1.50	Le Petit	11.25m	x 11.25m	8.9cm/m²	7.8 Kgr/m²
2.20	Carlos Vales	12.00m	x 12.00m	9.3cm/m²	8.0 Kgr/m²
2.50	Tepito Chica	12.80m	x 17.40m	10.2cm/m²	7.6 Kgr/m²
2.50	Tepito Grande	12.80m	x 16.80m	10.0cm/m²	8.3 Kgr/m²
2.40	Ugaldea	14.40m	x 13.75m	10.0 cm/m²	10.3 Kgr/m²
3.50	Moctezuma	15.90m	x 18.30m	11.5 cm/m²	11.4 Kgr/m²
3.00	Teoria	12.00m	x 15.60m	8.6 cm/m²	9.0 Kgr/m²
3.00	Tecoman	10.00m	x 19.60m	11.6 cm/m²	8.6 Kgr/m²
300	Harinera	15.00	x 15.00	7.0 cm/m²	9.0 Kgr/m²
200	POGA. SA	10.00	x 10.00 enladrillada pretensada	7.0cm/m²	(5.0 φ + 0.62 ┼) Kgr/m²

Concha de 15.69m x 15.46m flecha 3.50m
<u>enladrillada</u>

Trabe de borde de 18cm x 68cm

1ª capa inf. 1ª capa ext 2ª cap. inf

3 ø A tor de 1" a 3.75m 2.80m y 2.00m del eje

cuando no pasan a otra concha van anclados 1.00 metros

2 a 3/8 traslapados a el ø de 1" 40cm para sostener estribos

2 barras de 3/8 corridas para sostener estribos

20 estribos de 3/8 a cada lado a 3-10-17-25-33-41-49
58 67 77 88 100 113 127 142 159 178
200 y 225 2.50 y luego estribos de 1/4 a cada 25cm

Tendon 11 M63 para tensar a 38.5 Tons

Pechina 80cm x 80cm △ de 18cm de espesor

lateral 70cm de 9cm de espesor

Transicion 30cm de h 9cm a h 3.5cm

Abanico grueso h 18cm a h 9cm Abanico delgado h 9cm a h 3.5cm

Domo 3.5cm

Abanico grueso 6 ø Tor 1" (2 de 1.90m 2 de 1.75m 2 de 2.00m
anclados 50cm en las Trabes

Abanico delgado 5 ø 3/8 normal traslapados 40cm con ø 1"

amarre abanico grueso { 3 ø 5/8 Tor a 0cm 10cm y 25cm de la esquina anclados 40 ø o sea 65cm
3 ø 3/8 a 40-60 y 85 anclados 40cms

Marco 3/8 a 10-25-45-70-100

Marco 1/4 a 125-145-170-200-235 y a cada 40cm

Dic 4 1960

Abanico grueso 6 ø Tor 1" { 2 de 1.40 m, 2 de 1.75 m, 2 de 2.00 m } anclado, 50 cm

3 diagonales 5/8 a 0-10 y 25 3 de 3/8 @ 40-60 y 85

Abanico delgado 5 ø 3/8 normal de 2.40 m cada uno

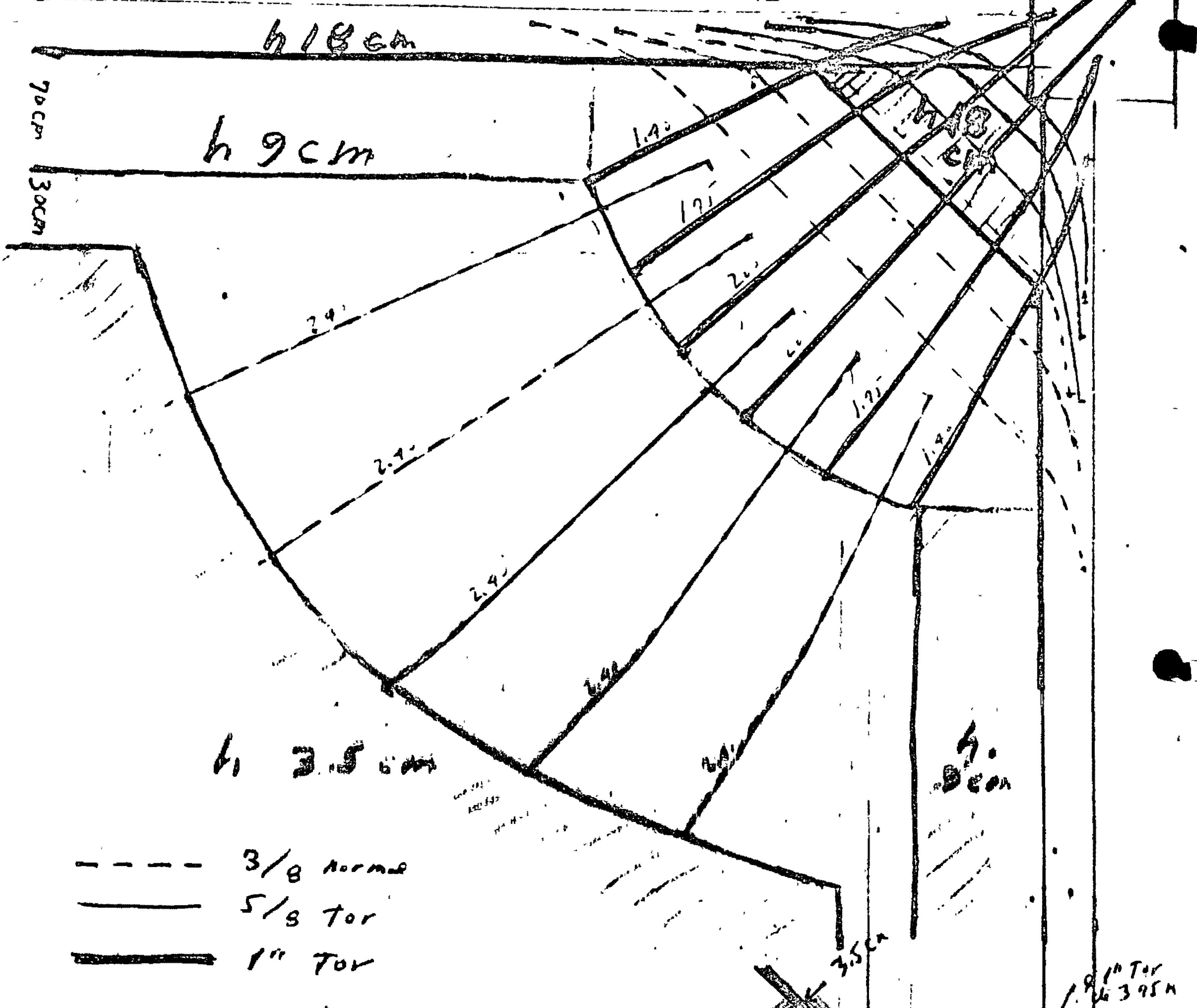

- - - - 3/8 normal

—— 5/8 Tor

▬▬ 1" Tor

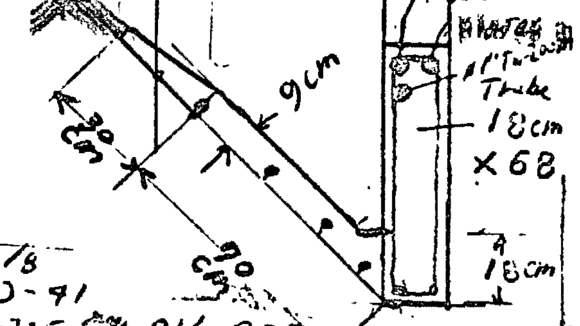

Marco 3/8 10 - 25 45 70 100

Marco 1/4 125 145 170 200 235

y a cada 40 cm

Trabe 3 A 1" Tor de 3.75 m 2.80 m y 2.00 m 2 ø 3/8

2 ø 3/8 para estrib. (20) e 3/8 @ 3-10-17-25-33-41

49 58-67-77-93-100-113 127 142 159 178 200-225 e 1/4 @ 25

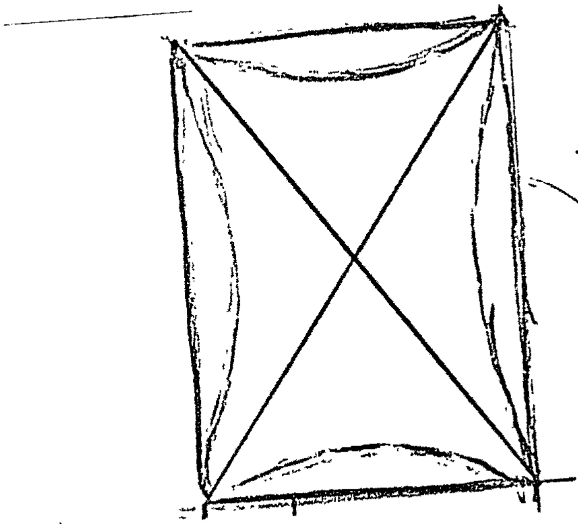

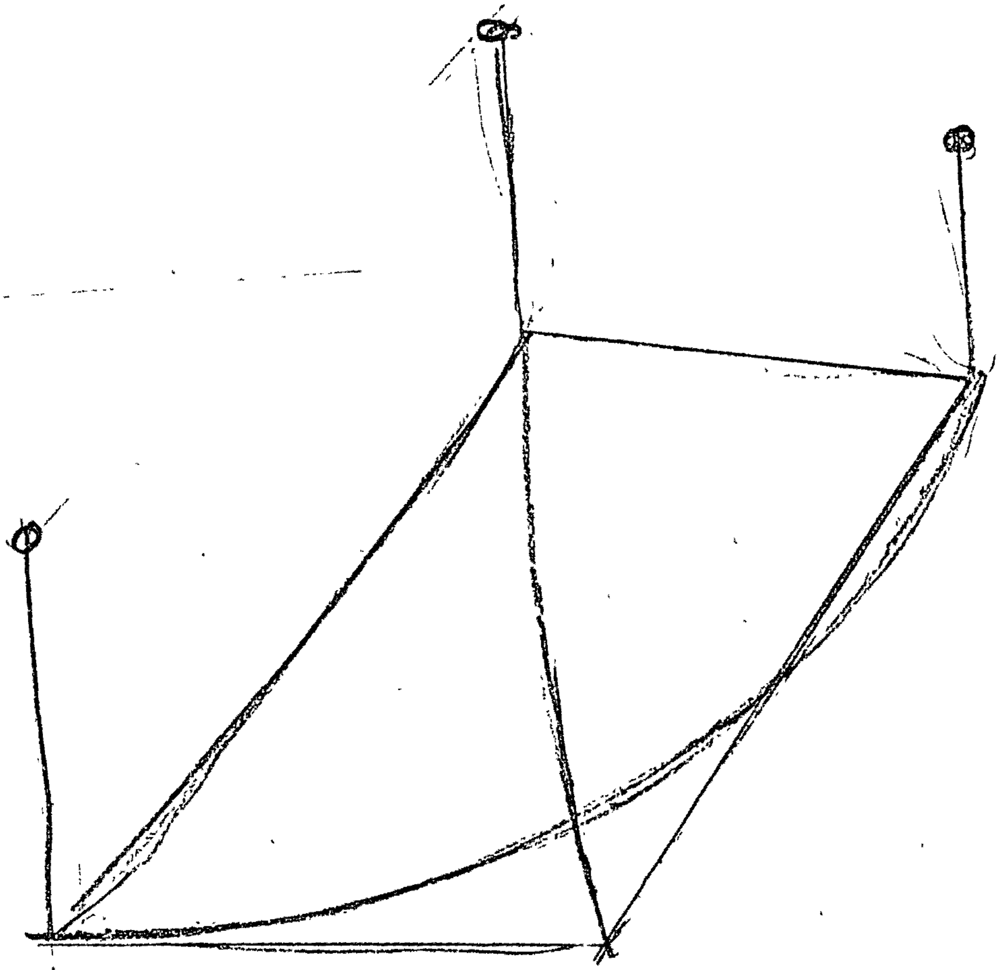

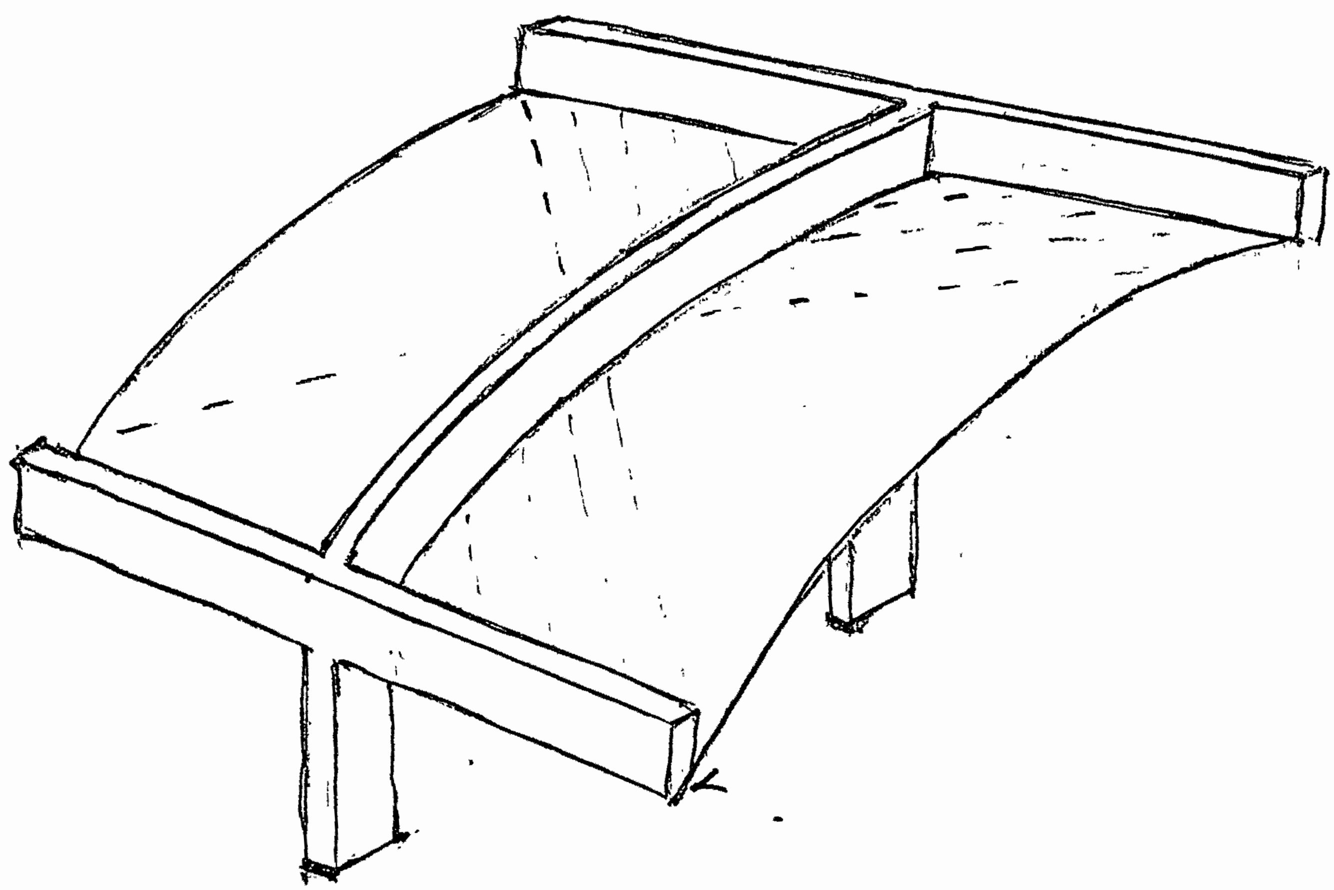

Prueba 10m x 10m
Para STan Home de México S. A.
Tecamachalco 145 Mexico D.F.

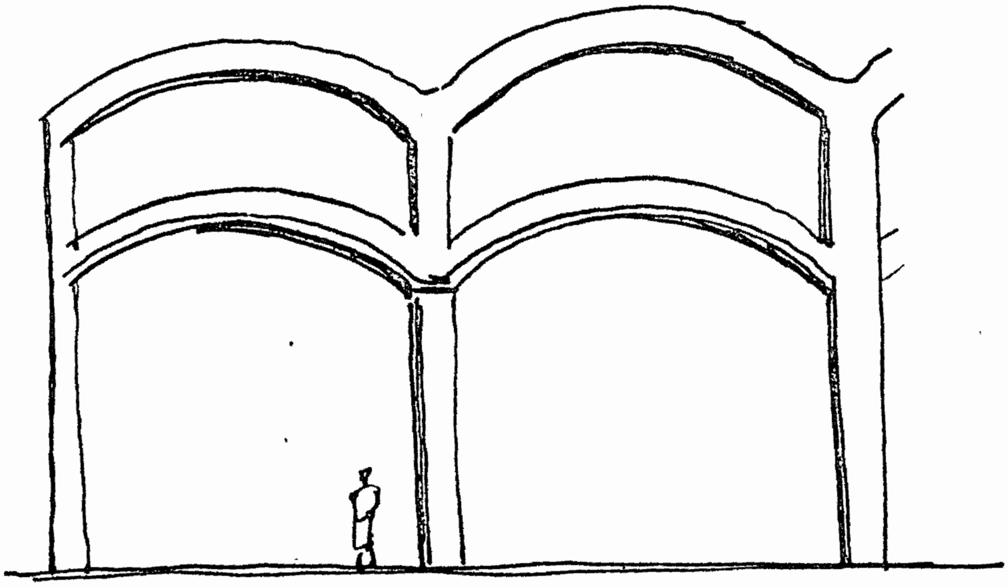

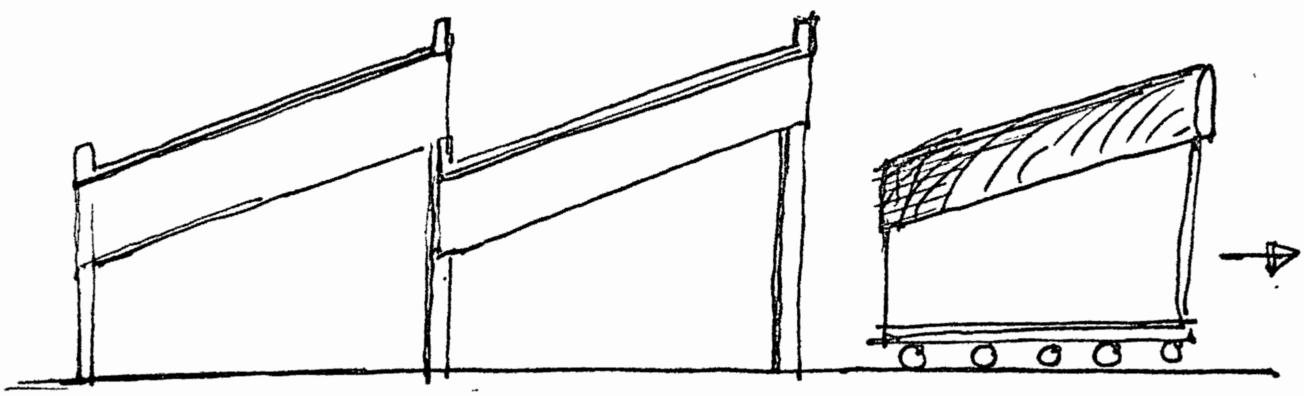

TORNILLOS, S.A.

PUENTE DE NONOALCO.

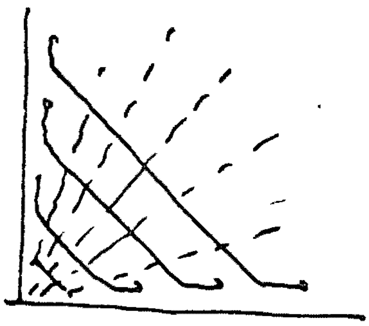

ABANICO DE FIERRO CORRUGADO.

PESO DOMO

1500 Kgr./cm2.

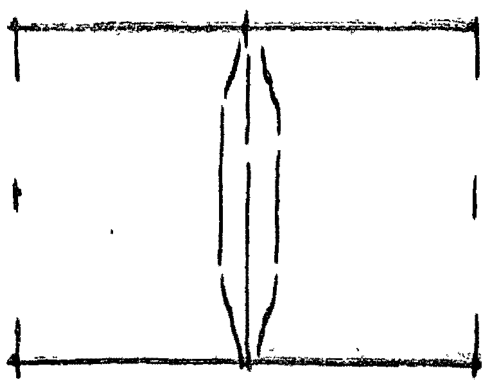

JUNTA ENTRE DOS TRABES.

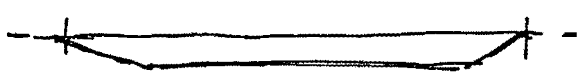

FLECHA EN FORMA DE TRAJINERA
CUANDO NO SE PONE TRABE DE BORDE.

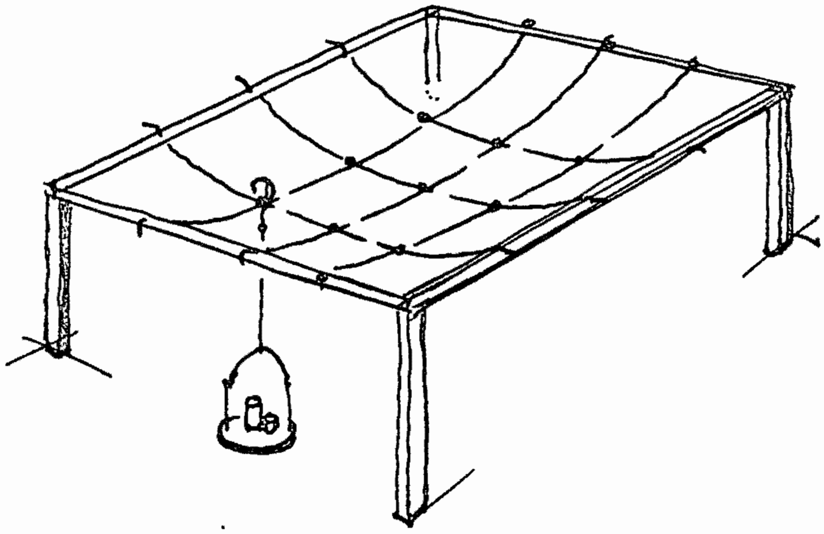

DETERMINACION DE LA FORMA.

ENTRAMADO DE LIGAS.

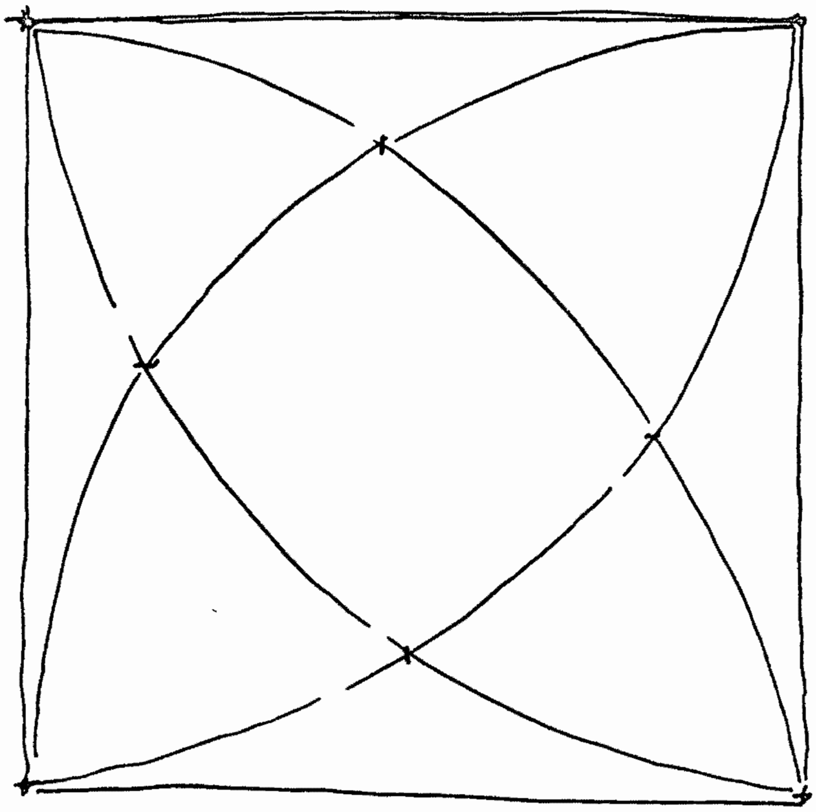

TRABES 25% CONCHA MAS PESO PROPIO TRABE

DOMO 75% CONCHA

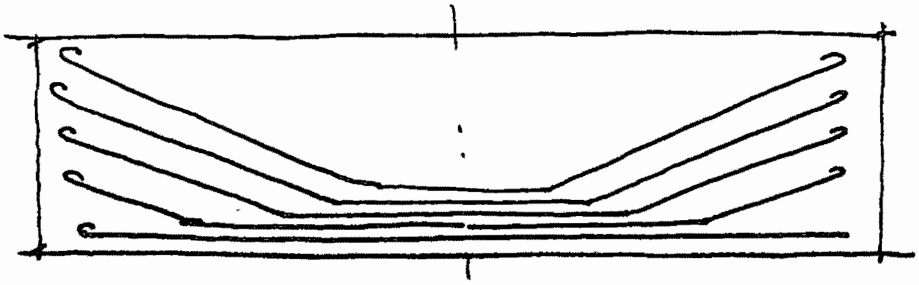

ARMADO PARA MOMENTO Y ESFUERZO CORTANTE.

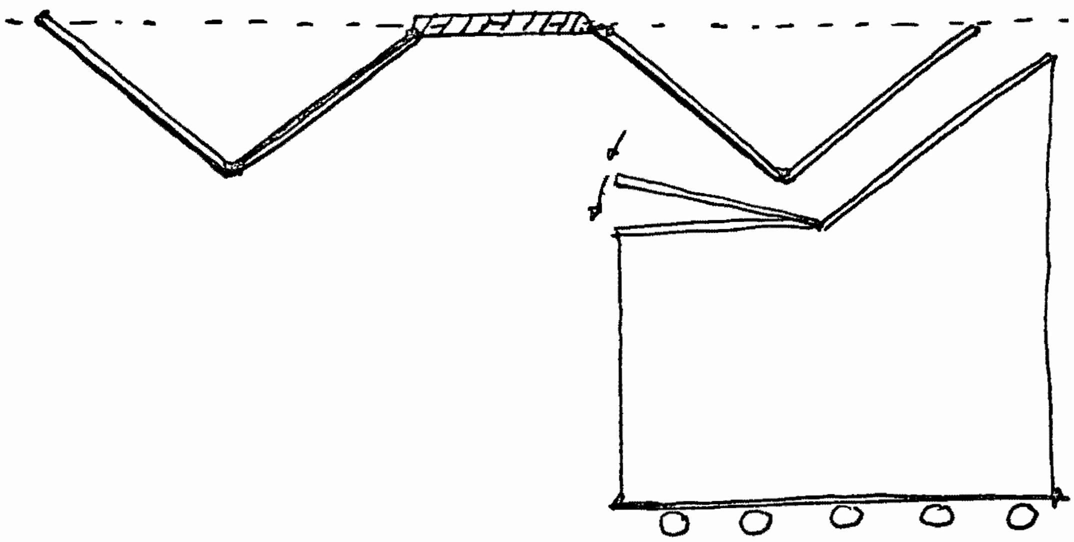

CLUB DEPORTIVO FEMENIL, S.A.DE C.V.   COAHUILA 164.   CLARO: 15 METROS.

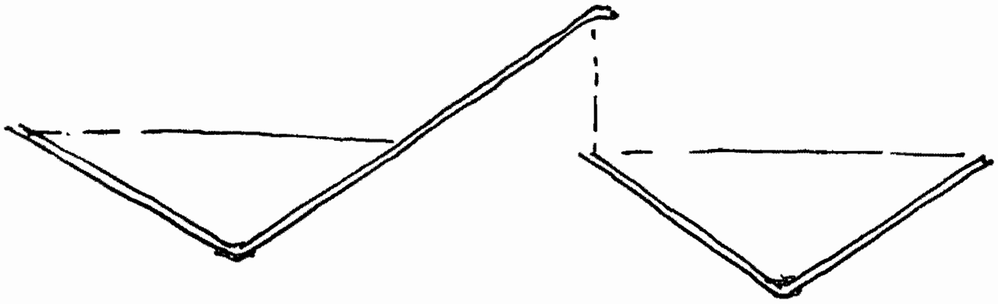

MENDEZ Y VILLELA.   COLONIA INDUSTRIAL VALLEJO.

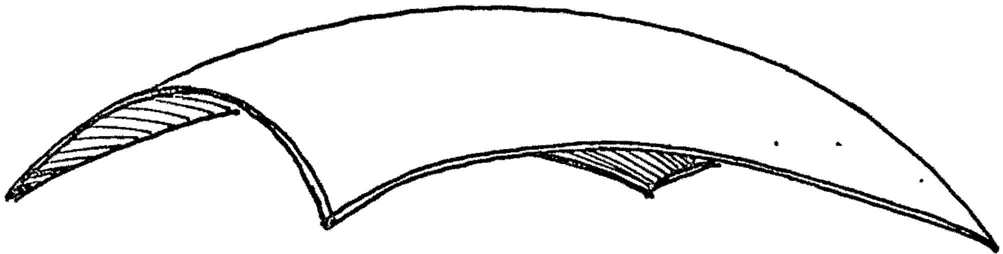

IGLESIA DE FATIMA. COL. IRRIGACION. CLARO: 20 METROS.

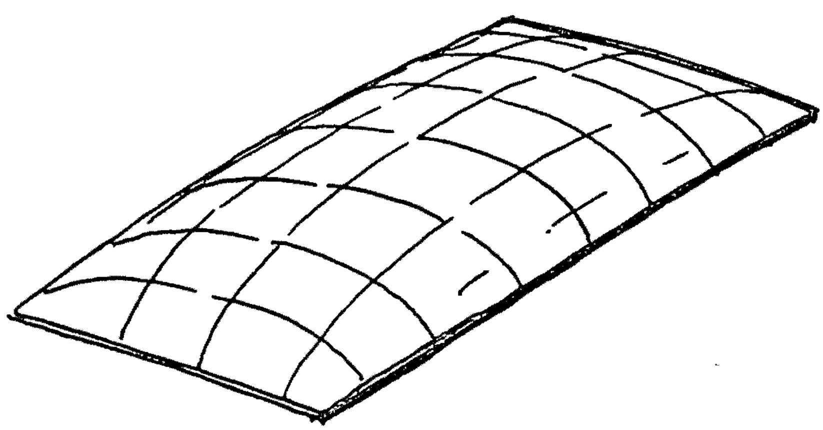

CONCHA O VELARIA.
GONZALO RIO 132 UNIDADES DE 10 M. x 12.60 M.
NORTE 45 Y PONIENTE 134.
COL. INDUSTRIAL VALLEJO.

TRABELOSA

PATENTE 61347.4 DE MARZO DE 1949

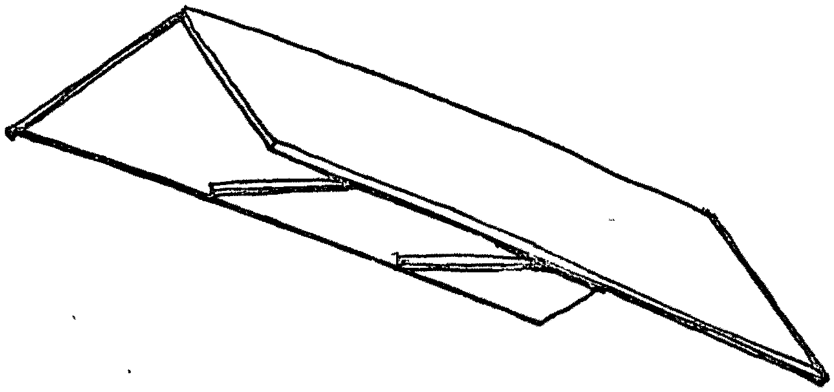

TRAVESAÑOS PARA COLAR UNIDAD POR UNIDAD.

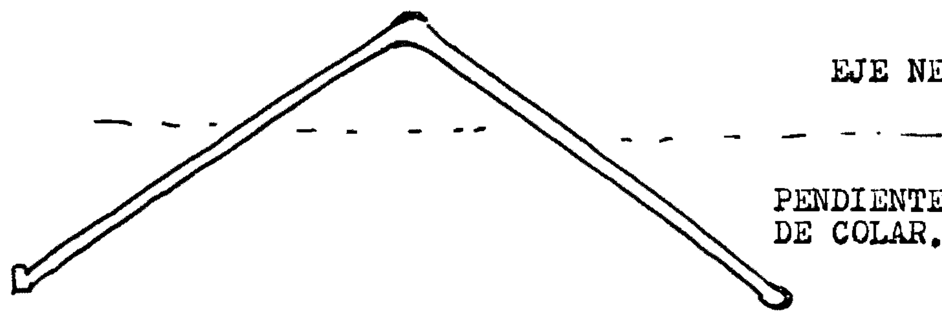

EJE NEUTRO.

PENDIENTE FACIL
DE COLAR.

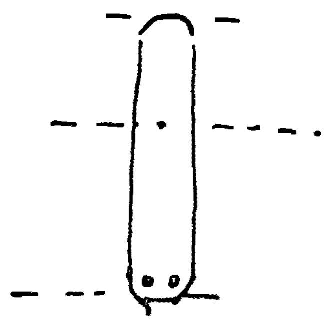

CALCULO COMO TRABE

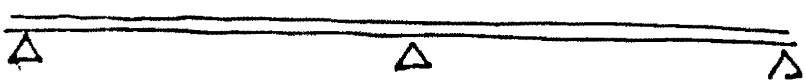

CALCULO COMO LOSA.

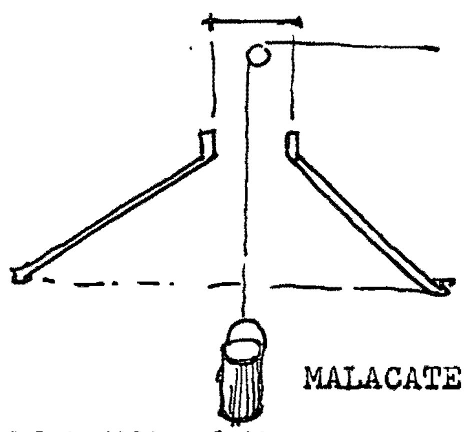

MALACATE.

CINE ERMITA. CLARO MAYOR 36 M.
AVENIDA REVOLUCION 67.

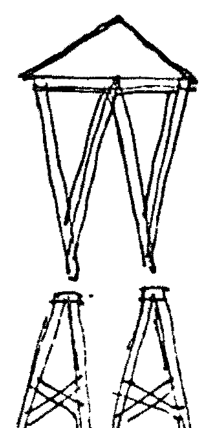

CIMBRA TELESCOPICA COMPLICADA.

1) SR. GONZALO RI.	Norte 45 y Poniente 154 Col. Industrial Vallejo	16,650.00
2) CELLOMEX.	Norte 45 Núm. 1013. Col. Industrial Vallejo	1,600.00
3) STANHOME DE MEXICO.	Poniente 134 Núm. 124.	2,200.00
4) BODEGAS DEL SR. CARLOS VALLES.	Poniente 146 Núm. 740.	9,500.00
5) DEPARTAMENTO DEL D. F.	Mercado de Ropa. Tepito	4,000.00
6) DEPARTAMENTO DEL D. F.	Mercado de Utensilios. Tepito.	4,000.00
7) DEPARTAMENTO DEL D. F.	Mercado General de San Pedro de los Pinos.	4,300.00
8) UGALDEA, S.A.	Norte 45 Núm. 667. Col. Industrial Vallejo.	9,800.00
9) BANCO ABOUMRAD, S.A.	Tochtli y Santa Lucía.	8,750.00
10) LA TOLTECA, S. A.	Planta Atotonilco Hgo.	2,400.00
11) LABORATORIOS CIBA.	Calzada de Tlalpan 1779	1,800.00
12) LABORATORIOS LEPETIT.	V. García Torres 235.	1,200.00
13) IGLESIA DE LA SANTISIMA.	Morelia Michoacán.	800.00
14) PINTURA SERVICIO, S.A.	La Presa, Edo. de México.	6,500.00
15) HARINERA DE MEXICO, S.A.	Ciprés 277.	2,200.00
16) CERVECERIA MOCTEZUMA.	Orizaba, Ver.	8,500.00
17) IGLESIA DE TECOMAN.	Tecomán, Colima.	650.00
18) AMPLIACION A STANHOME DE MEXICO.	Poniente 146 Núm. 740.	4,000.00
19) CEREALES INDUSTRIALIZADOS, S.A.	Norte 59 Núm.1100	1,000.00
20) CIA. MEXICANA DE DESARROLLO INDUSTRIAL.	Carreterá México Pachuca.	10,000.00
21) IGLESIA DE TEQUESQUITLAN.	Tequesquitlán, Jal.	1,000.00
22) IGLESIA DE ARMERIA.	Colima.	800.00
23) IGLESIA DE GUADALUPE.	Tuxtla Gutierrez, Chis.	1,200.00
24) IGLESIA DE QUESERIA	Colima.	800.00
25) IGLESIA DE FATIMA.	Col. Irrigación.	900.00
26) INDUSTRIAL PECUARIA.	La Presa, Edo. de México.	2,000.00
27) INMOBILIARIA SAN CARLOS.	Col. Industrial Vallejo.	1,600.00
28) CINE ERMITA.	Tacubaya, D.F.	1,500.00
29) COAHUILA 164.		600.00
	TOTAL EN METROS CUADRADOS.	110,250.00

centro de educación contínua
facultad de ingeniería, unam

DISEÑO Y CONSTRUCCION DE ESTRUCTURAS ESPACIALES Y DE CASCARON

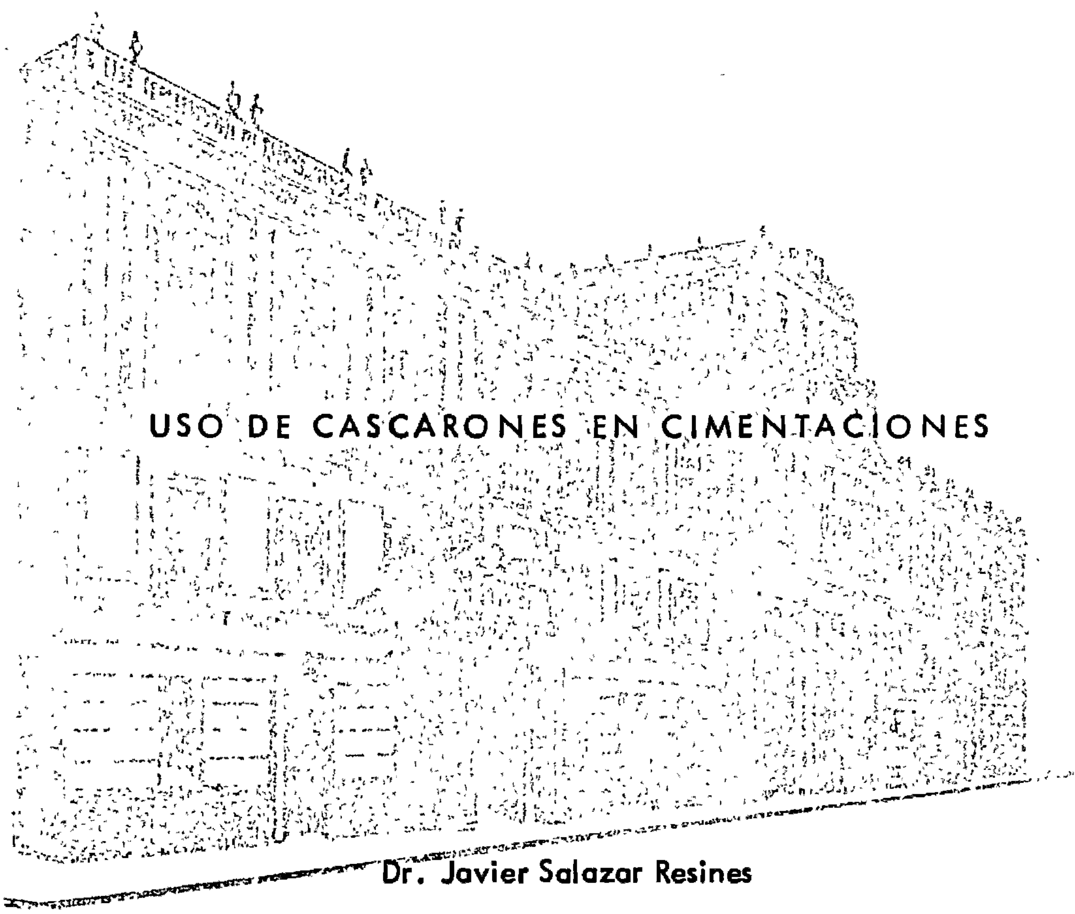

USO DE CASCARONES EN CIMENTACIONES

Dr. Javier Salazar Resines

1972

Tacuba 5, primer piso. México 1, D.F.
Teléfonos: 521-30-95 y 513-27-95

The continuing development of design and construction techniques of shell structures is resulting in an increasing fund of information of practical interest to Architects, Engineers and Contractors. The aim of furthering all branches of this progress has inspired the formation of the **international association for shell and spatial structures,** whose purpose is to organise meetings and congresses for the interchange of ideas and their dissemination by means of periodical publications.

Everyone interested in the various branches of shell techniques and their architectonic possibilities or realizations is invited to join this International Association.

To become a member or to obtain more detailed information, please write to the Secretariat of the International Association for Shell and Spatial Structures, Alfonso XII, 3, Madrid (7). Spain.

1.2 Se presenta en las siguientes hojas la nomenclatura más empleada en el desarrollo del texto, con su respectivo significado. Más adelante en los lugares correspondientes se insistirá sobre su significado y en caso de utilizar otras literales para describir conceptos particulares se aclararán donde aparezcan.

2.2. La figura 1.2 representa una franja unitaria de cascarón con las fuerzas y geometría que en ella intervienen y cuyo significado se describe en la nomenclatura. La figura referida a la cimentación, se ha dibujado invertida por claridad, dado que se tienen mayor experiencia en la solución de arcos y trabes con las cargas obrando hacia abajo. De la figura 1.2 se puede estudiar el equilibrio de la franja. Para esto, cabe hacer la comparación con una estructura más sencilla, por ejemplo, una trabe. Si una trabe se corta en dos secciones separadas por una distancia unitaria, se estudia en Estática que, la carga que obra en este tramo de viga queda equilibrado por los incrementos de fuerza cortante y momento flexionante. En la franja de cascarón el incremento de fuerza cortante está representado por $T' = dT/dx$. El conocimiento de esta variación de fuerza cortante es importante para el análisis transversal del cascarón. Esto no sucede en las trabes en general, porque la línea de acción de la carga y el de la fuerza cortante es la misma. El incremento de las fuerzas normales se estudia a partir de la flexión longitudinal esencialmente igual que en las trabes, con ligeras modificaciones.

3.2 En la figura 2.2 se representa en un plano la sección unitaria de cascarón sujeta a las fuerzas que intervendrán en el estudio de la flexión transversal. El cascarón está sujeto a una carga uniformemen te distribuída q (t/m^2) y su resultante es equilibrada por las dos fuerzas T'k cuya línea de acción se localiza en la línea de fuerza cortante Fig. 2.2. (b). La posición de las líneas de fuerza cortante se pueden obtener a partir de la posición de los centroides de esfuerzo 1-2-3. Efectivamente basándose en el Teorema de Bredt se puede establecer que la resultante de las fuerzas cortantes (T') que obran a lo largo de una sección de paredes delgadas tiene el mismo valor y dirección que si estuviera actuando a lo largo de la cuerda. La resultante pasa por el vértice de un triángulo que tiene la cuerda como base y un área igual a la encerrada por el arco y la cuerda. En la Figura 2.2. (b) el área encerrada por la cuerda 1-2 y el arco 1-1'-2 es igual a la del triángulo 1-0-2. La dirección de T'k es paralela a la de la cuerda 1-2 de longitud k. Su valor es el producto del valor T', que obra en el cascarón, por la longitud k, de la cuerda. Los puntos 1, 2 y 3 representan el centroide de los esfuerzos de tensión o compresión que resultan de la flexión longitudinal. En general, para lograr que las líneas de cortante se intersecten en la resultante, basta fijar dos centroides, por ejemplo los de tensión indicados con una cruz y determinar el tercero de compresión, por tanteos hasta que se logre que las líneas de fuerza cortante de los tramos 1-2 y 2-3 se corten en la línea de acción de q 1.

Si se propone estudiar una sección simétrica, con respecto a un eje vertical, el centroide 2 quedará situado al centro del claro y el estudio se simplifica un poco.

La longitud de la cuerda será:

$$k = \sqrt{(h+f)^2 + \left(\frac{1}{2}\right)^2}$$

Por simetría, las dos proyecciones verticales de T'k son iguales y con valor $\frac{ql}{2}$

Resumen de la Acción de Arco e influencia de la flexión longitudinal

Nomenclatura:

X: Coordenada paralela a las generatrices del cascarón.

y Coordenada horizontal transversal

z: Coordenada vertical

l. Claro a ejes del arco

R. Radio del eje del cascarón

f. Flecha del cascarón.

ϕ. Angulo desde un eje, de simetría, del arco.

ϕ_o Angulo hasta el arranque del arco

Δy Incremento en y. Δz: Incremento en Z

u Distancia del centro de compresión (en el arco) al arranque del cascarón

α_o. Relación $\frac{u}{f}$

b. Ancho de la zona de compresión desde la clave del arco

t. espesor del cascarón.

ϕ_b: Angulo hasta donde empieza la zona de compresión

e. Flecha del arco desde el arranque hasta $\frac{b}{2}$

c: Distancia de la cuerda del arco (del arranque a $\frac{b}{2}$) hasta la línea de acción de la fuerza cortante.

a: Distancia de la clave a la línea de acción de la fuerza cortante.

$d = a - c$

k. Factor de la fuerza cortante = longitud de la cuerda del semiarco.

h. Altura efectiva de la contratrabe.

$$\left.\begin{matrix} A \\ B \\ C \\ D \\ E \\ F \\ M \\ N \\ P \\ T \\ J \\ S \end{matrix}\right\} \text{Constantes para la determinación de } M\phi,\ N\phi \text{ y } Q\phi$$

EI Rigidez del arco (Franja de 1.00 m de ancho)

α: Curvatura de la elástica

ϕ: Pendiente de la elástica

v: Variación en la dirección "y" de la elástica.

w: Variación en la dirección "Z" de la elástica.

f'_c: Esfuerzo de ruptura del concreto.

q. Reacción del terreno

T': Variación de la fuerza cortante, en el sentido longitudinal.

$\left.\begin{matrix} N_z \\ N_y \\ N_x \end{matrix}\right\}$ Fuerzas normales paralelas a los ejes definidos por los subíndices

H: Fuerza horizontal en el arranque del cascarón que hace cero el momento transversal $M\phi,o$ en la clave.

P: Coceo del arco.

H_1: Modificación a la fuerza H.

q_z: Suma de cargas que obran en la dirección Z desde el arranque del cascarón hasta una sección en ϕ.

q_y: Id. dirección y.

Q_z, Q_y, Q_H, : Componentes de $Q\phi$ debidas a $N_z, N_y, y\ N_H$ respectivamente

$Q\phi$: Fuerza cortante radial en una sección en ϕ

$N\phi$: Fuerza normal tangencial a una sección en ϕ.

$M\phi,o$: Momento transversal del arco, para la condición del empotramiento en la clave.

$\bar{M}\phi,o$: Momento transversal corregido por H.

$M\phi$: Momento transversal final.

M_H Momento correctivo debido a H.

M_{H_1} Momento correctivo debido a H_1.

M: Momento flexionante longitudinal.

p: Factor de seguridad para f'_t.

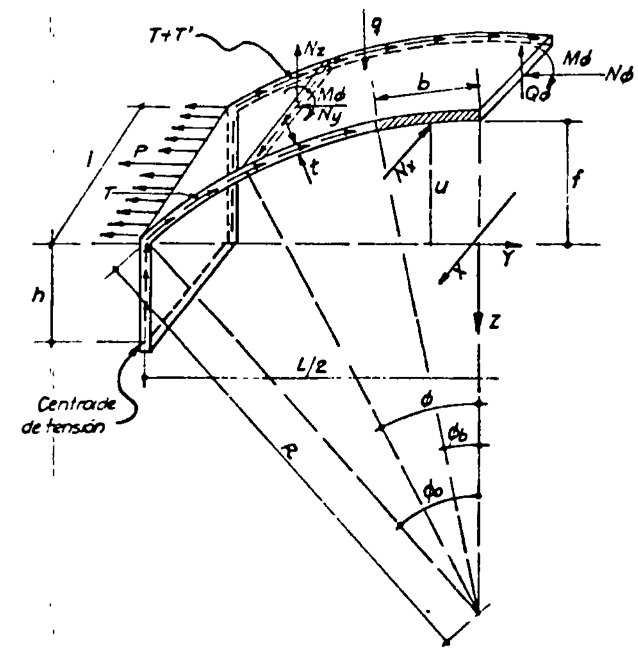

FIG. 1. 2.

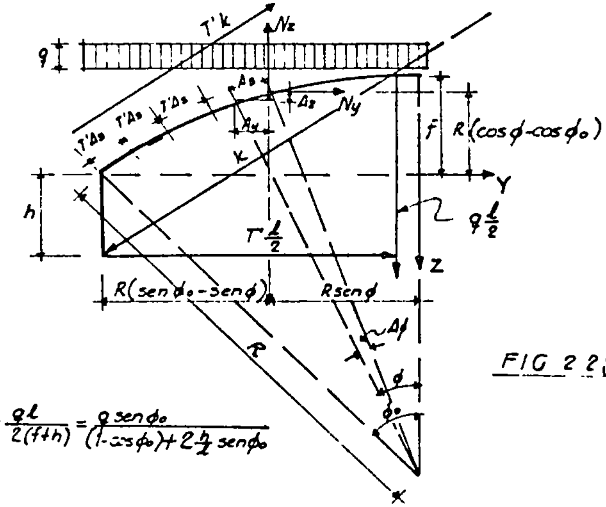

FIG 2.2(a)

$$12 \ldots\ldots T = \frac{q\ell}{2(f+h)} = \frac{q\,\operatorname{sen}\phi_0}{(1-\cos\phi_0) + 2\frac{h}{\ell}\operatorname{sen}\phi_0}$$

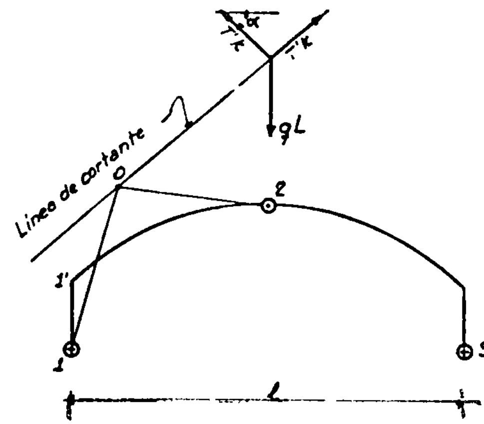

FIG 2.2(b)

Si se toma un intervalo de arco ΔS, dovéla, se tendrán fácilmente las expresiones de las cargas que obran en ese tramo:

$$(1)\begin{cases} q_z = q\,\Delta y - T'\Delta z & \text{en la dirección del eje } z. \\ q_y = T'\Delta y & \text{en la dirección del eje } y. \end{cases}$$

Las fuerzas totales que obran en una sección será la suma acumulativa de las fuerzas de cada dovéla. Hacemos esta integración desde el punto (1) Fig. 2.2. (b), hasta el arranque (ϕo) y desde (ϕo) hasta un punto cualquiera (ϕ). El hecho de proceder de ϕo a ϕ y nó de $\phi = 0$ a ϕ tiene por objeto considerar únicamente la acción de la fuerza cortante T'y la de la carga q; si se hiciera de $\phi = o$ a ϕ se tendría que tomar en cuenta la acción de la parte derecha del cascarón 2-3. Fig. 2.2. (b). Es decir, cortando el cascarón en un punto (definido por ϕ), consideramos el "cuerpo libre" de la izquierda determinando el valor de las fuerzas interiores Nz y Ny que lo mantienen en equilibrio.

$$(2)\begin{cases} N_z = \sum_{\phi_o}^{\phi} (q\,\Delta y - T'\Delta z) - T'h \\ N_y = \sum_{\phi_o}^{\phi} T'\Delta y \\ \text{como } \underline{T'} \text{ y } q \text{ son constantes y} \\ \sum_{\phi_o}^{\phi} \Delta z = R(\cos\phi - \cos\phi_o) \\ \sum_{\phi_o}^{\phi} \Delta y = R(\operatorname{sen}\phi_o - \operatorname{sen}\phi) \\ \text{Obtenemos:} \\ N_z = qR(\operatorname{sen}\phi_o - \operatorname{sen}\phi) - T'R(\cos\phi - \cos\phi_o) - T'h \quad - 2.2 \\ N_y = T'R(\operatorname{sen}\phi_o - \operatorname{sen}\phi) \text{ ------------ } 3.2 \end{cases}$$

2.5 Los momentos transversales M ϕo, se obtienen en forma análoga. Se corta nuevamente en una sección cualquiera (ϕ) y se estudia la acción del tramo de la izquierda sobre el de la derecha y la de la carga que obra en el de la derecha.

La acción de la izquierda está representada por las fuerzas Nz y Ny. Las fuerzas Nz y Ny para producir momento deben actuar en los intervalos Δy y Δs respectivamente. Los valores de estos incrementos de ordenadas se pueden valuar directamente de la figura 2.2. (a).

$$(3)\begin{cases} -\Delta s \ \operatorname{sen}\phi \doteq \Delta z \ (\text{en sentido contrario del eje } z) \\ \Delta s \ \cos\phi \doteq \Delta y \\ \text{pero } \Delta s = R\,\Delta\phi \\ \Delta z = -R\,\Delta\phi \ \operatorname{sen}\phi \\ \Delta y = R\,\Delta\phi \ \cos\phi \\ \text{La variación del momento estara dada por:} \\ \Delta M\phi,o = -N_z\,\Delta y + N_y\,\Delta z \end{cases}$$

En esta expresión no se ha indicado el término de la carga que actúa en el intervalo ΔS. Sin embargo, este está incluído en Nz para la parte izquierda de cascarón y como la integración del momento se hará desde ϕo hasta ϕ su efecto quedará incluído en la expresión que se obtenga. Substituyendo en $\Delta M\,\phi,o$, los valores de Nz y Ny e integrando de ϕo a ϕ se obtiene:

$$(4)\begin{cases} M\phi,o = -qR^2\int_{\phi_o}^{\phi}(\operatorname{sen}\phi_o - \operatorname{sen}\phi)\cos\phi\, d\phi + T'R^2\int_{\phi}^{\phi_o}(\cos\phi - \cos\phi_o)\times \\ \quad + T'hR\int_{\phi}^{\phi_o}\cos\phi\, d\phi - T'R^2\int_{\phi}^{\phi_o}(\operatorname{sen}\phi_o - \operatorname{sen}\phi)\operatorname{sen}\phi\, d\phi \end{cases}$$

Arreglando los términos para obtener una expresión más sencilla y efectuando las integraciones:

(5)
$$4.2 \ldots \quad M\phi,o = R^2\left\{T'\left[\phi_o-\phi-\text{sen}(\phi_o-\phi)+\frac{h}{R}(\text{sen}\,\phi_o-\text{sen}\,\phi)\right] - \frac{q}{2}(\text{sen}\,\phi_o-\text{sen}\,\phi)^2\right\}$$

En el centro $\phi = 0$

$$\therefore M\phi{=}0 = R^2\left\{T'\left[\phi_o-\text{sen}\,\phi_o+\frac{h}{R}\text{sen}\,\phi_o\right]-\frac{q}{2}\text{sen}^2\phi_o\right\}$$

Este momento en el centro del claro es en general muy grande de manera que habrá que buscar alguna forma de disminuirlo. Hasta ahora el problema ha sido isostático y puede compararse con un cantiliver. Por simetría el centro del claro se ha comportado como un empotramiento, puesto que las acciones se han ido sumando desde el fondo de la trabe y el arranque del cascarón hasta el centro del claro (ϕ = o).
Habrá que introducir alguna fuerza, ya sea en el arranque o en el fondo de la trabe, cuya acción disminuya los momentos transversales.
Por la forma del diagrama de momentos flexionantes isostáticos, como se verá más adelante, una fuerza horizontal (coceo) obrando en el arranque del cascarón es la que hace mínimos estos momentos transversales pues su diagrama de momento es el que más se aproxima al isostático. Elásticamente las redundancias en el borde (perturbaciones de borde) se obtienen a partir de condiciones de desplazamiento y giro en la orilla (condiciones de borde) como se resuelve en el método analítico presentado posteriormente. Plásticamente las redundancias se pueden imponer sin otra limitación que la de hacer mínimos los momentos transversales. Desde luego que esta limitación más o menos ar

bitraria, como se indicó en la introducción, puede conducir a deformaciones fuertes. Sin embargo, como se verá en el método numérico, las redundancias obtenidas elástica o plásticamente difieren poco.

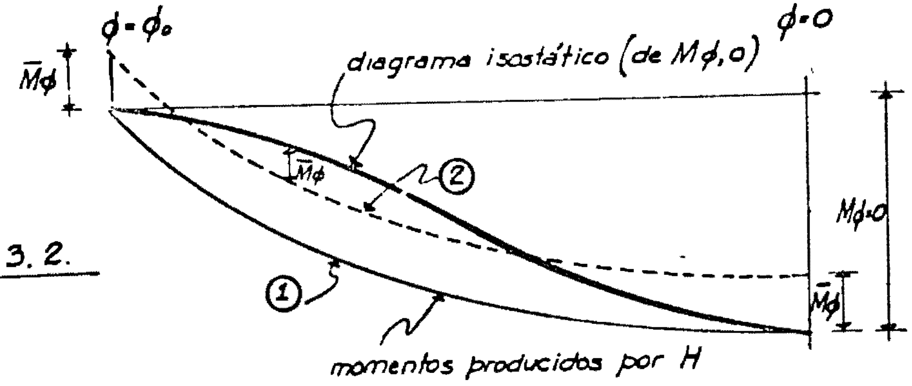

FIG. 3. 2.

En la Fig. 3.2. se indica la forma que tienen el diagrama isostático de $M\phi,o$ y el de los momentos de una fuerza horizontal H en el arranque (ϕo). De la misma figura se puede deducir que la condición de Momentos transversales mínimos se obtiene trasladando paralelamente a sí mismo el diagrama de corrección (de H) desde la posición (1) a la posición (2) en la que se han igualado los momentos en tres puntos (con valor $\bar{M}\phi$). Con cualquier otra corrección se obtendría cuando menos en un punto un momento transversal mayor a $\bar{M}\phi$.
El valor de H cuyo momento nulifica al $M\phi$ = o se obtiene de:

$$H = \frac{M\phi{=}0}{f} \quad \text{en la que } f \text{ es la flecha del cascarón}$$

De la figura 2.2 se deduce que:

$$f = R(1-\cos\phi_o)$$

$$\therefore H = \frac{R}{1-\cos\phi_o}\left\{T'\left[\phi_o - sen\,\phi_o + \frac{h}{R}\,sen\,\phi_o\right] - \frac{q}{2}\,sen^2\phi_o\right\}$$

De la misma figura 2.2:

$$R = \frac{l}{2\,sen\,\phi_o}$$

Substituyendo este valor y el de T' en la expresión de H:

$$H = \frac{ql}{2}\cdot\frac{1}{1-\cos\phi_o}\left\{\frac{\phi_o - sen\,\phi_o + 2\frac{h}{l}\,sen^2\phi_o}{(1-\cos\phi_o)+2\frac{h}{l}\,sen\,\phi_o} - \frac{1}{2}\,sen\,\phi_o\right\} \qquad 5.2$$

Los momentos producidos por H, serán:

$$M_H = -HR(\cos\phi - \cos\phi_o)$$

en la que $R(\cos\phi - \cos\phi_o)$ es la distancia vertical desde el arranque (ϕ_o) hasta un punto determinado por el ángulo ϕ.

(5')

$$M_H = -\frac{Hl}{2\,sen\,\phi_o}(\cos\phi - \cos\phi_o)$$

Sumándole esta corrección 4.2, y substituyendo los valores de T', H y R se obtiene:

$$\bar{M}_{\phi,o} = ql^2\left\{\frac{\frac{\phi_o}{(2sen\phi_o)^2} - \frac{[\phi + sen(\phi_o-\phi)]}{(2sen\phi_o)^2} + \frac{1}{2}\cdot\frac{h}{l} - \frac{sen\,\phi}{2sen\phi_o}\,\frac{h}{l} - \frac{\cos\phi}{(2sen\phi_o)^2}\cdot\frac{\phi_o - sen\phi_o}{1-\cos\phi_o} - \frac{\cos\phi}{2(1-\cos\phi_o)}\,\frac{h}{l}}{\frac{1-\cos\phi_o}{sen\phi_o} + 2\,\frac{h}{l}}\right.$$

$$\left. + \frac{\frac{\cos\phi_o}{(2sen\phi_o)^2}\cdot\frac{\phi_o - sen\phi_o}{1-\cos\phi_o} + \frac{\cos\phi_o}{2(1-\cos\phi_o)}\cdot\frac{h}{l}}{\frac{(1-\cos\phi_o)}{sen\,\phi_o} + 2\frac{h}{l}} + \frac{\cos\phi - \cos\phi_o}{8(1-\cos\phi_o)} - \frac{1}{8sen^2\phi_o}(sen\phi_o - sen\phi)^2\right]$$

En esta expresión se pueden hacer:

$$A = \frac{1}{(2sen\phi_o)^2}\left[\phi_o - \phi - sen\,(\phi_o - \phi) + \frac{\phi_o - sen\phi_o}{1-\cos\phi_o}(\cos\phi_o - \cos\phi)\right] \qquad 6.2$$

$$B = \frac{1}{2(1-\cos\phi_o)}\left\{(1-\cos\phi_o)\left[1 - \frac{sen\phi}{sen\phi_o}\right] + \cos\phi_o - \cos\phi\right\} \qquad 7.2$$

$$C = \frac{1}{8}\left[\frac{\cos\phi - \cos\phi_o}{1-\cos\phi_o} - \frac{(sen\,\phi_o - sen\,\phi)^2}{sen^2\phi_o}\right] \qquad 8.2$$

En el transcurso del texto se adoptará un valor de $\phi_o = 40°$. Este valor es recomendable por razones prácticas:

1o.- La mezcla de concreto se adhiere a la cimbra sin resbalar con esta pendiente. En caso de usar un ángulo mayor en el arranque habrá que utilizar una contra-cimbra.

2o.- Es la pendiente máxima que los trabajadores, sin necesidad de escalinatas, pueden subir.

Con este valor de ϕ_o Substituído en 6.2, 7.2 y 8.2 se obtiene:

(6)

$$\begin{cases} A = 0.60507\left[.69813 - \phi - sen(\phi_o - \phi) - 0.23654(\cos\phi - 0.76604)\right] \\ B = 2.13712\left\{.23396\left[1 - 1.55572\,sen\phi\right] - (\cos\phi - .76604)\right\} \\ C = 0.12500\left[4.27423(\cos\phi - \cos\phi_o) - 2.42032(sen\phi_o - sen\phi)^2\right] \end{cases}$$

Se indica en la Tabla 1.2 valores de A, B y C para variaciones de 5° en el valor de ϕ

TABLA 1.2.

ϕ	A	B	C
0	0	0	0
5	-0.01038	-0.05965	0.02956
10	-0.01703	-0.10260	0.05030
15	-0.02031	-0.12850	0.06219
20	-0.02058	-0.13716	0.06541
25	-0.01827	-0.12850	0.06028
30	-0.01378	-0.10260	0.04725
35	-0.00753	-0.05965	0.02693
40	0	0	0

Subatituyendo las literales A, B y C en la expresión de M ϕ, o:

$$\bar{M}\phi,o = q\,l^2\left[\frac{A+B\frac{h}{l}}{.36398+2\frac{h}{l}}+C\right] \qquad 9.2$$

(7) y

$$H = q\,l\left[\frac{.18399+2.74744\frac{h}{l}}{.36398+2\frac{h}{l}}-.68686\right] \qquad 10.2$$

Se incluye la tabla 2.2 de distintos valores de H en función de $\frac{h}{l}$.-
Se puede observar en la tabla que para una relación del peralte h de la trabe al claro l (h/l) igual 0.048 el valor de H es cero. Es decir que el momento M ϕ, o en la clave no necesita corrección por ser cero.

Para valores menores de h/l el valor de H es negativo, es decir, que habrá que jalar horizontalmente el cascarón en el arranque con una fuerza H para nulificar el momento en la clave. Este hecho es difícil de creer si los cascarones se pretenden comparar con los arcos; sin embargo, se ha comprobado la inversión del signo de H en experiencias efectuada en E.E.U.U.

Desde un punto de vista empírico debe hacerse notar que el valor real de h/l para que H se nulifique no tiene por que ser exactamente 0.048; lo cual conduce a tomar medidas adecuadas, por ejemplo considerar un elemento que resista una fuerza horizontal mínima que obre en los dos sentidos. cuando el valor de h/l sea próximo a 0.048.

Sin tomar en cuenta, por ahora, la interacción del terreno, la principal fuente de error, en lo deducido hasta ahora, es la suposición de la distribución de la fuerza cortante. Al principio de este capítulo se dijo que la T' tiene un valor constante desde el centro de tensión hasta el de compresión (Ver Ref. 1 Pág. 258. Fig. 160.3) lo cual es -

sólo una burda aproximación que posteriormente se podrá afinar cuando en algún laboratorio experimental se logrén hacer mediciones adecuadas de la tensión diagonal.

Cabe indicar que los métodos elásticos adolecen también de este importante defecto y por lo mismo no existe ninguna justificación para aceptar soluciones tan elaboradas que en ningún caso puede afirmarse son más aproximadas que las obtenidas plásticamente.

No obstante, como ya se indicó, no se ha encontrado ningún método adecuado para encontrar las deformaciones del cascarón. Si sólo interesa el orden de estas se puede recurrir a la teoría elástica.

TABLA 2.2.

h/l	[illegible]	h/l		h/l		h/l		h/l	
0000	- 18137	0038	-03140	0076	.07441	0114	.15303	0.152	21377
0001	-.17661	0.039	-0 2814	0077	07676	0115	15484	0.153	21518
0 002	-.17194	0.040	-0 2492	0.078	.07911	0 116	.15661	0.154	.21659
0 003	-.16729	0.041	-.0 2172	0.079	.08145	0.117	.15839	0.155	21797
0.004	- 16269	0.042	-.01857	0.080	.08376	0.118	16015	0.156	.21937
0.005	- 15814	0.043	-.01543	0.081	.08604	0.119	.16191	0.157	.22075
0.006	-.15367	0.044	-.01232	0.082	08832	0120	.16363	0.158	.22212
0.007	-.14921	0.045	-.00925	0.083	.09058	0.121	.16536	0.159	.22347
0.008	-.14481	0.046	-.00619	0.084	.09281	0122	.16708	0.160	.22483
0.009	-.14044	0.047	-.00316	0.085	09504	0 123	.16879	0.161	.22618
0010	-.13613	0.048	0000	0.086	.09726	0124	.17047	0162	22753
0.011	-.13188	0.049	.00280	0087	.09945	0.125	.17216	0.163	.22885
0.012	-.12766	0.050	00576	0 088	.10161	0126	17383	0.164	.23018
0013	-12347	0.051	00868	0.089	10378	0.127	.17548	0.165	.23149
0.014	-.11936	0.052	.01159	0090	.10593	0.128	.17714	0.166	.23281
0.015	- 11526	0.053	.01445	0.091	10806	0129	.17878	0.167	.23410
0.016	-.11120	0.054	.01730	0.092	11016	0.130	.18041	0.168	.23539
0.017	-.10718	0.055	.02013	0.093	.11226	0.131	.18202	0.169	23668
0.018	-.10323	0.056	02294	0.094	11435	0 132	18363	0.170	.23795
0019	-.09929	0.057	.02570	0 095	11642	0133	.18523	0 171	23928
0.020	- 09540	0.058	02846	0096	11846	0 134	18682	0172	24050
0.021	- 09154	0.059	03120	0.097	.12050	0.135	.18839	0 173	.24176
0.022	-.08774	0.060	.03391	0.098	12253	0.136	18996	0.174	24300
0023	-.08395	0.061	.03659	0099	.12454	0.137	.19152	0 175	.24424
0.024	- 08020	0.062	.03926	0 100	.12652	0138	.19307	0.176	.24548
0025	-.07649	0.063	.04190	0 101	12850	0.139	.19460	0 177	.24672
0026	- 07284	0.064	.04453	0.102	13048	0 140	19613	0 178	.24793
0.027	-.06920	0.065	.04712	0.103	.13242	0.141	.19766	0 179	.24915
0.028	- 06559	0.066	.04970	0 104	13436	0 142	.19917	0.180	25036
0.029	- 06202	0.067	05227	0.105	.13629	0.143	.20066	0 181	.25157
0.030	-.05850	0.068	.05481	0 106	.13820	0 144	20216	0 182	25275
0 031	- 05500	0.069	05731	0 107	14011	0145	20364	0 183	.25395
0.032	- 05153	0.070	.05982	0.108	14198	0.146	20512	0 184	.25513
0.033	- 04809	0.071	.06230	0.109	14386	0 147	.20657	0 185	.25631
0.034	- 04470	0.072	.06476	0.110	.14572	0 148	.20803	0.186	25747
0.035	- 04132	0.073	.06719	0 111	14757	0 149	.20948	0.187	25864
0036	- 03798	0.074	06961	0.112	14939	0150	21092	0.188	25980
0037	- 03466	0.075	.07202	0 113	15122	0151	.21234	0189	26096

h/l		h/l		h/l		h/l		h/l	
190	.26209	340	38416	620	49884	1950	61275		
191	.26323	.345	38703	.640	49463	2000	61445		
192	26437	350	38984	660	49920	2050	61607		
193	26550	.355	39261	.680	50355	2100	61762		
194	26661	360	39533	.700	50771	2150	.61910		
195	.26773	.365	.39800	.720	51168	2200	.62053		
·196	.26884	.370	40061	740	51548	2250	62189		
.197	.26995	375	.40318	760	51912	2300	.62320		
.198	.27103	380	.40570	·780	52261	2350	62445		
.199	.27213	385	40818	800	.52595	2400	.62566		
.200	.27322	390	.41062	820	52917	2450	.62683		
205	.27857	.395	.41301	.840	53225	2500	.62795		
210	28376	.400	41537	.860	53522				
.215	28884	405	41767	.880	.53808				
220	.29380	410	.41995	900	54083				
.225	29862	415	42219	920	54347				
.230	30333	.420	.42438	940	.54603				
.235	.30794	425	.42654	.960	.54850				
240	.31243	430	42867	980	.55088				
245	31681	435	43077	1 000	55318				
250	32109	440	43282	1 050	55860				
255	32528	445	.43485	1 100	56361				
260	32936	450	43684	1 150	56824				
265	33336	455	.43881	1 200	57253				
270	.33728	460	44074	1 250	.57652				
275	.34111	465	44264	1 300	.58024				
280	34484	470	44451	1 350	58372				
.285	34850	475	.44635	1 400	58698				
290	35209	.480	.44817	1 450	59004				
.295	35559	485	44996	1 500	59292				
300	35903	.490	45173	1 550	.59563				
305	36240	495	45346	1 600	59819				
.310	36570	500	45517	1 650	60061				
315	36893	520	46177	1 700	60290				
320	.37210	540	46801	1 750	60507				
325	37520	560	47391	1 800	60714				
330	37825	580	47950	1 850	60910				
335	38123	600	48480	1 900	61097				

Se resuelve a continuación un ejemplo que representa un caso frecuente en cimentación de edificios de oficinas o departamento de 6 pisos.

E J E M P L O:

Claro entre ejes	l =	700 cm.
Contratrabe	h =	80 cm.
Arranque	ϕ_o =	40^o
Reacción del terreno	q =	6 t/m^2

Supóngase el momento flexionante longitudinal despreciable. Es decir que se puede suponer concentrada la compresión en la clave;

TABLA 32

ϕ	$A+B\frac{h}{I}$	$A+B\frac{h}{I}/59261$	[ ]	$\bar{M}\phi_o$	$M\phi$
0	0	0	0	0	-.685
5	-.01720	-.02902	+.00054	.159	-.528
10	-.02878	-.04853	+.00177	.520	-.165
15	-.03500	-.05906	.00313	.920	+.235
20	-.03626	-.06119	.00422	1.241	+.556
25	-.03296	-.05562	.00466	1.370	+.685
30	-.02551	-.04305	.00420	1.235	+.550
35	-.01435	-.02421	.00272	.800	+.115
40	0	0	0	0	-.685

En la tabla 3.2 se indican las operaciones hasta obtener $M\phi$, o. La columna $M\phi$ (momentos transversales finales) se han obtenido desplazando la corrección para hacer los momentos iguales en tres puntos: $\phi = 0 - M\phi = -.685$; $\phi = 25^o - M\phi = +.685$; $\phi = 40^o - M\phi = -.685$ tm/m

$$M\phi = M\phi,o - \frac{M\phi,\ o\ máx.}{2}$$

5.2 El diseño del cascarón, para sus efectos transversales deberá incluir aparte de los momentos tranversales otros efectos: el de las fuerzas normal $N\phi$ y el de la cortante $Q\phi$. A continuación se desarrollan expresiones para estos efectos.

a) Fuerza normal $N\phi$.

En la figura 4.2 se indican las fuerzas que obran en una sección cualquiera, Nz, Ny y en la orilla la perturbación H.

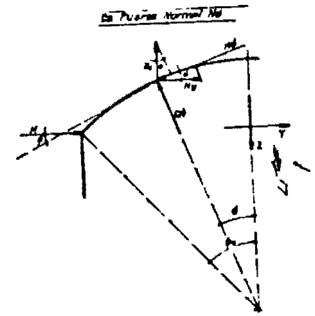

Proyectando las fuerzas Nz, Ny y H sobre la tangente al punto, determinado por el ángulo ϕ, se obtiene la expresión: $N\phi = Ny\cos\phi - Nz\,sen\,\phi + H\cos\phi$

Substituyendo los valores de Nz y Ny dados por las expresiones 2.2 y 3.2:

$$N\phi = TR\,sen\phi_o\cos\phi - T'R\,sen\phi\cos\phi - qR\,sen\phi_o\,sen\phi + qR\,sen^2\phi + T'R\cos\phi_o\,sen\phi\left(1-\frac{sen\phi}{sen\phi_o}\right) + H\cos\phi - Th\,sen\phi$$

$$(8)\quad N\phi = \frac{ql}{2}\left\{\frac{sen(\phi_o-\phi) + \frac{\phi_o - sen\phi_o}{1-\cos\phi_o}\cos\phi + \frac{2\frac{h}{l}sen^2\phi_o}{1-\cos\phi_o}\cos\phi + 2\frac{h}{l}sen\phi\,sen\phi_o}{1-\cos\phi_o + 2\frac{h}{l}sen\phi_o} - \frac{sen\phi_o}{2(1-\cos\phi_o)}\cos\phi - \left(1-\frac{sen\phi}{sen\phi_o}\right)sen\phi\right\}$$

Haciendo:

$$D = sen(\phi_o - \phi) + \frac{\phi_o - sen\phi_o}{1-\cos\phi_o}\cos\phi$$

$$E = \frac{sen\phi_o}{2(1-\cos\phi_o)}\cos\phi + \left(1-\frac{sen\phi}{sen\phi_o}\right)sen\phi$$

$$F = 2\,sen\phi_o\left[\frac{sen\phi_o}{1-\cos\phi_o}\cos\phi + sen\phi\right]$$

Si $\phi = 40^o$

$$N\phi = \frac{ql}{2}\left\{\frac{D + \frac{h}{l}F}{.23396 + 1.28558\frac{h}{l}} - E\right\} \qquad 11.2$$

Las literales D, E y F para $\phi_o = 40^o$ tienen los valores indicados en la Tabla 4.2.

TABLA 4.2.

ϕ	D	ξ	F
0	.87935	1.37570	3.53205
5	.80922	1.44381	3.63066
10	.73295	1.47957	3.70166
15	.65110	1.48151	3.74444
20	.56429	1.45088	3.75873
25	.47320	1.38976	3.74444
30	.37850	1.30074	3.70166
35	.28092	1.18703	3.63066
40	.18120	1.05231	3.53205

Ejemplo. Se encontrarán ahora los valores de la fuerza normal N ϕ — del ejemplo propuesto anteriormente. Estos valores se presentan tabulados en la Tabla 5.2

TABLA 5.2.

ϕ	$D+H/I\ F$	$\frac{D+H/I\ F}{[illegible]}$	[ ]	$N\phi$ (T/m)
0	1.28301	3.36843	1.99473	41.89
5	1.22417	3.21397	1.77016	37.17
10	1.15601	3.03502	1.55545	32.66
15	1.07905	2.83297	1.35146	28.38
20	.99387	2.60934	1.15846	24.33
25	.90115	2.36591	.97615	20.50
30	.80158	2.10444	.80370	16.88
35	.69587	1.82695	.63992	13.44
40	.58488	1.53556	.48321	10.15

Observando los valores de la columna N ϕ se ve que el valor máximo está en la clave ($\phi = 0$) y el mínimo en el arranque ($\phi = \phi_0 = 40^\circ$). El diseño de las secciones del cascarón se hará considerando el momento M ϕ y la fuerza N ϕ (la acción Q ϕ resulta despreciable como se verá más adelante). Dentro de ciertos límites, para un valor constante de M ϕ, las secciones del cascarón resultan más económicas para los -

valores mayores de N ϕ; como se puede deducir del diseño de columnas a flexo-compresión en las que la acción de los momentos flexionantes es mucho más desfavorables que el de la carga axial. Esto conduce a pensar en que la igualación de los momentos transversales en tres puntos no es la más económica. El procedimiento que se debe seguir, utilizando el presente método, será:

1.- Encontrar los momentos $\overline{M}\ \phi$, o,

2.- Transladar y girar la línea de corrección por tanteos, diseñando las secciones más desfavorables.

La forma de efectuar la translación de la línea de corrección ya se explicó anteriormente.

El giro de la línea correctiva se puede efectuar variando el valor de H. Las variaciones de H para llegar a la condición más favorable son pequeñas y tienen poca influencia en los valores finales de N ϕ, de manera que el giro de la línea correctiva se puede hacer sin considerar la variación de H. Encontrada la posición adecuada de la línea de corrección se procederá a afinar los valores de H y N ϕ.

b) Fuerza cortante transversal Q ϕ.

La fuerza cortante Q ϕ se puede encontrar por dos procedimientos:

1o.- Derivando la expresión de $\overline{M}\ \phi$, o y sumándole el efecto de H.

2o.- Proyectando radialmente.

Se optó por el 2o. procedimiento para que los resultados obtenidos para Q ϕ puedan servir de comprobación a los de $\overline{M}\ \phi$. Efectivamente, comparando las gráficas 1.2 y 2.2 se puede observar, para el ejemplo citado, que:

1.- La curva de Q ϕ corta a el eje horizontal "0" en dos puntos en los que M ϕ es máximo. ($\phi = 25^\circ$ y $\phi = 0^\circ$).

2.- El area bajo la curva Q ϕ, considerado como constante de integración C = - 0.685 t^m/m, dá el valor de Mϕ, en ϕ = 25°. De igual manera se obtienen dos valores de M ϕ en otros puntos. Por ejemplo, el momento en ϕ = 0° si se considera C = - 0.685 Ton^m/m será la integral $\int_{\phi_o}^{o} Q\phi \, d\phi$ que corresponde a la suma de las areas positiva y negativa bajo la curva Q ϕ. Ahora bien, en la gráfica 2.2 se aprecia " a ojo " que estas dos areas son iguales de manera que su suma será cero por tener signos contrarios. Por tanto, el valor de la integral será $\int_{\phi_o}^{o} Q\phi \, d\phi = O + C = C$ (el de la constante de integración C = -0.685 Tm/m) que es el valor de Mϕ en ϕ = 0°. El valor de C depende de la translación de la línea de corrección de $\overline{M}$ ϕ, o, y no tiene influencia directa en los de Q ϕ.

3.- El tramo de curva, de Q ϕ, de 40° a 25° es aproximadamente una línea rectà, por lo tanto la variación de M ϕ de 40° a 25° es aproximadamente parabólica.

4.- En ϕ = 12° la curva que representa Q ϕ tiene tangente horizontal, lo cual corresponde a un punto de inflexión en el diagrama de M ϕ. Como se puede apreciar en el diagrama de M ϕ.

De esta correspondencia se pueden obtener, no sólo la comprobación de la expresión y resultados de M ϕ, sino datos útiles para el trazado del diagrama de M ϕ. Por ejemplo: La curva tiene: tangente horizontal en ϕ = o y en ϕ = 25°; punto de inflexión en ϕ = 12° y variación parabólica entre ϕ = 40° y ϕ = 25°.

De acuerdo con la figura 5.2 se vé que proyectando Nz, Ny y H en dirección radiál se obtienen las siguientes expresiones:

Fuerza transversal cortante Qϕ:

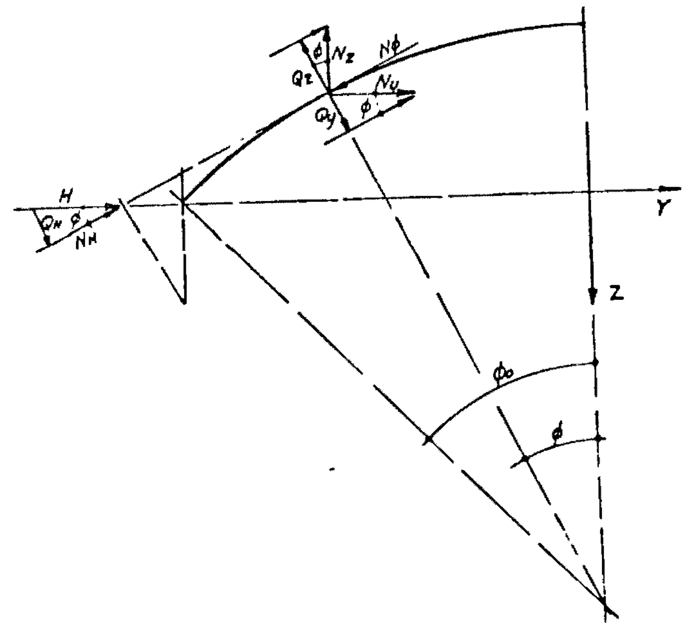

FIG. 5.2

$$
(9)\quad
\begin{cases}
Q_0 = Q_z - Q_y - Q_H \\[4pt]
Q_z = N_z \cos\phi = q\dfrac{\ell}{2\,\mathrm{sen}\,\phi_0}(\mathrm{sen}\,\phi_0 - \mathrm{sen}\,\phi)\cos\phi + q\left[\dfrac{\ell/2(\cos\phi - \cos\phi_0) + h\,\mathrm{sen}\,\phi_0}{(1-\cos\phi_0) + 2\,\mathrm{sen}\,\phi_0\,\frac{h}{\ell}}\right]\cos\phi \\[10pt]
Q_y = N_y\,\mathrm{sen}\,\phi = q\dfrac{\frac{\ell}{2}(\mathrm{sen}\,\phi_0 - \mathrm{sen}\,\phi)}{(1-\cos\phi_0) + 2\,\mathrm{sen}\,\phi_0\,\frac{h}{\ell}}\,\mathrm{sen}\,\phi \\[10pt]
Q_H = H\,\mathrm{sen}\,\phi = \dfrac{q\ell}{2}\cdot\dfrac{1}{1-\cos\phi_0}\left\{\dfrac{\phi_0 - \mathrm{sen}\,\phi_0 + 2\frac{h}{\ell}\,\mathrm{sen}^2\phi_0}{(1-\cos\phi_0) + 2\,\mathrm{sen}\,\phi_0\,\frac{h}{\ell}} - \dfrac{1}{2}\,\mathrm{sen}\,\phi_0\right\}\mathrm{sen}\,\phi \\[10pt]
Q\phi = \dfrac{q\ell}{2}\left[\dfrac{(\cos\phi - \cos\phi_0 + 2\frac{h}{\ell}\,\mathrm{sen}\,\phi_0)\cos\phi - (\mathrm{sen}\,\phi_0 - \mathrm{sen}\,\phi)\,\mathrm{sen}\,\phi - \dfrac{(\phi_0 - \mathrm{sen}\,\phi_0 + 2\frac{h}{\ell}\,\mathrm{sen}^2\phi_0)\,\mathrm{sen}\,\phi}{1-\cos\phi}}{(1-\cos\phi_0) + 2\,\mathrm{sen}\,\phi_0\,\frac{h}{\ell}}\right. \\[10pt]
\qquad\left. -\left(1 - \dfrac{\mathrm{sen}\,\phi}{\mathrm{sen}\,\phi_0}\right)\cos\phi + \dfrac{\mathrm{sen}\,\phi_0}{2(1-\cos\phi_0)}\,\mathrm{sen}\,\phi\right] \\[10pt]
\text{Haciendo:} \\[4pt]
M = \left(1 - \dfrac{\mathrm{sen}\,\phi}{\mathrm{sen}\,\phi_0}\right)\cos\phi \\[8pt]
N = \dfrac{\mathrm{sen}\,\phi_0\,\mathrm{sen}\,\phi}{1-\cos\phi_0} \\[8pt]
P = 1 - \cos(\phi_0 - \phi) \\[8pt]
T = \dfrac{\phi_0\,\mathrm{sen}\,\phi}{1-\cos\phi_0} \\[8pt]
J = \dfrac{2\,\mathrm{sen}^2\phi_0}{1-\cos\phi_0}\,\mathrm{sen}\,\phi
\end{cases}
$$

$$
Q\phi = \frac{q\ell}{2}\left[\frac{N}{2} - M - \frac{P + \frac{h}{\ell}[S-J] - T + N}{1-\cos\phi_0 + 2\,\mathrm{sen}\,\phi_0\,\frac{h}{\ell}}\right] \text{------------ } 12.2
$$

Los valores de M, N, P, T, J, y S para $\phi_0 = 40^{\circ}$, se indican en la tabla 6.2

TABLA 6.2.

ϕ	M	N	P	T	J	S
0°	1.000	0	.23396	0	0	1.28558
5°	.86111	.23947	18085	.26008	.30785	1.28068
10°	.71876	.47709	.13397	.51817	.61334	1 26605
15°	.57700	.71109	.09369	.77231	.91417	1 24178
20°	.43969	.93968	.06031	1.02058	1 20803	1.20805
25°	.31043	1.16112	.03407	1 26109	1.49272	1.16513
30°	.19238	1.37372	.01519	1.49199	1 76603	1.11335
35°	.08820	1.57588	.00381	1.71155	202592	1.05308
40°	0	1.76603	0	1.91807	2.27037	.98481

Los resultados de $Q\phi$, para el ejemplo citado antes, se presentan en la Tabla 7.2

TABLA 7.2.

ϕ	$\frac{N}{2}$	$-M+\frac{N}{2}$	N-T+P	S-J	$+\frac{h}{\ell}[S-J]$	$\overline{.38090}$	$\frac{h}{\ell}[\ ]-T+N$	$Q\phi$
0°	0	-1000	.23396	1.28558	+.14693	+1.000	0	0
5°	.11973	-.74138	.16024	.97283	+.11118	+.71257	-.02881	-.60601
10°	.23854	-.48022	.09289	.65270	+.07460	+.43972	-.04050	-.85080
15°	.35554	-.22146	.03247	32760	+.03744	+.18354	-.03792	-.79632
20°	.46984	+.03015	-.02059	0	0	+05406	-.02391	-.50211
25°	58056	+.27013	-.06590	-.32760	-.03744	-.27130	-.00117	-.02457
30°	68686	+.49448	- 10308	- 65270	-.07460	-.46647	+.02801	+.58821
35°	.78794	+.69974	-.13186	-97283	-.11118	-.63807	+.06167	+1.29507
40°	.88301	+.88301	-.15204	-1 28558	-.14693	-.78490	+.05811	+2 06031

6.2 Se han considerado hasta ahora los efectos transversales M ϕ. N ϕ y Q ϕ. En lo que sigue se tratará de explicar lo que sucede longitudinalmente y la coorrelación que guardan entre sí los efectos transversales con los longitudinales.

Para estudiar los efectos transversales se partió del análisis de una franja unitaria en la que el incremento, longitudinal, de la fuerza cortante T', equilibraba a la carga unitaria (reacción del terreno) que obraba en la franja. Posteriormente se introdujo una fuerza H con objeto de reducir los momentos flexionantes transversales. Este estudio se denomina <u>Análisis de la Acción de Arco.</u>

Faltan analizar los efectos que longitudinalmente tienen la fuerza cortante: $T = \int T' dx$ y la corrección H. Asimismo deben analizarse los efectos que resultan de la flexión longitudinal: Momento flexionante longitúdinal M, la fuerza cortante Qx (que obra radialmente en una cara x, determinada por un plano perpendicular al eje x), los momentos torsionantes Mϕ x y M x ϕ y el efecto del momento M x aplicado en todo el arco (este momento flexionante se considera actuando en un plano que contiene a las generatrices del cascarón y pasa por el centro del arco.)

El momento flexor M se puede estudiar por sus efectos en la sección: Esfuerzos de compresión o tensión N x.

En la figura 6.2 se muestran todos estos efectos actuando en un elemento de cascarón.

La teoría elástica estudia todos estos efectos conjuntamente con las deformaciones que producen. En esta teoría distintos autores, para el análisis, han propuesto una serie de simplificaciones despreciando los efectos que no tienen importancia en el diseño definitivo. El Dr. J. J. Mc Namee, Ref. 4, establece comparaciones entre los métodos

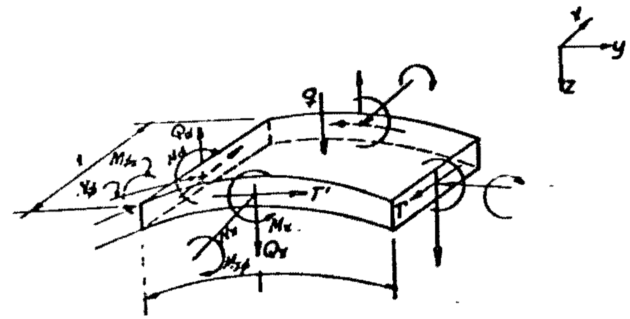

FIG. 6.2.

empleados por: Dischinger, Jakobsen, Finsterwalder, Schörer, etc., y señala las limitaciones de aplicabilidad de cada método de acuerdo con las simplificaciones empleadas.

En el presente método no se considerarán los efectos de:

1o.- Las deformaciones en general. Por lo tanto del coeficiente de Poisson que se aplica en la teoría elástica.

2o.- Los momentos torsionantes: $M_{x\phi}$ y $M_{\phi x}$. De acuerdo con el equilibrio directo hecho en cada sección en las que se han determinado la posición de los centroides de esfuerzo longitudinal, no cabe la posibilidad de que existan momentos torsionantes.

3o.- Los efectos Q_x y M_x son despreciables en toda la longitud del cascarón, excepto en la cercanía de los tímpanos cuyo efecto es puramente local, como se estudia en las tuberías para el efecto de anillos atiesadores.

Se estudiarán por tanto, sólo los efectos del momento longitudinal M- y su efecto transversal y los de T' y H. Esto comprende lo que se denomina <u>Acción de Viga.</u>

2 Se empezará por plantear el efecto longitudinal de T' y H. Lógicamente la variación longitudinal de la fuerza cortante T' es análoga a la que se establece para las vigas. Nuevamente, para mayor claridad, se recurre a una viga de sección rectangular para comparar sus características con las de un cascarón. En la figura 7.2 se muestran en a) y b) una viga y un cascarón; en a) se puede apreciar que la pendiente del diagrama de fuerza cortante, incremento V' de la fuerza cortante, tiene el valor de la carga uniforme ω . En el cascarón Fig. b), la pendiente representa la variación de la fuerza cortante, total de la semi-sección, T'k, que es igual a la carga q l, por unidad de longitud, multiplicada por una constante de proporcionalidad. En ambos casos la fuerza cortante en el apoyo es la integral del incremento V' -

ó T'k, desde el centro hasta el extremo. Los espesores del cascarón deberán revisarse para que resistan los esfuerzos cortantes. El esfuerzo cortante v se obtiene:

$$v = \frac{T'l}{2t} \qquad \text{———} \qquad 13.2$$

esta fórmula es semejante a la de trabes de concreto:

$$\tau = \frac{V}{b\,j\,d} \quad \text{en la que} \begin{cases} V = \frac{T'kl}{2} \\ b = t \\ jd = k \end{cases} \quad \text{como se ve en b) Fig. 7.2}$$

Con respecto al diseño del espesor del cascarón se tiene, por lo que se puede deducir, dos condiciones: Transversalmente la acción de M_ϕ y N_ϕ. Longitudinalmente la fuerza cortante T'k (ó T' por unidad de longitud de arco).

En las mismas figuras 7.2 a) y b), se indican esquemáticamente los apoyos. En la viga la fuerza cortante en el apoyo es vertical y queda equilibrada por la resultante vertical de las reacciones que obran en el ancho b. El trozo achurado de la viga trabaja al aplastamiento sujeto a la fuerza cortante y al propio del ancho b. Prácticamente en las vigas para la revisión del tramo apoyado, no se es tan riguroso en incluir el peso del ancho b, ya sea porque para el cálculo se tome una longitud mayor de la pieza (distancia centro a centro entre apoyos) o bien porque simplemente se desprecie el peso propio de este ancho b. Es decir, el efecto del tramo apoyado es despreciable.

En los cascarones se tiene una condición de apoyo distinta pues la cortante T'k $\frac{1}{2}$ tiene componentes vertical y horizontal y además porque el tímpano, elemento que trasmite las fuerzas normales y cortantes al apoyo, no se apoya en toda su longitud l. Además de estas componentes el apoyo deberá resistir la reacción de la fuerza correctiva H.

FIG. 7.2

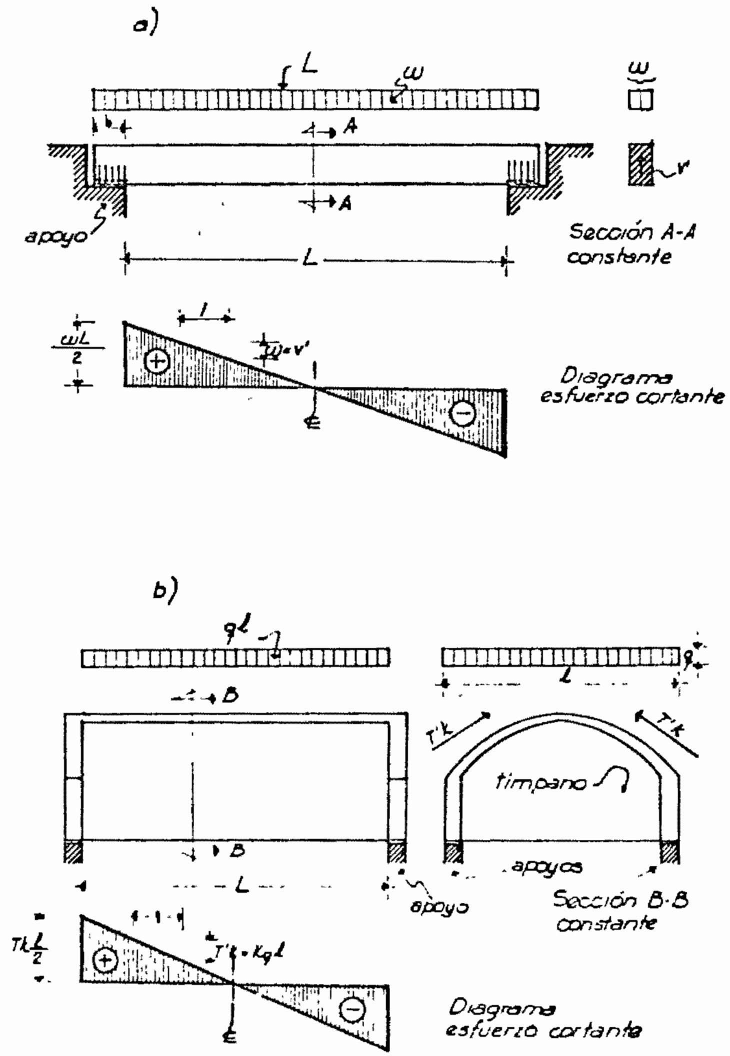
a)
L
ω
A
A
apoyo
L
Sección A-A
constante
Diagrama
esfuerzo cortante
b)
B
B
L
apoyo
tímpano
apoyos
Sección B-B
constante
Diagrama
esfuerzo cortante

8.2 Todo el borde, arranque ϕ_o, del cascarón estará sujeto longitudinalmente a la perturbación H. A esta fuerza ficticia se le denomina Coceo del cascarón. El valor de esta fuerza se puede deducir de la fórmula 10.2, o bien, con las proyecciónes horizontales de $Q\phi$ y $N\phi$ y una fuerza P, que como se demuestra a continuación es igual a H.

$$P = H = -Q\phi_o \operatorname{sen}\phi_o + N\phi_o \cos\phi_o = -2.06 \times .6428 + 10.15 \times 0.734$$
$$= 6.44\,Ton$$

$$H = 6 \times 7\left[\left[\frac{.184 + 2.747 \times .114}{.364 + 2 \times .114}\right] - .687\right] = 6.44\,Ton$$

Coceo.-

$$\therefore P = H$$

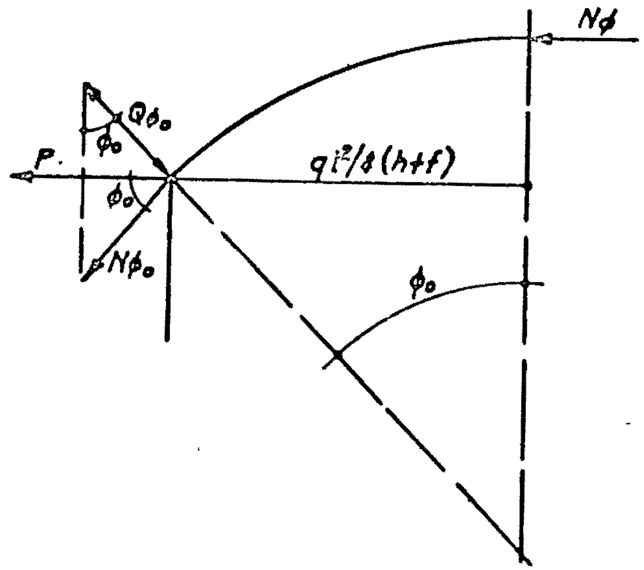

FIG. 8. 2.

).2 Encontrado el valor de H, se obtendrán las condiciones en el apoyo. - El apoyo directo del cascarón, como ya se dijo, lo constituye el tímpano. El tímpano o diafragma es un elemento rígido, en su plano, que recibe la acción del cascarón en toda la longitud del arco y la trasmite a losapoyos. La transmisión de esta fuerza puede hacerse también por medio de arcos, que se emplean más frecuentemente en las cubiertas. Las figuras 9.2ay 9.2bmuestran los tipos usuales de travesaños; tímpanos y arcos. En los emparrillados de cimentación se usan, como travesaños los tímpanos, que además de trabajar como se indicó, sirven como contratrabes en dirección perpendicular a la de las generatrices del cascarón.

Como se puede concluir del análisis de la franja unitaria la fuerza - cortante T' obra del centroide de Tensión al de Compresión. En la figura 10.2 se indica, sección X =Q en la perspectiva, la orientación - de la fuerza cortante. La acción de la fuerza cortante sobre el tímpano tiene sentido contrario, es decir, obra del centroide de compresión al de tensión. Dicho de otra forma: El incremento de fuerza cortante T', obra del centroide de tensión al de compresión de manera — que sus resultantes T'k equilibren a la de la carga 1. La acción de esta fuerza, integrada desde x=o hasta el tímpano, debe ser equilibrada en el apoyo por el tímpano con fuerzas cortantes de sentido contrario. En las figuras 9.2 y 10.2 se ha marcado, en el corte longitudinal un ancho be, ancho efectivo, achurado junto con el tímpano. De una analogía con la acción de los anillos atiesadores Lundgren (Ref.1 Pág. 133) encuentra el valor del ancho efectivo con las siguientes expresiones:

1er. Caso.- Cascarón contínuo a ambos lados del tímpano.

$$b_e = 0.76\left(1 - 0.29 m^2 \frac{t}{R}\right)\sqrt{tR} \quad \text{———} \quad 14.2$$

2º Caso.- Tímpano extremo. Fig. 10.2

$$b_e = 0.38\left(1 + 0.29 m^2 \frac{t}{R}\right)\sqrt{tR} \quad \text{———} \quad 15.2$$

en las que:

be: ancho efectivo, cm.

t: espesor total del cascarón, cm.

R: Radio, cm.

$m = \frac{2}{\phi_o}$ para cascarones sin trabe de orilla,

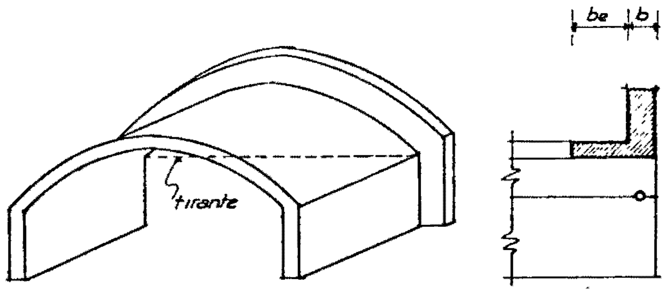

PERSPECTIVA .   CORTE LONGITUDINAL

a) *Arco por arriba del Cascarón.*

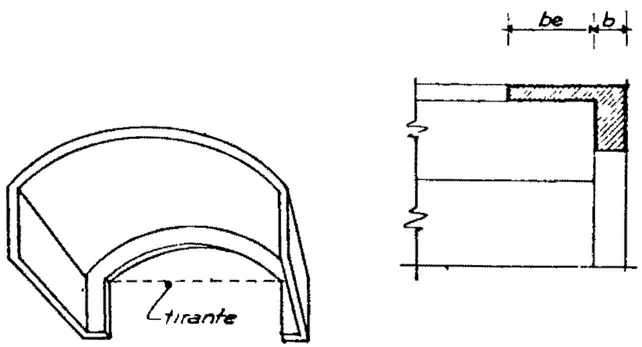

b) *Arco por abajo del cascarón*

FIG 9.2.

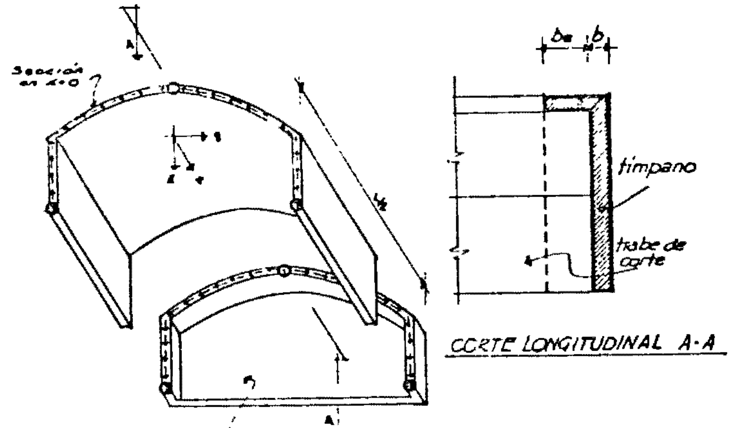

PERSPECTIVA   CORTE LONGITUDINAL A-A

FIG. 10.2

- centroide de tensión
- centroide de compresión

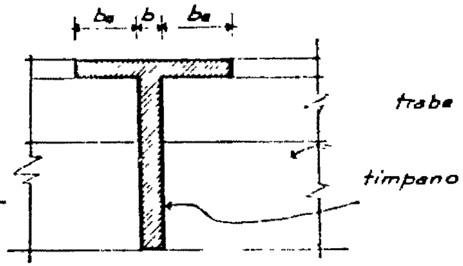

FIG 11 2

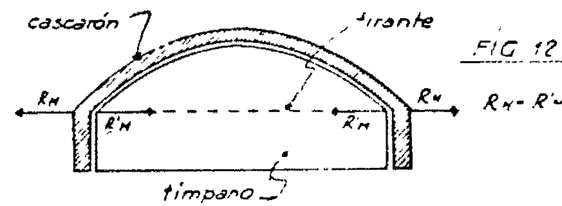

FIG 12 2

$R_H = R'_H$

$m = 1$ para cascarones con trabe de orilla.

Para el ejemplo citado:

1er. caso: Suponiendo $t = 8$ cm.

$$R = \frac{1}{2 \operatorname{sen} \phi_0} = \frac{700}{2 \times 0.6928} = 505 \text{ cm.}$$

$$be = 0.76 \left(1 - 0.29 \times 1^2 \times \frac{8}{505}\right) \sqrt{8 \times 505} = 48.1 \text{ cm}$$

2o. caso:

$$be = 0.38 \left(1 + 0.29 \times 1^2 \times \frac{8}{505}\right) \sqrt{8 \times 505} = 24.3 \text{ cm.}$$

Suponiendo que el tímpano tenga un espesor b, Fig. 11.2, el ancho total que puede considerarse con el tímpano es: b+ 2be.

Sí $b = 20$ cm.

ancho total = 20 + 48.6 = 68.6 cm.

En las fórmulas para be, el término $0.23\, m^2 \frac{t}{R}$ es generalmente despreciable, de manera que, las fórmulas pueden simplificarse. Enseguida se hace una comparación, en los dos casos presentados, con las fórmulas:

$$\left.\begin{array}{ll} be = 0.76\sqrt{tR} & \text{para el 1er caso, y} \\ be = 0.38\sqrt{tR} & \text{para el 2º caso} \end{array}\right\} \qquad 16.2$$

para el ejemplo numérico:

1er. caso:

$$be_1 = 0.76 \sqrt{8 \times 505} = 48.3 \text{ cm.}$$

2o. caso:

$$be_2 = be_1/2 = 24.2 \text{ cm.}$$

Los valores obtenidos con estas fórmulas aproximadas son bastante buenos.

Para el análisis del tímpano deberán considerarse la acción de la fuerza cortante a una distancia be del apoyo, el de la reacción, la

acción de q actuando en el ancho be y el del peso propio del tímpano. Posteriormente se hará una aplicación de los resultados anteriores para el cálculo de un tímpano.

10.2 El apoyo, además de las cargas verticales, deberá resistir las cargas horizontales que resultan de la H y de la proyección horizontal de T'x $\frac{L}{2}$. Si para el cálculo del tímpano no se requieren correcciones hiperestáticas, el valor de la reacción horizontal, estará dado por las siguientes expresiones:

$$(11) \quad \left\{\begin{array}{l} R_H = H\frac{L}{2} + \frac{q\ell^2}{4(h+f)} \cdot \frac{L}{2} \\ R_H = q\ell\frac{L}{2}\left[\frac{.18399 + 2.74744\frac{h}{\ell}}{.36398 + 2\frac{h}{\ell}} .68686\right] + \frac{q\ell L}{2} \cdot \frac{1}{2} \cdot \frac{1}{.36398 + 2\frac{h}{\ell}} \\ R_H = \frac{q\ell L}{2}\left[\frac{.68399 + 2.74744\frac{h}{\ell}}{.36398 + 2\frac{h}{\ell}} - .68686\right] \text{-----------} \quad 17.2 \end{array}\right.$$

Suponiendo que L (longitud del cascarón), sea de 9.00 mts., se obtiene para el ejemplo que se viene resolviendo:

$$(12) \quad R_H = \frac{.6 \times 7 \times 9/2}{2}\left[\frac{.68399 + 2.74744 \times .11429}{.36398 + 2 \times .11429} - .68686\right] = 94.23 \text{ Ton.}$$

Esta fuerza horizontal puede ser resistida por tirantes que vayan dentro del tímpano y anclados en sus extremos al cascarón. Ver. Fig.12.2. Si los tirantes fueran de acero grado duro, por ejemplo tor 40 de aceros ecatepec, el área de acero sería:

$f_s = 2000$ Kg./cm^2

$$A_s = \frac{P}{f_s} = \frac{94.23}{2.0} = 47.10 \text{ cm}^2 \text{ Aprox.}$$

10 var.1"

11.2 Se han mencionado anteriormente los centroides de esfuerzos, resultado de la flexión longitudinal, de compresión y tensión, los cuales han servido para orientar la línea de fuerza cortante de T'k. En el análisis transversal del cascarón, se ha supuesto que la compresión y tensión totales, longitudinales, se encuentran localizados en estos puntos. Esta hipótesis no es cierta pero si bastante aproximada para los dos casos siguientes:

1o.- Cuando el momento flexionante longitudinal M, es pequeño, que a su vez depende de dos circunstancias:

a).- Que el claro L sea pequeño.

b).- Que la carga q sea baja.

Estas dos características se pueden presentar más fácilmente en el caso de cascarones de cubiertas que en el de cimentaciones. Por ejemplo, en cimentaciones flotantés, si L representa el claro centro a centro entre dos columnas contiguas, los momentos flexionantes que obran en las contratrabes dependen más del claro total del emparrillado de cimentación que de la distancia a que se encuentren las columnas. Para fijar esta circunstancia, supóngase una estructura que tenga cuatro claros, definidos por columnas, en un eje. Un cascarón de cubierta trabajaría longitudinalmente como una estructura continua apoyada en cinco puntos. En cambio, si se trata de una bóveda invertida de cascarones, trabajaría en dos formas, una como una estructura continua en 5 apoyos fijos, las columnas, y otra como una viga que recibe las cargas de las columnas y la reacción del terreno, de un claro igual al claro total del eje (la suma de los 4 claros). Los momentos flexionantes que resultan de trabajar en la segunda forma, como viga flotante, son generalmente mayores de 100 tm (para cimentación de edificios de 6 pisos o más).

2o.- Cuando se refuerza con acero la zona de compresión. La extensión

de la zona compresiva se puede reducir apreciablemente con refuerzo a compresión, aún en las cimentaciones, de manera que se pueda obtener buena aproximación con los centroides de esfuerzos. En caso de que existan momentos flexionantes grandes se requeriría una área de acero en la zona de compresión bastante grande. Este aspecto puede conducir a dos resultados indeseables: elevar el costo de la cimentación y producir deformaciones apreciables para lograr el trabajo efectivo de este refuerzo.

Se puede concluir de lo anterior que en las cimentaciones de cascarones es conveniente estudiar la extensión de la zona compresiva. Véase la discusión que sobre la posición del eje neutro presenta el Dr. P. B. Morice, en su artículo "Investigaciones sobre estructuras de cascarones de concreto". Ref. 4, Pág. 99.

La Fig. 13.2 muestra la extensión de la zona b de compresión. En la misma figura se ha achurado el diagrama de esfuerzos cortantes T'. En este diagrama el valor de la fuerza cortante se hace variar linealmente, dentro de la zona compresiva, desde un valor máximo T', hasta cero en el centro del claro, de acuerdo con lo propuesto por Lundgren y A.L.L. Baker. Sin embargo Lundgren, Ref. 1, Pág. 258, propone que se use un diagrama equivalente en el que T' sea constante hasta el centroide de compresión (como se indica con línea llena en la misma figura). Mientras la zona compresiva no se extienda mucho, digamos que b = 100 cm., la aproximación en los momentos transversales Mø es adecuada.

Pero, si la distancia b es demasiado grande los momentos Mø dentro de la zona compresiva pueden diferir bastante de la realidad. No obstante, se puede emplear esta aproximación, en cualquier caso, como una primera aproximación para fines de anteproyecto.

Extensión de la zona compresiva

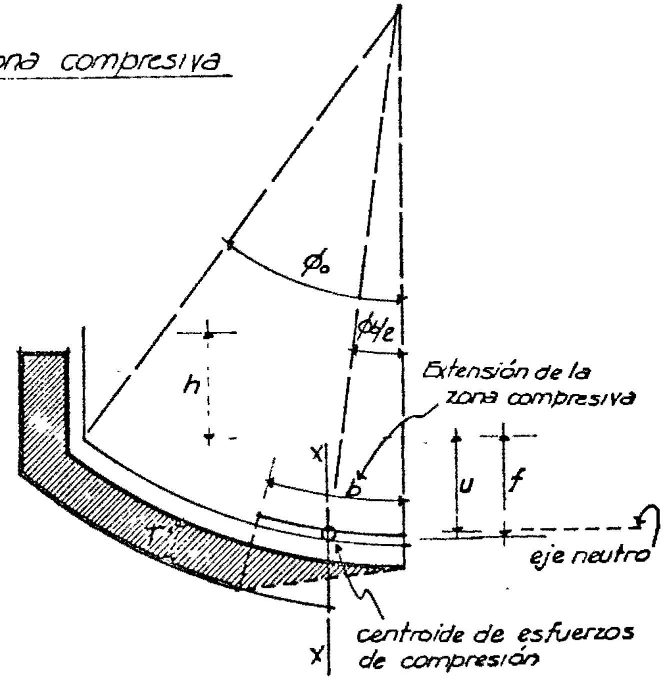

FIG. 13.2.

La extensión de la zona de compresión afecta simultáneamente el trabajo transversal del cascarón, al aumentar T', y el longitudinal al reducir el brazo de palanca del par resistente de la flexión longitudinal. Por esta razón, como anteriormente se indicó, puede pensarse en reforzar la zona de compresión para reducir la zona compresiva. El efecto de reducir la zona de compresión se puede concluir de lo siguiente:

1o.- Aumenta el brazo de palanca por lo cual:

a).- Disminuye la cantidad de refuerzo en flexión longitudinal,

b).- Aumenta la resistencia a la fuerza cortante, disminuyendo a la vez el valor de la fuerza cortante.

2o.- Se obtiene mejor aproximación, con el método de los centroides, para la obtención de $M\phi$, $N\phi$ y $Q\phi$.

Se había señalado que el empleo del refuerzo, a compresión podía encarecer el costo de la cimentación (como sucede en las trabes doblemente reforzadas). Pero ahora se han establecido las ventajas que puede acarrear el concentrar los esfuerzos de compresión. Para el diseño definitivo de los cascarones, como en general se hace en el diseño estructural, habrá que proceder por tanteos "pesando", las circunstancias favorables y desfavorables que gravan el análisis y adoptando de acuerdo con el criterio del calculista una de las soluciones posibles para la estructura. Como se puede concluir de la práctica y del análisis de costos un diseño económico no siempre es el que obtiene la mínima cantidad de material, pues la economía de una construcción está afectada por una serie de factores independientes de la teoría, por ejemplo: Facilidad y rapidez de ejecución, costo de mano de obra, precio de materiales, etc.

Las expresiones obtenidas anteriormente, cuando la zona de compresión se extiende apreciablemente, dejan de ser aplicables y deberán obtenerse otras que tomen en cuenta la posición del eje neutro, como lo hacen Ernst, Marlette y Berg en su artículo sobre "Teoría de la resistencia última y pruebas de cubierta de cascarones cilíndricos largos". Ref.11, las fórmulas necesarias para tomar en cuenta la posición del eje neutro son un poco más complicadas que las obtenidas en el presente trabajo.

Las fórmulas presentadas en este capítulo como las que se mencionan de la Ref. 11, sólo resuelven un caso particular de cascarones cilíndricos sujeto a las siguientes condiciones:

a).- Que el arranque tenga una pendiente definida por el ángulo $\phi_o = 40^\circ$.

b).- Que la sección sea simétrica, es decir que el centroide de compresión esté localizado precisamente en la clave del cascarón.

c).- Que la zona de compresión no se extienda demasiado.

El formulario necesario para cubrir la generalidad de los casos de cas

carones resulta excesiva y complicada, por lo cual, con las ideas fundamentales del criterio plástico se presenta en el siguiente capítulo un método numérico cuyo campo de aplicación no sólo cubre los casos frecuentes de cascarones cilíndricos, sino que se extiende al estudio de las deformaciones.

En las fórmulas de este capítulo no se consideró la acción del peso propio, puesto que el orden de cargas que representa la reacción es bastante mayor y puede considerarse despreciable su efecto. En todo caso el cálculo, sin considerar el peso propio, resulta del lado de la seguridad.

12.2 Por último se presenta en este capítulo la gráfica 3.2 que sirve para diseñar el refuerzo transversal del cascarón, cuando las secciones están sujetas a la fuerza normal $N\phi$ y el momento $M\phi$. Como se vé en la figura de la parte superior de la gráfica, el refuerzo está colocado a la mitad del peralte t de la sección.

La incertidumbre en la distribución de la T' conduce a pensar que la extensión de los momentos transversales $M\phi$, de un mismo signo es bastante indeterminada por lo cual se puede presentar inversión de signos en los momentos calculados, en el contorno en el que la gráfica de $M\phi$ cambia de signo.

Además la colocación del refuerzo en esta forma resulta más sencilla.

Lundgren discute este mismo asunto en la Pág. 296 de la Ref. 1 y cita la posibilidad de que en los cascarones calculados con base en la teoría elástica pueden resultar menos afectados puesto que la reducción de los momentos isostáticos $M\phi$, o con las perturbaciones de orilla son menores, es decir, que se trabaja en el diseño con momentos $M\phi$ mayores que en la teoría plástica. Esto no parece muy razonable cuando se piensa que la teoría elástica utiliza una distribución de la derivada de la fuerza cortante Nxø, equivalente a la T', que lo más probable - es que tenga que ver muy poco con la realidad. Sin embargo nada se podrá asegurar hasta que no se dispongan de mayor número de pruebas de laboratorio.

Los datos de las curvas de la gráfica 3.2 se obtuvieron de acuerdo con el método planteado por Ch. S. Whitney, para el diseño plástico de — piezas a flexo-compresión. Ref. 12.

Para el estudio del porcentaje de acero se ha dividido el análisis en tres etapas de acuerdo con la posición que puede tener el eje neutro.

La distribución de los esfuerzos de compresión se ha supuesto constante con un valor de $f_c = 0.85 f'_c$ de acuerdo con lo establecido por — Whitney en la Ref. 12. La sección sujeta a la fatiga $0.85 f'_c$ en el concreto y a la de fluencia, o límite elástico, fy en el acero estará trabajando a su máxima capacidad. (Resistencia última).

Posteriormente para el trazado de las curvas se adoptaron dos factores de seguridad, como se explica en la Ref. 10.

Factor de seguridad de carga:

Coeficiente de seguridad para la carga muerta: 1.20

Coeficiente de seguridad para la carga viva: 2.00

Coeficiente de seguridad para carga accidental: 1.50

Se deberá usar un factor de seguridad que sea la combinación de éstos según su importancia y frecuencia.

Se optó por un coeficiente de seguridad en la carga:

F.s. carga = 2.0

El factor de seguridad total estará influenciado por otros conceptos y su valor empírico puede representarse.

F.s. Total: = F.s. carga x F.s. resistencia de materiales x F.s. por- discrepancias entre el cálculo y la ejecución.

El factor de seguridad de carga ya se estableció $F.s._1 = 2.0$.

El F.s de la resistencia de los materiales será menor siempre para el acero que para el concreto pudiéndose comprobar que los resultados de ensayos en probetas de acero dan menores discrepancias en el acero que en el concreto. Sin embargo suponiendo que se tiene un control adecuado de la resistencia del concreto en la obra las discrepancias en la - resistencia del concreto pueden quedar incluídas en el último Factor - de Seguridad denominado:

F.S. para las discrepancias del cálculo y la ejecución.

En general aún el cálculo bastante detallado es insuficiente para establecer una relación real entre la hipótesis y la realidad. Por otro - lado una obra siempre adolece de defectos en la ejecución. Se pueden citar como ejemplo: errores en la colocación del refuerzo, en las dimensiones de las piezas, etc.,

Así el factor de seguridad que se adopta para cubrir este aspecto se supone de 1.25 para el concreto y 1.00 para el acero.

Con esto resultan dos factores de seguridad:

Para el concreto:)Fallas a compresión).

Fs total = 2 x 1 x 1.25 = 2.5

Para el acero (fallas a tensión)

Fs total = 2 x 1 x 1 = 2.0

Estos factores de seguridad se ven apropiados si se comparan con los determinados para las condiciones planteadas por A.L.L. Baker en su libro "The ultimate - load theory applied to the design of reinforced and prestressed concrete frames". Baker presenta en la Tabla I, pág. 5, de su libro una serie de valores para distintos acontecimientos en la ejecución y vida útil de la estructura. El valor del factor de seguridad se valúa de la expresión: $F = \frac{\Sigma W}{10} + 1$ en que los términos W representan los distintos aspectos que se "pesan" según su importancia.

TABLA.- Condiciones que controlan la adopción del factor de seguridad.

CONSIDERACIONES	Valores de W para las condiciones más adversas:
1.- Importancia de la falla (humana o económica)...	4.0
2.- Ejecución....................................	2.0
3.- Condiciones de carga.........................	2.0
4.- Importancia del miembro en la estructura.......	0.5
5.- Posibilidad de falla.........................	1.0
6.- Reducción en la resistencia..................	0.5
	$\Sigma W = 10.0$

Para la elaboración de esta Tabla se han supuesto:

1.- Factor de seguridad = $\frac{\text{carga última}}{\text{carga de trabajo}}$

2.- Los cálculos están hechos por la teoría plástica y los resultados tienen un error máximo del 15% cuando la resistencia, carga y condiciones de apoyo y excentricidad se han supuesto correctamente.

3.- Los cálculo están basados en los valores límites aceptables de:

1.3 Se presentará un procedimiento basado en el curso de METODOS NUMERICOS. impartido por el Dr. Emilio Rosenblueth en la Escuela Libre de Postgraduados en 1956.

No se han aplicado estos métodos al análisis de cascarones, sin embargo se procede a adoptar los empleados para el estudio de arcos con algunas modificaciones fundamentales.

La teoría general del análisis numérico se explicará a partir del estudio de las cargas, momentos, flechas, etc. de una viga de eje longitudinal recto.

2.3 Supóngase la viga de la figura 1.3 .

Determinado el valor de la reacción R_1 el valor de la fuerza cortante en cualquier punto será:

$$Vx = R_1 - \sum_1^n P_n$$

Por ejemplo en la sección x, de la figura:

$$Vx_1 = R_1 - P_1 - P_2$$

El momento flexionante en la sección (3):

$$M_3 = R_1 (\Delta X_1 + \Delta X_2 + \Delta X_3) \quad - \quad P_1 \; (\Delta X_2 + \Delta X_3) \; - \; P_2 \Delta X_3$$

$$= R_1 \Delta X_1 + (R_1 - P_1) \Delta X_2 + (R_1 - P_1 - P_2) \Delta X_3$$

Los términos dentro del paréntesis representan la fuerza cortante en los tramos (o) a (1), (1) a (2) y (2) a (3) si ésta en cada tramo se representa por V_1, V_2 y V_3, el momento flexionante estará dado por:

$$M_3 = V_1 \Delta X_1 + V_2 \Delta X_2 + V_3 \Delta X_3$$

$$Mn = \sum_1^n Vn \Delta Xn$$ que es una expresión conocida en Estática $M = \int Vdx.$

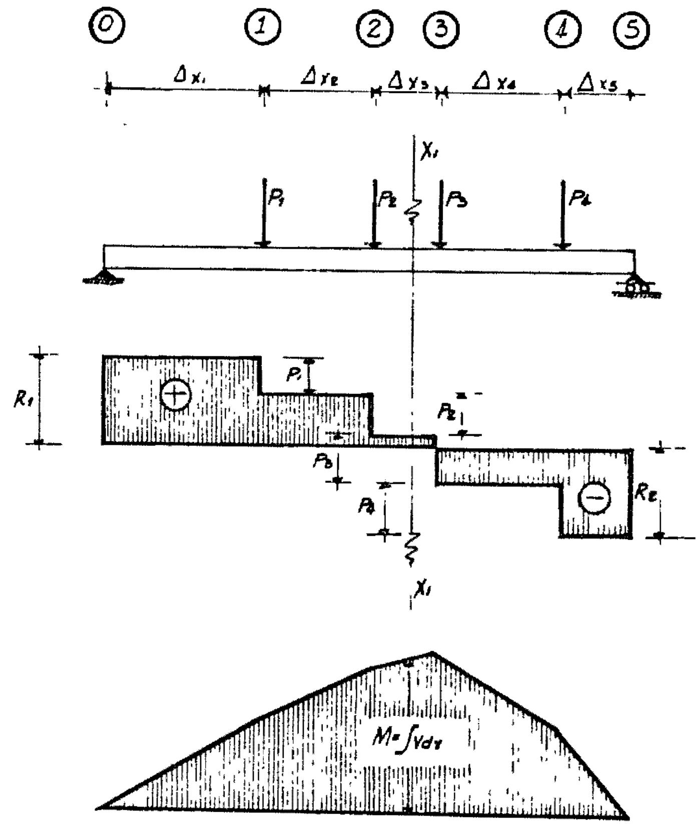

FIG. 1.3.

la expresión de la fuerza cortante $V_x = R_1 - \sum_1^x F_n$ tiene el término constante R_1, que se puede representar por ejemplo por C

$V_x = C - \sum_1^x F_n$ Para determinar la fuerza cortante en una sección cualquiera x deberá determinarse el valor de C.

Por lo tanto la variación de la fuerza cortante, no depende del valor de C sino del sistema de fuerzas que obran en la viga. Esto proporciona una primera idea para el análisis de vigas, por ejemplo, resolver la fuerza cortante a partir de un valor arbitrario de C que posteriormente se puede corregir satisfaciendo condiciones de frontera para el momento flexionante. Supóngase un valor arbitrario de $C = C_1$ el valor de la fuerza cortante sin corregir estará dado por:

$V_x^1 = C_1 - \sum_1^x F_n$ el valor correcto de V será

$V_x = C_1 + e - \sum_1^x F_n$ en la que e es el error en fuerza cortante.

El momento flexionante se puede expresar:

$$M_x^1 = \sum_1^{n=x} V'_n \, \Delta X_n = \sum_1^{n=x} \left(C_1 - \sum_1^x F_n\right) \Delta X_n = C_1 \sum_1^{n=x} \Delta x_n - \sum_1^{n=x} \left(\sum_1^x F_n\right) \Delta X_n$$

$$M^1 x = C_1 X_n - \sum_1^{n=x} \left(\sum_1^{n=x} F_n\right) \Delta X_n$$

El momento real:

$$M_x = (c_1 + e)\, X_n - \sum_1^{n=x} \left(\sum_1^{n=x} F_n\right) \Delta X_n$$

Encontrando la diferencia entre $M^1 x$ y M_x:

$$\Delta M_x = e X_n$$

Como se ve el error en el momento flexionante ΔM_x tiene variación lineal definida por el producto del error e de la fuerza cortante y la abscisa X_n al punto que se va a corregir.

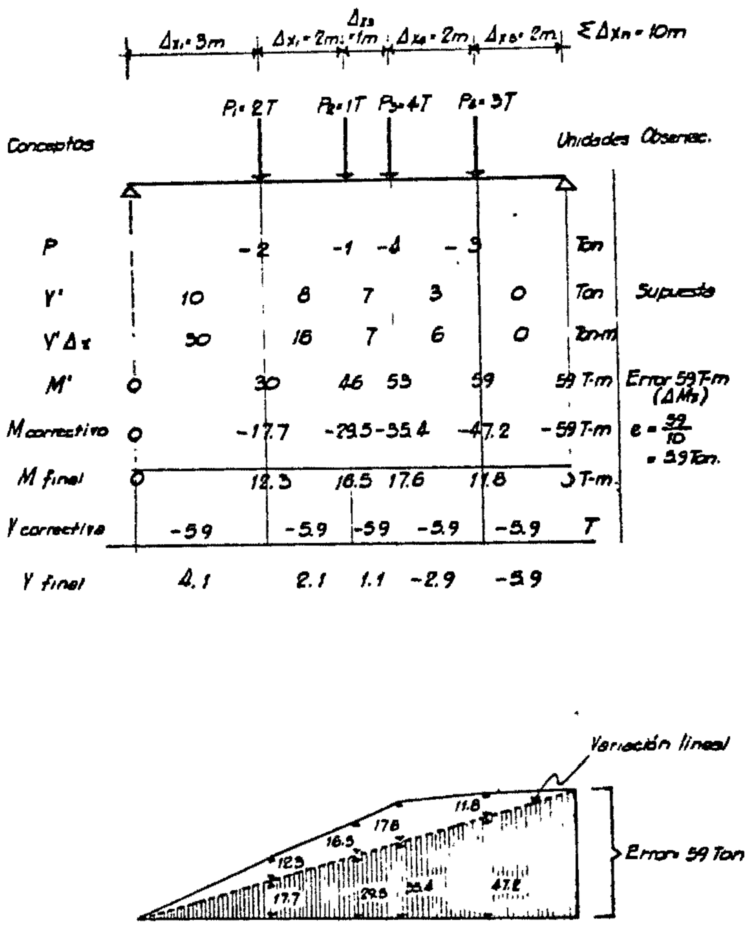

FIG. 2.3.

Es sencillo encontrar el error del momento satisfaciendo las condiciones de apoyo.

3.3 En la figura 2.3 se resuelve un ejemplo numérico con objeto de fijar las ideas expuestas.

En la figura 2.3 se indica la determinación del diagrama de momentos flexionantes en forma tabulada. En la columna izquierda denominada "Conceptos" se han marcado convencionalmente con:

P:- Las cargas concentradas, cuyos valores se indican en sus líneas de acción. Se consideran positivas cuando obran hacia arriba.

V^1:- La fuerza cortante supuesta: Se inventa un valor inicial de la fuerza cortante en el primer tablero de la izquierda y se prosigue a encontrar los valores en los demás tableros sumando acumulativamente de izquierda a derecha al valor supuesto el valor de la concentración P.

$V^1 \Delta x$:- El producto de la fuerza cortante por el intervalo en que obra.

M^1:- (momentos flexionante) Suma acumulativa de los productos $V^1 \; \Delta x$ empezando con un valor conocido, en este caso cero por estar la pieza libremente apoyada. Se llega al apoyo derecho, en donde debía ser cero, con un error de + 59 ton., como se había visto, este valor dividido por el claro dá el error, constante a lo largo de la viga, de la fuerza cortante.

M correctivo:.- Como se puede ver la corrección es lineal y se obtiene multiplicando el valor del error e = 5.9 ton por la distancia desde el apoyo izquierdo hasta el punto que se corrige.

Para encontrar las flechas de la elástica se emplea un método análogo al anterior basado en los artificios de la viga conjugada. La viga se supone cargada con el diagrama de $\frac{M}{EI}$ y los momentos flexionantes que se obtienen de esta carga corresponden a las flechas de la viga -

original, producidas por las cargas P. Es fácil establecer las semejanzas entre las dos etapas:

Analogía básica:

$\alpha = \frac{-M}{EI} \sim p$ curvatura análoga a la carga.

$\phi_x = \int_0^x \alpha_s\, ds \sim V_x = \int_0^x p_s\, ds$ Desviación de la tangente análoga la fuerza cortante.

$y_x = \int_0^x \phi_s\, ds \sim M_x = \int_0^x V_s\, ds$ flechas análogas a los momentos flexionantes.

El proceso numérico consiste en una integración sucesiva de la expresión EI $\frac{d^4y}{dx^4}$ que se establece en estática:

$$p = -EI\,\frac{d^4y}{dx^4}$$

$$V = -EI\,\frac{d^3y}{dx^3}$$

$$M = -EI\,\frac{d^2y}{dx^2}$$

$$\alpha = \frac{d^2y}{dx^2}$$

$$\phi = \frac{dy}{dx}$$

$$y = y$$

En la figura 3.3 (a) se tabulan los valores de M y en el siguiente renglón el de la curvatura $\frac{M}{EI}$. La carga irregular $\frac{M}{EI}$ se considerará concentrada en las divisiones como si ésta fuera la acción de una serie de vigas de longitudes ΔX como se ve en la parte inferior de la figura 3.3 (b). Las concentraciones de curvatura $\bar{\alpha}$ se pueden obtener del formulario dado en la figura 3.3 (c).

La suma acumulativa de las curvaturas concentradas proporciona los valores de la desviación de la tangente ϕ. Igual que para la fuerza cor

a) -

Concepto							Unidad
Δx	3	2	1	2	3		m
M	0	17.3	16.5	17.6	11.8	0	Tm
$\alpha = M/EI$	0	-17.3	-16.5	-17.6	-11.8	0	+ Tm/EI Curvatura
$\bar{\alpha}$		-73.8 -82.2	-90.6 -50.6	-51.7 -9.4	-91.6 -47.2		Tm²/6EI Curvatura concentrada
ϕ_1	300.00	144.0	2.8	-147.9	-281.7		Tm²/6EI Desviación con valor inicial supuesto
$\phi \cdot \Delta x$	900.00	288.0	2.8	-285.8	-563.4		Tm³/6EI
y_1	0	900	1188.0	1190.8	905.0	341.6	Tm³/6EI error 341.6 Tm³/6EI
y_c	0	-102.5	-170.8	-205.0	-273.3	-341.6	error en $\phi = \frac{341.6}{10} = 34.16$
y	0	797.5	1017.2	985.8	631.7	0	Tm³/6EI
ϕ_c	-34.2	-34.2	-34.2	-34.2	-34.2		
	265.8	109.8	-31.4	-177.1	-315.9		

b) -

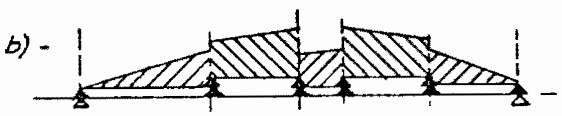

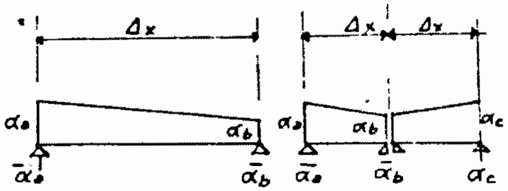

FIG 3.3.

$$\bar{\alpha}_a = \frac{\Delta x}{6}(2\alpha_a + \alpha_b) \qquad \bar{\alpha}_b = \frac{\Delta x}{6}(\alpha_a + 4\alpha_b + \alpha_c)$$

$$\bar{\alpha}_b = \frac{\Delta x}{6}(2\alpha_b + \alpha_a)$$

tante se supone un valor inicial de ϕ para el primer tablero que posteriormente se corrige al encontrar el error en la flecha, en igual forma que se hizo para el momento flexionante.

.3 Se resuelve ahora una viga en cantiliver, que es un caso más parecido al de los arcos que se presentará posteriormente. Fig. 4.3.

Para la viga conjugada se vuelven a encontrar las concentraciones del diagrama $\frac{M}{EI}$. Las fórmulas empleadas anteriormente aproximan la curva a una poligonal inscrita a dicha curva. Si la curva es de segundo — grado (parábola) como en el presente caso, pueden emplearse con mayor exactitud las fórmulas de la aproximación parabólica que se dan en la Fig. 4.3 (b).

Las sumas acumulativas, integraciones, hasta el renglón del momento flexionante se efectúan de izquierda a derecha puesto que se conoce la condición de apoyo del extremo izquierdo. Para la desviación angular ϕ y la flecha y se procede de derecha a izquierda porque se sabe que ϕ y y en el empotramiento son cero.

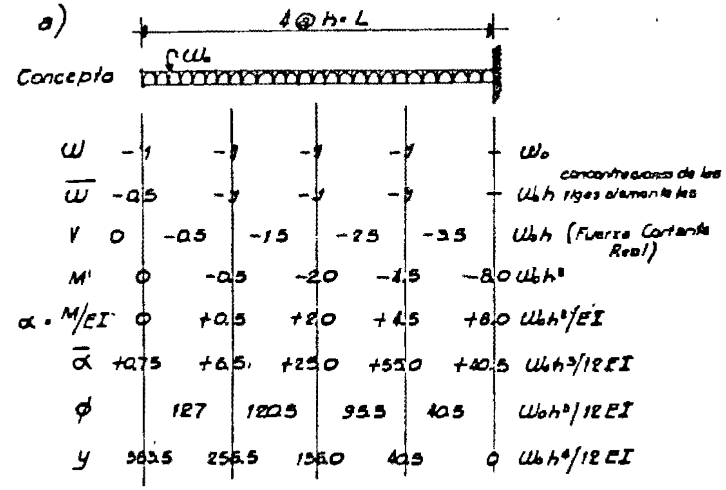

$$y_{máx} = \frac{383.5}{12} \cdot \frac{\omega_o h^4}{EI} = \frac{\omega_o L^4}{8EI}$$

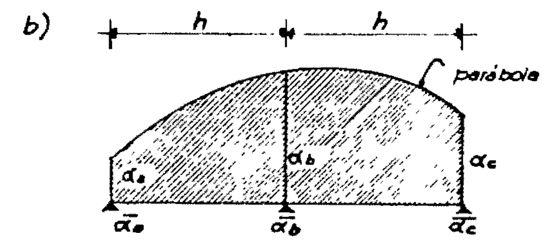

$$\bar{\alpha}_a = \frac{h}{24}(7\alpha_a + 6\alpha_b - \alpha_c)$$
$$\bar{\alpha}_b = \frac{h}{12}(\alpha_a + 10\alpha_b + \alpha_c)$$
$$\bar{\alpha}_c = \frac{h}{12}(7\alpha_c + 6\alpha_b - \alpha_a)$$

FIG. 4 3

a) Convención de Signos.

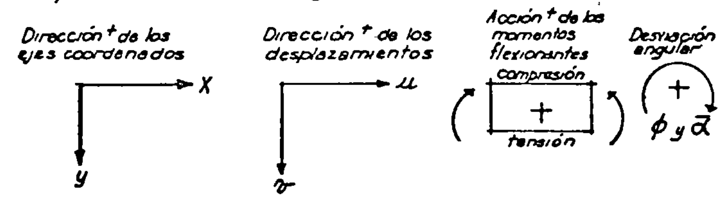

b) Tabulación del procedimiento.

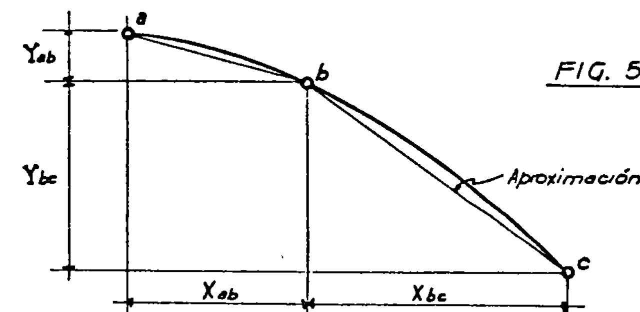

FIG. 5.3.

	a		b		c	
Geometría						
Coordenadas	X_a, Y_a		X_b, Y_b		X_c, Y_c	
Proyecciones		$X_{ab} = X_b - X_a$ $Y_{ab} = Y_b - Y_a$		$X_{bc} = X_c - X_b$ $Y_{bc} = Y_c - Y_b$		
Estática						
M	M_a		M_b		M_c	Momentos Flexionantes
α	$\alpha_a = \frac{M_a}{EI_a}$		$\alpha_b = \frac{M_b}{EI_b}$		$\alpha_c = \frac{M_c}{EI_c}$	Curvatura
$\bar{\alpha}$	$\bar{\alpha}_a$		$\bar{\alpha}_b$		$\bar{\alpha}_c$	Curvatura concentrada
ϕ	ϕ_a	$\phi_{ab} = \phi_a + \bar{\alpha}_{ab}$		$\phi_{bc} = \phi_{ab} + \bar{\alpha}_b$		Desviación angular
Δx		$-Y_{ab}\ \phi_{ab}$		$-Y_{bc}\ \phi_{bc}$		Cambio de proyección en las cuerdas
Δy		$X_{ab}\ \phi_{ab}$		$X_{bc}\ \phi_{bc}$		
u	u_a	$u_b = u_a + \Delta X_{ab}$		$u_c = u_b + \Delta X_{bc}$		Desplazamiento
v	v_a	$v_b = v_a + \Delta Y_{ab}$		$v_c = v_b + \Delta Y_{bc}$		

6.3 El procedimiento empleado para el análisis de arcos es prácticamente el mismo que se ha presentado hasta ahora. En la figura 6.3 se indica en una tabulación el desarrollo del análisis.
Los momentos flexionantes se pueden encontrar proyectando el arco y las fuerzas según los ejes xx y yy, y tratando estas proyecciones como si fueran dos vigas sujetas a las cargas proyectadas. De los momentos flexionantes obtenidos en cada una, se encuentran los del arco superponiendo los efectos.
El proceso seguido hasta ahora (para encontrar los desplazamientos) es igual al expuesto anteriormente, exceptuando lo referente a los cambios de proyección que antes no se obtenían.
A continuación se demostrará que los cambios de proyección:

$$\Delta X = -\phi Y$$

$$\Delta Y = \phi X$$

En las que se desprecian las deformaciones de la carga axial.

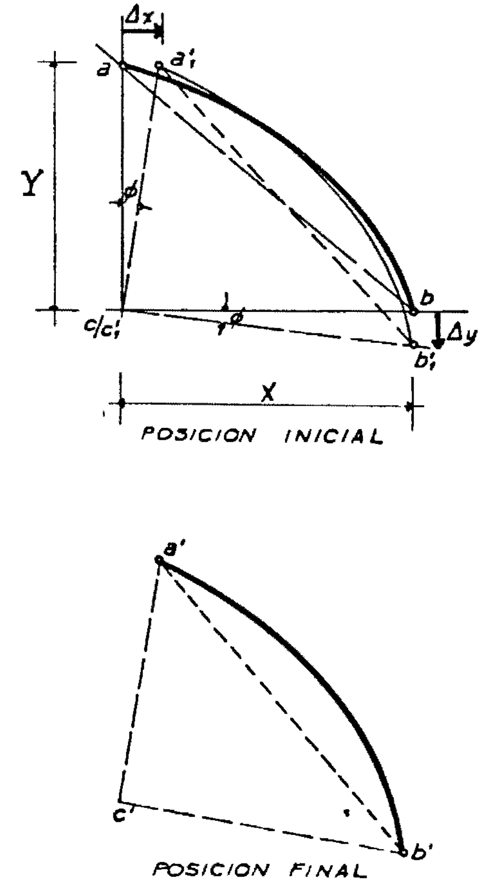

FIG. 6.3

En la figura anterior se muestra un tramo de arco ab en dos posiciones: inicial, antes de deformarse y final, después de la deformación. Como sólo interesa estudiar los desplazamientos relativos ΔX y ΔY, se traslada hasta hacer coincidir los puntos C y C'.

En esta posición se observa que:

$$\Delta x = - aa_1' = - \phi Y$$

$$\Delta y = bb_1' = \phi X$$

q.e.d.

Para visualizar este método se resuelve a continuación un ejemplo: Fig 7.3

En este ejemplo se encontrarán, proyectando radialmente y sobre la tangente la fuerza P, la fuerza cortante V y la fuerza normal N, que son conceptos que junto con el momento flexionante M, se utilizan para el diseño del arco.

La desviación angular ϕ, así como los desplazamientos u y v se encontrarán sumando de derecha a izquierda como se hizo en el cantiliver.- Para tener idea de la magnitud de los desplazamientos u y v se resuelve a continuación numéricamente el ejemplo dado:

a = 3.00 m.

P = 5000 Kgs.

EIo = 500000 Kg. M^2

u: desplazamiento horizontal:

$$u = 3514.\frac{a^3 \pi P}{10^5 E I_o} = \frac{3514 \times 3^3 \times 3.1416 \times 5000}{10^5 \times 5 \times 10^5} = 0.0298 \text{ m}$$

$$\underline{u \doteq 3 \text{ cm.}}$$

$$v = 5970.\frac{a^3 \pi P}{10^5 E I_o} = 0.0506 \text{ M.}$$

$$\underline{v \doteq 5.1 \text{ cm.}}$$

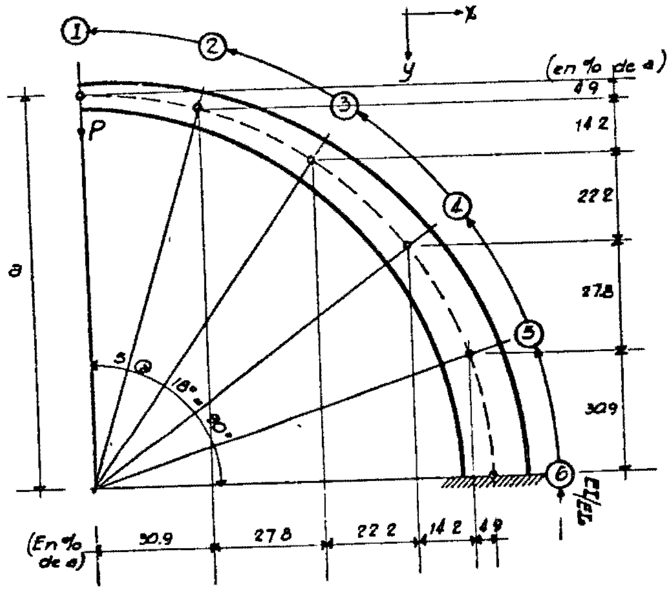

EI/EI₀

	1		2		3		4		5		6	
X		30.9		27.8		22.2		14.2		4.9		a/100
Y		-4.9		-14.2		-22.2		-27.8		-30.9		〃 〃
V	1.00		0.951		0.809		0.587		0.309		0	P (Fuerza Cortante)
N	0		-0.309		-0.587		-0.809		-0.951		-1.00	P (Fuerza Normal)
M	0		-30.9		-58.7		-80.9		-95.1		-100	aP/100
α	0		15.45		19.57		20.22		19.02		16.67	aP/100 EI
α	–		14.51		19.27		20.07		19.75		8.81	$a^2 \pi P/1000\ EI_0$
ϕ		88.41		67.90		48.83		28.58		8.81		
$\Delta x = -\phi Y$		404		962		1080		797		271		$a^3 \pi P/10^5\ EI_0$
$\Delta y = \phi X$		2550		1890		1080		407		43		
u	3514		3110		2148		1083		271			
v	5970		3420		1530		450		43			

F I G. 7. 3

6.3 Ahora se aplicara al análisis de cascarones un método, que como se dijo antes, es semejante al empleado en los arcos. En esta etapa se utilizaran dos procedimientos: uno en el que se inventan las redundancias, por ejemplo el coceo, que hagan mínimos los momentos transversales $M\phi$ y en el cual se encuentran los desplazamientos del cascarón sometido a tales condiciones predeterminadas; y el otro en el que a partir precisamente de los desplazamientos se encuentren las redundancias. Este último procedimiento no puede decirse que se base en la teoría elástica absolutamente puesto que se seguirá adoptando la misma distribución de fuerza cortante T, en la sección transversal, que se plantea en la teoría plástica. Puede decirse más bien, que se aplica un método que utiliza conceptos de ambas teorías. El hecho de que la teoría plástica no esté lo suficientemente desarrollada como para obtener las deformaciones de las piezas, obliga a aceptar algunas ideas básicas de la teoría elástica.

El primer caso se presenta en las Tablas 1.3 y 2.3 y enseguida se hace la descripción de lo efectuado en cada etapa del análisis.

Como se había denominado anteriormente el eje longitudinal por xx, se emplean ahora los ejes y y z para la sección.

Conceptos:

1 y 2-Proyección horizontal y vertical, Y y Z, de la longitud ΔS de la dovela. La suma de las proyecciones horizontales desde el punto (2) hasta el (10) debe ser igual al semiclaro $\ell/2$. La suma de las proyecciones verticales desde (0) hasta (10) debe ser f + h (flecha del arco más peralte efectivo de la trabe).

3.-La proyección horizontal de la fuerza cortante, que obra en cada intervalo ΔS, es igual al producto de la fuerza cortante T', que se supone constante y obrando a lo largo de todo el arco, por el incremento-

Concepto	ⓐ	ⓑ	ⓒ	Observaciones
1- Proyección horizontal Y	Y_{ab}	Y_{bc}		$\Sigma Y_{mn} = \ell/2$
2- Proyección vertical Z	Z_{ab}	Z_{bc}		$\Sigma Z_{mn} = f+h$
3.- Proyección horizontal en cada dovela de la Fza. cortante $= T'Y$ (Carga horizontal / dovela)	$T_{ab_y} = T'Y_{ab}$	$T_{bc_y} = T'Y_{bc}$		$\Sigma T_{mn_y} = T'\frac{\ell}{2}$
4.- Proyección vertical en cada dovela de la Fza cortante $= T'Z$	$T_{ab_z} = T'Z_{ab}$	$T_{bc_z} = T'Z_{bc}$		$\Sigma T'_{mn_z} = T'(f+h) = -\frac{q\ell}{2}$
5- Carga exterior/dovela $= qY$	$Q_{ab} = qY_{ab}$	$Q_{bc} = qY_{bc}$		$\Sigma Q_{mn} = \frac{q\ell}{2}$
6- Carga vertical total/dovela $= q_z = T'Z + qY$	$q_{z_{ab}} = Q_{ab} + T'_{ab_z}$	$q_{z_{bc}} = Q_{bc} + T_{bc_z}$		$\Sigma q_{z_{bc}} = 0$
7.- Proyecciones horizontales de las cargas de las cargas de dovela en las líneas (a), (b), (c) . $\bar{q}_y$	$\bar{q}_{ya}$	$\bar{q}_{yb} = -\frac{T_{ab_y} + T_{bc_y}}{2}$	$\bar{q}_{yc}$	$\Sigma \bar{q}_y = T'\frac{\ell}{2}$
8.- Proyecciones verticales de las cargas de dovela en las líneas (a), (b), (c) $\bar{q}_z$	$\bar{q}_{za}$	$\bar{q}_{zb} = \frac{q_{z_{ab}} + q_{z_{bc}}}{2}$	$\bar{q}_{zc}$	$\Sigma \bar{q}_z = 0$
9_1- Suma acumulativa de proyecciones horizontales N_{y_1}	$N_{y_1 ab}$	$N_{y_1 bc} = N_{y_1 ab} + q_{yb}$		
9_2- Suma acumulativa de las cargas $\bar{q}_y$ en las líneas (a), (b), (c). $\Sigma\bar{q}_y$	Σ_{a_y}	$\Sigma_{b_y} = \Sigma_{a_y} + \bar{q}_{yb}$	$\Sigma_{c_y} = \Sigma_{b_y} + \bar{q}_{yc}$	
10_1- Suma acumulativa de proyecciones verticales N_z	$N_{z ab}$	$N_{z bc} = N_{z ab} + \bar{q}_{zb}$		
10_2- Suma acumulativa de las cargas $\bar{q}_z$ en las líneas (a), (b), (c) .... $\Sigma\bar{q}_z$	Σ_{a_z}	$\Sigma_{b_z} = \Sigma_{a_z} + \bar{q}_{zb}$	$\Sigma_{c_z} = \Sigma_{b_z} + \bar{q}_{zc}$	

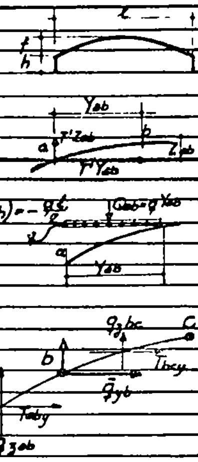

Concepto	ⓐ	ⓑ	ⓒ	Observaciones
11- Momentos transversales isostáticos $M_{\phi,o}$	$M_{\phi,oa}$	$M_{\phi,ob} = M_{\phi,oa} + \Sigma_{ay}Z_{ab} - \Sigma_{az}Y_{ab}$	$M_{\phi,oc} = M_{\phi,ob} + \Sigma_{by}Z_{bc} - \Sigma_{bz}Y_{bc}$	
12- Momento debido a la perturbación H M_H M_{Ha}		$M_{Hb} = M_{Ha} + HZ_{ab}$	$M_{Hc} = M_{Hb} + MHZ_{bc}$	
13- $M_\phi = M_{\phi o} + M_H$	$M_{\phi oa} + M_{Ha} = \bar{M}_{\phi a}$	$\bar{M}_{\phi b} = M_{\phi ob} + M_{Hb}$	$\bar{M}_{\phi c} = M_{\phi oc} + M_{Hc}$	$H = \frac{M_{\phi o}}{f}$
14.- Igualación de momentos en tres puntos M_ϕ (Momentos finales)	$\frac{\bar{M}_{\phi a} + \bar{M}_{\phi máx}}{2} = M_{\phi a}$	$\frac{\bar{M}_{\phi b} - \bar{M}_{\phi máx}}{2} = M_{\phi b}$	$\frac{\bar{M}_{\phi c} + -\bar{M}_{\phi máx}}{2} = M_{\phi c}$	
15.- Fuerza N_y corregida con H	$N_{yab} = N_{y_1 ab} + H$	$N_{ybc} = N_{y_1 c} + H$		
16.- Cos ϕ	$\cos\phi_a$	$\cos\phi_b$	$\cos\phi_c$	
17.- Sen ϕ	$\operatorname{sen}\phi_a$	$\operatorname{sen}\phi_b$	$\operatorname{sen}\phi_c$	
18.- Fuerza normal N_ϕ	$N_{\phi a}$	$N_{\phi b} = N_{yab}\cos\phi_b + N_{zab}\operatorname{sen}\phi_b$	$N_{\phi c} = N_{ybc}\cos\phi_c + N_{zbc}\operatorname{sen}\phi_c$	
19.- Fuerza Cortante Q_ϕ	$Q_{\phi a}$	$Q_{\phi b} = N_{zab}\cos\phi_b - N_{yab}\operatorname{sen}\phi_b$	$Q_{\phi c} = N_{zab}\cos\phi_c - N_{yab}\operatorname{sen}\phi_c$	

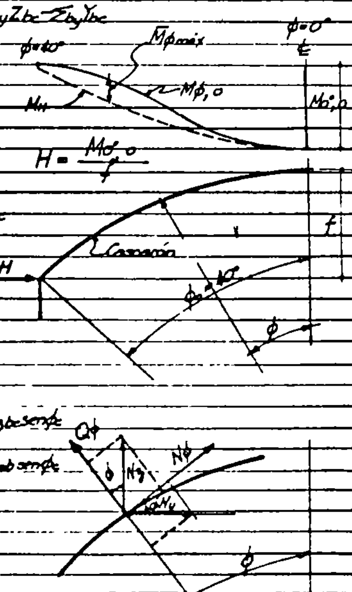

TABLA 1.3 (a)

Concepto	(a)		(b)		(c)	Observaciones
19.- Momentos transversales M_ϕ	$M_{\phi a}$		$M_{\phi b}$		$M_{\phi c}$	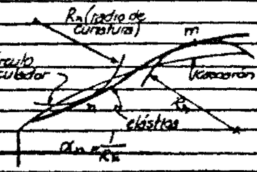
20.- Curvatura (de la elástica) $\alpha = \frac{M_{\phi a}}{EI_a} = \alpha_a$			$\frac{M_{\phi b}}{EI_b} = \alpha_b$		$\alpha_c = \frac{M_{\phi c}}{EI}$	
21.- Curvaturas concentradas (desviación de la tangente)	$\bar{\alpha}_a$	$\bar{\alpha}_b = \frac{\Delta s}{12}(\alpha_a + 10\alpha_b + \alpha_c)$			$\bar{\alpha}_c$	$\alpha_n = \frac{1}{R_n}$
22.- Desviación angular ϕ		ϕ_{ab}		$\phi_{bc} = \phi_{ab} + \bar{\alpha}_b$		$\alpha_m = \frac{1}{R_m} = \frac{M_{\phi m}}{EI_m}$
23.- Cambio de proy. horizontal $\Delta Y = \phi Z$		$\Delta Y_{ab} = \phi_{ab} Z_{ab}$		$\Delta Y_{bc} = \phi_{bc} Z_{bc}$		Ver figura 6.3
24.- Cambio de proy. vertical $\Delta Z = \phi Y$		$\Delta Z_{ab} = \phi_{ab} Y_{ab}$		$\Delta Z_{bc} = \phi_{bc} Y_{bc}$		
25.- $V = \Sigma_{acumulativa} \Delta Y$	V_a		$V_b = V_a + \Delta Y_{ab}$		$V_c = V_b + \Delta Y_{bc}$	
26.- $U = \Sigma_{acumulativa} \Delta Z$	U_a		$U_b = U_a + \Delta Z_{ab}$		$U_c = U_b + \Delta Z_{bc}$	

TABLA 1.3 (b)

Concepto	0	1	2	3	4	5	6	7	8	9	10	Unidad	Observaciones
1- Y	0	0	0.3768	0.4007	0.4214	0.4389	0.4530	0.4639	0.4704	0.4749		m	$\Sigma Y = \frac{L}{2} = 3.5m$
2- Z	-0.4000	-0.4000	-0.2892	-0.2553	-0.2193	-0.1818	-0.1429	-0.1028	-0.0620	-0.0207		m	$\Sigma Z = f/h = 2.0740$
3- $q_y = T'Y$	0	0	3.8163	4.0572	4.2668	4.4440	4.5868	4.6972	4.7630	4.8075		T/m	$\Sigma q_y = 35.4388$ T/m
4- $T'Z$	-4.0502	-4.0502	-2.9283	-2.5850	-2.2205	-1.8408	-1.4469	-1.0409	-0.6277	-0.2095		T/m	$\Sigma T'_Z = \frac{gL}{2} = 21.0000$
5- qY	0	0	2.2608	2.4042	2.5284	2.6334	2.7180	2.7834	2.8224	2.8494		T/m	$\Sigma qY = \frac{gL}{2} = 21.0000$
6- $q_z = T_z + qY$	-4.0502	-4.0502	-0.6675	-0.1808	0.3079	0.7926	1.2711	1.7425	2.1947	2.6399		T/m	$\Sigma q_z = 0$
7- $\bar{q}_y$	0	0	1.9081	3.9368	4.1620	4.3554	4.5154	4.6420	4.7301	4.7853	2.4037	T/m	$\Sigma \bar{q}_y = 35.4388$
8- $\bar{q}_z$	-2.0251	-4.0502	-2.3588	-0.4242	.0635	0.5503	1.0518	1.5068	1.9666	2.4173	1.3200	T/m	$\Sigma \bar{q}_z = 0$
9₁- N_{y_1}	0	0	3.8163	7.8735	12.1103	16.5843	21.1711	25.8683	30.6313	35.4388			
9₂- Σq_z	0	0	1.9081	5.8449	10.0069	14.0623	18.3111	23.5197	28.2498	33.0351	35.1339	T/m	
10- N_z	-4.0502	-8.1004	-8.7679	-8.9487	-8.6408	-7.8482	-6.5171	-4.8346	-2.6399	0			
10₂- Σq_z	-2.0251	-6.0753	-8.7641	-8.8583	-8.7948	-8.2445	-7.2127	-5.7059	-3.7373	-1.3200	0	T/m.	
11- $M_{\phi o}$	0	0	0	2.6261	4.6835	6.1951	7.2025	7.7723	8.0014	8.0079	8.0080	T m/m	$H = \frac{8.008}{1.274} = 6.2857$
12- M_H			0	-1.8478	-3.4726	-4.8010	-5.9438	-6.8420	-7.4882	-7.8779	-8.0000	T m/m	
13- $\bar{M}_\phi$	0	0	0	+.8083	1.2609	1.3941	1.2587	.9303	0.5102	0.1300	0	T m/m	
14- M_ϕ	0	0	-0.6970	+.1113	.5839	.6970	.5617	.2333	-.1838	-.5670	-.6970	T m/m	
15- $N_y = N_z + H$		6.2857	10.1020	14.1592	18.4260	22.8700	27.1568	32.1540	36.9170	41.7245		T/m	
16- $Y/\Delta s = \cos\phi$			.76504	.81915	.86603	.90631	.93969	.96593	.98481	.99619	1.00000		
17- $Z/\Delta s = \operatorname{sen}\phi$			.64279	.57358	.50000	.42262	.34202	.25882	.17365	.08716	0.00000		
18- N_ϕ			10.0220	13.3041	16.7366	20.3514	24.1750	28.2236	32.5051	37.0064	41.7245	T/m	
19- Q_ϕ			2.1648	1.3879	.6702	0.140	-0.4471	-.7534	-.8224	-.5878	0	T/m	

TABLA 2.3.

Concepto	⓪	①	②	③	④	⑤	⑥	⑦	⑧	⑨	⑩	Unidades	Observac.
14-Md	0	0	-0.6970	+.1115	+.5639	+.6970	+.5617	+.1333	-.1838	-.5670	-.6970	T·m/m	
20-α			+.6970	-.1115	-.5639	-.6970	-.5617	-.2333	+.1838	+.5670	+.6970	T/EI	
21-ᾱ			+2.3875	-.9799	-6.4473	-8.0856	-6.5473	-2.7109	+2.1717	+6.5508	10.4486	T ΔS/EI	
22-φ		0	2.3875	1.4076	-.50997	-1.31553	-1.98826	-2.23935	-2.02218	-1.56710	-.96224		error en φ
23-φZ·ΔY		0	-.8905	-.5594	+1.1052	+2.3300	+2.8186	+2.5020	+1.7888	+.1850		Tm ΔS/EI	
24-φY·ΔZ		0	+.8990	+.5640	-2.1257	-5.7651	-8.9162	-10.3885	+9.5123	-6.4924		″	
25-v			0	-.6925	-.10499	+.0553	+2.4433	+5.1553	+7.5579	+8.8117	+9.0947	Tm ΔS/EI	error en v
26-u			0	+.8996	+1.4636	-.6801	-6.4752	-15.3414	-25.7197	-36.2410	-41.7844	″	
27-v̄			0	-.3784	-.5753	+.0303	+1.5389	+2.8802	+4.1417	+4.8288	+4.9839	mm	
28-ū			0	+.4930	+.8020	-.3417	-3.5210	-8.4071	-14.0999	-19.3126	-22.8704		

NOTA.- Con el fin de facilitar las operaciones (para que no haya confusión en los signos) se optó por la convención de u y v.

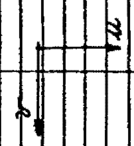

TABLA 2.3

horizontal Y no existiendo fuerzas, exteriores, horizontales que obren en la dóvela T'Y será el valor de la fuerza resultante qy en cada intervalo Δ S. La suma de las fuerzas qy deberá ser igual a T' $\frac{l}{2}$ = 10.125 x $\frac{7.00}{2}$ = 35.438 T/ M. que checa con el valor de la última columna.

4.- Se obtienen los valores de la proyección vertical de la fuerza cortante T'Z de cada intervalo ΔS. La suma Σ T'Z debe equilibrar a la resultante de la carga q que actúa en el semiclaro. Σ T'Z = $q\frac{l}{2}$.

5.- La carga que actúa en cada dóvela ΔS, varía con la proyección horizontal Y y su valor se encuentra fácilmente por qY en que q es la carga uniforme exterior.

6.- La carga vertical qz, total será la suma algebraica de la carga exterior q y la proyección vertical de la fuerza cortante T'Z. La suma acumulativa de qz en el punto (10) deberá ser cero para que haya equilibrio. Efectivamente como se ve del renglón 4, Σ T'Z = $q\frac{l}{2}$ (en realidad esta suma es negativa). Del renglón 5, Σ qY = q ΣY = $q\frac{l}{2}$ - (con signo positivo). La suma de ambos conceptos es cero.

7 y 8.-En estos renglones se obtienen los valores de las concentraciones de q_z y q_y en las líneas divisorias. La obtención se hace repartiendo la mitad de la carga en cada intervalo hacia las líneas divisorias de la izquierda y derecha. A cada línea divisoria le corresponde la semisuma de las cargas de dos intervalos consecutivos. Es decir que en cada línea divisoria la carga $\bar{q}_{y_n}$ es el promedio de las cargas $q_{y_{n-1}}$ y $q_{y_{n+1}}$ de los intervalos adyacentes.

Para la obtención de los momentos transversales (renglón 11) habrá que considerar el hecho de que las cargas q_y y q_z están aplicadas al centro de cada dóvela. Esta consideración hace necesaria la obten---

ción de los incremento. Y' y Z' entre los centros de los intervalos ΔS. La obtención de estos incrementos en un procedimiento gráfico conduce a errores mayores por tener que efectuar mayor número de mediciones (cada medición tiene un error); en un procedimiento analítico aumenta la laboriosidad si se encuentran geométricamente los incrementos de las ordenadas. En este último procedimiento se pueden considerar en forma aproximada, los centros de ΔS a la mitad de los incrementos Y y Z. Sin embargo, la tabulación del procedimiento se dificulta al tener que trazar nuevas líneas divisorias para los nuevos intervalos. Por lo tanto parece más indicado distribuir las cargas q en las líneas divisorias actuales tal como se explicó arriba.

y 15- Para encontrar posteriormente los valores de $N\phi$ y $Q\phi$ se hace la suma acumulativa, en los intervalos de q_y y q_z. Esta suma se hace precisamente en los intervalos ΔS, y nó en las líneas, puesto que interesa la acción de las fuerzas del intervalo sobre la sección. Determinando $N\phi$ y $Q\phi$ a partir de las concentraciones $\bar{q}$ se obtienen errores del: 15% aproximadamente para $N\phi$ y del 50% para $Q\phi$.

Para anteproyectos se pueden usar los valores de $N\phi$ obtenidos a partir de las $\bar{q}$. El valor de la fuerza cortante producida por $Q\phi$ resulta despreciable. Las proyecciones de las fuerzas totales que obran en cada dóvela se denominan Ny_i y Nz. La Ny_i se incrementa posteriormente en el renglón 15 con la perturbación H.

11.- Se encuentran fácilmente los valores de $M\phi,o$ sumando acumulativamente los productos de $q_y Z$ y $-q_z Y$. La convención de signos empleada es la siguiente: El momento $M\phi,o$ es positivo si produce compresión en la parte superior del cascarón y tensión en la inferior. El cálculo hasta esta etapa es muy semejante a la del arco presentado anteriormente. La discrepancia principal la constituye la fuerza cortante actuando

a lo largo del cascarón.

12- Como se hizo en el capítulo anterior la perturbación H se obtiene de manera que su efecto anule el momento $M\phi,o$ de la clave ($\phi = o$).
Se encuentran los momentos M_H, multiplicando el valor de H por las ordenadas del arco. (La fuerza H se considera actuando en el arranque del cascarón $\phi_o = 40^0$). El valor de H se calcula con la expresión:

$$H = \frac{M\phi = o,o}{f}$$ en la que $M\phi = o,o$ es el momento transversal en la clave, y f la flecha del arco.

13 y 14.- Los valores de $\overline{M}\phi$ se determinan restando a $M\phi,o$ los momentos M_H. El momento $\overline{M}\phi$ máximo sirve para igualar los momentos $M\phi$ en tres puntos. Para esto basta con restar a todos los momentos $\overline{M}\phi$ la mitad del valor $\overline{M}\phi$ máximo.

16 y 17- Para determinar los renglones 18 y 19 es necesario conocer los valores de las funciones cos ϕ y sen ϕ. En forma aproximada se pueden obtener de las expresiones $\frac{Y}{\Delta S}$ y $\frac{Z}{\Delta S}$ (aceptando la cuerda del intervalo por la tangente). Sin embargo, en este caso es bastante sencillo obtener los valores de cos ϕ y sen ϕ de tablas pues el ángulo central está dividido en 8 ángulos iguales de 5^o cada uno.

18- El valor de $N\phi$, como se indica en la Tabla 1.3 (a) se obtiene fácilmente proyectando los valores de Nz y Ny según la tangente del arco en el punto considerado. Así el de $N\phi$ se encuentra dado por la ecuación:

$$N\phi = Ny \cos\phi + Nz \operatorname{sen}\phi.$$

19 - El valor de $Q\phi$ se determina proyectando Nz y Ny en dirección radial. Se obtiene la fórmula:

$$Q\phi = Nz \cos\phi - Ny \operatorname{sen}\phi.$$

20 - La curvatura de la elástica, considerando al arco de sección constante, se calcula dividiendo los momentos transversales en cada punto por la rigidez EI en la que $I = \frac{bt^3}{12}$ y E es el módulo de elasticidad.

21.- Las curvaturas concentradas (desviación de la tangente entre dos puntos) se puede calcular con el formulario (aproximación parabólica) dado para el cálculo del arco (Fig. 7.3).

22 - La desviación angular ϕ se encuentra sumando acumulativamente las curvaturas concentradas.

24-Los cambios en la proyección (al deformarse la pieza) se obtienen multiplicando el valor de ϕ por las proyecciones Z o Y. La desmostración de este asunto se indicó en la Fig. 6.3.

26-Los desplazamientos v y u se encontraron sumando acumulativamente los cambios de proyección ΔY y ΔZ respectivamente.

En la figura 8.3 se muestra, muy ampliada, la elástica del cascarón. Se ve en esta figura que el hecho de inventar la redundancia H y el valor correctivo de $\overline{M}\phi$ conduce a incompatibilidades en las deformaciones del cascarón:

$v_{10} = 4.98$ m.m.	Debe ser cero.	Por simetría la clave no puede desplazarse lateralmente.
$\phi_{10} = 9.62 \ \frac{\Delta s}{12EI}$	Debe ser cero.	Por simetría la tangente a la clave después de la deformación debe seguir siendo horizontal.

Es decir que la clave se comporta en forma análoga a un apoyo (deslizante) guiado en el que sólo es posible el desplazamiento vertical. - Fig. 9.3

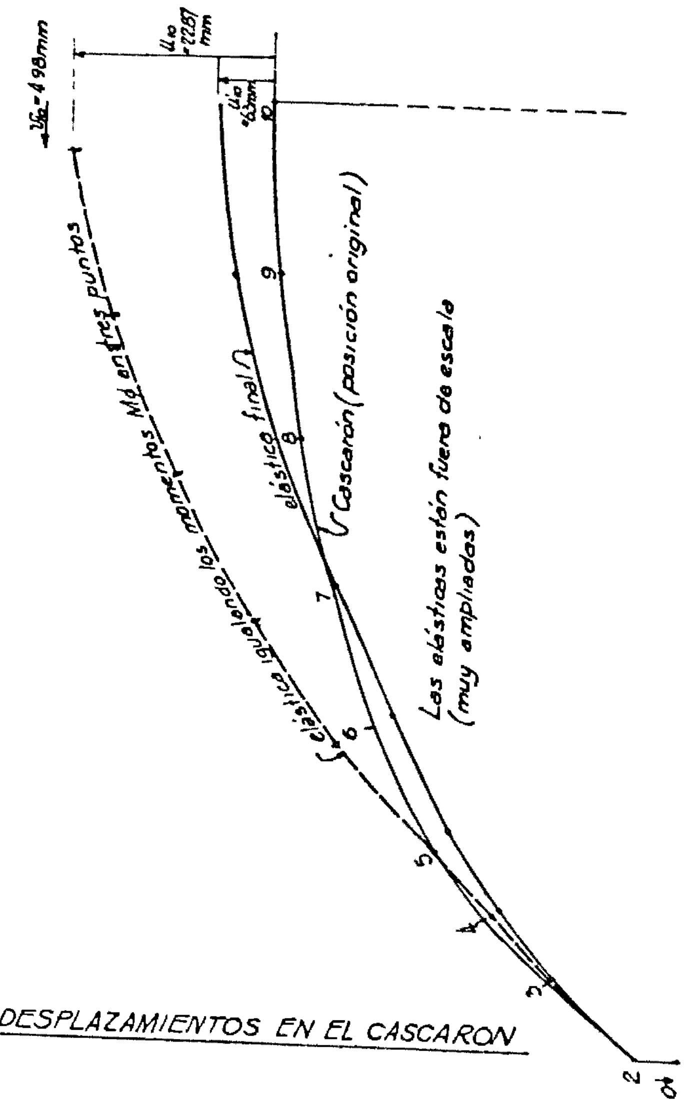

FIG 8.3- DESPLAZAMIENTOS EN EL CASCARON

Dentro del criterio plástico es posible pensar en que la tangente en la clave no sea horizontal, esto es, que el cascarón se quiebre en la clave. Pero el que haya un desplazamiento del tipo de v_{10} es inadmisible, lo cual significa que para llegar a las condiciones fijadas de antemano, tanto en lo que se refiere a la perturbación H como la de la igualación de los momentos transversales $M\phi$ en tres puntos, debe haber un proceso de redistribución de deformaciones en el arco que no se puede atacar con base en la teoría elástica. Además en lo referente a cuantificación e importancia de grietas y deformación final, sobre todo en cimentaciones que están sujetas a cargas q apreciables, el procedimiento plástico no proporciona una base sólida desde la que pueda fijarse su campo de aplicabilidad. Pero ya se ha insistido anteriormente en lo que esto representa en el aspecto general del comportamiento de la cimentación. Este asunto conduce a buscar otro procedimiento en el que cuando menos se cumplan los requisitos de que v_{10} y ϕ_{10} sean cero en la clave. Si bien es cierto que no se puede asegurar la validez absoluta del procedimiento, sobre todo en lo que respecta a la fuerza cortante T' y a la obtención de las deformaciones si podrá obtenerse una idea de la magnitud de los desplazamientos y de las redundancias que deban actuar en el cascarón.

De cualquier modo al cumplir estos requisitos el cascarón no estará en peores condiciones que en el caso de igualar los momentos en tres puntos, o en el de resolverlo de acuerdo con algún método analítico "exacto" puesto que cuando menos se satisface el equilibrio estático.

7.3 El problema mencionado se puede plantear en los siguientes términos: Introducir las correcciones necesarias para que v_{10} y ϕ_{10} sean cero en la clave. Estas correcciones tendrán que obrar simultáneamente de manera que su efecto combinado corrija ambos conceptos. Para corregir v_{10} se ocurre introducir una fuerza P horizontal en la clave, de sentido contrario al desplazamiento v_{10}. La corrección de ϕ_{10} se logra mediante la acción de un momento M_c correctivo, aplicado en la clave, con sentido contrario al giro ϕ_{10}. La figura 10.3 indica las correcciones aplicadas en la clave, ambas produciendo momentos positivos, más adelante se encontrarán los signos adecuados.

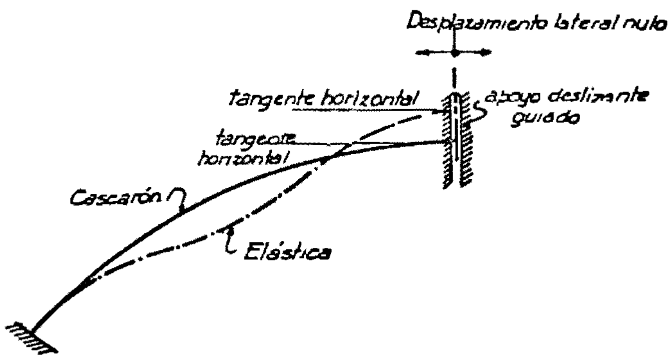

FIG. 9.3.

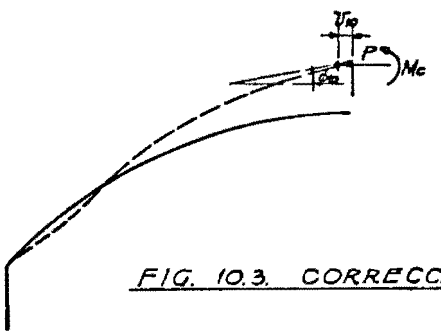

FIG. 10.3. CORRECCIONES

En la Tabla 3.3 se resuelve el problema con las correcciones M_c y P.

C O N C E P T O :

29.- Se obtienen los momentos producidos por M_c y P. Los de M_c son constantes a lo largo del arco y los de P se encuentran con la suma acumulativa de los productos PZ a partir de la clave.

30.- Para la determinación de las curvaturas concentradas, no se incluye el de las curvaturas M/EI puesto que las α se pueden encontrar directamente de los momentos, se empleó la aproximación parabólica mencionada anteriormente.

31.- Se encontró el valor de ϕ'_{10} en función M_c y P.

32 y 33.- Se calcularon los valores de ϕZ y el de v'_{10} en función de M_c y P.

Determinado los valores de ϕ'_{10} y v'_{10} se procede a la corrección teniendo en cuenta que:

$$\phi_{10} + \phi'_{10} = 0$$

$$(-96 M_c - 41.4242P)\frac{\Delta S}{12EI} - 9.6224\ \frac{\Delta S}{12EI} = 0$$

$$\therefore\quad -96 M_c - 41.4242P = 9.6224 \ldots\ldots\ldots\ldots\ldots\ldots(A)$$

$$v_{10} + v'_{10} = 0$$

$$(41.7636 M_c + 32.0218P)\frac{\Delta S}{12EI} + 9.0947\ \frac{\Delta S}{12EI} = 0$$

$$\therefore\quad 41.7636 M_c + 32.0218P = -9.0947 \ldots\ldots\ldots\ldots(B)$$

Resolviendo el sistema de ecuaciones (A)-(B):

$$\frac{96}{41.7636} \times (B) = 2.29865 \times (B)$$

$$\therefore\quad 96 M_c + 73.6069P = -20.9055 \ldots\ldots\ldots\ldots\ldots\ldots(B')$$

Sumando la ecuación (A) con (B')

$$32,1827P = -11.2831$$

$$P = -\frac{11.2831}{32.1827} = -0.3506\ Tm/m.$$

Concepto		(2)	(3)	(4)	(5)	(6)	(7)	(8)	(9)	(10)	Unidades	Observaciones
29- $M_c + \beta P$		Mc+1.274P	Mc+.9848P	Mc+.7295P	Mc+.5102P	Mc+.3284P	Mc+.1855P	Mc+.0810P	+Mc+.0207P	+Mc		
30- $\bar{\alpha}$		-6Mc-7.0486P	12Mc-11.8515P	-12Mc-8.790P	-12Mc-6.1363P	-12Mc-3.9797P	-12Mc-1.2618P	-12Mc 1.0262	-12Mc-.289P	-6Mc-.0211P		$\frac{\Delta s}{12EI}$
31- ϕ'	0	6Mc-7.0486P	18Mc-18.9001P	30Mc-27.6901P	42Mc-32.8464P	54Mc-37.8251P	66Mc-40.0879P	78Mc-41.1141P	90Mc-41.4031P	96Mc-41.4242P		
32- $\delta Z \cdot \Delta Y$	0	+1.7568Mc +8.0355P	+4.5454Mc +6.8886P	+6.5790Mc +6.0726P	+7.8354Mc +6.1533P	+7.7168Mc +5.6053P	+6.7618Mc +4.1810P	+4.8360Mc +2.5491P	+1.0030Mc .8370P			
33- v'_{10}									41.7836Mc+32.0218P			$\frac{\Delta s}{12EI}$
34- M_x		-.3957	-.2943	-.2048	-.1279	-.0641	-.0140	+.0223	+.0438	+.0510		$T\frac{m}{m}$
35- M_ϕ		-1.0927	-.1830	+.3591	+.5691	+.4976	+.2193	-.1615	-.5832	-.6460		$T\frac{m}{m}$
36- $\bar{\alpha}$		+4.5330	+1.5686	-3.9771	-6.5477	-5.7614	-2.5291	+1.9189	+6.0396	+3.7499		$\frac{\Delta s}{12EI}$
37- ϕ	0	4.5330	+7.1166	+3.1395	-3.4082	-9.1776	-11.7017	-9.7828	-3.7432	= 0		✓
38- δZ		-1.3167	-1.8169	-.6885	+.6196	+1.3108	+1.2029	+.6065	+.0775			✓
39- δY		1.7156	2.8516	1.3230	-1.4959	-4.1552	-5.4284	-4.6018	-1.7776			✓
40- v'		0	-1.3167	-3.1336	-3.8221	-3.2025	-1.8917	-.6888	-.0823	= 0		✓
41- u'		0	1.7156	4.5672	5.8902	+4.3943	.2391	-5.1893	-9.7911	-11.5687		✓
42- v'		0	-.722	-1.717	-2.095	-1.755	-1.037	-.377	-.045	0	milímetros	
43- u'		0	.940	2.503	3.228	2.408	.131	-2.844	-5.366	-6.340	✓	

$$\frac{41.4242}{32.0218} \times (B) = 1.2936$$

$$\therefore \quad 54.0262\, M_c + 41.4242 = -11.7651 \quad \ldots\ldots\ldots\ldots\ldots\ldots (B'')$$

Sumando la ecuación (A) con la (B''),

$$-41.9738\, M_c = -2.1427$$

$$\therefore \quad M_c = \frac{2.1427}{41.9738} = \underline{0.0510} \quad T\frac{m}{m}$$

El valor de $P = -0.3506\ T/_m$ (tensión) es bastante pequeño en comparación con el de $N\phi_{10} = 41.72\ T/_m$ (compresión); asimismo el de $M_c = 0.0510$. Su efecto sobre el cascarón podría creerse despreciable; sin embargo, sobre los momentos transversales es importante sobre todo en la cercanía del arranque del arco. En ϕo la corrección P, que es la más importante, produce una discrepancia apreciable con respecto al momento calculado primero (en la igualación de momentos transversales).

Se vuelve a insistir en la sensibilidad de los momentos transversales con pequeñas variaciones en la fuerza $N\phi$ puesto que con una disminución de $N\phi$ (en la clave) del 0.08% se obtiene un incremento del 65% del momento en el arranque lo cual afirma la necesidad de hacer pruebas en el laboratorio para poder establecer la distribución real de T' cuyo desconocimiento puede conducir a errores, probablemente hasta del 100% en los momentos transversales.

La elástica final de la figura 8.3 se produce si se considera que la trabe vertical en el borde no tiene desplazamientos verticales. En realidad para calcular los desplazamientos verticales absolutos habrá que considerar la flexión longitudinal y sumar sus efectos a los transversales. De esta elástica sólo es interesante su forma y el orden de sus desplazamientos pues no se podrá asegurar que la clave tenga una $u_{10} = 6.3$ mm. Sólo se podrá decir que el desplazamiento —

vertical de la clave es alrededor de 1 cm. Lo que si es interesante de observar es que el hecho de haber considerado las correcciones M_c y P reduce apreciablemente las flechas.

La transformación de u y v a milímetros se hizo considerando:

$$\Delta S = 0.475 \text{ m.}$$

$$EI = \frac{bt^3}{12} = \frac{1 x 0.\overline{10}^3}{12}$$

y $E = 86700 \text{ Kg/cm}^2 = C\sqrt{f'_c}$ en la que $C = 6000\sqrt{\text{Kg/cm}^2}$ obtenido del valor tangente inicial del módulo de elasticidad. R. Saliger. El hormigón armado pág. 80.

Tomando $f'_c = 210 \text{ Kg/cm}^2$ $E = 86700 \text{ Kg/cm}^2$

$$\therefore \frac{\Delta S}{12EI} = \frac{12 \times 0.475}{12 \times 867000 \times 1. \times 0.\overline{10}^3} = 0.000548 \rightarrow u \text{ y } v \text{ en metros}$$

$$0.548 \rightarrow u \text{ y } v \text{ en m.m.}$$

En la figura 11.3 se muestra el nuevo diagrama de momentos transversales $M\phi$. No se considera importante modificar el de $N\phi$ ni el de $Q\phi$ - porque no hay mucha variación en estos valores. Como se puede apreciar en la figura el diagrama conserva aproximadamente la misma forma, todos los momentos transversales son menores excepto en $\phi o = 40^\circ$.

8.3 Hasta ahora sólo se ha considerado la influencia de $M\phi$ para la determinación de u y v falta incluir la de $N\phi$ y $Q\phi$. En un cálculo preliminar, no presentado, se tomó la influencia de estas fuerzas y se pudo observar que su efecto, comparado con el de $M\phi$, es despreciable. Sin embargo, se presenta a continuación la forma en la que se pueden considerar sus efectos.

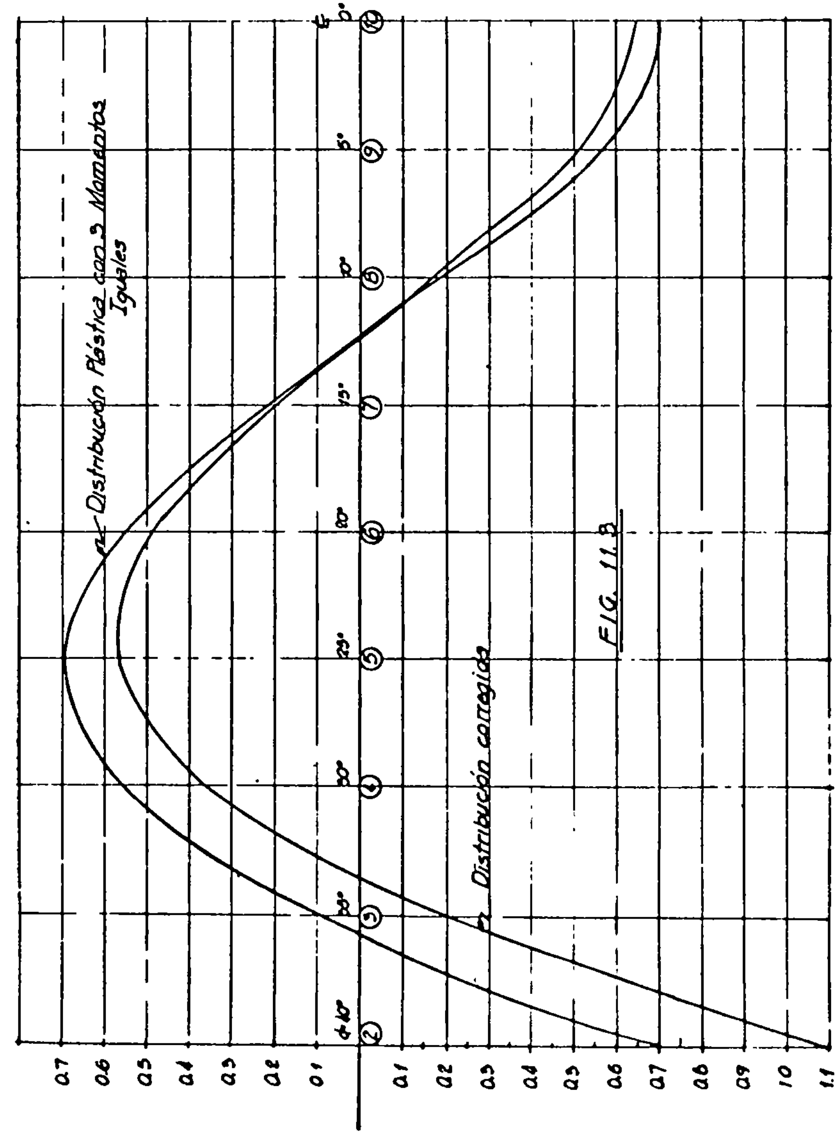

FIG. 11.3

a).- Deformaciones debidas a $N\phi$

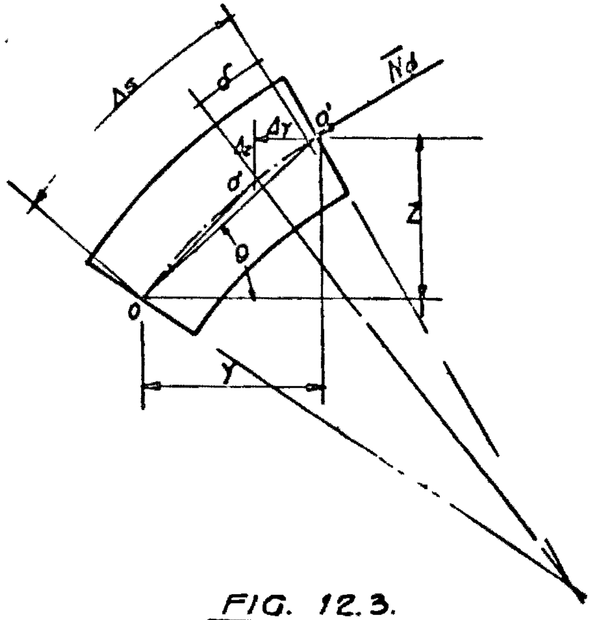

FIG. 12.3.

De acuerdo con la ley de Hooke:

$E = \dfrac{\overline{N}\phi / A}{\epsilon}$ en la que $\overline{N}\phi$ es la fuerza normal a la sección de area $A = bt$.
E: módulo de elasticidad del concreto.
ϵ: deformación unitaria. $= \dfrac{\delta}{\Delta S}$

$$\therefore \quad E = \frac{\overline{N}\phi \, \Delta S}{A\,\delta} \qquad \therefore \quad \frac{\overline{N}\phi}{AE}\, \Delta S = \delta$$

Los cambios de las longitudes de las proyecciones serán:

$$\Delta Y = -\delta \cos\theta = -\frac{N\phi}{AE}\,\Delta S \cos\theta$$

$$\Delta Z = \delta \operatorname{sen}\theta = -\frac{N\phi}{AE}\,\Delta S \operatorname{sen}\theta$$

Si se emplea la longitud de la cuerda $\overline{OO'}$ en lugar de ΔS se tendrá

$$\Delta Y = -\frac{N\phi\, Y}{AE}$$

$$\Delta Z = \frac{N\phi\, Z}{AE}$$

La suma acumulativa de ΔY y ΔZ del arranque a la clave dará los desplazamientos v y u debidos a la fuerza normal.

b).- Deformaciones debidas a $Q\phi$.

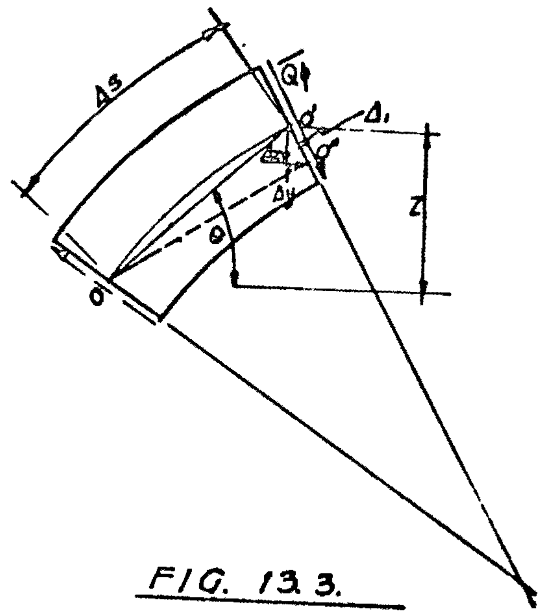

FIG. 13.3.

La determinación de las deformaciones debidas a $Q\phi$ se hace en forma análoga a las de $N\phi$:

El módulo de cortante: $G = K \dfrac{\overline{Q}\phi}{A\gamma}$ en la que:

G: módulo de cortante:

γ: = deformación unitaria = $\frac{\Delta_1}{AS}$

Δ_1: = K $\frac{\overline{Q\phi}}{AG}$ Δ S.

Los incrementos de proyección serán:

$\Delta Y = \Delta_1 \operatorname{sen} \theta = \frac{K}{AG} Q\phi Z$

$\Delta Z = \Delta_1 \cos \theta = \frac{K}{AG} Q\phi Y$

La suma acumulativa de ΔY y ΔZ del arranque a la clave dará los desplazamientos v y u debidos a la fuerza cortante.

En los casos a) y b) se pueden encontrar las variaciones de ϕ:

$$\phi = \frac{u_2-u_1}{Z} = \frac{v_2-v_1}{Y}$$

Es decir, que el valor de ϕ se corrige para los efectos de $Q\phi$ y $N\phi$ después de haber obtenido los desplazamientos u y v causados por estos conceptos. Una manera más sencilla de encontrar los valores de ϕ reales se obtiene si se consideran los desplazamientos totales v y u de los que con la expresión anterior se puede encontrar los valores finales de ϕ. Para el caso resuelto bastará con encontrar el valor de ϕ en el tramo (9)-(10) y sumarle el valor de α del punto (10). Ejemplo:

Si ϕ es el valor sin corregir en el tramo (9)-(10) y α_{10} el del cambio de curvatura en el punto (10) el valor de ϕ_{10} (en lugar del que se había obtenido) será:

$$\phi_{10} = \phi_1 + \frac{u_a-u_1}{Z} + \alpha_{10}.$$

9.3 Uno de los aspectos sobre el que se ha insistido frecuentemente se refiere a la acción que el terreno tiene sobre el cascarón. Para explicar esta interacción se recurre a una analogía en la que la acción del

terreno se representa por una serie de resortes cuya constante de resorte representa el módulo del terreno. Como se vé en física la constante de resorte representa la carga W que hay que aplicar a un resorte para que se deforme la unidad.

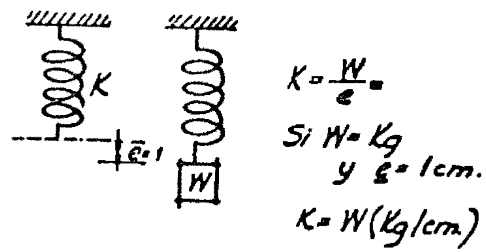

FIG. 14.3

Supóngase una viga sujeta a una carga cualquiera que se deforma como se indica en la figura 15.3 (a). Si ahora se somete la viga deformada a la acción de un sistema de resortes su efecto será el de reducir las flechas y en la cantidad y_q.

Como vía de introducción al método para encontrar la posición de la elástica final se resuelve un ejemplo sencillo de manera que pueda visualizarse el procedimiento y a la vez ir estableciendo los conceptos básicos que de otra manera resultarían difíciles de explicar. Por ejemplo se propone una viga simplemente apoyada sujeta a la acción de una carga concentrada P_c al centro del claro y a un resorte de constante K = 48 EI/L^3 también al centro del claro. Se desean encontrar el valor de la constante crítica del resorte para este sistema y el valor de la flecha máxima. Todo en términos de EI y L.

Se establece en métodos numéricos Ref. 7, que el procedimiento es convergente cuando la constante de resorte $K < K_{cr}$

Es importante el conocimiento de la constante crítica pues en el desarrollo del método se cuenta con la expresión:

$y_q = \frac{y_t}{K_{cr}/K + 1}$ que puede utilizarse siempre que $K < [K_2]$ en la que K_2 representa la constante crítica del 2o. modo.

Se procede entonces a determinar la constante crítica del resorte.

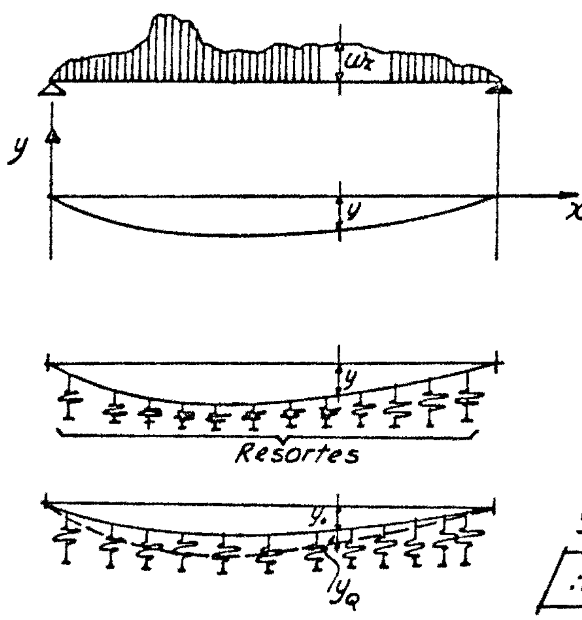

FIG. 15.3

$y_Q + y_o = y$

$\boxed{\therefore\ y_o = y - y_Q}$

Fig. 16.3.

1.- Se supone una elástica en función de una constante a de proporcionalidad.

2.- Se determina el valor de la acción sobre el resorte $Q = -aK$. Esta literal Q representa una fuerza que obra en sentido contrario a la deformación a del resorte.

3.- Se encuentra el valor de la fuerza cortante, que por simetría es igual a la mitad de la fuerza Q a cada lado de la línea de acción de Q.

4.- El momento flexionante es la suma acumulativa de Vh. Siendo h un valor constante se saca como factor común en la columna derecha.

5.- Se determina directamente la curvatura concentrada $\bar{\alpha}$ con la aproximación poligonal.

$$-\bar{\alpha} = \frac{h}{6}\ (0 + 4 \times 0.5 + 0) = 2\,\frac{h}{6}$$

6 y 7.- Se obtienen los valores de ϕ y y^1.

Se demuestra en métodos numéricos que si

$$y_s = y^1 \qquad K = Kcr$$

$$\therefore \quad a = aKcr\ h^3/6EI$$

$$\therefore \quad Kcr = \frac{6EI}{h^3} = \frac{48EI}{L^3} \qquad (= y_s/y^1)$$

8 a 13.- El procedimiento hasta encontrar y_ℓ ya se expuso anteriormente.

14.- Los valores y_ϕ se calculan con la expresión

$$y_\phi = -\frac{y_\ell}{\frac{K\,cr}{K} + 1} = -0.5\ y_\ell$$

Los de $y_o = y_\ell - y_\phi = 0.5 y_\ell$

$$\therefore \quad y_o\ \text{máx.} = 0.5\ Po\ h^3/6EI = \frac{0.5}{48}\ Po\ \frac{L^3}{EI}$$

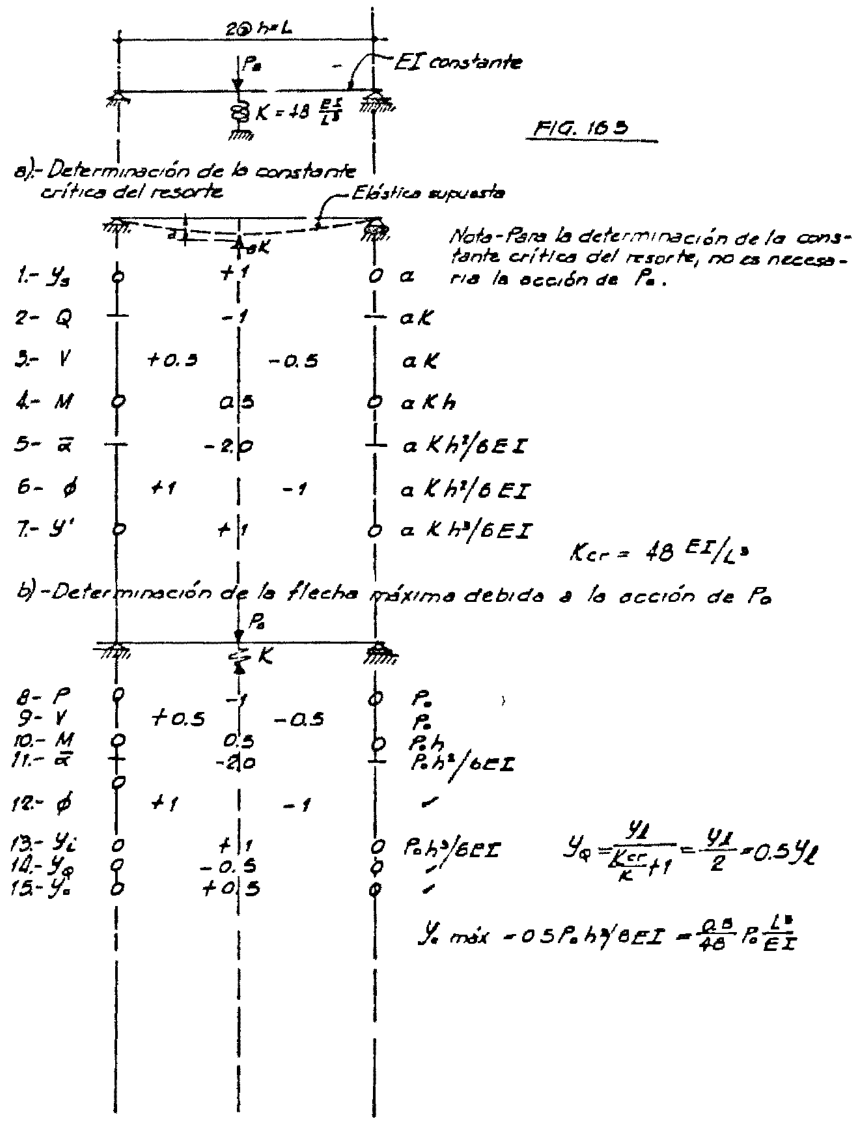

FIG. 16.3

El problema que se acaba de resolver pertenece al grupo de los sistemas estables. Cuando no obra la acción de los resortes una estructura pue de resultar: estable o inestable, isostática o hiperestática. La figu ra 17.3 muestra los tipos de sistemas que pueden existir.

El cascarón pertenece al grupo 3, 2o. caso Estable hiperestático y se puede representar como se ve en la figura 18.3.

.3 En la Tabla 5.3 se resuelve la interacción del terreno a partir de los valores iniciales de u y usando la expresión de y_q.

1er. Ciclo.

1.- El valor final de los desplazamientos verticales u_o será la dife- rencia entre las de u_1 (encontrados sin la interacción del terre- no) y los de u_Q (resultado de la acción de los resortes.).

2.- El valor de u_o multiplicado por la constante K del terreno propor ciona él valor de la fuerza Q producida al deformar el resorte.

3.- Suponiendo empotrado el arranque se procede a calcular la fuerza- cortante en los intervalos sumando acumulativamente los valores - de Q desde la clave hasta el arranque.

4.- Se encuentran los productos VY (no indicados) y su suma acumulati va de derecha a izquierda. Se obtienen en esta forma los momen- tos transversales M isostáticos.

5,6 y 7.- Con el fin de corregir los momentos de la etapa 4. se proce de a calcular los valores de ϕ_{10} y v_{10}

Se obtuvieron los errores:

$$\phi_{10} = 141.461 \frac{\Delta S}{12EI}$$

$$v_{10} = -91.411 \frac{\Delta S}{12EI}$$

Utilizando las configuraciones correctivas de la tabla 3.3 es posible plantear un sistema de 2 ecuaciones simultáneas que proporcionen los-

$K = k\,\Delta S = 0.2\ \mathrm{kg/cm^3} \times 47.5 \times 100$

$K = 0.95\ \mathrm{T/cm\ m}$

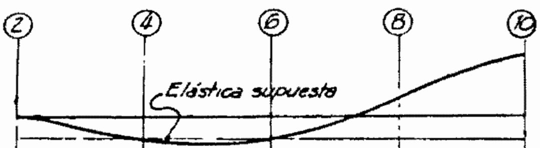

	②		④		⑥		⑧		⑩	
1- u	0		+1		+1		-1		-3	a
2.- Q = Ku	-		+1		+1		-1		-3	aK
3.- Y = ΣQ		+2		+3		+4		+3		aK
4.- YY		1 555		2 381		3 668		2 836		aK
5- Mo	-10 640		-9 085		-6 504		-2 836		0	aK
6.- ᾱ	30 365		53 584		37 937		17 848		2 836	aK ΔS/6EI
7- φ		30 365		83 949		121 886		139 734	142.570	aK ΔS/6EI
8.- v10									-91 709	aK ΔS/6EI
9.- M1	Mc+1.274P		Mc+0.730P		Mc+0.328P		Mc+0.082P		Mc	
10.- ᾱ1	-3Mc-3.278P		-6Mc-4.522P		-6Mc-2.124P		-6Mc-0.656P		-3Mc-0.082P	ΔS/6EI
11.- φ1		-3Mc-3.278P		-9Mc-7.800P		-15Mc-9.924P		-21Mc-10.58P	-24Mc-10.662P	ΔS/6EI
12- v'10									10.666 Mc+8.227P	ΔS/6EI
13- M1	2 041		-0 828		-1 506		+0 160		+2.330	aK
14.- ᾱ2	-3 254		+2 177		+6 692		-1 464		-4 810	aK ΔS/6EI
15- φ		-3 254		-0 477		+6 215		+4 750	≐ 0	aK ΔS/6EI
16.- v10									= 0	aK ΔS/6EI
17- Uq	0		-2 530		-2 940		+2 758		+7 248	aK ΔS/6EI
18.- u/Uq			-0 395		-0 340		-0 363		-0 414	6EI/ΔS

$$K_{cr} = \frac{\Sigma u}{\Sigma u_q} = -0.387 \times \frac{6EI}{\Delta S} = \frac{-0.387 \times 6 \times 867 \times 10^5 \times 0.13}{0.475 \times 12} = 353\ \mathrm{T/m^2}$$

$K_{cr} = -353\ \mathrm{T/m \times cm}$ $\quad (K_{cr} = -0.743\ \mathrm{Kg/cm^3})$

Como $K_{cr} > K$ el sistema es convergente

$$u_q = -\frac{u_e}{\frac{|K_{cr}|}{K} + 1} = -\frac{u_e}{4.716}$$

TABLA 4.3

(Determinación de K_{cr})

	②	③	④	⑤	⑥	⑦	⑧	⑨	⑩	
1er Ciclo U_ℓ	0	.094	0.250	0.323	0.241	0.013	-0.264	-0.537	-0.634	cm $K=0.95\,T/m$
U_q	0	-.020	-.053	-.069	-0.051	-.003	+.060	+.114	+.134	cm
1- $U_o = U_q + U_\ell$	0	.074	.197	.254	.190	.010	-.224	-.423	-.500	cm
2- Q	0	.070	.187	.241	.181	.010	-.213	-.402	-.475	T/m
3- V		.401	.471	.658	.899	1.080	1.090	.877	.475	T/m
4- M	-2.61	-2.494	-2.305	-2.028	-1.633	-1.144	-.637	-.225	0	Tm/m.
5- $\bar{\alpha}$	+15587	29890	27.572	24.218	19502	13.710	2.739	2887	.356	ΔS/12EI
6- ϕ		15587	45477	73049	97.267	116769	130.479	138218	141.105	141.461 ΔS/12EI
7- v_{10}										-91.411 ΔS/12EI
8- M'	0.627	+.160	-.196	-.386	-.380	-.195	.091	.372	+.553	Tm/m
9- $\bar{\alpha}$	-2.772	-2031	+2166	+4436	+4.381	+2.239	-1.087	-4.364	-3.006	ΔS/12EI
10- ϕ	0	-2.772	-1803	-2.617	+1.819	+6.200	+8439	+7.352	2.988	0 ΔS/12EI
11- v_{10}										0 ΔS/12EI
12- u'_q	0	-1045	-2970	-4.072	-3.273	-465	+3450	+6908	8.327	ΔS/12EI
13- u'_q	0	-0.057	-163	-223	-.179	-025	+.189	+.378	+.456	cm
2º Ciclo 1- u'_o	0	+0.037	+087	+100	+.062	-012	-.095	-.159	-.178	cm
2- Q'	0	0.035	+083	+.095	+.059	-.011	-.090	-.151	-169	T/m.
3- V		.149	.184	.267	.362	.421	.410	.320	.169	0 T/m
4- M'	-1013	-967	-833	-771	-612	-421	-.231	-.080	0	Tm/m
5- $\bar{\alpha}$	+5975	11466	10.558	9.205	7.312	5.053	2811	1.081	+.125	ΔS/12EI
6- ϕ	0	5975	17441	27.999	37,204	44.516	49569	52.380	53411	53.536 ΔS/12EI
7- v_{10}										-34895 ΔS/12EI
8- M''	+213	+059	-078	-.148	-.140	-067	0035	0137	0.200	Tm/m
9- $\bar{\alpha}$	-1067	-755	+869	+1698	+1.615	+.775	-.490	-1.605	1.093	ΔS/12EI
10- ϕ		-1.067	-1.822	-.953	+.745	+2.360	+3135	+2.715	+1.110	=0 ΔS/12EI
11- v_{10}										=0 ΔS/12EI

	②	③	④	⑤	⑥	⑦	⑧	⑨	⑩	
12- $\Sigma \phi Y = u''_\phi$	0	-.402	-1.102	-1.534	-1.398	-.329	+1.125	2.402	+2.929	ΔS/EI
13- u''_ϕ	0	-022	-052	-064	-.077	-018	+062	+.132	+161	cm
u'_q	0	-057	-.163	-.223	-179	-025	+189	+.378	+456	cm
u_q	0	-.020	-053	-.069	-051	-003	+.060	+.114	+.134	cm
(promedio) u''_q	0	-010	-090	-130	-.100	-.015	+.130	+.210	+.250	cm
3er Ciclo 1- u_o	0	+0.054	+.160	+.193	+.141	-002	-.154	-.327	-.384	cm
2- Q	0	+0.051	+.152	+.183	+.134	-002	-.146	-.311	-365	T/m
3- V		.304	355	507	690	.824	.822	.676	.365	T/m
4- M	-2019	-1905	-1762	-1549	-1.246	-.873	-491	-173	0	Tm/m
5- $\bar{\alpha}$	+11900	22851	21.074	18498	14882	10467	5.956	2221	.273	ΔS/12EI
6- ϕ		11900	34731	55805	74303	89185	99652	105.508	107.829	108102 ΔS/12EI
7- v_{10}										
									-69823	ΔS/12EI
8- M	0479	+122	-150	-294	-.287	-147	+068	+285	+0424	Tm/m
9- $\bar{\alpha}$	-2118	-1549	+1672	+3377	+3311	+1.691	-798	-3.340	-2306	ΔS/12EI
10- ϕ		-2118	-3667	-1995	1382	4.693	6384	5586	2.246	=0 ΔS/12EI
11- v_{10}									=0	ΔS/12EI
12- u^{IV}_q	0	-798	-2268	-3.108	-2502	-.376	+2586	+5.214	+6.280	ΔS/12EI
13- u'''_q	0	-044	-124	-.170	-137	-021	+.142	+.287	+.344	cm
u''_q	0	-042	-107	-150	-118	-018	+.136	+.248	+.297	cm
3er Ciclo 1- u_o	0	052	+143	+.173	+123	-005	-.148	-.289	-.337	cm
2- Q	0	049	136	.164	+117	-025	-141	-.275	-.320	T/m
3- V		.275	324	.460	.624	741	.736	.595	.320	T/m
4- M	-1810	-1706	-1.577	-1383	-1109	-773	-432	-152	0	Tm/m
5- $\bar{\alpha}$	+10655	20447	18859	16516	8246	9271	5245	1.952	.240	ΔS/12EI
6- ϕ		10665	31112	49971	66487	79.733	89004	94249	96201	96441 ΔS/12EI
7- v_{10}										
									-62451	ΔS/12EI
8- M	+438	+109	-136	-.263	-.255	-128	.061	.251	0.373	Tm/m
9- $M_{\phi E}$	-665	-074	+223	+306	+.243	+091	-100	-272	-0.273	Tm/m.

TABLA 5.3

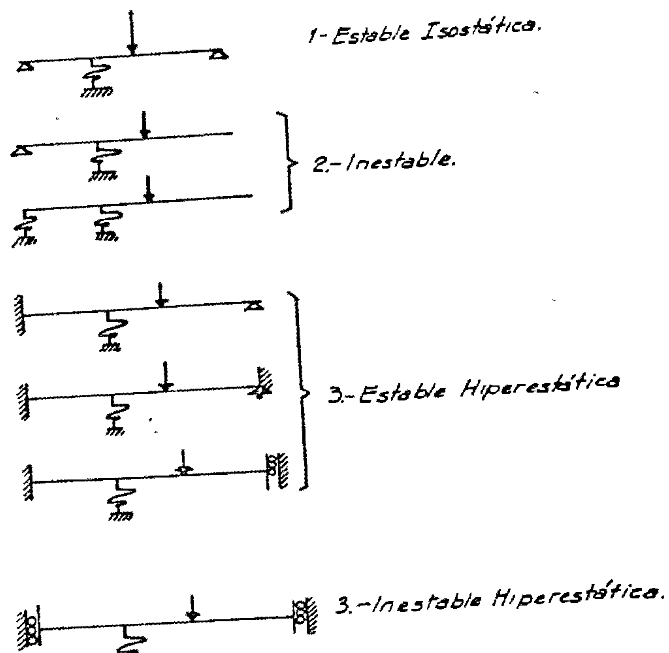

FIG. 17.3.

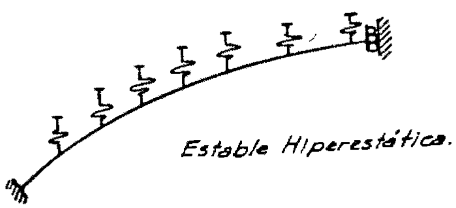

FIG. 18.3.

valores de P y Mc correctivos.

$$-96\ Mc - 41.424P + 141.461 = 0$$

$$41.764Mc + 32.022P - 91.411 = 0$$

Resolviendo el sistema resultan:

$$Mc = 0.553\ T\ \frac{m}{m}$$

$$P = 2.134\ T/_{m.}$$

8.- Sumando los efectos de estas correcciones a M (de acuerdo con la configuración correctiva de la Tabla 3.3) se obtienen los valores de M'.

9,10 y 11.- Se recalculan los valores de ϕ_{10} y v_{10} para checar que sean cero.

12 y 13.- Se obtienen los valores de u'_Q en el renglón 12 en función de $\frac{\Delta s}{12EI}$ y en el 13 en milímetros.

Los valores de u'_Q deberán ser iguales a los de u_Q supuestos, sin embargo, se nota una apreciable discrepancia. El procedimiento es en general lentamente convergente y una forma de acelerar su convergencia, consiste en tomar promedios pesados de los valores u'_Q obtenidos y los u_Q supuestos.

Por vía de ilustración se continúa el análisis aceptando los desplazamientos u'_Q. Si los valores que a partir de u'_Q resultan nuevamente mayores, el proceso será divergente.

2o. Ciclo.

1 a 12.- Con los valores de u'_Q en la misma forma expuesta se obtuvieron los valores u''_Q. Se puede observar que los valores de u''_Q vuelven a ser pequeños de manera que el sistema es convergente.

Las variaciones de los valores u_Q son aproximadamente como se indican en la figura 19.3. En un nuevo ciclo convendrá tomar el --

omedio de u_Q, u'_Q y u''_Q.

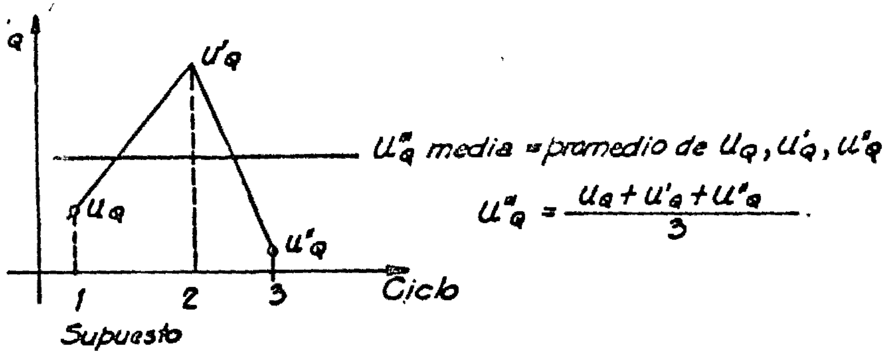

FIG. 19.3

3er. y 4o. Ciclos.

A partir del promedio u'''_Q se vuelven a obtener los conceptos u_o, Q, V, etc., hasta u^{IV}_Q. Las diferencias entre u^{IV}_Q y u'''_Q son bastante - pequeñas de manera que no habrá necesidad de otro ciclo. Se calculan los momentos M (renglón 8 del 4o. ciclo) a partir del promedio de - - u^{IV}_Q y u'''_Q.

En el renglón 9 se presentan los valores de $M\phi_t$ que es la suma de M y $M\phi$ (corregido elásticamente). En la figura 20.3 se indican las elásticas de los dos métodos presentados. En la figura 21.3 se muestran dos diagramas de momentos transversales calculados anteriormente.

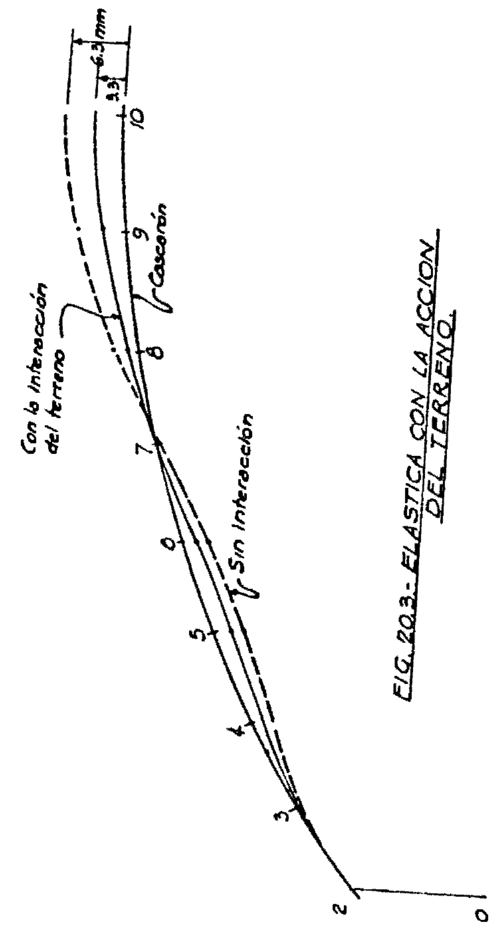

FIG. 20.3.- ELASTICA CON LA ACCION DEL TERRENO.

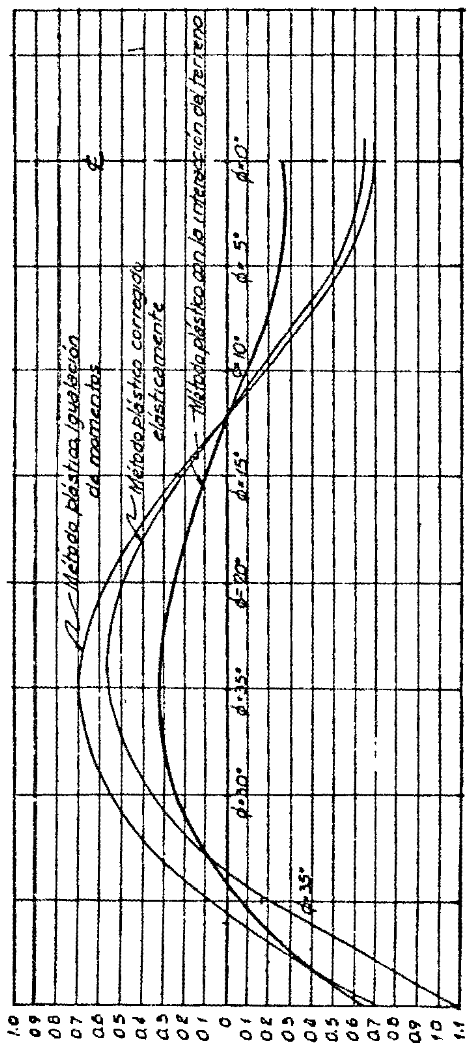

FIG. 21.3. DIAGRAMAS DE Mφ.

Para fines de diseño en general no será necesario tomar en cuenta la corrección de P para los valores de Nφ pues influye bastante poco en el valor total. La corrección P del 4o. ciclo fué 1.464 T/m. de compresión.

11.3 A continuación se efectúa el diseño de los cascarones de una cimentación ideal simplificada. Se presentan los conceptos básicos que intervienen en el análisis propio de los cascarones y no se insiste en el del emparrillado en el cuál sólo se pretende mantener el equilibrio estático sin considerar hundimientos diferenciales ni variación de presiones. Cualesquiera que sean los métodos con los que se resuelva el equilibrio del emparrillado el método plástico numérico sigue siendo aplicable, de manera que no siendo asunto de esta tésis el estudio general de la cimentación, se resuelve la cimentación en la forma más sencilla en la que puedan atacarse los problemas que hasta ahora se han analizado. Supóngase la Fig. 22.3 en la que se indican las cargas de la superestructura incluyendo el peso propio de la cimentación. Estas cargas corresponderían a un edificio como el que se esquematiza abajo. Por simetría de cargas y geometría se cumplen las condiciones de equilibrio:

$$\Sigma Mx = 0$$

$$\Sigma My = 0$$

$$\Sigma P = 300 + 2 \times 150 + 2 \times 200 + 4 \times 44 = 1176 \text{ Ton.}$$

Superficie cubierta: $14 \times 14 = 196 \ m^2$

Reacción media $q = \frac{1176}{196} = 6 \ ton/m^2.$

El análisis se puede dividir en dos etapas:

1a.- Considerando las columnas como apoyos fijos, encontrar las reacciones verticales en los nudos.

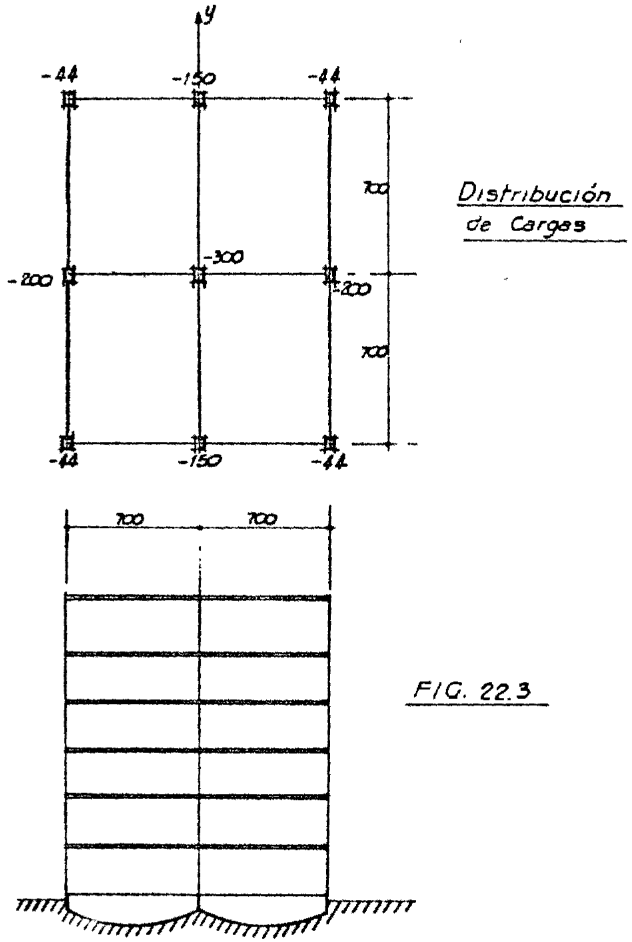
y
-44
-150
-44
700
-300
-200
-200
700
-44
-150
-44
Distribución
de Cargas
700
700

FIG. 22.3

"On Questions of Shape and Scale in the Design of Space Frame Shells"

by

F Castaño H , **Triodetic de México, S. A., México, D. F.**

and

D. T. Wright, Toronto, Ontario, Canada

Paper for

International Congress on the application of Shell Structures in Architecture
Mexico DF - September 19 7

In the history of building, architecture has always been constrained by the limited capabilities, at any time, of current structural technology - and great architecture has always exploited to the limit the capabilities of current structural technology While the history of architecture is usually traced stylistically, it is thus equally convenient to trace it in terms of the development of structural technology, which development has been usually characterized by fairly abrupt changes as new technologies become adopted on a widespread basis It is interesting to note, however, that changes in the building industry do not reflect technological developments quite as rapidly as those in other fields - e. g the conquest of the electronics industry by the transistor This is, of course, because of the highly decentralized nature of the building industry and because of conservatism in taste which leads to initial hesitation until such time as leading designers have clearly shown the way with new developments.

It seems worthwhile to point these circumstances out because it seems that in the case of the space frame shell we are on the threshold of another pervasive and radical change in building technology, corresponding in significance to the introduction of metallic skeleton building structure to a world of masonry gravity building, or corresponding to the introduction of reinforced concrete surface structures (plates and shells) earlier in this century

Interestingly, the space frame shell structure provides for the conjunction of the benefits of skeleton building construction with the benefits of surface or membrane structures Just as the strong and efficient but light-weight steel skeleton permitted a tenfold increase in practicable building heights when it was introduced, so the space frame shell appears to carry the well-established benefits of shell construction to a differen order of scale The concern of this paper then is with a discussion of questions of shape and scale in space frame shells

Shell structures have conventionally been constructed in reinforced concrete, usually as monoliths, although an effective technology for precast reinforced concrete shell structures has recently been developed in the Soviet Union. The structural significance of the shell has been the realization of a generally moment-free structure of remarkable efficiency as compared with structures acting flexurally over comparable spans. The architectural significance and exploitation of potentials of shape and structure with shells is perhaps best illustrated by reference to the works of architect Felix Candela.

Notwithstanding the great fertility of imagination and realization in the history of development of reinforced concrete shell structures, it is evident that the technology of such shell structures is severely restricted. While clear spans up to 25 metres may be fairly common, and clear spans up to 100 metres or so have been shown to be possible, spans much over 50 metres are practical only in terms of certain kinds of stiffened spheroidal forms and these often are relatively expensive. In general, in fact, the choice of geometric surfaces for reinforced concrete shells is severely limited by problems of forming and construction. The great majority of all reinforced concrete shells built have been shaped to surfaces of revolution. While some elliptic paraboloids have been constructed, the only commonly used translational surface for reinforced concrete shells is the hyperbolic paraboloid. And perhaps the greatest constraint on the application of reinforced concrete shells in building has been the very high cost of construction - the fact that their construction is highly "labour intensive", a characteristic which puts them at odds with the general trend towards increased industrialization in building.

The notion of the space frame shell is that of a structure formed as a skeleton in space with the nodes or connections tracing out a smooth surface - or shell - in space. The space frame shell, while skeleton, is very different from the usual building skeleton. Reflecting the ability of a membrane structure to function without bending, members in a space frame shell have only axial forces as primary loading, and for the sake of industrialization and mass production, individual members in space frame shells tend usually to be of more or less constant section throughout the structure

The development of an effective technology for space frame shell structures has been concluded only very recently The pioneering work of such people as Buckminster Fuller has shown the practicability of the general structural forms, and has popularized the entire notion But for the realization on a consistent basis of effective and economic structures rather more was needed than the development of notions of form Perhaps the most difficult challenge has been in developing practical and economic connection methods for members coming together from all directions to points in space The other critical technological problem was the development of effective methods of analysis and design for the proportioning of such structures.

Within the past decade a number of connection systems, including Triodetic, Mero, Octaplette, SPC, etc , have been shown to be effective It is not within the scope of the present paper to deal in detail with these various methods of connection It is perhaps sufficient to note that effective connections are available that permit space frame shell structures to be designed as if the connections were perfect, so that attention can be focused solely on general questions of shape, geometry, and member selection It is, of course, inevitable that in due time experience in construction and with costs will identify the most suitable connection or connections

The structural design of space frame shells is challenging to conventional analysis by reason of the very great number of members involved. In a conventional multi-storey building, design considerations are usually restricted to plane frames, and a framework with 200 connections and 400 members is already considered to be large Quite modest space frame shells have over 1,000 joints with some 3,000 members, and practical space frames may now be considered with up to 100,000 joints with, perhaps, 500,000 members In a space frame there may be three to five times as many members as joints and full three-dimensional behaviour must be considered with three unknowns per joint, if bending is exluded, and six per joint if it is to be considered

Three approaches are evidently available for the analysis of member forces in space frame systems The first consists in dealing with the framework more or less as one deals conventionally with structural frameworks, determining explicitly all forces and deformations in discrete form While traditional manual methods of analysis and calculation would be quite unthinkable for systems of the sort described, the capability of modern digital computers to invert very large matrices has allowed discrete analysis to be used for some smaller space frame shell structures, although larger structures are still beyond the capability of even the largest of current computers A second approach, which is evidently in widest use, treats the space frame shell as a continuum and involves the analysis of a shell having elastic properties such that its deformation under load would be identical with that of the space frame structure, with the results from such a continuum analysis transposed to indicate individual member forces and moments, etc The third approach, provides for the writing of difference equations reflecting the discrete form of the structure and node spacing, etc , which are parallel in form to the differential equations that are encountered with continuum analysis.

As well as the problem of determining member forces, etc , experience has shown that over-all instability is often the governing consideration in the design of space frame shells - especially those of positive Gaussian curvature So far, at least, only the continuum analogue approach has been shown to be effective in providing analysis for instability The usefulness of the continuum concept in dealing with instability confirms as well the value of the continuum concept as providing a basis for general understanding of behaviour in a qualitative sense, especially as related to the already well-understood behaviour of ordinary continuous shells.

It may be appropriate now to turn to a discussion of some of the kinds of design decissions required with space frame shell structures. The first and most critical consideration is that of over-all span and general shape The upper limit of spanning capacity of the single layer or reticulated space frame shell is of the order of 100 metres, although considerations of economy and erection may limit its effective span to about 75 metres It has been shown that the double-layer space frame shell has an upper limit of spanning capacity of the order of 800 metres Design studies are already in hand in Great Britain for space frame shell structures with clear spans of the order of 500 metres and these have been shown to be feasible and, indeed, remarkably economic Such spans are, of course, much greater than those of any existing roof structure in the world The development of a technology for space frame shell structures, as outlined above, thus seems to open the door to radical new departures in building design, and even in the nature of building - in the sense of providing environments for human activity which are not buildings in the ordinary sense While specific cost data cannot be introduced without specific notions of loads, and material and labour costs in different countries, it is important to note that the influence of span on unit cost with space frame shell structures is not even linear This contrasts sharply with the influence of span on structural systems such as trusses or beams or ordinary slabs which operate in bending where the cost per unit of area covered may increase with the square of the clear span.

With space frame shells, the structural cost per unit area increases not much more rapidly than as the square root of the increase in clear span: that is the increase in cost per unit area for a doubling of clear span will be of the order of 50 per cent or less And space frame shells become competitive in cost which conventional alternatives at spans of 20 or 25 metres It can only be concluded from this discussion that space frame shell structures provide an opportunity for a radical change in scale of building in an entirely practical and economic fashion It would seem that structures with clear spans of 300 or 400 metres should soon become commonplace

On the question of general shape, great flexibility is available. The conventional rotational and simple translational surfaces with which we are familiar in reinforced concrete shells are, of course, all applicable to the space frame shell structure. But interestingly, surfaces of arbitrary shape-so costly to form in reinforced concrete- are really not fundamentally more difficult to construct than simple spherical segments This is because space frame shell structures are erected without falsework, on a more or less self-scaffolding basis Shape is controlled not by field constraints on formwork but by the precise control of node spacings and positions in the manufacture of the structural members. These are, of course, always factory manufactured - whatever the structural jointing system used As a result the only penalty in the choice of an arbitrary shell form lies in the greater variety of member lenghts and end angles required Modern computer methods for determining member dimensions, and modern production methods, enable shells of arbitrary shape to be manufactured economically

A striking example of such a shell is that recently constructed in Toluca for the new Escuela Normal of the Estado de Mexico The geometric form is indicated in Figure 1 and is seen to be defined by assymetric parabolas in varying attitudes Node spacing was approximately 1 metre, and some 5,000 aluminum tubes were used, all of 2 inch diameter with a wall thickness of 0.0 0 inches. The geometric requirements of the surface necessitated the use of 2, 00 different members so far as lenghts and end angles were considered: nevertheless, the structure was erected in fifteen days with a crew of fifteen men only one or two light erection towers Confirming what has already been indicated, the structural design was governed by considerations of general instability

Beyond general considerations of over-all shape and span, several other questions of shape and scale must be dealt with One of the most interesting aspects of space frame design is that the scale of the individual member is remarkably uniform for great varieties of structural forms, types and spans. It has already been noted that in most space frame structures it is usually appropriate to have members of almost constant cross-section throughout, contrasting sharply with usual structural practice But even beyond this, experience with many kinds of space frame plate and shell structures for wide ranges of span and loading indicates that the lenght between nodes or connection points for individual members is almost always in the range 1 to 2 metres Many reasons exist that, together, tend to lead to this result Because of membrane shell action and the prevalence of axial loading, design loads and individual members are not often very large, and there is a natural tendency with tubular members (which are, of course, most suitable for resisting loads of arbitrary direction in space) to work to slenderness ratios of the order of 90 or 100 for optimum load-carrying capacity against material density

An important by-product of the tendency to have relatively uniform member lenghts in different kinds of space frame structures is that what might be called the "local scale" is then more or less independent of the over-all scale and span The apparent fineness of division of the surface thus increases with span Given the obvious necessity of cladding to resist weather, it follows then that, in general, ordinary space frame structures of large span do not reveal their skeletal construction from the outside after completion This is seen by many as a distinct disadvantage. On the other hand, interior appearance can, and usually does, effectively exploit the geometric pattern of the reticulated surface The shell at Toluca, already referred to, illustrates this circumstance clearly

The question of local scale and the treatment of the surface offer especially interesting opportunities in double layer shell structures As has already been indicated, considerations of structural stability indicate the need for double layer forms for spans over about 75 metres While it is possible and indeed very easy to realize a double layer space frame shell as a regular nesting of tetrahedra, with cladding of the outer surface equally easy, it is interesting to note two recent designs which have avoided this for obvious architectural benefit while retaining the distinct structural benefit of double layer structural form. The first example is that of the U. S. pavilion at Expo 67 where Fuller s conventional spherical geometry of nearly-equilateral triangles is used on the inner face, while the outer face is composed of hexagons with the cladding being fitted to the resulting externally concave hexagonally based pyramids While this structure has won great acclaim, and is appropriately transparent for an exhibition, it is interesting to contemplate that an opaque surface might be no less attractive, given this treatment of the local scale in three-dimensional form to obviate the utter regularity of a smooth surface.

Another, and very different example is that of Candela s Palacio de los Deportes being constructed for the Olympic Games in Mexico City in 1968. This is a variant of a space frame shell of double layer form, constructed as a series of intersecting arches of trussed steelwork The interstices, approximately 12 metres square, between the primary trusses are to be filled not by simple purlins with a surface everywhere tangent to the outer face of the space frame structure, but rather the interstices, and thus the over-all surface, are fitted to secondary space frame shells of hyperbolic paraboloid form. The result will then be in the character of a double layer space frame, but with a highly textured surface

Some comments have already been offered on the matter of geometric division of the surface The pattern of reticulation is of considerable importance from both structural and architectural points of view. It has already been indicated that typical node spacings are of the order of 1 to 2 metres It is evident from the most elementary considerations that the ability to resist membrane forces without bending in individual members requires a highly triangulated surface (An interesting instance of the consequences of failing to realize this circumstance and constraint may be seen in the controversial theme buildings at Expo 67 where the use of a truncated tetrahedron led, in effect, to a double layer space frame composed altogether of hexagonal forms which when assembled either in a plane or in space do not, in fact, lead to a simple stable structural configuration without moment joints) Only for the simplest shell forms - those with zerp Gaussian curvature - is it possible to cover a surface with contiguous congruent triangles Since it is possible, structurally, to build space frame shells of arbitrary form, we must necessarily then face the prospect of surface divisions which are not quite regular

The nature of the problem can perhaps best be seen by considering the example of the simple spherical shell surface Two kinds of geometric division have been used most commonly for this form One of this is that devised by Buckminster Fuller, and sometimes termed the "tracon" subdivision This pattern is realized by commencing with a icosahedron which is a regular solid having 20 congruent equilateral face triangles. The edges of a regular icosahedron are projected on to a circumscribing sphere and the resulting spherical triangles are then subdivided by lines paralleling their bisectors producing more finely divided sets of points which are, of course, finally connected by straight-line members The result is a geometry in which the primary triangular intersections forming the original 20 equilateral triangles have only five members meeting each node, and all the other nodes have six members meeting With this geometry, there is a fair but tolerable number of different bar lenghts although the different lenghts do not vary greatly The major disadvantages of the Fuller system are that a fairly large number of angular conditions must be met at node points, and that a horizontal intersection at a base produces a very large number of different member lenghts and special conditions.

An alternative, and at least equally popular system of subdivision, is that of a division by parallels of latitude on a spherical segment, joined by diagonal members such that in each ring all triangles between adjacent parallels of latitude are more or less equilateral. The result is a regular system in which members are constant in each ring, but in which successive rings tend to become more closely spaced With this system angles tend to be relatively constant and there is of course, no problem of starting from a base or a ring structure.

One of the last aspects of design is that of fitting the cladding to the three-dimensional skeleton structure Common structural practice might suggest the use of purlins spanning from node to node - but such designs become rather startling because purlin sections, designed for bending, can often be substantially heavier than the primary space frame structural members! Thus, for reasons both of structural efficiency and appearance it often becomes appropriate to integrate the purlin requirement with the provision of a member for primary structure This may be achieved in numbers of ways, but one of the simplest and most effective is to add some kind of "top hat" form to the primary member (using a special extrusion in the case of aluminum, or using a supplementary cold form member tack-welded in place with steel sections)

Actual cladding materials with space frame shells vary widely according to local circumstances It has already been noted that Fuller s dome at Expo 67 is clad in transparent plastic One of the cheapest and certainly one of the most attractive cladding materials is wood, either in the form of plywood, or in the form of butting boards of fairly narrow width Because of the remarkable lightness of the space frame skeleton primary structure, it may become beneficial to utilize composite action with a wooden deck. Scrupulous care must, of course, be taken with connections at nodes between the skeleton and the wooden deck, and to provide for continuity in the wooden deck itself if composite action is to be relied upon structurally Experience suggests that all this is indeed worthwhile, and that resistance to instability - by far the most critical aspect of the design of reticulated shells - may be greatly improved with composite action.

By way of conclusion, it seems clear both from theoretical derivations and from experience that space frame shell structures provide the opportunity for radical new departures in the achievement of shell structures of spans greater than have been known heretofore, and in forms different from any ever before achieved in shell structures Interestingly, these achievements are evidently attainable at cost levels comparable with conventional structure of modest span While considerable care is required in design, especially because of the danger of failure by instability in reticulated shells, design methods are now well established for space frame shell structures.

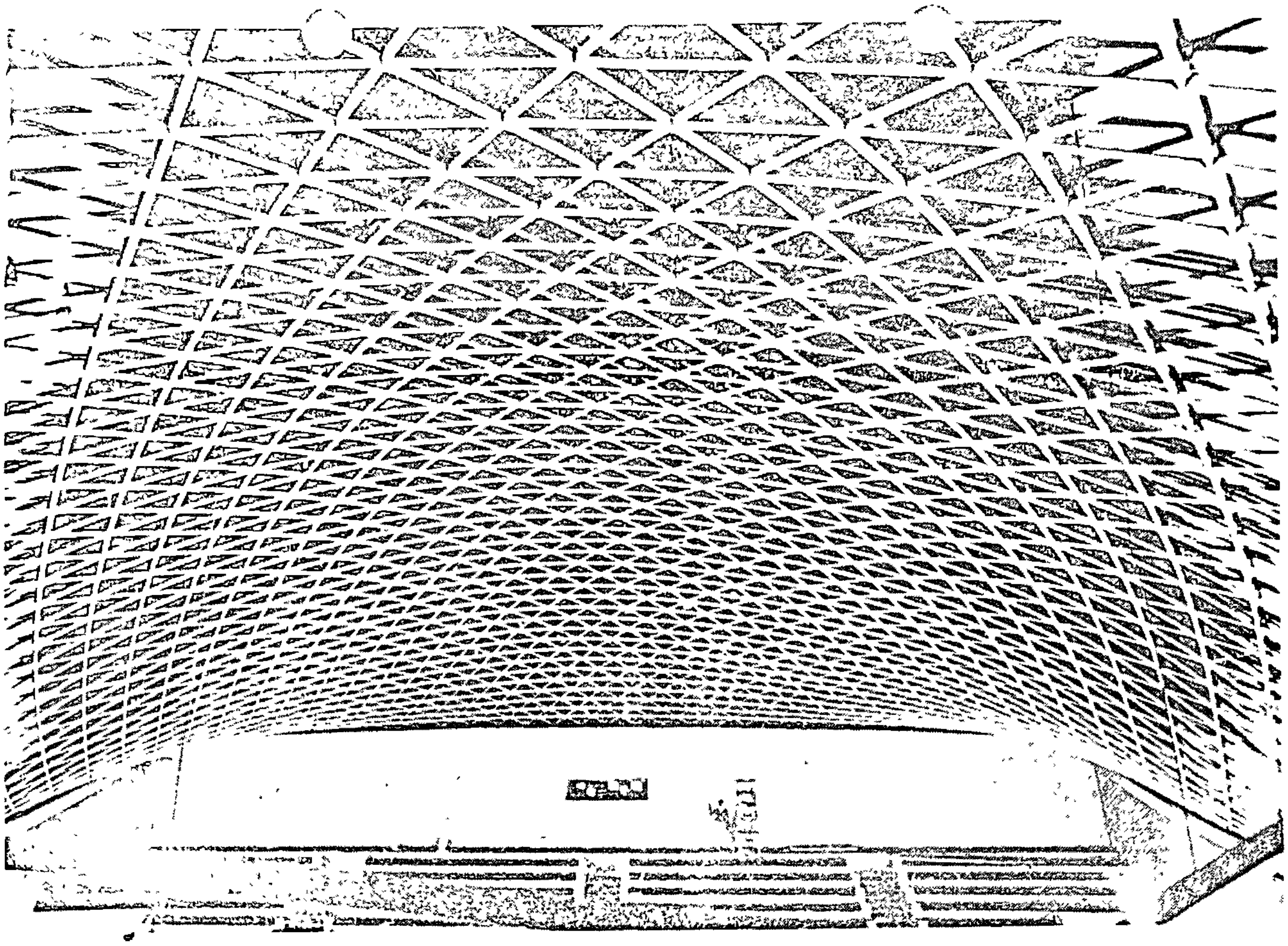

AUDITORIO - TOLUCA

ARCHITECTS: G. GALLO Y A. AZORIN
ENGINEERS: F. CASTAÑO Y D. T. WRIGHT

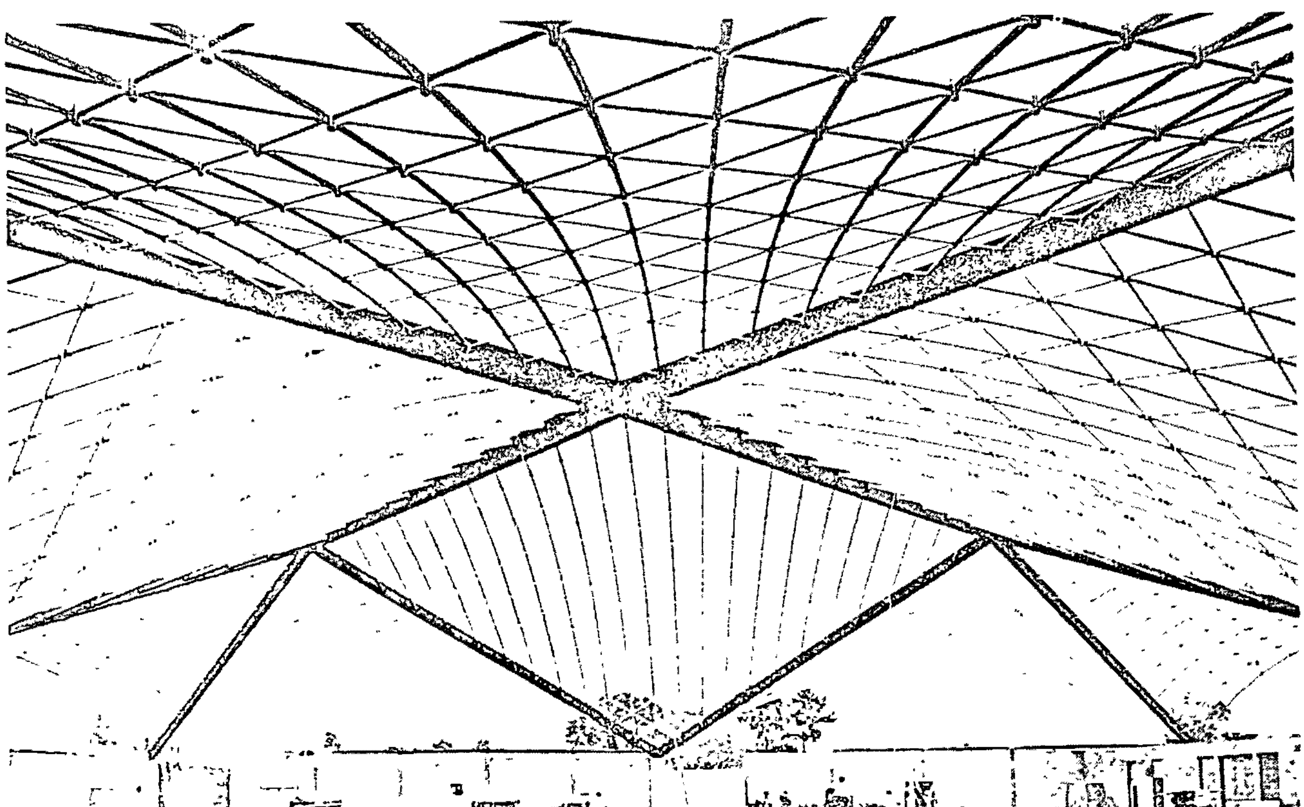

ROOF FOR INDUSTRY:

ARCHITECT: RICARDO SEIN
ENGINEER: FRANCISCO CASTAÑO

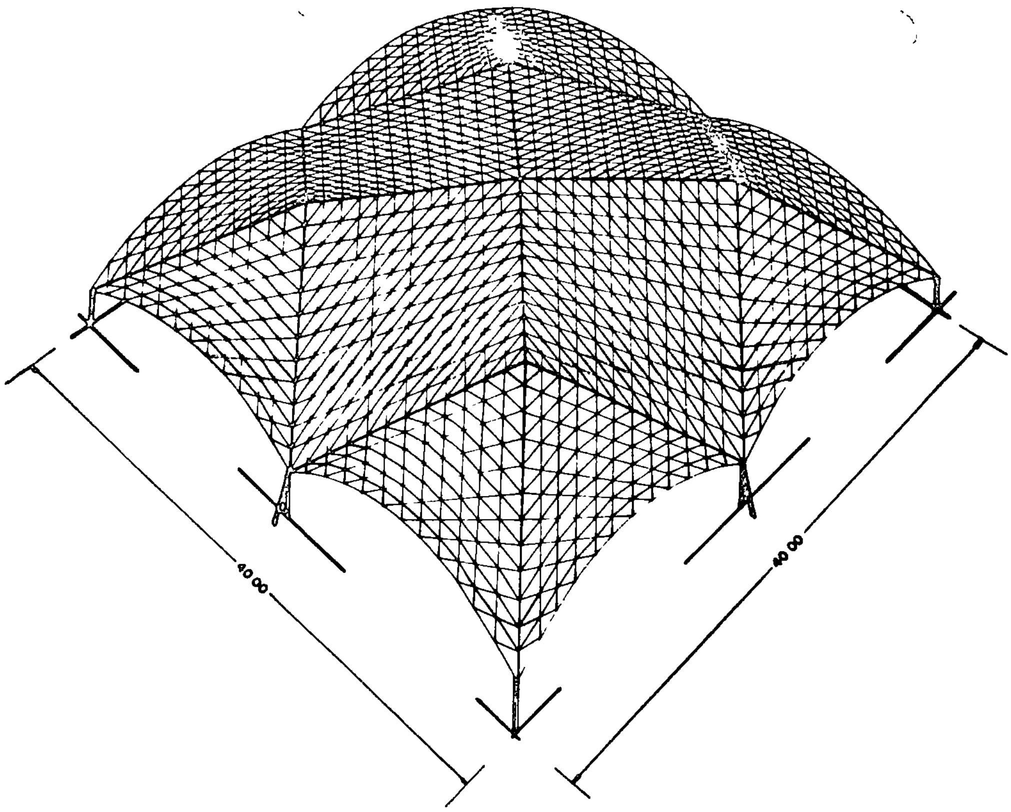

ROOF FOR INDUSTRY - GEOMETRY

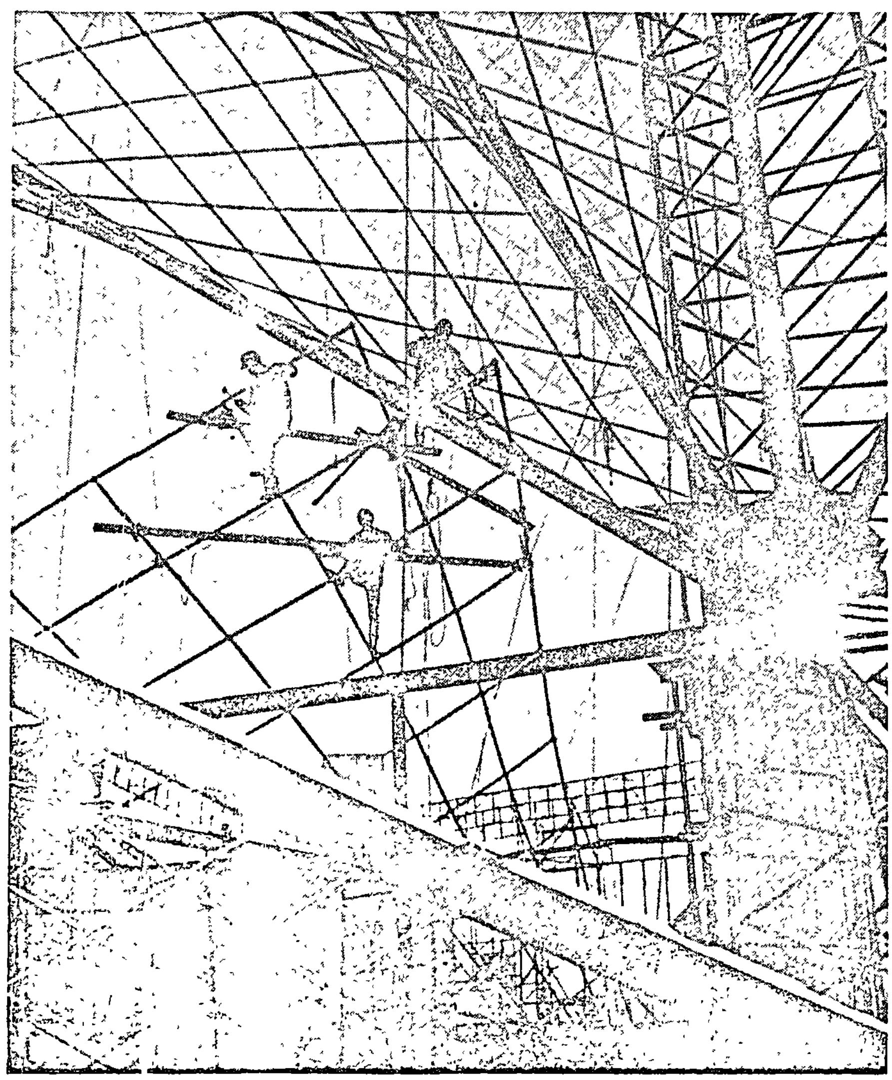

MEXICAN PAVILLION - EXPO'67
ERECTION OF HYPARS

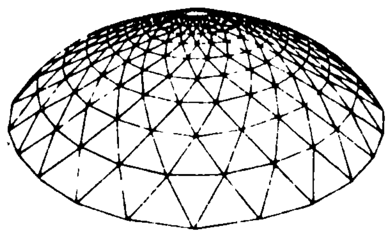

CUPULA.

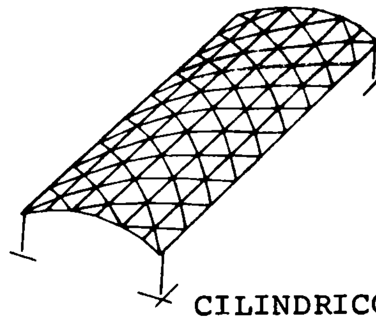

CILINDRICO.

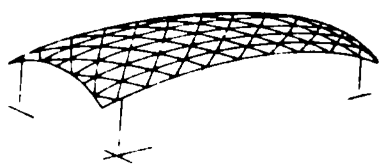

TOROIDE
o PARABOLOIDE ELIPTICO.

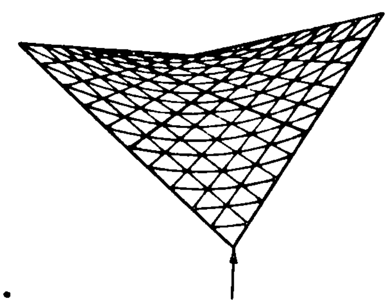

HIPAR.

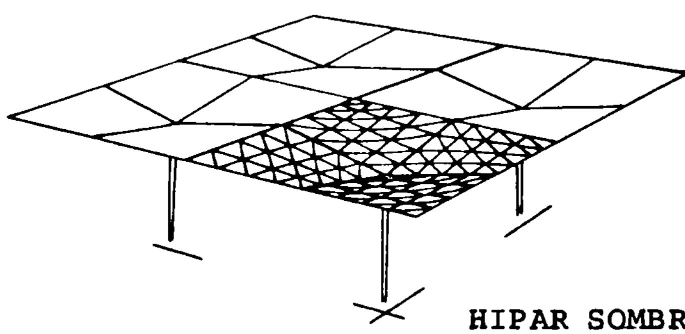

HIPAR SOMBRILLA.

2

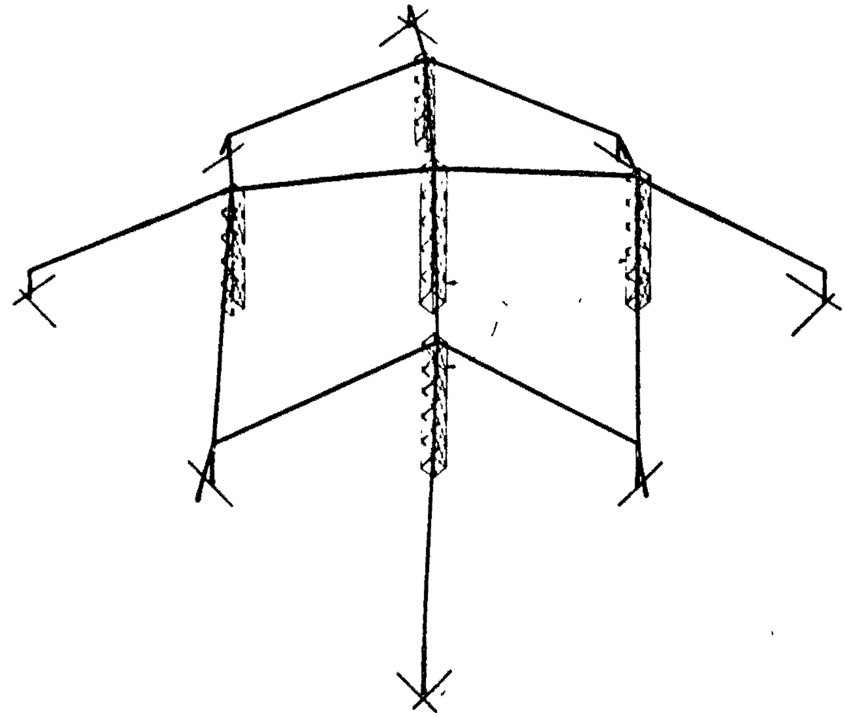

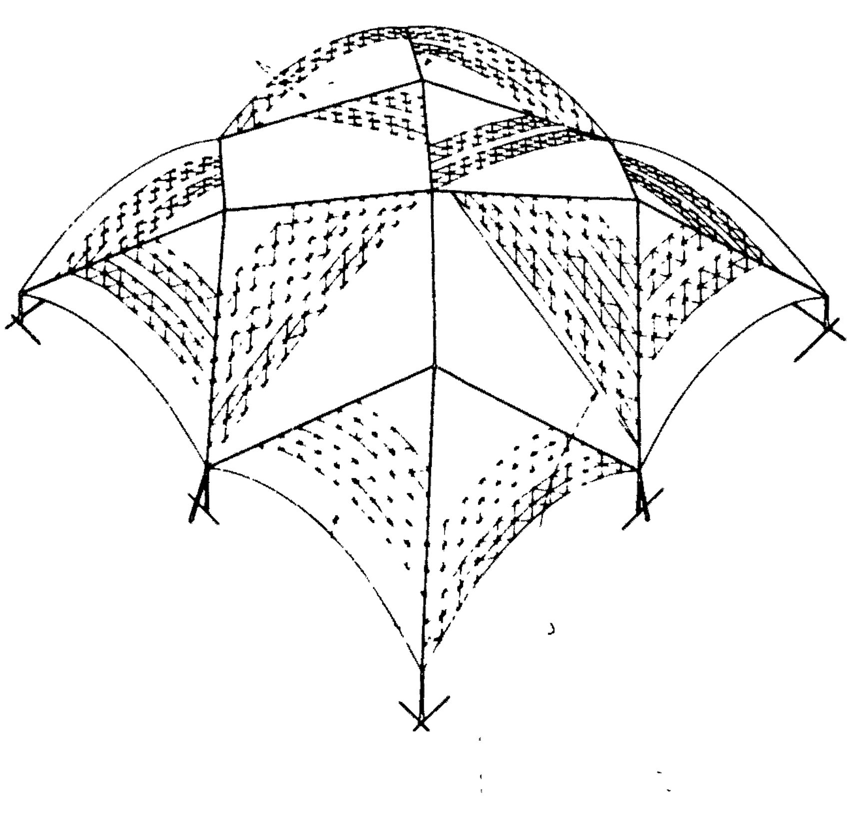

3

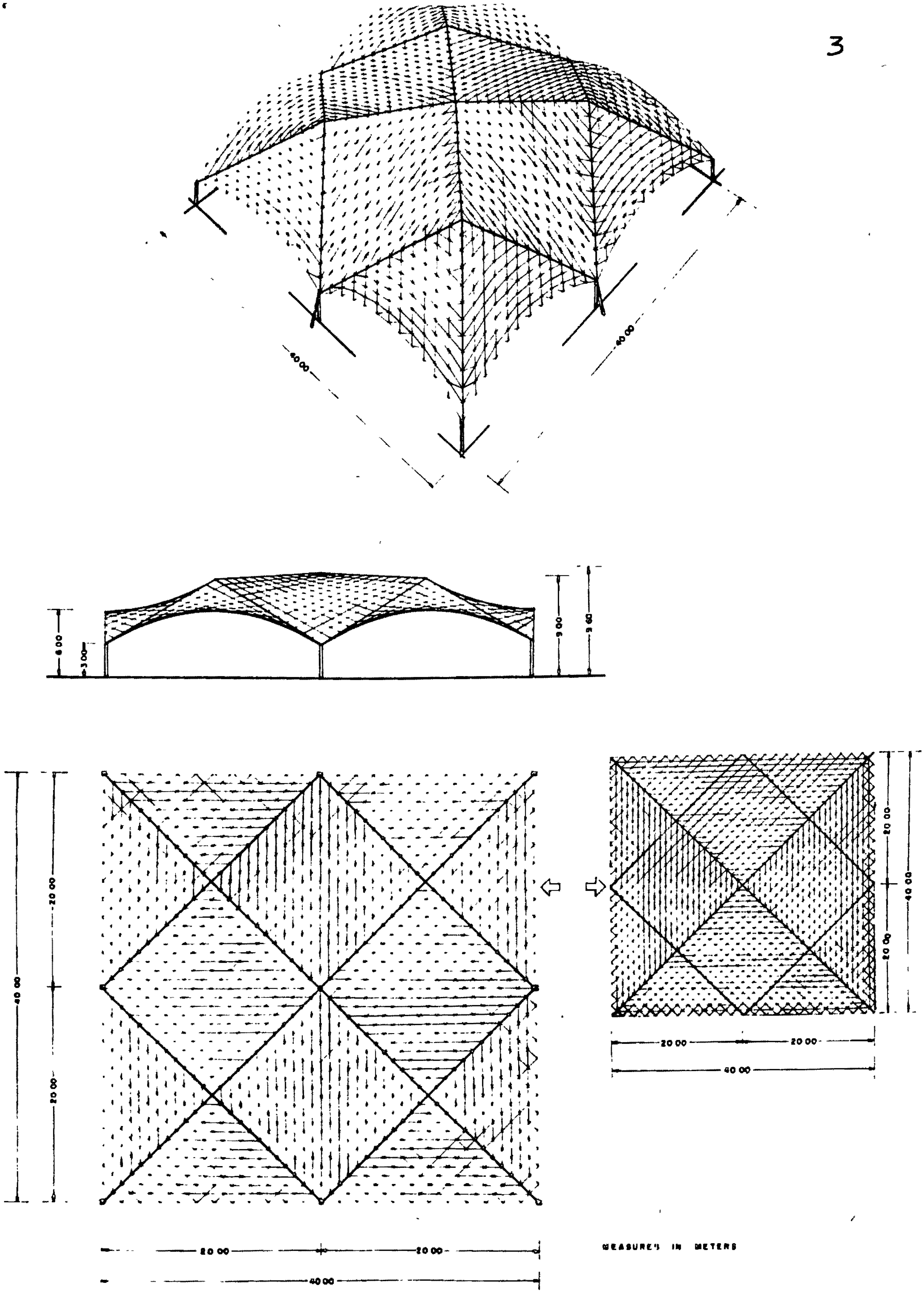
40.00
40.00
6.00
3.00
9.00
9.60
20.00
20.00
40.00
20.00
20.00
40.00
20.00
20.00
40.00
20.00
20.00
40.00
MEASURES IN METERS

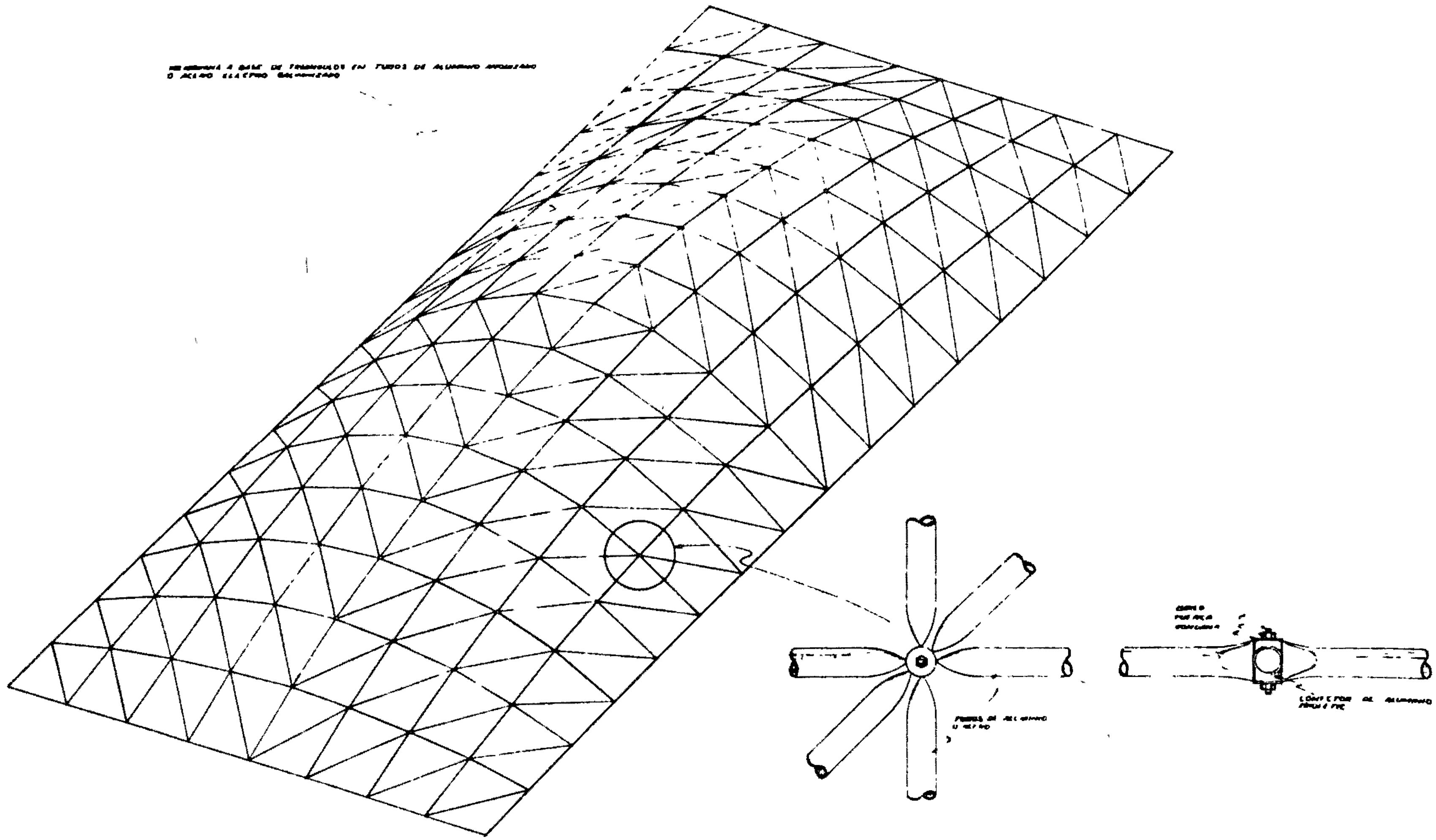

5

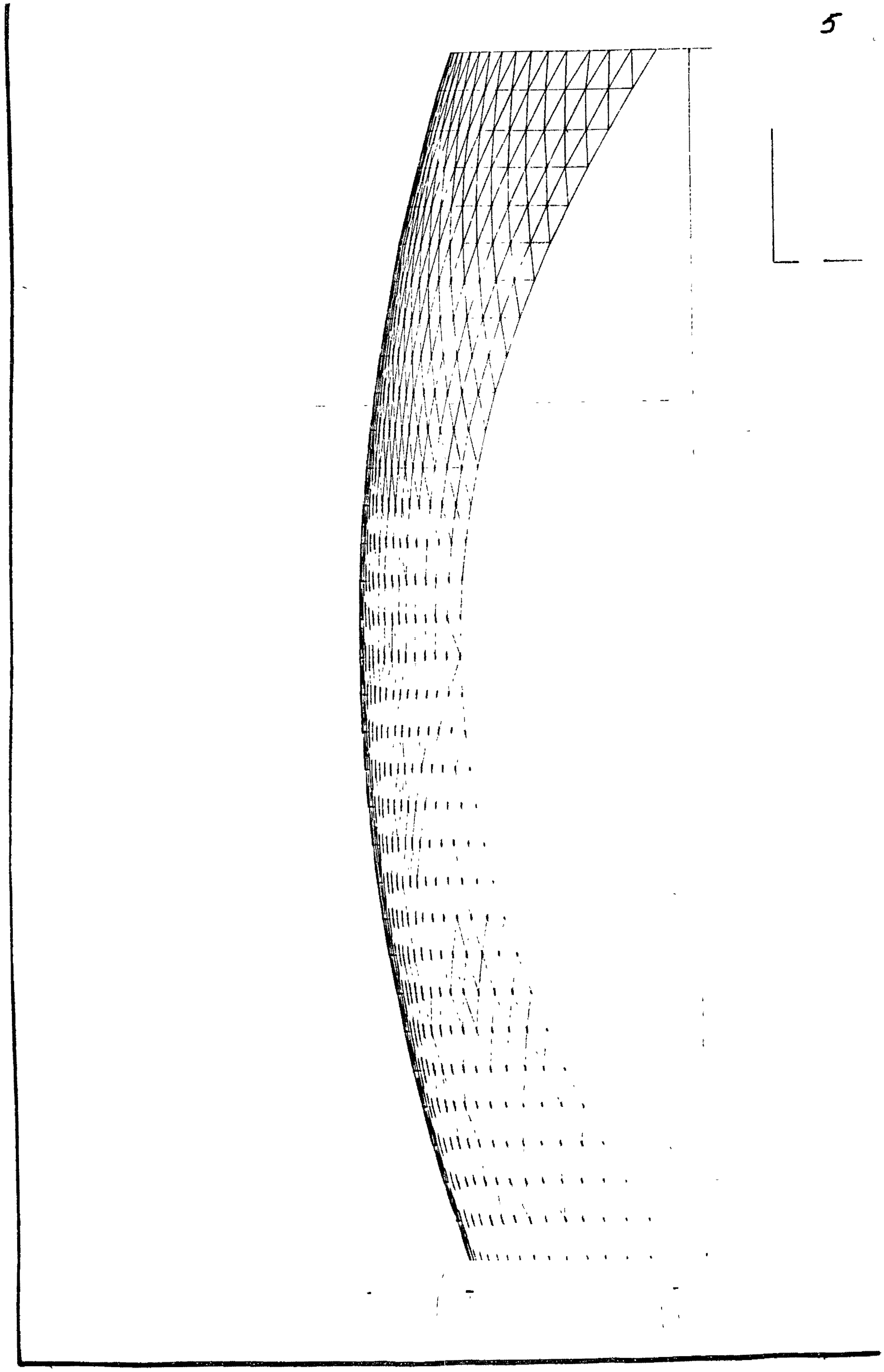

GEOMETRIAS ADAPTADAS A LA PLANTA DEL TERRENO ACTUAL

OPCION N. 1

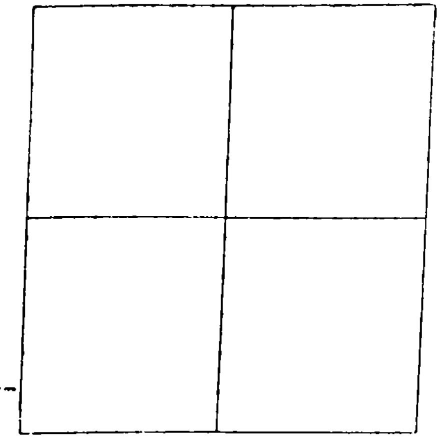

PLANTA

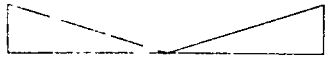

ISOMETRIA – COMBINACION PARABOLOIDES HIPERBOLICOS

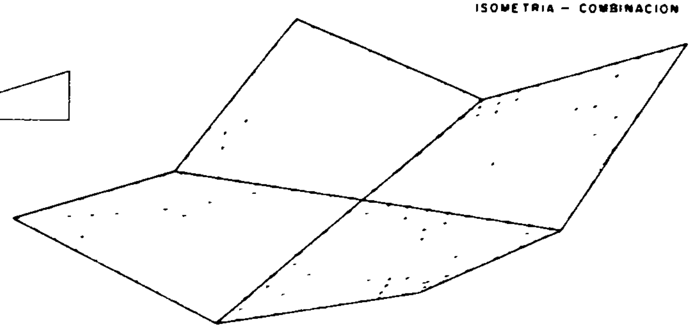

OPCION N. 2

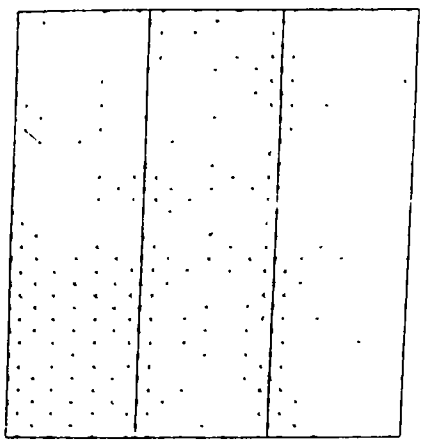

PLANTA

ISOMETRIA – COMBINACION CAÑONES CORRIDOS

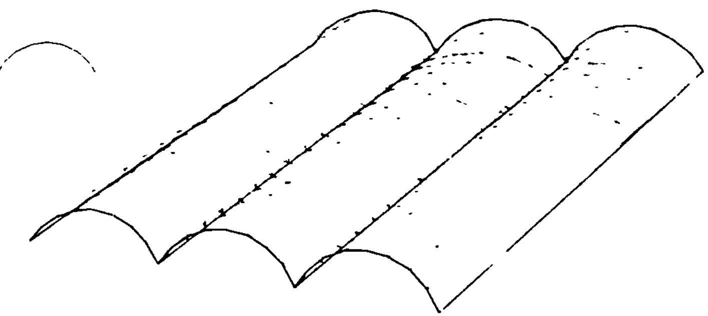

OPCION No 3

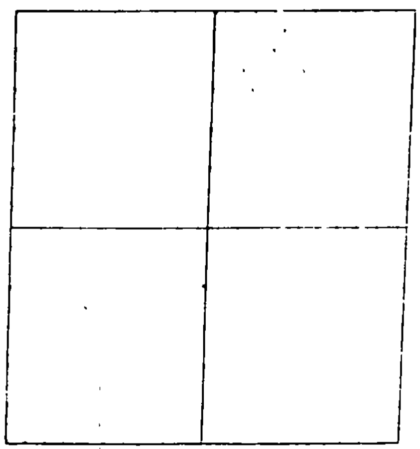

PLANTA

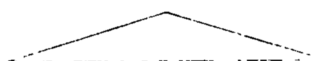

ISOMETRIA – COMBINACION PARABOLOIDES HIPERBOLICOS

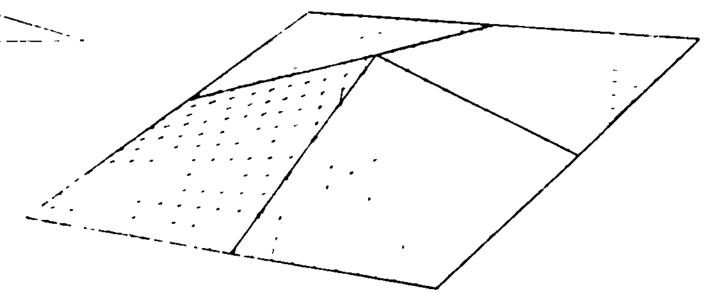

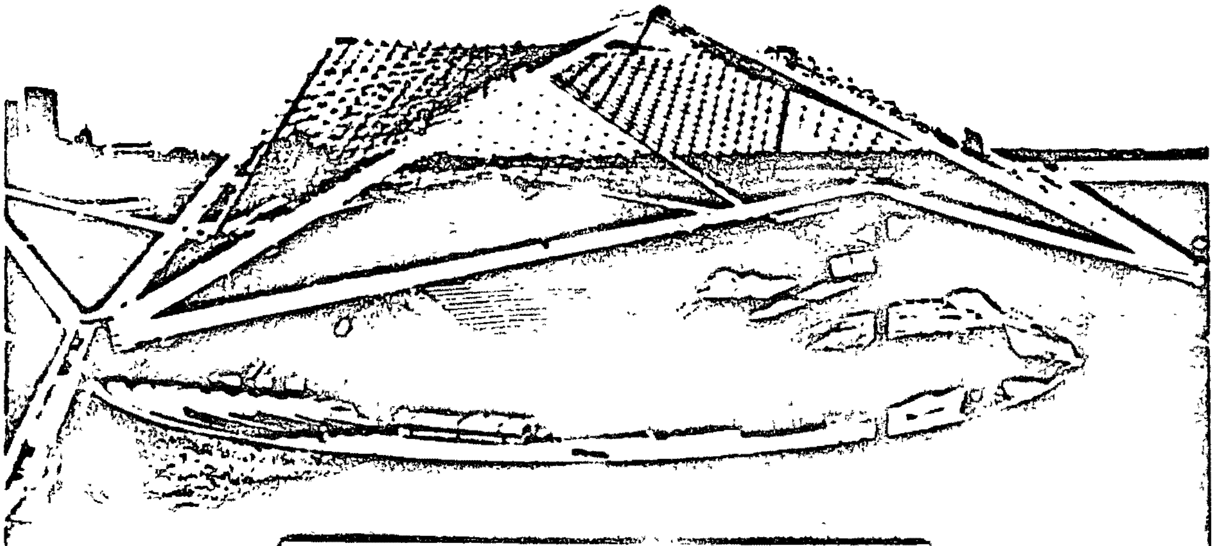

FIG. (11) FORUM AMPHITHEATRE, TORONTO

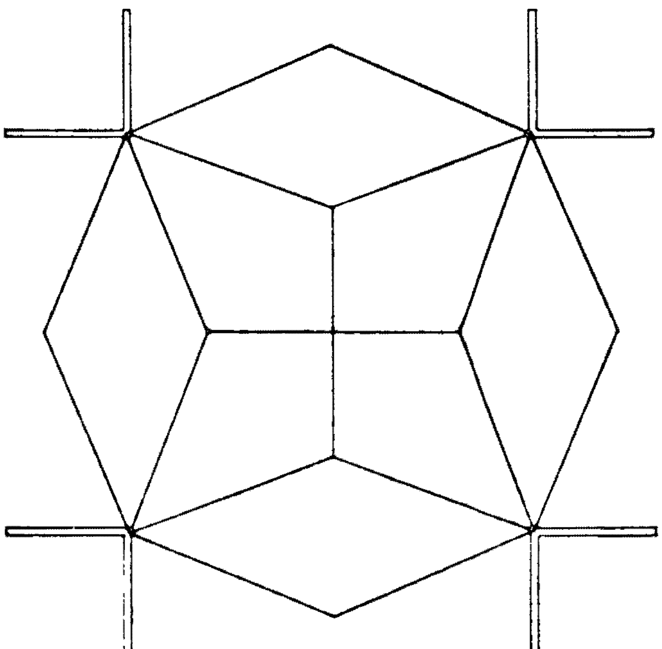

FIG. (12) PLAN

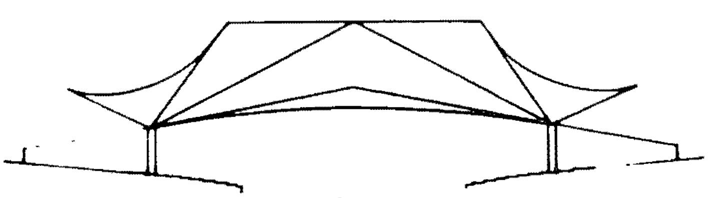

FIG. (13) ELEVATION

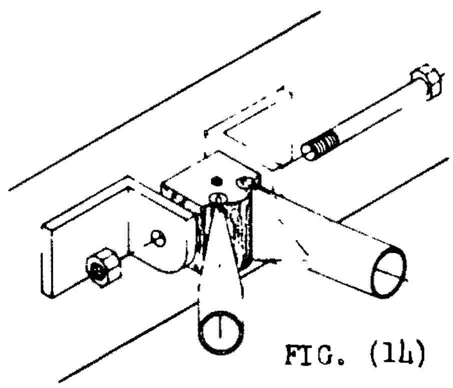

FIG. (14)

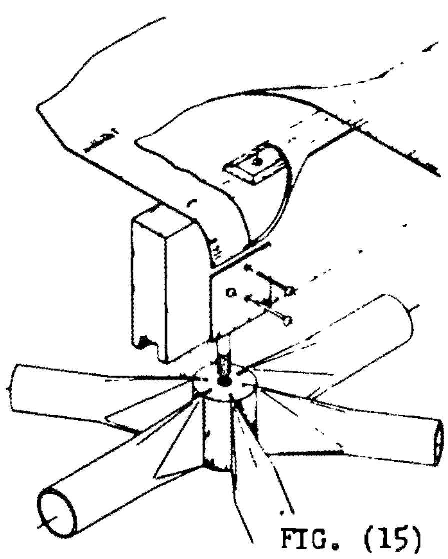

FIG. (15)

Triodetic de méxico, s.a.
AVE. NUEVO LEON 108 DESP. 205
TELEFONOS 511-7220 y 528-8618
MEXICO 11, D. F.

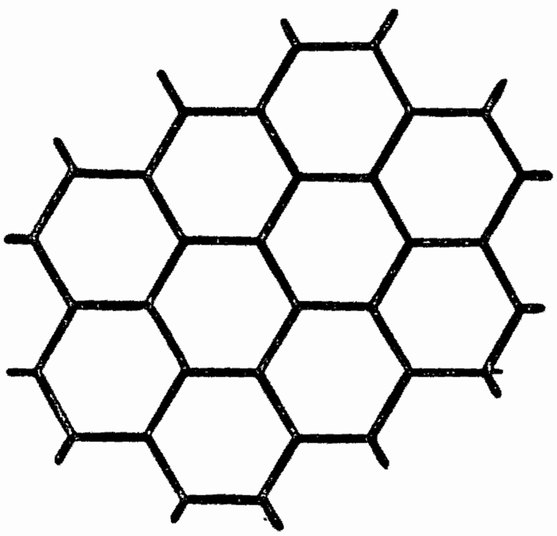

Membrana no estable
y sin rigidez

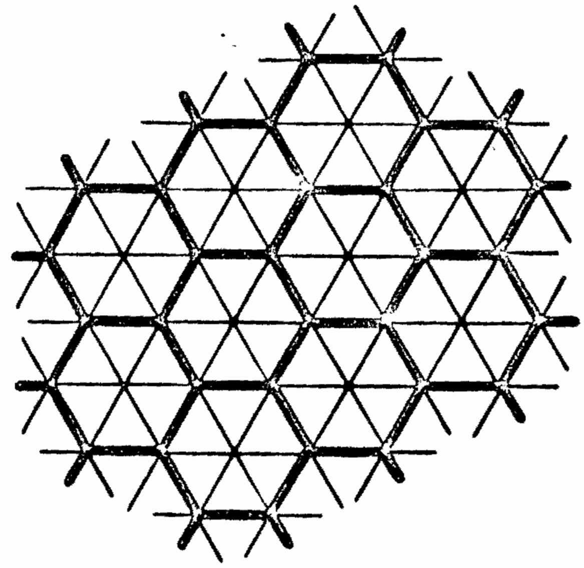

Membrana estable y
rígida.

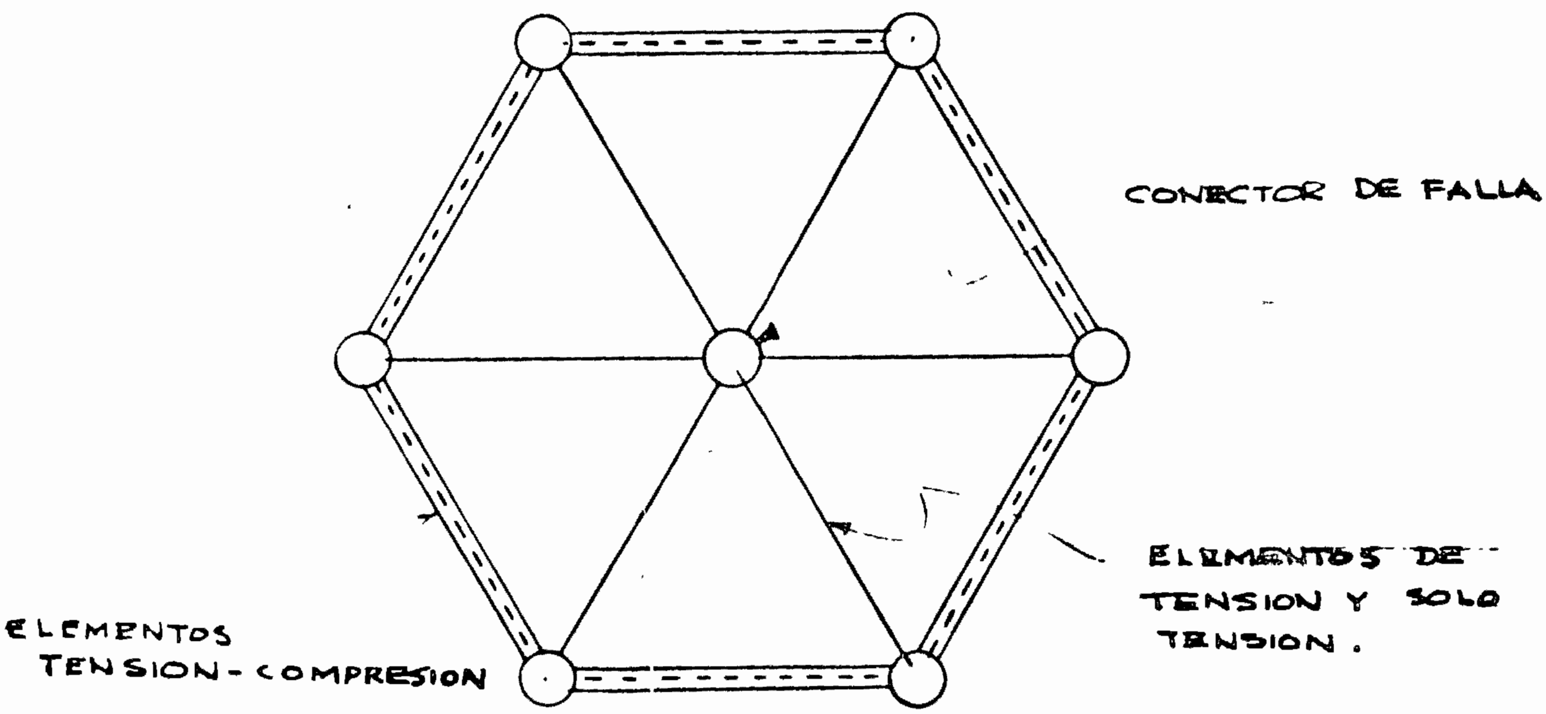

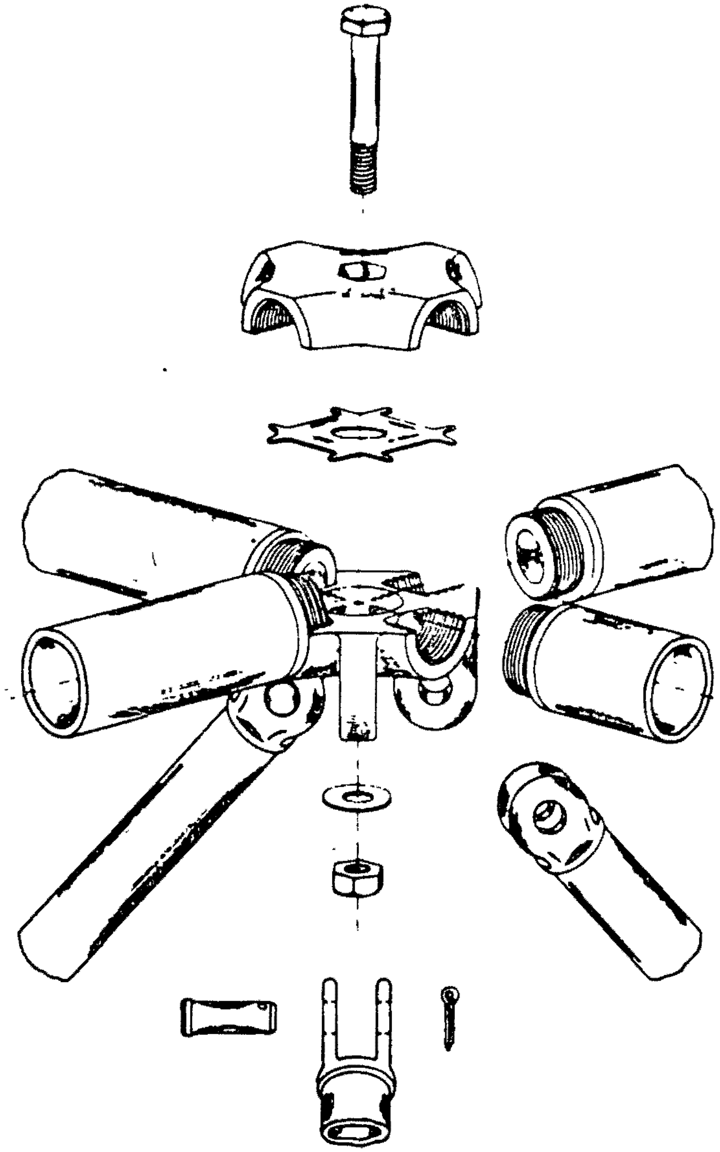

FIG. (1) STEWARTS & LLOYDS

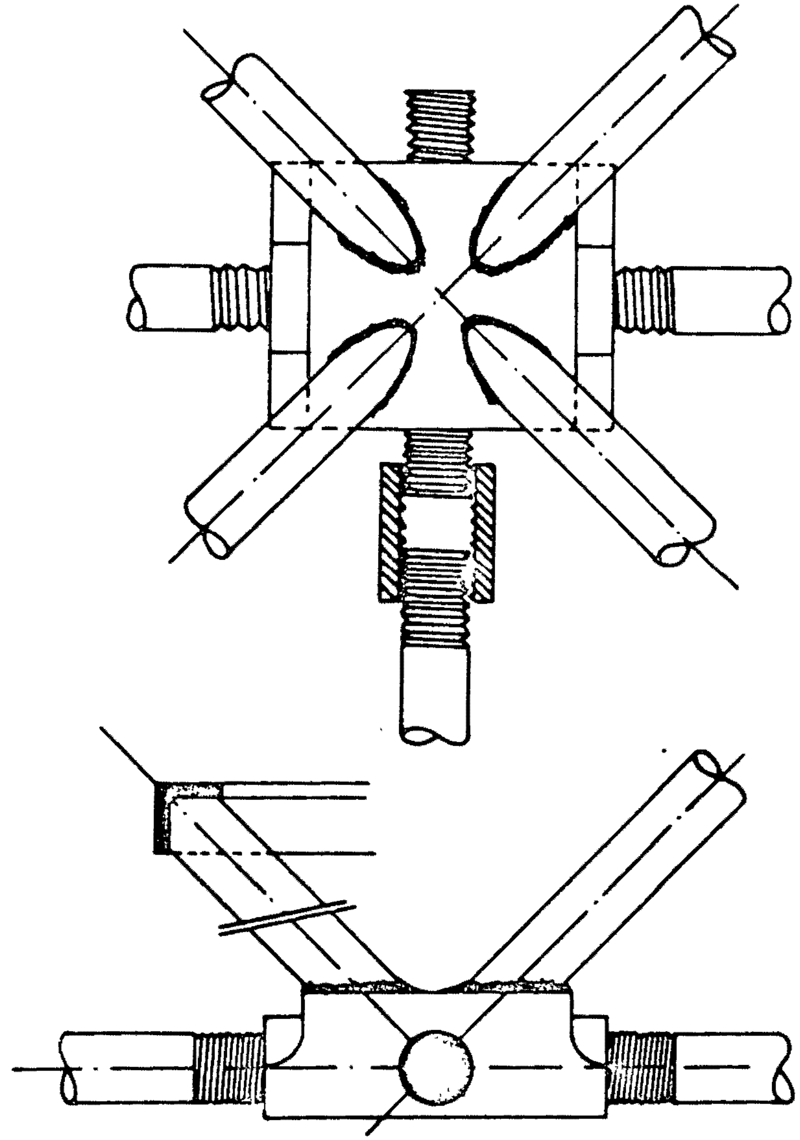

FIG. (2) SPACE DECK

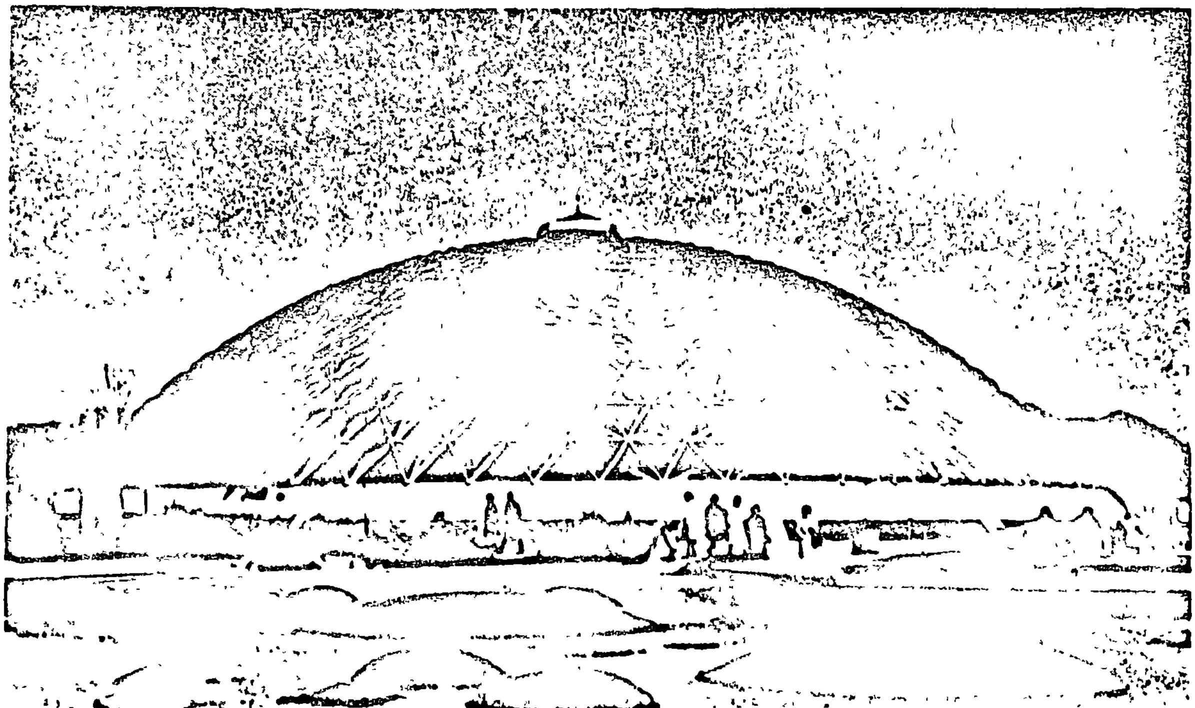

FIG. (7) CONSERVATORY DOME, VANCOUVER

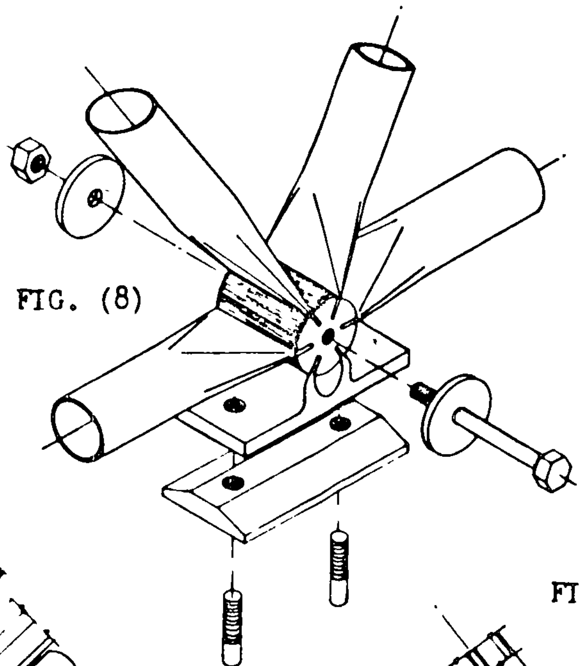

FIG. (8)

FIG. (9)

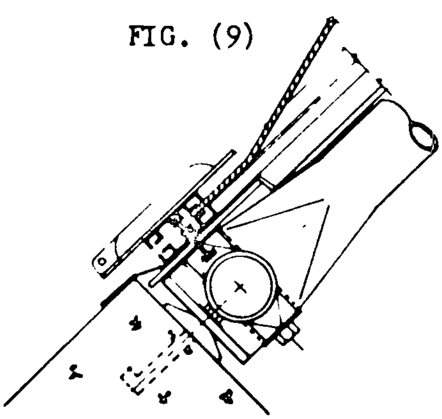

FIG. (10)

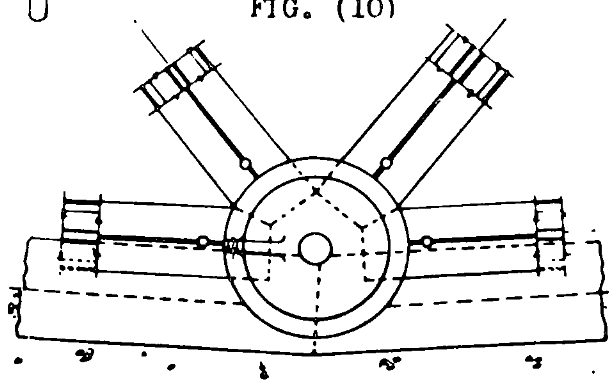

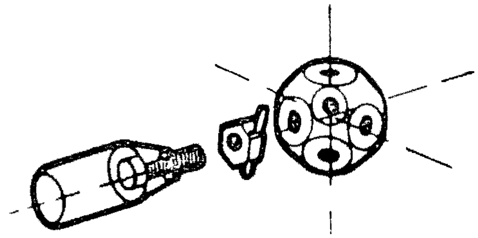
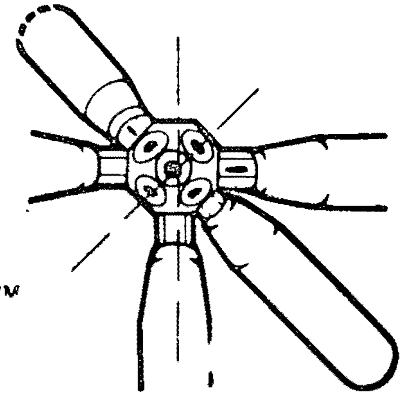

FIG. (3) MERO SYSTEM

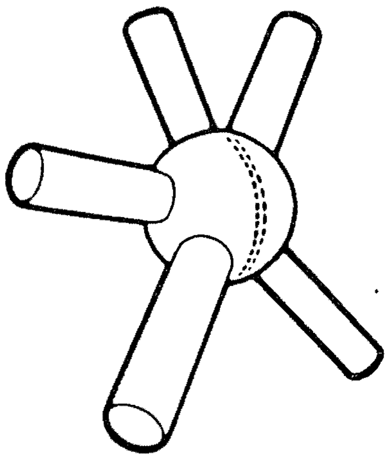
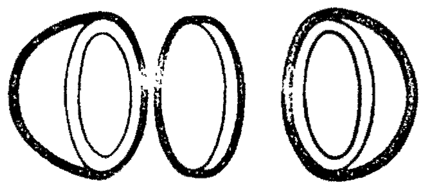

FIG. (4) OKTAPLATTE

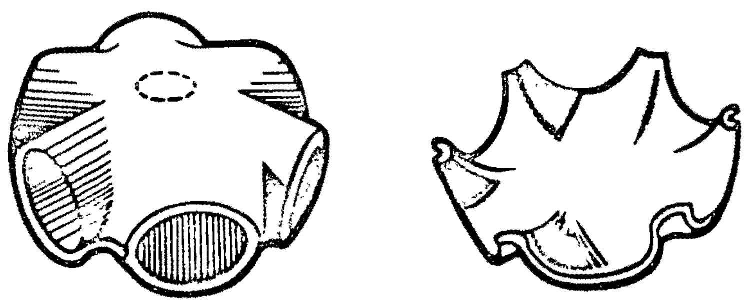

FIG. (5) SDC SYSTEM

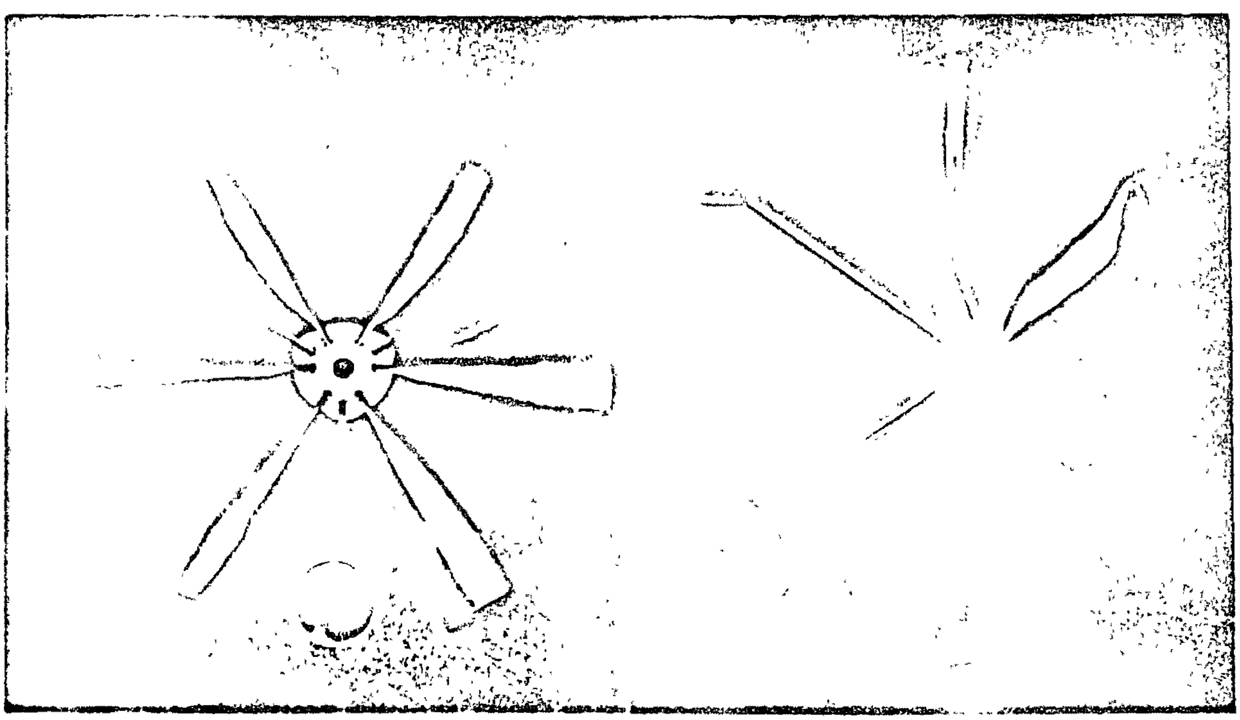

FIG. (6) TRIODETIC

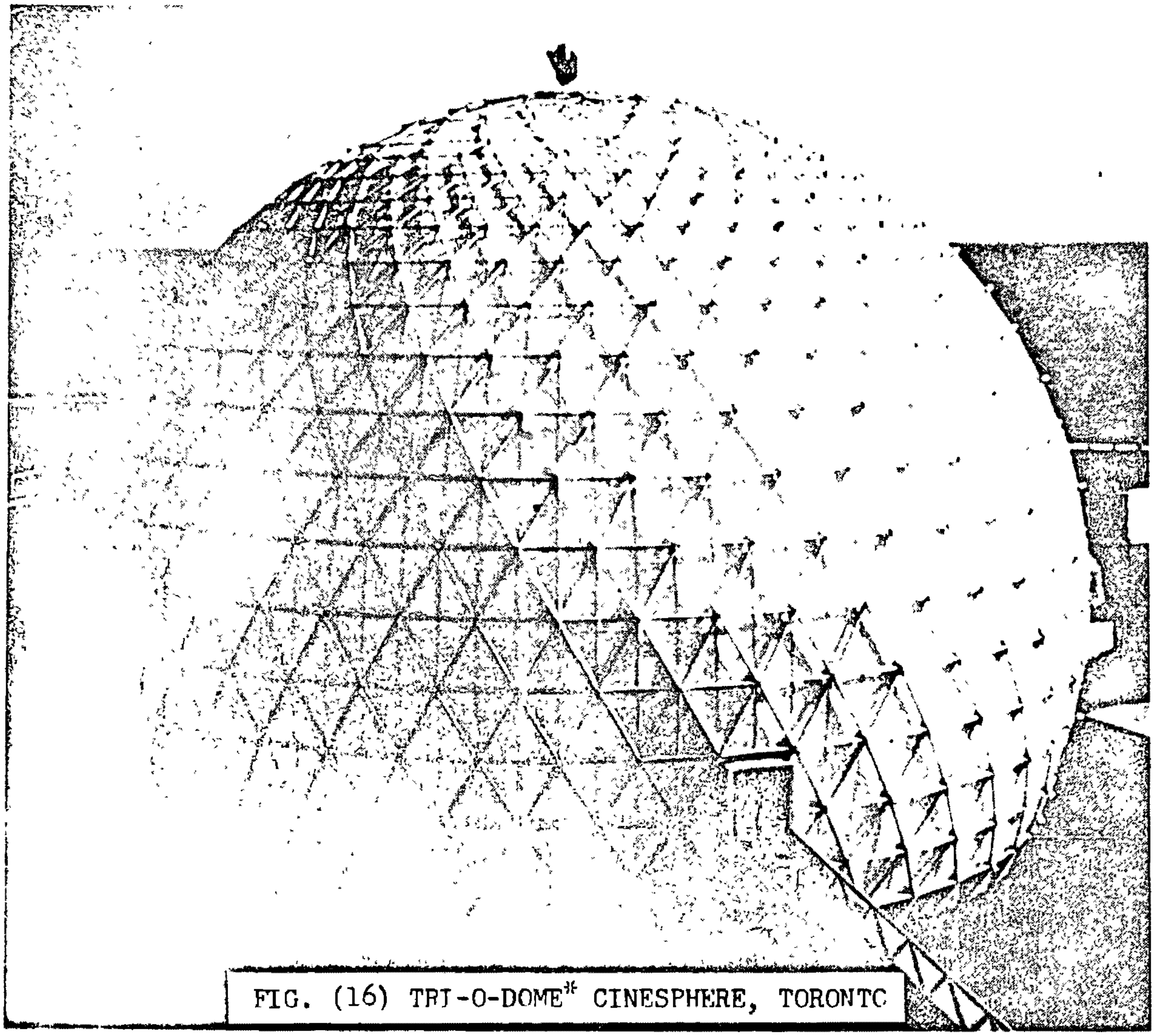

FIG. (16) TRI-O-DOME* CINESPHERE, TORONTO

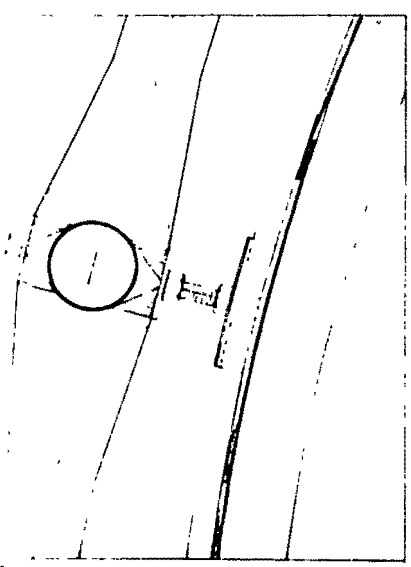

FIG. (17)
VERTICAL SECTION

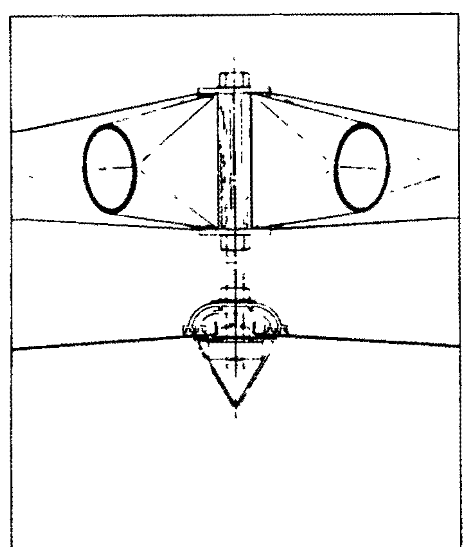

FIG. (18)
HORIZONTAL SECTION

* REGISTERED TRADE NAME

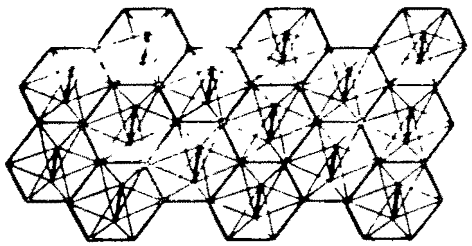

(a)

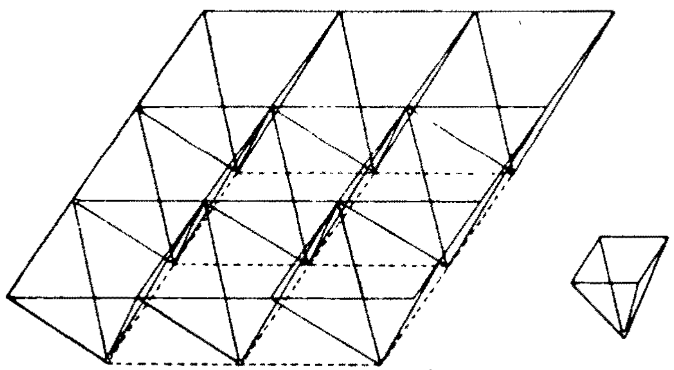

(b)

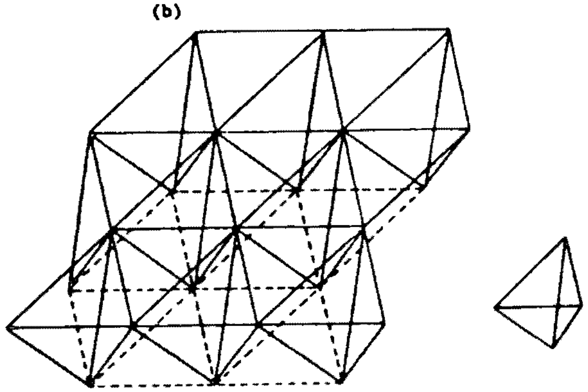

(c)

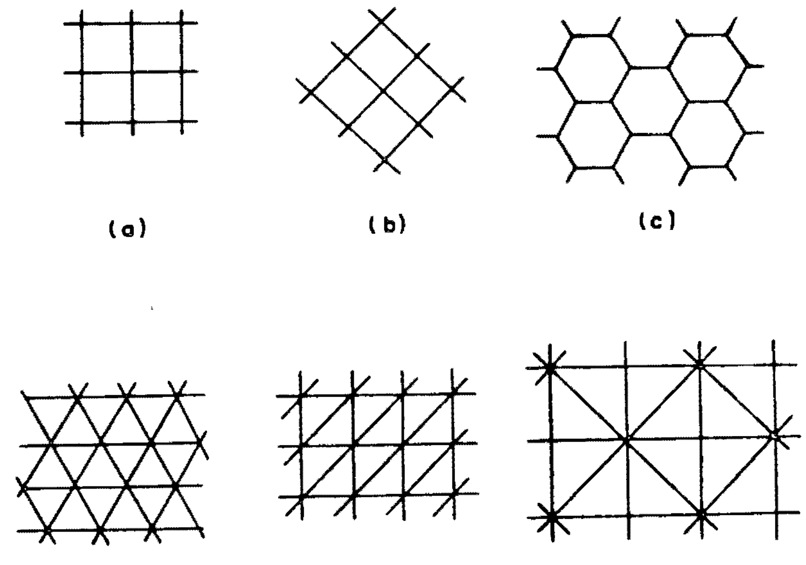

(a) (b) (c)

(d) (e) (f)

±

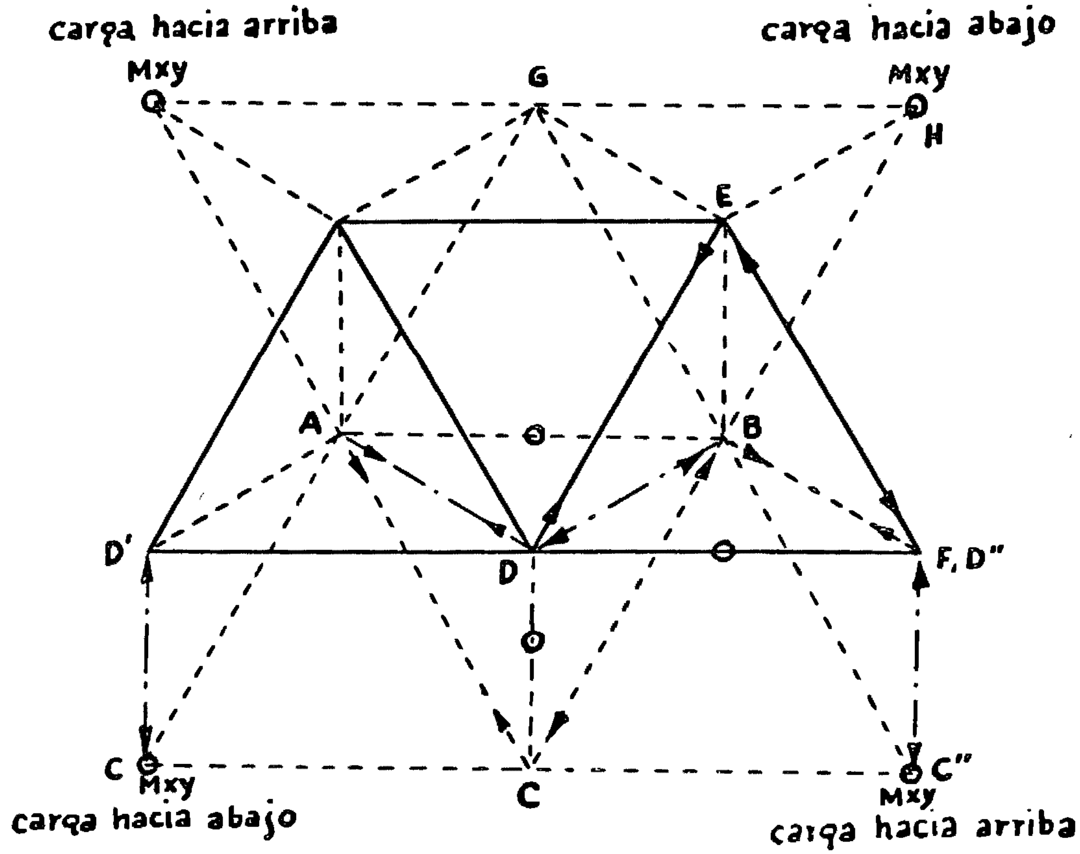

carga hacia arriba
Mxy
Q
G
carga hacia abajo
Mxy
H
E
A
B
D'
D
F, D"
C
Mxy
carga hacia abajo
C
C"
Mxy
carga hacia arriba

$CC' = CC'' = L^2Nxy/2AE$

$CC''' = L^2Nxy/AE$

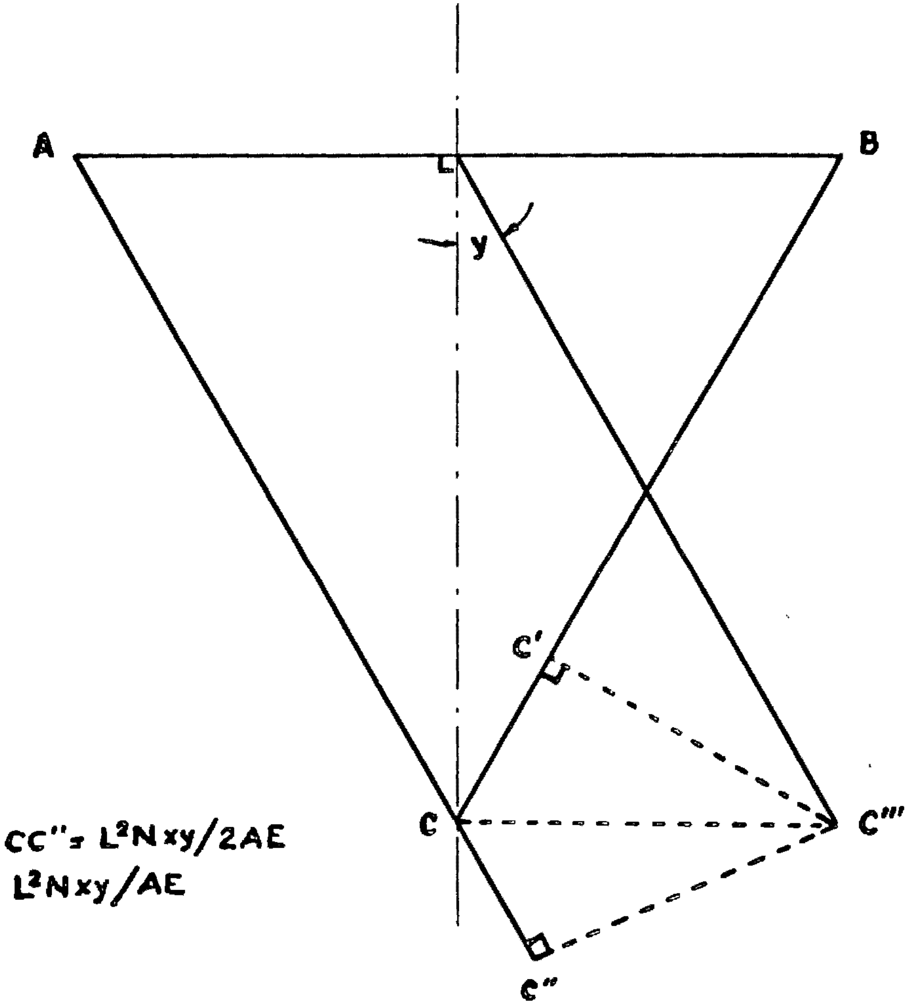

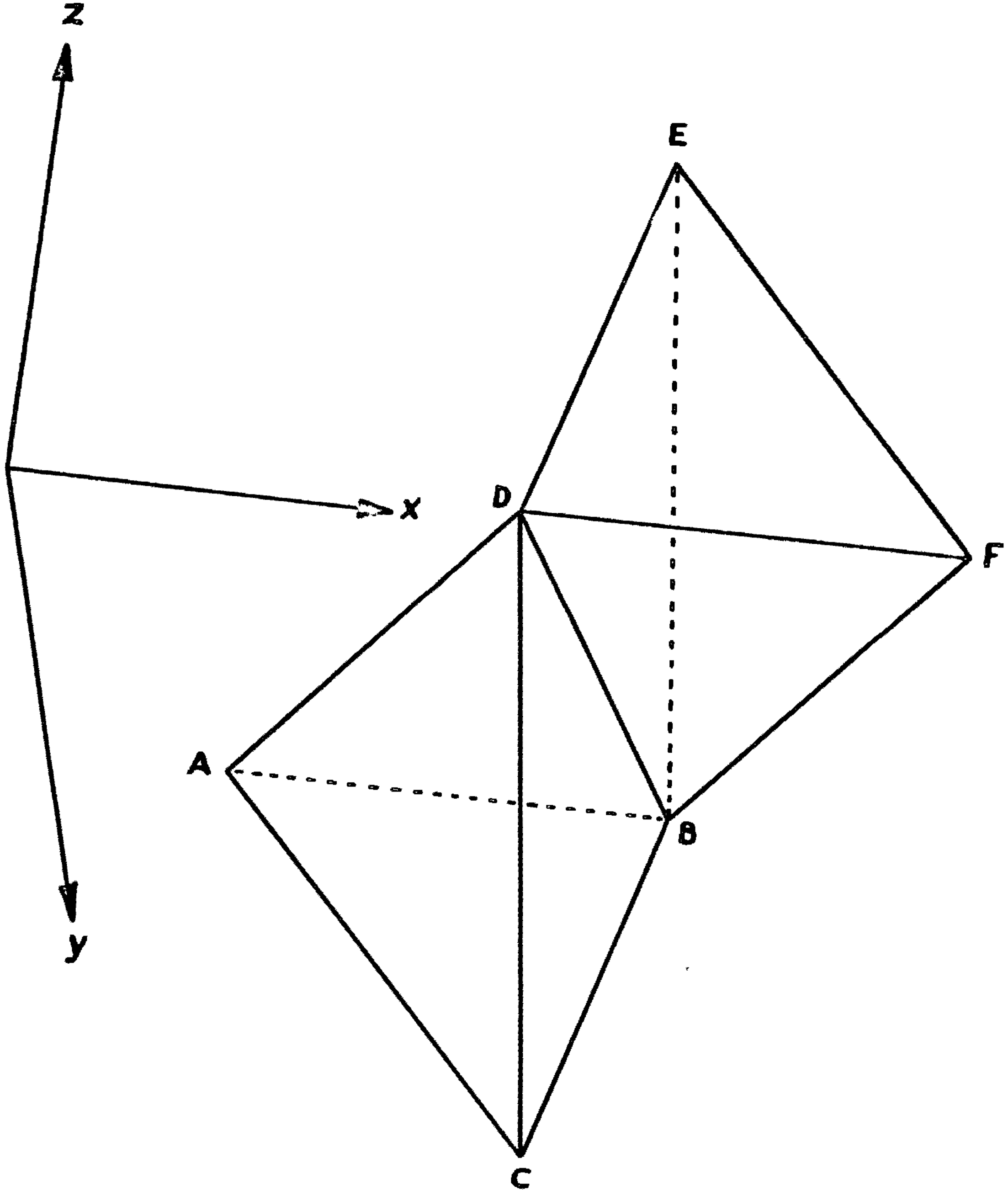
z
x
y
E
D
F
A
B
C

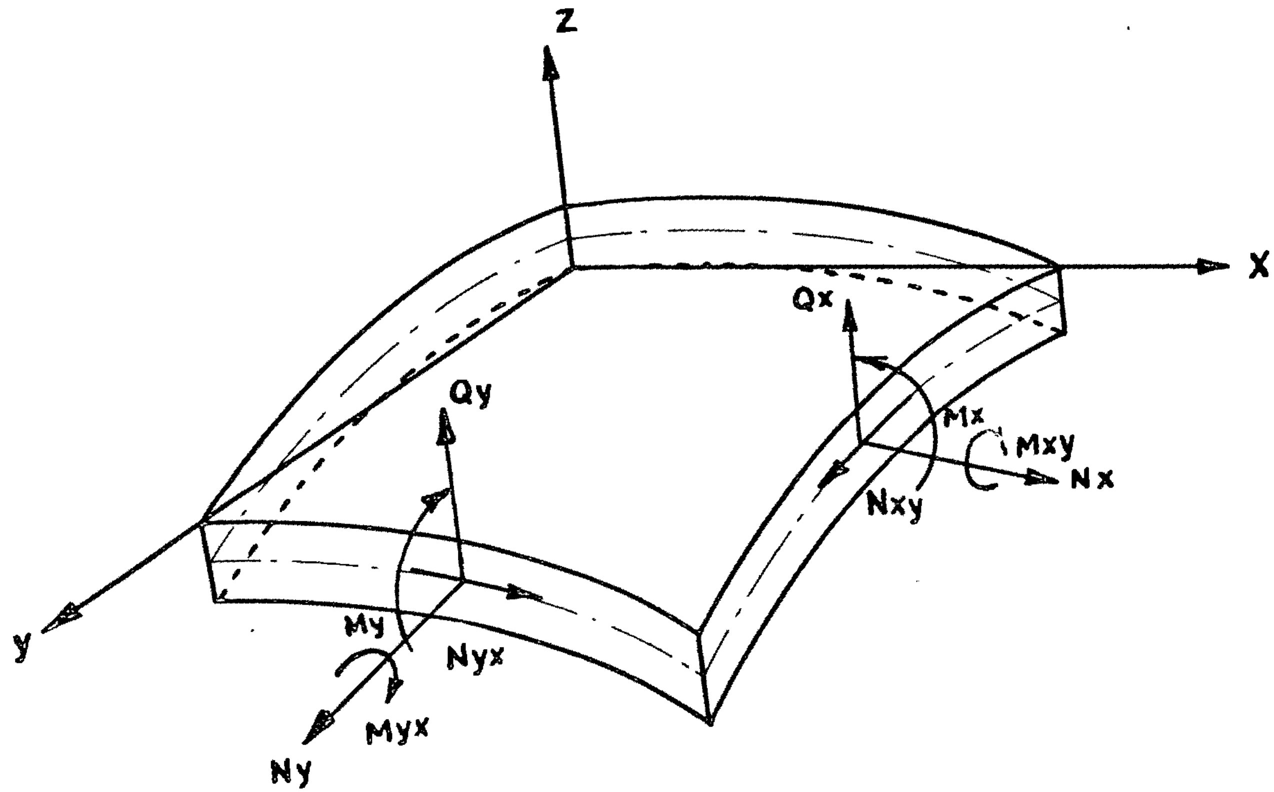

Z
X
Qx
Qy
Mx
Mxy
Nx
Nxy
y
My
Nyx
Myx
Ny

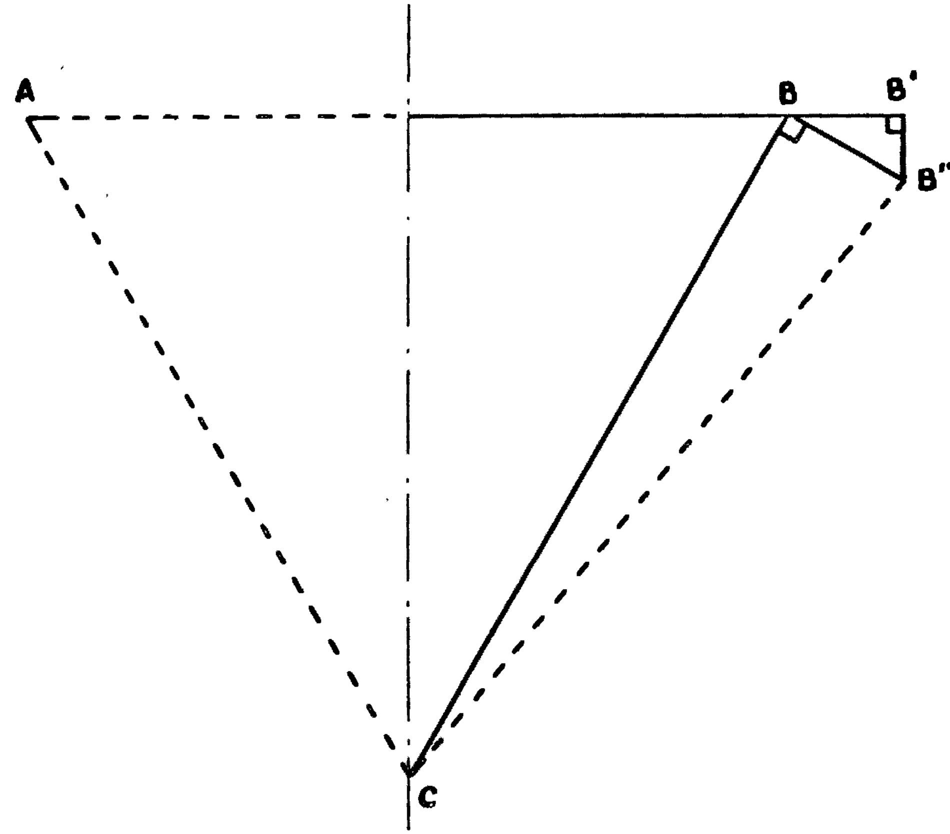

$BB' = 3L^2 Nx/8AE$

$B'B'' = L^2 Nx/8AE$

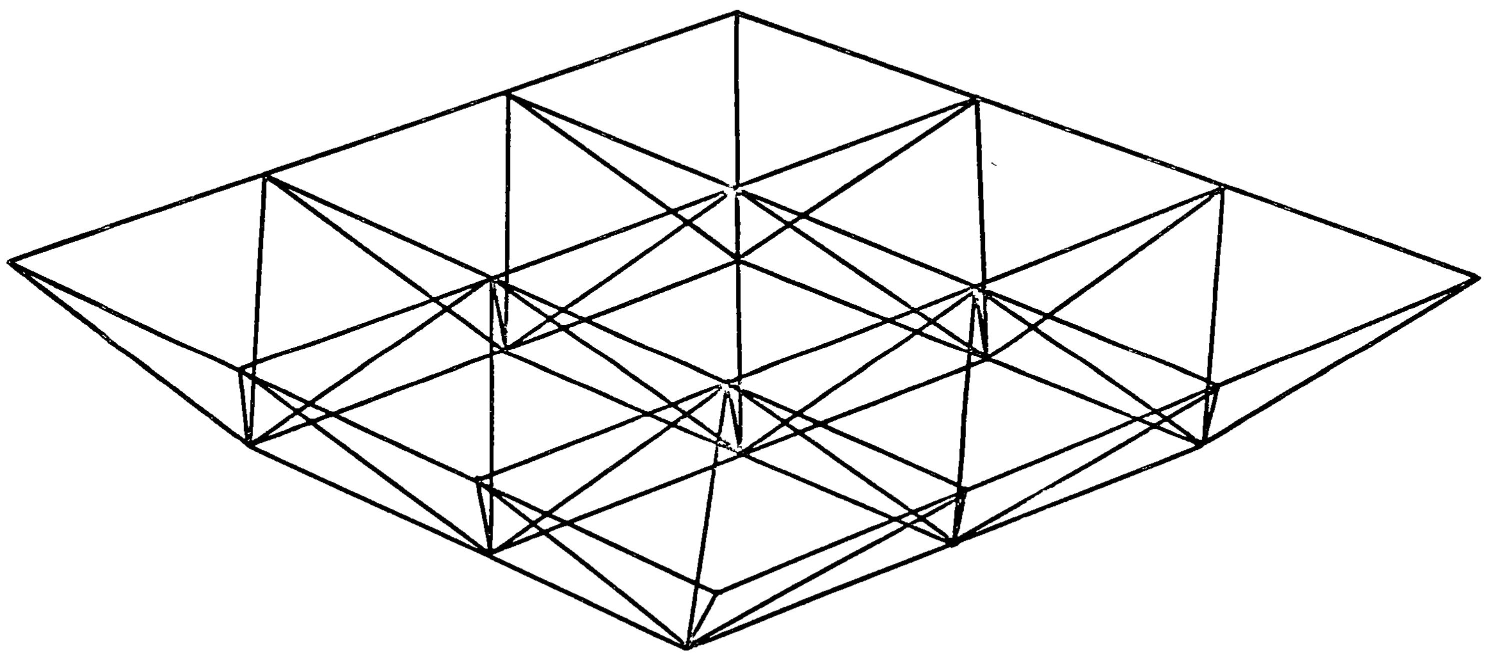

$$K = \sqrt{k^2 - \frac{1}{3}} \qquad (1)$$

$$P_{AB} = P_{FD} = \frac{L}{4\sqrt{3}} (3 N_x - N_y), \qquad (2a)$$

$$P_{BC} = P_{DE} = \frac{L}{2\sqrt{3}} (N_y - \sqrt{3} N_{xy}) \qquad (2b)$$

$$P_{CA} = P_{EF} = \frac{L}{2\sqrt{3}} (N_y + \sqrt{3} N_{xy}) \qquad (2c)$$

$$P_{CD} = - \frac{k L Q_y}{K} \qquad (2d)$$

$$P_{AD} = P_{BD} = \frac{k L Q_y}{2 K} \qquad (2e)$$

$$P_{CD} = 0 \qquad (2f)$$

$$P_{AD} = \frac{\sqrt{3} k L Q_x}{2 K} \qquad (2g)$$

$$P_{BD} = -\frac{\sqrt{3}\ k\ L\ Q_x}{2\ K} \qquad (2h)$$

$$N_m = \left| \frac{M}{K\ L} \right|$$

$$P_{AB} = \frac{3\ (M_x - M_y)}{2\sqrt{3}\ K} \qquad (2i)$$

$$P_{BC} = P_{CA} = \frac{M_y}{\sqrt{3}\ K} \qquad (2k)$$

$$P_{DE} = P_{EF} = -\frac{M_y}{\sqrt{3}\ K} \qquad (2l)$$

$$P_{DF} = -\frac{(3\ M_x - M_y)}{2\sqrt{3}\ K}$$

$$P_{AB} = P_{CD} = P_{DF} = 0 \tag{2m}$$

$$P_{CD} = \pm \frac{k\ M_{xy}}{K} \tag{2n}$$

$$P_{AC} = P_{DE} = \frac{M_{xy}}{K} \tag{2o}$$

$$P_{BC} = P_{EF} = -\frac{M_{xy}}{K} \tag{2p}$$

$$P_{BD} = -\frac{k\ M_{xy}}{K} \tag{2q}$$

$$P_{AD} = \frac{k\ M_{xy}}{K} \tag{2r}$$

$$P_{A} = \frac{K\,L\,(3\,N_x - N_y) + 2\,(3\,M_x - M_y)}{4\sqrt{3}\,K} \qquad (3a)$$

$$P_{BC} = \frac{K\,L\,(N_y - \sqrt{3}\,N_{xy}) + 2\,(M_y - \sqrt{3}\,M_{xy})}{2\sqrt{3}\,K} \qquad (3b)$$

$$P_{CA} = \frac{K\,L\,(N_y + \sqrt{3}\,N_{xy}) + 2\,(M_y + \sqrt{3}\,M_{xy})}{2\sqrt{3}\,K} \qquad (3c)$$

$$P_{DA} = \frac{k\,(Q_y L + \sqrt{3}\,Q_x L + 2\,M_{xy})}{2K} \qquad (3d)$$

$$P_{DB} = \frac{k\,(Q_y L - \sqrt{3}\,Q_x L - 2\,M_{xy})}{2\,K} \qquad (3e)$$

$$P_{DC} = -\frac{k\,L\,Q_y}{K} \pm \text{(en esquinas)}\ \frac{k\,M_{xy}}{K} \qquad (3f)$$

$$P_{DE} = \frac{K L (N_y - \sqrt{3} N_{xy}) - 2 (M_y - \sqrt{3} M_{xy})}{2\sqrt{3} K} \qquad (3g)$$

$$P_{EF} = \frac{K L (N_y - \sqrt{3} N_{xy}) - 2 (M_y + \sqrt{3} M_{xy})}{2\sqrt{3} K} \qquad (3h)$$

$$P_{FD} = \frac{K L (3 N_x - N_y) - 2 (3 M_x - M_y)}{4\sqrt{3} K} \qquad (3i)$$

$$\epsilon_x = \frac{\sigma_x}{E'_x} - v'_x \frac{\sigma_y}{E'_y} \qquad (4a)$$

$$\epsilon_y = \frac{\sigma_y}{E'_y} - v'_y \frac{\sigma_x}{E'_x} \qquad (4b)$$

$$\gamma_{xy} = \frac{\tau_{xy}}{G'} \qquad (4c)$$

$$\sigma_x = \frac{E'_x\,(\epsilon_x + v'_x\,\epsilon_y)}{(1 - v'_x\; v'_y)} \qquad (5a)$$

$$\sigma_y = \frac{E'_y\,(\epsilon_y + v'_y\,\epsilon_x)}{(1 - v'_x\; v'_y)} \qquad (5b)$$

$$\tau_{xy} = G'\,\gamma_{xy} \qquad (5c)$$

$$N_x = \sigma_x\,h' \qquad (6a)$$

$$N_y = \sigma_y\,h' \qquad (6b)$$

$$N_{xy} = \tau_{xy}\,h' \qquad (6c)$$

$$\epsilon_x = -z\,\frac{d^2 w}{dx^2} \qquad (7a)$$

$$\epsilon_y = -z\,\frac{d^2 w}{dy^2} \qquad (7b)$$

$$\gamma_{xy} = -\,2z\,\frac{d^2 w}{dx\,dy} \qquad (7c)$$

$$\sigma_x = - \frac{E'_x z}{(1 - v'_x \, v'_y)} \left(\frac{d^2 w}{d x^2} + v'_x \frac{d^2 w}{d y^2} \right), \tag{8a}$$

$$\sigma_y = - \frac{E'_y z}{(1 - v'_x \, v'_y)} \left(\frac{d^2 w}{d y^2} + v'_y \frac{d^2 w}{d x^2} \right), \tag{8b}$$

$$\tau_{xy} = - 2 G' z \left(\frac{d^2 w}{d x \, d y} \right) \tag{8c}$$

$$M_x = \int_{-h'/2}^{h'/2} \sigma_x z \, dz = - D'_x \left(\frac{d^2 w}{d x^2} + v'_x \frac{d^2 w}{d y^2} \right) \tag{9a}$$

$$M_y = \int_{-h'/2}^{h'/2} \sigma_y z \, dz = - D'_y \left(\frac{d^2 w}{d y^2} + v'_y \frac{d^2 w}{d x^2} \right) \tag{9b}$$

$$M_{xy} = - \int_{-h'/2}^{h'/2} \tau_{xy} z \, dz = - 2 D_{xy} \left(\frac{d^2 w}{d x \, d y} \right) \tag{9c}$$

$$D'_x = \frac{E'_x \, h'^3}{12 \, (1 - v'_x \, v'_y)} \tag{10a}$$

$$D'_y = \frac{E'_y \, h'^3}{12 \, (1 - v'_x \, v'_y)} \tag{10b}$$

$$D'_{xy} = \frac{G' \ h'^3}{12} \quad (10c)$$

$$\frac{\sqrt{3}\ L\ N_x}{4}$$

$$\frac{\sqrt{3}\ L^2\ N_x}{4\ A\ E}$$

$$\epsilon_x = \frac{\sqrt{3}\ L\ N_x}{4\ A\ E}$$

$$\frac{L^2\ N_x}{8\ A\ E}$$

$$\epsilon_y = -\frac{L\ N_x}{4\sqrt{3}\ A\ E}$$

$$E'_x = \frac{4\ A\ E}{\sqrt{3}\ L\ h'} \quad (11a)$$

$$\epsilon_x = - \frac{L\ N_y}{4\sqrt{3}\ A\ E}$$

$$\epsilon_y = \frac{\sqrt{3}\ L\ N_y}{4\ A\ E}$$

$$E'_y = \frac{4\ A\ E}{\sqrt{3}\ L\ h'} \qquad (11\ c)$$

$$\nu'_x = \frac{1}{3} \qquad (11\ d)$$

$$G' = \frac{\sqrt{3}\ A\ E}{2\ h'\ L} \qquad (11\ e)$$

$$G' = \frac{E'}{2\ (1 + v')} \qquad (12\ )$$

$$\frac{d^2 w}{d x^2} = \frac{\epsilon_s - \epsilon_i}{\text{peralte}} = - \frac{\sqrt{3}\ M_x}{K^2\ A\ E\ L}$$

$$\frac{d^2 w}{d y^2} = - v'_y \frac{d^2 w}{d x^2} = \frac{M_x}{\sqrt{3}\ K^2\ A\ E\ L}$$

$$D'_x = \frac{3\sqrt{3}\,K^2 A E L}{8} \qquad (11\ f)$$

$$h' = \sqrt{3}\,K L \qquad (11\ g)$$

$$\frac{6\,L\,M_{xy}(1 + k^3)}{K^2 E A}$$

$$\frac{\Delta w}{\Delta x} = \frac{6\,M_{xy}(1 + k^3)}{K^2 E A}$$

$$\frac{\Delta}{\Delta y}\left(\frac{\Delta w}{\Delta x}\right) = \frac{6\,M_{xy}(1 + k^3)}{\sqrt{3}LK^2 E A}$$

$$D'_{xy} = \frac{\sqrt{3}\,K^2 L A E}{12(1 + k^3)} \qquad (11\ h)$$

$$G'' = \frac{A E}{3 L^2 (1 + k^3)} \qquad (11\ i)$$

$$h' = \sqrt{3}\, K\, L \quad , \qquad\qquad (13a)$$

$$E'_x = E'_y = E' = \frac{4\,A\,E}{3\,K\,L^2} \quad ,$$

$$v'_x = v'_y = v' = \frac{1}{3} \quad ,$$

$$G' = \frac{A\,E}{2\,K\,L^2} \quad ,$$

$$G'' = \frac{A\,E}{3\,L^2(1 + k^3)}$$

$$D'_x = D'_y = D' = \frac{3\sqrt{3}\,K^2 A\,E\,L}{8}$$

$$D'_{xy} = \frac{3\,L\,K^2 A\,E}{12\,(1 + k^3)}$$

$$G' = \frac{E'}{2\,(1 + v')} \neq G''$$

STRESS ANALYSIS AND DESIGN OF OUR LADY OF FATIMA CHURCH

BY

PORFIRIO BALLESTEROS [1]

SYNOPSIS

HYPERBOLIC PARABOLOIDAL SHELLS OF WIDE SPAN FOR THE STRUCTURE, OF FATIMA CHURCH AT MONTERREY-MEXICO HAS RECENTLY BEEN DESIGNED BY THE WRITER AND THEY ARE NOW UNDER CONSTRUCTION, WITH THE WRITER IN-CHARGE.

IN THE SHELLS EFGH (FIG.2) AND IJKL NUMERICAL VALUES FOR THE MEMBRANE STRESSES WERE DETERMINED ANALYTICALLY, AND IN THE SHELLS ABCD AND MNOP THEY WERE FOUND BY RELAXATION PROCEDURES. THE RESULTS ARE PRESENTED GRAPHICALLY. THE ORDER OF MAGNITUDE OF THE CRITICAL LOAD IS DISCUSSED. ALL THE IMPORTANT DESIGN AND CONSTRUCTIVE DETAILS ARE PRESENTED.

INTRODUCTION

IN FIG. 1 WE HAVE A SHELL ELEMENT OF ARBITRARY SHAPE REFERED TO A CARTESIAN COORDINATE SYSTEM, IN WHICH WE ASSUME THAT Z IS GIVEN AS A FUNCTION OF X AND Y. THE MEMBRANE STRESSES ARE DESCRIBED BY A SYSTEM OF SKEW FORCES. THE FORCES N_X AND N_{YX}, ARE PARALLEL TO THE X,Z PLANE, THE OTHER TWO, N_Y, AND N_{XY} ARE PARALLEL TO THE Y,Z PLANE. THE SKEW FORCES ARE FORCES PER UNIT LENGHT OF THE LINE ELEMENT ON WHICH THEY ARE TRANSMITTED. THE ACTUAL FORCES ARE DETERMINED BY MULTIPLYING THEM BY THE LENGTH OF ITS ELEMENT $DX/\cos\phi$ OR $DY/\cos\psi$.

---

[1] STRUCTURAL ENGINEER MONTERREY-MEXICO

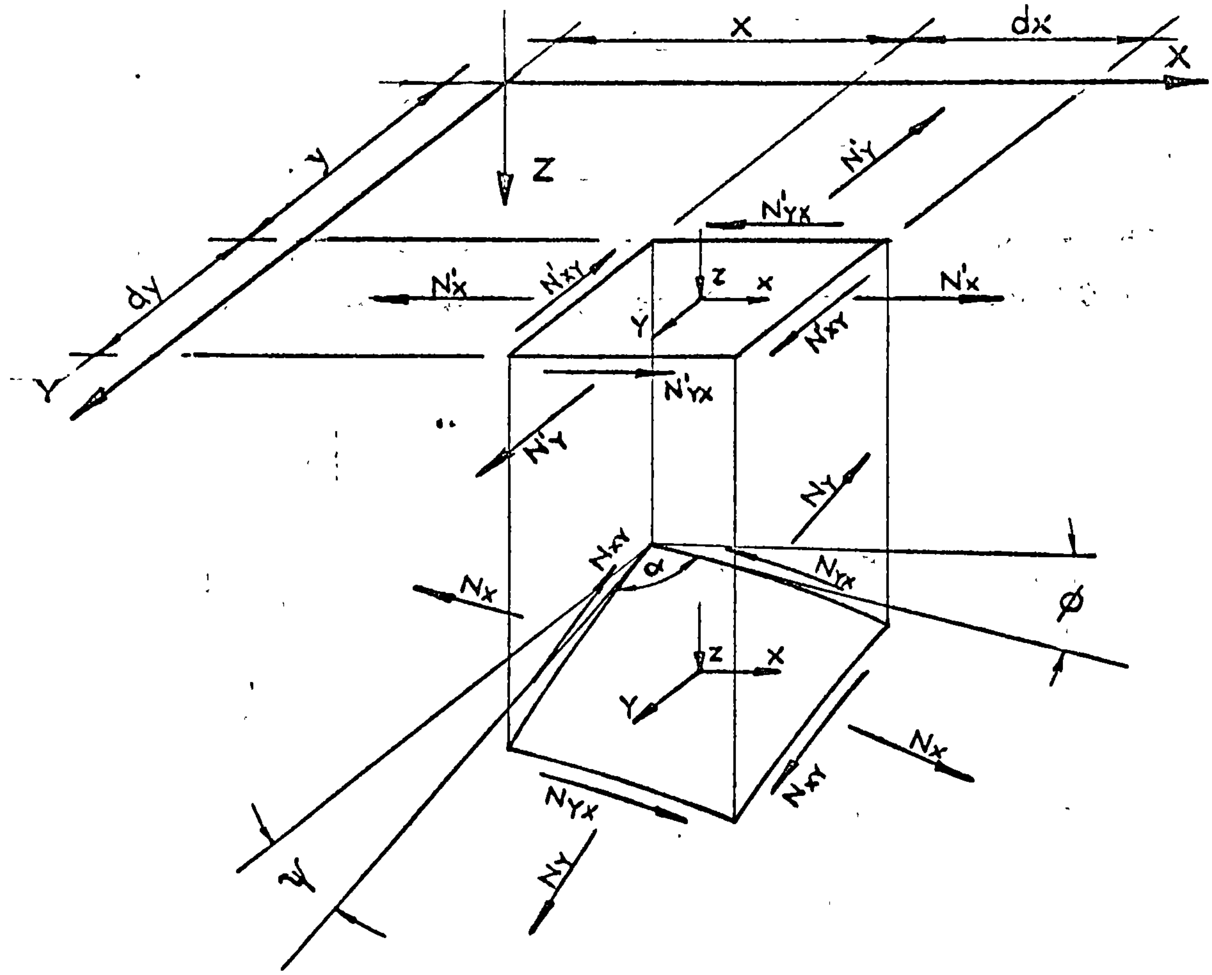

FIGURE 1.- SHELL ELEMENT AND ITS PROYECTION ON THE X,Y PLANE.

THE GENERAL EQUATIONS OF THE MEMBRANE THEORY FOR SHELLS OF ARBI_ TRARY SHAPE ARE:

THE HORIZONTAL COMPONENT OF THE MEMBRANE FORCES;

$$\left.\begin{aligned} N'_x &= N_x \frac{\cos\phi}{\cos\psi} \\ N'_Y &= N_Y \frac{\cos\psi}{\cos\phi} \\ N'_{xY} &= N_{xY} \end{aligned}\right\} \quad (1)$$

THE EQUILIBRIUM EQUATIONS,

$$\frac{\partial N'_x}{\partial x} + \frac{\partial N'_{xy}}{\partial y} + X = 0 \qquad (2\text{-a})$$

$$\frac{\partial N'_y}{\partial y} + \frac{\partial N'_{xy}}{\partial x} + Y = 0 \qquad (2\text{-b})$$

$$N'_x \frac{\partial^2 z}{\partial x^2} + N'_y \frac{\partial^2 z}{\partial y^2} + 2N'_{xy} \frac{\partial^2 z}{\partial x \partial y} - X\frac{\partial z}{\partial x} - Y\frac{\partial z}{\partial y} + Z = 0 \qquad (2\text{-c})$$

THE DEFINITION OF THE STRESS FUNCTION F,

$$N'_x = \frac{\partial^2 F}{\partial y^2} - \int_{x_0}^{x} X\,dx \qquad (3\text{-a})$$

$$N'_y = \frac{\partial^2 F}{\partial x^2} - \int_{y_0}^{y} Y\,dy \qquad (3\text{-b})$$

$$N'_{xy} = -\frac{\partial^2 F}{\partial x \partial y} \qquad (3\text{-c})$$

EQUATIONS (3) SATISFY THE EQUILIBRIUM EQUATIONS (2A) AND (2B) AND REDUCE (2C) TO THE GENERAL DIFFERENTIAL EQUATION OF THE MEMBRANE THEORY FOR SHELLS OF ANY SHAPE (1) AND (7).

$$\boxed{\begin{aligned} &\frac{\partial^2 F}{\partial y^2}\cdot\frac{\partial^2 z}{\partial x^2} + \frac{\partial^2 F}{\partial x^2}\cdot\frac{\partial^2 z}{\partial y^2} - 2\frac{\partial^2 F}{\partial x \partial y}\cdot\frac{\partial^2 z}{\partial x \partial y} = \\ &= -Z + X\frac{\partial z}{\partial x} + Y\frac{\partial z}{\partial y} + \frac{\partial^2 z}{\partial x^2}\int_{x_0}^{x} X\,dx + \frac{\partial^2 z}{\partial y^2}\int_{y_0}^{y} Y\,dy \end{aligned}} \qquad (4)$$

STRESS ANALYSIS OF SHELLS EFGH AND IJKL

THE EQUATION OF THE SURFACE IS,

$$z = \frac{f}{ab}xy = \frac{1}{c}xy \qquad (5)$$

THE COMPONENTS OF THE EXTERNAL LOAD ARE,

$$X = Y = 0 \qquad (6\text{-a})$$

$$Z = \frac{1}{c} q_0 \sqrt{x^2 + y^2 + c^2} \qquad (6\text{-b})$$

FROM (1), (3), (4), (5), (6), AND FROM $(N_X)_{x=a} = (N_Y)_{y=b} = 0$

WE OBTAIN,

$$N_x = \frac{q_0 y}{2} \sqrt{\frac{y^2 + c^2}{x^2 + c^2}} \ln \frac{x + \sqrt{x^2 + y^2 + c^2}}{a + \sqrt{a^2 + y^2 + c^2}} \qquad (7\text{-a})$$

$$N_y = \frac{q_0 x}{2} \sqrt{\frac{x^2 + c^2}{y^2 + c^2}} \ln \frac{y + \sqrt{x^2 + y^2 + c^2}}{b + \sqrt{x^2 + b^2 + c^2}} \qquad (7\text{-b})$$

$$N_{xy} = -\frac{q_0}{2} \sqrt{x^2 + y^2 + c^2} \qquad (7\text{-c})$$

THE NUMERICAL VALUES OF (7) ARE EXPRESSED IN FIG.2 AND 3

STRESS ANALYSIS OF SHELLS ABCD AND MNOP

THE EQUATIONS OF THE SURFACE IS (FIG.4)

$$Az + Bxz + Cyz + Dxy + Ez^2 = 0 \qquad (8\text{-a})$$

WHERE: $A = ab$; $B = b_1 sen\alpha - b$; $C = -b_1 \cos\alpha$; $D = f$; $E = \frac{b_1^2}{f}$ (8-b)

THE COMPONENTS OF THE EXTERNAL LOAD ARE,

$$X = Y = 0 \qquad (9\text{-a})$$

$$Z = q_0 \sqrt{1 + \left(\frac{Bz + Dy}{A + Bx + Cy + 2Ez}\right)^2 + \left(\frac{Cz + Dx}{A + Bx + Cy + 2Ez}\right)^2} \qquad (9\text{-b})$$

SUBSTITUTING (8) AND (9) IN (4) WE GET,

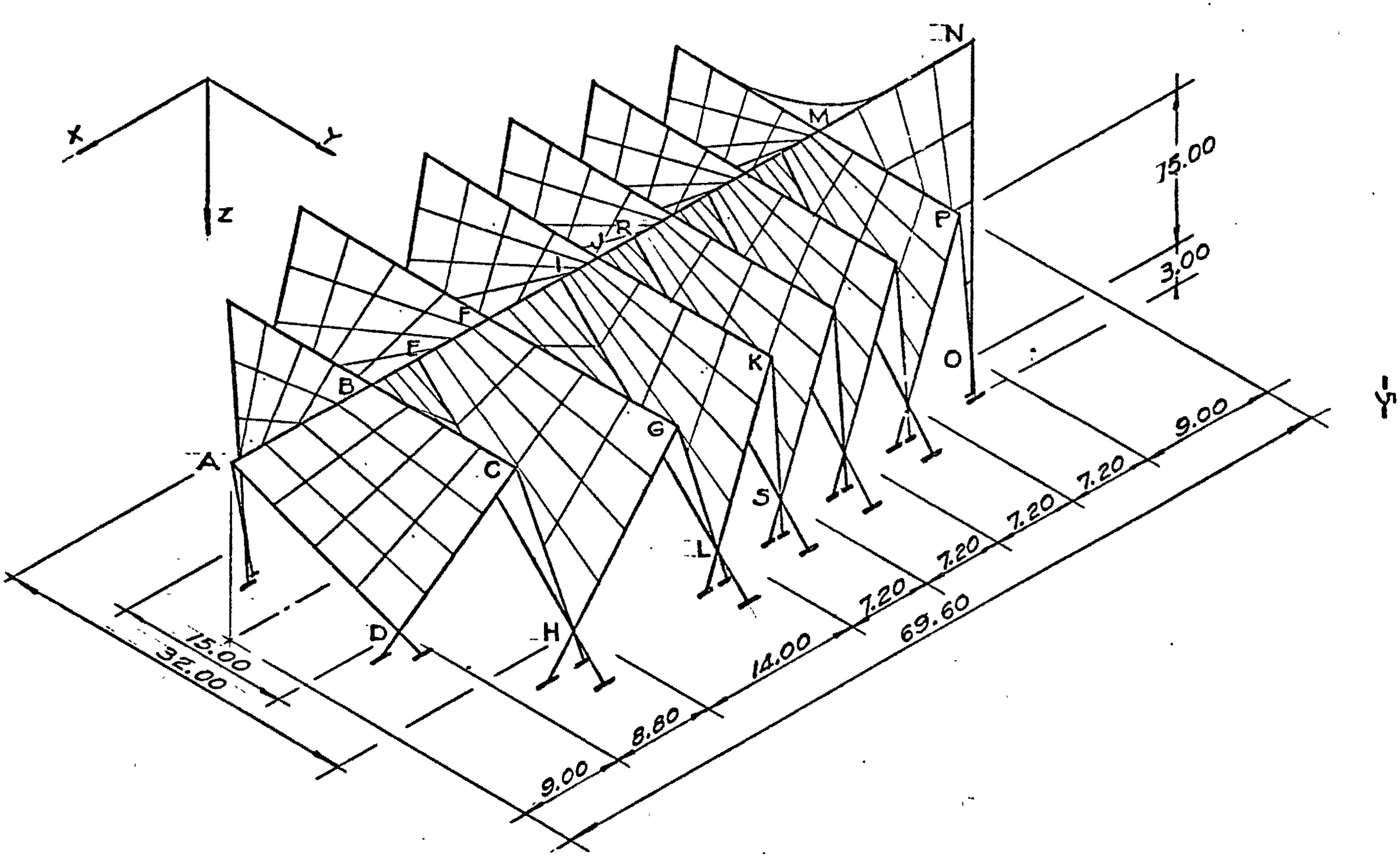

ISOMETRIC
FIGURE 2A

SCALE : 1:500
MEAS. IN METERS.

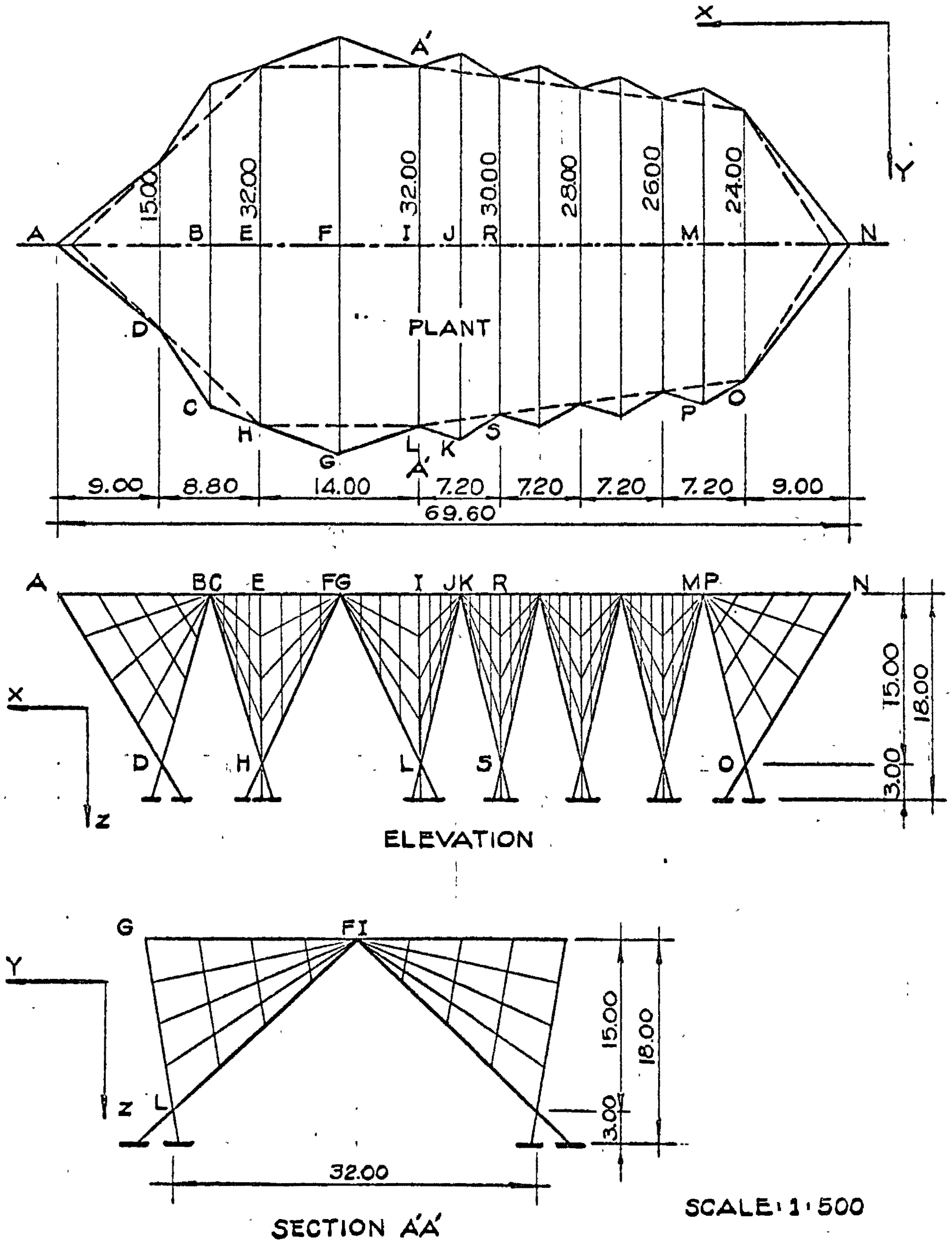

FIGURE 2B

STRUCTURE PROJECTIONS

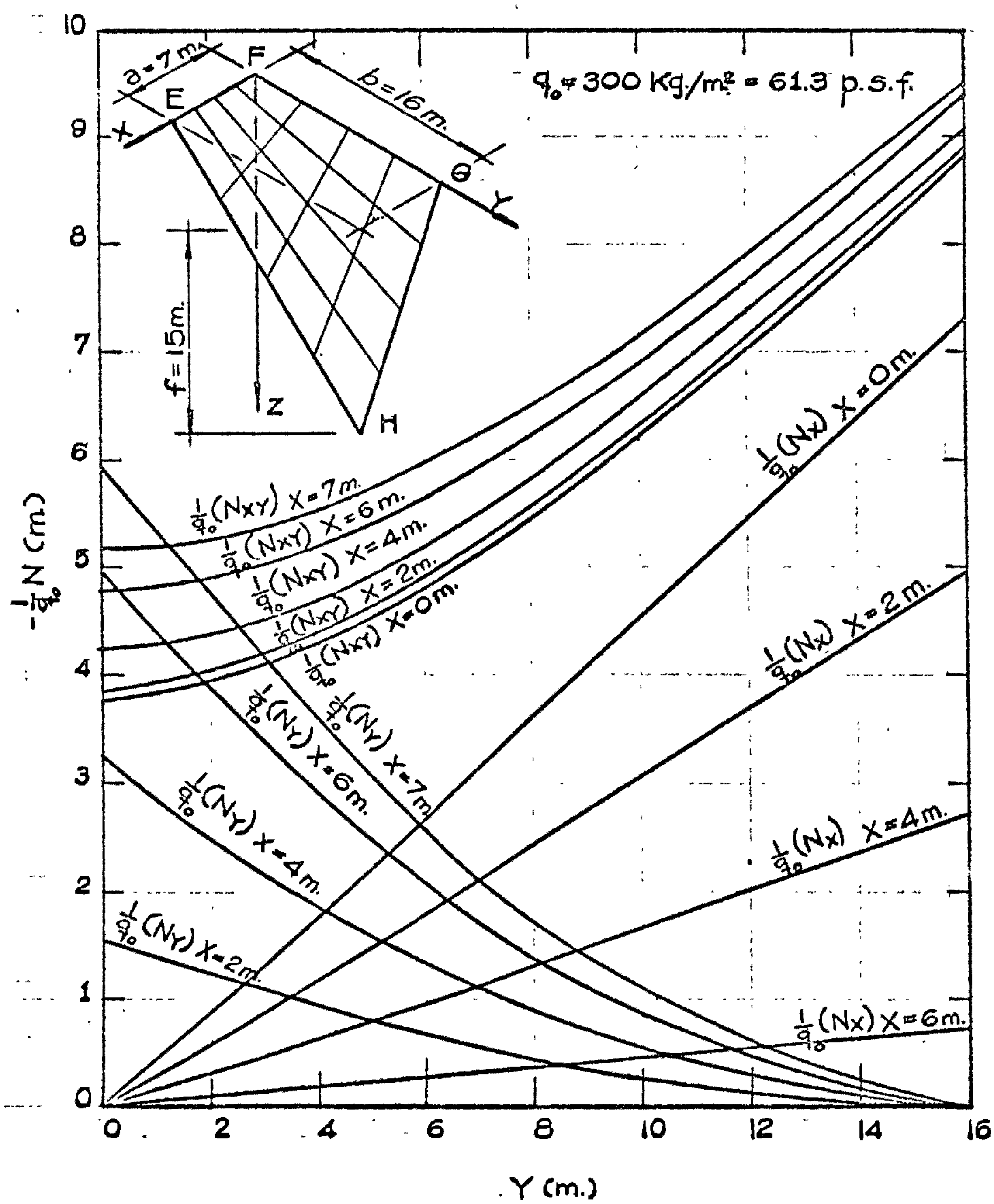

FIGURE 2 – STRESSES IN SHELL EFGH

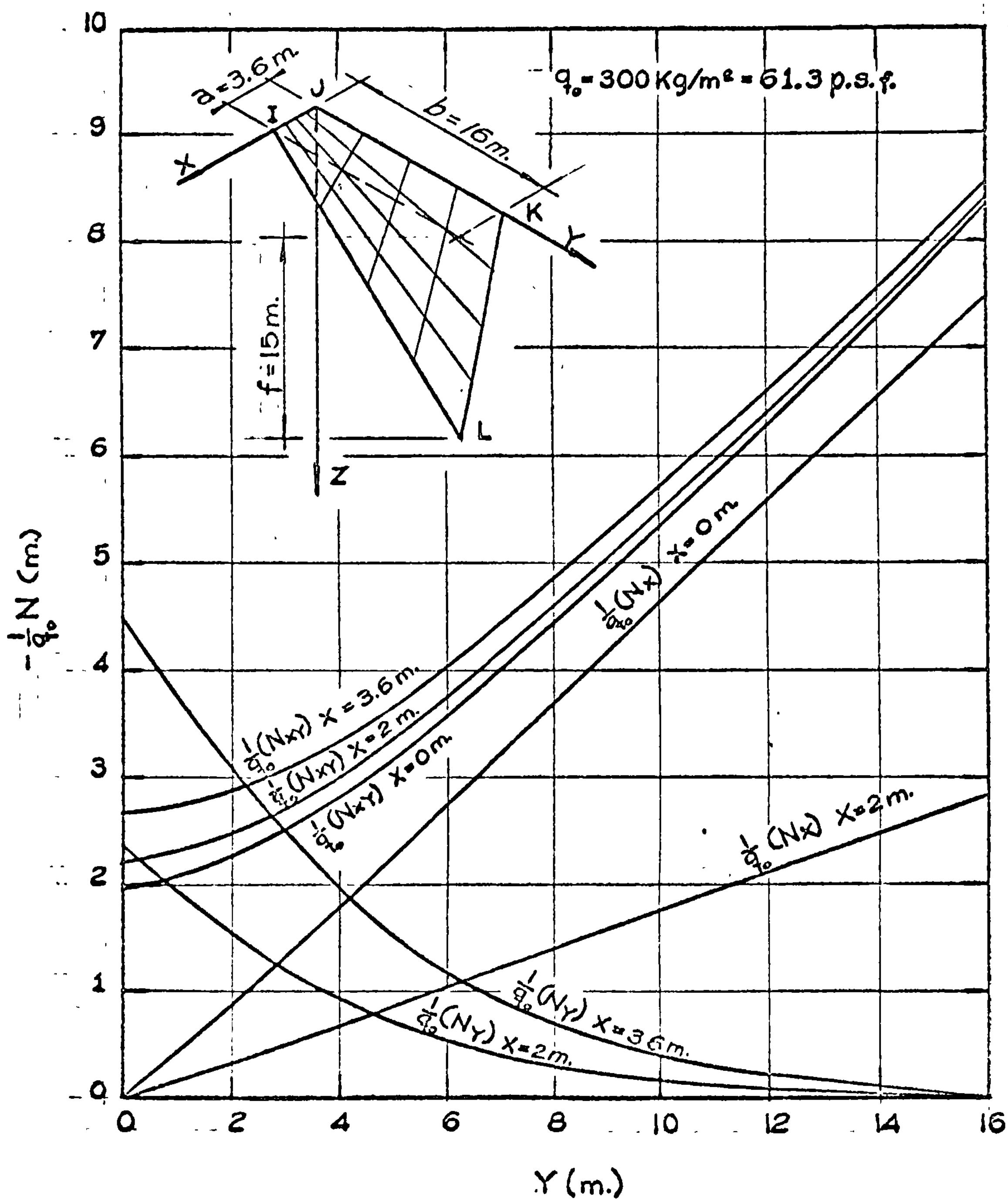

FIGURE 3 - STRESSES IN SHELL IJKL

$$\left[\frac{2(C^2z+DCx)}{\beta}-\frac{2E(Cz+Dx)^2}{\beta^2}\right]\frac{\partial^2F}{\partial y^2}+\left[\frac{2(B^2+DBy)}{\beta}-\frac{2E(Bz+Dy)^2}{\beta^2}\right]\frac{\partial^2F}{\partial x^2}+$$

$$+\left[D-\frac{2BCz+BDx+CDy}{\beta}+\frac{2E(Bz+Dy)(Cz+Dx)}{\beta^2}\right]\frac{\partial^2F}{\partial x\partial y}+$$

$$+\sqrt{(A+Bx+Cy+2Ez)^2+(Bz+Dy)^2+(Cz+Dx)^2}=0 \qquad (10)$$

WHERE $\beta = A+Bx+Cy+2Ez$

EQUATION (10) MAY BE SOLVED NUMERICALLY.
VALUES OF THE SHEARING MEMBRANE STRESS AT THE BOUNDARIES ARE PRESENTED IN FIG. 4.

ORDER OF MAGNITUDE OF CRITICAL LOAD

SINCE THERE IS A PORTION OF THE SHELLS IJKL AND EFGH THAT IS ALMOST PLANE, IT WAS CONVENIENT TO KNOW THE BUCKLING LOAD OF THE EQUIVALENT SIMPLY SUPPORTED RECTANGULAR PLATE COMPRESSED IN TWO PERPENDICULAR DIRECTIONS AND ALSO THE CORRESPONDING BUCKLING OF THE SAME PLATE UNDER THE ACTION OF SHEARING STRESSES.
THIS VALUES ARE SHOWN IN FIG. 5 .

DESIGN AND CONSTRUCTIVE DETAILS

IN THE TYPICAL SUPPORT SHOWN IN FIG. 6 THE STATIC ANALYSIS WAS MADE SUCH THAT THE RESULTANT FORCE IS VERTICAL AND IT GOES THROUGH THE CENTROIDAL POINT OF THE CONTACT SECTION, THE FIGURE IS EXPLANATORY ITSELF. THE REINFORCED OF THE SHELLS IS SHOWN IN FIG. 7 .

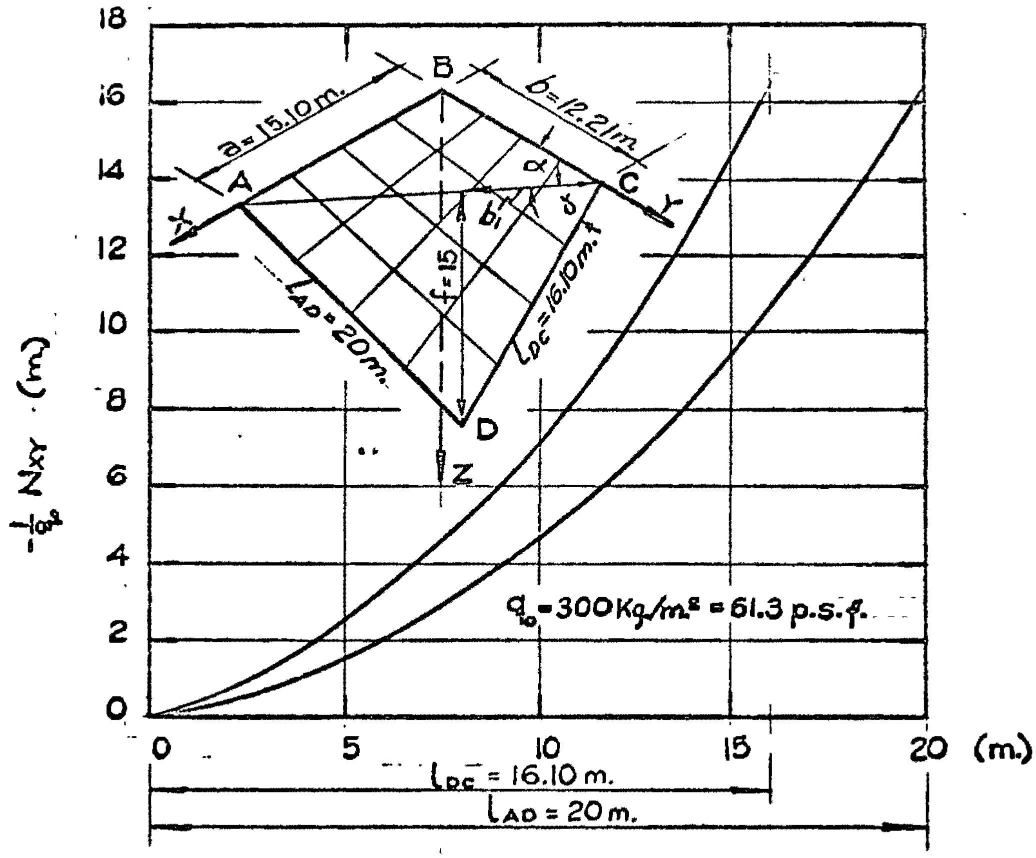

FIGURE 4.- SHEARING STRESS AT BOUNDARY IN SHELL ABCD -

$E = 2.1 \times 10^5 \frac{kg.}{cm^2}$; $h = 5\,cm$; $\nu = 0.15$; $D = 2.19 \times 10^6\ kg.cm.$

$N_m = 430 \frac{kg.}{m}$; $(N_{xy})_m = 2,235 \frac{kg.}{m}$

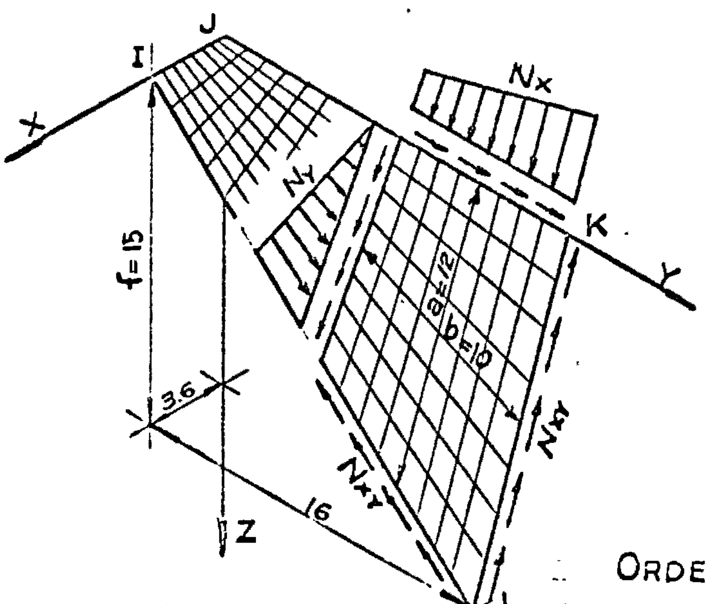

FIGURE 5

$$N_{CR} = \frac{\pi^2 D}{a^2}\left(1 + \frac{a^2}{b^2}\right) \qquad (1)$$

$$(N_{xy})_{CR} = 5.7\,\frac{\pi^2 D}{b^2} \qquad (1)$$

$$N_{CR} = 4,050\ \frac{kg.}{m}$$

$$(N_{xy})_{CR} = 15,400\ \frac{kg.}{m.}$$

$$\boxed{\frac{N_{CR}}{N_m} = 9.42\ ;\ \frac{(N_{xy})_{CR}}{(N_{xy})_m} = 6.9}$$

ORDER OF MAGNITUDE
OF CRITICAL LOAD

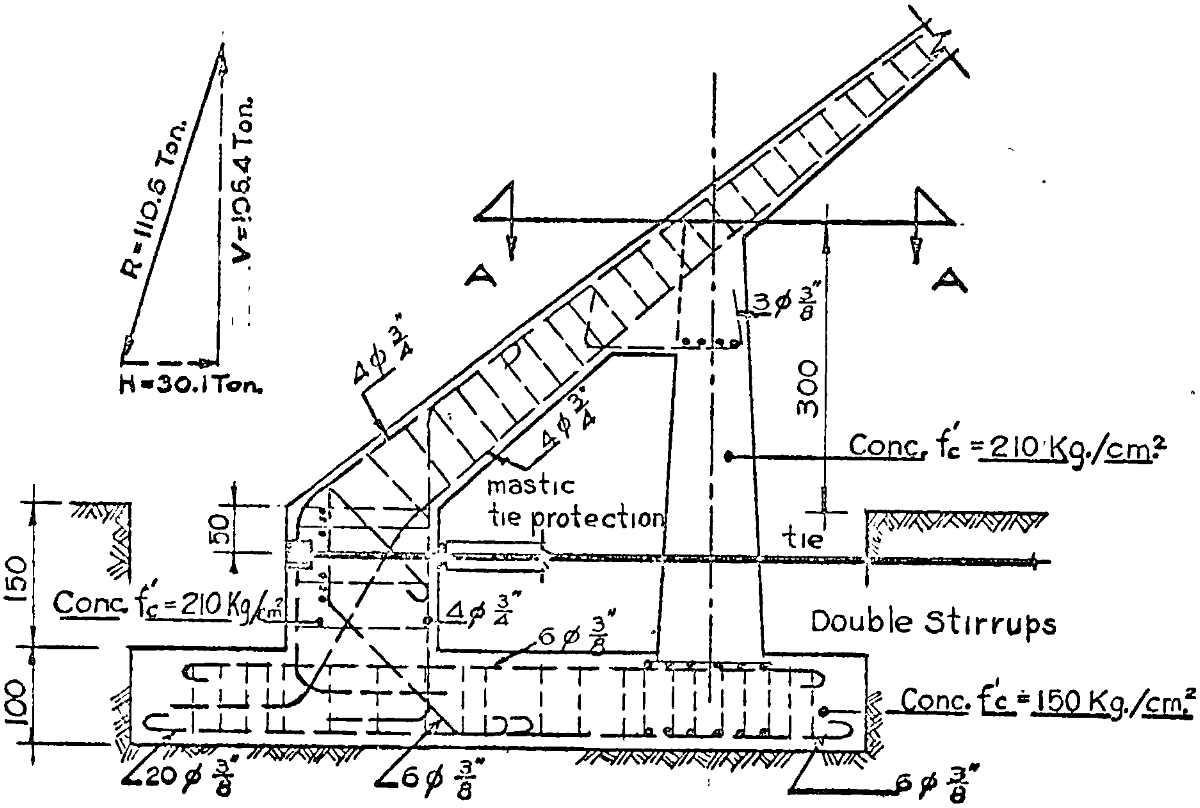

SECTION B-B

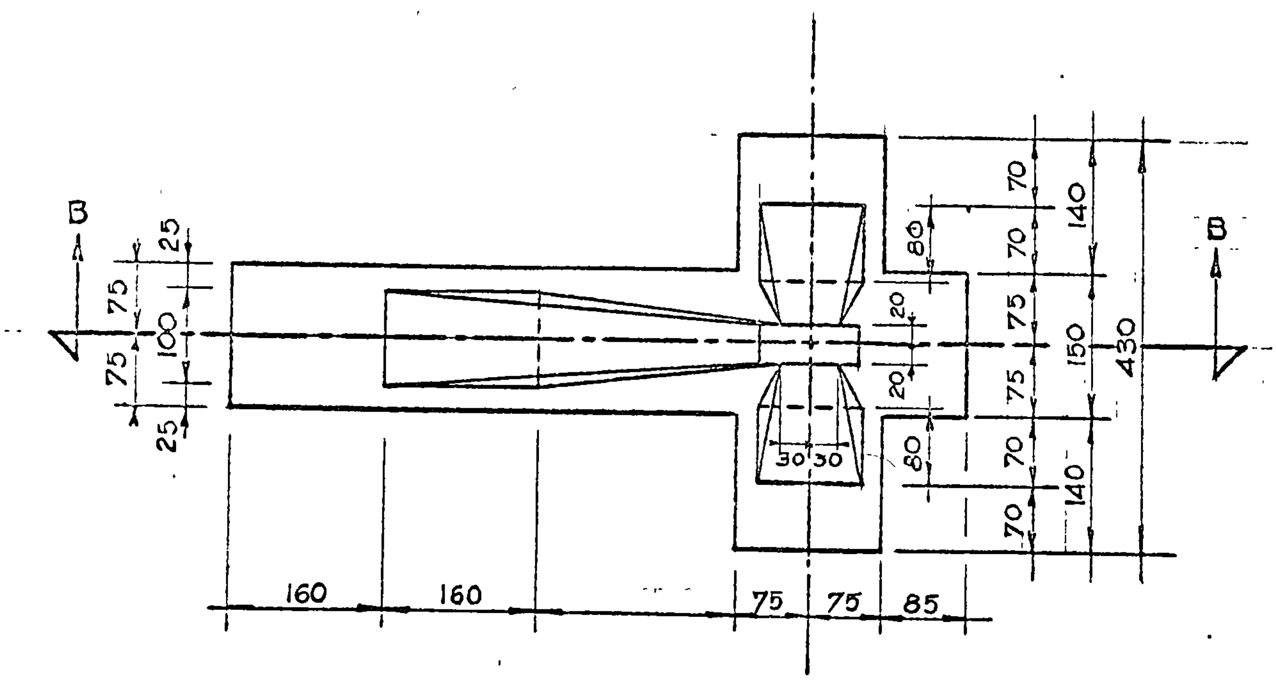

SECTION A-A

FIGURE 6.- TYPICAL SUPPORT.-

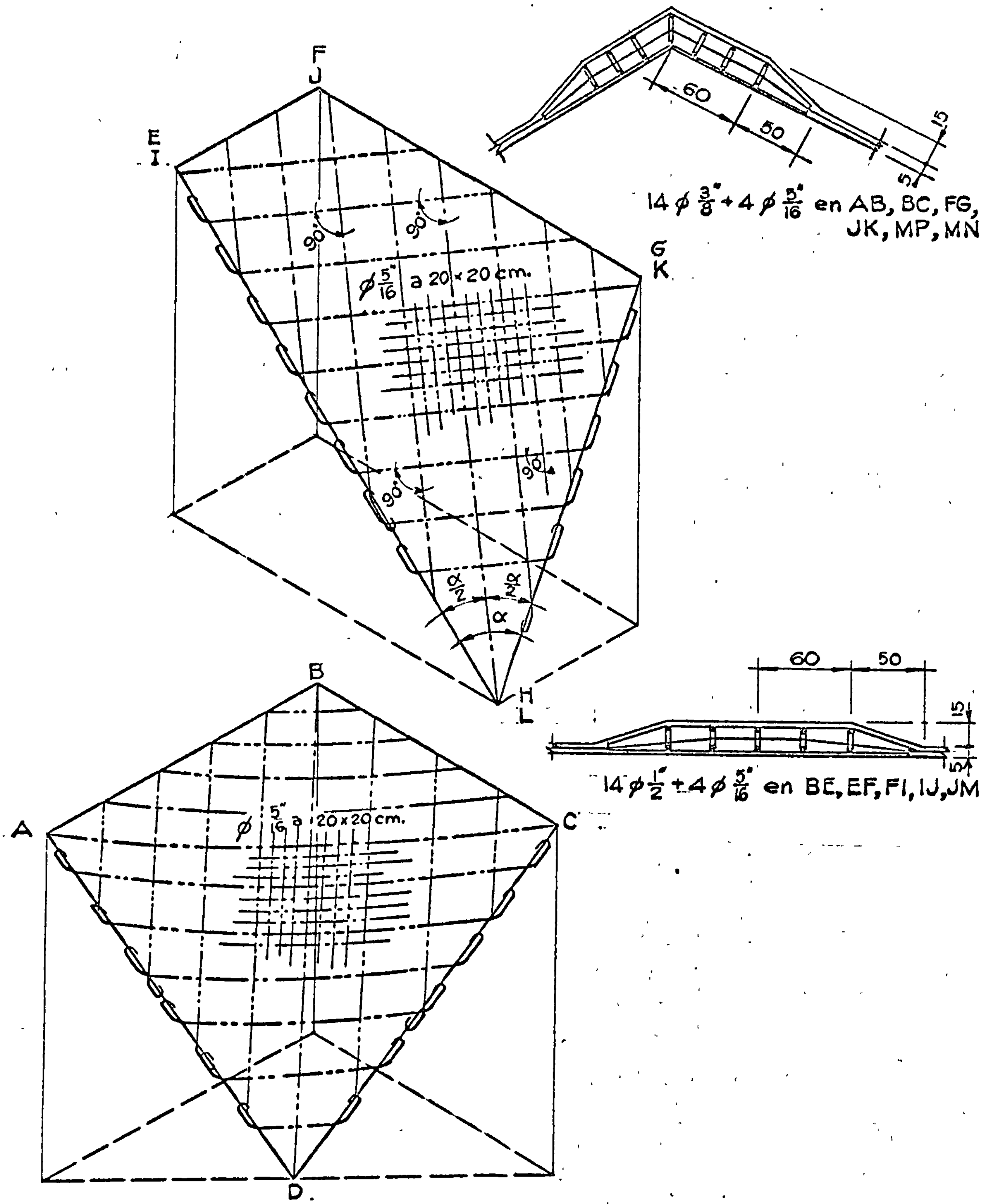

FIGURE 7

ISOMETRIC VIEWS OF REINFORCEMENT STEEL IN SHELLS

ACKNOWLEDGEMENTS

It is with sincere gratitude that the Writer wishes to - thank Arq. Eduardo Padilla for the Architectural Project of - the Church.

Grateful acknowledgements should also be extended to Mr. Edgardo Taroco from Montevideo, Uruguay, for doing most of the Numerical work and Mr. Gregorio Cruz for doing the Structural Drawings of this project.

NOTATIONS

h	Shell Thickness
a, b, f	Shell Dimensions (length, width, rise)
E	Modulus of Elasticity
ν	Poisson's Ratio
D	Flexural Rigidity $\left[\frac{Eh^3}{12(1-\nu^2)}\right]$
X, Y, Z	Components of surface load per unit area.
N_X, N_Y, N_{XY}	Normal and shearing forces per unit distance in the middle surface of the shell.
N_{CR}.	Critical force per unit distance in the middle surface of the shell.
$A, B, C, \ldots$	Constants
γ	Weight per unit volume.
q_o	Weight per unit area of shell. (γh)
F	Stress Function.

BIBLIOGRAPHY

1.- "THEORY OF ELASTIC STABILITY", BY STEPHEN P. TIMOSHENKO, AND JAMES M.GERE, MC.GRAW-HILL, 1961.-

2.- "SHELLS OF DOUBLE CURVATURE", BY ALFRED L. PARME, TRANSACTIONS -- ASCE, 1958, VOL. 123, PP.989-1025.

3.- "DEFORMATIONS OF HYPERBOLIC PARABOLOID SHELLS", BY SHISUO BAN, -- PUBLICATIONS, INTERNATIONAL ASSN. FOR BRIDGE AND STRUCTURAL ENG., - ZURICH, VOL. 13, 1953, P.1.

4.- "THEORY OF NEW FORMS OF SHELL", BY R.S. JENKINS, PAPER NO. 7, --- SYMPOSIUM ON CONCRETE SHELL ROOF CONSTRUCTION, CEMENT AND CONCRETE- ASSN., LONDON, JULY, 2-4, 1952.

5.- "HYPERBOLIC PARABOLOID SHELLS", BY [illegible].FYTOS, TECHNIKA CHRONIKA, -- ATHENS, VOL. 26, NOS. 295-296, 1949, PP. 35-44.

6.- "DOUBLY CURVED THIN SLAB STRUCTURES", BY M.P. BORKOWSKI, TRANSLATION NO. 31, CEMENT AND CONCRETE ASSN., LONDON 1951.

7.- "CALCULATIONS FOR SHELLS OF DOUBLE CURVATURE USING DIFFERENTIAL -- EQUATIONS", BY A. PUCHER, BAUINGENIEUR, VOL. 18, 1937, P, 118.

8.- "TREATISE ON STATICS OF PARABOLIC HYPERBOLOID SHELLS NOT STIFF IN BENDING" BY F. AIMOND, PUBLICATIONS, INTERNATIONAL, ASSN. FOR BRIDGE- AND STRUCTURAL ENG. ZURICH, VOL. 4, 1936, P.1.

9.- "GENERAL INVESTIGATION CONCERNING SKEW SURFACE SHELLS", BY B. LAFFAILLE, PUBLICATIONS, INTERNATIONAL, ASSN. FOR BRIDGE AND STRUCTU_ RAL ENG. ZURICH, VOL. 3, 1935, P. 295.

10.- "THIN SHELLS IN THE SHAPE OF HYPERBOLIC PARABOLOIDS," BY LAFFAILLE LE GENIE CIVILE, PARIS, VOL. 104, 1934, PP. 409-410.

Wind and seismic stresses in hyperbolic paraboloid shells

P. BALLESTEROS [1] and E. TAROCO [2]

Summary

Considering that the wind pressure vector is always normal to the surface of the shell, a solution is determinated for membrane stresses. Seismic stresses are also studied. The application of all these studies is illustrated for the particular case of the Sanctuary «Nuestra Señora de Fátima» (Fig. 1) and some values are compared with that previously obtained in the analysis of vertical loads (2).

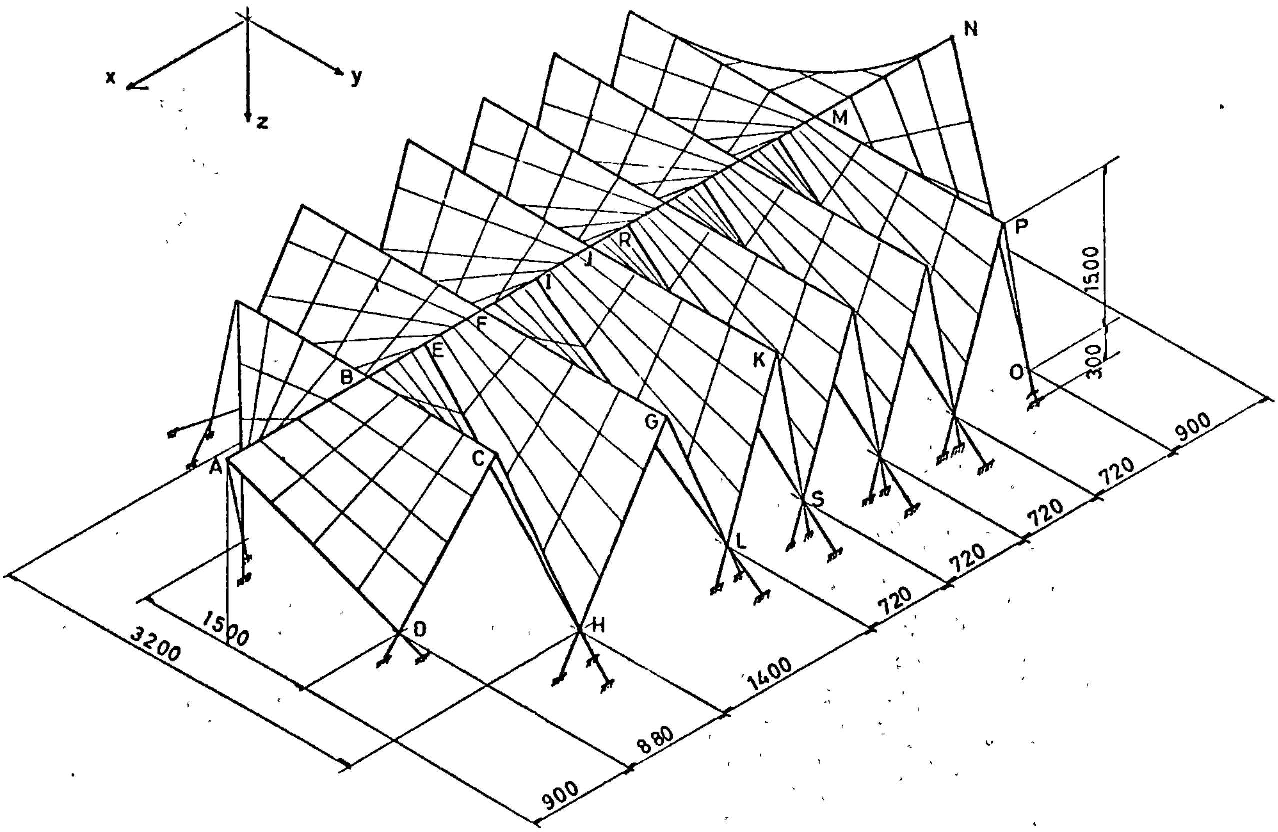

Fig. 1. Isometric view of the structure.

[1] University of «Nuevo León», Monterrey, Mexico.

[2] University of Montevideo, Montevideo, Uruguay.

Notation

$\overline{W}$ = Total load acting on the differential element of the shell.

p = Wind pressure vector, function of (x, y) which is always normal to the surface of the shell.

$(\bar{i}, \bar{j}, \bar{k})$ = Unitary vectors which are respectively parallel to axes x, y, z.

(a, b, h) = Dimensions of the shell: length, wide and height.

$C = \frac{ab}{h}$ = Constant depending of the dimensions of the shell.

(x, y, z) = Rectangular coordinates.

(X', Y', Z') = Components of the load by unit of area in the proyected element of the shell.

(X, Y, Z) = Components of the load by unity of area in the element of the shell.

N'_x, N'_y, N'_{xy} = Stress-resultants by unity of length in the element of the proyected shell.

N_x, N_y, N_{xy} = Stress-resultants by unity of lenght in the element of the shell.

α = Maximum seismic acceleration.

g = Acceleration of the gravity.

$C = \frac{\alpha}{g}$ = Maximum seismic constant, comparation between the maximum seismic acceleration and the acceleration of the gravity.

γ = Specific weight.

t = Thickness of the shell.

$p_x = \frac{\partial p}{\partial x}$ = Partial derivative of the wind pressure function with respect to x.

$p_y = \frac{\partial p}{\partial y}$ = Partial derivative of the wind pressure functon with respect to y.

$z_x = \frac{\partial z}{\partial x}$ = Partial derivative of z with respect to x.

$z_y = \frac{\partial z}{\partial y}$ = Partial derivative of z with respect to y.

$z_{xx} = \frac{\partial^2 z}{\partial x^2}$ = Second derivative of z with respect to x.

$z_{yy} = \frac{\partial^2 z}{\partial y^2}$ = Second derivative of z with respect to y.

$z_{xy} = \frac{\partial^2 z}{\partial x \partial y}$ = Second derivative of z with respect to x and with respect to y.

Stress-Resultants due to wind loads

Representing the middle surface of the shell by a function $z(x, y)$, referred to a Cartesian coordinates system. The total load acting on the differential element of the area dA (Fig. 2) is as follows:

$$W = (\bar{u} \times \bar{v})\, p(x, y) = \begin{vmatrix} \bar{i} & \bar{j} & \bar{k} \\ dx & 0 & z_x dx \\ 0 & dy & z_y dy \end{vmatrix} p(x, y) \qquad [1]$$

From the development of the determinant [1] it is noticed that the load component acting on the projection element $dxdy$ are:

$$
\begin{aligned}
X' &= -z_x p \\
Y' &= -z_y p \\
Z' &= p
\end{aligned}
\qquad [2]
$$

Substituting [2] in the three equilibrium equation, the following equations are obtained:

$$
\begin{aligned}
&\frac{\partial N'_x}{\partial x} + \frac{\partial N'_{xy}}{\partial x} - z_x p = 0 \\
&\frac{\partial N'_y}{\partial y} + \frac{\partial N'_{xy}}{\partial y} - z_y p = 0 \\
&N'_x z_{xx} + N'_y z_{yy} + 2N'_{xy} z_{xy} + z^2_x p + z^2_y p + p = 0
\end{aligned}
\qquad [3]
$$

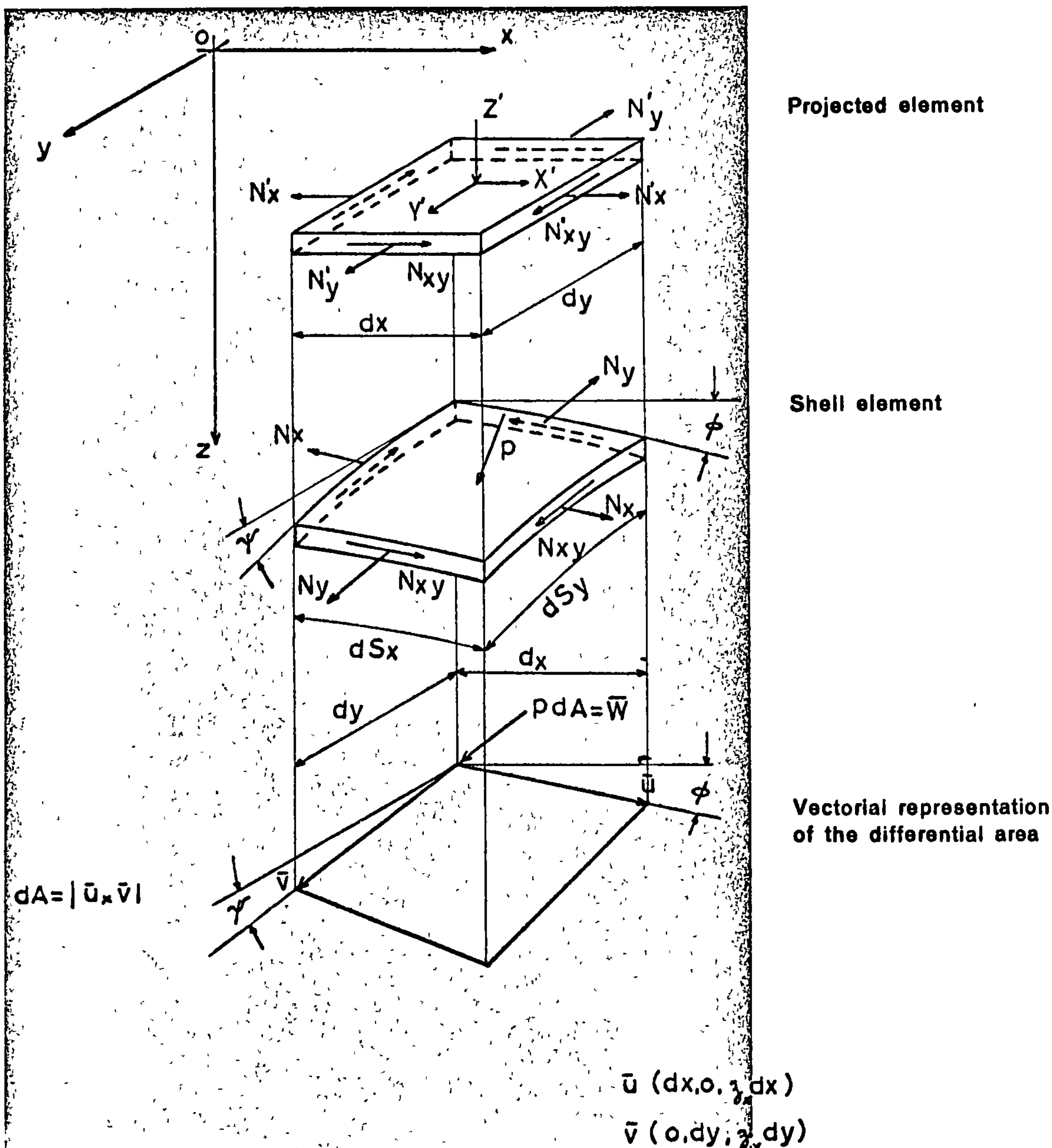

Fig. 2. Shell element referred to a system of rectangular coordinates.

Substituting the hyperbolic paraboloid equation in [3] and integrating, becomes:

$$N'x = \int\left[\frac{2py}{c} + \frac{p_y}{2c}(x^2 + y^2 + c^2)\right]dx + f_1(y).$$

$$N'y = \int\left[\frac{2px}{c} + \frac{p_x}{2c}(x^2 + y^2 + c^2)\right]dy + f_2(x). \qquad [4]$$

$$N'xy = -\frac{p}{2c}(x^2 + y^2 + c^2).$$

For the boundary conditions $(N'x)_{x=a} = (N'y)_{y=b} = 0$ and $p =$ constant, the general equations [4] became transformed as follows:

$$N'x = \frac{2p}{c}\,y\,(x - a).$$

$$N'y = \frac{2p}{c}\,x\,(y - b). \qquad [5]$$

$$N'xy = -\frac{p}{2c}(x^2 + y^2 + c^2).$$

The relationship between the projected and the real stress-resultants in the element for the hyperbolic paraboloid, are:

$$Nx = \frac{\cos\Psi}{\cos\Phi}N'x = \sqrt{\frac{c^2 + y^2}{c^2 + x^2}}\,N'x.$$

$$Ny = \frac{\cos\Phi}{\cos\Psi}N'y = \sqrt{\frac{c^2 + x^2}{c^2 + y^2}}\,N'y. \qquad [6]$$

$$Nxy = N'xy.$$

Substituting [5] into [6], it is obtained:

$$Nx = \frac{2p}{c}\,y\,(x - a)\sqrt{\frac{c^2 + y^2}{c^2 + x^2}}.$$

$$Ny = \frac{2p}{c}\,x\,(y - b)\sqrt{\frac{c^2 + x^2}{c^2 + y^2}}. \qquad [7]$$

$$Nxy = -\frac{p}{2c}(x^2 + y^2 + c^2).$$

Equations [7] are determining the membrane stress-resultants for hyperbolic paraboloid shells, when they are supporting a wind pressure p which is constant in magnitude, but with a variable direction, being always normal to the surface of the shell. In Figure 3 are plotted the stress-resultants for the case of the structure of Fatima.

Seismic stress-resultants

The differential element weight is:

$$dP = \sqrt{1 + z_x^2 + z_y^2}\,\gamma t dxdy \qquad [8]$$

The load produced by the seismo in the differential element will be:

$$Y = -\frac{k}{c}\sqrt{x^2 + y^2 + c^2}. \qquad [9]$$

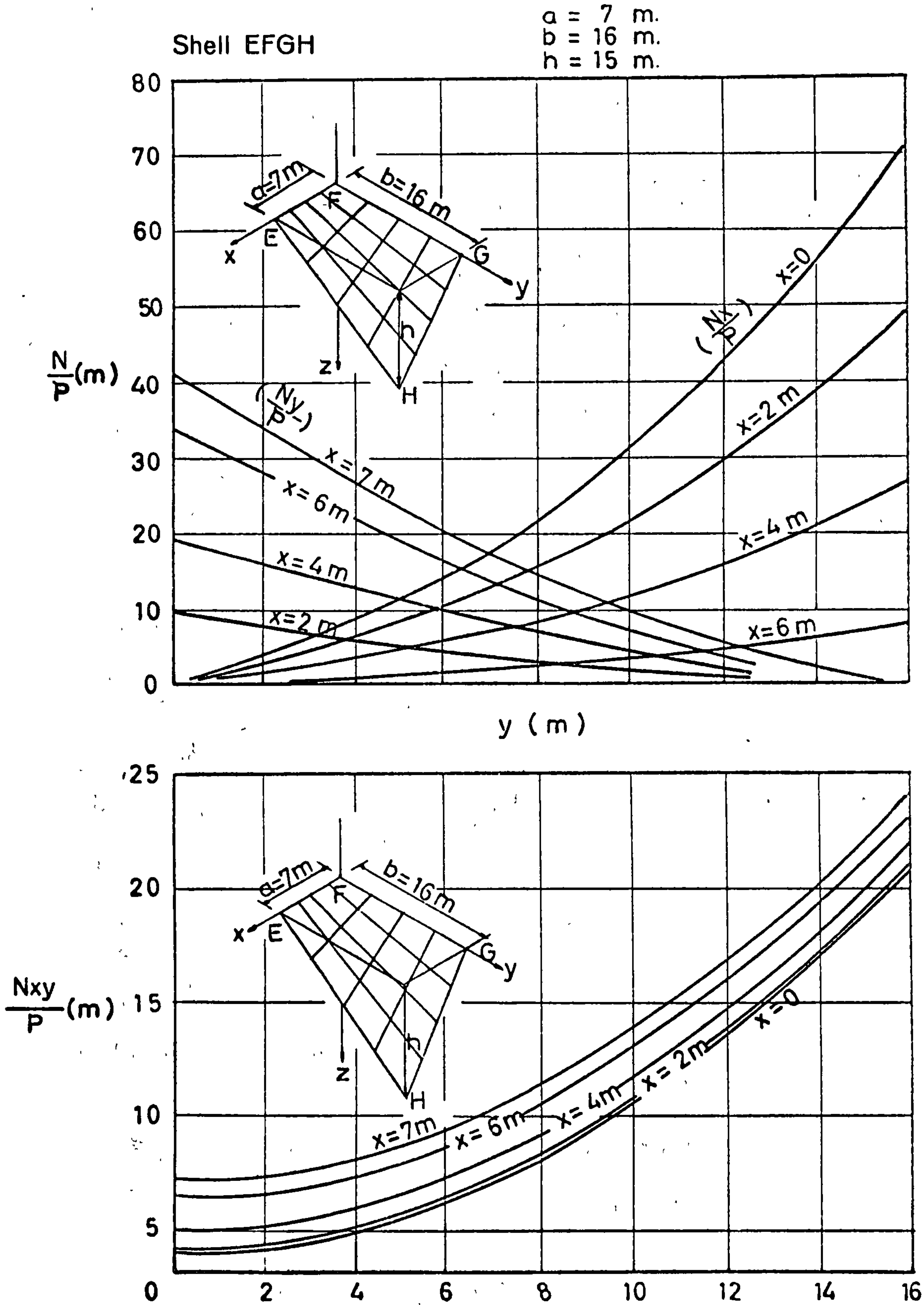

Fig. 3. Variation of the wind stress-resultants.

Where $k = c\gamma t$. The equilibrium equations for the hyperbolic paraboloid, in this case, will be reduced into:

$$\begin{aligned}
&\frac{\partial N'x}{\partial x} + \frac{\partial N'xy}{\partial y} = 0 . \\
&\frac{\partial N'y}{\partial y} + \frac{\partial N'xy}{\partial x} = \frac{k}{c}\sqrt{x^2 + y^2 + c^2} . \\
&\frac{2N'xy}{c} = -\frac{kx}{c^2}\sqrt{x^2 + y^2 + c^2} .
\end{aligned} \qquad [10]$$

Introducing [10c] in [10a] and integrating, it is obtained:

$$N'x = \frac{ky}{2c}\sqrt{x^2 + y^2 + c^2} + f_1(y) . \qquad [11]$$

and conisdering the boundary conditions $(N'x)_{x=a} = 0$, then

$$f_1(y) = -\frac{ky}{2c}\sqrt{y^2 + a^2 + c^2} . \qquad [12]$$

Substituting [10c] in [10b] and integrating, becomes:

$$N'y = \frac{3ky}{4c}\sqrt{x^2 + y^2 + c^2} + \frac{k}{4c}(3c^2 + 5x^2)\log\left(y + \sqrt{x^2 + y^2 + c^2}\right) + f_2(x) . \qquad [13]$$

From the boundary condition $(N'y)_{y=b} = 0$ it is obtained:

$$f_2(x) = -\frac{3kb}{4c}\sqrt{x^2 + b^2 + c^2} - \frac{k}{4c}(3c^2 + 5x^2)\log\left(b + \sqrt{x^2 + b^2 + c^2}\right) \qquad [14]$$

From the equations [6], [10], [11], [12], [13] and [14] the following seismic stress-resultants are determinated:

$$\begin{aligned}
Nx &= \frac{ky}{2c}\sqrt{\frac{c^2 + y^2}{c^2 + x^2}}\left(\sqrt{x^2 + y^2 + c^2} - \sqrt{y^2 + a^2 + c^2}\right) . \\
Ny &= \frac{k}{4c}\sqrt{\frac{c^2 + y^2}{c^2 + x^2}}\left[3\left(y\sqrt{x^2 + y^2 + c^2} - b\sqrt{x^2 + b^2 + c^2}\right) + \right. \\
&\qquad \left. + (3c^2 + 5x^2)\log\frac{y + \sqrt{x^2 + y^2 + c^2}}{b + \sqrt{x^2 + b^2 + c^2}}\right] . \\
Nxy &= -\frac{kx}{2c}\sqrt{x^2 + y^2 + c^2} .
\end{aligned} \qquad [15]$$

Where $k = \frac{\alpha}{g}\gamma t$.

Figures 4 showes the variation of the seismic stress-resultants determinated by [15] for the particular case of the shell of Fatima.

Comparison between stress-resultants due to seismic vertical loads and wind

Numerical data for shell EFGH:

$$\begin{array}{ll}
t = 0.05 \text{ m.} & f = 15 \text{ m.} \\
\gamma = 2\,500 \text{ kg/m}^3. & c = \dfrac{ab}{f} = 7.47 \text{ m.} \\
a = 7 \text{ m.} & C = 0.10 \\
b = 16 \text{ m.} & p = 50 \text{ kg/m}^2.
\end{array} \qquad [16]$$

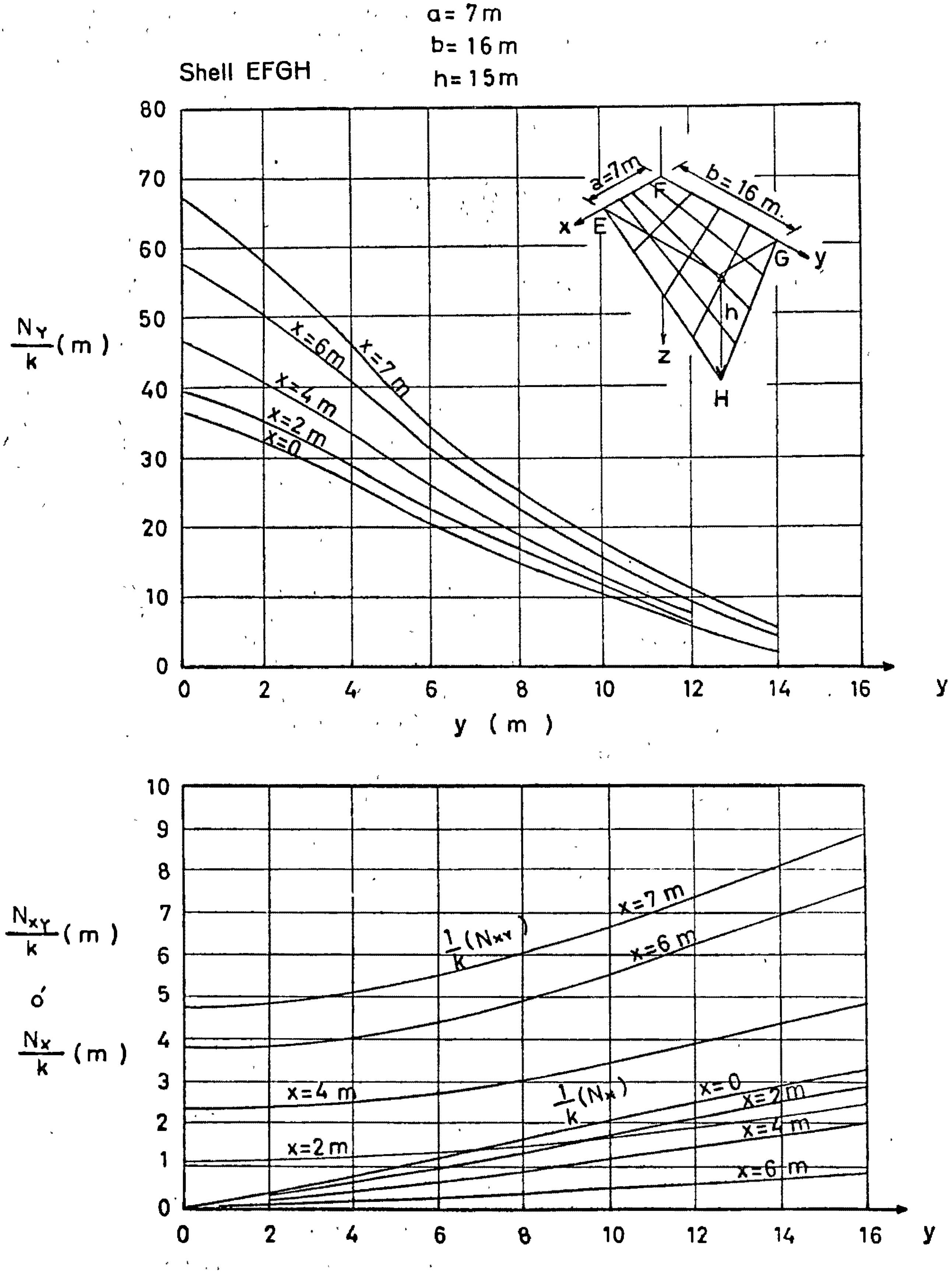

Fig. 4. Seismic stress-resultants in shell E F G H.

With data of [16] and following the graphic for N (Reference 2, page 356, figure 2) and graphics of figures 3 and 4, it is obtained the stress-resultants dues to dead load, wind and seismo as well as combinations of dead load with wind and dead with seismo, which have been all indicated in Table I.

Stress	Dead load	Wind	Seismo	Dead load and wind	Dead load and seismo
Nx $\begin{matrix} x=0 \\ y=16 \end{matrix}$	912 kg/m	3 550 kg/m	40 kg/m	4 462 kg/m	952 kg/m
Ny $\begin{matrix} x=7 \\ y=0 \end{matrix}$	738 kg/m	2 100 kg/m	837 kg/m	2 838 kg/m	1 675 kg/m
Nxy $\begin{matrix} x=7 \\ y=16 \end{matrix}$	1 200 kg/m	1 200 kg/m	111 kg/m	2 400 kg/m	1 311 kg/m

TABLE I. Comparison between maximum stress-resultans

Conclusions

In Table I a comparison between maximum stresses is established for a specific problem, due to the following load conditions:

a) Vertical loads (dead and live load).

b) Vertical and seismic loads.

c) Vertical loads and wind.

It is observed that the less favourable load condition is that resulting of combination of vertical loads with wind, because it increases approximately four times, the middle stresses due to vertical loads. Of course, the value of the middle pressure of wind p, that was supposed of 50 kg/m^2, could be diminished by forms of aereodinamic characteristics which have their own surface.

Reduced models can be used to study the real distribution of the wind pressure p, and by means of hydraulical similitude existing between the Euler, Reynolds and Froude numbers it can be determinated the distribution of the wind pressure of the prototype, and substituting this function of the wind pressure in equations [4], it is possible to obtain a more rigorous solution of that problem. However, for practical results can be considered the pressure wind vector of constant modulus but of variable direction i.e. normal to the middle surface of the shell.

For that reason, we consider very important in paraboloidal hyperbolic shells, to take into account the stresses due to wind loads, and to compare them with the order of magnitude of critical stresses (Reference 1).

Generally, in these cases, seismic stresses are not of importance, as it can be observed in that values expressed in Table I.

It is very important to mention that every solution obtained by means of the membrane theory, represent only one form of all that can be obtained with equilibrium configurations, giving different values to functions $f_1(y)$ and $f_2(x)$ in equations [4]. In the case presented the selected functions has been choosen such as the boundary conditions at $x = a$ and $y = b$, having zero normal stress-resultans Nx and Ny, and in this way the selected equilibrium stresses-resultants shape is consistent with the real conditions of the structure support. If all these conditions can not be obtained, the theory of the membrane could not reach satisfactory results, and then it would be necessary to get the compatibility conditions by strain between edge beam and shell, and to derive the stresses from these conditions.

Advantageously in the above particular case studied, the theory of membrane solution, gives satisfactories values.

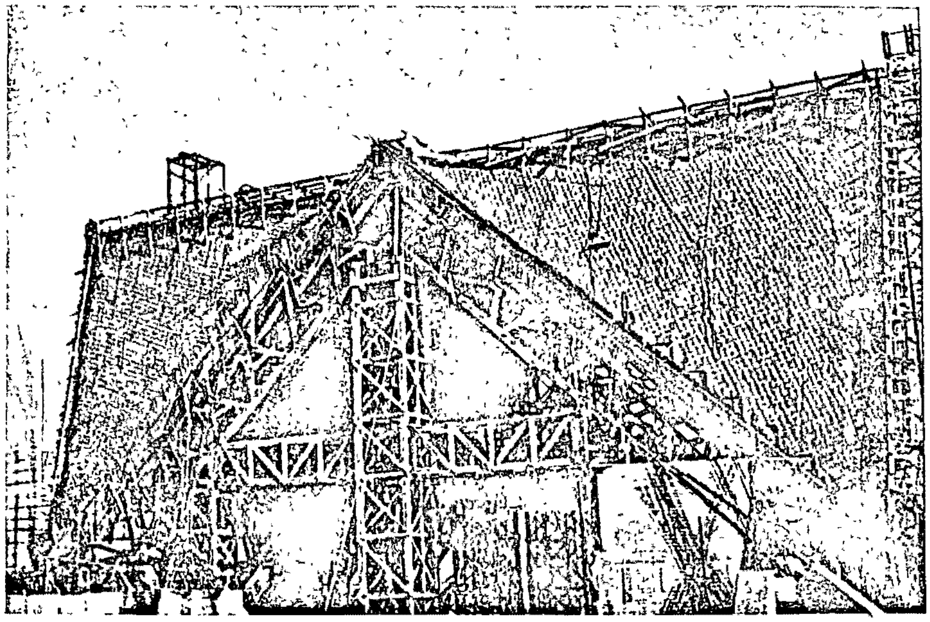

View of scafolder in shell A B C D.

Bibliography

(1) K. G. Tester: «Beitrag zur berechung der hyperbolischen Paraboloidschale». Ingenieur-Archiv, vol. 16, 1947, pp. 39-44.

(2) P. Ballesteros: «Stress Analysis and Design of Our Lady of Fatima Church». World Conference in Shell structures San Francisco, Cal. 1962. National Academy of Sciences. National research council publication No. 1187.

Detail of the reinforcement of shell E F G H.

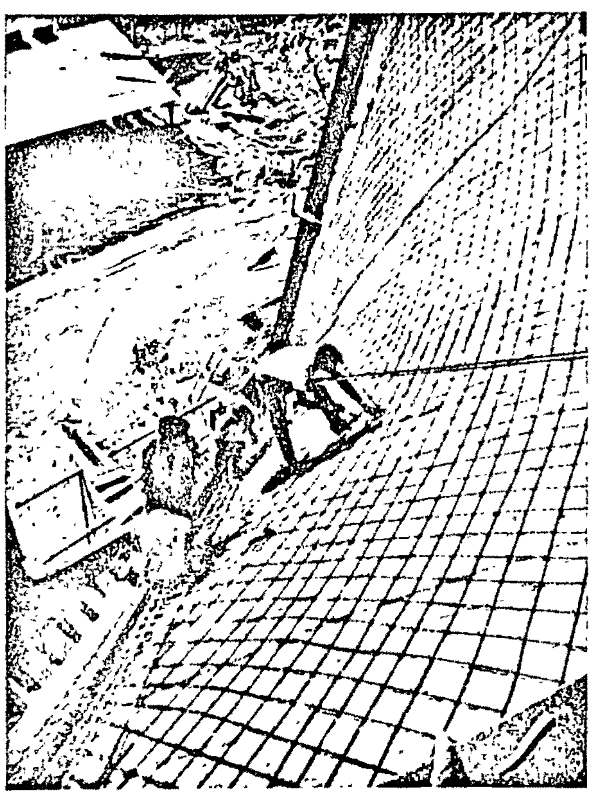

Reinforcement of the edge beam M N.

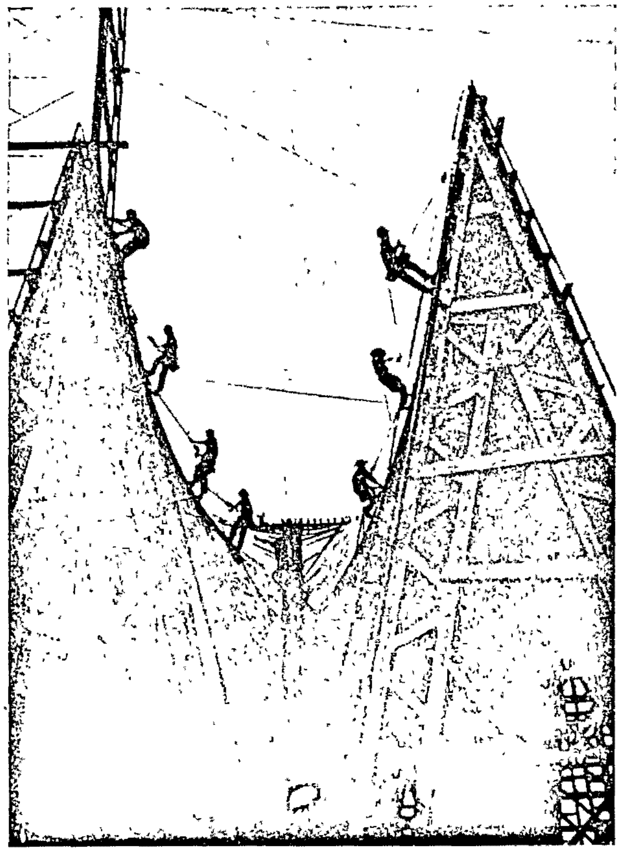

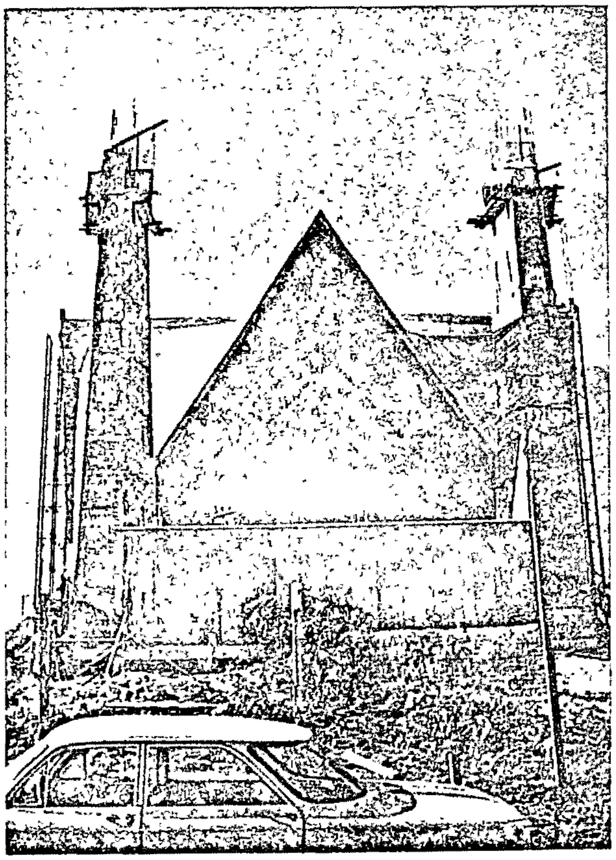

Scaffolder and laying of reinforcement.

View of the main façade.

View of the main façade without screen.

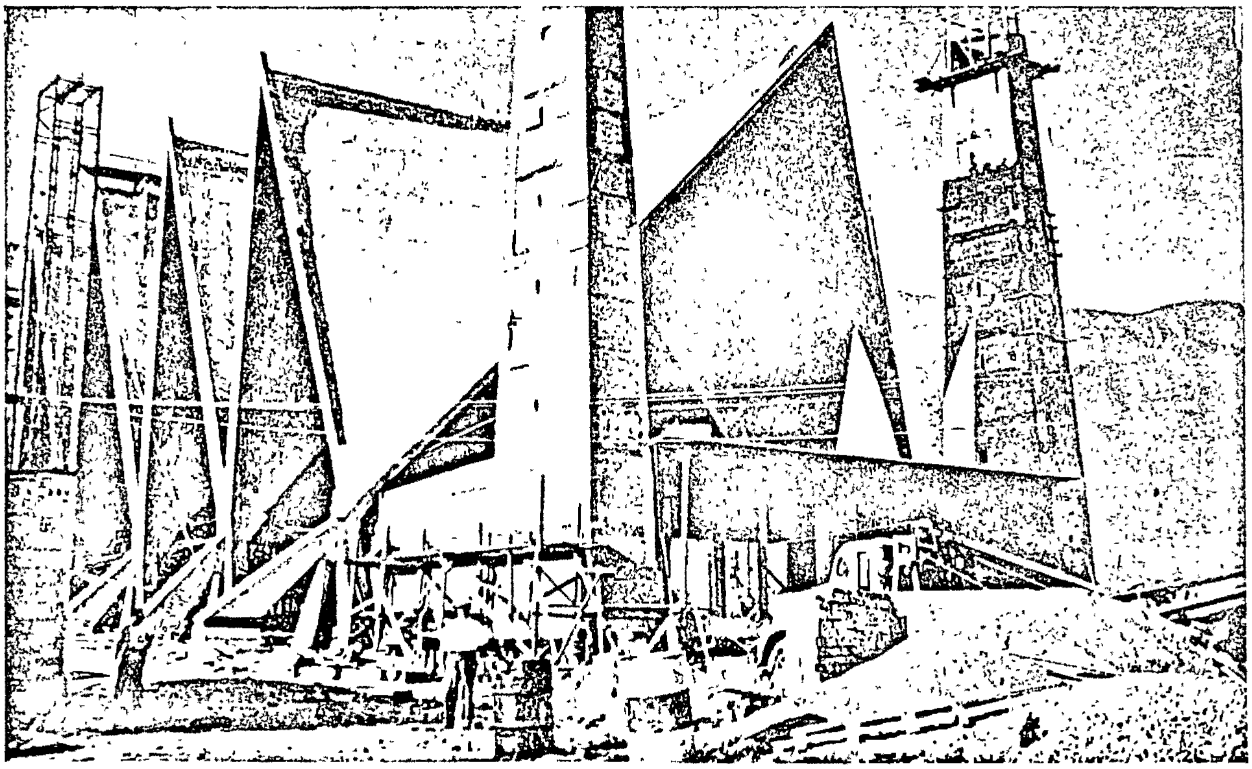

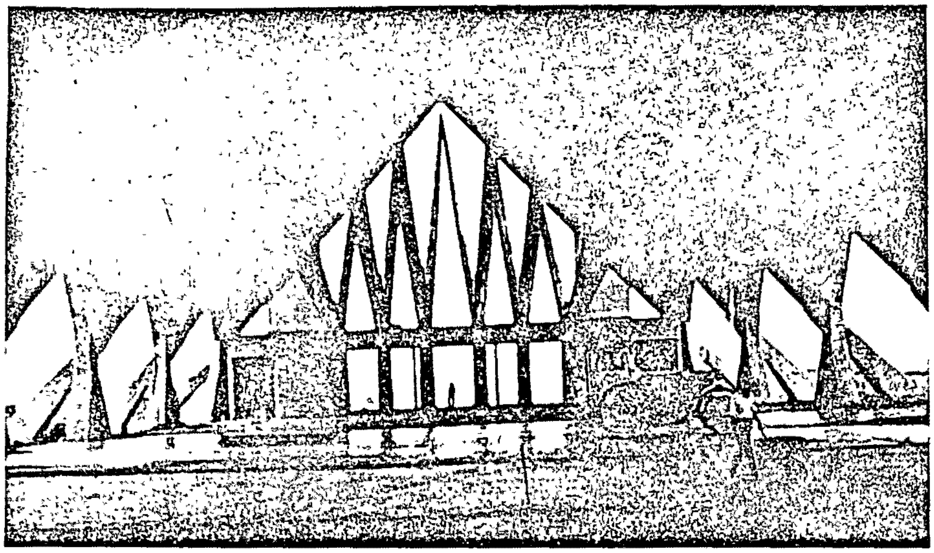

Interior view of the main façade.

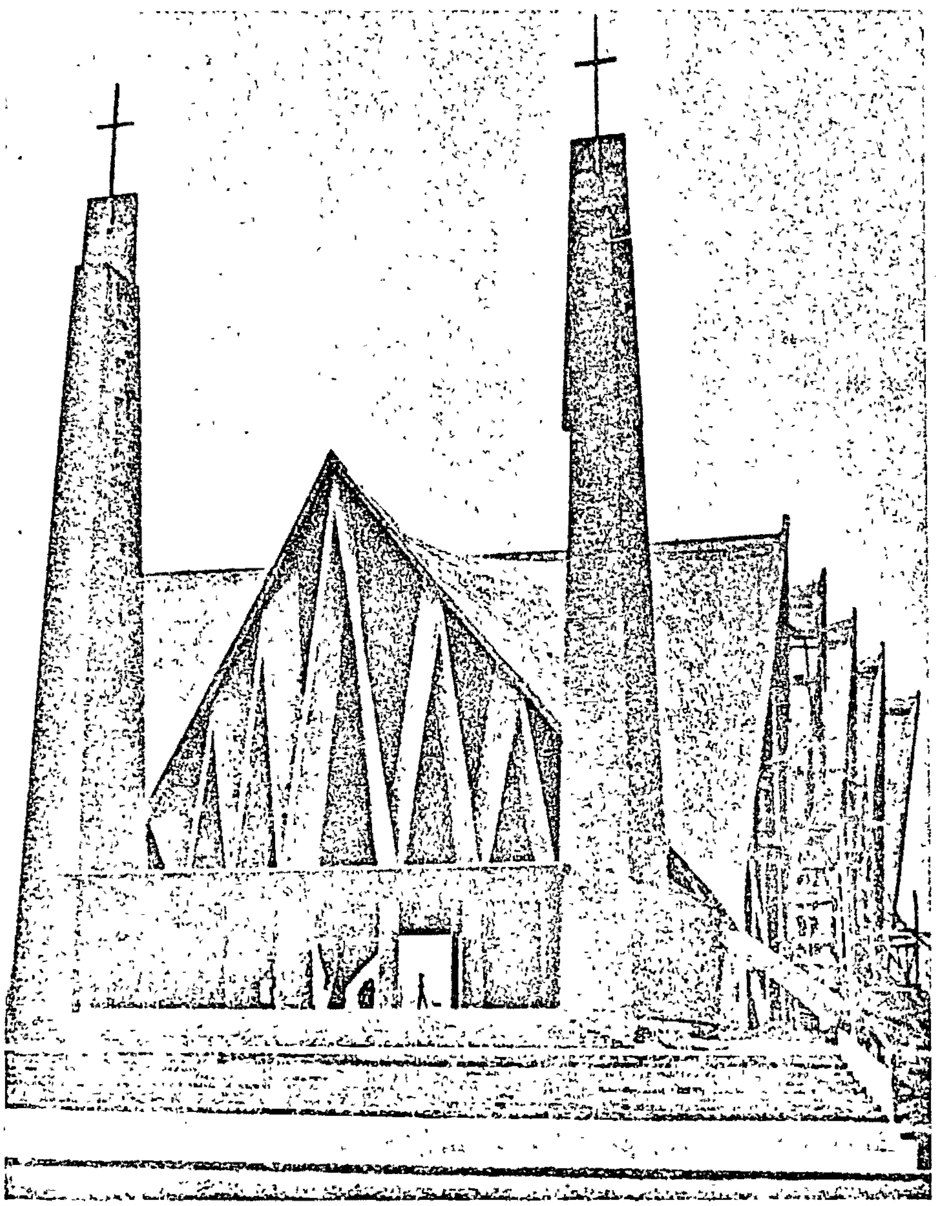

View of the main façade with screens.

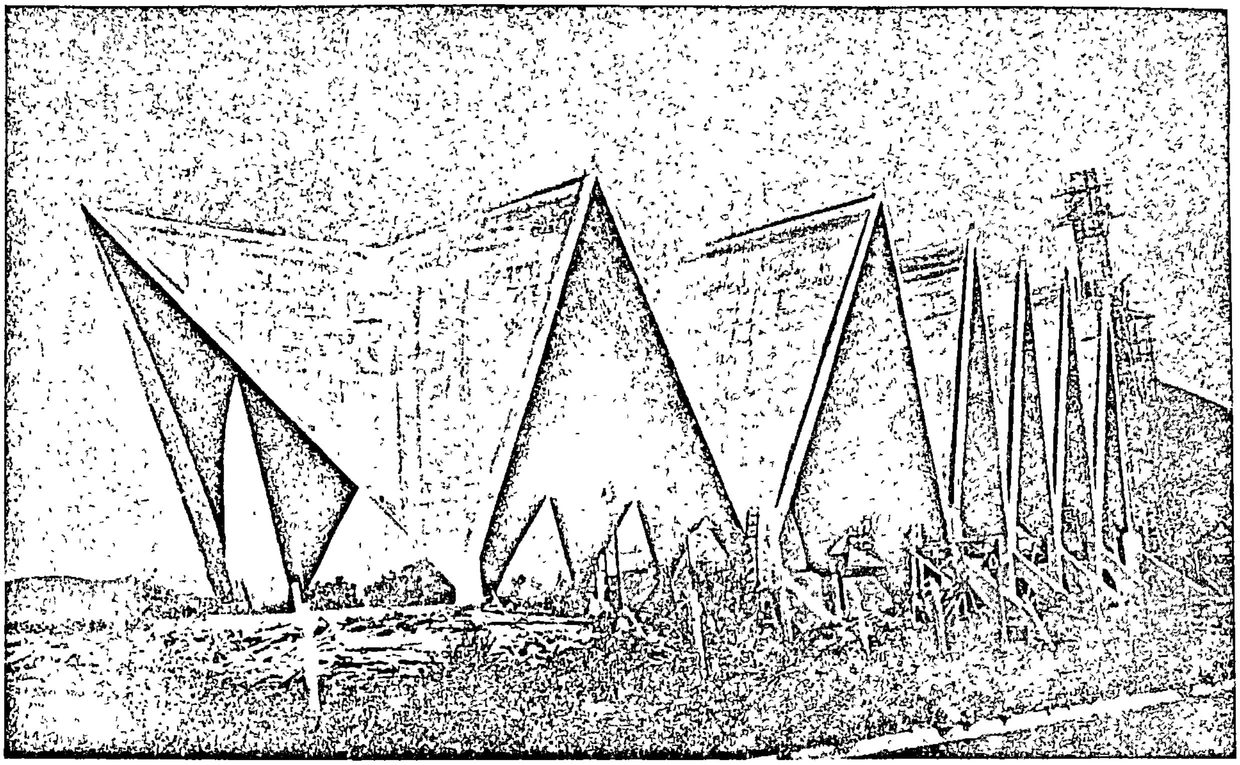

Shell completely poured.

Interior view of the supports.

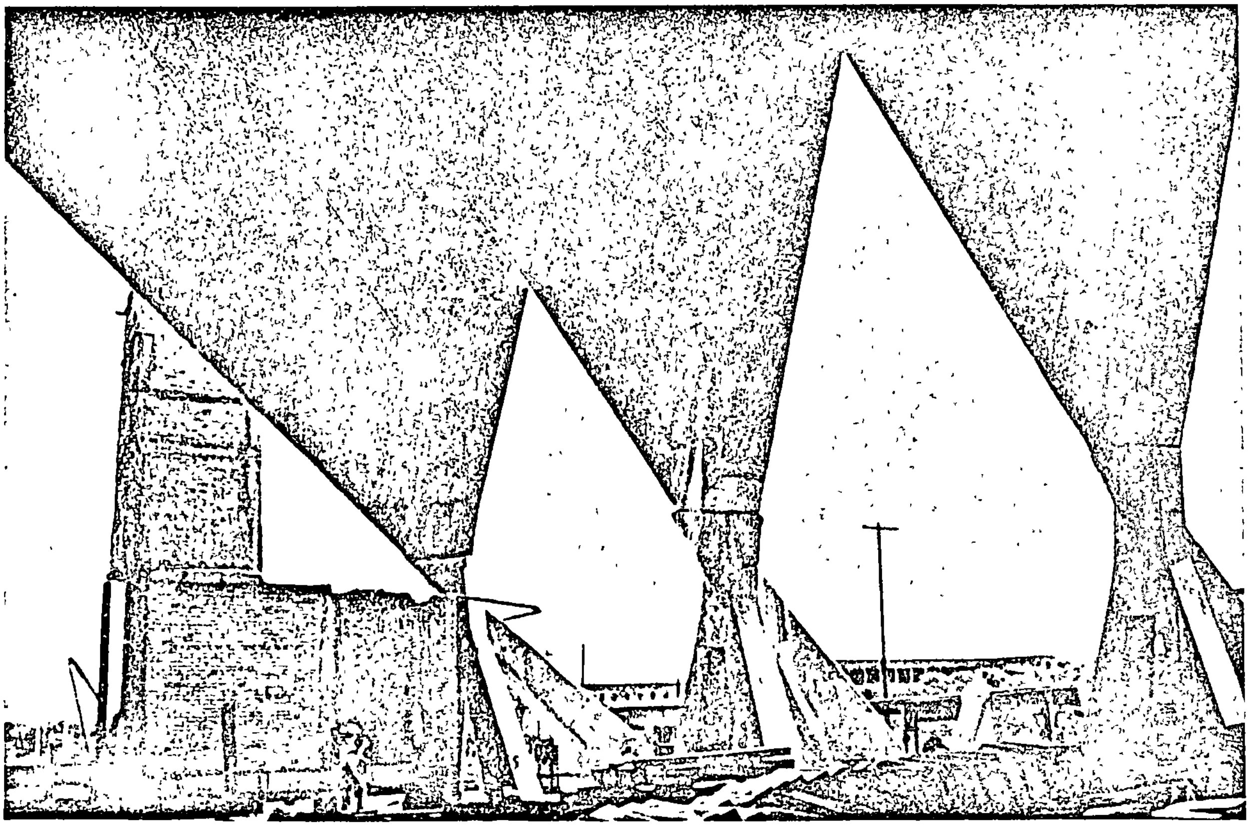

unit area of the surface To this area corresponds an area

$$\cos \gamma = \frac{c}{\sqrt{x^2 + y^2 + c^2}}$$

of the horizontal projection of the shell. Hence

$$Z = \frac{q_0}{c} \sqrt{x^2 + y^2 + c^2} \tag{t}$$

and Eq. (r) yields

$$N_{xy} = \frac{q_0}{2} \sqrt{x^2 + y^2 + c^2}$$

Differentiating this with respect to y and then integrating the result with respect to x, or vice versa, both in accordance with Eqs. (e), we get

$$\bar{N}_x = -\frac{q_0 y}{2} \log \frac{x + \sqrt{x^2 + y^2 + c^2}}{\sqrt{y^2 + c^2}}$$
$$\bar{N}_y = -\frac{q_0 x}{2} \log \frac{y + \sqrt{x^2 + y^2 + c^2}}{\sqrt{x^2 + c^2}}$$

The true forces N_x and N_y are obtained from those expressions by means of Eqs. (c), in which the angles φ, θ are given by $\tan \varphi = -y/c$ and $\tan \theta = -x/c$.

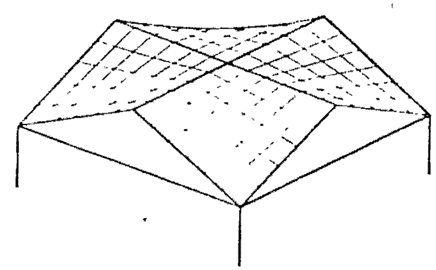

FIG. 234

Several shells of this kind may be combined to form a roof, such as shown in Fig 234 It should be noted, however, that neither the dead load of the groin members, needed by such a roof, nor a partial loading—due, for instance, to snow [illegible] be transmitted by the membrane forces alone; hence flexural stresses will necessarily arise.[1]

Of practical interest and worthy of mention are also the conoidal shells, which sometimes have been used in the design of cantilever roofs and dam walls.[2] Roof shells of this kind, however, with curved generatrices instead of [illegible] used in structural applications.[3]

[1] See Flügge, *op cit*, p 119, Flügge and Geyling, *op* [illegible] *Trans Eng Inst Canada*, vol 3, p 32, 1959

[2] The theory of the conoidal shell has been elaborated by [illegible], *[illegible]*, vol 9, p 29, 1911 See also M Soare, *Bauingenieur*, vol 33, p 256, 1958, and Flügge, *op cit*, p 127

[3] See [illegible] Doganoff, *Bautechnik*, vol 34, p 232, 1957

CHAPTER 15

GENERAL THEORY OF CYLINDRICAL SHELLS

114. A Circular Cylindrical Shell Loaded Symmetrically with Respect Its Axis. In practical applications we frequently encounter problems which a circular cylindrical shell is submitted to the action of forces tributed symmetrically with respect to the axis of the cylinder. The ess distribution in cylindrical boilers submitted to the action of steam essure, stresses in cylindrical containers having a vertical axis and subitted to internal liquid pressure, and stresses in circular pipes under uform internal pressure are examples of such problems.

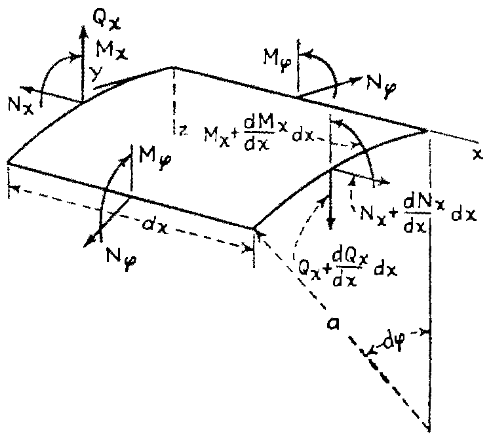

FIG 235

To establish the equations required for the solution of these problems e consider an element, as shown in Figs 228*a* and 235, and consider the quations of equilibrium. It can be concluded from symmetry that the nembrane shearing forces $N_{x\varphi} = N_{\varphi x}$ vanish in this case and that forces N_φ are constant along the circumference. Regarding the transverse hearing forces, it can also be concluded from symmetry that only the orces Q_x do not vanish. Considering the moments acting on the elenent in Fig 235, we also conclude from symmetry that the twisting moments $M_{x\varphi} = M_{\varphi x}$ vanish and that the bending moments M_φ are constant along the circumference. Under such conditions of symmetry

three of the six equations of equilibrium of the element are identically satisfied, and we have to consider only the remaining three equations, *viz.*, those obtained by projecting the forces on the x and z axes and by taking the moment of the forces about the y axis. Assuming that the external forces consist only of a pressure normal to the surface, these three equations of equilibrium are

$$\begin{aligned} \frac{dN_x}{dx} a\,dx\,d\varphi &= 0 \\ \frac{dQ_x}{dx} a\,dx\,d\varphi + N_\varphi\,dx\,d\varphi + Za\,dx\,d\varphi &= 0 \\ \frac{dM_x}{dx} a\,dx\,d\varphi - Q_x a\,dx\,d\varphi &= 0 \end{aligned} \tag{a}$$

The first one indicates that the forces N_x are constant,[1] and we take them equal to zero in our further discussion. If they are different from zero, the deformation and stress corresponding to such constant forces can be easily calculated and superposed on stresses and deformations produced by lateral load. The remaining two equations can be written in the following simplified form:

$$\begin{aligned} \frac{dQ_x}{dx} + \frac{1}{a} N_\varphi &= -Z \\ \frac{dM_x}{dx} - Q_x &= 0 \end{aligned} \tag{b}$$

These two equations contain three unknown quantities N_φ, Q_x, and M_x. To solve the problem we must therefore consider the displacements of points in the middle surface of the shell.

From symmetry we conclude that the component v of the displacement in the circumferential direction vanishes. We thus have to consider only the components u and w in the x and z directions, respectively. The expressions for the strain components then become

$$\epsilon_x = \frac{du}{dx} \qquad \epsilon_\varphi = -\frac{w}{a} \tag{c}$$

Hence, by applying Hooke's law, we obtain

$$\begin{aligned} N_x &= \frac{Eh}{1-\nu^2}(\epsilon_x + \nu\epsilon_\varphi) = \frac{Eh}{1-\nu^2}\left(\frac{du}{dx} - \nu\frac{w}{a}\right) = 0 \\ N_\varphi &= \frac{Eh}{1-\nu^2}(\epsilon_\varphi + \nu\epsilon_x) = \frac{Eh}{1-\nu^2}\left(-\frac{w}{a} + \nu\frac{du}{dx}\right) \end{aligned} \tag{d}$$

From the first of these equations it follows that

$$\frac{du}{dx} = \nu\frac{w}{a}$$

[1] The effect of these forces on bending is neglected in this discussion

d the second equation gives

$$N_\varphi = -\frac{Ehw}{a} \tag{e}$$

nsidering the bending moments, we conclude from symmetry that ere is no change in curvature in the circumferential direction. The rvature in the x direction is equal to $-d^2w/dx^2$. Using the same equans as for plates, we then obtain

$$\begin{aligned} M_\varphi &= \nu M_x \\ M_x &= -D\frac{d^2w}{dx^2} \end{aligned} \tag{f}$$

here

$$D = \frac{Eh^3}{12(1-\nu^2)}$$

the flexural rigidity of the shell.

Returning now to Eqs. (b) and eliminating Q_x from these equations, e obtain

$$\frac{d^2M_x}{dx^2} + \frac{1}{a}N_\varphi = -Z$$

om which, by using Eqs. (e) and (f), we obtain

$$\frac{d^2}{dx^2}\left(D\frac{d^2w}{dx^2}\right) + \frac{Eh}{a^2}w = Z \tag{273}$$

ll problems of symmetrical deformation of circular cylindrical shells us reduce to the integration of Eq. (273).

The simplest application of this equation is obtained when the thickss of the shell is constant. Under such conditions Eq. (273) becomes

$$D\frac{d^4w}{dx^4} + \frac{Eh}{a^2}w = Z \tag{274}$$

sing the notation

$$\beta^4 = \frac{Eh}{4a^2D} = \frac{3(1-\nu^2)}{a^2h^2} \tag{275}$$

q. (274) can be represented in the simplified form

$$\frac{d^4w}{dx^4} + 4\beta^4 w = \frac{Z}{D} \tag{276}$$

his is the same equation as is obtained for a prismatical bar with a exural rigidity D, supported by a continuous elastic foundation and bmitted to the action of a load of intensity Z.* The general solution this equation is

$$\begin{aligned} w = {} & e^{\beta x}(C_1\cos\beta x + C_2\sin\beta x) \\ & + e^{-\beta x}(C_3\cos\beta x + C_4\sin\beta x) + f(x) \end{aligned} \tag{277}$$

* See S. Timoshenko, "Strength of Materials," part II, 3d ed., p. 2, 1956.

in which $f(x)$ is a particular solution of Eq. (276), and $C_1, \ldots, C_4$ are the constants of integration which must be determined in each particular case from the conditions at the ends of the cylinder.

Take, as an example, a long circular pipe submitted to the action of bending moments M_0 and shearing forces Q_0, both uniformly distributed along the edge $x = 0$ (Fig. 236). In this case there is no pressure Z distributed over the surface of the shell, and $f(x) = 0$ in the general solution (277). Since the forces applied at the end $x = 0$ produce a local bending which dies out rapidly as the distance x from the loaded end increases, we conclude that the first term on the right-hand side of Eq. (277) must vanish.[1] Hence, $C_1 = C_2 = 0$, and we obtain

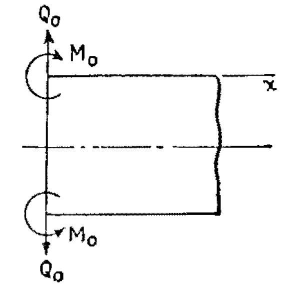

FIG. 236

$$w = e^{-\beta x}(C_3\cos\beta x + C_4\sin\beta x) \tag{g}$$

The two constants C_3 and C_4 can now be determined from the conditions at the loaded end, which may be written

$$\begin{aligned} (M_x)_{x=0} &= -D\left(\frac{d^2w}{dx^2}\right)_{x=0} = M_0 \\ (Q_x)_{x=0} &= \left(\frac{dM_x}{dx}\right)_{x=0} = -D\left(\frac{d^3w}{dx^3}\right)_{x=0} = Q_0 \end{aligned} \tag{h}$$

Substituting expression (g) for w, we obtain from these end conditions

$$C_3 = -\frac{1}{2\beta^3D}(Q_0 + \beta M_0) \qquad C_4 = \frac{M_0}{2\beta^2D} \tag{i}$$

Thus the final expression for w is

$$w = \frac{e^{-\beta x}}{2\beta^3D}[\beta M_0(\sin\beta x - \cos\beta x) - Q_0\cos\beta x] \tag{278}$$

The maximum deflection is obtained at the loaded end, where

$$(w)_{x=0} = -\frac{1}{2\beta^3D}(\beta M_0 + Q_0) \tag{279}$$

The negative sign for this deflection results from the fact that w is taken positive toward the [illegible]

[1] Observing the fact that the system of forces applied at the end of the pipe is a balanced one and that the length of the pipe may be increased at will, this follows also from the principle of Saint-Venant; see, for example, S. Timoshenko and J. N. Goodier, "Theory of Elasticity," 2d ed., p. 33, 1951.

obtained by differentiating expression (278). This gives

$$\left(\frac{dw}{dx}\right)_{x=0} = \frac{e^{-\beta x}}{2\beta^2 D}\,[2\beta M_0 \cos\beta x + Q_0(\cos\beta x + \sin\beta x)]_{x=0}$$
$$= \frac{1}{2\beta^2 D}\,(2\beta M_0 + Q_0) \qquad (280)$$

By introducing the notation

$$\begin{aligned}
\varphi(\beta x) &= e^{-\beta x}(\cos\beta x + \sin\beta x)\\
\psi(\beta x) &= e^{-\beta x}(\cos\beta x - \sin\beta x)\\
\theta(\beta x) &= e^{-\beta x}\cos\beta x\\
\zeta(\beta x) &= e^{-\beta x}\sin\beta x
\end{aligned} \qquad (281)$$

the expressions for deflection and its consecutive derivatives can be represented in the following simplified form:

$$\begin{aligned}
w &= -\frac{1}{2\beta^3 D}\,[\beta M_0\psi(\beta x) + Q_0\theta(\beta x)]\\
\frac{dw}{dx} &= \frac{1}{2\beta^2 D}\,[2\beta M_0\theta(\beta x) + Q_0\varphi(\beta x)]\\
\frac{d^2w}{dx^2} &= -\frac{1}{2\beta D}\,[2\beta M_0\varphi(\beta x) + 2Q_0\zeta(\beta x)]\\
\frac{d^3w}{dx^3} &= \frac{1}{D}\,[2\beta M_0\zeta(\beta x) - Q_0\psi(\beta x)]
\end{aligned} \qquad (282)$$

The numerical values of the functions $\varphi(\beta x)$, $\psi(\beta x)$, $\theta(\beta x)$, and $\zeta(\beta x)$ are given in Table 84.[1] The functions $\varphi(\beta x)$ and $\psi(\beta x)$ are represented graphically in Fig. 237. It is seen from these curves and from Table 84

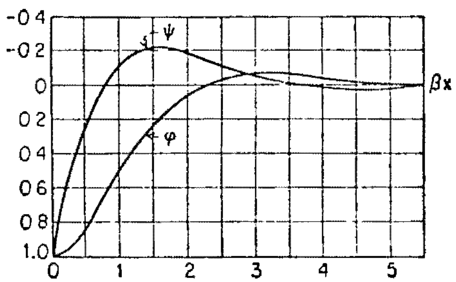

FIG. 237

that the functions defining the bending of the shell approach zero as the quantity βx becomes large. This indicates that the bending produced in the shell is of a local character, as was already mentioned at the beginning when the constants of integration were calculated.

If the moment M_x and the deflection w are found from expressions

[1] The figures in this table are taken from the book by H. Zimmermann, "Die Berechnung des Eisenbahnoberbaues," Berlin, 1888.

(282), the bending moment M_φ is obtained from the first of the equations (f), and the value of the force N_φ from Eq. (e). Thus all necessary information for calculating stresses in the shell can be found.

115. Particular Cases of Symmetrical Deformation of Circular Cylindrical Shells. *Bending of a Long Cylindrical Shell by a Load Uniformly Distributed along a Circular Section* (Fig. 238). If the load is far enough from the ends of the cylinder, solution (278) can be used for each half of

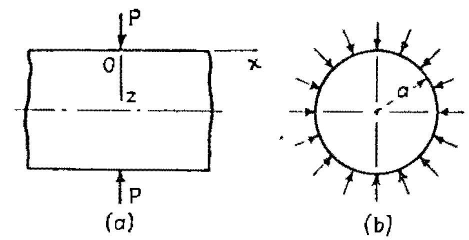

FIG. 238

the shell. From considerations of symmetry we conclude that the value of Q_0 in this case is $-P/2$. We thus obtain for the right-hand portion

$$w = \frac{e^{-\beta x}}{2\beta^3 D}\left[\beta M_0(\sin\beta x - \cos\beta x) + \frac{P}{2}\cos\beta x\right] \qquad (a)$$

where x is measured from the cross section at which the load is applied. To calculate the moment M_0 which appears in expression (a) we use expression (280), which gives the slope at $x = 0$. In our case this slope vanishes because of symmetry. Hence,

$$2\beta M_0 - \frac{P}{2} = 0$$

and we obtain

$$M_0 = \frac{P}{4\beta} \qquad (b)$$

Substituting this value in expression (a), the deflection of the shell becomes

$$w = \frac{Pe^{-\beta x}}{8\beta^3 D}\,(\sin\beta x + \cos\beta x) = \frac{P}{8\beta^3 D}\,\varphi(\beta x) \qquad (283)$$

and by differentiation we find

$$\begin{aligned}
\frac{dw}{dx} &= -2\beta\,\frac{P}{8\beta^3 D}\,e^{-\beta x}\sin\beta x = -\frac{P}{4\beta^2 D}\,\zeta(\beta x)\\
\frac{d^2w}{dx^2} &= 2\beta^2\,\frac{P}{8\beta^3 D}\,e^{-\beta x}(\sin\beta x - \cos\beta x) = -\frac{P}{4\beta D}\,\psi(\beta x)\\
\frac{d^3w}{dx^3} &= 4\beta^3\,\frac{P}{8\beta^3 D}\,e^{-\beta x}\cos\beta x = \frac{P}{2D}\,\theta(\beta x)
\end{aligned} \qquad (c)$$

TABLE 84. TABLE OF FUNCTIONS φ, ψ, θ, AND ζ

βx	φ	ψ	θ	ζ
0	1.0000	1.0000	1.0000	0
0.1	0.9907	0.8100	0.9003	0.0903
0.2	0.9651	0.6398	0.8024	0.1627
0.3	0.9267	0.4888	0.7077	0.2189
0.4	0.8784	0.3564	0.6174	0.2610
0.5	0.8231	0.2415	0.5323	0.2908
0.6	0.7628	0.1431	0.4530	0.3099
0.7	0.6997	0.0599	0.3798	0.3199
0.8	0.6354	−0.0093	0.3131	0.3223
0.9	0.5712	−0.0657	0.2527	0.3185
1.0	0.5083	−0.1108	0.1988	0.3096
1.1	0.4476	−0.1457	0.1510	0.2967
1.2	0.3899	−0.1716	0.1091	0.2807
1.3	0.3355	−0.1897	0.0729	0.2626
1.4	0.2849	−0.2011	0.0419	0.2430
1.5	0.2384	−0.2068	0.0158	0.2226
1.6	0.1959	−0.2077	−0.0059	0.2018
1.7	0.1576	−0.2047	−0.0235	0.1812
1.8	0.1234	−0.1985	−0.0376	0.1610
1.9	0.0932	−0.1899	−0.0484	0.1415
2.0	0.0667	−0.1794	−0.0563	0.1230
2.1	0.0439	−0.1675	−0.0618	0.1057
2.2	0.0244	−0.1548	−0.0652	0.0895
2.3	0.0080	−0.1416	−0.0668	0.0748
2.4	−0.0056	−0.1282	−0.0669	0.0613
2.5	−0.0166	−0.1149	−0.0658	0.0492
2.6	−0.0254	−0.1019	−0.0636	0.0383
2.7	−0.0320	−0.0895	−0.0608	0.0287
2.8	−0.0369	−0.0777	−0.0573	0.0204
2.9	−0.0403	−0.0666	−0.0534	0.0132
3.0	−0.0423	−0.0563	−0.0493	0.0071
3.1	−0.0431	−0.0469	−0.0450	0.0019
3.2	−0.0431	−0.0383	−0.0407	−0.0024
3.3	−0.0422	−0.0306	−0.0364	−0.0058
3.4	−0.0408	−0.0237	−0.0323	−0.0085
3.5	−0.0389	−0.0177	−0.0283	−0.0106
3.6	−0.0366	−0.0124	−0.0245	−0.0121
3.7	−0.0341	−0.0079	−0.0210	−0.0131
3.8	−0.0314	−0.0040	−0.0177	−0.0137
3.9	−0.0286	−0.0008	−0.0147	−0.0140

TABLE 84. TABLE OF FUNCTIONS φ, ψ, θ, AND ζ (*Continued*)

βx	φ	ψ	θ	ζ
4.0	−0.0258	0.0019	−0.0120	−0.0139
4.1	−0.0231	0.0040	−0.0095	−0.0136
4.2	−0.0204	0.0057	−0.0074	−0.0131
4.3	−0.0179	0.0070	−0.0054	−0.0125
4.4	−0.0155	0.0079	−0.0038	−0.0117
4.5	−0.0132	0.0085	−0.0023	−0.0108
4.6	−0.0111	0.0089	−0.0011	−0.0100
4.7	−0.0092	0.0090	0.0001	−0.0091
4.8	−0.0075	0.0089	0.0007	−0.0082
4.9	−0.0059	0.0087	0.0014	−0.0073
5.0	−0.0046	0.0084	0.0019	−0.0065
5.1	−0.0033	0.0080	0.0024	−0.0057
5.2	−0.0023	0.0075	0.0026	−0.0049
5.3	−0.0014	0.0069	0.0028	−0.0042
5.4	−0.0006	0.0064	0.0029	−0.0035
5.5	0.0000	0.0058	0.0029	−0.0029
5.6	0.0005	0.0052	0.0029	−0.0023
5.7	0.0010	0.0046	0.0028	−0.0018
5.8	0.0013	0.0041	0.0027	−0.0014
5.9	0.0015	0.0036	0.0026	−0.0010
6.0	0.0017	0.0031	0.0024	−0.0007
6.1	0.0018	0.0026	0.0022	−0.0004
6.2	0.0019	0.0022	0.0020	−0.0002
6.3	0.0019	0.0018	0.0018	+0.0001
6.4	0.0018	0.0015	0.0017	0.0003
6.5	0.0018	0.0012	0.0015	0.0004
6.6	0.0017	0.0009	0.0013	0.0005
6.7	0.0016	0.0006	0.0011	0.0006
6.8	0.0015	0.0004	0.0010	0.0006
6.9	0.0014	0.0002	0.0008	0.0006
7.0	0.0013	0.0001	0.0007	0.0006

Obse[illegible]ng from Eqs. (*b*) and (*f*) of the preceding article that

$$M_x = -D\frac{d^2w}{dx^2} \qquad Q_x = -D\frac{d^3w}{dx^3}$$

we finally [illegible] expressions for the bending mo[illegible] shearing force:

$$M_x = \frac{P}{4\beta}\psi(\beta x) \qquad Q_x = -\frac{P}{2}\theta(\beta x) \tag{281}$$

The results obtained are all graphically represented in Fig. 239. It is seen that the maximum deflection is under the load P and that its value as given by Eq. (283) is

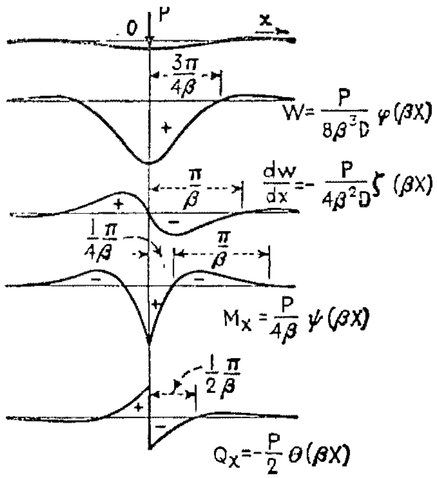

FIG. 239

$$w_{\max} = \frac{P}{8\beta^3 D} = \frac{Pa^2\beta}{2Eh} \tag{285}$$

The maximum bending moment is also under the load and is determined from Eq. (284) as

$$M_{\max} = \frac{P}{4\beta} \tag{286}$$

The maximum of the absolute value of the shearing force is evidently equal to $P/2$. The values of all these quantities at a certain distance from the load can be readily obtained by using Table 84. We see from this table and from Fig. 239 that all the quantities that determine the bending of the shell are small for $x > \pi/\beta$. This fact indicates that the bending is of a local character and that a shell of length $l = 2\pi/\beta$ loaded at the middle will have practically the same maximum deflection and the same maximum stress as a very long shell.

Having the solution of the problem for the case in which a load is concentrated at a circular cross section, we can readily solve the problem of a load distributed along a certain length of the cylinder by applying the principle of superposition. As an example let us consider the case of a load of intensity q uniformly distributed along a length l of a cylinder (Fig. 240). Assuming that the load is at a considerable distance from the ends of the cylinder, we can use solution (283) to calculate the deflections.

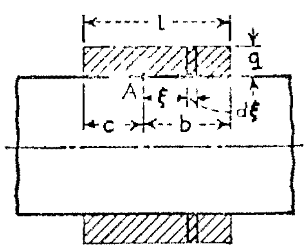

FIG 240

The deflection at a point A produced by an elementary ring load of an intensity[1] $q\,d\xi$ at a distance ξ from A is obtained from expression (283) by substituting $q\,d\xi$ for P and ξ for x and is

$$\frac{q\,d\xi}{8\beta^3 D} e^{-\beta\xi}(\cos\beta\xi + \sin\beta\xi)$$

The deflection produced at A by the total load distributed over the

[1] $q\,d\xi$ is the load per unit length of circumference.

length l is then

$$w = \int_0^b \frac{q\,d\xi}{8\beta^3 D} e^{-\beta\xi}(\cos\beta\xi + \sin\beta\xi) + \int_0^c \frac{q\,d\xi}{8\beta^3 D} e^{-\beta\xi}(\cos\beta\xi + \sin\beta\xi)$$
$$= \frac{qa^2}{2Eh}(2 - e^{-\beta b}\cos\beta b - e^{-\beta c}\cos\beta c)$$

The bending moment at a point A can be calculated by similar application of the method of superposition.

Cylindrical Shell with a Uniform Internal Pressure (Fig. 241). If the edges of the shell are free, the internal pressure p produces only a hoop stress

$$\sigma_t = \frac{pa}{h}$$

and the radius of the cylinder increases by the amount

$$\delta = \frac{a\sigma_t}{E} = \frac{pa^2}{Eh} \tag{d}$$

If the ends of the shell are built in, as shown in Fig. 241a, they cannot move out, and local bending occurs at the edges. If the length l of the

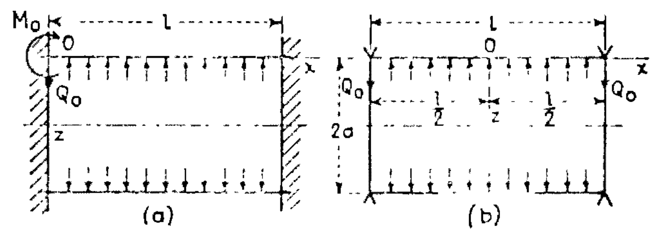

FIG. 241

shell is sufficiently large, we can use solution (278) to investigate this bending, the moment M_0 and the shearing force Q_0 being determined from the conditions that the deflection and the slope along the built-in edge $x = 0$ (Fig. 241a) vanish. According to these conditions, Eqs. (279) and (280) of the preceding article become

$$-\frac{1}{2\beta^3 D}(\beta M_0 + Q_0) = \delta$$
$$\frac{1}{2\beta^2 D}(2\beta M_0 + Q_0) = 0$$

where δ is given by Eq. (d).

Solving for M_0 and Q_0, we obtain

$$M_0 = 2\beta^2 D\delta = \frac{p}{2\beta^2} \qquad Q_0 = -4\beta^3 D\delta = -\frac{p}{\beta} \tag{287}$$

We thus obtain a positive bending moment and a negative shearing force acting as shown in Fig. 241a. Substituting these values in expressions (282), the deflection and the bending moment at any distance from the end can be readily calculated using Table 84.

If, instead of built-in edges, we have simply supported edges as shown in Fig. 241b, the deflection and the bending moment M_x vanish along the edge $M_0 = 0$, and we obtain, by using Eq. (279),

$$Q_0 = -2\beta^3 D\delta$$

By substituting these values in solution (278) the deflection at any distance from the end can be calculated.

It was assumed in the preceding discussion that the length of the shell is large. If this is not the case, the bending at one end cannot be considered as independent of the conditions at the other end, and recourse must be had to the general solution (277), which contains four constants of integration. The particular solution of Eq. (276) for the case of uniform load ($Z = -p$) is $-p/4\beta^4 D = -pa^2/Eh$. The general solution (277) can then be put in the following form by the introduction of hyperbolic functions in place of the exponential functions:

$$w = -\frac{pa^2}{Eh} + C_1 \sin\beta x \sinh\beta x + C_2 \sin\beta x \cosh\beta x + C_3 \cos\beta x \sinh\beta x + C_4 \cos\beta x \cosh\beta x \qquad (e)$$

If the origin of coordinates is taken at the middle of the cylinder, as shown in Fig. 241b, expression (e) must be an even function of x. Hence

$$C_2 = C_3 = 0 \qquad (f)$$

The constants C_1 and C_4 must now be selected so as to satisfy the conditions at the ends. If the ends are simply supported, the deflection and the bending moment M_x must vanish at the ends, and we obtain

$$(w)_{x=l/2} = 0 \qquad \left(\frac{d^2w}{dx^2}\right)_{x=l/2} = 0 \qquad (g)$$

Substituting expression (e) in these relations and remembering that $C_2 = C_3 = 0$, we find

$$\begin{aligned} -\frac{pa^2}{Eh} + C_1 \sin\alpha \sinh\alpha + C_4 \cos\alpha \cosh\alpha &= 0 \\ C_1 \cos\alpha \cosh\alpha - C_4 \sin\alpha \sinh\alpha &= 0 \end{aligned} \qquad (h)$$

where, for the sake of simplicity,

$$\frac{\beta l}{2} = \alpha \qquad (i)$$

From these equations we obtain

$$\begin{aligned} C_1 &= \frac{pa^2}{Eh} \frac{\sin\alpha \sinh\alpha}{\sin^2\alpha \sinh^2\alpha + \cos^2\alpha \cosh^2\alpha} = \frac{pa^2}{Eh} \frac{2 \sin\alpha \sinh\alpha}{\cos 2\alpha + \cosh 2\alpha} \\ C_4 &= \frac{pa^2}{Eh} \frac{\cos\alpha \cosh\alpha}{\sin^2\alpha \sinh^2\alpha + \cos^2\alpha \cosh^2\alpha} = \frac{pa^2}{Eh} \frac{2 \cos\alpha \cosh\alpha}{\cos 2\alpha + \cosh 2\alpha} \end{aligned} \qquad (j)$$

Substituting the values (j) and (f) of the constants in expression (e) and observing from expression (275) that

$$\frac{Eh}{a^2} = 4D\beta^4 = \frac{64\alpha^4 D}{l^4} \qquad (k)$$

we obtain

$$w = -\frac{pl^4}{64D\alpha^4}\left(1 - \frac{2\sin\alpha \sinh\alpha}{\cos 2\alpha + \cosh 2\alpha} \sin\beta x \sinh\beta x - \frac{2\cos\alpha \cosh\alpha}{\cos 2\alpha + \cosh 2\alpha} \cos\beta x \cosh\beta x\right) \qquad (l)$$

In each particular case, if the dimensions of the shell are known, the quantity α, which is dimensionless, can be calculated by means of notation (i) and Eq. (275). By substituting this value in expression (l) the deflection of the shell at any point can be found.

For the middle of the shell, substituting $x = 0$ in expression (l), we obtain

$$(w)_{x=0} = -\frac{pl^4}{64D\alpha^4}\left(1 - \frac{2\cos\alpha \cosh\alpha}{\cos 2\alpha + \cosh 2\alpha}\right) \qquad (m)$$

When the shell is long, α becomes large, the second term in the parentheses of expression (m) becomes small, and the deflection approaches the value (d) calculated for the case of free ends. This indicates that in the case of long shells the effect of the end supports upon the deflection at the middle is negligible. Taking another extreme case, *viz.*, the case when α is very small, we can show by expanding the trigonometric and hyperbolic functions in power series that the expression in parentheses in Eq. (m) approaches the value $5\alpha^4/6$ and that the deflection (l) approaches that for a uniformly loaded and simply supported beam of length l and flexural rigidity D.

Differentiating expression (l) twice and multiplying it by D, the bending moment is found as

$$M_x = -D\frac{d^2w}{dx^2} = -\frac{pl^2}{4\alpha^2}\left(\frac{\sin\alpha \sinh\alpha}{\cos 2\alpha + \cosh 2\alpha} \cosh\beta x \cos\beta x - \frac{\cos\alpha \cosh\alpha}{\cos 2\alpha + \cosh 2\alpha} \sin\beta x \sinh\beta x\right) \qquad (n)$$

At the middle of the shell this moment is

$$(M_x)_{x=0} = -\frac{pl^2}{4\alpha^2}\frac{\sin\alpha\sinh\alpha}{\cos 2\alpha + \cosh 2\alpha} \tag{o}$$

It is seen that for large values of α, that is, for long shells, this moment becomes negligibly small and the middle portion is, for all practical purposes, under the action of merely the hoop stresses pa/h.

The case of a cylinder with built-in edges (Fig. 241*a*) can be treated in a similar manner. Going directly to the final result,[1] we find that the bending moment M_0 acting along the built-in edge is

$$M_0 = \frac{p}{2\beta^2}\frac{\sinh 2\alpha - \sin 2\alpha}{\sinh 2\alpha + \sin 2\alpha} = \frac{p}{2\beta^2}\chi_2(2\alpha) \tag{288}$$

where

$$\chi_2(2\alpha) = \frac{\sinh 2\alpha - \sin 2\alpha}{\sinh 2\alpha + \sin 2\alpha}$$

In the case of long shells, α is large, the factor $\chi_2(2\alpha)$ in expression (288) approaches unity, and the value of the moment approaches that given by the first of the expressions (287). For shorter shells the value of the factor $\chi_2(2\alpha)$ in (288) can be taken from Table 85.

TABLE 85

2α	$\chi_1(2\alpha)$	$\chi_2(2\alpha)$	$\chi_3(2\alpha)$
0.2	5.000	0.0068	0.100
0.4	2.502	0.0268	0.200
0.6	1.674	0.0601	0.300
0.8	1.267	0.1065	0.100
1.0	1.033	0.1670	0.500
1.2	0.890	0.2370	0.596
1.4	0.803	0.3170	0.689
1.6	0.755	0.1080	0.775
1.8	0.735	0.5050	0.855
2.0	0.738	0.6000	0.925
2.5	0.802	0.8220	1.015
3.0	0.893	0.9770	1.090
3.5	0.966	1.0500	1.085
4.0	1.005	1.0580	1.050
4.5	1.017	1.0400	1.027
5.0	1.017	1.0300	1.008

Cylindrical Shell Bent by Forces and Moments Distributed along the Edges. In the preceding section this problem was discussed assuming that the shell is long and that each end can be treated independently. In the case of shorter shells both ends must be considered simultaneously by using solution (*e*) with four constants of integration. Proceeding as in the previous cases, the following results can be obtained. For the case of bending by uniformly distributed shearing forces Q_0 (Fig. 242*a*), the deflection and the slope at the ends are

$$\begin{aligned}(w)_{x=0,x=l} &= -\frac{2Q_0\beta a^2}{Eh}\frac{\cosh 2\alpha + \cos 2\alpha}{\sinh 2\alpha + \sin 2\alpha} = -\frac{2Q_0\beta a^2}{Eh}\chi_1(2\alpha)\\ \left(\frac{dw}{dx}\right)_{x=0,x=l} &= \pm\frac{2Q_0\beta^2a^2}{Eh}\frac{\sinh 2\alpha - \sin 2\alpha}{\sinh 2\alpha + \sin 2\alpha} = \pm\frac{2Q_0\beta^2a^2}{Eh}\chi_2(2\alpha)\end{aligned} \tag{289}$$

In the case of bending by the moments M_0 (Fig. 242*b*), we obtain

$$\begin{aligned}(w)_{x=0,x=l} &= -\frac{2M_0\beta^2a^2}{Eh}\frac{\sinh 2\alpha - \sin 2\alpha}{\sinh 2\alpha + \sin 2\alpha} = -\frac{2M_0\beta^2a^2}{Eh}\chi_2(2\alpha)\\ \left(\frac{dw}{dx}\right)_{x=0,x=l} &= \pm\frac{4M_0\beta^3a^2}{Eh}\frac{\cosh 2\alpha - \cos 2\alpha}{\sinh 2\alpha + \sin 2\alpha} = \pm\frac{4M_0\beta^3a^2}{Eh}\chi_3(2\alpha)\end{aligned} \tag{290}$$

In the case of long shells, the factors χ_1, χ_2, and χ_3 in expressions (289) and (290) are close to unity, and the results coincide with those given by

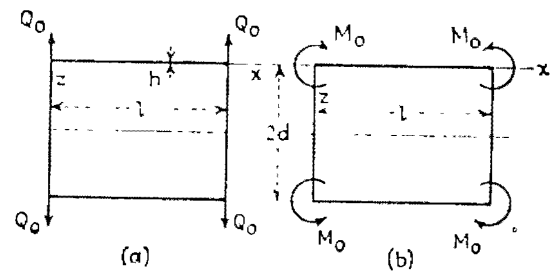

FIG. 242

expressions (279) and (280). To simplify the calculations for shorter shells, the values of functions χ_1, χ_2, and χ_3 are given in Table 85.

Using solutions (289) and (290), the stresses in a long pipe reinforced by equidistant rings (Fig. 243) and submitted to the action of uniform internal pressure p can be readily discussed.

Assume first that there are no rings. Then, under the action of internal pressure, hoop stresses $\sigma_t = pa/h$ will be produced and the radius of the pipe will increase by the amount

$$\delta = \frac{pa^2}{Eh}$$

Now, taking the rings into consideration and assuming that they are absolutely rigid, we conclude that reactive forces will be produced between each ring and the pipe. The magnitude of the forces per unit length of

[1] Both cases are discussed in detail by I. G. Boobnov in his "Theory of Structure of Ships," vol. 2, p. 368, St. Petersburg, 1913. Also included are numerical tables which simplify the calculations of moments and deflections.

the circumference of the tube will be denoted by P. The magnitude of P will now be determined from the condition that the forces P produce a deflection of the pipe under the ring equal to the expansion δ created by the internal pressure p. In calculating this deflection we observe that a portion of the tube between two adjacent rings may be considered as the shell shown in Fig. 242a and b. In this case $Q_0 = -\frac{1}{2}P$, and the magnitude of the bending moment M_0 under a ring is determined from the condition that $dw/dx = 0$ at that point. Hence from Eqs. (289) and (290) we find

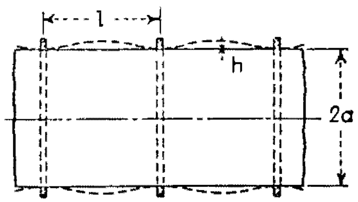

FIG 243

$$-\frac{P\beta^2a^2}{Eh}\chi_2(2\alpha) + \frac{4M_0\beta^3a^2}{Eh}\chi_3(2\alpha) = 0$$

from which

$$M_0 = \frac{P\chi_2(2\alpha)}{4\beta\chi_3(2\alpha)} \tag{p}$$

If the distance l between the rings is large,[1] the quantity

$$2\alpha = \beta l = \frac{l}{\sqrt{ah}}\sqrt[4]{3(1-\nu^2)}$$

is also large, the functions $\chi_2(2\alpha)$ and $\chi_3(2\alpha)$ approach unity, and the moment M_0 approaches the value (286). For calculating the force P entering in Eq. (p) the expressions for deflections as given in Eqs. (289) and (290) must be used These expressions give

$$\frac{P\beta a^2}{Eh}\chi_1(2\alpha) - \frac{P\beta a^2}{2Eh}\frac{\chi_2^2(2\alpha)}{\chi_3(2\alpha)} = \delta = \frac{pa^2}{Eh}$$

or

$$P\beta\left[\chi_1(2\alpha) - \frac{1}{2}\frac{\chi_2^2(2\alpha)}{\chi_3(2\alpha)}\right] = \frac{\delta Eh}{a^2} = p \tag{291}$$

For large values of 2α this reduces to

$$\frac{P\beta a^2}{2Eh} = \delta$$

which coincides with Eq. (285). When 2α is not large, the value of the reactive forces P is calculated from Eq. (291) by using Table 85 Solving Eq (291) for P and substituting its expression in expression (p), we find

$$M_0 = \frac{p}{2\beta^2}\chi_2(2\alpha) \tag{292}$$

This coincides with expression (288) previously obtained for a shell with built in edges

To take into account the extension of rings we observe that the react[illegible]

[1] For $\nu = 0.3$, $2\alpha = 1.285l/\sqrt{ah}$.

forces P produce in the ring a tensile force Pa and that the corresponding increase of the inner radius of the ring is[1]

$$\delta_1 = \frac{Pa^2}{AE}$$

where A is the cross-sectional area of the ring To take this extension into account we substitute $\delta - \delta_1$ for δ in Eq (291) and obtain

$$P\beta\left[\chi_1(2\alpha) - \frac{1}{2}\frac{\chi_2^2(2\alpha)}{\chi_3(2\alpha)}\right] = p - \frac{Ph}{A} \tag{293}$$

From this equation, P can be readily obtained by using Table 85, and the moment found by substituting $p - (Ph/A)$ for p in Eq. (292).

If the pressure p acts not only on the cylindrical shell but also on the ends, longitudinal forces

$$N_x = \frac{pa}{2}$$

are produced in the shell. The extension of the radius of the cylinder is then

$$\delta' = \frac{pa^2}{Eh}\left(1 - \frac{1}{2}\nu\right)$$

and the quantity $p(1 - \frac{1}{2}\nu)$ must be substituted for p in Eqs (292) and (293)

Equations (293) and (291) can also be used in the case of external uniform pressure provided the compressive stresses in the ring and in the shell are far enough from the critical stresses at which buckling may occur [2] This case is of practical importance in the design of submarines and has been discussed by several authors.[3]

116. Pressure Vessels. The method illustrated by the examples of the preceding article can also be applied in the analysis of stresses in cylindrical vessels submitted to the action of internal pressure.[4] In discussing the "membrane theory" it was repeatedly indicated that this theory fails to represent the true stresses in those portions of a shell close to the

[1] It is assumed that the cross-sectional dimensions of the ring are small in comparison with the radius a

[2] Buckling of rings and cylindrical shells is discussed in S. Timoshenko, "The[illegible] of Elastic Stability," 1936

[3] See paper by K von Sanden and K Günther, "Werft und R[illegible]," [illegible] pp 163 168, 189 198, 216 221, and vol [illegible], 1921 pp 505 510

[4] See also M Esslinger, "Statische Berechnung von [illegible] G. Salet and J Barthelemy, *Bull Assoc Tech Maritime Aeronaut*, vol 44, [illegible] 1945, J L Maulbetsch and M Hetényi, *ASME Design Data*, no 1, 1944, [illegible] Schultz-Grunow, *Ingr.-Arch.*, vol 4, p 545, 1933, N L S[illegible] *J Appl Mechanics*, vol 25, p 89, 1958

edges, since the edge conditions usually cannot be completely satisfied by considering only membrane stresses. A similar condition in which the membrane theory is inadequate is found in cylindrical pressure vessels at the joints between the cylindrical portion and the ends of the vessel. At these joints the membrane stresses are usually accompanied by local bending stresses which are distributed symmetrically with respect to the axis of the cylinder. These local stresses can be calculated by using solution (278) of Art. 114.

Let us begin with the simple case of a cylindrical vessel with hemispherical ends (Fig. 244).[1] At a sufficient distance from the joints mn

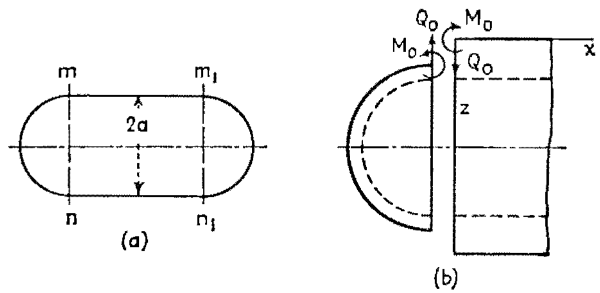

FIG 244

and m_1n_1 the membrane theory is accurate enough and gives for the cylindrical portion of radius a

$$N_x = \frac{pa}{2} \qquad N_t = pa \tag{a}$$

where p denotes the internal pressure.

For the spherical ends this theory gives a uniform tensile force

$$N = \frac{pa}{2} \tag{b}$$

The extension of the radius of the cylindrical shell under the action of the forces (a) is

$$\delta_1 = \frac{pa^2}{Eh}\left(1 - \frac{\nu}{2}\right) \tag{c}$$

and the extension of the radius of the spherical ends is

$$\delta_2 = \frac{pa^2}{2Eh}(1 - \nu) \tag{d}$$

Comparing expressions (c) and (d), it can be concluded that if we consider only membrane stresses we obtain a discontinuity at the joints as represented in Fig. 244b. This indicates that at the joint there must act

[1] This case was discussed by E. Meissner, *Schweiz. Bauztg.*, vol. 86, p. 1, 1925.

shearing forces Q_0 and bending moments M_0 uniformly distributed along the circumference and of such magnitudes as to eliminate this discontinuity. The stresses produced by these forces are sometimes called *discontinuity stresses.*

In calculating the quantities Q_0 and M_0 we assume that the bending is of a local character so that solution (278) can be applied with sufficient accuracy in discussing the bending of the cylindrical portion. The investigation of the bending of the spherical ends represents a more complicated problem which will be fully discussed in Chap. 16. Here we obtain an approximate solution of the problem by assuming that the bending is of importance only in the zone of the spherical shell close to the joint and that this zone can be treated as a portion of a long cylindrical shell[1] of radius a. If the thickness of the spherical and the cylindrical portion of the vessel is the same, the forces Q_0 produce equal rotations of the edges of both portions at the joint (Fig. 244b). This indicates that M_0 vanishes and that Q_0 alone is sufficient to eliminate the discontinuity. The magnitude of Q_0 is now determined from the condition that the sum of the numerical values of the deflections of the edges of the two parts must be equal to the difference $\delta_1 - \delta_2$ of the radial expansions furnished by the membrane theory. Using Eq. (279) for the deflections, we obtain

$$\frac{Q_0}{\beta^3 D} = \delta_1 - \delta_2 = \frac{pa^2}{2Eh}$$

from which, by using notation (275),

$$Q_0 = \frac{pa^2\beta^3 D}{2Eh} = \frac{p}{8\beta} \tag{e}$$

Having obtained this value of the force Q_0, the deflection and the bending moment M_x can be calculated at any point by using formulas (282), which give[2]

$$w = \frac{Q_0}{2\beta^3 D}\theta(\beta x)$$

$$M_x = -D\frac{d^2w}{dx^2} = -\frac{Q_0}{\beta}\zeta(\beta x)$$

Substituting expression (e) for Q_0 and expression [illegible] for β in the formula for M_x, we obtain

$$M_x = -\frac{ahp}{8\sqrt{3(1-\nu^2)}}\zeta(\beta x)$$

[1] E. Meissner, in the above-mentioned paper, showed that the error in the magnitude of the bending stresses as calculated from such an approximate solution is small for thin hemispherical shells and is smaller than 1 per cent if $a/h > 30$.

[2] Note that the direction of Q_0 in Fig. 244 is opposite to the direction in Fig. 236.

This moment attains its numerical maximum at the distance $x = \pi/4\beta$, at which point the derivative of the moment is zero, as can be seen from the fourth of the equations (282).

Combining the maximum bending stress produced by M_x with the membrane stress, we find

$$(\sigma_x)_{max} = \frac{ap}{2h} + \frac{3}{4}\frac{ap}{h\sqrt{3(1-\nu^2)}}\zeta\left(\frac{\pi}{4}\right) = 1.293\frac{ap}{2h} \tag{g}$$

This stress which acts at the outer surface of the cylindrical shell is about 30 per cent larger than the membrane stress acting in the axial direction. In calculating stresses in the circumferential direction in addition to the membrane stress pa/h, the hoop stress caused by the deflection w as well as the bending stress produced by the moment $M_\varphi = \nu M_x$ must be considered. In this way we obtain at the outer surface of the cylindrical shell

$$\sigma_t = \frac{ap}{h} - \frac{Ew}{a} - \frac{6\nu}{h^2}M_x = \frac{ap}{h}\left[1 - \frac{1}{4}\theta(\beta x) + \frac{3\nu}{4\sqrt{3(1-\nu^2)}}\zeta(\beta x)\right]$$

Taking $\nu = 0.3$ and using Table 84, we find

$$(\sigma_t)_{max} = 1.032\frac{ap}{h} \qquad \text{at } \beta x = 1.85 \tag{h}$$

Since the membrane stress is smaller in the ends than in the cylinder sides, the maximum stress in the spherical ends is always smaller than the calculated stress (h). Thus the latter stress is the determining factor in the design of the vessel.

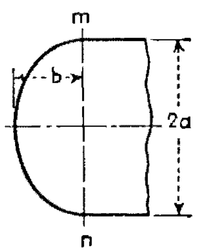

Fig. 245

The same method of calculating discontinuity stresses can be applied in the case of ends having the form of an ellipsoid of revolution. The membrane stresses in this case are obtained from expressions (263) and (264) (see page 440). At the joint mn which represents the equator of the ellipsoid (Fig. 245), the stresses in the direction of the meridian and in the equatorial direction are, respectively,

$$\sigma_\varphi = \frac{pa}{2h} \qquad \sigma_\theta = \frac{pa}{h}\left(1 - \frac{a^2}{2b^2}\right) \tag{i}$$

The extension of the radius of the equator is

$$\delta_2' = \frac{a}{E}(\sigma_\theta - \nu\sigma_\varphi) = \frac{pa^2}{Eh}\left(1 - \frac{a^2}{2b^2} - \frac{\nu}{2}\right)$$

Substituting this quantity for δ_2 in the previous calculation of the shearing force Q_0, we find

$$\delta_1 - \delta_2' = \frac{pa^2}{Eh}\frac{a^2}{2b^2}$$

and, instead of Eq. (e) we obtain

$$Q_0 = \frac{p}{8\beta}\frac{a^2}{b^2}$$

It is seen that the shearing force Q_0 in the case of ellipsoidal ends is larger than in the case of hemispherical ends in the ratio a^2/b^2. The discontinuity stresses will evidently increase in the same proportion. For example, taking $a/b = 2$, we obtain, from expressions (g) and (h)

$$(\sigma_x)_{max} = \frac{ap}{2h} + \frac{3ap}{h\sqrt{3(1-\nu^2)}}\zeta\left(\frac{\pi}{4}\right) = 2.172\frac{ap}{2h}$$

$$(\sigma_t)_{max} = 1.128\frac{ap}{h}$$

Again, $(\sigma_t)_{max}$ is the largest stress and is consequently the determining factor in design.[1]

117. Cylindrical Tanks with Uniform Wall Thickness. If a tank is submitted to the action of a liquid pressure, as shown in Fig. 246, the stresses in the wall can be analyzed by using Eq. (276). Substituting in this equation

$$Z = -\gamma(d - x) \tag{a}$$

where γ is the weight per unit volume of the liquid, we obtain

$$\frac{d^4w}{dx^4} + 4\beta^4 w = -\frac{\gamma(d - x)}{D} \tag{b}$$

A particular solution of this equation is

$$w_1 = -\frac{\gamma(d - x)}{4\beta^4 D} = -\frac{\gamma(d - x)a^2}{Eh} \tag{c}$$

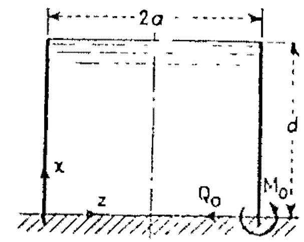

Fig. 246

This expression represents the radial expansion of a cylindrical shell with free edges under the action of hoop stresses. Substituting expression (c) in place of $f(x)$ in expression (277), we obtain for the complete solution of Eq. (b)

$$w = e^{\beta x}(C_1\cos\beta x + C_2\sin\beta x) + e^{-\beta x}(C_3\cos\beta x + C_4\sin\beta x) - \frac{\gamma(d - x)a^2}{Eh}$$

In most practical cases the wall thickness h is small in comparison with both the radius a and the depth d of the tank, and we can consider the shell as infinitely long. The constants C_1 and C_2 are then equal to zero

[1] More detail regarding stresses in boiler [illegible] in the book by Höhn, "Über die Festigkeit der gewölbten Böden [illegible] Zylinderschale," Zurich, 1927. Also included are the results of experimental investigations of discontinuity stresses which are in a good agreement with the approximate solution. See also Schultz-Grunow, *loc. cit.*

and we obtain

$$w = e^{-\beta x}(C_3 \cos \beta x + C_4 \sin \beta x) - \frac{\gamma(d - x)a^2}{Eh} \tag{d}$$

The constants C_3 and C_4 can now be obtained from the conditions at the bottom of the tank. Assuming that the lower edge of the wall is built into an absolutely rigid foundation, the boundary conditions are

$$(w)_{x=0} = C_3 - \frac{\gamma a^2 d}{Eh} = 0$$

$$\left(\frac{dw}{dx}\right)_{x=0} = \left[-\beta C_3 e^{-\beta x}(\cos \beta x + \sin \beta x) + \beta C_4 e^{-\beta x}(\cos \beta x - \sin \beta x) + \frac{\gamma a^2}{Eh}\right]_{x=0} = \beta(C_4 - C_3) + \frac{\gamma a^2}{Eh} = 0$$

From these equations we obtain

$$C_3 = \frac{\gamma a^2 d}{Eh} \qquad C_4 = \frac{\gamma a^2}{Eh}\left(d - \frac{1}{\beta}\right)$$

Expression (*d*) then becomes

$$w = -\frac{\gamma a^2}{Eh}\left\{d - x - e^{-\beta x}\left[d \cos \beta x + \left(d - \frac{1}{\beta}\right)\sin \beta x\right]\right\}$$

from which, by using the notation of Eqs. (281), we obtain

$$w = -\frac{\gamma a^2 d}{Eh}\left[1 - \frac{x}{d} - \theta(\beta x) - \left(1 - \frac{1}{\beta d}\right)\zeta(\beta x)\right] \tag{e}$$

From this expression the deflection at any point can be readily calculated by the use of Table 84. The force N_φ in the circumferential direction is then

$$N_\varphi = -\frac{Ehw}{a} = \gamma a d\left[1 - \frac{x}{d} - \theta(\beta x) - \left(1 - \frac{1}{\beta d}\right)\zeta(\beta x)\right] \tag{f}$$

From the second derivative of expression (*e*) we obtain the bending moment

$$M_x = -D\frac{d^2w}{dx^2} = \frac{2\beta^2\gamma a^2 Dd}{Eh}\left[-\zeta(\beta x) + \left(1 - \frac{1}{\beta d}\right)\theta(\beta x)\right]$$

$$= \frac{\gamma a d h}{\sqrt{12(1 - \nu^2)}}\left[-\zeta(\beta x) + \left(1 - \frac{1}{\beta d}\right)\theta(\beta x)\right] \tag{g}$$

Having expressions (*f*) and (*g*), the maximum stress at any point can readily be calculated in each particular case. The bending moment has its maximum value at the bottom, where it is equal to

$$(M_x)_{x=0} = M_0 = \left(1 - \frac{1}{\beta d}\right)\frac{\gamma a d h}{\sqrt{12(1 - \nu^2)}} \tag{h}$$

The same result can be obtained by using solutions (279) and (280) (pages 169, 170). Assuming that the lower edge of the shell is entirely free, we obtain from expression (*c*)

$$(w_1)_{x=0} = -\frac{\gamma a^2 d}{Eh} \qquad \left(\frac{dw_1}{dx}\right)_{x=0} = \frac{\gamma a^2}{Eh} \tag{i}$$

To eliminate this displacement and rotation of the edge and thus satisfy the edge conditions at the bottom of the tank, a shearing force Q_0 and bending moment M_0 must be applied as indicated in Fig. 216. The magnitude of each of these quantities is obtained by equating expressions (279) and (280) to expressions (*i*) taken with reversed signs. This gives

$$-\frac{1}{2\beta^3 D}(\beta M_0 + Q_0) = +\frac{\gamma a^2 d}{Eh}$$

$$\frac{1}{2\beta^2 D}(2\beta M_0 + Q_0) = -\frac{\gamma a^2}{Eh}$$

From these equations we again obtain expression (*h*) for M_0, whereas for the shearing force we find[1]

$$Q_0 = -\frac{\gamma a d h}{\sqrt{12(1 - \nu^2)}}\left(2\beta - \frac{1}{d}\right) \tag{j}$$

Taking, as an example, $a = 30$ ft, $d = 26$ ft, $h = 14$ in., $\gamma = 0.03613$ lb per in.^{3}, and $\nu = 0.25$, we find $\beta = 0.01824$ in.$^{-1}$ and $\beta d = 5.691$. For such a value of βd our assumption that the shell is infinitely long results in an accurate value for the moment and the shearing force, and we obtain from expressions (*h*) and (*j*)

$$M_0 = 13{,}960 \text{ in.-lb per in.} \qquad Q_0 = -563.6 \text{ lb per in.}$$

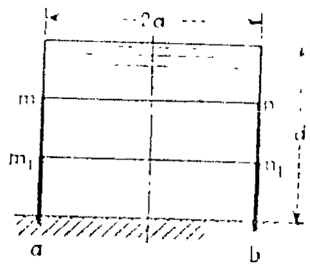

FIG. 217

In the construction of steel tanks, metallic sheets of several different thicknesses are very often used as shown in Fig. 217. Applying the particular solution (*c*) to each portion of uniform thickness, we find that the differences in thickness give rise to discontinuities in the displacement w_1 along the joints mn and m_1n_1. These discontinuities, together with the displacements at the bottom ab, can be removed by applying moments and shearing forces. Assuming that the vertical dimension of each portion is sufficiently large to justify the application of the formulas for an infinitely long shell, we calculate the discontinuity moments and shearing forces as before by using Eqs. (279) and (280) and applying at each joint the two conditions that the adjacent portions of the shell have equal deflection and a common tangent. If the use of formulas (279) and (280) derived for an infinitely long shell cannot be justified, the general solution containing four constants of integration must be applied to each portion of the tank. The determination of the constants under such conditions becomes much more complicated, since the fact that each joint cannot be treated

[1] The negative sign indicates that Q_0 has the direction shown in Fig. 216 which is opposite to the direction used in Fig. 236 when deriving expressions (279) and (280).

independently necessitates the solution of a system of simultaneous equations. This problem can be solved by approximate methods.[1]

118. Cylindrical Tanks with Nonuniform Wall Thickness. In the case of tanks of nonuniform wall thickness the solution of the problem requires the integration of Eq. (273), considering the flexural rigidity D and the thickness h as no longer constant but as functions of x. We have thus to deal with a linear differential equation of fourth order with variable coefficients. As an example, let us consider the case when the thickness of the wall is a linear function of the coordinate x.* Taking the origin of the coordinates as shown in Fig. 248, we have for the thickness of the wall and for the flexural rigidity the expressions

$$h = \alpha x \qquad D = \frac{E\alpha^3}{12(1-\nu^2)} x^3 \tag{a}$$

and Eq. (273) becomes

$$\frac{d^2}{dx^2}\left(x^3 \frac{d^2w}{dx^2}\right) + \frac{12(1-\nu^2)}{\alpha^2 a^2} xw = -\frac{12(1-\nu^2)\gamma(x-x_0)}{E\alpha^3} \tag{b}$$

The particular solution of this equation is

$$w_1 = -\frac{\gamma a^2}{E\alpha}\frac{x - x_0}{x} \tag{c}$$

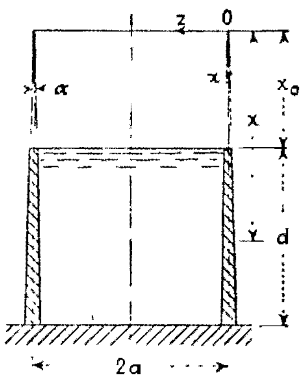

FIG. 248

This solution represents the radial expansion of a shell with free edges under the internal pressure $\gamma(x - x_0)$. As a result of the displacement (c) a certain amount of bending of the generatrices of the cylinder occurs. The corresponding bending moment is

$$M_x = -D\frac{d^2w_1}{dx^2} = -\frac{\gamma\alpha^2 a^2 x_0}{6(1-\nu^2)} \tag{d}$$

This moment is independent of x and is in all practical cases of such small magnitude that its action can usually be neglected.

To obtain the complete solution of Eq. (b) we have to add to the particular solution (c) the solution of the homogeneous equation

$$\frac{d^2}{dx^2}\left(x^3 \frac{d^2w}{dx^2}\right) + \frac{12(1-\nu^2)}{\alpha^2 a^2} xw = 0$$

[1] An approximate method of solving this problem was given by C. Runge, *Z. Math. Physik*, vol. 51, p. 254, 1904. This method was applied by K. Girkmann in a design of a large welded tank; see *Stahlbau*, vol. 4, p. 25, 1931.

* H. Reissner, *Beton u. Eisen*, vol. 7, p. 150, 1908; see also W. Flügge, "Statik und Dynamik der Schalen," 2d ed., p. 167, Berlin, 1957. For tanks slightly deviating from the cylindrical form see K. Federhofer, *Österr. Bauzeitschrift*, vol. 6, p. 149, 1951; and for tanks with thickness varying in accordance with a quadratic law, see Federhofer, *Österr. Ingr.-Arch.*, vol. 6, p. 43, 1952. A parameter method, akin to that explained in Art. 40, has been used by H. Favre, *Proc. Ninth Congr. Appl. Mech. Brussels*, vol. 6, p. 297, 1957. Many data regarding the design of water tanks are found in W. S. Gray, "Reinforced Concrete Reservoirs and Tanks," London, 1954, and in V. Lewe, "Handbuch für Eisenbetonbau," vol. 9, Berlin, 1934.

which, upon division by x, can be also written

$$\frac{1}{x}\frac{d^2}{dx^2}\left(x^3 \frac{d^2w}{dx^2}\right) + \frac{12(1-\nu^2)}{\alpha^2 a^2} w = 0 \tag{e}$$

The solution of this equation of the fourth order can be reduced to that of two equations of the second order[1] if we observe that

$$\frac{1}{x}\frac{d^2}{dx^2}\left(x^3 \frac{d^2w}{dx^2}\right) = \frac{1}{x}\frac{d}{dx}\left\{x^2 \frac{d}{dx}\left[\frac{1}{x}\frac{d}{dx}\left(x^2 \frac{dw}{dx}\right)\right]\right\}$$

For simplification we introduce the following symbols:

$$L(w) = \frac{1}{x}\frac{d}{dx}\left(x^2 \frac{dw}{dx}\right) \tag{f}$$

$$\rho^4 = \frac{12(1-\nu^2)}{\alpha^2 a^2} \tag{g}$$

Equation (e) then becomes

$$L[L(w)] + \rho^4 w = 0 \tag{h}$$

and can be rewritten in one of the two following forms:

$$\begin{aligned} L[L(w) + i\rho^2 w] - i\rho^2[L(w) + i\rho^2 w] &= 0 \\ L[L(w) - i\rho^2 w] + i\rho^2[L(w) - i\rho^2 w] &= 0 \end{aligned} \tag{i}$$

where $i = \sqrt{-1}$.

We see that Eq. (h) is satisfied by the solutions of the second-order equations

$$L(w) + i\rho^2 w = 0 \tag{j}$$

$$L(w) - i\rho^2 w = 0 \tag{k}$$

Assuming that

$$w_1 = \varphi_1 + i\varphi_2 \qquad w_2 = \varphi_3 + i\varphi_4 \tag{l}$$

are the two linearly independent solutions of Eq. (j), it can be seen that

$$w_3 = \varphi_1 - i\varphi_2 \qquad \text{and} \qquad w_4 = \varphi_3 - i\varphi_4 \tag{m}$$

are the solutions of Eq. (k). All four solutions (l) and (m) together then represent the complete system of independent solutions of Eq. (h). By using the sums and the differences of solutions (l) and (m), the general solution of Eq. (h) can be represented in the following form:

$$w = C_1\varphi_1 + C_2\varphi_2 + C_3\varphi_3 + C_4\varphi_4 \tag{n}$$

in which $C_1, \ldots, C_4$ are arbitrary constants. Thus the problem reduces to the determination of four functions $\varphi_1, \ldots, \varphi_4$, which can all be obtained if the complete solution of either Eq. (j) or Eq. (k) is known.

Taking Eq. (j) and substituting for $L(w)$ its meaning (f), we obtain

$$x\frac{d^2w}{dx^2} + 2\frac{dw}{dx} + i\rho^2 w = 0 \tag{o}$$

[1] This reduction was shown by G. Kirchhoff, "Berliner Monatsberichte," p. 815, 1879; see also I. Todhunter and K. Pearson, "A History of the Theory of Elasticity," vol. 2, part 2, p. 92.

TABLE 86 TABLE OF THE $\psi(x)$ FUNCTIONS (Continued)

x	$\psi_1(x)$	$\psi_2(x)$	$\dfrac{d\psi_1(x)}{dx}$	$\dfrac{d\psi_2(x)}{dx}$
4 00	−2 5634	−2 2927	−3 1346	+0 4912
4 10	−2 8843	−2 2309	−3 2819	+0 7482
4 20	−3 2195	−2 1422	−3 4199	+1 0318
4 30	−3 5679	−2 0236	−3 5465	+1 3433
4 40	−3 9283	−1 8726	−3 6587	+1 6833
4 50	−4 2991	−1 6860	−3 7536	+2 0526
4 60	−4 6784	−1 4610	−3 8280	+2 4520
4 70	−5 0639	−1 1946	−3 8782	+2 8818
4 80	−5 4531	−0 8837	−3 9006	+3 3422
4 90	−5 8429	−0 5251	−3 8910	+3 8330
5 00	−6 2301	−0 1160	−3 8154	+4 3542
5 10	−6 6107	+0 3467	−3 7589	+4 9046
5 20	−6 9803	+0 8658	−3 6270	+5 4835
5 30	−7 3344	+1 4443	−3 4446	+6 0893
5 40	−7 6674	+2 0845	−3 2063	+6 7198
5 50	−7 9736	+2 7890	−2 9070	+7 3729
5 60	−8 2466	+3 5597	−2 5409	+8 0453
5 70	−8 4794	+4 3986	−2 1024	+8 7336
5 80	−8 6644	+5 3068	−1 5856	+9 4332
5 90	−8 7937	+6 2851	−0 9844	+10 1394
6 00	−8 8583	+7 3347	−0 2931	+10 3462

in which ψ_3' and ψ_4' are the derivatives with respect to the argument $2\rho\sqrt{x}$ of the following functions:

$$\begin{aligned}\psi_3(2\rho\sqrt{x}) &= \frac{1}{2}\psi_1(2\rho\sqrt{x}) - \frac{2}{\pi}\left[R_1 + \log\frac{\beta 2\rho\sqrt{x}}{2}\psi_2(2\rho\sqrt{x})\right] \\ \psi_4(2\rho\sqrt{x}) &= \frac{1}{2}\psi_2(2\rho\sqrt{x}) + \frac{2}{\pi}\left[R_2 + \log\frac{\beta 2\rho\sqrt{x}}{2}\psi_1(2\rho\sqrt{x})\right]\end{aligned} \tag{295}$$

where

$$R_1 = \left(\frac{2\rho\sqrt{x}}{2}\right)^2 - \frac{S(3)}{(3\cdot 2)^2}\left(\frac{2\rho\sqrt{x}}{2}\right)^6 + \frac{S(5)}{(5\cdot 4\cdot 3\cdot 2)^2}\left(\frac{2\rho\sqrt{x}}{2}\right)^{10} - \cdots$$

$$R_2 = \frac{S(2)}{2^2}\left(\frac{2\rho\sqrt{x}}{2}\right)^4 - \frac{S(4)}{(4\cdot 3\cdot 2)^2}\left(\frac{2\rho\sqrt{x}}{2}\right)^8 + \frac{S(6)}{(6\cdot 5\cdot 4\cdot 3\cdot 2)^2}\left(\frac{2\rho\sqrt{x}}{2}\right)^{12} - \cdots$$

$$S(n) = 1 + \frac{1}{2} + \frac{1}{3} + \cdots + \frac{1}{n}$$

$$\log\beta = 0.57722$$

TABLE 86 TABLE OF THE $\psi(x)$ FUNCTIONS (Continued)

x	$\psi_3(x)$	$\psi_4(x)$	$\dfrac{d\psi_3(x)}{dx}$	$\dfrac{d\psi_4(x)}{dx}$
0 00	+0 5000	−∞	0 0000	+∞
0 10	+0 4916	−1 5409	−0 0929	+6 3413
0 20	+0 4826	−1 1034	−0 1419	+3 1340
0 30	+0 4667	−0 8513	−0 1746	+2 0498
0 40	+0 4480	−0 6765	−0 1970	+1 4974
0 50	+0 4275	−0 5419	−0 2121	+1 1585
0 60	+0 4058	−0 4112	−0 2216	+0 9273
0 70	+0 3834	−0 3574	−0 2268	+0 7582
0 80	+0 3606	−0 2883	−0 2286	+0 6286
0 90	+0 3377	−0 2308	−0 2276	+0 5258
1 00	+0 3151	−0 1825	−0 2243	+0 4422
1 10	+0 2929	−0 1419	−0 2193	+0 3730
1 20	+0 2713	−0 1076	−0 2129	+0 3149
1 30	+0 2504	−0 0786	−0 2054	+0 2656
1 40	+0 2302	−0 0542	−0 1971	+0 2235
1 50	+0 2110	−0 0337	−0 1882	+0 1873
1 60	+0 1926	−0 0166	−0 1788	+0 1560
1 70	+0 1752	−0 0023	−0 1692	+0 1290
1 80	+0 1588	+0 0094	−0 1594	+0 1056
1 90	+0 1433	+0 0189	−0 1496	+0 0854
2 00	+0 1289	+0 0265	−0 1399	+0 0679
2 10	+0 1153	+0 0325	−0 1304	+0 0527
2 20	+0 1026	+0 0371	−0 1210	+0 0397
2 30	+0 0911	+0 0405	−0 1120	+0 0285
2 40	+0 0804	+0 0429	−0 1032	+0 0189
2 50	+0 0705	+0 0444	−0 0948	+0 0109
2 60	+0 0614	+0 0451	−0 0868	+0 0039
2 70	+0 0531	+0 0452	−0 0791	−0 0018
2 80	+0 0455	+0 0447	−0 0719	−0 0066
2 90	+0 0387	+0 0439	−0 0650	−0 0105
3 00	+0 0326	+0 0427	−0 0586	−0 0137
3 10	+0 0270	+0 0412	−0 0526	−0 0164
3 20	+0 0220	+0 0394	−0 0469	−0 0180
3 30	+0 0176	+0 0376	−0 0417	−0 0194
3 40	+0 0137	+0 0356	−0 0369	−0 0204
3 50	+0 0102	+0 0335	−0 0325	−0 0210
3 60	+0 0072	+0 0314	−0 0284	−0 0213
3 70	+0 0045	+0 0293	−0 0246	−0 0213
3 80	+0 0022	+0 0271	−0 0212	−0 0210
3 90	+0 0003	+0 0251	−0 0180	−0 0206

TABLE 86 TABLE OF THE $\psi(x)$ FUNCTIONS (*Continued*)

x	$\psi_3(x)$	$\psi_4(x)$	$\dfrac{d\psi_3(x)}{dx}$	$\dfrac{d\psi_4(x)}{dx}$
4.00	−0.0014	+0.0230	−0.0152	−0.0200
4.10	−0.0028	+0.0211	−0.0127	−0.0193
4.20	−0.0039	+0.0192	−0.0104	−0.0185
4.30	−0.0049	+0.0174	−0.0083	−0.0177
4.40	−0.0056	+0.0156	−0.0065	−0.0168
4.50	−0.0062	+0.0140	−0.0049	−0.0158
4.60	−0.0066	+0.0125	−0.0035	−0.0148
4.70	−0.0069	+0.0110	−0.0023	−0.0138
4.80	−0.0071	+0.0097	−0.0012	−0.0129
4.90	−0.0071	+0.0085	−0.0003	−0.0119
5.00	−0.0071	+0.0073	+0.0005	−0.0109
5.10	−0.0070	+0.0063	+0.0012	−0.0100
5.20	−0.0069	+0.0053	+0.0017	−0.0091
5.30	−0.0067	+0.0044	+0.0022	−0.0083
5.40	−0.0065	+0.0037	+0.0025	−0.0075
5.50	−0.0062	+0.0029	+0.0028	−0.0067
5.60	−0.0059	+0.0023	+0.0030	−0.0060
5.70	−0.0056	+0.0017	+0.0032	−0.0053
5.80	−0.0053	+0.0012	+0.0033	0.0047
5.90	−0.0049	+0.0008	+0.0033	−0.0041
6.00	−0.0046	+0.0004	+0.0033	−0.0036

Having solutions (a') and (b') of Eq. (r), we conclude that the general solution (n) of Eq. (e) is

$$w = \frac{\zeta}{\sqrt{x}} = \frac{1}{\sqrt{x}}[C_1\psi_1'(2\rho\sqrt{x}) + C_2\psi_2'(2\rho\sqrt{x}) + C_3\psi_3'(2\rho\sqrt{x}) + C_4\psi_4'(2\rho\sqrt{x})] \quad (c')$$

Numerical values of the functions $\psi_1, \ldots, \psi_4$ and their first derivatives are given in Table 86.[1] A graphical representation of the functions $\psi_1', \ldots, \psi_4'$ is given in Fig. 219. It is seen that the values of these functions increase or decrease rapidly as the distance from the end increases. This indicates that in calculating the constants of integration in solution (c') we can very often proceed as we did with functions (281), i.e., by considering the cylinder as an infinitely long one and using at each edge only two of the four constants in solution (c').

[1] This table was calculated by F. Schleicher, see "Kreisplatten auf elastischer Unterlage," Berlin, 1926. The well-known Kelvin functions may be used in place of the functions ψ, to which they relate as follows: $\psi_1(x) = \text{ber}\, x$, $\psi_2(x) = -\text{bei}\, x$, $\psi_3(x) = -(2/\pi)\,\text{kei}\, x$, $\psi_4 = -(2/\pi)\,\text{ker}\, x$. For more accurate tables of the functions under consideration see p. 266

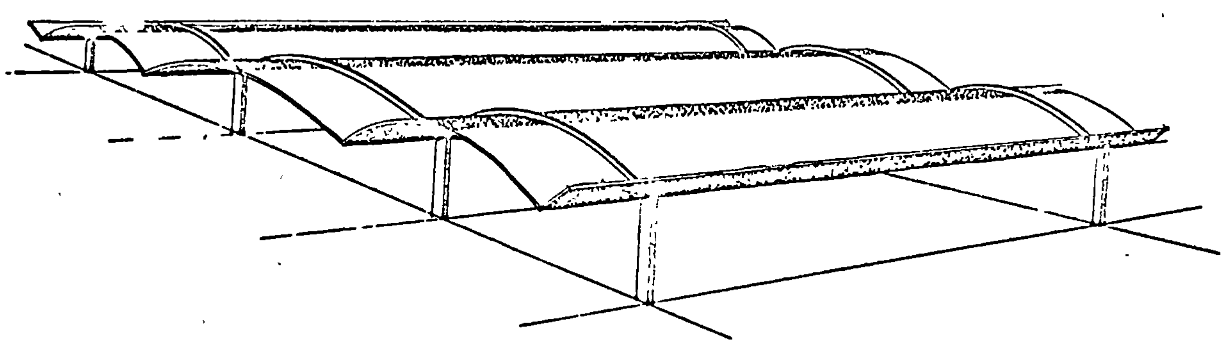

CONSTANTES DE DISEÑO PARA CASCARONES CILINDRICOS
APOYADOS EN DIAFRAGMAS

Porfirio Ballesteros

Design Constants for Interior Cylindrical Concrete Shells

In the discussion of the ACI article "Cylindrical Shell Analysis Simplified by Beam Method" by James Chinn, design constants based on a linear transverse distribution of longitudinal strains, or in other words based on the assumption that the shells behave like a beam, were presented by Messrs. Parme and Conner. These constants provided a convenient method of readily evaluating the internal forces and moments created in long and in intermediate length cylindrical shells by uniform and dead load. While these constants are perfectly satisfactory for long shells and were recommended in this range, some vagueness regarding the applicable limit for intermediate length shells existed. This uncertainty was caused primarily because the validity of the assumption of linear strain depends not only on the ratio of radius to longitudinal span but is as well a function of the subtended angle and the ratio of thickness to radius. Because of the interdependence of the effect of these factors, no precise limits for the beam method could be given.

To remove this uncertainty and at the same time reduce the labor involved in the design of cylindrical shells which cannot be adequately treated by the beam method, a new series of comparable constants are presented in Table 1. These constants have been computed on the basis of the shell theory expounded in ASCE Manual No. 31 "Design of Cylindrical Concrete Shell Roofs." Consequently these newer constants in contrast to those previously given are a function of r/L and r/t as well as the subtended angle, ϕ_k. To avoid interpolation as much as possible, values are given for the three r/t values of 100, 200 and 300 and for six values of r/L with r/L varying from a low of 0.4 to a high of 2.6. For ϕ_k less than 45 deg., it was found that the modified beam method was sufficiently accurate for all values of r/L less than 0.6. Thus for the portion of Table 1 dealing with ϕ_k less than 45 deg., the internal forces are only given for values of r/L greater than 0.6. When ϕ_k is greater than 45 deg., it was found necessary to include an r/L as low as 0.4 to provide a good transition from values as computed by the beam method to those computed by shell theory.

It should be noted that although values are tabulated for r/t = 300, which represents a shell beyond practical limit, they have been included to avoid extrapolation for cases of r/t beyond 200. Likewise the selection of r/L = 2.6 represents an arbitrary limit. For values of r/L greater than those listed the internal forces are concentrated near the edge. For this reason, the arrangement of Table 1 is not suitable for such shells.

Values have been given only for load varying as the dead weight. This is due to the fact that numerous comparisons made with different r/L values indicate that the effect of a uniform load could be very closely approximated by an equivalent dead weight by the simple expression that

$$p_d = p_u \left(\frac{\sin \phi_k}{\phi_k} \right)$$

The constants have been determined on the basis that transverse and horizontal displacement of the longitudinal edges of the shell are prevented. They are thus applicable to interior barrels in which restraint to such movement is provided by adjacent barrels. However they can be applied with tolerable accuracy to the interior half of the exterior bay since the effect of disturbance of loads on the far edge has only minor influence on the first interior valley. This is especially true since to prevent excessive deflection of the free edge an edge beam should always be provided (except for long shells with short chord width) at the exterior edge.

Determination of the internal forces in cylindrical shells subject to uniform longitudinal loading by the shell theory requires that the actual load be approximated as the sum of partial loads varying sinusoidally according to a Fourier Series in the longitudinal direction. From a practical point of view generally only the first or at most two partial loads are used with adjustments made especially to the value of shear on the basis of statical requirements. However since Table 1 was prepared by means of an electronic computer, the algebraic sum of four partial loads was used to avoid the need of any adjustment. Even with this number of loads to achieve sufficient accuracy it was found necessary in some cases to employ Euler's convergence technique. The use of such care should not be interpreted however as needed or justified on the basis of underlying assumptions. Its worth rests solely on the fact that it permitted a more accurate comparison of values as the parameters r/t and r/L are varied, and enabled a more precise examination of the variation of the internal forces in the longitudinal direction.

In this connection, the constants in Table 1 give only the transverse distribution of forces at midspan and at the support as noted by the footnote in Table 1, with no indication of the longitudinal distribution of forces. The reason for this is that the exact expression for longitudinal distribution even for simply supported shells is highly complex involving four functions. Fortunately within the range of the tabulated values the longitudinal distribution can be approximated by well recognized relationship.

For example, as shown in Fig. 1, the distribution of T_x as might be anticipated follows very closely that given by a parabolic distribution as the case of a uniform load on a beam even for widely different shells represented by r/L equal to 0.6 and 2.6. Although the curves shown in Fig. 1 have been computed on the basis of ϕ_k = 27.5 deg., they are typical of those for other angles. A sinusoidal distribution of T_x would also be satisfactory.

With respect to T_ϕ, for design purposes this force can be assumed to be uniform in the longitudinal direction as can be inferred from Fig. 2. Because the analysis has been based on the prescribed boundary condition that the shell is supported by a rigid member at x = 0 and x = L, the value of T_ϕ decreases theoretically to zero at the support. The transition from zero to the full value however takes place over a very short interval. Thus, especially for values near the crown, the assumption of a uniform distribution of T_ϕ is justified. Distribution of T_ϕ in the valley can also be considered uniform even though a careful evaluation of the distribution in this area indicates some departure from uniform distribution near the support. The computed variation near the support may be due however to the sensitivity of the results to the number of load terms used. This is primarily due to the fact that the absolute value is generally quite small compared to the crown value with the final result equal to the difference of almost like values. Because the values are small and have almost no effect on the design, the assumption of uniform distribution of T_ϕ in the valley is justified.

As in the case of the distribution of the T_x forces, the distribution of shear can be assumed to be like that in a beam with the shear varying linearly from a maximum value at the support to zero value at midspan. As shown in Fig. 3, the distribution as computed by the shell theory gives slightly higher values, but the variation from the linear distribution is negligible.

There is one important aspect of shear distribution which warrants some comments. As shown in Fig. 4, in which a plot of the transverse distribution of shear at various sections along the shell are superimposed on each other, the shear tends to be concentrated towards the valley as the support is approached. From this plot it should not be inferred that the magnitude of shear does not decrease proportionally to the distance from the support. For purpose of clarity in presentation of the variation in transverse distribution, all values have been plotted in terms of the value of shear at $\phi = 0.5\ \phi_k$. The values hence are all relative. While this change in transverse shear distribution is insignificant with respect to its effect on the direct stresses in the shell, it has a pronounced effect on the longitudinal moment distribution.

As in the case of T_ϕ, the boundary condition of supports rigid in the transverse direction leads to zero moment at the support. For long shells as discussed in Reference 1, the moment increases at a variable rate from zero at the support to a maximum value near the quarter point, and there remains essentially uniform to midspan. On the other hand, for shells in the range covered by Table 1, the magnitude of the moment increases almost parabolically from the support to midspan as shown in Fig. 5, especially for the moment at the crown. At the valley, the moment increases at a slightly faster rate for smaller r/L values as can be seen by a comparison of the curves of Fig. 5 and Fig. 6. In determining the amount of transverse reinforcement for shells with r/L about 1.0, due account should be taken of the greater curvature of the longitudinal distribution of M_ϕ.

Continuity

The design constants of Table 1 are for simply supported shells, i.e., the supports are assumed to offer no lateral restraint. Thus it will be found that taking the summation of the moment of T_x forces at midspan about any axis will equal to $wL^2/8$. Nevertheless the constants can be applied without any great loss of accuracy to shells continuous in the longitudinal direction. The effect of continuity as one might expect from beam behavior is to radically change the magnitude and sense of the T_x forces without affecting greatly the other internal forces such as T_ϕ and M_ϕ. However, while continuity alters greatly the longitudinal distribution of T_x forces, previous investigations have shown that only minor change in the transverse distribution occurs.

Without becoming involved in complex mathematics, a qualitative appraisal of the effect of continuity on the transverse distribution can be made by recalling that the transverse distribution of T_x is a function solely of the relative proportions of transverse to longitudinal displacement. When as in the case of long shell, the vertical deflection of the edge measured with respect to the crown of a unit strip at midspan is small compared to the deflection of the same point measured longitudinally, the distribution of T_x in the transverse direction is linear and thus is similar to that of the fiber stress in a beam. As the relative displacement in the transverse direction to that in the longitudinal direction increases, the transverse distribution of T_x departs from a linear pattern becoming curvilinear with a decrease in the slope of the stress curve below the neutral axis. Since continuity decreases the deflection of the section at midspan with respect to the support, the effect of continuity is to increase the ratio of transverse to longitudinal deflection.

From this it follows that the transverse distribution of T_x forces in a continuous shell has slightly greater curvature than that of a simply supported shell of the same span and radius. An inkling of the relative difference between the two distributions can be obtained by comparing the design constants in Table 1 for any two r/L values with one r/L being 1.4 times the other. A plot of the two transverse distribution curves will show that while there might be significant change in the magnitude of T_x at the edge of the shell, the total area below the neutral axis will be about the same for both curves. In general, the difference will not be greater than 3 or 4 per cent. Because of this, it is sufficiently accurate to use the transverse distribution of stresses of a simply supported shell, irrespective of the degree of continuity. As shown by Dr. Olev Olsen in the article "Continuous Shells" in the Proceedings of the Second Symposium of Concrete Shell Roof Construction, the transverse distribution of T_x for all practical purposes is uniform throughout the length of the shell.

By similar deductive reasoning, the longitudinal distribution can also be accurately estimated. In long barrel shells, because the transverse distribution is almost linear, it is apparent that the magnitude of T_x at any section will be to the T_x in a simply supported shell as the ratio of the moment in a continuous beam of equal length and support condition is to the simple beam bending moment. For short barrel shells, because of the effect of shear strain, the longitudinal stresses over the support will be somewhat greater than that indicated by the analogy to a continuous beam. This increase, which will be slight for the range of shells covered in Table 1, is of little consequence since an underestimate of the intensity of the forces at the support will be compensated by an overestimate of the forces in the region of positive moment. Consequently proportioning the longitudinal forces on the basis of the variation of the moment occurring in a continuous beam can be applied without any decrease in the ultimate capacity.

The change in the transverse distribution of the T_x forces caused by continuity will naturally be reflected in the transverse distribution of the shearing forces. However because very slight change in the location of the neutral axis occurs, the position of the peak shear will undoubtedly be quite insensitive to the effect of continuity, and may therefore be considered to occur at the same place as in a simply supported shell. On the other hand the downward drift of the tensile forces will cause the shear curve to have more of a bulge near the valley.

Since the shear stresses in this region are not generally the critical ones, inaccuracy in this area is relatively unimportant.

With respect to the longitudinal distribution of shear, the reasoning presented for T_x applies. Refinements aimed at increasing the accuracy of determining the intensity of the shear forces are hardly warranted in view of the common practice of providing shear resistance. Generally to avoid variable spacing, shear reinforcement is placed uniformly and thus leads always to overdesign because of the large number of bars crossing a section of principal stresses. For this reason, modification of the shear forces in a shell to correspond to the total shear in a continuous beam is satisfactory.

Example

The ease with which the internal forces can be computed makes the use of Table 1 self-explanatory. In all cases, the internal force is equal to the product of a multiplier and the design constants. The multiplier shown in the third row of Table 2 equals the product of the load times various powers of the dimension indicated in the heading of Table 1. However to avoid misinterpretation the computation required for a typical interior shell will be outlined. From the dimensions given in Table 2

$$r/t = 45 \times 12/4 = 135$$

$$r/L = 45/50 = 0.90$$

Inspection of the constants in Table 1 show that there is only slight differences in the constants for values of r/t and r/L in the range with $\phi_k = 25^\circ$ and 27.5°. As such, the design constants will be selected from r/L = 1.0 and r/t = 100. But interpolation for the specific ϕ_k is recommended. To simplify this task, advantage will be taken of the fact that linear interpolation can be achieved by adding algebraically a fixed ratio of the two adjacent values. For this example, the constants for $\phi_k = 25^\circ$ are multiplied by

$$\frac{27.5 - 26.4}{27.5 - 25.0} = 0.45$$

while the constants for 27.5° are multiplied by

$$1 - 0.45 = 0.55$$

Thus the design constant for T_x at the crown for $\phi_k = 26.4^\circ$, r/L = 1.0 and r/t = 100 is

$$-(4.482 \times 0.45 + 3.509 \times 0.55) = -3.947$$

which is recorded in the first row of numbers, second column of Table 2. The other coefficients are obtained in a similar manner.

In accordance with the formula given on page 2 and the intensity of load listed in Table 2, the equivalent dead load for which the shell is to be designed is

$$p_d = 50 + 30\,\frac{.44}{.46} = 79 \text{ psf.}$$

The multiplier for T_x therefore is

$$\frac{L^2}{r}\,p_d = \frac{50^2}{45} \times 79 = 4390 \text{ lb/ft.}$$

In a similar manner the other multipliers can be obtained as readily. The product of these and the tabulated constants gives the internal forces in the shell which appear in the columns marked Force.

A graphical representation of the tabulated values for T_x and M_ϕ is given in Fig. 7 for comparison with values as obtained by the beam method. As to be expected, the value of T_x as computed by the shell theory is slightly larger while the value of the moment M_ϕ is slightly less. For design purposes the difference is negligible. However, this good agreement holds only for the interior shells. If the outer edge of the exterior shell is not stiffened by an edge beam, marked increase in the intensity of T_x will occur at the edge.

If the shell is continuous in the longitudinal direction, the forces determined in Table 2 can be modified as previously discussed. For example if two 50-ft. long shells are continuous over a central arch, then the forces are multiplied by the ratio of moments in a beam of similar continuity to the moment in a simply supported beam. Since the moment over a central support is $-wL^2/8$, obviously the ratio is -1.0. The ratio to be applied to the forces at midspan is

$$\frac{wL^2/16}{wL^2/8} = 0.50$$

Similarly, the shear forces are altered by the ratio of continuous beam shear at the interior support to that in a simple beam. The ratio is

$$\frac{5wL/8}{wL/2} = 1.25$$

The shear forces at the outer support are given by the following ratio:

$$\frac{3wL/8}{wL/2} = .75$$

As discussed above, continuity does not cause T_ϕ and M_ϕ to change significantly.

Notation

h = total vertical height of shell from edge to crown

y = vertical height of shell measured from edge

L = length of shell between supports

r = centerline radius of shell

t = thickness of shell

x = longitudinal distance measured from the left support

ϕ = angle measured from the right edge of shell

ϕ_k = angle subtended by the edge of shell measured from the centerline axis

p_u = intensity of uniform load on unit area

p_d = intensity of dead load on unit area

T_ϕ = the direct force component in the transverse direction, considered positive when tensile

$T_\phi^{\mathcal{C}}$ = T_ϕ at midspan of the shell

T_x = the direct force component in the longitudinal direction, considered positive when tensile

$T_x^{\mathcal{C}}$ = T_x at midspan of the shell

S = the tangential shearing force, considered positive when it creates tension in the direction of increasing values of x and ϕ.

S^* = S at the transverse support

M_ϕ = the moment in the transverse direction, considered positive when it produces tension in the inner fibers

$M_\phi^{\mathcal{C}}$ = M_ϕ at midspan of the shell

Table 1 Internal Forces in a Multiple Cylindrical Shell Due to Dead Load $\phi_k = 22.5°$

$$T_x = \frac{L^2}{r}\left[p_d \text{ col. (1)}\right] \qquad S^* = -L\left[p_d \text{ col. (3)}\right]$$

$$T_\phi = r\left[p_d \text{ col. (2)}\right] \qquad M_\phi = r^2\left[p_d \text{ col. (4)}\right]$$

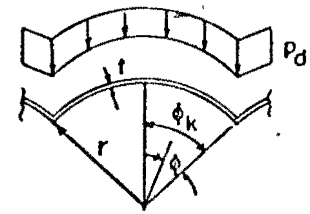

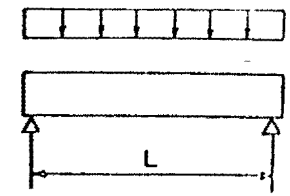

		$r/t = 100$				$r/t = 200$				$r/t = 300$			
r/L	ϕ	T_x (1)	T_ϕ (2)	S (3)	M_ϕ (4)	T_x (1)	T_ϕ (2)	S (3)	M_ϕ (4)	T_x (1)	T_ϕ (2)	S (3)	M_ϕ (4)
.6	$1.00\phi_k$	-5.976	-1.415	.000	-.00289	-6.035	-1.452	.000	-.00315	-6.011	-1.476	.000	-.00328
	$.75\phi_k$	-4.893	-1.187	1.959	-.00102	-4.946	-1.210	1.882	-.00118	-4.947	-1.219	1.787	-.00123
	$.50\phi_k$	-1.591	-.597	3.258	.00251	-1.615	-.598	3.227	.00256	-1.648	-.583	3.160	.00263
	$.25\phi_k$	4.086	.077	3.034	.00234	4.129	.083	3.126	.00251	4.123	.099	3.189	.00258
	0	12.395	.390	.000	-.00742	12.539	.393	.000	-.00729	12.608	.398	.000	-.00738
1.0	$1.00\phi_k$	-5.682	-1.430	.000	-.00286	-5.461	-1.471	.000	-.00307	-4.934	-1.471	.000	-.00302
	$.75\phi_k$	-4.777	-1.193	1.783	-.00102	-4.760	-1.219	1.624	-.00117	-4.626	-1.225	1.436	-.00118
	$.50\phi_k$	-1.808	-.589	3.094	.00248	-2.069	-.586	2.998	.00248	-2.510	-.593	2.854	.00242
	$.25\phi_k$	3.853	.087	3.117	.00235	3.771	.100	3.247	.00251	3.531	.097	3.360	.00251
	0	13.013	.393	.000	-.00743	13.564	.396	.000	-.00727	14.339	.394	.000	-.00715
1.4	$1.00\phi_k$	-5.103	-1.420	.000	-.00252	-4.174	-1.419	.000	-.00251	-2.768	-1.360	.000	-.00220
	$.75\phi_k$	-4.555	-1.198	1.592	-.00093	-4.337	-1.214	1.299	-.00103	-3.935	-1.205	.939	-.00096
	$.50\phi_k$	-2.241	-.612	2.911	.00221	-3.094	-.644	2.725	.00203	-4.260	-.704	2.462	.00175
	$.25\phi_k$	3.416	.069	3.222	.00223	2.972	.051	3.396	.00229	2.255	.002	3.594	.00216
	0	14.172	.386	.000	-.00709	15.834	.376	.000	-.00661	17.999	.358	.000	-.00611
1.8	$1.00\phi_k$	-4.305	-1.382	.000	-.00204	-2.523	-1.328	.000	-.00180	-.473	-1.224	.000	-.00135
	$.75\phi_k$	-4.238	-1.189	1.374	-.00079	-3.743	-1.196	.911	-.00083	-3.080	-1.175	.408	-.00072
	$.50\phi_k$	-2.831	-.652	2.707	.00181	-4.409	-.739	2.408	.00145	-6.124	-.838	2.041	.00105
	$.25\phi_k$	2.788	.026	3.341	.00199	1.817	-.040	3.572	.00195	.607	-.126	3.838	.00175
	0	15.841	.369	.000	-.00648	19.067	.344	.000	-.00568	22.579	.314	.000	-.00493
2.2	$1.00\phi_k$	-3.440	-1.327	.000	-.00154	-1.018	-1.237	.000	-.00119	1.149	-1.118	.000	-.00074
	$.75\phi_k$	-3.868	-1.169	1.148	-.00064	-3.113	-1.173	.548	-.00063	-2.283	-1.144	.009	-.00052
	$.50\phi_k$	-3.460	-.691	2.492	.00141	-5.596	-.832	2.095	.00095	-7.441	-.946	1.677	.00055
	$.25\phi_k$	2.044	-.027	3.456	.00171	.523	-.137	3.729	.00162	-1.056	-.242	4.012	.00140
	0	17.833	.345	.000	-.00575	22.631	.310	.000	-.00477	27.029	.276	.000	-.00397
2.6	$1.00\phi_k$	-2.647	-1.268	.000	-.00112	.064	-1.164	.000	-.00075	1.982	-1.050	.000	-.00037
	$.75\phi_k$	-3.490	-1.143	.939	-.00049	-2.541	-1.150	.272	-.00048	-1.614	-1.118	-.226	-.00038
	$.50\phi_k$	-4.022	-.723	2.282	.00107	-6.425	-.903	1.821	.00059	-8.098	-1.017	1.386	.00024
	$.25\phi_k$	1.269	-.076	3.550	.00145	-.741	-.221	3.838	.00134	-2.611	-.333	4.102	.00113
	0	19.939	.318	.000	-.00502	26.078	.281	.000	-.00403	31.058	.248	.000	-.00329

*Shear forces are at supports, others are at midspan

Table 1 Internal Forces in a Multiple Cylindrical Shell Due to Dead Load $\phi_k = 25^\circ$

$T_x = \frac{L^2}{r}\left[p_d \text{ col. (1)}\right]$ $S^* = -L\left[p_d \text{ col (3)}\right]$

$T_\phi = r\left[p_d \text{ col (2)}\right]$ $M_\phi = r^2\left[p_d \text{ col (4)}\right]$

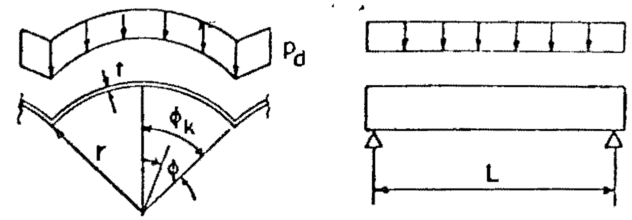

		r/t = 100				r/t = 200				r/t = 300			
r/L	ϕ	T_x (1)	T_ϕ (2)	S (3)	M_ϕ (4)	T_x (1)	T_ϕ (2)	S (3)	M_ϕ (4)	T_x (1)	T_ϕ (2)	S (3)	M_ϕ (4)
.6	1.00ϕ_k	-4.856	-1.428	.000	-.00368	-4.851	-1.469	.000	-.00397	-4.740	-1.493	.000	-.00409
	.75ϕ_k	-3.986	-1.194	1.733	-.00133	-4.005	-1.214	1.618	-.00148	-3.981	-1.222	1.510	-.00153
	.50ϕ_k	-1.317	-.595	2.920	.00309	-1.359	-.582	2.851	.00320	-1.455	-.564	2.765	.00327
	.25ϕ_k	3.318	.078	2.776	.00295	3.326	.097	2.869	.00313	3.280	.115	2.936	.00320
	0	10.171	.381	.000	-.00898	10.291	.387	.000	-.00900	10.457	.393	.000	-.00912
1.0	1.00ϕ_k	-4.482	-1.441	.000	-.00352	-3.951	-1.457	.000	-.00355	-3.067	-1.417	.000	-.00326
	.75ϕ_k	-3.849	-1.202	1.538	-.00131	-3.728	-1.218	1.304	-.00139	-3.487	-1.214	1.045	-.00134
	.50ϕ_k	-1.603	-.591	2.740	.00296	-2.078	-.601	2.579	.00286	-2.805	-.641	2.377	.00260
	.25ϕ_k	3.046	.087	2.868	.00293	2.808	.087	3.018	.00300	2.385	.055	3.165	.00289
	0	10.917	.383	.000	-.00889	11.792	.380	.000	-.00860	13.030	.368	.000	-.00817
1.4	1.00ϕ_k	-3.747	-1.410	.000	-.00291	-2.273	-1.349	.000	-.00252	-.573	-1.240	.000	-.00190
	.75ϕ_k	-3.581	-1.202	1.310	-.00114	-3.171	-1.200	.871	-.00112	-2.640	-1.179	.419	-.00097
	.50ϕ_k	-2.170	-.635	2.532	.00246	-3.428	-.710	2.233	.00202	-4.841	-.813	1.895	.00149
	.25ϕ_k	2.520	.048	2.981	.00267	1.759	-.011	3.219	.00255	.810	-.099	3.463	.00227
	0	12.361	.368	.000	-.00319	14.777	.344	.000	-.00730	17.536	.314	.000	-.00635
1.8	1.00ϕ_k	-2.822	-1.349	.000	-.00216	-.582	-1.225	.000	-.00153	1.240	-1.096	.000	-.00089
	.75ϕ_k	-3.218	-1.188	1.049	-.00092	-2.510	-1.170	.429	-.00082	-1.803	-1.139	-.067	-.00065
	.50ϕ_k	-2.874	-.698	2.299	.00186	-4.789	-.836	1.872	.00120	-6.341	-.957	1.471	.00065
	.25ϕ_k	1.790	-.019	3.105	.00230	.446	-.135	3.418	.00205	-.871	-.245	3.685	.00173
	0	14.357	.342	.000	-.00719	18.414	.302	.000	-.00588	22.035	.267	.000	-.00483
2.2	1.00ϕ_k	-1.944	-1.279	.000	-.00150	.571	-1.129	.000	-.00085	2.017	-1.014	.000	-.00035
	.75ϕ_k	-2.828	-1.164	.801	-.00070	-1.908	-1.141	.107	-.00059	-1.115	-1.107	-.319	-.00044
	.50ϕ_k	-3.527	-.755	2.066	.00132	-5.703	-.933	1.562	.00064	-6.986	-1.044	1.151	.00020
	.25ϕ_k	.977	-.089	3.215	.00191	-.857	-.244	3.552	.00163	-2.441	-.355	3.788	.00135
	0	16.587	.313	.000	-.00616	21.928	.267	.000	-.00476	25.992	.234	.000	-.00383
2.6	1.00ϕ_k	-1.259	-1.215	.000	-.00100	1.147	-1.069	.000	-.00044	2.038	-.977	.000	-.00010
	.75ϕ_k	-2.464	-1.137	.599	-.00052	-1.415	-1.117	-.079	-.00042	-.564	-1.082	-.403	-.00030
	.50ϕ_k	-4.014	-.796	1.853	.00091	-6.126	-.993	1.315	.00030	-7.013	-1.087	.904	-.00002
	.25ϕ_k	.179	-.147	3.291	.00157	-2.057	-.327	3.614	.00131	-3.920	-.437	3.806	.00108
	0	18.799	.285	.000	-.00525	25.115	.241	.000	-.00395	29.611	.212	.000	-.00319

*Shear forces are at supports, others are at midspan

Table 1 Internal Forces in a Multiple Cylindrical Shell Due to Dead Load $\phi_k = 27.5$

$T_x = \frac{L^2}{r}\left[p_d \text{ col. (1)}\right]$ $S^* = -L\left[p_d \text{ col. (3)}\right]$

$T_\phi = r\left[p_d \text{ col. (2)}\right]$ $M_\phi = r^2\left[p_d \text{ col. (4)}\right]$

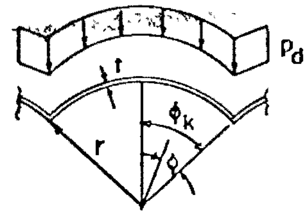

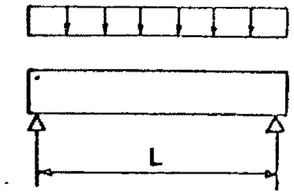

		r/t = 100				r/t = 200				r/t = 300			
r/L	ϕ	T_x (1)	T_ϕ (2)	S (3)	M_ϕ (4)	T_x (1)	T_ϕ (2)	S (3)	M_ϕ (4)	T_x (1)	T_ϕ (2)	S (3)	M_ϕ (4)
.6	$1.00\phi_k$	-4.008	-1.441	.000	-.00454	-3.916	-1.482	.000	-.00482	-3.672	-1.492	.000	-.00484
	$.75\phi_k$	-3.304	-1.199	1.536	-.00166	-3.292	-1.217	1.394	-.00180	-3.231	-1.222	1.271	-.00182
	$.50\phi_k$	-1.118	-.588	2.633	.00375	-1.214	-.567	2.532	.00387	-1.415	-.561	2.427	.00387
	$.25\phi_k$	2.738	.084	2.565	.00361	2.704	.108	2.663	.00379	2.597	.116	2.737	.00382
	0	8.515	.372	.000	-.01073	8.699	.380	.000	-.01085	9.038	.381	.000	-.01085
1.0	$1.00\phi_k$	-3.509	-1.441	.000	-.00412	-2.619	-1.411	.000	-.00380	-1.433	-1.323	.000	-.00313
	$.75\phi_k$	-3.133	-1.206	1.314	-.00158	-2.898	-1.210	.991	-.00156	-2.557	-1.195	.651	-.00141
	$.50\phi_k$	-1.509	-.598	2.432	.00341	-2.259	-.641	2.198	.00304	-3.234	-.724	1.935	.00249
	$.25\phi_k$	2.405	.080	2.669	.00349	1.979	.050	2.857	.00340	1.381	-.019	3.043	.00312
	0	9.452	.369	.000	-.01036	10.809	.356	.000	-.00968	12.587	.332	.000	-.00873
1.4	$1.00\phi_k$	-2.600	-1.378	.000	-.00311	-.737	-1.250	.000	-.00223	.842	-1.115	.000	-.00135
	$.75\phi_k$	-2.808	-1.197	1.035	-.00130	-2.240	-1.176	.465	-.00113	-1.670	-1.146	.007	-.00090
	$.50\phi_k$	-2.222	-.671	2.190	.00258	-3.788	-.800	1.788	.00176	-5.123	-.927	1.421	.00102
	$.25\phi_k$	1.767	.013	2.800	.00305	.730	-.096	3.103	.00268	-.302	-.207	3.349	.00226
	0	11.231	.344	.000	-.00912	14.333	.306	.000	-.00755	17.210	.269	.000	-.00622
1.8	$1.00\phi_k$	-1.608	-1.292	.000	-.00208	.638	-1.117	.000	-.00109	1.818	-1.000	.000	-.00042
	$.75\phi_k$	-2.407	-1.176	.737	-.00098	-1.594	-1.139	.056	-.00076	-.932	-1.104	-.322	-.00056
	$.50\phi_k$	-2.990	-.758	1.929	.00174	-4.907	-.934	1.424	.00081	-5.965	-1.047	1.044	.00023
	$.25\phi_k$	.947	-.079	2.933	.00250	-.606	-.237	3.285	.00204	-1.895	-.347	3.497	.00167
	0	13.499	.311	.000	-.00765	17.937	.261	.000	-.00580	21.202	.227	.000	-.00463
2.2	$1.00\phi_k$	-.824	-1.213	.000	-.00130	1.255	-1.040	.000	-.00047	1.839	-.957	.000	-.00005
	$.75\phi_k$	-2.021	-1.149	.491	-.00071	-1.070	-1.109	-.161	-.00051	-.349	-1.073	-.408	-.00036
	$.50\phi_k$	-3.576	-.825	1.689	.00110	-5.391	-1.015	1.146	.00029	-5.987	-1.100	.768	-.00009
	$.25\phi_k$	.106	-.162	3.031	.00201	-1.842	-.342	3.368	.00158	-3.411	-.446	3.523	.00129
	0	15.827	.279	.000	-.00634	21.146	.230	.000	-.00462	24.769	.202	.000	-.00371
2.6	$1.00\phi_k$	-.331	-1.153	.000	-.00079	1.354	-1.003	.000	-.00018	1.434	-.949	.000	.00006
	$.75\phi_k$	-1.693	-1.122	.324	-.00051	-.663	-1.085	-.241	-.00035	.101	-1.049	-.375	-.00023
	$.50\phi_k$	-3.913	-.868	1.488	.00068	-5.417	-1.055	.934	.00004	-5.571	-1.118	.550	-.00021
	$.25\phi_k$	-.674	-.224	3.083	.00162	-2.974	-.418	3.377	.00126	-4.872	-.522	3.483	.00101
	0	18.005	.251	.000	-.00530	24.050	.208	.000	-.00385	28.226	.184	.000	-.00311

*Shear forces are at supports, others are at midspan

Table 1 Internal Forces in a Multiple Cylindrical Shell Due to Dead Load $\phi_k =$ [illegible]0°

$T_x = \frac{L^2}{r}\left[p_d \ \text{col. (1)}\right]$ $S^* = -L\left[p_d \ \text{col (3)}\right]$

$T_\phi = r\left[p_d \ \text{col (2)}\right]$ $M_\phi = r^2\left[p_d \ \text{col. (4)}\right]$

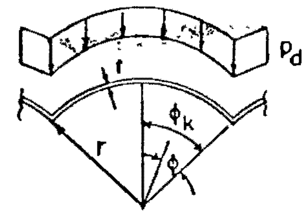

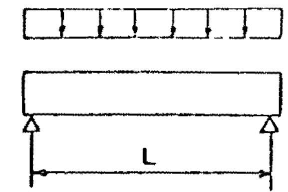

		r/t = 100				r/t = 200				r/t = 300			
r/L	ϕ	T_x (1)	T_ϕ (2)	S (3)	M_ϕ (4)	T_x (1)	T_ϕ (2)	S (3)	M_ϕ (4)	T_x (1)	T_ϕ (2)	S (3)	M_ϕ (4)
.6	1.00ϕ_k	-3.340	-1.452	.000	-.00544	-3.125	-1.482	.000	-.00562	-2.714	-1.465	.000	-.00540
	.75ϕ_k	-2.777	-1.202	1.363	-.00201	-2.728	-1.216	1.197	-.00212	-2.621	-1.215	1.045	-.00203
	.50ϕ_k	-.980	-.579	2.384	.00445	-1.167	-.563	2.256	.00450	-1.502	-.581	2.125	.00431
	.25ϕ_k	2.286	.091	2.392	.00431	2.194	.110	2.497	.00444	2.009	.097	2.586	.00437
	0	7.269	.363	.000	-.01263	7.594	.368	.000	-.01268	8.163	.363	.000	-.01238
1.0	1.00ϕ_k	-2.678	-1.425	.000	-.00457	-1.444	-1.336	.000	-.00371	-.148	-1.208	.000	-.00263
	.75ϕ_k	-2.559	-1.204	1.102	-.00181	-2.210	-1.193	.678	-.00164	-1.807	-1.168	.287	-.00137
	.50ϕ_k	-1.506	-.615	2.156	.00374	-2.531	-.708	1.845	.00296	-3.607	-.826	1.540	.00207
	.25ϕ_k	1.867	.064	2.513	.00401	1.248	-.010	2.750	.00367	.538	-.111	2.960	.00319
	0	8.463	.350	.000	-.01171	10.345	.324	.000	-.01033	12.402	.291	.000	-.00880
1.4	1.00ϕ_k	-1.622	-1.325	.000	-.00308	.326	-1.144	.000	-.00170	1.453	-1.015	.000	-.00074
	.75ϕ_k	-2.177	-1.185	.765	-.00139	-1.520	-1.147	.130	-.00106	-.981	-1.113	-.241	-.00079
	.50ϕ_k	-2.345	-.723	1.876	.00251	-3.986	-.896	1.405	.00130	-4.981	-1.020	1.057	.00049
	.25ϕ_k	1.117	-.038	2.668	.00331	-.089	-.189	3.007	.00268	-1.095	-.303	3.210	.00219
	0	10.570	.315	.000	-.00975	14.040	.265	.000	-.00747	16.657	.231	.000	-.00594
1.8	1.00ϕ_k	-.671	-1.221	.000	-.00181	1.168	-1.031	.000	-.00062	1.635	-.947	.000	-.00006
	.75ϕ_k	-1.763	-1.157	.454	-.00098	-.942	-1.108	-.171	-.00067	-.339	-1.072	-.386	-.00046
	.50ϕ_k	-3.036	-.826	1.599	.00147	-4.684	-1.013	1.074	.00039	-5.182	-1.100	.730	-.00011
	.25ϕ_k	.246	-.150	2.801	.00260	-1.366	-.327	3.137	.00197	-2.634	-.428	3.272	.00160
	0	12.982	.277	.000	-.00782	17.332	.225	.000	-.00559	20.216	.197	.000	-.00446
2.2	1.00ϕ_k	-.079	-1.144	.000	-.00100	1.285	-.983	.000	-.00016	1.180	-.940	.000	.00012
	.75ϕ_k	-1.407	-1.129	.243	-.00068	-.498	-1.078	-.268	-.00043	.155	-1.042	-.346	-.00027
	.50ϕ_k	-3.521	-.894	1.368	.00080	-4.755	-1.068	.832	-.00001	-4.762	-1.122	.481	-.00029
	.25ϕ_k	-.580	-.238	2.878	.00203	-2.544	-.424	3.162	.00151	-4.156	-.521	3.238	.00121
	0	15.263	.246	.000	-.00634	20.255	.199	.000	-.00447	23.644	.176	.000	-.00362
2.6	1.00ϕ_k	.192	-1.094	.000	-.00054	1.065	-.970	.000	.00000	.603	-.952	.000	.00013
	.75ϕ_k	-1.127	-1.103	.178	-.00046	-.168	-1.057	-.261	-.00028	.488	-1.020	-.245	-.00015
	.50ϕ_k	-3.678	-.931	1.188	.00042	-4.488	-1.087	.647	-.00016	-4.097	-1.119	.288	-.00031
	.25ϕ_k	-1.320	-.298	2.900	.00161	-3.636	-.494	3.128	.00118	-5.589	-.596	3.157	.00092
	0	17.327	.221	.000	-.00525	23.021	.181	.000	-.00375	27.073	.161	.000	-.00305

*Shear forces are at supports, others are at midspan

Table I Internal Forces in a Multiple Cylindrical Shell due to Dead Load $\qquad \phi_k = 32.5°$

$$T_x = \frac{L^2}{r}\left[p_d \;\; \text{col. (1)}\right] \qquad S^{*} = -L\left[p_d \;\; \text{col (3)}\right]$$

$$T_\phi = r\left[p_d \;\; \text{col. (2)}\right] \qquad M_\phi = r^2\left[p_d \;\; \text{col. (4)}\right]$$

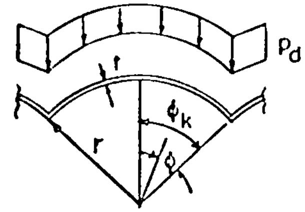

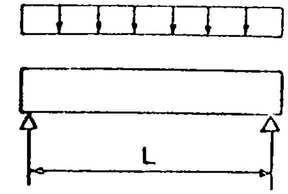

		r/t = 100				r/t = 200				r/t = 300			
r/L	ϕ	T_x (1)	T_ϕ (2)	S (3)	M_ϕ (4)	T_x (1)	T_ϕ (2)	S (3)	M_ϕ (4)	T_x (1)	T_ϕ (2)	S (3)	M_ϕ (4)
.6	$1.00\phi_k$	-2.792	-1.459	.000	-.00634	-2.418	-1.463	.000	-.00624	-1.831	-1.409	.000	-.00562
	$.75\phi_k$	-2.358	-1.203	1.210	-.00236	-2.264	-1.211	1.013	-.00239	-2.107	-1.204	.816	-.00225
	$.50\phi_k$	-.894	-.570	2.168	.00515	-1.204	-.576	2.009	.00500	-1.683	-.626	1.845	.00449
	$.25\phi_k$	1.921	.096	2.247	.00503	1.754	.097	2.367	.00504	1.483	.057	2.478	.00480
	0	6.330	.352	.000	-.01460	6.863	.350	.000	-.01434	7.686	.337	.000	-.01352
1.0	$1.00\phi_k$	-1.944	-1.391	.000	-.00481	-.480	-1.240	.000	-.00327	.676	-1.096	.000	-.00189
	$.75\phi_k$	-2.083	-1.197	.894	-.00198	-1.645	-1.170	.384	-.00163	-1.231	-1.139	.003	-.00127
	$.50\phi_k$	-1.574	-.646	1.903	.00390	-2.790	-.791	1.524	.00258	-3.771	-.926	1.212	.00145
	$.25\phi_k$	1.399	.034	2.396	.00443	.620	-.087	2.675	.00377	-.115	-.203	2.877	.00314
	0	7.831	.327	.000	-.01282	10.136	.287	.000	-.01050	12.184	.251	.000	-.00851
1.4	$1.00\phi_k$	-.818	-1.256	.000	-.00280	.887	-1.052	.000	-.00109	1.461	-.953	.000	-.00024
	$.75\phi_k$	-1.660	-1.167	.511	-.00140	-.988	-1.118	-.097	-.00095	-.495	-1.083	-.334	-.00067
	$.50\phi_k$	-2.475	-.785	1.590	.00225	-3.937	-.979	1.099	.00077	-4.505	-1.079	.788	.00003
	$.25\phi_k$	.559	-.101	2.570	.00345	-.700	-.276	2.900	.00260	-1.669	-.380	3.037	.00210
	0	10.187	.283	.000	-.01004	13.647	-.229	.000	-.00720	15.930	.200	.000	-.00569
1.8	$1.00\phi_k$	-.028	-1.14[illegible]	.000	-.00142	1.189	-.975	.000	-.00022	1.087	-.932	.000	.00016
	$.75\phi_k$	-1.262	-1.134	.224	-.00093	-.485	-1.079	-.263	-.00056	.070	-1.043	-.327	-.00036
	$.50\phi_k$	-3.092	-.893	1.315	.00110	-4.197	-1.065	.807	.00002	-4.220	-1.120	.491	-.00035
	$.25\phi_k$	-.315	-.224	2.689	.00260	-1.918	-.402	2.966	.00189	-3.220	-.496	3.029	.00151
	0	12.585	.244	.000	-.00777	16.614	.195	.000	-.00539	19.302	.173	.000	-.00435
2.2	$1.00\phi_k$	.328	-1.081	.000	-.00068	.961	-.957	.000	.00004	.444	-.948	.000	.00018
	$.75\phi_k$	-.949	-1.106	.071	-.00061	-.110	-1.051	-.260	-.00034	.456	-1.014	-.210	-.00018
	$.50\phi_k$	-3.337	-.953	1.105	.00049	-3.957	-1.094	.593	-.00023	-3.540	-1.119	.263	-.00040
	$.25\phi_k$	-1.102	-.310	2.735	.00199	-3.070	-.492	2.943	.00142	-4.738	-.588	2.952	.00110
	0	14.736	.215	.000	-.00622	19.385	.174	.000	-.00435	22.713	.155	.000	-.00354
2.6	$1.00\phi_k$	.402	-1.047	.000	-.00032	.593	-.961	.000	.00010	-.072	-.970	.000	.00012
	$.75\phi_k$	-.719	-1.082	.011	-.00041	.141	-1.031	-.197	-.00020	.637	-.996	-.089	-.00008
	$.50\phi_k$	-3.325	-.978	.947	.00019	-3.510	-1.096	.430	-.00028	-2.773	-1.102	.104	-.00035
	$.25\phi_k$	-1.796	-.366	2.727	.00156	-4.124	-.559	2.876	.00109	-6.079	-.663	2.840	.00081
	0	16.677	.194	.000	-.00514	22.090	.159	.000	-.00366	26.101	.142	.000	-.00298

* Shear forces are at supports, others are at midspan

Table 1 Internal Forces in a Multiple Cylindrical Shell Due to Dead Load $\phi_k =$ [illegible]°

$T_x = \frac{L^2}{r}\left[p_d \text{ col. (1)}\right]$ $S^* = -L\left[p_d \text{ col (3)}\right]$

$T_\phi = r\left[p_d \text{ col (2)}\right]$ $M_\phi = r^2\left[p_d \text{ col. (4)}\right]$

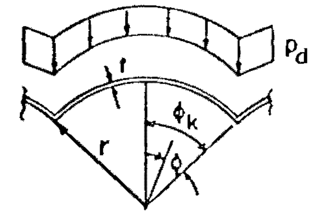

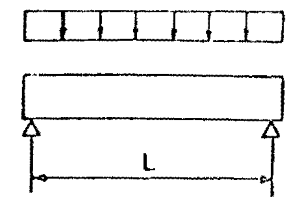

		r/t = 100				r/t = 200				r/t = 300			
r/L	φ	T_x (1)	T_ϕ (2)	S (3)	M_ϕ (4)	T_x (1)	T_ϕ (2)	S (3)	M_ϕ (4)	T_x (1)	T_ϕ (2)	S (3)	M_ϕ (4)
.6	1.00ϕ_k	-2.323	-1.458	.000	-.00718	-1.769	-1.422	.000	-.00658	-1.037	-1.329	.000	-.00542
	.75ϕ_k	-2.015	-1.202	1.072	-.00270	-1.870	-1.201	.831	-.00260	-1.668	-1.186	.583	-.00233
	.50ϕ_k	-.852	-.567	1.976	.00581	-1.307	-.607	1.781	.00527	-1.906	-.692	1.582	.00433
	.25ϕ_k	1.615	.096	2.127	.00573	1.361	.067	2.268	.00553	1.011	-.001	2.404	.00505
	0	5.630	.338	.000	-.01654	6.414	.327	.000	-.01566	7.466	.305	.000	-.01413
1.0	1.00ϕ_k	-1.293	-1.339	.000	-.00476	.207	-1.141	.000	-.00256	1.047	-1.008	.000	-.00111
	.75ϕ_k	-1.681	-1.184	.689	-.00208	-1.193	-1.144	.139	-.00153	-.805	-1.110	-.172	-.00113
	.50ϕ_k	-1.683	-.691	1.668	.00383	-2.941	-.877	1.248	.00199	-3.686	-1.005	.959	.00078
	.25ϕ_k	.983	-.010	2.309	.00473	.111	-.169	2.608	.00374	-.593	-.283	2.773	.00303
	0	7.451	.300	.000	-.01356	9.963	.250	.000	-.01028	11.807	.216	.000	-.00810
1.4	1.00ϕ_k	-.215	-1.181	.000	-.00233	1.037	-.987	.000	-.00053	1.124	-.927	.000	.00011
	.75ϕ_k	-1.244	-1.145	.291	-.00134	-.602	-1.090	-.211	-.00083	-.145	-1.054	-.316	-.00055
	.50ϕ_k	-2.553	-.851	1.337	.00183	-3.666	-1.038	.863	.00027	-3.847	-1.109	.583	-.00031
	.25ϕ_k	.096	-.170	2.490	.00347	-1.147	-.348	2.771	.00250	-2.121	-.442	2.844	.00201
	0	9.917	.250	.000	-.01001	13.132	.199	.000	-.00689	15.196	.175	.000	-.00551
1.8	1.00ϕ_k	.340	-1.081	.000	-.00098	.920	-.948	.000	.00005	.463	-.940	.000	.00025
	.75ϕ_k	-.881	-1.110	.060	-.00084	-.162	-1.053	-.255	-.000[illegible]	.335	-1.016	-.206	-.00026
	.50ϕ_k	-2.982	-.952	1.079	.00070	-3.570	-1.091	.602	-.00026	-3.246	-1.118	.305	-.00049
	.25ϕ_k	-.748	-.294	2.580	.00254	-2.342	-.464	2.781	.00179	-3.701	-.556	2.785	.00140
	0	12.191	.213	.000	-.00758	15.897	.171	.000	-.00523	18.537	.152	.000	-.00425
2.2	1.00ϕ_k	.474	-1.033	.000	-.00039	.514	-.953	.000	.00015	-.138	-.969	.000	.00016
	.75ϕ_k	-.615	-1.083	-.028	-.00053	.141	-1.026	-.185	-.00025	.574	-.991	-.062	-.00010
	.50ϕ_k	-3.041	-.996	.893	.00019	-3.129	-1.098	.408	-.00037	-2.446	-1.099	.110	-.00044
	.25ϕ_k	-1.491	-.374	2.593	.00192	-3.474	-.551	2.722	.00132	-5.149	-.649	2.674	.00098
	0	14.200	.189	.000	-.00605	18.611	.153	.000	-.00424	21.916	.136	.000	-.00345
2.6	1.00ϕ_k	.405	-1.014	.000	-.00014	.141	-.968	.000	.00012	-.465	-.990	.000	.00008
	.75ϕ_k	-.431	-1.062	-.040	-.00034	.301	-1.009	-.096	-.00013	.588	-.980	.047	-.00002
	.50ϕ_k	-2.899	-1.010	.757	-.00001	-2.596	-1.088	.272	-.00035	-1.678	-1.075	-.002	-.00034
	.25ϕ_k	-2.142	-.425	2.559	.00149	-4.465	-.617	2.629	.00098	-6.332	-.720	2.537	.00068
	0	16.045	.170	.000	-.00501	21.274	.140	.000	-.00357	25.213	.125	.000	-.00290

*Shear forces are at supports, others are at midspan

Table 1 Internal Forces in a Multiple Cylindrical Shell Due to Dead Load $\varphi_k = 37.5°$

$T_x = \frac{L^2}{r}\left[p_d \text{ col. (1)}\right]$ $S^{*} = -L\left[p_d \text{ col. (3)}\right]$

$T_\phi = r\left[p_d \text{ col. (2)}\right]$ $M_\phi = r^2\left[p_d \text{ col. (4)}\right]$

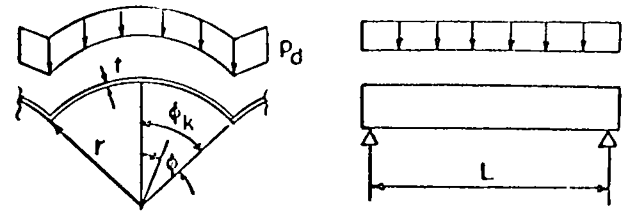

r/L	ϕ	$r/t = 100$				$r/t = 200$				$r/t = 300$			
		T_x (1)	T_ϕ (2)	S (3)	M_ϕ (4)	T_x (1)	T_ϕ (2)	S (3)	M_ϕ (4)	T_x (1)	T_ϕ (2)	S (3)	M_ϕ (4)
.6	$1.00\phi_k$	-1.905	-1.446	.000	-.00787	-1.175	-1.361	.000	-.00654	-.375	-1.234	.000	-.00480
	$.75\phi_k$	-1.728	-1.199	.944	-.00300	-1.531	-1.187	.647	-.00271	-1.298	-1.165	.360	-.00230
	$.50\phi_k$	-.849	-.573	1.803	.00636	-1.448	-.656	1.567	.00524	-2.110	-.771	1.343	.00383
	$.25\phi_k$	1.349	.038	2.028	.00638	1.005	.023	2.197	.00586	.601	-.071	2.351	.00513
	0	5.119	.321	.000	-.01834	6.165	.299	.000	-.01651	7.362	.270	.000	-.01419
1.0	$1.00\phi_k$	-.738	-1.273	.000	-.00441	.602	-1.056	.000	-.00176	1.072	-.951	.000	-.00044
	$.75\phi_k$	-1.341	-1.167	.494	-.00209	-.847	-1.118	-.034	-.00139	-.491	-1.083	-.245	-.00098
	$.50\phi_k$	-1.799	-.747	1.451	.00353	-2.941	-.952	1.023	.00130	-3.405	-1.058	.768	.00019
	$.25\phi_k$	.616	-.065	2.244	.00488	-.277	-.243	2.532	.00363	-.948	-.347	2.646	.00292
	0	7.225	.270	.000	-.01387	9.713	.217	.000	-.00985	11.317	.188	.000	-.00773
1.4	$1.00\phi_k$	.180	-1.109	.000	-.00176	.915	-.949	.000	-.00010	.653	-.926	.000	.00030
	$.75\phi_k$	-.916	-1.122	.122	-.00124	-.319	-1.055	-.235	-.00070	.105	-1.028	-.232	-.00043
	$.50\phi_k$	-2.544	-.913	1.122	.00132	-3.251	-1.073	.682	-.00014	-3.131	-1.115	.421	-.00055
	$.25\phi_k$	-.272	-.238	2.412	.00340	-1.488	-.407	2.626	.00240	-2.505	-.496	2.645	.00190
	0	9.655	.219	.000	-.00976	12.569	.174	.000	-.00664	14.553	.154	.000	-.00537
1.8	$1.00\phi_k$	.482	-1.029	.000	-.00058	.536	-.944	.000	.00020	-.061	-.960	.000	.00024
	$.75\phi_k$	-.597	-1.087	-.036	-.00074	.061	-1.029	-.187	-.00035	.465	-.992	-.069	-.00015
	$.50\phi_k$	-2.768	-.996	.890	.00032	-2.902	-1.097	.442	-.00045	-2.353	-1.101	.167	-.00055
	$.25\phi_k$	-1.074	-.355	2.467	.00244	-2.681	-.518	2.592	.00168	-4.064	-.612	2.548	.00126
	0	11.765	.187	.000	-.00733	15.251	.151	.000	-.00509	17.883	.134	.000	-.00414
2.2	$1.00\phi_k$	.444	-1.001	.000	-.00016	.098	-.962	.000	.00017	-.480	-.990	.000	.00011
	$.75\phi_k$	-.375	-1.062	-.066	-.00045	.277	-1.005	-.083	-.00016	.532	-.975	.066	-.00002
	$.50\phi_k$	-2.675	-1.024	.726	-.00005	-2.353	-1.088	.271	-.00044	-1.531	-1.072	.019	-.00043
	$.25\phi_k$	-1.779	-.429	2.449	.00182	-3.770	-.604	2.505	.00119	-5.375	-.701	2.410	.00083
	0	13.662	.166	.000	-.00587	17.929	.135	.000	-.00413	21.172	.120	.000	-.00335
2.6	$1.00\phi_k$	.294	-.994	.000	-.00002	-.192	-.981	.000	.00011	-.598	-1.005	.000	.00004
	$.75\phi_k$	-.234	-1.043	-.043	-.00027	.338	-.992	.007	-.00007	.404	-.971	.145	.00003
	$.50\phi_k$	-2.446	-1.027	.609	-.00016	-1.802	-1.070	.166	-.00036	-.825	-1.043	-.040	-.00031
	$.25\phi_k$	-2.390	-.477	2.394	.00139	-4.662	-.667	2.393	.00085	-6.368	-.767	2.252	.00055
	0	15.442	.150	.000	-.00488	20.531	.124	.000	-.00347	24.353	.110	.000	-.00281

Shear forces are at supports, others are at midspan

Tab. 1 Internal Forces in a Multiple Cylindrical Shell Due to Dead Load $\phi_k = 40°$

$T_x = \frac{L^2}{r}\left[p_d \text{ col (1)}\right]$ $S^* = -L\left[p_d \text{ col (3)}\right]$

$T_\phi = r\left[p_d \text{ col (2)}\right]$ $M_\phi = r^2\left[p_d \text{ col. (4)}\right]$

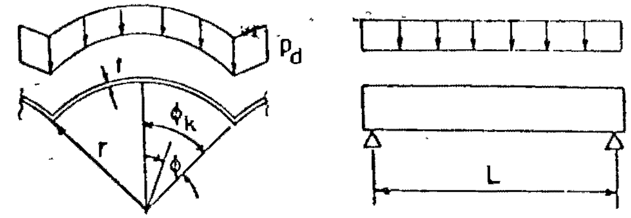

		r/t = 100				r/t = 200				r/t = 300			
r/L	ϕ	T_x (1)	T_ϕ (2)	S (3)	M_ϕ (4)	T_x (1)	T_ϕ (2)	S (3)	M_ϕ (4)	T_x (1)	T_ϕ (2)	S (3)	M_ϕ (4)
.6	$1.00\phi_k$	-1.524	-1.422	.000	-.00834	-.655	-1.284	.000	-.00609	.113	-1.139	.000	-.00386
	$.75\phi_k$	-1.481	-1.192	.819	-.00325	-1.239	-1.169	.466	-.00273	-.994	-1.142	.169	-.00218
	$.50\phi_k$	-.879	-.590	1.644	.00674	-1.595	-.718	1.369	.00488	-2.241	-.851	1.137	.00307
	$.25\phi_k$	1.112	.070	1.949	.00694	.689	-.033	2.145	.00602	.264	-.143	2.301	.00506
	0	4.760	.300	.000	-.01987	6.034	.268	.000	-.01681	7.260	.235	.000	-.01379
1.0	$1.00\phi_k$	-.296	-1.201	.000	-.00381	.744	-.992	.000	-.00099	.882	-.924	.000	.00005
	$.75\phi_k$	-1.058	-1.146	.319	-.00202	-.586	-1.093	-.131	-.00124	-.254	-1.058	-.243	-.00084
	$.50\phi_k$	-1.885	-.808	1.256	.00301	-2.803	-1.008	.848	.00064	-3.007	-1.037	.623	-.00028
	$.25\phi_k$	.304	-.125	2.191	.00490	-.568	-.306	2.440	.00349	-1.231	-.399	2.503	.00281
	0	7.066	.239	.000	-.01379	9.372	.188	.000	-.00939	10.804	.164	.000	-.00744
1.4	$1.00\phi_k$	.385	-1.049	.000	-.00118	.649	-.935	.000	.00018	.191	-.942	.000	.00036
	$.75\phi_k$	-.665	-1.098	.009	-.00112	-.111	-1.041	-.198	-.00058	.269	-1.004	-.119	-.00031
	$.50\phi_k$	-2.444	-.963	.947	.00080	-2.770	-1.087	.539	-.00044	-2.437	-1.105	.292	-.00068
	$.25\phi_k$	-.555	-.299	2.329	.00329	-1.766	-.456	2.473	.00228	-2.824	-.546	2.450	.00176
	0	9.355	.191	.000	-.00941	12.033	.153	.000	-.00643	14.007	.136	.000	-.00523
1.8	$1.00\phi_k$	.467	-.994	.000	-.00026	.159	-.953	.000	.00025	-.404	-.983	.000	.00018
	$.75\phi_k$	-.387	-1.065	-.075	-.00053	.198	-1.007	-.092	-.00025	.469	-.975	.054	-.00006
	$.50\phi_k$	-2.483	-1.024	.739	.00000	-2.262	-1.088	.318	-.00056	-1.586	-1.074	.079	-.00056
	$.25\phi_k$	-1.320	-.408	2.348	.00233	-2.946	-.566	2.405	.00154	-4.293	-.661	2.322	.00110
	0	11.320	.164	.000	-.00708	14.681	.133	.000	-.00495	17.274	.118	.000	-.00401
2.2	$1.00\phi_k$	.319	-.983	.000	.00000	-.210	-.977	.000	.00015	-.599	-1.006	.000	.00005
	$.75\phi_k$	-.206	-1.042	-.050	-.00036	.313	-.988	.019	-.00009	.376	-.966	.159	.00003
	$.50\phi_k$	-2.281	-1.038	.594	-.00023	-1.673	-1.068	.178	-.00046	-.808	-1.040	-.012	-.00039
	$.25\phi_k$	-1.992	-.477	2.306	.00171	-3.953	-.650	2.296	.00105	-5.427	-.745	2.160	.00069
	0	13.143	.146	.000	-.00569	17.303	.119	.000	-.00401	20.442	.106	.000	-.00324
2.6	$1.00\phi_k$	.140	-.986	.000	.00005	-.380	-.994	.000	.00007	-.558	-1.013	.000	.00000
	$.75\phi_k$	-.107	-1.026	-.016	-.00021	.281	-.980	.094	-.00001	.164	-.969	.204	.00005
	$.50\phi_k$	-2.003	-1.032	.495	-.00025	-1.150	-1.045	.108	-.00035	-.202	-1.011	-.023	-.00026
	$.25\phi_k$	-2.558	-.523	2.236	.00128	-4.723	-.709	2.170	.00072	-6.226	-.804	1.985	.00043
	0	14.875	.132	.000	-.00474	19.872	.109	.000	-.00336	23.509	.097	.000	-.00272

*Shear forces are at supports, others are at midspan

Table 1 Internal Forces in a Multiple Cylindrical Shell Due to Dead Load $\phi_k = 45^\circ$

$T_x = \frac{L^2}{r}\left[p_d \ \text{col. (1)} \right]$ $S^* = -L\left[p_d \ \text{col (3)} \right]$

$T_\phi = r \left[p_d \ \text{col (2)} \right]$ $M_\phi = r^2\left[p_d \ \text{col (4)} \right]$

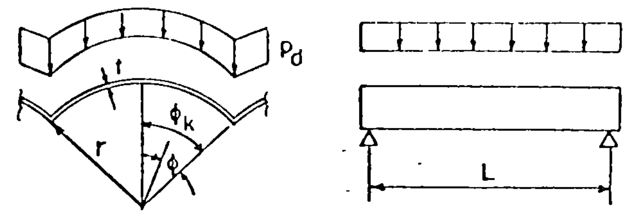

		r/t = 100				r/t = 200				r/t = 300			
r/L	ϕ	T_x (1)	T_ϕ (2)	S (3)	M_ϕ (4)	T_x (1)	T_ϕ (2)	S (3)	M_ϕ (4)	T_x (1)	T_ϕ (2)	S (3)	M_ϕ (4)
.4	1.00ϕ_k	-1.416	-1.446	.000	-.01148	-.959	-1.368	.000	-.00974	-.439	-1.249	.000	-.00734
	.75ϕ_k	-1.244	-1.185	.832	-.00425	-1.125	-1.174	.619	-.00387	-.980	-1.155	.400	-.00331
	.50ϕ_k	-.540	-.546	1.556	.00930	-.915	-.618	1.380	.00787	-1.344	-.726	1.212	.00593
	.25ϕ_k	1.004	.094	1.706	.00889	.797	.038	1.829	.00822	.547	-.046	1.947	.00725
	0	3.456	.278	.000	-.02554	4.094	.261	.000	-.02328	4.847	.237	.000	-.02017
.6	1.00ϕ_k	-.856	-1.335	.000	-.00834	.070	-1.121	.000	-.00423	.545	-.993	.000	-.00175
	.75ϕ_k	-1.078	-1.168	.576	-.00350	-.789	-1.127	.165	-.00249	-.567	-1.095	-.059	-.00181
	.50ϕ_k	-.999	-.654	1.356	.00674	-1.777	-.852	1.038	.00337	-2.207	-.977	.839	.00130
	.25ϕ_k	.701	.007	1.837	.00765	.194	-.156	2.061	.00588	-.197	-.263	2.175	.00473
	0	4.357	.251	.000	-.02168	5.836	.205	.000	-.01601	6.864	.175	.000	-.01245
1.0	1.00ϕ_k	.213	-1.068	.000	-.00224	.559	-.932	.000	.00009	.273	-.929	.000	.00051
	.75ϕ_k	-.644	-1.103	.075	-.00174	-.235	-1.048	-.149	-.00093	.059	-1.011	-.109	-.00055
	.50ϕ_k	-1.892	-.918	.949	.00166	-2.271	-1.062	.608	-.00037	-2.110	-1.090	.410	-.00084
	.25ϕ_k	-.152	-.240	2.083	.00465	-.973	-.398	2.220	.00321	-1.686	-.482	2.210	.00254
	0	6.719	.182	.000	-.01287	8.595	.144	.000	-.00862	9.920	.128	.000	-.00699
1.4	1.00ϕ_k	.396	-.976	.000	-.00025	.049	-.951	.000	.00037	-.413	-.985	.000	.00024
	.75ϕ_k	-.329	-1.056	-.067	-.00085	.131	-.999	-.040	-.00033	.338	-.967	.098	-.00007
	.50ϕ_k	-2.047	-1.021	.694	-.00007	-1.812	-1.073	.336	-.00075	-1.270	-1.057	.138	-.00073
	.25ϕ_k	-.937	-.393	2.142	.00300	-2.180	-.539	2.168	.00197	-3.215	-.632	2.085	.00141
	0	8.668	.146	.000	-.00868	11.123	.119	.000	-.00604	13.049	.105	.000	-.00489
1.8	1.00ϕ_k	.209	-.966	.000	.00013	-.341	-.985	.000	.00018	-.576	-1.013	.000	.00003
	.75ϕ_k	-.126	-1.026	-.040	-.00043	.246	-.974	.094	-.00006	.214	-.959	.213	.00007
	.50ϕ_k	-1.833	-1.041	.525	-.00043	-1.194	-1.045	.174	-.00060	-.470	-1.011	.040	-.00047
	.25ϕ_k	-1.650	-.490	2.106	.00205	-3.232	-.645	2.053	.00121	-4.371	-.735	1.907	.00076
	0	10.464	.127	.000	-.00661	13.662	.103	.000	-.00462	16.071	.091	.000	-.00373
2.2	1.00ϕ_k	.001	-.977	.000	.00013	-.457	-1.004	.000	.00005	-.463	-1.017	.000	-.00002
	.75ϕ_k	-.027	-1.008	.021	-.00021	.169	-.968	.171	.00003	-.042	-.966	.246	.00007
	.50ϕ_k	-1.526	-1.033	.415	-.00042	-.657	-1.015	.111	-.00041	.115	-.975	.050	-.00027
	.25ϕ_k	-2.245	-.554	2.030	.00144	-4.003	-.719	1.912	.00075	-5.134	-.803	1.710	.00041
	0	12.191	.113	.000	-.00533	16.103	.092	.000	-.00373	19.003	.082	.000	-.00301

*Shear forces are at supports, others are at midspan

Table 1 Internal Forces in a Multiple Cylindrical Shell Due to Dead Load $\phi_k = 50°$

$$T_x = \frac{L^2}{r}\left[p_d \quad \text{col. (1)}\right] \qquad S^* = -L\left[p_d \quad \text{col (3)}\right]$$

$$T_\phi = r\left[p_d \quad \text{col. (2)}\right] \qquad M_\phi = r^2\left[p_d \quad \text{col. (4)}\right]$$

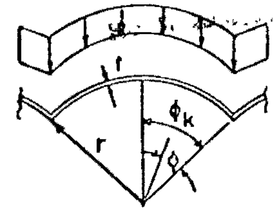

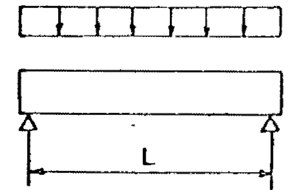

		r/t = 100				r/t = 200				r/t = 300			
r/L	ϕ	T_x (1)	T_ϕ (2)	S (3)	M_ϕ (4)	T_x (1)	T_ϕ (2)	S (3)	M_ϕ (4)	T_x (1)	T_ϕ (2)	S (3)	M_ϕ (4)
.4	$1.00\phi_k$	-.998	-1.399	.000	-.01249	-.404	-1.239	.000	-.00849	.064	-1.097	.000	-.00500
	$.75\phi_k$	-.976	-1.168	.678	-.00474	-.813	-1.142	.393	-.00382	-.661	-1.116	.166	-.00298
	$.50\phi_k$	-.575	-.570	1.352	.01015	-1.066	-.716	1.132	.00690	-1.466	-.847	.961	.00405
	$.25\phi_k$	.747	.065	1.598	.01001	.465	-.050	1.757	.00840	.202	-.155	1.876	.00695
	0	3.061	.237	.000	-.02868	3.922	.206	.000	-.02344	4.682	.178	.000	-.01879
.6	$1.00\phi_k$	-.342	-1.214	.000	-.00700	.341	-1.000	.000	-.00204	.468	-.928	.000	-.00015
	$.75\phi_k$	-.772	-1.135	.354	-.00338	-.497	-1.085	.005	-.00207	-.306	-1.052	-.098	-.00142
	$.50\phi_k$	-1.119	-.747	1.111	.00565	-1.720	-.951	.815	.00153	-1.885	-1.034	.661	-.00012
	$.25\phi_k$	.374	-.082	1.766	.00771	-.115	-.256	1.955	.00545	-.474	-.343	2.006	.00437
	0	4.162	.197	.000	-.02153	5.499	.152	.000	-.01441	6.297	.132	.000	-.01125
1.0	$1.00\phi_k$	.307	-.984	.000	-.00080	.152	-.936	.000	.00053	-.231	-.967	.000	.00046
	$.75\phi_k$	-.388	-1.063	-.016	-.00139	-.031	-1.007	-.041	-.00062	.181	-.973	.069	-.00024
	$.50\phi_k$	-1.684	-.983	.745	.00039	-1.644	-1.058	.453	-.00091	-1.304	-1.051	.278	-.00101
	$.25\phi_k$	-.428	-.326	1.951	.00426	-1.259	-.464	1.990	.00288	-1.990	-.552	1.937	.00214
	0	6.251	.137	.000	-.01169	7.902	.110	.000	-.00802	9.207	.098	.000	-.00650
1.4	$1.00\phi_k$	.159	-.956	.000	.00023	-.334	-.984	.000	.00026	-.534	-1.014	.000	.00005
	$.75\phi_k$	-.139	-1.020	-.017	-.00059	.168	-.968	.123	-.00009	.149	-.953	.231	.00009
	$.50\phi_k$	-1.549	-1.029	.533	-.00059	-1.032	-1.028	.232	-.00079	-.467	-.995	.118	-.00062
	$.25\phi_k$	-1.171	-.460	1.943	.00266	-2.385	-.604	1.886	.00158	-3.262	-.691	1.760	.00101
	0	7.993	.112	.000	-.00802	10.330	.091	.000	-.00559	12.097	.080	.000	-.00449
1.8	$1.00\phi_k$	-.084	-.973	.000	.00022	-.458	-1.009	.000	.00005	-.406	-1.018	.000	-.00003
	$.75\phi_k$	-.016	-.995	.060	-.00023	.088	-.960	.214	.00006	-.126	-.963	.269	.00010
	$.50\phi_k$	-1.228	-1.022	.398	-.00060	-.465	-.989	.154	-.00050	.148	-.949	.127	-.00031
	$.25\phi_k$	-1.819	-.551	1.872	.00172	-3.209	-.698	1.738	.00086	-4.075	-.775	1.547	.00045
	0	9.694	.097	.000	-.00612	12.669	.079	.000	-.00425	14.873	.070	.000	-.00343
2.2	$1.00\phi_k$	-.223	-.989	.000	.00011	-.398	-1.013	.000	-.00001	-.263	-1.012	.000	-.00002
	$.75\phi_k$	.000	-.984	.123	-.00008	-.076	-.965	.243	.00007	-.321	-.975	.259	.00005
	$.50\phi_k$	-.919	-1.002	.328	-.00045	-.066	-.958	.160	-.00029	.463	-.920	.193	-.00013
	$.25\phi_k$	-2.303	-.609	1.777	.00113	-3.727	-.758	1.578	.00046	-4.492	-.826	1.339	.00017
	0	11.317	.087	.000	.00492	14.917	.070	.000	-.00343	17.586	.062	.000	-.00277

* Shear forces are at supports, others are at midspan

Table 1 Internal Forces in a Multiple Cylindrical S[illegible] to Dead Load

$\phi_k = 55^\circ$

$$T_x = \frac{L^2}{r}\left[p_d \ \text{col. (1)}\right] \qquad S^* = -L\left[p_d \ \text{col (3)}\right]$$

$$T_\phi = r\left[p_d \ \text{col (2)}\right] \qquad M_\phi = r^2\left[p_d \ \text{col (4)}\right]$$

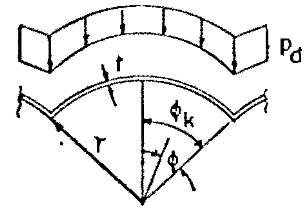

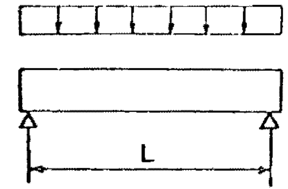

r/L	ϕ	$r/t = 100$ T_x (1)	T_ϕ (2)	S (3)	M_ϕ (4)	$r/t = 200$ T_x (1)	T_ϕ (2)	S (3)	M_ϕ (4)	$r/t = 300$ T_x (1)	T_ϕ (2)	S (3)	M_ϕ (4)
.4	$1.00\phi_k$	-.640	-1.318	.000	-.01218	-.048	-1.109	.000	-.00603	.243	-.991	.000	-.00246
	$.75\phi_k$	-.764	-1.143	.528	-.00490	-.585	-1.106	.215	-.00344	-.449	-1.076	.045	-.00250
	$.50\phi_k$	-.642	-.622	1.174	.00995	-1.143	-.815	.939	.00492	-1.411	-.932	.796	.00194
	$.25\phi_k$	.532	.011	1.525	.01053	.221	-.142	1.697	.00799	-.013	-.240	1.784	.00639
	0	2.847	.191	.000	-.02996	3.772	.154	.000	-.02174	4.395	.130	.000	-.01672
.6	$1.00\phi_k$	-.032	-1.097	.000	-.00479	.298	-.941	.000	-.00037	.192	-.924	.000	.00066
	$.75\phi_k$	-.552	-1.097	.193	-.00298	-.313	-1.047	-.023	-.00165	-.140	-1.013	-.026	-.00105
	$.50\phi_k$	-1.157	-.836	.922	.00383	-1.488	-.997	.679	.00005	-1.463	-1.037	.547	-.00098
	$.25\phi_k$	.140	-.170	1.701	.00728	-.304	-.322	1.820	.00500	-.671	-.396	1.826	.00400
	0	3.977	.147	.000	-.01988	5.054	.113	.000	-.01293	5.755	.100	.000	-.01033
1.0	$1.00\phi_k$	.179	-.951	.000	.00011	-.189	-.966	.000	.00051	-.448	-1.002	.000	.00022
	$.75\phi_k$	-.231	-1.028	.003	-.00105	.055	-.974	.097	-.00031	.131	-.951	.205	.00001
	$.50\phi_k$	-1.369	-1.001	.616	-.00048	-1.086	-1.021	.359	-.00108	-.697	-.995	.232	-.00094
	$.25\phi_k$	-.599	-.384	1.801	.00385	-1.439	-.517	1.775	.00244	-2.098	-.602	1.693	.00166
	0	5.748	.103	.000	-.01063	7.308	-.083	.000	-.00737	8.519	.073	.000	-.00592
1.4	$1.00\phi_k$	-.092	-.966	.000	.00035	-.437	-1.008	.000	.00009	-.407	-1.019	.000	-.00004
	$.75\phi_k$	-.049	-.990	.081	-.00035	.057	-.953	.230	.00007	-.108	-.955	.284	.00013
	$.50\phi_k$	-1.083	-1.006	.435	-.00081	-.483	-.973	.220	-.00068	.006	-.934	.190	-.00044
	$.25\phi_k$	-1.301	-.509	1.751	.00226	-2.378	-.645	1.635	.00116	-3.061	-.721	1.479	.00065
	0	7.382	.084	.000	-.00735	9.540	.068	.000	-.00508	11.136	.060	.000	-.00408
1.8	$1.00\phi_k$	-.264	-.989	.000	.00016	-.376	-1.015	.000	-.00002	-.246	-1.012	.000	-.00003
	$.75\phi_k$	-.013	-.973	.159	-.00008	-.119	-.959	.268	.00009	-.328	-.971	.274	.00006
	$.50\phi_k$	-.752	-.983	.342	-.00060	-.043	-.933	.218	-.00035	.368	-.897	.260	-.00015
	$.25\phi_k$	-1.846	-.592	1.658	.00135	-2.964	-.723	1.467	.00054	-3.552	-.785	1.255	.00020
	0	8.970	.073	.000	-.00558	11.697	.058	.000	-.00397	13.680	.052	.000	-.00311
2.2	$1.00\phi_k$	-.310	-1.001	.000	.00005	-.285	-1.012	.000	-.00002	-.200	-1.007	.000	-.00001
	$.75\phi_k$	-.059	-.969	.202	.00001	-.253	-.968	.265	.00005	-.380	-.979	.250	.00001
	$.50\phi_k$	-.495	-.959	.313	-.00039	.186	-.908	.264	-.00016	.426	-.880	.340	-.00003
	$.25\phi_k$	-2.201	-.642	1.553	.00082	-3.252	-.768	1.302	.00023	-3.664	-.819	1.057	.00000
	0	10.467	.065	.000	-.00447	13.734	.053	.000	-.00311	16.157	.047	.000	-.00251

*Shear forces are at supports, others are at midspan

Table I Internal Forces in a Multiple Cylindrical Shell Due to Dead Load

$\phi_k = 60°$

$$T_x = \frac{L^2}{r}\left[p_d \ \text{col. (1)}\right] \qquad S^{*} = -L\left[p_d \ \text{col (3)}\right]$$

$$T_\phi = r\left[p_d \ \text{col. (2)}\right] \qquad M_\phi = r^2\left[p_d \ \text{col. (4)}\right]$$

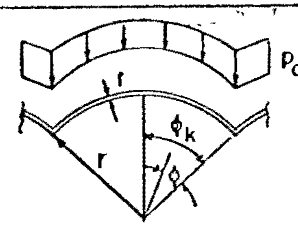

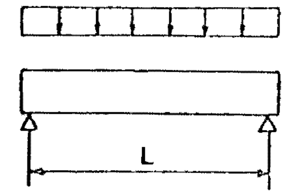

		r/t = 100				r/t = 200				r/t = 300			
r/L	ϕ	T_x (1)	T_ϕ (2)	S (3)	M_ϕ (4)	T_x (1)	T_ϕ (2)	S (3)	M_ϕ (4)	T_x (1)	T_ϕ (2)	S (3)	M_ϕ (4)
.4	$1.00\phi_k$	-.358	-1.218	.000	-.01047	.099	-1.012	.000	-.00336	.205	-.941	.000	-.00054
	$.75\phi_k$	-.597	-1.113	.392	-.00469	-.428	-1.070	.117	-.00291	-.312	-1.040	.026	-.00202
	$.50\phi_k$	-.705	-.691	1.022	.00862	-1.107	-.886	.808	.00272	-1.234	-.968	.697	.00026
	$.25\phi_k$	.358	-.056	1.474	.01038	.064	-.215	1.624	.00731	-.146	-.294	1.670	.00584
	0	2.715	.144	.000	-.02912	3.546	.110	.000	-.01928	4.032	.094	.000	-.01484
.6	$1.00\phi_k$	.083	-1.012	.000	-.00256	.120	-.932	.000	.00056	-.086	-.949	.000	.00083
	$.75\phi_k$	-.404	-1.062	.113	-.00249	-.194	-1.012	.029	-.00125	-.047	-.979	.085	-.00067
	$.50\phi_k$	-1.092	-.896	.793	.00195	-1.192	-.998	.594	-.00088	-1.057	-1.007	.471	-.00135
	$.25\phi_k$	-.009	-.238	1.622	.00564	-.432	-.364	1.677	.00453	-.815	-.437	1.657	.00351
	0	3.723	.106	.000	-.01769	4.617	.083	.000	-.01170	5.291	.073	.000	-.00943
1.0	$1.00\phi_k$	-.010	-.952	.000	.00050	-.360	-.995	.000	.00030	-.440	-1.018	.000	.00002
	$.75\phi_k$	-.138	-.998	.076	-.00073	.036	-.952	.208	-.00005	-.016	-.944	.280	.00015
	$.50\phi_k$	-1.042	-.986	.535	-.00095	-.656	-.970	.325	-.00102	-.290	-.936	.259	-.00075
	$.25\phi_k$	-.708	-.424	1.651	.00338	-1.494	-.553	1.583	.00193	-2.033	-.629	1.481	.00120
	0	5.279	.075	.000	-.00964	6.733	.061	.000	-.00664	7.809	.054	.000	-.00530
1.4	$1.00\phi_k$	-.255	-.985	.000	.00027	-.381	-1.016	.000	-.00002	-.270	-1.014	.000	-.00005
	$.75\phi_k$	-.038	-.967	.176	-.00014	-.103	-.951	.284	.00012	-.284	-.963	.295	.00010
	$.50\phi_k$	-.708	-.965	.391	-.00082	-.144	-.918	.274	-.00050	.210	-.881	.301	-.00025
	$.25\phi_k$	-1.333	-.541	1.575	.00181	-2.213	-.662	1.418	.00079	-2.703	-.725	1.249	.00034
	0	6.804	.062	.000	-.00662	8.739	.050	.000	-.00455	10.176	.044	.000	-.00365
1.8	$1.00\phi_k$	-.323	-1.003	.000	.00007	-.276	-1.012	.000	-.00003	-.202	-1.006	.000	-.00001
	$.75\phi_k$	-.074	-.960	.232	.00002	-.261	-.963	.285	.00007	-.364	-.974	.268	.00002
	$.50\phi_k$	-.420	-.937	.344	-.00051	.136	-.884	.318	-.00020	.322	-.858	.389	-.00004
	$.25\phi_k$	-1.753	-.613	1.470	.00099	-2.579	-.722	1.244	.00028	-2.906	-.770	1.035	.00001
	0	8.252	.053	.000	-.00500	10.671	.043	.000	-.00345	12.469	.038	.000	-.00277
2.2	$1.00\phi_k$	-.309	-1.008	.000	.00001	-.231	-1.008	.000	-.00001	-.222	-1.005	.000	.00000
	$.75\phi_k$	-.143	-.962	.251	.00004	-.315	-.971	.269	.00002	-.324	-.976	.248	-.00001
	$.50\phi_k$	-.234	-.915	.347	-.00029	.207	-.869	.375	-.00006	.216	-.854	.455	.00003
	$.25\phi_k$	-1.986	-.653	1.361	.00055	-2.675	-.753	1.090	.00005	-2.787	-.787	.862	-.00011
	0	9.616	.047	.000	-.00399	12.536	.038	.000	-.00277	14.699	.034	.000	-.00223

*Shear forces are at supports, others are at midspan

Table 2 - Calculation of forces in a simply supported interior cylindrical shell

Given:

$t = 4$ in.
$r = 45$ ft.
$L = 50$ ft.

$\phi_k = 26.4°$
$p_u = 30$ psf
$p_d = 50$ psf

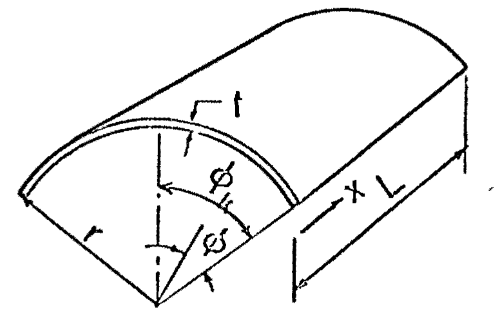

Force	T_x		T_ϕ		S		M_ϕ	
Multiplier	$(L^2/r)p_d = 4390$		$(r)p_d = 3560$		$-(L)p_d = -3950$		$(r^2)p_d = 160{,}000$	
ϕ	Constant	Force (lb./ft.)	Constant	Force (lb./ft.)	Constant	Force (lb./ft.)	Constant	Force (ft.-lb./ft.)
ϕ_k (crown)	-3.947	-17,300	-1.441	-5130	0	0	-.00385	-620
$.75\phi_k$	-3.455	-15,200	-1.204	-4290	1.415	-5590	-.00146	-230
$.50\phi_k$	-1.551	-6,800	-.595	-2120	2.571	-10,160	.00321	510
$.25\phi_k$	2.693	11,800	.083	300	2.759	-10,900	.00324	520
0 (valley)	10.111	44,400	.375	1340	0	0	-.00970	-1550

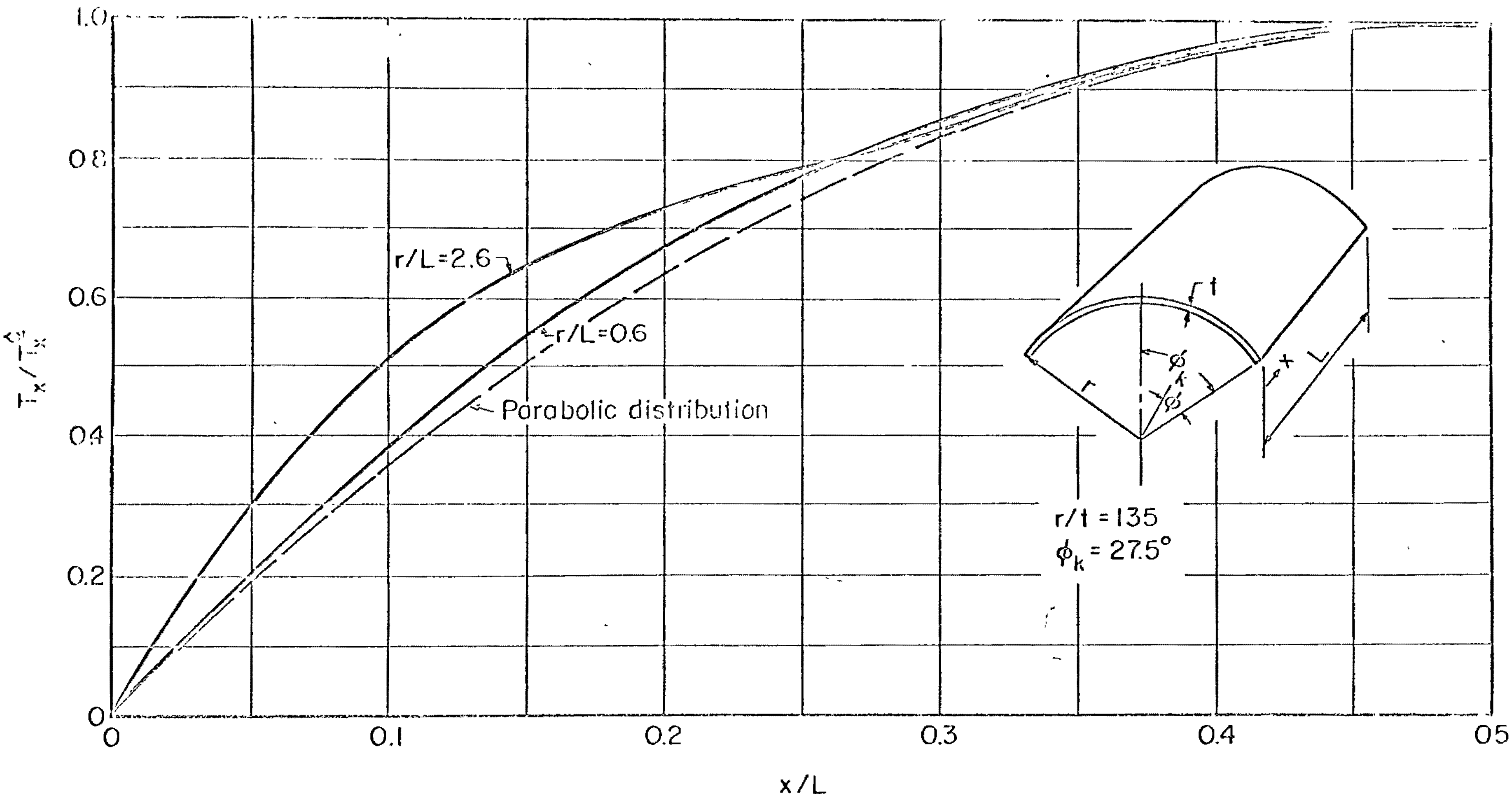

Fig. 1 - Longitudinal distribution of T_x at valley

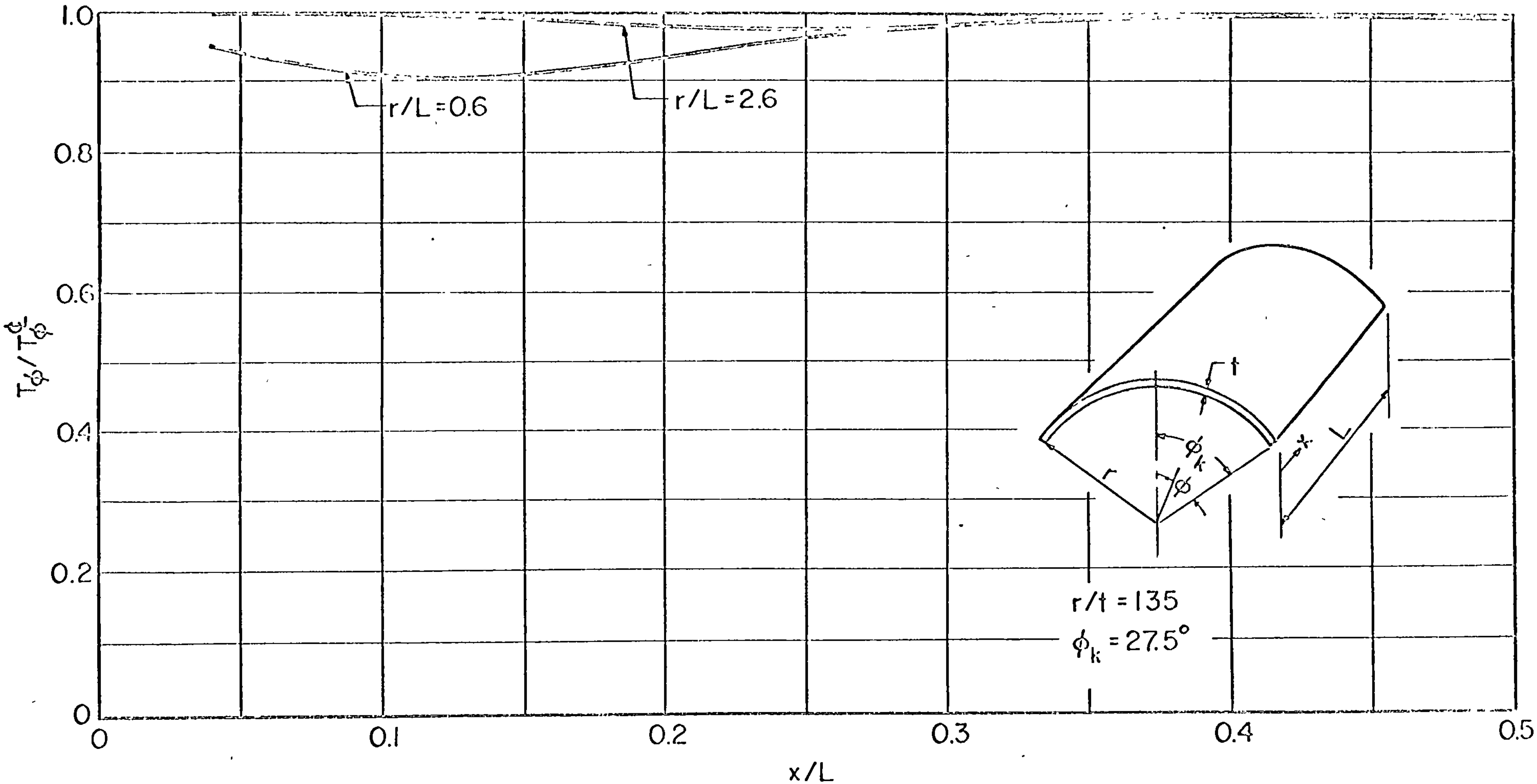

Fig.2 - Longitudinal distribution of T_ϕ at crown

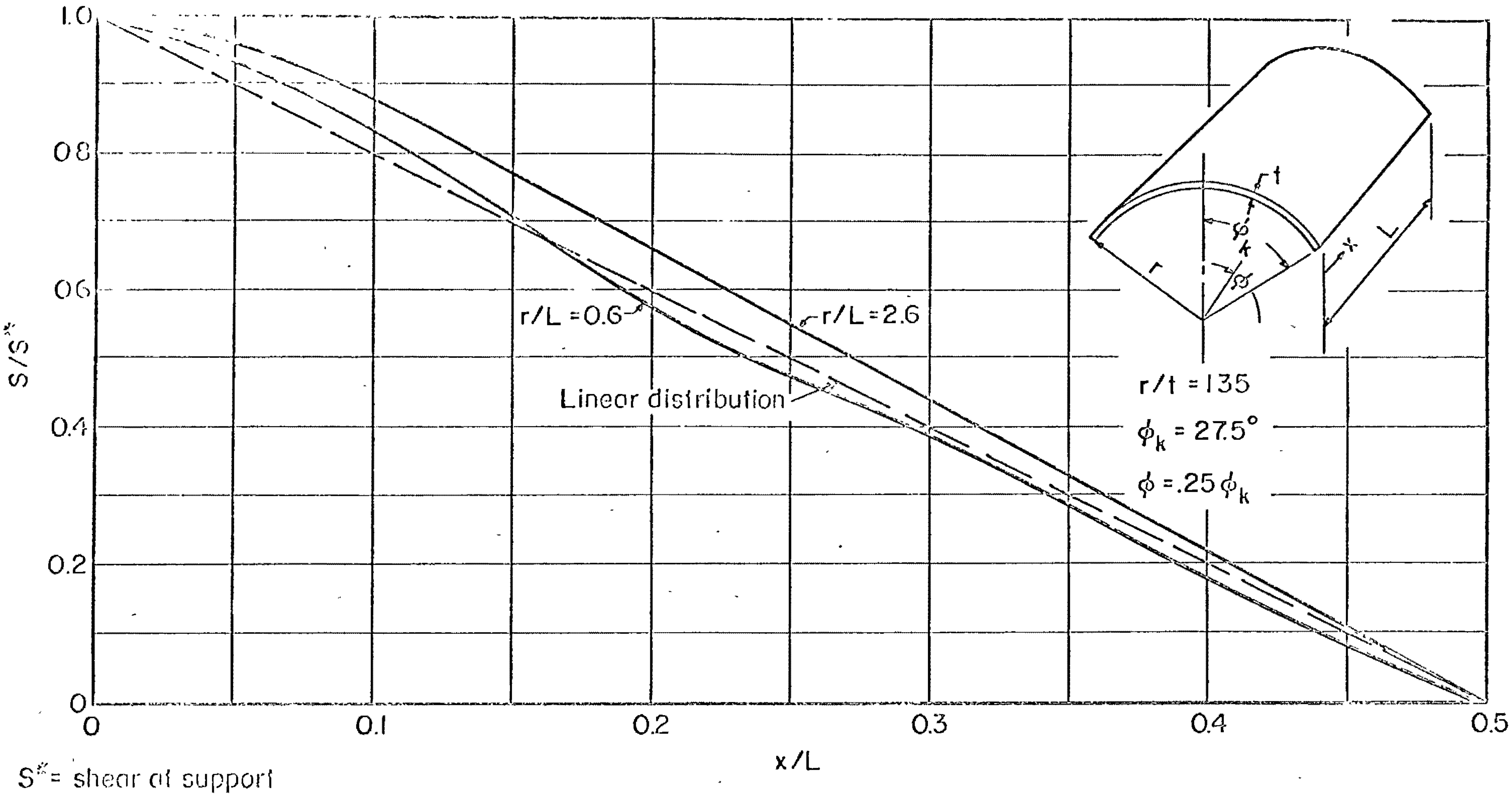

Fig. 3 Longitudinal distribution of shear at $\phi = 0.25\,\phi_k$

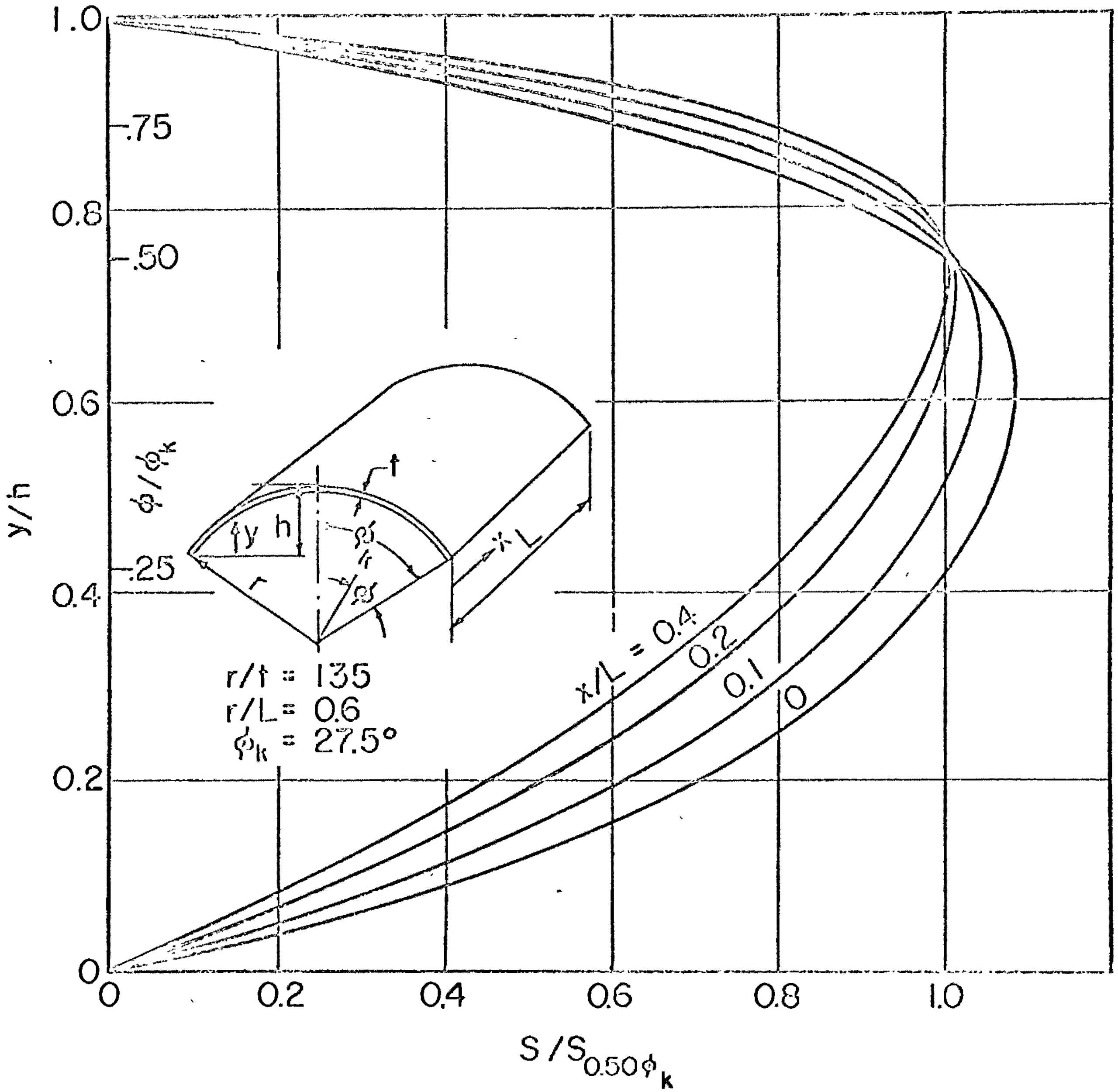

Fig. 4 Relative distribution of shear

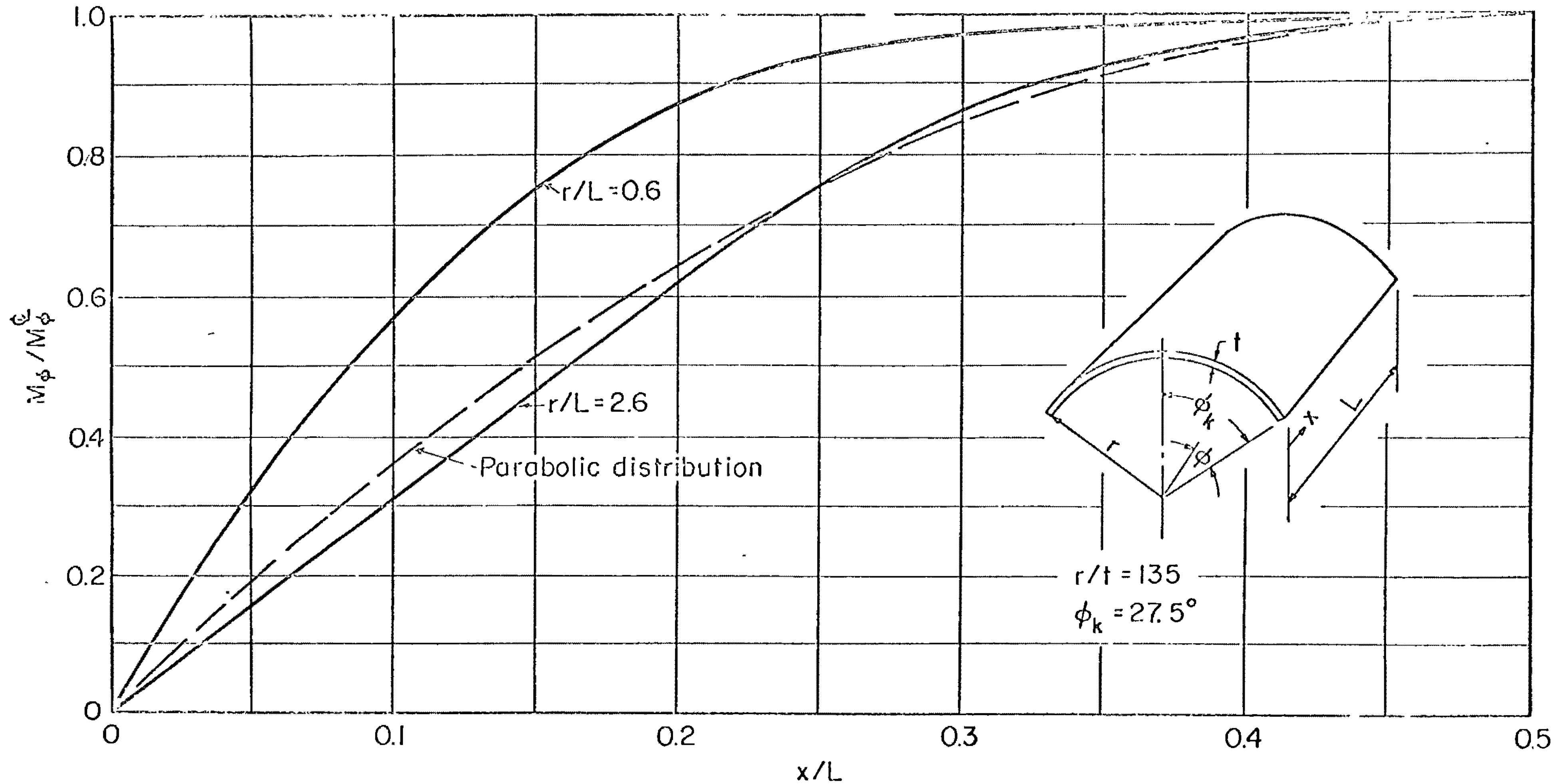

Fig.6 - Longitudinal distribution of transverse moment at valley

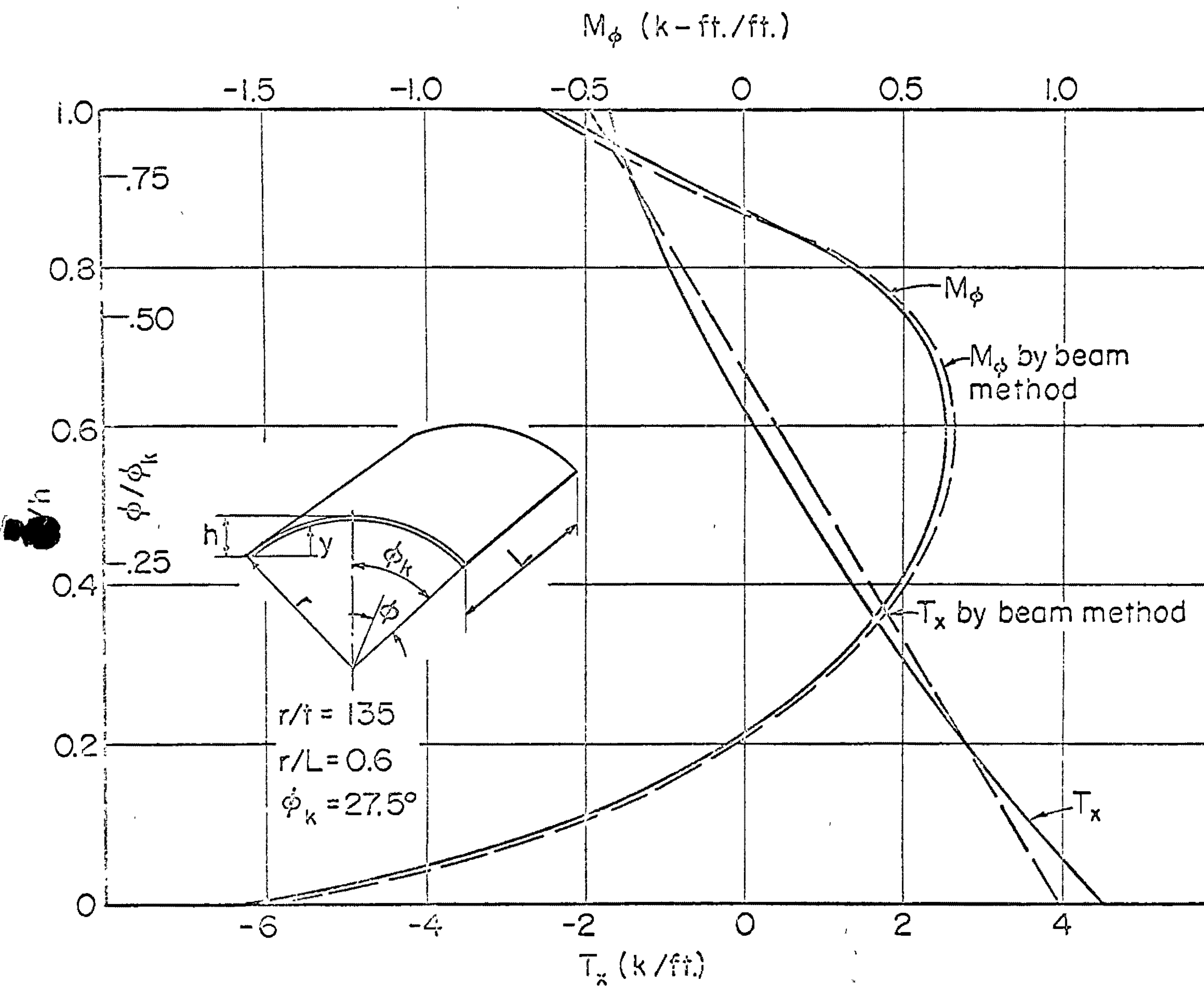

Fig. 7 Transverse distribution of T_x and M_ϕ for interior shell example

CUBIERTAS CON NERVADURAS SUJETAS A ESFUERZOS AXIALES DE COMPRESION

por

José Flavio Madrigal R.*

SINOPSIS

Estudio hecho sobre algunos viejos principios constructivos, traídos a Norteámerica por el Ingeniero Paul Chelazzi, quien declara haberlos adquirido en China.

En el presente trabajo se analiza ese pensamiento y se aplica a la solución de un problema práctico.

* Ingeniero Consultor y Contratista de Obras de Ingeniería Civil, - San Luis Potosi, S.L.P., México.

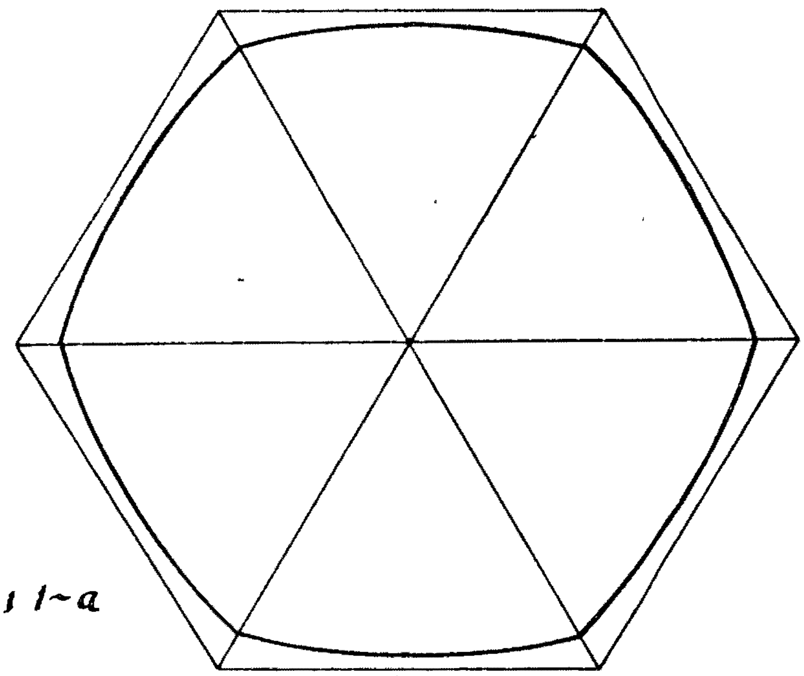

Fig: 1~a

Cubiertas con nervaduras sujetas a esfuerzos de compresión.

El estudio de una cubierta semejante a la ilustrada, cuyas caracterizticas escenciales son la ligereza estructural, la economía en la ejecución de la obra y, sobre todo, la belleza del recinto encerrado bajo una cubierta de esta clase.

Indudablemente que este conjunto de circunstancias, a cual más de atractivas, hace de una techumbre de esta índole

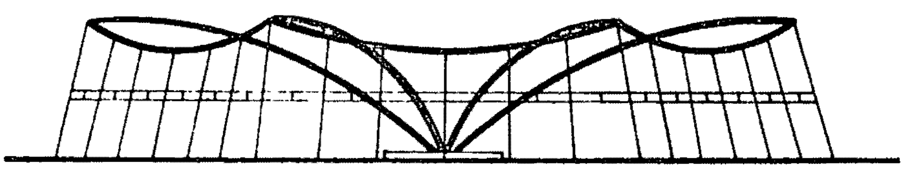

Fig: 1~b

motivo de especial interés.

Respecto a la ligereza estructural ha de decirse que la cuantía del material que interviene en su construcción es mínima en virtud de que las secciones de los elémentos constructivos se hallan siempre trabajando a esfuerzos axiales simples, ya sea de compresión o de tensión.

No existen esfuerzos de flexión y, como queda dicho, siendo axial la acción del--

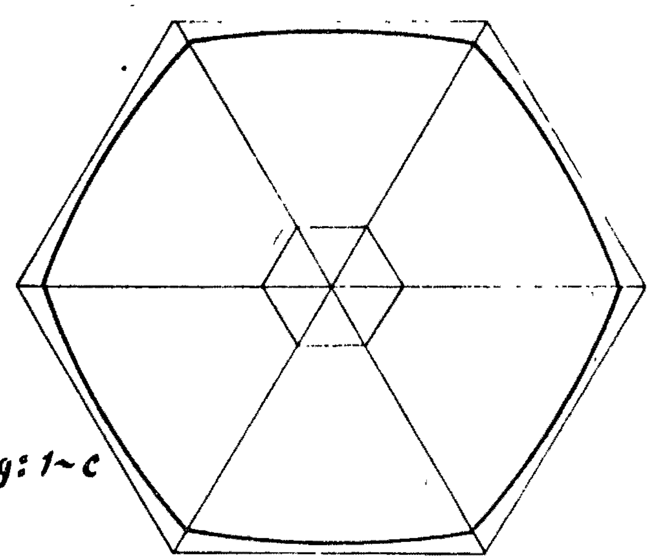

Fig: 1~c

Fig: 1~d

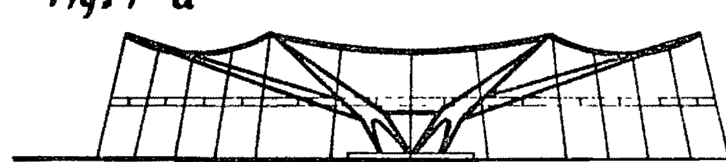

esfuerzo, la distribución de éste es uniforme en toda sección del -- eléménto constructivo.

En una pieza de concreto reforzado, pongamos por caso, solamen-- te una porción de la sección, y no la mayor, trabaja realmente so-- portando la compresión; el resto de dicha sección cumple otros fi-- nes: transmitir el esfuerzo razante, soportar el esfuerzo cortante, Etc.; pero la porción activa para tomar la compresión se reduce a-- un triángulo-esto considerado dentro de la hipotésis de Navier-, -- cuya altura es, como sabemos, Kd. Si asignamos una fatiga de tra--- bajo al acero igual a f_s y otra de f_c para el concreto, se tendrá -

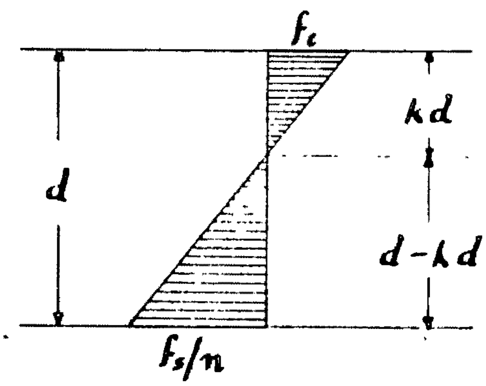

Fig: 2

y si hacemos , d= 60 Cms.

f_s= 1800 Kg/Cm2.

f_c= 60 Kg/Cm2.

n = 10 , se tiene.

$$Kd= \frac{600}{180} (60-Kd)= 0.333x60-0.333\ Kd.$$

$$1.333\ Kd = 20\ .^{\circ}.\ Kd= \frac{20}{1.333} \doteq 15\ Cms.$$

lo cual pone de manifiesto que de la sección total sólo interviene 1/3 para tomar el esfuerzo de compresión. Ahora bién, como el es-- fuerzo de compresión no se haya distribuido uniformemente en esta zona de la sección sino que, por el contrario, trabaja a un máximo de 60 Kg/Cm2. y un mínimo igual a cero en la fibra neutra, el pro-medio será, pues, de 30 Kg/Cm2. lo cual, desde este punto de vista, convierte a la sección en una cuestión antieconómica.

Si en lugar de una pieza de concreto tomamos una de madera- o de fierro, es decir una pieza homogenea y la sometemos a un- momento flector la situación mejora un poco; pero no tanto que pudiera decirse haber encontrado una solución satisfactoria -- para el buen empleo del material. La razón es la siguiente:

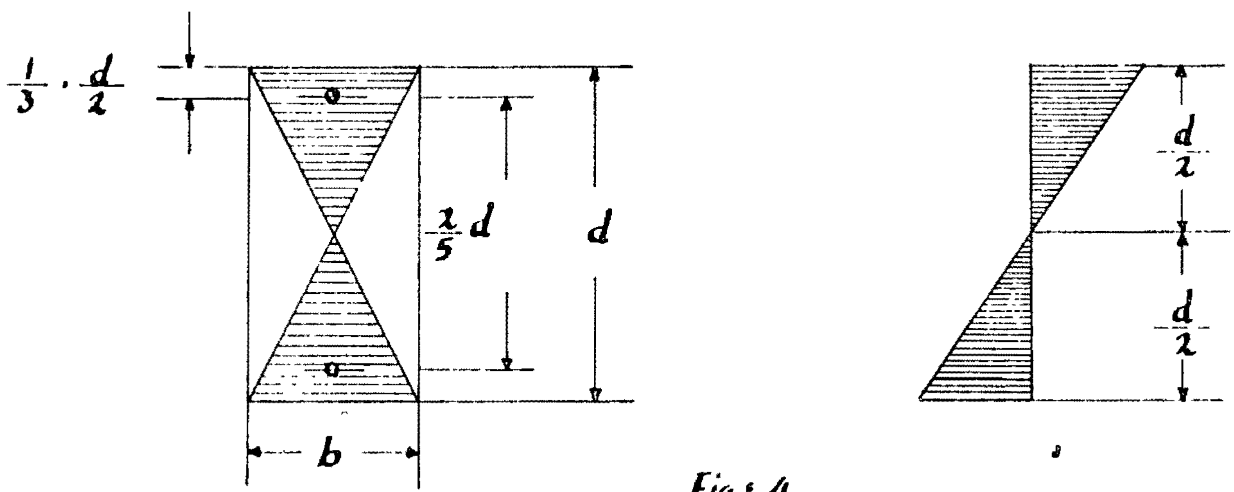

Fig: 4

El area efectiva de trabajo puede estimarse como:

$bd - 2\left(\frac{1}{2}d \cdot \frac{b}{2}\right) = bd - \frac{bd}{2} = \frac{bd}{2}$, es decir solamente el-- 50 por ciento de la sección total. Esto es una consecuencia de - la ley de variación de esfuerzos supuestas: Máximos esfuerzos en las fibras extremas y valor nulo en la fibra neutra, variando -- linealmente.

Estas desventajas que se presentan cuando la pieza se hace -- trabajar a flexión, desaparecen del todo cuando se suprime por - algún medio el momento flector que origina los esfuerzos de signos contrarios.

Tal procedimiento es factible en algunos casos. El objeto del presente trabajo es mostrar el camino a seguir para alcanzar ese fin.

Antes de exponer los simples principios en que el procedi --- miento se basa, quiero decir algo sobre la economía que se obtie ne utilizando este tipo de cubiertas.

La cimbra, empleada para cascarones de concreto, cualquiera -- que sea el tipo de éstos, resulta cara en función del volúmen de concreto empleado. La cimbra utilizada para soportar el concre-- to de una cubierta como la propuesta, es barata no porque sea de otra clase, sino porque se le usa en pequeñas cantidades, puesto- que el colado del concreto se hace o se puede hacer por gajos -- procurando, naturalmente, que estos gajos ocupen posiciónes --- opuestas para conseguir el equilibrio de la estructura en eje-- cución. Puede, inclusive, llegarse hasta suprimir del todo-prac- ticamente-la cimbra si el colado del concreto se hace sobre una- capa de metal desplegado, el cual descansa sobre el refuerzo de- las varillas empleadas en todos los casos para soportar los cam- bios operados en la masa de concreto, por concepto del fraguado- y la variación de temperatura. Resumiendo: La cimbra, mejor di-- cho, su costo puede reducirse a su mínima expresión.

Para concluír con el último punto enunciado en el primer pá-- rrafo de este escrito, quiero decir que si bien la belleza de -- las cosas, como la de las personas, es algo convencional y que - muchas ocasiones es un concepto cambiante con la latitud o con - el tiempo (con la latitud: en Africa estiman como muy hermoso el rostro de un negro que muestra dibujos creados bajo su piel con- trozos pequeños de bambú; a nuestra vista no solo es feo sino -- repugnante; respecto al tiempo: diré que cosas hay que concide-- randose ahora bonitas, pasado un lapso nos resultan feas y desa- gradables a nuestros ojos, por ejemplo el modelo pasado de un -- automovil, el dibujo de una alfombra o el largo anticuado de la- falda de la señora) y que, precisamente, por ser la belleza o la idea que de ella tenemos, un concepto algo convencional adquirido por educación-es decir por condicionamiento del gusto del indi-- viduo, esta cubierta debe, tiene que ser hermosa por la simple - razón expuesta del gusto del hombre acostumbrado o entrenado en- la búsqueda de la expresión materializada de un proceso matemá-- tico, creado por el ingeniero o el arquitecto para encerrar un -- volumen cuyas dimensiones son tales, que por la ausencia casi --- absoluta de soportes hacen de ese volúmen, un algo que alardea de audacia, pregonando la capacidad técnica de quien supo y pudo -- concebir y, por añadidura se atrevió a ejecutar la obra... y en- el atrevimiento, en la audacia existe siempre la belleza del --- arrojo.

Ahora especularemos sobre el principio que sirve de base- al método empleado en el estudio de las nervaduras que sopor- tan la membrana del techo ilustrado en la figura # 1. Estas-- nervaduras que bien pudieran, aparentemente, tomarse como --- cantiliveres y, por lo tanto, como piezas trabajando a flexión, no son otra cosa que simples tornapuntas trabajando a un esfuer zo axial de compresión.

En la figura siguiente se tiene una porción de uno de estos postes, en el que se ha practicado un orificio por el cual --- pasa uno de los cables de los gajos contigüos de la estructura.

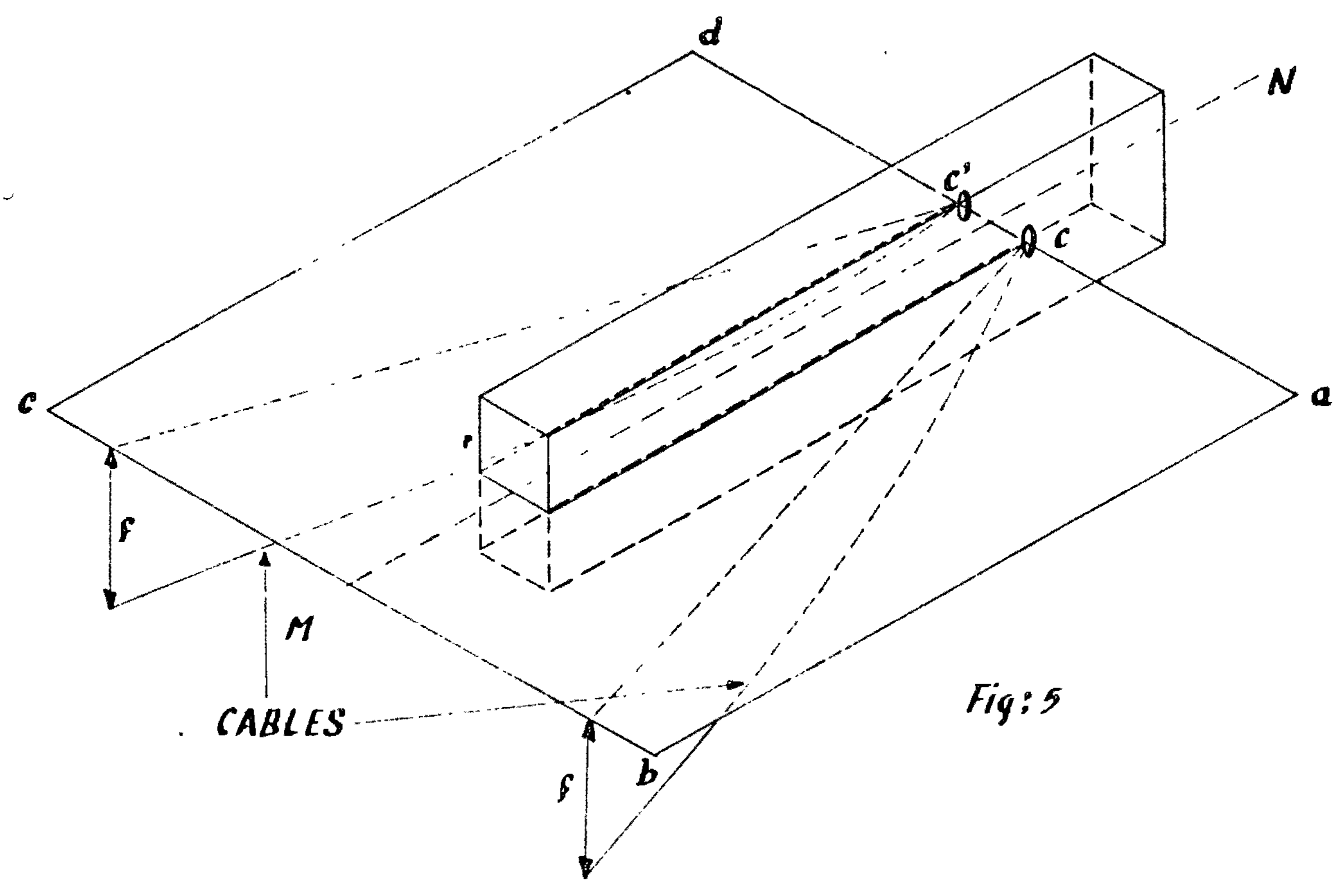

Fig: 5

El orificio mencionado pasa a la altura del eje simétrico-- de la pieza, el cual se haya contenido en el plano a-b-c-d- -- tal y como indica la figura. Los cables pasan por debajo del -- plano indicado, con excepción hecha de los puntos C y C' que se encuentran en el plano mismo.

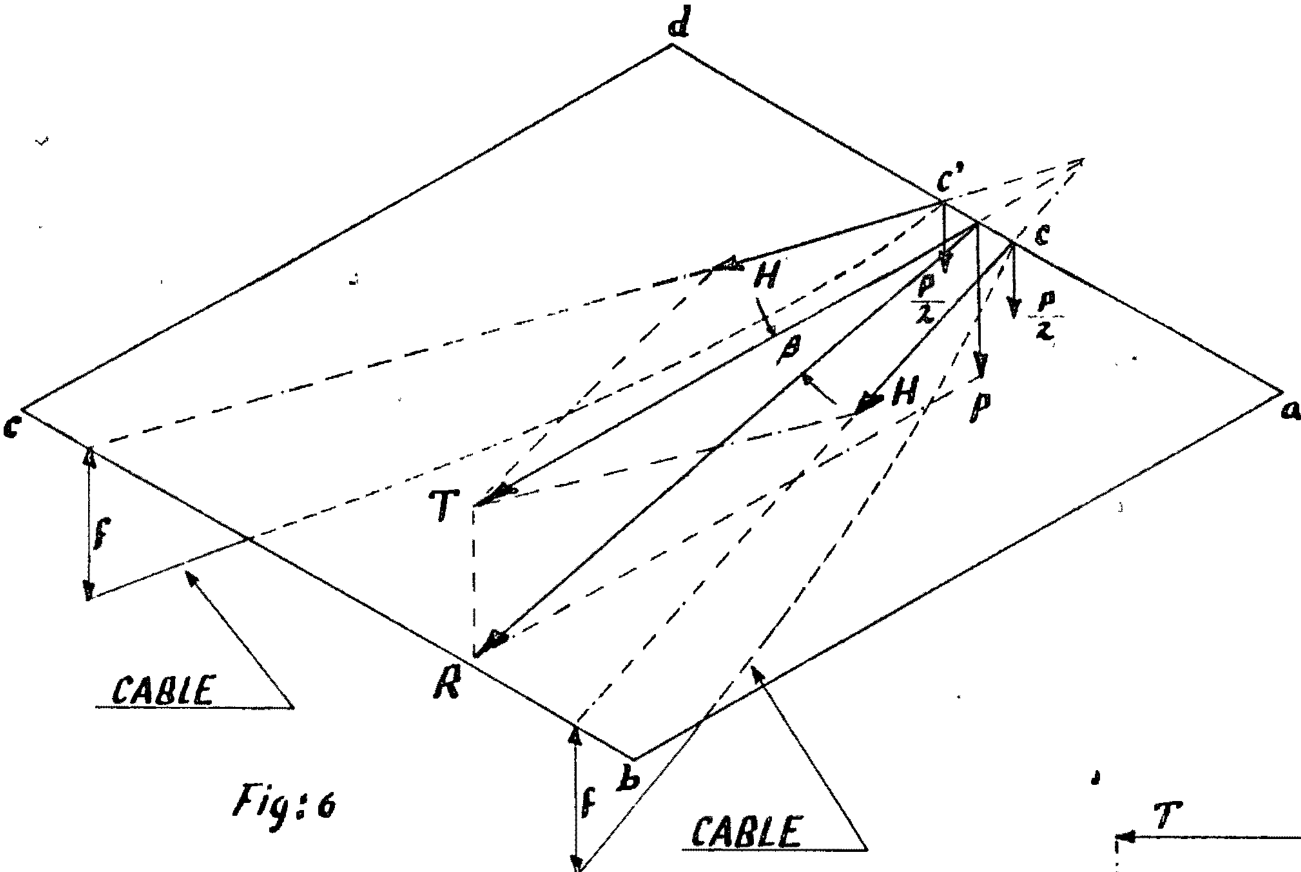

Fig: 6

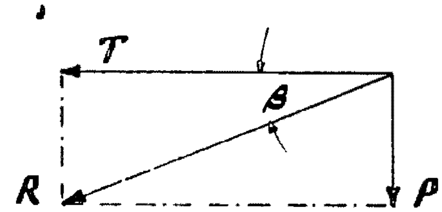

Fig: 7

En la última figura se advierte que cuando el eje de la pieza coincide con la dirección de la resultante R, la fatiga del material es uniforme en toda la sección de la pieza; por lo que, una-vez determinada la posición de la nervadura-por razones de necesidad-basta con ajustar el valor de H para hacer variar el ángulo de manera que coincida con el eje de la tornapunta.

Este sencillo artificio nos permite resolver estructuras semejantes a la de la figura # 1. La planta del salón puede ser muy variada e igualmente variada puede ser la curva del eje de la nervadura. La parábola, la elipse, la cisoide, la cicloide y la cardioide, entre otras curvas, pueden emplearse para la curva de las piezas utilizadas como nervaduras.

Supóngase que se ha elegido para eje de la pieza una parábola de expresión $Y^2 = 4px$, la cual necesariamente ha de pasar por el origen y por el punto. p(10.5,5.5)

$$Y^2 = 30.25 = 4 \cdot p \cdot 10.50 = 42\,p$$

$$\therefore\ p = \frac{30.25}{42} = 0.72 \quad \text{por lo que}$$

$$Y^2 = 2.88X \quad \therefore\ Y = 1.7\sqrt{X.}$$

Si hemos de tèner en cuenta de que la ordenada de un punto - distante del origen 2 Mts., aproximadamente, ha de ser superior a- 2.25 para evitar que la nervadura en ese punto seleccionado ---- constituya un estorbo para el público que transita por ese sitio, se tendrá :

$X = 2$ Mts.

$Y = 1.7 \cdot \sqrt{2} = 1.7 \times 1.4142 \doteq 2.4$ Mts. lo cual es -- satisfactorio para facilitar el tránsito en la zona próxima a -- los arranques de las nerva duras. Ahora, bién, si por razones de estética se -- hubiera elegido como eje - de la pieza una cicloide - o una cisoide; esta última nos daría una ordenada --- igual a $Y = x\sqrt{\frac{x}{2a-x}}$. En- la que, aceptando para x - un valor de 2.50 Mts., se- tiene :

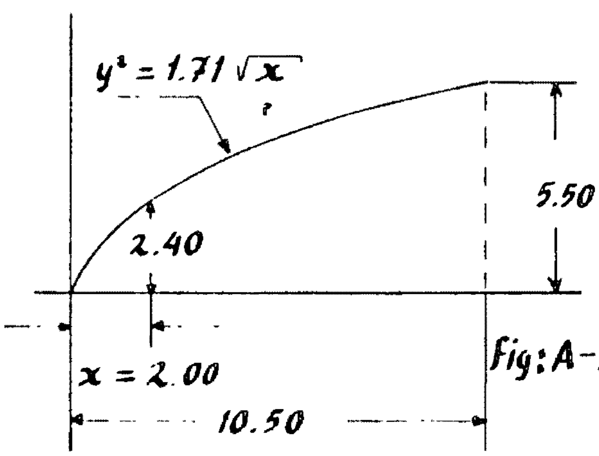

Fig:A-A

$$Y = 2.5\sqrt{\frac{2.5}{2 \times 5.5 - 2.5}} = \frac{2.5 \times 1.58}{\sqrt{8.5}} \doteq 2.06 \text{ Mt.}$$

Este valor es aceptable si consideramos que el arranque de la --- curva puede tener lugar sobre un soporte auxiliar que levante -- medio metro-aproximadamente-sobre el nivel de piso terminado. Si esto es así procedemos al cálculo de la cubierta.

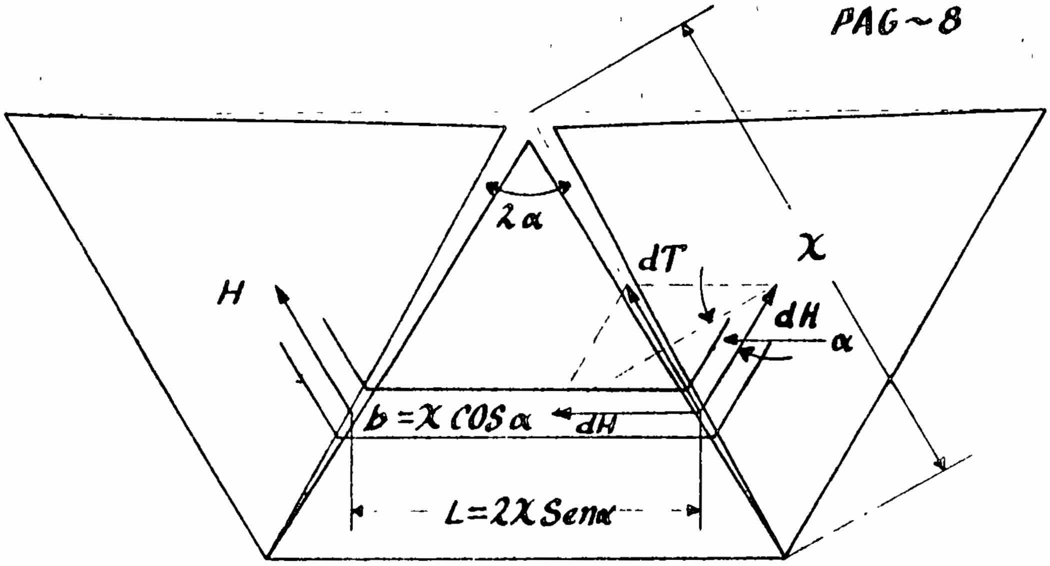

Fig: 8

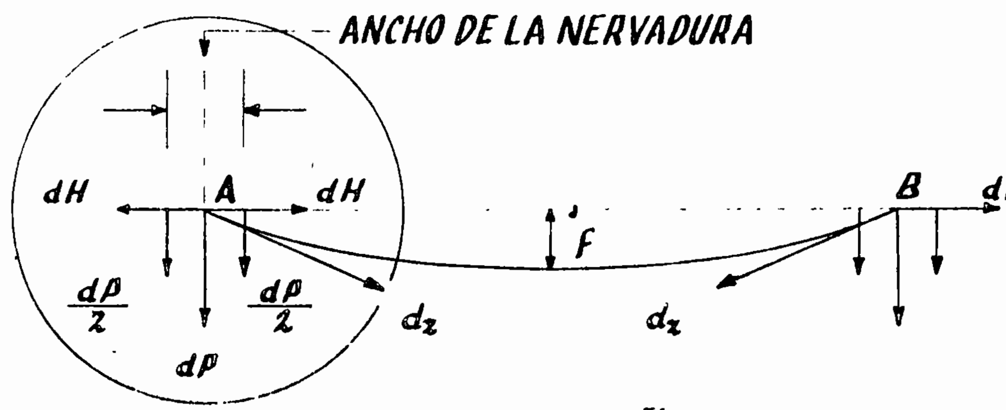

Fig: 9

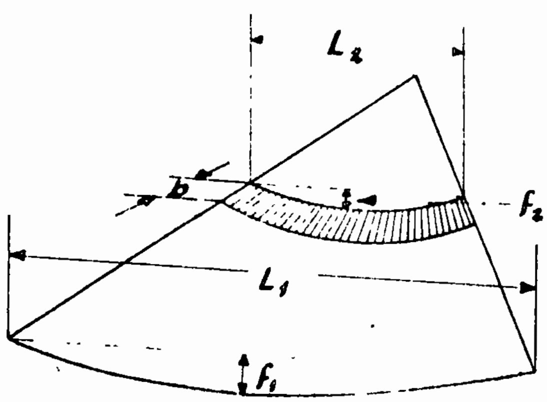

Fig: 10

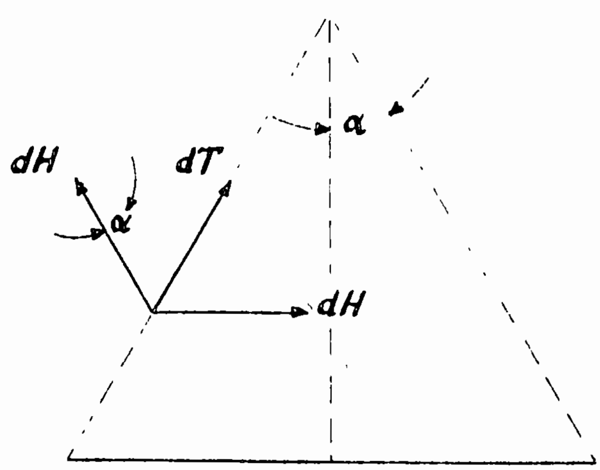

Fig: 11

De la figura # 8, se tiene:

$$L = 2x\ SEN\alpha \qquad b = dx\ COS\alpha \qquad dH = \frac{\omega' L^2}{8f}$$

De la figura # 10, se tiene:

$$C = \frac{L}{f}$$

$\omega' = \omega b = \omega \cdot dx \cdot COS\alpha$, por lo que

$$dH = \frac{\omega dx \cdot COS\alpha}{8} \cdot \frac{L}{f} \cdot L = \frac{\omega dx \cdot COS\alpha}{8} \times c \cdot 2x\ SEN\alpha =$$

$$= \frac{\omega}{4}\ SEN\alpha \cdot COS\alpha \cdot c x dx$$

$$dT = 2dH\ SEN\alpha = 2\frac{\omega}{4}\ SEN\alpha \cdot COS\alpha \cdot cx \cdot dx \cdot SEN\alpha =$$

$= \frac{\omega}{2}\ SEN^2\alpha \cdot COS\alpha \cdot cx\ dx$, en la figura #9, se tiene:

$$dP = 2 \cdot \frac{dP}{2} = 2 \times \frac{1}{2}\ \omega' L = \omega' L = \omega \cdot dx \cdot COS\alpha \times 2x\ SEN\alpha =$$

$$= 2\omega\ SEN\alpha \cdot COS\alpha \cdot x dx$$

recordando, según figura #7, que

$TAN\beta = \frac{P}{T}$ ó $\frac{dP}{dT}$ que es lo mismo, se tiene:

$$\frac{dP}{dT} = \frac{2\omega\ SEN\alpha \cdot COS\alpha \cdot x\ dx}{\frac{\omega}{2}\ \omega\ SEN^2\alpha\ COS\alpha \cdot c \cdot x dx} = \frac{4}{c\ SEN\alpha}$$, y como

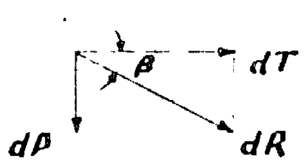

$$\frac{dP}{dR} = SEN\beta \qquad dR = \frac{dP}{SEN\beta} =$$

$$= \frac{2\omega \cdot SEN\alpha \cdot COS\alpha}{SEN\beta} \cdot x\ dx = dR$$; pero

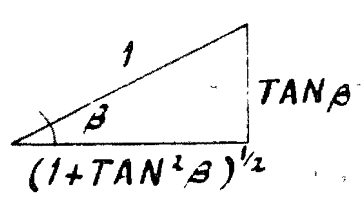

$$SEN\beta = \frac{TAN\beta}{\sqrt{1+TAN^2\beta}} = \frac{4/c\ SEN\alpha}{(1+16/c^2\ SEN^2\alpha)^{1/2}} =$$

$$= \frac{4}{c\ SEN\alpha\ (1+16/c^2\ SEN^2\alpha)^{1/2}}$$

$$dR = \frac{2\omega\, SEN\alpha \cdot COS\alpha \cdot x\,dx}{\dfrac{4/c\ SEN\alpha}{(1+16/c^2\ SEN^2\alpha)^{1/2}}} = \frac{1}{2}\,\omega c\ SEN^2\alpha \cdot COS\alpha \left(1+\frac{16}{c^2\,SEN^2\alpha}\right)x\,dx$$

$$R = \int_0^L \frac{1}{2}\,\omega c\ SEN^2\alpha \cdot COS\alpha \left(1+\frac{16}{c^2\,SEN^2\alpha}\right)x\,dx$$

Esta expresión dá el valor de la resultante que comprime la sección - de la tornapunta en un punto x cualquiera; pero su solución exacta requiere de un trabajo más laborioso que si se resuelve mediante un procedimiento apróximado, por ejemplo, el de diferencias finitas u otro semejante -- que nos dé un resultado prácticamente aprovechable.

Antes de seguir adelante debe hacerse notar un punto de capital importancia. Este punto es el siguiente:

En la página #9 se estableció la igualdad siguiente $C = \frac{L}{f}$, es de-- cir, que la relación entre la luz, L, y la flecha, f, era constante, lo - cual es cierto para la figura #10, pués esta relación es constante para - cualquier valor de x y si esto ocurre, entonces dR actuará de tal manera- que su inclinación irá en aumento a medida que el punto en que se encuentre aplicada esté más próximo al origen. Bastará, pues, con ajustar, las- direcciones de las fuerzas elementales dR al eje de la nervadura para que ésta se encuentre trabajando exclusivamente a compresión axial; para ---- ajustar, para hacer coincidir el polígono de fuerzas con el eje mencionado es menester conservar en toda sección de la nervadura la siguiente --- igualdad $C = \frac{L}{f}$

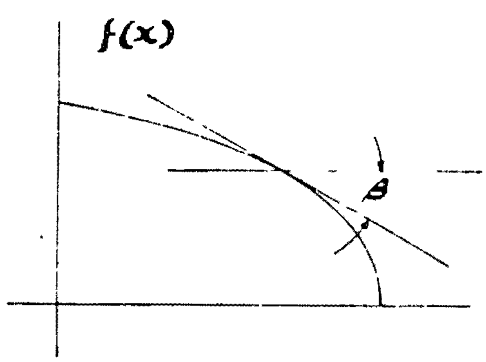

$$f'(x) = TAN\beta = \frac{4}{c}\,SEN\alpha$$

$$\therefore\ C = \frac{4}{SEN\alpha \cdot TAN\beta}$$

ó bien : $\quad \frac{1}{C} = \frac{1}{4}\ SEN\alpha\ TAN\beta$

como inversa de C, según lo dicho en la página # . Esta última-- fórmula nos permite hacer el ajuste buscado a fín de que coincidan la curva de presiones con el eje de la nervadura.

$$\frac{1}{c} \quad \frac{f}{L} = \frac{1}{4}\ SEN\,\alpha \ \ TAN\beta = \frac{1}{4}\ SEN\alpha \cdot f'(x)$$

o lo que es lo mismo: la primera derivada de la función multiplicada -- por $\frac{1}{4}$ senα, en la que $\alpha = \frac{1}{2}$ del ángulo existente entre dos- nervaduras consecutivas de la cubierta.

Para nuestro caso que hemos planteado en que la cisoide tiene- por expresión

$$y^2 = \frac{x^3}{2a-x}$$

$$2y\frac{dy}{dx} = \frac{(2a-x)\,3x^2 - x^3\,(-1)}{(2a-x)^2} = \frac{6ax^2-3x^3+x^3}{(2a-x)^2} = \frac{6ax^3-2x^3}{(2a-x)^2}$$

$$\therefore\ \frac{dy}{dx} = \frac{3ax^3-x^5}{y(2a-x)^2} = f'(x)$$

En la última ecuación para el cálculo de R aparece C; este ha- de determinarse en función del ángulo α y de la relación $\frac{f}{L}$ para- introducirlo en la integral que, resuelta, nos dá R

Si hacemos

$$\frac{f}{L} = C = f(x) = \frac{1}{\psi(x)}, \quad \text{en la que} \quad \psi(x) = \frac{1}{4}\,SEN\alpha\ \frac{\partial\phi(x)}{\partial x} =$$

$$= \frac{1}{4}\,SEN\alpha\ \frac{3ax^3-x^3}{y(2a-x)^2}, \quad \text{por lo que} \quad \frac{1}{\psi(x)} = \frac{1}{\frac{1}{4}\,SEN\alpha\ \frac{3ax^3-x^3}{y(2a-x)^2}} =$$

$$= \frac{4y(2a-x)^2}{SEN\alpha(3ax^3-x^3)}, \quad \text{y puesto que} \quad a = 5.50 \ \text{y} \ \alpha = 30^\circ,\ SEN\alpha = 0.5$$

$$C = \frac{4y(11-x)^2}{0.5(16.5x^3-x^5)} = \frac{4y(11-x)^2}{8.25x^3-0.5x^5} = \frac{4y(11-x)^2}{7.75x^3}$$

.Quedó dicho, hoja # 10, que

$$\frac{R}{dx} = \frac{1}{2}\,\omega c\ SEN^2\alpha \cdot COS\alpha \cdot \left(1 + \frac{16}{c^2\,SEN^2\alpha}\right)x$$

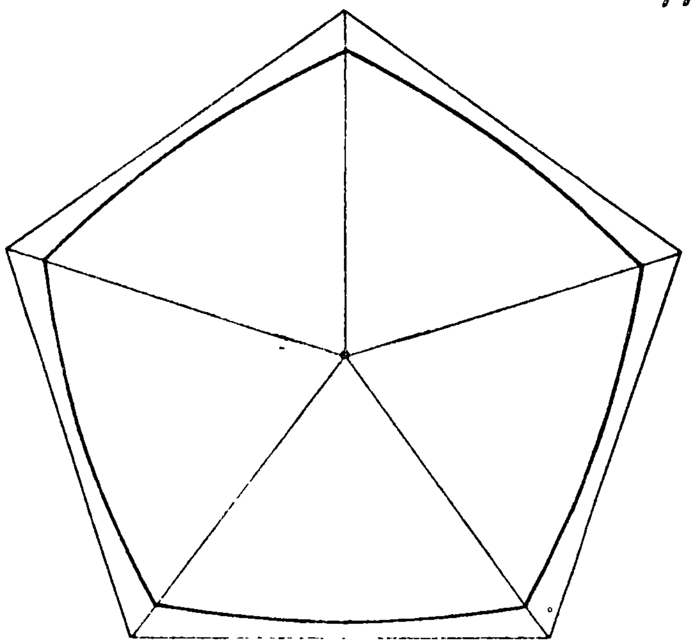

⊕ puntos equidistantes de X, se tendrán 10, 15, 20 ó más valores...

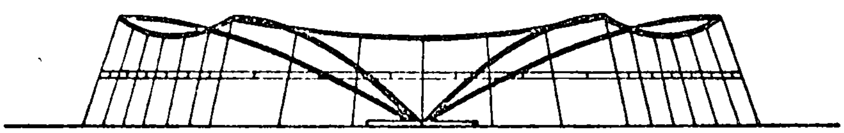

fig: B-B

Dividiendo la longitud de la nervadura en un número conveniente de partes, es decir utilizando 10, 15, 20 ó más valores de la compresión, uno por cada punto de los estimados. Con estos valores así obtenidos se determinará el valor de la integral por alguno de los procedimientos conocidos para la integración numérica; por ejemplo, el de la regla de los trapecios o el de la regla de Simpson. Igualmente válidas resultan las fórmulas de Gregory y de Euler-Maclaurin. Como aplicación de estas ideas se emplea aquí un problema resuelto por el señor Ing. Paul Chelazzi, a quien debe reconocérsele como el introductor en América del Norte de este sistema constructivo. La práctica que él ha realizado de estas estructuras es, a todas luces, suficientemente exitosa para encontrar en sus realizaciones una demostración plena de los alcances ya muy prometedores de estas estructuras, en las que los materiales que las componen, trabajan uniformemente en toda la sección, dandonos, como primera consecuencia, una económía grande, además de la inherente belleza del conjunto espacial que siempre ~~le~~ acompaña a la concepción del diseño:

Se ilustra con una aplicación práctica todo lo dicho hasta aquí. Esta aplicación que expongo a continuación ha sido estudiada como parte principal en un restaurante. Sólo se muestra la cubierta sin atender al resto del edificio.

Las nervaduras, mejor dicho, la curva con que estas se construyen se indican en la figura siguiente: B-B.

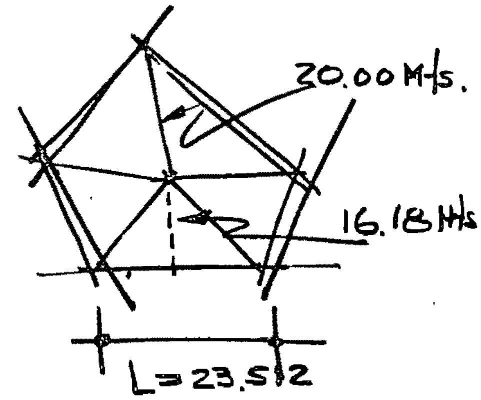

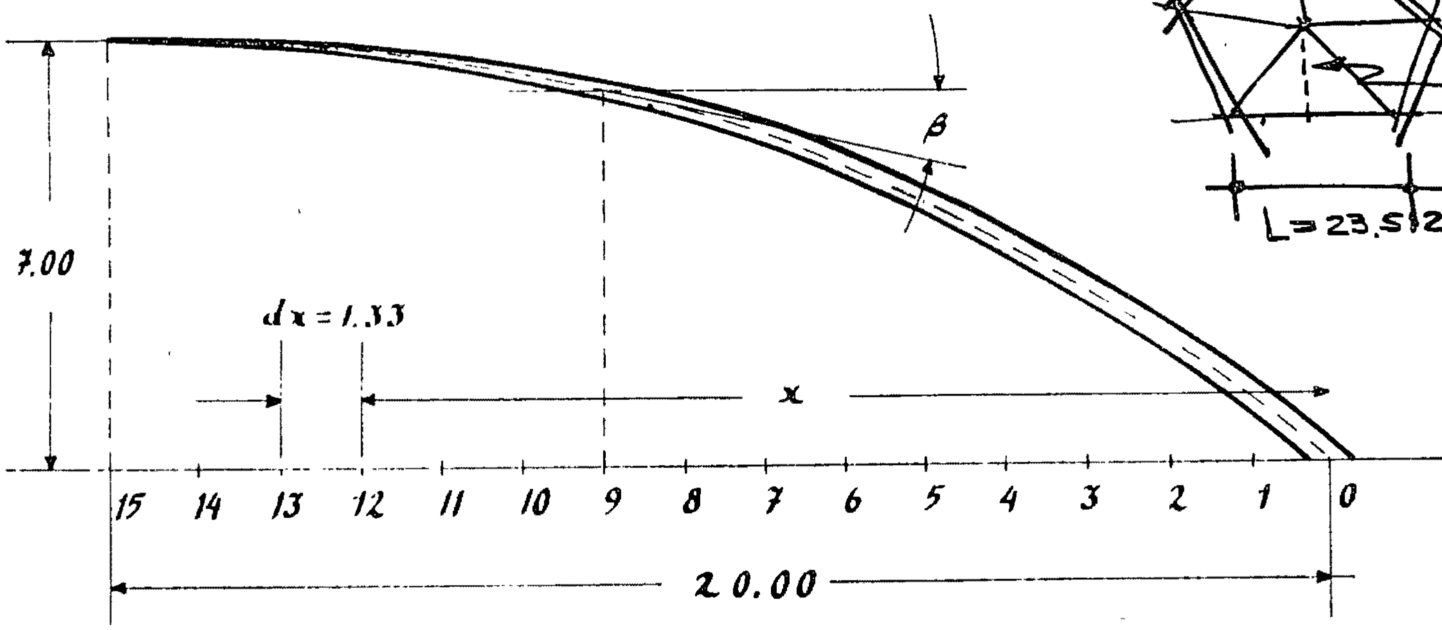

$\omega = 100\ Kg/mt^2$, $\alpha = \dfrac{360^o}{10} = 36^o$, $f = 1.00$

$\omega' = \omega b \times \dfrac{L}{f} = \dfrac{23.512}{1.00} = 23.512$

P	dx	X	L	b	W'	f	dH	dT
1	1.33	1.33	1.5635	1.076	107.6	0.066	494.43	581.38
2	"	2.66	3.1271	"	"	0.133	988.87	1162.69
3	"	3.99	4.6906	"	"	0.199	1483.31	1744.53
4	"	5.32	6.2542	"	"	0.266	1977.74	2325.54
5	"	6.65	7.8177	"	"	0.333	2472.18	2906.92
6	"	7.98	9.3813	"	"	0.399	2966.62	3488.30
7	"	9.31	10.9448	"	"	0.466	3461.06	4069.69
8	"	10.64	12.5084	"	"	0.532	3955.49	4651.08
9	"	11.97	14.0719	"	"	0.598	4449.93	5232.46
10	"	13.30	15.6355	"	"	0.665	4944.37	5813.84
11	"	14.63	17.1990	"	"	0.732	5534.80	6403.97
12	"	1596	18.7626	"	"	0.798	5933.24	6976.61
13	"	17.29	20.3261	"	"	0.864	6427.68	7557.99
14	"	18.62	21.8897	"	"	0.931	6922.11	8139.38
15	1.38	20.00	23.5120	1.117	111.7	1.000	7714.64	9071.29

$$L \cdot 2x\,SEN\alpha \quad ; \quad SEN\,\alpha = SEN\,36^{o} = 0{,}5878 \;;\; COS\,\alpha = 0.8090$$

$$b = dx \cdot COS\,\alpha = 1.076\ mt$$

$$dH = \frac{\omega}{4}\,SEN\alpha \cdot COS\,\alpha \cdot c \cdot x \cdot dx = 279.516 \cdot x \cdot dx$$

$$dT = \frac{1}{2}\,\omega c\ SEN^{2}\alpha \cdot COS\alpha \cdot x \cdot dx =$$

$$= \frac{1}{2}\,100 \times 23.512 \times 0.34527 \times 0.8090 \cdot x\,dx = 328.368 \cdot x\,dx =$$

$$= 328.67\,x\,dx$$

$$TAN\,\beta = \frac{dP}{dT} = \frac{4}{c\,SEN\,\alpha} = \frac{1}{c} \times 6.8050 = \frac{6.8050}{c}$$

P	dP	Tan β
1	168.23	0.28[illegible]
2	336.46	"
3	504.70	0 "
4	672.93	"
5	841.17	"
6	1009.40	"
7	1177.63	"
8	1345.86	"
9	1514.10	"
10	1682.33	"
11	1850.56	"
12	2018.79	"
13	2187.03	"
14	2355.26	"
15	2624.92	"

La columna correspondiente a tan β pone de manifiesto que estos valores son los mismos para un valor cualquiera de X, lo que significa que la nervadura es una pieza recta-no curva-inclinada - 16°08' con respecto a la linea de tierra, tal como lo indica la figura #

Si en lugar de una pieza recta, se desea una curva de la manera que ya se explicó en la Pag. # entonces habrá que obtener, como ya quedó también dicho anteriormente, la igualdad entre la relación $\frac{f}{L}$ y la primera derivada de la función que nos fija la curva multiplicada por $\frac{1}{4\ SEN\alpha}$ como se es[illegible] en la pág. 11

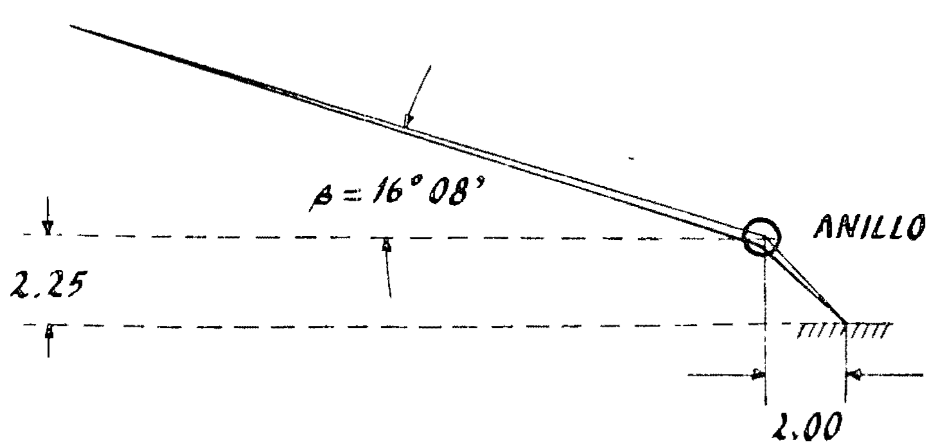

Si la ecuación de la curva fuera, por ejemplo, $Y = 1.7\sqrt{X}$, la -- primera derivada de esta función es :

$$\phi = y = 1.7\,x^{1/2}$$

$$\frac{dy}{dx} = \frac{1}{2} \times 1.7\,x^{-1/2} = \frac{0.85}{\sqrt{x}}$$

$C = f(x) = \dfrac{1}{\psi(x)}$; en la que $\psi(x)$ decimos que es

$$= \frac{SEN\alpha}{4}\,\frac{\partial\phi(x)}{\partial x} = \frac{SEN\alpha}{4}\cdot\frac{0.85}{\sqrt{x}} \therefore C = \frac{1}{\frac{SEN\alpha}{4} \times \frac{0.85}{\sqrt{x}}} = \frac{4\sqrt{x}}{0.85\cdot SEN\alpha} =$$

$$= \frac{4\sqrt{x}}{0.85 \times 0.5878} = 8.00592\sqrt{x}$$

$C = \dfrac{f}{L} = 8.00592\sqrt{x}$, este valor introducido en

$$\frac{dR}{dx} = \frac{1}{2}\,\omega c\cdot SEN^2\alpha\cdot COS\alpha\left(1 + \frac{16}{c^2\,SEN^2\alpha}\right)^{1/2}\cdot x$$

nos dá el valor dR para el segmento de la nervadura dx . La suma- de todos ellos dará el valor de la integral ya conocida.

El mismo problema anterior se operaría de la manera siguiente:

$$\frac{1}{2}\,100 \times \overset{c}{\widehat{8.00592\sqrt{x}}}\cdot SEN^2\alpha\cdot COS\alpha\left(1 + \frac{16}{c^2\,SEN^2\alpha}\right)^{1/2}\cdot x =$$

$$= 400.296\sqrt{x} \times 0.27952\left(1 + \frac{16}{0.34551\cdot c^2}\right)^{1/2}\cdot x =$$

$$= 111.89074\sqrt{x}\left(1 + \frac{16}{2.76613}\cdot\frac{1}{\sqrt{x}}\right)^{1/2}\cdot x =$$

$$= 111.89074\sqrt{x}\left(1 + \frac{5.78425}{\sqrt{x}}\right)^{1/2}\cdot x$$

P	dx	X	dR/dx	Tang	
1	1.33	1.33	420.93	0.7370	36º23'
2	"	2.66	1035.04	0.5211	27º31'
3	"	3.99	1760.14	0.4255	23º03'
4	"	5.32	2571.44	0.3685	20º14'
5	"	6.65	3455.41	0.3295	18º14'
6	"	7.98	4403.26	0.3009	16º45'
7	"	9.31	5408.70	0.2786	15º34'
8	"	10.64	6466.98	0.2606	14º36'
9	"	11.97	7574.26	0.2457	13º48'
10	"	13.30	8727.49	0.2331	13º07'
11	"	14.63	9924.05	0.2222	12º32'
12	"	15.96	11161.82	0.2127	12º00'
13	"	17.29	12438.84	0.2044	11º33'
14	"	18.62	13753.44	0.1970	11º10'
15	138	20.00	15155.71	0.1900	10º45'

Programa en computadora IME - 86

Begin
RI
√
III
5.78425
÷
RIII
=
+
1
+
=
√
÷II
RI
√
x
111.89074
=
x
RII
=
x
RI
=
End

$$TAN_{\beta} = \frac{4}{SEN\alpha} \cdot \frac{1}{C} = \frac{4}{0.5878} \cdot \frac{1}{8.00592\sqrt{x}} =$$

$$= 6.80503 \times \frac{0.12490}{\sqrt{x}} =$$

$$= \frac{0.84995}{\sqrt{x}}$$

dR/dx, esta columna se calcula utilizando, en este caso particular, la regla de Simpson en la que h= 1.33 Mts: $Y = \frac{h}{3}(E+4I+2P)$

P	X	E	I	P
0	0	0.00		
1	1.33		420.93	
2	2.66			1035.04
3	3.99		1760.14	
4	5.32			2571.44
5	6.65		3455.41	
6	7.98			4403.26
7	9.31		5408.70	
8	10.64			6466.98
9	11.97		7574.26	
10	13.30			8727.40
11	14.63		9924.05	
12	15.96			11161.82
13	17.29		12438.84	
14	18.62			13753.44
15	20.00	15155.71	15155.71	
Σ		15155.71	56138.04	48119.47
Coef.		x1	x4	x2

Total: 15155.71 + 56138.04 x 4 + 48119.47 x 2 = 335946.81.

$335946.81 \times \frac{h}{3} = 148936.3$ Kgs.

Area necesaria de la nervadura en la base:

$$\frac{148936.3}{2000} = 74.4 \text{ c}^2$$

Chapter 1

GENERAL PROPERTIES OF STRESS SYSTEMS IN SHELLS

1.1 Definitions

1.1.1 Definition of a Shell

Every part of a structure, of a machine or of any other object is a three-dimensional body, however small its dimensions may be. Nevertheless, the three-dimensional theory of elasticity is not often applied when stresses in such a body are calculated. There is a simple reason for this: Every structural element is created for a certain purpose, one of the most frequent being the transmission of a force from one point to another. Cables, shafts and columns are typical examples of such elements which receive a force or a couple at one end and transmit it to the other, whereas beams and arches usually transmit loads to supports at both ends. The stress analyst does not envisage these elements as three-dimensional but rather as lines having some thickness, a kind of "physical lines" as opposed to the mathematical meaning of the word. When he wants to describe the stresses in them, he first defines a cross section and then calculates the resultant of the stresses acting in it. Instead of describing this resultant by its magnitude, direction and location in space, he usually gives its three components and its moments about three axes. These quantities, commonly known as the normal force, two (transverse) shearing forces, two bending moments, and the torque, are called the "stress resultants" in the cross section.

Not all structural elements are of the kind just described. A second large group consists of all those which are made to bound or enclose some space: walls, in the widest sense of the word, e. g., the wall of a tank, the metal hull of an airplane, or the cloth-and-rubber hull of a balloon. All these objects cannot be described by a line, but can be described by a plane or curved surface, and consequently, their stress analysis must be built on the concept of a "physical surface", a surface made of some more or less solid material, capable of transmitting loads from one part to another and of undergoing consequent deformations.

In the development of the mathematical theory of such structural elements, it has become necessary to distinguish between two types:

Plane walls are called plates, while all walls shaped to curved surfaces are called shells.

Summarizing these considerations, we may define a shell as an object which, for the purpose of stress analysis, may be considered as the materialization of a curved surface. This definition implies that the thickness of a shell is small compared with its other dimensions, but it does not require that the smallness be extreme. It also does not require that the shell be made of elastic material. The occurrence of plastic flow in a steel shell would not prevent its being a shell; a soap bubble is also a shell, although made of liquid. Even the surface of a liquid, because of the surface tension acting in it, has all the properties of a true shell and may be treated by the methods of shell theory (see p. 39).

Most shells, of course, are made of solid material, and generally in this book we shall assume that this material is elastic according to HOOKE's law.

In most cases, a shell is bounded by two curved surfaces, the faces. The thickness t of the shell may be the same everywhere, or it may vary from point to point. We define the middle surface of such a shell as the surface which passes midway between the two faces. If we know the shape of the middle surface and the thickness of the shell for every one of its points, then the shell is geometrically fully described. Mechanically, the middle surface and the thickness represent the shell in the same way as a bar is represented by its axis and the cross section.

However, not every shell fits this description. A parachute, for instance, is made of cloth, i. e., of threads crossing each other and leaving holes in between. Nevertheless, it is a shell, and the "middle surface" which represents it is fairly well defined, although not by the definition just given. However, the thickness t is not easily defined in such a case. Another example of this kind is culvert pipe used in highway work. For most purposes it may be treated as a shell in the shape of a circular cylinder, and its middle surface may easily be defined. The real pipe, however, is corrugated, and in alternate regions all of the material lies either on one side of the "middle surface" or on the other. For some special purposes one may, of course, consider the corrugated surface which really bisects the thickness, as the middle surface of this pipe, but in many cases this is not done, and shell theory may still be applied.

1.1.2 Stress Resultants

Before we can define stresses in a shell, we need a coordinate system. Since the middle surface extends in two dimensions, we need two coordinates to describe the position of a point on it. Let us assume that

some system of coordinates x, y has been defined on the middle surface so that the lines x = const. meet the lines y = const. at right angles (GAUSSian coordinates). We may then cut an element from the shell by cutting along two pairs of adjacent coordinate lines as shown in fig. 1. The cuts are made so that the four sides of the element are normal to the middle surface of the shell.

Since it is not always possible for the distance ds_x or ds_y between two adjacent coordinate lines to be the same everywhere, opposite sides of the element will differ slightly in length. However, for the present purpose this difference is of no importance.

The front side of the element is part of a cross section x = const through the shell and has the area $ds_y \cdot t$. The stresses acting on this

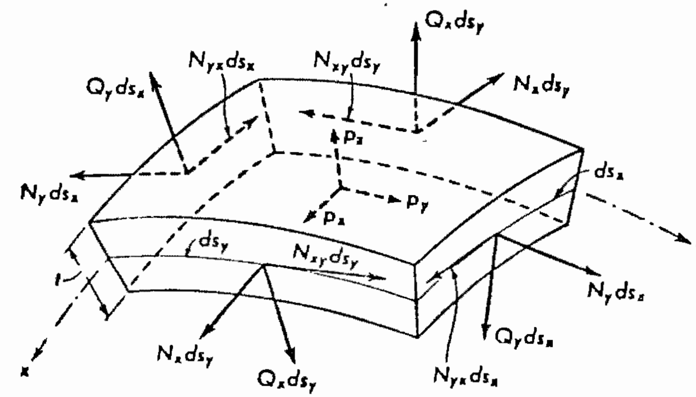

Fig. 1. Stress resultants and loads acting on a shell element

area have a certain resultant which, of course, depends on the length ds_y. When ds_y approaches zero, the resultant decreases proportionately, and the quotient "force divided by length of section" has a finite limit. It is therefore reasonable to call this quotient the "stress resultant". It is a force per unit length of section and may be measured in lb/ft or kg/m, for example.

For all analytical work we must resolve the stress resultant into components. We choose as a reference frame the tangent to the line element ds_y, another tangent to the middle surface at right angles to ds_y (i. e., normal to the cross section), and a normal to the shell. For the force components in these directions we give the following definitions.

In a section x = const, the force in direction x, transmitted by a unit length of section (measured on the middle surface) is called the normal force N_x. It is considered positive if tensile and negative if compressive. The normal force N_y in a section y = const is defined correspondingly.

In a section $x = \text{const.}$, the force transmitted by a unit length of this section and directed tangent to ds_y is called the shearing force N_{xy}. It is considered positive if it points in the direction of increasing y on the same side of the shell element where a tensile force N_x would point in the direction of increasing x. Correspondingly, in the section $y = \text{const.}$ the shearing force N_{yx} is defined with a similar rule for its positive sign (fig. 1). Evidently the sign of both shearing forces depends on the choice of the coordinates. It changes when the positive direction of one of them is reversed.

In a section $x = \text{const.}$, the force normal to the middle surface transmitted by a unit length is called the transverse force Q_x. The positive sign of this force will be defined later [eq.(1c)].

Each of the three components thus defined for a section is the resultant of a certain kind of stresses (fig. 2), normal stresses (σ_x, σ_y), shear stresses parallel to the middle surface $(\tau_{xy} = \tau_{yx})$, and shear stresses normal to it (τ_{xz}, τ_{yz}). Consequently they also deserve the name of "stress resultant", and so they will be called in this book.

The foregoing definitions apply to every shell, including shells in which the faces and thickness are not defined. In the common case of a shell consisting of solid material included between its faces, it is possible to express the stress resultants as integrals of the stresses acting on a section. Then one may consider these integral expressions which are derived from the foregoing definitions, as the definitions themselves. We shall now derive these integrals.

In the section $x = \text{const.}$ (fig. 2), the total force normal to this section is by definition $N_x\, ds_y$. It is the resultant of the stresses σ_x which act on this area. Since the width ds_y is of differential magnitude, we may disregard a possible variation in this direction, but we have to consider a variability of all stresses across the thickness of the shell. It is therefore necessary to consider first an element in the cross section which has differential magnitude in all directions. Such an element has been shaded in fig. 2. Because of the curvature of the shell, its width is not simply ds_y, but $ds_y(r_y + z)/r_y$, and the force transmitted through it is

$$\sigma_x\, ds_y \frac{r_y + z}{r_y}\, dz.$$

The total normal force for the element $ds_y \cdot t$ is found when this expression is integrated between the limits $-t/2$ and $+t/2$:

$$N_x\, ds_y = \int_{-t/2}^{+t/2} \sigma_x\, ds_y \frac{r_y + z}{r_y}\, dz.$$

When the factor ds_y on both sides is dropped, this is the equation which relates the normal force and the normal stress. In the same way the

shearing stresses τ_{xy} and τ_{xz} must be integrated to obtain the forces N_{xy} and Q_x. Altogether, we have

$$N_x = \int_{-t/2}^{+t/2} \sigma_x \frac{r_y + z}{r_y}\, dz, \qquad N_{xy} = \int_{-t/2}^{+t/2} \tau_{xy} \frac{r_y + z}{r_y}\, dz,$$
$$Q_x = -\int_{-t/2}^{+t/2} \tau_{xz} \frac{r_y + z}{r_y}\, dz. \qquad (1\,\text{a–c})$$

The minus sign which has been added to the equation for Q_x, stipulates that a positive transverse force shall have the direction shown in fig. 1, which is opposite to the direction of τ_{xz} in fig. 2.

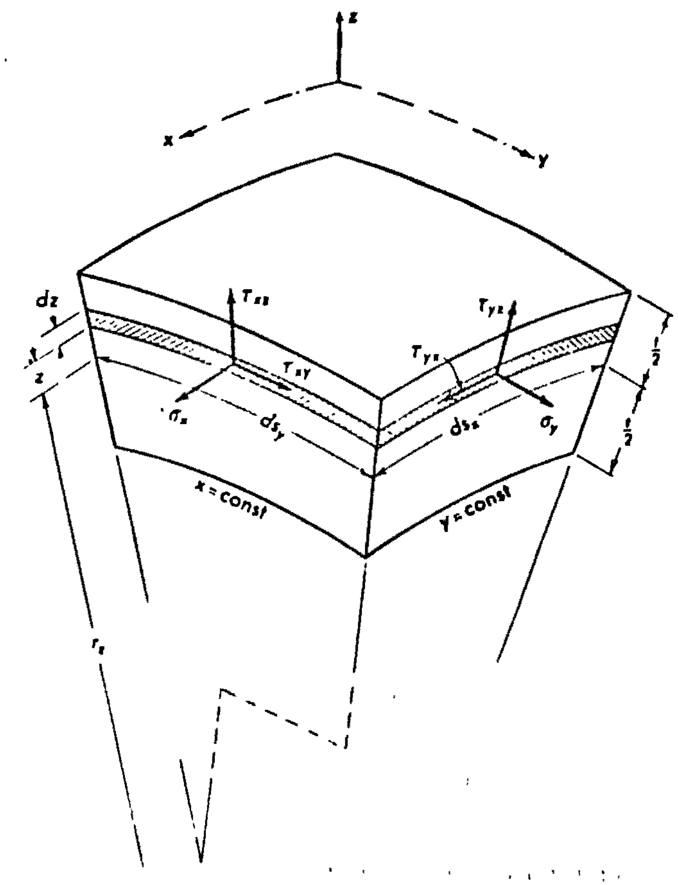

We may apply the same reasoning to a section $y = \text{const.}$ and write three more equations for the other three stress resultants; we must, of course, keep in mind that the line element ds_x has a different radius of curvature, say r_x. We have then

$$N_y = \int_{-t/2}^{+t/2} \sigma_y \frac{r_x + z}{r_x} dz, \quad N_{yx} = \int_{-t/2}^{+t/2} \tau_{yx} \frac{r_x + z}{r_x} dz,$$

$$Q_y = -\int_{-t/2}^{+t/2} \tau_{yz} \frac{r_x + z}{r_x} dz. \qquad \text{(1 d–f)}$$

When we compare eqs. (1 b) and (1 e), we see that the equality of the shearing stresses, $\tau_{xy} = \tau_{yx}$, does not imply the equality of the shearing forces. The difference between N_{xy} and N_{yx} vanishes only if $r_x = r_y$ (e.g., for a sphere), or if τ_{xy} does not depend on z. In a thin shell t and z are small compared with the radii r_x, r_y; then the difference between the two shearing forces is not large and may often be neglected.

When the stresses are not distributed uniformly across the thickness t, some of them have moments with respect to the center of the section. Since these moments influence the equilibrium of the shell element, we must consider them. The moment of the stresses σ_x in a section $x =$ const. is referred to a tangent to the line element ds_y of the middle surface. The moment is of differential magnitude and proportional to ds_y. If it is designated by $M_x\, ds_y$, the quantity M_x is finite and represents a moment per unit length of section. Consequently, it may be measured in such units as ft.lb/ft or in.lb/ft or others of the same kind. M_x is called the bending moment of the section.

When the stresses τ_{xy} are distributed non-uniformly across the thickness t, their resultant may lie anywhere in the plane of the cross section and has a moment with respect to an axis which is normal to the section and passes through the center of the line element ds_y. This moment is also proportional to ds_y and is denoted by $M_{xy}\, ds_y$. The finite quantity M_{xy} is called the twisting moment.

One may easily read from fig. 2 the relations

$$M_x = -\int_{-t/2}^{+t/2} \sigma_x \frac{r_y + z}{r_y} z\, dz, \quad M_{xy} = -\int_{-t/2}^{+t/2} \tau_{xy} \frac{r_y + z}{r_y} z\, dz, \qquad \text{(1 g, h)}$$

which may be considered as the definitions of the bending and twisting moments. The minus signs are arbitrary and fix the sign convention used in this book. (See also figs. V–1 b and VI–1 b).

When the same ideas are applied to a section $y =$ const., another bending moment and another twisting moment are obtained:

$$M_y = -\int_{-t/2}^{+t/2} \sigma_y \frac{r_x + z}{r_x} z\, dz, \quad M_{yx} = -\int_{-t/2}^{+t/2} \tau_{yx} \frac{r_x + z}{r_x} z\, dz. \qquad \text{(1 i, j)}$$

Again, as in the case of the shearing forces, the shear stresses in eqs. (1 h, j) are equal, but the resultant moments are different. And again the difference is not large and may often be neglected (see p. 216), but may sometimes be the key to the exact formulation of a problem (see p. 421). It will be noticed that, because of the factors $(r_x + z)/r_x$ and $(r_y + z)/r_y$, the moments are not zero when the stresses are independent of z, i. e., uniformly distributed across the thickness. These factors are required because of the curvature of the shell and represent the fact that the sides of an element are not rectangles, but trapezoids, and that their centroids do not lie exactly on the middle surface.

It should be noted that eqs. (1 g–j) do not imply any particular law of distribution of the stresses across the thickness. Whether or not the distribution is linear, these equations are always valid as definitions of the moments.

The transverse shearing stresses τ_{xz} and τ_{yz} do not lead to moments.

The ten quantities

$$N_x, \quad N_y, \quad N_{xy}, \quad N_{yx}, \quad Q_x, \quad Q_y, \quad M_x, \quad M_y, \quad M_{xy}, \quad M_{yx}$$

describe the forces and moments acting on the sides of a rectangular shell element. A common name for the whole group is needed, and we shall call them the "stress resultants". It is the main purpose of Chapters 2–6 of this book to explain the methods which allow their computation in shells of different shapes.

Once the stress resultants are known, the stresses may be found by elementary methods. In thin shells of homogeneous material the stress distribution is generally not far from linear, and we may obtain the stresses from the simple relations derived for beams of rectangular cross section, subjected to a normal force and a bending moment.

$$\sigma_x = \frac{N_x}{t} - \frac{12 M_x z}{t^3}, \quad \sigma_y = \frac{N_y}{t} - \frac{12 M_y z}{t^3}. \qquad \text{(2 a, b)}$$

The N-term in these formulas is called the direct stress, and the M-term is called the bending stress. If the shell thickness is not very small compared with the radii of curvature, it may be worth while to take the trapezoidal shape of the cross section into account, but then one should also make use of the basic ideas of bars of great curvature and consider the corresponding non-linearity in the stress distribution.

The tangential shearing stresses follow the same pattern as the bending stresses and must be handled in the same way. However, the two formulas

$$\tau_{xy} = \frac{N_{xy}}{t} - \frac{12 M_{xy} z}{t^3}, \quad \tau_{yx} = \frac{N_{yx}}{t} - \frac{12 M_{yx} z}{t^3} \qquad \text{(2 c, d)}$$

will not necessarily yield identical results. This indicates that there is a logical objection to the assumption of linear stress distribution. Since the discrepancy is not large in thin shells, we may usually disregard it at this stage of the stress analysis.

If the bending and twisting stresses are distributed linearly, the transverse shearing stresses will have the parabolic distribution of the shearing stresses in a beam of rectangular cross section:

$$\tau_{xz} = \frac{3Q_x}{2t}\left(1 - \frac{4z^2}{t^2}\right), \qquad \tau_{yz} = \frac{3Q_y}{2t}\left(1 - \frac{4z^2}{t^2}\right). \tag{2e, f}$$

If the shell ist not made of homogeneous material, or if there is a system of ribs or stiffeners incorporated into the shell, other formulas must be set up. In the case of reinforced concrete shells some particular problems arise.

1.1.3 Membrane Forces

Let us consider two examples of shells which behave very differently. First, roll a sheet of paper to cylindrical form and paste the edges together. This is a cylindrical shell. Very feeble lateral forces will suffice to produce in it a considerable deformation. The resistance of this shell to loads is contingent upon the bending moments, and in more complicated cases of this kind the whole group of bending and twisting moments may come into action.

Second, take the shell of an egg or an electric light bulb. Both are very thin and are made of rather fragile materials, but they can withstand remarkable forces without breaking and without undergoing a visible deformation. In these shells a quite different mechanism of load carrying is at work. It consists essentially of normal and shearing forces N_x, N_y, N_{xy}, N_{yx}. Since there is not much deformation, we would expect the bending and twisting moments to be small, at least in thin shells. A detailed study shows that this is true.

While the first kind of shell is not very attractive for design purposes, the second one is, and whenever it is possible, engineers attempt to shape and to support a shell so that it carries its load essentially by normal and shearing forces. If this is done, it seems reasonable to neglect the moments altogether in the stress analysis. The simple version of shell theory which is obtained in this way is called the Membrane Theory of Shells. We shall study it in the following Chapters, and we shall see its merits and its limitations.

If the bending and twisting moments are zero, only the forces shown in fig. 1 act on the sides of the shell element. In addition there may be a load, proportional to the area $ds_x \cdot ds_y$ of the element, applied at its centroid in an arbitrary direction. We shall now consider the moment equilibrium of this force system. First, we choose as a reference axis a normal to the middle surface, passing through the center of the element (marked "p_z" in fig. 1). The only moments with respect to this axis

are those of the shearing forces N_{xy} and N_{yx}. The two forces $N_{xy}\,ds_y$ form a couple with the arm ds_x, turning counterclockwise if we look on the upper face of the shell. The other two shearing forces, $N_{yx}\,ds_x$, form a clockwise couple, and there is equilibrium if

$$N_{xy}\,ds_y \cdot ds_x = N_{yx}\,ds_x \cdot ds_y,$$

that is, if the two shearing forces are equal:

$$N_{xy} = N_{yx}. \tag{3}$$

Next, we choose the line marked "p_y" as a reference axis. It is a tangent to a line x = const. on the middle surface. With respect to this axis, there is the moment of the transverse forces $Q_x\,ds_y$ which form a couple with the arm ds_x, but all other forces either are parallel to the axis or intersect it, or they pass it so closely that their moments are infinitely small compared with $Q_x\,ds_y \cdot ds_x$. It follows that $Q_x = 0$. From the moment equilibrium for the axis "p_x" we find in the same way that $Q_y = 0$.

Thus we arrive at a remarkable simplification of shell theory: Of the ten unknown stress resultants, only three are left, N_x, N_y, and $N_{xy} = N_{yx}$. The three equations of force equilibrium, which have not yet been used, are available and sufficient in number for calculating these forces (see pp. 19, 109, 167). When the normal and shearing forces have been found, the corresponding deformations may be calculated, and we may check whether or not they lead to bending stresses. In many cases it is found that the bending stresses are negligibly small and this justifies the basic assumption of the membrane theory. In other cases it is found that the deformations derived from the membrane theory contain a discrepancy or a contradiction, and that, therefore, bending and twisting moments must be an important part of the stress system.

When speaking of membrane theory, membrane stresses, or membrane forces (i. e., N_x, N_y, N_{xy}), we do not imply that the normal forces are necessarily tensile forces. In many shells they are compressive; nevertheless the theory is exactly the same and is also called membrane theory.

1.2 Membrane Forces in Arbitrary Directions

1.2.1 Rectangular Coordinates

The membrane forces at a point of a shell represent a plane stress system in a tangential plane to the middle surface. When these forces, or the stress resultants N_x, N_y, N_{xy} have been calculated for sections x = const and y = const passing through that point, the question may be raised as to what forces would be found if the shell were cut in another direction, making an arbitrary angle α with the x direction.

For a plane stress system σ_x, σ_y, τ_{xy} the answer is well known and may be found in textbooks on elementary strength of materials. We need only repeat the essential facts in the notation used for the stress resultants of shells.

We consider a certain point of the shell (i. e., of its middle surface) and define there two rectangular reference frames x, y and ξ, η (fig. 3a). The directions x and y may be those of the GAUSSian coordinates used on the preceding pages for defining the normal and shearing forces N_x, N_y, N_{xy}, N_{yx}, and we assume now that these forces are known. We wish to find the forces in sections $\xi =$ const and $\eta =$ const as defined

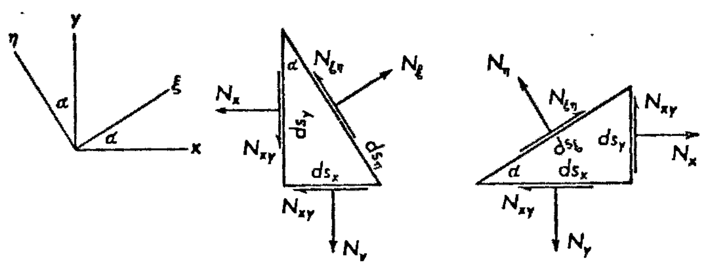

Fig. 3. Equilibrium of triangular shell elements

by the second reference frame (which need only be defined locally). We obtain them by cutting from the shell one of the triangular elements shown in fig. 3b, c.

The first of these elements has two sides ds_x and ds_y in which the forces are known, and one side ds where two of the desired forces, N_ξ and $N_{\xi\eta}$, appear. The equilibrium of the six forces yields the following equations:

$$N_\xi\, ds_\eta = \quad N_x\, ds_y \cos\alpha + N_{xy}\, ds_y \sin\alpha + N_y\, ds_x \sin\alpha + N_{xy}\, ds_x \cos\alpha,$$

$$N_{\xi\eta} ds_\eta = -N_x\, ds_y \sin\alpha + N_{xy}\, ds_y \cos\alpha + N_y\, ds_x \cos\alpha - N_{xy}\, ds_x \sin\alpha.$$

With the angle α as shown in fig. 3a, we have

$$\frac{ds_x}{ds_\eta} = \sin\alpha, \qquad \frac{ds_y}{ds_\eta} = \cos\alpha,$$

and so we obtain the first and third of the following formulas:

$$\begin{aligned} N_\xi &= N_x \cos^2\alpha + N_y \sin^2\alpha + 2N_{xy} \cos\alpha \sin\alpha, \\ N_\eta &= N_x \sin^2\alpha + N_y \cos^2\alpha - 2N_{xy} \cos\alpha \sin\alpha, \\ N_{\xi\eta} &= (N_y - N_x) \cos\alpha \sin\alpha + N_{xy}(\cos^2\alpha - \sin^2\alpha). \end{aligned} \qquad (4a-c)$$

Eq. (4b) is obtained in the same way from the shell element shown in fig. 3c. The equations may also be written in the following form:

$$\begin{aligned} N_\xi &= \frac{1}{2}(N_x + N_y) + \frac{1}{2}(N_x - N_y)\cos 2\alpha + N_{xy}\sin 2\alpha, \\ N_\eta &= \frac{1}{2}(N_x + N_y) - \frac{1}{2}(N_x - N_y)\cos 2\alpha - N_{xy}\sin 2\alpha, \\ N_{\xi\eta} &= -\frac{1}{2}(N_x - N_y)\sin 2\alpha + N_{xy}\cos 2\alpha. \end{aligned} \qquad (5a-c)$$

Eq. (5a) gives the normal force as a function of the direction of the section. When α varies through 180°, N_ξ must have at least one maximum and one minimum. We find the angles $\alpha = \alpha_0$ for which these extrema occur, from the condition $dN_\xi/d\alpha = 0$. It yields

$$\tan 2\alpha_0 = \frac{2N_{xy}}{N_x - N_y} \qquad (6)$$

and thus determines two directions at right angles to each other which are called the principal directions of the membrane forces at this point of the shell. From eqs. (6) and (5c) it may easily be seen that the shear is zero for $\alpha = \alpha_0$. The extreme normal forces are called the principal forces and are denoted by N_a, N_b. One of them is the maximum and the other one the minimum that the normal force N_ξ or N_η can assume for any direction at this point. From eqs. (5) and (6) one may obtain the following formulas for these forces:

$$\begin{aligned} N_a &= \frac{1}{2}(N_x + N_y) + \frac{1}{2}\sqrt{(N_x - N_y)^2 + 4N_{xy}^2}, \\ N_b &= \frac{1}{2}(N_x + N_y) - \frac{1}{2}\sqrt{(N_x - N_y)^2 + 4N_{xy}^2}. \end{aligned} \qquad (7)$$

One of the principal forces makes an angle α_0 with the x axis, the other one with the y axis, but eqs. (7) do not indicate which of them is N_a and which N_b. To find this out, one must use either eqs. (4) or MOHR's circle (see p. 12).

When the principal directions are known at every point of the shell, one may draw a net of curves which have these directions as tangents. They are called the trajectories of the normal forces. They indicate the paths along which the loads are carried to the supported edges by a system of tensile and compressive forces in the shell. These trajectories may give a very suggestive picture of the stresses in a shell (figs. II-26, II-31), but they are laborious to obtain and not easy to represent on paper. Therefore they are not often used in practical stress analysis work. However, they indicate in which direction a thin shell may best be reinforced by ribs, and in which directions the steel rods in reinforced concrete shells should preferably be placed.

1.2.2 Mohr's Circle

Equations (4) indicate that the membrane forces at a point of a shell represent a two-dimensional, symmetric tensor, just as do two-dimensional stresses (σ_x, σ_y, τ_{xy}) or strains (ϵ_x, ϵ_y, $\frac{1}{2}\gamma_{xy}$), and the moments and products of inertia of a cross section (I_x, I_y, I_{xy}). In all these cases there exists a set of formulas identical with eqs. (6) and (7), and there are several graphical methods available which do the same service as these equations (e. g., the different ellipses of inertia, LAND's circle, MOHR's circle). Among all these devices, MOHR's circle appears to be the most useful one, and although graphical methods have lost

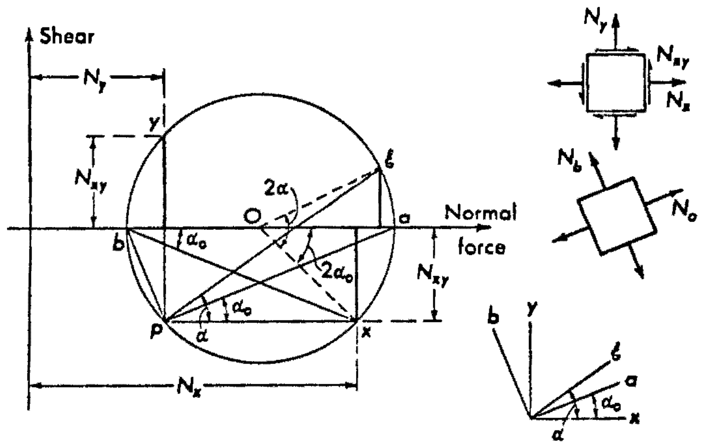

Fig. 4. MOHR's circle for normal and shearing forces

much of their former importance, we shall describe it here in some detail because of its usefulness for the qualitative understanding of stress patterns.

We consider a certain point of the shell and the normal and shearing forces which may be found from eqs. (4) for various sections passing through this point. In a rectangular coordinate system we mark the points x and y with the coordinates N_x, $-N_{xy}$ and N_y, N_{xy}, respectively, and then we draw a circle which has the line $x\,y$ as a diameter (fig. 4). The center of this circle has the coordinates $\frac{1}{2}(N_x + N_y)$, 0, and its radius is

$$\sqrt{\left(\frac{N_x - N_y}{2}\right)^2 + N_{xy}^2}.$$

It follows that the points a and b have the abscissas N_a and N_b as given by eqs. (7), their ordinates being zero. Consequently, the points x, y, a, b represent the forces transmitted through sections which pass through the shell point under consideration in four different directions.

Since the circle is unequivocally determined by the principal forces N_a, N_b, we should necessarily have found this same circle, if we had started from the forces N_ξ, N_η, $N_{\xi\eta}$ for an arbitrary pair of orthogonal sections passing through the same point of the shell. Hence, this circle is the locus for all points whose coordinates are the normal and shearing forces in sections of arbitrary direction and is a graphical representation of the stress resultants at the particular point of the shell. It is called MOHR's circle.

From eq. (6) we see that $\sphericalangle\, x\, o\, a = 2\alpha_0$, and from a well known theorem of elementary geometry it follows that $\sphericalangle\, x\, b\, a = \alpha_0$.

In the lower right-hand corner of fig. 4 are shown the reference frames x, y and a, b which define the directions of the sections in which the different forces N_x, N_{xy}, etc. are transmitted. The force N_x, for example, has the direction x and is transmitted in a section at right angles to the x axis.

We may define a pole p on MOHR's circle by drawing through one of the points, x, y, a, b, a straight line parallel to the corresponding line of the reference frame. All such lines lead to the same point p, and the angle α_0 is found again there. When we now choose an arbitrary ξ direction and draw parallel to it the line $p\xi$ through the pole p, we may read from the figure the following relations for the coordinates of the point ξ: Its abscissa is

$$\frac{1}{2}(N_x + N_y) + \overline{o\,x}\cos 2(\alpha - \alpha_0) =$$

$$= \frac{1}{2}(N_x + N_y) + \overline{o\,x}\cos 2\alpha_0 \cos 2\alpha + \overline{o\,x}\sin 2\alpha_0 \sin 2\alpha$$

$$= \frac{1}{2}(N_x + N_y) + \frac{1}{2}(N_x - N_y)\cos 2\alpha + N_{xy}\sin 2\alpha,$$

i. e., exactly the normal force N_ξ as given by eq. (5). The ordinate of the point ξ is

$$\overline{o\,x}\sin 2(\alpha - \alpha_0) = -\overline{o\,x}\sin 2\alpha_0 \cos 2\alpha + \overline{o\,x}\cos 2\alpha_0 \sin 2\alpha$$

$$= -N_{xy}\cos 2\alpha + \frac{1}{2}(N_x - N_y)\sin 2\alpha,$$

and this is equal to $-N_{\xi\eta}$.

Evidently, every point of MOHR's circle corresponds to one possible section through the shell, and the direction of the normal force is parallel to the line ξp [illegible] when this direction is rotated through 180°, the corresponding point runs just once around [illegible]

[illegible]

of [illegible]. While [illegible] forces [illegible] right and [illegible] to the left, the same positive shearing force N_{xy} had to be plotted downward when it was associated with N_x and upward when associated with N_y. We may easily verify the rule that the right angle between the normal and shearing forces in a section and the right angle between the directions in which they are plotted must always be of opposite sense, one of them clockwise and the other one counterclockwise. As an example, we may look at the forces N_x and N_{xy} in fig. 4. At the shell element they point right and up, in the MOHR diagram they point right and down.

1.2.3 Oblique Coordinates and Skew Forces

On the curved middle surface of a shell the coordinates cannot be simple cartesian coordinates but must be some kind of orthogonal curvilinear coordinates. In many cases it is advisable to use, instead,

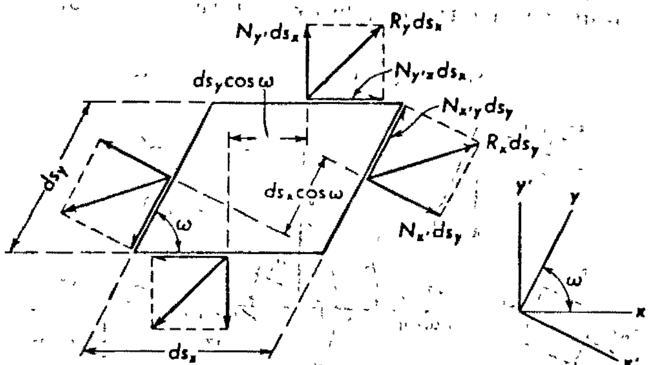

Fig. 5. Orthogonal force components at an oblique shell element

a non-orthogonal system which is better adapted to the general shape of the middle surface or to the boundaries of the shell (see Chapter IV). In such cases the lines x = const and y = const meet each other at an angle ω which may be constant or even vary from point to point. The shell element is then in the first approximation a parallelogram (fig. 5).

The membrane force $R_x\,ds_y$ which is transmitted in the side ds_y of the element, is certainly situated in the tangential plane to the middle surface. There are different ways of resolving it into two components. One might think of using rectangular components $N_{x'}\,ds_y$ and $N_{x'y}\,ds_y$. These correspond to the definitions of normal and shearing forces given on p. 4, if we use a rectangular reference frame x', y. The force $R_y\,ds_x$ on the adjacent side of the element should then be resolved into the rectangular components $N_{y'}\,ds_x$ and $N_{y'x}\,ds_x$ shown in fig. 5, and these forces require the use of another reference frame x, y'.

The two shearing forces $N_{x'y}$ and $N_{y'x}$ are, of course, not equal since equality can be expected only for sections at right angles to each other. Therefore, the tensor of the membrane forces is now described by four quantities insted of three. These four quantities, however, are not

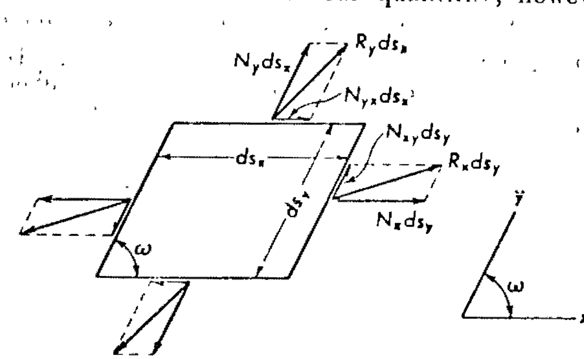

Fig. 6. Skew force components

independent of each other but are connected by the condition of moment equilibrium with respect to a normal to the shell:

$$N_{x'}\,ds_y \cdot ds_x \cos\omega - N_{x'y}\,ds_y \cdot ds_x \sin\omega - N_{y'}\,ds_x \cdot ds_y \cos\omega + \\ + N_{y'x}\,ds_x \cdot ds_y \sin\omega = 0$$

which yields the relation

$$N_{x'y} - N_{y'x} = (N_{x'} - N_{y'})\cot\omega. \tag{8}$$

We may avoid complications and arrive at a more natural description of the state of stress at a point (i. e., of the membrane force tensor) if we resolve the forces $R_x\,ds_y$ and $R_y\,ds_x$ in oblique components following the directions of the lines x = const and y = const (fig. 6). On the sides ds_y of the element we have then per unit length the "skew fiber force" N_x and the "skew shearing force" N_{xy} which has the same direction as the orthogonal shear $N_{x'y}$ but not the same magnitude. From fig. 7 we easily read the relations between the orthogonal and the skew forces:

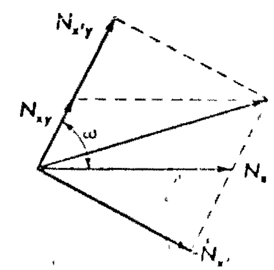

Fig. 7
Relation between orthogonal and skew forces

$$N_x = \frac{N_{x'}}{\sin\omega}, \qquad N_{xy} = N_{x'y} - N_{x'}\cot\omega.$$

Applying the same ideas to R_y, we obtain the skew forces N_{yx} in the section y = const:

$$N_y = \frac{N_{y'}}{\sin\omega}, \qquad N_{yx} = N_{y'x} - N_{y'}\cot\omega.$$

Like the normal forces on a rectangular shell element, the skew forces N_x or N_y on opposite sides of the oblique element fall on the same line and do not yield a couple. Thus the shearing forces are again alone in the equation of moment equilibrium:

$$N_{xy}\,ds_y \cdot ds_x \sin\omega - N_{yx}\,ds_x \cdot ds_y \sin\omega = 0,$$

and hence they are again equal to each other:

$$N_{xy} = N_{yx}.$$

Having solved a shell problem in oblique coordinates x, y, we may desire to find from the skew forces N_x, N_y, N_{xy} the components N_ξ, N_η, $N_{\xi\eta}$ for an orthogonal pair ξ, η of sections or the principal forces N_a, N_b. The set of transformation formulas needed may be found by the

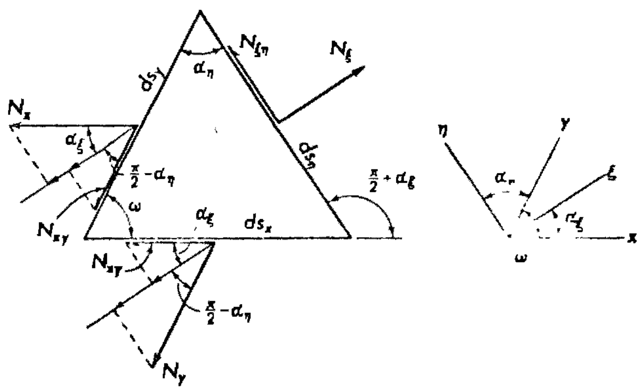

Fig. 8. Triangular shell element in oblique coordinates x, y

method which led to eqs. (4). We cut from the shell a triangular element having one side parallel to one of the new rectangular axes, and the other two sides parallel to the directions x and y (fig. 8). The equilibrium of all forces in the direction ξ yields the equation

$$N_\xi\,ds_\eta = N_x\,ds_y\cos\alpha_\xi + N_{xy}\,ds_y\sin\alpha_\eta + N_y\,ds_x\sin\alpha_\eta + N_{xy}\,ds_x\cos\alpha_\xi,$$

and a similar equation will be found for the η-components:

$$N_{\xi\eta}\,ds_\eta = -N_x\,ds_y\sin\alpha_\xi + N_{xy}\,ds_y\cos\alpha_\eta + N_y\,ds_x\cos\alpha_\eta - N_{xy}\,ds_x\sin\alpha_\xi.$$

Between the three sides of the element we have the geometric relation

$$\frac{\sin\omega}{ds_\eta} = \frac{\sin\alpha_\xi}{ds_x} = \frac{\cos\alpha_\eta}{ds_y}.$$

We multiply each term in the preceding equations by one of the three identical factors and thus obtain two of the three following equations,

the third of which can be derived from another triangular element:

$$\begin{aligned} N_\xi \sin\omega &= N_x\cos^2\alpha_\xi + N_y\sin^2\alpha_\eta + 2N_{xy}\cos\alpha_\xi\sin\alpha_\eta, \\ N_\eta \sin\omega &= N_x\sin^2\alpha_\xi + N_y\cos^2\alpha_\eta - 2N_{xy}\sin\alpha_\xi\cos\alpha_\eta, \\ N_{\xi\eta}\sin\omega &= N_y\cos\alpha_\eta\sin\alpha_\eta - N_x\cos\alpha_\xi\sin\alpha_\xi + \\ &\quad + N_{xy}(\cos\alpha_\xi\cos\alpha_\eta - \sin\alpha_\xi\sin\alpha_\eta). \end{aligned} \tag{9}$$

To find the principal forces N_a, N_b we must put $N_{\xi\eta} = N_{ab} = 0$. This is an equation for the unknown angles α_ξ and α_η, which we now call α_a and α_b. Using well-known trigonometric formulas, we may bring this equation into the form

$$N_y \sin 2\alpha_b - N_x \sin 2\alpha_a + 2N_{xy}\cos(\alpha_a + \alpha_b) = 0.$$

From fig. 8 we find

$$\alpha_b = \frac{\pi}{2} + \alpha_a - \omega,$$

which enables us to eliminate α_b. Subsequent trigonometric transformation leads to an equation in which only the functions $\cos 2\alpha_a$ and $\sin 2\alpha_a$ occur. It has the solution

$$\tan 2\alpha_a = \frac{N_y \sin 2\omega + 2N_{xy}\sin\omega}{N_x + N_y\cos 2\omega + 2N_{xy}\cos\omega}. \tag{10a}$$

By a similar calculation we find also

$$\tan 2\alpha_b = -\frac{N_x \sin 2\omega + 2N_{xy}\sin\omega}{N_y + N_x\cos 2\omega + 2N_{xy}\cos\omega}. \tag{10b}$$

If we put $\omega = \pi/2$, both formulas coincide with our formula (6) for rectangular coordinates.

1.3 Transformation of Moments

All the questions we have asked and answered on the preceding pages for the normal and shearing forces may also be formulated for the bending and twisting moments. The answers may be found easily by reducing each moment problem to the corresponding force problem. We simply replace each moment by a couple of forces parallel to the middle surface. The [illegible] all the [illegible] otherwise [illegible] We [illegible] them equal to the thickness of the shell. We have then in the [illegible] surface a system of normal and [illegible] forces and in the lower surface a [illegible] identical except that the direction of each force is reversed. We may now cut triangular and other elements from the shell and write for each one of the two force systems the equations of equilibrium as we did in the preceding sections. The resultant forces may then be recombined to yield bending and twisting moments.

It follows that in all the equations and in all the diagrams of Section 1.2 we may simply replace everywhere the letter N by M to obtain valid results for the transformation of the bending and twisting moments to a new set of axes.

Chapter 2

DIRECT STRESSES IN SHELLS OF REVOLUTION

2.1 General Differential Equations

2.1.1 Geometrical Relations

The particular type of shell which we are going to treat in this chapter appears in many technical applications, especially in the construction of tanks, pressure vessels and domes.

Before we enter into the investigation of the stress resultants in these shells, we must examine the geometry of their middle surfaces.

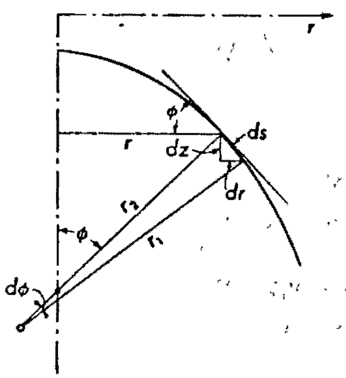

Fig. 1. Meridian of a shell of revolution

A surface of revolution is generated by the rotation of a plane curve about an axis in its plane. This generating curve is called a meridian, and an arbitrary point on the middle surface of the shell is described by specifying the particular meridian on which it is found and by giving the value of a second coordinate which varies along the meridian and is constant on a circle around the axis of the shell. Since all these circles for different values of the second coordinate are parallel to each other, they are called the "parallel circles".

We shall identify a meridian by the angular distance θ of its plane from that of a datum meridian and choose as second coordinate the angle ϕ between a normal to the shell and its axis of revolution. If the middle surface of our shell is a sphere, these coordinates are the spherical coordinates used in geography: θ is the longitude and ϕ is the complement to the latitude: hence the nomenclature of the meridians and the parallel circles.

Fig. 1 shows a meridian of the shell. Let r be the distance of one of its points from the axis of rotation and r_1 its radius of curvature. In our equations we also need the length r_2, measured on a normal to the meridian between its intersection with the axis of rotation and the middle surface. It is the second radius of curvature of the shell, and we read from fig. 1 the relation

$$r = r_2 \sin\phi. \tag{1}$$

For the line element ds of the meridian we have

$$ds = r_1\, d\phi, \tag{2}$$

and since

$$dr = ds\cos\phi, \qquad dz = ds\sin\phi \tag{3a, b}$$

we have the relations

$$\frac{dr}{d\phi} = r_1\cos\phi, \qquad \frac{dz}{d\phi} = r_1\sin\phi. \tag{4a, b}$$

Finally we obtain from (1) and (4a)

$$\frac{1}{r}\frac{dr}{d\phi} = \frac{r_1}{r_2}\cot\phi. \tag{5}$$

2.1.2 Equilibrium of the Shell Element

The shell element (fig 2) is cut out by two meridians and two parallel circles, each pair indefinitely close together. The conditions of its equilibrium will furnish three equations, just enough to determine the three unknown stress resultants: the meridional force N_ϕ, the hoop force N_θ, and the shear $N_{\phi\theta}$.

To find these equations, let us begin with the forces parallel to the tangent to the meridian. The shear transmitted by one of the meridional edges of the element is $N_{\theta\phi}\, r_1\, d\phi$, on the opposite edge it is

$$\left(N_{\theta\phi} + \frac{\partial N_{\theta\phi}}{\partial\theta}\, d\theta\right) r_1\, d\phi.$$

These two forces are of opposite direction and

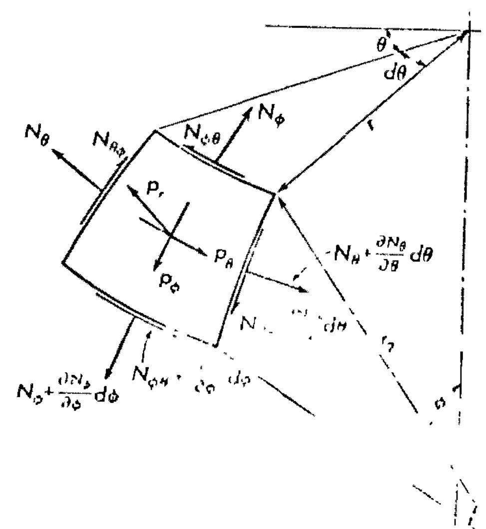

Fig. 2. Shell element

therefore almost cancel each other. Only their difference

$$\frac{\partial N_{\theta\phi}}{\partial\theta} r_1 \, d\theta \, d\phi$$

enters the equilibrium condition. In the same way we have the difference of the two meridional forces, but in computing it, we must bear in mind that both the force per unit length of section, N_ϕ, and the length of section $r\,d\theta$ vary with ϕ. Therefore we have to introduce the increment

$$\frac{\partial}{\partial\phi}(r N_\phi)\, d\phi\, d\theta$$

into the condition of equilibrium. But that is not all. The hoop forces N_θ also contribute. The two forces $N_\theta r_1 \, d\phi$ on either side of the element lie in the plane of a parallel circle where they include an angle $d\theta$. They therefore have a resultant force $N_\theta r_1 \, d\phi \cdot d\theta$, situated in the same plane and pointing towards the axis of the shell. We resolve this force into two rectangular components normal to the shell and in the direction of the tangent to the meridian. The latter one,

$$N_\theta r_1 \, d\phi \, d\theta \cdot \cos\phi,$$

enters our condition of equilibrium, and since its direction is opposite to that of the increments of $N_{\theta\phi}$ and N_ϕ, it requires a negative sign. Finally we have to introduce a component of the external force, which is the product of the load component per unit area of shell surface, p_ϕ, and the area of the element, $r\,d\theta \cdot r_1 \, d\phi$. The equilibrium condition thus reads:

$$\frac{\partial N_{\theta\phi}}{\partial\theta} r_1 \, d\theta \, d\phi + \frac{\partial}{\partial\phi}(r N_\phi)\, d\phi \, d\theta - N_\theta r_1 \, d\phi \, d\theta \cos\phi + \\ + p_\phi r r_1 \, d\theta \, d\phi = 0.$$

All its terms contain the product of the two differentials $d\theta\, d\phi$. Dividing by this, we get the partial differential equation

$$\frac{\partial}{\partial\phi}(r N_\phi) + r_1 \frac{\partial N_{\theta\phi}}{\partial\theta} - r_1 N_\theta \cos\phi + p_\phi r r_1 = 0. \tag{6a}$$

By quite similar reasoning we obtain an equation for the forces in the direction of a parallel circle. For the difference of the two shearing forces which are transmitted in the horizontal edges of the shell element, we must take into account the variability of the length of the line element:

$$\frac{\partial}{\partial\phi}(r N_{\phi\theta})\, d\phi \, d\theta.$$

Then we have a term representing the difference of the two forces $N_\theta \cdot r_1 \, d\phi$ and another one with the load component p_θ. Furthermore,

we have a contribution from the shear acting on the meridional edges. The two forces $N_{\theta\phi} \cdot r_1 \, d\phi$ are not exactly parallel. Their horizontal components make an angle $d\theta$ and therefore have a resultant

$$N_{\theta\phi} \cdot r_1 \, d\phi \cdot \cos\phi \cdot d\theta$$

which has the direction of the tangent to a parallel circle and thus enters our equation. If we drop the factor $d\theta\, d\phi$, common to all terms, we have:

$$\frac{\partial}{\partial\phi}(r N_{\phi\theta}) + r_1 \frac{\partial N_\theta}{\partial\theta} + r_1 N_{\theta\phi} \cos\phi + p_\theta r r_1 = 0. \tag{6b}$$

The third equation refers to the forces which are perpendicular to the middle surface of the shell. It contains contributions from both normal forces N_ϕ and N_θ and the third load component, p_r.

In formulating eq. (6a), we have already seen that the two forces $N_\theta r_1 \, d\phi$ have a horizontal resultant $N_\theta r_1 \, d\phi \, d\theta$. It has a component

$$N_\theta r_1 \, d\phi \, d\theta \sin\phi,$$

directed normally to the shell and pointing toward its inner side. Similarly, the two forces $N_\phi r\,d\theta$, including the angle $d\phi$, have the resultant

$$N_\phi r \, d\theta \, d\phi$$

in the same direction. These two forces and the component

$$p_r r r_1 \, d\theta \, d\phi$$

of the load must be in equilibrium. This yields the equation

$$N_\theta r_1 \sin\phi + N_\phi r - p_r r r_1 = 0.$$

We divide by $r r_1$, use the geometric relation (1), and thus get the third of our equations:

$$\frac{N_\phi}{r_1} + \frac{N_\theta}{r_2} = p_r. \tag{6c}$$

This equation not only is valid for shells in the form of a surface of revolution, but may be applied to all shells when the coordinate lines $\phi = \text{const}$ and $\theta = \text{const}$ are the lines of curvature of the surface. Therefore, we shall meet it again in the next chapter and we shall see in Chapter 4 what becomes of it when the coordinates no longer follow the lines of curvature of the shell.

It is notable that eq. (6c) does not contain any derivatives of the unknowns. It may therefore always be used to eliminate one of the normal forces [illegible] differentiable [illegible] with the shear and one of the normal [illegible] unknowns.

Till now, we have used two angular coordinates θ and ϕ. This is adequate for many shells with meridians of simple shape and has been done quite generally in the theory of shells of revolution. However the angle ϕ is very inconvenient if the meridian has a point of inflection. At such a point, ϕ passes a maximum and afterwards begins to decrease. The stress resultants must therefore be double-valued functions of ϕ, the two branches belonging to the two parts of the meridian above and below the point of inflection. Even worse is the fact that the sign of the shear $N_{\phi\theta}$ depends on the direction in which ϕ increases. Since this is reversed beyond the inflection point, the shear must suddenly have the opposite sign, without passing through zero. It is evident that an analytical solution fulfilling all these requirements cannot be very simple and that numerical methods for the solution of the differential equations will also meet with difficulties. For such cases it is useful to replace ϕ by a coordinate which avoids all these difficulties, and that is the length s of the meridian, measured from any datum point, say from the vertex of the shell if such a point exists, or otherwise from its edge. Consequently, we then replace the subscript ϕ by s.

Between s and ϕ we have the relation (2) and introducing this into the eqs. (6a–c), we get

$$\begin{aligned} &\frac{\partial}{\partial s}(r N_s) + \frac{\partial N_{\theta s}}{\partial \theta} - N_\theta \cos\phi + p_s r = 0, \\ &\frac{\partial}{\partial s}(r N_{\theta s}) + \frac{\partial N_\theta}{\partial \theta} + N_{\theta s}\cos\phi + p_\theta r = 0, \\ &\frac{N_s}{r_1} + \frac{N_\theta}{r_2} = p_r. \end{aligned} \tag{7a–c}$$

There is still a third way of formulating the fundamental equations, using rectangular coordinates r, z in the plane of the meridian (fig. 1). From (4b) we find that

$$\frac{\partial}{\partial \phi} = r_1 \sin\phi \cdot \frac{\partial}{\partial z},$$

and when we introduce that into (6a, b), we find

$$\begin{aligned} &\frac{\partial}{\partial z}(r N_\phi)\sin\phi + \frac{\partial N_{\theta\phi}}{\partial \theta} - N_\theta \cos\phi + p_\phi r = 0, \\ &\frac{\partial}{\partial z}(r N_{\phi\theta})\sin\phi + \frac{\partial N_\theta}{\partial \theta} + N_{\theta\phi}\cos\phi + p_\theta r = 0. \end{aligned} \tag{8a, b}$$

There is some advantage in using this form of the equations, if the shape of the meridian is given by its equation in rectangular coordinates r, z. However, there is no particular reason to prefer for structures shells whose meridians have a simple cartesian equation to those which yield simple relations between ϕ and the radii.

2.2 Loads Having Axial Symmetry

2.2.1 Differential Equations

In many practical problems the external forces have the same symmetry as the shell itself. Then the stresses are independent of θ, and all derivatives with respect to this coordinate disappear from eqs. (6). The equations (6a, c) then read

$$\begin{aligned} &\frac{d}{d\phi}(r N_\phi) - r_1 N_\theta \cos\phi = -p_\phi r r_1, \\ &\frac{N_\phi}{r_1} + \frac{N_\theta}{r_2} = p_r. \end{aligned} \tag{9a, b}$$

Eq. (6b) becomes independent of these equations and contains only the shear:

$$\frac{d}{d\phi}(r N_{\phi\theta}) + r_1 N_{\theta\phi}\cos\phi = -p_\theta r r_1.$$

It describes a kind of torsion of the shell about its axis, a very simple state of stress which may be treated separately. We eliminate it from our further considerations by putting $p_\theta \equiv 0$ and $N_{\phi\theta} \equiv 0$. When we solve eq. (9b) for N_θ and substitute the result into eq. (9a), we obtain a first order differential equation for N_ϕ. After multiplication by $\sin\phi$ it reads

$$\frac{d(r N_\phi)}{d\phi}\sin\phi + r N_\phi \cos\phi = r_1 r_2 p_r \cos\phi \sin\phi - r_1 r_2 p_\phi \sin^2\phi.$$

The two terms at the left may be combined to form a total derivative,

$$\frac{d}{d\phi}(r N_\phi \sin\phi) = \frac{d}{d\phi}(r_2 N_\phi \sin^2\phi),$$

and N_ϕ may be found by an integration:

$$N_\phi = \frac{1}{r_2 \sin^2\phi}\left[\int r_1 r_2 (p_r \cos\phi - p_\phi \sin\phi)\sin\phi \, d\phi + C\right]. \tag{10}$$

N_θ may then be found from (9b).

Eq. (10) may be interpreted as a condition of equilibrium for the part of the shell above a parallel circle ϕ = const. Indeed, if we cut the shell along this circle, $2\pi r_2 \sin\phi$ is its circumference, and $2\pi N_\phi r_2 \sin^2\phi$ is the vertical resultant of all internal forces transmitted in this section. The integral times 2π represents the distributed load applied above this circle, if we write it as a definite integral between appropriate limits. The upper limit, of course, will be the value ϕ for the circle in question, and the lower limit will be the value $\phi = \phi_0$ with which the meridian begins (see figs. 4, 9). When the shell has a flat top (figs. 6–11) we have $\phi_0 = 0$. The constant C represents the effect of loads which may be applied above the circle $\phi = \phi_0$ (see fig. 4), $2\pi C$ being the resultant of these forces.

If the shell is closed at the vertex, such an additional load can only be a concentrated force P applied at this point. If no other load is present, we have in eq. (10)

$$p_\phi = p_r = 0, \quad 2\pi C = -P,$$

and hence the meridional force

$$N_\phi = -\frac{P}{2\pi r_2 \sin^2\phi} \tag{11a}$$

and from eq. (9b) the hoop force

$$N_\theta = +\frac{P}{2\pi r_1 \sin^2\phi}. \tag{11b}$$

At the top, both forces have a singularity of the second order, i. e. they tend toward infinity as ϕ^{-2}. We shall see later (p. 350) that the immediate vicinity of this point where the concentrated load is applied will be subjected to severe bending stresses but that at some distance the membrane forces as given by eqs. (11) still represent the real state of stress.

2.2.2. Solution for some Typical Cases

2.2.2.1. Spherical Dome

As a first example we consider a spherical dome as shown in fig. 3. We ask for the stress resultants produced by a dead load p (weight per unit area of the middle surface). To apply our formula (10), we must first resolve this load into its components tangential and normal to the shell. These are

$$p_\phi = p \sin\phi, \quad p_r = -p \cos\phi. \tag{12}$$

Introducing this into (10) we find with $r_1 = r_2 = a$:

$$N_\phi = -\frac{1}{a \sin^2\phi} \int_0^\phi a^2 p \sin\phi \, d\phi = -p a \frac{1 - \cos\phi}{\sin^2\phi}.$$

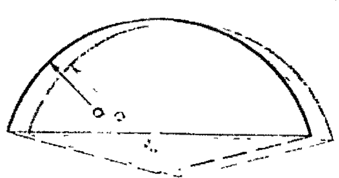

Fig. 3. Spherical dome

Simplifying the trigonometric expression and then using (9b) we find for the stress resultants the formulas

$$N_\phi = -\frac{p a}{1 + \cos\phi},$$
$$N_\theta = p a \left(\frac{1}{1 + \cos\phi} - \cos\phi \right). \tag{13}$$

It is interesting to discuss these forces in some detail. When we put $\phi = 0$ we find $N_\phi = N_\theta = -pa/2$. The meridional force N_ϕ is negative throughout the hemisphere, but N_θ decreases in absolute value with increasing ϕ and changes sign at a value $\phi = 51.82°$ which follows

from the equation

$$\cos^2\phi + \cos\phi - 1 = 0.$$

If the shell is so flat that ϕ does not exceed this limit, no tensile stress appears, assuming that the dead load is the only load and that a proper abutment is provided. This abutment has to resist the thrust N_ϕ which has the direction of the tangent to the meridian. Such an abutment usually consists of a continuous vertical support and a ring, which resists the horizontal component of N_ϕ and from it receives a tensile force

$$N = N_\phi a \sin^2\phi.$$

This ring is the source of a perturbation of the membrane stresses given by our formulas. In flat domes its stress is of opposite sign to the hoop stress in the shell, and in high domes, where the hoop stress at the springing line is positive, it is usually much smaller than the stress in the ring. Therefore, after the elastic deformations, the ring and the shell do not fit together. The continuity of deformation is re-established by an additional bending of the shell, which will be treated in Chapter 6. It may be mentioned here that the bending stresses are confined to a border zone of limited width and that the major part of the shell has, in fact, the simple stresses given by the membrane theory.

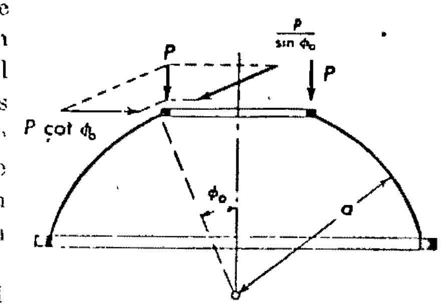

Fig. 4. Shell dome with skylight

Most domes are not closed at the vertex but have a skylight or a ventilation opening, covered by a superstructure, the lantern. Its weight, say $2\pi \cdot P \cdot a \sin\phi_0$, acts on the upper edge of the shell as a vertical line load. Since the shell can resist only tangential forces, this edge also needs a stiffening ring, which takes the other component (fig. 4) and gets a compressive force from it. We find the stress resultants in such a shell with its own dead load p and the lantern load P by returning to the integral (10) and determining C so that for $\phi = \phi_0$ we have $N_\phi = -P/\sin\phi_0$. The simple computation leads to the following formulas:

$$N_\phi = -p a \frac{\cos\phi_0 - \cos\phi}{\sin^2\phi} - P \frac{\sin\phi_0}{\sin^2\phi},$$
$$N_\theta = p a \left(\frac{\cos\phi_0 - \cos\phi}{\sin^2\phi} - \cos\phi \right) + P \frac{\sin\phi_0}{\sin^2\phi}.$$

The difference of the two cosines is disadvantageous for numerical work, in particular for small angles ϕ, and it is better to write the formulas in the following form:

$$N_\phi = -\frac{2pa}{\sin^2\phi}\sin\frac{\phi+\phi_0}{2}\sin\frac{\phi-\phi_0}{2} - P\frac{\sin\phi_0}{\sin^2\phi}, \qquad (14)$$
$$N_\theta = -N_\phi - pa\cos\phi.$$

Some figures may interpret this result. The roof represented in fig. 5 carries a uniformly distributed load $p = 45$ lb/ft², and the lantern ring has a line load of 460 lb/ft, applied along its center line, i. e. on a circle of 13′ 5″ radius. The edge of the shell has a slightly greater radius,

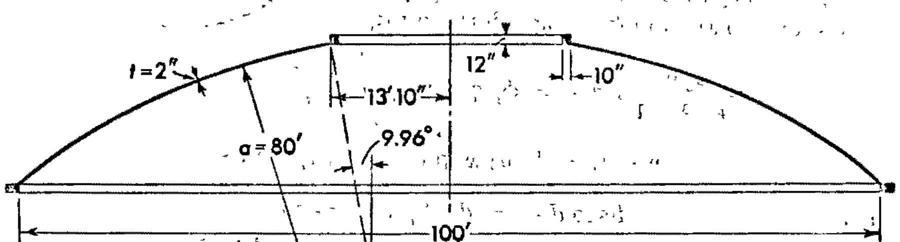

Fig. 5. Shell dome with skylight

$r = 13'\,10''$, and the vertical line load P transmitted at this edge is correspondingly smaller, $P = 446$ lb/ft. When we introduce these values in eqs. (14), we obtain

$$N_\phi = -\frac{7200\text{ lb/ft}}{\sin^2\phi}\sin\frac{\phi+9.96^\circ}{2}\sin\frac{\phi-9.96^\circ}{2} - \frac{77.1\text{ lb/ft}}{\sin^2\phi},$$
$$N_\theta = -N_\phi - 3600\,[\text{lb/ft}]\cos\phi.$$

At the upper edge ($\phi = 9.96°$) these formulas yield $N_\phi = -2580$ lb/ft, $N_\theta = -966$ lb/ft; and at the springing line ($\phi = 38.7°$): $N_\phi = -2087$ lb/ft, $N_\theta = -723$ lb/ft. The highest stress occurs at the upper edge and is $\sigma_\phi = N_\phi/t = -107.5$ lb/in². With an admissible stress of 500 or 600 lb/in² there is sufficient margin for additional bending stresses.

2.2.2 Boiler End

Pressure vessels of all kinds are built as shells of revolution, consisting of a cylindrical drum and two ends which may be shaped as hemispheres, half ellipsoid or in any other suitable form. They have to resist an internal pressure p, constant and perpendicular to the wall.

When we put $p_\phi = 0$, $p_r = p$, the integral (10) may be simplified considerably. Making use of (3a), we find

$$N_\phi = \frac{1}{r_2\sin^2\phi}\int_0^\phi r_1 r_2\, p\cos\phi\sin\phi\, d\phi = \frac{p}{r_2\sin^2\phi}\int_0^r r\, dr,$$

and this integral may be evaluated independently of the shape of the meridian. Eq. (9b) then yields the hoop force N_θ. Thus we get the following simple expressions for the stress resultants in pressure vessels:

$$N_\phi = \frac{1}{2}p\,r_2, \qquad N_\theta = p\,r_2\frac{2r_1 - r_2}{2r_1}. \qquad (15)$$

We shall use these formulas to study some typical forms of boiler ends.

Boiler ends are often shaped as flat ellipsoids of revolution (fig. 6). As we find easily by well-known methods of analytical geometry, the

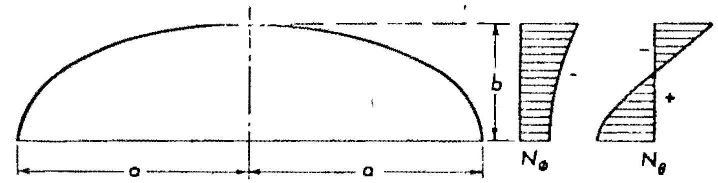

Fig. 6. Ellipsoid as boiler end

elliptic meridian has the radius of curvature

$$r_1 = \frac{a^2 b^2}{(a^2\sin^2\phi + b^2\cos^2\phi)^{3/2}},$$

and the radius of transversal curvature of the ellipsoid is

$$r_2 = \frac{a^2}{(a^2\sin^2\phi + b^2\cos^2\phi)^{1/2}}.$$

Introducing these expressions and the given load into the eq. (15), we find

$$N_\phi = \frac{pa^2}{2}\,\frac{1}{(a^2\sin^2\phi + b^2\cos^2\phi)^{1/2}},$$
$$N_\theta = \frac{pa^2}{2b^2}\,\frac{b^2 - (a^2 - b^2)\sin^2\phi}{(a^2\sin^2\phi + b^2\cos^2\phi)^{1/2}}.$$

At the vertex $\phi = 0$ we have $N_\phi = N_\theta$. This is no peculiarity of the ellipsoid but is true for any surface of revolution. At the vertex all meridians meet, and any direction is parallel to one of them and at right angles to another. Since in a surface of continuous curvature we have at the vertex $r_1 = r_2$, the common magnitude of both longitudinal forces may be found immediately from (9b)

$$N_\phi = N_\theta = \frac{p r_1}{2}$$

and this may be used as a boundary condition to determine C in (10).

Fig. 6 shows the distribution of the stress [illegible]. The hoop force changes sign and becomes negative near the equator. The zero is found where

$$\sin\phi = \frac{b}{\sqrt{a^2 - b^2}}.$$

This formula yields a real angle only if $a/b \geqq \sqrt{2}$. If the ellipsoid is flatter than indicated by this ratio of its axes, an equatorial zone exists where the hoop stress is a compression. The elastic deformation of such a shell must be such that the diameter of its border decreases. On the other hand, the cylindrical part of the boiler has a positive hoop force $N_\theta = p\,a$ everywhere as we see from eq. (9b) by putting $r_1 = \infty$, $r_2 = a$. On the parallel circle where the two parts meet, they have quite different deformations and will not fit together without an additional deformation. This is furnished by bending stresses, which

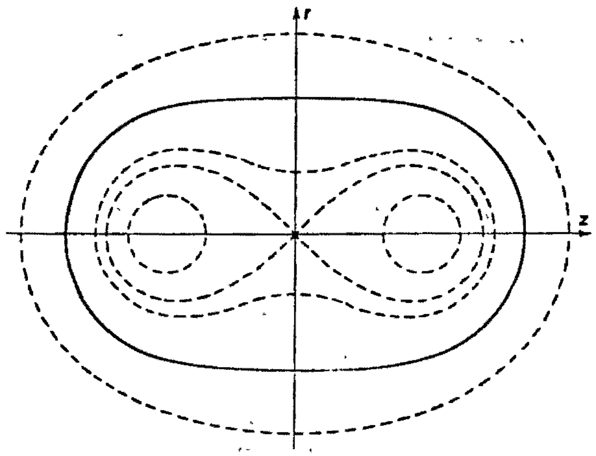

Fig. 7. CASSINI's curves

bend the cylinder inward and the ellipsoid outward. We shall study them in detail in Chapters 5 and 6.

The discrepancy of the hoop forces of the boiler end and the boiler drum may be avoided by choosing another shape of the meridian. The only requirement is that the radius $r_1 = \infty$ for $\phi = 90°$. There are, of course, many curves which fulfill this condition. One of them may be found among the Cassinian curves (fig. 7). Its equation is

$$(r^2 + z^2)^2 + 2a^2(r^2 - z^2) = 3a^4.$$

This curve is rather lengthy and therefore not particularly fit for the end of a pressure vessel, but its property of zero curvature at $z = 0$ is preserved when we subject it to an affine transformation, substituting $n\,z$ for z with $n > 1$:

$$(r^2 + n^2 z^2)^2 + 2a^2(r^2 - n^2 z^2) = 3a^4.$$

To find the stress resultants in a boiler end having this curve as a meridian, we need the radii r_1 and r_2. A simple but somewhat lengthy

computation yields the following formulas:

$$r_1 = 2\,\frac{[r^2(a^2 + n^2 z^2) + n^4 z^2(a^2 - r^2)]^{3/2}}{3n^2 a^3(a^2 - r^2 + n^2 z^2)},$$

$$r_2 = 2a\,\frac{[r^2(a^2 + n^2 z^2) + n^4 z^2(a^2 - r^2)]^{1/2}}{a^2 + r^2 + n^2 z^2}.$$

Introducing this into (15), we find the stress resultants

$$N_\phi = p\,a\,\frac{[r^2(a^2 + n^2 z^2) + n^4 z^2(a^2 - r^2)]^{1/2}}{a^2 + r^2 + n^2 z^2},$$

$$N_\theta = N_\phi\left[2 - \frac{3n^2 a^4(a^2 - r^2 + n^2 z^2)}{(a^2 + r^2 + n^2 z^2)\,[r^2(a^2 + n^2 z^2) + n^4 z^2(a^2 - r^2)]}\right].$$

Fig. 8 gives an example of the distribution of the stress resultants in such a boiler end. It shows the continuity of the hoop force. There is

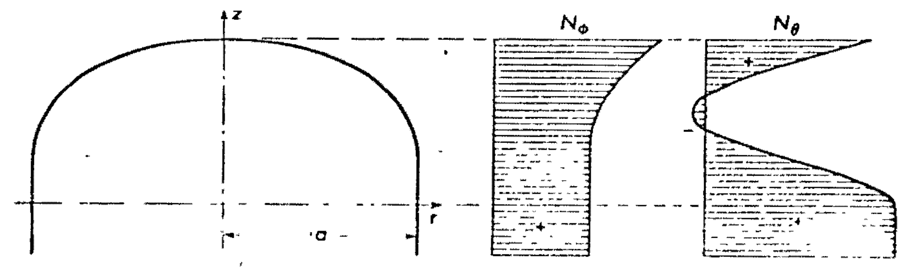

Fig. 8 Boiler end without discontinuity in the hoop forces

a small zone in which N_θ is negative. This may be avoided by choosing $n < 1.9$. If n is chosen much greater than 2, the compressive zone is wider and the maximum compressive stress higher

2.2.2.3 Pointed Shells

It is not necessary that the meridian meet the axis of the shell at a right angle. If it does not, a shell with a pointed apex results. Such shells have some particularities which we shall now study in a typical example. The meridian of the dome, fig. 9, is a circle whose center does not lie on the axis of revolution. Although the radius of curvature $r_1 = a$ of the meridian is a constant, the radius of transversal curvature is variable:

$$r_2 = \frac{r}{\sin\phi} = a\left(1 - \frac{\sin\phi_0}{\sin\phi}\right)$$

We ask for the stress resultants produced by the weight of the structure, assuming a constant wall thickness. The load is then given by [illegible]. We find N_ϕ from eq. (10) and avoid the determination of the constant C from a boundary condition by using the mechanical interpretation of this formula, writing the integral between the limits ϕ_0 and ϕ and dropping C:

$$N_\phi = -\frac{p\,a}{(\sin\phi - \sin\phi_0)\sin\phi}\int_{\phi_0}^{\phi}(\sin\phi - \sin\phi_0)\,d\phi$$

$$= -p\,a\,\frac{(\cos\phi_0 - \cos\phi) - (\phi - \phi_0)\sin\phi_0}{(\sin\phi - \sin\phi_0)\sin\phi}.$$

The hoop force then follows from (9b):

$$N_\theta = -\frac{p\,a}{\sin^2\phi}\,[(\phi - \phi_0)\sin\phi_0 - (\cos\phi_0 - \cos\phi) + {}$$

$$+ (\sin\phi - \sin\phi_0)\cos\phi\sin\phi].$$

At the vertex $\phi = \phi_0$ these formulas yield $N_\theta = 0$, but N_ϕ becomes indefinite. We find in the usual way by differentiating the numerator

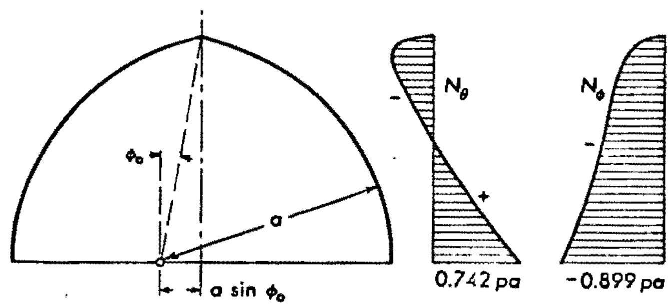

Fig. 9. Ogival shell. Force diagrams for $\phi_0 = 10°$

and denominator that N_ϕ also becomes zero. The stress distribution is shown in fig. 9.

In the limiting case $\phi_0 = 0$ the ogival dome becomes a sphere, and the preceding formulas give the stress resultants of a spherical dome. In this limiting case N_ϕ and N_θ are no longer zero at the top. One may easily see from fig. 9, how the limiting case is approached when $\phi_0 \to 0$: For very small values of ϕ_0, the normal forces rise rather suddenly from zero to approximately $-p\,a/2$. Such a sudden local change of the stress resultants sometimes occurs in membrane theory formulas, but it does not represent a physical reality. It would lead to almost discontinuous deformations, and the shell avoids such states of stress by additional bending stresses, as will be discussed in Chapter 6.

We now consider a modification of the ogival dome, in which the meridian begins at the axis with a negative value of ϕ, say $\phi = -\phi_0$. This results in a cupola of the type of fig. 10, having a downward point at its center. Let us compute the stresses for a snow load, distributed

uniformly over the projected area. Its components are

$$p_\phi = p\cos\phi\sin\phi, \qquad p_r = -p\cos^2\phi.$$

From eq. (10) we find

$$N_\phi = -\frac{p\,a}{(\sin\phi + \sin\phi_0)\sin\phi}\int_0^{\phi}(\sin\phi + \sin\phi_0)\cos\phi\,d\phi + \frac{C}{a(\sin\phi + \sin\phi_0)\sin\phi}$$

and after evaluation of the integral

$$N_\phi = -\frac{p\,a}{2}\,\frac{\sin\phi + 2\sin\phi_0}{\sin\phi + \sin\phi_0} + \frac{C}{a(\sin\phi + \sin\phi_0)\sin\phi}.$$

The denominator is zero for $\phi = -\phi_0$, and if we put $C = 0$, N_ϕ will become infinite at this point. It is possible to give C such a value that the numerator vanishes too, leading to $N_\phi = 0$, as we had in the ogival shell. But then N_ϕ would be infinite on the whole top circle $\phi = 0$, and that would be much worse. We choose tentatively $C = 0$ and we shall see at once what the singularity at the center means. Our formula now reads

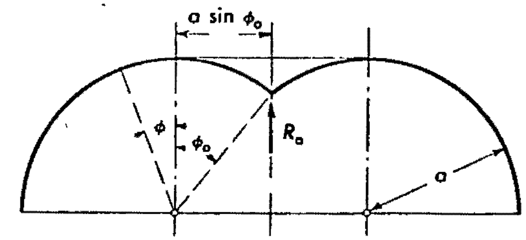

Fig. 10. Shell requiring central support

$$N_\phi = -\frac{p\,a}{2}\,\frac{\sin\phi + 2\sin\phi_0}{\sin\phi + \sin\phi_0},$$

and the hoop force follows from (9b):

$$N_\theta = \frac{p\,a}{2}\,(2\sin\phi_0\sin\phi - \cos 2\phi).$$

To study the singularity, we cut the shell in a parallel circle having a negative ϕ, say $\phi = -\phi' < 0$ and compute the resultant of the forces N_ϕ which act on it. It is a vertical force of magnitude

$$R = \frac{p\,a}{2}\,\frac{-\sin\phi' + 2\sin\phi_0}{-\sin\phi' + \sin\phi_0}\cdot\sin\phi'\cdot 2\pi a(\sin\phi_0 - \sin\phi')$$

$$= p\,a^2\pi(2\sin\phi_0 - \sin\phi')\sin\phi'.$$

For $\phi' = 0$, in the top circle, R is zero. This means that the meridional forces there which are horizontal, cannot carry any load from the inner part of the shell to the outer part. The inner part [illegible] its equilibrium by a special support, and that is possible only in the center. Indeed, for $\phi' = \phi_0$, the resultant R is

$$R_0 = p\,a^2\pi\sin^2\phi_0.$$

and this indicates what the singularity of the stress resultants means: that forces of infinite intensity, acting on a circle of radius zero, carry the total load applied on the part of the shell within the top circle. A support, say a column, which can exert a vertical force R_0 is needed there. Then the infinity disappears if the thin shell extends only to the circumference of this column.

The stress system, which we now have found, shows nothing special on the top circle $\phi = 0$ and seems to be quite harmless. But on p. 99, when discussing the deformations of toroidal shells, we shall see that this stress system cannot be realized because it would lead to an impossible deformation. We therefore have to expect additional bending stresses in a certain zone near the top circle, but since they are needed only to remedy an impossible deformation, they will be much smaller than those which would be needed in the absence of a central support, and which would have to transmit an important part of the total load. It is this argument which finally justifies our choice for the constant C.

2.2.2.4 Toroidal Shell

A toroid is generated by the rotation of a closed curve about an axis passing outside. A toroidal shell encloses an annular volume and may be considered as a pressure vessel. Figs. 11 and 12 show meridional sections of two typical cases.

The shell, fig. 11, may be cut in two parts as indicated by the broken line. The meridian of each part begins and ends with a horizontal

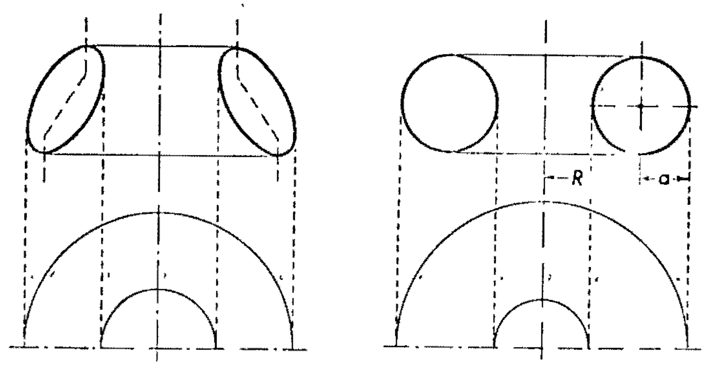

Figs. 11 and 12. Toroidal shells

tangent. Therefore the meridional forces acting at each edge do not have a vertical component and cannot transmit any vertical force from one half of the shell to the other. Now, when the shell is filled with gas of pressure p, this pressure has a downward resultant on the inner half and an upward resultant of the same magnitude on the outer half,

and neither part can be in equilibrium under the action of the pressure p and the forces on its edges. It follows that a membrane stress system with finite values N_ϕ, N_θ is not possible in this shell under this load.

This difficulty disappears when the two top circles have the same radius, e. g. when the meridian of the shell is a circle (fig. 12). Then eq. (10) gives with $p_\phi = 0$, $p_r = p$:

$$N_\phi = \frac{p\,a}{(a\sin\phi + R)\sin\phi}\left[\int (a\sin\phi + R)\cos\phi\,d\phi + C\right]$$

$$= \frac{p\,a}{(a\sin\phi + R)\sin\phi}\left[-\frac{a}{4}(\cos^2\phi - \sin^2\phi) + R\sin\phi + C\right],$$

and here we can determine C so that the singularities at $\phi = 0$ and at $\phi = \pi$ disappear simultaneously. This yields

$$N_\phi = \frac{p\,a}{a\sin\phi + R}\left(\frac{a}{2}\sin\phi + R\right), \qquad N_\theta = \frac{p\,a}{2}.$$

However, this solution also cannot be realized in the vicinity of the top and bottom circles without additional bending, because it again leads to an incompatibility of deformations which we shall discuss on p. 99.

2.2.2.5 Tanks

Our next example we choose in the domain of steel tanks. Fig. 13 shows a spherical tank, as used for storing water or gas. It is a complete sphere, supported along one of its parallel circles, $A\,A$. The essential

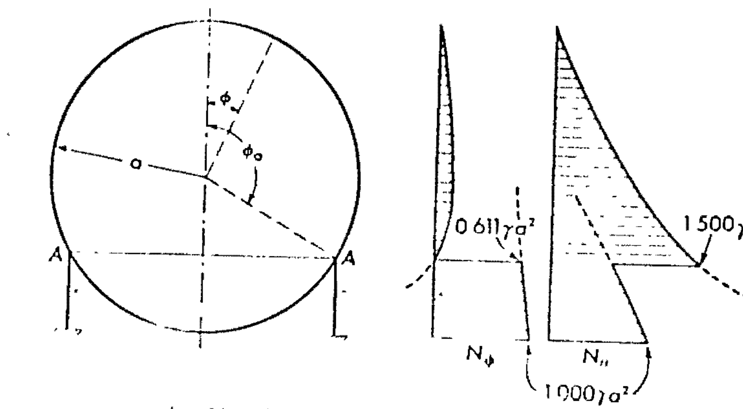

Fig. 13. Spherical water tank, [illegible] ϕ_0 [illegible]

load for a water tank is the pressure of the [illegible] (sp[illegible] [illegible]). It is normal to the shell ($p_\phi = 0$) and proportional to the depth. If the tank is completely filled, we have

$$p_r = \gamma a(1 - \cos\phi).$$

and this indicates what the singularity of the stress resultants means: that forces of infinite intensity, acting on a circle of radius zero, carry the total load applied on the part of the shell within the top circle. A support, say a column, which can exert a vertical force R_0 is needed there. Then the infinity disappears if the thin shell extends only to the circumference of this column.

The stress system, which we now have found, shows nothing special on the top circle $\phi = 0$ and seems to be quite harmless. But on p. 99, when discussing the deformations of toroidal shells, we shall see that this stress system cannot be realized because it would lead to an impossible deformation. We therefore have to expect additional bending stresses in a certain zone near the top circle, but since they are needed only to remedy an impossible deformation, they will be much smaller than those which would be needed in the absence of a central support, and which would have to transmit an important part of the total load. It is this argument which finally justifies our choice for the constant C.

2.2.2.4 Toroidal Shell

A toroid is generated by the rotation of a closed curve about an axis passing outside. A toroidal shell encloses an annular volume and may be considered as a pressure vessel. Figs. 11 and 12 show meridional sections of two typical cases.

The shell, fig. 11, may be cut in two parts as indicated by the broken line. The meridian of each part begins and ends with a horizontal

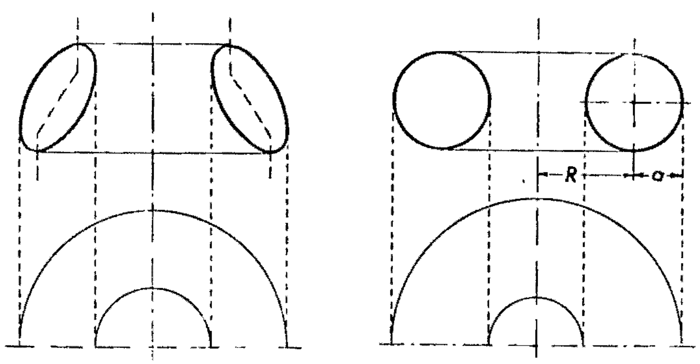

Figs. 11 and 12. Toroidal shells

tangent. Therefore, the meridional forces acting at each edge do not have a vertical component and cannot transmit any vertical force from one half of the shell to the other. Now, when the shell is filled with gas of pressure p, this pressure has a downward resultant on the inner half and an upward resultant of the same magnitude on the outer half,

and neither part can be in equilibrium under the action of the pressure p and the forces on its edges. It follows that a membrane stress system with finite values N_ϕ, N_θ is not possible in this shell under this load.

This difficulty disappears when the two top circles have the same radius, e. g. when the meridian of the shell is a circle (fig. 12). Then eq. (10) gives with $p_\phi = 0$, $p_r = p$:

$$N_\phi = \frac{p\,a}{(a\sin\phi + R)\sin\phi}\left[\int (a\sin\phi + R)\cos\phi\, d\phi + C\right]$$
$$= \frac{p\,a}{(a\sin\phi + R)\sin\phi}\left[-\frac{a}{4}(\cos^2\phi - \sin^2\phi) + R\sin\phi + C\right],$$

and here we can determine C so that the singularities at $\phi = 0$ and at $\phi = \pi$ disappear simultaneously. This yields

$$N_\phi = \frac{p\,a}{a\sin\phi + R}\left(\frac{a}{2}\sin\phi + R\right), \qquad N_\theta = \frac{p\,a}{2}.$$

However, this solution also cannot be realized in the vicinity of the top and bottom circles without additional bending, because it again leads to an incompatibility of deformations which we shall discuss on p. 99.

2.2.2.5 Tanks

Our next example we choose in the domain of steel tanks. Fig. 13 shows a spherical tank, as used for storing water or gas. It is a complete sphere, supported along one of its parallel circles, A A. The essential

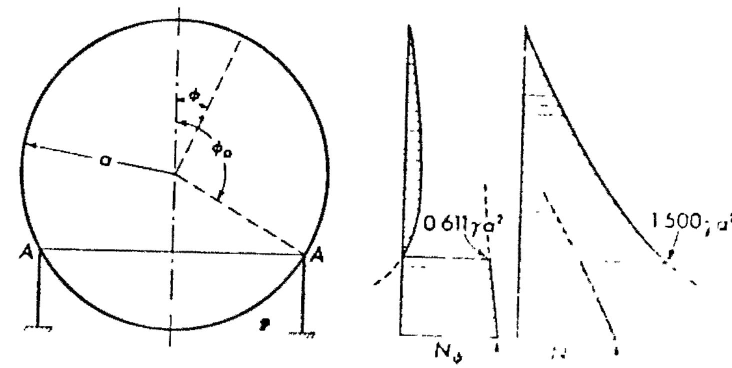

Fig. 13. Spherical water tank [illegible]

load for a water tank is the pressure of the water (specific weight γ). It is normal to the shell ($p_\phi = 0$) and proportional [illegible]. tank is completely filled, we have

$$p_r = -\gamma a(1 - \cos\phi).$$

a simple integration, we find from eq. (10) the meridional force

$$N_\phi = \frac{\gamma a^2}{\sin^2\phi}\left[\int(1-\cos\phi)\cos\phi\sin\phi\,d\phi + C\right]$$

$$= \frac{\gamma a^2}{6\sin^2\phi}\left[(2\cos\phi - 3)\cos^2\phi + 6C\right].$$

the vertex $\phi = 0$ the denominator vanishes. To obtain a finite value N_ϕ the factor in brackets must also become zero. This leads to $= 1/6$, and after some simple transformation we find

$$N_\phi = \frac{\gamma a^2}{6}\,\frac{1-\cos\phi}{1+\cos\phi}\,(1 + 2\cos\phi)$$

, from eq. (9b),

$$N_\theta = \frac{\gamma a^2}{6}\,\frac{1-\cos\phi}{1+\cos\phi}\,(5 + 4\cos\phi).$$

se formulas are valid above the supporting circle $\phi = \phi_0$. In the er part of the shell we have to apply another value of C, which kes N_ϕ finite at $\phi = \pi$. It is $C = 5/6$ and hence we have

$$N_\phi = \frac{\gamma a^2}{6}\,\frac{5 - 5\cos\phi + 2\cos^2\phi}{1-\cos\phi},$$

$$N_\theta = \frac{\gamma a^2}{6}\,\frac{1 - 7\cos\phi + 4\cos^2\phi}{1-\cos\phi}.$$

distribution of these forces is shown in fig. 13.

The location of the supporting circle does not influence the two ues of C. If we give it a higher or lower position, only the domains validity of the two pairs of formulas are changed. The corresponding nges in the stress resultants are indicated by dotted lines in fig. 13. ey show that a position of the support below $\phi = 120°$ leads to npressive forces in the meridian, which in a thin-walled structure this one should be avoided, and that a higher position cuts off the k value of N_θ which determines the wall thickness, but of course eads to a larger and more expensive support.

At the supporting ring both stress resultants change their values continuously. The difference of the meridional forces is a load lied to the ring. We resolve it into a vertical component

$$\frac{2\gamma a^2}{3\sin\phi_0},$$

ected downward, which the ring must pass to its numerous supports bending and torsion, and into a horizontal component

$$\frac{2\gamma a^2}{3}\,\frac{\cot\phi_0}{\sin\phi_0},$$

ich is a radial load applied to the ring, producing in it a compressive op stress.

Here we have again a case in which the direct stresses lead to a deformation which is incompatible with the continuity of the structure. A discontinuity in the hoop force means a discontinuity of the elastic extension of the parallel circles. A membrane-stress system which avoids this discrepancy cannot exist, since we have already used all available constants to fulfill other, more important conditions. The continuity of deformations can be reestablished only by an additional bending of the border zones of both halves of the shell, and again we have to refer to the treatment of this problem in Chapter 6.

A similar disturbance, but of greater intensity, is caused by the connection of the shell to the supporting ring, if this is supported by vertical forces, as shown in fig. 13. Then the ring is subject to compressive stresses which fit the positive hoop stresses in both parts of the shell even more poorly than these fit each other. For this reason it is preferable to support the ring by inclined bars, tangential to the meridians of the shell, or even by a conical steel plate. Then the ring is relieved of its hoop stress and causes less disturbance of the membrane forces of the shell.

If we change the formula for p_r slightly, writing

$$p_r = -\gamma(h_1 + a - a\cos\phi),$$

we may obtain the membrane forces in a spherical tank bottom such as that shown in fig. 14. The evaluation of the integral (10) and subsequent application of (9b) yield

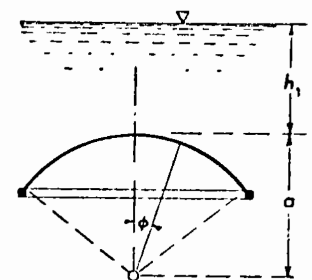

Fig. 14. Spherical tank bottom

$$N_\phi = -\frac{\gamma a}{6}\left[3h_1 + a\,\frac{1-\cos\phi}{1+\cos\phi}\,(1 + 2\cos\phi)\right],$$

$$N_\theta = +\frac{\gamma a}{6}\left[3h_1 + a\,\frac{1-\cos\phi}{1+\cos\phi}\,(5 + 4\cos\phi)\right].$$

These are both compressive forces, and at the edge of the shell [illegible] must be a ring to take care of the horizontal component of the meridional force N_ϕ.

Another kind of tank bottom which is of practical inter[illegible] in fig. 15a. It is the lower half of an ellipsoid of revolution [illegible] mulas concerning its geometry have already been give[illegible] add here the relation

$$z = \frac{b^2\cos\phi}{(a^2\sin^2\phi + b^2\cos^2\phi)^{1/2}}$$

The load on the shell is $p_r = -\gamma(h + z)$. When this is introduced [illegible] the integral (10), a somewhat lengthy integration must be performed cease to be so. The shell degenerates into a plane plate, and no tank of reasonable shape can be obtained. Therefore, drop tanks are not particularly fit for storing water, but they have been built for the storage of gasoline. When the tank contains a volatile liquid, the pressure γh at the top is welcome to prevent evaporation losses in hot weather.

When a drop tank is to be constructed there will be given the specific weight γ of the contents, the desirable pressure head h, the working stress σ in the steel plates, and the capacity V. The first three of these data enter into the parameter

$$\frac{h}{a} = h\sqrt{\frac{\gamma}{\sigma t}},$$

but V does not. Instead of this the wall thickness t appears. One has to start the computation with an assumed thickness and at the end check

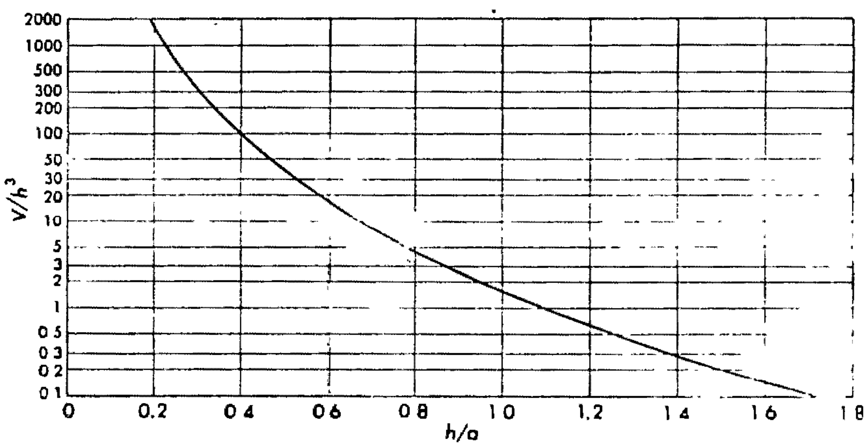

Fig 21. Capacity of drop-shaped tanks vs. h/a

the volume of the resulting tank. Then the computation must be repeated with a better fitting wall thickness until agreement between the resulting and the required capacity is reached. This will be facilitated by fig. 21, where V/h^3 is plotted against h/a. With the help of this diagram the computation may be started at once with the right value of h/a.

The drop-shaped tank cannot be expected to have uniform stress if the actual load is different from the design load, whether it be that the top pressure is not exactly as assumed or that the tank is only partially filled, with or without some gas pressure on the liquid level. In all these cases N_ϕ must be found from eq. (10) by numerical integration and N_θ from eq. (9b). One essential result of such computations may be predicted without going through the details of the numerical

work: When we separate the tank from its foundation, we find two external forces acting on it, the weight of the contents and the upward force exerted by the foundation on the flat bottom. The latter force equals the pressure γH at this level multiplied by the area of the bottom plate. Under arbitrary loading conditions one cannot expect that this reaction and the weight will be equal. The force N_ϕ at the edge E, fig. 19, cannot take care of the difference because it is horizontal, and therefore a transverse shear Q_ϕ is needed at the edge. Since the membrane theory denies the existence of transverse shears, it will yield $N_\phi = \pm\infty$, and N_θ will then become infinite, with the opposite sign. The practical application of the drop shape should therefore be limited to the upper part of the tank, say to $\phi < 150°$ or $160°$, and the rest should be completely cut away or replaced by an arc which leads

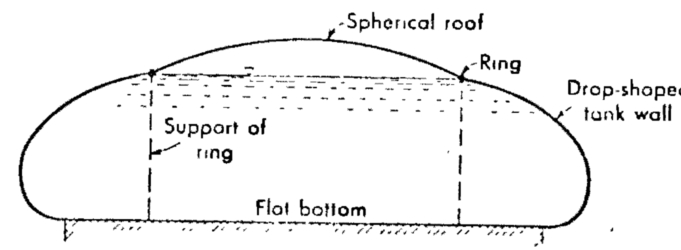

Fig 22. Partially drop-shaped tank

without discontinuity of the curvature to a ring before its tangent becomes horizontal.

The height h depends on the liquid to be stored. Tanks of great capacity will always become rather flat and may not be able to support their own weight when empty. Such tanks may be built in an open form and closed by a roof which is not touched by the liquid (fig. 22). The calculation of the shape is very similar to that described here. The meridian starts with a set of finite values [illegible]. If [illegible] is small enough, the approximate formula (22) may be used [illegible] the integration, but now both terms must be employed, and the [illegible] B must be chosen so as to meet the initial values of [illegible].

2.3.2 Dome of Constant Strength

A shell dome looks almost like a three dimensional arch [illegible]. This raises the question whether or not for a given load there also exists a best shape, analogous to the funicular curve for [illegible].

This question shows plainly the fundamental difference [illegible] the shell and the arch. Only an arch shaped like the funicular [illegible] is free from bending moments; any other one needs them [illegible] librium. Exactly the contrary is true for a shell dome. We have seen how we can have equilibrium without bending in almost any shell for almost any load, and the additional bending which occurs in boundary zones is of somewhat the same importance as the bending moments in a statically indeterminate funicular arch.

From this situation it follows that we can ask for more than absence of bending. We can try to find a shape of the shell such that the membrane stress σ has the same magnitude at every point and in every direction.

As a first problem of this type we determine the shape of a dome which has to carry its own weight. The problem is a simple one if the dome consists of a plain concrete shell without additional dead load. Then, if γ is the specific weight of the concrete, the load per unit area of the surface is

$$p_\phi = \gamma t \sin\phi, \qquad p_r = -\gamma t \cos\phi.$$

Introducing this into eq. (9b) and putting

$$N_\phi = N_\theta = -\sigma t$$

(here σ is considered positive when it is a compression, contrary to our usual convention), we get

$$\sigma t \left(\frac{1}{r_1} + \frac{1}{r_2}\right) = \gamma t \cos\phi \qquad (25)$$

and resolving with respect to r_1:

$$r_1 = \frac{r}{(\gamma/\sigma)\, r \cos\phi - \sin\phi}.$$

By means of the geometric relation (4a) this may be transformed into a simple differential equation for $r(\phi)$ or, better, for $\phi(r)$:

$$\frac{d\phi}{dr} = \frac{\gamma}{\sigma} - \frac{\tan\phi}{r}. \qquad (26)$$

It may be solved by numerical integration, beginning at the vertex. There we have $r_1 = r_2$, and hence from (25) and (4a):

$$\frac{d\phi}{dr} = \frac{1}{r_1} = \frac{\gamma}{2\sigma}.$$

We see that there is only one parameter, σ/γ. It has the dimension of a length and determines the size of the shell. When we have found r as a function of ϕ, we determine the meridian in cartesian coordinates by a simple quadrature:

$$z = \int \tan\phi \, dr.$$

The wall thickness follows from eq. (9a), which here assumes the form

$$-\frac{d}{d\phi}(r\sigma t) + r_1 \sigma t \cos\phi + \gamma t r r_1 \sin\phi = 0$$

and yields
$$\frac{dt}{d\phi} = \frac{\gamma}{\sigma} t \tan\phi \cdot \frac{dr}{d\phi}.$$

This equation has a simple solution, when we transform it to rectangular coordinates r, z. We have

$$\frac{d}{d\phi} = r_1 \frac{d}{ds} = r_1 \sin\phi \cdot \frac{d}{dz}, \qquad \frac{dr}{dz} = \cot\phi$$

and therefore

$$\frac{dt}{dz} = \frac{\gamma}{\sigma} t$$

which is solved by

$$t = t_0 \exp\frac{\gamma z}{\sigma}.$$

The solution is represented in fig. 23. The shell may be extended to greater angles ϕ, but then the exponential growth of t leads to structures which soon cease to be thin-walled and probably are beyond the sphere of technical interest.

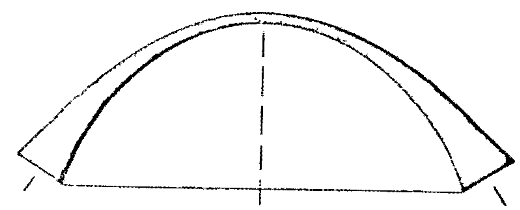

Fig. 23 Dome of constant strength

For domes of usual sizes, the problem of a shell of constant stress is of no practical importance, because shells of any reasonable shape will have direct stresses far below the admissible limit. But we see, for example, from eq. (13) for a spherical dome, that the stress resultants are proportional to pa; therefore the stresses caused by the weight of the shell are proportional to γa. This indicates that they increase in proportion to the diameter of the dome, independently of the wall thickness. Therefore, for every shape of the shell there exists a certain size beyond which it can no longer be built in a material of a given σ/γ, and the shell of constant stress is that which allows the biggest dome.

Usually a large dome will have an opening at the top. We may use the previous solution also in this case if we choose the thickness t so that $N_\phi = -\sigma t$, together with a compr[illegible] ring will be capable of carrying the loads applied at the upper [illegible]. But this is not the most general solution for a dome having an opening. W[illegible] it by numer[illegible] integration of eq. (26), beginning at the edge [illegible] value $\phi = \phi_0$. This means that we have two parameters and hence a greater variety of shapes. If we choose ϕ_0 [illegible] 0, we [illegible] as that in fig. 21a which abuts against a ring having [illegible] force $\sigma t b$. To avoid a local disturbance, its cross section [illegible] have the area $t b$ and it will be quite heavy. To carry its weight, we must

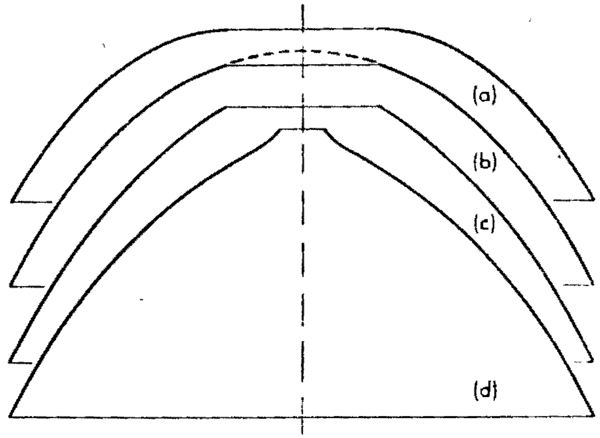

Fig 24 Domes of constant strength with skylight

choose $\phi_0 > 0$. Among these solutions is the one which we obtained for the closed shell. If we choose ϕ_0 so that

$$\frac{\tan\phi_0}{b} = \frac{\gamma}{\sigma}$$

the meridian begins with a point of inflection and for still greater values of ϕ_0 we come to shapes as indicated by Fig. 24d.

2.4 Loads without Axial Symmetry

2.4.1 General Equations

We shall now drop the assumption that all loads and stress resultants are independent of the coordinate θ. The equations (6a–c) have already been established for the general case. Since one of them, eq. (6c), contains no derivatives, we use it to eliminate N_θ from the other two. Making use of the geometrical relations (4) and (5) we obtain the following set:

$$r_2 \frac{\partial N_\phi}{\partial \phi} \sin\phi + (r_1 + r_2) N_\phi \cos\phi + r_1 \frac{\partial N_{\phi\theta}}{\partial \theta} = -r_1 r_2 (p_\phi \sin\phi + p_r \cos\phi),$$

$$r_2 \frac{\partial N_{\phi\theta}}{\partial \phi} \sin\phi + 2 r_1 N_{\phi\theta} \cos\phi - r_2 \frac{\partial N_\phi}{\partial \theta} = -r_1 r_2 \left(p_\theta \sin\phi - \frac{\partial p_r}{\partial \theta}\right) \qquad (27)$$

We might go one step further and eliminate $N_{\phi\theta}$. This would lead to a second order differential equation for N_ϕ. We shall come back to this on p. 78 and we shall see then that important conclusions may be drawn from this equation. But for the present purpose it is simpler to use the system (27).

Alberca y Gimnasio Olímpicos
Procedimientos de Construcción

Francisco DE PABLO *

RESUMEN

Este artículo describe la construcción de la alberca y gimnasio olímpicos. La cubierta, que mide 99 6 × 101.6 m en el caso de la alberca, y 66 4 × 76.2 en el gimnasio, es una de las cubiertas colgantes más grandes en el mundo. Está formada por cables de acero anclados en una trabe de borde que se apoya en columnas de concreto armado. La cimentación y gradería son también de concreto armado.

SYNOPSIS

This paper describes the construction of the Olympic swimming-pool and gymnasium. The roof, which measures 99.60 × 101 60 m in the swimming pool and 66.40 × 76.20 m in the gymnasium, is one of the largest suspended roofs in the world. The whole foundation and grandstands are of reinforced concrete. The roof is made of suspended steel cables anchored in a steel beam supported on the columns of reinforced concrete.

1. *INTRODUCCION*

Estas instalaciones, construidas por la Secretaría de Obras Públicas, tienen distinta utilización, pero el tipo y criterio de diseño de estructuración es el mismo, además de tener elementos comunes. En estas condiciones hablaremos del conjunto

La alberca es una estructura de 99.60 × 101.60 m, no incluidos los servicios, por lo que se puede catalogar su cubierta colgante como una de las mas grandes que existen. Junto a esta instalación, y aprovechando uno de los ejes de columnas, se encuentra el gimnasio para volibol de dimensiones 66.40 × 76.20 m. La superficie total construida es de 39 000 m² aproximadamente. En cada una de estas estructuras podemos distinguir, atendiendo a la carga que reciben de la estructura, las siguientes zonas:

a) Zona bajo la escalinata y losa de acceso que se caracteriza por una carga ligera de 1 ton/m².
b) Zona bajo las graderías con una carga trasmitida de 3 ton/m² aproximadamente
c) Zona correspondiente a las columnas que soportan la cubierta cuya carga en la cimentación es de 6 a 7 ton/m².

2. *CIMENTACION*

Durante la etapa de excavación, previa al colado de la cimentación, se encontró un terreno con características limo-arenosas. En efecto, a los 2 m de profundidad se encontró una capa de arena que drena muy bien el terreno, y alrededor de los 4 m un limo arcilloso con alto contenido de agua. El nivel de aguas freáticas se encuentra a 2.20 m aproximadamente. De acuerdo con los estudios previos de mecánica de suelos, era conveniente limitar las

* Secretaría de Obras Públicas.

Etapa de excavación

zonas excavadas, ya que por cada tonelada de descarga se esperaba una expansión de 5 cm.

En estas condiciones el proceso de excavación se realizó de la siguiente manera.

— Se inició en las zonas oriente y poniente con una profundidad total de 1 05 m. La cimentación de esta parte esta formada por zapatas corridas de concreto armado.
— Simultáneamente se comenzó la excavación de la zona correspondiente a las graderías, con una profundidad máxima de 2.55 m. La cimentación de esta zona está formada por cascarones invertidos en la alberca, y trabes y losas de cimentación en el gimnasio. La profundidad de excavación se escogió con el criterio de compensar las cargas de la estructura Las zonas excavadas tenían unas dimensiones máximas de 20 × 40 m.
— Zona de cajones profundos correspondientes a las columnas que soportan directamente la cubierta. La profundidad de excavación en

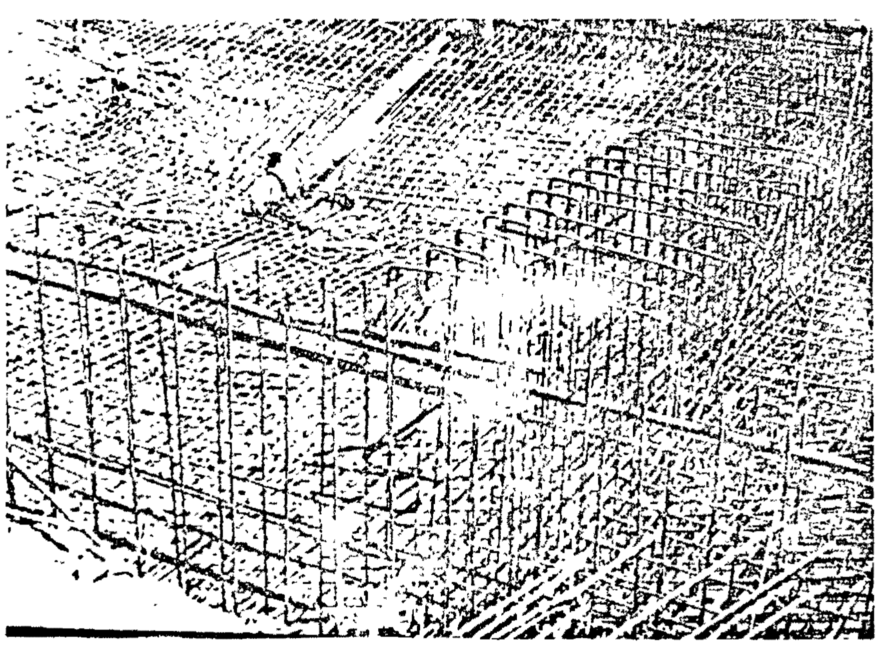

Detalle del armado en cimentación

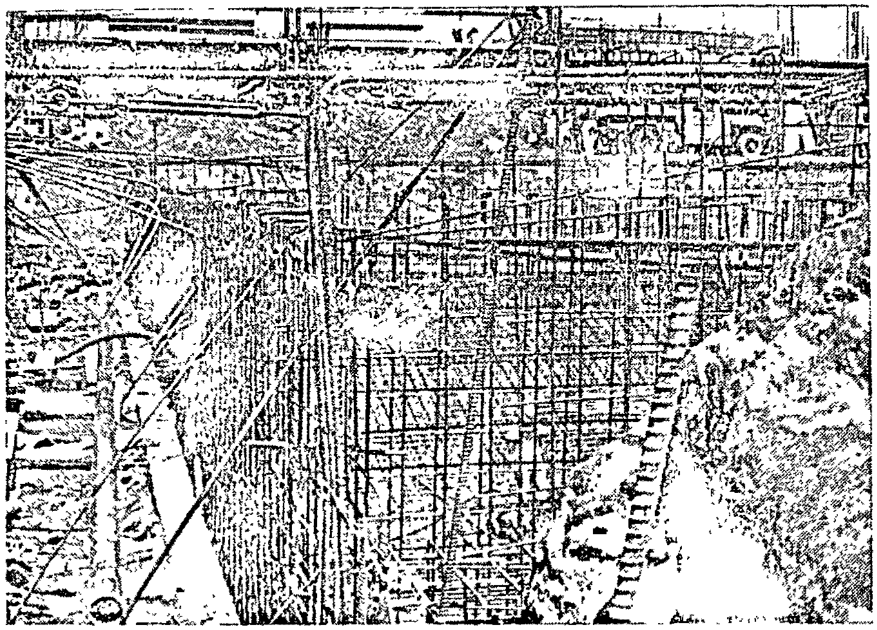

Detalle del armado en foso de alberca. Se aprecian los anclajes de postensado

esta parte es de 3.85 m en la zona sur, de 5 05 m en la zona intermedia, y de 3.55 m en la zona norte. Las partes excavadas tenían una superficie máxima de 20 × 25 m, además del talud que había que dar a las paredes de la excavación Durante este proceso se mantuvo el nivel de agua freática abatido a una profundidad de 6 m con respecto al nivel del terreno.

— Fosos de alberca para natación y para clavados, con una profundidad de 2.20 m el primero, y máxima de 6.25 m el segundo. Esta excavación se realizó en su totalidad permitiendo que el terreno tuviera expansiones durante el proceso constructivo. De esta manera se trataba de evitar que los movimientos futuros de esta zona, producidos por descarga de la alberca, afectaran al resto de la estructura.

Los fosos presentan el problema de que cuando están vacíos se encuentran sobrecompensados, y por lo tanto tienden a emerger induciendo esfuerzos al resto de la estructura. De aquí que, con el

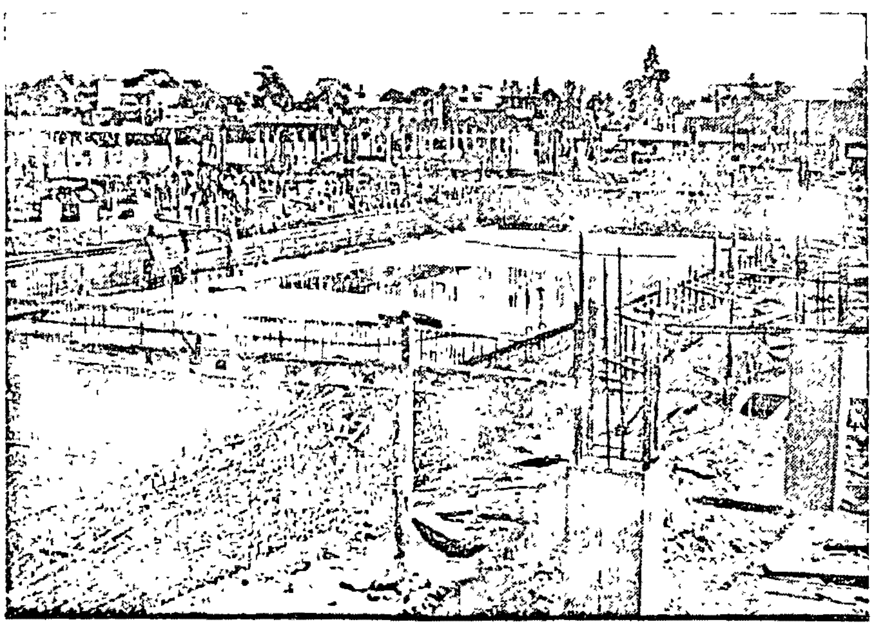

Vista panorámica de los fosos en la etapa constructiva procedimiento de excavación descrito, se tratara de producir expansiones iniciales en el suelo, con objeto de que, al colar los elementos estructurales propios de los fosos, y al llenar los mismos con agua, hubiera recompresiones del terreno, y por consiguiente asentamientos semejantes a los del resto de la estructura. Con las losas de fondo se buscó lastrar estas zonas sobrecompensadas y evitar la flotación; de este modo el foso de clavados tiene una losa de concreto de 1 m, y el de natación de 0.20 m de espesor.

Durante este proceso de excavación se llevaron nivelaciones periódicas de bancos situados en el centro de la excavación, y el valor máximo de las expansiones fue de 5 cm.

Una vez efectuado el colado de cada tramo de cimentación, se procedía a lastrarlo con agua, y a continuación se excavaba la zona siguiente.

3. *ESTRUCTURA*

Conforme se iba terminando el colado de la cimentación, se iniciaba de inmediato la construcción de la losa de nivel 4.00 y el colado de las graderías. Todo el colado se efectuó con concreto premezclado; se logró un promedio de 100 m^3 de concreto colado por día.

La fosa de natación y clavados está constituida por dos muros paralelos, que forman un pasadizo perimetral que tiene por objeto alojar instalaciones. También permite el acomodo de cámaras de televisión, de fotógrafos, etc. Todo el concreto en contacto con el terreno tiene en su parte exterior un recubrimiento de lámina de PVC para impedir filtraciones de agua. De estos muros, el interior en contacto con el agua de la alberca es el menos seguro, ya que puede permitir fugas de agua. El cálculo de estos fosos, se ha realizado suponiendo una losa de fondo apoyada en una serie de trabes y muros ligados al resto de la estructura. Para evitar la fisuración de los muros de la alberca, además de su armado propio como trabes, se les aplicó una fuerza de postensado. El proceso de construcción seguido fue el siguiente:

— Colado de la losa de fondo de alberca sobre una lámina impermeable de PVC. Después de alcanzada la resistencia de diseño, se postensó a 50 ton por tendón, estando estos a 2.50 m de separación.
— Colado de los muros perimetrales hasta el nivel 0.63 m postensando estos elementos a 40 ton. Existen dos tendones.
— Colado de la parte superior de los muros perimetrales y postensado de los mismos a una carga de 60 ton. Existen tres tendones. Con este procedimiento de tensado, se trató de evitar fuerzas muy excesivas de postensado, como hubiera ocurrido de haberse aplicado el tensado con todos los elementos colados. De esta manera se eliminaron las grietas en cada uno de los elementos estructurales que forman el foso.

Después de haber colado los fosos, y transcurrido algún tiempo para permitir movimientos del terreno, se ligaron aquellos al resto de la estructura.

El proceso de colado de las columnas que soportan la cubierta fue una de las etapas más difíciles en la construcción, debido a la altura que es de 26.50 m en el eje norte; 37.50 m en el central y 34.50 m en el eje sur. Todo el trabajo se realizó por medio de andamios tubulares, sobre los que se ejecutaron las maniobras de trabajo. El peso de es-

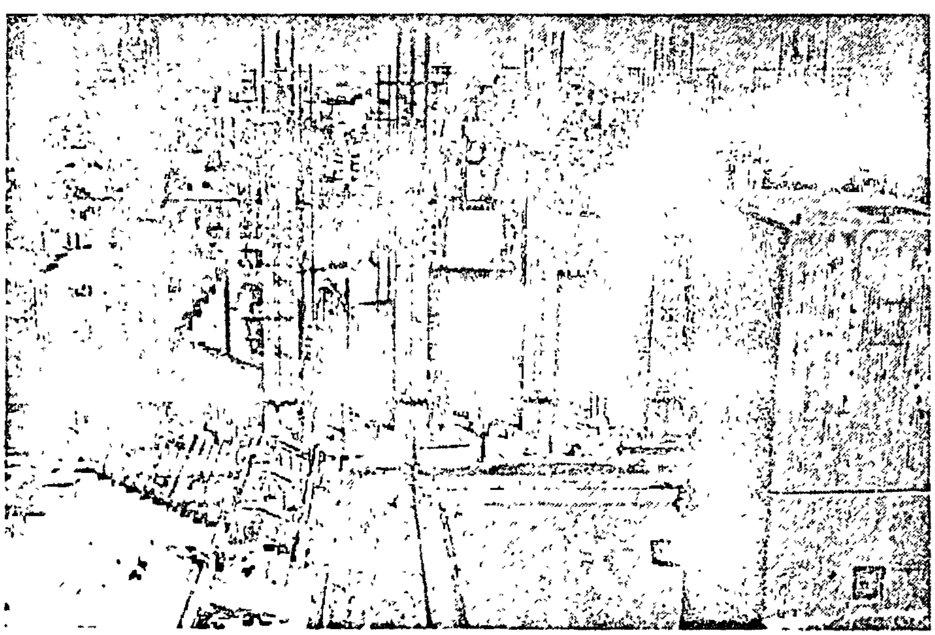

Proceso de colado de las columnas centrales

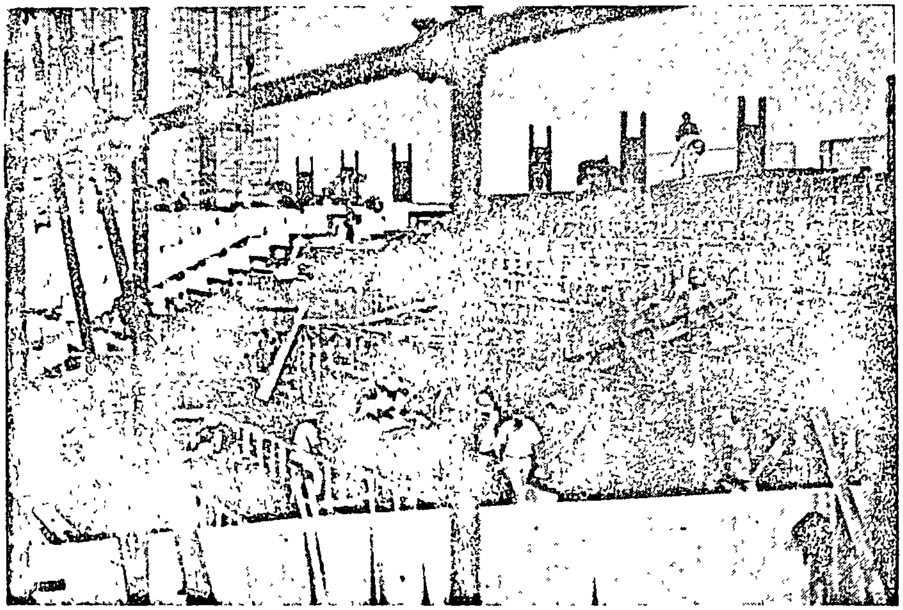

Construcción de las graderías

tructura tubular por metro de columna fue aproximadamente de 400 kg. Se usó madera machihembrada como cimbra, troquelada por medio de tornillos de acero. Las uniones de colado se hicieron de lámina ligadas a la cimbra, que marcaron la junta en el concreto. El tiempo promedio en que se ejecutó un ciclo completo, por tramo, fue de tres días. La principal dificultad estuvo en el colado de los diafragmas que interrumpían interiormente la columna y que estaban a una separación aproximada de 4 ó 6 m. La sección de las columnas extremas es de 2 × 3 m, y de 3 × 5 m las centrales.

Las columnas centrales, comunes a la alberca y gimnasio, se encuentran en condiciones distintas de las de los extremos, por no tener retenidas. Deben soportar un momento adicional producido por la diferencia de pesos de las dos cubiertas, además de la distinta altura a que se encuentran ambas. En estas condiciones se creyó conveniente postensarlas aplicándoles, por tendón, una fuerza de 85 ton en las centrales y 49 ton en las correspondientes al mismo eje, en su cara norte colindante con el gimnasio. Se empleó el anclaje tipo Prescon. Cada columna tiene cuatro tendones de diecinueve alam-

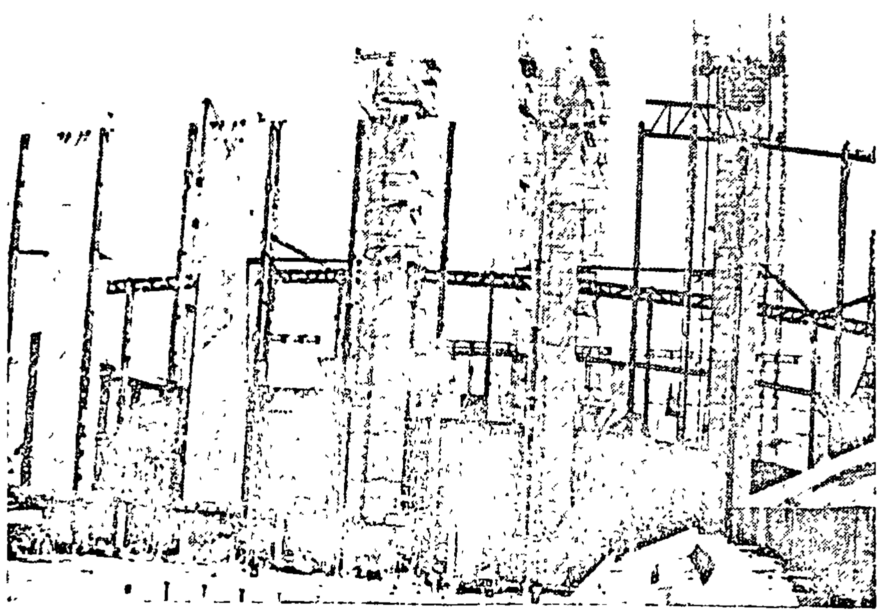

Proceso constructivo de la zona común de alberca y gimnasio

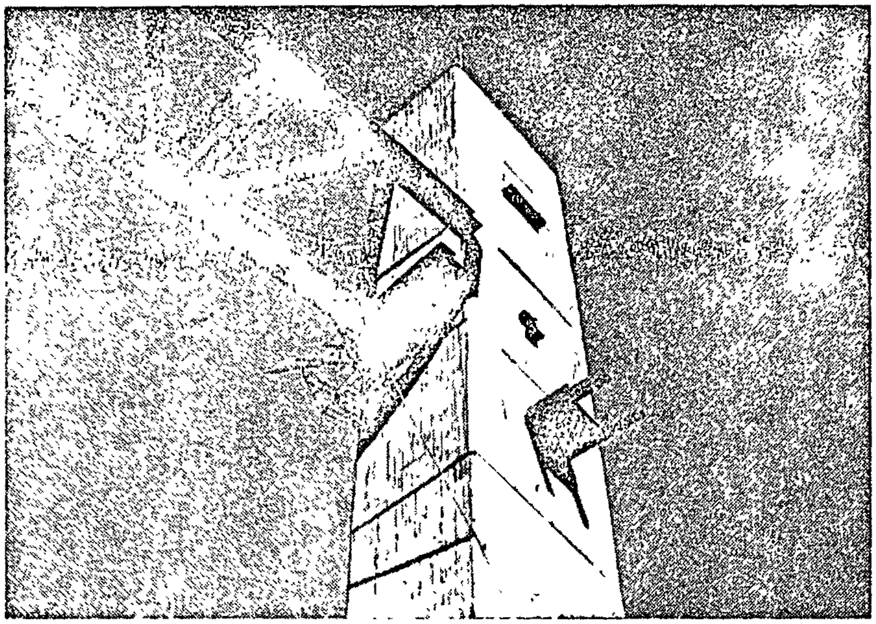

Detalle del anclaje de la trabe de borde

bres de 7 mm a una altura de 20 m. y siete tendones de diecinueve alambres de 7 mm a 35 15 m de altura. Durante el proceso de tensado, estas columnas sufrieron en su extremo superior un desplazamiento máximo de 2.5 cm. En la cimentación de estas columnas también hubo necesidad de considerar la diferencia de peso de las cubiertas; para ello se colocó un lastre de arena en la parte de cimentación que corresponde al gimnasio.

Simultáneamente al colado de las columnas, se inició el montaje de la estructura de acero. Esta estructura está formada por las columnas de los ejes extremos oriente y poniente que, al mismo tiempo que forman la fachada, soportan la trabe de borde de la cubierta. Son columnas con una alta relación de esbeltez y están restringidas, a manera de puntales, por las trabes que soportan la tribuna provisional. Una vez montadas las columnas que se fabricaron en dos tramos, se montó la trabe de borde utilizando para ello un cable-vía. El peso promedio de cada una de estas piezas era de 4 ton. Especial dificultad presentó el lograr la unión de los tramos de la trabe de borde con los anclajes alojados en las columnas de concreto. En toda la

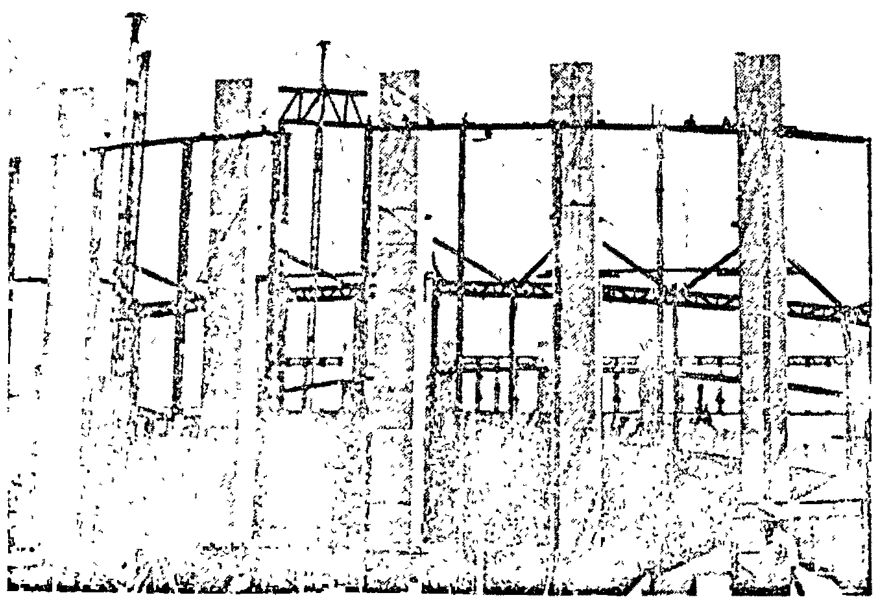

Montaje de la estructura de acero

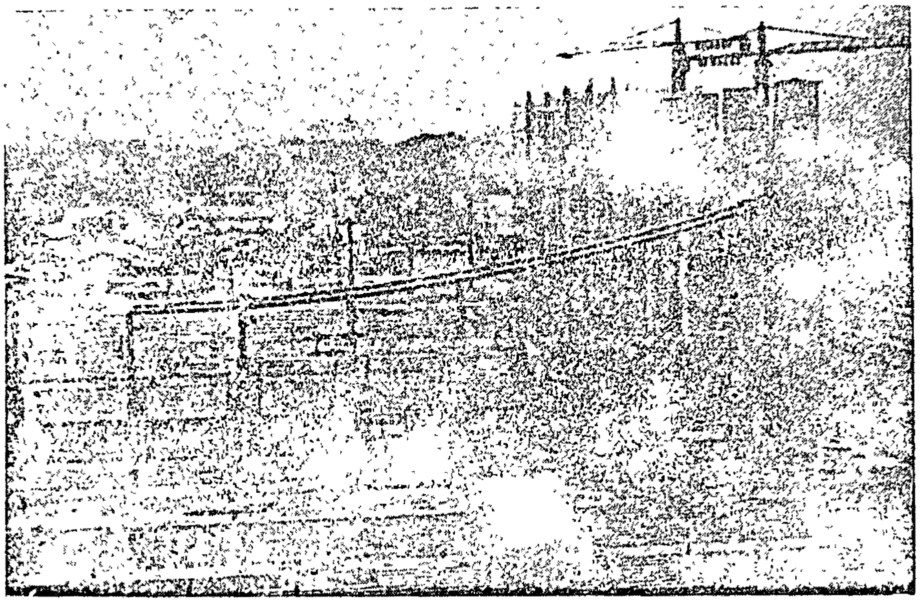

Vista panorámica de la obra cuando se inició la colocación de los cables del techo

estructura de acero se hicieron las pruebas necesarias de calidad del material y se radiografiaron las soldaduras 100 por ciento. El promedio de acero fue de 45.00 kg/m² en lo que respecta a la cubierta. La totalidad de la estructura se fabricó y montó en un tiempo de 150 días.

Todas las graderías para público se probaron de acuerdo con los reglamentos en vigor. En este caso la carga aplicada fue de 950 kg/m². La flecha máxima observada fue de 10 mm que se recuperó en un 90 por ciento.

4. *CUBIERTA*

El techo, que cubre una superficie de 98.40 × 107.90 m en alberca, y de 66.40 × 73.80 m en gimnasio, está formado por una cubierta del tipo colgante que, por sus dimensiones, se puede considerar como una de las más grandes construidas hasta el momento. La integrada por una retícula de cables de acero de presfuerzo con curvaturas opuestas en dos direcciones. En el sentido largo o de carga se encuentran unos tendones formados por doce

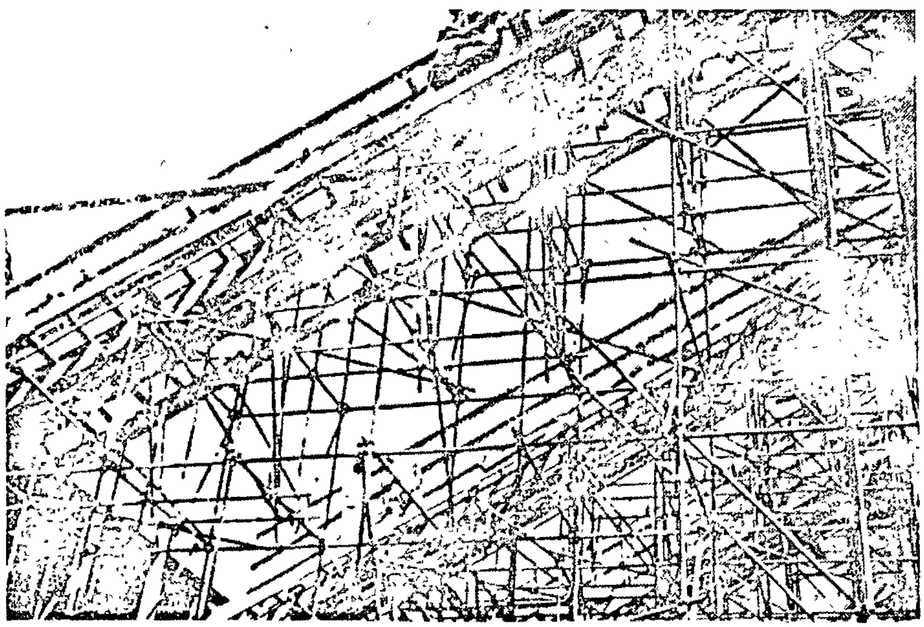

Detalle de la construcción de las trabes que soportan las graderías cables de 7 mm en la alberca, y por diez cables de 7 mm en el gimnasio. La separación de estos cables es de 1.59 m entre sí, con una flecha máxima de 7.50 m en la alberca, y de 5 m en el gimnasio. Los anclajes se encuentran a distinta altura con objeto de describir una parábola cuyo vértice superior se encuentra en el eje central de la cubierta. En sentido transversal hay cables de forma cada 2.07 m, constituidos por un torón de ½" de diámetro, de acero galvanizado de presfuerzo. La flecha de los cables en sentido transversal es de 5 m en alberca, y de 3.50 m en gimnasio.

Hay que proteger estos cables adecuadamente, ya que en caso contrario pueden oxidarse rápidamente y fallar de manera brusca. La oxidación se incrementa, en este caso, debido a los siguientes factores indicados en seguida:

- Los cables son de acero de presfuerzo y por ello con alto contenido de carbono.
- Están sometidos a un esfuerzo de tensión.
- Los de la alberca se encuentran en un ambiente con un contenido de humedad relativa de 65 por ciento.
- La atmósfera de la alberca contiene algo de cloro (0.3 partes por millón) debido a la evaporación del agua.

Por estas razones, se efectuaron pruebas en la Facultad de Química de la Universidad Nacional Autónoma de México, en el Instituto Mexicano del Petróleo, así como en el laboratorio de la propia Secretaría de Obras Públicas, que sugirieron finalmente la necesidad de proteger todo el cable de acero con un galvanizado electrolítico, y sobre este aplicar una segunda protección a base de revestimiento de vinilo El proceso de protección del cable se realizó de la siguiente manera:

- Limpieza del cable, que consistió en un desengrasado en solución alcalina y, después de un enjuague, inmersión en una solución ácida ligera.
- Inmersión en una solución para galvanizado electrolítico a temperatura ambiente y secado al aire. El recubrimiento de zinc alcanzaba un espesor de 0.0008 a 0.001 mm. El galvanizado en caliente se desechó por temor a que se modificaran las propiedades mecánicas del acero.
- Revestimiento de vinilo por el sistema de extrusión con un espesor de 1 mm. La temperatura máxima del material sobre el cable fue de 170°C, lo que es perfectamente admisible.

En las pruebas mecánicas y químicas que se hicieron posteriormente al cable, se confirmó que no se alteraban sus propiedades físicas y que el recubrimiento resistía absolutamente el ambiente de la alberca.

Se comprobó el perfecto estado del recubrimiento a la salida de la fábrica. En la obra, por medio de un aparato que mandaba una corriente eléctrica al cable de acero, se registraba cualquier ruptura que hubiera en el forro, causada por su manejo.

Los lugares donde había fractura se ligaban por medio de cinta de vinilo que sellaba la grieta, incorporándose excelentemente al material de fábrica.

La unión o adherencia entre vinilo y galvanizado se debe a la presión que ejerce el vinilo sobre el cable en el proceso de enfriamiento.

Hay que tener cuidado en los lugares en que existe concentración de fuerzas, como son los puntos en que se encuentran aplicados los nudos de sujeción para las láminas de la cubierta, o los puntos de liga con la trabe de borde. En estos lugares se protegió el conjunto de los doce cables con una

Detalle del anclaje de los retenidas en cimentación.

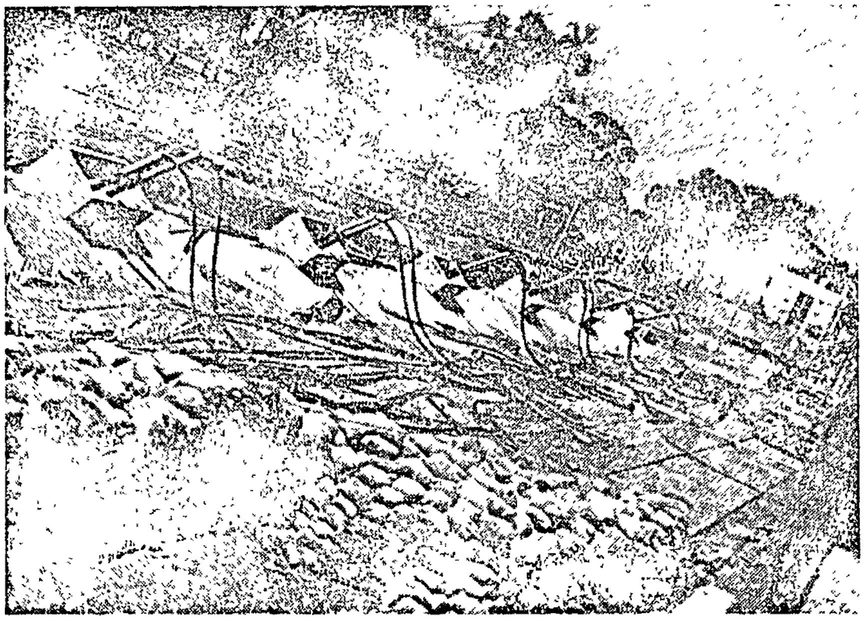

Anclaje de las retenidas

envoltura adicional de polivinilo cuyo espesor es de 3 mm.

Los cables de carga recubiertos como se indica, se cortaron a la medida teórica de 102 90 m en la alberca, y de 69 30 m en el gimnasio, y se anclaron en las trabes de borde mediante un anclaje tipo Freyssinet de concreto, para doce cables.

Hubo necesidad de quitar el recubrimiento del cable en la zona de la cuña de anclaje.

Previamente a la subida y anclaje de los cables se colocaron, a la distancia requerida por el proyecto, los nudos que servirían para sujetar la cubierta los cables de forma. Simultáneamente se sujetó en estos mismos puntos un anclaje de alambre de presfuerzo de 4 mm de diámetro, con objeto de colgar allí el lastre del que luego se hablará. Para evitar que el alambre citado llegara a deteriorar el recubrimiento de vinilo, se le adicionaba un recubrimiento de cinta adhesiva y sobre esta, un tramo de tubería de PVC gruesa.

Con todos los aditamentos citados, se ancló el cable en sus extremos, haciendo coincidir las marcas que se habían hecho previamente de acuerdo con la longitud teórica. A su vez esta longitud teó-

Detalle de las retenidas

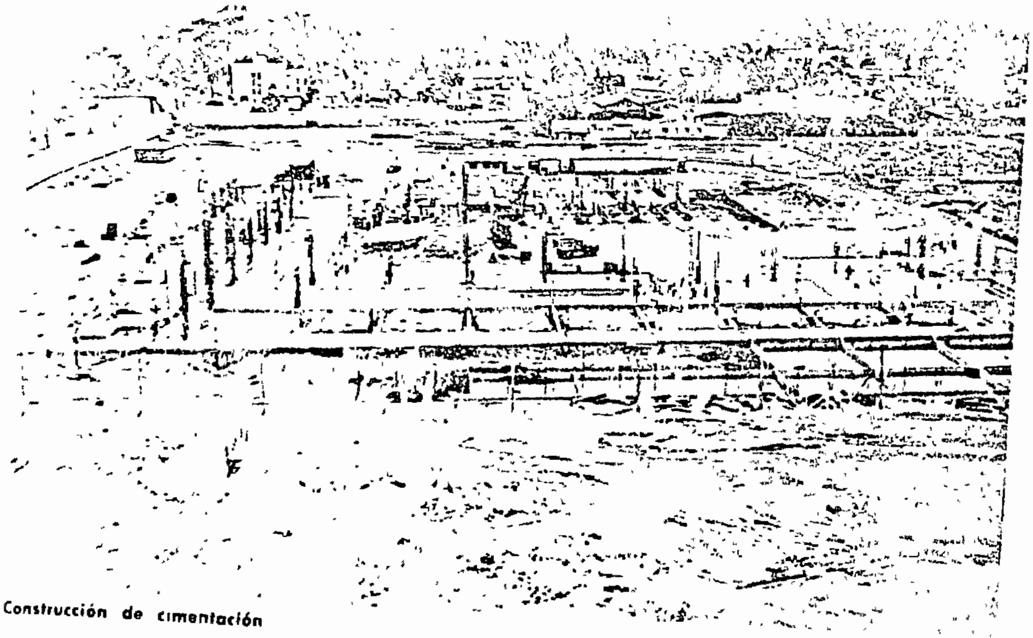

Construcción de cimentación

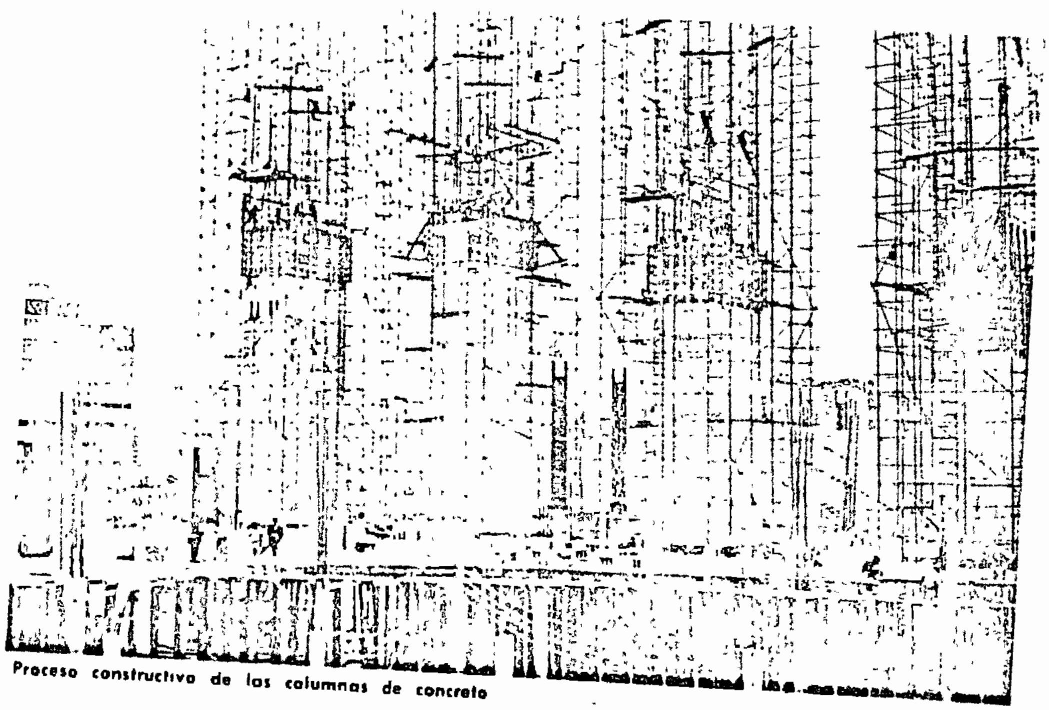

Proceso constructivo de las columnas de concreto

Vista general de la obra durante el montaje de la estructura metálica

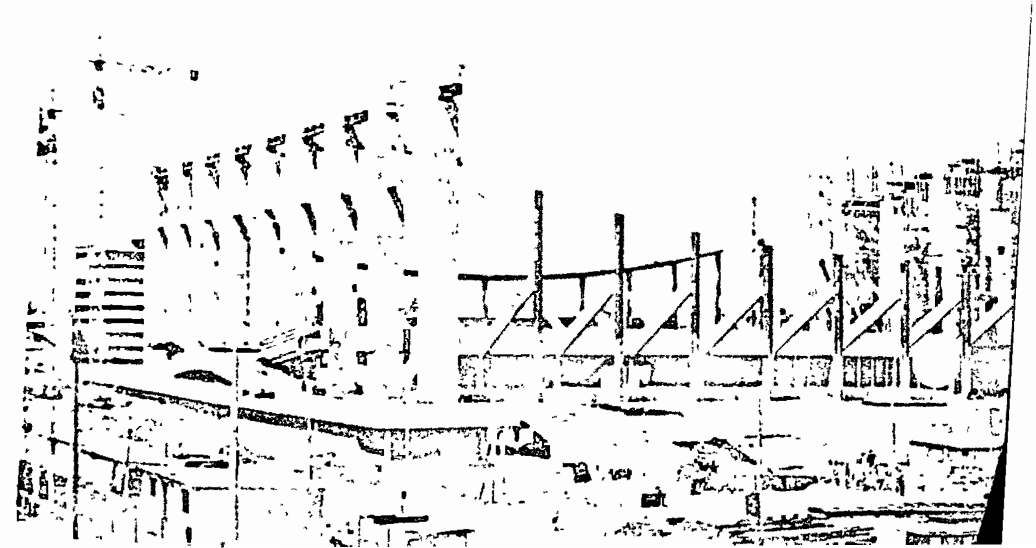

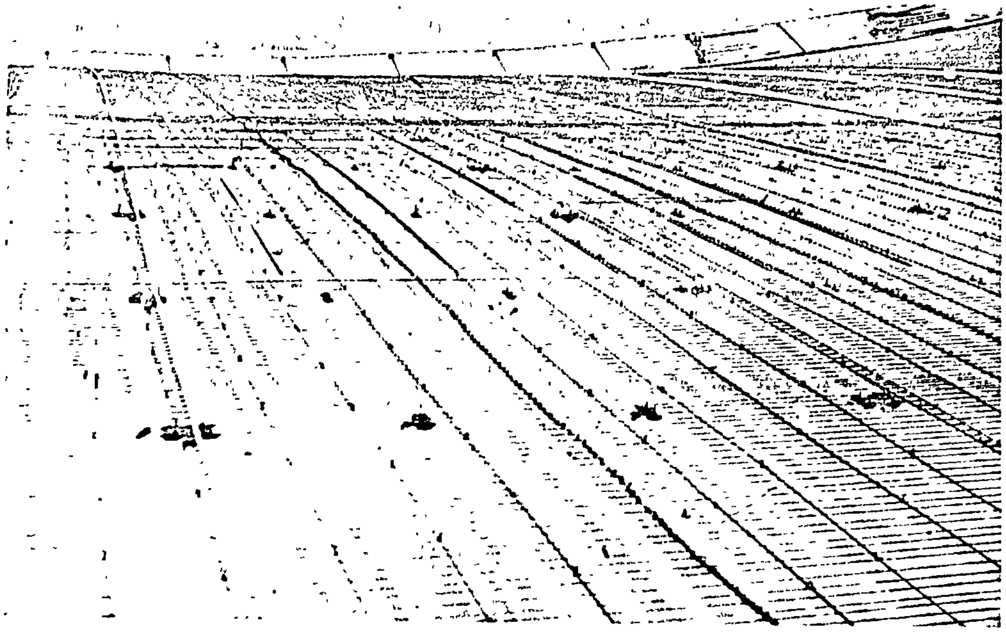

Vista del armado del firme de concreto de la cubierta

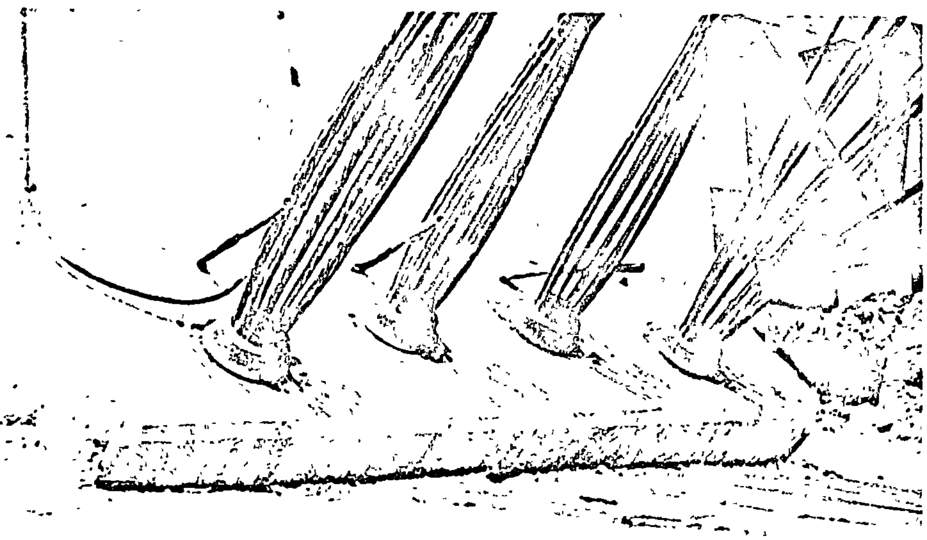

Detalle del anclaje de la retenida en las columnas

Vista que muestra la colocación del lastre de la cubierta

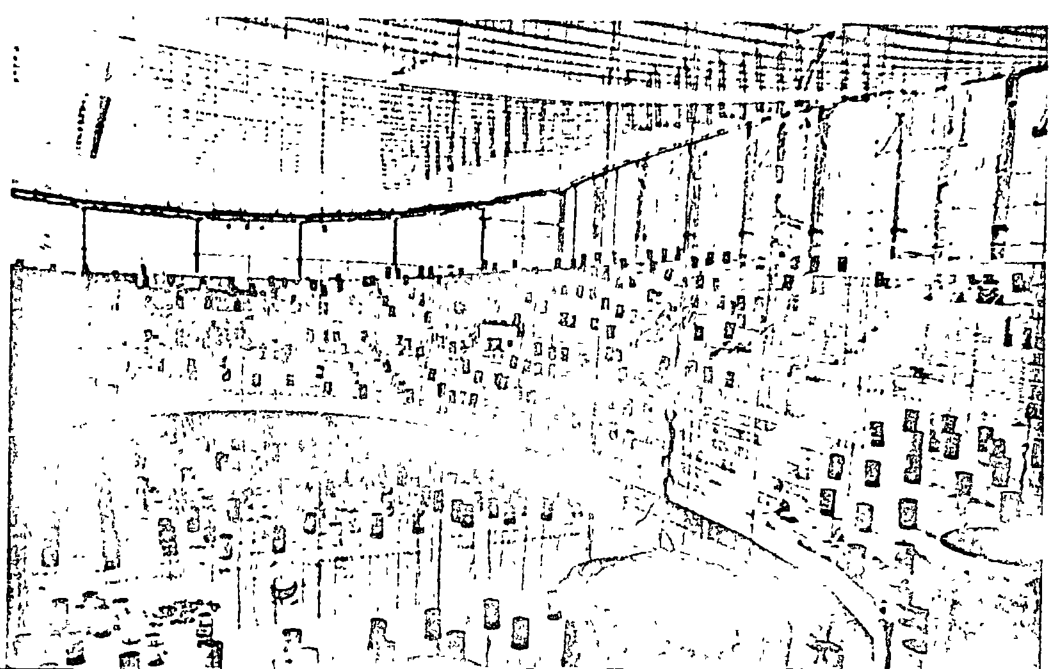

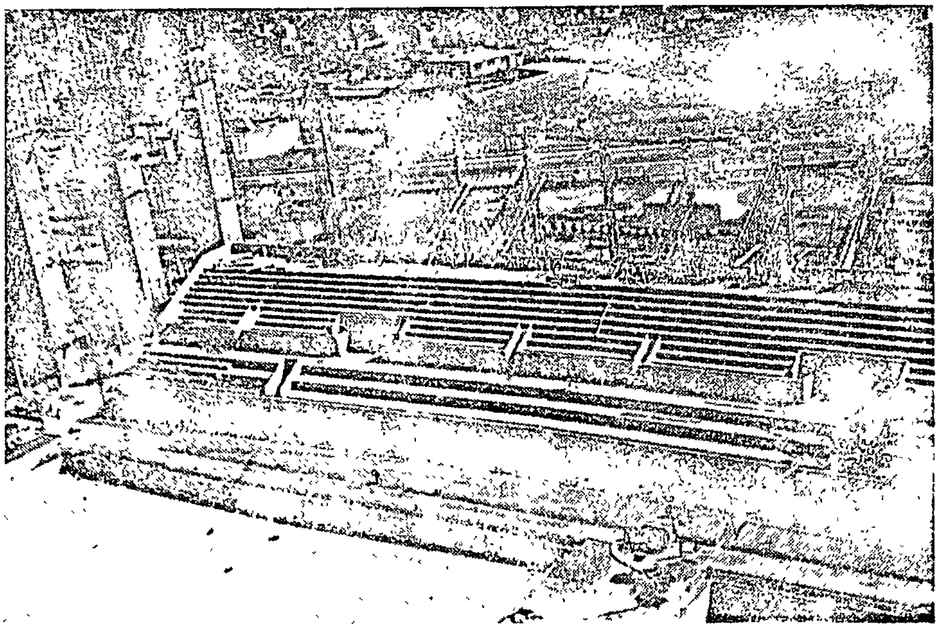

Vista general de la tribuna

rica de los cables de carga se había comprobado, colocando el primer cable junto a la trabe de borde de la cubierta, de tal modo que coincidieran ambos al aplicarle una carga provisional, semejante a la definitiva. Conforme se colocaban los cables de carga, de los alambres citados se colgaban recipientes con capacidad de 200 lt. Una vez terminada la colocación de todos los cables con los aditamentos correspondientes, se procedió al tensado y lastrado de la cubierta.

La maniobra de lastrado se realizó simultáneamente en la alberca y gimnasio. Se inició en las fachadas oriente y poniente.

Mientras que en la alberca el lastrado se hizo llenando con agua los recipientes, en el gimnasio el lastre se aplicó llenándolos con arena. De esta manera la relación de pesos era 220/365, que es la misma que existe en la cubierta definitiva, y con esta diferencia en carga se busca reducir al máximo el momento flexionante en la columna común a las dos estructuras. Al aplicar el lastre, lo que se hizo gradualmente, el desplazamiento vertical máximo que los cables de carga tuvieron fue de 1.04 m en la alberca, y de 0.69 m en el gimnasio. Debido a esta carga, las columnas de concreto sufrían deformaciones cuyo máximo valor permitido

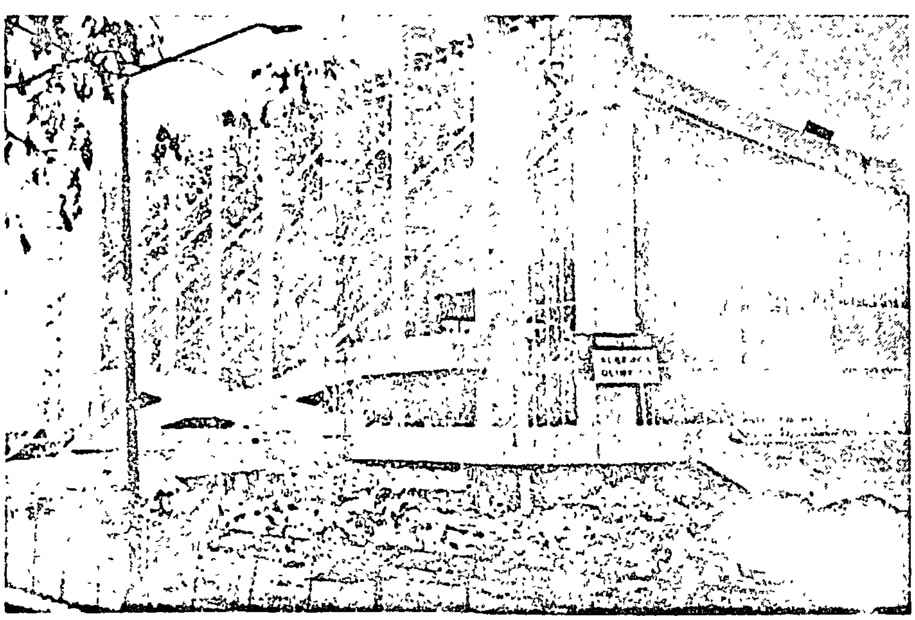

Vista de la fachada sur

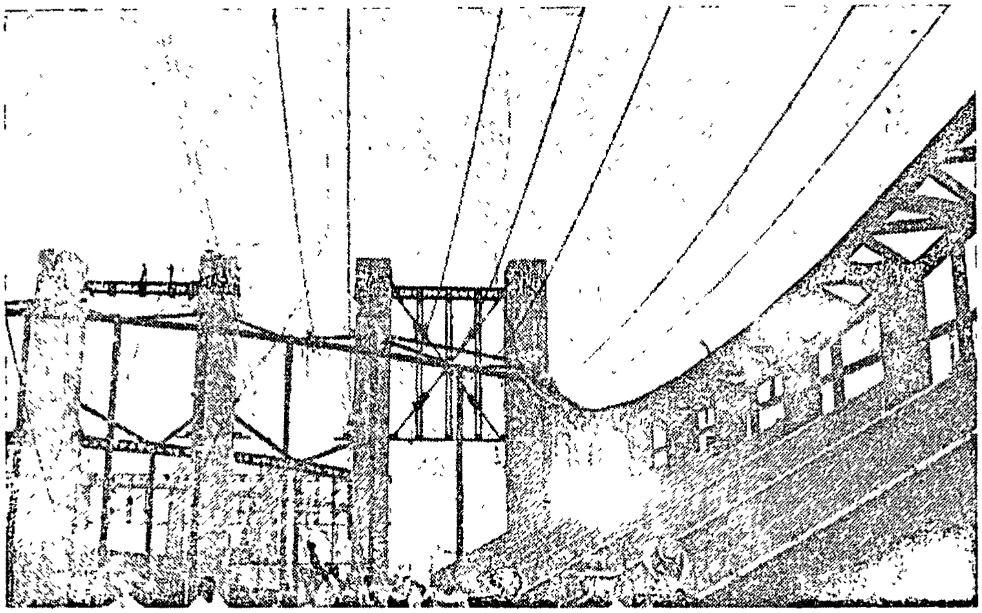

Iniciación de la colocación de cables de la cubierta

fue de 4 cm hacia uno u otro lado. Cuando la columna alcanzaba este valor, se tensaba la retenida hasta que la columna alcanzaba una deformación de valor semejante en el sentido opuesto.

Las retenidas son cables que impiden el libre desplazamiento de los extremos de las columnas. Los cables están anclados al terreno mediante unas masas de concreto cuyo volumen es de 300 m^3 cada una. El peso de este volumen es superior a la tensión del cable, con objeto de que esta sea efectiva. El conjunto cubierta-columna-retenida, se encuentra en equilibrio y la cimentación del grupo queda compensada.

La tensión aplicada a las retenidas, las que están formadas por 48 cables o torones de $\frac{1}{2}''$, se aplicó en cuatro etapas hasta alcanzar una tensión total máxima de 357 ton en algunos de los cables de alberca y de 321 ton en gimnasio, aproximadamente. Todavía en una última etapa se comprobó la tensión final para tomar en cuenta efectos de distribución producidos por la continuidad de la trabe de borde. Durante el tensado se comprobó que, en las etapas iniciales, las deformaciones eran relativamente más pequeñas debido a las restricciones impuestas por la citada trabe de borde.

El objeto de lastrar los cables de carga antes de colocar el techo, fue el de lograr la forma final de la cubierta, antes de efectuar el colado del firme. Los cables de carga con la cubierta de lámina, tienen restricciones y fricciones en cada uno de los

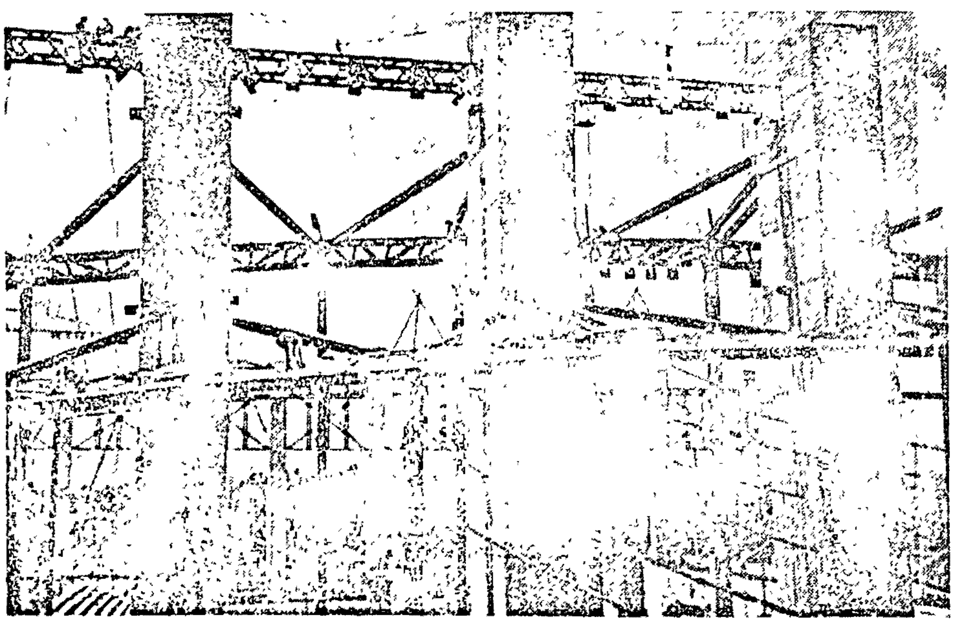

Detalle de los cables

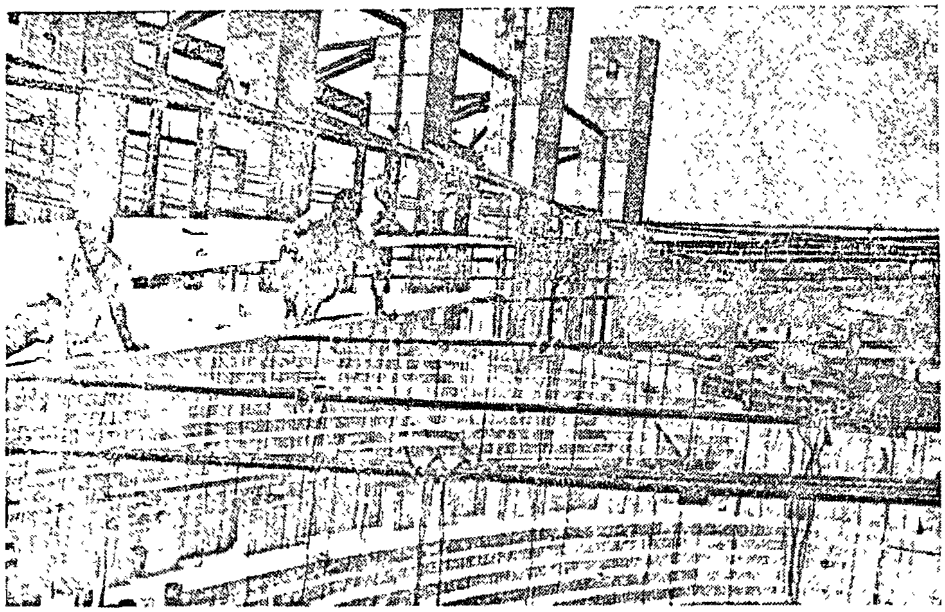

Detalle de los nudos

puntos en los que se encuentra apoyada la lámina que hacen imposible lograr una uniformidad de esfuerzos y de forma en la cubierta. Además, hay que tener en cuenta que las condiciones iniciales y longitudes originales de que se parte, son distintas para cada uno de los cables, debido a errores en localización de apoyos, de medida, diferencias en tensión, etc. Esto hace que la figura que se obtiene al tensar los cables, no sea una curva continua adaptada al proyecto estructural. En esta forma, una vez aplicado el lastre, se puede corregir la tensión en los cables hasta lograr una superficie continua igual a la supuesta. Tambien debe tomarse en cuenta que al aplicar el firme de concreto sobre una superficie pretensada y que no vaya a tener movimientos posteriores, se evitan posibles grietas o fisuras. En cierto modo, equivale a una prueba de carga, ya que se aplica una carga provisional equivalente a la definitiva, durante la etapa constructiva.

Otra alternativa habria sido la colocación de obra falsa para dar forma a la cubierta. Esto habria requerido que se conociera con toda precisión dicha forma. Este cálculo seria muy complicado y de resultados inciertos, además del alto costo que hubiera tenido el procedimiento. La solución adoptada tiene la ventaja de su economia, el poco tiempo requerido en su ejecución y el permitir que se rea-

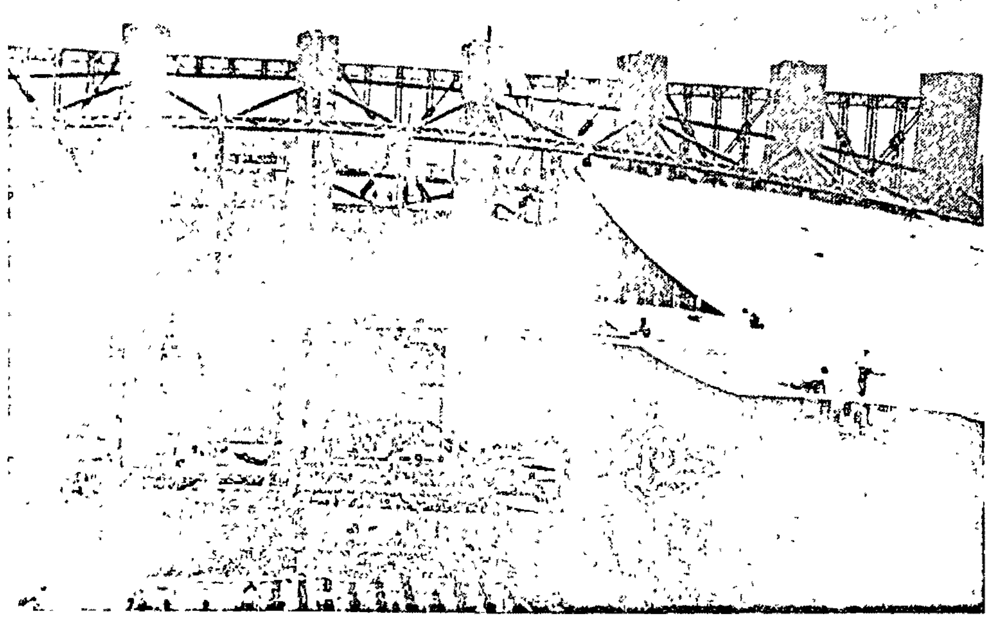

Colocación de láminas de la cubierta

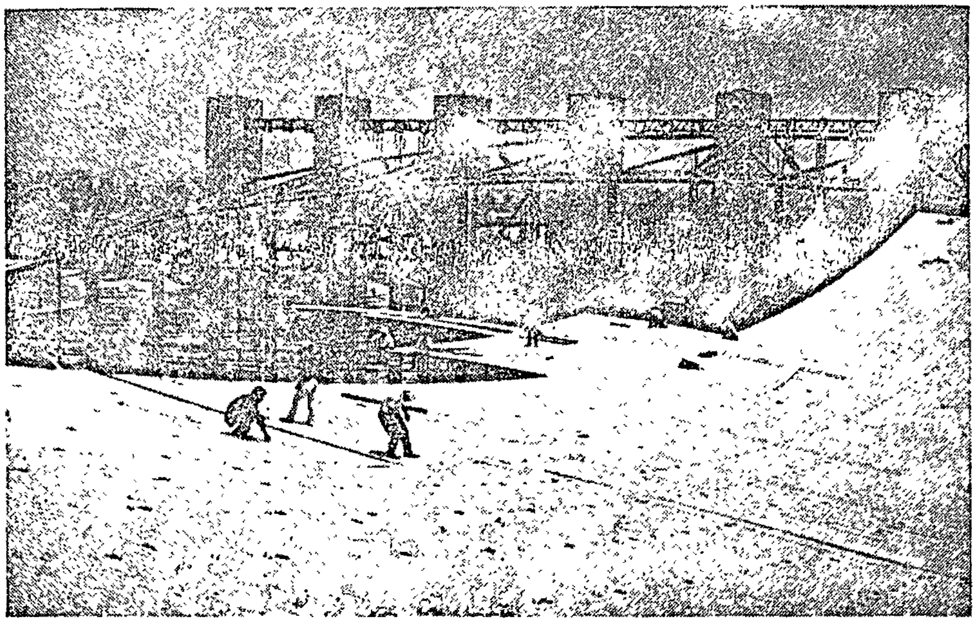

Vista de la cubierta

lizaran trabajos en el resto de la estructura de manera independiente a los trabajos en la cubierta.

Las tensiones que se presentaron sobre los distintos cables fueron las siguientes:

Cables de carga	30	ton	ó	6,490 kg/cm^2
Cables de retenida	357	ton	ó	8,000 kg/cm^2
Cables de forma	2	ton	ó	2,150 kg/cm^2

Sobre los cables de carga y de manera simultánea a su tensado, se fue colocando la lámina de la cubierta. Es lámina acanalada galvanizada y pintada al fuego, del Nº 20 en dimensiones efectivas de 0.73 × 6.30 m. La sujeción de la lámina se hizo por medio de nudos. Se tuvo un promedio de colocación de 500 m^2 diarios. Las perforaciones de la lámina se protegieron de la oxidación con una pintura epóxica, además de proteger cada orificio con una tapa de hule.

Sobre la lámina se aplicó un firme a base de carlita con un peso volumétrico de 1,200 kg/m^3 en gimnasio y de 1,000 kg/m^3 en alberca que daban un espesor promedio de 6.2 y 5.8 cm, respectivamente. Este firme, cuyo objeto es el de suministrar

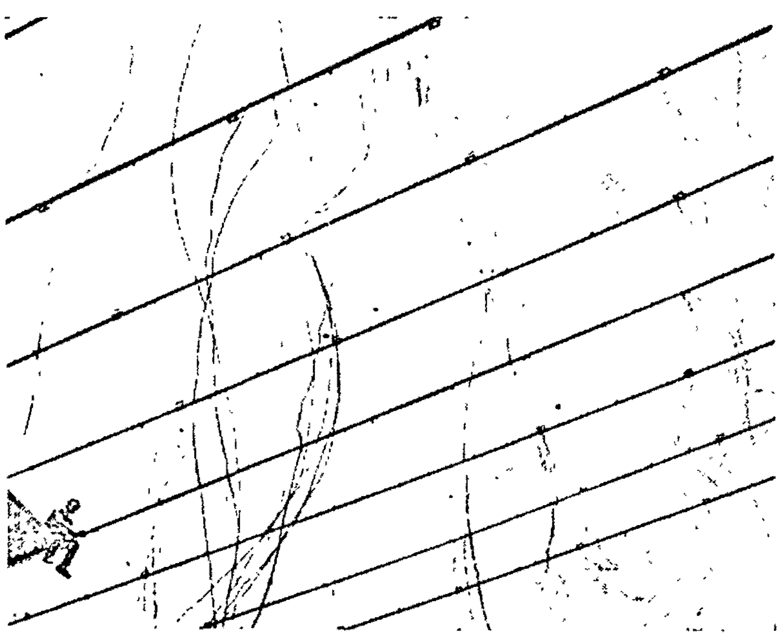

Detalle de las preparaciones que se dejaron en los cables

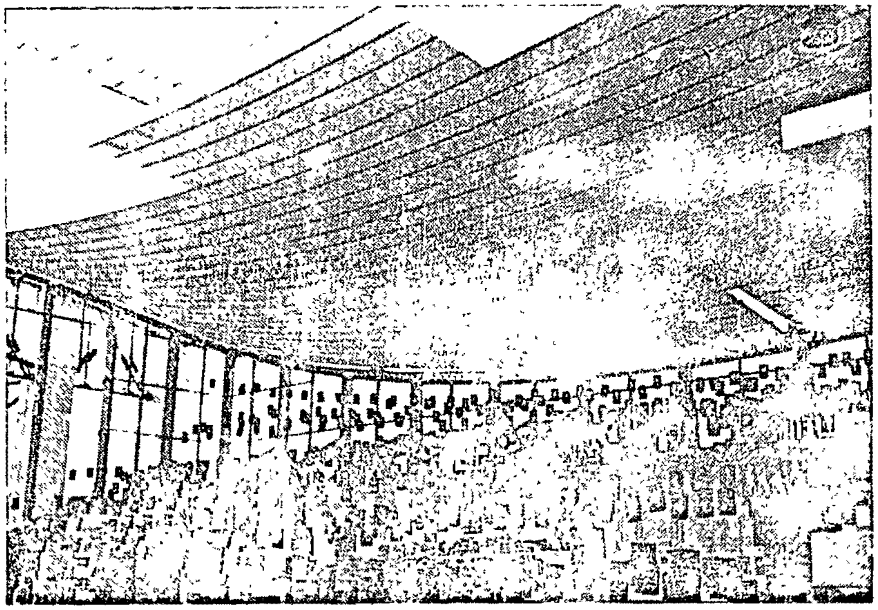

Vista de la colocación de lastre en la construcción de la cubierta

el peso suficiente para contrarrestar la acción de succión del viento, se armó como se describe a continuación.

Sobre la lámina se aplicó, en el sentido de los cables de carga, alambre de presfuerzo de 4 mm a 4.5 cm de separación de una longitud tal que el alambre con su peso propio quedara separado de la lámina, en la parte central, 6 cm en el gimnasio, y 10 cm en la alberca. Este alambre está anclado en una trabe horizontal de concreto que está ligada a la trabe de borde de la cubierta. Transversalmente existe un refuerzo de temperatura para evitar el agrietamiento del firme. Sobre este armado están los cables de forma ya citados, tensados de tal suerte que bajen el refuerzo de 4 mm a una distancia de 1 cm de la lámina de la cubierta. Con este tensado se está aplicando a la cubierta una presión uniforme de 5 kg/m². Hay que tener presente que no está aplicada directamente sobre los cables de carga inferiores y por lo mismo estos no deben sobrecargarse.

Conforme se iba efectuando el colado del firme, por fajas de 2 m de ancho transversales a los cables de carga, se soltaba el lastre. En esta operación se está sustituyendo el peso aplicado a la cubierta y por ende se evita el agrietamiento del concreto. Además, como el peso húmedo de este es de 1,320 kg/m³, y durante el secado a la intemperie pierde alrededor de un 10 por ciento del mismo, se logró una recuperación de 4 cm de la flecha inicial de la cubierta, y de ahí, por eso, un postensado de la misma.

En las nivelaciones efectuadas a la cubierta durante la etapa de colado, se observó que los movimientos eran del orden de 1 cm.

Sobre la cubierta se aplicará un impermeabilizante formado por una capa de hule butilo que quedará aparente.

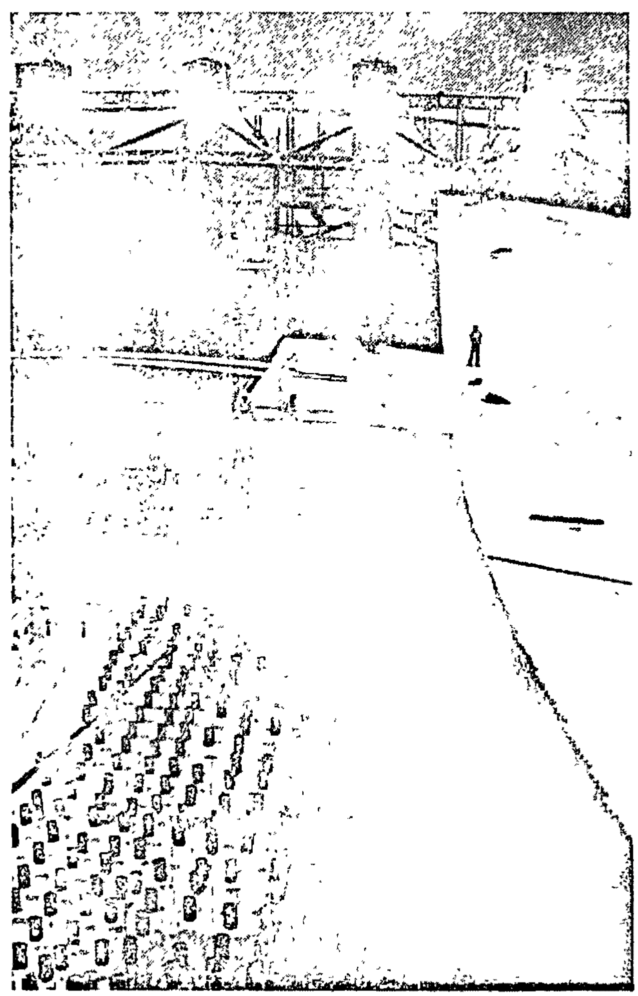

Proceso constructivo de la cubierta

NIVELACION DE COLUMNAS
DE GRADERIAS

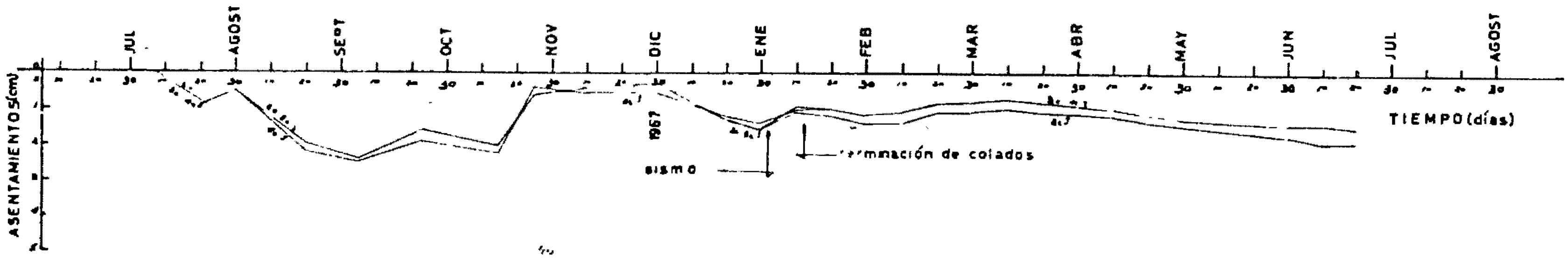

NIVELACION DE COLUMNAS
NORTE

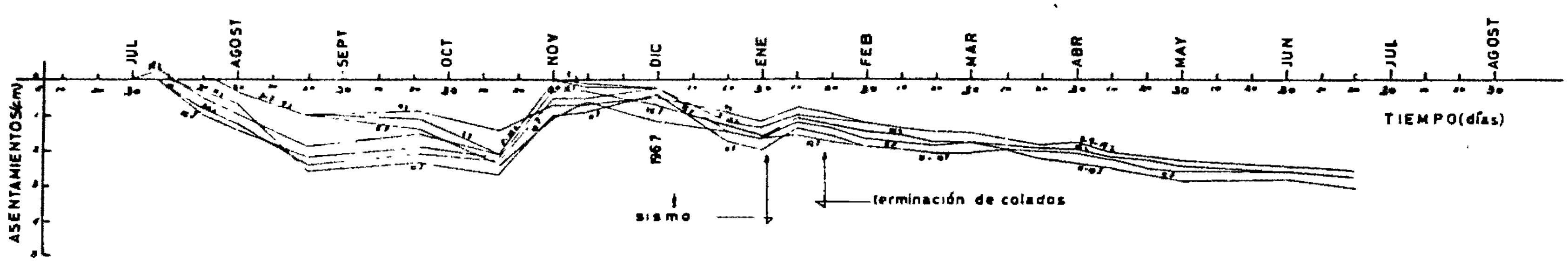

NIVELACION DE COLUMNAS
CENTRALES

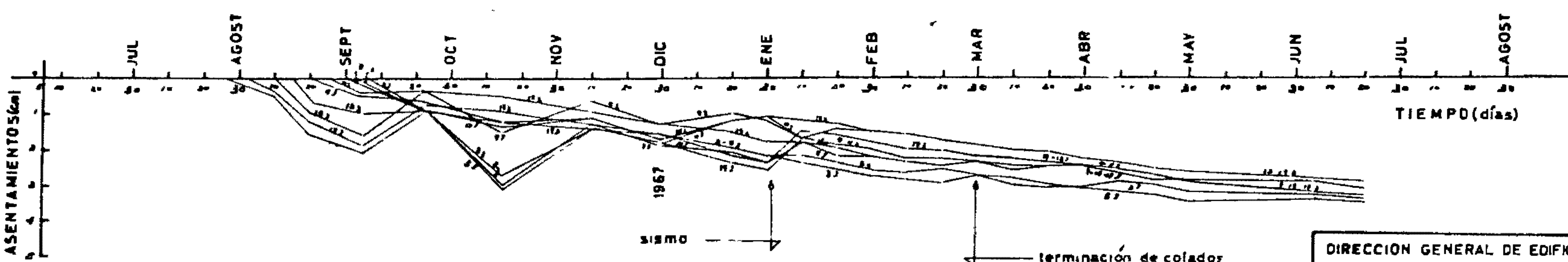

DIRECCION GENERAL DE EDIFICIOS

SOP

COMPORTAMIENTO DE LA CIMENTACION

JULIO 1968

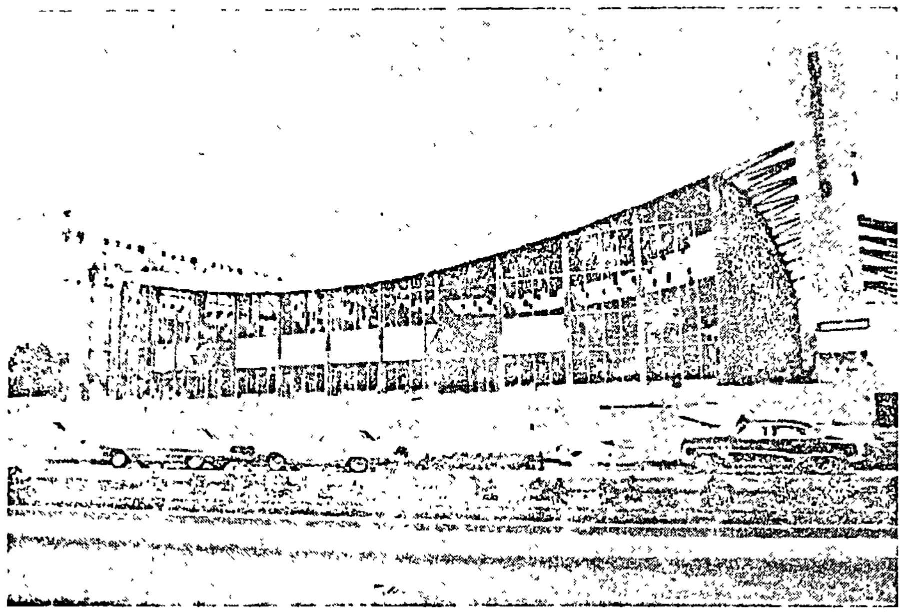

Vista general de la alberca

La distribución del peso final de la cubierta resultó:

Peso de cables: 2.7 kg/m² en alberca, y 2.3 kg/m² en gimnasio

Peso de la lámina: 10.9 kg/m²

Peso del firme de concreto ligero: 58 kg/m² en la alberca, y 74.5 kg/m² en el gimnasio

Peso del impermeabilizante 3 kg/m²

Peso de retenidas 2 2 kg/m²

Peso de estructura de acero correspondiente a la cubierta 45 kg/m²

Las trabes verticales de acero que ligan las columnas de concreto se recubrieron con lámina extruida de asbesto de 3 pulg de espesor, apoyada en soportes de acero estructural.

5. CONTROL DE MATERIALES

Durante toda la obra se efectuó un cuidadoso control de la misma que se llevó a cabo con la participación de la Dirección General de Laboratorio y Control de Calidad. En efecto se realizaron las siguientes pruebas:

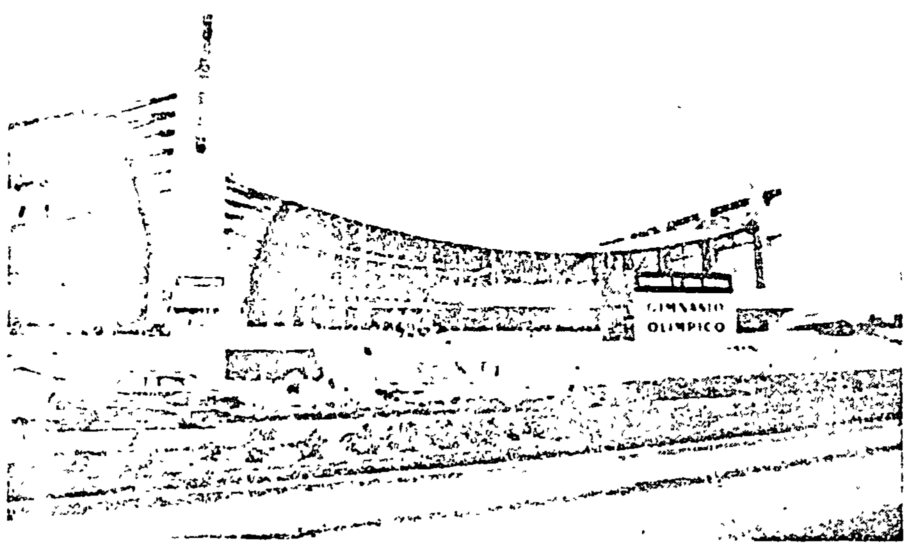

Vista general del gimnasio

Control de acero de refuerzo para concreto. Todo el acero utilizado fue de grado duro

Control de concreto. La resistencia especificada para el concreto variaba de 210 kg/cm² a 350 kg/cm² a los 28 días de edad

Control del acero de estructura

Control de soldadura. Además de pruebas visuales, tanto en taller como en obra se radiografiaron todas las soldaduras de campo.

6. *CONCLUSIONES*

En el poco tiempo que lleva el edificio de construido, el comportamiento del mismo ha sido satisfactorio. Podríamos resumirlo como sigue:

- La estructura ha tenido durante la etapa de construcción un movimiento anual de 3 cm con respecto al terreno que la circunda. En los últimos meses se ha observado tendencia a estabilizarse y es de esperar que en lo futuro se mueva junto con el terreno.
- La cubierta muestra movimientos máximos de 4 mm con el paso de personal sobre la misma.
- El desplome máximo de las columnas, medido por medio de reglas fijadas a estas, fue, durante la construcción, de 2 cm con respecto al que había originalmente.
- Los movimientos máximos diferenciales que se han obtenido en el transcurso de un año han sido de 3 mm.

La ejecución de la obra se llevó a cabo controlando su avance por medio de programas de ruta crítica. Se inició el 1º de marzo de 1967.

ANALISIS DE LA CUBIERTA

Este capítulo lo subdividiremos en los siguientes conceptos:

1. Determinación de la superficie que adoptarán los cables.
2. Procedimiento constructivo y su influencia en el tipo de cubierta.
3. Análisis de esfuerzos en los cables sujetos a carga vertical, viento y sismo.

Determinación de la superficie que adoptarán los cables

Es indispensable determinar cualitativamente los valores de las fuerzas que se inducen en los cables por la forma de la superficie. Para esto consideremos una membrana flexible sujeta firmemente en su perímetro y bajo la acción de una presión uniforme y constante, que pudiera cambiar de sentido obrando en su superficie:

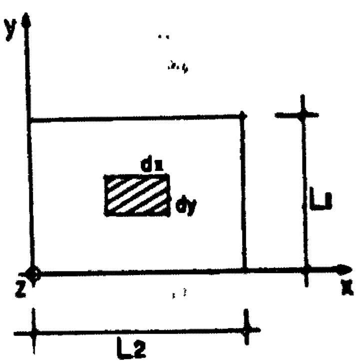

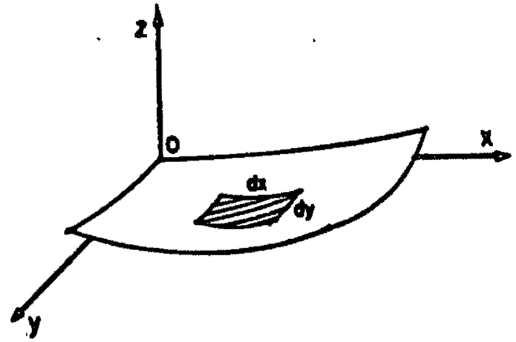

Efectuando un corte en un plano paralelo al plano xz, tendríamos

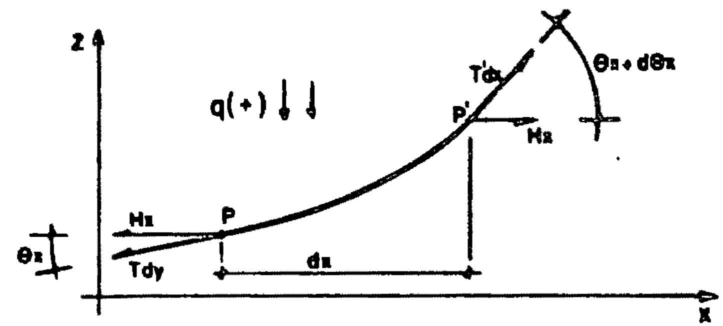

Por condiciones de equilibrio, la resultante de la tensión T en la dirección del eje x debe ser igual a cero, o sea que

$T_x = T'_x = H_x$ (proyección horizontal de la tensión, que podría ser f(y); por simplicidad la obligaremos a ser constante para cortes paralelos al plano xz)

de donde,

$$T = \frac{H_x}{\cos \theta_x} \qquad (1)$$

y

$$T' = \frac{H_x}{\cos(\theta_x + d\theta_x)} \qquad (2)$$

La suma de las componentes verticales de las fuerzas interiores en esta dirección es:

$$\left[-T \operatorname{sen} \theta_x + T' \operatorname{sen}(\theta_x + d\theta_x)\right] dy \qquad (3)$$

en la que T y T' representan la tensión por unidad de longitud en los puntos P y P'.

Sustituyendo en (3) los valores obtenidos en (1) y (2) tenemos:

$$\left[-H_x \tan \theta_x + H_x \tan(\theta_x + d\theta_x)\right] dy \qquad (4)$$

r definición

$$f(x+\Delta x) = f(x) + \Delta f(x)$$

r lo que:

$$\tan(\theta x + d\theta x) = \tan\theta x + d\tan\theta x$$

stituyendo en (4), tenemos:

$$Hx\left[-\tan\theta x + \tan\theta x + d\tan\theta x\right] dy$$

fectuando,

$$Hx\,(d\tan\theta x)\,dy \qquad (5)$$

Ahora bien, si en una superficie cualquiera cuya ecuación sea

$: = f(x,y)$

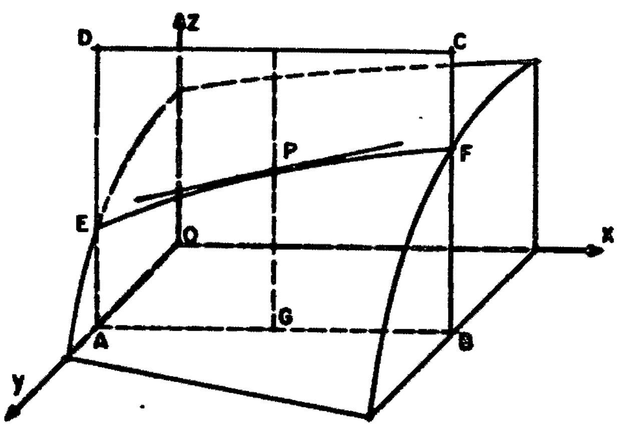

por el punto $x = a$, $y = b$ pasamos un plano ABCD paralelo al plano XOZ, puesto que la ecuación de este plano es

$$y = b$$

la ecuación de la curva EPF, intersección del plano con la superficie es

$$Z = f(x,b)$$

considerando a AD como eje de las x y AB como eje de las x.

En este plano, $\frac{\partial z}{\partial x}$ representa lo mismo que $\frac{dz}{dx}$, o sea el valor de la pendiente de la tangente a la superficie en el punto P, en la intersección con el plano y b. Análogamente $\frac{\partial z}{\partial y}$ representa el valor de la pendiente de la tangente a la superficie en el punto P en su intersección con el plano $x = a$.

Aplicando este concepto en la expresión (5), tenemos que, $\tan\theta x = \frac{\partial z}{\partial x}$

$$\frac{d}{dx}\tan\theta x = \frac{\partial^2 z}{\partial x^2}$$

y por lo tanto,

$$d\tan\theta x = \frac{\partial^2 z}{\partial x^2}\,dx$$

de donde,

$$\Sigma F_{z_{(x)}} = Hx\,\frac{\partial^2 z}{\partial x^2}\,dx\,dy$$

Análogamente la suma de las componentes verticales de las fuerzas interiores en la dirección y, tendrá por valor:

$$\Sigma F_{z_{(y)}} = Hy\,\frac{\partial^2 z}{\partial y^2}\,dx\,dy\,.$$

Igualando la suma de las componentes verticales de las fuerzas interiores en ambas direcciones al valor de la fuerza exterior que obra sobre el elemento de área queda

$$Hx\,\frac{\partial^2 z}{\partial x^2}\,dx\,dy + Hy\,\frac{\partial^2 z}{\partial y^2}\,dx\,dy = q\,dx\,dy$$

simplificando, finalmente obtenemos

$$Hx\,\frac{\partial^2 z}{\partial x^2} + Hy\,\frac{\partial^2 z}{\partial y^2} = q$$

que es la ecuación de Poisson deducida para el caso en que las componentes horizontales de las tensiones de membrana en dos direcciones ortogonales sean diferentes. Los valores de Hx y Hy están dados por unidad de longitud y q por unidad de superficie.

$$\text{Si} \quad k = \frac{Hy}{Hx}$$

podemos escribir la ecuación diferencial de membrana, en la siguiente forma:

$$\boxed{\frac{\partial^2 z}{\partial x^2} + k\,\frac{\partial^2 z}{\partial y^2} = \frac{q}{Hx}} \qquad (6)$$

forma en la cual podemos interpretar propiedades interesantes para definir la forma y obtener la ecuación de la superficie más conveniente, para este caso, que deberemos darle a los cables.

Nuestro punto de partida será la ecuación general de una superficie algebraica en el espacio y eliminaremos o asignaremos el valor a las constantes de tal forma de lograr una superficie que a la vez que sea simple sea fácil de manejar y se ajuste a las condiciones impuestas de las que se dedujo la ecuación diferencial.

En ningún punto de la superficie deberá existir curvatura negativa en ambas direcciones, lo que haría inestable la cubierta ya que si llega a existir inversión de fuerzas inducidas por la succión de viento, los cables se verían sujetos a fuerzas de compresión, lo cual sería absurdo.

De la ecuación diferencial sabemos que como primera condición la superficie de ecuación

$$Z = f(x, y)$$

debe cumplir con la condición de que la combinación lineal de derivadas parciales de segundo orden sea constante. La forma más simple de cumplir con la condición anterior es obligar a que las segundas derivadas sean constantes individualmente, lo que equivale a obligar que la superficie sea de segundo grado.

Esto lo cumple una infinidad de ecuaciones que serán necesario eliminar para llegar a obtener la más conveniente. Una ecuación de primer grado también satisface, pero las tensiones en los cables tendrían un valor infinito por ser éstos rectos. Por lo tanto escogeremos una ecuación de segundo grado, cuya forma general es

$$Z = ax^2 + by^2 + cx + dy + exy + f$$

la primera derivada parcial vale:

$$\frac{\partial z}{\partial x} = 2ax + c + ey$$

y la segunda derivada parcial es:

$$\frac{\partial^2 z}{\partial x^2} = 2a \qquad \text{(constante)}$$

Análogamente

$$\frac{\partial^2 z}{\partial y^2} = 2b \qquad \text{(constante)}$$

Ahora bien en la ecuación general de segundo grado podemos eliminar c y d por medio de traslación de ejes; a e lo eliminaremos para lograr la forma más simple.

Las segundas derivadas no dependen de los valores asignados a c, d, e y f. El valor de f dependerá exclusivamente de la localización de los ejes, por lo que la ecuación general puede ser:

$$Z = ax^2 + by^2 + f \qquad (7)$$

Como se explicó anteriormente, las curvaturas en ambas direcciones deberán ser de signo contrario o sea que a y b son de signo contrario, con lo que la superficie será un pa loide hiperbólico, una de las superficies más sencillas. El borde de la superficie estará gado a quedar contenido en un paraboloide hiperbólico. La forma, en planta, de la super queda definida por las necesidades arquitectónicas y el borde se fijará de tal manera que pliendo con los requisitos estructurales satisfaga la expresión arquitectónica.

En la siguiente figura, se muestran las dimensiones en planta de la cubierta:

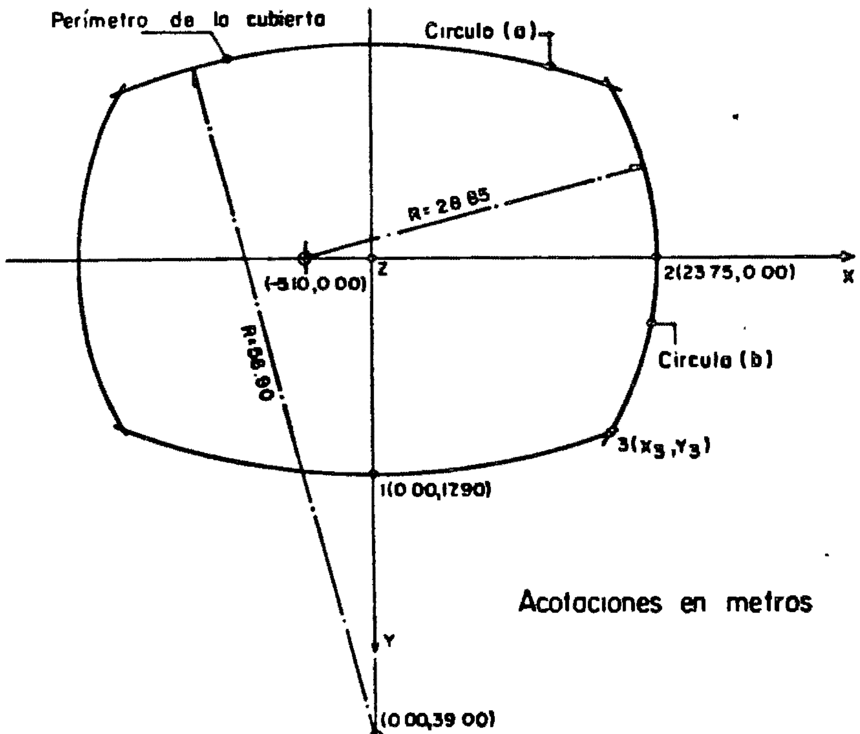

La ecuación del círculo (a) es

$$x^2 + (y + 39.0)^2 = \overline{56.9}^2$$

$$x^2 + y^2 + 78.0y + 1521.0 = 3237.61$$

$$X = \sqrt{1716.61 - 78.0y - y^2} \qquad \text{———} \qquad (8)$$

La ecuación del círculo (b) estará dada por

$$(x + 5.10)^2 + y^2 = \overline{28.85}^2$$

$$Y = \sqrt{806.3125 - 10.2x - x^2} \qquad \text{———} \qquad (9)$$

Las coordenadas del punto de intersección entre los círculos (a) y (b), que nos serán útiles, las obtenemos haciendo simultáneas las ecuaciones (8) y (9)

$$X_3 = 19.967 \text{ m}$$

$$Y_3 = 14.282 \text{ m}$$

En la siguiente figura se muestran las condiciones de borde adoptadas:

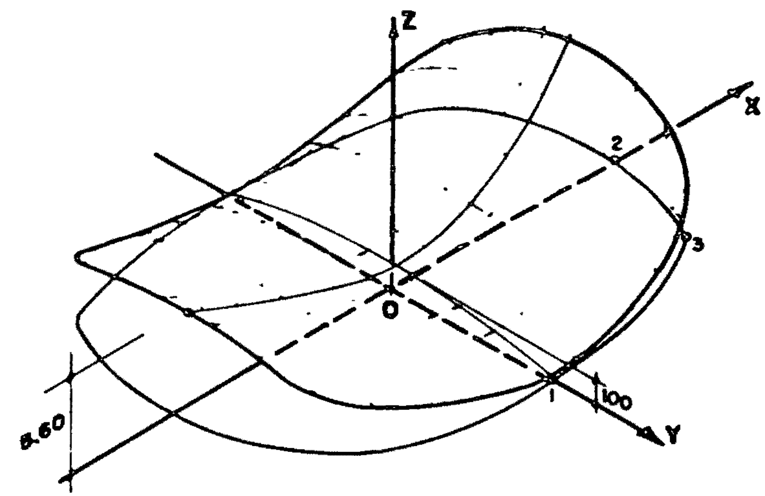

Cabe mencionar que los valores de las flechas en el eje x y y se fijaron después de una primera aproximación de los valores de la tensión en los cables, la aproximación fue hecha estimando el valor de q y teniendo en cuenta la forma que a juicio del arquitecto encargado del proyecto cumpliese con los propósitos deseados desde el punto de vista estético. Los valores de las flechas aceptados se consignan en la figura anterior.

Los valores de las coordenadas de los puntos que fijan las condiciones de frontera ...uestas a la superficie son:

Punto	x	y	z
0	0.00	0.00	1.00
1	0.00	17.90	4.00
2	23.75	0.00	4.60

Sustituyendo en la ecuación (7), los valores de x, y y z del punto 0 obtenemos:

$$f = 1.00$$

...ituyendo para el punto 1 obtenemos:

$$b \times \overline{17.9}^2 + 1.0 = 0.0$$

$$b = -\frac{1}{320.41} = -0.003121$$

...ituyendo para el punto 2

$$a \times \overline{23.75}^2 + 1.0 = 5.6$$

$$a - \frac{4.6}{564.0625} = 0.008155$$

donde, la ecuación de la superficie que adoptarán los cables, queda finalmente:

$$\boxed{Z = 0.008155\, x^2 - 0.003121\, y^2 + 1.0} \text{ ———— } (10)$$

...ación que cumple con los requisitos arquitectónicos y que nos garantiza un comportamiento ...ecuado de la cubierta al cumplir con las condiciones estructurales impuestas

2. Procedimiento constructivo y su influencia en el tipo de cubierta

Uno de los problemas que influyen en forma decisiva en el costo y por lo tanto, en el tipo de cubierta es el proceso de construcción que se siga para la ejecución de la cubierta.

Toda cubierta debe ser impermeable, pero en nuestro caso por tratarse de la Ciudad de Villahermosa, en la cual existe una precipitación pluvial relativamente alta, la característica de impermeabilidad es altamente deseable.

Como material de cubierta, entre las soluciones más viables, se emplearía lámina de madera adecuadamente tratada, lámina metálica unida mediante soldadura, una placa de concreto colado en el sitio o bien precolados de concreto. Analizando cada una de las alternativas, se descartó la lámina de madera por los problemas de mantenimiento que implicaría en climas como el de Villahermosa, ya que por ser una cubierta sumamente ligera, al obrar la fuerza de succión inducida por la acción del viento ocurren disminuciones en las tensiones de los cables que necesariamente ocasionan separaciones en las duelas o tableros de madera con los problemas de impermeabilización subsecuentes.

El empleo de lámina metálica se ve restringido por su alto costo ya que además del costo propio requiere aislantes adecuados para reflejar el calor y para amortiguar el sonido de la lluvia.

La placa de concreto colado en el sitio es solución adecuada por lo que respecta a la función del peso propio de la cubierta para equilibrar la succión, puesto que su espesor deberá ser como mínimo 5 cm por el tipo de agregados existentes en la localidad (es factible disminuir el espesor si se cuenta con agregados que garanticen el correcto comportamiento del concreto ante problemas tales como cambios volumétricos debidos a variaciones en tempe-

Alberca y Gimnasio Olímpicos
Efecto del Viento Sobre la Estructura

RESUMEN

Se presenta una investigación experimental realizada para determinar los efectos de viento en las estructuras de cubierta de la alberca y el gimnasio olímpicos.

La primera parte del estudio consistió en la determinación de la distribución de presiones de viento en un modelo rígido en túnel de viento

En la segunda parte se investigaron, también en túnel de viento, modelos que reproducían la flexibilidad de las cubiertas, con el fin de estudiar la posible modificación de la distribución de presiones debida a la vibración, las deformaciones producidas y la ampliación de éstas por efectos dinámicos.

Se comprobó que las presiones medidas en el modelo rígido no se modificaban en los modelos flexibles por la vibración de la cubierta. Se determinó el orden de magnitud de las deformaciones para la velocidad de viento de diseño y se concluyó que no existían efectos importantes de amplificación dinámica ni de resonancia.

SYNOPSIS

An experimental research program was performed to study wind effects on the roof of the Olympic swimming-pool and gymnasium.

Firstly, the wind pressure distribution was investigated by means of wind tunnel tests on a rigid model.

Secondly, flexible models, reproducing the stiffness of the roof in the prototype, were studied to define the effect of the vibration on the wind pressures, the deflections of the roof, and the dynamic effects on them.

It was found that pressures measured on the rigid model were not modified by the vibration. The order of magnitude of the deflections, for the design wind velocity, was established. It was concluded that appreciable effects of dynamic amplification or resonance were probable.

INTRODUCCION

Por encargo de la Secretaría de Obras Públicas, se emprendió en el Instituto de Ingeniería el estudio del efecto del viento sobre las estructuras de los edificios de la alberca y el gimnasio olímpicos. Ambos edificios, situados uno al lado del otro, están formados por cubiertas colgantes que son muy flexibles debido a un gran claro.

El Instituto propuso hacer un estudio experimental en un túnel de viento; dicho estudio comprende dos partes, que se presentan aquí; la primera consiste en la determinación de la distribución y magnitud de las presiones en un modelo rígido, y la segunda en la repetición de las pruebas, en modelos con las cubiertas flexibles, para medir además las deformaciones de estas. Los resultados de los dos estudios permitirían, por comparación, conocer la importancia de la falta de rigidez de las cubiertas en las solicitaciones producidas por el viento, ya que un cambio de forma de la estructura puede modificar tales efectos y existe el peligro de oscilaciones molestas o perjudiciales para la seguridad de la misma.

En la segunda parte del estudio se ensayaron tres modelos; los dos primeros de acuerdo con el proyecto inicial de la cubierta, y el tercero con la geometría modificada de la cubierta en su forma definitiva, es decir, con una curvatura mayor de los cables transversales.

I. MODELO RIGIDO

Antonio CAPELLA
Rolando SPRINGALL *

1. *ANTECEDENTES*

UN ESTUDIO como el propuesto sólo es posible mediante técnicas experimentales, debido a que la irregularidad de la forma de las estructuras representaría una complejidad inabordable en un análisis teórico. El Instituto cuenta para tales estudios con un túnel de viento de circuito cerrado, con una sección de pruebas de 0.80 m × 1.15 m, donde el viento alcanza velocidades de 220 km/h, aproximadamente

En la realización de las pruebas se supone que la corriente de aire es uniforme, y se desprecia la influencia que puedan tener en la que nos ocupa otras estructuras u obstáculos. Tal hipótesis es aceptable en este caso, pues alrededor de los edificios en cuestión hay grandes espacios libres No se debe ignorar, sin embargo, la influencia que pueda suponer la proximidad de los dos edificios en los efectos sobre cada uno de ellos. Esto obliga a hacer el estudio con un modelo del conjunto de la alberca y el gimnasio.

2 *LEYES DE SEMEJANZA*

Con las velocidades que se alcanzan, tanto en el prototipo como en el modelo, los únicos factores decisivos en la magnitud y distribución de las presiones son, respectivamente, la velocidad del viento y la forma de la estructura. Así, construyendo un modelo que respete la forma del prototipo se obtendrá la distribución de presiones, y sus magnitudes dependerán de la velocidad original del viento, de tal modo que se conserve constante en cada punto un parámetro adimensional llamado número de Euler.

$$E = \frac{V_0^2\ \rho}{2\ p} \qquad (1)$$

donde

E numero de Euler
p presión en cada punto
V_0 velocidad original del viento
ρ masa especifica del aire

Habiendo medido en el modelo las presiones que se originan para determinada velocidad, se puede calcular en cada punto el valor del número de Euler. Este valor será el mismo que se presenta en el prototipo y, dada la velocidad del viento, se puede encontrar la presión que se producirá, a través de la fórmula.

$$p = \frac{1}{E}\ \frac{1}{2}\ \rho\ V_0^2 \qquad (2)$$

Es costumbre presentar los resultados mediante los valores del inverso de E, que se conoce como coeficiente de presión

$$C_p = \frac{1}{E} \qquad (3)$$

3. *EL MODELO*

La escala a la que se construyó el modelo fue determinada por el tamaño de la sección de pruebas. Esta escala resultó ser 1:250. El modelo se construyó de madera, montado sobre una base circular que se colocó en un orificio del mismo tamaño, hecho en la pared de la sección de pruebas del túnel. De este modo fue posible hacer girar el modelo y determinar el efecto del viento soplando en diversas direcciones. La fig. 1 muestra el modelo colocado en la sección de pruebas del túnel, para una de las direcciones ensayadas.

Para medir las presiones se hicieron una serie de orificios en la superficie del modelo, que funcionaron como otras tantas tomas piezométricas en los puntos donde se midió la presión. Cada orificio se comunicaba con la parte superior de un tubo de vidrio que en el otro extremo estaba conectado a un tanque lleno de agua coloreada, a un nivel constante Estos tubos estaban sujetos en dos tableros, uno para los correspondientes al gimnasio y otro para los de la alberca (fig 2). Mediante este sistema, una subpresión en un punto del modelo se traduce en elevación de la columna de agua del tubo correspondiente, y una presión en descenso. Los números que aparecen en el tablero indican a qué punto de medición en el modelo corresponde cada tubo.

4. *PRUEBAS Y RESULTADOS*

Con el método descrito se midieron las presiones correspondientes a cinco direcciones del viento y

* Facultad de Ingeniería, UNAM

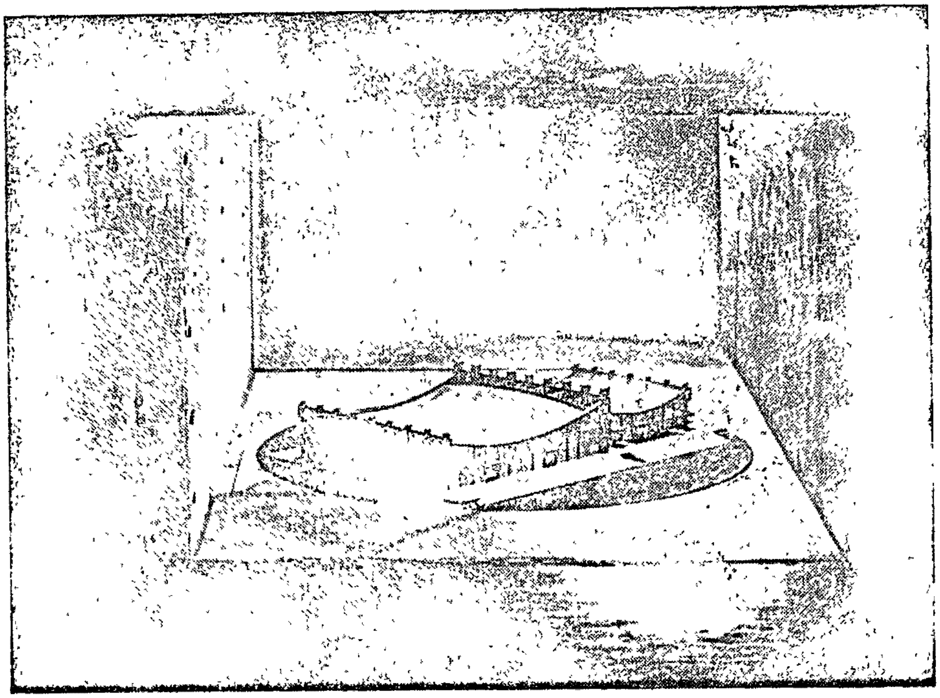

Fig. 1. *Vista del modelo desde el interior del túnel en la posición 4*

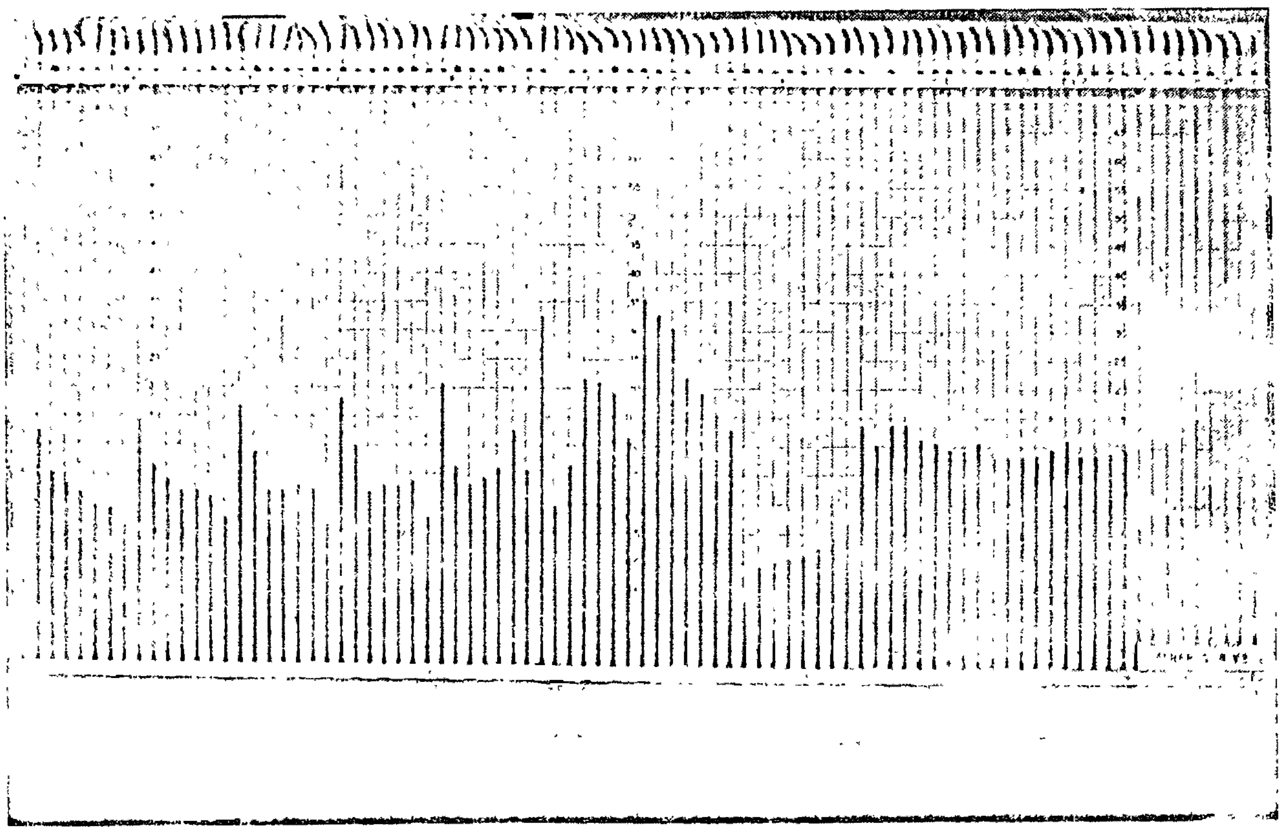

Fig. 2 *Tablero de piezómetros para la alberca (posición 4)*

para dos velocidades en cada caso. La fig. 3 muestra las direcciones mencionadas.

Las mediciones se hicieron fotografiando los tableros de tubos piezométricos, para leer la altura de la columna de agua. Con esta altura se calcula fácilmente la presión al multiplicarla por el peso volumétrico del agua.

La velocidad del viento se midió en función de la diferencia de presiones que se produce entre dos secciones del cono de contracción del túnel. Esta diferencia de presiones se observa en dos de los tubos del tablero correspondiente al gimnasio, los numerados 77 y 78 (fig. 2) y queda así registrada fotográficamente en cada caso.

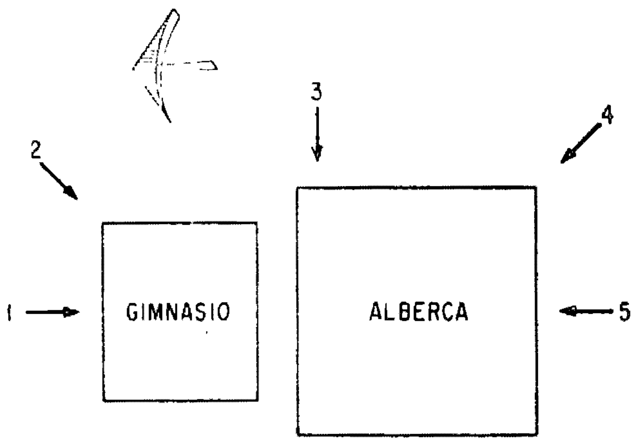

FIG. 3 *Direcciones del viento para las que fueron determinadas las presiones*

Al hacer las mediciones para dos velocidades distintas en cada dirección, se pudo comprobar la validez de la hipótesis según la cual sólo el número de Euler tiene influencia decisiva, constatando que las presiones cambian proporcionalmente al cuadrado de la velocidad

Con las mediciones así hechas se calcularon los coeficientes de presión C_p, los que se muestran en las figs. 4 y 5; en ellas aparece indicada la dirección correspondiente del viento. Para calcular las presiones se utilizan las fórmulas 2 y 3, esto es

$$p = \frac{1}{2} C_p \ \rho \ V_0^2 \qquad (4)$$

Un valor medio de la densidad del aire es

$$\rho = 0.123 \text{ kg seg}^2/\text{m}^4$$

con lo cual, la fórmula

$$p = 0.0615 \, C_p V_0^2$$

permite calcular la presión (en kg/m²) en cada punto, a partir de la velocidad del viento V_0 (en m/seg) y el coeficiente de presión C_p correspondiente.

Durante las pruebas se observó que las presiones de las cubiertas oscilaban formándose unas ondas con un periodo de aproximadamente un segundo. Esto puede deberse al desprendimiento de vórtices en los bordes de la cubierta que forman una arista de separación bien definida. El sistema de medición no permite, sin embargo, registrar oscilaciones de mayor frecuencia, debido a la inercia de las columnas de agua, y asimismo, las amplitudes de las oscilaciones observadas pueden ser el resultado de una amortiguación. De estas oscilaciones no se puede establecer nada concluyente y conviene investigar el problema en el modelo con las cubiertas flexibles que se mencionó como segunda parte de este estudio.

5. *CONCLUSIONES*

Se cree que los coeficientes de presión obtenidos son una buena base para el análisis estructural. Las hipótesis hechas, especialmente la que considera una velocidad de viento uniforme y que se mantiene largo tiempo, no corresponden del todo a la realidad. La experiencia muestra, en cambio, que las velocidades máximas de viento se presentan en ráfagas de corta duración, pero en este caso las condiciones supuestas son más desfavorables que las reales.

6. *RECONOCIMIENTO*

En esta parte del estudio intervino personal de la Sección de Hidráulica bajo la supervisión del ingeniero José Luis Sánchez Bribiesca, quien hizo la revisión del informe.

II. MODELOS FLEXIBLES

Roberto MELI
Alfredo OLIVARES *

1 *DISEÑO DE LOS MODELOS*

1.1 *Análisis dimensional*

PARA QUE los resultados del ensaye de un modelo en túnel de viento puedan ser relacionados con el prototipo, deben cumplirse ciertas relaciones de geometría, propiedades de materiales y acciones exteriores, que se definen por medio de un análisis dimensional.

Para plantear las condiciones que debe cumplir el análisis dimensional, es necesario definir cuáles son las respuestas de la estructura que se quieren reproducir. En este caso se trata de estudiar el comportamiento dinámico de la estructura, e intere-

* Facultad de Ingeniería, UNAM

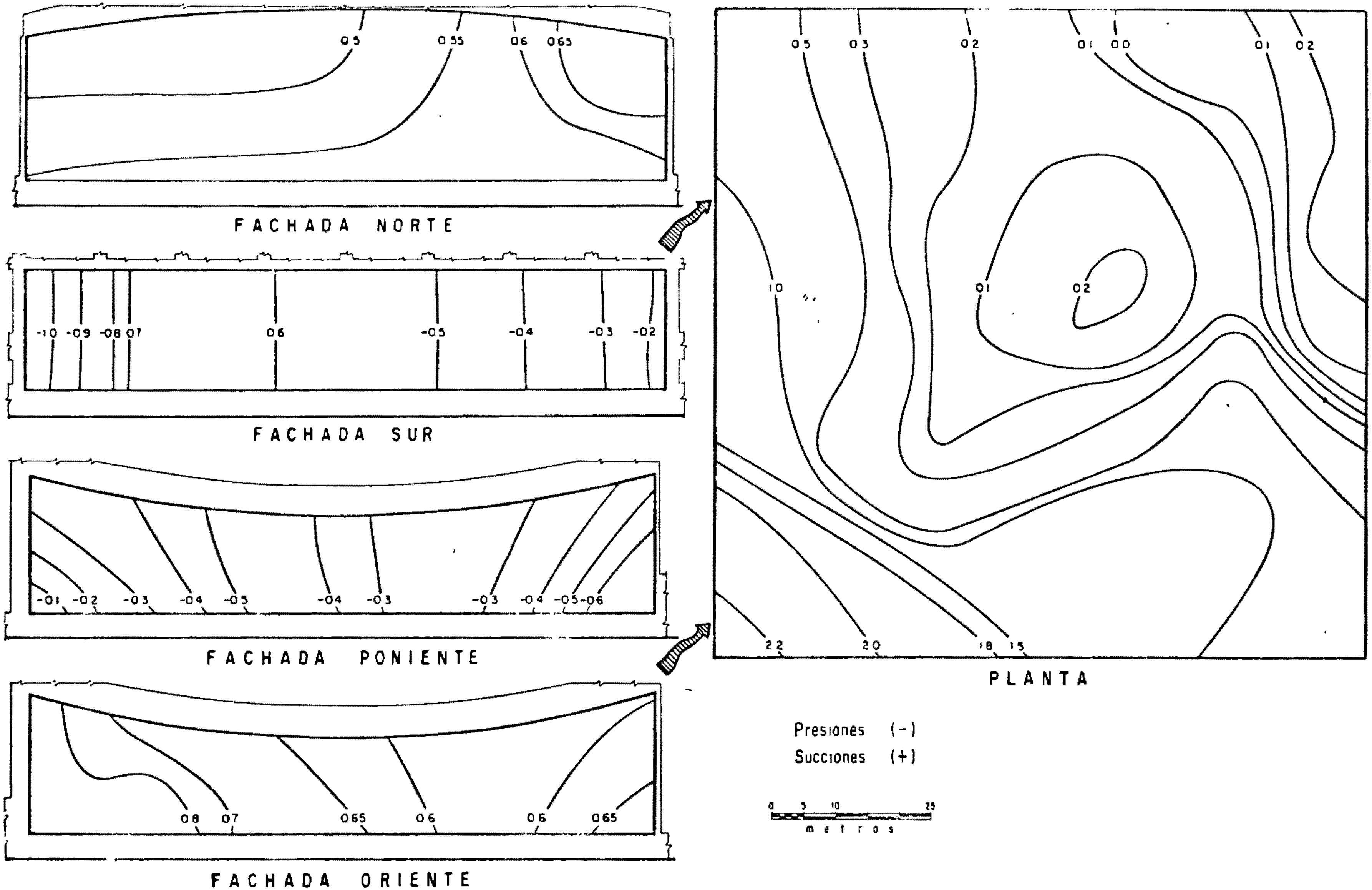

FIG. 4 *ALBERCA OLIMPICA. Distribución de los coeficientes de presión Dirección del viento: SO*

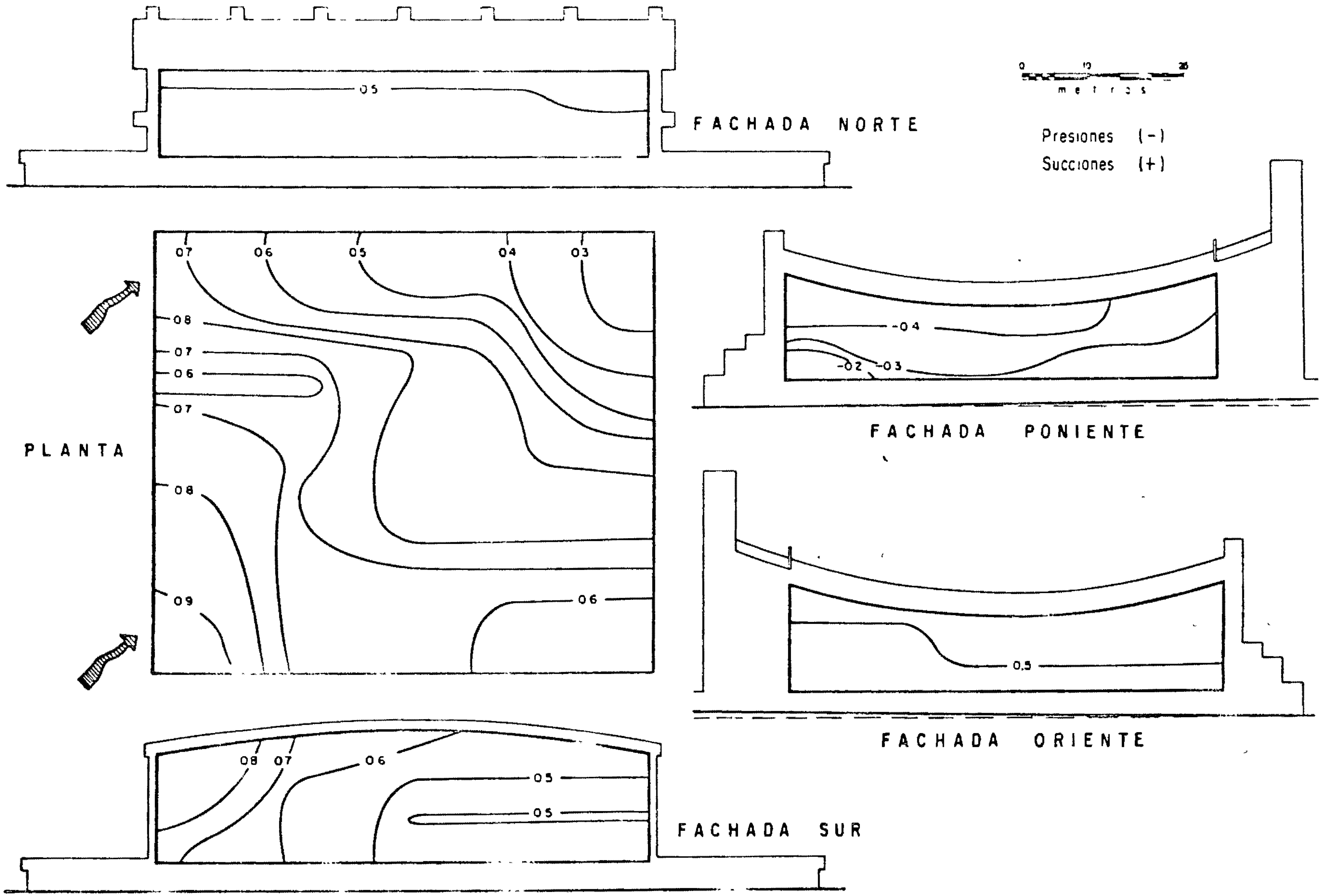

Fig 5 *GIMNASIO OLIMPICO Distribucion de los coeficientes de presion. Dirección del viento. SO*

san los desplazamientos, periodos y factores de amplificación dinámica de la vibración de la estructura.

El comportamiento dinámico de una estructura sujeta a la acción del viento depende de las propiedades siguientes: número de Reynolds; amortiguamiento de la estructura, y relación entre el periodo natural de la estructura y el de la excitación.

En la práctica es casi siempre imposible satisfacer todas las condiciones impuestas por el análisis dimensional, principalmente debido a que no se encuentran materiales con las propiedades adecuadas para cumplir con todos los requisitos. Debe por lo tanto estudiarse la importancia de cada una de las condiciones, para tratar de cumplir con las que tienen mayor influencia en el comportamiento.

La distribución de presiones en un sólido varia en función del número de Reynolds. Este número es mayor para el prototipo que para el modelo, y se encuentra en un rango en que no se ha podido relacionar con la variación de presiones; sin embargo extrapolando resultados, es posible suponer que su influencia en el comportamiento no es muy marcada.

Es prácticamente imposible introducir en el modelo la misma cantidad de amortiguamiento que en el prototipo, considerando que el amortiguamiento del prototipo es de por sí difícilmente predecible. Por esto no se tomó en cuenta esta variable en el diseño del modelo, pero se comprobó que los valores fuesen del mismo orden en los dos casos, y que no se introdujeran errores serios por esta razón.

La tercera condición es la más importante para definir el comportamiento dinámico de la estructura y consiste en que se cumpla en el modelo y el prototipo la igualdad de las relaciones entre el periodo de excitación causado por el viento y el periodo natural de vibración de la estructura, T_i/T_n.

Esta variable ha sido relacionada directamente con el factor de amplificación, que debe multiplicarse por las deformaciones estaticas, a fin de obtener la magnitud de la deformación dinámica[2].

Para una vibración armónica, este factor vale 1.0 para $T_i/T_n = 0$, y aumenta hasta un máximo para $T_i/T_n = 1$, correspondiente al caso de resonancia. La magnitud del valor máximo depende de la cantidad de amortiguamiento. Después de alcanzar el punto mas alto, el factor de amplificación disminuye bruscamente.

El periodo natural de vibración de una estructura depende de su masa (M) y de su rigidez (K).

$$T_n \propto \sqrt{\frac{M}{K}} \propto \sqrt{\frac{\gamma}{g}\frac{L^2}{k}}$$

donde γ es el peso volumetrico del material, g la aceleración de la gravedad y L una dimensión típica.

El periodo de excitación, T_i, es el que el viento induce en la estructura por las turbulencias que se producen en su flujo al chocar con ella. Este fenómeno ha sido estudiado a fondo sólo para cuerpos regulares, cilíndricos, de los que se desprenden en forma alternada vórtices, llamados de Von Karman, que provocan fuerzas transversales a la dirección del viento. En estos casos, la frecuencia con que se desprenden los vórtices depende de la velocidad del viento y se expresa en función del número de Strouhal

$$S = f\,\frac{L}{V} = \text{constante}$$

$$T_v = \frac{1}{f} \propto \frac{L}{V}$$

Para una estructura irregular, como la que nos interesa, en lugar de vórtices alternados se producen turbulencias, que probablemente no serán periódicas sino caóticas, por el gran valor del número de Reynolds. Es conservador suponer que las circunstancias de la excitación son las mismas que en un cuerpo cilindrico.

La relación entre los periodos de la estructura y del viento resulta

$$\frac{T_i}{T_n} \propto \sqrt{\frac{K}{M}}\;\frac{L}{V}$$

Básicamente, en el diseño de los modelos se tratará de cumplir la siguiente relación

$$\left(\frac{KL^2}{MV^2}\right)_{\text{modelo}} = \left(\frac{KL^2}{MV^2}\right)_{\text{prototipo}} \qquad (1)$$

1.2 *Diseño de la cubierta*

La escala de longitudes, 1:250, estuvo determinada por las dimensiones del túnel de viento. Como el espesor de la cubierta del prototipo es muy reducido, no se pudo mantener para esta dimensión la misma escala que para las otras longitudes.

La relación T_i/T_n aplicable a la estructura en estudio se deduce a continuación.

La masa de la estructura se obtiene sumando a las masas de los cables, M_2, la del material de la cubierta, M_1

$$M_1 \propto \gamma_1\,\frac{L^2 t}{g}$$

$$M_2 \propto \gamma_2\,\frac{A_s L}{g}$$

$$M = M_1 + M_2 \propto \gamma_1\,\frac{L^2 t}{g}\left(1 + \frac{A_s}{L}\,\frac{\gamma_2}{\gamma_1}\right) =$$

$$= \frac{\gamma_1 L^2 t}{g}\left(1 + p\,\frac{\gamma_2}{\gamma_1}\right)$$

donde

A_s area total de los cables
L una dimensión típica longitudinal

p porcentaje de área de los cables multiplicado por unidad de área de cubierta
γ_1 peso volumétrico de la cubierta
γ_2 peso volumétrico de los cables.

La rigidez de la cubierta es equivalente a la rigidez lineal axial, k_L, de un elemento compuesto por dos materiales

$$k_L \propto \frac{L^2 E_1}{L} + \frac{A_k E_2}{L} \propto t E_1 (1 + p n)$$

donde E_1 y E_2 son los módulos de elasticidad, respectivamente, de la cubierta y de los cables, y $n = E^1/E^2$

La relación entre los periodos se expresa como

$$\left(\frac{T_m}{T_p}\right)^2 \propto \frac{\gamma_1 L^2 \frac{t}{g}\left(1 + p\frac{\gamma_2}{\gamma_1}\right)}{t(1 + pn) E_1} \propto \frac{\gamma_1 V^2 \left(1 + p\frac{\gamma_2}{\gamma_1}\right)}{(1 + pn) E_1}$$

Para obtener esta relación solo se consideró la rigidez axial en tensión de la cubierta. Esta rigidez no es igual en compresión, ya que en este caso no hay contribución de los cables Aunque la cubierta trabaja principalmente en tensión, existen compresiones locales en las áreas entre los cables. Para que estos efectos locales sean reproducidos fielmente, debería existir la misma relación entre las rigideces lineales en tensión debidas a los cables y al material de cubierta. Esto implica que

$$\frac{k}{k_1} \propto \frac{t(1 + pn) E_1}{t E_1} \propto 1 + pn$$

$$\left(\frac{k}{k_1}\right)_{\text{modelo}} = \left(\frac{k}{k_1}\right)_{\text{prototipo}}$$

$$(1 + pn)_{\text{modelo}} = (1 + pn)_{\text{prototipo}} \qquad (2)$$

No se pudo reproducir con mucha aproximación esta condición en los modelos, pero su influencia no es determinante en los resultados.

Otra condición que debe respetarse se refiere al amortiguamiento de la cubierta, que debe ser igual en modelo y prototipo

El amortiguamiento del modelo se puede medir experimentalmente, proporcionando a la cubierta un impulso que provoque una vibración libre y midiendo la diferencia entre dos amplitudes sucesivas de vibración El decremento logarítmico en este caso se calcula como

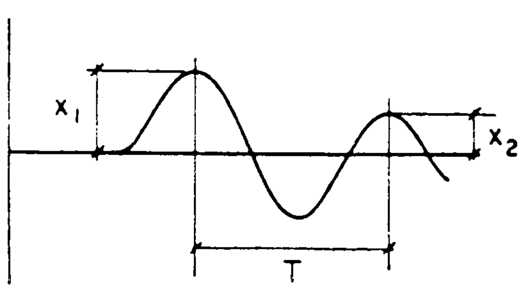

$$\delta_s = \log x_1 - \log x_2 = 2\pi \frac{C}{C_{cr}}$$

donde C/C_{cr} es la fracción del amortiguamiento crítico de la estructura.

Por lo que respecta al prototipo no existen mediciones de amortiguamiento en estructuras semejantes; extrapolando resultados de otras estructuras de concreto, se puede esperar que el amortiguamiento será alrededor de 5 por ciento del crítico.

Si se cumplen las condiciones de semejanza, los factores de amplificación dinámica serán los mismos para modelo y prototipo, y las distintas solicitaciones y respuestas se relacionarán como sigue

Presiones	$W \propto V^2$
Fuerzas	$F \propto V^2 L^2$
Esfuerzos	$\sigma \propto \frac{V^2 L^2}{t}$
Deformaciones	$\varepsilon \propto \frac{V^2 L^2}{t E_1}$
Periodos de vibración	$T \propto \sqrt{\frac{M}{K}} \propto$

$$\propto \sqrt{\frac{\gamma_1 L^2 \left(1 + p\frac{\gamma_2}{\gamma_1}\right)}{(1 + p n) E_1}}$$

En las expresiones anteriores, σ es un esfuerzo ficticio promedio que vale

$$\sigma = \varepsilon E_1$$

donde E' módulo de elasticidad equivalente, es igual a $(1 + p n) E_1$.

1.3 *Diseño de los apoyos*

La flexibilidad de los apoyos influye en las deformaciones y en la vibración de la cubierta. La única característica de los apoyos que interesa reproducir en el modelo es su rigidez a desplazamiento horizontal en los puntos de apoyo de la cubierta. La relación entre esta rigidez y la de la cubierta debe mantenerse constante en modelo y prototipo

En el prototipo, la rigidez lineal de los apoyos se debe a las columnas de concreto, y a los tirantes y marcos de tribunas, los valores teóricos de las rigideces fueron proporcionadas por los calculistas. Los dos primeros modelos tuvieron apoyos rígidos, despreciándose la influencia del movimiento de los apoyos en el comportamiento de la cubierta. En el tercer modelo, los apoyos fueron columnas rectangulares de latón que se diseñaron de modo que hubiese la misma relación entre rigideces de apoyos, K_m/K_p, que entre rigideces de cubierta, k_m/k_p.

1.4 *Características de los modelos*

En la Tabla 1 se resumen las propiedades más importantes para definir el comportamiento dinámico tanto del prototipo como de los tres modelos.

TABLA 1

PROPIEDADES GEOMÉTRICAS Y DE MATERIALES DE PROTOTIPO Y MODELOS

Propiedad		*Prototipo*	*Modelo 1*	*Modelo 2*	*Modelo 3*
L, Longitudes, escala		1	$\frac{1}{250}$	$\frac{1}{250}$	$\frac{1}{250}$
t, Espesor cubierta, cm		8	0.25	0.25	0.15
p Porcentaje de cables de refuerzo	Alberca longitudinal	0.005	0.0123	0.0123	0.133
	Alberca transversal	0.0025	0.008	0.008	0.079
	Gimnasio longitudinal	0.0038	0.009	0.009	0.041
	Gimnasio transversal	0.0020	0.006	0.006	0.024
γ Peso volumétrico kg/m^3	γ_1, cubierta	1,500 (Alberca)	800	800	1,200
	γ_2, cables	2,100 (Gimnasio)	9,000	9,000	9,000
E_1, Módulo de elasticidad del material de cubierta kg/cm^2		50,000	10	30	30,000
$n = \frac{E_2}{E_1}$		40	40,000	30,000	30

El porcentaje de refuerzo longitudinal de los cables se calculó para que cumpliera con la relación de periodos, definida a partir de la ec. 1. La relación entre porcentajes de refuerzo longitudinal y transversal se conservó aproximadamente igual en modelos y prototipo.

Para el prototipo, se encontró un peso volumétrico ficticio dividiendo la carga muerta de diseño entre el espesor de la cubierta, y no se hizo distinción entre cables y material de cubierta. Para los modelos, la masa total de la cubierta se obtuvo su-

TABLA 2

RELACIÓN ENTRE RESPUESTAS DE MODELOS Y PROTOTIPO

Propiedad	*Prototipo*	*Modelo 1*		*Modelo 2*		*Modelo 3*	
		Velocidad inicial	*Velocidad final*	*Velocidad inicial*	*Velocidad final*	*Velocidad inicial*	*Velocidad final*
Velocidad de viento km/h	120	140	200	140	200	140	200
Relacion de periodos T T.	1	1/2.1	1/3.0	1/2.1	1/3.0	1/0.94	1/1.33
V_p km/h		250	370	250	370	105	150
Relación de presiones	1	1.36	2.78	1.36	2,78	1.36	2.78
Relación de deformaciones	1	1/258	1/126	1/258	1/126	1/2,150	1/1,050
Relación de periodos	1	1/135		1/135		1/500	

mando la masa de los cables y la del material de cubierta.

En la Tabla 2 se muestran las relaciones entre algunas respuestas del prototipo y los modelos, que definen el comportamiento ante la acción del viento.

Las velocidades de ensaye están fijadas por las características del túnel de viento y son de 140 y 200 km/h, aproximadamente

En ninguno de los tres modelos se pudo cumplir exactamente la ec. 1; en los primeros dos modelos, el diseño se hizo suponiendo que la rigidez de la estructura se debía únicamente a los cables, despreciando la contribución del material de cubierta. Esta suposición es válida para el modelo, pero errónea para el prototipo

En el tercer modelo se tomaron en cuenta todas las condiciones definidas en el análisis dimensional, pero debido a las propiedades de los materiales disponibles, no fue posible obtener esta relación con exactitud

Procediendo indirectamente se puede encontrar la velocidad del viento en el prototipo, V_P, para la cual se cumple la ec 1

Los valores de V_P se dan en la Tabla 2 para las dos velocidades del túnel

En los modelos 1 y 2 las velocidades V_P, calculadas con las rigideces obtenidas según el criterio usado en la ec 1, son muy superiores a la de diseño; sin embargo, los resultados de estos modelos son muy útiles, ya que las velocidades, V_P, corresponden a las de diseño para el caso límite en que la contribución a la rigidez del material de cubierta se pierda por agrietamientos y deformaciones.

En el modelo 3, las dos velocidades para las que se tomaron mediciones corresponden a velocidades del prototipo aproximadamente iguales a las de diseño

2. *PROPIEDADES DE LOS MATERIALES Y PROCEDIMIENTOS DE CONSTRUCCION*

2.1 *Propiedades de los materiales*

Para formar la malla de cables que constituyen la estructura de soporte de las cubiertas, se utilizaron alambres de cobre de distintos calibres.

Como material de cubierta, en el modelo 1 se aplicó látex (mezclado con otros elementos, para obtener una viscosidad adecuada) sobre la malla de alambres. Para el modelo 2, se usó como material de cubierta una resina apóxica reforzada con polvo de aluminio y con un flexibilizador. Para la cubierta del modelo 3 se usó una lámina de plexiglás forjada para dar la forma necesaria. El espesor nominal de la lámina era de 1.5 mm, pero el espesor real era mayor en muchos puntos, por lo cual fue necesario lijar algunas zonas para obtener un grueso más uniforme. Las propiedades estructurales de estos materiales, determinados experimentalmente, se consignan en la Tabla 1.

2.2 *Procedimiento de construcción de los modelos*

Los tres modelos se montaron sobre una plataforma circular de madera, en la cual se reprodujeron los relieves más importantes de las zonas inmediatas a los dos edificios.

En los modelos 1 y 2 la estructura de soporte de la cubierta estaba constituida por tablas de madera rigidizadas (fig. 1).

La malla de la alberca se formó con alambres (calibre 24 BWG a cada 8 mm), como cables colgantes, dispuestos en la dirección longitudinal, y cables de forma (calibre 26 BWG, a cada 8 mm), en la dirección transversal. Sobre la malla en el

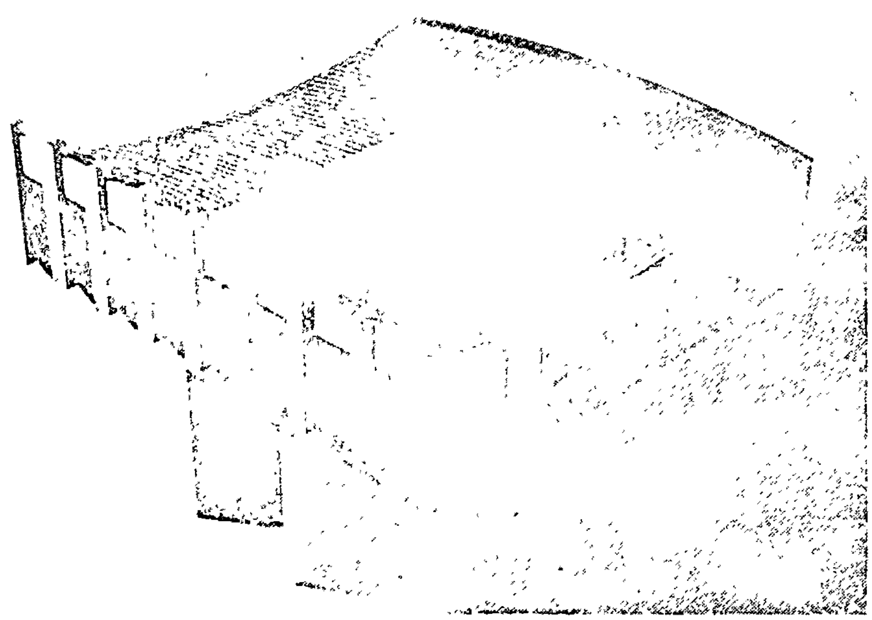

FIG 1 *Estructura de soporte y malla de refuerzo de la alberca Modelos 1 y 2*

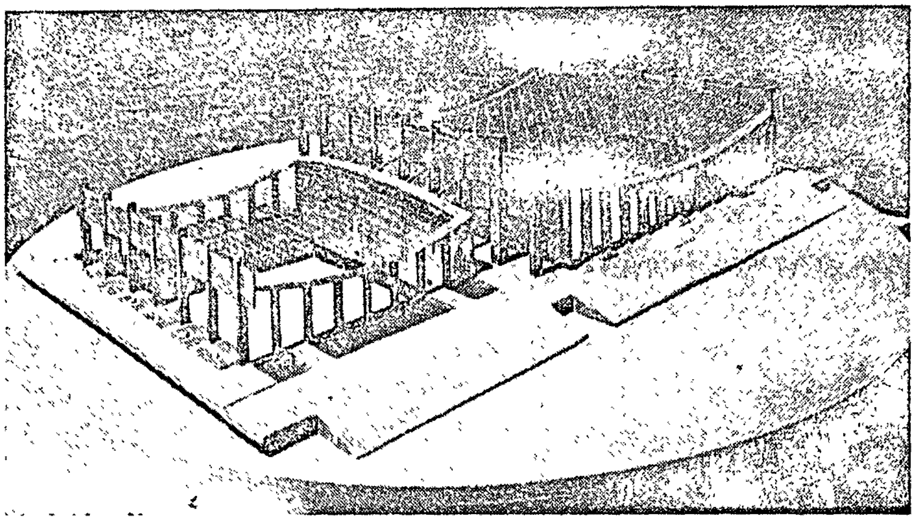

FIG 2 *Estructura de soporte y malla de refuerzo. Modelo 3*

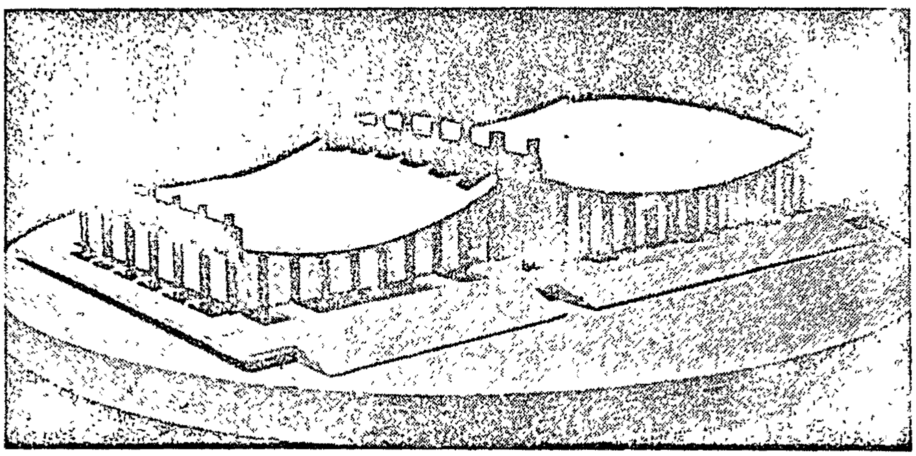

FIG. 3. *Modelo 3*

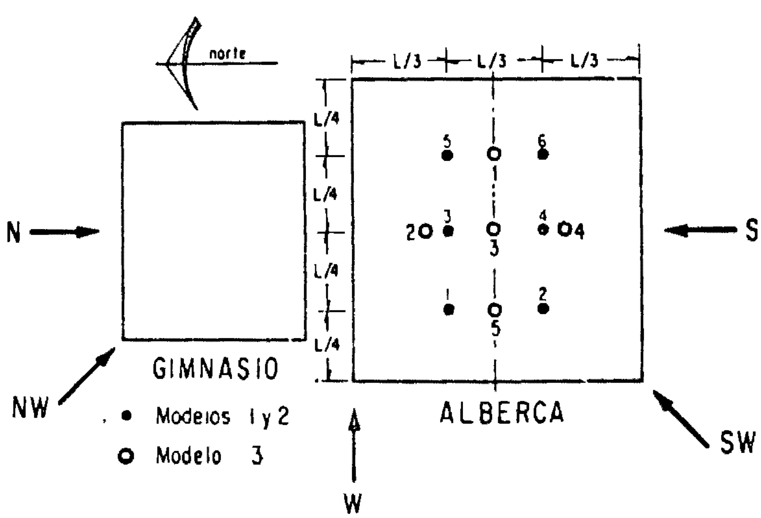

FIG 4 *Direcciones del viento para las que fueron determinadas las presiones y localizacion de puntos de medicion de deformaciones*

modelo 1 se aplicó con brocha el látex preparado con alta viscosidad, y se vulcanizó parcialmente con focos infrarrojos, hasta lograr una película total sobre aquélla. Posteriormente, se engrosó la capa hasta el espesor deseado, 2.5 mm, usando una solución de látex más diluida, aplicada con pistola de aire, y con el mismo procedimiento de vulcanización parcial. Finalmente, se terminó la vulcanización en un horno.

Las perforaciones, para la colocación de los tubos de plástico de los piezómetros, se hicieron con punzón, este procedimiento hizo que la cubierta perdiera parte de su tensión.

El modelo 2 se construyó sobre los mismos apoyos que el anterior. Una malla de alambre con las mismas características se colocó con igual procedimiento. El material usado para la cubierta, resina epóxica, se colocó sobre una cimbra de cartón colocada abajo de la malla; esta cimbra se mantuvo durante la polimerización del material

En el modelo 3, sobre la misma plataforma circular, se atornillaron ángulos de latón entre los cuales se soldaron las columnas del mismo material, quedando estas firmemente empotradas. En los extremos superiores de las columnas se soldaron unas trabes curvas de latón, sobre las que a su vez se soldaron los alambres de la malla.

La trabe que une las columnas centrales entre la alberca y el gimnasio se ligó a las trabes perimetrales adyacentes, mediante diagonales de varilla de latón formándose una armadura muy rígida. Las paredes del modelo fueron de tela ahulada, para que no proporcionaran rigidez adicional a la estructura

La malla de la alberca estaba formada por alambres calibre 18 BWG a cada 6 mm, en dirección longitudinal y calibre 20 BWG a cada 6 mm, en dirección transversal.

En la cubierta del gimnasio se usaron alambres calibre 24 BWG, a cada 6 mm, en la dirección longitudinal y calibre 24 BWG, a cada 10 mm, en la transversal (fig. 2)

Las cubiertas se construyeron por separado forjando, con calor, una hoja de plexiglás sobre un molde con la forma adecuada. La cubierta así formada se colocó en contacto con la malla de alambre y se procuró una adherencia perfecta, por medio de una resina líquida colada por el interior del modelo (fig. 3).

Después de ensayar el modelo, se hicieron en las paredes de la alberca aberturas de 4 × 16 mm, al centro de cada entreeje, inmediatamente abajo de las trabes perimetrales. El modelo así modificado se volvió a ensayar y se denominó modelo 3A.

3 ENSAYES

3.1 *Túnel de viento*

Las pruebas se realizaron en el túnel de viento descrito en la primera parte de este artículo.

En todas las pruebas se hicieron mediciones para dos velocidades, la primera, en el arranque, antes de que la velocidad llegara a la máxima; esta velocidad no pudo ser igual en todos los casos y varió de 130 a 160 km/h. La segunda lectura se tomó cuando la velocidad se había estabilizado en 200 km/h, aproximadamente.

Se midieron presiones en varios puntos de la cubierta de las dos estructuras con el mismo procedimiento usado para el modelo rígido.

3.2 *Registro de deformaciones*

Se efectuó un registro continuo de deformaciones de la cubierta de la alberca. La cubierta del gimnasio no se instrumentó para medición de este tipo.

El equipo de medición constó de seis transformadores diferenciales linealmente variables, LVDT, fijados en un marco independiente del modelo de ensaye y con sus núcleos colocados en contacto con distintos puntos de la cubierta. La distribución de los puntos de medición fue diferente en los modelos y se muestra en la fig. 4. En la fig. 5 se aprecia la colocación de los LVDT.

Los transformadores se conectaron a un sistema de registro consistente en un oscilógrafo Visicorder, de 12 canales, con marcador de tiempos de

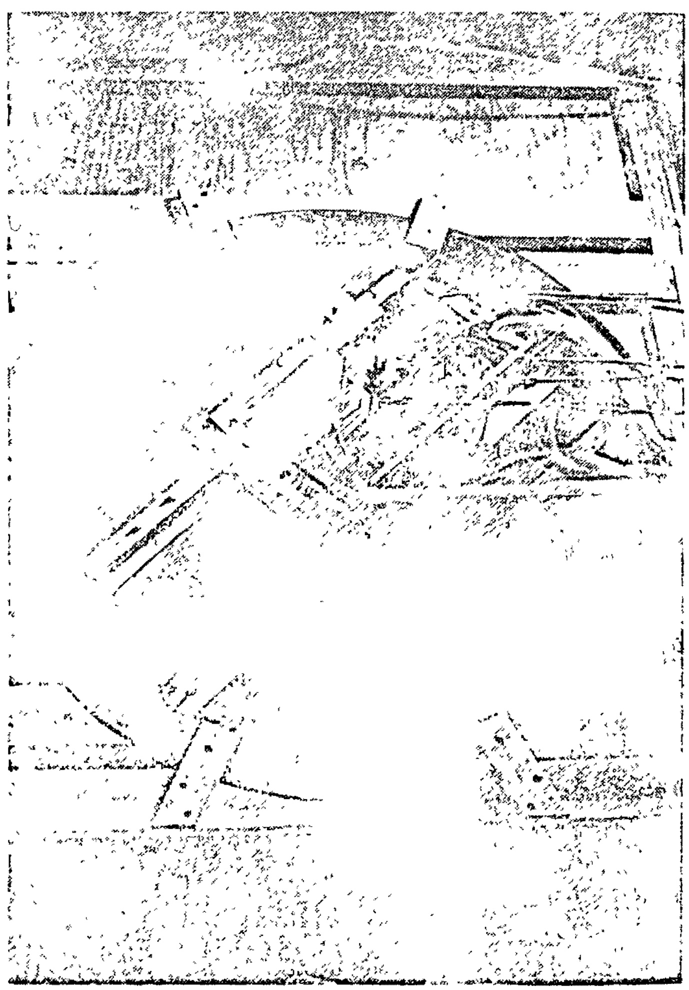

FIG. 5. *Vista posterior del modelo y disposición de los piezómetros y LVDT, en la alberca*

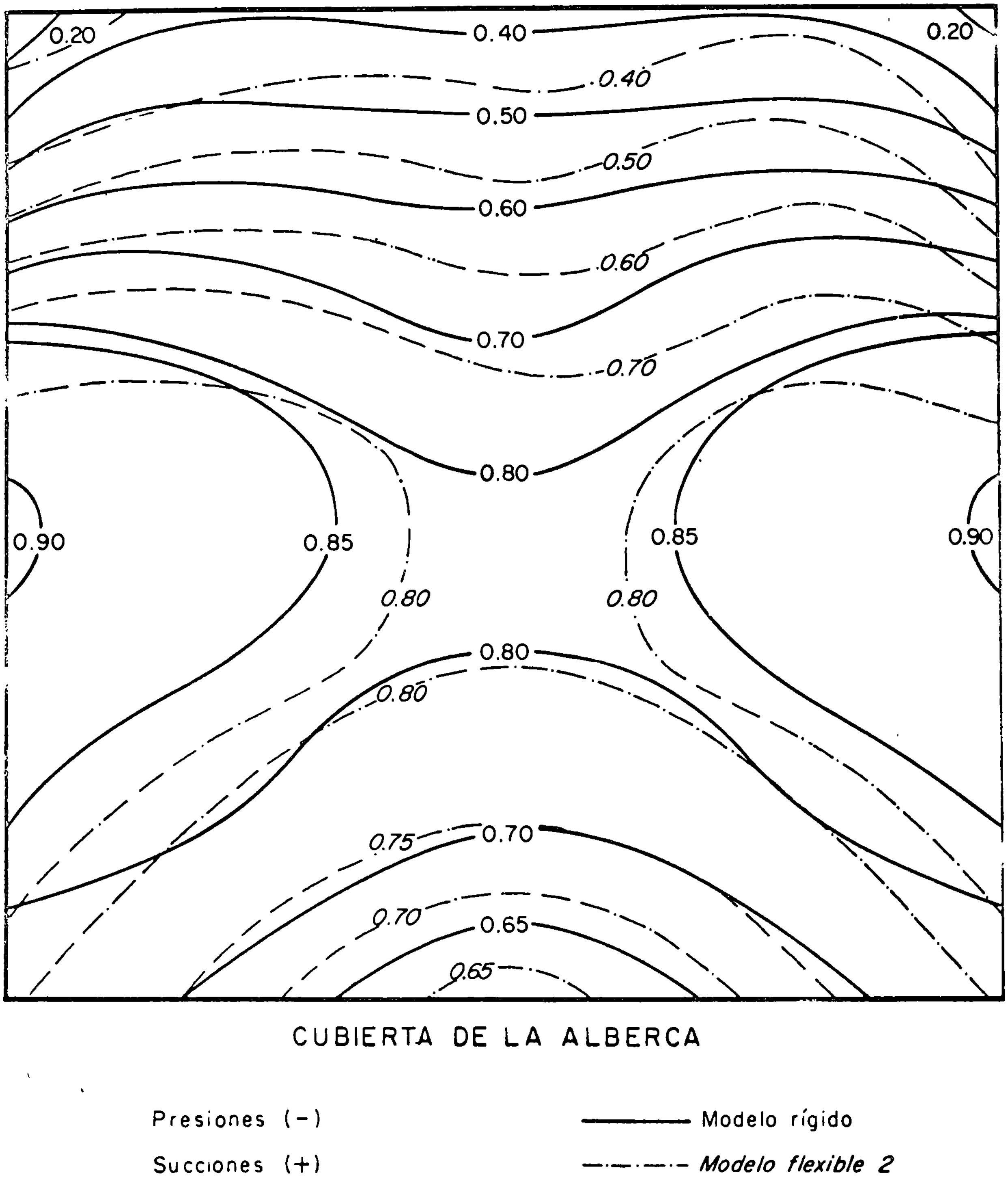

FIG 6 *Distribucion de los coeficientes de presion. Direccion del viento* S

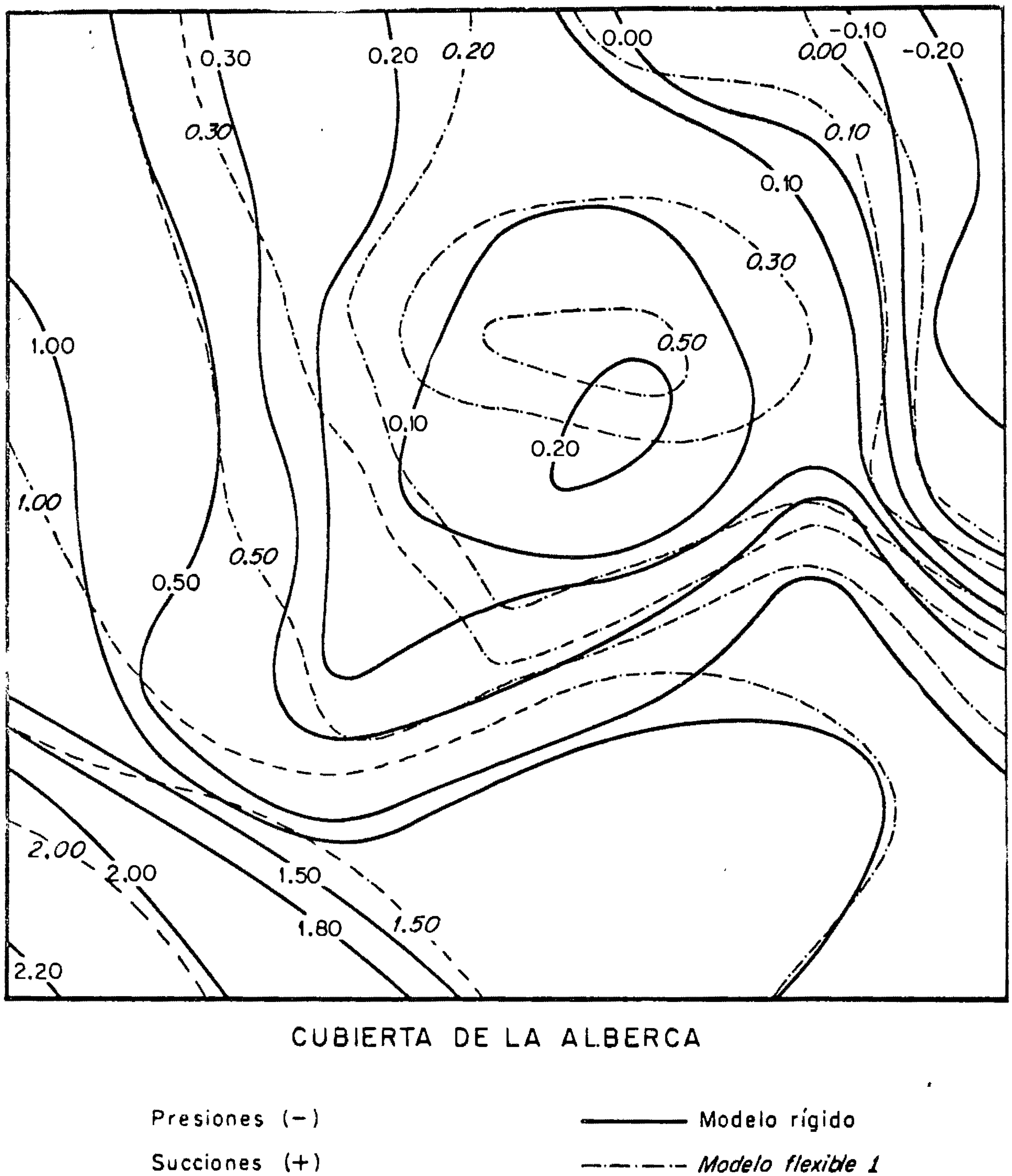

FIG. 7. *Distribución de los coeficientes de presión. Dirección del viento: SO*

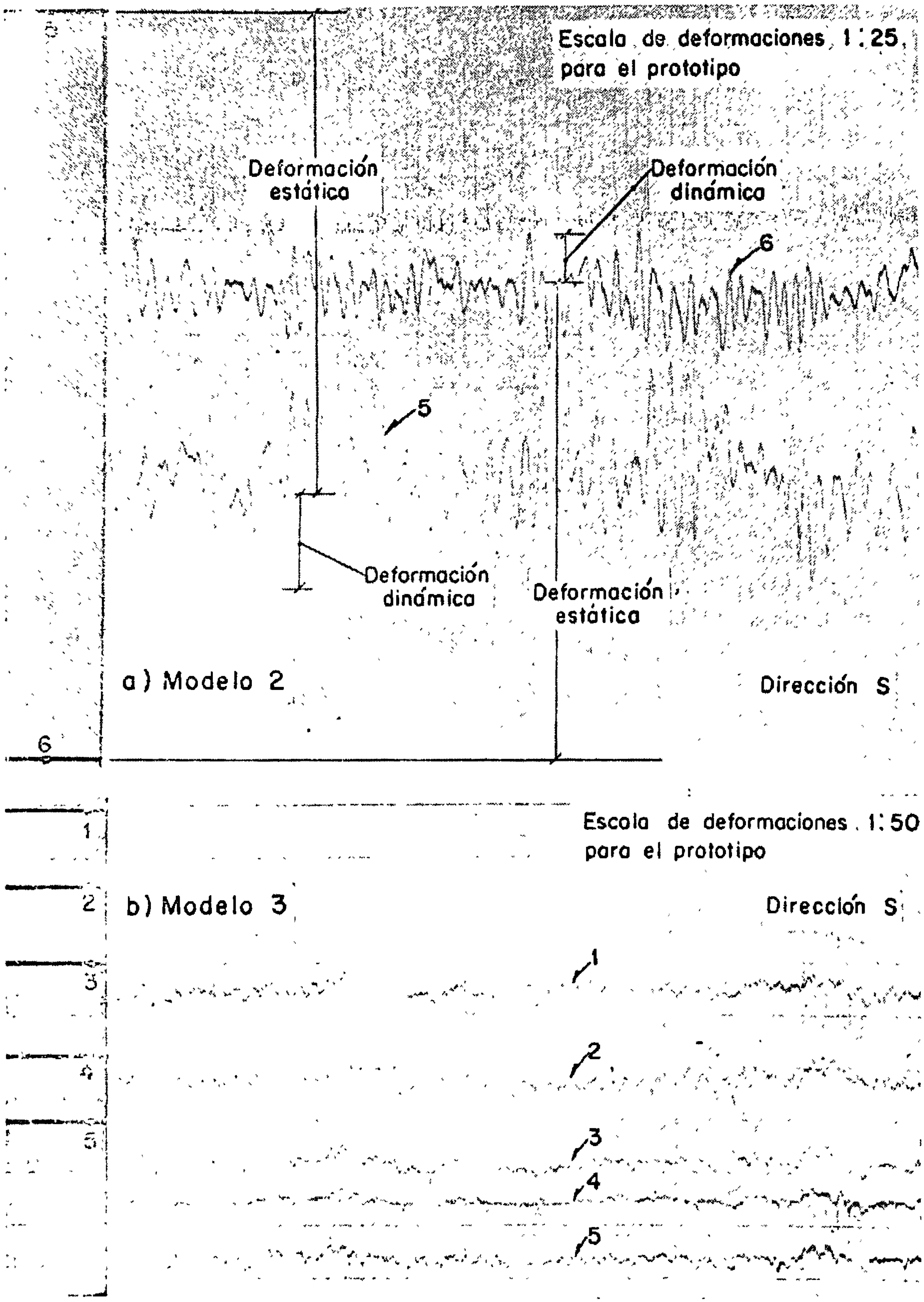

FIG. 8 *Registros típicos de deformaciones en la cubierta de la alberca*

1 0, 0.1 y 0.01 seg y velocidades de registro de 0.4, 2, 10 y 50 pulg/seg. El registro se hizo en papel fotográfico de impresión directa.

El oscilógrafo está equipado con un amplificador de onda portadora con atenuadores de 0.01, 0.05, 0.1, 0.2, 0.5 y 1.0 del rango para la entrada. Los atenuadores permiten regular el factor de escala para obtener un registro claro de los seis puntos de medición.

4. *RESULTADOS*

A partir de las presiones, medidas en alturas de columnas de agua en los piezómetros, se encontraron los coeficientes de presión C_p definidos en la primera parte.

En las figs. 6 y 7 se comparan, para la cubierta de la alberca, las curvas que unen los puntos de igual coeficiente de presión en los modelos flexibles y el rígido. Las curvas son para las direcciones sur y suroeste del viento, que corresponden a deformaciones máximas de la cubierta.

La fig. 8 presenta un registro típico de las deformaciones de la cubierta de la alberca al ser sometida al efecto del viento. A partir de estos registros se encontraron la deformación estática, medida desde el origen hasta el punto medio de un ciclo de vibración, y la deformación dinámica, medida desde el punto medio hasta el pico máximo.

Las medidas se tomaron en zonas del registro donde la oscilación era aproximadamente estable. En los primeros dos modelos se tuvieron algunas dificultades en la interpretación de los registros, porque la vibración fue siempre irregular, y las seis curvas se cruzaban frecuentemente llegando a confundirse.

En la Tabla 3 se encuentran las deformaciones estáticas máximas y los porcentajes de amplificación dinámica, para dos puntos de medición en los modelos 1 y 2. También se consignan los valores para el prototipo, transformados mediante el uso de los factores de conversión en la Tabla 2.

La Tabla 4 contiene las deformaciones transformadas a la escala del prototipo, y los porcentajes de amplificación dinámica, registrados en las pruebas 3 y 3A para todos los puntos de medición y las distintas direcciones de viento.

La fig. 9 muestra esquemáticamente la configuración deformada de la cubierta, para la acción más desfavorable del viento; los valores están calculados para la escala del prototipo, a partir de los resultados del modelo 3A.

5. *DISCUSION DE RESULTADOS*

5.1 *Presiones*

En las figs. 6 y 7 se aprecia que la distribución general de presiones es parecida en los distintos modelos; lo que indica que la deformación y vibración de la cubierta no modifican sustancialmente la distribución de presiones, aunque producen algunas diferencias tanto locales como de conjunto.

La distribución de coeficientes de presión fue más irregular en los modelos flexibles que en el rígido, y en los primeros se obtuvieron coeficientes en general más bajos, particularmente en los modelos 1 y 2.

TABLA 3

DEFORMACIONES DE LA CUBIERTA EN LOS MODELOS 1 Y 2

Dirección del viento	Posición del LVDT	Modelo 1			Modelo 2		
		Deformación, cm		% amplificación	Deformación, cm		% amplificación
		modelo	prototipo		modelo	prototipo	
S	3	0.03	38	56	0.021	26	18
	4	0.026	33	40	0.024	30	9
SW	3	0.031	39	40	0.008	10	15
	4	0.011	14	29	0.007	9	20
W	3	0.023	29	18			
	4	0.024	30	12	0.027	34	10
NW	3	0.015	19	18	0.023	29	5
	4	0.010	13	19	0.022	28	12
N	3	0.005	6	220	0.008	10	25
	4	0.000			0.001	1	50

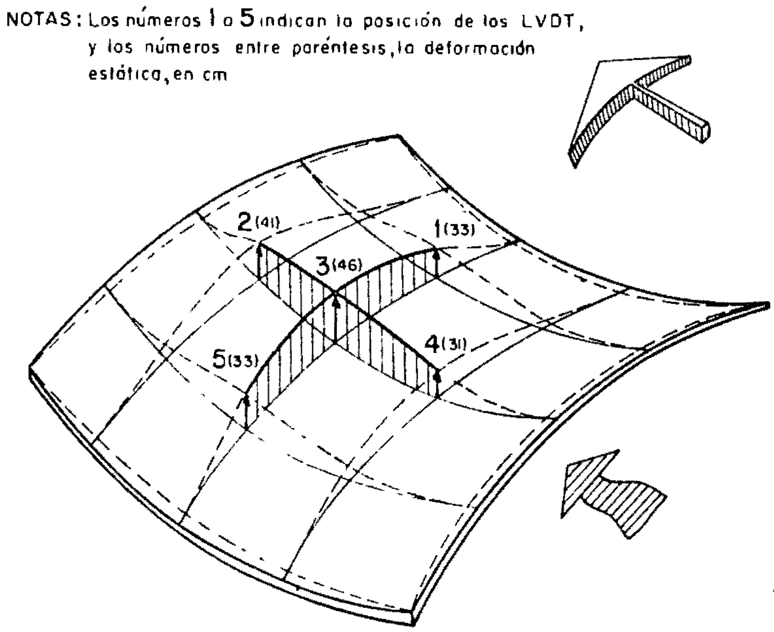

FIG. 9 *Configuración deformada de la cubierta de la alberca. Modelo 3A*

TABLA 4

DEFORMACIONES EN EL PROTOTIPO PARA DISTINTAS DIRECCIONES DE VIENTO

Dirección del viento	*Posición del LVDT*	*Modelo 3*		*Modelo 3 A*	
		Deformación estática, cm	*% amplificación*	*Deformación, estática cm*	*% amplificación*
S	1	42	9	33	4
	2	45	11	41	5
	3	48	6	46	4
	4	32	4	31	6
	5	32	8	33	9
SW	1	12	10	14	6
	2	10	10	17	2
	3	17	8	21	4
	4	14	0	10	7
	5	13	15	14	4
W	1	24	6	25	3
	2	32	7	35	5
	3	35	8	38	4
	4	20	8	23	4
	5	21	10	23	5
NW	1	22	7	20	4
	2	22	4	23	5
	3	26	5	28	5
	4	13	7	19	5
	5	20	9	22	4
N	1	10	17	10	20
	2	10	24	7	23
	3	10	59	10	15
	4	5	90	7	16
	5	6	45	5	33

El cambio de geometría del modelo 3 dio lugar a coeficientes un poco mayores que los anteriores, pero en general no se llegó a los valores del modelo rígido.

La prueba del modelo 3A dio resultados idénticos a los del modelo 3 en lo que se refiere a presiones, así que las pequeñas aberturas abajo del techo no provocan diferencias de presiones de viento.

En las mediciones en las paredes también hubo variaciones en los resultados de los distintos modelos, aunque estas variaciones fueron menores que en la cubierta; esto indica que parte de la discrepancia en los resultados es debida a defectos del ensaye, más que a diferencias de comportamiento de los modelos, ya que las paredes fueron siempre rígidas y deberían haber tenido presiones iguales.

La causa más importante de las diferencias en los resultados fue la oscilación de la columna de agua de los piezómetros que era, en general, de 2 a 3 cm, ocasionando que la altura medida dependiera del instante en que se tomaba la fotografía del tablero; especialmente para las presiones pequeñas, las oscilaciones pudieron variar los resultados en un porcentaje considerable.

A pesar de estas diferencias, la magnitud y distribución de las presiones en la cubierta están definidas con suficiente confiabilidad.

5.2 *Deflexiones*

Comparando los resultados de los modelos 1 y 2, Tabla 3, se nota que las deflexiones estáticas medidas fueron del mismo orden, y que la amplificación dinámica fue mayor en el primer modelo.

Nominalmente, los dos modelos tuvieron la misma rigidez lineal, puesto que el factor de transformación para las deflexiones es el mismo, Tabla 2. Sin embargo, en el primer modelo, el procedimiento usado para hacer las perforaciones para medición de presiones y deflexiones, provocó deformaciones locales en la cubierta, y esta no quedó perfectamente tensada. Además, el módulo de elasticidad del material de la cubierta fue tres veces menor en el modelo 1 que en el 2; esto no influye en la rigidez lineal en tensión de la cubierta, según se discutió en el capítulo 2, pero cambia la rigidez y puede causar algunas diferencias en el comportamiento.

El modelo 3 fue más rígido debido a la nueva geometría de la cubierta; por otra parte, sus apoyos fueron flexibles, lo cual compensó el efecto anterior y llevó a deformaciones estáticas un poco mayores que las registradas en los otros ensayes, Tabla 3. Las deformaciones dinámicas disminuyeron considerablemente, debido en parte a la nueva geometría de la cubierta, y principalmente a que la relación entre el periodo de la excitación y el de la estructura es mucho mayor en este modelo y se apega más a la del prototipo.

En la prueba 3A se obtuvieron resultados muy semejantes a los del modelo 3, lo cual indica que las aberturas para ventilación no influyen en el comportamiento de la cubierta.

Las deflexiones del prototipo, presentadas en las Tablas 3 y 4, han sido calculadas con el factor de escala obtenido en el inciso 1.2, considerando que el concreto contribuye a la rigidez como un material elástico que trabaja en conjunto con el acero.

Así para la obtención de la rigidez de la cubierta del prototipo se usó el módulo de elasticidad del material compuesto.

$$E' = E_1(1 + pn) = 1.2\,E_1$$

La fórmula anterior indica que la contribución a la rigidez del concreto es cinco veces mayor que la del acero. Para cálculo se utilizó un módulo de elasticidad del concreto de 50,000 kg/cm^2, para cargas dinámicas, y concreto de peso volumétrico de 800 kg/m^3.

Para que la cubierta del prototipo trabaje en la forma supuesta, debe existir adherencia perfecta entre concreto y cables, y el concreto debe ser una lámina continua que acepte tensiones sin agrietarse.

La rigidez real del conjunto concreto-cables será menor que la supuesta debido a los agrietamientos del concreto, las holguras entre placas si se usan precoladas y que la adherencia entre los dos materiales no será perfecta. Se obtiene un límite superior de las deflexiones considerando que solo los cables contribuyen a la rigidez; entonces las deflexiones serán seis veces mayores que las consignadas.

El comportamiento real estará entre estos dos casos extremos, más cercano al prmiero mientras más precauciones se tomen para asegurar el trabajo de conjunto de los dos materiales y evitar holguras y agrietamiento en el concreto.

Pueden disminuirse las deformaciones si se procura tener un módulo de elasticidad mayor del concreto aumentando su peso volumétrico o su resistencia.

Las deflexiones medidas en los modelos son bastante confiables debido a la concordancia entre las distintas pruebas efectuadas; sin embargo, no puede excluirse la posibilidad de que pequeñas holguras entre la estructura y el sistema de referencia puedan haber afectado las lecturas, ya que se estaban midiendo deformaciones extremadamente pequeñas.

5.3 *Periodos de vibración.*

En el primer modelo se registró una vibración periódica con una frecuencia aproximada de 50 ciclos por segundo. En el segundo, la vibración fue del mismo tipo pero con una frecuencia de 75 cps, aproximadamente. En el tercer modelo no se nota ninguna periodicidad en la vibración; se trata de vibraciones de alta frecuencia que parecen debidas a vibración del túnel, más que al comportamiento de la estructura.

Hay que recordar que el comportamiento dinámico de los modelos 1 y 2 corresponde al del prototipo, para una velocidad de viento de más de

300 km/h, así que las vibraciones registradas no son de esperarse en la realidad. El comportamiento dinámico del prototipo, para la velocidad de viento de diseño, será del tipo del que se encontró en el modelo 3; es decir, la amplificación dinámica de la deformación será de poca importancia.

6 CONCLUSIONES

La primera pregunta que se trataba de contestar mediante esta investigación, era si la vibración de la cubierta de la alberca modificaba la distribución de presiones obtenida para el modelo rígido. Se puede afirmar que la vibración solo produce diferencias locales, y que las presiones tienen la misma distribución y sus valores son ligeramente más bajos.

Con respecto al comportamiento dinámico de la cubierta se comprobó que:

a) Las deformaciones máximas que deben esperarse en el prototipo no son mayores de 40 cm, para una velocidad de viento de 120 km/h. Hay que considerar que la deformación disminuye con el cuadrado de la velocidad y para un viento de 85 km/h la deformación se reduce a la mitad.

b) Las deflexiones mencionadas corresponderán a las del prototipo si el concreto contribuye a la rigidez de la cubierta como un material elástico que trabaja en conjunto con los cables con un módulo de elasticidad de 50,000 kg/cm². Si solo los cables contribuyen a la rigidez, las deflexiones serán seis veces mayores que las consignadas. Para un comportamiento satisfactorio debe procurarse que exista la máxima adherencia posible entre cables y concreto, evitar holguras entre distintas piezas. Una disminución importante de las deformaciones puede obtenerse aumentando el módulo de elasticidad del material de cubierta.

c) La cubierta de la alberca no presenta vibraciones periódicas importantes, y la amplificación de la deformación debida a la vibración es del orden del 10 por ciento si el concreto trabaja en conjunto con los cables.

d) La presencia de aberturas para ventilación, hasta de 1 × 4 en cada entreeje, no produce efectos desfavorables de importancia en el comportamiento de la cubierta.

7. RECONOCIMIENTO

Esta parte del trabajo fue realizado en la Sección de Estructuras bajo la dirección del Ing. Luis Esteva. La Sección de Instrumentación colaboró en la operación de los aparatos de medición.

8. REFERENCIAS

1. Goodier, J. N. "Dimensional Analysis", apéndice de "Handbook of Experimental Stress Analysis", *M. Hetényi, editor, J. Wiley and Sons, Inc.* (1950 p. 1043)
2. Timoshenko, S. "Vibration Problems in Engineering", *D. Van Nostrand Co., Inc.* (1956)
3. Scruton, C. "On the wind-excited oscillations of stacks, towers, and masts". Proceedings of the Symposium on Wind Effects on Buildings and Structures, Teddington, G. B. II (1963), p. 797

Proyecto Estructural de la Alberca y Gimnasio Olímpicos

*Carlos OLAGARAY P**

RESUMEN

El proyecto de alberca y gimnasio olímpicos comprende dos cubiertas colgantes, siendo la de la alberca una de las más grandes del mundo.

Se presenta un resumen cualitativo del criterio general adoptado para el análisis y diseño estructural, poniendo especial énfasis en lo que se refiere a la forma de trabajo de las cubiertas y sus apoyos, sujetas a la acción de carga permanente y carga acidental de viento o sismo. Se exponen en forma breve las consideraciones básicas relativas a su cimentación.

SYNOPSIS

The Olympic swimming pool and gymnasium project includes two suspension roofs. That of the swimming pool is one of the largest in the world.

Qualitative aspects of the design assumptions of the buildings are presented, specially those pertaining to the action of the suspension roofs and of their bearings while undergoing dead load, wind and seismic forces. Basic suggestions for the foundation design are briefly described.

1. *INTRODUCCION*

El ANTEPROYECTO arquitectónico seleccionado para la obra de alberca y gimnasio olímpicos adoptó como solución estructural básica la de cubiertas colgantes; la mayor para cubrir la alberca de competencia y foso de clavados, y la menor para cubrir el gimnasio. Durante los análisis estructurales preliminares, se estudió, por ejemplo, una alternativa de 132 m de claro principal sin tirantes en los extremos, que resultó factible, pero de costo superior al de otras soluciones. De esta manera se fijaron las dimensiones definitivas de los claros, curvaturas y niveles del proyecto.

El conjunto de cubiertas y sus apoyos representó para el análisis y diseño varios problemas de interés, lo que era de esperarse por ser la cubierta colgante de la alberca posiblemente la mayor del mundo con planta rectangular.

2. *DESCRIPCION DE LA ESTRUCTURA*

Las figs. 1 a 3 muestran las dimensiones generales del conjunto. La cubierta de la alberca, con claro principal de 111.90 m a ejes, cubre un espacio interior de 99.60 × 101.60 m, o sea poco más de 10,100 m². En forma análoga la del gimnasio, con claro principal de 78.70 m a ejes, cubre un área de 66.40 × 76.20 m poco más de 5,000 m². Las cubiertas son colgantes en la dirección norte-sur teniendo como flechas 7.50 m en la alberca y 5.00 m en el gimnasio.

En la dirección oriente-poniente las cubiertas tienen curvatura inversa con flechas de 5.00 y 3.50 m respectivamente. Esta curvatura obedece

* Diseño Racional, A. C.

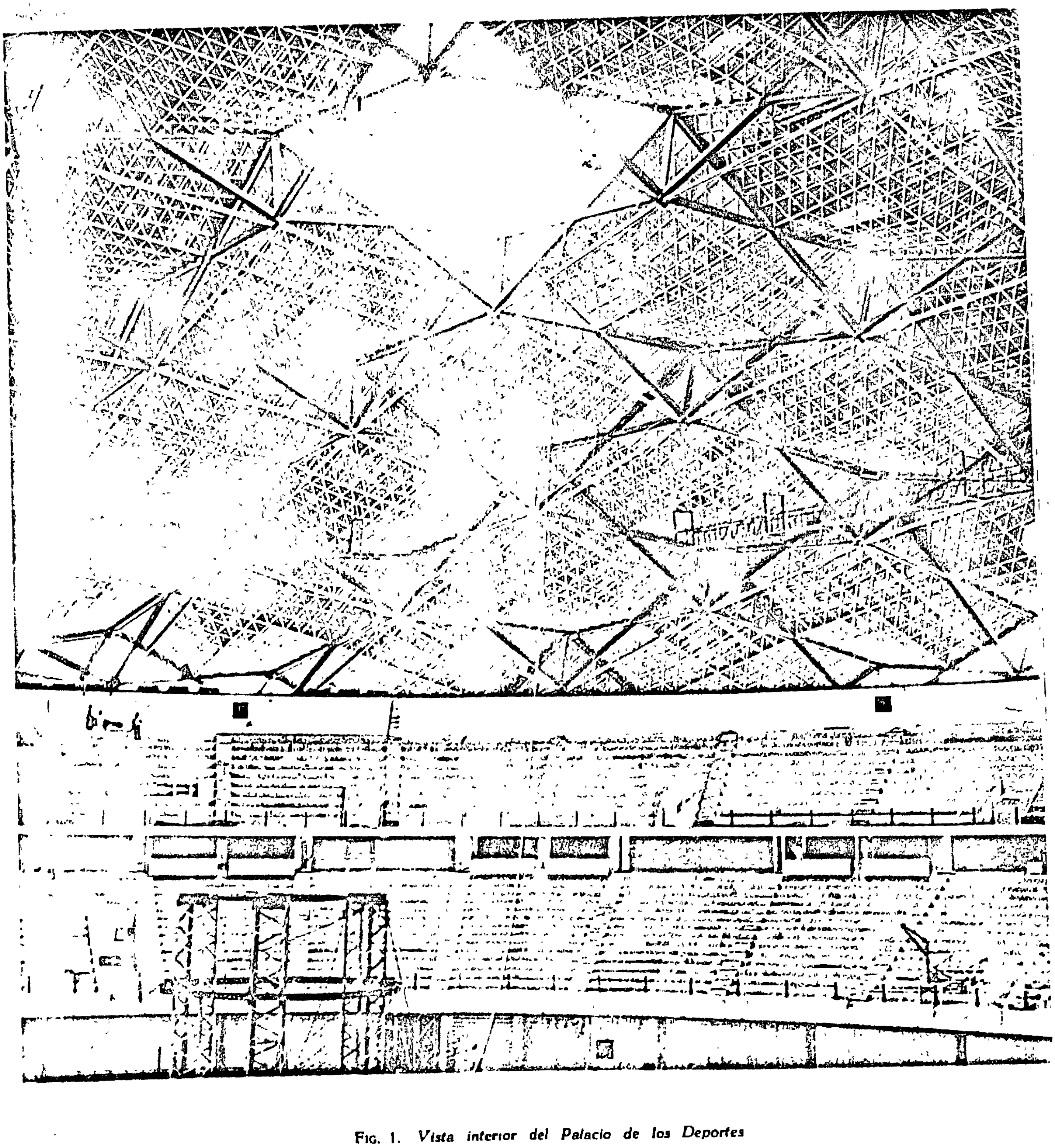

Fɪɢ. 1. *Vista interior del Palacio de los Deportes*

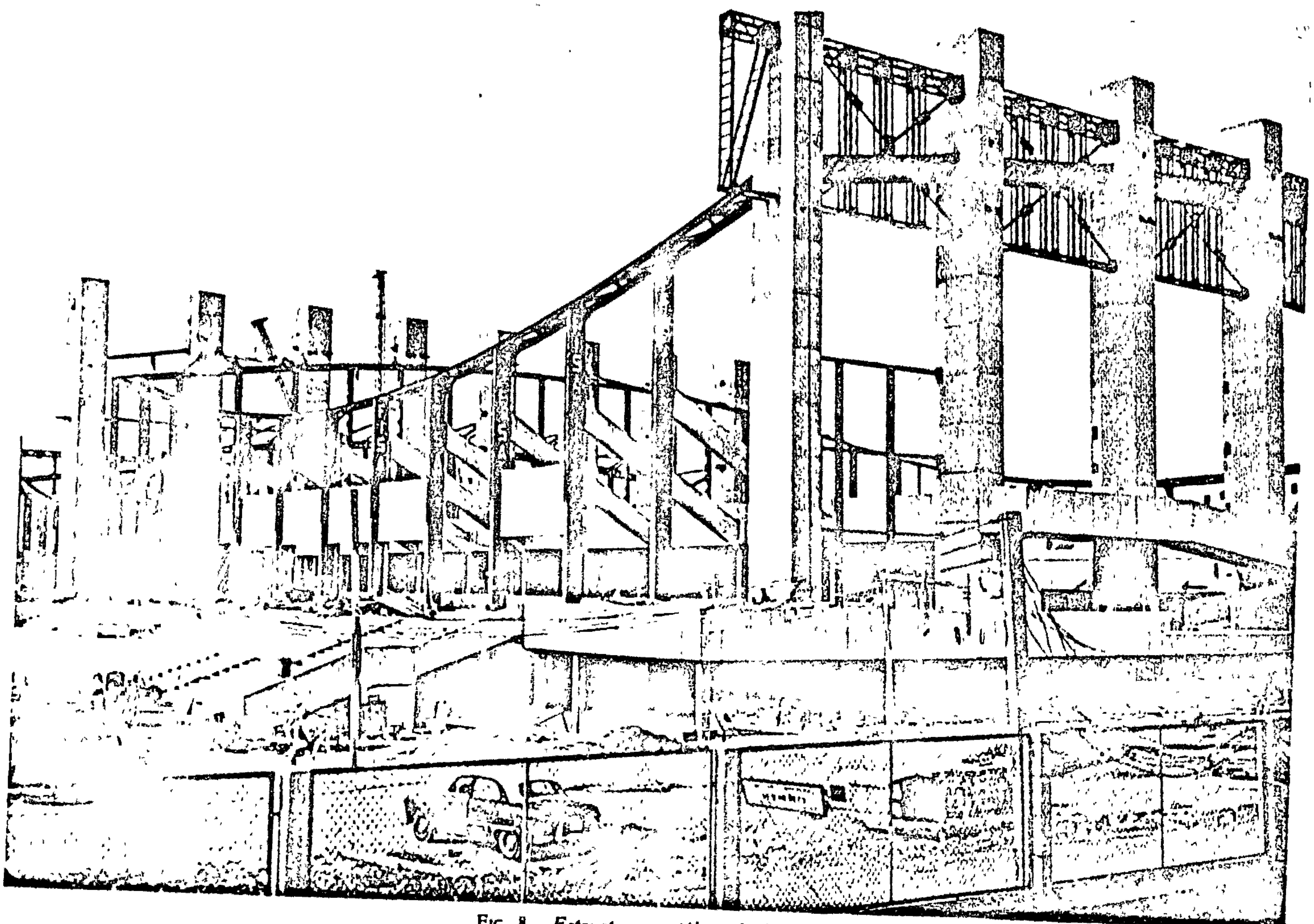

Fig 8. *Estructura metálica de la alberca*

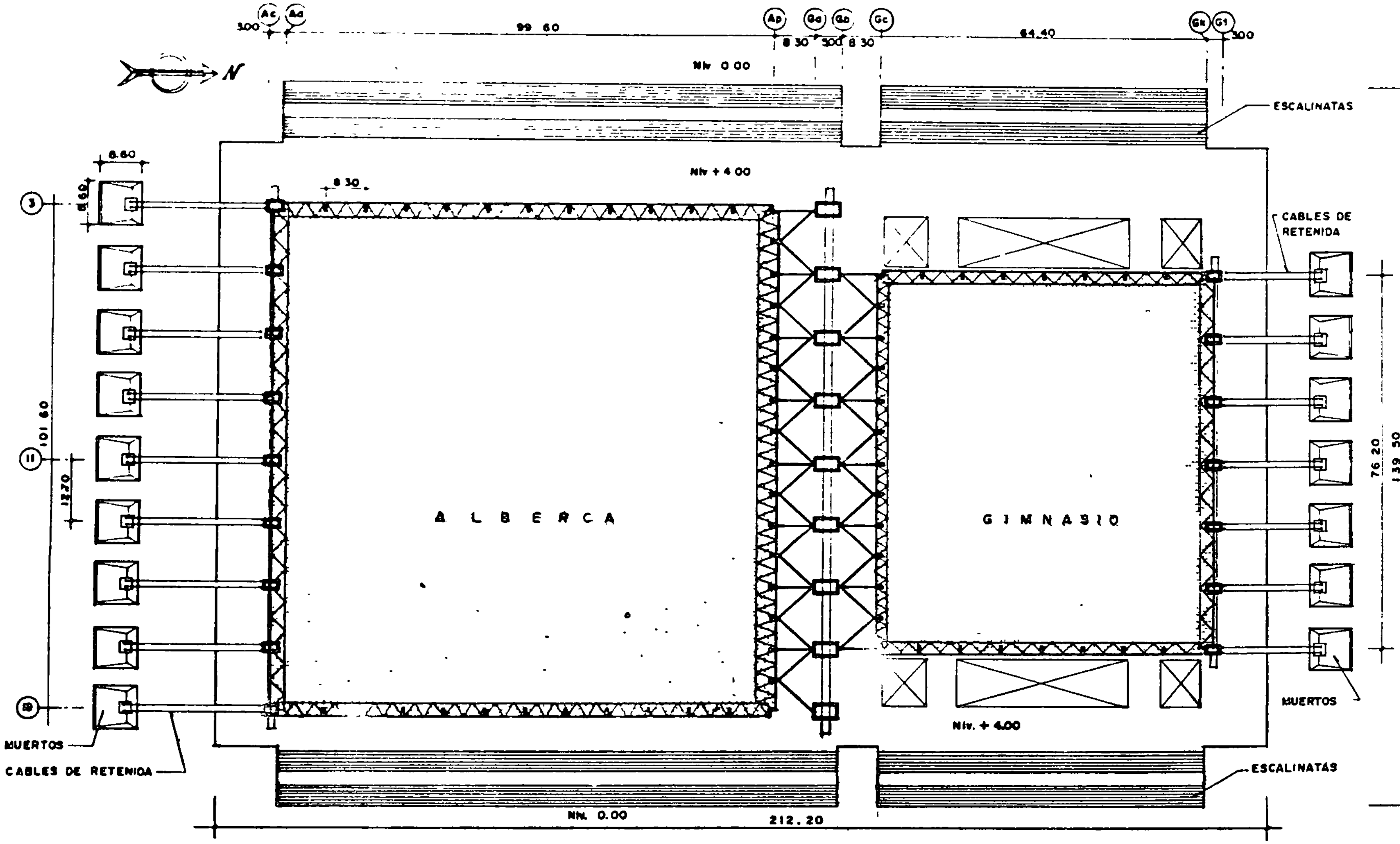

FIG. 1. *Planta General*

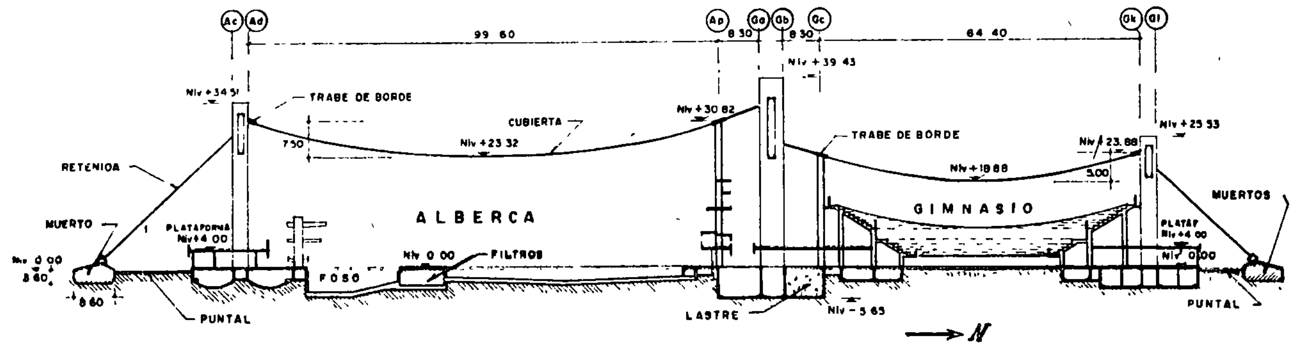

FIG. 2. *Corte longitudinal norte-sur*

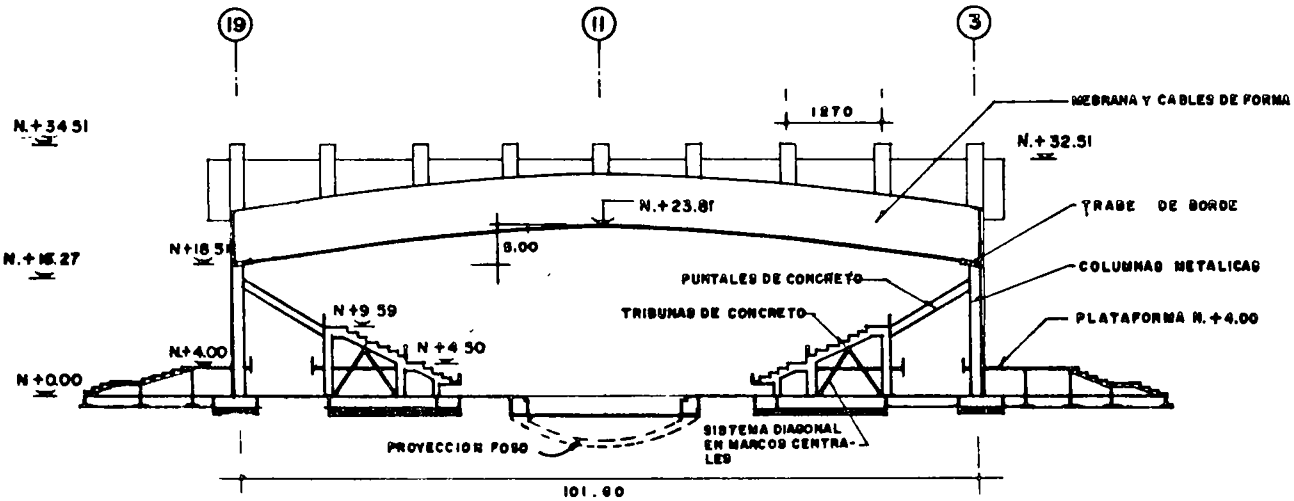

• FIG. 3. *Corte oriente poniente en alberca*

en parte a los requisitos de drenaje pero es necesaria desde el punto de vista estructural para dar rigidez a las membranas. Las superficies formadas son prácticamente paraboloides hiperbólicos, ya que las catenarias se aproximan mucho a parábolas de segundo grado.

El proyecto definitivo de la techumbre utiliza una retícula de cables, unos colgantes en la dirección norte-sur (cables de carga) y otros convexos en la dirección oriente-poniente (cables de forma). Sobre los cables de carga se apoyaron láminas acanaladas, las cuales quedan fijas mediante herrajes especiales. Sobre la lámina se coló un firme de concreto reforzado con objeto de dar el peso y rigidez necesarios para la estabilidad de la cubierta, especialmente ante la acción del viento. En el firme quedan ahogados los cables de forma de la dirección oriente-poniente. Los cables de carga están formados por alambre de 7 mm, de acero de presfuerzo, a cada 1.60 m; los de forma lo están por acero de las mismas características, a cada 2.07 m. Tanto los cables de carga como los de forma están anclados en sus extremos en trabes de borde, metálicas, de alma abierta y contenidas en la misma superficie, a la cual limitan formando un marco cuya proyección horizontal es rectangular. Estas trabes trasmiten sus esfuerzos tanto a las columnas de concreto de los tres ejes principales de apoyo (fig. 2) como a las metálicas que constituyen las fachadas oriente-poniente (fig. 3).

Las columnas extremas, ejes A_c—A_d y G_k—G_l, son huecas, de concreto reforzado, con dimensiones exteriores de 2.00 × 3.00 m. Cada una está provista de dos cables-retenida para equilibrio de la componente horizontal de los cables de carga.

Las retenidas, también de acero de presfuerzo, están protegidas por un tubo de asbesto-cemento y se anclan en los muertos de concreto que muestran las figs. 1 y 2.

Las columnas del eje central G_a—G_b también son huecas, de concreto reforzado, con dimensiones exteriores de 3.00 × 5.00 m. Para resistir flexión que originan en ellas las componentes horizontales de las cubiertas de alberca y gimnasio, se han diseñado presforzadas mediante tendones de acero; estos se tensaron en concordancia con el avance de la obra. Las columnas de cada uno de los tres ejes principales están ligadas en la parte superior por una trabe peraltada metálica, de alma abierta, recubierta con paneles de asbesto-cemento.

Las columnas de las fachadas oriente-poniente e interiores en los ejes A_p y G_c son metálicas

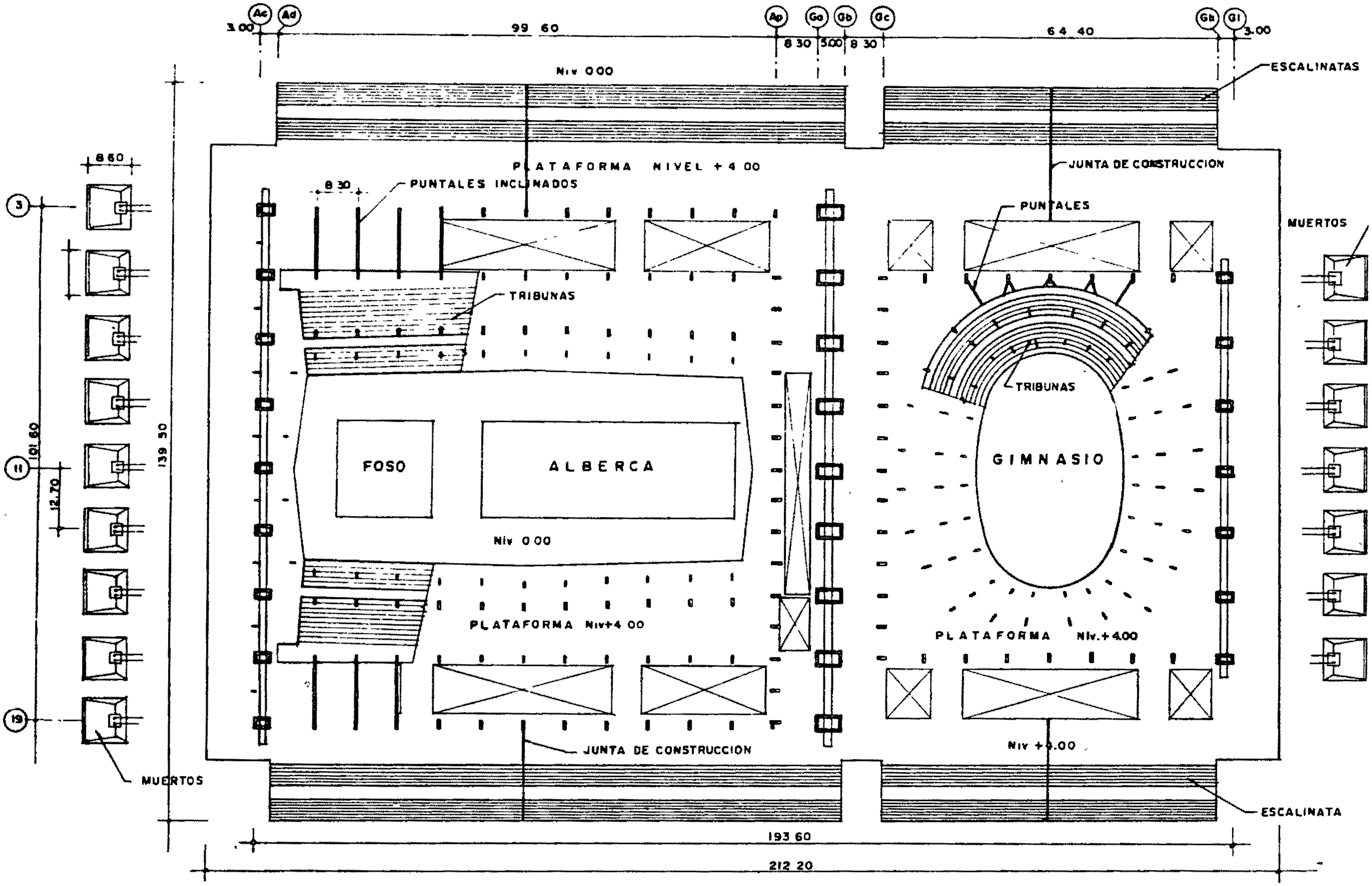

FIG. 4. *Plataforma nivel* +4.00

de 40 × 80 cm y dan apoyo tanto a las trabes de borde como a la cancelería, muros y otros elementos propios de fachada.

Un elemento importante del proyecto es la plataforma del nivel +4.00 m, que, junto con las escalinatas, tiene como dimensiones exteriores 210 × 152 m (fig. 4) y cubriendo un total de 23,000 m². En la mayor extensión es una losa plana de concreto, aligerada, de 40 cm de espesor incluidos los 5 cm de recubrimiento de cajas de aligeramiento. El resto está formado por trabes de concreto y losas perimetralmente apoyadas. Bajo la plataforma del nivel +4.00 se ubican los servicios e instalaciones olímpicas y arriba de la misma se encuentran las tribunas para los espectadores.

Las tribunas, tanto en alberca como en gimnasio, son de concreto reforzado y sus estructuras sirven de apoyo a las columnas metálicas de las fachadas oriente y poniente. En la alberca este troquelamiento se logró con puntales inclinados de concreto (fig. 3) los cuales, además, servirán de apoyo a un sistema de tribunas temporales. En el gimnasio las tribunas están dispuestas en óvalo, de acuerdo con el proyecto arquitectónico.

Los escenarios de gimnasio y alberca se encuentran al nivel +0.00. El del primero es ovalado, con cancha rectangular, y el de la segunda es de planta sensiblemente rectangular; se encuentra al norte la alberca de competencia y al sur el foso y las plataformas de clavados. Tanto el foso como la alberca están provistos de un túnel perimetral de servicio; en la separación de las dos piscinas está un sótano para cuarto de filtros.

La cimentación del conjunto es por compensación total. Está formada de cascarones de cimentación en la zona de alberca, y losa maciza de cimentación en la de gimnasio. Posee una retícula de contratrabes; cierra la cimentación la losa del nivel +0.00 (figs. 2 y 3).

3. *PRINCIPALES CONSIDERACIONES ESTRUCTURALES DETERMINANTES DEL ANALISIS Y DISEÑO*

En el conjunto de alberca y gimnasio olímpicos se tienen varios grupos estructurales cuyo comportamiento satisfactorio requiere de interacciones de importancia. Pueden considerarse como grupos estructurales los siguientes: *a)* cubiertas y sus apoyos, *b)* tribunas, *c)* plataforma del nivel + 4 00, *d)* cimentación, *e)* alberca de competencia y foso de clavados, *f)* estructuras de acceso, rampas y puentes, y *g)* fachadas A continuación se describirá la forma de trabajo de estos grupos ante las solicitaciones a que serán sometidos.

La secuencia del análisis estuvo regida primordialmente por las cubiertas, siendo la geometría final de las mismas, como ya se indicó, el producto de una serie de análisis previos, en los que se valuaron las respuestas ante las solicitaciones estimadas.

4. *CUBIERTAS Y SUS APOYOS*

El punto de partida para el estudio de la techumbre fue la ecuación diferencial del equilibrio de membranas

$$q = H_x \frac{\partial^2 z}{\partial x^2} + H_y \frac{\partial^2 z}{\partial y^2} \tag{1}$$

donde

$z = z(x, y)$ ecuación de la superficie
$q = q(x, y)$ carga vertical por unidad de área horizontal (kg/m²)
H_x componente horizontal de tensión o compresión por unidad de longitud en dirección del eje X (kg/m)
H_y componente horizontal de tensión o compresión por unidad de longitud en dirección del eje Y (kg/m).

Al considerar q como constante, lo que equivale a despreciar el efecto del peso en área real respecto a su proyección, la solución de esta ecuación da origen a parábolas en ambas direcciones. Las concavidades pueden estar hacia arriba o hacia abajo en las dos direcciones (paraboloides elípticos), o una hacia arriba y la otra hacia abajo (paraboloide hiperbólico). Esta última alternativa fue la solución adoptada para las cubiertas.

Bajo la acción de carga vertical constante q, como el peso propio, la ec. 1 conduce a lo mostrado esquemáticamente por la fig. 5, en la que se aprecia que sobre los cables de carga actúa no solo el peso propio q, sino también la carga q_y debida a la presión que ejercen los cables de forma sobre los de carga al ser tensados con la fuerza H_y. El valor de esta fuerza puede ser arbitrario, mientras se trate de tensión. El valor q_y, denominado carga de presfuerzo, se fijó en 5 kg/m² para la alberca y 10 kg/m² para el gimnasio; estos valores son los estimados como los más convenientes, atendiendo a consideraciones de economía y de rigidez.

Antes de describir con más detalle la forma general del trabajo de las cubiertas, cabe hacer mención de los efectos de viento y sismo sobre las membranas. Ante ambas solicitaciones, la ec. 1 deja de ser rigurosamente válida, ya que intervienen componentes horizontales de carga; no obstante, algunas idealizaciones como las de la fig. 6 permiten apreciar cualitativamente los efectos entre los que destacan, por su importancia, los desplazamientos máximos que pueden ocurrir.

Encaminándose a fines prácticos para diseño de las membranas bajo la acción del viento, se procedió por una parte a idealizarlo como una carga vertical uniforme de succión, lo que es conservador para los esfuerzos, y se aplicaron las consideraciones de forma de trabajo que más adelante se describen. Por otra parte, en lo referente a deformaciones, se coordinó con el Instituto de Ingeniería de la UNAM la preparación de un modelo

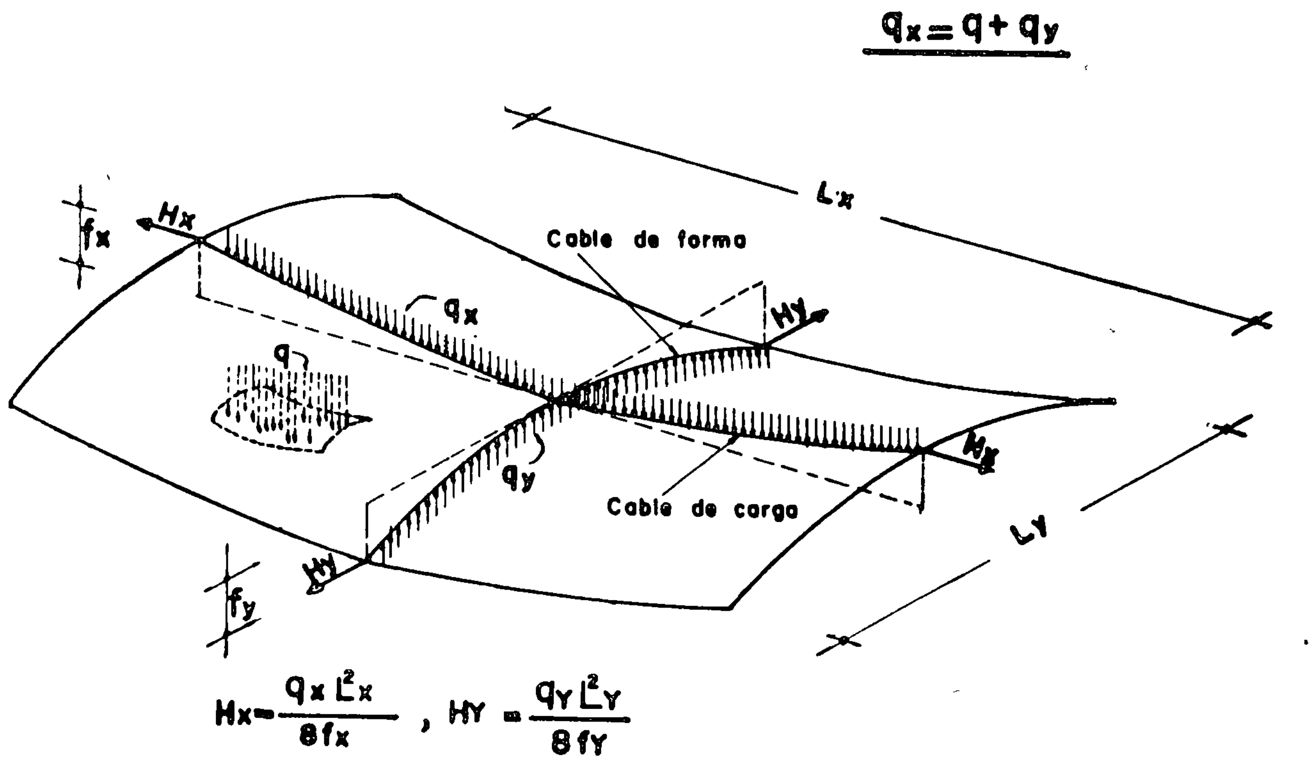

$$H_x = \frac{q_x L_x^2}{8 f_x}, \quad H_Y = \frac{q_Y L_Y^2}{8 f_Y}$$

FIGURA 5

flexible que se estudió en el túnel de viento, encontrándose que los desplazamientos serían tolerables.

En lo correspondiente a sismo, la idealización de la fig. 6b es simplemente para obtener una cota superior, tanto de desplazamiento como de tensión en cables de carga ya que para el diseño práctico se consideró que las fuerzas de inercia de las membranas serán trasmitidas a los bordes fundamentalmente por esfuerzo cortante a través del firme colado sobre la lámina de techumbre. Puede resumirse que las acciones de membranas en sus cuatro bordes pueden valuarse en forma precisa bajo carga vertical y en forma suficientemente aproximada y conservadora bajo cargas dinámicas, incluyendo en esto su distribución.

Para los fines prácticos de diseño, el primer problema planteado fue determinar y resistir las componentes horizontales de los cables de carga tanto en los ejes extremos como en el central. Dado el orden de magnitud de estas fuerzas lo conveniente, en apariencia era optar por un mínimo de carga en las techumbres, pero ello hubiera obrado en contra de la estabilidad y de la rigidez de las membranas sujetas a la acción del viento. Se requiere un mínimo de peso muerto tal que la succión del viento no lo exceda, para evitar una condición de inestabilidad cosa que solo puede evitarse disponiendo de elementos estructurales capaces de resistir la succión.

Por otra parte y muy relacionado con lo anterior se presentaba el problema del apoyo central. La marcada asimetría de las cubiertas y sus niveles trae por consecuencia un desequilibrio muy impor-

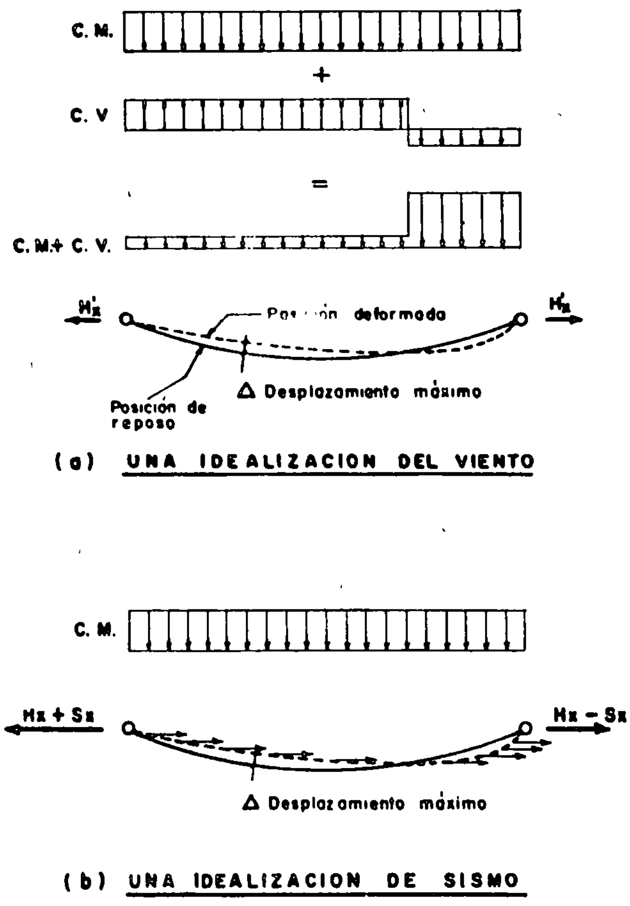

FIGURA 6

tante en las columnas del eje central. Para disminuirlo se requería poco peso y amplia flecha en la alberca y un peso mayor con flecha menor en el gimnasio (fig. 7).

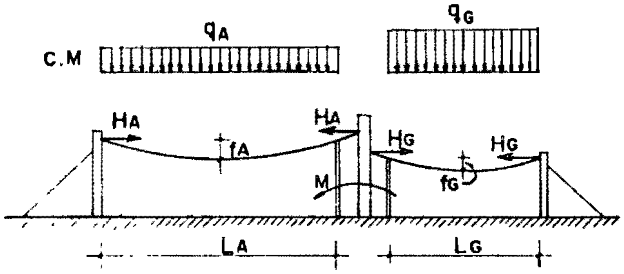

FIG. 7. *Componentes horizontales de cubiertas*

Valorando distintas alternativas, quedaron en el proyecto estructural definitivo, como peso muerto de techumbres, incluidos los cables:

C. M. alberca	125	kg/m²*
C. M. gimnasio	165	,,
Presfuerzo alberca	10	,,
Presfuerzo gimnasio	10	,,

Las solicitaciones por carga muerta, carga viva, viento y sismo, empleadas para el análisis y diseño estructural, se estimaron de acuerdo con el Reglamento de Construcciones para el Distrito Federal, tanto para las cubiertas y sus apoyos como para el resto de las estructuras en el conjunto.

Este Reglamento prevé el empleo de modelos a escala para el estudio del viento, labor que le fue encomendada al Instituto de Ingeniería de la Universidad Nacional Autónoma de México y cuyos resultados con modelos tanto rígidos como flexibles en túnel aerodinámico sirvieron para establecer con precisión características importantes del comportamiento del conjunto.

La acción del sismo sobre las membranas resultó menos desfavorable en ciertos aspectos —los relativos a deformaciones—, que la del viento. Sin embargo, las diferencias de sus características, con respecto a las del viento, requirieron análisis con varias alternativas de hipótesis simplificadoras.

La velocidad de viento supuesta para el proyecto fue 120 km/hora. Esta acción es, cualitativamente, como una carga ascendente que actúa en la membrana. La acción del viento se tradujo en una disminución de la tensión de los cables de carga y un aumento en la tensión de los cables de forma, planteando problemas consecuentes; por una parte la posibilidad de que el viento de sur a norte succione más en la alberca que en el gimnasio, creando cambios en el equilibrio general y especialmente en el eje central (similarmente al obrar de norte a sur) y por otra parte los cables de forma, apoyados en las estructuras de tribunas, introducían fuerzas que provocaban la aparición de nuevos elementos mecánicos en las mismas, lo cual hubo de ser tomado en cuenta para su diseño. Las succiones más importantes del viento fueron en la dirección de 45°, pero la más desfavorable a la estructura resultó ser de 90°, oriente poniente, pero todas las alternativas se tomaron en cuenta con hipótesis simplificadoras.

Otro aspecto interesante se presentó al analizar y diseñar las trabes de los bordes. Las que reciben a los cables de carga tienen como función principal trasmitir a las columnas la tensión de aquellos y además servir de elemento de liga horizontal. Estas trabes se diseñaron para dichas condiciones, después de analizar los posibles desplazamientos diferenciales.

Tratándose de las trabes de borde de oriente y poniente, que reciben a los cables de forma, no era práctico que se librara horizontalmente el claro total de 100 m para constituir un anillo rectangular de compresión, pues los órdenes de magnitud de los momentos y de los desplazamientos hubieran sido intolerables. Así, se decidió que estas trabes se apoyaran en las columnas metálicas de fachada, las cuales a su vez se troquelarían contra las tribunas (fig. 8). La carga máxima en estas trabes se tiene cuando actúa el viento, pero la acción del sismo es similar y sus efectos comparables. Dado que los apoyos proporcionados por las columnas metálicas a las trabes de borde varían en altura y por lo tanto en rigidez, se hizo el análisis como vigas sobre cimentación elástica empleando computadora electrónica.

Una característica importante del sistema de cubiertas radica en que las columnas extremas, ejes 3 y 19 del eje central, no tienen retenidas ni reciben la restricción del gimnasio. En consecuencia se ha analizado y diseñado para que las trabes de borde ejes 3 y 19 de alberca trabajen como arcos invertidos apoyándose en las columnas metálicas de fachada (fig. 9a). Algo similar ocurre con las inmediatas hacia el interior 5 y 17, la componente horizontal aportada por el gimnasio es menor que en la típica interior y por ello las trabes de borde del gimnasio trabajarán como tensores restringidos por las columnas de la fachada (fig. 9b).

Las trabes de borde oriente y poniente están también analizadas y diseñadas para servir de liga estructural entre los tres ejes principales cuyas rigideces difieren entre sí. El trabajo de las trabes será similar al ya mostrado por las figs. 9a y b.

5. *COLUMNAS*

Para el análisis y diseño definitivos de las columnas de los tres ejes principales fue necesario considerar la envolvente de todas las solicitaciones que se han mencionado. La flexibilidad de estas columnas intervino en forma definitiva al estudiar viento y sismo, pues de sus valores de-

* Posteriormente, en la etapa de construcción, y teniendo resultados aportados por el Instituto de Ingeniería, UNAM, estos valores se modificaron a 95, 130, 5 y 10 kg/m², respectivamente.

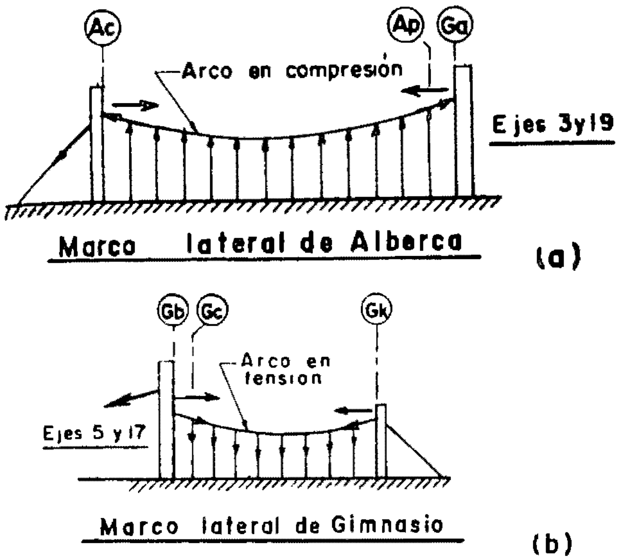

FIGURA 9

pendió. no solo la respuesta de la estructura, sino también el dimensionamiento adecuado de todos los elementos resistentes que intervienen, y muy especialmente el de las trabes de borde.

La rigidez de las columnas de los ejes extremos se analizó integrándolas con los cables-retenida correspondientes los que además tienen altura variable con la consiguiente variación de rigidez (fig. 10). Se refuerza así la necesidad de las trabes de borde convenientemente diseñadas incluyendo en esto su ductilidad. Otra característica en estas columnas, la carga axial, está constituida por la componente vertical de los cables de carga y su peso propio; además soportan la componente vertical de sus retenidas.

Los muertos de concreto reforzado en que se anclan los tirantes se analizaron para resistir con su peso y, considerando el efecto de flotación en el nivel freático, la componente vertical de las retenidas. Se dimensionaron con un factor de carga estática de 1.30. Los muertos de concreto se ligaron a la estructura mediante puntales que resisten la componente horizontal. Una trabe peraltada de cimentación liga entre sí a los muertos de concreto para disminuir los posibles movimientos diferenciales que afectarían principalmente a las propias columnas.

El criterio seguido para el análisis y diseño de las columnas del eje central (3.00 × 5.00 m, huecas), fue similar. Se determinó su rigidez con la sección total, se tomó en cuenta el pequeño aumento de rigidez por la restricción de las membranas. En los detalles finales del diseño se tomó en cuenta la deformación causada por los tendones del presfuerzo. Ya se ha visto la razón por la cual estas columnas son presforzadas, pero además de la diferencia en fuerzas de borde entre las dos cubiertas, contribuyó el hecho de que la deformación total se logra disminuir en virtud del presfuerzo y que se logra un aumento de rigidez al trabajar la sección total, merced al mismo presfuerzo.

La fig. 11 muestra esquemáticamente la columna central.

6. *ESTRUCTURAS DE TRIBUNAS*

En lo referente al análisis y diseño de estas estructuras de concreto puede mencionarse que, además de su peso propio, y la correspondiente carga viva, fueron diseñadas para recibir el empuje que proviene de la cubierta a través de las columnas de fachada y los puntales. El análisis de los marcos se llevó a cabo con las alternativas más desfavorables de carga viva, viento o sismo, estableciendo para tal efecto un sistema simultáneo de ecuaciones de piso, una por cada grado de libertad.

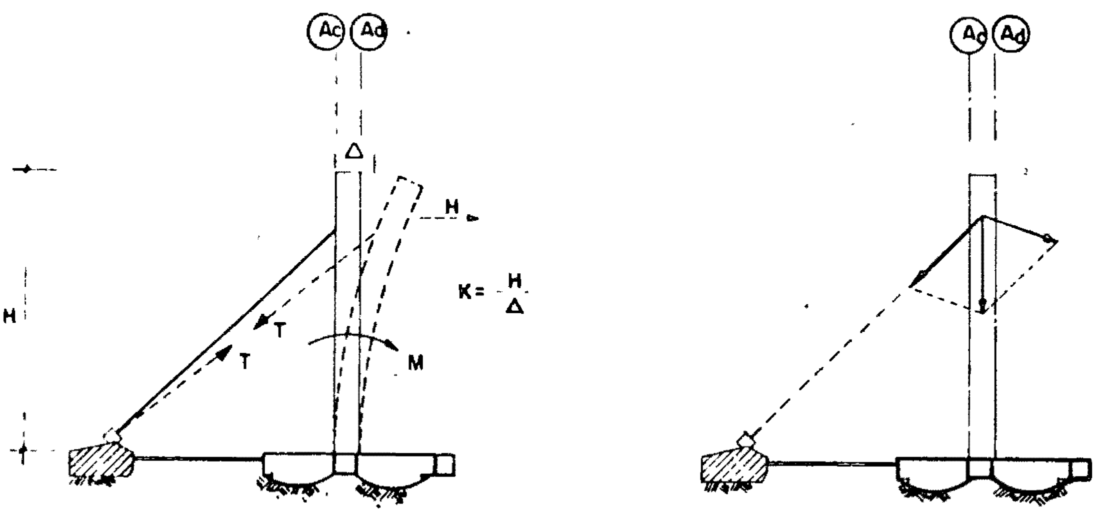

FIGURA 10

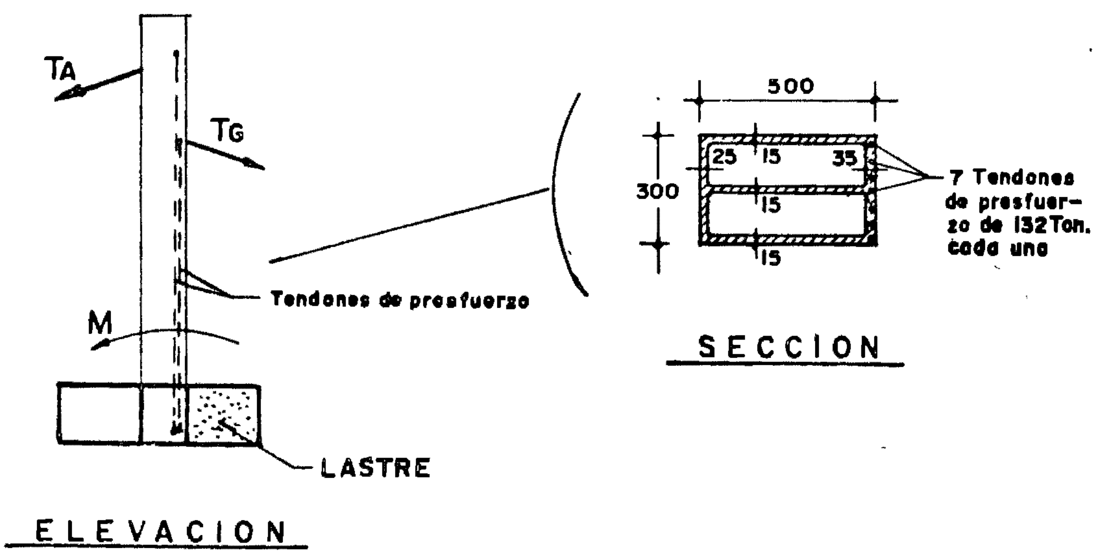

FIGURA 11

7 *PLATAFORMA DE NIVEL* +4.00

Esta estructura es la liga general del conjunto: despreciando sus deformaciones axiales y de cortante, iguala los desplazamientos de todas las columnas, tanto metálicas de fachadas como las de concreto de tribunas y las huecas de cubierta. Este criterio llevó a concluir que todas las fuerzas sísmicas serían absorbidas por las columnas huecas debido a la rigidez relativa de estas. Sin embargo, de un análisis más detallado que toma en cuenta la deformabilidad de esta losa, se determinó que habría una fuerza cortante sísmica no despreciable en las columnas restantes.

Otro aspecto de interés en esta plataforma son sus dimensiones al tomar en cuenta los cambios de temperatura. Para disminuir los daños probables, se proyectaron las juntas expuestas a la intemperie que se muestran en la fig. 4. Además se tomaron precauciones especiales en el terminado de la plataforma y se adoptó un método adecuado de construcción.

8. *CIMENTACION*

El análisis y diseño de la cimentación del conjunto requirió un estudio geotécnico para determinar las características mecánicas del suelo en el predio destinado a esta obra. El terreno pertenece a la zona de transición del Valle de México, con estratos arcillosos y arcillo-limosos de alta y media compresibilidad, con espesor total medio de 12 m hasta la llamada primera capa dura.* El nivel freático se encontró a una profundidad media de 2 m y hay indicios de consolidación en el primer depósito compresible por abatimiento del nivel freático causado por los bombeos en el Valle.

Es fácil apreciar que las mayores cargas se localizan bajo los tres ejes principales de apoyo de cubiertas. Ello se hace palpable no solo por el peso de estas, sino también por el de las columnas huecas. En cambio, bajo las escalinatas, plataforma y tribunas, las cargas son relativamente pequeñas.

Por otra parte, las características de compresibilidad del subsuelo no permiten una sobrecarga mayor de 1 ton/m² sin que ocurran asentamientos de importancia, por lo que, bajo los ejes citados habría que compensar —al menos parcialmente— o recurrir al empleo de pilotes.

Después de estudiar distintas alternativas, se decidió una cimentación compensada por zonas, según las distintas cargas proyectadas por la estructura.

Así, la cimentación proyectada posee bajo cada uno de los tres ejes principales un cajón profundo corrido. En el extremo sur de alberca, este cajón consta de dos cascarones y una losa horizontal (fig. 2): en el extremo norte del gimnasio, el cajón es de losa plana y contratrabes. Esta diferencia es consecuencia de la disposición de los ejes del gimnasio, unos radiales y otros circunferenciales.

La cimentación del eje central fue la de mayor importancia en el proyecto: esta, además de la carga vertical, resistirá el momento de volteo que le trasmitan las columnas, debido a la asimetría de las cubiertas. Dicho momento se modifica notablemente ante las acciones de sismo o viento, lo que reforzó la conveniencia de ampliar la base. Para equilibrar el momento estático de volteo, formó parte del proyecto estructural un lastre de carácter definitivo en la parte norte del cajón, que, junto con el peso de las tribunas del gimnasio comprendidas en la misma zona, reunió las condiciones requeridas para un buen comportamiento.

La cimentación para las estructuras de plataforma y tribunas en la zona de alberca está for-

* Los depósitos compresibles en la zona del lago del Valle de México tienen espesores hasta de 40 m a la primera capa dura

ada por cascarones de cimentación de 4.15 m de claro apoyados en una retícula de contratrabes; cierra la cimentación hueca la losa del nivel + 0.00. Para tribunas del gimnasio y la porción restante de plataforma, la cimentación es hueca también pero no fue aconsejable el uso de cascarones, sino que se empleó losa maciza, dada la irregularidad de los ejes interiores.

Para las escalinatas la cimentación es de zapatas corridas compensando la carga mediante sustitución del terreno natural por tezontle.

9 *ALBERCA DE COMPETENCIA Y FOSO DE CLAVADOS*

Este núcleo, formado por el foso de clavados, el cuarto de filtros, la alberca de competencia y el tunel perimetral, presentó dos problemas predominantes: por una parte la sobrecompensación, en especial la del foso y cuarto de filtros, y por otra los efectos accidentales de vaciado y llenado (fig. 2).

La compensación se logró disminuir por un incremento —dentro de la economía— de los espesores de las losas de fondo, las cuales tienen además que cumplir los requisitos de rigidez como elementos de cimentación. Por otra parte se aplicó una secuela adecuada durante la etapa constructiva con el fin de que las expansiones diferidas ocurrieran sin afectar a las cimentaciones vecinas.

En cuanto a los efectos de llenado y vaciado, este núcleo estructural se ligó a las cimentaciones vecinas mediante contratrabes para disminuir los movimientos relativos que podrían dañar así el piso del escenario.

En el foso de clavados se analizó la posibilidad de flotación suponiendo que el nivel freático subiera 1.00 m de su nivel actual. La supresión ejercida en el fondo del foso, estando este vacío, constituyó la condición más desfavorable y con ella se diseñaron el cascarón cilíndrico y la conoide que forman el fondo.

PLACAS PLEGADAS.

Por Miguel Angel Velasco Ruiz (*)

(*) Profesor de la División de Estudios Superiores, Facultad de Ingeniería, U.N.A.M.

PLACAS PLEGADAS.

1. INTRODUCCION.

Las estructuras de placas plegadas fueron usadas por primera vez en Alemania en 1925 y desde entonces se han venido haciendo más populares, Se han usado ampliamente, en particular como estructuras de cubierta desde su empleo tiene muchas ventajas sobre otras formas estructurales,

En una estructura de placas plegadas, como la que se muestra en la Fig. I la superficie de cubierta es ella misma el principal sistema estructural y soporta toda la carga exterior. Las placas plegadas son así mucho más económicas de material que los sistemas convencionales de cubierta, a base de armadura en las cuales los Largueros son un sistema estructural secundario. Además las estructuras de placas plegadas, ya que consisten simplemente de una serie de superficies planas que se intersectan libremente de los marcos de apoyo, son estéticamente agradables.

Aún cuando las estructuras de placas plegadas no son formas estructurales tan eficientes como los cascarones de curvatura contínua los cuales pueden transmitir una proporción mayor de la carga externa por una acción en su plano, la construcción de las placas plegadas es mucho más convenientes y por lo tanto a menudo menos costosa que la de los complicados cascarones curvos. Así, las placas plegadas pueden verse como un compromiso, poseyendo una gran proporción de la eficiencia de cascarones de curvatura continua, mientras, al mismo tiempo, abarcando costos constructivos relativamente bajos.

El interés mostrado en este tipo de costrucción ha acelerado el desarrollo de un cierto número de métodos de análisis para estructuras Placa-plegada de un solo claro. No obstante ya se han reportádo estudios accesibles de estructuras plegadas contínuas y en voladizo, Reiss (41) entre otros.

2. NOMENCLATURA.

Una estructura plegada es una disposición tridimencional de placas que estan arregladas a modo de producir una construcción estable capaz de soportar cargas.

El instintivo esencial de tal estructura es que los elementos componentes individuales son planos, no curvos.

De acuerdo con su forma externa, las estructuras de placas plegadas (6) pueden distinguirse como:

a) Prismáticas,

b) Piramidales,

c) Prismoidales,

d) Curvas en planta.

Las estructura plegadas "Prismáticas " (que son conocidas usualmente simplemente como "estructuras Prismáticas ") Son usadas para varios propósitos constructivos tales como cubiertas, Fig. (1). Puentes, torres de enfriamiento, etc. Se caracterizan por el hecho de que consisten de placas rectangulares que estan restringidas de movimiento relativo entre si (como lo supone la teoría) por medio de " diafragmas "transversales de rigidez o, alternativamente,por medio de marcos rígidos, armaduras u otros dispositivos estructurales que cumplan una misión similar.

Las estructuras plegadas " Prismáticas" ocurren como pabellones cubiertos, torres de enfriamiento y silos, Fig. (2). Las estructuras plegadas " Prismoideas " , Fig. (3), son una forma intermedia de construcción entre entre las estructuras prismáticas y piramidales. Las estructuras plegadas " curvas en planta ". se utilizan principalmente en la edificación de puentes, Fig. (4). Aparte de las formas principales antes mencionadas, existen muchos otros tipos de " Plegaduras " y formas aliadas de construcción que presentan un comportamiento más o menos semejante. Estas incluyen por ejemplo varios tipos de escaleras, Fig. (5).

Si solo dos placas se intersectan en una " junta ", " vertice ", "unión", " dobles " o "borde", la estructura se denomina estructura plegada " Simple ". Si más de dos placas se intersectan en una " junta ", la estructura se denomina estructura plegada " Multiple ". El grado de multiplicidad es, M = S - 1, donde S es el número de placas que se intersectan en un borde.

Como va a ser evidente de las consideraciones anteriores, las componentes fundamentales de una estructura plegada son las placas y las uniones formadas por ellas.

Una característica significativa de las estructuras placa-plegada es que cada una de las placas componentes posee considerablemente mayor rigidez a la flexión dentro de su propio plano que en la dirección perpendicular a él. De aquí en adelante, el nombre de " placa plegada " estará restringido a estructuras prismáticas exclusivamente.

Una placa plegada puede definirse haciendo una traslación de una poligonal, abierta o cerrada, llamada su " Sección trasversal " , a lo largo de un eje longitudinal recto para generar una plegadura prismática que cubre el claro entre diafragmas de apoyo.

En un análisis completo de un prisma estructural deben determinarse todas las fuerzas internas y desplazamientos mostrados en la Fig. (6). Las fuerzas internas Nx, Ny y Nxy se llaman " Fuerzas de menbrana " mientras que Mx, My, Mxy, Qx y Qy son fuerzas internas debidas a la flexión de la plegadura. En muchos análisis aproximados ciertas fuerzas internas se consideran despreciables y se toman iguales a cero.

De primordial importancia desde el punto de vista del diseño de prismas de comcreto son aquellas fuerzas internas que determinan los requisitos de acero de refuerzo que se muestran en la Fig. (7). Estas son Nx para el acero principal por tracción longitudinal ; Nxy para el acero en tracción diagonal; y My y Ny para el Acero transversal.

3. MÉTODOS DE ANALISIS.

LOs métodos disponibles de análisis pueden calificarse como sigue.

1.- Métodos de la teoría de la Elasticidad.

a) Los que desprecian los desplazamientos relativos de las uniones (placas plegadas cortas) Goatharamulu- y Kulkarni, Reiss y Yitzhak. (50, 40)

b) Los que permiten los desplazamientos relativos de las uniones (placas plegadas largas) Werfel- Goldberg y Leve. (55, 26)

2. Métodos ordinarios (vigas de gran peralte)

a) Los que desprecian los desplazamientos relativos de los nudos. Cremer, Gruber y Winter y Pei. (10, 12, 28, 57)

b) Los que permiten los desplazamientos relativos de nudos. Gaafar, Yitzhaki- Reiss y Mast. (19, 59, 31)

3.- Métodos especiales.

a) Teoría degenerada de cascarones cilíndricos (Gibson) (20, 21, 22, 23)

b) Método del elemento finito (Rockey- Evans) (42)

c) Método del elemento transversal (13, 48)

4.- Método de la viga de pared delgada. (48)

4. METODO DE LA ELASTICIDAD.

Hipótesis.

H-1.- El material de la estructura Placa- Plegada es Homogéneo y linealmente elástico.

H-2.- Los desplazamientos son pequeños comparados con las dimensiones de la estructura de modo que la geometría estructural no se altera significativamente.

H-3.- Se aplica el principio de Superposición.

H-4.- Las uniones entre las placas son totalmente monolíticas.

H-5.- Cada Diafragma de borde es infinitamente rígido en su propio plano y perfectamente flexible normalmente a su plano.

El Método de la elasticidad introducido por Werfel (55) y modificado por Golderg-Leve (26) Consiste básicamente en analizar la acción de placa y de losa de cada placa individual en primera instancia, y entonces asegurado que se satisfacen las condiciones de equilibrio y compatibilidad en cada borde cuando se ensamblan las placas para formar la estructura completa." La acción de placa"de cada placa se analiza por la aplicación de los principios de la Elasticidad bidimensional y la " acción de losa " es analizada por la teoría de la flexión de placas.

Desafortunadamente el Método, puesto que envuelve las soluciones clásicas de esfuerzo plano y de flexión de placas, el cual requiere la representación de cada una de las cargas aplicadas por una serie de Fourier, envuelve una gran cantidad trabajo de Cómputo. En general su aplicación solo viene a ser practicable cuando se programa para una computadora digital.

Se ha desarrollado además un Método basado también en la teoría de la elasticidad pero despreciando los desplazamientos relativos de las uniones el cual puede ser apropiado para estructuras " cortas " Este enfoque ha sido muy recientemente propuesto por Seetharamulu y Kulkarni (50) y tambien por Rise y Yistak (40). En este método los análisis de esfuerzo plano y de flexión de las placas individuales han sido desarrollados como en el método elástico ordinario, pero despreciando los desplazamientos relativos de las juntas se ahorra tiempo y esfuerzo de cómputo. Sin embargo, la cantidad de trabajo requerido es aún considerable y el método requiere nuevamente el uso de una computadora digital y por lo tanto los beneficios del empleo de esta solucion se pueden ser marginales.

5. METODOS ORDINARIOS DE CALCULO.

En virtud de que el método de la Elasticidad requiere un gran esfuerzo de cómputo, fundamentalmente con máquinas electronicas, los métodos ordinarios, en los cuales se supone un comportamiento estructural simplificado, han atraido mucha atención. Ademas de las primeras cinco hipótesis antes presentadas, los metodos ordinarios suponen que:

H-6.- La acción en el plano de una placa individual es similar a la de una viga simplemente apoyada en los diafragmas de borde.

H-7.- La Acción de cada placa normal a su plano es similar a la de una franja unitaria de losa tranversal que trabaja en una sola dirección Fig. (8).

El comportamiento de una placa plegada puede considerarse entonces que consiste de la acción de una serie de franjas transversales de losa unidireccionales, las cuales interactúan en los bordes de una serie de vigas placas que se extienden longitudinalmente entre los diafragmas externos. Las franjas de losa solo tranmiten cortantes y momentos en la dirección transversal, esta acción se llama " Acción transversal de losa ", mientras que las vigas - placa solo tranmiten fuerza en sus planos, esta acción se llama " Acción longitudinal de placa " de la estructura.

Este comportamiento idealizado se ilustra en la Fig. (9), la carga externa es resistida por el sistema de losas que se supone soportado por las barras rígidas imaginarias que tranmiten las reacciónes de losas R2, R3, R4, a los bordes del sistema de placas. Estas reacciones se resuelven en sus componentes en los planos de las distintas placas como se muestra en el diagrama.

El desplazamiento de una placa típica " i " durante la acción de las placas longitudinales se muestra en la Fig. (10). Es aparente que, con objeto de que los desplazamientos de esta placa sean compatibles con los de las placas adyacentes, los bordes de la placa " i " deben desplazarse normalmente al plano de la placa. La diferencia de estos dos desplazamientos normales de borde se llama " El desplazamiento relativo de la junta ", Δ i, de la placa, y este desplazamiento producirá momentos adicionales en el sistema transversal de losas, como se muestra en el diagrama.

METODOS ORDINARIOS DE CALCULO (Continúa)

En el primero de los métodos ordinarios, método 2a, se supone que estos momentos transversales adicionales son despreciables en comparación con los producidos en la franja transversal por las cargas externas. Estas soluciones como fueron propuestas por Craemer, (10,12) Gruber (28) y Pei (57) simplemente envuelven analizar primero los sistemas transversales de losas, rígidamente apoyadas en los nudos, bajo carga externa y entonces analizar el sistema longitudinal de placas bajo las reacciónes de las losas. Consecuentemente, los cálculos envueltos no son extensivos.

En el segundo de los métodos ordinarios, el método 2b, los momentos adicionales producidos por los desplazamientos relativos de nudo son tomados en cuenta. Esto complica el problema considerablemente ya que se crea una situación en la cual los desplazamientos del sistema de placa producidos por las reacciónes inciales de losa producen ahora reacciones de losas adicionales debido a los momentos de giro. Sin embargo, los procedimientos de solución desarrollados por Gaafar, (19) Yitzhaki, (58) Yitzhaki- Reiss (59) y Mast (31) para tratar con estas complicación adicional son tratables por cálculo manual y este método aun envuelve muchos menos cómputo que el método de la elasticidad.

Rockey y Evans (44), Concluyen de un estudio realezado recientemente que por lo que se refiere a los métodos ordinarios, las corrección por los efectos de los desplazamientos relativos de las juntas es extremadamente importante para estructuras que tengan una alta relación: longitud de placa- ancho de placa y también y que este efecto se incremento con una disminución: ancho de placa- espesor de placa. (18)

En todos los casos, la corrección se hace insignificante cuando la relación: longitud de placa- ancho de placa se reduce a tres aproximadamente y el efecto puede ignorarse para estructuras que tengan una relación menor que ésta.

Puede concluirse que el método ordinario, que permite desplazamientos relativos de los nudos, es satisfactoriamente razonable para el análisis de estructuras placa- plegada que tengan una relación de longitud de placa a ancho mayor que tres, y, por lo tanto, este método puede usarse en lugar del método de elasticidad para el analisis de estas estructuras más largas con un considerable ahorro en tiempo y esfuerzo de cómputo. Para estructuras más cortas, no obstante, el método no es suficiente-mente preciso y tiene una desventaja seria en el sentido de que sobrestima la rigidez de las placas componentes; su empleo podría llegar así a especificaciones de diseño fuera de la seguridad.

En los métodos ordinarios es usual despreciar Mx, Mxy y Qx, con lo cual el método se reduce a determinar los valores de Nx, Nxy, Ny, My y Qy haciendo uso de las ecuaciones respectivas.

6. METODOS ORDINARIOS

6.1. METODO DEL ELEMENTO FINITO

Este método ha sido aplicado reccientemente por Rockey y Evans ( ) para el análisis de placas plegadas, quienes mostraron la adaptabilidad del método al análisis de estructuras con varias condiciones de borde. Los extensos cálculos requeridos en una solución del elemento finito debe balancearse contra su gran adaptabilidad. De hecho hay muchos casos, tales como las placas plegadas con aberturas para ventanas, Fig. (12) o placas plegadas apoyadas sobre columnas colocadas al azar, donde el método del elemento finito ofrese el único medio de solución; por otro lado, comentando el aspecto negativo del método, los programas de computadora que utilizan esta técnica siendo muy apreciados consumen sin embargo demasiado tiempo en virtud del gran número de ecuaciones simultáneas que intervienen. Así para analizar una sola placa , digamos , tendría que usarse una malla de 8x6 comprendiendo unos 50 nudos con seis grados de libertad en cada nudo. Esto conduce a 300 ecuaciones simultáneas y para una estructura plegada formada de 6 placas requeriría la inversión de una matriz en banda diagonal del orden de 3000. Para el mismo problema, en cambio, usando el método de Gibson se requieren solamente 8 ecuaciones simultáneas por placa dando solamente 48 ecuaciones que invertir.

Las estructuras plegadas exhiben tanto acción en el plano como a la flexión. La configuración de placa plegada, ya que consiste de una serie de componentes de placas, puede dividirse simplemente en un cierto número de elementos tipo placa plana. Rockey y Evans utilizaron en su investigación, elementos rectangulares y un elemento típico se muestra en la Fig. (13).

Cada elemento estará sometido a esfuerzos de flexión y en el plano, así, con objeto de establecer la continuidad entre los elementos, deben considerarse seis componentes de desplazamiento en cada nudo. Estos desplazamientos consisten de tres movimientos lineales y tres rotaciones. Las direcciones positivas de las rotaciones se definen de modo que sus vectores positivos coincidan con las direcciones positivas X, Y, Z. Así el vector fuerza en cada elemento consistirá de 24 términos y la matríz de rigidez elemental es de 24x 24.

Los principales pasos que se siguen el método del elemento finito son,

a) Escoger la función deflexión para los elementos tipo placa y evaluar la matriz de rigidez de cada elemento.

b) Ensamblar las matrices de rigidez elementales para formar la matriz de rigidez total de la estructura.

c) Localizar las cargas nodales.

d) Especificar las condiciones de frontera .

e) Resolver el sistema de ecuaciones simultáneas resultantes.

f) Evaluar los esfuerzos internos en los elementos.

Los resultados Obtenidos por Rockey y Evans revelan que al aplicar el método del elemento finito a una placa plegada de 4 placas y usar 16 elementos se comete un error hasta del- 28. 10 % en la deflexión vertical. Este error se reduce a medida que se aumenta el número de elementos, por ejemplo si se emplean 192 elementos el error se reduce a-4.23 % en la deflexión vertical. Estos valores se compararon con los resultados obtenidos por Goldberg y Leve (26) al aplicar el método de Elasticidad considerado como exacto.

El MEF tiene laventaja de ser capaz de trabajar con aberturas tales como la mostrada en la Fig. (14) , en donde se muestra también una distribución típica de hilos de malla que podría usarse en tales problemas. Utilizando una malla fina cerca de la abertura, podrían manejarse rápidamente lo efectos de concentración de esfuerzos, etc. Similarmente podrían estudiarse los efectos de pilares de apoyo, marcos elásticos de apoyo y varias condiciones de frontera en los apoyos. Es en el análisis de tales estructuras, que no pueden resolverse directamente por los métodos normales de la Elasticidad, que la técnica el elemento finito es más valiosa.

6.2. METODO DE GIBSON.

En este método se usa la teoría general de los cascarones cilíndricos y se resuelve la ecuación diferencial parcial de octavo orden de los cascarones que resulta. Esta es la equivalente combinada de las dos ecuaciones diferenciales parciales de cuarto orden para flexión y acción de placa de la teoría elástica de las placas plegadas (método de la Elasticidad 1b) . La técnica es esencialmente un método de computadora ya que demanda el empleo de un programa general para analizar cascarones cilíndricos. (20, 21, 22, 23)

En la teoría degenerada de placas plegadas, se utiliza la teoría normal de cascarones y la superficie circular se hace degenerar en una superficie plana o lisa por el decrecimiento del medio ángulo de la superficie cilíndrica hasta 1° e incrementando el radio de curvatura de la superficie cilíndrica de modo que se obtenga el ancho requerido del elemento de placa.

Considérese la Fig. (15) la cual representa una sección transversal de una superficie cilíndrica degenerada de radio R y medio angulo de 1°.

La planura de la superficie resultante puede ser medida por la relación de la altura ó flecha " δ " a la cuerda " C " así :

$$\text{relación de planura} = \frac{\delta}{C} = R\ (\ 1-\cos 1^\circ\ ) = 2\ R\ \text{sen}\ 1^\circ \doteq \frac{1}{230}$$

Este es un grado suficiente de planura para todos los propósitos prácticos : el radio necesario " R " requerido para generar el ancho de cuerda " C " estará dado entonces por:

$$R = \frac{C}{2}\ \text{sen}\ 1^\circ = \frac{C}{0.035}$$

Usando esta técnica cualquier programa de computadora que analice cascarones cilíndricos puede usarse para analizar placas. Si el programa es general y así capaz de analizar cascarones multicilíndricos de cualquier sección transversal geométrica, entonces las estructuras placa- plegada pueden ser analizadas con este programa usando esta técnica degenerada.

El método Gibson controla la sección transversal por medio de tres [illegible] el radio R, el semi- ángulo ϕ y la inclinación de la línea central de cada cascarón respecto a la vertical. La Fig. (16) muestra una estructura cuyos datos son los siguientes:

Placa 1 $\phi = 1^{\circ}$, $R = 60.6$, $\beta = +90^{\circ}$,
Placa 2 $\phi = 1^{\circ}$, $R = 182.0$, $\beta = +45^{\circ}$,
Placa 3 $\phi = 1^{\circ}$, $R = 182.0$, $\beta = -45^{\circ}$,

Y así sucesivamente.

Comparaciones hechas por Gibson con el método de la Elasticidad muestran un gran acuerdo en los resultados numéricos obtenidos, como era de esperarse, ya que ambos métodos se han derivado a partir de la teoría de la Elasticidad Lineal. Esto muestra que un programa de análisis de cascarones puede ser utilizado para soluciones de placa plegada y tal vez por un razonamiento similar también debe ser posible aplicar programas de placas plegadas al análisis de cascarones curvos, simulados adecuadamente por una serie de placas planas.

6.3. MÉTODO DEL ELEMENTO TRANSVERSAL.

En el presente método cada placa componente del sistema es considerado como un elemento individual. Estos elementos son en forma de franjas con sus bordes transversales simplemente apoyados. Esto permite el uso del análisis armónico para la aplicación al problema de flexión transversal y en el plano de tales elementos. Así las representaciones en serie de Fourier de los desplazamientos y las fuerzas reducen el problema al caso unidireccional. La relación entre la fuerza de borde y los desplazamientos de borde de cada elemento (esto es la matriz de rigidez del elemento) se obtiene por medio de una técnica numérica llamada " Método de la progresión Matricial ". Una vez que las matrices individuales de rigidez para los elementos son obtenidos, se lleva a cabo el ensamblaje del conjunto y se analiza por los procedimientos usados en las técnicas usuales del elemento finito, la única diferencia es que los elementos del vector de carga externa son expresados como términos de la serie de Fourier. El proceso se repite para el número requerido de armónicos y los resultados se suman algebraicamente.

Este método de análisis fue desarrollado por DAS (13) usando ecuaciones de equilibrio y por CHEUNG (8, 9) usando el funcional de energía, siendo aplicado por Loo y Cusens (30)

El método es sistemático y conveniente para el cómputo. El almacenamiento requerido en una computadora aún para una caja multicelular es pequeño comparado con los otros métodos numéricos ya que las placas entre las juntas pueden considerarse como elementos individuales y son innecesarias mayores subdivisiones. La Convergencia de los momentos y las fuerzas es más lenta que las de los desplazamientos. Das, para los problemas que menciona en su reporte, consideró suficiente la suma de 19 armónicos.

De las comparaciones numéricas y de los resultados experimentales obtenidos se cocluye que la precisión numérica obtenida por este método es muy satisfactoria.

Pueden presentarse cualquiera condiciones de carga, normales o en el plano, usando una apropiada representación de Fourier, inclusive las debidas al presfuerzo cuando es necesario su empleo.

El problema de apoyos intermedios puede ser analizado usando una técnica de influencia en él que las reacciones internas se calculan primero de las condiciones de que las deflexiones resultantes en los puntos soportados son cero.

La solución final es --- la de una estructura de un sólo claro bajo la acción combinada de la carga aplicada y las reaciones.

El método puede aplicarse no solo a placas plegadas sino tambien a estructuras de cajón o multicelulares, de eje recto o curvo como en el caso de puentes. La Fig. (17) muestra algunas secciones transversales que pueden analizarse con el método.

7) MÉTODO DE LA VIGA.

Este método supone que el comportamiento de una estructura placa-plegada es similar al de una viga de pared delgada que cubre el claro entre los apoyos extremos. La aplicación de este método es, consecuentemente, extremadamente simple, pero conduce, se comprende, solamente a soluciones aproximadas.

Según el estudio crítico de Rockey- Evans (13) los valores de las deflexiones, esfuerzos y momentos obtenidos por el método de la viga, generalmente se desvían significativamente de los valores correctos. El método de la viga supone que la estructura placa-plegada se comporta como una viga simple apoyada sobre los diafragmas extremos, como ya se menciono antes, o sea que los esfuerzos longitudinales se suponen estar distribuídos linealmente através del peralte de la sección transversal la cual debe retener su forma original siempre. Un estudio comparativo de este método respecto a los métodos ordinarios y de la Elasticidad revelan que las estructuras placa- plegada sufren, de hecho, distorsiones transversales de consideración durante el desplazamiento, y se observó también en dicho estudio claramente que la distribución de esfuerzos en el peralte es no-lineal. Las suposiciones del método de la viga no se justificaron para ninguna de las estructuras consideradas en esa investigación. Se apreciará también que el método de la viga no es capaz de tomar en cuenta condiciones asimétricas de carga.

Finalmente, Concluyen Evans- Rockey, el método de la viga es inapropiado completamente para el análisis de los tipos de estructura placa- plegada considerada en su reporte, ya que el comportamiento estructural real es completamente diferente al supuesto en este método. Sin embargo, existen ciertas ciertas estructuras que se comportan de una manera similar a la supuesta en el método de la viga, y los mismos autores demostraron previamente (43) que el método de la viga puede usarse para el análisis de los pórticos interiores de placa - plegadas de pórticos múltiples, Fig. (11). El método no puede, sin embargo, ser utilizado con confianza en el análisis de cualquier estructura particular de placa- plegada, a menos que la experiencia previa haya mostrado que las distorsiones de la sección transversal de la estructura debidas a los efectos de desplazamiento, etc., sean despreciables.

Las hipótesis inherentes al método de la viga para placas plegadas, (48) pueden resumirse como sigue:

H-1) La distorsión de la sección transversal en su propio plano es despreciable.

H-2) Las fuerzas internas Mx, Mxy y Qx, son pequeños y pueden ignorarse.

H-3) El efecto de las deformaciones por cortante pueden despreciarse.

El objetivo del método de la viga se reduce entonces a la determinación de Nx, Nxy, Ny, My y Qy. El método de la viga consiste en dos análisis separados. El primero es el análisis de viga propiamente dicho, en el cual se determinan Nx y Nxy. El segundo análisis es el análisis de arco, en el cual Ny, My y Qy resultan como incógnitas. En este caso de estructuras plegadas se trata de un arco "discreto" o sea un marco rígido de ancho unitario.

De la teoría elemental de las vigas se tiene que,

$$Nx = \frac{M}{I} z \; t$$

$$Nxy = \frac{V \; Q}{I}$$

en donde M y V son el momento flector y fuerza cortante total en cualquier sección transversal, I es el momento de inercia de la sección transversal respecto a su eje centroidal y Q es el momento estático del área de la sección transversal, abajo o arriba del punto en el cual se va a calcular Nxy, tomado respecto al eje centroidal.

El resto de los elementos mecánicos se obtienen con los procedimientos clásicos de la Teoría de las Estructuras.

8. DISCUSION DE LOS METODOS.

Los métodos de análisis que se han revisado no son todos los que existen pero son los más representativos, hasta el momento, del avance en este campo de la Mecánica Aplicada. Efectivamente existen otros métodos como son el método de diferencias finitas, el método del valor inicial usando integración numérica, etc.

Desde el punto de vista teórico existen en realidad tres Modelos que explican el comportamiento estructural de las plegaduras, como se explicó anteriormente,

a) Modelo de las placas- losas.

b) Modelo de las vigas- losas.

c) Modelo de la viga única.

El primero de ellos se considera exacto, el segundo mediano y el tercero muy aproximado.

Desde el punto de vista del procedimiento de solución matemática de estos modelos, podemos decir que existen.

a) Procedimientos Analíticos.

b) Procedimientos Numéricos.

Dentro del primer grupo podemos cosiderar los métodos que se basan en las Series de Fourier, por ejemplo. Y que pueden aplicarse sea al método de la Elasticidad o al modelo ordinario.

Dentro de los métodos Númericos de solución que se emplean para resolver estos problemas encontramos el método del elemento finito, de las diferencias finitas, etc.

Es decir, los procedimientos de solución se aplican a las ecuaciones diferenciales obtenidas según sea la Teorí considerada.

En el método de la Elasticidad se requiere por cada placa una ecuación diferencial parcial de 4o orden y dos de segundo orden. En el método ordinario Se necesita una ecuación diferencial ordinaria de 4o orden y una ecuacion diferencial parcial de 4o orden, En el método de la viga se requiere resolver solamente una ecuación diferencial ordinaria de 4o orden.

Finalmente, atendiendo a la cantidad de trabajo a realizar los métodos se pueden agrupar en

a) Manuales.

b) Electrónicos.

Los manuales son aquellos que pueden realizarse con mayor o menor esfuerzo con regla de cálculo o cuando mucho con una calculadora de oficina. Los electrónicos son aquellos que requieren forzozamente el empleo de una instalación de cómputo electrónico para su aplicación.

Esto lo resume el cuadro de la Fig. (18).

9. DISEÑO DEL REFUERZO.

Como se dijo al principio el refuerzo debe proporcionarse en tres familias,

a) Acero Longitudinal,

b) Acero Transversal,

c) Acero Diagonal.

El primero absorberá esfuerzos de tracción Nx en las placas, el segundo resistirá el momento transversal My y la fuerza Ny mientras que el tercero absorberá la componente diagonal de fuerzas internas Nxy. Esta ultima fuerza se calcula por los procedimientos usuales de cálculo de ---------- esfuerzos principales en esfuerzo plano (Círculo de Mohr por ejemplo). (39)

El diseño del acero de refuerzo puede basarse en los principios contenidos en el reporte del comité 334 del ACI Sobre estructuras Laminares de Concreto, Sección 403 y en el reglamento ACI 318-71.

10. PROBLEMAS FUTUROS.

El comportamiento elástico de las plegaduras se conoce con bastante aproximación para deformaciones infinitesimales. Se requiere considerar problemas de cambios de geometrías es decir deformaciones grandes. En el futuro deberá examinarse el comportamiento plástico de estas estructuras, o sea incluir la No-Linealidad del material. Esto implicará el estudio del Análisis Límite de las estructuras plegadas, pues hace falta conocer las superficies de fluencia de estas formas estructurales.

Los problemas de Estabilidad requieren de especial atención así como los aspectos relativos a vibraciones e imperfecciones del material. De acuerdo con las informaciones disponible, no existen estudios acerca de optimización de estructuras plegadas, con respecto a alguna función objetivo, digamos el peso propio.

Finalmente, queda del campo abierto para la investigación de plegaduras no-prismáticas, multicelulares, contínuas y con Voladizos.

II. CONCLUSION.

El presente trabajo ha tenido por objeto mostrar varios aspectos,

a) La existencia de una forma estructural espacial de alta eficiencia;

b) La posibilidad de aplicar esta estructura a la solución de problemas arquitectónicos y constructivos con ventajas respecto a otras formas y sistemas estructurales;

c) La variedad de los métodos de análisis, tanto analíticos como numéricos, manuales y electrónicos, a disposición de los diseñadores de estructuras; y

d) El amplio horizonte que cubre la búsqueda de nuevas formas estructurales, nuevos materiales y nuevos métodos de análisis y diseño óptimo de las estructuras modernas.

12. REFERENCIAS

1. Abu Ghazeleh, B.N., "Analysis of Plate Type Prismatic Structures". Ph. D. Thesis. Univ. of California, Berkeley, Jan. 1966.
2. Aldridge, W.W., "Ultimate Strength Tests of Model Reinforced Concrete Folded Plate Structures". Ph.D. Thesis. Univ. of Texas, 1966.
3. Ashdown, S., "The Design of Prismatic Structures", London, 1951.
4. Beaufait, F.W., y G.A. Gray, "Experimental Analysis of Continuous Folded Plates". Jour. Struc. Div. ASCE, 92, ST 1, 1966, pp. 11-19.
5. Beaufait, F.W., "Analysis of Continuous Folded Plate Surface". J. Struc. Div. ASCE, 91, ST 6, 1965, pp. 117-140.
6. Born, J., Hipped Plate (Folded Plate) Structures, Their Theory and Analysis. Crosby Lockwood and Son, London, 1962.
7. Brielmaier, A.A., "Prismatic Folded Plates". Jour. ACI, 59, March 1962, pp. 407-419.
8. Cheung, Y.K.,"The finite strip method in the Analysis of Elastic Plates with two opposite simply supported end". Proc. Instn.Civ.Engrs., 40, May 1968, pp. 1-7.
9. Cheung, Y.K.,"Folded Plate Structures by Finite Strip Method". Proc. ASCE 95, ST 12, Dec. 1969, pp. 2963-2979.
10. Craemer, W. "Theorie der Faltwerke". Beton und Eisen, 29, 1930, pp. 276-9.
11. Craemer, W. "Prismatic Structures with Traverse Stiffners" Concrete and Constructional Engn., 1950.
12. Craemer, W. "Design of Prismatic Shells". J. ACI. 1953.
13. Das, P.C., "Analysis of Box-Type Structures", Proc. Instn.Civ.Engrs. 1972, pp. 19-40.
14. De Fries- Skene, A. y A.C. Scordelis.,"Direct Stiffness Solution for Folded Plates". Proc. ASCE, 90, ST 4, Aug. 1964, pp. 15-47.
15. Ehlers, G., "Ein Neues Konstruktions Prinzip". Der Bauingenieru, 11, 8, Berlin 1930, pp. 125-132.
16. Evans, H.R. "An investigation of Aluminum Folded Plate Structures". M.Sc. Thesis. Univ. of Wales, Swansea, 1964.
17. Evans, H.R. "The Analysis of Folded Plate Structures". Ph.D. Thesis. Univ. of Wales, Swansea, 1967.
18. Evans, H.R. y K.C. Rockey, "A Critical Review of the Methods of Analysis for Folded Plate Structures". Proc. Instn.Civ.Engrs.,49, June 1971, pp. 171-192. Discuss. Proc. Instn. Civ. Engrs., 1972, pp. 581-589.

19. Gaafar, I. "Hipped Plate Analysis, considering joint displacements ". Paper 2696, Trans. ASCE, 119, 1954, pp. 743-784.
20. Gibson, J.E. "Computer Investigatiob of Folded Slab Roofs". Struc. Engrn. 40, 1962, pp. 151-160.
21. Gibson, J.E. "An investigation of Folded Plate Structures", Struc. Engr., 42, 1964, pp. 299-304.
22. Gibson, J.E. "The design of Shell Roofs". Spon, London, C. 12, 1968.
23. Gibson, J.E. y N.J. Gardener, "Investigation of Multi-Folded Plate Structures". Proc. Instn. Civ. Engrs., 28, 31, 1962, pp. 57-69. Discussion , Proc. Instn. Civ. Engrs., 34, 1966, pp. 295-300.
24. Girkmann, K. "Flächentragwerke", Springer-Verlag, Vienna, 1948.
25. Goble, G.G. y Joudikis, A., "Reinforced Concrete Folded Plate Behaviour". IAAS Symposium, Leningrado, 1966.
26. Goldberg, J.E. y H.L. Leve, "Theory of Prismatic Folded Plate Structures" Memoires IABSA, Int. Congr. Bridge Struc. Engrn., 1957, 17, pp. 59-86.
27. Goldberg, J.E. y otros, "Analytical and Model Studies of Continuous Folded Plates". Proc. ASCE, EM 10, Paper 6181, 1968.
28. Gruber, E. "Berechnung Prismatischer Scheibenwerke", Int.Ass. Bridge and Struct. Eng., 1, Zürich, 1932, pp. 225, 251.
29. Konigsberg, M. "Model Analysis of Folded Plates", M. Sc. Thesis, Technion, Haifa, Jan. 1966.
30. Loo, Y.C. y A.R. Cusens, "Developments in the Finite Strip Method in Bridge Decks", Proc. Bridge Design, Cardiff, 1971.
31. Last, P.S. "An iteration Method for Folded Plate Analysis". Proc. World Conf. on Shell Struct., 1962, Nat. Academy of Sc, Washington, 1964, pp. 517-526.
32. Meyer, C. y A.C. Scordelis, "Computer Program for Prismatic Folded Plates with Plate and Beam Finite Elements". Struc. and Mats. Research Report, SESM 70-3. Struct. Eng. Div., Univ. of California, Berkeley, Fe. 1970.
33. Ohlig, P. "Beitrag Zur Theorie der Prismatischen Faltwerke", Ing. Arch. 345, 1935.
34. Ohlig, P. " Mehrfache Prismatische Faltwerke", Ing. Arch., 254, 1941.
35. Osborne, K.P. "Experimental and Theoretical Studies of Prismatic Folded Plate Structures", Univ. of Strathclyde, Ph. Thesis, 1970.
36. P.C.A., "Direct Solution of Folded Plate Concrete Roofs", Advanced Engr. Bull. No. 3, Skokie, Ill., 1960.
37. ASCE Report on Folded Plate Construction, "Report of the Task Commitee on Folded Plate Construction", Proc.ASCE, Jour.Struc.Div., 60, ST 6, Dec. 1963, pp. 365-79.

38. Rao, G. S. "Analysis of Folded Plate Roofs by Iteration", Indian Concrete J., 36, 10, Oct. 1962, pp. 365-376.

39. Ramaswamy, G. S. "Design and Construction of Concrete Shell Roofs", Mc Graw Hill, Ch. 12, 1968, pp. 241-323.

40. Reiss, M. y M. Yitzhak.,"Analysis of Short Folded Plates". Proc. of ASCE, 91, Oct.1965, pp. 233-254.

41. Reiss, M.,"Cantilevered and Continuous Folded Plates", Space Structures. Int. Conf., Univ. of Surrey, Sep. 1966, Oxford, 1967, pp. 189-200.

42. Rockey, K.C. y H.R. Evans, "A Finite Element Solution for Folded Plate Structures". Proc. Conf. Space Struct., Blackwell, Oxford 1967, Univ. of Surrey, pp. 165-188.

43. Rockey, M. y H.R. Evans, "The Behaviour of Corrugated Flooring Systems" Thin Walled Steel Structures, Crosby-Lockwood, 1969, London, pp. 236-257.

44. Rockey, M. y H.R. Evans, "A Study of the Behaviour of Folded Plate Structures", Struc. Engrn., 1971, 49, April, pp. 189-197.

45. Scordelis, A.C., "A matrix Formulation of the Folded Plate Equations". Proc.ASCE, 86, ST 10, 1960, pp. 2617-2699.

46. Scordelis, A.C. y otros, "Experimental and Analytical Study of Folded Plate", Proc.ASCE, 87, ST 12, 1961, pp. 3023-3074.

47. Scordelis, A.C. y otros, "Load Distribution in Concrete Box Girder Bridges", Concrete Bridge Design, SP-23, ACI, Detroit, 1969, pp. 117-136.

48. Scordelis, A.C., "Analysis of Cylindrical Shells and Folded Plates", paper 11 of ACI pub. SP-28-Concrete Thin Shells-Detroit, 1971, 424 p.

49. Schegg, A. y Gudmani, R.o., "Analysis of Short Span Folded Plates Structure"by Transfer Matrices", Indian Concrete J., 1965.

50. Seetharamulu, K. y M. Kulkarni, "Analysis of Short Span Folded Plate Structures", Proc. ASCE, 90, June 1964, pp. 165-178.

51. Simpson, H., "Design of Folded Plate Roofs", Proc. ASCE, 84, Jan. 1958.

52. Syracuse University, "Test of a Reinforced Concrete Folded Plate Structure" Report No. 335-5910 F, Syracuse, N.Y., 1959.

53. Traum, E. "The Design of Folded Plates", Proc. of the ASCE, 85, ST 8, Oct. 1959, p. 103-125.

54. Vlasov, V.Z., "Handbuck für Platten und Schalen", Moskau, 1939.

55. Werfel, A. "Die Genaue Theorie der Prismatischen Faltwerke und Ihre Praktische", Anwendung, Int. Congr. Bridge Structr. Engr., 14, 1954, pp. 277-318.

56. Whitney, C. S. y otros, "Reinforced Concrete Folded Plate Construction", J. of the Str. Div., Proc. ASCE, 85, Oct. 1959, ST 8, p. 15-39.

57. Winter, G.M. y M. Pei, "Hipped Plate Construction", J. ACI, 43, Jan. 1947, pp. 505-531.

58. Yitzhaki, D. "The Design of Prismatic and Cylindrical Shell Roofs", Haifa Pub., Israel, 1958, 251 p.

59. Yitzhaki, D. y M. Reiss, "Analysis of Folded Plates", Proc. ASCE, 88, Oct. 1962, pp. 107-142.

60. Chu, K. H. y S.G. Pinjarkar, "Multiple Folded Plate Structures", Proc. ASCE, 92, ST 2, April 1966, pp. 297-321.

61. Pultar, M. y otros, "Folded Plates Continuous over Flexible Supports", Proc. ASCE, 93, ST 5, Oct. 1967, pp. 253-277. Discussion Proc. ASCE, 94, ST 6, June 1968, pp. 1639-1652.

13. APENDICE

A. Ecuaciones de la Teoría de Placas.

La ecuación biharmónica de la flexión de placas es,

$$\frac{\partial^4 w}{\partial x^4} + 2\frac{\partial^4 w}{\partial x^2 \partial y^2} + \frac{\partial^4 w}{\partial y^2} = \frac{p}{D}$$

Las ecuaciones que gobiernan la deformación en el plano de la placa son,

$$\frac{\partial^2 u}{\partial x^2} + \frac{1-\nu}{2}\frac{\partial^2 u}{\partial y^2} + \frac{1+\nu}{2}\frac{\partial^2 v}{\partial x \partial y} = \frac{q}{D_1}$$

$$\frac{\partial^2 v}{\partial y^2} + \frac{1-\nu}{2}\frac{\partial^2 v}{\partial x^2} + \frac{1+\nu}{2}\frac{\partial^2 u}{\partial x \partial y} = \frac{r}{D_1}$$

Los Momentos y fuerzas transversales son,

$$M_x = -D\left(\frac{\partial^2 w}{\partial x^2} + \nu\frac{\partial^2 w}{\partial y^2}\right)$$

$$M_y = -D\left(\frac{\partial^2 w}{\partial y^2} + \nu\frac{\partial^2 w}{\partial x^2}\right)$$

$$M_{xy} = -(1-\nu)D\frac{\partial^2 w}{\partial x \partial y}$$

$$V_x = -D\left[\frac{\partial^3 w}{\partial x^3} + (2-\nu)\frac{\partial^3 w}{\partial x \partial y^2}\right]$$

$$V_y = -D\left[\frac{\partial^3 w}{\partial y^3} + (2-\nu)\frac{\partial^3 w}{\partial x^2 \partial y}\right]$$

$$N_x = D_1\left(\frac{\partial u}{\partial x} + \nu\frac{\partial v}{\partial y}\right)$$

$$N_y = D_1\left(\frac{\partial v}{\partial y} + \nu\frac{\partial u}{\partial x}\right)$$

$$N_{xy} = D_1\frac{1-\nu}{2}\left(\frac{\partial u}{\partial y} + \frac{\partial v}{\partial x}\right)$$

en donde
$$D = \frac{E t^3}{12(1-\nu^2)} \quad , \quad D_1 = \frac{E t}{(1-\nu^2)}$$

son las rigideces a la flexión y de membrana respectivamente.

u,v,w, son las deformaciones de la placa elemental a lo largo de los ejes de coordenadas de la placa.

ν, es la relación de Poisson.

Mx, es el momento transversal.

Vx, es la fuerza cortante transversal

Nx, es la fuerza normal en el plano de la placa en dirección transv.

Nxy, es la fuerza cortante en el plano, actuando sobre una sección longitudinal.

t, es el espesor de lapplaca.

E, es el módulo de Young del material de la placa.

p,q,r, son las cargas repartidas en las direcciones coordenadas.

B. Ecuaciones de la Teoría de Vigas con carga Axial.

La Ecuación diferencial de la flexión de vigas es,

$$\frac{d^4 w}{dx^4} = \frac{p}{EI}$$

La Ecuación diferencial que determina el comportamiento axial de una barra prismática es,

$$\frac{d^2 u}{dx^2} = \frac{q}{EA}$$

El momento flector, las fuerzas cortante y Normal son,

$$M = -EI \frac{d^2 w}{dx^2}$$

$$V = -EI \frac{d^3 w}{dx^3}$$

$$N = EA \frac{du}{dx}$$

en donde,

w, u, son los desplazamientos transversal y longitudinal de la viga.

p, q, son las cargas transversal y longitudinal sobre la barra.

A, I, son el área y el momento de inercia de la sección transversal.

M, es el momento flector de la barra.

V, es la fuerza cortante "

N, es la fuerza normal " .

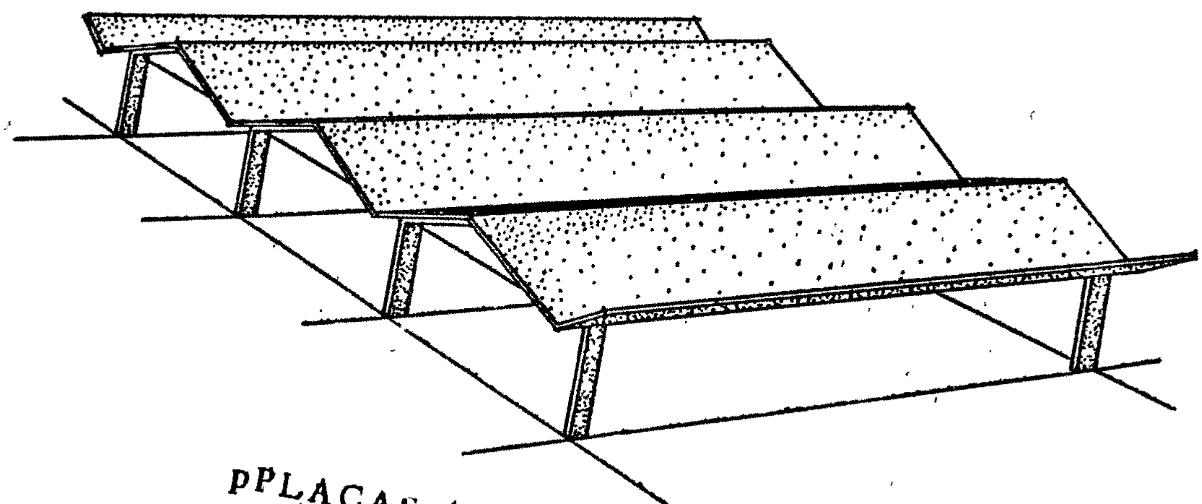

pPLACAS PLEGADAS
Porfirio Ballesteros

The continuing development of design and construction techniques of shell structures is resulting in an increasing fund of information of practical interest to Architects, Engineers and Contractors. The aim of furthering all branches of this progress has inspired the formation of the **international association for shell and spatial structures,** whose purpose is to organise meetings and congresses for the interchange of ideas and their dissemination by means of periodical publications.

Everyone interested in the various branches of shell techniques and their architectonic possibilities or realizations is invited to join this International Association.

the advisory board

A. L. L. Baker (Gt. Britain)
N. Esquillan (France)
R. S. Jenkins (Gt. Britain)
K. W Johansen (Denmark)
F. Levi (Italy)
W. Olszak (Poland)

the executive council

Honorary President:
A. M. Haas (The Netherlands)

President:
A. Paduart (Belgium)

Vice presidents:
A. L. Parme (U. S. A.)
F. del Pozo (Spain)
H. Rühle (German D. R.)

Treasurer:
G. Lacombe (France)

Secretary:
R. López Palanco (Spain)

Members of the Executive Council:
A. Aas-Jackobsen (Norway)
P. Ballesteros (Mexico)
T. Brøndum - Nielsen (Denmark)
L. Finzi (Italy)
K. A. Glukhovskoi (U. S. S. R.)
G. K. Khaidukov (U. S. S. R.)
J Kozak (Czechoslovakia)
R. Krapfenbauer (Austria)
J. Munro (Gt. Britain)
E. P. Popov (U. S. A.)
G. S. Ramaswamy (India)
K. Szmodits (Hungary)
Y. Tsuboi (Japan)
W. Zerna (German F. R.)

To become a member or to obtain more detailed information, please write to the Secretariat of the International Association for Shell and Spatial Structures, Alfonso XII, 3, Madrid (7). Spain.

Direct Solution of Folded Plate Concrete Roofs

In the past few years due to the proven economy of folded plate construction, several noteworthy papers have appeared in American literature. In general, the formulas and equations presented therein have a common basis in that the behavior of a folded plate is divided into interdependent transverse and longitudinal action. Equilibrium of forces in the transverse direction is established assuming that representative transverse strips are supported at the junction of plates on rigid or flexible supports. The reaction resulting from this is then resolved into forces parallel to the plates which resist the forces as longitudinal beams. Thus the problem of folded plate analysis is reduced to procedures familiar to most engineers and from this point of view the analyses are perfectly satisfactory.

However, the calculations required are not as fully automatic as might be desired, especially when undertaken at infrequent instances. In the interest of simplicity of application, the direct solution procedure is presented. The procedure involves merely the establishment of two equations at each fold of the plates which expresses the relationship between moment and longitudinal stresses at neighboring points and the superimposed load. The determination of the magnitude of the moments and stress at each point requires the solution of a number of simultaneous equations. This can be accomplished by a direct solution or by a rapidly converging iteration process.

Prior to undertaking the calculation of a folded plate, an understanding of the behavior of a folded plate is desirable. This can lead to a better appraisal of the effect of the various parameters and may also avoid needless computations. In certain cases, such as plates at some distance from free edges or those which incorporate deep vertical members, complex analysis is not needed. Treatment of the folded plates in such cases as beams is sufficient.

As is the case for two-dimensional structures, a qualitative and for that matter a quantitative investigation must commence with an examination of a portion of the structure as a free body. In the case of folded plate, a unit transverse strip as shown in figure 1a is the most suitable free body. The forces acting on this free body sketched in greater detail in figure 1b consists of the external load, variable tangential shears, s, acting parallel to the surfaces, normal shears v acting perpendicular to the plates and moments M_L. The extreme flexibility of the individual plates in the direction normal to the surface of the plates as compared to the stiffness in the direction parallel to the plates makes the normal shear v insignificant. It also follows from this that longitudinal bending moments M_L are also very small. For this reason, these shears and moments can be neglected.

Examining more minutely the free body of figure 1b by isolating a single straight element as a free body as per sketch 1c it is apparent that the transverse moment acting at the junction of the plates is independent of the distribution and intensity of the shear forces acting in the individual element since these forces act parallel to the plate. Furthermore resolving the end reactions supplied by the neighboring plates into forces R and P normal and parallel to the plate respectively, the equations of equilibrium of forces and moments in any individual member becomes identical to those of a member in a continuous beam. Thus the behavior and even the analysis of the unit transverse strip can be approached and treated as that of a continuous beam. In so doing because the deflection of adjacent folds may not be same, it is necessary to consider the continuous beam as being on elastic supports as shown graphically in figure 2 with the supports indicated as springs.

In the structural system shown symbolically in figure 2 the moment at any support can be expressed as a function of the moments at the two adjacent supports, the load on the two spans on either side of the support and the relative deflection of the beam at the support with respect to the deflection at the adjacent supports or what is more convenient as a function of the absolute deflection at the three supports. The expression given by the theorem of three moments is a classical example of the form of this relationship.

In this relationship, the deflection of the beam at any support is of course equal to the amount by which the spring is compressed or elongated. The magnitude of this movement can be expressed either as the product of the reaction and a constant equal to the load required to produce a unit displacement or what is more preferable for this discussion as a function of the stress in the spring times a constant equal to the displacement caused by a unit stress. Consequently at any support, an equation can be written in which the moments in the beam and stresses in the springs at three supports; i.e., at the support under consideration, and at the two adjacent supports, are related to the load on the beam.

In this equation, the only difficult quantities to determine are the spring constants. The springs in the analogous continuous beam naturally represents the resistance to displacement of the plates in the actual structure acting as longitudinal beams. Thus the constants of the several springs can be expressed in terms of the geometry of the plates; i.e., their length, depth, thickness and angle of inclination to each other or to a vertical plane. However, since at any fold, the displacement in the direction of the spring is a function of the interaction of the two intersecting plates at that support, the constants for the three springs involve not only the geometry of the two enclosed spans but likewise the next adjoining span. Thus at any point the geometry of four spans is involved.

In expressing the spring constants in terms of the geometrical and physical properties of the plates, it is tacitly implied that these factors are in turn related to the plates' longitudinal stresses. Were the stresses in the plates solely flexural, the three stresses at the folds corresponding to the three points of support would be sufficient to account for the displacement of the four plates. But because the transverse tangential shear, s, and therefore the longitudinal tangential shear need not be zero at either extremity of the free body of figure 1c, each plate considered individually is subject to axial as well as flexural stresses. This makes it necessary to relate the displacement of a plate to the fiber stress at both sides of the centroidal axis. As a consequence of this, the longitudinal stress at the fold twice removed from the fold under consideration, or in other words at the outer edge of the two outer plates must be included as an unknown if the action of the spring is to be correctly formulated. From this it can be generalized that at any fold of a folded plate structure, a relationship can be established between the moments at three folds and the longitudinal stresses at five folds and the superimposed load on the two adjacent folds.

From the foregoing presentation, two pertinent conclusions can be drawn. First, if the relative deflection of one fold to its neighboring fold is small, then the transverse moments in the folded plates can be computed by considering a unit transverse strip of the folded plate as a continuous beam rigidly supported at the folds. This condition is approached where a number of identical plates, or identical combination of plates are continuous in the transverse direction and subject to the same load.

The second fact to emerge is that the deviation of the transverse moments from that given by a continuous beam on rigid support analysis is a function of the vertical stiffness of the plates. If the plates are flexible in the longitudinal direction, that is when the vertical intercepts of the plates are small compared to the longitudinal span, say less than one-fifteenth of the span, marked increase in the transverse moment near the free edges can be expected. With certain configurations, it is possible to have the transverse moment at some of the folds near the free edge greater than the statical moment of the load about the fold. For this reason, in some cases, a deepening of the plates is desirable not only from consideration of its effect on the amount of longitudinal reinforcement required but as well as from its effect on the transverse strength.

In the preceding discussion, emphasis has centered on the behavior of a representative transverse strip with the effect of longitudinal action only indirectly introduced. This is primarily due to the fact that quite frequently the magnitude of the transverse moments dictates either the thickness of the slab or the width of each fold. Hence an understanding of the factors which control the magnitude of moment especially near free edges is essential for a proper layout. However, of equal interest for a complete perspective is the behavior of the folded plate in the longitudinal direction. Fortunately, although somewhat more complicated, the kind of qualitative examination made for transverse action can be applied to longitudinal action.

For this purpose a longitudinal strip consisting of two adjoining plates is examined as a free body. This differs from the procedure employed previously in which the strip was only a unit wide. One could commence with a strip consisting of an individual plate. However for exposition, nothing is gained by starting with the equilibrium of forces in an individual element. Considering then two plates as a unit, the free body of figure 3 being only a portion of the total structure is subject not only to the superimposed vertical loads but is as well subject to forces along the edges which represent reactions from the adjacent plates. Although the cross section of the free body is not of the customary shape nevertheless the longitudinal stresses can be obtained by the conventional flexural formulas. However in this case, because the direction of the loads are not necessarily co-planar with the plates or located at the flexural center (shear center) the stresses at a point created by the moment and thrust about any two perpendicular axes must be combined with the effect of rotation about the longitudinal axis. The work involved is not as simple as it may be inferred and therefore it is not recommended as a design procedure.

Expressing the midspan stresses at the fold and free edges of the free body in figure 3 in terms of the known loads and the unknown edge forces, S_1 S_2 N_1 and N_2, three simultaneous equations are obtained. The transverse moment acting along the edge will not appear in these equations because the longitudinal stresses are related only to the moments perpendicular to the plane of the transverse moment. By successive elimination of S_1 and S_2, the three simultaneous equations can be reduced to a single equation, in which the stresses at the three points are related to the superimposed load on the two plates and to the unknown edge forces N_1 and N_2. A consideration of the equilibrium of forces in the transverse direction, of which a detailed explanation is given in the appendix shows that the N forces at one edge is a function solely of the load on the two plates on each side of the edge; of the difference between the values of the transverse moments at the edge and its neighboring edges; and of the geometry of the plates. Consequently the replacement of the edge forces (N_1 and N_2) by their equivalent in the preceding equation results in an expression in which the stresses at three adjacent points and the moment at five points are related to the superimposed load on four plates.

From a consideration of the above, several obvious facts emerge which merit slight attention in that recognition may help prevent needless computation. If the transverse moments are all equal, as for example in the interior folds of deep V-type folded plate, or can be obtained from statics, the longitudinal stresses can be determined directly from the superimposed loads only. As a corollary it follows that if in addition the longitudinal shears are zero at both folds of a plate, then the stresses can be obtained by the ordinary flexural theory.

In summary, a folded plate analysis is required principally to determine the effect of edge disturbances. The free edges and outer plates tend to deflect more than what is indicated by considering the folded plate as an ordinary beam. Because of this the intensity of the maximum longitudinal stress in the outer plates can be larger and the distribution of the stress entirely different than anticipated by conventional beam analysis. However, the sum of the tensile or compressive forces will remain about the same. Hence the value of a folded plate analysis resides not so much in a precise determination of the ultimate capacity but chiefly in that it ensures satisfactory behavior at service loads and leads to a better evaluation of the transverse moments.

ANALYSIS

Simply Supported Folded Plates

The principal problem associated with the analysis of folded plate is that of making the displacement as computed from the longitudinal behavior compatible with the displacement obtained from the transverse behavior. In a strict sense not only must this equality of displacements be satisfied at a few points, say along a strip, but the requirement should be satisfied at all points on the surface. However in many cases and especially for folded plates, reasonable values can be obtained by satisfying the condition of compatible displacement at midspan only. This approximation while acceptable for determining the critical stresses and moments tends to obscure the exact distribution of stresses. To avoid this and at the same time provide a sound basis for further development, the procedure used in this paper has been based on satisfying the condition of compatible displacement at all points. To secure this, it is necessary to express the uniform load as sum of partial sinusoidal loads each load corresponding to a term in the Fourier Series given by the expression

$$w = \frac{4w}{\pi}\left(\sin\frac{\pi x}{L} + \frac{1}{3}\sin\frac{3\pi x}{L} + \frac{1}{5}\sin\frac{5\pi x}{L} \ldots\ldots\right)$$

The distribution of the loads is shown graphically in figure 4. In reality for purpose of design only the first partial load needs to be used. The effect of the succeeding partial loads will be mainly felt in the vicinity of the supports, and will not produce any significant stresses at midspan. Furthermore, in most practical cases the use of partial sinusoidal loads does not present any great difficulty since the transverse moment for the second and succeeding partial loads can be obtained without recourse to any complex folded plate analysis by treating a transverse strip as a continuous beam on fixed support. This simplification is possible because each partial load can be analyzed separately as a load on a folded plate whose span is equal to one-half the wave length of the particular sine loading under consideration. With such a reduction in the effective design length, the plates become so stiff in the longitudinal direction that for all practical purposes, the plates can be considered as being rigidly supported at the folds.

Another advantage of this approach is that in satisfying the requirement at midspan one automatically satisfies the requirement of all other sections. Consequently attention will be centered only on the relationship of forces at midspan of a simply supported folded plate, with the understanding that the moments and stresses at any other section will vary according to sine $(n\pi x/L)$.

In the earlier discussion, it has been indirectly pointed out that if the transverse moment and longitudinal stresses at each fold are known, the moment and stress at any other point can be found directly by statics or by the ordinary flexural theory. Hence, if figure 5a represents a transverse strip at midspan of a simply supported folded plate of any configuration it is necessary only to determine the stresses and moments at the various folds. As shown in greater detail in figure 5b, a unit element at any fold designated by the subscript n is subject to a longitudinal stress, f_n, a shearing stress, S_n, and a transverse moment M_n. Since the shearing stress S_n can be calculated from the longitudinal stresses there remains at most actually only two unknown quantities at each fold. Thus two equations at each fold relating the stress and moment at the folds to the superimposed load are sufficient to achieve a solution. The two equations which are derived in detail in the appendix are based on satisfying the condition of continuity in the transverse direction, and statics at a fold. The first of these, which can be considered primarily as fulfilling the condition of compatible strains is at representative fold n

$$
\begin{aligned}
&2\,\frac{h_{n-1}}{h_n}\left(\frac{t_n}{t_{n-1}}\right)^3 M_{n-1} + 4\left[1+\frac{h_{n-1}}{h_n}\left(\frac{t_n}{t_{n-1}}\right)^3\right] M_n + 2M_{n+1} \\
&-\left(\frac{L}{\pi}\right)^2\left(\frac{t_n}{h_n}\right)^3\left[C_n^{n-2} f_{n-2} - C_n^{n-1} f_{n-1} + C_n^{n} f_n - C_n^{n+1} f_{n+1} + C_n^{n+2} f_{n+2}\right] \\
&= -h_n\left[\left(\frac{h_{n-1}}{h_n}\right)^2\left(\frac{t_n}{t_{n-1}}\right)^3 \frac{W_{n-1}\cos\beta_{n-1}}{2} + \frac{W_n\cos\beta_n}{2}\right]
\end{aligned}
\qquad (8)
$$

in which the symbols

M = transverse bending moment at a fold and is considered positive when it creates tension on the underside of the plate.

f = the longitudinal stress and is considered positive when it is compressive.

f^p = the longitudinal stress produced by prestressing the plates considered as individual plates. The first subscript locates the position of the stress and the combined subscript designates the folds on each side of the plate.

W = the total vertical load acting on a plate, and is considered positive where acting downward.

h = length of the plates

t = thickness of the plate

β = the angle formed by a plate and a horizontal line and is considered positive when the angle measured from the plate is clockwise

α = the angle formed by the extension of one plate with the next one and is considered positive when the angle measured from the extension is clockwise.

$$C_n^{n-2} = \frac{h_n^2}{h_{n-2}h_{n-1}\sin\alpha_{n-1}}$$

$$C_n^{n-1} = \frac{h_n^2}{h_{n-2}h_{n-1}\sin\alpha_{n-1}} + \left(\frac{h_n}{h_{n-1}}\right)^2\left(\cot\alpha_{n-1} + \cot\alpha_n\right) + \frac{h_n}{h_{n-1}\sin\alpha_n}$$

$$C_n^{n} = \left(\frac{h_n}{h_{n-1}}\right)^2\left(\cot\alpha_{n-1} + \cot\alpha_n\right) + \cot\alpha_n + \cot\alpha_{n+1} + \frac{2h_n}{h_{n-1}\sin\alpha_n}$$

$$C_n^{n+1} = \frac{h_n}{h_{n-1}\sin\alpha_n} + \cot\alpha_n + \cot\alpha_{n+1} + \frac{h_n}{h_{n+1}\sin\alpha_{n+1}}$$

$$C_n^{n+2} = \frac{h_n}{h_{n+1}\sin\alpha_{n+1}}$$

The subscript employed with the symbols identifies the particular stress, moment, angle, plate or fold involved. The second equation at fold n which is derived mainly from a consideration of statics is

$$\begin{aligned}
&\frac{h_{n-1}t_{n-1}}{h_n t_n} f_{n-1} + 2\left(1 + \frac{h_{n-1}t_{n-1}}{h_n t_n}\right) f_n + f_{n+1} \\
&+ \frac{6}{t_n h_n}\left(\frac{L}{\pi h_n}\right)^2\left[C_n^{n-2}M_{n-2} - C_n^{n-1}M_{n-1} + C_n^{n}M_n - C_n^{n+1}M_{n+1} + C_n^{n+2}M_{n+2}\right] \\
&= \frac{-3}{t_n}\left(\frac{L}{\pi h_n}\right)^2\left[\left(W_{n-2} + W_{n-1}\right)\frac{h_n\cos\beta_{n-2}}{h_{n-1}\sin\alpha_{n-1}} - \left(W_{n-1} + W_n\right)\left(\frac{\cos\beta_{n-1}}{\sin\alpha_n} + \frac{h_n\cos\beta_n}{h_{n-1}\sin\alpha_n}\right)\right. \\
&\qquad\left. + \left(W_n + W_{n+1}\right)\frac{\cos\beta_{n+1}}{\sin\alpha_{n+1}}\right] \\
&+ \left(\frac{h_{n-1}t_{n-1}}{h_n t_n}\right)\left(2f^P_{n,n-1} + f^P_{n-1,n}\right) + 2f^P_{n,n+1} + f^P_{n+1,n}
\end{aligned} \tag{16}$$

The two equations presented are valid at any fold except for point 0 and fold 1. At these latter places the moment can be determined from statics, and only the longitudinal stresses are unknown. Hence only one equation is needed at each point. For point zero, we have

$$
\begin{aligned}
&2f_0 + f_1 + \frac{6}{t_0 h_0}\left(\frac{L}{h_0\pi}\right)^2 \frac{h_0}{h_1 \sin\alpha_1} M_2 \\
&= -\frac{3}{t_0}\left(\frac{L}{h_0\pi}\right)^2\left(2W_0 + W_1 + W_0\frac{h_0\cos\beta_0}{h_1\cos\beta_1}\right)\frac{\cos\beta_1}{\sin\alpha_1} + 2f_{01}^p + f_{10}^p
\end{aligned}
\tag{20}
$$

and for fold 1, the relation is

$$
\begin{aligned}
&\frac{h_0 t_0}{h_1 t_1} f_0 + 2\left(1+\frac{h_0 t_0}{h_1 t_1}\right) f_1 + f_2 - \frac{6}{h_1 t_1}\left(\frac{L}{h_1\pi}\right)^2 \left(C_1^2 M_2 - C_1^3 M_3\right) \\
&= \frac{3}{t_1}\left(\frac{L}{\pi h_1}\right)^2 \left[(2W_0+W_1)\left(\frac{\cos\beta_0}{\sin\alpha_1}+\frac{h_1\cos\beta_1}{h_0\sin\alpha_1}\right) - (W_1+W_2)\frac{\cos\beta_2}{\sin\alpha_2} + W_0\frac{h_0}{h_1}\cos\beta_0\, C_1\right] \\
&\quad + 2f_{12}^p + f_{21}^p + \frac{h_0 t_0}{h_1 t_1}\left(2f_{10}^p + f_{01}^p\right)
\end{aligned}
\tag{23}
$$

in which

$$C_1 = (\cot\alpha_1 + \cot\alpha_2) + \frac{h_1}{h_0\sin\alpha_1}$$

$$C_1^2 = \cot\alpha_1 + \cot\alpha_2 + \frac{h_1}{h_2\sin\alpha_2} + \frac{h_1}{h_0\sin\alpha_1}$$

$$C_1^3 = \frac{h_1}{h_2\sin\alpha_2}$$

With two equations at each fold except for the first fold and only one at that fold and the exterior point, the number of equations which must be solved simultaneously will equal twice the number of plates minus two. In many cases, this number of equations can be reduced by half because of symmetry or antisymmetry. To illustrate the use of the equations, the simple example shown in the sketch of table 1 will be analyzed. To avoid error, a systemization of the computations as indicated in table 1 is recommended.

Example

In table 1, the dimensions and the required trigonometric properties of the folded plate shown in the sketch are recorded in columns 1 through 9. The calculations required to determine the various constants in the equations are contained in columns 10 to 23 with the particular operation stated algebraically in the heading of the columns. Although the numerical values in table 1 are applicable only to the selected example, the arrangement is suitable for any type of folded plate. It should be noted that for many columns only the values at specific folds need be computed. In columns 24 to 31, the load terms are computed.

For convenience, the four basic equations (8), (16), (20) and (23) are repeated in table 2 with however the algebraic terms replaced by an equivalent column designation. Because of symmetry of load and geometry in this example $M_1 = M_4$; $M_2 = M_3$; $f_0 = f_5$; $f_1 = f_4$ and $f_2 = f_3$. Consequently, equations need to be written only for point 0 and folds 1 and 2, with n, in equations (8) and (16) taken as 2. For this particular example, M_{n-2}, M_{n-1} and M_{n+2} which correspond to M_0, M_1 and M_4 are all equal to zero. Executing the indicated operations by utilizing the appropriate numerical values tabulated in table 1, we obtain the four simultaneous equations listed in the upper portion of table 2. In this case for ease in solving the simultaneous equations, each equation has been divided by the coefficient of M_2. The question of how many significant figures are needed has not been fully explored. It is believed that in most cases, the use of three significant figures is sufficient. However, four significant figures were used because with machine calculations it is just as easy to use four figures as three figures.

When the number of equations is small, say less than eight, a direct solution can be performed in an hour or so employing some of the new techniques as Crout's method which is specifically designed for machine calculation. For a larger number of equations, the chances of error in a direct solution is so great that an iteration process is more feasible. There are a number of such procedures outlined in various mathematical textbooks. The most common one, and easiest one to master is the procedure outlined on page 227 of Timoshenko's book "Theory of Plates and Shells." Briefly the method consists of arbitrarily assuming a set of values for all of the unknowns except the first one. These values are then multiplied by the appropriate numerical coefficient in each equation for all terms to the right of the heavy stepped line. Starting with the top equation, it is then possible by proceeding from one equation to the next to determine a new set of values for the unknown forces and moments. These are then employed in the same manner to arrive at the next set of values. The procedure is repeated till sufficient convergence is achieved. For the initial values it has been found advantageous to commence with $M_n = -wa^2/12$ and $f_n = WL^2/8s$ where s is the section modulus of a plate or of a combination of plates.

For this example, the simultaneous equations were solved by direct solution and by iteration. As may be observed, all of the critical values have converged within 5 per cent by the fourth cycle even though analysis of the same structure by the conventional distribution technique led to extremely poor convergence. One of the advantages of the procedure is that convergence can be speeded by noting any oscillation of values and arbitrarily interpolating between the values of two sets for the next succeeding trial.

The values shown in table 1, multiplied by $4/\pi$ to account for the difference between a sinusoidal load and a uniform load can be considered as sufficiently accurate. If greater refinement is desired, the same overall procedure or simplified versions of the procedure is applied to the other partial sinusoidal loads. For this example, it was found that the second partial load, varying as sine $3\pi x/L$ produced the following stresses at midspan

$$M_2 = + \ 234 \text{ ft.-lb./ft.}$$
$$f_0 = +8,300 \text{ lb./sq.ft.}$$
$$f_1 = - \ 700 \text{ lb./sq.ft.}$$
$$f_2 = - \ 410 \text{ lb./sq.ft.}$$

A comparison of these values with those tabulated in table 2 shows that the longitudinal stresses produced by this partial load and thus also of other partial loads are either a small percentage of that produced by the first load or is numerically insignificant. The ratio of the moments produced by the two loads is somewhat larger, indicating a slight justification for increasing the accuracy here. However, it is interesting to point out that the moment created by the second partial load is almost equal to the moment produced considering the plates to be continuous over rigid supports at each fold.

Combining the first and second partial loads, we obtain

$$M_2 = (4/\pi)(-1{,}513 + 234) = -1628 \text{ ft.-lb./ft.}$$
$$f_0 = (4/\pi)(-161{,}000 + 8{,}300)(1/144) = -1350 \text{ psi}$$
$$f_1 = (4/\pi)(-1{,}129 - 700)(1/144) = -16 \text{ psi}$$
$$f_2 = (4/\pi)(+16{,}790 - 410)(1/144) = +145 \text{ psi}$$

With the value of the moments and stresses known, the tangential shear can be obtained. A detailed explanation of the procedure is given in the appendix after equation (33).

Design Aid

Although the analysis of a folded plate structure has been reduced to arithmetical manipulation, insight into their behavior can only be achieved by comparison of results of many cases. To supply this and at the same time facilitate the design of the most popular type of folded plate, table 3 has been compiled. This table gives design coefficients for the V-type folded plate structure, consisting of a number of identical interior V's with unsymmetrical exterior V strengthened by the presence of a vertical edge beam. While the sketch in table 3 whows that the values have been computed on the basis of a structure symmetrical about fold 6, coefficients are applicable to roofs with a smaller or greater number of folds. In most cases, the effect of the free edge only penetrates to the fourth fold. Consequently the folds inside the fourth have little effect on the value of stresses and moments at the exterior folds.

In computing table 3, it was found desirable to align the design coefficients in conformance to the four parameters h_v/h, h_e/h, a/d and L^2t/a^3 with the symbols defined in the sketch. The selection of these variable was based on the common practice of designating structures in terms of horizontal and vertical dimensions. Furthermore, these parameters permit a ready interpolation for values other than those listed. The range selected represents the practical range of economic applicability. Values were computed for larger values of L^2t/a^3. In most cases, the transverse moments obtained for such cases indicated that it would be difficult to satisfy the strength needed, and for this reason, higher values of L^2t/a^3 were purposely omitted.

To conserve space and avoid needless repetition, coefficients are given only for M_2 to M_5 and for the longitudinal stress f_0 to f_3. The moment coefficient at fold 6 or at further interior folds equals the fixed end moment value of 0.0833. The coefficients for the longitudinal stresses at folds greater than 3 are also constant independent of the parameters with the exception of the a/d ratio. For the ratios given, the coefficients are

a/d	2.5	2.0	1.5	1.0
stress coef.	±1.411	±1.087	±0.759	±0.430

Since the coefficients are given in non-dimensional form, it is important that all of the units be consistent. If w is in lb./ft.^{2} and the dimensions in ft., then the calculated moment and longitudinal stress will be in ft.lb./ft. and lb./ft.^{2} respectively.

To illustrate the ease with which the moment and stresses can be obtained, a brief example will be calculated. Given a folded plate roof in which

$L = 55$ ft. $\qquad h_o/h = 0.25$
$a = 10$ ft. $\qquad h_v/h = 0$
$t = 0.33$ ft. $\qquad a/d = 2.0$
w = (dead load + live load) = 86 psf(projected area)

then

$$L^2t/a^3 = \frac{55^2 \times 0.333}{10^3} = 1$$

and the multipliers shown in the heading of table 3 are

$$(4/\pi)wa^2 = 1.27 \times 86 \times 10^2 = 10{,}900 \text{ ft.-lb./ft.}$$

$$(4/\pi)\frac{wL^2}{at} = \frac{1.27 \times 86 \times 55^2}{10 \times 0.333} = 99{,}400 \text{ lb./ft.}^2$$

Entering table 3, with the given parameters, we find that the coefficient for M_2 is -0.285. Consequently the moment is

$$M_2 = -0.285 \times 10{,}900 = -3110 \text{ ft.lb./ft.}$$

The other values can be determined in like manner. The effect of the second partial load can also be determined from table 3. For this purpose, the span length and load is assumed as one-third of the given value. On that basis

$$L^2t/a^3 = \frac{(55/3)^2 \times 0.333}{10^3} = \frac{1}{9}$$

and

$$w = -86/3 = -28.7 \text{ lb./ft.}^2 \text{ (at midspan)}$$

When the value of L^2t/a^3 is less then that given in table 3 as is the case here, the moment can be computed assuming the folds are rigidly supported, and the change in the longitudinal stress can be ignored.

Table 3, assumes that the load is uniform on the structure. As a consequence, the effect of the weight of the vertical edge member is neglected.

Continuity

The preceding equations have been derived on the basis that the folded plates are simply supported. A similar though considerably more complex set of equations can be established for continuous folded plates. This complexity is due primarily to the fact that in continuous folded plates the transverse distribution (not the intensity) of longitudinal stresses is not as uniform throughout the length of the folded plate as for simple spans. In other words the transverse distribution of stresses for each partial load at any section is no longer equal to the transverse distribution at midspan times sin $n\pi x/L$. Other terms which are quite complicated must be inserted in the expression for stresses to fulfill the requirements of end restraint.

One expedient way which has been employed to overcome this difficulty is by relaxing the requirement of satisfying the condition of compatible strains along the entire junction of two plates and satisfying merely the requirement of compatible deflection at midspan. The deflection of each plate at midspan is determined as for a continuous beam. Thus for example if full fixity is assumed at both ends of a plate, the deflection is taken as $5PL^4/384$.

Another approach which has been used and has given satisfactory results is to proportion the longitudinal stresses over the support and at midspan on the basis of the moments created in a continuous beam whose spans are equal to those of the folded plate. In this approximation, the transverse distribution is based on an effective span length equal to the distance between the points of inflection of the continuous beam.

Intersection of Three Plates

One of the advantages of the direct solution approach is that it facilitates the determination of the stresses in folded plate structures having three plates intersecting at one fold as shown in figure A8. The same pattern of attack employed for the conventional folded plate is applicable to this more complex problem. Because of the infrequent use of the three plate arrangement at interior folds no design equations have been developed for this case. However to demonstrate the manner in which such equations can be derived, the more common case of three plates intersecting at the exterior fold is worked out in the appendix. Even for this case, it is possible at the points or folds involved to establish equations relating the stresses and moments to the superimposed loads.

The presence of an additional vertical plate at fold one naturally makes equations (20) and (23) previously given for point 0 and fold 1 no longer valid. In place of these, equations (27) and (29) must be employed. In addition because the third plate introduces another unknown namely the longitudinal stress at the bottom of the vertical plate designated as f_v, equation (31) must be used. This equation which is easily derived by equating the deflection of the respective intersecting plates to each other, expresses the relationship between f_v and the neighboring stresses. Lastly, at fold 2 slight modification of equation (16) as presented in equation (33) is required to account for the additional vertical member.

Table 1 Numerical Example

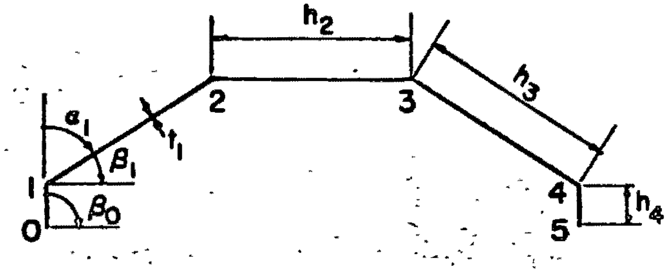

Live load = 25 lb. per sq. ft.

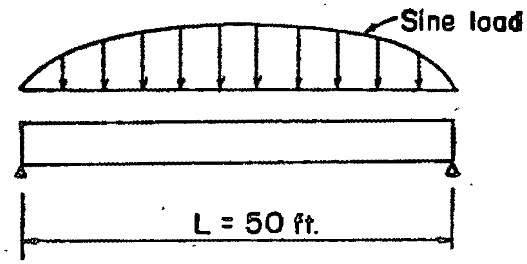

Given properties									Computed coef.				
1	2	3	4	5	6	7	8	9	10	11	12	13	14
Point or plate	α (deg.)	β (deg.)	t_n (ft.)	h_n (ft)	W_n (lb.)	$\cos\beta$	$\sin\alpha$	$\cot\alpha$	$\frac{h_{n-1}}{h_n}\left(\frac{t_n}{t_{n-1}}\right)^3$	$\frac{h_{n-1}}{h_n}\frac{t_{n-1}}{t_n}$	$\left(\frac{h_n}{h_{n-1}}\right)^2(\cot\alpha_{n-1}+\cot\alpha_n)$	$\frac{h_n}{h_{n-1}\sin\alpha_n}$	$(\cot\alpha_n+\cot\alpha_{n+1})$
0	--	+90	0.33	2	100	0			---	---	-----	-----	-----
1	60	+30	0.33	10	716.7	0.8660	0.8660	0.5774	---	0.2	-----	5.773	2.309
2	30	0	0.33	10	750	1	0.5000	1.732	1.0	1.0	2.309	2.000	3.464
3	30	-30	0.33	10	716.7	0.8660	0.5000	1.732					
4	60	-90	0.33	2	100	0	0.8660	0.5774					
5													

Table 1 (cont'd)

① Point or plate	Computed coef. ⑮ $C_n^{n-2} = \frac{h_n^2}{h_{n-2} h_{n-1} \sin a_{n-1}}$	⑯ $C_n^{n-1} =$ ⑮ + ⑫ + ⑬	⑰ $C_n^n =$ ⑫ + 2 × ⑬ + ⑭	⑱ $C_n^{n+1} =$ ⑬ + ⑭ + ⑲	⑲ $C_n^{n+2} = \frac{h_n}{h_{n+1} \sin a_{n+1}}$	⑳ $\frac{3}{t_n}\left(\frac{L}{\pi h_n}\right)^2$	㉑ $\frac{6}{t_n h_n}\left(\frac{L}{\pi h_n}\right)^2$	㉒ $\left(\frac{L}{\pi}\right)^2\left(\frac{t_n}{h_n}\right)^3$	㉓ $\left(\frac{h_{n-1}}{h_n}\right)^2\left(\frac{t_n}{t_{n-1}}\right)^3$
0	---	---	---	---	0.2309	569.9	569.9	---	--
1	---	---	---	10.08	2.000	22.80	4.560	---	--
2	5.773	10.08	9.774	7.464	2.000	22.80	4.560	0.009382	1.0
3									
4									
5									

① Point or plate	Load terms ㉔ $\frac{W_{n-1} \cos \beta_{n-1}}{2}$	㉕ $\frac{W_n \cos \beta_n}{2}$	㉖ $\left(W_{n-2} + W_{n-1}\right)\frac{h_n \cos \beta_{n-2}}{h_{n-1} \sin a_{n-1}}$	㉗ $\frac{W_{n-1} + W_n}{\sin a_n}\left(\cos \beta_{n-1} + \frac{h_n}{h_{n-1}} \cos \beta_n\right)$	㉘ $\left(W_n + W_{n+1}\right)\frac{\cos \beta_{n+1}}{\sin a_{n+1}}$	㉙ $\frac{2W_0 + W_1}{\sin a_1}\left(\cos \beta_0 + \frac{h_1}{h_0} \cos \beta_1\right)$	㉚ $W_0 \frac{h_0}{h_1} \cos \beta_0$	㉛ $\left(2W_0 + W_1 + W_0 \frac{h_0 \cos \beta_0}{h_1 \cos \beta_1}\right)\frac{\cos \beta_1}{\sin a_1}$
0	---	---	-	--	--	--	-	916.7
1	---	---	-	--	2933	4583	0	--
2	810.3	375	0	5474	2540	--	--	--
3								
4								
5								

Table 2 Simultanous Equations

Equation 8

$$2\times(10)M_{n-1}+4\left[1+(10)\right]M_n+2M_{n+1}-(22)\left[(15)f_{n-2}-(16)f_{n-1}+(17)f_n-(18)f_{n+1}+(19)f_{n+2}\right]=-h_n\left[(23)\times(24)+(25)\right]$$

Equation 16

$$(11)f_{n-1}+2\left[1+(11)\right]f_n+f_{n+1}+(21)\left[(15)M_{n-2}-(16)M_{n-1}+(17)M_n-(18)M_{n+1}+(19)M_{n+2}\right]=-(20)\left[(26)-(27)+(28)\right]$$

Equation 23

$$(11)f_0+2\left[1+(11)\right]f_1+f_2-(21)\left[(18)M_2-(19)M_3\right]=(20)\left\{(29)-(28)+(30)\left[(13)+(14)\right]\right\}$$

Equation 20

$$2f_0+f_1+(21)\times(19)M_2=-(20)\times(31)$$

Equation No.	Point or fold	M_2 ft-lb./ft.	f_0 lb./sq. ft.	f_1 lb. / sq. ft	f_2 lb. / sq. ft.	Constant
8	2	1	-0.005416	+0.007583	-0.002167	=- 685
20	0	1	+0.01520	+0.007598	0	=-3969
23	1	-1	+0.005427	+0.06512	+0.02713	=+1021
16	2	1	0	+0.09497	+0.4749	=+6351
Direct Solution		-1513	-161,100	-1,129	+16,790	
Iteration Solution						
Assumed Values		--	- 73,700	-43,100	+33,000	
1st Cycle		- 685	-195,000	+7,600	+13,300	
2nd Cycle		-1770	-148,500	-4,700	+18,000	
3rd Cycle		-1415	-165,700	+7,010	+14,950	
4th Cycle		-1603	-159,200	-1,900	+17,130	

Table 3 - Design Coefficients for V Folded Plate Roofs

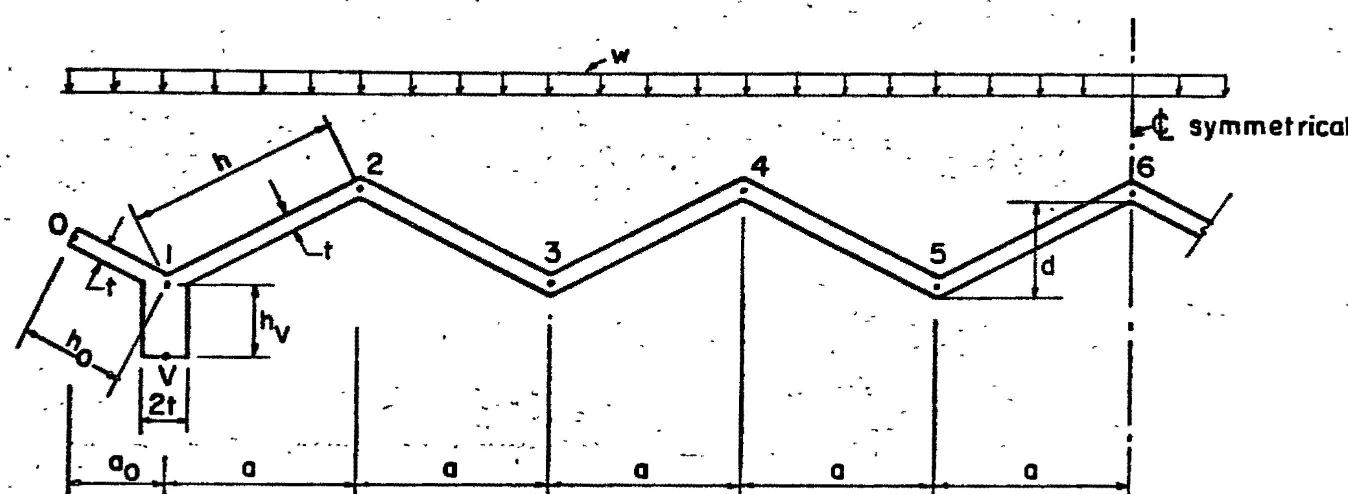

Transverse moments $M_n = \frac{4}{\pi} wa^2 \times$ coef.

Longitudinal stresses $f_n = \frac{4}{\pi} \left(\frac{wL^2}{ta}\right)$ coef.

$\frac{h_V}{h}$	$\frac{h_0}{h}$	$\frac{a}{d}$	$\frac{L^2 t}{a^3}$	Transverse moments				Longitudinal stresses				
				M_2	M_3	M_4	M_5	f_0	f_V	f_1	f_2	f_3
		2.5	0.5	-0.500	0.028	-0.114	-0.075			-1.458	1.486	-1.390
			1.0	-0.500	0.028	0.116	-0.074			-1.458	1.485	-1.390

Table 3 (cont'd)

$\frac{h_y}{h}$	$\frac{h_o}{h}$	$\frac{a}{d}$	$\frac{L^2 t}{a^3}$	Transverse moments M_2	M_3	M_4	M_5	Longitudinal stresses f_o	f_v	f_1	f_2	f_3
0	0	2.5	0.5	-0.500	0.028	-0.114	-0.075			-1.458	1.486	-1.390
			1.0	-0.500	0.028	-0.116	-0.074			-1.458	1.485	-1.390
			2.0	-0.500	0.026	-0.125	-0.072			-1.457	1.484	-1.391
			4.0	-0.500	0.022	-0.152	-0.065			-1.453	1.479	-1.396
		2.0	0.5	-0.500	0.028	-0.114	-0.075			-1.124	1.145	-1.071
			1.0	-0.500	0.028	-0.115	-0.075			-1.124	1.145	-1.071
			2.0	-0.500	0.027	-0.120	-0.073			-1.123	1.144	-1.071
			4.0	-0.500	0.024	-0.139	-0.069			-1.121	1.142	-1.074
		1.5	0.5	-0.500	0.028	-0.114	-0.075			-0.784	0.799	-0.747
			1.0	-0.500	0.028	-0.114	-0.075			-0.784	0.799	-0.747
			2.0	-0.500	0.028	-0.117	-0.074			-0.784	0.799	-0.748
			4.0	-0.500	0.026	-0.127	-0.072			-0.783	0.798	-0.748
			8.0	-0.500	0.021	-0.157	-0.064			-0.781	0.795	-0.751
		1.0	0.5	-0.500	0.028	-0.113	-0.075			-0.444	0.453	-0.423
			1.0	-0.500	0.028	-0.114	-0.075			-0.444	0.453	-0.423
			2.0	-0.500	0.028	-0.114	-0.075			-0.444	0.453	-0.423
			4.0	-0.500	0.028	-0.118	-0.074			-0.444	0.452	-0.423
			8.0	-0.500	0.026	-0.130	-0.071			-0.444	0.452	-0.424
	$\frac{1}{8}$	2.5	0.5	-0.379	-0.007	-0.105	-0.078	6.928		-2.413	1.724	-1.470
			1.0	-0.565	0.042	-0.122	-0.073	2.397		-1.714	1.597	-1.411
			2.0	-0.658	0.075	-0.144	-0.067	0.121		-1.364	1.531	-1.380
			4.0	-0.687	0.111	-0.194	-0.048	-0.606		-1.257	1.502	-1.365
		2.0	0.5	-0.305	-0.026	-0.100	-0.079	6.733		-2.075	1.368	-1.150
			1.0	-0.503	0.025	-0.116	-0.075	3.001		-1.499	1.263	-1.102
			2.0	-0.633	0.064	-0.134	-0.070	0,553		-1.121	1.193	-1.070
			4.0	-0.680	0.095	-0.170	-0.058	-0.332		-0.987	1.164	-1.056
		1.5	0.5	-0.223	-0.047	-0.093	-0.081	5.789		-1.616	0.985	-0.817
			1.0	-0.401	-0.002	-0.107	-0.077	3.441		-1.254	0.919	-0.787
			2.0	-0.579	0.046	-0.124	-0.073	1.099		-0.892	0.853	-0.756
			4.0	-0.663	0.078	-0.147	-0.066	-0.002		-0.723	0.821	-0.741
			8.0	-0.689	0.116	-0.203	-0.044	-0.345		-0.673	0.806	-0.734
		1.0	0.5	-0.148	-0.067	-0.088	-0.082	3.837		-1.002	0.573	-0.470
			1.0	-0.248	-0.041	-0.095	-0.080	3.088		-0.886	0.552	-0.460
			2.0	-0.438	0.008	-0.110	-0.076	1.675		-0.668	0.513	-0.442
			4.0	-0.601	0.053	-0.127	-0.072	0.459		-0.480	0.473	-0.426
			8.0	-0.671	0.083	-0.154	-0.064	-0.056		-0.401	0.463	-0.419

Table 3 (cont'd)

$\frac{h_y}{h}$	$\frac{h_o}{h}$	$\frac{a}{d}$	$\frac{L^2 t}{a^3}$	Transverse moments M_2	M_3	M_4	M_5	Longitudinal stresses f_0	f_v	f_1	f_2	f_3
0	$\frac{1}{4}$	2.5	0.5	-0.187	-0.058	-0.091	-0.082	4.508		-2.313	1.652	-1.472
			1.0	-0.372	-0.014	-0.106	-0.078	3.334		-2.047	1.642	-1.446
			2.0	-0.661	0.063	-0.145	-0.068	1.498		-1.633	1.623	-1.404
			4.0	-0.863	0.146	-0.234	-0.040	0.213		-1.347	1.599	-1.370
		2.0	0.5	-0.153	-0.066	-0.088	-0.082	3.642		-1.820	1.275	-1.138
			1.0	-0.285	-0.035	-0.099	-0.080	2.998		-1.674	1.269	-1.124
			2.0	-0.552	0.032	-0.127	-0.073	1.688		-1.379	1.256	-1.094
			4.0	-0.804	0.114	-0.192	-0.054	0.450		-1.101	1.239	-1.064
		1.5	0.5	-0.125	-0.073	-0.086	-0.083	2.637		-1.292	0.891	-0.797
			1.0	-0.200	-0.055	-0.092	-0.081	2.382		-1.234	0.888	-0.791
			2.0	-0.400	-0.007	-0.109	-0.077	1.697		-1.079	0.882	-0.776
			4.0	-0.689	0.071	-0.151	-0.066	0.709		-0.857	0.872	-0.753
			8.0	-0.876	0.156	-0.248	-0.035	0.071		-0.715	0.858	-0.735
		1.0	0.5	-0.107	-0.077	-0.085	-0.083	1.530		-0.740	0.505	-0.452
			1.0	-0.133	-0.071	-0.087	-0.082	1.479		-0.728	0.504	-0.451
			2.0	-0.225	-0.049	-0.094	-0.081	1.301		-0.688	0.503	-0.447
			4.0	-0.451	0.006	-0.114	-0.076	0.863		-0.589	0.499	-0.437
			8.0	-0.733	0.086	-0.163	-0.063	0.315		-0.466	0.492	-0.424
	$\frac{1}{2}$	2.5	0.5	-0.092	-0.083	-0.084	-0.083	2.392		-1.866	1.526	-1.434
			1.0	-0.146	-0.072	-0.088	-0.082	2.304		-1.845	1.539	-1.431
			2.0	-0.322	-0.037	-0.109	-0.078	2.022		-1.778	1.578	-1.423
			4.0	-0.697	0.048	-0.206	-0.056	1.421		-1.635	1.653	-1.406
		2.0	0.5	-0.084	-0.084	-0.083	-0.083	1.852		-1.440	1.174	-1.105
			1.0	-0.117	-0.078	-0.086	-0.083	1.811		-1.430	1.180	-1.104
			2.0	-0.234	-0.055	-0.097	-0.080	1.667		-1.396	1.201	-1.099
			4.0	-0.537	0.009	-0.154	-0.068	1.293		-1.307	1.251	-1.089
		1.5	0.5	-0.078	-0.085	-0.083	-0.083	1.298		-1.006	0.819	-0.771
			1.0	-0.094	-0.082	-0.084	-0.083	1.284		-1.003	0.821	-0.771
			2.0	-0.157	-0.070	-0.089	-0.082	1.230		-0.990	0.829	-0.769
			4.0	-0.353	-0.031	-0.114	-0.077	1.061		-0.950	0.852	-0.764
			8.0	-0.743	0.060	-0.226	-0.051	0.725		-0.870	0.893	-0.755
		1.0	0.5	-0.074	-0.085	-0.083	-0.084	0.737		-0.570	0.464	-0.437
			1.0	-0.079	-0.085	-0.083	-0.083	0.734		-0.570	0.464	-0.437
			2.0	-0.101	-0.081	-0.085	-0.083	0.724		-0.567	0.465	-0.437
			4.0	-0.179	-0.066	-0.091	-0.082	0.686		-0.558	0.471	-0.435
			8.0	-0.410	-0.019	-0.125	-0.074	0.573		-0.531	0.487	-0.432

Table 3 (cont'd)

$\frac{h_y}{h}$	$\frac{h_o}{h}$	$\frac{a}{d}$	$\frac{L^2 t}{a^3}$	Transverse moments M_2	M_3	M_4	M_5	Longitudinal stresses f_o	f_v	f_t	f_2	f_3
$\frac{1}{8}$	0	2.5	0.5	-0.172	-0.055	-0.089	-0.081		-2.814	0.124	0.859	-1.265
			1.0	-0.[illegible]50	-0.025	-0.094	-0.079		-2.006	-0.183	0.966	-1.280
			2.0	-0.310	0.020	-0.098	-0.073		-1.384	-0.424	1.048	-1.284
			4.0	-0.330	0.117	-0.098	-0.047		-1.156	-0.532	1.076	-1.260
		2.0	0.5	-0.170	-0.057	-0.089	-0.081		-2.698	0.257	0.618	-0.964
			1.0	-0.255	-0.028	-0.095	-0.079		-1.891	-0.039	0.719	-0.980
			2.0	-0.328	0.009	-0.100	-0.075		-1.191	-0.297	0.805	-0.991
			4.0	-0.358	0.074	-0.104	-0.061		-0.902	-0.413	0.840	-0.983
		1.5	0.5	-0.160	-0.061	-0.089	-0.082		-2.470	0.361	0.381	-0.660
			1.0	-0.245	-0.034	-0.095	-0.080		-1.772	0.114	0.462	-0.675
			2.0	-0.335	-0.001	-0.101	-0.077		-1.035	-0.147	0.548	-0.689
			4.0	-0.379	0.040	-0.106	-0.070		-0.676	-0.278	0.589	-0.692
			8.0	-0.391	0.137	-0.111	-0.040		-0.573	-0.326	0.599	-0.679
		1.0	0.5	-0.138	-0.068	-0.087	-0.082		-1.948	0.376	0.168	-0.362
			1.0	-0.205	-0.048	-0.092	-0.081		-1.555	0.241	0.211	-0.371
			2.0	-0.310	-0.015	-0.100	-0.078		-0.937	0.029	0.278	-0.384
			4.0	-0.384	0.014	-0.106	-0.075		-0.506	-0.119	0.325	-0.392
			8.0	-0.411	0.056	-0.110	-0.067		-0.346	-0.177	0.342	-0.392
	$\frac{1}{8}$	2.5	0.5	-0.168	-0.057	-0.089	-0.081	1.998	-3.120	-0.106	0.965	-1.293
			1.0	-0.277	-0.018	-0.097	-0.078	1.221	-2.451	-0.251	1.052	-1.298
			2.0	-0.402	0.048	-0.113	-0.069	0.320	-1.682	-0.420	1.150	-1.296
			4.0	-0.467	0.167	-0.140	-0.035	-0.164	-1.290	-0.521	1.193	-1.271
		2.0	0.5	-0.157	-0.061	-0.088	-0.082	2.161	-2.711	-0.085	0.745	-0.998
			1.0	-0.259	-0.028	-0.096	-0.079	1.490	-2.191	-0.183	0.805	-1.002
			2.0	-0.400	0.030	-0.110	-0.073	0.558	-1.470	-0.320	0.888	-1.004
			4.0	-0.487	0.118	-0.134	-0.054	-0.022	-1.031	-0.410	0.935	-0.993
		1.5	0.5	-0.140	-0.067	-0.087	-0.082	2.116	-2.126	-0.079	0.526	-0.700
			1.0	-0.222	-0.042	-0.093	-0.080	1.664	-1.818	-0.127	0.557	-0.701
			2.0	-0.369	0.008	-0.106	-0.076	0.843	-1.259	-0.214	0.613	-0.704
			4.0	-0.490	0.074	-0.125	-0.066	0.169	-0.804	-0.287	0.658	-0.702
			8.0	-0.539	0.194	-0.162	-0.024	-0.114	-0.625	-0.323	0.671	-0.686
		1.0	0.5	-0.120	-0.073	-0.086	-0.083	1.644	-1.322	-0.074	0.306	-0.399
			1.0	-0.163	-0.061	-0.089	-0.082	1.481	-1.227	-0.085	0.314	-0.400
			2.0	-0.276	-0.027	-0.097	-0.079	1.049	-0.976	-0.114	0.336	-0.400
			4.0	-0.436	0.028	-0.112	-0.074	0.440	-0.621	-0.155	0.366	-0.401
			8.0	-0.537	0.095	-0.134	-0.062	0.057	-0.401	-0.182	0.384	-0.398

Table 3 (cont'd)

$\frac{h_v}{h}$	$\frac{h_o}{h}$	$\frac{a}{d}$	$\frac{L^2 t}{a^3}$	Transverse moments				Longitudinal stresses				
				M_2	M_3	M_4	M_5	f_0	f_v	f_1	f_2	f_3
$\frac{1}{8}$	$\frac{1}{4}$	2.5	0.5	-0.133	-0.067	-0.087	-0.082	2.052	-2.510	-0.513	1.090	-1.327
			1.0	-0.219	-0.037	-0.093	-0.079	1.711	-2.303	-0.522	1.124	-1.322
			2.0	-0.397	0.041	-0.113	[illegible]	0.999	-1.873	-0.543	1.193	-1.307
			4.0	-0.570	0.188	-0.164	-0.029	0.299	-1.465	-0.572	1.253	-1.272
		2.0	0.5	-0.123	-0.071	-0.086	-0.082	1.873	-1.957	-0.465	0.863	-1.030
			1.0	-0.188	-0.050	-0.091	-0.081	1.657	-1.839	-0.465	0.881	-1.027
			2.0	-0.349	0.011	-0.106	-0.074	1.119	-1.545	-0.465	0.926	-1.018
			4.0	-0.553	0.128	-0.146	-0.051	0.438	-1.180	-0.470	0.978	-0.997
		1.5	0.5	-0.112	-0.075	-0.085	-0.083	1.526	-1.356	-0.383	0.621	-0.725
			1.0	-0.152	-0.063	-0.088	-0.082	1.426	-1.308	-0.380	0.628	-0.724
			2.0	-0.271	-0.023	-0.098	-0.078	1.126	-1.163	-0.372	0.649	-0.719
			4.0	-0.485	0.065	-0.125	-0.067	0.589	-0.905	-0.360	0.685	-0.708
			8.0	-0.659	0.217	-0.191	-0.018	0.152	-0.703	-0.355	0.708	-0.688
		1.0	0.5	-0.103	-0.078	-0.085	-0.083	0.985	-0.746	-0.253	0.364	-0.414
			1.0	-0.118	-0.073	-0.086	-0.083	0.962	-0.736	-0.252	0.365	-0.414
			2.0	-0.174	-0.057	-0.090	-0.081	0.877	-0.700	-0.248	0.370	-0.413
			4.0	-0.326	-0.007	-0.103	-0.077	0.646	-0.603	-0.236	0.383	-0.409
			8.0	-0.556	0.092	-0.138	-0.062	0.297	-0.458	-0.220	0.401	-0.401
	$\frac{1}{2}$	2.5	0.5	-0.084	-0.081	-0.083	-0.083	1.477	-1.841	-0.762	1.177	-1.340
			1.0	-0.116	-0.067	-0.085	-0.082	1.433	-1.825	-0.759	1.187	-1.336
			2.0	-0.222	-0.017	-0.095	-0.075	1.289	-1.771	-0.753	1.219	-1.323
			4.0	-0.463	0.126	-0.147	-0.038	0.964	-1.655	-0.740	1.285	-1.288
		2.0	0.5	-0.079	-0.083	-0.083	-0.083	1.218	-1.369	-0.634	0.926	-1.038
			1.0	-0.100	-0.075	-0.084	-0.083	1.196	-1.362	-0.632	0.930	-1.036
			2.0	-0.175	-0.043	-0.090	-0.079	1.116	-1.334	-0.627	0.947	-1.030
			4.0	-0.376	0.057	-0.122	-0.060	0.903	-1.263	-0.614	0.991	-1.011
		1.5	0.5	-0.076	-0.085	-0.083	-0.083	0.904	-0.914	-0.475	0.659	-0.728
			1.0	-0.087	-0.081	-0.083	-0.083	0.896	-0.911	-0.475	0.661	-0.728
			2.0	-0.129	-0.064	-0.086	-0.082	0.864	-0.902	-0.472	0.667	-0.726
			4.0	-0.263	-0.007	-0.101	-0.074	0.762	-0.870	-0.464	0.688	-0.718
			8.0	-0.543	0.147	-0.172	-0.029	0.550	-0.807	-0.449	0.727	-0.698
		1.0	0.5	-0.073	-0.086	-0.083	-0.084	0.539	-0.492	-0.287	0.380	-0.415
			1.0	-0.077	-0.084	-0.083	-0.083	0.538	-0.491	-0.287	0.380	-0.414
			2.0	-0.092	-0.079	-0.084	-0.083	0.531	-0.490	-0.286	0.382	-0.414
			4.0	-0.147	-0.058	-0.088	-0.081	0.507	-0.483	-0.284	0.386	-0.412
			8.0	-0.314	0.012	-0.110	-0.070	0.434	-0.463	-0.277	0.400	-0.407

Table 3 (cont'd)

$\frac{h_y}{h}$	$\frac{h_o}{h}$	$\frac{a}{d}$	$\frac{L^2 t}{a^3}$	Transverse moments M_2	M_3	M_4	M_5	Longitudinal stresses f_o	f_v	f_1	f_2	f_3
$\frac{1}{4}$	0	2.5	0.5	-0.106	-0.074	-0.084	-0.083		-0.737	-0.176	0.919	-1.291
			1.0	-0.108	-0.063	-0.083	-0.082		-0.732	-0.181	0.920	-1.287
			2.0	-0.108	-0.024	-0.076	-0.078		-0.726	-0.192	0.920	-1.273
			4.0	-0.099	0.106	-0.051	-0.049		-0.738	-0.208	0.913	-1.227
		2.0	0.5	-0.110	-0.074	-0.085	-0.083		-0.727	-0.063	0.689	-0.989
			1.0	-0.120	-0.065	-0.085	-0.082		-0.697	-0.083	0.697	-0.988
			2.0	-0.140	-0.035	-0.083	-0.079		-0.639	-0.123	0.711	-0.983
			4.0	-0.154	0.053	-0.072	-0.064		-0.592	-0.164	0.721	-0.962
		1.5	0.5	-0.111	-0.075	-0.085	-0.083		-0.670	0.031	0.461	-0.685
			1.0	-0.126	-0.067	-0.086	-0.082		-0.635	0.010	0.469	-0.686
			2.0	-0.160	-0.045	-0.087	-0.080		-0.552	-0.041	0.488	-0.686
			4.0	-0.199	0.009	-0.085	-0.074		-0.456	-0.103	0.510	-0.680
			8.0	-0.212	0.152	-0.072	-0.037		-0.414	-0.141	0.518	-0.657
		1.0	0.5	-0.110	-0.076	-0.085	-0.083		-0.515	0.081	0.244	-0.384
			1.0	-0.121	-0.072	-0.086	-0.082		-0.496	0.070	0.248	-0.384
			2.0	-0.154	-0.058	-0.088	-0.081		-0.440	0.037	0.260	-0.385
			4.0	-0.213	-0.026	-0.091	-0.079		-0.338	-0.021	0.281	-0.387
			8.0	-0.259	0.039	-0.091	-0.069		-0.257	-0.070	0.298	-0.384
	$\frac{1}{8}$	2.5	0.5	-0.111	-0.072	-0.085	-0.083	0.195	-1.052	-0.055	0.906	-1.285
			1.0	-0.127	-0.056	-0.085	-0.081	0.145	-1.012	-0.077	0.919	-1.282
			2.0	-0.161	-0.005	-0.083	-0.075	0.038	-0.929	-0.126	0.946	-1.270
			4.0	-0.186	0.138	-0.075	-0.041	-0.071	-0.861	-0.181	0.962	-1.227
		2.0	0.5	-0.112	-0.073	-0.085	-0.083	0.354	-0.975	0.002	0.689	-0.988
			1.0	-0.133	-0.061	-0.086	-0.082	0.298	-0.931	-0.020	0.702	-0.987
			2.0	-0.181	-0.021	-0.088	-0.078	0.164	-0.827	-0.072	0.733	-0.983
			4.0	-0.236	0.082	-0.089	-0.059	0.003	-0.710	-0.139	0.765	-0.963
		1.5	0.5	-0.111	-0.075	-0.085	-0.083	0.467	-0.831	0.039	0.473	-0.688
			1.0	-0.130	-0.066	-0.086	-0.082	0.423	-0.798	0.024	0.481	-0.688
			2.0	-0.184	-0.038	-0.089	-0.080	0.298	-0.706	-0.018	0.506	-0.688
			4.0	-0.266	0.032	-0.096	-0.071	0.105	-0.566	-0.084	0.542	-0.683
			8.0	-0.317	0.192	-0.106	-0.025	-0.031	-0.477	-0.134	0.561	-0.660
		1.0	0.5	-0.108	-0.076	-0.085	-0.083	0.456	-0.576	0.045	0.263	-0.388
			1.0	-0.119	-0.072	-0.086	-0.082	0.437	-0.564	0.039	0.266	-0.389
			2.0	-0.157	-0.057	-0.088	-0.081	0.374	-0.521	0.022	0.276	-0.389
			4.0	-0.246	-0.016	-0.095	-0.078	0.228	-0.423	-0.019	0.299	-0.390
			8.0	-0.344	0.067	-0.107	-0.065	0.062	-0.313	-0.065	0.323	-0.387

Table 3 (cont'd)

$\frac{h_v}{h}$	$\frac{h_b}{h}$	$\frac{a}{d}$	$\frac{L^2 t}{a^3}$	Transverse moments				Longitudinal stresses				
				M_2	M_3	M_4	M_5	f_0	f_v	f_1	f_2	f_3
1/4	1/4	2.5	0.5	-0.106	-0.074	-0.084	-0.083	0.510	-1.203	-0.078	0.914	-1.283
			1.0	-0.127	-0.056	-0.085	-0.081	0.459	-1.173	-0.091	0.926	-1.280
			2.0	-0.183	0.001	-0.086	-0.075	0.324	-1.094	-0.125	0.956	-1.265
			4.0	-0.257	0.158	-0.090	-0.035	0.132	-0.993	-0.180	0.990	-1.221
		2.0	0.5	-0.105	-0.075	-0.085	-0.083	0.598	-1.030	-0.067	0.713	-0.992
			1.0	-0.125	-0.063	-0.085	-0.082	0.557	-1.007	-0.076	0.721	-0.990
			2.0	-0.184	-0.021	-0.088	-0.078	0.436	-0.938	-0.101	0.746	-0.983
			4.0	-0.286	0.094	-0.098	-0.057	0.224	-0.822	-0.147	0.784	-0.961
		1.5	0.5	-0.103	-0.077	-0.085	-0.083	0.607	-0.792	-0.062	0.507	-0.695
			1.0	-0.117	-0.070	-0.085	-0.082	0.583	-0.780	-0.065	0.511	-0.694
			2.0	-0.167	-0.044	-0.088	-0.080	0.503	-0.738	-0.078	0.525	-0.692
			4.0	-0.280	0.033	-0.098	-0.070	0.321	-0.643	-0.108	0.555	-0.684
			8.0	-0.400	0.212	-0.126	-0.019	0.118	-0.544	-0.144	0.583	-0.659
		1.0	0.5	-0.100	-0.077	-0.084	-0.083	0.476	-0.485	-0.051	0.295	-0.396
			1.0	-0.107	-0.076	-0.085	-0.083	0.469	-0.481	-0.052	0.296	-0.396
			2.0	-0.132	-0.065	-0.086	-0.082	0.442	-0.468	-0.055	0.300	-0.395
			4.0	-0.212	-0.028	-0.092	-0.079	0.359	-0.429	-0.064	0.312	-0.394
			8.0	-0.362	0.068	-0.110	-0.065	0.201	-0.356	-0.082	0.333	-0.388
	1/2	2.5	0.5	-0.077	-0.082	-0.082	-0.083	0.687	-1.229	-0.221	0.959	-1.282
			1.0	-0.092	-0.068	-0.082	-0.082	0.671	-1.224	-0.223	0.964	-1.278
			2.0	-0.140	-0.017	-0.082	-0.075	0.616	-1.206	-0.230	0.980	-1.262
			4.0	-0.253	0.140	-0.091	-0.035	0.485	-1.168	-0.249	1.015	-1.217
		2.0	0.5	-0.076	-0.083	-0.083	-0.083	0.647	-0.967	-0.213	0.763	-0.995
			1.0	-0.087	-0.075	-0.083	-0.083	0.638	-0.964	-0.214	0.766	-0.993
			2.0	-0.125	-0.043	-0.083	-0.079	0.603	-0.953	-0.217	0.776	-0.985
			4.0	-0.232	0.065	-0.092	-0.059	0.505	-0.923	-0.227	0.802	-0.961
		1.5	0.5	-0.074	-0.085	-0.083	-0.083	0.542	-0.679	-0.185	0.552	-0.700
			1.0	-0.081	-0.081	-0.083	-0.083	0.538	-0.678	-0.186	0.553	-0.699
			2.0	-0.105	-0.064	-0.083	-0.081	0.522	-0.673	-0.186	0.557	-0.696
			4.0	-0.184	-0.003	-0.089	-0.073	0.470	-0.658	-0.189	0.571	-0.687
			8.0	-0.356	0.175	-0.121	-0.022	0.356	-0.626	-0.198	0.598	-0.661
		1.0	0.5	-0.073	-0.086	-0.083	-0.084	0.359	-0.380	-0.128	0.324	-0.399
			1.0	-0.075	-0.084	-0.083	-0.083	0.358	-0.380	-0.128	0.324	-0.399
			2.0	-0.085	-0.079	-0.083	-0.083	0.355	-0.379	-0.128	0.325	-0.399
			4.0	-0.121	-0.057	-0.085	-0.081	0.341	-0.375	-0.129	0.329	-0.397
			8.0	-0.231	0.020	-0.096	-0.069	0.298	-0.364	-0.130	0.339	-0.391

Table 3 (cont'd)

$\frac{h_v}{h}$	$\frac{h_o}{h}$	$\frac{a}{d}$	$\frac{L^2 t}{a^3}$	Transverse moments M_2	M_3	M_4	M_5	Longitudinal stresses f_0	f_v	f_1	f_2	f_3
3/8	0	2.5	0.5	-0.098	-0.076	-0.084	-0.083		-0.232	-0.286	0.945	-1.299
			1.0	-0.079	-0.072	-0.080	-0.083		-0.262	-0.261	0.932	-1.294
			2.0	-0.029	-0.045	-0.067	-0.080		-0.339	-0.200	0.897	-1.277
			4.0	0.045	0.079	-0.022	-0.055		-0.443	-0.129	0.847	-1.222
		2.0	0.5	-0.102	-0.076	-0.084	-0.083		-0.254	-0.179	0.718	-0.998
			1.0	-0.093	-0.073	-0.083	-0.083		-0.267	-0.169	0.713	-0.996
			2.0	-0.068	-0.055	-0.076	-0.081		-0.301	-0.143	0.699	-0.988
			4.0	-0.025	0.025	-0.052	-0.069		-0.357	-0.107	0.674	-0.960
		1.5	0.5	-0.105	-0.076	-0.085	-0.083		-0.255	-0.082	0.490	-0.694
			1.0	-0.104	-0.074	-0.084	-0.083		-0.256	-0.081	0.490	-0.693
			2.0	-0.099	-0.063	-0.082	-0.082		-0.261	-0.078	0.488	-0.690
			4.0	-0.087	-0.018	-0.072	-0.077		-0.273	-0.072	0.483	-0.681
			8.0	-0.065	0.136	-0.040	-0.040		-0.290	-0.071	0.473	-0.650
		1.0	0.5	-0.106	-0.077	-0.085	-0.083		-0.207	-0.011	0.268	-0.390
			1.0	-0.108	-0.075	-0.085	-0.083		-0.206	-0.012	0.269	-0.390
			2.0	-0.113	-0.070	-0.085	-0.082		-0.202	-0.015	0.270	-0.390
			4.0	-0.125	-0.050	-0.083	-0.081		-0.190	-0.024	0.273	-0.388
			8.0	-0.139	0.014	-0.076	-0.072		-0.177	-0.037	0.277	-0.382
	1/8	2.5	0.5	-0.100	-0.075	-0.084	-0.083	-0.197	-0.438	-0.139	0.920	-1.290
			1.0	-0.092	-0.066	-0.082	-0.082	-0.184	-0.449	-0.132	0.913	-1.286
			2.0	-0.067	-0.031	-0.072	-0.078	-0.150	-0.478	-0.114	0.894	-1.268
			4.0	-0.023	0.103	-0.036	-0.048	-0.104	-0.528	-0.093	0.858	-1.215
		2.0	0.5	-0.103	-0.076	-0.084	-0.083	-0.060	-0.428	-0.070	0.701	-0.992
			1.0	-0.102	-0.069	-0.083	-0.082	-0.059	-0.429	-0.070	0.700	-0.990
			2.0	-0.098	-0.044	-0.079	-0.080	-0.058	-0.432	-0.070	0.697	-0.982
			4.0	-0.086	0.047	-0.063	-0.065	-0.055	-0.442	-0.071	0.688	-0.956
		1.5	0.5	-0.105	-0.076	-0.085	-0.083	0.060	-0.385	-0.015	0.482	-0.691
			1.0	-0.108	-0.072	-0.084	-0.083	0.056	-0.382	-0.017	0.483	-0.690
			2.0	-0.117	-0.056	-0.083	-0.081	0.041	-0.372	-0.024	0.487	-0.687
			4.0	-0.136	-0.001	-0.079	-0.075	0.010	-0.353	-0.039	0.494	-0.679
			8.0	-0.144	0.165	-0.062	-0.031	-0.023	-0.340	-0.058	0.495	-0.650
		1.0	0.5	-0.105	-0.077	-0.085	-0.083	0.127	-0.283	0.017	0.267	-0.390
			1.0	-0.108	-0.075	-0.085	-0.083	0.124	-0.281	0.015	0.268	-0.390
			2.0	-0.119	-0.068	-0.085	-0.082	0.113	-0.274	0.011	0.270	-0.389
			4.0	-0.150	-0.041	-0.086	-0.080	0.081	-0.253	-0.002	0.278	-0.388
			8.0	-0.200	0.035	-0.086	-0.069	0.029	-0.221	-0.024	0.290	-0.383

Table 3 (cont'd)

$\frac{h_v}{h}$	$\frac{h_0}{h}$	$\frac{a}{d}$	$\frac{L^2 t}{a^3}$	Transverse moments				Longitudinal stresses				
				M_2	M_3	M_4	M_5	f_0	f_v	f_1	f_2	f_3
$\frac{3}{8}$	$\frac{1}{4}$	2.5	0.5	-0.097	-0.076	-0.084	-0.083	-0.006	-0.617	-0.051	0.886	-1.277
			1.0	-0.097	-0.064	-0.082	-0.082	-0.008	-0.617	-0.053	0.885	-1.273
			2.0	-0.095	-0.021	-0.075	-0.077	-0.013	-0.618	-0.056	0.882	-1.257
			4.0	-0.084	0.123	-0.048	-0.043	-0.021	-0.626	-0.065	0.870	-1.205
		2.0	0.5	-0.099	-0.077	-0.084	-0.083	0.116	-0.557	-0.024	0.684	-0.984
			1.0	-0.102	-0.069	-0.083	-0.082	0.110	-0.554	-0.027	0.685	-0.982
			2.0	-0.114	-0.039	-0.080	-0.079	0.091	-0.546	-0.034	0.689	-0.975
			4.0	-0.134	0.063	-0.070	-0.062	0.050	-0.530	-0.050	0.695	-0.949
		1.5	0.5	-0.099	-0.078	-0.084	-0.083	0.203	-0.458	-0.008	0.479	-0.688
			1.0	-0.104	-0.073	-0.084	-0.083	0.197	-0.455	-0.009	0.480	-0.687
			2.0	-0.120	-0.055	-0.084	-0.081	0.178	-0.445	-0.015	0.485	-0.684
			4.0	-0.161	0.007	-0.082	-0.073	0.127	-0.421	-0.030	0.497	-0.675
			8.0	-0.211	0.184	-0.077	-0.025	0.057	-0.393	-0.054	0.507	-0.646
		1.0	0.5	-0.098	-0.079	-0.084	-0.083	0.211	-0.302	-0.002	0.274	-0.390
			1.0	-0.101	-0.077	-0.084	-0.083	0.209	-0.301	-0.003	0.274	-0.390
			2.0	-0.112	-0.070	-0.085	-0.082	0.200	-0.297	-0.005	0.276	-0.390
			4.0	-0.148	-0.042	-0.086	-0.080	0.173	-0.284	-0.011	0.282	-0.388
			8.0	-0.226	0.042	-0.090	-0.068	0.111	-0.256	-0.026	0.294	-0.382
	$\frac{1}{2}$	2.5	0.5	-0.074	-0.082	-0.082	-0.083	0.260	-0.801	-0.041	0.864	-1.257
			1.0	-0.079	-0.070	-0.080	-0.082	0.254	-0.800	-0.042	0.866	-1.252
			2.0	-0.096	-0.023	-0.074	-0.076	0.234	-0.796	-0.048	0.870	-1.236
			4.0	-0.133	0.130	-0.057	-0.037	0.188	-0.790	-0.062	0.877	-1.186
		2.0	0.5	-0.074	-0.084	-0.082	-0.083	0.305	-0.661	-0.053	0.684	-0.974
			1.0	-0.079	-0.076	-0.081	-0.083	0.301	-0.660	-0.054	0.685	-0.972
			2.0	-0.096	-0.046	-0.079	-0.079	0.286	-0.657	-0.057	0.690	-0.964
			4.0	-0.144	0.059	-0.072	-0.060	0.244	-0.647	-0.066	0.700	-0.938
		1.5	0.5	-0.073	-0.085	-0.082	-0.083	0.302	-0.489	-0.059	0.494	-0.684
			1.0	-0.077	-0.081	-0.082	-0.083	0.300	-0.489	-0.059	0.494	-0.683
			2.0	-0.090	-0.065	-0.081	-0.082	0.292	-0.487	-0.060	0.497	-0.681
			4.0	-0.133	-0.006	-0.080	-0.074	0.266	-0.480	-0.064	0.504	-0.671
			8.0	-0.226	0.175	-0.082	-0.023	0.208	-0.467	-0.075	0.518	-0.642
		1.0	0.5	-0.073	-0.086	-0.083	-0.084	0.228	-0.288	-0.050	0.291	-0.391
			1.0	-0.074	-0.084	-0.082	-0.083	0.228	-0.288	-0.050	0.291	-0.390
			2.0	-0.080	-0.079	-0.082	-0.083	0.226	-0.287	-0.050	0.291	-0.390
			4.0	-0.102	-0.058	-0.082	-0.081	0.218	-0.285	-0.051	0.294	-0.388
			8.0	-0.171	0.018	-0.085	-0.069	0.193	-0.279	-0.054	0.300	-0.381

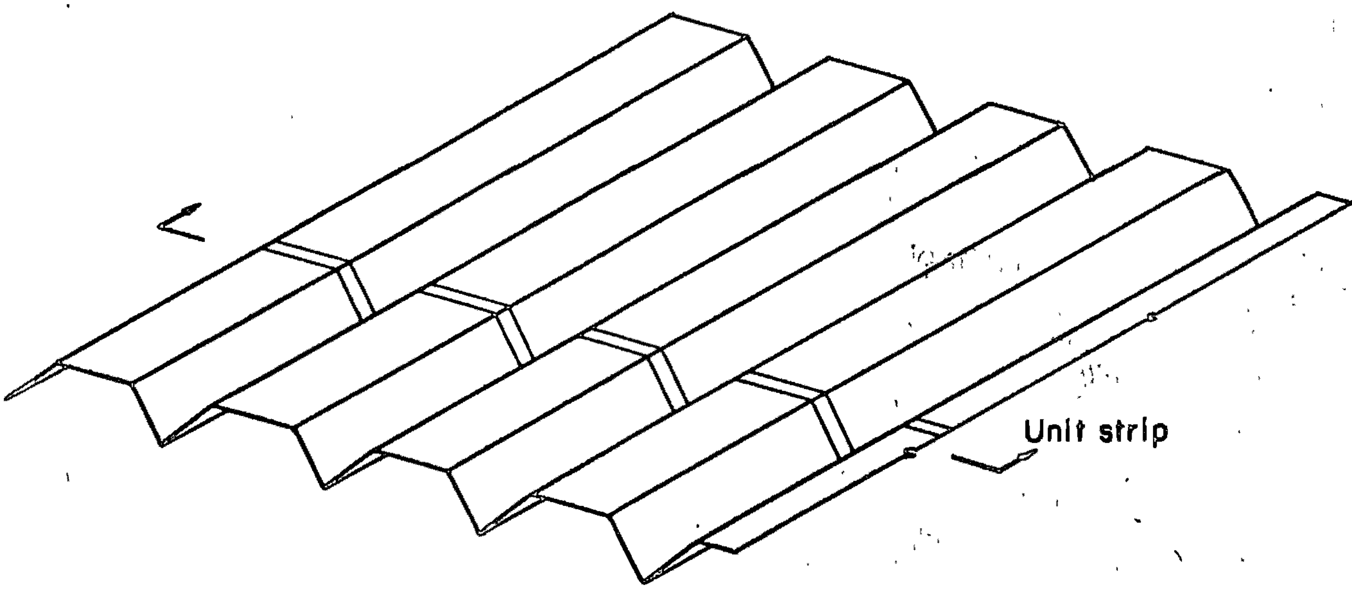

(a)

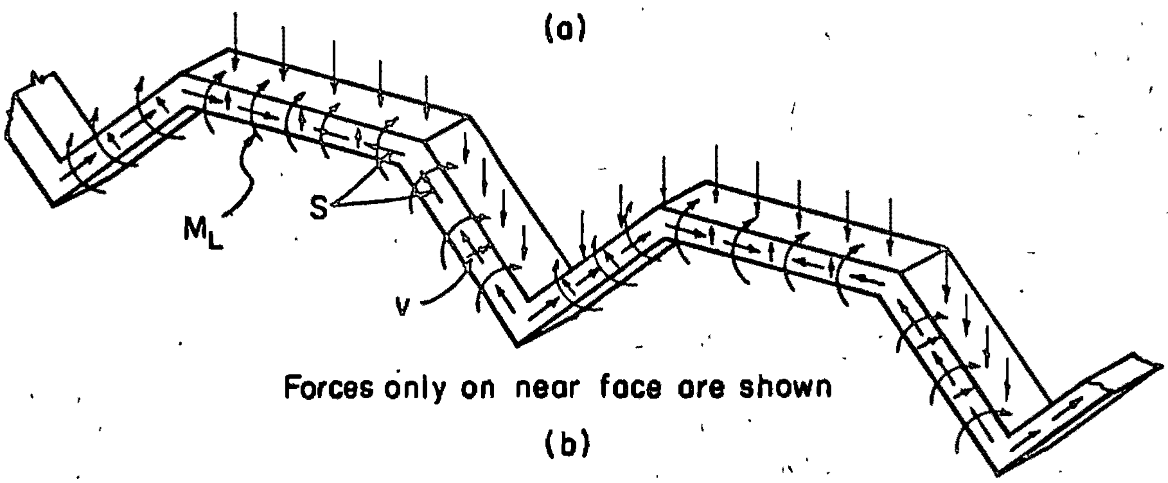

Forces only on near face are shown

(b)

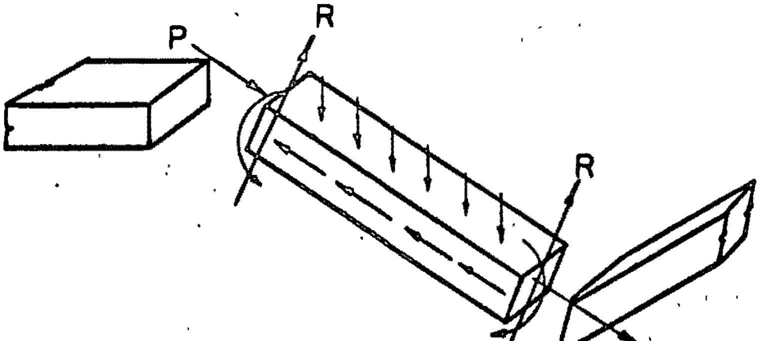

(c)

Fig. 1

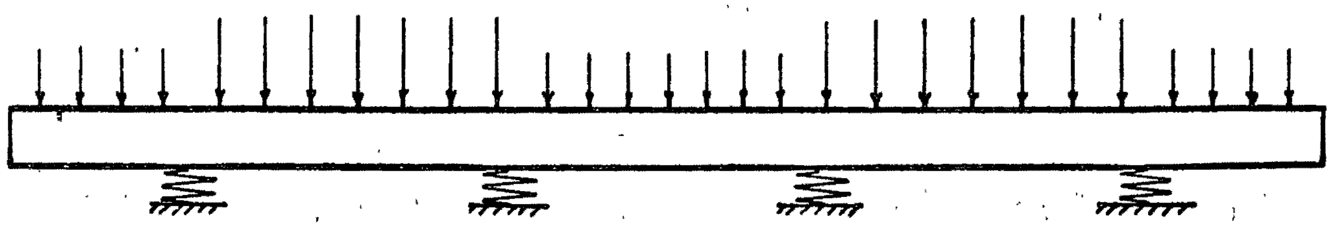

Fig. 2

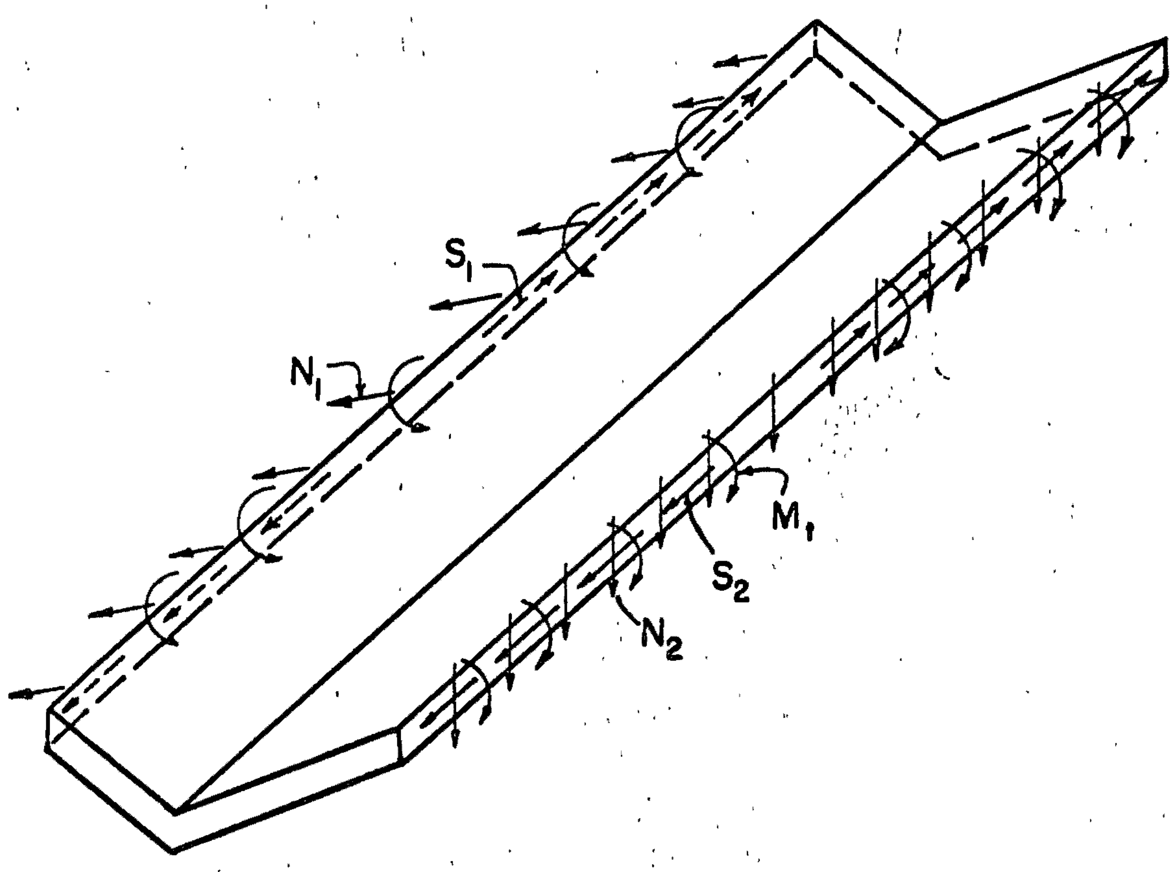

Fig. 3

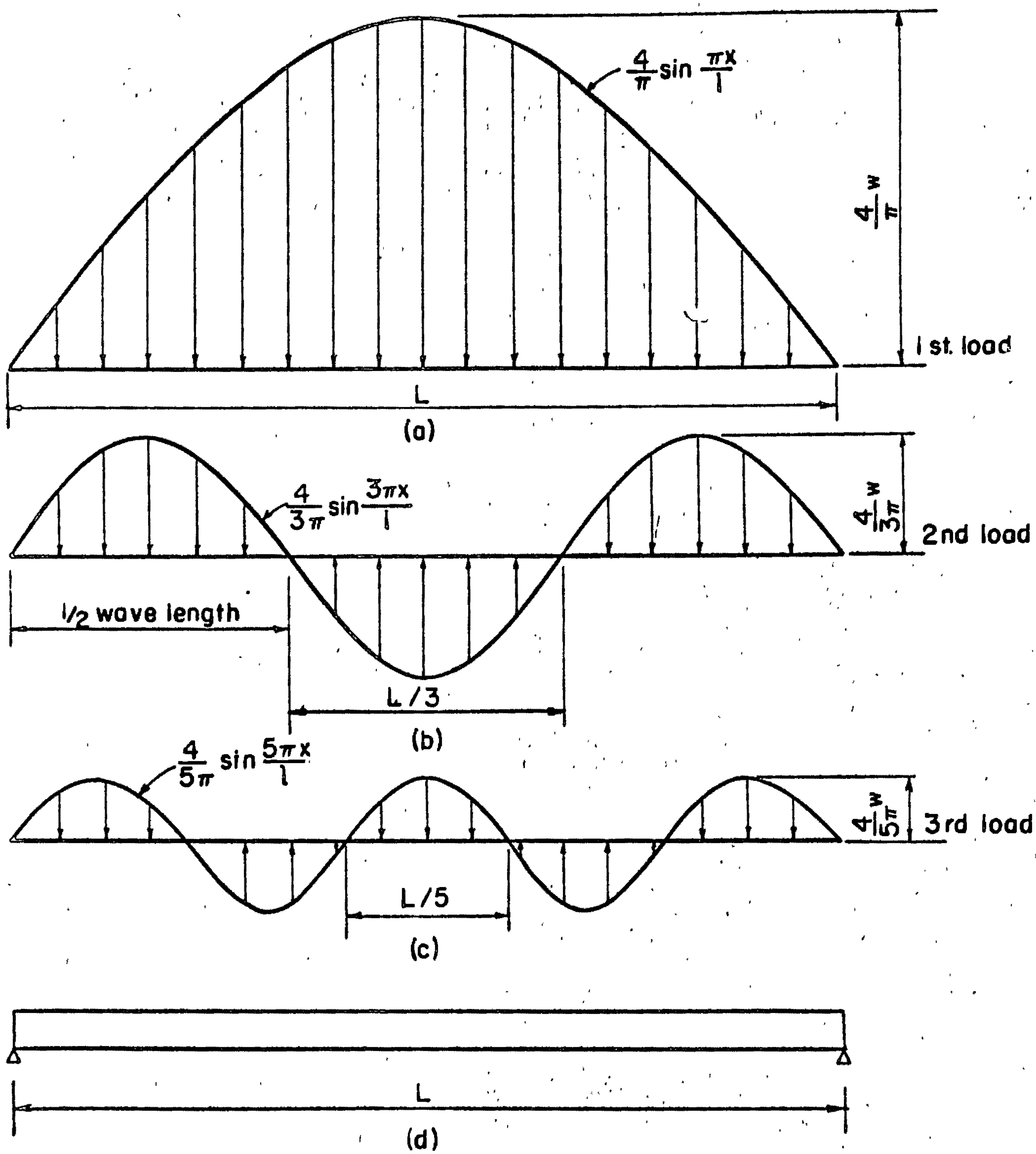

$\frac{4}{\pi}\sin\frac{\pi x}{l}$
$\frac{4}{\pi}w$
1 st. load
L
(a)
$\frac{4}{3\pi}\sin\frac{3\pi x}{l}$
$\frac{4}{3\pi}w$
2nd load
1/2 wave length
L / 3
(b)
$\frac{4}{5\pi}\sin\frac{5\pi x}{l}$
$\frac{4}{5\pi}w$
3rd load
L / 5
(c)
L
(d)

Fig. 4

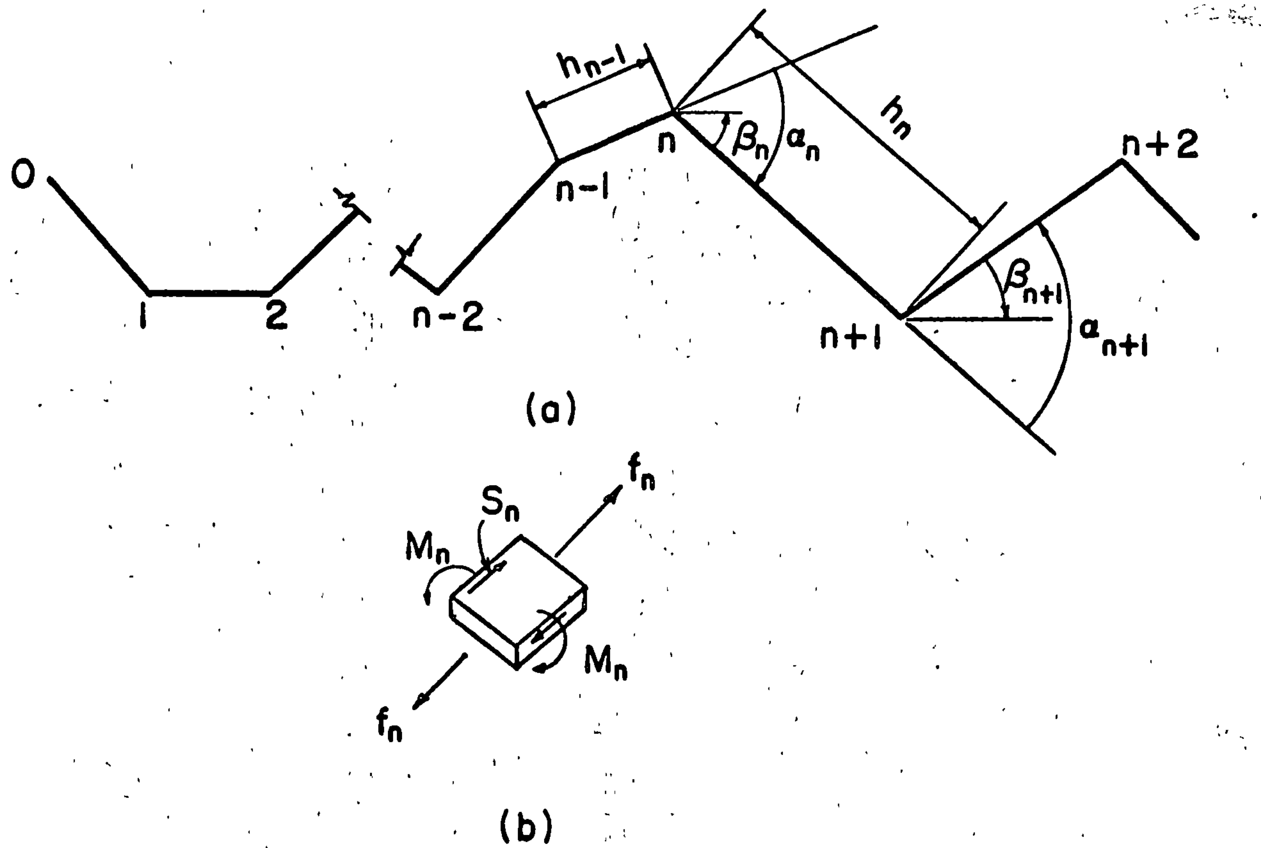
0
1
2
n-2
n-1
n
n+1
n+2
h_{n-1}
h_n
β_n
α_n
β_{n+1}
α_{n+1}
(a)
S_n
M_n
f_n
M_n
f_n
(b)

Fig. 5

Appendix:

Although the behavior of a folded plate is three dimensional, nevertheless the analysis and design of such a structure can be reduced to merely the solution of a series of simultaneous equations by means of routine and familiar concepts. No greater knowledge is required other than familiarity with statics, the conventional flexural theories and the principles of elastic weight, generally referred to as the moment area principles. The complications that occur are due primarily to the obscure and multiple inter-relationship of forces. Because of this a greater systematization of the analytical steps is needed for folded plates than for conventional structures.

In this vein, the study of folded plates will commence by considering first transverse and longitudinal action separately. The first deals with the bending of the individual plates out of their plane, that is, the resistance of the plates acting as a continuous slab between the junctions. The second involves primarily the deflection of the plates in the plane parallel to the plates which has come to be designated as plate action.

In the former instance because the length of each plate in the longitudinal direction is generally several times the distance between the folds of the plates, slab resistance in the longitudinal direction is small, and the slab can be regarded as a one-way slab. Therefore the relationship between the transverse moments at the junctions is identical to those in continuous beams. Hence if beam AB in fig. A1 be considered as a representative strip extending from one fold to the next, using moment distribution notation by the first moment area principal,

$$M_{AB} = K_{AB}\phi_{AB} - C_{BA}K_{BA}\phi_{BA} - \frac{\Delta}{h_A}(K_{AB} - C_{BA}K_{BA}) + M^F_{AB} \tag{1a}$$

$$M_{BA} = C_{AB}K_{AB}\phi_{AB} - K_{BA}\phi_{BA} - \frac{\Delta}{h_A}(C_{AB}K_{AB} - K_{BA}) - M^F_{BA} \tag{1b}$$

in which

M = bending moment and is considered positive when it creates tension on the underside of the beam

K = the stiffness factor which is the moment produced by a unit rotation

C = the carry-over factor and is considered negative

ϕ = angle change with respect to the chord and is considered positive when angle is rotated in a clockwise direction

h = length of slab between A and B

Δ = displacement of end B with respect to A and is considered positive when it is downward

For prismatic beams of unit width $K = 4Et^3/12h = Et^3/3h$ and $c = -0.5$ in which

E = modulus of elasticity
t = thickness of slab

Substituting these values in equations (1a) and (1b) we have

$$M_{AB} = \frac{Et^3}{3h_A}\left(\phi_{AB} + 0.5\phi_{BA} - 1.5\frac{\Delta}{h_A}\right) + M^F_{AB} \quad (2a)$$

$$M_{BA} = \frac{Et^3}{3h_A}\left(-0.5\phi_{AB} - \phi_{BA} + 1.5\frac{\Delta_A}{h_A}\right) + M^F_{BA} \quad (2b)$$

Eliminating ϕ_{BA} from equations (2a) and (2b) and factoring the results yields

$$\phi_{AB} = \frac{4h_A}{Et^3}\left(M_{AB} + 0.5M_{BA} - M^F_{AB} - 0.5M^F_{AB}\right) + \frac{\Delta}{h_A} \quad (3a)$$

Similarly

$$\phi_{BA} = -\frac{4h_A}{Et^3}(M_{BA} + 0.5M_{AB} - M^F_{BA} - 0.5M^F_{AB}) + \frac{\Delta}{h_A} \tag{3b}$$

The preceding equations express the basic relationship needed for investigating and determining the variation in the magnitude of the transverse moments from fold to fold. The other basic relationship needed is naturally that dealing with longitudinal action. Fortunately in this case the problem is essentially confined to the action and more specifically to the deflection of the individual plates acting as beams spanning from support to support. In general, for prismatic beams it is customary to express the deflection of a beam as a function of the load divided by the product of the moment of inertia and the modulus of elasticity. However in this case it is more suitable to express the deflection as a function of the extreme fiber stresses. To do so it is necessary to know the longitudinal distribution of the stresses. For a simply supported prismatic beam subject to uniform load, the distribution is parabolic. Since the dead and live load on a folded plate will be generally uniform, it would seem desirable at first to assume a parabolic distribution. Such an assumption leads however to a slight inconsistency and difficulties in adjusting the longitudinal strains of two adjacent plates. This can be easily avoided by assuming that the load and thus the stresses vary sinusoidally in the longitudinal direction.

As such, if the midspan fiber stress at the top and bottom of a plate are designated respectively as f_A and f_B then on the basis of a linear stress-strain relationship as shown in fig. A2, the rotation of an element dx long will be

$$d\theta = -\left(\frac{f_A - f_B}{Eh_A}\right)\sin\frac{\pi x}{L}\,dx \tag{4a}$$

in which

f_A and f_B are considered positive when they are compressive. Integrating equation (4a) and making the slope zero at midspan the angle change at any point is therefore

$$\theta = \left(\frac{f_A - f_B}{Eh_A}\right)\frac{L}{\pi}\cos\frac{\pi x}{L} \tag{4b}$$

Since, the derivitive of the deflection curve with respect to X equals the angle change, then integrating equation (4b) and making the deflection equal to zero at X = 0 and X = L

$$\delta_A = \left(\frac{f_A - f_B}{Eh_A}\right)\left(\frac{L}{\pi}\right)^2 \tag{4c}$$

in which

δ_A equals the midspan deflection of the beam and is considered positive downward, or in the direction from A to B.

The three equations (3a), (3b) and (4c) are the only ones needed for the analysis of folded plates which depend on stress-strain relationship. Further derivations involve primarily equilibrium of forces and satisfaction of trigonometric relationship. In the latter category, the problem can be reduced to a consideration of the effect of the deflection of one plate on the adjacent plates. In this it is advantageous to employ a technique similar to that used in moment distribution. Thus in fig. A3 if plate BC is fixed in the direction parallel to its plane but capable of either rotating about C or being bent then a displacement of plate AB from B to B' can only take place with an accompanying movement in the direction perpendicular to plate BC. Based on the geometry of triangle B B' B",

$$\Delta^B_{BC} = \delta_A / \sin \alpha_B \tag{5a}$$

in which

α_B = the angle formed by the projection of the slope of plate AB with the slope of plate BC, and is considered positive where the angle is clockwise

δ_A = deflection of plate AB and considered positive when A moves toward B.

With plate AB fixed but plate BC displaced,

$$\Delta^B_{BC} = -\delta_B \cot \alpha_B \tag{5b}$$

The total movement of point B normal to the line BC caused by the displacement of the two plates AB and BC is therefore

$$\Delta^B_{BC} = \delta_A / \sin \alpha_B - \delta_B \cot \alpha_B \tag{5c}$$

By similar operation with plates BC and CD, the displacement of C with respect to the original line BC is

$$\Delta^C_{BC} = -\delta_B \cot \alpha_C + \delta_C / \sin \alpha_C \tag{5d}$$

Since the displacement of C, with respect to B designated as Δ_{BC} equals the sum of the values given by equations (5c) and (5d), then

$$\Delta_{BC} = \delta_A / \sin \alpha_B - \delta_B(\cot \alpha_B + \cot \alpha_C) + \delta_C / \sin \alpha_C \tag{5e}$$

The general equations just derived will now be applied to a folded plate such as shown in fig. A4. In this case for convenience the folds are designated by number rather than letters. Considering a typical interior point as fold 4, the angle of rotation and moment to the left of 4 must be equal respectively to those on the right side. Hence equating the rotation at 4 of plates 3 and 4 in accordance to equations (3a) and (3b) by replacing the subscripts A and B by the appropriate numerals, and designating the final moment at a fold solely by the number at the fold.

$$\begin{aligned} -\frac{4h_3}{Et_3^3}(M_4 + 0.5M_3 - M^F_{43} - 0.5M^F_{34}) + \frac{\Delta_3}{h_3} \\ = \frac{4h_4}{Et_4^3}(M_4 + 0.5M_5 - M^F_{45} - 0.5M^F_{54}) + \frac{\Delta_4}{h_4} \end{aligned} \tag{6a}$$

Replacing the Δ 's in eq. (6a) by their equivalent as given by eq. (5e) and factoring the result, we obtain

$$
\begin{aligned}
&-2\frac{h_3}{t_3^3}M_3-4\left(\frac{h_3}{t_3^3}+\frac{h_4}{t_4^3}\right)M_4-2\frac{h_4}{t_4^3}M_5 \\
&+\frac{E}{h_3}\left[\delta_2/\sin\alpha_3-\delta_3(\cot\alpha_3+\cot\alpha_4)+\delta_4/\sin\alpha_4\right] \\
&-\frac{E}{h_4}\left[\delta_3/\sin\alpha_4-\delta_4(\cot\alpha_4+\cot\alpha_5)+\delta_5/\sin\alpha_5\right] \\
&=-2\frac{h_3}{t_3^3}(M_{34}^F+2M_{43}^F)-2\frac{h_4}{t_4^3}(M_{54}^F+2M_{45}^F)
\end{aligned}
\tag{6b}
$$

Equation (6b) can now be conveniently altered into an expression containing only moment and stress terms by means of eq. (4c). If we substitute for the δ's their equivalent equation (6b) reduces to

$$
\begin{aligned}
&-2\frac{h_3}{t_3^3}M_3-4\left(\frac{h_3}{t_3^3}+\frac{h_4}{t_4^3}\right)M_4-2\frac{h_4}{t_4^3}M_5 \\
&\left(\frac{L}{\pi}\right)^2\left\{+\frac{1}{h_3}\left[\frac{f_2-f_3}{h_2\sin\alpha_3}-\frac{f_3-f_4}{h_3}(\cot\alpha_3+\cot\alpha_4)+\frac{f_4-f_5}{h_4\sin\alpha_4}\right]\right. \\
&\left.-\frac{1}{h_4}\left[\frac{f_3-f_4}{h_3\sin\alpha_4}-\frac{f_4-f_5}{h_4}(\cot\alpha_4+\cot\alpha_5)+\frac{f_5-f_6}{h_5\sin\alpha_5}\right]\right\} \\
&=-2\frac{h_3}{t_3^3}(M_{34}^F+2M_{43}^F)-2\frac{h_4}{t_4^3}(M_{54}^F+2M_{45}^F)
\end{aligned}
\tag{6c}
$$

In equation (6c), since we are considering only a uniform load on the plates, the fixed end moment in any span is equal to

$$
-\frac{W\cos\beta\, h}{12} \tag{7}
$$

in which

β = the angle formed by the plate and a horizontal line and is considered positive in the clockwise direction

W = the total load on the plate

Substituting this value in equation (6c) and factoring, we obtain

$$
\begin{aligned}
&2\frac{h_3}{h_4}\left(\frac{t_4}{t_3}\right)^3 M_3 + 4\left[1+\frac{h_3}{h_4}\left(\frac{t_4}{t_3}\right)^3\right] M_4 + 2M_5 \\
&-\frac{L^2}{\pi^2}\left(\frac{t_4}{h_4}\right)^3\left(C_4^2 f_2 - C_4^3 f_3 + C_4^4 f_4 - C_4^5 f_5 + C_4^6 f_6\right) \\
&= -h_4\left[\left(\frac{h_3}{h_4}\right)^2\left(\frac{t_4}{t_3}\right)^3 \frac{W_3\cos\beta_3}{2} + \frac{W_4\cos\beta_4}{2}\right]
\end{aligned}
\tag{8}
$$

in which

$$C_4^2 = \frac{h_4^2}{h_2 h_3 \sin\alpha_3}$$

$$C_4^3 = \frac{h_4^2}{h_2 h_3 \sin\alpha_3} + \left(\frac{h_4}{h_3}\right)^2(\cot\alpha_3 + \cot\alpha_4) + \frac{h_4}{h_3\sin\alpha_4}$$

$$C_4^4 = \left(\frac{h_4}{h_3}\right)^2(\cot\alpha_3 + \cot\alpha_4) + \cot\alpha_4 + \cot\alpha_5 + 2\frac{h_4}{h_3\sin\alpha_4}$$

$$C_4^5 = \frac{h_4}{h_3\sin\alpha_4} + (\cot\alpha_4 + \cot\alpha_5) + \frac{h_4}{h_5\sin\alpha_5}$$

$$C_4^6 = \frac{h_4}{h_5\sin\alpha_5}$$

The above equation satisfies the requirement of continuity. Another relation can be found from a consideration of statics and the conventional flexural theory. If we isolate from a folded plate structure a single plate and consider only the forces which produce bending in the longitudinal direction, the plate will be subject as shown in fig. A5 to two shearing forces of different magnitude and two normal forces at each edge, and if prestressed it will also be subject to prestressing forces. In order to have the stresses at the folds of adjacent plates compatible along the entire edge, it is necessary to have the load varying sinusoidally. However, by means of a Fourier series, the actual load can be approximated as the sum of partial loads varying sinusoidally. From a practical point of view only the first sine load or at most two partial loads are necessary. For purpose of illustration and derivation only the first sine load will be used. An explanation of how to adjust this load is given in the text proper. Thus on the basis that the normal load varies as the sine, and the shearing forces vary as the cosine, taking moment at midspan the stress at 4 in plate 4 is

$$f_4 = \frac{1}{t_4}\left(\frac{L}{h_4\pi}\right)^2\left(6P_4 - 4\pi\frac{h_4}{L}S_4 - 2\pi\frac{h_4}{L}S_5\right) + f_{45}^P \tag{9a}$$

and at 5 is

$$f_5 = \frac{1}{t_4}\left(\frac{L}{h_4\pi}\right)^2\left(-6P_4 + 2\pi\frac{h_4}{L}S_4 + 4\pi\frac{h_4}{L}S_5\right) + f_{54}^P \tag{9b}$$

in which

f^P = stress created by prestressing force considering the plates as individual and isolated plates with the subscript 45 designating the stress at fold 4, and 54 the stress at fold 5 in plate 4

Eliminating S_5 from equations (9a) yields

$$2f_4 + f_5 = \frac{1}{t_4}\left(\frac{L}{h_4\pi}\right)^2\left(6P_4 - 6\pi\frac{h_4}{L}S_4\right) + 2f_{45}^P + f_{54}^P \tag{10}$$

Repeating the identical operation on plate 34 we have

$$f_4 = \frac{1}{t_3}\left(\frac{L}{h_3\pi}\right)^2\left(-6P_3 + 4\pi\frac{h_3}{L}S_4 + 2\pi\frac{h_3}{L}S_3\right) + f_{43}^P \tag{11a}$$

$$f_3 = \frac{1}{t_3}\left(\frac{L}{h_3\pi}\right)^2\left(6P_3 - 2\pi\frac{h_3}{L}S_4 - 4\pi\frac{h_3}{L}S_3\right) + f_{34}^P \tag{11b}$$

from which, we obtain

$$2f_4 + f_3 = \frac{1}{t_3}\left(\frac{L}{h_3\pi}\right)^2\left(-6P_3 + 6\pi\frac{h_3}{L}S_4\right) + 2f_{43}^P + f_{34}^P \tag{12}$$

Equations (10) and (12) can be solved as simultaneous equations to eliminate S_4. Multiplying equation (10) by t_4h_4 and equation (12) by t_3h_3 and adding the two results we obtain on factoring

$$\begin{aligned} &h_3t_3f_3 + 2(h_3t_3 + h_4t_4)f_4 + h_4t_4f_5 - 6\left(\frac{L}{\pi}\right)^2\left(\frac{P_4}{h_4} - \frac{P_3}{h_3}\right) \\ &= \left(2f_{45}^P + f_{54}^P\right)h_4t_4 + \left(2f_{43}^P + f_{34}^P\right)h_3t_3 \end{aligned} \tag{13}$$

In order to employ equation (13) it is necessary to express P_3 and P_4 in terms of the load and transverse moments. From a consideration of the equilibrium of forces in fig. A6 with each slab considered as a free body, the vertical reaction at fold 4 is

$$V_4 = \frac{M_3 - M_4}{h_3\cos\beta_3} - \frac{M_4 - M_5}{h_4\cos\beta_4} + \frac{W_3 + W_4}{2} \tag{14a}$$

and by the same token at fold 5, we have

$$V_5 = \frac{M_4 - M_5}{h_4\cos\beta_4} - \frac{M_5 - M_6}{h_5\cos\beta_5} + \frac{W_4 + W_5}{2} \tag{14b}$$

Since there are no vertical supports at any folds, these reactions must be supplied by forces parallel to the plates. Resolving these reactions, into a force component parallel to the plate we find

$$P_4 = V_4 \frac{\sin(90^\circ-\beta_3)}{\sin\alpha_4} - V_5 \frac{\sin(90^\circ-\beta_5)}{\sin\alpha_5}$$
$$= V_4 \frac{\cos\beta_3}{\sin\alpha_4} - V_5 \frac{\cos\beta_5}{\sin\alpha_5} \qquad (14c)$$

Substituting the values of V_4 and V_5 as given by equations (14a) and (14b) in equation (14c) gives

$$P_4 = \frac{M_3-M_4}{h_3\sin\alpha_4} - \frac{M_4-M_5}{h_4\cos\beta_4}\left(\frac{\cos\beta_3}{\sin\alpha_4}+\frac{\cos\beta_5}{\sin\alpha_5}\right) + \frac{M_5-M_6}{h_5\sin\alpha_5}$$
$$\left(\frac{W_3+W_4}{2}\right)\frac{\cos\beta_3}{\sin\alpha_4} - \left(\frac{W_4+W_5}{2}\right)\frac{\cos\beta_5}{\sin\alpha_5} \qquad (14d)$$

But from figure A6

$$\beta_3 = -\alpha_4+\beta_4 \quad \text{and} \quad \beta_5 = \alpha_5+\beta_4$$

Substituting these values in the second term of equation (14d), we obtain

$$\frac{\cos(-\alpha_4+\beta_4)}{\cos\beta_4\sin\alpha_4} + \frac{\cos(\alpha_5-\beta_4)}{\cos\beta_4\sin\alpha_5} = \frac{\cos\alpha_4}{\sin\alpha_4} + \frac{\sin\beta_4}{\cos\beta_4} + \frac{\cos\alpha_5}{\sin\alpha_5} - \frac{\sin\beta_4}{\cos\beta_4}$$
$$= \cot\alpha_4 + \cot\alpha_5 \qquad (14e)$$

Hence equation (14d) reduces

$$P_4 = \frac{M_3-M_4}{h_3\sin\alpha_4} - \frac{M_4-M_5}{h_4}(\cot\alpha_4+\cot\alpha_5) + \frac{M_5-M_6}{h_5\sin\alpha_5}$$
$$+ \left(\frac{W_3+W_4}{2}\right)\frac{\cos\beta_3}{\sin\alpha_4} - \left(\frac{W_4+W_5}{2}\right)\frac{\cos\beta_5}{\sin\alpha_5} \qquad (15a)$$

By similar operation on plate 2 and 3

$$
\begin{aligned}
P_3 &= \frac{M_2 - M_3}{h_2 \sin \alpha_3} - \frac{M_3 - M_4}{h_3}\left(\cot \alpha_3 + \cot \alpha_4\right) + \frac{M_4 - M_5}{h_4 \sin \alpha_4} \\
&+ \left(\frac{W_2 + W_3}{2}\right)\frac{\cos \beta_2}{\sin \alpha_3} - \left(\frac{W_3 + W_4}{2}\right)\frac{\cos \beta_4}{\sin \alpha_4}
\end{aligned} \tag{15b}
$$

On substituting the value of P_3 and P_4 as given in equations (15a) and (15b) in equation (13) and collecting similar terms, we obtain,

$$
\frac{h_3 t_3}{h_4 t_4} f_3 + 2\left(1 + \frac{h_3 t_3}{h_4 t_4}\right) f_4 + f_5 + \frac{6}{t_4 h_4}\left(\frac{L}{\pi h_4}\right)^2 \left(C_4^2 M_2 - C_4^3 M_3 + C_4^4 M_4 - C_4^5 M_5 + C_4^6 M_6\right)
$$

$$
= -\frac{3}{t_4}\left(\frac{L}{\pi h_4}\right)^2 \left[\left(W_2 + W_3\right)\frac{h_4 \cos \beta_2}{h_3 \sin \alpha_3} - \left(W_3 + W_4\right)\left(\frac{\cos \beta_3}{\sin \alpha_4} + \frac{h_4 \cos \beta_4}{h_3 \sin \alpha_4}\right) + \left(W_4 + W_5\right)\frac{\cos \beta_5}{\sin \alpha_5}\right] \tag{16}
$$

$$
+ \frac{h_3 t_3}{h_4 t_4}\left(2 f_{43}^P + f_{34}^P\right) + 2 f_{45}^P + f_{54}^P
$$

Equations (8) and (16) give two distinct relationships between stresses, moments and loads about fold 4. This relationship with appropriate subscripts holds for any other interior fold. Hence at each fold two equations similar in nature to equations (8) and (16) can be written. Since there are only two unknowns at each fold, it is apparent that a system of linear equations can be established to solve the unknown forces and moments. In this connection, advantage should be taken of symmetry to reduce the work involved. Thus should fold 4 be at the axis of symmetry for symmetrical load $f_2 = f_6$; $f_3 = f_5$; $M_2 = M_6$; $M_3 = M_5$. Modification of the equations on the basis of these identities reduces the number of unknowns.

Because the basic equations at any fold involves the moment and stresses at folds once and twice removed from the fold, they are not applicable at the transverse extremity of a folded plate structure. The relationship in this region is considerably simplified because some of the values are already known. For example in figure A7, the moment at 0 will be zero, while the moment at 1, must by a consideration of statics be equal to the cantilever moment of the load to the left of 1. Consequently at each fold, there is only one unknown, the longitudinal stress, and therefore only one equation is needed at point 0 and 1.

With the moments known, consideration need be given only to the requirements of static equilibrium and bending of the plates as beams spanning longitudinally. Thus, if in figure A7, plate 0 be regarded as a free body, with no shearing force at 0 ($S_0 = 0$) then in accordance to equation (10)

$$2f_0 + f_1 = \frac{6}{t_0}\left(\frac{L}{h_0\pi}\right)^2 P_0 + 2f_{01}^P + f_{10}^P \qquad (17)$$

With no member to the left of 0, by equation (14c)

$$P_0 = -V_1 \frac{\cos\beta_1}{\sin\alpha_1} \qquad (18)$$

but as in equation (14a)

$$V_1 = W_0 + \frac{W_1}{2} - \frac{M_1 - M_2}{h_1 \cos\beta_1} \qquad (19a)$$

hence substituting V_1 in equation (18) and letting

$$M_1 = -\frac{W_0 h_0 \cos\beta_0}{2}$$

we obtain

$$P_0 = -\left[\left(W_0 + \frac{W_1}{2}\right) + \frac{W_0 h_0 \cos\beta_0}{2h_1\cos\beta_1}\right]\frac{\cos\beta_1}{\sin\alpha_1} - \frac{M_2}{h_1\sin\alpha_1} \qquad (19b)$$

Substituting this value in equation (17) gives

$$2f_0 + f_1 + \frac{6}{t_0 h_0}\left(\frac{L}{h_0\pi}\right)^2 \frac{h_0}{h_1 \sin\alpha_1} M_2$$
$$= -\frac{3}{t_0}\left(\frac{L}{h_0\pi}\right)^2 \left(2W_0 + W_1 + W_0 \frac{h_0\cos\beta_0}{h_1\cos\beta_1}\right)\frac{\cos\beta_1}{\sin\alpha_1} + 2f^P_{01} + f^P_{10} \qquad .(20)$$

The derivation of the equation for fold 1 can be commenced with a restatement of equation (13)with the proper subscripts. Thus for fold 1, we

$$h_0t_0f_0 + 2(h_0t_0 + h_1t_1)f_1 + h_1t_1f_2 - 6\left(\frac{L}{\pi}\right)^2\left(\frac{P_1}{h_1} - \frac{P_0}{h_0}\right)$$
$$= (2f^P_{12} + f^P_{21})h_1t_1 + (2f^P_{10} + f^P_{01})h_0t_0 \qquad (21)$$

but in accordance to equations (15a),

$$P_1 = \frac{M_0 - M_1}{h_0 \sin\alpha_1} - \frac{M_1 - M_2}{h_1}(\cot\alpha_1 + \cot\alpha_2) + \frac{M_2 - M_3}{h_2\sin\alpha_2}$$
$$+ \left(\frac{W_0 + W_1}{2}\right)\frac{\cos\beta_0}{\sin\alpha_1} - \left(\frac{W_1 + W_2}{2}\right)\frac{\cos\beta_2}{\sin\alpha_2} \qquad (22)$$

On substituting the value of P_0 and P_1 as given by equations (19b) and (22) respectively, equation (21) reduces to

$$\frac{h_0t_0}{h_1t_1}f_0 + 2\left(1 + \frac{h_0t_0}{h_1t_1}\right)f_1 + f_2 - \frac{6}{h_1t_1}\left(\frac{L}{h_1\pi}\right)^2(C_1^2M_2 - C_1^3M_3)$$
$$= \frac{3}{t_1}\left(\frac{L}{\pi h_1}\right)^2\left[(2W_0 + W_1)\left(\frac{\cos\beta_0}{\sin\alpha_1} + \frac{h_1\cos\beta_1}{h_0\sin\alpha_1}\right) - (W_1 + W_2)\frac{\cos\beta_2}{\sin\alpha_2} + W_0\frac{h_0}{h_1}\cos\beta_0 C_1\right] \qquad (23)$$
$$+ 2f^P_{12} + f^P_{21} + \frac{h_0t_0}{h_1t_1}(2f^P_{10} + f^P_{01})$$

in which

$$C_1 = (\cot\alpha_1 + \cot\alpha_2) + \frac{h_1}{h_0\sin\alpha_1}$$
$$C_1^2 = \cot\alpha_1 + \cot\alpha_2 + \frac{h_1}{h_2\sin\alpha_2} + \frac{h_1}{h_0\sin\alpha_1}$$
$$C_1^3 = \frac{h_1}{h_2\sin\alpha_2}$$

When the longitudinal spans of unprestressed folded plates are long, the transverse moment at fold 2 may become greater than that which can be resisted by a slab of ordinary thickness. For such cases, a vertical edge member will be in most cases of considerable benefit. The analysis of a structure formed by the intersection of three plates, although somewhat more complex, follows the same procedure as developed previously. Thus considering plate 0 in figure A8 as a free body, then as in equation (10).

$$f_0 = \frac{1}{t_0}\left(\frac{L}{\pi h_0}\right)^2\left(6P_0 - \frac{2\pi h_0}{L}S_{10}\right) \tag{24a}$$

and

$$f_1 = \frac{1}{t_0}\left(\frac{L}{\pi h_0}\right)^2\left(-6P_0 + \frac{4\pi h_0}{L}S_{10}\right) \tag{24b}$$

The solution of these equations yields

$$2f_0 + f_1 = \frac{6}{t_0}\left(\frac{L}{\pi h_0}\right)^2 P_0 \tag{24c}$$

and

$$f_0 + f_1 = \frac{2L}{t_0 h_0 \pi}S_{10} \tag{24d}$$

If in plate v, P_v is considered as acting downward, then

$$f_1 + 2f_v = \frac{-6}{t_v}\left(\frac{L}{\pi h_v}\right)^2 P_v \tag{24e}$$

$$f_1 + f_v = \frac{2L}{t_v h_v \pi} S_{1v} \tag{24f}$$

In plate 1

$$2f_1 + f_2 = \frac{6}{t_1}\left(\frac{L}{\pi h_1}\right)^2 P_1 - \frac{6}{\pi t_1 h_1}S_{12} \tag{24g}$$

But with the sign convention used in figure A8

$$S_{12} = S_{10} + S_{1V} \tag{24h}$$

Hence if the expression for S_{10} and S_{1V} as given by equations (24d) and (24f) are substituted in equation (24g) on collecting similar terms, we obtain

$$3\left(\frac{h_0 t_0}{h_1 t_1}\right)f_0 + \left(2 + 3\frac{h_0 t_0}{h_1 t_1} + 3\frac{h_v t_v}{h_1 t_1}\right)f_1 + f_2 + 3\frac{h_v t_v}{h_1 t_1}f_v = \frac{6}{t_1}\left(\frac{L}{h_1 \pi}\right)^2 P_1 \tag{25}$$

As in previous derivations it is now necessary to express P_1 in terms of the loads and moments in the adjacent panels. By equation (14a) with the addition of the load on plate V we have

$$V_1 = \frac{W_0+W_1}{2} + \frac{M_0-M_1}{h_0\cos\beta_0} - \frac{M_1-M_2}{h_1\cos\beta_1} + W_V \tag{26a}$$

and

$$V_2 = \frac{W_1+W_2}{2} + \frac{M_1-M_2}{h_1\cos\beta_1} - \frac{M_2-M_3}{h_2\cos\beta_2} \tag{26b}$$

Since part of the vertical reaction at fold 1 is resisted by plate V, the relationship as given by equation (14c) must be modified as

$$P_0 = -(V_1 - P_V)\frac{\cos\beta_1}{\sin\alpha_1} \tag{26c}$$

and

$$P_1 = V_1\frac{\cos\beta_0}{\sin\alpha_1} - V_2\frac{\cos\beta_2}{\sin\alpha_2} - P_V\frac{\cos\beta_0}{\sin\alpha_1} \tag{26d}$$

which by means of equations (24e), (26a) and (26b) can be restated similarly to equation (15a) to

$$\begin{aligned} P_1 = &-\frac{M_1}{h_0\sin\alpha_1} - \frac{M_1-M_2}{h_1}(\cot\alpha_1+\cot\alpha_2) + \frac{M_2-M_3}{h_2\sin\alpha_2} \\ &+\left(\frac{W_0+W_1}{2}\right)\frac{\cos\beta_0}{\sin\alpha_1} - \frac{W_1+W_2}{2}\frac{\cos\beta_2}{\sin\alpha_2} + \left[W_V + \frac{t_V}{6}\left(\frac{h_V\pi}{L}\right)^2(f_1+2f_V)\right]\frac{\cos\beta_0}{\sin\alpha_1} \end{aligned} \tag{26e}$$

Substituting this value in equation (25), we obtain

$$\begin{aligned} &3\frac{h_0t_0}{h_1t_1}f_0 + \left[2 + 3\frac{h_0t_0}{h_1t_1} + 3\frac{h_Vt_V}{h_1t_1} - \frac{t_V}{t_1}\left(\frac{h_V}{h_1}\right)^2\frac{\cos\beta_0}{\sin\alpha_1}\right]f_1 \\ &+ f_2 + \left[\frac{3h_Vt_V}{h_1t_1} - 2\frac{t_V}{h_1}\left(\frac{h_V}{h_1}\right)^2\frac{\cos\beta_0}{\sin\alpha_1}\right]f_V \\ &- \frac{6}{h_1t_1}\left(\frac{L}{h_1\pi}\right)^2\left[+M_2\left(\cot\alpha_1+\cot\alpha_2+\frac{h_1}{h_2\sin\alpha_2}\right) - M_3\frac{h_1}{h_2\sin\alpha_2}\right] \\ &= \frac{3}{t_1}\left(\frac{L}{h_1\pi}\right)^2\left[W_0\cos\beta_0\frac{h_0}{h_1}(\cot\alpha_1+\cot\alpha_2) + (2W_0+W_1+2W_V)\frac{\cos\beta_0}{\sin\alpha_1} - (W_1+W_2)\frac{\cos\beta_2}{\sin\alpha_2}\right] \end{aligned} \tag{27}$$

The preceding equation is applicable to point 1. Another equation must be derived for point 0. Substituting the expression for P_0 given in equation (26c), in equation (24c) we have

$$2f_0 + f_1 = -\frac{6}{t_0}\left(\frac{L}{\pi h_0}\right)^2 (V_1 - P_V)\frac{\cos\beta_1}{\sin\alpha_1} \tag{28}$$

which be means of equations (26a) and (24e) reduces to

$$2f_0 + \left[1 + \frac{t_V}{t_0}\left(\frac{h_V}{h_0}\right)^2 \frac{\cos\beta_1}{\sin\alpha_1}\right] f_1 + \frac{2t_V}{t_0}\left(\frac{h_V}{h_0}\right)^2 \frac{\cos\beta_1}{\sin\alpha_1} f_V + \frac{6}{t_0 h_0}\left(\frac{L}{\pi h_0}\right)^2 \frac{h_0}{h_1\sin\alpha_1} M_2$$
$$= -\frac{3}{t_0}\left(\frac{L}{\pi h_0}\right)^2 \left[(2W_0 + W_1 + 2W_V)\frac{\cos\beta_1}{\sin\alpha_1} + W_0\frac{h_0\cos\beta_0}{h_1\sin\alpha_1}\right] \tag{29}$$

Since the inclusion of plate V introduces another unknown quantity, the longitudinal stress at V, an equation is needed for point V. This equation can be derived on the basis of the compatibility of displacement at point 1. From figure A9,

$$\delta_V = \delta_1\sin\beta_1 - \Delta'_{12}\cos\beta_1 \tag{30a}$$

which be means of the relationship given in equation (5c) reduces to

$$\delta_V = \delta_1\sin\beta_1 - (\delta_0/\sin\alpha_1 - \delta_1\cot\alpha_1)\cos\beta_1 \tag{30b}$$

which by the introduction of the identity

$$\alpha_1 = \beta_1 - \beta_0$$

reduces to

$$\delta_V = \frac{\delta_1\cos\beta_0}{\sin\alpha_1} - \frac{\delta_0\cos\beta_1}{\sin\alpha_1} \tag{30c}$$

Expressing the deflection in terms of the stresses

$$\frac{f_1 - f_V}{h_V} = \frac{f_1 - f_2}{h_1}\frac{\cos\beta_0}{\sin\alpha_1} - \frac{f_0 - f_1}{h_0}\frac{\cos\beta_1}{\sin\alpha_1} \tag{30d}$$

Collecting similar terms

$$\frac{h_V}{h_0}\frac{\cos\beta_1}{\sin\alpha_1} f_0 + \left(1 - \frac{h_V}{h_0}\frac{\cos\beta_1}{\sin\alpha_1} - \frac{h_V}{h_1}\frac{\cos\beta_0}{\sin\alpha_1}\right) f_1 + \frac{h_V}{h_1}\frac{\cos\beta_0}{\sin\alpha_1} f_2 - f_V = 0 \tag{31}$$

Since the equation at any fold contains terms related to the condition at other folds, the presence of the vertical plate at 1 has an effect on the relationship of moments, stresses and loads at fold 2. A review of the derivations leading up to equation (8) will show that this equation is unaffected. However, equation (16) must be modified since the simple relationship established for the plate load in equation (15a) no longer holds. For this point, the value of P_1 as given by equation (26e) must be used. It should be noted that the only difference between equation (26e) and (15a) taking into account the required change in subscript to convert the formula for application at fold 2, is

$$\left[W_V+\frac{t_V}{6}\left(\frac{h_V\pi}{L}\right)^2\left(f_1+2f_V\right)\right]\frac{\cos\beta_0}{\sin\alpha_1} \qquad (32)$$

Consequently with this term being multiplied by $6L^2/h_1\pi^2$ the equation comparable to (16) with no prestressing is

$$\left(\frac{h_1t_1}{h_2t_2}+\frac{t_Vh_V^2\cos\beta_0}{t_2h_1h_2\sin\alpha_1}\right)f_1+2\left(1+\frac{h_1t_1}{h_2t_2}\right)f_2+f_3+2\frac{t_Vh_V^2\cos\beta_0}{t_2h_1h_2\sin\alpha_1}f_V$$

$$+\frac{6}{t_2h_2}\left(\frac{L}{\pi h_2}\right)^2\left(C_2^1M_1+C_2^2M_2-C_2^3M_3+C_2^4M_4\right)$$

$$=\frac{-3}{t_2}\left(\frac{L}{\pi h_2}\right)^2\left[(W_0+W_1)\frac{h_2\cos\beta_0}{h_1\sin\alpha_1}-(W_1+W_2)\left(\frac{\cos\beta_1}{\sin\alpha_2}+\frac{h_2\cos\beta_2}{h_1\sin\alpha_2}\right)+(W_2+W_3)\frac{\cos\beta_3}{\sin\alpha_3}\right. \qquad (33)$$

$$\left.+2\frac{W_Vh_2\cos\beta_0}{h_1\sin\alpha_1}\right]$$

It should be noted that, $M_1=-\frac{W_0h_0\cos\beta_0}{2}$

By means of the previous derivation it is possible through direct or indirect solution of simultaneous equations to determine the longitudinal stress and moment at each fold. In addition to this it is desirable to check on the magnitude of the tangential shear in each plate and when it is excessive to provide reinforcement to resist diagonal tension. Now the determination of the shear at any point in a plate can best be approached by a two-step procedure. In this procedure, it must be recognized that the summation of the tangential shear at any section of a plate due to longitudinal shearing forces acting at the two edges is zero. This can be confirmed by taking a free body of an individual plate, acted on only by longitudinal shears at the two edges. The effect of these forces is to produce fiber stresses in the plate. Because these stresses vary along the length of the plate, shears parallel to the plane of the plates are developed. Since however there are no forces normal to the plane of the plate, by a consideration of statics, the summation of the shears must be zero. As such, the sum of the shears acting at any section of a plate must be equal to that produced by the normal force P.

Equation (13) gives the relationship between the plate forces in two plates and the fiber stresses. Consequently even with the stresses known, the magnitude of the P forces cannot be determined directly. However by commencing at the first exterior plate, employing equation (17) and progressing inward to the next adjacent plate, equation (13) can be reduced to contain only one unknown P. In brief, P_o is first determined by equation (17). Then with this known value, P_1 can be calculated from equation (13). Succeeding values of P can then be determined in order. From these computed P's value, the total shear acting at any section of an individual plate is

$$S_n^T = \frac{L}{\pi} P_n \cos \frac{\pi x}{L} \qquad (34)$$

Since the members are assumed homogeneous, the theoretical distribution of shear will be parabolic varying from zero at one edge to the maximum value at the neutral axis then zero at the other edge. For practical design purpose the ordinary conventional method of treating shear is appropriate, with the average stress considered equal to

$$S_n^T / 0.87\, th$$

In a few exceptional cases in the region of the exterior folds, concentration of shear may occur near the folds due to the effect of the longitudinal edge shears. The magnitude of these longitudinal shears can be determined by starting, as for the P forces, at the exterior plate, in accordance with equation (24d). For fold 2 with no vertical edge beams at point 1

$$f_1 + f_2 = \frac{2}{t_2 h_2}\left(\frac{L}{\pi}\right)(S_2 - S_1) + f_{12}^P + f_{21}^P \tag{35}$$

in which S_1 is already known. The substitution of known values in this equation naturally gives the intensity of the shear at the fold. With a vertical edge beam at point 1 to determine S_{21}, it is first necessary to compute S_{1V} by means of equation (24f). With S_{10} and S_{1V} known, S_{12} can be computed from equation (24h). The substitution of the known values of f_1, f_2 and S_{12} in equation (35) will yield the value of S_{21}.

By conventional flexural formulas, it can be shown that the variation of shear at a cross section in a rectangular beam due to a shearing force varying sinusoidally applied along one edge is

$$S = S_n\left[1 - 4\left(\frac{y}{h}\right) + 3\left(\frac{y}{h}\right)^2\right]\cos\frac{\pi x}{L} \tag{36}$$

where y is measured from the loaded edge. A graphical interpretation of formula (36) is given in figure A10. It should be noted that the shear decreases from its maximum value at the loaded edge to zero at the other edge. The maximum value of shear in the opposite direction occurs at y/h = 0.67.

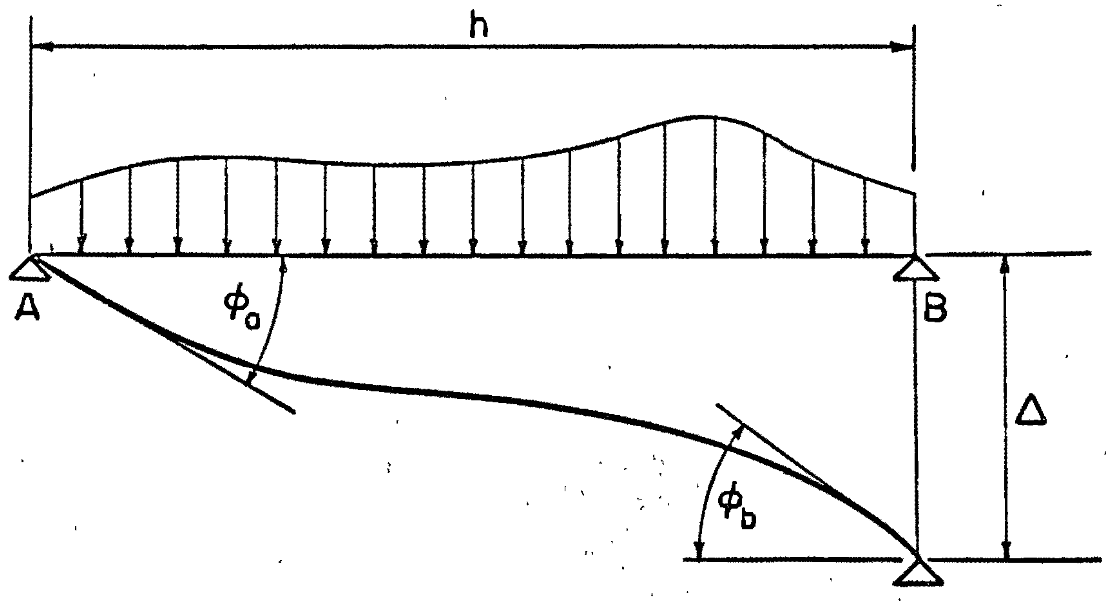

Fig. A1

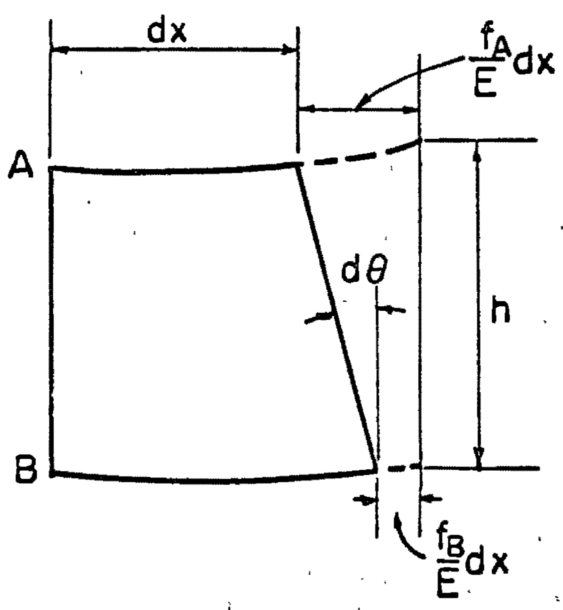

Fig. A 2

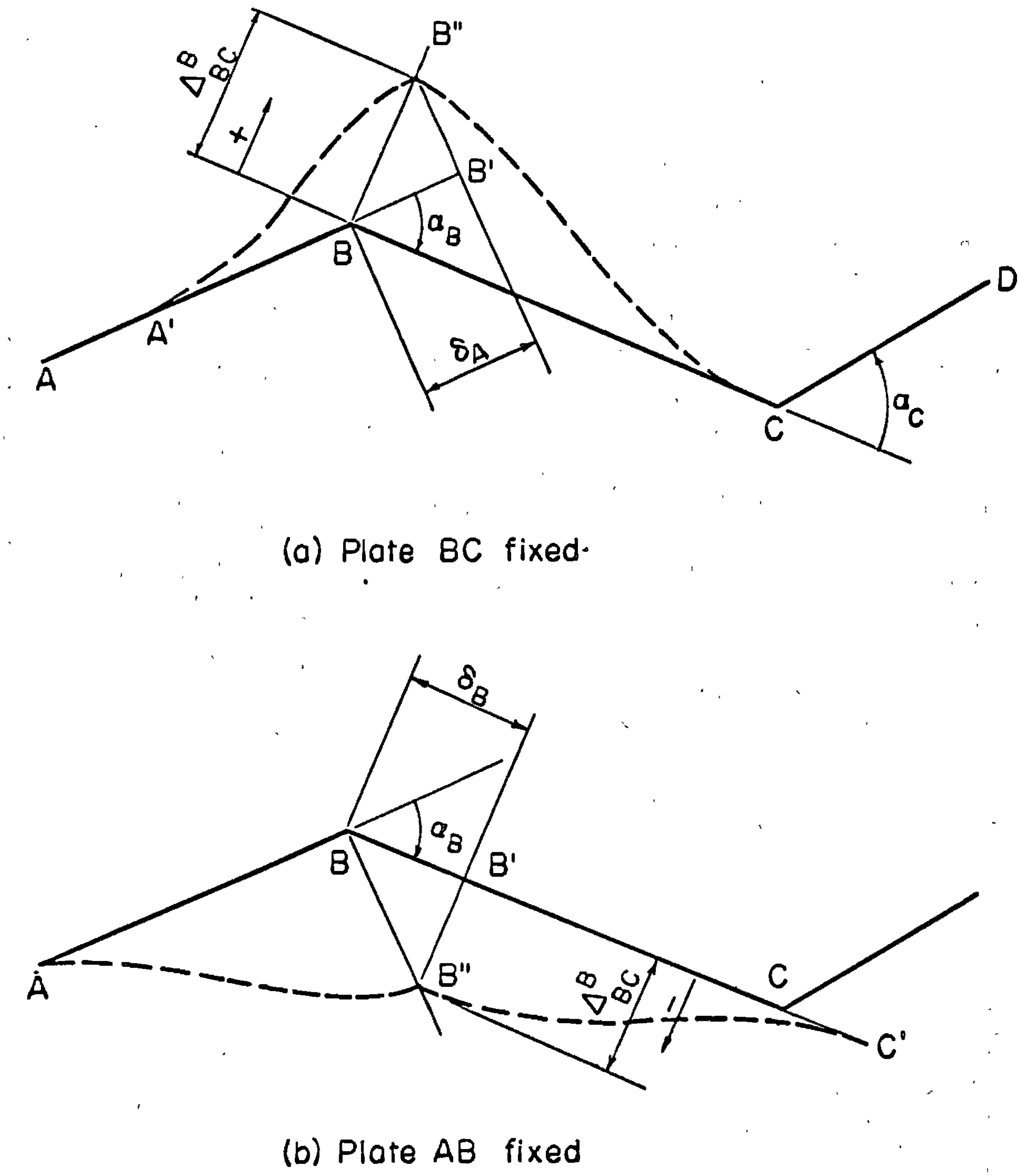

B''
Δ^B_{BC}
+
B'
a_B
B
D
A'
δ_A
A
a_C
C
(a) Plate BC fixed
δ_B
a_B
B
B'
A
B''
Δ^B_{BC}
C
–
C'
(b) Plate AB fixed

Fig. A3

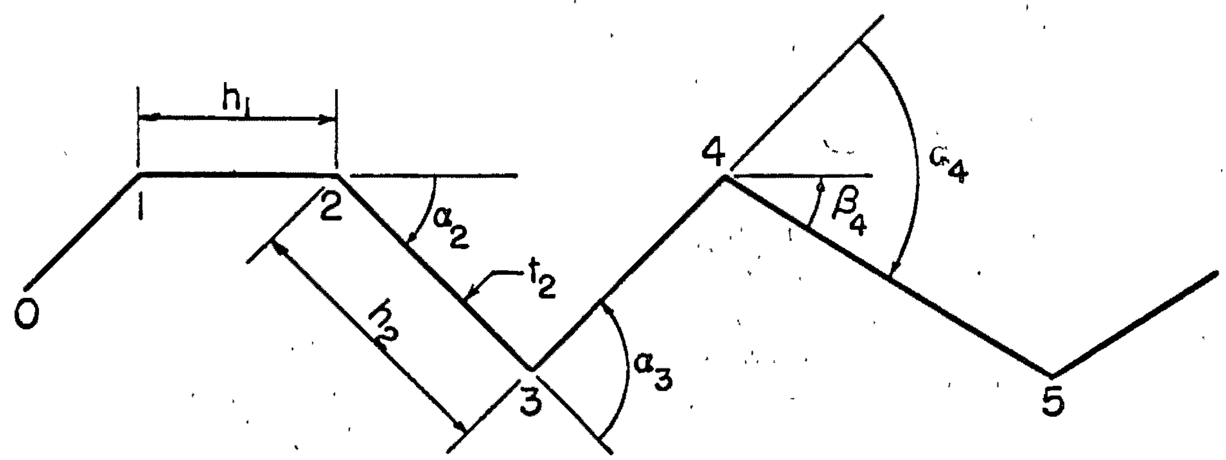

Fig. A4

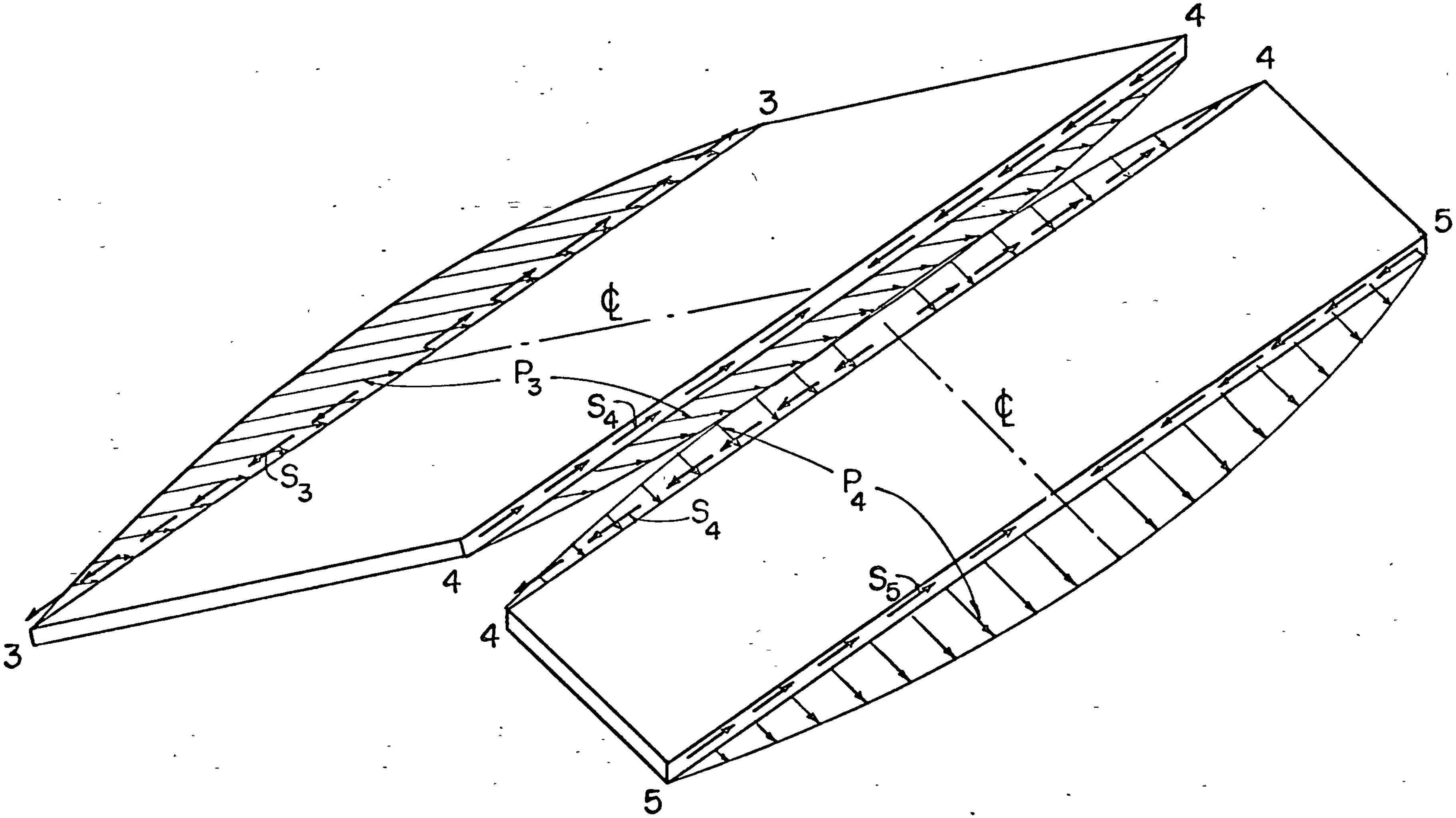

Fig. A5

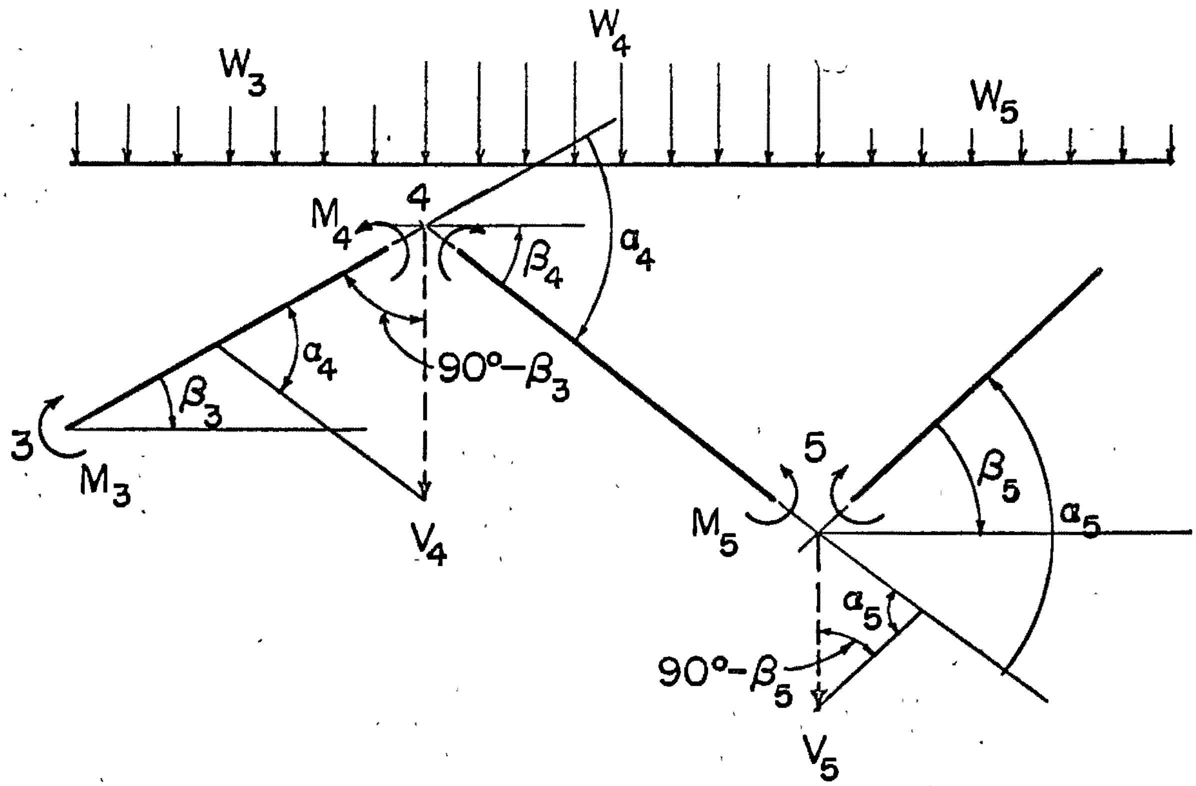
W4
W3
W5
4
M4
β4
α4
α4
90°−β3
β3
3
M3
V4
5
β5
M5
α5
α5
90°−β5
V5

Fig. A6

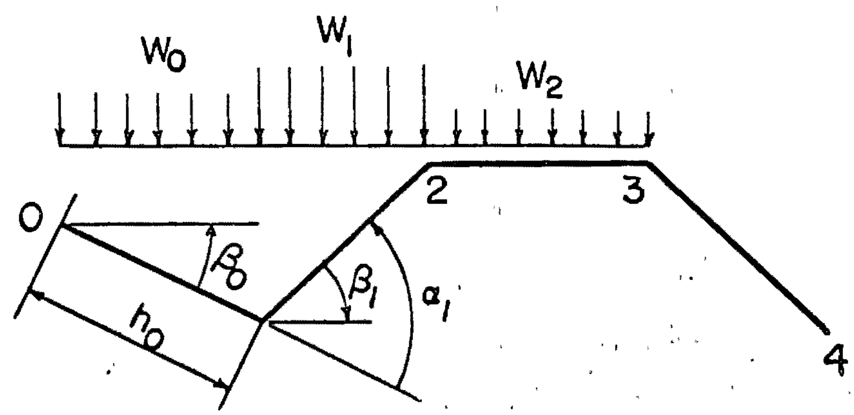
W1
W0
W2
2
3
0
β0
β1
α1
h0
4

Fig. A7

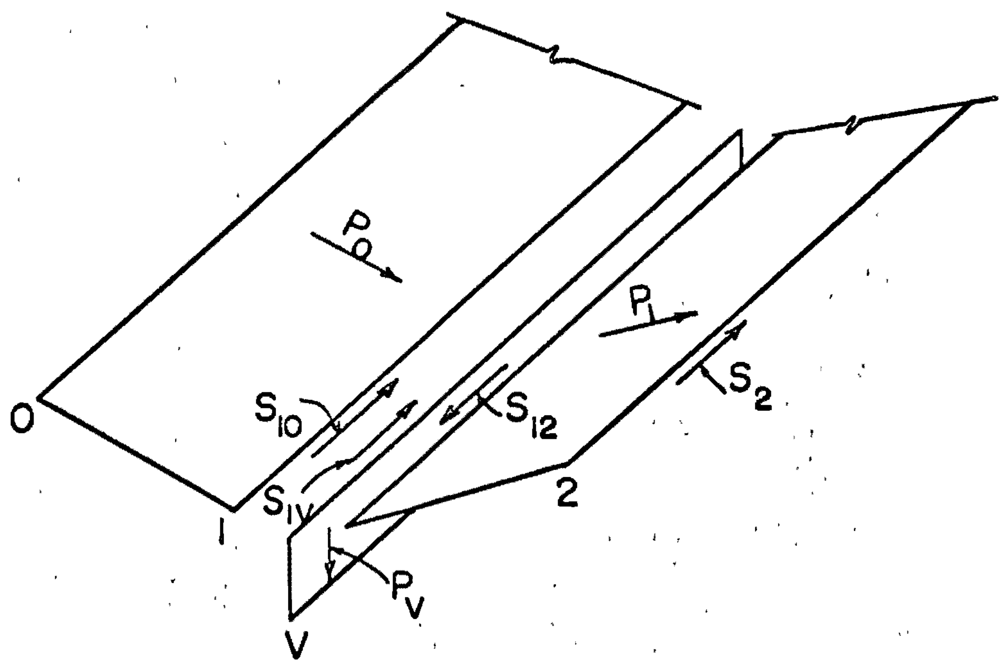

Fig. A8

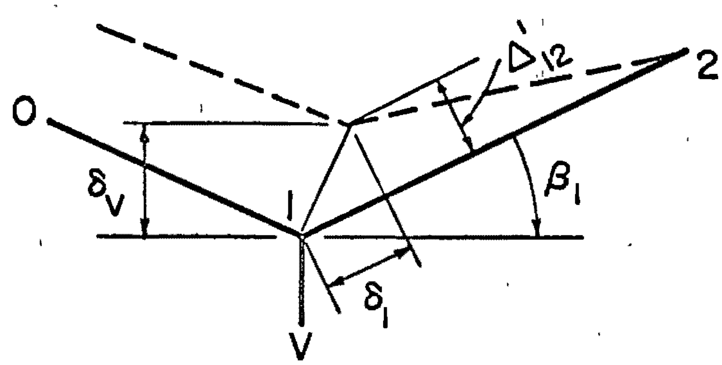

Fig. A9

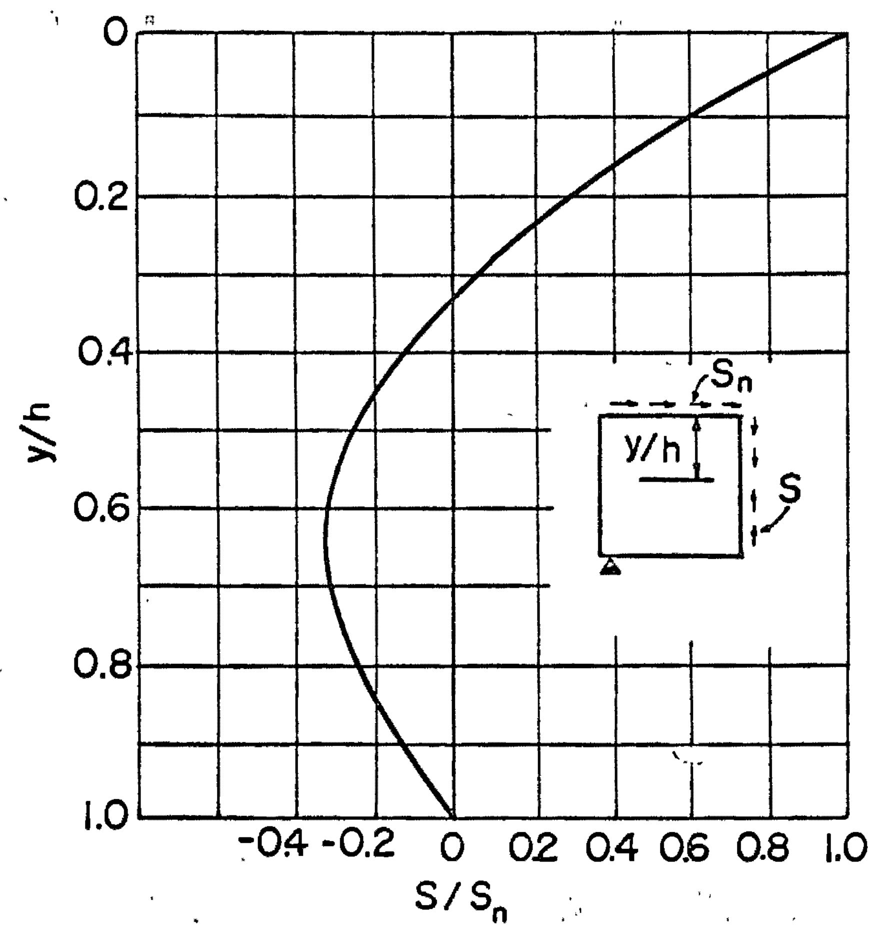

Fig. A10

Funicular surface structures: a computer graphics approach

E. SHAVIV [1] and D. P. GREENBERG [2]

Summary This paper describes the problem to find the shape of the middle surface of a shell when the loading and the stress resultants distributions is known. Differential equations are set up where are solved using the finite difference technique. Several solutions are presented by means of a electronic computer and plotter.

1. Introduction

Current practice in modern architectural design of surface structures is first to arbitrarily assume a shape for the surface, and then calculate the resulting stress distribution for an assumed state of loading.

It would seem more logical to use an inverse approach; that is, assume a stress distribution for a given state of loading, and then determine the required geometry to satisfy the equilibrium requirements. This paper illustrates the latter approach by both deriving the equations and demonstrating their advantages for different types of surface structures. Numerical results are transformed and presented graphically by using an IBM 1130 digital computer in combination with a CALCOMP 565 plotter.

There are several disadvantages to using the conventional procedure for determining the size and shape of surface structures. After calculating the stress distribution for the assumed geometry and loading, it is then necessary to provide edge members to equilibrate the unbalanced forces at the boundaries. In addition to introducing bending stresses which penetrate into the surface of the shell and require a thickening of the shell near the edges, the thickness of the edge members generally destroy the elegance of a thin shell and create an illusion of a more massive structure. Also, the thickness of the membrane except near the edges is normally constant, whereas the stress distribution, except for very special cases, e.g., hypar with uniform load, varies significantly from point to point.

A better approach would be analagous to making a soap bubble experiment. For this, the geometry of the boundaries is fixed, and the stress distribution of the membrane, i.e., the tension of the soap film, is equal in all directions. Thus the resulting surface which is formed for a given loading condition has the minimum strain energy.

There would be considerable architectural and structural advantages if one could accomplish the same results mathematically as in a soap bubble experiment. Thus, if the equations are rearranged such that the geometrical edge conditions and the stress distribution are known,

[1] Former graduate student, Architectural Science Program, Cornell University, Ithaca, New York.

[2] Assistant Professor and Head, Architectural Science Program, Cornell University, Ithaca, New York.

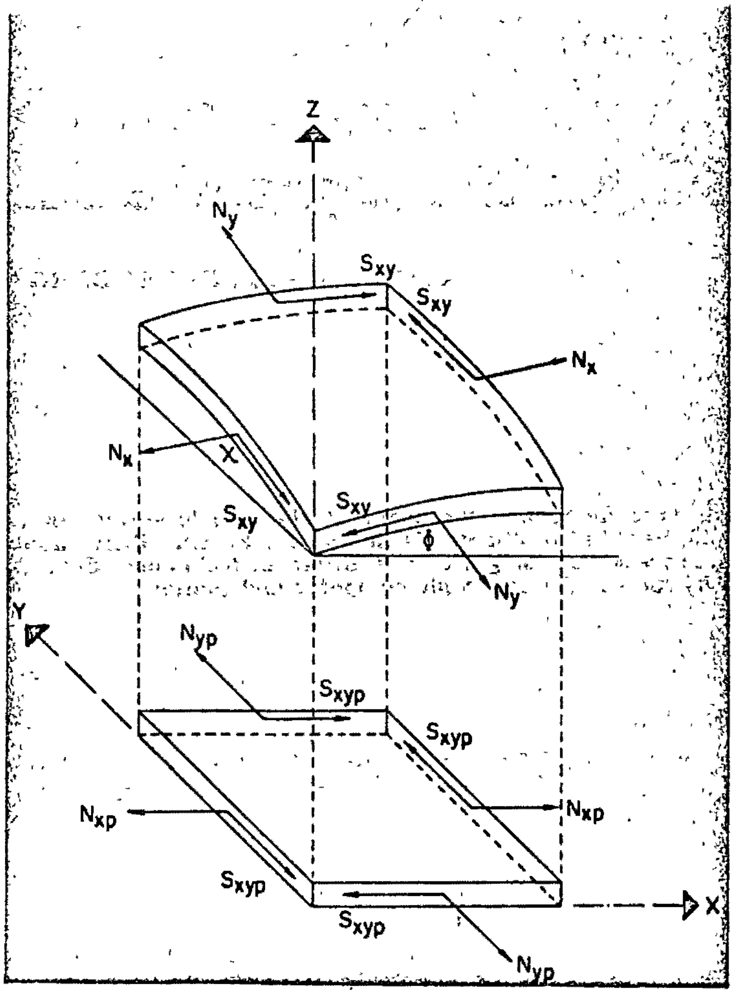

Fig. 1. Shell Element.

a surface geometry can be found to fit these conditions. This would result in more efficient use of shell material as the stress magnitudes could be predetermined throughout the shell. However, the architectural advantages are even greater, for if one can demand that the membrane stresses of compression and tension normal to the boundaries diminish to zero at the boundaries, then the size of the required edge beams will be greatly reduced, and the appearance of the structure will be enhanced. It is the purpose of this article to show this approach, both mathematically and visually.

2. Mathematical Properties and Analysis

The following analysis is based upon the general assumptions of membrane theory which are not repeated herein. Only in-plane stress resultants are assumed.

The well-known membrane equations resulting from equilibrium (Fig. 1) in three directions are (3):

$$(\Sigma x = 0) \quad \frac{\partial N_{xp}}{\partial x} + \frac{\partial S_{xyp}}{\partial y} + P_{xp} = 0 \qquad [1]$$

$$(\Sigma y = 0) \quad \frac{\partial N_{yp}}{\partial y} + \frac{\partial S_{xyp}}{\partial x} + P_{yp} = 0 \qquad [2]$$

$$(\Sigma z = 0) \quad N_{xp}z_{xx} + 2S_{xyp}z_{xy} + N_{yp}z_{yy} = -P_{zp} + P_{xp}z_x + P_{yp}z_y \qquad [3]^*$$

where:

z = coordinate in vertical direction
x, y = orthogonal horizontal coordinates
N_{xp} = projected normal stress resultant in the x-direction
N_{yp} = projected normal stress resultant in the y-direction
S_{xyp} = projected shear stress resultant
P_{xp} = projected uniform load in x-direction
P_{yp} = projected uniform load in y-direction
P_{zp} = projected uniform load in z-direction

* The notation z_{xx} represents the second partial derivative $\partial^2 z/\partial x^2$ in the x-direction. Similar notation is used for all partial derivatives of the vertical direction z.

For dead load only, which is a uniform gravity load per unit of surface area for a shell of constant thickness, equation [3] becomes:

$$N_{xp}z_{xx} + 2S_{xyp}z_{xy} + N_{yp}z_{yy} = -P_z\sqrt{1 + z_x^2 + z_y^2} \qquad [3a]$$

where P_z = vertical load per unit of surface area.

The relations between the projected stresses and the membrane stresses are given by:

$$N_{xp} = N_x \frac{\sqrt{1 + z_y^2}}{\sqrt{1 + z_x^2}} \qquad [4]$$

$$N_{yp} = N_y \frac{\sqrt{1 + z_x^2}}{\sqrt{1 + z_y^2}} \qquad [5]$$

$$S_{xyp} = S_{xy} \qquad [6]$$

where:

N_x = in-plane normal stress resultant in the x-direction
N_y = in-plane normal stress resultant in the y-direction
S_{xy} = in-plane shear stress resultant.

Equation [3] is a second-order, quasi-linear, partial differential equation with variable coefficients. This type of partial differential equation may be mathematically classified according to then sign of the discriminant, δ_{xy},

where:

$$\delta_{xy} = N_{xp}N_{yp} - S^2_{xyp} \qquad [7]$$

According to this classification, the equations are (4):

I. Elliptic if $\delta_{xy} > 0$
II. Parabolic if $\delta_{xy} = 0$
III. Hyperbolic if $\delta_{xy} < 0$

Equation [3] may be transformed into a general system of coordinates by using the following equations:

$$\xi = \Phi(x, y) \quad ; \quad \eta = \chi(x, y) \qquad [8]$$

where, ξ, η are independent variables.

Thus,

$$N_{\xi p}z_{\xi\xi} + 2S_{\xi\eta p}z_{\xi\eta} + N_{\eta p}z_{\eta\eta} = -P_{zp} + P_{\xi p}z_\xi + P_{\eta p}z_\eta \qquad [9]$$

where:

$N_{\xi p}$, $N_{\eta p}$ and $S_{\xi\eta p}$

are the projected stresses in the ξ, η system of co-ordinates. The relations between the stress resultants for the two systems of coordinates are given by:

$$N_{\xi p} = N_{xp}\Phi_x^2 + 2S_{xyp}\Phi_x\Phi_y + N_{yp}\Phi_y^2 \qquad [10a]$$

$$S_{\xi\eta p} = N_{xp}\Phi_x\chi_x + S_{xyp}[\Phi_x\chi_y + \Phi_y\chi_x] + N_{yp}\Phi_y\chi_y \qquad [10b]$$

$$N_{\eta p} = N_{xp}\chi_x^2 + 2S_{xyp}\chi_x\chi_y + N_{yp}\chi_y^2 \qquad [10c]$$

Noting that the discriminant, $\delta_{\xi\eta}$, of equation [9] is:

$$\delta_{\xi\eta} = N_{\xi p}N_{\eta p} - S^2_{\xi\eta p} \qquad [11]$$

and from substitution of equations [10],

$$\delta_{\xi\eta p} = \delta_{xy}(\Phi_x\chi_y - \Phi_y\chi_x)^2 \qquad [12]$$

Since the term $(\Phi_x\chi_y - \Phi_y\chi_x)^2$, must always be positive, the sign of the discriminant in each system of coordinates is similar for any set of stress resultants, and thus the type of equation is independent of the coordinate system.

For simplicity, if the functions, Φ, χ, of equation [8] are chosen so that the direction of the principal stresses are achieved, the resulting shear stresses are zero. The resulting surfaces may be classified according to the mathematical properties, and thus the principal stresses, of the governing differential equation [9]. Using this classification, there are three distinct types of structures:

I. Elliptic Structures:

The principal stress resultants, are either both tensile or compressive.

$$\text{Thus, } \delta_{\xi\eta} = N_{\xi p} \cdot N_{\eta p} > 0$$

II. Parabolic Structures:

The principal stress resultant in one direction equals zero. Thus, $\delta_{\xi\eta} = 0$.

III. Hyperbolic Structures:

The principal stress resultants are of opposite form, one tensile and the other compressive.

$$\text{Thus, } \delta_{\xi\eta} = N_{\xi p} \cdot N_{\eta p} < 0$$

It should be emphasized that this classification is based on the mathematical properties of the differential equation, and thus depends upon the stress distribution, and not upon the geometrical configuration of the surface.

In order to more clearly understand the properties of the three types of surface structures, it is advantageous to introduce the notion of characteristic curves. Structurally, these characteristic curves define the particular directions on the surface where the normal stresses perpendicular to these directions are zero. It can be shown that the equation of the characteristic curves in the x-y coordinate system is given by (4):

$$\omega_{1,2} = \frac{dy}{dx} \qquad [13]$$

where, $\omega_{1,2}$, is the solution to the following quadratic equation:

$$N_{xp}\omega^2 - 2S_{xyp}\omega + N_{yp} = 0 \quad [14]$$

The number of real solutions to equation [14] depends on the value of the discriminant, δ_{xy}. For hyperbolic structures, two solutions exist, and there are two families of characteristic curves. There is only one solution for the parabolic case and thus only one family of curves. No solution, and no characteristic curves exist for the elliptic case.

This may be graphically illustrated for the special case of an orthogonal coordinate system by using the Mohr's circle technique for the analogous states of stress of each type of equation (see Fig. 2).

It is advantageous to use the characteristic curves to define the boundaries of the surface. Thus, the edge beams will only be subjected to axial shear stresses, and may be substantially reduced in size and appearance. This is possible only with the hyperbolic and parabolic structures, as normal forces must exist on any boundaries of the elliptic structures.

In the following discussion, equation [9] is simplified to:

$$N_{\xi p} z_{\xi\xi} + 2S_{\xi\eta p} z_{\xi\eta} + N_{\eta p} z_{\eta\eta} = -P \qquad [15]$$

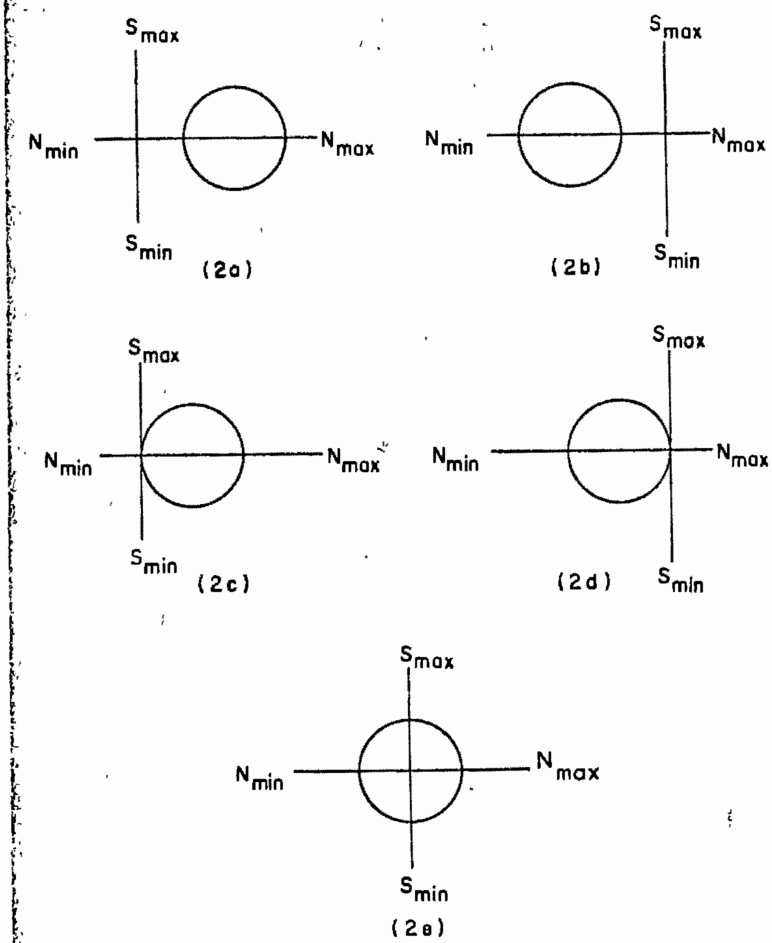

Fig. 2. Mohr's Circle for Principal Forces.

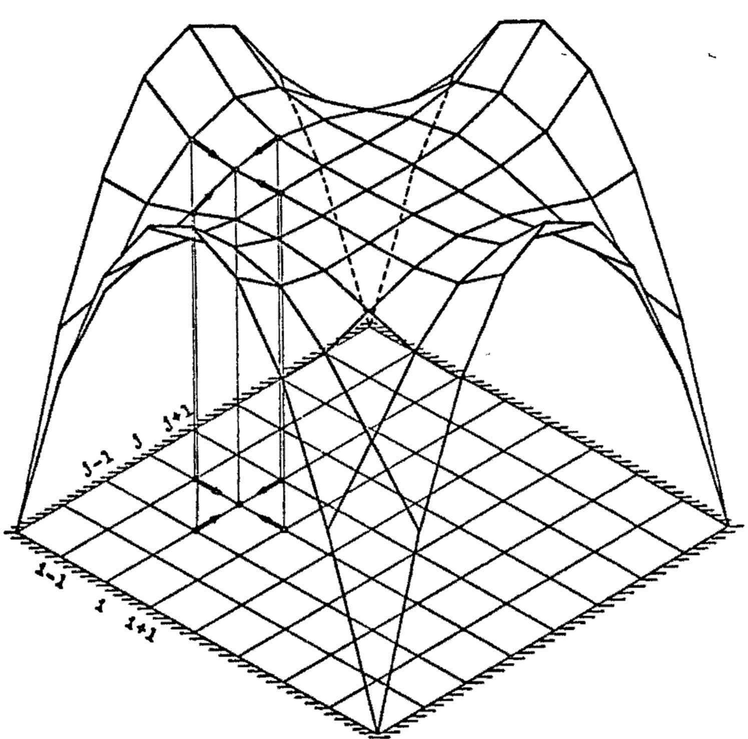

Fig. 3. Elliptic Structure.

where,

$$P = P_{\xi p} - P_{\xi p} z_\xi - P_{\eta p} z_\eta \qquad [16]$$

Note that for shallow shells subjected to vertical loading only, $P = P_\xi$ (see equation [3a]). For non-shallow shells, the terms involving the first derivatives cannot be neglected, and techniques must be used to solve the resulting non-linear equations.

I. Elliptical Structures

As has been previously mentioned, there are no characteristic curves for the elliptic structures since there are normal stresses in all directions (Figs. 2a and 2b). This type of equation where, $N_{\xi p} N_{\eta p} > 0$, is a boundary value problem, and the boundary conditions must be known and continuous along the closed boundary of the surface.

When written in the direction of the principal stresses, equation [15] becomes:

$$N_{\xi p}\, z_{\xi\xi} + N_{\eta p}\, z_{\eta\eta} = -P \qquad [17]$$

Equation [17] may be transformed into a finite difference equation, such that:

$$z_{i,j} = \frac{z_{i,j+1} + z_{i,j-1} + z_{i+1,j} + z_{i-1,j}}{4} + \frac{P\Delta^2}{4N} \qquad [18]$$

where:

$$\Delta_\xi = \Delta_\eta = \Delta$$
$$N_\xi = N_\eta = N$$

Equation [18] is written for each interior nodal point on the surface of the shell resulting in a set of n simultaneous equations, where n equals the number of interior nodal points. (Fig. 3). Thus the elevation of any interior point on the surface depends upon the elevations of all points on the closed boundary. For the same reason, the effect of any one point on the boundary is relatively insignificant and diminishes rapidly with distance. For the figure shown, the properties on all four boundaries must be prescribed.

II. Parabolic Structures

For the parabolic structure, the direction of the characteristic curve and the principal stress with the maximum absolute value is identical (Figs. 2c and 2d). For this direction, equation [15] degenerates into a two-dimensional equation and becomes:

$$N_{\xi p} z_{\xi\xi} = -P \qquad [19]$$

For all other directions, the equation is extremely unstable, and has not been solved for this discussion.

III. Hyperbolic Structures

For the hyperbolic case, there are two sets of characteristic curves, and normal forces do not exist in two directions (Fig. 2e). In the direction of the characteristic curves, equation

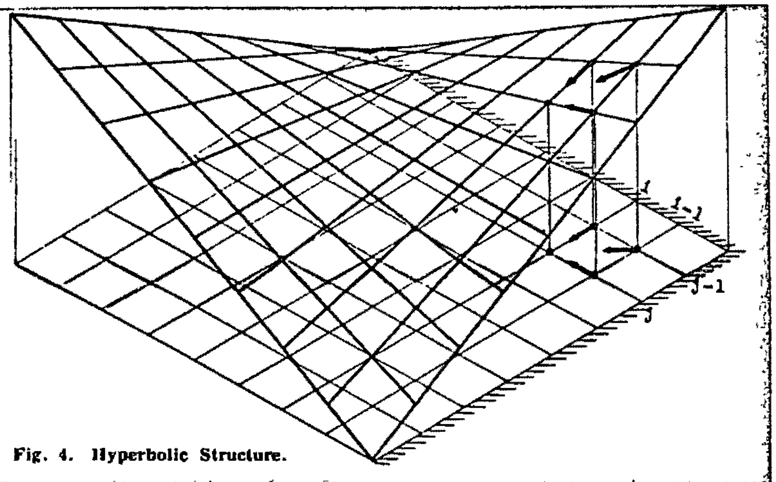

Fig. 4. Hyperbolic Structure.

[15] reduces to:

$$2S_{\xi\eta p} z_{\xi\eta} = -P \qquad [20]$$

Transforming equation [20] into finite difference form,

$$z_{i,j} = z_{i,j-1} + z_{i-1,j} - z_{i-1,j-1} - \frac{P\Delta\xi\Delta\eta}{2S_{\xi\eta p}} \qquad [21]$$

It can be seen that the solution to equation [21] depends upon known starting conditions on two adjacent boundaries (Figure 4). This is a typical characteristic of the resulting initial value problem. Geometrically, this means that the elevation of any interior point on the shell surface is determined by the boundary elevations of the two characteristic curves passing through that point. This illustrates the known fact that the boundary disturbances in a hyperbolic surface will penetrate through the shell only along the «characteristic curves». This further allows only *two* conditions to be predetermined.

It should be noted that composite surfaces consisting of two or more types may exist, but that the boundaries described by their common intersection are governed by the parabolic equation.

Both equations [18] and [21] have been solved on an IBM 1130 computer using standard mathematical techniques. The numerical results have been converted to graphical output by a CALCOMP 565 plotter and are discussed below.

3. Examples of Graphical Output

To obtain the following figures, an orthogonal x-y coordinate system with equal mesh spacing was used for simplicity only. The plan projections of all figures shown are square.

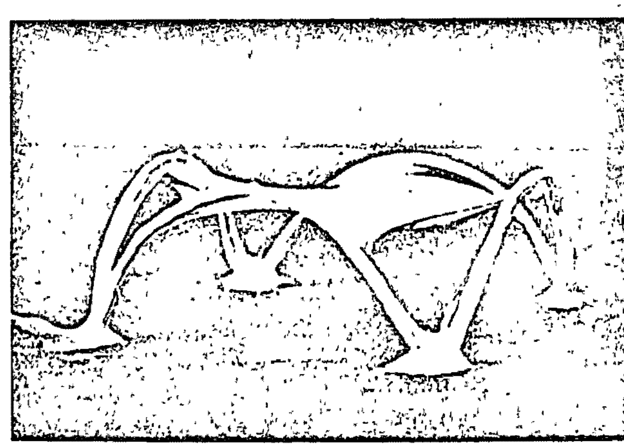

Fig. 5. Elliptic Structure Soap Bubble.

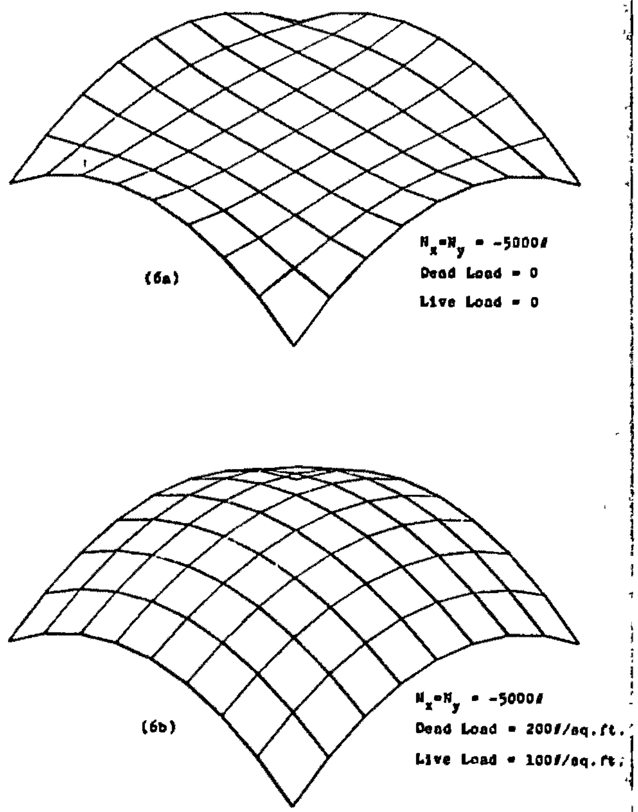

Fig. 6. Elliptic Structures.

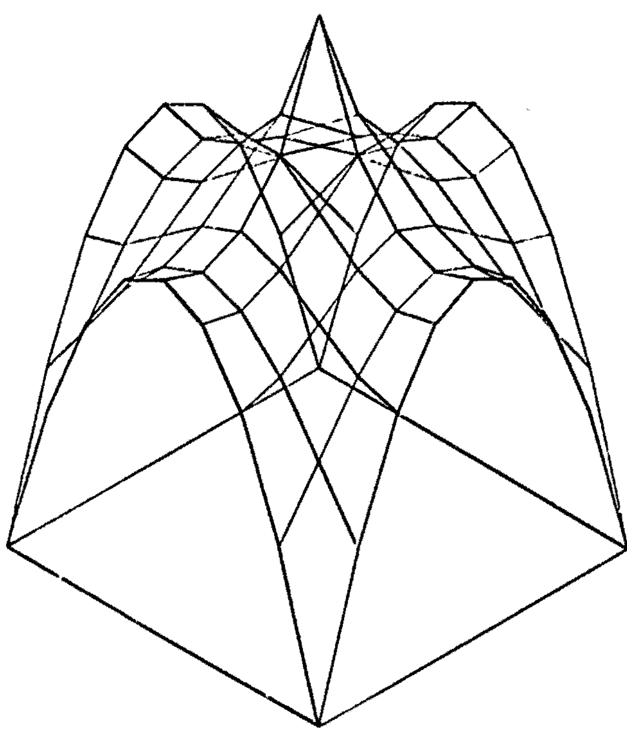

Fig. 7. Elliptic Structure with Lantern.

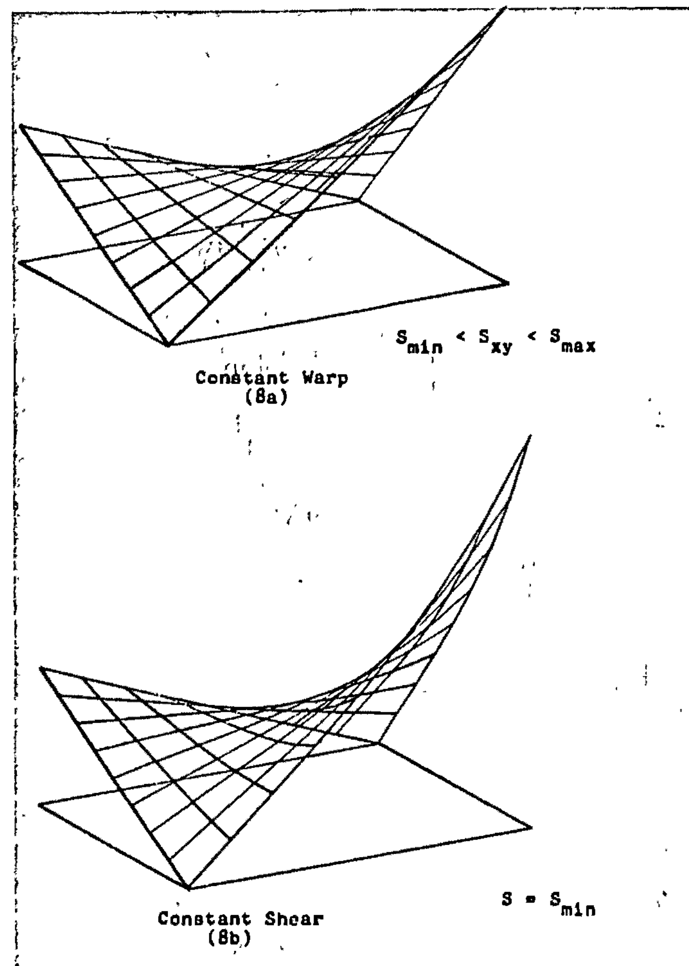

Fig. 8. Hyperbolic Structures.

Elliptic Structures

Figure (6a) shows the graphical output for the solution to equation [18] for the particular case of equal horizontal tension stress resultants and zero applied loading. It becomes obvious that the resulting geometry is similar to that of a shallow soap bubble with identical boundary conditions (Fig. 5). In general, for *shallow* structures subjected to uniform vertical loading, the resulting geometry is also similar to that of a soap bubble experiment with internally applied pressure.

Figures (6) show two elliptic structures, one anticlastic surface and the other synclastic. Both figures were generated by assuming similar boundary conditions and stress distribution. However, as the magnitude of the vertical load increases, the surface changes from anticlastic to synclastic. This further emphasizes the difference between the proposed classification, which depends on the assumed stress distribution, and a geometrical classification.

As is typical in boundary value problems, boundaries may also exist inside the domain. Thus it is possible to obtain the required geometry for a lantern, post, or for concentrated loads. Figure 7 shows the graphical results of this type of case.

Hyperbolic Structures

For the particular case of hyperbolic structures, a major advantage of the method proposed in this paper becomes evident when compared to the conventional approach.

Using the conventional approach, assume the surface to have a constant warp, the geometry of a hyperbolic paraboloid (Fig. 8a). Thus,

$$z = kxy \qquad [22a]$$

where,

$$k = \frac{h}{ab} = \text{constant «warping coefficient»} \qquad [22b]$$

and

$$\frac{\partial^2 z}{\partial x \partial y} = k \qquad [22c]$$

Substitution into equation [20] yields,

$$S_{xy} = -\frac{P}{2k} \qquad [23]$$

Obviously then, when P is a variable, S_{xy} must also be a variable. However, if S_{xy} is a variable, then according to equations [1] and [2], normal forces must also exist. Therefore, for a surface with a constant warping coefficient, normal forces must exist on at least two of the four boundaries, and edge members must be provided to accommodate these forces.

If the geometry is not predetermined, one can demand that the shearing stresses are constant, and then calculate the required geometry from equations [20] or [21]. The resulting geometry is shown in Figure 8b for an assumed constant shear stress equal to the minimum shear of the previous figure (Fig. 8a).

A similar comparison is shown in Figures 9a and 9b. For this case, the vertex elevations of both figures are equal. In Figure 9a, the warping coefficient is constant, and the minimum shear is S_{min}. The maximum shear is 1.58 S_{min}. In Figure 9b, the shear stress is assumed constant, and equals 1.28 S_{min}.

It should be emphasized that the procedure is not restricted to straight line boundaries. This is illustrated in Figure 10a and 10b where the initial edge conditions are convex and concave parabolic curves respectively.

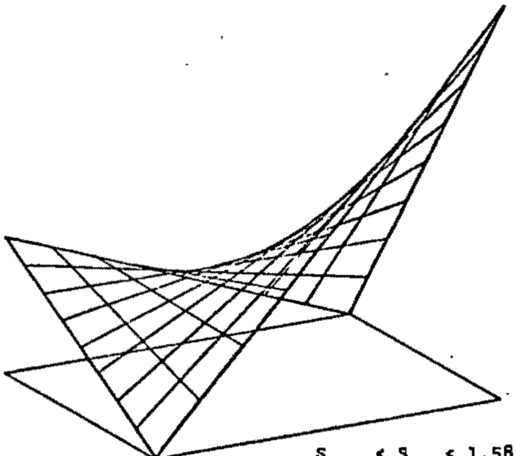

Constant Warp
(9a)

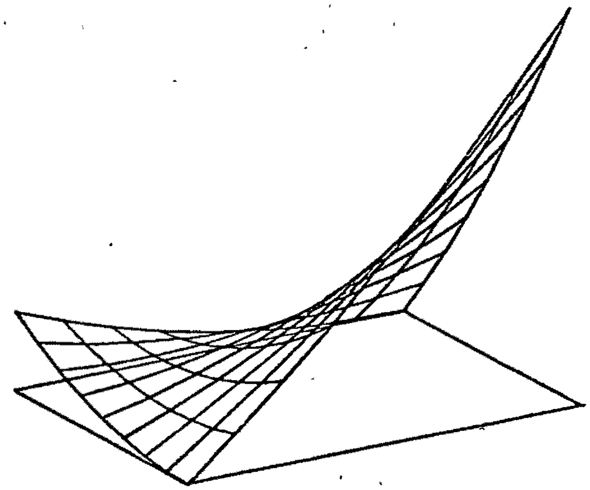

(10a)

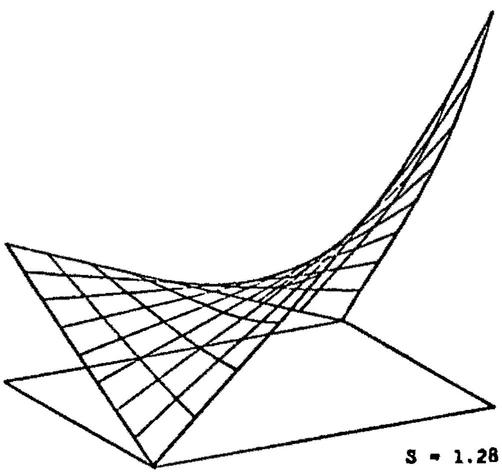

Constant Shear
(9b)

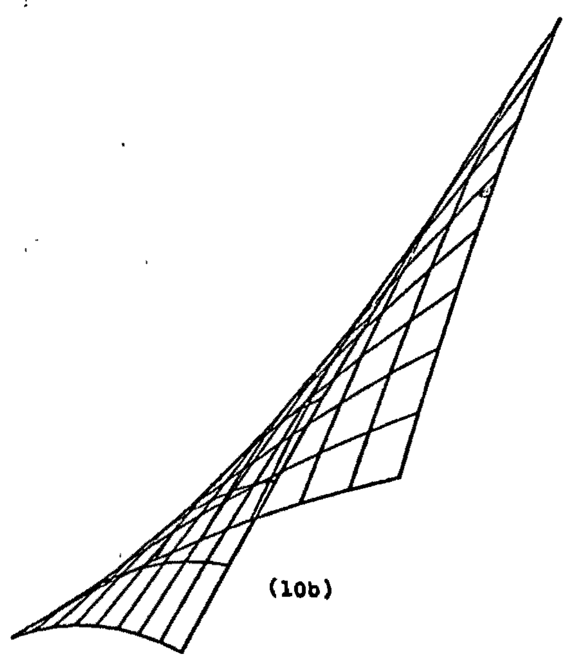

(10b)

Fig. 9. Hyperbolic Structures.

Fig. 10. Hyperbolic Structures with Curved Edges.

4. General

The graphical output may be drawn as an isometric projection from any angle ot view. Similarly, the mesh size is variable. Lines interconnecting the mesh points may be straight or curved. In order to generate curved lines a Lagrangian interpolation formula was used (5). An illustration of this type is shown in Figure 11. For comparison, results of a soap bubble experiment with the same boundary conditions are included (Fig. 12).

5. Conclusions

The procedure presented in this paper is as follows:

1) Derive the general differential equations for shell membrane forces.

2) Invert the differential equations of [1] so that the geometry is unknown and the stresses are known.

3) Use numerical methods techniques to convert the differential equations [2] to finite difference equations according to the type of structure.

4) Solve the finite difference equations - [3] - using standard numerical techiques (iteration, relaxation, etc.).

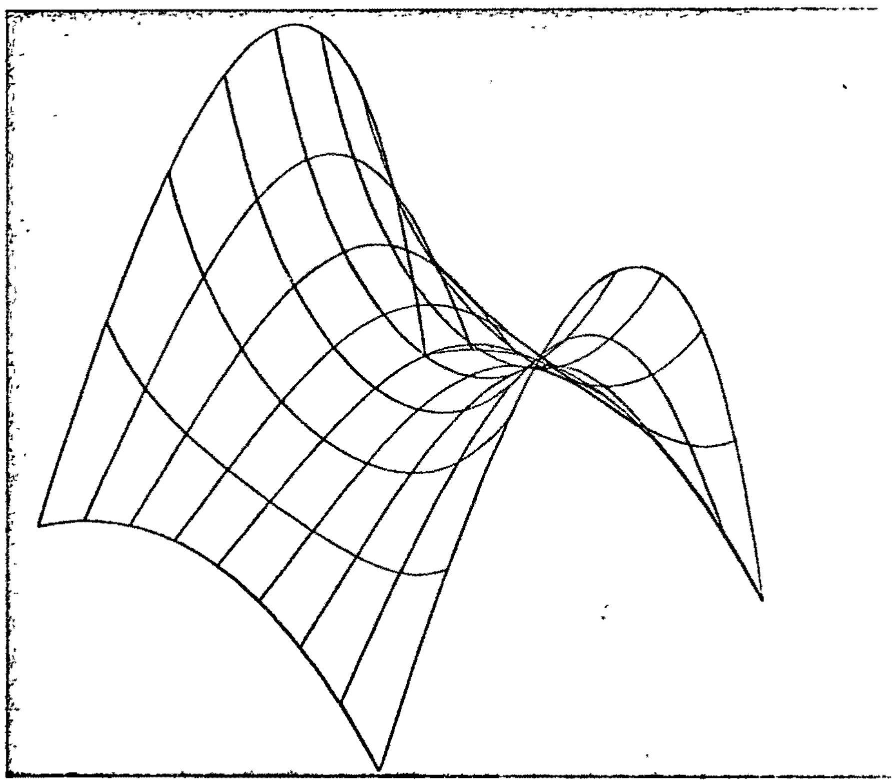

Fig. 11. Elliptic Surface.

5) Through the interaction of both the computer and plotter, present the solutions in graphical form.

The procedure is applicable to all types of shells and pneumatic structures, and can be adapted to suspension structures.

According to the governing differential equations, all structures may be classified into three categories, depending upon their predetermined stress distribution. These are the elliptic, parabolic, and hyperbolic structures.

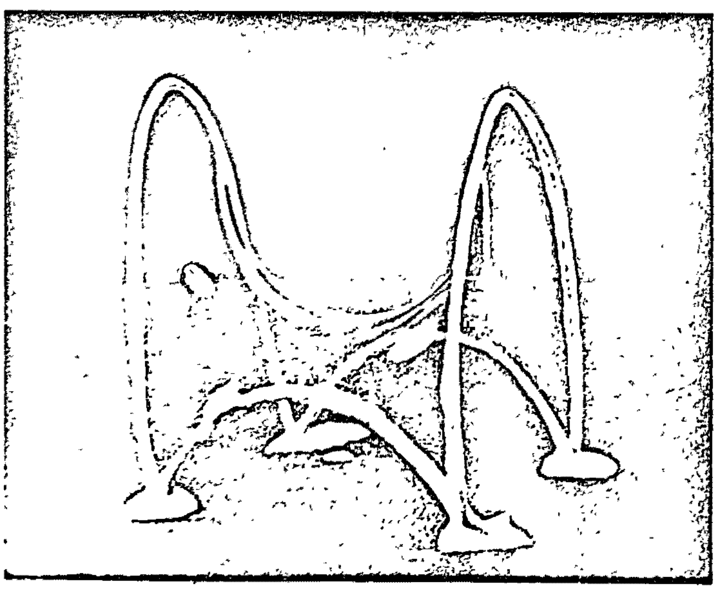

Fig. 12. Elliptic Structure Soap Bubble.

To solve for the geometry of an elliptic structure, the boundary conditions along a closed boundary must be given. For this type, where the stresses are either both tensile or both compressive, there are no characteristic curves. Normal forces must exist at the edges, and thus edge members are required. The shape of the surface is influenced by all points along the boundary. Since internal boundary conditions may also be prescribed, surfaces with lanterns, concentrated loads, or posts may be analyzed.

The parabolic structure is a degenerate case as only one type of normal stress exists (either tension or compression). Thus, only one family of characteristic curves exist for this type.

For the hyperbolic type of structure, two families of characteristic curves exist. When the boundaries and characteristic curves are similar, the geometry of hyperbolic structures, where the principal stresses are of opposite sign, depends on the boundary conditions of two adjacent sides only. The conditions along the entire closed boundary cannot be specified. The vertical elevation at any point on the surface depends only on the predetermined boundary elevations of the two characteristic curves passing through that point. For a given load condition, the boundaries may be chosen so that normal forces do not exist on the edges, and thus the size of the edge beams may be substantially reduced. This factor has decided architectural advantages.

In general, by using the inverse approach, the resulting structure will have a better stress distribution and a more efficient use of material than analagous surfaces obtained in the conventional approach.

The use of the computer to obtain solutions to the governing differential equations and the graphical presentation of the solutions has been demonstrated. There are numerous advantages inherent in this procedure including speed, accuracy, and visual presentation, but perhaps the most important aspect is the possibility of a man-machine interaction which ultimately leads to a better understanding of structural behavior and a better conceived architectural design.

Bibliography

(3) PARME, A. L.: «Hyperbolic Paraboloids and Other Shells of Double Curvature», Proceeding Paper 1057, American Society of Civil Engineers, Vol. 82, No. ST5, September 1956.

(4) COURANT, R., and HILBERT, D.: «Methods of Mathematical Physics», Volume II: Partial Differential Equations by R. Courant, John Wiley and Sons, Inc., New York, 1962.

(5) ISAACSON, E., and KELLER, H. B.: Analysis of Numerical Methods», John Wiley and Sons, Inc., New York, 1966.

Analysis of circular conoids

A. SINGHAL [1] and M. GAGNON [2]

Summary This paper presents a general numerical procedure for the analysis of circular conoids undergoing bending deformation. The influence of rise, length, thickness, Poisson's ratio and mesh size over the stress quantities of the shell are investigated. A set of two governing partial differential equations is reduced to a stiffness matrix type formulation using linear central finite difference techniques. The shell deflections and finally the stresses are obtained by using the flow-graph method of solution.

Nineteen different simply supported circular truncated conoids, subjected to uniformly distributed loads, have been numerically analyzed. The results show that the maximum radial deflections for geometrically similar conoids with various rises always occur at a constant distance from the mid-length point and closer to the lower rise end. The maximum radial deflections for conoids with various lengths always occur at various distances away from the mid-length point and closer to the low rise end. The influence of thickness is very pronounced. For moderately thin shells, the maximum deflection usually occurs along the crown of the shell. However, for very thin shells, the maximum deflections occur at both sider of the crown at equal distances away from the crown, this distance being larger for thinner shells. The influence of Poisson's ratio is also very pronounced being larger than 5 % for bending moments (M_r) for a variation of Poisson's ratio from either 0.0 to 0.15 or 0.15 to 0.30. Furthermore, Abu-Sitta's hypotesis han been numerically verified. The study of the influence of mesh size shows that using the central finite difference echeme even with a fairly coarse mesh of base 10, leads to a satisfactorily accurate result within 2 %.

1 Introduction

Conoid shells are very common and are frequently seen in roofs covering mill (Ref. 1) type buildings. An examination of existing conoid shell roofs indicates that usually only truncated conoid sections are used.

As in many fields of engineering, the construction of conoid shells has preceded the development of refined analytical techniques. Until recently, the design of circular conoids had usually been based on experiments conducted on models. However, in the recent years, due to the development of digital computer facilities, it has become possible to analyse complex shell structures using advanced numerical techniques.

This paper is concerned with the study of thin shallow circular truncated conoid shells, Figure 1, simply supported on four edges in the radial direction and subjected to uniformly distributed normal loads. The influences of geometrical (rise, length and thickness), physical (Poisson's ratio), and numerical (mesh size) parameters on the behavior of conoids are investigated. A suitable general numerical procedure is developed for the analysis of a circular conoid shell, undergoing bending deformation. The procedure is applied to obtain the stress quantities (forces, moments and deflections) of radially supported circular conoid shells with various geometrical, physical and numerical parameters. From considerations of the above parameters, explicit conclusions have been arrived at for the design of intermediate * and long * circular conoids.

[1] Professor of Civil Engineering, Laval University, Quebec.

[2] Structural Engineer, Dufresne, Beaulieu, Trudeau and Associates, Quebec.

* Intermediate and long conoids: In this paper, a long shell is defined as a shell which has a high end radius over length ratio less than 0.4 and the intermediate shell is defined as a shell which has a radius over length ratio between 0.4 and 2.0. (This definition was first used by Gibson (Ref. 2) for open circular cylindrical shells).

Although, for the numerical test examples, only truncated circular conoids are treated in this paper, yet the theory presented herein is general enough to be applicable to other conoid surfaces (viz, parabolic and hyperbolic) also.

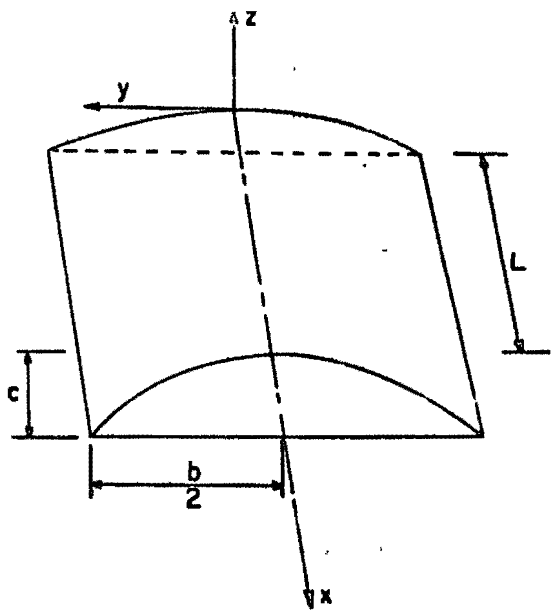

Fig. 1. Definition of a circular conoid.

2 Notation

b = base of shell
c = rise of shell
CM = computational finite difference molecule
$D = Et^3/[12(1-\nu^2)]$ = bending rigidity
E = modulus of elasticity
F = stress function
$G = Et/(1-\nu^2)$ = extensional rigidity
k = coordinate of a point on the basic networtk along x-axis (see Fig. 5), ($k = 1 \dots m+1$)
K = Gaussian curvature ($K = K_1 \times K_2$)
K_1, K_2 = curvatures in α-β plane, also principal curvatures in x-y plane
l = coordinate of a point on the basic network along y-axis (see Fig. 5) used as a subscript or index number ($l = 1 \dots n+1$)
L = length of shell
m = number of intervals along x-axis
M = moment per unit length
n = number of intervals along y-axis
N = normal force per unit length
p = uniformly distributed load (psi)
q = sub-partitioned matrix size
Q = shearing force per unit length
R = radius of curvature
R_2 = radius of curvature in y-z plane = $1/K_1$
t = thickness of shell
u, v, w = displacements along α, β, γ
x, y, z = rectilinear orthogonal coordinates
α, β, γ = orthogonal curvilinear coordinates
ζ = half of the base width of the shell
Ψ = mathematical differential operator
ν = Poisson's ratio
ϱ = dead weight of shell material (psi)
ΔS = finite difference interval
∇^4 = biharmonic (Del Fourth) operator
∇_R^2 = Pucher's operator

Subscript

o = quantity referred to high end
$,x$ = partial derivative (viz, $N_{,x} = \partial N/\partial x$)
$,xx$ = partial second derivative (viz, $N_{,xx} = \partial^2 N/\partial x^2$)
α, β, γ = x, y, z used as subscript indicate the direction of a vector
2η = order of the mathematical operator Ψ

3 Mathematical formulation

Using the classical theory of elastic shallow shells, the basic governing partial differential equations, specialized to the conoid surfaces, result into two «Del Fourth» equations. It is found that these equations have a striking similarity to Vlasov's equations for shallow shells (Ref. 3).

3.1. Theoretical Equations

3.1.1. *Assumptions*

The governing equations used in this paper are based on the following assumptions:

a) The shell is shallow *.

b) The shell is thin **.

c) The strains are small.

d) The material of the shell is linear, elastic and isotropic.

3.1.2. *Governing Equations*

Using the definition of stress quantities as defined in Figs. 2 & 3, the governing differential equations for shallow thin circular conoids can be written as:

$$D\nabla^4 w - \nabla^2_R F = p_z \qquad [1]$$

$$\nabla^4 F + G\nabla^2_R w = 0 \qquad [2]$$

where:

$$\nabla^2_R = K_2 \partial^2/\partial x^2 \qquad [3]$$

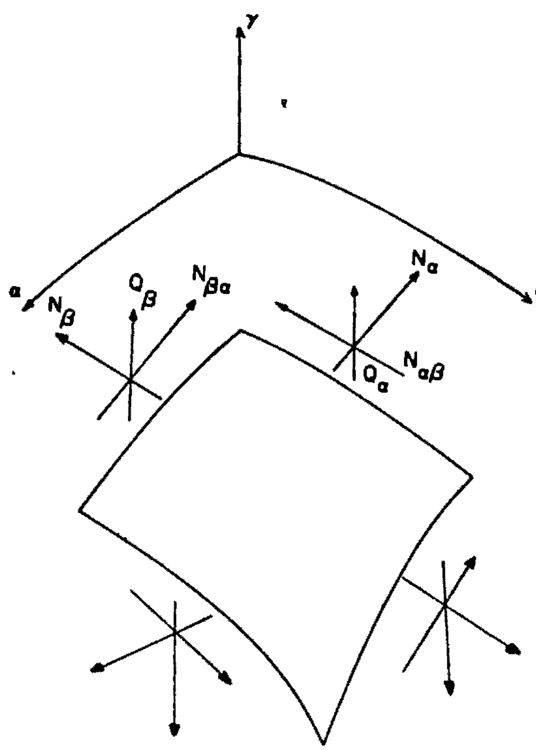

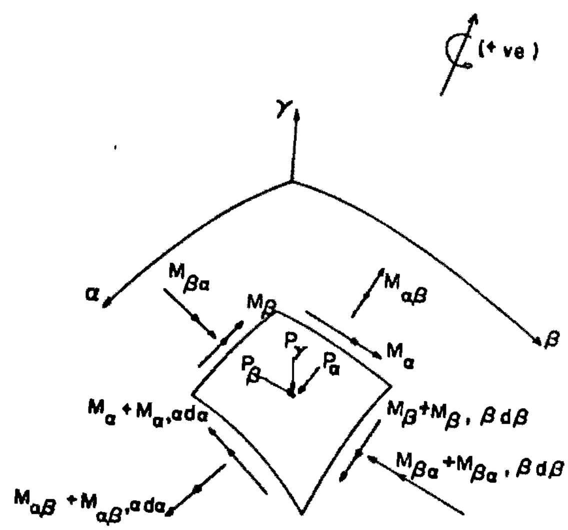

Fig. 3. Definition of moments and applied loads.

Fig. 2. Definition of forces on the shell element.

* A ratio of 1/13 was proposed by Lachance and Popov (Ref. 4) for the spherical shells to keep the errors in M and Q within 5 %.

** For thin sells, the effect of transverse shear stresses and of the tranverse normal stresses can be neglected.

In a special case when the axes α and β are in the planes of principal curvature and the Gaussian curvature becomes zero, Eq. [1] and Eq. [2] become similar to Vlasov's (Ref. 3) equations for shallow thin spherical shells.

3.2. Boundary Conditions

Stress analysis of conoids is an equilibrium or a boundary value problem. The domain is a bi-dimensional continuum and the boundaries are defined by four closed curves. Thus, mathematically Eq. [1] and Eq. [2] can be represented by:

$$\Psi_{2\eta} w = f_1 \quad [4]$$

$$\Psi_{2\eta} F = f_2 \quad [5]$$

where f_1 and f_2 define the prescribed loading and distortion functions for the entire shell domain. In such systems, there are η boundary conditions of maximum differential order up to $2\eta - 1$ for each boundary point. Comparing Eqs. [1] and [2] with [4] and [5], gives $\eta = 3$.

Thus, three boundary conditions in terms of forces and/or displacements are needed to be prescribed for each boundary point. For the circular conoids, which are simply supported in the radial direction at the four edges, the following boundary conditions must be satisfied at each boundary point:

$$w = M_i = N_i = 0 \quad [6]$$

where:

$$i = \alpha \text{ or } \beta$$

4. Numerical method

4.1. Introduction

The exact solutions of conoid shells are very few and are available for membrane analysis of conoid shells only. For general loading conditions, no explicit solution for truncated circular conoids is possible by analytical means. Numerical approximations are conceivable and are of practical importance when the finite difference formulations is carried out by an electronic digital computer for the conoid problem. A finite difference method can be used to convert the continuous equilibrium problem into a discrete boundary value problem. The solution of the discrete problem is an approximation to the solution of the continuous problem with an error which can be theoretically brought to any desired level. The purpose of this work is to investigate whether the numerical method, using an IBM 360, yields accurate results for the analysis of circular conoids.

4.2. Finite Difference Operators

The ultimate purpose of the finite difference procedure is to reduce the continuous system of differential equations (for example, the continuous equilibrium differential equations of the shell element) into a pattern of discrete points. The advantage of this procedure is that instead of solving the differential equations, we solve linear algebraic equations and find the solution of the problem at the desired discrete points.

In this paper, a central finite difference technique with a truncation error of order $(\Delta S)^2$ has been used for the purpose of discretization. Molecular forms of finite difference operators can be obtained by using Taylor's Series expansion viz, Crandall (Ref. 5). Figure 4, gives a list of elementary central finite difference operators with a truncation error of order $(\Delta S)^2$.

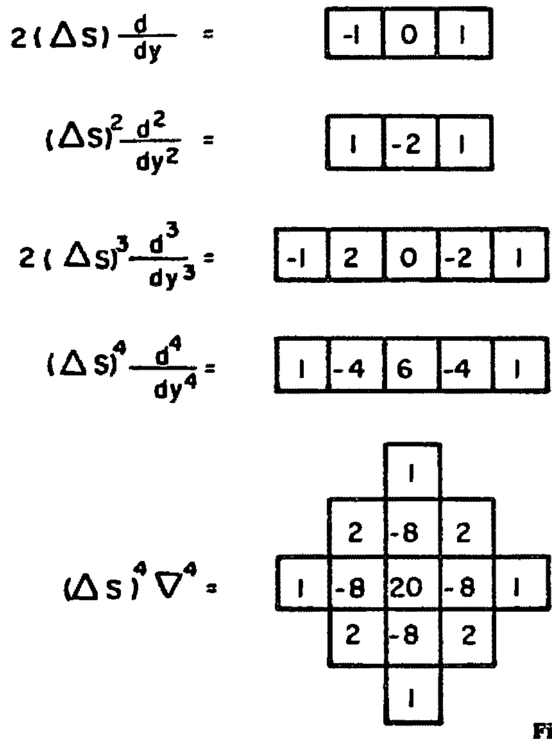

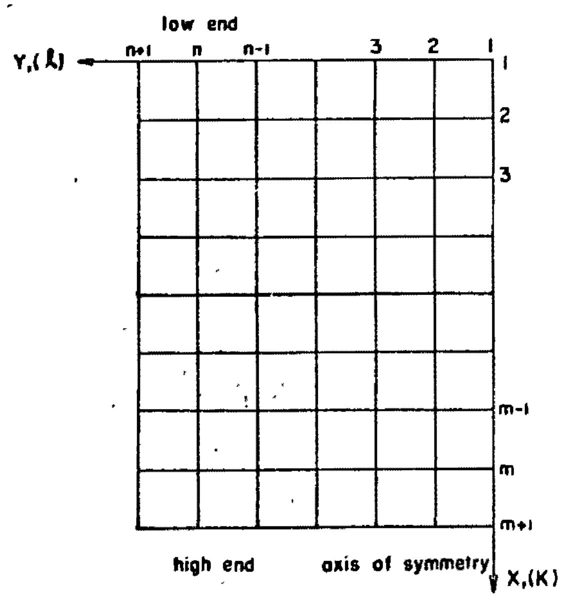

Fig. 5. Basic network used for finite difference technique.

Fig. 4. Central finite difference operators.

4.3. Discretization of Equations

An important step in the numerical analysis using finite difference techniques is the conversion of the governing differential equations [1] and [2] into linear algebraic equations. Using the central finite difference operator for a «Del Fourth» derivative, Eq. [1] can be writen in an algebraic form as:

$$
\begin{aligned}
(\nabla^4 w)_{k,l} = \frac{1}{(\Delta S)^4} &[(w_{k-2,l} + w_{k,l+2} + w_{k+2,l} + w_{k,l-2}) \\
&+ 2(w_{k-1,l-1} + w_{k-1,l+1} + w_{k+1,l-1} + w_{k+1,l+1}) \\
&- 8(w_{k-1,l} + w_{k,l+1} + w_{k+1,l} + w_{k,l-1}) + 20w_{k,l}] + 0(\Delta S)^2
\end{aligned} \qquad [7]
$$

where indexes k and l define the coordinates of a point along x and y axis respectively on the projected base plan of the shell (see Fig. 5).

Using Eq. [7] for Eq. [1] and a similar equation for Eq. [2], a set of computational molecules (CM) can be defined to represent Eq. [1] and Eq. [2] in difference equation forms. The computational molecules corresponding to Eq. [1] and Eq. [2] are presented in Figure 6 and Figure 7.

4.4. Finite Difference Formulation of Boundary Conditions

The continuous boundary conditions given in Eq. [6] are first expressed in terms of the unknown radial displacement w and the stress function F, and then the finite difference approximations are obtained using the computational molecules listed in Figure 4. From this finite difference approximation of the boundary conditions, the unknowns of the discrete points lying outside the solution domain are solved simultaneously, and substituted into equations given in Figure 6 and Figure 7, to obtain a set of molecules suitable for boundary points.

4.5. Generation of the Coefficient Matrix

Using the central finite difference computational molecules given in Figure 6 and Figure 7 for the various derivatives appearing in Eq. [1] and Eq. [2], one can write finite difference algebraic equations at each discrete point, including boundary points. This set of linear equations is cast into a stiffness matrix type of formulation.

The discrete points are labelled according to the scheme presented in Figure 5. The coefficient matrix relates the radial displacements and stress functions to the loading and deformations functions corresponding to each row of discrete points along the y axis. The coefficient matrix is generated by successive application of the computational molecules associated with Eq. [1] and Eq. [2] for all the discrete points except for the points near the boundary where special boundary computational molecules are utilized. A sophisticated internal labelling scheme has been devised to reduce the coefficient matrix size and to make the matrix operation highly efficient.

The resulting large order augmented coefficient matrix is subpartitioned into smaller (qxq) square matrices and subsequently reduced to a diagonal band. Thus, all the zero submatrices outside the band are eliminated. The sub-partitioned coefficient matrix is further processed by using the flow-graph approach first described by Singhal at al. (Ref. 6) and later developed by Dhatt as described in (Ref. 7). It is found that the flow-graph method is especially suitable for the processing of the present problem because of the mixed formulation in terms of displacements and stress functions. The advantage of the flow-graph method is that it automatically minimizes the computer time needed to obtain the solutions from the coefficient matrix. Once the radial deflection and the stress function are computed, their simple substitution into the equations expressing forces in terms of the stress function, directly leads to all the other stress quantities. The theoretical formulation have been described in detail by the authors in (Ref. 8).

4.6. Sources of Error in Finite Difference Formulations

As in any other finite difference solution, the results obtained from the computer are distorted by the existence of a truncation error and a round-off error. In an IBM 360 type machine, which carries 16 significant decimal digit accuracy, no appreciable round-off error was detected. The numerical analysis of a long conoid shell resulted in 790 simultaneous equations. As shown in the next section, the maximum truncation error was found to be less than 2 %.

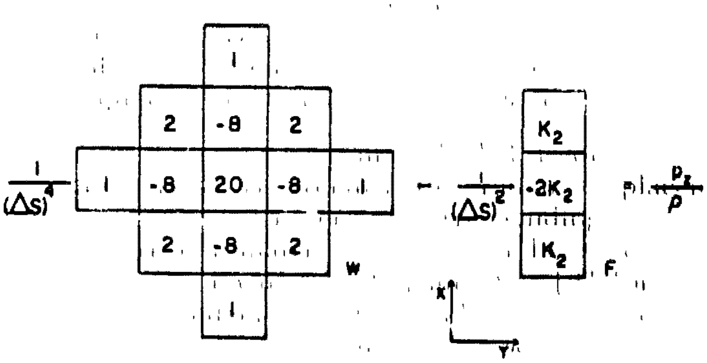

$\nabla^4 w - \nabla_R^2 F = \frac{p_z}{\rho}$

Fig. 6. Molecule for equation [1].

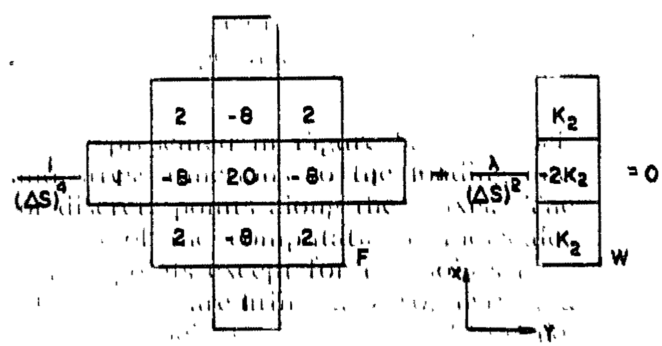

$\nabla^4 F + \lambda \nabla_R^2 w = 0$

Fig. 7. Molecule for equation [2].

5 Results and discussion

5.1. Introduction

To study the influence of various parameters on the behaviour of intermediate and long conoid shells, a range of parameters is carefully selected. Various curves are plotted with respect to each parameter.

5.2. Range of Parameters

Following is a list of major parameters which are selected to investigate the behaviour of the shell:

5.2.1. *Geometrical Parameters*

1. Rise; 2. Length; 3. Thickness.

5.2.2. *Physical Parameter*

4. Poisson's Ratio.

5.2.3. *Numerical Parameter*

5. Mesh size.

The chosen range of parameters as described in (Ref. 8) is summarized as follows;

rise,	$0.05\zeta < c < 0.2\zeta$	[8]
length (intermediate shell),	$1.3\zeta < L < 6.5\zeta$	[9]
length (long shell),	$6.5\zeta < L$	[10]
thickness,	$0.75'' < t < 2.5''$	[11]
Poisson's ratio,	$0 < \nu < 0.33$	[12]
mesh size *,	$\zeta/5 < \Delta S < \zeta/14$	[13]

Based on the above selection of the ranges of the various parameters, Table 1 outlines 19 test cases used in the numerical analyses. For all these 19 test cases, the shells are loaded by a uniformly distributed load of an arbitrarily chosen intensity of 90 psf. Since the shell behaves linearly with respect to the load intensity, the stress quantities corresponding to any other load intensity can be easily calculated.

* The choice of $\zeta/5$ as a starting point for the mesh size in the numerical analysis was partially influenced by the conclusions arrived at by Rao and Sharma in (Ref. 9) who used a mesh size of $\zeta/4$ for the numerical analysis of a parabolic truncated conoid using finite difference technique. Rao and Sharma concluded that a finer mesh than $\zeta/4$ would usually provide more accurate derivatives near the boundaries.

In this paper the shells tested are geometrically similar. For all test cases, the width is arbitrarily kept constant at $b = 16$ ft. Moreover, the low end rise is always taken as one half of the value of the high end rise. The absolute values of the five major parameters (rise, length, thickness, Poisson's ratio and mesh size) are shown in Table 1 in Column 2 to 6 respectively.

5.3. Results of Numerical Analysis of Simply Supported Conoids

For each of the nineteen test cases listed in Table 1, a numerical analysis of the simply supported conoid shells was carried out by using a high speed electronic digital computer. These numerical values have been plotted on various figures 8 through 20 to clearly establish

TABLE 1. Definition of Test Cases Used in Numerical Analysis.

$E = 4.5 \times 10^6$ psi

Case No.	High end rise (in)	Length (ft)	Thickness (in)	Poisson's ratio	Mesh size
I	18	32	2.5	0.15	$\zeta/5$
II	12	32	2.5	0.15	$\zeta/5$
III	5	32	2.5	0.15	$\zeta/5$
IV	18	16	2.5	0.15	$\zeta/5$
V	18	51.37	2.5	0.15	$\zeta/5$
VI	18	64	2.5	0.15	$\zeta/5$
VII	18	128	2.5	0.15	$\zeta/5$
VIII	18	32	1.75	0.15	$\zeta/5$
IX	18	32	1.25	0.15	$\zeta/5$
X	18	32	1.0	0.15	$\zeta/5$
XI	18	32	0.90	0.15	$\zeta/5$
XII	18	32	0.75	0.15	$\zeta/5$
XIII	18	16	2.5	0.15	$\zeta/7$
XIV	18	16	2.5	0.15	$\zeta/9$
XV	18	16	2.5	0.15	$\zeta/14$
XVI	18	32	2.5	0.0	$\zeta/7$
XVII	18	32	2.5	0.15	$\zeta/7$
XVIII	18	32	2.5	0.30	$\zeta/7$
XIX	18	64	2.5	0.15	$\zeta/7$

the influence of the selected five major parameters. The results are also presented in a tabular form, Tables 2, 3 and 4. This facilitates a comparative study between various test cases.

5.3.1. *Geometrical Parameters.—Rise, Length and Thickness*

Figure 8 shows the influence of various values of high end *rises* between the values of 5 inches to 18 inches. On this figure, three curves for the radial deflections at the crown corresponding to cases I, II and III of Table 1 are plotted.

TABLE 2. Influence of Mesh Size. Intermediate shell (cases I and XVII).

Stress Quantities	Coordinates	Figure Number
w	$y = 0$ $x = 0$ to 32 ft	13
w	$x = 8$ ft $y = 0$ to 8 ft	14
N_x, N_y	$y = 0$ $x = 0$ to 32 ft	15
N_x, N_y	$x = 8$ ft $y = 0$ to 8 ft	16
M_x, M_y	$y = 0$ $x = 0$ to 32 ft	17
M_x, M_y	$x = 8$ ft $y = 0$ to 8 ft	18

TABLE 3. Influence of Mesh Size (cases I and XVII). A Comparative Study of Stress Quantities along x-axis for Intermediate Length Conoids.

Mesh Size Influence							% Difference in Stress Quantities Between Values Obtained from $\Delta S = \zeta/5$ and $\Delta S = \zeta/7$				
x (ft)	Mesh size	w (in)	N_x (lb/in)	N_y (lb/in)	M_x (lb-in/in)	M_y (lb-in/in)	w (%)	N_x (%)	N_y (%)	M_x (%)	M_y (%)
8	$\zeta/5$	—0.203	988.18	358.58	—149.33	—264.14	.97	.62	.32	.56	1.39
	$\zeta/7$	—0.205	994.42	359.76	—150.18	—267.82					
16	$\zeta/5$	—0.210	1139.44	210.58	—100.42	—263.21	.94	.62	.08	1.36	1.72
	$\zeta/7$	—0.212	1146.60	210.76	—101.81	—267.82					
24	$\zeta/5$	—0.120	745.64	152.34	— 36.60	—120.02	1.63	.73	.34	1.77	1.72
	$\zeta/7$	—0.122	751.19	152.85	— 37.26	—122.13					

TABLE 4. Influence of Mesh Size (cases VI and XIX). A Comparative Study of Stress Quantities along x-axis for Long Length Conoids.

Mesh Size Influence							% Difference in Stress Quantities Between Values Obtained from $\Delta S = \zeta/5$ and $\Delta S = \zeta/7$				
x (ft)	Mesh size	w (in)	N_x (lb/in)	N_y (lb/in)	M_x (lb-in/in)	M_y (lb-in/in)	w	N_x	N_y	M_x	M_y
8	$\zeta/5$	—1.072	1819.46	135.42	—395.52	—1649.47	.18	.29	1.04	.44	.61
	$\zeta/7$	—1.074	1814.15	134.00	—397.29	—1659.60					
16	$\zeta/5$	—1.200	2105.33	74.88	—370.63	—1845.11	.24	.28	1.3	.52	.63
	$\zeta/7$	—1.203	2099.27	73.90	—372.57	—1856.95					
24	$\zeta/5$	—0.734	1585.80	108.45	—208.79	—1096.02	.40	.05	.08	.71	.72
	$\zeta/7$	—0.737	1585.00	108.36	—210.30	—1104.05					

Figure 9 establishes the influence of the various *lengths* ranging from intermediate to long shells. On this figure, five typical cases represented by cases I, IV, V, VI, VII of Table 1 are plotted.

The influence of various *thicknesses* over conoid shell behaviour is shown in Figure 10 for cases I, VIII, IX, X, XI, XII.

5.3.2. *Physical Parameter.—Poisson's ratio*

The moment M_x as well as the radial deflections have been selected to study the influence of Poisson's ratio over these two stress quantities. The results are plotted in Figure 11 for the moment M_x and Figure 12 for the radial deflection w for three test cases number XVI, XVII and XVIII of Table 1.

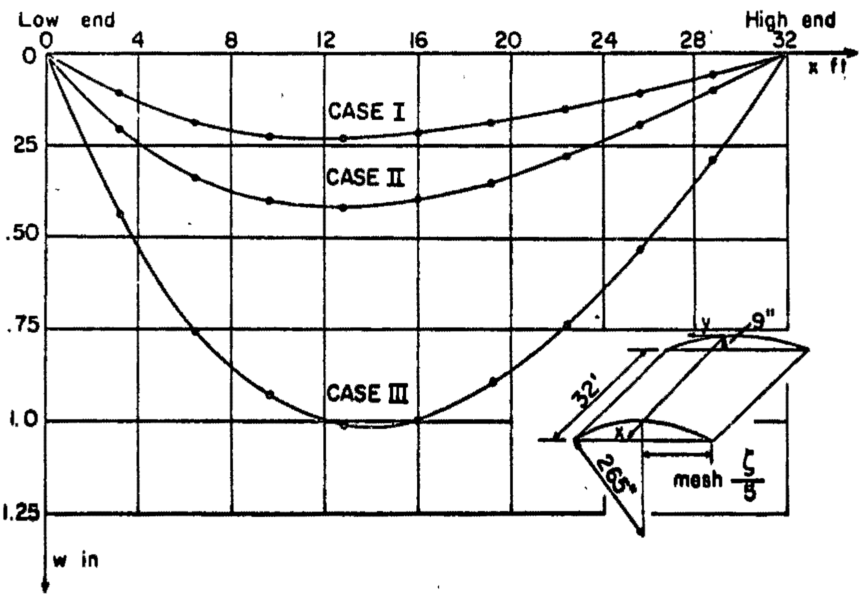

Fig. 8. Deflections w at $y = 0$ for various rises: cases I, II and III.

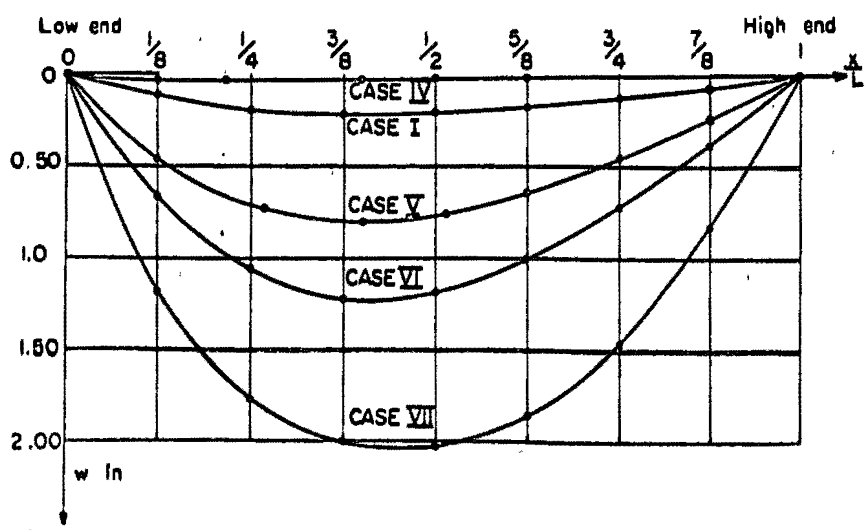

Fig. 9. Deflections w at $y = 0$ for various lengths: cases I, IV, V, VI and VII.

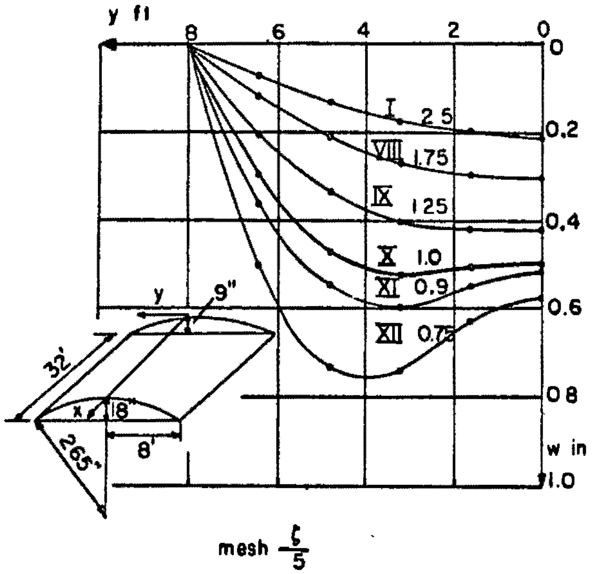

Fig. 10. Deflections w at $x = 8$ ft. for various thicknesses: cases I, VIII, IX, X, XI and XII.

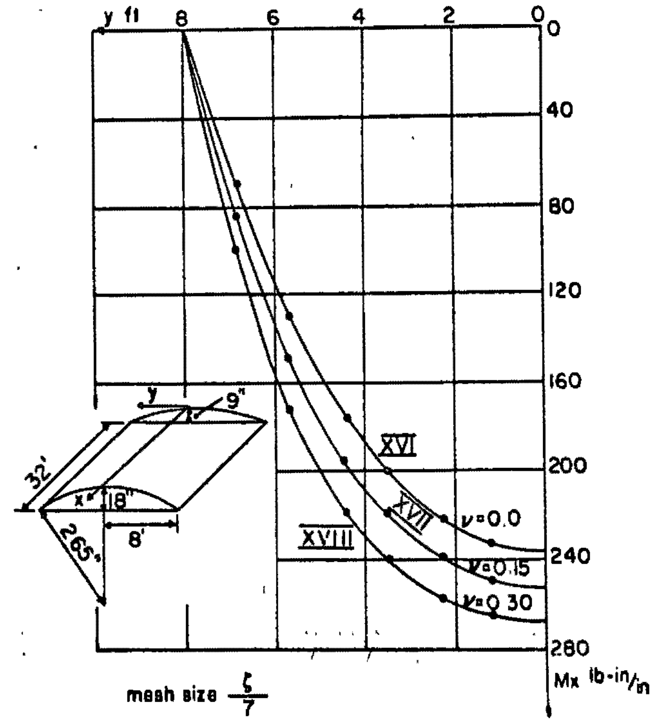

Fig. 11. Moment M_x at $x = 2.85$ ft. for various Poisson's ratios for cases XVI, XVII and XVIII.

5.3.3. *Numerical Parameter.—Mesh size*

The influence of mesh sizes over the accuracy of numerical results has been carefully and extensively studied within this paper. The influence of mesh size over various stress quantities (w, N_x, N_y, M_x and M_y) along x and y axis for both intermediate and long shells has been studied. Table 2 summarizes the list of Figures 13 through 18 which are presented in this paper to study the influence of mesh sizes $\zeta/5$ and $\zeta/7$ over various stress quantities. Figures 13 through 18 refer to conoids of intermediate length; for the purpose of comparison Figure 19 which refers to a long conoid, is also included.

Table 3 and Table 4 summarize the percentage error between the results of $\zeta/5$ and $\zeta/7$ mesh sizes at various stations along x axis for the stress quantities w, N_x, N_y, M_x, M_y, for intermediate and long shells respectively.

5.4. Discussion

5.4.1. *Influence of Geometrical Parameters.—Rise, Length and Thickness*

Figure 8 shows that decreasing the rise of a shell is always accompanied by a corresponding increase in the deflection quantities. For the shallow conoid shells of moderate rise the maximum deflection always occurs closer to the low end.

For the various test cases treated in this paper corresponding to several different conoids with lengths varying between 16 to 128 feet, it is found that the maximum deflection always occurs closer to the low end of the shell; this phenomenon being more pronounced in the case of intermediate shells. For very long shells, the maximum deflection occurs at the crown, approximately at half of the length from either end.

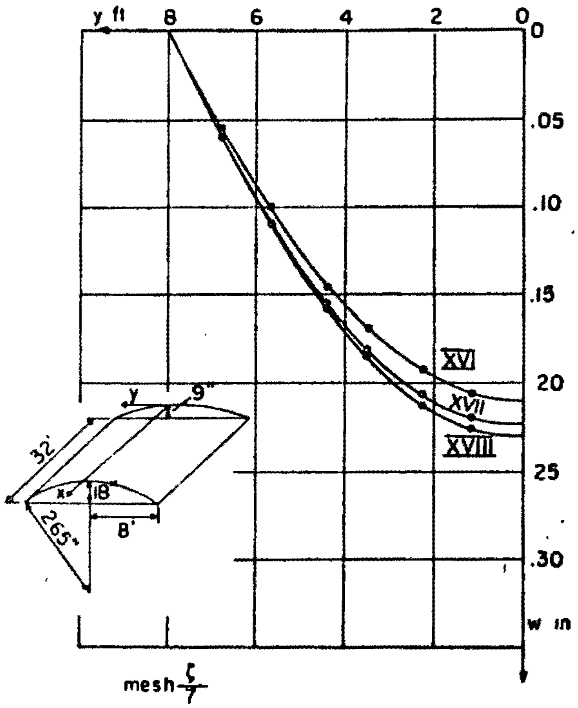

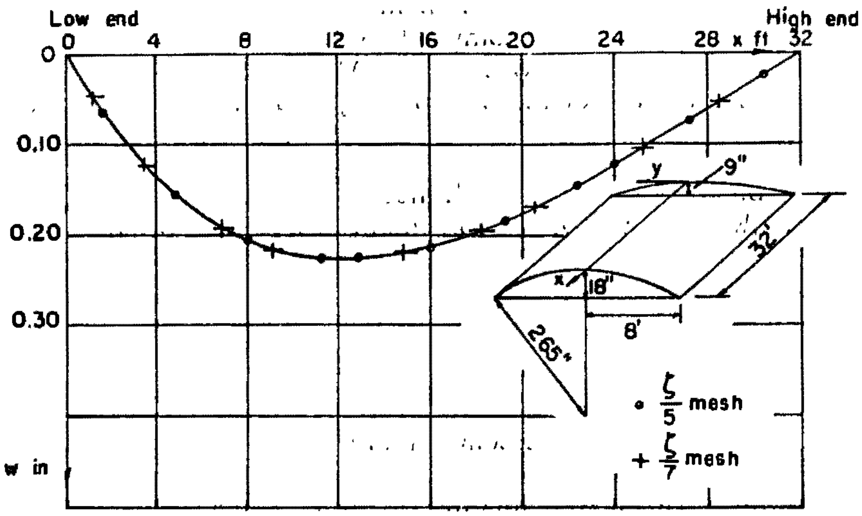

Fig. 13. Vertical deflections w at $y = 0$ for cases I, XVII.

Fig. 12. Deflections w at $x = 12.57$ ft. for various Poisson's ratios for cases XVI, XVII and XVIII.

The influence of thickness is very pronounced. For moderate thickness the maximum deflection occurs at the crown. However, for thinner shells, the deflection shape along y-axis shows wave formation Figure 10. Therefore the thinner shells with rippled deflected shape are considerably more susceptible to buckling than the moderately thick shells.

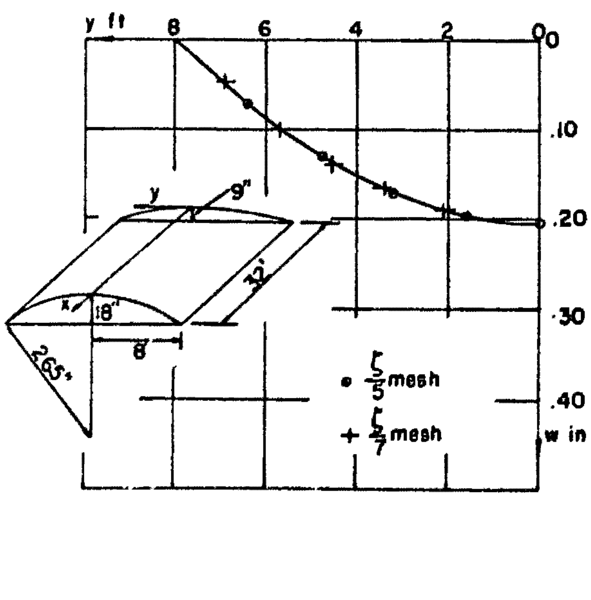

Fig. 14. Deflections w at $x = 8$ ft. for cases I and XVII.

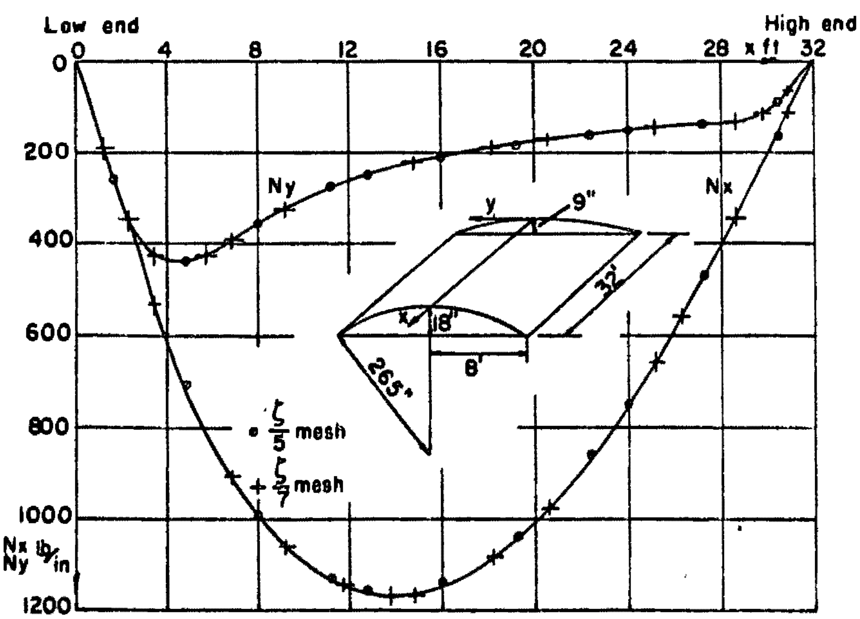

Fig. 15. N_x, N_y at $y = 0$ for cases I and XVII.

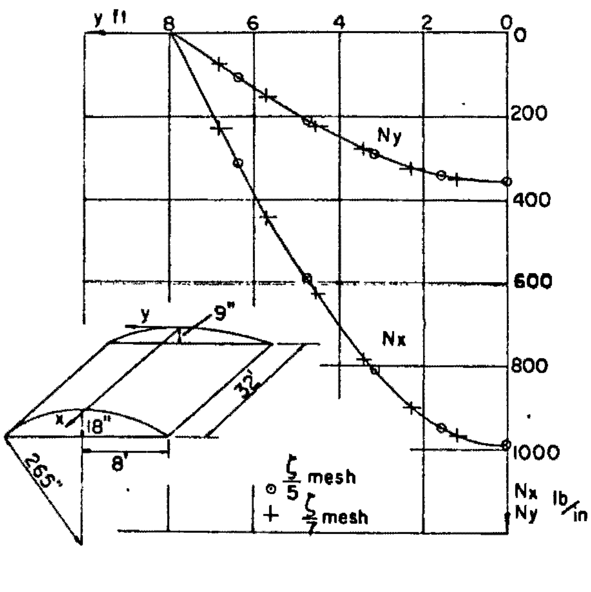

Fig. 16. N_x, N_y at $x = 8$ ft. for cases I and XVII.

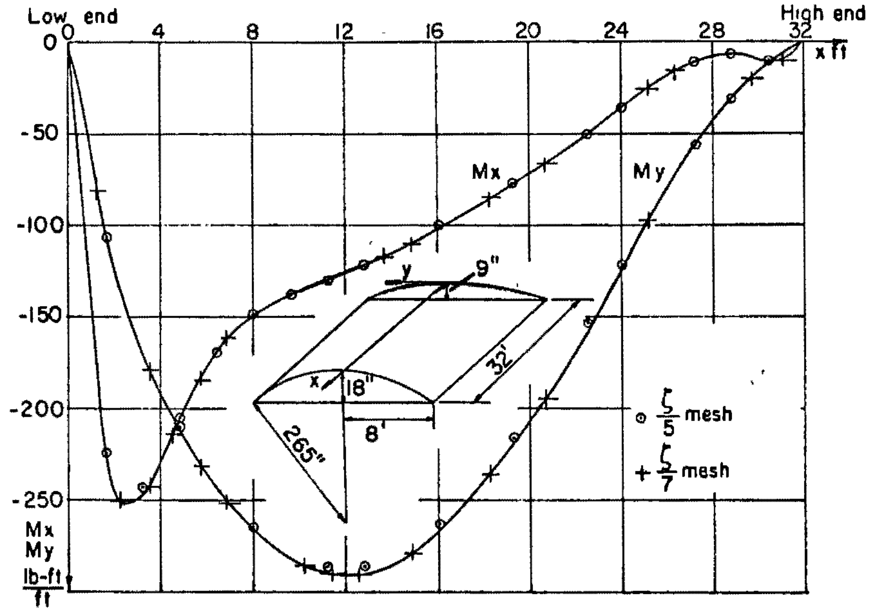

Fig. 17. M_x, M_y at $y = 0$ for cases I and XVII.

5.4.2. *Influence of Physical Parameter.—Poisson's ratio*

A comparison of the various curves in Figure 11 corresponding to Poisson's ratio values varying between 0.0 and 0.30, shows that an increase of Poisson's ratio from either 0.0 to 0.15 or from 0.15 to 0.30 brings a change in the bending moment value greater than 5 % at all stations along y-axis. Also a comparison of Figures 11 and 12 shows that the influence of Poisson's ratio is more pronounced on the bending moment quantities as compared to deflection quantities.

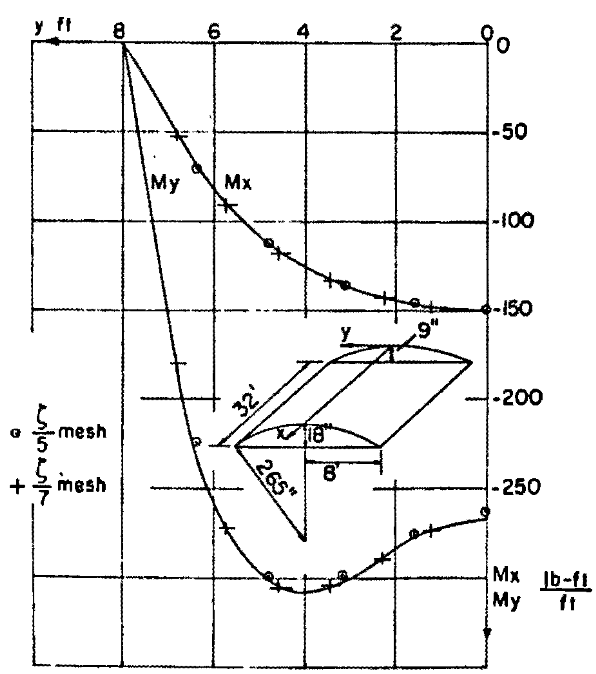

Fig. 18. M_x, M_y at $x = 8$ ft. for cases I and XVII.

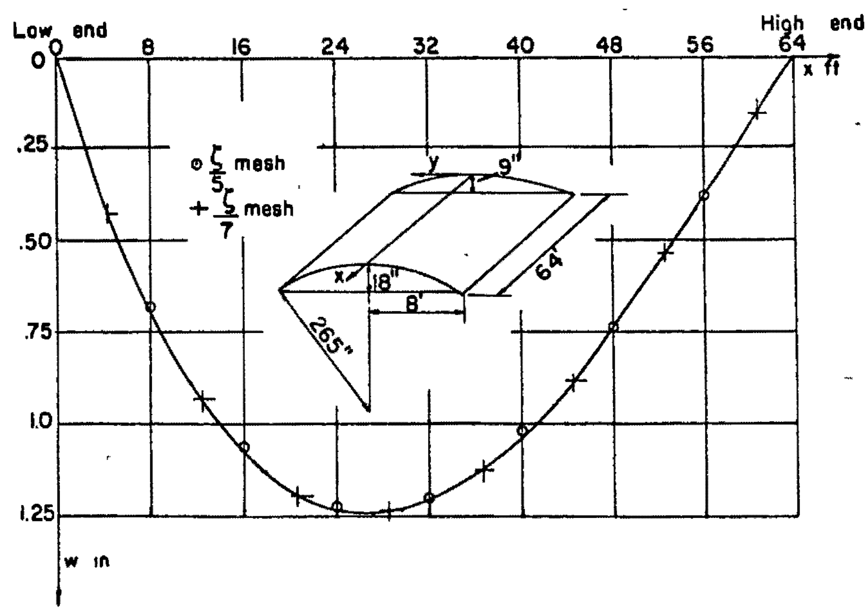

Fig. 19. Vertical deflections w at $y = 0$ for cases VI and XIX.

An attempt was also made to confirm the hypothesis of Abu-Sitta (Ref. 10), in which he suggested that Poisson's ratio may be taken as equal to zero in the governing differential equations and the proper value of Poisson's ratio be substituted in the stress-deflection relationships to retain the accuracy of the stress quantities. Two special numerical test cases were computed, one with Poisson's ratio equal to 0.15 throughout the entire computation, and another with Poisson's ratio equal to 0.0 during the solution of the coefficient matrix and equal to 0.15 during the resubstitution of the deflection into the stress-deflection relationships. When the results of these two computations were compared for bending moment and deflection quantities, it was found that these results were within 99.9 % of each other, thus confirming the validity of the hypothesis of Abu-Sitta.

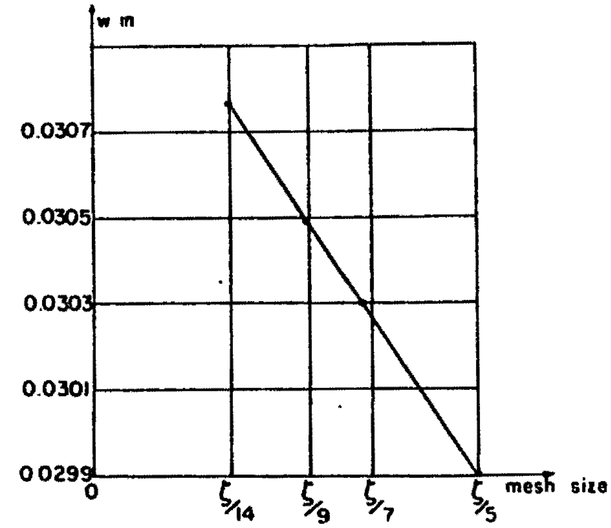

Fig. 20. Deflections w at $x = 8$ ft. for various mesh sizes for cases IV, XIII, XIV and XV.

5.4.3. *Infuence of Numerical Parameter.—Mesh size*

Based on the results presented in Figures 13 through 19 and Tables 3 and 4, all the stress quantities for $\Delta S = \zeta/7$ are always higher than those obtained with $\Delta S = \zeta/5$. Furthermore, for the intermediate and long shells, the difference between the stress quantities corresponding to $\Delta S = \zeta/5$ and $\zeta/7$ values is never greater than 2 %. Analysis of the shell described in case IV but using mesh size values $\zeta/5$, $\zeta/7$, $\zeta/9$ and $\zeta/14$, leads to Figure 20 which clearly establishes the influence of the mesh size over the radial deflections of conoids. This figure shows that the deflection at the crown at $x = 8$ ft always increases when decreasing the mesh size from $\zeta/5$ to $\zeta/14$, a result similar to that shown by Table 3 and 4 for the intermediate and the long shells. Furthermore, the variation between $\zeta/5$ and $\zeta/14$ values is not greater than 2 %. Another interesting observation from Figure 20 is that all the four points corresponding to four different mesh sizes between $\zeta/5$ to $\zeta/14$ lie over a straight line which leads to the hypothesis that the truncation error for the conoid shell is linearly proportionate to the mesh size. This implies that the boundary conditions indeed play an important role in the behaviour of the shell.

Conclusions

In this paper, the influences of rise, length, thickness, Poisson's ratio and mesh size on the behavior of conoid shells are analyzed. Based on numerical analysis of nineteen different conoid shells, the following conclusions are quantitatively established:

— the maximum radial deflections for geometrically similar conoids with various *rises* always occur at a constant distance away from the mid-length point and closer to the low rise end.

— the maximum radial deflections for geometrically similar conoids with various *lengths* (intermediate to long lengths) always occur away from the mid-length point and closer to low rise end. The distance of maximum deflection point from the mid-length point depends upon the dimensions of the conoid shells, being zero for infinitely long shells, large for intermediate shells, largest for short shells.

— the influence of *thickness* is very pronounced; for moderately thin shells the maximum deflection occurs along the crown of the shell, however for very thin shells, the maximum deflections occur at both sides of the crown at equal distance away from the crown, this distance being larger for thinner shells.

— the influence of *Poisson's ratio* is very pronounced, being larger than 5 % for bending moments (M_x) for a variation of Poisson's ratio from either 0.0 to 0.15 or 0.15 to 0.30; furthermore, Abu-Sitta's hypothesis that neglecting Poisson's ratio in governing equations but including it in stress-deflection relationships leads to accurate stress quantities within 0.1 %, has been numerically verified.

— the influence of *mesh size* between mesh sizes of $b/10$ and $b/28$ is found to be only within 2 %; thus it can be concluded that using the central finite difference scheme with a fairly coarse mesh of $b/10$ leads to a satisfactorily (within 2 %) accurate result.

Acknowledgment

The work presented herein was carried out at the Civil Engineering Department of Laval University, Quebec, Canada. It was partially sponsored by the National Research Council of Canada under grant No. A 2940, Canadian Steel Industries Construction Council under grant No. 4015 and United Aircraft of Canada Limited. The assistance and financial support P of these organizations, which made this research possible, is gratefully acknowledged. The authors also wish to acknowledge the assistance of the staff of Laval University Computation Centre.

Bibliography

(1) ZALEWSKI, Waclaw: «A Study of Saw-Tooth Shell Roof Shapes», World Conference on Shell Structures. San Francisco, 1962, pp. 43-56.

(2) GIBSON, J. E.: «Design of Cylindrical Shell Roofs», 2nd ed., Van Nostrand, New York, 1961.

(3) VLASOV, V. Z.: «General Theory of Shells and its Applications in Engineering», NASA, April 1964, N64-19883, pp. 285, 337, 350.

(4) LACHANCE, L. and POPOV, E. P.: «Limitations of Shallow Shell Equations for Spherical Shells», International Symposium on Shell Structures in Engineering Practice, Budapest, Hungary, 1965.

(5) CRANDALL, S. T.: «Engineering Analysis», McGraw Hill Book Co., New York, 1956, pp. 160, 207, 246.

(6) SINGHAL, A. C.; ROBICHAUD, L. P. A., and DHATT, G. S.: «The Dedevelopment of Flow-Graph Techniques to the Solution of Continuous Structural Systems»/ Proceedings of the Fifth U. S. National Congress of Applied Mechanics, ASME, New York, 1966.

(7) DHATT, GURBACHAN S.: «Multi-Level Flow Graphs with Application to Large Structural Systems», Doctor of Science Thesis, Laval University, Quebec, Canada, Oct. 1968.

(8) SINGHAL, A. C., and GAGNON, M.: «Numerical Analyses of Circular Conoids», Department of Civil Engineering Report No. S-14, Laval University, Quebec, Canada, January 1969.

(9) RAO KESHAVA, M. N., and SHARMA, S. P.: «Application of the Method of Finite Differences for the Analysis of a Conoid Shell Using the Bending Theory», Indian Concrete Journal, Vol. 36, No. 3, March 1962, pp. 84-92.

(10) ABU-SITTA, S. H.: «Finite Difference Solutions of the Bending Theory of the Elliptic Paraboloid», Bulletin of the International Association for Shell Structures, No 20, Dec. 1964.

Proceedings of the

"Symposium on tower shaped steel and reinforced concrete structures"

held in Bratislava, June 1966

Approx. 360 pages, 21 x 27 cm

All the papers presented to the Symposium.

Discussions

General reports

Edited by the Secretariat of the I.A.S.S. with the collaboration of the Organizing Czechoslovak Committee.

Price $ 17

If you plan to buy this book, please send **today** your order filling the joined card and sending it to:

Secretariat of the I. A. S. S.
Alfonso XII, 3
MADRID - 7 - (SPAIN)

Numerical solution of bending stage in hypar shell

M. GELLERT [1] and N. SAPOZNIKOV [2]

Summary An analysis is presented of a shallow hypar in flexure based on solving two fourth-order partial differential equations in two unknowns: w (vertical displacement) and F (Airy function of forces) by the finite-differences method. A parametric analysis was applied to a hinge-supported hypar mounted on walls rigid in their planes and flexible normal to them. The numerical solution was obtained by the relaxation method, using an electronic computer.

1. Introduction

In view of its popularity in engineering practice, the hypar has been throuroughly studied theoretically (e.g. Bongard's (1) work) and practical methods have been recommended for specific cases. The scarcity of published practical results, so essential for the experience of the practical engineer, is due to two reasons:

a) some of the methods are intended for highly specific cases (e.g. special edge conditions).

b) the more comprehensive theories are not too handy for numerical solution.

In many cases the designer contents himself with a membrane-state based analysis. Application of the membrane theory (adapted for the hypar by Candela (2)) is particularly simple in the case of a shallow hypar under continuous uniform load. This solution suffices where actual conditions duplicate, with satisfactory accuracy, edge conditions compatible with the membrane state. Otherwise flexure sets in, calling for a more general solution arrived at in the present case with the aid of Vlasov's (3) equations for shallow shells.

As can be seen from the concluding examples, the flexure effect varies with the shell parameters.

2. Theory

The hypar equation in Cartesian coordinates (see Fig. 1) is as follows:

$$z = \frac{c\,x\,y}{a\,b} \qquad [1]$$

[1] D. Sc., Lecturer, Faculty of Civil Engineering, Technion, Israel Institute of Technology, Haifa.

[2] M. Sc.

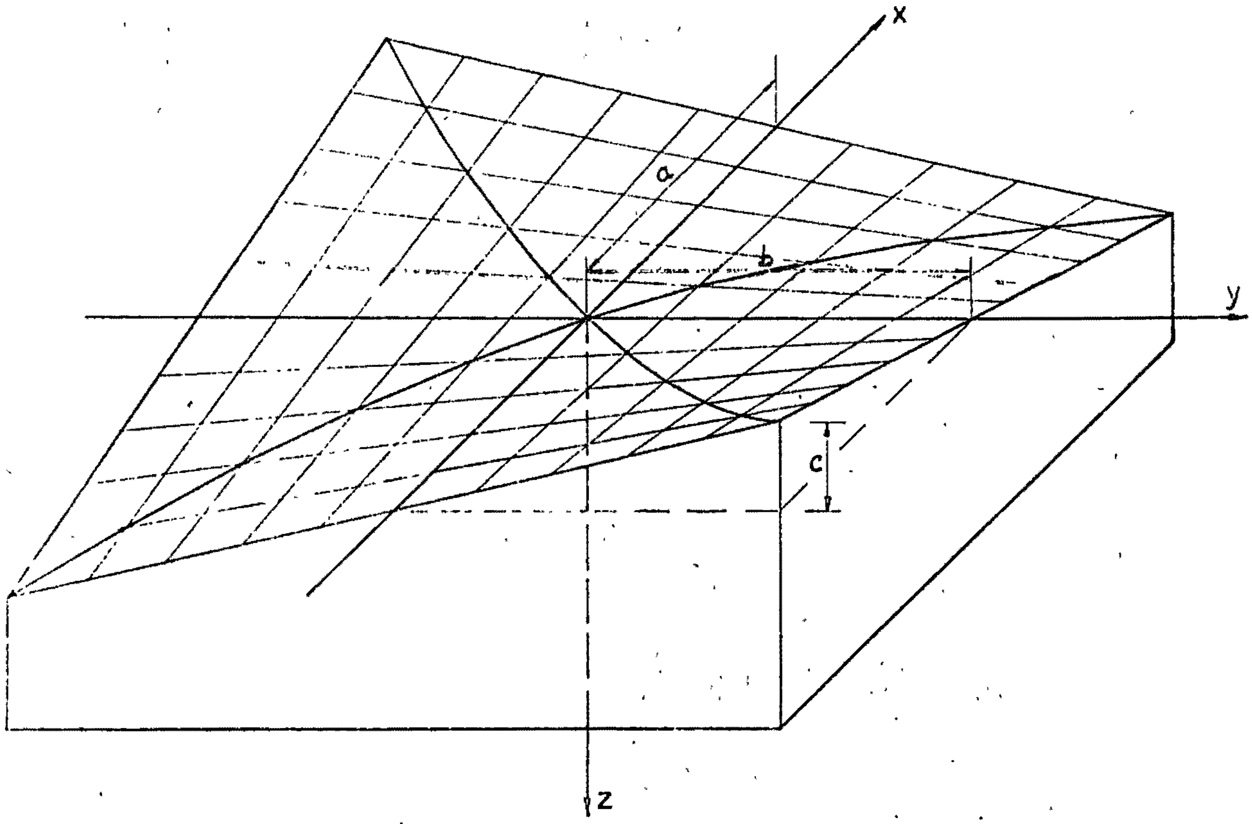

Fig. 1

The curvature and surface twist are given by the corresponding derivatives:

$$
\begin{aligned}
r &= \frac{\partial^2 z}{\partial x^2} = 0 \\
s &= \frac{\partial^2 z}{\partial x\,\partial y} = \frac{c}{a\,b} \\
t &= \frac{\partial^2 z}{\partial y^2} = 0
\end{aligned}
\qquad [2]
$$

Substitution of Eq. [2] in Vlasov's equations yields the differential equations for the shallow hypar under a vcertical load q:

$$
\begin{aligned}
K\,\nabla^2\nabla^2 w + \frac{2c}{a\,b}\,\frac{\partial^2 F}{\partial x\,\partial y} &= q\,(x\,,\,y) \\
\frac{1}{Ed}\,\nabla^2\nabla^2 F - \frac{2c}{a\,b}\,\frac{\partial^2 w}{\partial x\,\partial y} &= 0
\end{aligned}
\qquad [3]
$$

The structure of Eq. [3] shows that for the hypar in question, y symmetric load results in symmetric w and antisymmetric F about both the x— and y— axes.

Knowing w and F, the forces and the moments are obtainable as follows (see Fig. 2):

$$
\begin{aligned}
N_x &= \frac{\partial^2 F}{\partial y^2} \quad ; \quad M_x = -K\left(\frac{\partial^2 w}{\partial x^2} + \mu\,\frac{\partial^2 w}{\partial y^2}\right) \quad ; \quad Q_x = -K\,\frac{\partial\,(\nabla^2 w)}{\partial x} \\
N_{xy} &= -\frac{\partial^2 F}{\partial x\,\partial y} \quad ; \quad M_{xy} = -K\,(1-\mu)\,\frac{\partial^2 w}{\partial x\,\partial y} \\
N_y &= \frac{\partial^2 F}{\partial x^2} \quad ; \quad M_y = -K\left(\frac{\partial^2 w}{\partial y^2} + \mu\,\frac{\partial^2 w}{\partial x^2}\right) \quad ; \quad Q_y = -K\,\frac{\partial\,(\nabla^2 w)}{\partial y}
\end{aligned}
\qquad [4]
$$

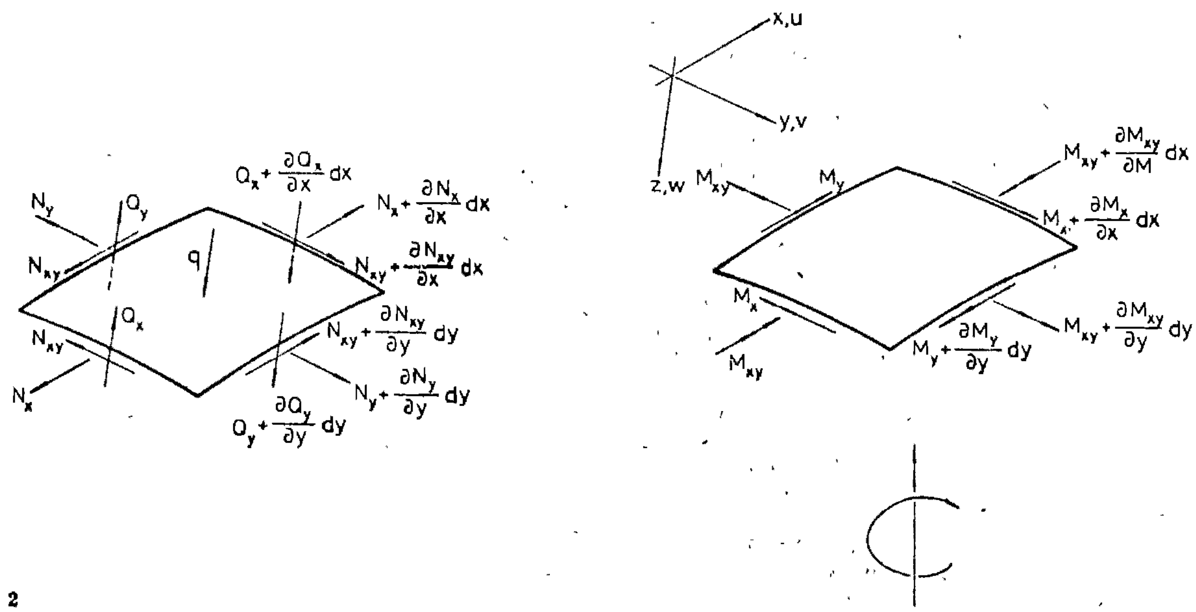

Fig. 2

and the displacements u and v are obtainable from the strains:

$$
\begin{aligned}
\epsilon_x &= \frac{1}{Ed}\,(N_x - \mu\,N_y) = \frac{\partial u}{\partial x} - rw = \frac{\partial u}{\partial x} \quad ; \quad (r = 0) \\
\epsilon_y &= \frac{1}{Ed}\,(N_y - \mu\,N_x) = \frac{\partial v}{\partial y} - tw = \frac{\partial v}{\partial y} \quad ; \quad (t = 0) \\
\gamma_{xy} &= \frac{2\,(1+\mu)}{Ed}\,N_{xy} = \frac{\partial u}{\partial y} + \frac{\partial v}{\partial x} - 2sw = \frac{\partial u}{\partial y} + \frac{\partial v}{\partial x} - \frac{2c}{ab}\,w
\end{aligned}
\tag{5}
$$

In what follows, only a continuous uniform load is considered.

The membrane-state equations are derived from Eq. [3] by omitting the term $K\nabla^2\nabla^2 w$ in the first equation:

$$
\begin{aligned}
&\frac{2c}{ab}\;\frac{\partial^2 F_0}{\partial x\,\partial y} = q \\
&\frac{1}{Ed}\,\nabla^2\nabla^2 F_0 - \frac{2c}{ab}\;\frac{\partial^2 w_0}{\partial x\,\partial y} = 0
\end{aligned}
\tag{6}
$$

and Eq. [6] yield the membrane solution for a hypar according to Fig. 1:

$$
\begin{aligned}
F_0 &= \frac{qabxy}{2c} \\
w_0 &= W = \text{const.}
\end{aligned}
\tag{7}
$$

It is readily seen that the solution [7] is also an exact particular solution of Eq. [3]. We also obtain:

$$
\begin{aligned}
&N_{x_0} = N_{y_0} = M_{x_0} = M_{xy_0} = Q_{x_0} = Q_{y_0} = 0 \\
&N_{xy_0} = -\frac{qab}{2c} \\
&U_0 = Uy \quad ; \quad v_0 = Vx
\end{aligned}
\tag{8}
$$

The membrane shear strain γ_{xy_0} is given by the expression constant throughout the hypar surface:

$$\frac{\partial u_0}{\partial y} + \frac{\partial v_0}{\partial x} - \frac{2c}{ab} w_0 = U + V - \frac{2c}{ab} W = -\frac{2(1+\mu)}{Ed} \frac{qab}{2c} \qquad [9]$$

It is also seen that all edge conditions acc. to Fig. 1 namely,

$$\begin{aligned} x &= \pm a \quad ; \quad w = v = M_x = N_x = 0 \\ y &= \pm b \quad ; \quad w = u = M_y = N_y = 0 \end{aligned} \qquad [10]$$

cannot be satisfied, as this would require $U = V = W = 0$, which contradicts Eq. [9]. At most, we can have:

a) $W \neq 0$; $U = 0$; $V = 0$

or b) $W = 0$; $U + V \neq 0$

For a), we obtain

$$W_0 = W = \frac{qa^2b^2}{2c^2} \frac{1+\mu}{Ed} \qquad [11]$$

Eq. [11] is recognizable as membrane settlement of the hypar. For the exact solution alternative b) was resorted to.

w and F were chosen as unknowns on grounds of convenience of numerical solution, considering the similarity of the two equations in [3]. The disadvantage of this choice lies in the difficulty in satisfying edge conditions for u and v (cf. conditions [10]).

In the present case, the difficulty was overcome by representing the sought result as a linear combination of the membrane solution and of that of Eq. [3] under edge conditions not involving u and v:

$$\begin{aligned} x &= \pm a \quad ; \quad w = F = M_x = N_y = 0 \\ y &= \pm b \quad ; \quad w = F = M_y = N_x = 0 \end{aligned} \qquad [12]$$

Under conditions [12], Eq. [3] yields F_1 and w_1. Each of the two sets — F_0 and w_0, F_1 and w_1 — satisfy separately all edge conditions not involving u and v, and the final result is:

$$\begin{aligned} F &= \alpha F_1 + \beta F_0 \\ w &= \alpha w_1 + \beta w_0 \end{aligned} \qquad [13]$$

As each solution is proportional to q (the whole load is involved), then necessarily $\alpha + \beta = 1$, or

$$\begin{aligned} F &= \alpha F_1 + (1-\alpha) F_0 \\ w &= \alpha w_1 + (1-\alpha) w_0 \end{aligned} \qquad [14]$$

The coefficient α is connected with the corner values of F, and obtainable by having Eq. [5] hold throughout the hypar surface:

$$\int_0^a \int_0^b \left(\frac{\partial u}{\partial y} + \frac{\partial v}{\partial x} - \frac{2c}{ab} w + \frac{2(1+\mu)}{Ed} \frac{\partial^2 F}{\partial x \, \partial y} \right) dx\, dy = 0 \qquad [15]$$

namely

$$\int_0^a (u_{y=b} - u_{y=0})\, dx + \int_0^b (v_{x=a} - v_{x=0})\, dy - \frac{2c}{ab} \int_0^a\int_0^b w\, dx\, dy + \\ + \frac{2(1+\mu)}{Ed} \left(F_{\substack{x=a\\y=b}} - F_{\substack{x=a\\y=0}} - F_{\substack{x=0\\y=b}} + F_{\substack{x=0\\y=0}}\right) = 0 \qquad [16]$$

By antisymmetry, we have

$$u_{y=0} \equiv 0 \;;\quad v_{x=0} \equiv 0 \;;\quad F_{\substack{x=a\\y=0}} = F_{\substack{x=0\\y=b}} = F_{\substack{x=0\\y=0}} = 0$$

and the remaining condition to be satisfied is:

$$\int_0^a u_{y=b} dx + \int_0^b v_{x=a} dy - \frac{2c}{ab} \int_0^a\int_0^b w\, dx\, dy + \frac{2(1+\mu)}{Ed} F_{\substack{x=a\\y=b}} = 0 \qquad [17]$$

For edge conditions $u_{y=b} = 0$, $v_{x=a} = 0$ we have at $x = a$; $y = b$:

$$F_{\substack{x=a\\y=b}} = \frac{Ed}{1+\mu} \;\frac{c}{ab} \int_0^a\int_0^b w\, dx\, dy \qquad [18]$$

Applying Eqs. [14] to [18], and bearing in mind that $w_0 \equiv 0$ and $F_{1_{\substack{x=a\\y=b}}} = 0$, we have

$$(1-\alpha)\, F_{0_{\substack{x=a\\y=b}}} = (1-\alpha)\, \frac{qa^2b^2}{2c} = \frac{Ed}{1+\mu} \;\frac{c}{ab}\, \alpha \int_0^a\int_0^b w_1 dx\, dy \qquad [19]$$

The integral $I = \int_0^a\int_0^b w_1 dx\, dy$ is readily obtainable by the finite-differences method. Defining the average of w_1 as $W_1 = I/ab$, we finally have for α, β:

$$\alpha = \frac{1}{1 + \dfrac{2c^2 I E d}{(1+\mu)\, qa^3b^3}} = \frac{1}{1 + \dfrac{W_1}{W_0}} = \frac{W_0}{W_0 + W_1} \quad ; \quad \beta = 1 - \alpha = \frac{W_1}{W_0 + W_1} \qquad [20]$$

and for w, F:

$$F = \alpha F_1 + \beta F_0 = \alpha F_1 + \beta\, \frac{qabxy}{2c} \qquad [21]$$

$$w = \alpha w_1 + \beta w_0 = \alpha w_1$$

3. Numerical solution

Eqs. [3] were solved by finite differences in a square grid with side Δ (see Fig. 3). As is known, the method converts a system of differential equations into one of linear equations with F_1 and w_1 at the grid points as the unknowns in the present case. These are given at the hypar edges acc. to [12], and equations for F_1 and w_1 should be set up for interior points, substituting the appropriate derivatives in Eqs. [3]. For a typical point (row i, colum j of the grid) we have after rearrangement:

$$20w_{1_{i,j}} - 8\left(w_{1_{i+1,j}} + w_{1_{i-1,j}} + w_{1_{i,j+1}} + w_{1_{i,j-1}}\right) + 2\left(w_{1_{i+1,j+1}} + w_{1_{i+1,j-1}} + w_{1_{i-1,j+1}} + w_{1_{i-1,j-1}}\right) +$$

$$+ w_{1_{i+2,j}} + w_{1_{i-2,j}} + w_{1_{i,j+2}} + w_{1_{i,j-2}} + \frac{c\Delta^2}{K2ab}\left(F_{1_{i+1,j+1}} - F_{1_{i+1,j-1}} - F_{1_{i-1,j+1}} + F_{1_{i-1,j-1}}\right) = q_{i,j}\frac{\Delta^4}{K}$$

$$20F_{1_{i,j}} - 8\left(F_{1_{i+1,j}} + F_{1_{i-1,j}} + F_{1_{i,j+1}} + F_{1_{i,j-1}}\right) + \qquad [22]$$

$$+ 2\left(F_{1_{i+1,j+1}} + F_{1_{i+1,j-1}} + F_{1_{i-1,j+1}} + F_{1_{i-1,j-1}}\right) + F_{1_{i+2,j}} + F_{1_{i-2,j}} + F_{1_{i,j+2}} + F_{1_{i,j-2}} -$$

$$- \frac{c\Delta^2 Ed}{2ab}\left(w_{1_{i+1,j+1}} - w_{1_{i+1,j-1}} - w_{1_{i-1,j+1}} + w_{1_{i-1,j-1}}\right) = 0$$

For facilitating the numerical solution, the above is converted to non-dimensional variables as follows:

$$\bar{w} = \sqrt{\frac{Ed}{K}}\, w_1 = \frac{\sqrt{12(1-\mu^2)}}{d}\, w_1$$

$$\bar{F} = \frac{1}{K} F_1 \qquad [23]$$

$$\bar{q} = \frac{\Delta^4}{K}\sqrt{\frac{Ed}{K}}\, q = \frac{\Delta^4\sqrt{12(1-\mu^2)}}{Kd}\, q$$

$$\varepsilon = \frac{c\Delta^2}{2ab}\sqrt{\frac{Ed}{K}} = \frac{c\Delta^2\sqrt{3(1-\mu^2)}}{abd}$$

and substitution in Eqs. [22] yields:

$$20\bar{w}_{i,j} - 8\left(\bar{w}_{i+1,j} + \bar{w}_{i-1,j} + \bar{w}_{i,j+1} + \bar{w}_{i,j-1}\right) + 2\left(\bar{w}_{i+1,j+1} + \bar{w}_{i+1,j-1} + \bar{w}_{i-1,j+1} + \bar{w}_{i-1,j-1}\right) +$$

$$+ \bar{w}_{i+2,j} + \bar{w}_{i-2,j} + \bar{w}_{i,j+2} + \bar{w}_{i,j-2} + \varepsilon\left(\bar{F}_{i+1,j+1} - \bar{F}_{i+1,j-1} - \bar{F}_{i-1,j+1} + \bar{F}_{i-1,j-1}\right) = \bar{q}_{i,j}$$

$$[24]$$

$$20\bar{F}_{i,j} - 8\left(\bar{F}_{i+1,j} + \bar{F}_{i-1,j} + \bar{F}_{i,j+1} + \bar{F}_{i,j-1}\right) + 2\left(\bar{F}_{i+1,j+1} + \bar{F}_{i+1,j-1} + \bar{F}_{i-1,j+1} + \bar{F}_{i-1,j-1}\right) +$$

$$+ \bar{F}_{i+2,j} + \bar{F}_{i-2,j} + \bar{F}_{i,j+2} + \bar{F}_{i,j-2} - \varepsilon\left(\bar{w}_{i+1,j+1} - \bar{w}_{i+1,j-1} - \bar{w}_{i-1,j+1} + \bar{w}_{i-1,j-1}\right) = 0$$

The set of points at distance Δ from the edge includes exterior points, in which case conditions [12] stipulate that the second derivatives of F_1, w_1 ($\bar{F}$, $\bar{w}$) vanish normal to the edge. With these additional equations included, the total number of equations equals that of unknowns, i.e. a pair for each point. (For their formulation and solution, see below).

With the system solved, W_1 is obtained numerically:

$$W_1 = \frac{1}{ab} \int_0^a \int_0^b w_1 dx dy = \frac{\Delta^2}{ab} \sum_{i=1}^{m} \sum_{j=1}^{n} \varrho_{i,j} w_{1_{i,j}} \qquad [25]$$

where $\varrho_{i,j}$ is a non-dimensional coefficient expressing the fraction of the square Δ^2 represented by $w_{1_{i,j}}$. It equals 1 for interior points, ½ for the edges and ¼ for the corners. W_1 yields α and β acc. to [20] and the final values of F and w at all grid points acc. to [21].

For the forces and moments the same procedure is applied to Eq. [4], which yields for a typical point:

$$N_x = \frac{F_{i+1,j} - 2F_{i,j} + F_{i-1,j}}{\Delta^2} \quad ; \quad M_x = -K\left(\frac{w_{i,j+1} - 2w_{i,j} + w_{i,j-1}}{\Delta^2} + \mu \frac{w_{i+1,j} - 2w_{i,j} + w_{i-1,j}}{\Delta^2}\right)$$

$$N_{xy} = -\frac{F_{i+1,j+1} - F_{i+1,j-1} - F_{i-1,j+1} + F_{i-1,j-1}}{4\Delta^2} \; ;$$

$$M_{xy} = -K(1-\mu)\frac{w_{i+1,j+1} - w_{i+1,j-1} - w_{i-1,j+1} + w_{i-1,j-1}}{4\Delta^2} \qquad [26]$$

$$N_y = \frac{F_{i,j+1} - 2F_{i,j} + F_{i,j-1}}{\Delta^2} \quad ; \quad M_y = -K\left(\frac{w_{i+1,j} - 2w_{i,j} + w_{i-1,j}}{\Delta^2} + \mu \frac{w_{i,j+1} - 2w_{i,j} + w_{i,j-1}}{\Delta^2}\right)$$

As the numerical solution utilizes the symmetry and antisymmetry properteis of the structure, load and unknowns, analysis of one quadrant suffices (see Fig. 3).

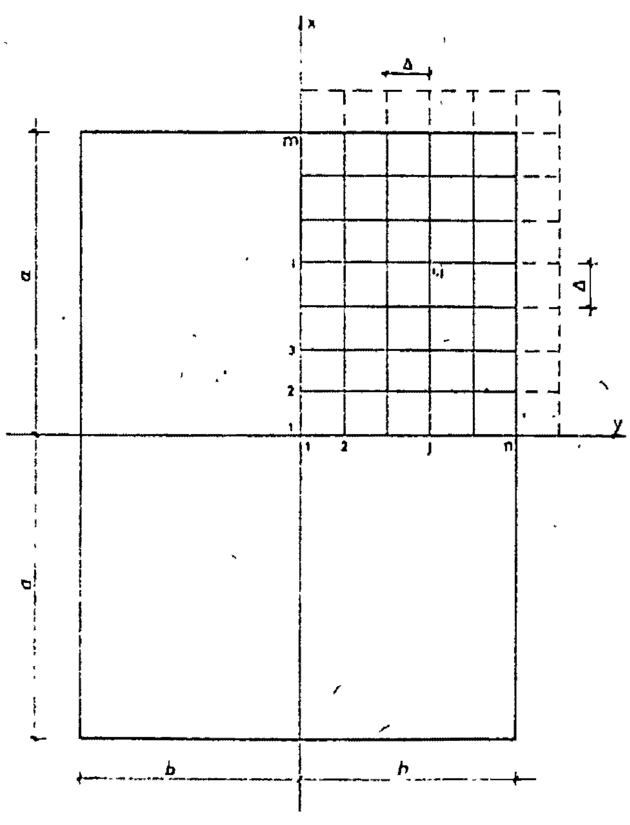

Fig. 3

Fig. 4

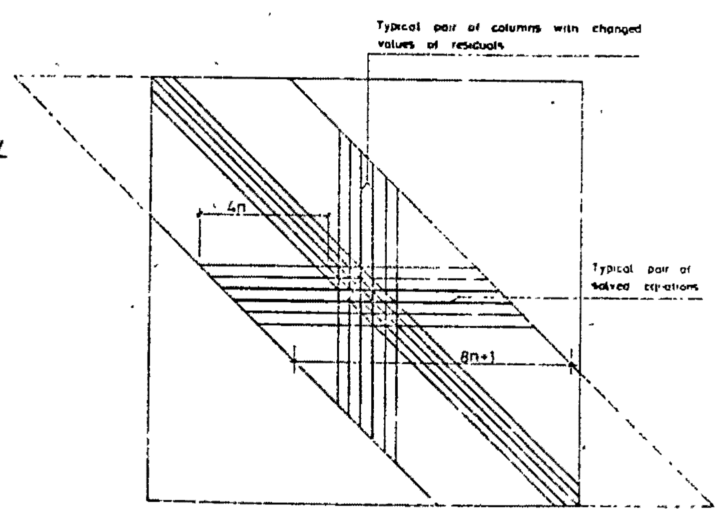

The structure of Eq. [22] indicates that for a typical unknown, only some of the coefficients are non-zero. If the pairs of equations are written down in ascending order of rows and columns, and the w_i equation precedes that of F_i, a band matrix is obtained for these coefficients (see Fig. 4), and it is easily verified that its half-width is $4n$ (measured from the principal diagonal). In addition, only certain diagonals of the band contain non-zero elements. Solution is again by the relaxation method (see e.g. Shaw (4)), with only non-zero coefficients taken into account. This permits large systems of equations to be solved without recourse to a large memory capacity. The initial solution required was obtained by the elimination method in a sparse grid and interpolation of the results for the final dense grid, with Eq. [24] rewritten as follows:

$$
\begin{aligned}
&20\bar{w}_{i,j} - 8(\bar{w}_{i+1,j} + \bar{w}_{i-1,j} + \bar{w}_{i,j+1} + \bar{w}_{i,j-1}) + 2(\bar{w}_{i+1,j+1} + \bar{w}_{i+1,j-1} + \bar{w}_{i-1,j+1} + \bar{w}_{i-1,j-1}) + \\
&+ \bar{w}_{i+2,j} + \bar{w}_{i-2,j} + \bar{w}_{i,j+2} + \bar{w}_{i,j-2} + \varepsilon(\bar{F}_{i+1,j+1} - \bar{F}_{i+1,j-1} - \bar{F}_{i-1,j+1} + \bar{F}_{i-1,j-1}) - \bar{q}_{i,j} = R_{w_{i,j}}, \\
&20\bar{F}_{i,j} - 8(\bar{F}_{i+1,j} + \bar{F}_{i-1,j} + \bar{F}_{i,j+1} + \bar{F}_{i,j-1}) + 2(\bar{F}_{i+1,j+1} + \bar{F}_{i+1,j-1} + \bar{F}_{i-1,j+1} + \bar{F}_{i-1,j-1}) + \\
&+ \bar{F}_{i+2,j} + \bar{F}_{i-2,j} + \bar{F}_{i,j+2} + \bar{F}_{i,j-2} - \varepsilon(\bar{w}_{i+1,j+1} - \bar{w}_{i+1,j+1} - \bar{w}_{i-1,j+1} + \bar{w}_{i-1,j-1}) = R_{F_{i,j}},
\end{aligned}
\tag{27}
$$

As the first step, the pair of equations with the largest sum of absolute values of the residuals $|R_{w_{i,j}}| + |R_{F_{i,j}}|$ is determined. The unknowns are then recalculated on the basis of the basis of the above pair, assuming that the others remain unchanged. It can be shown that in these circumstances only the equations for the columns indicated in Fig. 4 are subject to change of their residuals, so that the iterative process can be confined to these columns. It continues untill sufficient accuracy is achieved, i.e. untill the above sum of absolute values is reduced below a given low parameter.

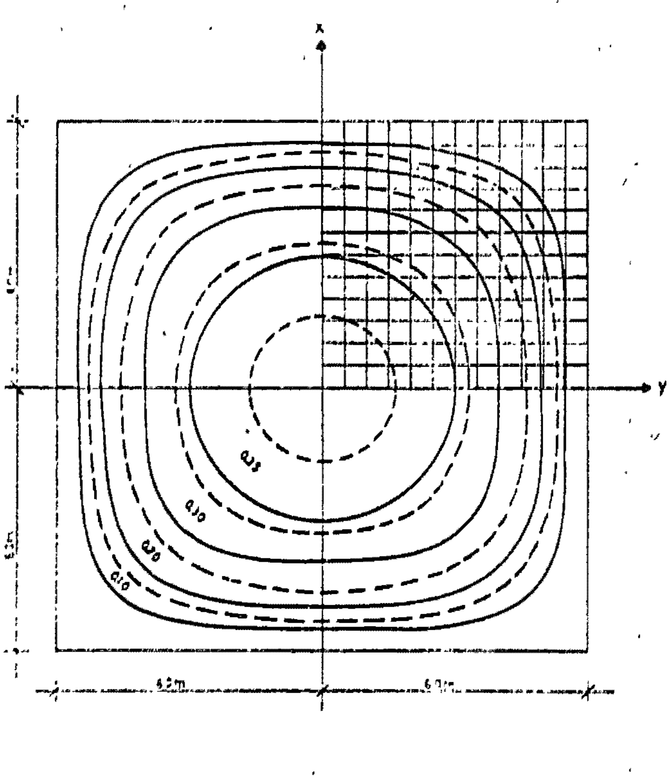

w(cm) example 1 – – –
w(cm) example 2 ———

Fig. 5

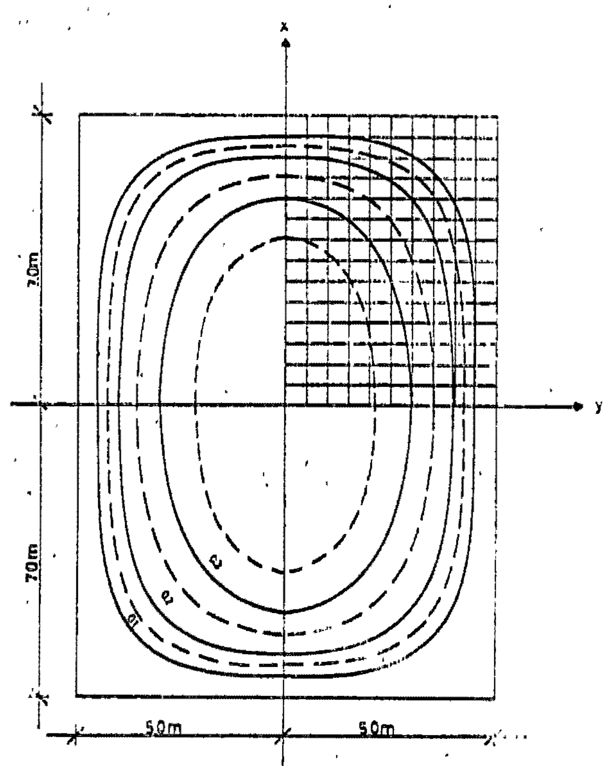

w(cm) example 3 – – –
w(cm) example 4 ———

Fig. 6

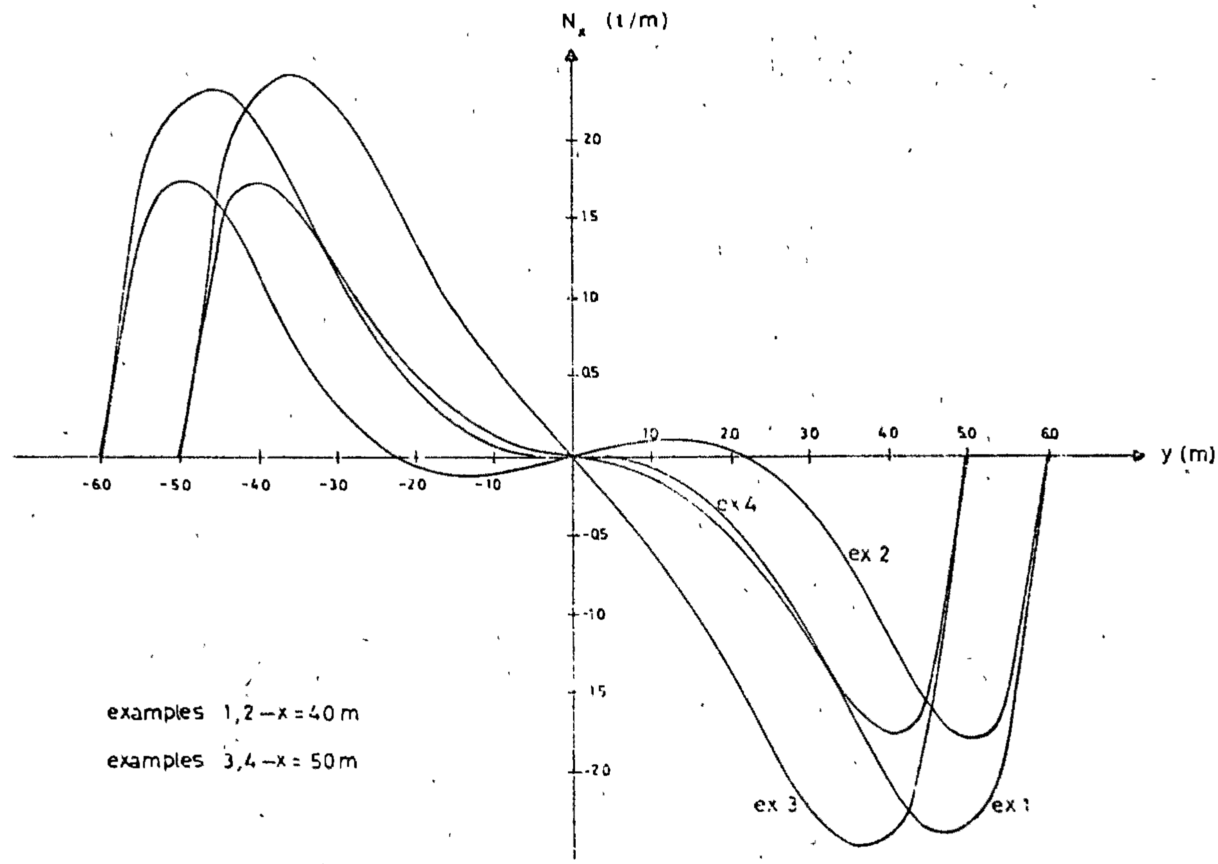
N_x (t/m)
y (m)
ex 1
ex 2
ex 3
ex 4
examples 1,2 – x = 40 m
examples 3,4 – x = 50 m

Fig. 7

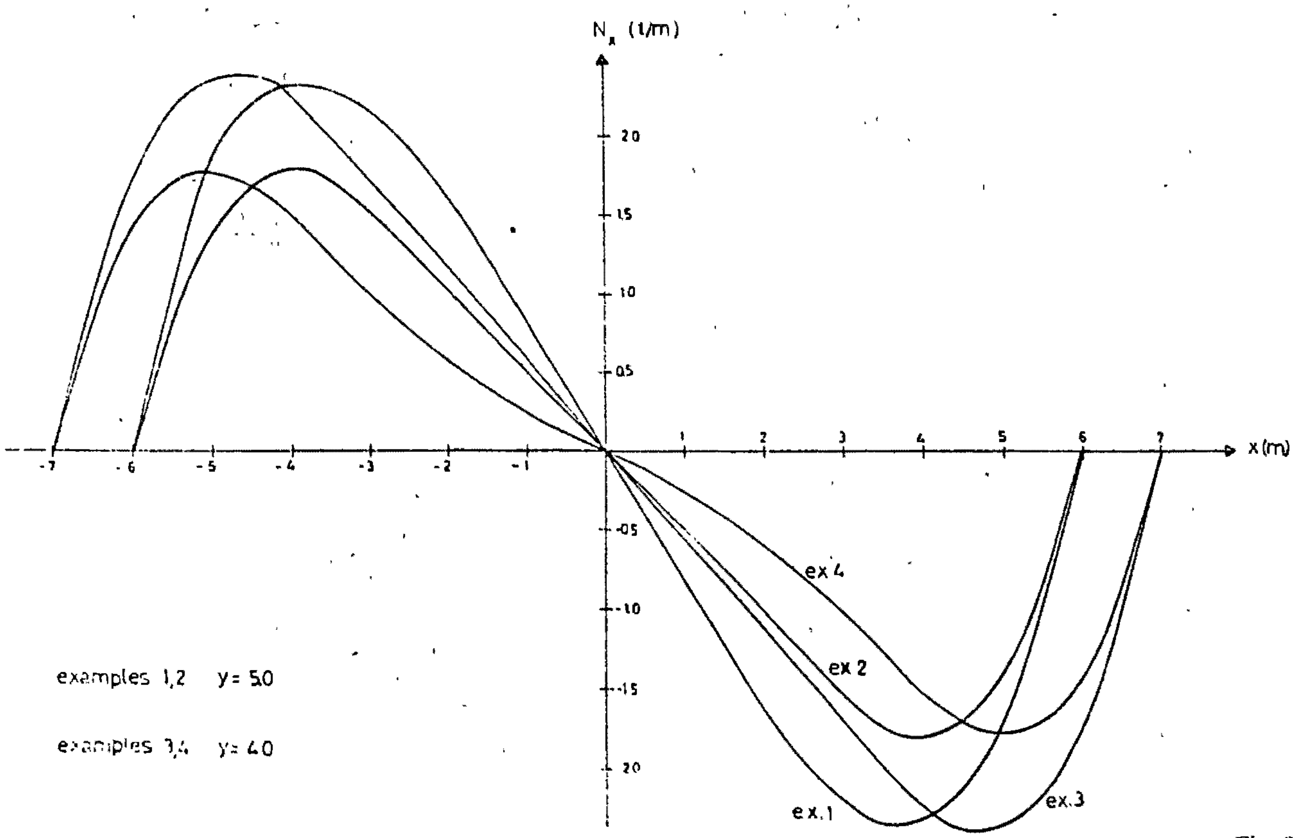
N_x (t/m)
x (m)
ex.1
ex 2
ex.3
ex 4
examples 1,2 y= 50
examples 3,4 y= 40

Fig. 8

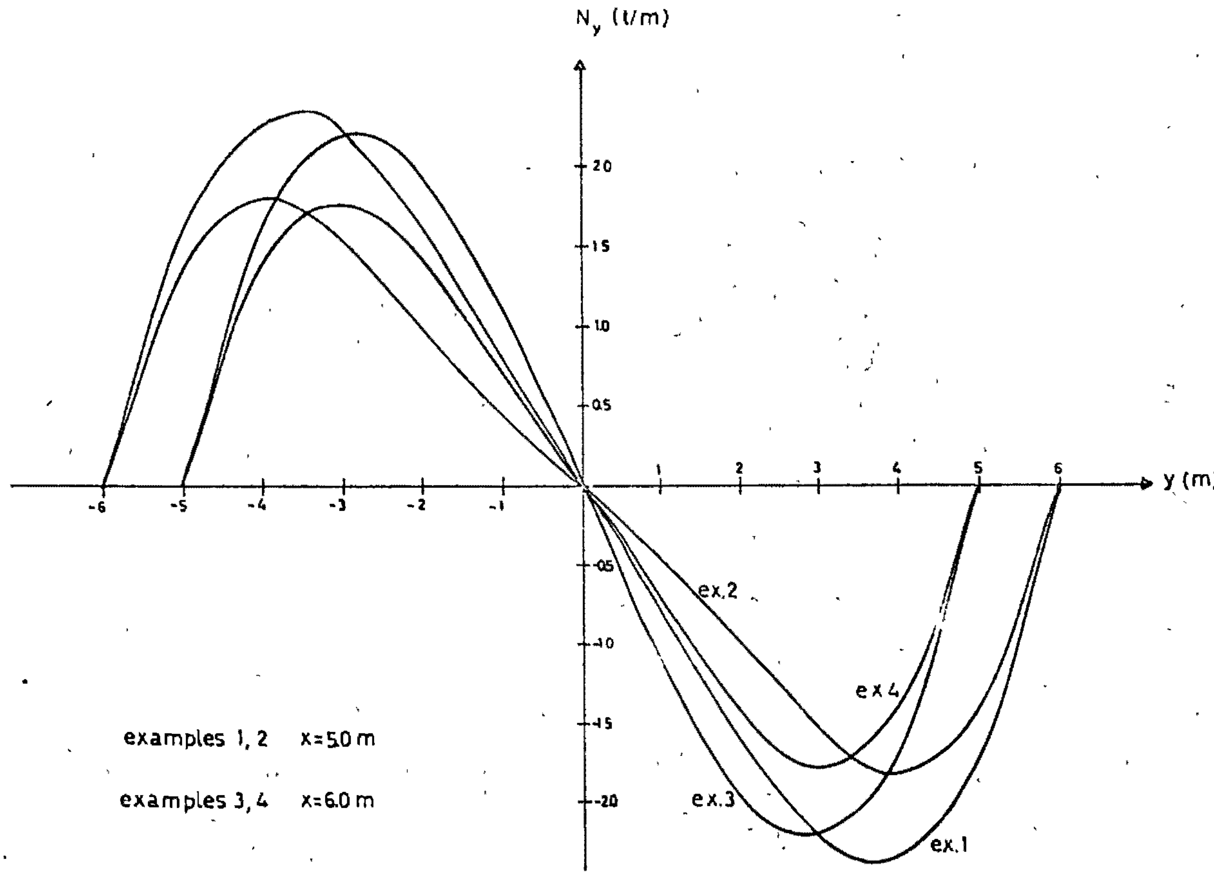

N_y (t/m)
y (m)
ex.1
ex.2
ex.3
ex.4
examples 1, 2 x=5.0 m
examples 3, 4 x=6.0 m

Fig. 9

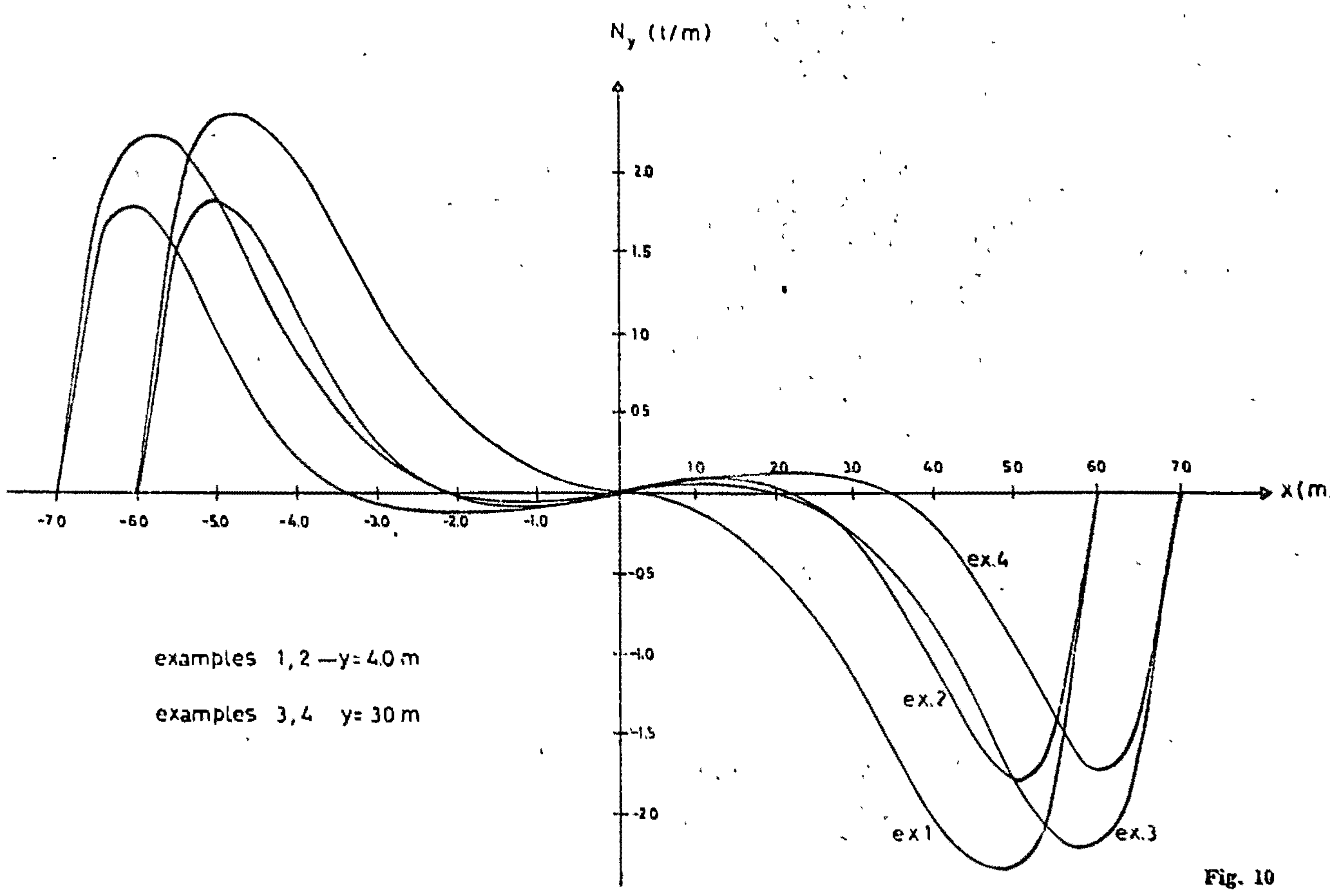

N_y (t/m)
x (m)
ex.1
ex.2
ex.3
ex.4
examples 1, 2 —y= 4.0 m
examples 3, 4 y= 30 m

Fig. 10

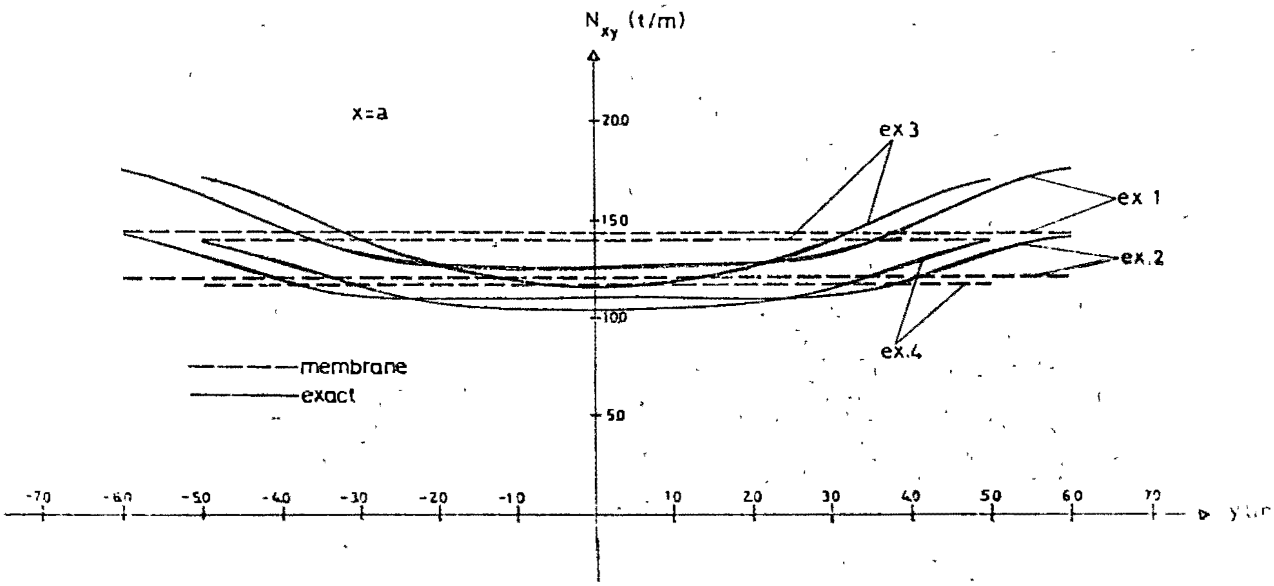

Fig. 11

4. Numerical examples

The influence of variation of the shell parameters on the magnitude and point of application of the forces and moments was verified in four examples acc. to Fig. 1. Data are summarized in Table 1; the load was 1 t/m² in all cases, and the elastic constants $E = 2.1 \times 10^6$ t/m² and $\mu = 0$. Force-, moment-, and settlement diagrams are given in Figs. 5-18. The N_{xy} diagram is compared with the membrane-state result.

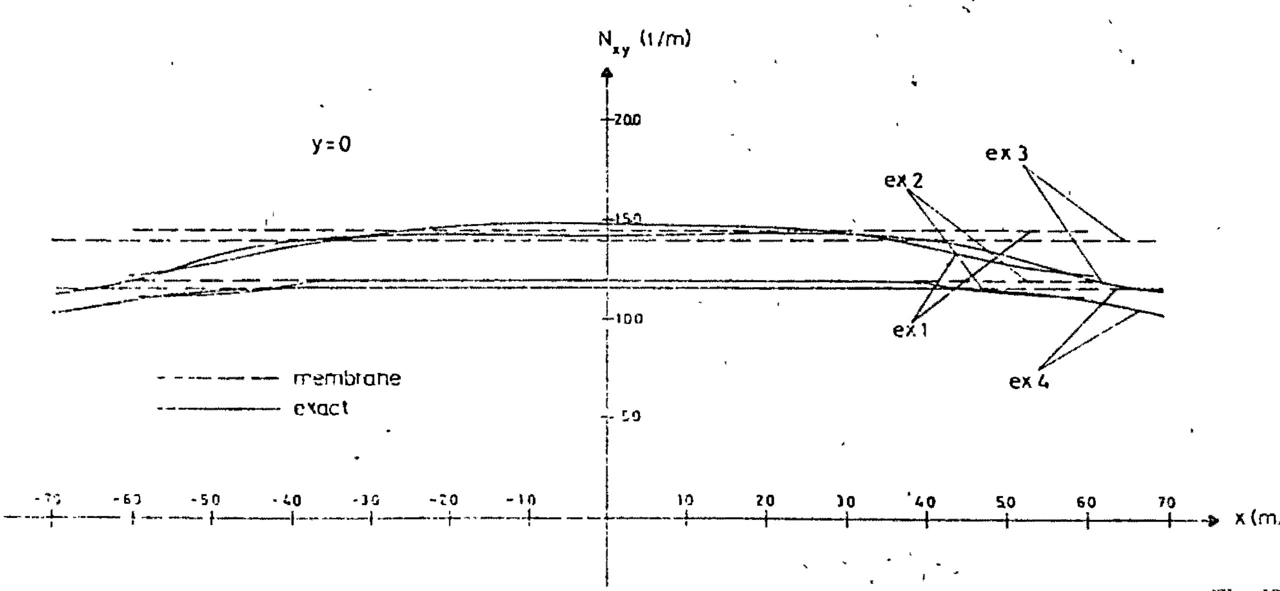

Fig. 12

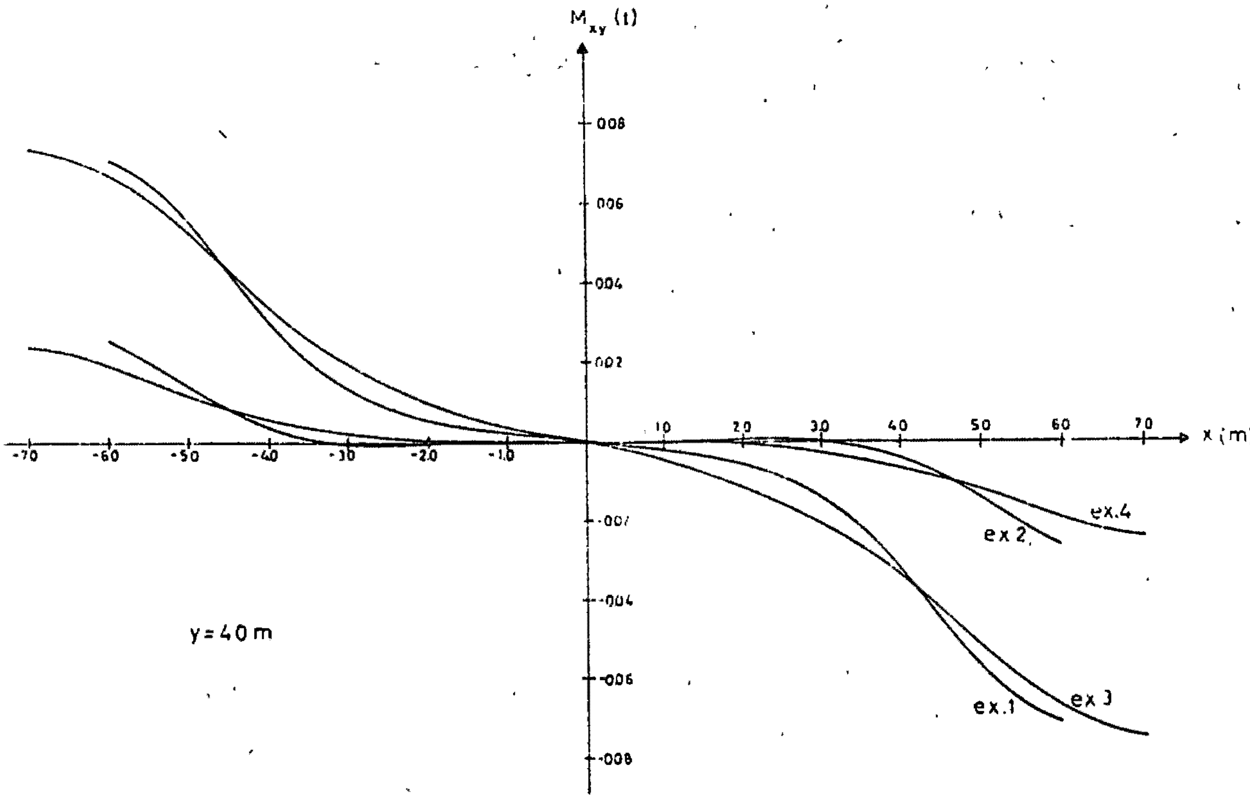

Fig. 18

TABLE 1

Example No.	a (m)	b (m)	c (m)	d (m)	a/b	$2c/d$
1	6	6	1.25	0.10	1.0	25
2	6	6	1.50	0.06	1.0	50
3	7	5	1.25	0.10	1.4	25
4	7	5	1.50	0.06	1.4	50

5. Conclusions

The maximum and membrane settlements (Eq. [11]) are compared in Table 2.

TABLE 2

Example No.	W_{max} (cm)	W_0 (cm)	$W_{max} - W_0$ (cm)	$W_{max} - W_0$ (%)
1	0.358	0.198	0.160	81
2	0.360	0.229	0.131	57
3	0.343	0.187	0.156	83
4	0.349	0.216	0.136	63

u, v, w / u_1, v_1, w_1 = displacements in x-, y-, z-directions respectively

F_0 = Airy function in membrane-state displacements

u_0, v_0, w_0, W_0 = membrane-state displacements

q = vertical load

$N_x, N_y, N_{x_0}, N_{y_0}$ = normal forces

N_{xy}, N_{xy_0} = shear forces

M_x, M_y = flexural moments

M_{xy} = torque

Q_x, Q_y = shearing forces

$\varepsilon_x, \varepsilon_y$ = normal strains

γ_{xy} = shear strain

U, V, W / $\alpha, \beta, \varrho, \varepsilon$ = constants

I = value of double integral

W_1 = average of w_1

Δ = distance between two points in finite-differences grid

i = serial number of typical row in finite-differences grid

j = serial number of typical column in finite-difference grid

m = number of rows in finite-differences grid

n = number of columns in finite-differences grid

$\bar{F}$ = non-dimensional Airy stress function

$\bar{w}$ = non-dimensional vertical displacement

$\bar{q}$ = non-dimensional vertical load

R_F, R_w = residuals

$$\nabla^2 = \frac{\partial^2}{\partial x^2} + \frac{\partial^2}{\partial y^2}$$

Bibliography

(1) CANDELA, F.: General Formulas for Membrane Stresses in Hyperbolic Paraboloidal Shells. ACI Journal, 32, October 1960.

(2) BONGARD, W.: Zur Theory und Berechnung von Schalentrakwerken in Form Gleichseitiger Hyperbolisher Paraboloid Bautechnich-Archiv 15, Verlag von Wilhelm Ernst & Sohn, Berlin 1959.

(3) WLASSOW, W. S.: Allgemeine Schalentheorie und ihre Anwendung in der Technik Akademie-Verlag, Berlin 1958

(4) S[illegible]w, F. S.: Relaxation Methods, Dover Publications Inc, 1953.

It can be seen that settlements in the middle zone exceed considerably their membrane counterparts. This confirms the known conclusion that, in contrast to synclasitc shells (whose middle region is practically in a membrane state, and in which the flexural effect is reflected in edge disturbances), in anticlastic shells like the hypar the entire surface is affected, and the shallower the shell, the stronger the effect. However, although no flexure-free zone can be defined, both the curvature of the settlement envelope and the moments are small owing to the gradual reduction in w near the edges. Most of the load is transmitted to the gable walls by the shear force N_{xy}. N_x and N_y are likewise small, but not as negligible as the moments; their order of magnitude ranges from 10 to 15 % of N_{xy} and their sign changes antisymmetrically according to the quadrant.

The maximum and membrane shear forces are compared in Table 3. The difference between them is seen to be about 20 %, so that in a membrane-designed hypar the actual safety factor will be about 80 % of the allowed figure. This is the most important conclusion to be drawn from the above examples.

TABLE 3

Example No.	Flexural N_{xy} (t)	Membrane N_{xy_0} (t)	$N_{xy} - N_{xy_0}$ (t)	$N_{xy} - N_{xy_0}$ (%)
1	— 17.5	— 14.3	3.1	21.5
2	— 14.3	— 12.0	2.3	19.2
3	— 17.0	— 14.0	3.0	21.4
4	— 13.9	— 11.7	2.2	18.8

6. Acknowledgment

The authors are indebted to Prof. L. Fischer for valuable advice in the course of the work.

7. Notation

a = width of hypar quadrant

b = length of hypar quadrant

c = height of hypar quadrant

d = thickness

x, y, z = coordinates of middle surface of hypar

r = curvature in x-direction

s = twist

t = curvature in y-direction

E = modulus of elasticity of material

μ = Poisson's ratio of material

K = flexural rigidity

F, F_1 = Airy functions

news

research
for engineers
trends
for contractors
shapes
for architects

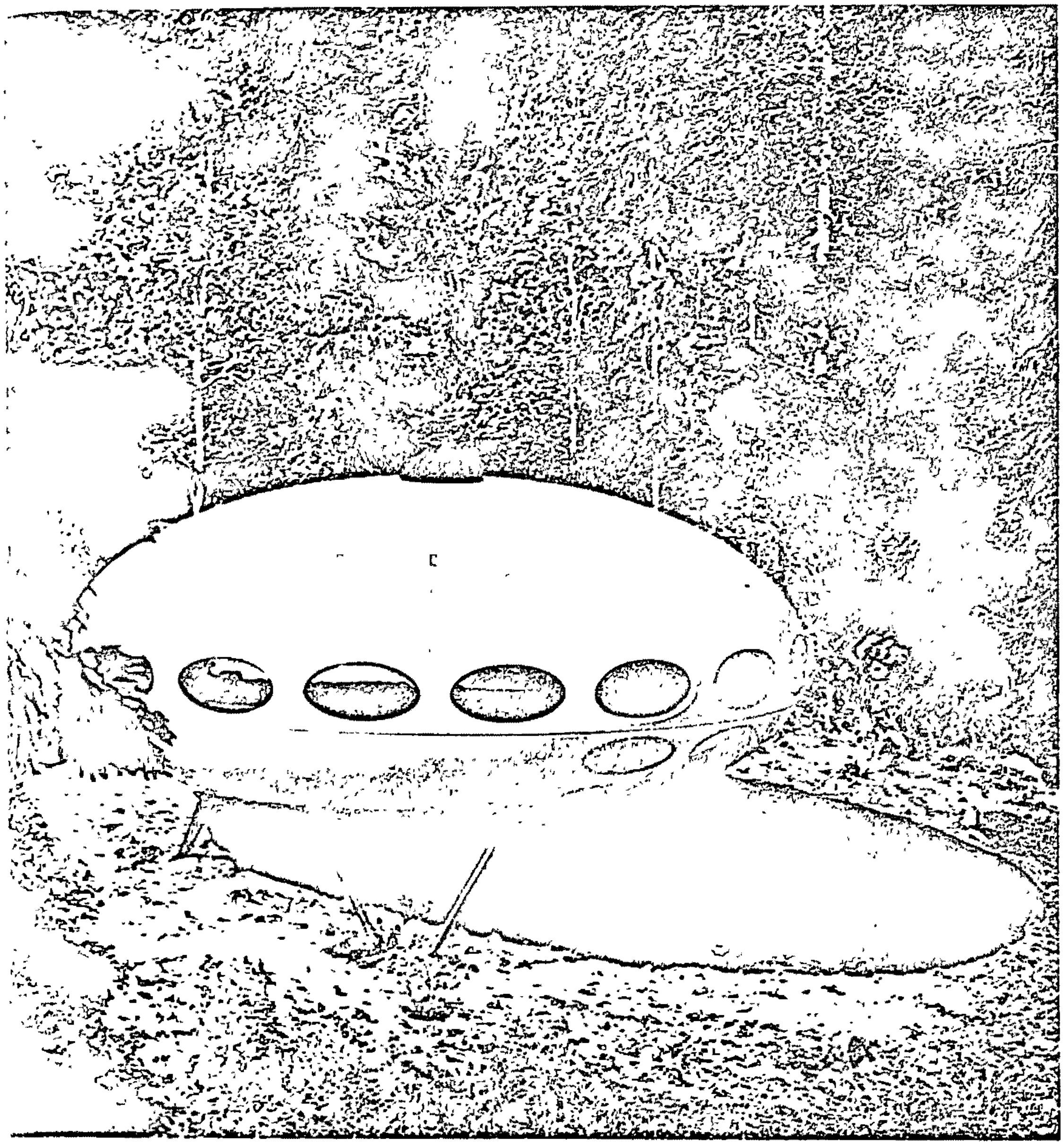

FINLAND

«Futuro» house, prefabricated shell structure.

Design Matti Suuronen, arch. and Yrjö Ronkka struct. eng.

Material: Sandwich structure of glassfiber polyester shells with polyurethan core.

The house is manufactured in Finland by Oy Polykem Ab and is now licensed for mass production in several countries amongst which Germany, Sweden and the U.S.A.

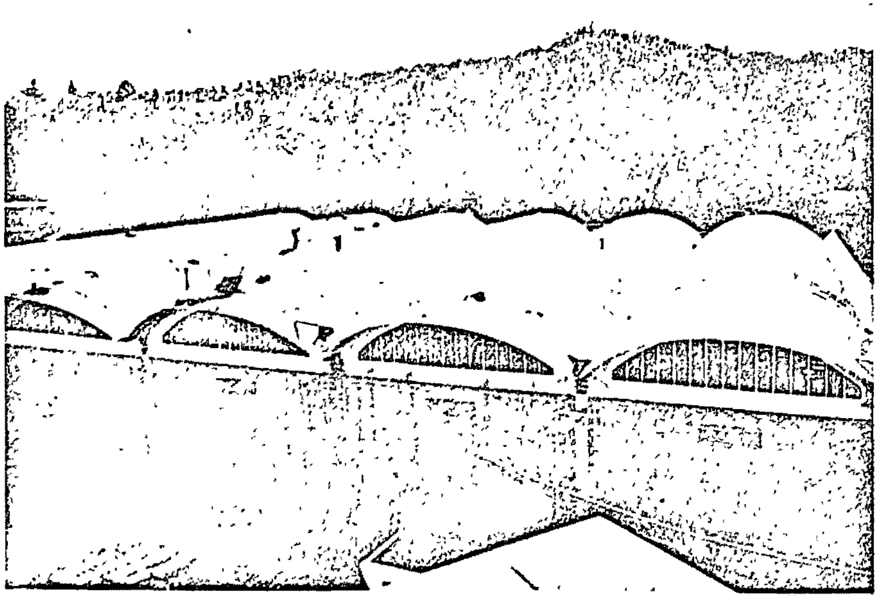

59

U. S. A.

Gymnasium for the Appalachian State University, Boone (North Carolina) Cylindrical shells; transversaly continuous and longitudinaly supported at gables.

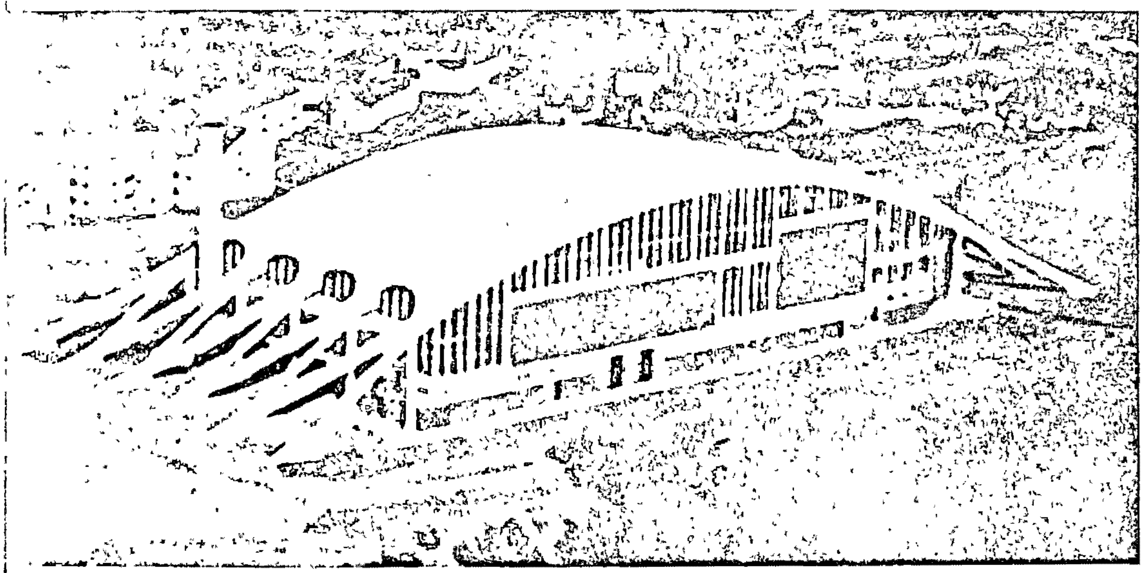

UNITED KINGDOM

Dollan baths at East Kilbride, Lanarkshire. Structurally, the building consists of five parabolic arch ribs, which span 324 ft at ground level. Four elliptical shells each 3 in thick at the crown, span between the ribs.

Arch. A. Buchanan Campbell.

Cons. Eng. T. Harley Haddow and Partners.

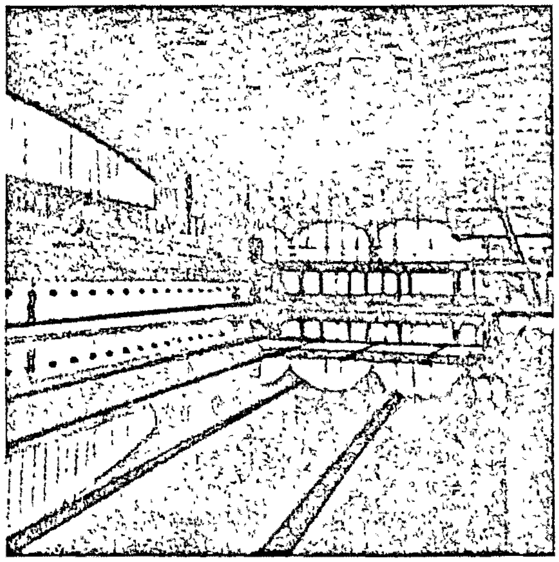

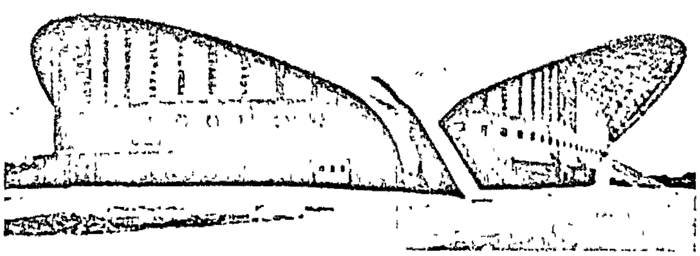

U. S. A.

Coliseum for the University of Georgia. The lightweight concrete roof structure, which cantilevers out over the entrance of the building, is made up of nearly 10,000 precast elements.

Arch.: Cooper, Barrett, Skinner, Woodbury and Cooper.

Eng.: Chastain and Trudel Incorporated.

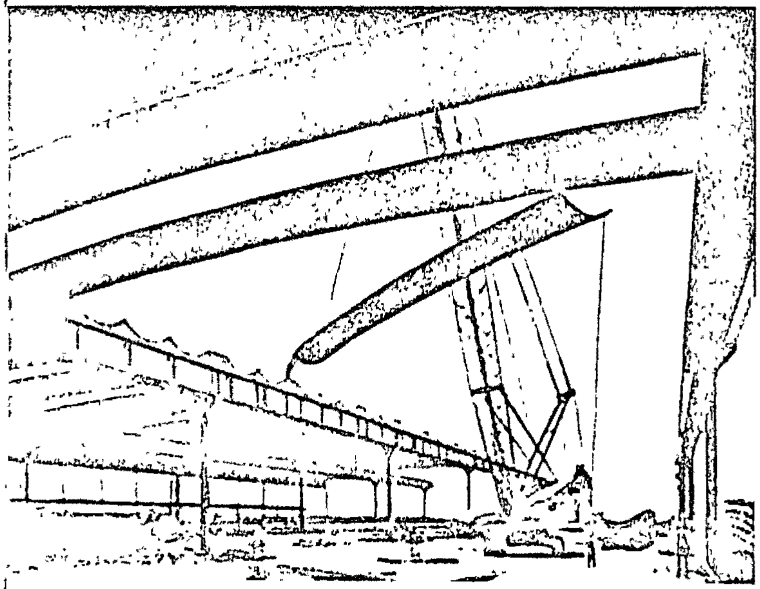

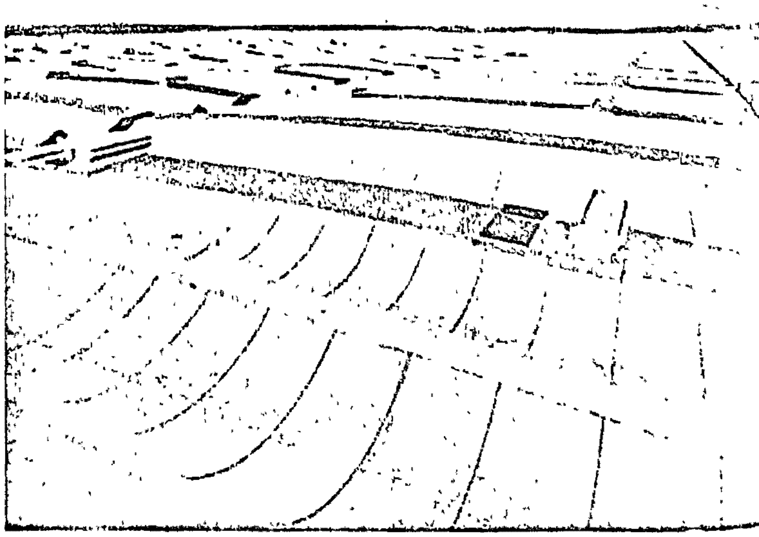

UNITED KINGDOM

Freeman's Warehouse at Peterborough.

The illustration of the erection of one of the precast hypar shells shows several constructional details. The other figure shows the completed roof.

Arch. Scott, Brownrigg and Turner Consulting Struct. Eng. Kenchington, Little and Partners.

news research - for engineers
trends - for contractors
shapes - for architects

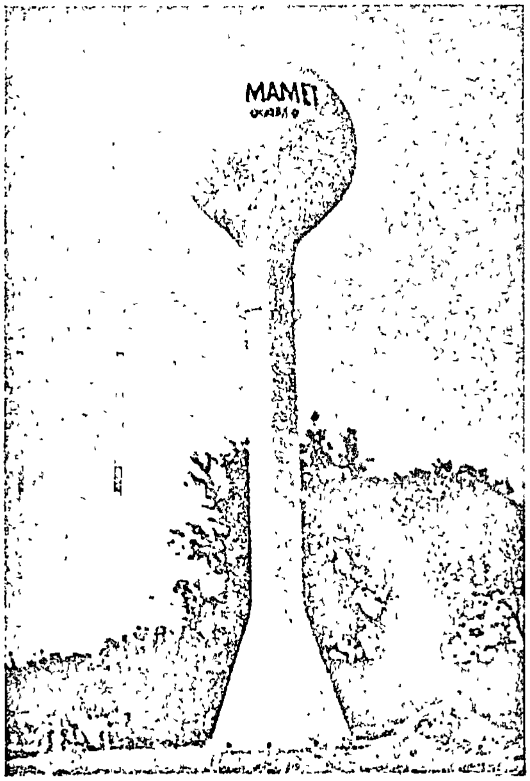

Spherical tank, capacity 100 m³. Heigt 16 m. Conserveries de Saint-Mamet.

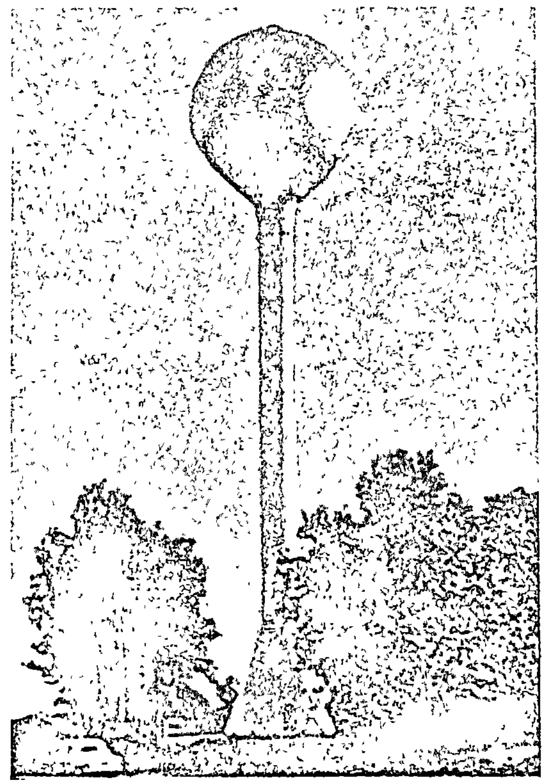

Spherical tank, capacity 600 m³. Height 34 m. Syndicat intercommunal de Montenboeuf.

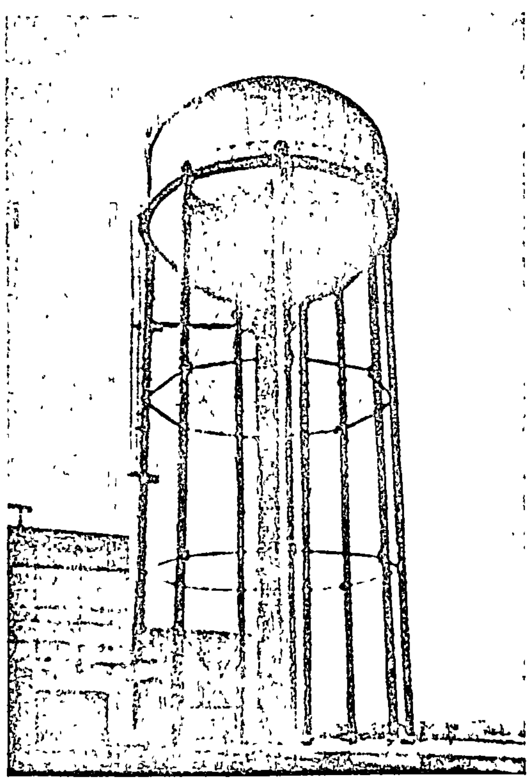

Ellipsoid tank. Capacity 1 900 m³. Height 34 m. Société Lorraine de Laminage à Florange.

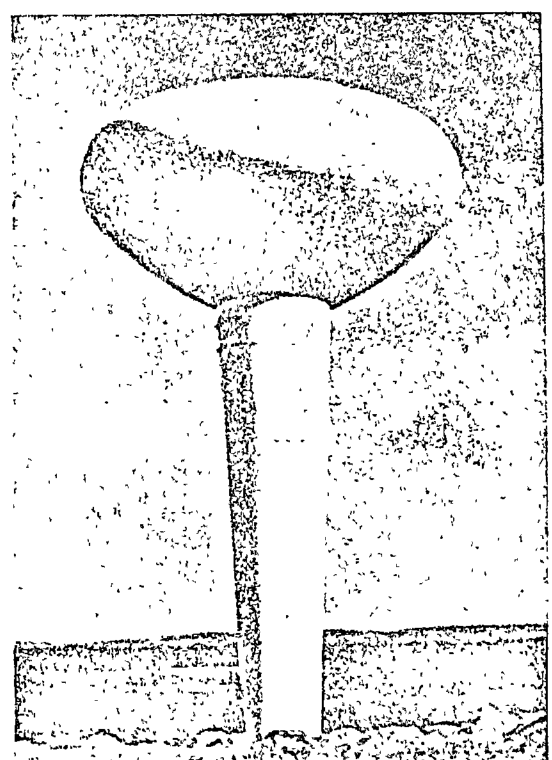

Spheroid tank. Capacity 2 800 m³. Height 27.5 m. Société d'Equipement de la Région Mantaise.

FRANCE. Water tanks, completely welded steel which ensures an absolute watertightnees.

books

Bauingenieur - Praxis Heft 15
SHELLS OF REVOLUTION WITH FLEXURAL STIFFNESS
1968 Verlag von Wilhem Ernst and Sohn. Berlin - München.
120 pages, 82 figures, 28 tables. Price of this book 23.60 D. M.

This book can be easily handled due to its size: DIN A5. It is divided into three parts.

The first part corresponds to formulae of general kind. There are shown, in an intuitive manner, the definitions, geometry, types of actions, and stresses of this kind of shells. There is also presented the theory of membrane and shell under axil-symmetrical loading, presenting general equations, edge conditions and the corresponding solutions with application to the two usual cases: vault and circular cylinder of constant thickness.

In this book is also studied other kind of loading as wind and temperature and some formulae of elastic estability are presented.

The second part is concerned with complementary formulae corresponding to the most generalized cases of revolution of shells and no homogeneous boundary conditions such as beams.

Finally, a numerical example is completely developed.

This book presents an elemental character in the exposition and is specially useful for students and engineers who are interested in contacting with this theme.

Proceedings of the IASS Congress on the Problems of Interdependence between design and Construction of Large Span Shells for Industrial and Civil Buildings.

Held in September, 6-9, 1966, in Leningrad (In two volumes: v.1 - 50 sheets; v.2 - 30 sheets, 1 500 copies).

Reports are published in English, German and French, i.e. in the language they were presented.

The Proceedings will be published in the fourth quarter of the year. The price of Volume 1 - 9 roubles, the price of Volume 2 - 6 roubles (NK 23/67 - 68).

The books contain data on world experience on the following problems: design of shells (detailing, standardization, economy, calculations); research in shells; manufacture and erection of shells made of concrete, steel, wood, plastics and other materials as well as examples of projects using such structures completed for the last 10 years.

Volume 1 contains 55 reports and discussion material on the problems of design and research in shells. Volume 2 contains 34 reports and discussion material on the problems of design and construction of concrete, steel lattice and suspended shells as well as outstanding examples of completed structures.

The Proceedings are edited by the Research Institute of Concrete and Reinforced Concrete and the Central Institute of Scientific Information on Construction and Architecture of the Gosstroy of the USSR.

The books are bound in hard covers with a colourful dust-cover, have many illustrations and extensive bibliography. The books are printed on a Rotaprint machine; the format is a convenient size.

You may order these books through booksellers in your country dealing with the literature from the Soviet Union. V/0 «Mezhdunarodnaya Knika», Moscow - 200, USSR.

centro de educación continua de la facultad de ingeniería, unam

DISEÑO Y CONSTRUCCION DE ESTRUCTURAS ESPACIALES Y DE CASCARON

TEORIA Y APLICACIONES A SILOS Y TANQUES

DR. PORFIRIO BALLESTEROS

TELS 521-30 95 Y 513-27-95 TACUBA 5, MEXICO 1, D F

The continuing development of design and construction techniques of shell structures is resulting in an increasing fund of information of practical interest to Architects, Engineers and Contractors. The aim of furthering all branches of this progress has inspired the formation of the **international association for shell and spatial structures,** whose purpose is to organise meetings and congresses for the interchange of ideas and their dissemination by means of periodical publications.

Everyone interested in the various branches of shell techniques and their architectonic possibilities or realizations is invited to join this International Association.

To become a member or to obtain more detailed information, please write to the Secretariat of the International Association for Shell and Spatial Structures, Alfonso XII, 3, Madrid (7). Spain.

TANQUES CILINDRICOS, TEORIA Y APLICACIONES

F. del Pozo y P. Ballesteros *

1. Introducción

La simetría que presenta la solicitación de presión hidrostática hace que una de las formas más racionales y económicas para un depósito destinado a contener líquidos sea la cilíndrica con directriz circular.

Adoptada esta forma cilíndrica circular, el procedimiento de cálculo lógico es recurrir a la teoría de flexión de láminas. El caso de lámina cilíndrica de espesor constante con simetría de revolución y solicitación también simétrica respecto al mismo eje de revolución que determina la geometría de la lámina, es afortunadamente, y aceptando las simplificaciones usuales en el cálculo de láminas, uno de los pocos casos en que la teoría, en su estado actual, conduce a una solución explícita muy sencilla.

* Profesores; Universidad de Madrid, España y UNAM, México..

Si el espesor de pared es variable, la solución no es tan simple. Aceptando una ley lineal para la variación del espesor de pared, la solución que se obtiene en el caso de depósito lleno incluye en su formulación funciones conocidas, cuya tabulación se añadirá como final de esta publicación.

Volviendo al caso de espesor de pared constante, la intención de esta publicación es a la vez servir como orientación en el estudio teórico del problema, y proporcionar un instrumento para el proyecto rápido de depósitos de este tipo.

En seguimiento de esta doble intención, en la primera parte del trabajo se hará un desarrollo formal de la teoría de la lámina cilíndrica circular, hasta llegar a unas expresiones literales de los esfuerzos en función del corrimiento radial, y de éste en función de las características de la solicitación y de la geometría del depósito.

En la segunda parte se incluirán unas tablas y unos gráficos que permiten obtener con gran rapidez y comodidad los valores de los esfuerzos y del corrimiento, con vistas a un dimensionamiento inmediato o a una comprobación de la validez de las dimensiones previamente fijadas para el depósito. Y esto para cuatro casos de solicitación del depósito que cubren realmente la mayor parte de su campo de aplicación.

Se ha juzgado interesante añadir, como complemento, siete ejemplos de depósitos de muy diversas características, para que la utilización de teoría, tablas y gráficos quede más claramente expuesta.

Notación

a = radio medio del depósito.

e = base de los logaritmos neperianos.

$k_0, k_1, k_2, k_3, k_4, k_l$ = constantes.

x = coordenada lineal con origen en el borde inferior.

x_0, x_1 = valores particulares de la coordenada x.

w = corrimiento radial, positivo si aumenta el radio.

β = coeficiente en los depósitos de espesor de pared con variación lineal $= \dfrac{\delta_0}{L_1}$.

γ = peso específico del líquido contenido en el depósito.

δ = espesor de la pared.

δ_0 = espesor de la pared para $x = 0$.

$\eta = 2\lambda \sqrt{i(L_1 - x)}$.

$\vartheta = 2\lambda \sqrt{L_1 - x}$.

φ = coordenada polar, ángulo en el centro.

$\varkappa$ = constante del depósito $= \dfrac{\sqrt[4]{3(1-\nu^2)}}{\sqrt{a\delta}}$.

$\varkappa L$ = constante del depósito $= \sqrt[4]{3(1-\nu^2)} \sqrt{\dfrac{L}{a}\,\dfrac{L}{\delta}}$.

λ = coeficiente en los depósitos de espesor de pared con variación lineal =

$= \dfrac{\sqrt[4]{12(1-\nu^2)}}{\sqrt{a\beta}}$.

ν = módulo de Poisson.

$\xi = w \sqrt{L_1 - x}$.

Coef. I = valores dados en la tabla I y gráficos G-I y G-I'.

Coef. II = valores dados en la tabla II y gráfico G-II.,

Coef. III = valores dados en la tabla III y gráfico G-III.

Coef. IV = valores dados en la tabla IV y gráficos G-IV y G-IV'.

Coef. V = valores dados en la tabla V y gráfico G-V.

Coef. VI $=$ valores dados en la tabla VI y gráfico G-VI.

Coef. VII $=$ valores dados en la tabla VII y gráfico G-VII.

Coef. VIII $=$ valores dados en la tabla VIII y gráfico G-VIII.

Coef. IX $=$ valores dados en la tabla IX y gráfico G-IX.

Coef. X $=$ valores dados en la tabla X y gráfico G-X.

Coef. XI $=$ valores dados en la tabla XI y gráfico G-XI.

Coef. XII $=$ valores dados en la tabla XII y gráfico G-XII.

$E =$ módulo de elasticidad.

$K =$ constante del depósito $= \dfrac{E\delta^3}{12(1-\nu^2)}$.

$K_\beta =$ constante de un depósito de espesor de pared con variación lineal $=$

$= \dfrac{E\beta^3}{12(1-\nu^2)}$.

$K_1, K_2, K_3, K_4 =$ constantes de integración.

$L =$ altura del depósito.

$L_1 =$ altura ficticia en un depósito de espesor de pared con variación lineal.

$M =$ momento exterior uniforme por unidad de longitud aplicado en un borde del depósito, positivo si produce tracción en la cara interior.

$M_x =$ momento flector longitudinal por unidad de longitud, positivo si produce tracción en la cara interior del depósito.

$M_\varphi =$ momento flector circunferencial por unidad de longitud, positivo si produce tracción en la cara interior del depósito.

$N_\varphi =$ esfuerzo circunferencial por unidad de longitud, positivo si es tracción.

$Q_x =$ esfuerzo cortante por unidad de longitud, positivo si en la cara frontal actúa hacia afuera.

$R =$ esfuerzo radial uniforme por unidad de longitud aplicado en un borde del depósito, positivo hacia el interior.

Z fuerza exterior, por unidad de superficie actuando sobre el depósito, positiva si actúa hacia el exterior.

$\psi_1(\vartheta), \psi_2(\vartheta), \psi_3(\vartheta), \psi_4(\vartheta) =$ funciones de ϑ utilizadas en el cálculo de depósitos de espesor de pared con variación lineal.

$$\psi_1' = \frac{d\psi_1(\theta)}{d\theta}$$

$$\psi_2' = \frac{d\psi_2(\theta)}{d\theta}$$

$$\psi_3' = \frac{d\psi_3(\theta)}{d\theta}$$

$$\psi_4' = \frac{d\psi_4(\theta)}{d\theta}$$

2. Desarrollo del cálculo

Los depósitos cuya superficie media es un cilindro de directriz circular con generatrices verticales, constituyen en realidad un caso particular de las láminas de revolución, en el que las cargas exteriores tienen simetría de revolución, y por lo tanto les serán aplicables los desarrollos y simplificaciones de la teoría elástica para este tipo de estructuras.

En lo que sigue se desarrollará el cálculo de una manera formal, aceptando todas las hipótesis que se admiten en la teoría elástica de las láminas.

Los esfuerzos que actuarán en un elemento diferencial serán los que se indican en la figura 1; es decir, un esfuerzo circunferencial normal N_φ, los momentos flectores M_x y M_φ y el esfuerzo cortante Q_x. De estos esfuerzos, al considerar cargas con simetría de revolución, N_φ y M_φ serán independientes de la coordenada angular φ.

Se prescinde de las cargas verticales sobre la pared del depósito, ya que si tienen simetría de revolución, producirán unos esfuerzos N_x cuyos efectos sobre el elemento corresponden a los de una solicitación axil pura y pueden analizarse muy simplemente.

Con la condición de simetría impuesta a las cargas, solamente se considerará una carga normal Z en dirección radial, variable con la coordenada x, pero independiente de φ.

En el elemento diferencial considerado en la figura 1, el equilibrio de fuerzas radiales da la siguiente ecuación:

$$\frac{dQ_x}{dx} - \frac{1}{a} N_\varphi + Z = 0 \qquad \text{[Ia]}$$

El equilibrio de momentos con eje la tangente al paralelo

$$\frac{dM_x}{dx} + Q_x = 0 \qquad \text{[Ib]}$$

Las expresiones del esfuerzo N_φ y del momento M_x en función del corrimiento radial w, único existente debido a las hipótesis admitidas, serán:

$$\left.\begin{aligned} N_\varphi &= \frac{E\delta}{a} w \\ M_x &= \frac{E\delta^3}{12(1-\nu^2)} \frac{d^2 w}{dx^2} \end{aligned}\right\} \qquad \text{[II]}$$

Se prescinde del valor del momento M_φ, cuyo valor aproximado es νM_x.

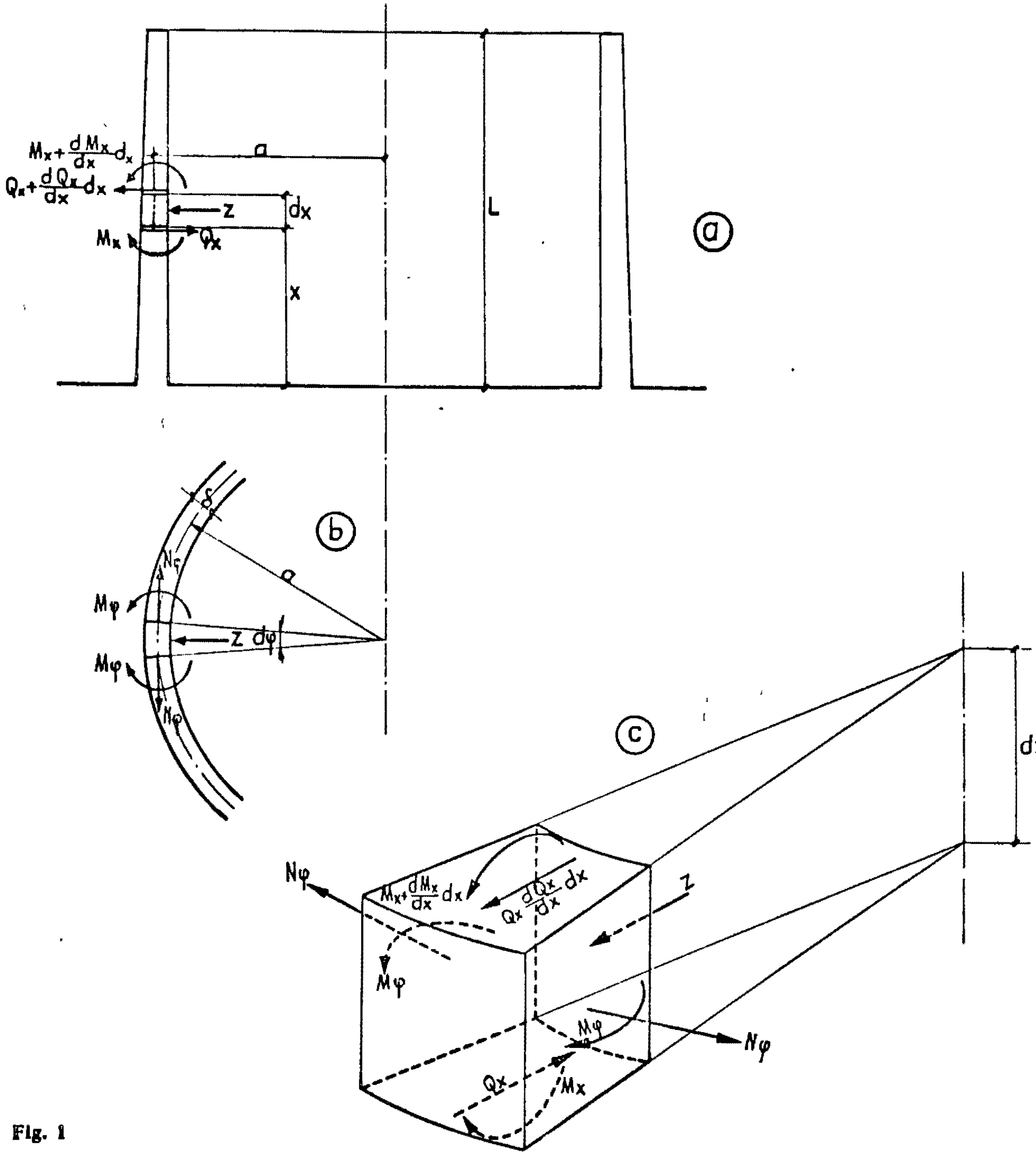

Fig. 1

Sustituyendo en la ecuación [Ia] el valor de Q_x sacado de [Ib] y los de N_φ y M_x sacados de [II], se tiene:

$$\frac{d^2}{dx^2}\left[\frac{E\,\delta^3}{12\,(1-\nu^2)}\;\frac{d^2w}{dx^2}\right]+\frac{E\,\delta}{a^2}w-Z=0 \qquad [III]$$

Esta ecuación diferencial de cuarto grado resuelve el problema para el caso general de espesor variable $\delta(x)$.

2.1. Depósitos de espesor de pared constante

Si se supone δ = constante, la ecuación anterior se convierte en la siguiente:

$$\frac{d^4 w}{dx^4} + \frac{12(1-\nu^2)}{a^2\delta^2} w = \frac{12(1-\nu^2)}{E\delta^3} Z \qquad \text{[IV]}$$

La solución de esta ecuación diferencial es la siguiente:

$$w = w_p + e^{\varkappa x}\left[K_1 \cos\varkappa x + K_2 \,\mathrm{sen}\,\varkappa x\right] + e^{-\varkappa x}\left[K_3\cos\varkappa x + K_4 \,\mathrm{sen}\,\varkappa x\right] \qquad \text{[V]}$$

Siendo $\varkappa = \frac{\sqrt{3(1-\nu^2)}}{\sqrt{a\delta}}$ y w_p una solución particular de la ecuación [IV] completa.

Con el valor del corrimiento w dado en [V] y teniendo en cuenta que:

$$N_\varphi = \frac{E\delta}{a}\left\{w_p + e^{\varkappa x}\left[K_1\cos\varkappa x + K_2\,\mathrm{sen}\,\varkappa x\right] + e^{-\varkappa x}\left[K_3\cos\varkappa x + K_4\,\mathrm{sen}\,\varkappa x\right]\right\} \qquad \text{[VI]}$$

$$M_x = K\left\{\frac{d^2 w_p}{dx^2} + 2\varkappa^2 e^{\varkappa x}\left[K_2\cos\varkappa x - K_1\,\mathrm{sen}\,\varkappa x\right] - 2\varkappa^2 e^{-\varkappa x}\left[K_4\cos\varkappa x - K_3\,\mathrm{sen}\,\varkappa x\right]\right\}$$

$$Q_x = -K\left\{\frac{d^3 w_p}{dx^3} + 2\varkappa^3 e^{\varkappa x}\left[(K_2-K_1)\cos\varkappa x - (K_1+K_2)\,\mathrm{sen}\,\varkappa x\right] + 2\varkappa^3 e^{-\varkappa x}\left[(K_3+K_4)\cos\varkappa x - (K_3-K_4)\,\mathrm{sen}\,\varkappa x\right]\right\}$$

se puede determinar el estado tensional de un depósito de espesor constante, cualquiera que sea el tipo de sustentación en los dos bordes horizontales.

En las expresiones [VI], $K = \frac{E\delta^3}{12(1-\nu^2)}$.

A continuación se estudiarán distintos casos particulares que permitirán conocer los esfuerzos y proyectar los tipos normales de depósito de espesor constante. Los casos que se estudiarán son los siguientes:

I. Depósito vacío, libre en sus bordes inferior y superior y solicitado en el primero de ellos por una fuerza radial uniforme, R.

II. Depósito vacío, libre en sus bordes inferior y superior y solicitado en el primero de ellos por un momento radial uniforme, M.

IIIa. Depósito lleno, libre en su borde superior y rígidamente empotrado en el inferior.

IIIb. Depósito lleno, libre en su borde superior y articulado en el inferior.

2.1.1. Caso I.

Depósito vacío, libre en sus bordes inferior y superior y solicitado en el borde inferior por una fuerza radial uniforme, R (fig. 2).

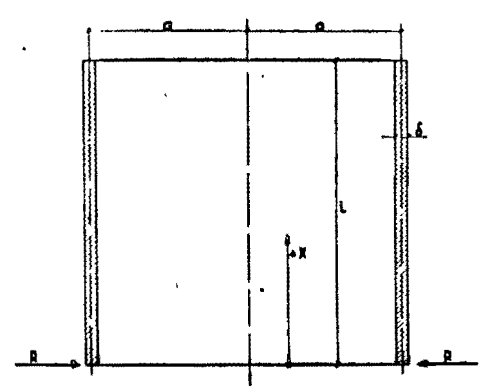

Fig. 2

R representa una fuerza por unidad de longitud de circunferencia, y sus dimensiones serán, por lo tanto, $\frac{F}{L}$.

Al no existir, en este caso, cargas exteriores Z, la solución particular de la ecuación [V], w_p, será nula, puesto que la ecuación en sí es homogénea.

Por otra parte, las condiciones en los bordes serán:

Para $x = 0$ $\quad (M_x)_{x=0} = 0 \quad (Q_x)_{x=0} = R = -K\left(\frac{d^3 w}{d x^3}\right)_{x=0}$

Para $x = L$ $\quad (M_x)_{x=L} = 0 \quad (Q_x)_{x=L} = 0$

Estas cuatro condiciones proporcionan las cuatro ecuaciones siguientes:

$$K_2 - K_4 = 0$$

$$K_1 - K_2 - K_3 - K_4 = \frac{R}{2K\varkappa^3}$$

$$e^{\varkappa L}\left[-K_1 \operatorname{sen}\varkappa L + K_2 \cos\varkappa L\right] + e^{-\varkappa L}\left[K_3 \operatorname{sen}\varkappa L - K_4 \cos\varkappa L\right] = 0$$

$$e^{\varkappa L}\left[-K_1(\operatorname{sen}\varkappa L + \cos\varkappa L) + K_2(\cos\varkappa L - \operatorname{sen}\varkappa L)\right] +$$
$$+ e^{-\varkappa L}\left[K_3(\cos\varkappa L - \operatorname{sen}\varkappa L) + K_4(\cos\varkappa L + \operatorname{sen}\varkappa L)\right] = 0$$

Sistema con el que se pueden determinar las constantes K_1, K_2, K_3 y K_4, cuyas soluciones son:

$$K_1 = \frac{R}{2\varkappa^3 K} k_1 \quad ; \quad k_1 = \frac{1 - e^{2\varkappa L} + e^{2\varkappa L}\operatorname{sen}\varkappa L}{1 + e^{4\varkappa L} - 4e^{2\varkappa L} + 2e^{2\varkappa L}\cos 2\varkappa L}$$

$$K_2 = \frac{R}{\varkappa^3 K} k_2 \quad ; \quad k_2 = \frac{\frac{1}{2}e^{2\varkappa L}(1 - \cos 2\varkappa L)}{1 + e^{4\varkappa L} - 4e^{2\varkappa L} + 2e^{2\varkappa L}\cos 2\varkappa L}$$

$$K_3 = \frac{R}{2\varkappa^3 K} k_3 \quad ; \quad k_3 = \frac{e^{2\varkappa L} - e^{4\varkappa L} + e^{2\varkappa L}\operatorname{sen} 2\varkappa L}{1 + e^{4\varkappa L} - 4e^{2\varkappa L} + 2e^{2\varkappa L}\cos 2\varkappa L}$$

$$K_4 = \frac{R}{\varkappa^3 K} k_4 = K_2 \quad ; \quad k_4 = \frac{\frac{1}{2}e^{2\varkappa L}(1 - \cos 2\varkappa L)}{1 + e^{4\varkappa L} - 4e^{2\varkappa L} + 2e^{2\varkappa L}\cos 2\varkappa L} = k_2$$

Con estos valores las expresiones de los esfuerzos y del recorrido resultan:

$$w = \frac{2\sqrt[4]{3(1-\nu^2)}}{E}\frac{a}{\delta}\sqrt{\frac{a}{\delta}}\, R\left[e^{\varkappa x}(k_1\cos\varkappa x + 2k_2 \operatorname{sen}\varkappa x) + e^{-\varkappa x}(k_3 \cos\varkappa x + 2k_4 \operatorname{sen}\varkappa x)\right]$$

$$N_\varphi = 2\sqrt[4]{3(1-\nu^2)}\sqrt{\frac{a}{\delta}}\, R\left[e^{\varkappa x}(k_1\cos\varkappa x + 2k_2\operatorname{sen}\varkappa x) + e^{-\varkappa x}(k_3\cos\varkappa x + 2k_4\operatorname{sen}\varkappa x)\right]$$

$$M_x = \sqrt[4]{\frac{a^2\delta^2}{3(1-\nu^2)}}\cdot R\left[e^{\varkappa x}(-k_1\operatorname{sen}\varkappa x + 2k_2\cos\varkappa x) + e^{-\varkappa x}(k_3\operatorname{sen}\varkappa x - 2k_4\cos\varkappa x)\right] \qquad \text{[VII]}$$

$$Q_x = -R\left[e^{\varkappa x}\left[-k_1(\operatorname{sen}\varkappa x - \cos\varkappa x) + 2k_2(\cos\varkappa x - \operatorname{sen}\varkappa x)\right] +\right.$$
$$\left. + e^{-\varkappa x}\left[k_3(\cos\varkappa x - \operatorname{sen}\varkappa x) + 2k_4(\cos\varkappa x + \operatorname{sen}\varkappa x)\right]\right]$$

Si el depósito tiene unas dimensiones que permitan suponer que la acción en un borde no tiene influencia en el otro, se llega a la conocida solución simplificada siguiente:

$$k_1 = k_2 = k_4 = 0 \; ; \quad k_3 = -1 \; ;$$

con esto las expresiones de los esfuerzos y del recorrido resultan también notablemente simplificadas y serían las siguientes:

$$w = \frac{2\sqrt[4]{3(1-\nu^2)}}{E} \frac{a}{\delta}\sqrt{\frac{a}{\delta}}\, R \left[-e^{-\varkappa x}\cos\varkappa x\right]$$

$$N_\varphi = 2\sqrt[4]{3(1-\nu^2)}\sqrt{\frac{a}{\delta}}\, R\left[-e^{-\varkappa x}\cos\varkappa x\right]$$

$$M_x = \sqrt[4]{\frac{a^2\,\delta^2}{3(1-\nu^2)}}\, R\left[-e^{-\varkappa x}\operatorname{sen}\varkappa x\right]$$

$$Q_x = -R\left[-e^{-\varkappa x}\left(\cos\varkappa x - \operatorname{sen}\varkappa x\right)\right]$$

Esta solución simplificada es válida para este caso en general con valores de $\varkappa \cdot L$ mayores o iguales a 3, o, lo que es igual:

$$\frac{L}{a} \times \frac{L}{\delta} \geqslant \frac{5{,}2}{\sqrt{1-\nu^2}}$$

Para los depósitos de hormigón armado o pretensado en que ν se puede considerar igual a 0,2, la solución simplificada da resultados aceptables para dimensiones que cumplan la limitación

$$\frac{L}{a} \times \frac{L}{\delta} \geqslant 5{,}3$$

En los casos en que estas simplificaciones sean válidas, el esfuerzo $N_{\varphi\,max}$ para $x = 0$ y el corrimiento w_{max} también para $x = 0$ se pueden determinar con las sencillas fórmulas aproximadas:

$$N_{\varphi_{max}} \simeq -2{,}6\sqrt{\frac{a}{\delta}}\, R$$

$$w_{max} \simeq -\frac{2{,}6}{E}\,\frac{a}{\delta}\sqrt{\frac{a}{\delta}}\, R$$

El valor del mayor de los máximos del momento M_x se producirá a una altura definida por el valor de $x = x_0$; tanto esta coordenada como el $M_{x\,max}$ se pueden determinar con las fórmulas aproximadas siguientes:

$$\frac{x_0}{L} \simeq 0{,}6\sqrt{\frac{a\,\delta}{L^2}}$$

(*)

$$M_{x\,max} \simeq -0{,}25\sqrt{a.\delta}.\,R$$

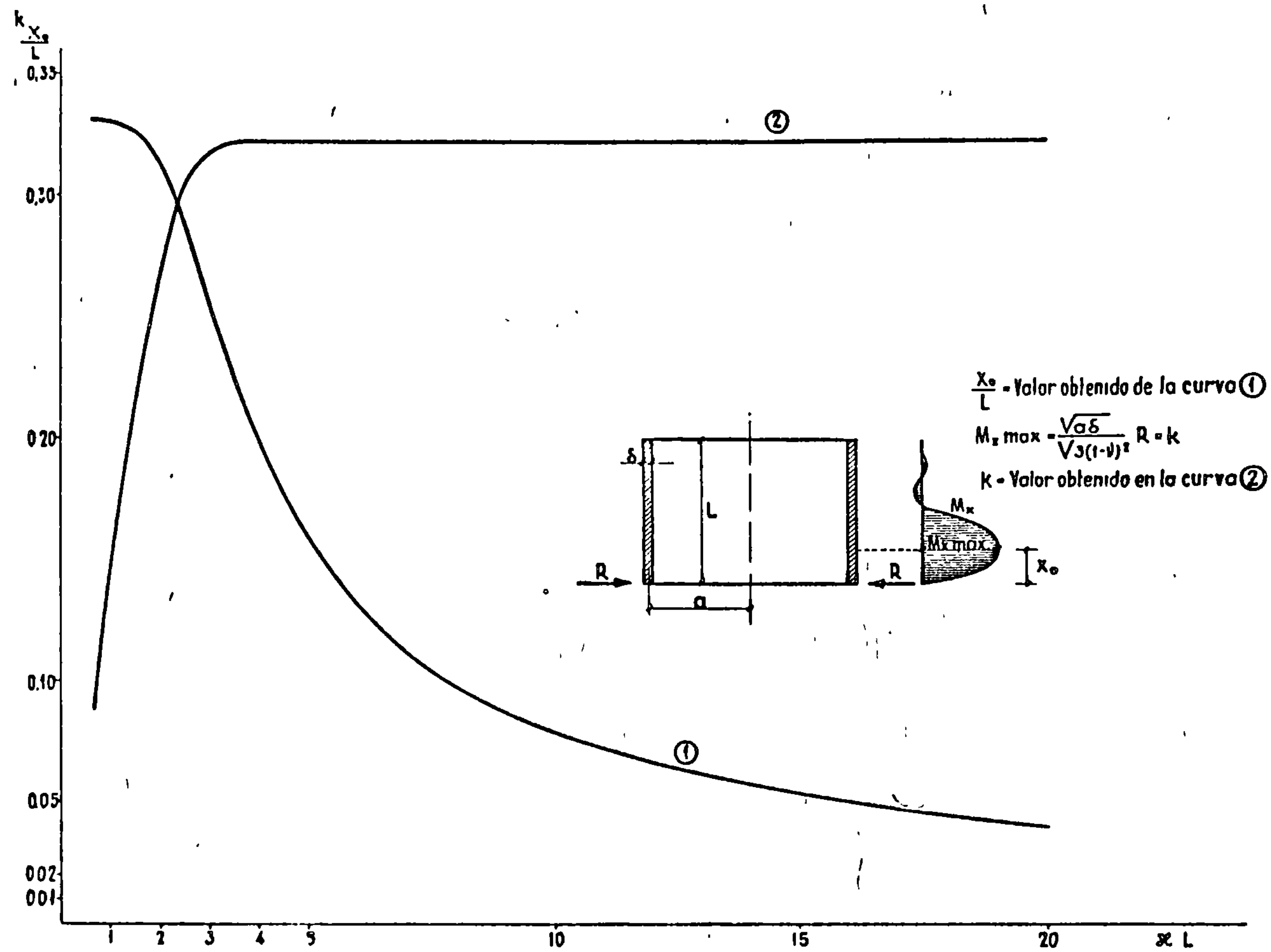

Fig. 3

2.1.2. Tabulación del caso I.

En la tabla I aparecen los coeficientes que para un depósito determinado dan el valor del corrimiento w y del esfuerzo N_φ, para distintos planos definidos por los valores de x/L, de acuerdo con las fórmulas:

$$W = \frac{2\sqrt[4]{3(1-\nu^2)}}{E}\,\frac{a}{\delta}\sqrt{\frac{a}{\delta}}\,R \times \mathrm{Coef}_I$$

$$N_\varphi = 2\sqrt[4]{3(1-\nu^2)}\sqrt{\frac{a}{\delta}}\,R \times \mathrm{Coef}_I$$

En la tabla II se da el coeficiente que determinará el momento flector M_x de acuerdo con la fórmula:

$$M_x = \frac{1}{\sqrt[4]{3(1-\nu^2)}}\sqrt{a.\delta} \times R \times \mathrm{Coef}_{II}$$

Con los gráficos de la figura 3 se pueden obtener el momento $M_{x\,max}$ definido en (*) y la ordenada x_0 en que se produce.

(*) Ver página anterior.

Análogamente, en la tabla III se da el coeficiente que determinará el esfuerzo cortante Q_x con la fórmula:

$$Q_x = -R \times \text{Coef. III}.$$

También se incluyen en la tabla A los coeficientes k_0 y k_L, que permiten hallar los valores de la derivada del corrimiento radial w en los dos bordes del depósito considerado, de acuerdo con las siguientes expresiones:

$$\left[\frac{dw}{dx}\right]_{x=0} = \frac{2a}{E\delta^2}\sqrt{3(1-\nu^2)}\, R \times k_0$$

$$\left[\frac{dw}{dx}\right]_{x=L} = \frac{2a}{E\delta^2}\sqrt{3(1-\nu^2)}\, R \times k_L$$

Estos valores facilitan la resolución en los casos de sustentación en los bordes en que intervenga el giro. En los ejemplos que se incluyen al final de esta publicación, se pueden ver algunos casos resueltos, mediante la utilización de la tabla A.

Las tablas I, II y III corresponden a los gráficos G-I, G-II y G-III.

TABLA A

Depósito libre en sus dos bordes, solicitado por una fuerza radial uniforme, R, en el borde inferior

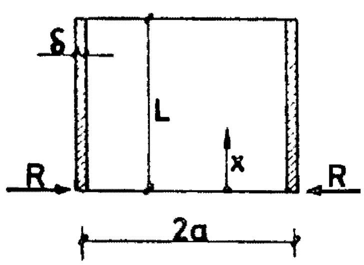

$$\left[\frac{dw}{dx}\right]_{x=0} = \frac{2a}{E\delta^2}\sqrt{3(1-\nu^2)}\, R \times k_0$$

$$\left[\frac{dw}{dx}\right]_{x=L} = \frac{2a}{E\delta^2}\sqrt{3(1-\nu^2)}\, R \times k_L$$

VALORES DE LOS COEFICIENTES k_0 Y k_L

$\varkappa L$	k_0	k_L	$\varkappa L$	k_0	k_L	$\varkappa L$	k_0	k_L
0,6	8,3710	8,3111	3,0	1,0004	0,0282	5,5	1,0001	—0,0115
0,8	4,7544	4,6480	3,2	1,0000	—0,0095	6,0	1,0000	—0,0028
1,0	3,1042	2,9387	3,4	1,0006	—0,0342	7,0	1,0000	0,0024
1,2	2,2324	1,9959	3,6	1,0012	—0,0484	8,0	1,0000	0,0013
1,4	1,7315	1,4135	3,8	1,0015	—0,0548	9,0	1,0000	0,0002
1,6	1,4303	1,0226	4,0	1,0015	—0,0555	10,0	1,0000	—0,0001
1,8	1,2461	0,7434	4,2	1,0014	—0,0523	12,0	1,0000	—
2,0	1,1341	0,5351	4,4	1,0011	—0,0468	14,0	1,0000	—
2,2	1,0680	0,3751	4,6	1,0008	—0,0400	16,0	1,0000	—
2,4	1,0310	0,2510	4,8	1,0005	—0,0328	18,0	1,0000	—
2,6	1,0119	0,1549	5,0	1,0003	—0,0259	20,0	1,0000	—
2,8	1,0034	0,0819						

2.1.3. Caso II.

Depósito vacío, libre en sus bordes inferior y superior y solicitado en el borde inferior por un momento radial uniforme M (fig. 4).

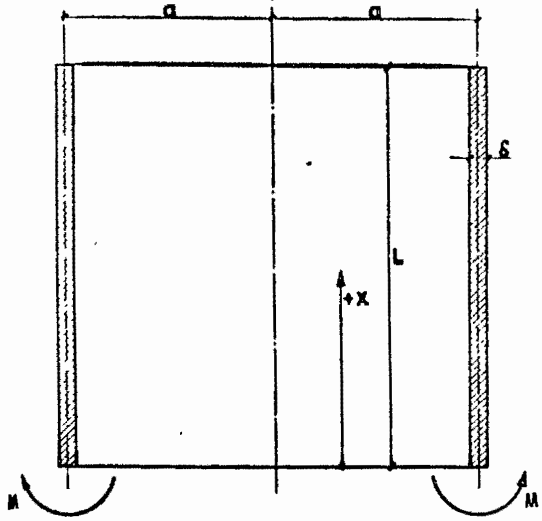

Fig. 4

M representa un momento por unidad de longitud de circunferencia y sus dimensiones serán, por lo tanto, las de una fuerza.

Como en el caso anterior, $Z = 0$, y por lo tanto $w_p = 0$, las condiciones de borde son en este caso:

Para $x = 0$ $\left(M_x\right)_{x=0} = M = K\left(\frac{d^2w}{dx^2}\right)_{x=0}$ $\left(Q_x\right)_{x=0} = 0$

Para $x = L$ $\left(M_x\right)_{x=L} = 0$ $\left(Q_x\right)_{x=L} = 0$

Estas cuatro condiciones conducen al siguiente sistema de ecuaciones:

$$K_2 - K_4 = \frac{M}{2æ^2 K} \qquad - K_1 + K_2 + K_3 + K_4 = 0$$

$$e^{æL}\left[-K_1 \operatorname{sen} æL + K_2 \cos æL\right] + e^{-æL}\left[K_3 \operatorname{sen} æL - K_4 \cos æL\right] = 0$$

$$e^{æL}\left[-K_1(\operatorname{sen} æL + \cos æL) + K_2(\cos æL - \operatorname{sen} æL)\right] + e^{-æL}\left[K_3(\cos æL - \operatorname{sen} æL) + K_4(\cos æL + \operatorname{sen} æL)\right] = 0$$

Resolviendo este sistema se determinan las constantes K_1, K_2, K_3 y K_4, cuyas soluciones para este caso son:

$$K_1 = \frac{M}{2æ^2K} k_1 \qquad k_1 = \frac{1 - e^{2æL}\operatorname{sen} 2æL - e^{2æL}\cos 2æL}{1 + e^{4æL} - 4e^{2æL} + 2e^{2æL}\cos 2æL}$$

$$K_2 = \frac{M}{2æ^2K} k_2 \qquad k_2 = \frac{1 - 2e^{2æL} - e^{2æL}\cos 2æL - e^{2æL}\operatorname{sen} 2æL}{1 + e^{4æL} - 4e^{2æL} + 2e^{2æL}\cos 2æL}$$

$$K_3 = \frac{M}{2æ^2K} k_3 \qquad k_3 = \frac{e^{4æL} + e^{2æL}\operatorname{sen} 2æL - e^{2æL}\cos 2æL}{1 + e^{4æL} - 4e^{2æL} + 2e^{2æL}\cos 2æL}$$

$$K_4 = \frac{M}{2æ^2K} k_4 \qquad k_4 = \frac{2e^{2æL} - e^{4æL} - e^{2æL}\operatorname{sen} 2æL - e^{2æL}\cos 2æL}{1 + e^{4æL} - 4e^{2æL} + 2e^{2æL}\cos 2æL}$$

Con estos valores las expresiones del recorrido y de los esfuerzos serán:

$$w = \frac{2\sqrt{3(1-\nu^2)}}{E}\frac{a}{\delta^2} M\left[e^{æx}(k_1 \cos æx + k_2 \operatorname{sen} æx) + e^{-æx}(k_3 \cos æx + k_4 \operatorname{sen} æx)\right]$$

$$N_\varphi = 2\sqrt{3(1-\nu^2)}\,\frac{1}{\delta} M\left[e^{æx}(k_1 \cos æx + k_2 \operatorname{sen} æx) + e^{-æx}(k_3 \cos æx + k_4 \operatorname{sen} æx)\right]$$

$$M_x = M\left[e^{æx}(-k_1 \operatorname{sen} æx + k_2 \cos æx) + e^{-æx}(k_3 \operatorname{sen} æx - k_4 \cos æx)\right]$$

$$Q_x = -\frac{\sqrt[4]{3(1-\nu^2)}}{\sqrt{a\delta}} M\left[e^{æx}\left[-k_1(\operatorname{sen} æx + \cos æx) + k_2(\cos æx - \operatorname{sen} æx)\right] + e^{-æx}\left[k_3(\cos æx - \operatorname{sen} æx) + k_4(\cos æx + \operatorname{sen} æx)\right]\right]$$

Si se supone que el depósito es de unas dimensiones tales que la acción en un borde no tiene influencia en el otro, se puede simplificar el problema, llegandose a la conocida solución:

$$k_1 = k_2 = 0 \,; \qquad k_3 = 1 \,; \qquad k_4 = -1 \,.$$

Con lo que las expresiones de los esfuerzos y del recorrido resultan también notablemente simplificadas y se transforman en las siguientes:

$$w = \frac{2\sqrt{3(1-\nu^2)}}{E} \frac{a}{\delta^2} M e^{-\varkappa x} (\cos \varkappa x - \operatorname{sen} \varkappa x)$$

$$N_\varphi = 2\sqrt{3(1-\nu^2)} \frac{1}{\delta} M e^{-\varkappa x} (\cos \varkappa x - \operatorname{sen} \varkappa x)$$

$$M_x = M e^{-\varkappa x} (\cos \varkappa x + \operatorname{sen} \varkappa x)$$

$$Q_x = \frac{\sqrt[4]{3(1-\nu^2)}}{\sqrt{a\delta}} M \, 2 e^{-\varkappa x} \operatorname{sen} \varkappa x$$

Esta solución simplificada puede utilizarse, en este caso, para valores de $\varkappa L$ mayores o iguales a 2,8, es decir:

$$\frac{L^2}{a\delta} \geq \frac{4{,}5}{\sqrt{1-\nu^2}}$$

Para los depósitos de hormigón armado o pretensado con $\nu = 0{,}2$ es válida la simplificación siempre que:

$$\frac{L^2}{a\delta} \geq 4{,}6$$

El corrimiento máximo w_{max} se produce en $x = 0$ y su valor se puede hallar por la fórmula aproximada:

$$w_{max} \simeq \frac{3{,}4\, a M}{E \delta^2}$$

El mayor valor de N_φ se produce en $x = 0$ y su valor aproximado será:

$$N_{\varphi max} \simeq 3{,}4 \frac{M}{\delta}$$

El máximo negativo de N_φ se produce en una coordenada x_0 y su valor será:

$$\frac{x_0}{L} = 0{,}92 \sqrt{\frac{a\delta}{L^2}} \qquad\qquad N_{\varphi max.n} = -0{,}74 \frac{M}{\delta}$$

El mayor valor de M_x se produce en $x = 0$ y su valor es igual al momento aplicado M.

El momento flector negativo alcanza como máximo el valor:

$$M_{max\,n.} \simeq -0{,}045\, M \,.$$

Sólo existen momentos flectores negativos que se deducen de este valor, en depósitos muy altos. En depósitos de dimensiones normales el máximo momento flector negativo es mucho menor e incluso no llega a presentarse el cambio de signo.

2.1.4. Tabulación del caso II.

En las tablas números IV, V y VI se incluyen los coeficientes que, introducidos en las fórmulas siguientes, dan los valores del recorrido y los esfuerzos, para distintas alturas unitarias:

$$W = \frac{2\sqrt{3(1-\nu^2)}}{E}\,\frac{a}{\delta^2}\,M \times Coef_{IV}$$

$$N_\varphi = 2\sqrt{3(1-\nu^2)}\,\frac{M}{\delta} \times Coef_{IV}$$

$$M_x = M \times Coef_V$$

$$Q_x = -\frac{\sqrt[4]{3(1-\nu^2)}}{\sqrt{a\delta}}\,M \times Coef_{VI}$$

En la tabla B se incluyen los valores de los coeficientes k_0 y k_L que permiten hallar los va-

TABLA B

Depósito libre en sus dos bordes, solicitado por un momento radial uniforme, M, en el borde inferior

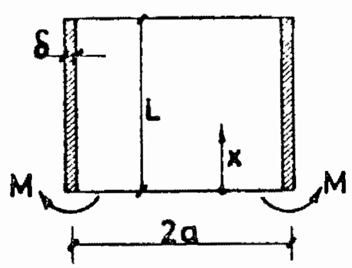

$$\left[\frac{dw}{dx}\right]_{x=0} = \frac{2\sqrt{\frac{a}{\delta}}\,\sqrt[4]{[3(1-\nu^2)]^3}}{E\,\delta^2}\,M \times k_0$$

$$\left[\frac{dw}{dx}\right]_{x=L} = \frac{2\sqrt{\frac{a}{\delta}}\,\sqrt[4]{[3(1-\nu^2)]^3}}{E\,\delta^2}\,M \times k_L$$

VALORES DE LOS COEFICIENTES k_0 Y k_L

$\varkappa L$	k_0	k_L	$\varkappa L$	k_0	k_L	$\varkappa L$	k_0	k_L
0,6	— 28,2233	— 27,6237	3,0	— 2,0076	0,1694	5,5	— 2,0001	— 0,0001
0,8	— 12,3121	— 11,5139	3,2	— 2,0075	0,1726	6,0	— 2,0000	— 0,0067
1,0	— 6,7400	— 5,7455	3,4	— 2,0073	0,1635	7,0	— 2,0000	— 0,0051
1,2	— 4,3565	— 3,1701	3,6	— 2,0065	0,1466	8,0	— 2,0000	— 0,0011
1,4	— 3,2113	— 1,8403	3,8	— 2,0054	0,1257	9,0	— 2,0000	0,0002
1,6	— 2,6243	— 1,0796	4,0	— 2,0042	0,1035	10,0	— 2,0000	0,0003
1,8	— 2,3149	— 0,6118	4,2	— 2,0030	0,0818	12,0	— 2,0000	—
2,0	— 2,1524	— 0,3101	4,4	— 2,0020	0,0619	14,0	— 2,0000	—
2,2	— 2,0699	— 0,1114	4,6	— 2,0013	0,0445	16,0	— 2,0000	—
2,4	— 2,0309	0,0188	4,8	— 2,0008	0,0299	18,0	— 2,0000	—
2,6	— 2,0144	0,1009	5,0	— 2,0004	0,0182	20,0	— 2,0000	—
2,8	— 2,0088	0,1479						

lores de la derivada del corrimiento radial w en los dos bordes del depósito considerado, de acuerdo con las expresiones:

$$\left[\frac{dw}{dx}\right]_{x=0} = \frac{2\sqrt{\frac{a}{\delta}}\ \sqrt[4]{[3(1-\nu^2)]^3}}{E\delta^2} M_x k_0$$

$$\left[\frac{dw}{dx}\right]_{x=L} = \frac{2\sqrt{\frac{a}{\delta}}\ \sqrt[4]{[3(1-\nu^2)]^3}}{E\delta^2} M_x k_L$$

Los gráficos G-IV, G-V y G-VI corresponden, respectivamente, a las tablas IV, V y VI.

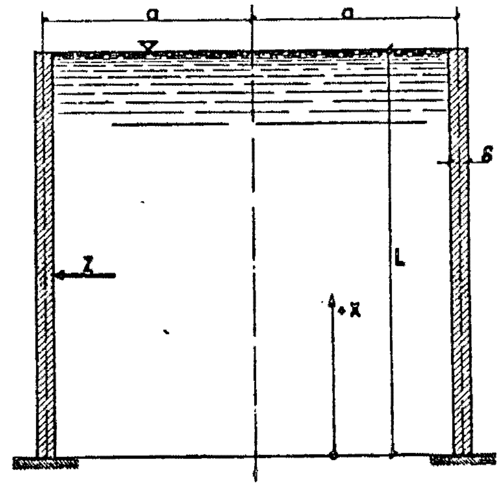

Fig. 5

2.1.5. Caso IIIa.

Depósito lleno, libre en su borde superior y rígidamente empotrado en el borde inferior (figura 5).

De acuerdo con la solución [V], la expresión del recorrido w será:

$$w = w_p + e^{\varkappa x}\left[K_1 \cos \varkappa x + K_2 \operatorname{sen} \varkappa x\right] + e^{-\varkappa x}\left[K_3 \cos \varkappa x + K_4 \operatorname{sen} \varkappa x\right] \qquad \text{[VIII]}$$

La carga exterior Z valdrá en este caso

$$Z = \gamma(L - x)\,,$$

con lo que una solución particular w_p, que coincide con la solución membrana, tiene la expresión:

$$w_p = \frac{\gamma a^2}{E\delta}(L - x)$$

Las condiciones de borde serán:

Borde inferior.—Para $x = 0$, $(w)_{x=0} = 0$; $\left(\frac{dw}{dx}\right)_{x=0} = 0$.

Borde superior.—Para $x = L$, $(M_x)_{x=L} = 0$; $(Q_x)_{x=L} = 0$.

Estas cuatro condiciones conducen al siguiente sistema de ecuaciones:

$$L\frac{\gamma a^2}{E\delta} + K_1 + K_3 = 0$$

$$-\frac{\gamma a^2}{E\delta}\frac{1}{\varkappa} + K_1 + K_2 - K_3 + K_4 = 0$$

$$e^{2\varkappa L}\left[-K_1 \operatorname{sen} \varkappa L + K_2 \cos \varkappa L\right] + K_3 \operatorname{sen} \varkappa L - K_4 \cos \varkappa L = 0$$

$$e^{2\varkappa L}\left[-K_1(\operatorname{sen} \varkappa L + \cos \varkappa L) + K_2(\cos \varkappa L - \operatorname{sen} \varkappa L)\right] + K_3(\cos \varkappa L - \operatorname{sen} \varkappa L) + K_4(\cos \varkappa L + \operatorname{sen} \varkappa L) = 0$$

De donde se obtienen los valores de las cuatro constantes de integración K_1, K_2, K_3 y K_4:

$$K_1 = \frac{-\gamma a^2}{E\delta} L k_1 \qquad k_1 = \frac{L\left[1+2e^{2\varkappa L}+e^{2\varkappa L}\cos 2\varkappa L - e^{2\varkappa L}\operatorname{sen} 2\varkappa L\right] - \frac{e^{2\varkappa L}}{\varkappa}\left(1-\cos 2\varkappa L\right)}{L\left(1+e^{4\varkappa L}+4e^{2\varkappa L}+2e^{2\varkappa L}\cos 2\varkappa L\right)}$$

$$K_2 = \frac{\gamma a^2}{E\delta} L k_2 \qquad k_2 = \frac{\left(\frac{1}{\varkappa}+L\right)\left(1+\frac{e^{2\varkappa L}}{2}-\frac{e^{2\varkappa L}}{2}\cos 2\varkappa L\right)+\left(\frac{1}{\varkappa}-L\right)\left(\frac{e^{2\varkappa L}}{2}+\frac{e^{2\varkappa L}}{2}\cos 2\varkappa L+e^{2\varkappa L}\operatorname{sen} 2\varkappa L\right)}{L\left(1+e^{4\varkappa L}+4e^{2\varkappa L}+2e^{2\varkappa L}\cos 2\varkappa L\right)}$$

$$K_3 = \frac{-\gamma a^2}{E\delta} L k_3 \qquad k_3 = \frac{L\left(1+e^{2\varkappa L}+\operatorname{sen} 2\varkappa L\right)+\left(L+\frac{1}{\varkappa}\right)\left(1+\cos 2\varkappa L\right)}{L\left(1+e^{4\varkappa L}+4e^{2\varkappa L}+2e^{2\varkappa L}\cos 2\varkappa L\right)}\, e^{2\varkappa L}$$

$$K_4 = \frac{\gamma a^2}{E\delta} L k_4 \qquad k_4 = \frac{\left(\frac{1}{\varkappa}-L\right)\left(e^{2\varkappa L}+\frac{1}{2}-\frac{1}{2}\cos 2\varkappa L\right)+\left(\frac{1}{\varkappa}+L\right)\left(\frac{1}{2}+\frac{1}{2}\cos 2\varkappa L-\operatorname{sen} 2\varkappa L\right)}{L\left(1+e^{4\varkappa L}+4e^{2\varkappa L}+2e^{2\varkappa L}\cos 2\varkappa L\right)}\, e^{2\varkappa L}$$

Con estos valores, las expresiones de los esfuerzos y del recorrido serán:

$$w = \frac{\gamma a^2}{E\delta} L\left[1-\frac{x}{L}+e^{\varkappa x}\left(-k_1\cos\varkappa x+k_2\operatorname{sen}\varkappa x\right)+e^{-\varkappa x}\left(-k_3\cos\varkappa x+k_4\operatorname{sen}\varkappa x\right)\right]$$

$$N\varphi = \gamma a L\left[1-\frac{x}{L}+e^{\varkappa x}\left(-k_1\cos\varkappa x+k_2\operatorname{sen}\varkappa x\right)+e^{-\varkappa x}\left(-k_3\cos\varkappa x+k_4\operatorname{sen}\varkappa x\right)\right]$$

$$M_x = \frac{\gamma a\delta L}{2\sqrt{3(1-\nu^2)}}\left[e^{\varkappa x}\left(k_1\operatorname{sen}\varkappa x+k_2\cos\varkappa x\right)+e^{-\varkappa x}\left(-k_3\operatorname{sen}\varkappa x-k_4\cos\varkappa x\right)\right]$$

$$Q_x = -\frac{\gamma L\sqrt{a\delta}}{2\sqrt[4]{3(1-\nu^2)}}\left[e^{\varkappa x}\left[k_1\left(\operatorname{sen}\varkappa x+\cos\varkappa x\right)+k_2\left(\cos\varkappa x-\operatorname{sen}\varkappa x\right)\right]+\right.$$
$$\left.+\,e^{-\varkappa x}\left[-k_3\left(\cos\varkappa x-\operatorname{sen}\varkappa x\right)+k_4\left(\cos\varkappa x+\operatorname{sen}\varkappa x\right)\right]\right]$$

Conviene destacar que para la solicitación del empuje hidrostá...co del líquido contenido en el depósito, la solución membrana o solución particular a que se ha hecho referencia anteriormente, es la siguiente:

$$w_p = \frac{\gamma a^2}{E\delta}(L-x) \qquad \frac{dw}{dx} = -\frac{\gamma a^2}{E\delta} \qquad N\varphi_p = \gamma a(L-x) \qquad M_{x_p} = Q_{x_p} \equiv 0$$

Si se supone que el depósito cumple, por sus dimensiones, la condición de que la acción en un borde no tiene influencia en el otro, se simplifica el problema, obteniéndose la solución:

$$k_1 = k_2 = 0 \qquad\qquad k_3 = 1 \qquad\qquad k_4 = \frac{1}{\varkappa L} - 1$$

con lo que se llega a las conocidas y más simples expresiones siguientes:

$$w = \frac{\gamma a^2}{E\delta} L\left[1-\frac{x}{L}+e^{-\varkappa x}\left(-\cos\varkappa x-\operatorname{sen}\varkappa x+\frac{1}{\varkappa L}\operatorname{sen}\varkappa x\right)\right]$$

$$N\varphi = \gamma a L\left[1-\frac{x}{L}+e^{-\varkappa x}\left(-\cos\varkappa x-\operatorname{sen}\varkappa x+\frac{1}{\varkappa L}\operatorname{sen}\varkappa x\right)\right]$$

$$M_x = \frac{\gamma a \delta L}{2\sqrt{3(1-\nu^2)}} e^{-\varkappa x}\left[-\operatorname{sen}\varkappa x + \cos\varkappa x - \frac{1}{\varkappa L}\cos\varkappa x\right]$$

$$Q_x = -\frac{\gamma L\sqrt{a\delta}}{2\sqrt[4]{3(1-\nu^2)}} e^{-\varkappa x}\left[-2\cos\varkappa x + \frac{1}{\varkappa L}(\cos\varkappa x - \operatorname{sen}\varkappa x)\right]$$

Los máximos de M_x y Q_x se obtienen para $x = 0$, es decir, en el empotramiento, y sus valores serán:

$$(M_x)_{x=0} \simeq \frac{\gamma a \delta L}{2\sqrt{3(1-\nu^2)}}\left[1 - \frac{1}{\varkappa L}\right]$$

$$(Q_x)_{x=0} \simeq \frac{\gamma L\sqrt{a\delta}}{2\sqrt[4]{3(1-\nu^2)}}\left[2 - \frac{1}{\varkappa L}\right]$$

En el gráfico figura 6 aparecen también el valor máximo de N_φ y su localización, cuya expresión analítica es bastante más compleja que las correspondientes a M_x y Q_x.

2.1.6. Tabulación del caso IIIa.

En las tablas VII, VIII y IX se incluyen los coeficientes que, introducidos en las expresiones que se dan a continuación, dan los valores del recorrido y los esfuerzos, para distintas alturas unitarias, en cualquier depósito:

$$w = \frac{\gamma a^2}{E\delta} L \times Coef_{VII}$$

$$N\varphi = \gamma . a . L \times Coef_{VII}$$

$$M_x = \frac{\gamma . a \delta L}{2\sqrt{3(1-\nu^2)}} \times Coef_{VIII}$$

$$Q_x = -\frac{\gamma L\sqrt{a\delta}}{2\sqrt[4]{3(1-\nu^2)}} \times Coef_{IX}$$

Los gráficos G-VII, G-VIII y G-IX corresponden, respectivamente, a las tablas VII, VIII y IX.

En el gráfico de la figura 6 se incluyen dos curvas que permiten determinar fácil y rápidamente los valores máximos del corrimiento w y del esfuerzo N_φ y la altura relativa x_0/L en que se presenta, en función de la característica geométrica del depósito.

Análogamente, en la figura 7 se incluyen cuatro curvas, con las que se determinan: el valor máximo positivo $M_{x\,max}$ correspondiente al momento flector M_x en el empotramiento, el valor máximo negativo $M_{x\,min}$ del momento flector, la altura relativa x_0/L en que se presenta, y la altura relativa x_1/L en que la ley del momento flector M_x pasa por primera vez por valor nulo. Todos estos datos se pueden obtener en función de la característica geométrica, $\varkappa L$, del depósito considerado.

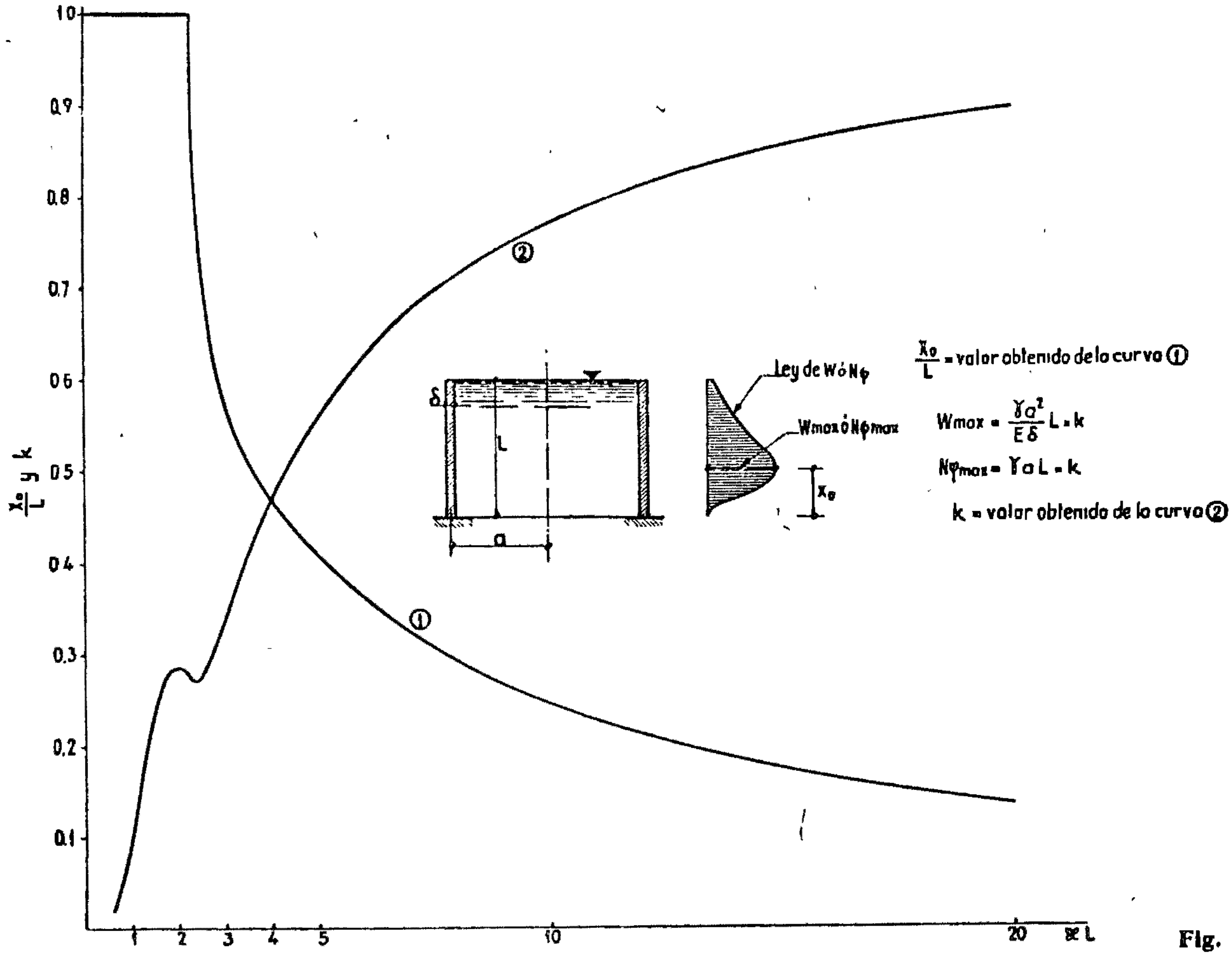

Fig. 6

2.1.7. Caso IIIb.

Depósito lleno, libre en su borde superior y articulado en el borde inferior (fig. 8).

Según se ha visto al estudiar el caso IIIa, la solución del recorrido será:

$$w = \frac{\gamma a^2}{E\delta} L \left[\left(1 - \frac{x}{L}\right) + e^{æx}\left(K_1 \cos æx + K_2 \operatorname{sen} æx\right) + e^{-æx}\left(K_3 \cos æx + K_4 \operatorname{sen} æx\right) \right] \qquad [IX]$$

Las condiciones de borde para este caso son:

Borde inferior.—Para $x = 0$, $\quad (w)_{x=0} = 0$; $\quad (M)_{x=0} = 0$.
Borde superior.—Para $x = L$, $\quad (M_x)_{x=L} = 0$; $\quad (Q_x)_{x=L} = 0$.

Estas cuatro condiciones conducen al sistema de ecuaciones siguiente:

$$\frac{\gamma a^2}{E\delta} L + K_1 + K_3 = 0$$

$$K_2 - K_4 = 0$$

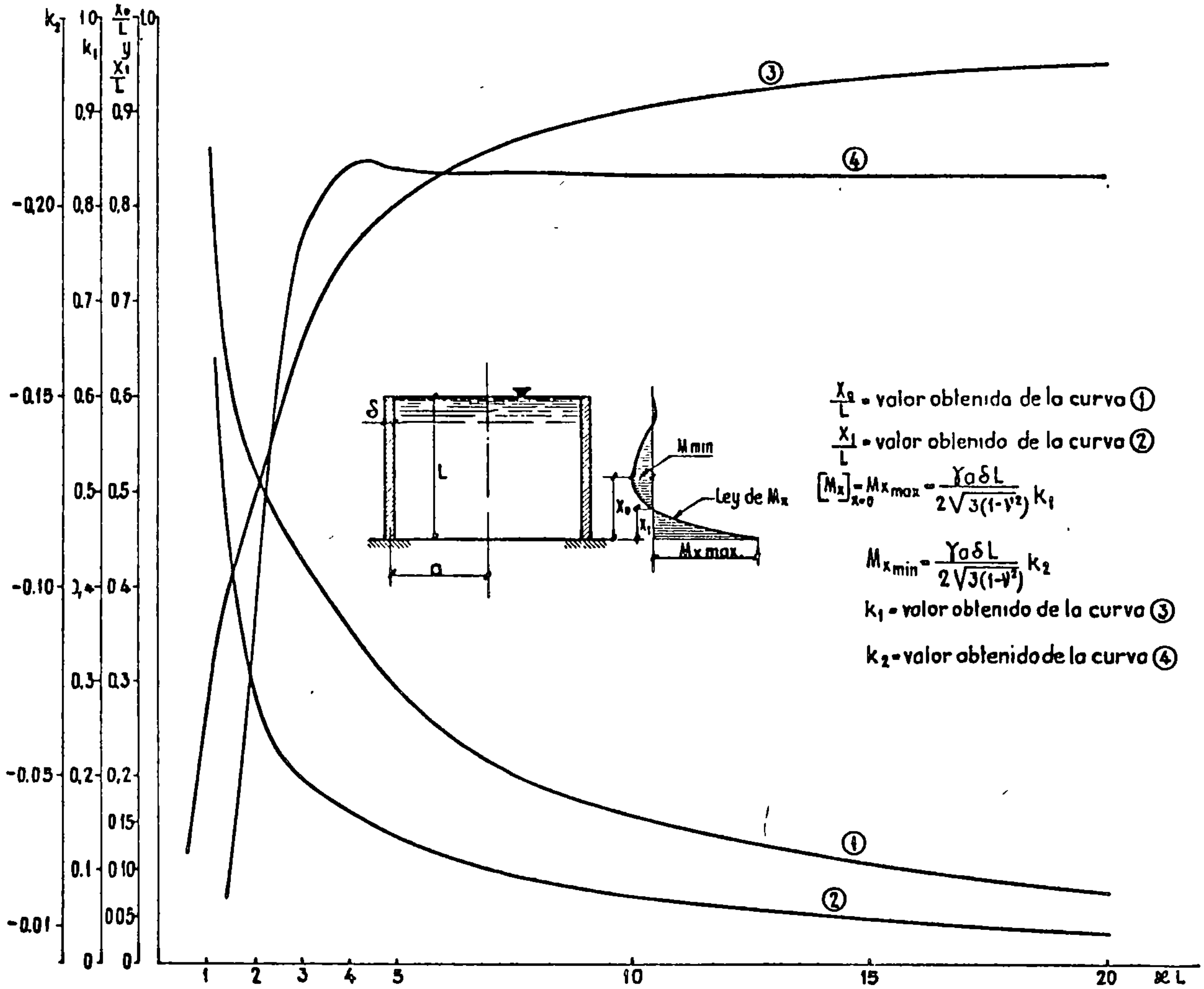

Fig. 7

$$e^{2\varkappa L}\left[-K_1 \operatorname{sen}\varkappa L + K_2 \cos\varkappa L\right] + K_3 \operatorname{sen}\varkappa L - K_4 \cos\varkappa L = 0$$

$$e^{2\varkappa L}\left[-K_1(\operatorname{sen}\varkappa L + \cos\varkappa L) + K_2(\cos\varkappa L - \operatorname{sen}\varkappa L)\right] + K_3(\cos\varkappa L - \operatorname{sen}\varkappa L) + K_4(\cos\varkappa L + \operatorname{sen}\varkappa L) = 0$$

De donde se obtienen los siguientes valores para las constantes de integración:

$$K_1 = \frac{\gamma a^2}{E\delta} L k_1 \qquad k_1 = \frac{1 + e^{2\varkappa L}\operatorname{sen} 2\varkappa L - e^{2\varkappa L}}{-1 + e^{4\varkappa L} - 2e^{2\varkappa L}\operatorname{sen} 2\varkappa L}$$

$$K_2 = \frac{\gamma a^2}{E\delta} L k_2 \qquad k_2 = \frac{e^{2\varkappa L} - e^{2\varkappa L}\cos 2\varkappa L}{-1 + e^{4\varkappa L} - 2e^{2\varkappa L}\operatorname{sen} 2\varkappa L}$$

$$K_3 = \frac{\gamma a^2}{E\delta} L k_3 \qquad k_3 = \frac{e^{2\varkappa L} - e^{4\varkappa L} + e^{2\varkappa L}\operatorname{sen} 2\varkappa L}{-1 + e^{4\varkappa L} - 2e^{2\varkappa L}\operatorname{sen} 2\varkappa L}$$

$$K_4 = \frac{\gamma a^2}{E\delta} L k_4 \qquad k_4 = \frac{e^{2\varkappa L} - e^{2\varkappa L}\cos 2\varkappa L}{-1 + e^{4\varkappa L} - 2e^{2\varkappa L}\operatorname{sen} 2\varkappa L}$$

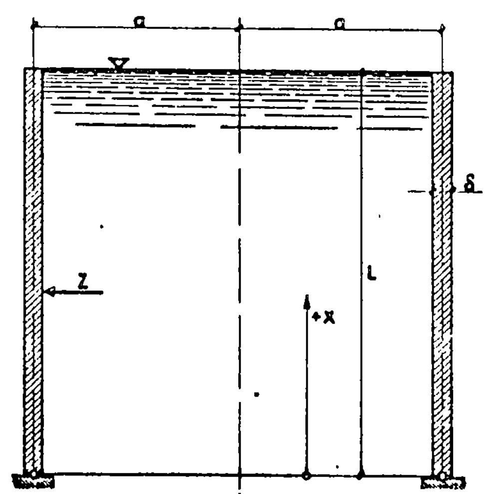

Fig. 8

Con estos valores las expresiones de los esfuerzos se obtendrán a partir de la fórmula [VI] y el recorrido de la expresión [IX]:

$$w=\frac{\gamma a^2}{E\delta}L\left[1-\frac{x}{L}+e^{\ae x}\left(k_1\cos\ae x+k_2\,\mathrm{sen}\,\ae x\right)+e^{-\ae x}\left(k_3\cos\ae x+k_4\,\mathrm{sen}\,\ae x\right)\right]$$

$$N_\varphi=\gamma a L\left[1-\frac{x}{L}+e^{\ae x}\left(k_1\cos\ae x+k_2\,\mathrm{sen}\,\ae x\right)+e^{-\ae x}\left(k_3\cos\ae x+k_4\,\mathrm{sen}\,\ae x\right)\right]$$

$$M_x=\frac{\gamma a\delta L}{2\sqrt{3(1-\nu^2)}}\left[e^{\ae x}\left(-k_1\,\mathrm{sen}\,\ae x+k_2\cos\ae x\right)+e^{-\ae x}\left(k_3\,\mathrm{sen}\,\ae x-k_4\cos\ae x\right)\right]$$

$$Q_x=-\frac{\gamma L\sqrt{a\delta}}{2\sqrt[4]{3(1-\nu^2)}}\left[e^{\ae x}\left[-k_1(\mathrm{sen}\,\ae x-\cos\ae x)+k_2(\cos\ae x-\mathrm{sen}\,\ae x)\right]+\right.$$
$$\left.+\,e^{-\ae x}\left[k_3(\cos\ae x-\mathrm{sen}\,\ae x)+k_4(\cos\ae x+\mathrm{sen}\,\ae x)\right]\right]$$

Si se supone que el depósito tiene unas dimensiones tales que el efecto en un borde no tiene influencia en el otro, se obtienen los siguientes valores para las constantes:

$$k_1=k_2=k_4=0\,;\qquad k_3=-1\,.$$

Con lo que se llega a las expresiones siguientes:

$$w=\frac{\gamma a^2}{E\delta}L\left[1-\frac{x}{L}-e^{-\ae x}\cos\ae x\right]$$

$$N_\varphi=\gamma a L\left[1-\frac{x}{L}-e^{-\ae x}\cos\ae x\right]$$

$$M_x=\frac{-\gamma a\delta L}{2\sqrt{3(1-\nu^2)}}\,e^{-\ae x}\,\mathrm{sen}\,\ae x$$

$$Q_x=\frac{\gamma L\sqrt{a\delta}}{2\sqrt[4]{3(1-\nu^2)}}\,e^{-\ae x}(\cos\ae x-\mathrm{sen}\,\ae x)$$

En esta solución simplificada, y para depósitos de hormigón armado o pretensado con $\nu\simeq 0{,}2$, el valor máximo del momento flector M_x es:

$$M_{x\,max}\simeq -0{,}095\gamma a\delta L$$

y se obtiene a una altura relativa $\dfrac{x_0}{L}$

$$\frac{x_0}{L}\simeq 0{,}6\sqrt{\frac{a\delta}{L^2}}$$

Como en el caso IIIa, aparece aquí en la figura 9 la localización de los máximos de w y N_φ y sus valores.

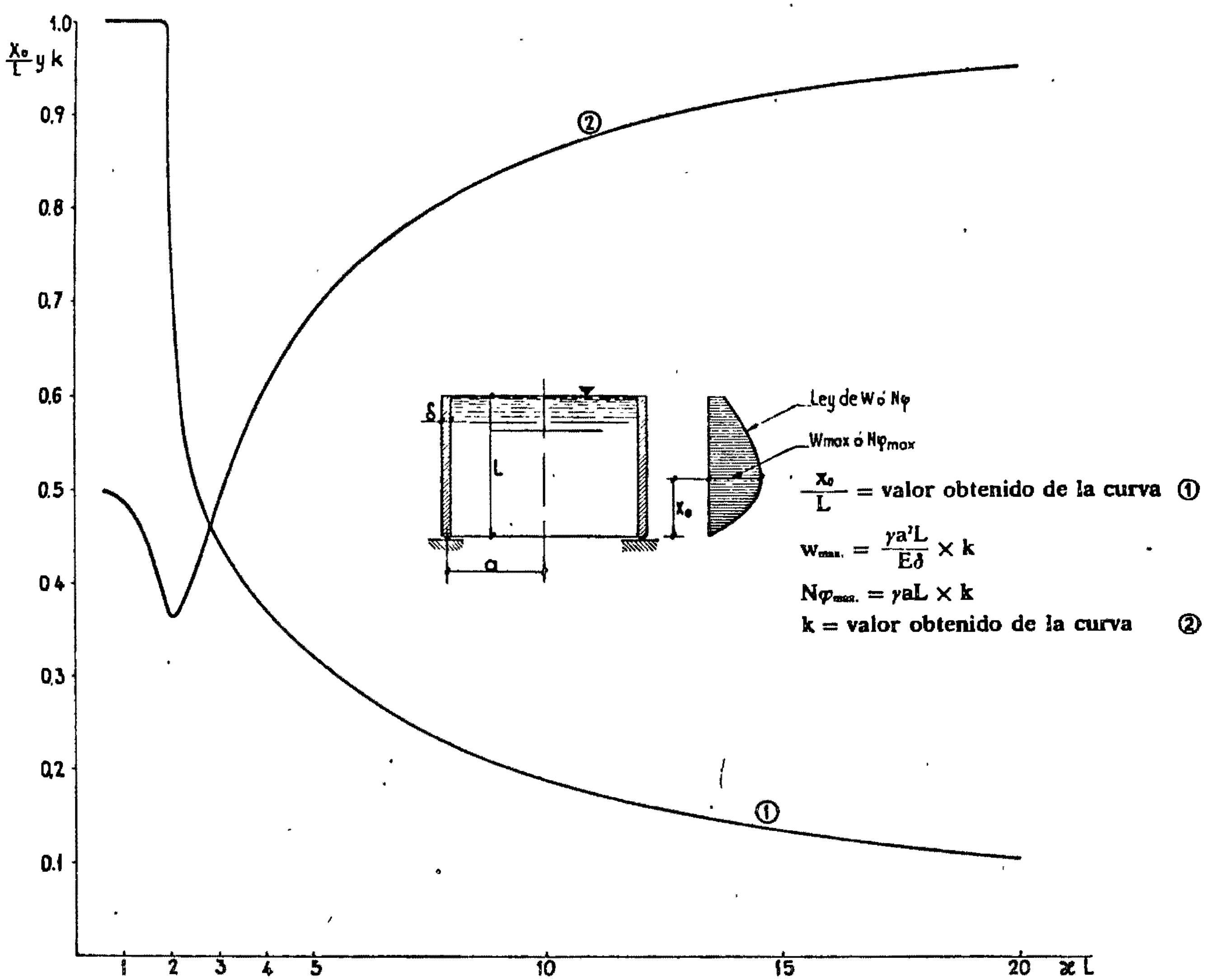

Fig. 9

2.1.8. Tabulación del caso IIIb.

En las tablas X, XI y XII se incluyen los coeficientes que, introducidos en las expresiones que se dan a continuación, permiten obtener los valores del recorrido y los esfuerzos, para distintas alturas unitarias, en cualquier depósito:

$$w = \frac{\gamma a^2}{E\,\delta} L \times \left[\mathrm{Coef}_{\mathrm{X}}\right]$$

$$N\varphi = \gamma a L \times \left[\mathrm{Coef}_{\mathrm{X}}\right]$$

$$M_x = \frac{\gamma a \delta L}{2\sqrt{3(1-\nu^2)}} \times \left[\mathrm{Coef}_{\mathrm{XI}}\right]$$

$$Q_x = -\frac{\gamma \sqrt{a\delta}\, L}{2\sqrt[4]{3(1-\nu^2)}} \times \left[\mathrm{Coef}_{\mathrm{XII}}\right]$$

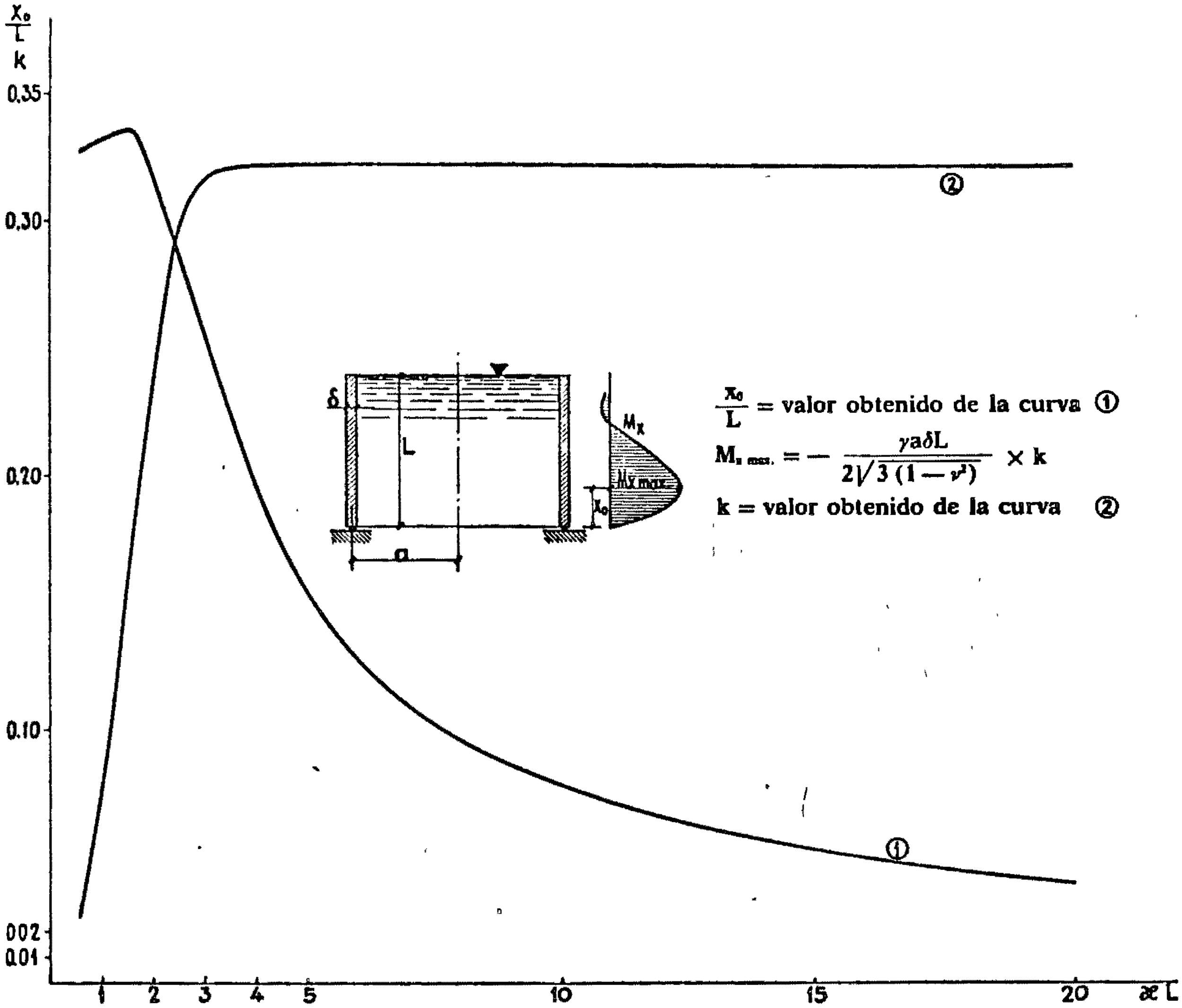

Fig. 10

Los gráficos G-X, G-XI y G-XII corresponden, respectivtmente, a las tablas X, XI y XII.

En el gráfico de la figura 9 se incluyen dos curvas que permiten determinar, fácil y rápidamente, los valores máximos del corrimiento w y del esfuerzo N_φ y la altura relativa en que se presentan, y esto en función de la característica geométrica $\varkappa L$ del depósito considerado.

En la figura 10 se incluyen otras dos curvas, con las que se pueden determinar el momento flector máximo M_x y la abscisa unitaria en que se produce.

3. Ejemplos

Ejemplo 1

Depósito de hormigón armado empotrado en la cimentación y libre en el borde superior, de 8 m de altura, 4,10 m de radio exterior y 20 cm de espesor uniforme de pared. Se considerará el depósito lleno de agua y se tomará un valor del coeficiente de Poisson igual a 0,2.

Datos.

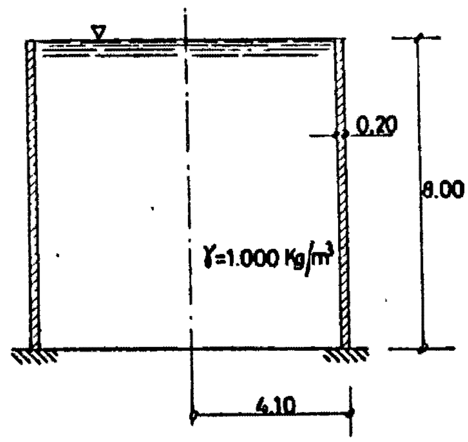

Radio medio: $a = 4{,}00$ m

Altura: $L = 8{,}00$ m

Espesor pared: $\delta = 0{,}20$ m

Módulo de Poisson: $\nu = 0{,}2$

Peso específico líquido: $\gamma = 1.000$ kg/m³

$$\varkappa = \frac{\sqrt[4]{3(1-\nu^2)}}{\sqrt{a\delta}} = 1{,}456$$

$$\varkappa L = 1{,}456 \times 8 = 11{,}65$$

$$\gamma a L = 1.000 \times 4 \times 8 = 32.000$$

$$\frac{\gamma a \delta L}{2\sqrt{3(1-\nu^2)}} = 1.885$$

Solución directa.

El gráfico de la figura 6 da para $\varkappa L = 11{,}65$

$$\frac{x_0}{L} = 0{,}216 \,; \qquad k = 0{,}806 \,,$$

luego

$$N_{\varphi\,max} = 0{,}806 \times 32.000 = 25.800 \text{ kg/m} \,.$$

Y se presenta a una altura $x_0 = 8 \times 0{,}216 = 1{,}728$ m.

Los gráficos de la figura 7 dan para $\varkappa L = 11{,}65$

$$\frac{x_0}{L} = 0{,}138 \,; \qquad \frac{x_1}{L} = 0{,}063 \,; \qquad k_1 = 0{,}913 \,; \qquad k_2 = -0{,}208 \,,$$

luego

$$[M_x]_{x=0} = 1.885 \times 0{,}915 = 1.720 \text{ kg} \cdot \text{m/m} \,;$$

$$M_{x\,min} = -1.885 \times 0{,}208 = -392 \text{ m} \cdot \text{kg/m} \,,$$

y se presenta a una altura $x_0 = 0{,}138 \times 8 = 1{,}104$ m.

La altura del momento nulo corresponde a $x_1 = 0{,}063 \times 8 = 0{,}504$ m.

En general, con los datos anteriores se pueden dibujar con aproximación suficiente en los casos prácticos las leyes de N_φ y M_x, esfuerzos fundamentales para el proyecto del depósito.

El valor del esfuerzo cortante Q_x interesa menos, por lo que se suele hallar su valor máximo para comprobación, pues en los depósitos de hormigón este esfuerzo está resistido ampliamente por el hormigón. Este valor máximo de Q_x se puede obtener del gráfico G-IX o de la tabla IX para $x = 0$.

$$Q_{x\,max} = -\frac{\gamma L\sqrt{a\delta}}{2\sqrt[4]{3(1-\nu^2)}} \times [\text{Coef. IX}]_{x=0} = -\frac{1.000 \times 8}{2 \times 1{,}456}[-1{,}910] = 5.240 \text{ kg/m}.$$

Los valores de N_φ, M_x y Q_x en las distintas alturas se obtendrán por medio de los coeficientes Coef. VII, Coef. VIII y Coef. IX, de los gráficos G-VII, G-VIII y G-IX para $\varkappa L = 11{,}65$, y sus expresiones serán:

$$N_\varphi = 32.000 \text{ Coef. VII}$$
$$M_x = 1.885 \text{ Coef. VIII}$$
$$Q_x = -2.750 \text{ Coef. IX}.$$

Solución por superposición de estados.

Se obtendrá mediante la superposición de los tres estados siguientes:

1.° Solución particular correspondiente a las cargas exteriores, que constituye la solución membrana (VIII).
2.° Estado correspondiente a la aplicación de un esfuerzo uniforme R en el borde inferior.
3.° Estado correspondiente a la aplicación de un momento uniforme M en el borde inferior.

Los valores numéricos de M y R se determinarán con las dos condiciones siguientes:

$$[w]_{x=0} = 0$$
$$\left[\frac{dw}{dx}\right] = 0.$$

Corrimiento en $x = 0$ de la solución particular:

$$\frac{\gamma a^2}{E\delta} L = \frac{12.800}{E\delta}.$$

Corrimiento en $x = 0$ debido a la aplicación de R (gráfico G-I):

$$-\frac{2\sqrt[4]{3(1-\nu^2)}a}{E\delta}\sqrt{\frac{a}{\delta}}R = -\frac{46{,}61}{E\delta}R.$$

Corrimiento en $x = 0$ debido a la aplicación de M (gráfico G-IV):

$$\frac{2\sqrt{3(1-\nu^2)}a}{E\delta}\frac{1}{\delta}M = \frac{67{,}88}{E\delta}M.$$

Giro en $x = 0$ de la solución particular:

$$-\frac{\gamma a^2}{E\delta} = -\frac{3.200}{E\delta^2}$$

Giro en $x = 0$ debido a la aplicación de R (tabla A):

$$\frac{2a}{E\delta^2}\sqrt{3(1-\nu^2)}R = \frac{13{,}58}{E\delta^2}R.$$

Giro en x = 0 debido a la aplicación de M (tabla B):

$$\frac{2\sqrt{a/\delta}\sqrt[4]{[3(1-\nu^2)]^3}}{E\delta^2} M(-2) = -\frac{39{,}55}{E\delta^2} M.$$

Las dos ecuaciones serán:

$$128.000 - 46{,}61\,R + 67{,}88\,M = 0$$
$$-3.200 + 13{,}58\,R - 39{,}55\,M = 0,$$

de donde:

$$R = 5.259 \text{ kg/m}$$
$$M = 1.725 \text{ m} \cdot \text{kg/m},$$

y las expresiones de los esfuerzos son:

$$N_\varphi = \gamma a L\left(1 - \frac{x}{L}\right) + \frac{2\sqrt[4]{3(1-\nu^2)}}{\sqrt{a\delta}}\, a\, 5.259[\text{Coef. I}] + 2\,\frac{\sqrt{3(1-\nu^2)}}{\delta}\, 1.725\,[\text{Coef. IV}];$$

$$M_x = \frac{\sqrt{a\delta}}{\sqrt[4]{3(1-\nu^2)}}\, 5.259\,[\text{Coef. II}] + 1.725\,[\text{Coef. VI}];$$

$$Q_x = -5.259\,[\text{Coef. III}] - \frac{\sqrt[4]{3(1-\nu^2)}}{\sqrt{a\delta}}\, 1.725\,[\text{Coef. V}].$$

Todos los valores de los coeficientes se obtendrán para $\varkappa L = 11{,}65$.

Los valores de los esfuerzos se dan en el cuadro siguiente, y su representación gráfica, en la figura 11.

EJEMPLO 1.°

$\frac{x}{L}$	x	Coef. I	Coef. II	Coef. III	Coef. IV	Coef. V	Coef. VI	N_φ	M_x	Q_x
0	0	— 1	0	— 1	1	1	0	0	1.725	5.259
0,05	0,4	— 0,466	— 0,307	— 0,160	0,158	0,775	— 0,614	6.479	228	2.384
0,10	0,8	— 0,123	— 0,287	0,165	— 0,165	0,410	— 0,573	16.435	— 329	571
0,15	1,2	0,030	— 0,172	0,200	— 0,200	0,140	— 0,348	23.183	— 380	— 178
0,20	1,6	0,068	— 0,070	0,140	— 0,140	0	— 0,140	25.667	— 253	— 385
0,30	2,4	0,028	0,010	0,018	— 0,019	— 0,039	0,025	23.559	— 31	— 157
0,40	3,2	0	0,010	— 0,010	0,010	— 0,007	0,020	19.493	24	2
0,50	4,0	— 0,003	0,001	— 0,005	0,005	—	—	15.963	4	26
0,60	4,8	—	— 0,001	—	—	—	—	12.800	—	—
0,70	5,6	—	—	—	—	—	—	9.600	—	—
0,80	6,4	—	—	—	—	—	—	6.400	—	—
0,90	7,2	—	—	—	—	—	—	3.200	—	—
1,00	8,0	—	—	—	—	—	—	0	—	—

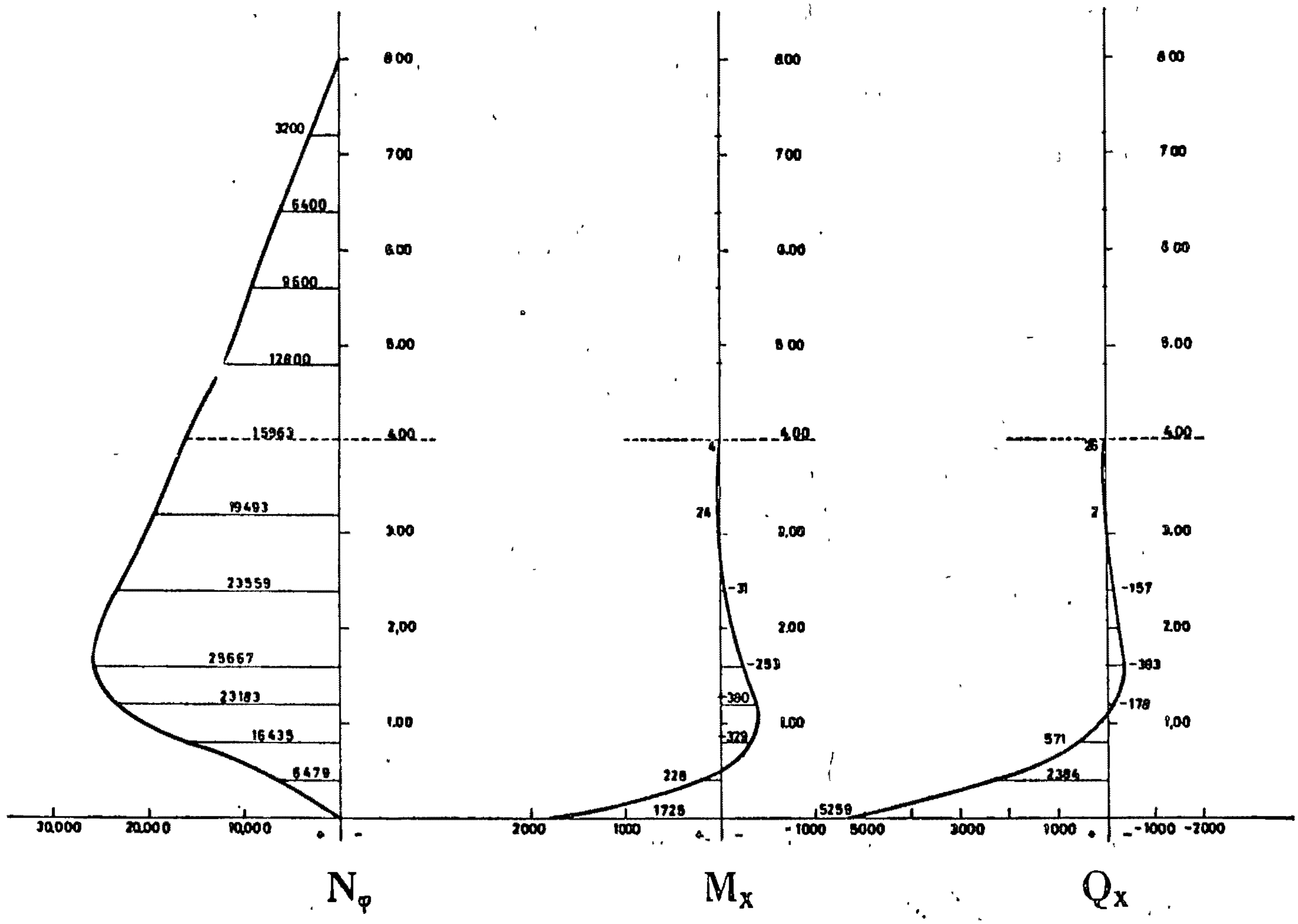
8.00
7.00
6.00
5.00
4.00
3.00
2.00
1.00
3200
6400
9600
12800
15963
19493
23559
25667
23183
16435
6479
30,000
20,000
10,000
2000
1000
-1000
5000
3000
1000
-1000
-2000
4
24
-31
-253
380
329
228
1728
26
2
-157
-383
-178
571
2384
5259
N_φ
M_x
Q_x

Fig. 11

Ejemplo 2

Depósito de hormigón armado, articulado en la cimentación y libre en el borde superior, de 8 m de altura, 4,10 m de radio exterior y 20 cm de espesor uniforme de pared. Se considerará el depósito lleno de agua y se tomará un valor del coeficiente de Poisson igual a 0,2.

Datos.

Radio medio: $a = 4{,}00$ m
Altura: $L = 8{,}00$ m
Espesor pared: $\delta = 0{,}20$ m
Módulo de Poisson: $\nu = 0{,}2$
Peso específico líquido: $\gamma = 1.000$ kg/m³

$$\varkappa = \frac{\sqrt[4]{3(1-\nu^2)}}{\sqrt{a\delta}} = 1.456$$

$$\varkappa L = 1{,}456 \times 8 = 11{,}65$$

$$\gamma a L = 1.000 \times 4 \times 8 = 32.000$$

$$\frac{\gamma a L \delta}{2\sqrt{3(1-\nu^2)}} = 1.885$$

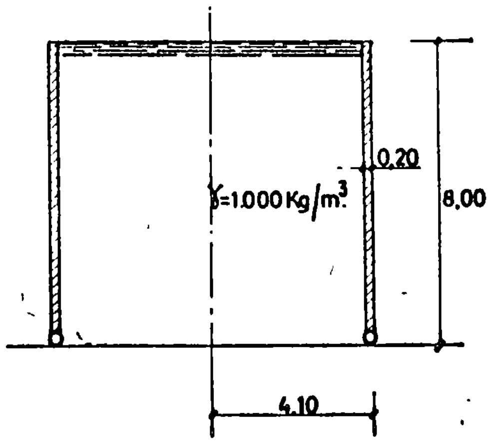

Solución directa.

El gráfico de la figura 9 da para $\varkappa L = 11{,}65$

$$\frac{x_0}{L} = 0{,}165 \,; \qquad k = 0{,}885 \,,$$

luego

$$N_{\varphi\ max} = 0{,}855 \times 32.000 = 28.320 \text{ kg/m} \,.$$

Y se presenta a una altura $x_0 = 8 \times 0{,}165 = 1{,}32$ m.

Los gráficos de la figura 10 dan para $\varkappa L = 11{,}65$

$$\frac{x_0}{L} = 0{,}067 \,; \qquad k = 0{,}322 \,,$$

$$\text{luego } [M_x]_{max} = -1.885 \times 0{,}322 = -607 \text{ m} \cdot \text{kg/m} \,.$$

y se presenta a una altura $x_0 = 0{,}067 \times 8 = 0{,}536$ m .

El valor máximo del esfuerzo cortante Q_x será:

$$Q_{x\ max} = -\frac{\gamma L \sqrt{a\delta}}{2\sqrt[4]{3(1-\nu^2)}} \times [\text{Coef. XII}]_{x=0} = -2.750 \text{ kg/m} \,.$$

Los valores de N_φ, M_x y Q_x en las distintas alturas se obtendrán por medio de los coeficientes Coef. V, Coef. XI y Coef. XII de los gráficos G-X, G-XI y G-XII para $\varkappa L = 11{,}65$, y sus expresiones serán:

$$N_\varphi = 32.000 \text{ Coef. X}$$
$$M_x = 1.885 \text{ Coef. XI}$$
$$Q_x = -2.750 \text{ Coef. XII}$$

Solución por superposición de estados.

Se obtendrá mediante la superposición de los dos estados siguientes:

1.º Solución particular correspondiente a las cargas exteriores, que constituye la solución membrana.

2.º Estado correspondiente a la aplicación de un esfuerzo uniforme R en el borde inferior.

El valor numérico de R se determinará con la condición siguiente:

$$[w]_{x=0} = 0 .$$

Corrimiento en $x = 0$ de la solución particular:

$$\frac{\gamma a^2 L}{E\delta} = \frac{128.000}{E\delta} .$$

Corrimiento en $x = 0$ debido a la aplicación de R (gráfico G-I):

$$-\frac{2\sqrt[4]{3(1-\nu^2)}}{E\delta}\, a \sqrt{\frac{a}{\delta}}\, R = -\frac{46{,}61}{E\delta} \cdot R$$

La ecuación que define el valor de R será:

$$128.000 - 46{,}61\, R = 0 ,$$

de donde

$$R = 2.746 \text{ kg/m} ,$$

y las expresiones de los esfuerzos son:

$$N_\varphi = \gamma a L \left(1 - \frac{x}{L}\right) + \frac{2\sqrt[4]{3(1-\nu^2)}\, a}{\sqrt{a\delta}}\, 2.746\, [\text{Coef. I}] .$$

$$M_x = \frac{\sqrt{a\delta}}{\sqrt[4]{3(1-\nu^2)}}\, 2.746\, [\text{Coef. II}] .$$

$$Q_x = -2.746\, [\text{Coef. III}] .$$

Todos los valores de los coeficientes se obtendrán para $\varkappa L = 11{,}65$.

Los valores de los esfuerzos se dan en el cuadro siguiente, y su representación gráfica, en la figura 12.

EJEMPLO 2.º

$\frac{x}{L}$	x	Coef. I	Coef. II	Coef. III	N_φ	M_x	Q_x
0	0	— 1,000	0,0000	— 1,000	0,000	0	2.747
0,05	0,4	— 0,466	— 0,3075	— 0,160	15.488	— 580	439
0,10	0,8	— 0,122	— 0,2870	0,163	24.896	— 541	— 448
0,15	1,2	0,030	— 0,1715	0,203	28.160	— 323	— 558
0,20	1,6	0,068	— 0,0705	0,140	27.776	— 133	— 385
0,30	2,4	0,028	0,0100	0,018	23.296	19	— 49
0,40	3,2	0,000	0,0100	— 0,010	19.200	19	27
0,50	4,0	— 0,003	0,0010	— 0,005	15.904	2	14
0,60	4,8	—	— 0,0010	—	12.800	— 2	—
0,70	5,6	—	—	—	9.600	—	—
0,80	6,4	—	—	—	6.400	—	—
0,90	7,2	—	—	—	3.200	—	—
1,00	8,0	—	—	—	—	—	—

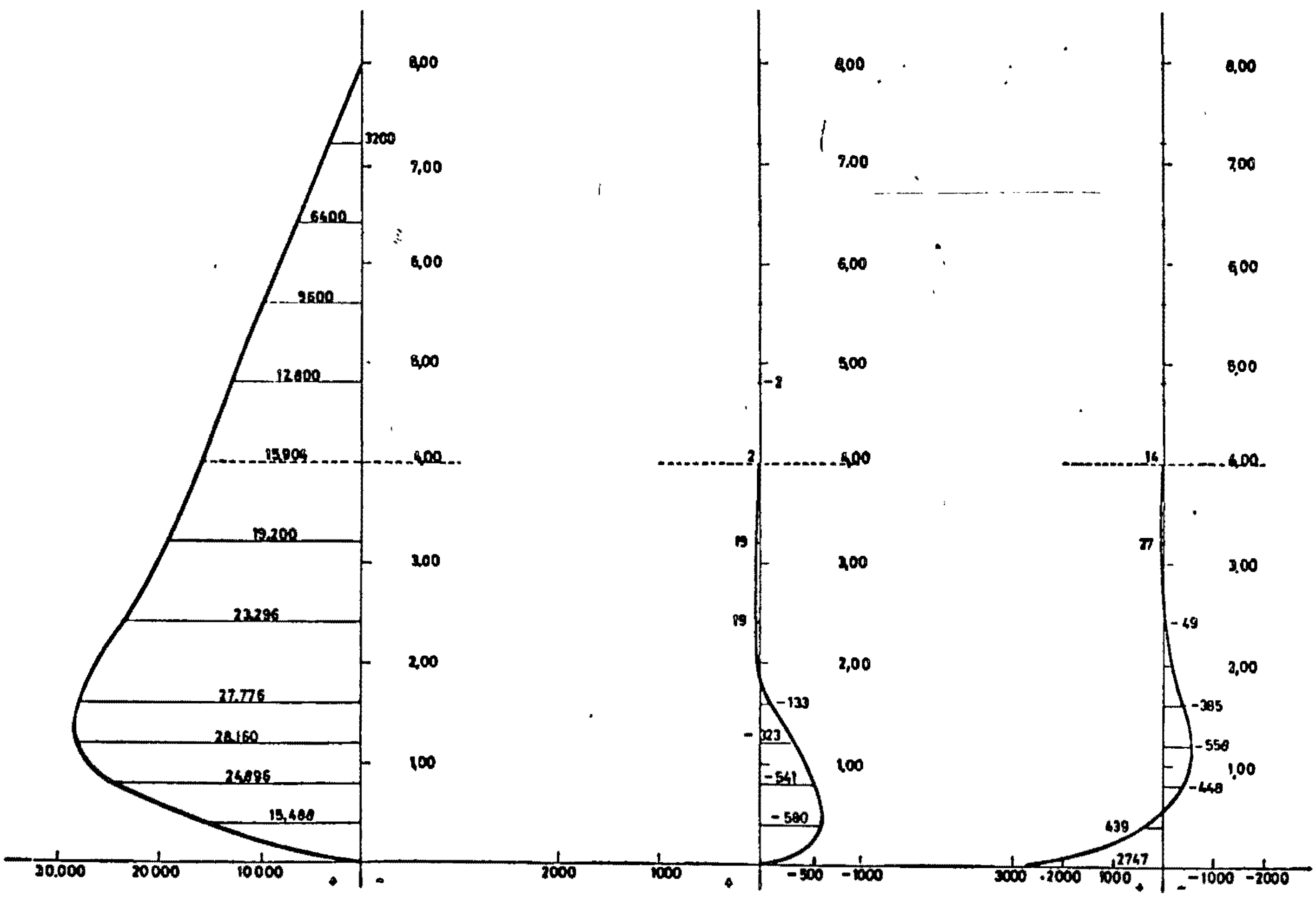

N_φ M_x Q_x

Fig. 12

Ejemplo 3

Depósito de hormigón armado empotrado en la cimentación y libre en el borde superior, de 2,30 m de altura, 5,10 m de radio exterior y 20 cm de espesor uniforme de pared. Se considerará el depósito lleno de agua y se tomará un valor del coeficiente de Poisson igual a 0,2.

Datos.

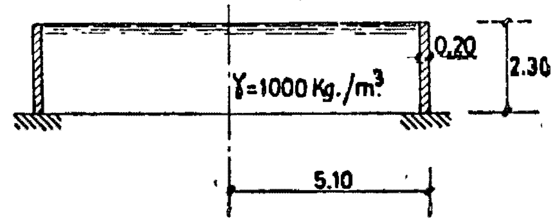

Radio medio: $a = 5{,}00$ m

Altura: $L = 2{,}30$ m

Espesor pared: $\delta = 0{,}20$ m

Módulo de Poisson: $\nu = 0{,}2$

Peso específico líquido: $\gamma = 1.000$ kg/m³

$$\varkappa = \frac{\sqrt[4]{3(1-\nu^2)}}{\sqrt{a\delta}} = 1{,}3027$$

$$\varkappa L = 1{,}3027 \times 2{,}30 = 2{,}996$$

$$\gamma a L = 1.000 \times 5 \times 2{,}3 = 11.500$$

$$\frac{\gamma a L \delta}{2\sqrt{3(1-\nu^2)}} = 678$$

Solución directa.

El gráfico de la figura 6 da para $\varkappa L = 2{,}996$

$$\frac{x_0}{L} = 0{,}560\,; \qquad k = 0{,}335\,,$$

luego

$$N_{\varphi\,max} = 0{,}335 \times 11.500 = 3.852 \text{ kg/m}\,.$$

Y se presenta a una altura $x_0 = 2{,}30 \times 0{,}56 = 1{,}29$ m.

Los gráficos de la figura 7 dan para $\varkappa L = 2{,}996$

$$\frac{x_0}{L} = 0{,}43\,; \qquad \frac{x_1}{L} = 0{,}195\,; \qquad k_1 = 0{,}65\,; \qquad k_2 = -0{,}192\,,$$

luego

$$[M_x]_{x=0} = 678 \times 0{,}65 = 440 \text{ m} \cdot \text{kg/m}$$
$$M_{x\,min} = -678 \times 0{,}192 = -130 \text{ m} \cdot \text{kg/m}$$

Y se presenta a una altura $x_0 = 0{,}43 \times 2{,}30 = 0{,}99$ m.

La altura del momento nulo corresponde a $x_1 = 0{,}195 \times 2{,}30 = 0{,}45$ m.

Los valores de N_φ, M_x y Q_x en las distintas alturas se obtendrán por medio de los coeficientes Coef. VII, Coef. VIII y Coef. IX, de los gráficos G-VII, G-VIII y G-IX para $\varkappa L = 2{,}996$, y sus expresiones serán:

$$N_\varphi = 11.500 \text{ Coef. VII}$$
$$M_x = 678 \text{ Coef. VIII}$$
$$Q_x = -883 \text{ Coef. IX}$$

Solución por superposición de estados.

Se obtendrá mediante la superposición de los tres estados siguientes:

1.° Solución particular correspondiente a las cargas exteriores, que constituye la solución membrana.

2.° Estado correspondiente a la aplicación de un esfuerzo uniforme R en el borde inferior.

3.° Estado correspondiente a la aplicación de un momento uniforme M en el borde inferior.

Los valores numéricos de M y R se determinarán con las dos condiciones siguientes:

$$[w]_{x=0} = 0$$
$$\left[\frac{dw}{dx}\right]_{x=0} = 0$$

Se tendrá:

Corrimiento en $x = 0$ de la solución particular:

$$\frac{\gamma a^2 L}{E\delta} = \frac{57.500}{E\delta}.$$

Corrimiento en $x = 0$ debido a la aplicación de R:

$$\frac{2a^2}{E\delta}\varkappa R[K_1 + K_3] = -\frac{2a^2}{E\delta} 1{,}3113\, R = -\frac{65{,}565}{E\delta} R.$$

Corrimiento en $x = 0$ debido a la aplicación de M:

$$\frac{a^2 L\gamma}{E\delta}\frac{2\sqrt{3(1-\nu^2)}}{\gamma a\delta L} M[K_1 + K_3] = \frac{a^2 L\gamma}{E\delta} M \cdot 1{,}476 \times 10^{-3} = \frac{84{,}87}{E\delta} M.$$

Giro en $x = 0$ de la solución particular:

$$-\frac{\gamma a^2}{E\delta} = -\frac{25.000}{E\delta}.$$

Giro en $x = 0$ debido a la aplicación de R:

$$\frac{2a^2}{E\delta}\varkappa^2 R[K_1 + 2K_2 - K_3 + 2K_4] = \frac{2a^2}{E\delta} 1{,}6977\, R = \frac{84{,}885}{E\delta} R.$$

Giro en $x = 0$ debido a la apl. ación de M:

$$\frac{2\sqrt{3(1-\nu^2)}}{\gamma a\delta L}\varkappa M[K_1 + K_2 - K_3 + K_4]\frac{a^2 L\gamma}{E\delta} = -\frac{a^2 L\gamma}{E\delta} M \cdot 3{,}859 \times 10^{-3} = -\frac{221{,}89}{E\delta} M.$$

Las dos ecuaciones serán:

$$57.500 - 65{,}565\,R + 84{,}870\,M = 0$$
$$-25.000 + 84{,}885\,R - 221{,}890\,M = 0\,,$$

de donde:

$$R = 1.450 \text{ kg/m}$$
$$M = 442 \text{ m} \cdot \text{kg/m}$$

Y las expresiones de los esfuerzos son:

$$N_\varphi = \gamma a L \left(1 - \frac{x}{L}\right) + \frac{2\sqrt[4]{3(1-\nu^2)}\,a}{\sqrt{a\delta}}\, 1.450\,[\text{Coef. I}] + 2\,\frac{\sqrt{3(1-\nu^2)}}{\delta}\, 442\,[\text{Coef. IV}]\,.$$

$$M_x = \frac{\sqrt{a\delta}}{\sqrt[4]{3(1-\nu^2)}}\, 1.450\,[\text{Coef. II}] + 442\,[\text{Coef. V}]\,.$$

$$Q_x = -1.450\,[\text{Coef. III}] - \frac{\sqrt[4]{3(1-\nu^2)}}{\sqrt{a\delta}}\, 442\,[\text{Coef. VI}]\,.$$

Todos los valores de los coeficientes se obtendrán para $\varkappa L = 2{,}996$.

Los valores de los esfuerzos se dan en el cuadro siguiente, y la representación gráfica, en la figura 13.

EJEMPLO 3.°

$\frac{x}{L}$	x	Coef. I	Coef. II	Coef. III	Coef. IV	Coef. V	Coef. VI	N_φ	M_x	Q_x
0	0	— 1,007	0	— 1,000	1,0004	1,000	0	0	442	1.450
0,05	0,115	— 0,855	— 0,128	— 0,720	0,722	0,980	— 0,257	190	291	1.192
0,1	0,23	— 0,715	— 0,2185	— 0,485	0,487	0,926	— 0,437	497	166	955
0,15	0,345	— 0,580	— 0,2760	— 0,290	0,294	0,850	— 0,553	1.025	69	739
0,2	0,46	— 0,460	— 0,3075	— 0,135	0,139	0,760	— 0,617	1.553	— 6	551
0,3	0,69	— 0,256	— 0,3138	0,076	— 0,072	0,570	— 0,631	2.675	— 97	253
0,4	0,92	— 0,113	— 0,2715	0,185	— 0,180	0,390	— 0,550	3.416	— 129	49
0,5	1,15	— 0,017	— 0,2092	0,220	— 0,216	0,246	— 0,430	3.809	— 124	— 71
0,6	1,38	0,042	— 0,1430	0,211	— 0,208	0,136	— 0,300	3.833	— 99	— 133
0,7	1,61	0,077	— 0,0840	0,176	— 0,174	0,064	— 0,186	3.599	— 65	— 148
0,8	1,84	0,092	— 0,0385	0,125	— 0,129	0,022	— 0,094	3.070	— 33	— 127
0,9	2,07	0,105	— 0,0100	0,065	— 0,079	0,004	— 0,032	2.541	— 9,4	— 76
1	2,30	0,110	0	0	— 0,028	0	0	1.868	0	0

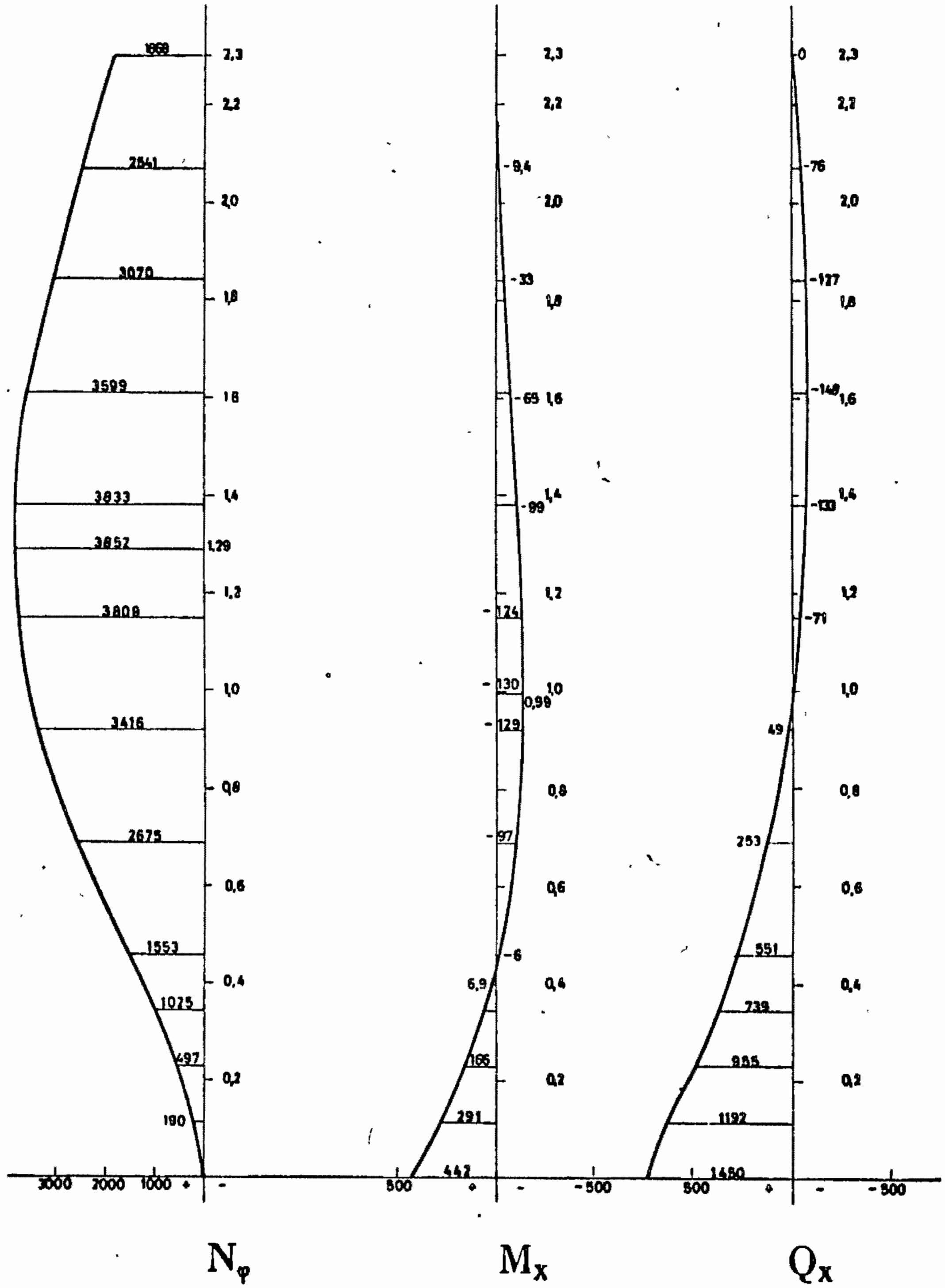

1868
2541
3070
3599
3833
3852
3808
3416
2675
1553
1025
497
190
2,3
2,2
2,0
1,8
1,6
1,4
1,29
1,2
1,0
0,8
0,6
0,4
0,2
3000
2000
1000
+
-
500
- 9,4
- 33
- 65
- 99
- 124
- 130
0,99
- 129
- 97
- 6
6,9
166
291
442
- 500
0
- 76
- 127
- 148
- 130
- 71
49
253
551
739
985
1192
1450
N_φ
M_x
Q_x

Fig. 13

Ejemplo 4

Depósito de hormigón armado articulado en la cimentación y libre en el borde superior, de 2,30 m de altura, 5,10 m de radio exterior y 20 cm de espesor de pared uniforme. Se considerará el depósito lleno de agua y se tomará un valor del coeficiente de Poisson igual a 0,2.

Datos.

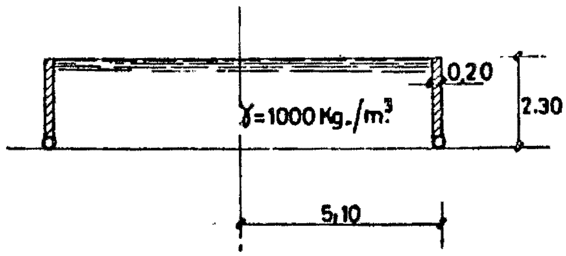

Radio medio: $a = 5{,}00$ m
Altura: $L = 2{,}30$ m
Espesor pared: $\delta = 0{,}20$ m
Módulo de Poisson: $\nu = 0{,}2$
Peso específico líquido: $\gamma = 1.000$ kg/m³

$$\varkappa = 1{,}3027$$
$$\varkappa L = 2{,}996$$
$$\gamma a L = 11.500$$
$$\frac{\gamma a L \delta}{2\sqrt{3(1-\nu^2)}} = 678$$

Solución directa.

El gráfico de la figura 9 da para $\varkappa L = 2{,}996$

$$\frac{x_0}{L} = 0{,}44 \,; \quad k = 0{,}49 \,,$$

luego

$$N_{\varphi\, max} = 11.500 \times 0{,}49 = 5.635 \text{ kg/m} \,.$$

Y se presenta a una altura $x_0 = 2{,}30 \times 0{,}44 = 1{,}01$ m.

El gráfico de la figura 10 da para $\varkappa L = 2{,}996$

$$\frac{x_0}{L} = 0{,}256 \,; \quad k = 0{,}316 \,.$$

luego

$$[M_x]_{max} = -678 \times 0{,}316 = -214 \text{ m} \cdot \text{kg/m} \,.$$

Y se presenta a una altura $x_0 = 2{,}30 \times 0{,}256 = 0{,}59$ m.

Los valores de N_φ, M_x y Q_x, en las distintas alturas, se obtendrán por medio de los coeficientes Coef. X, Coef XI y Coef. XII de los gráficos G-X, G-XI y G-XII para $\varkappa L = 2{,}996$, y sus expresiones serán:

$$N_\varphi = 11.500 \text{ Coef. X}$$
$$M_x = 678 \text{ Coef. XI}$$
$$Q_x = -883 \text{ Coef. XII}$$

Solución por superposición de estados.

Se obtendrá mediante la superposición de los dos estados siguientes:

1.° Solución particular correspondiente a las cargas exteriores, que constituye el estado membrana.

2.° Estado correspondiente a la aplicación de un esfuerzo uniforme R en el borde inferior.

El valor numérico de R se determinará con la condición siguiente:

$$[w]_{x=0} = 0 .$$

Corrimiento en x = 0 de la solución particular:

$$\frac{\gamma a^2 L}{E\delta} = \frac{57.500}{E\delta} .$$

Corrimiento en x = 0 debido a la aplicación de R:

$$-\frac{2a^2}{E\delta} 1{,}3113\, R = -\frac{65{,}565}{E\delta} R .$$

Así se tendrá:

$$57.500 - 65{,}565\, R = 0 ; \qquad R = 877 \text{ kg/m} .$$

Y las expresiones de los esfuerzos son:

$$N_\varphi = \gamma a L \left(1 - \frac{x}{L}\right) + \frac{2\sqrt[4]{3(1-\nu^2)}\,a}{\sqrt{a\delta}}\, 877\, [\text{Coef. I}] .$$

$$M_x = \frac{\sqrt{a\delta}}{\sqrt[4]{3(1-\nu^2)}}\, 877\, [\text{Coef. II}] .$$

$$Q_x = -877\, [\text{Coef. III}] .$$

Todos los valores de los coeficientes se obtendrán para $\varkappa L = 2{,}996$.

Los valores de los esfuerzos se dan en el cuadro siguiente, y la representación gráfica, en la figura 14.

EJEMPLO 4.°

$\frac{x}{L}$	x	Coef. I	Coef. II	Coef. III	N_φ	M_x	Q_x
0	0,000	— 1,007	0,0000	— 1,000	0	— 0,0	877
0,05	0,115	— 0,855	— 0,1285	— 0,720	1 161	— 86,4	631
0,1	0,23	— 0,715	— 0,2185	— 0,485	2.185	— 147	425
0,15	0,345	— 0,580	— 0,2760	— 0,290	3.151	— 186	254
0,2	0,46	— 0,460	— 0,3075	— 0,135	3.947	— 207	118
0,3	0,69	— 0,256	— 0,3138	0,076	5.127	— 211	— 67
0,4	0,92	— 0,113	— 0,2715	0,185	5.610	— 183	— 162
0,5	1,15	— 0,017	— 0,2092	0,220	5.556	— 141	— 193
0,6	1,38	0,042	— 0,1430	0,211	5.080	— 96	— 185
0,7	1,61	0,077	— 0,0840	0,176	4.329	— 56	— 154
0,8	1,84	0,092	— 0,0385	0,125	3.351	— 26	— 109
0,9	2,07	0,105	— 0,0100	0,065	2.349	— 6,7	— 57
1	2,30	0,110	0,0000	0	1.256	0	0

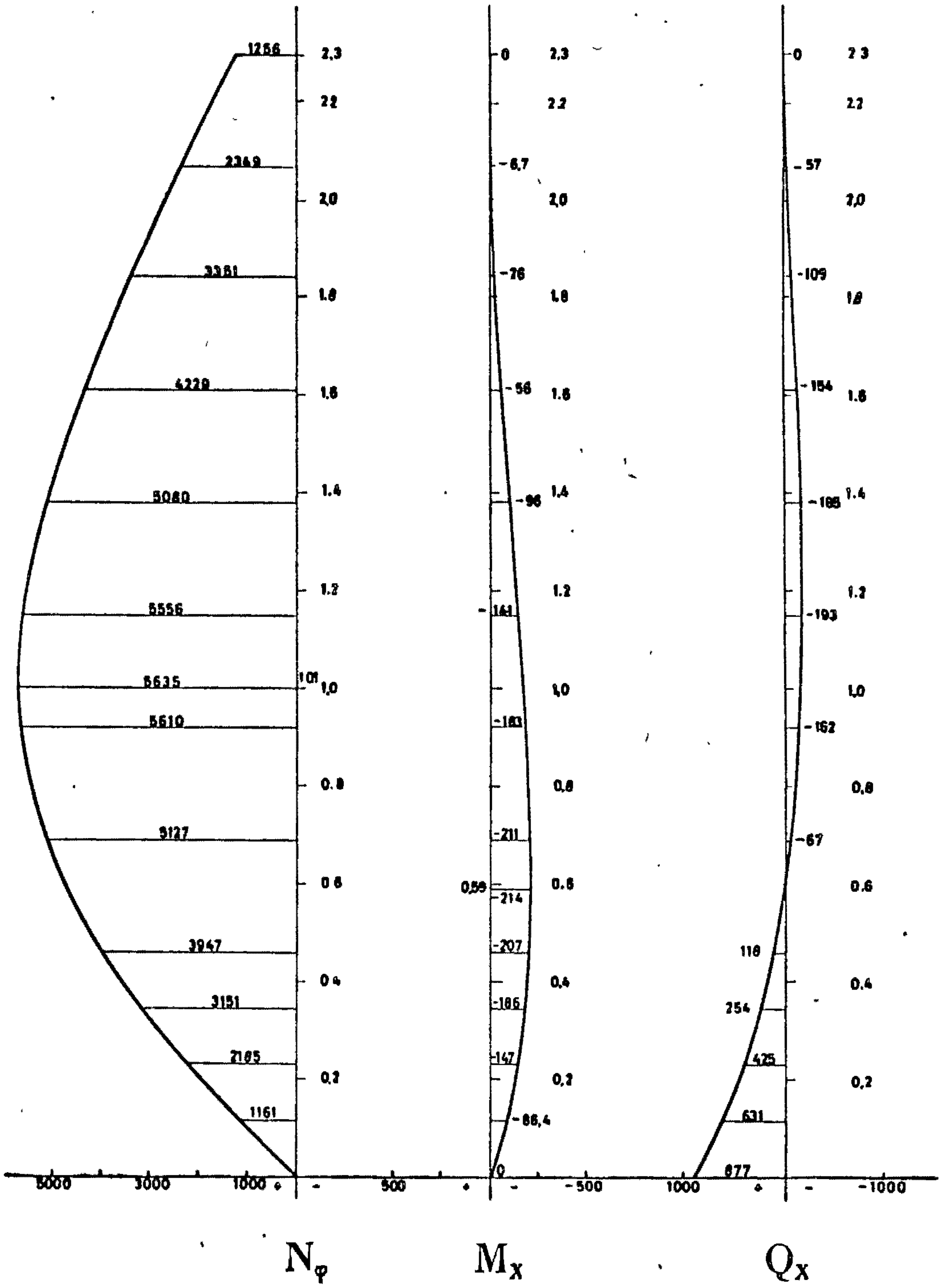

1266
2349
3381
4229
5080
5556
5635
5610
5127
3947
3151
2165
1161
101
2,3
2,2
2,0
1,8
1,6
1,4
1,2
1,0
0,8
0,6
0,4
0,2
0
-6,7
-76
-56
-96
-161
-183
-211
0,59
-214
-207
-186
-147
-86,4
-57
-109
-154
-186
-193
-162
-67
118
254
425
631
877
5000
3000
1000
500
-500
1000
-1000
N_φ
M_x
Q_x

Fig. 14

Ejemplo 5

Depósito de hormigón armado empotrado en la cimentación y libre en el borde superior, de 8 m de altura, 6 m de radio medio y 35 cm de espesor de pared uniforme. Se considerará el depósito lleno de agua y se tomará un valor del coeficiente de Poisson igual a 0,2.

Datos.

Radio medio: $a = 6{,}00$ m

Altura: $L = 8{,}00$ m

Espesor pared: $\delta = 0{,}35$ m

Módulo de Poisson: $\nu = 0{,}2$

Peso específico líquido: $\gamma = 1.000$ kg/m³

$\varkappa = 0{,}8989$

$\varkappa L = 7{,}1916$

$\gamma a L = 48.000$

$$\frac{\gamma a L \delta}{2\sqrt{3(1-\nu^2)}} = 4.950$$

$$\frac{\gamma L \sqrt{a\delta}}{2\sqrt{3(1-\nu^2)}} = 4.450$$

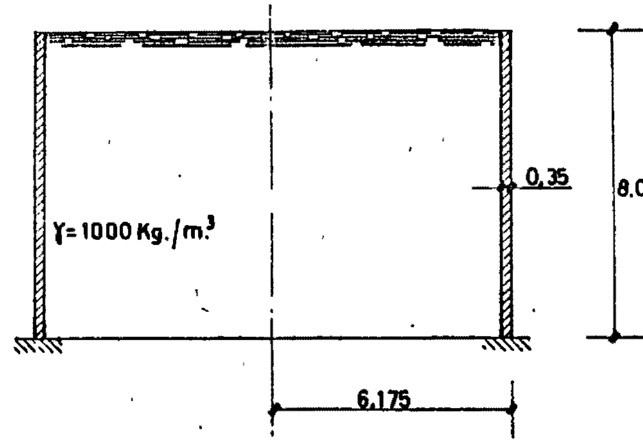

Solución directa.

El gráfico de la figura 6 da para $\varkappa L = 7{,}1916$

$$\frac{x_0}{L} = 0{,}315 \; ; \qquad k = 0{,}685 \, ,$$

luego

$$N_{\varphi\,max} = 32.880 \text{ kg/m} \quad \text{y} \quad x_0 = 2{,}52 \text{ m} .$$

El gráfico de la figura 7 da para $\varkappa L = 7{,}1916$

$$\frac{x_0}{L} = 0{,}21 \; ; \quad \frac{x_1}{L} = 0{,}10 \; ; \qquad k_1 = 0{,}86 \; ; \qquad k_2 = -0{,}209 \, ,$$

luego

$$M_{x\,max} = 4.257 \text{ m} \cdot \text{kg/m} \quad \text{en} \quad x = 0$$
$$M_{x\,min} = -1.034 \text{ m} \cdot \text{kg/m} \quad \text{en} \quad x_0 = 1{,}68 \text{ m} .$$

El momento es nulo en $x_1 = 0{,}8$ m .

Las expresiones de N_φ, M_x y Q_x son:

$$N_\varphi = 48.000 \text{ Coef. VII}$$
$$M_x = 4.950 \text{ Coef. VIII}$$
$$Q_x = -4.450 \text{ Coef. IX}$$

Solución por superposición de estados.

Siguiendo el mismo camino que en los ejemplos anteriores, se tiene:

Corrimiento en $x = 0$ de la solución particular:

$$\frac{\gamma a^2 L}{E\delta} = \frac{a^2}{E\delta} 8.000 .$$

Corrimiento en $x = 0$ debido a la aplicación de R:

$$-\frac{a^2}{E\delta} 1{,}7979 \, R .$$

Corrimiento en $x = 0$ debido a la aplicación de M:

$$\frac{a^2}{E\delta} 1{,}6163 \, M .$$

Giro en $x = 0$ de la solución particular:

$$-\frac{a^2}{E\delta} 1.000 .$$

Giro en $x = 0$ debido a la aplicación de R:

$$\frac{a^2}{E\delta} 1{,}6163 \, R .$$

Giro en $x = 0$ debido a la aplicación de M:

$$-\frac{a^2}{E\delta} 2{,}9059 \, M .$$

Las dos ecuaciones que expresan que

$$[w]_{x=0} = 0 \quad y \quad \left[\frac{dw}{dx}\right]_{x=0} = 0$$

son:

$$\begin{aligned} 8.000 - 1{,}7979 \, R + 1{,}6163 \, M &= 0 \\ -1.000 + 1{,}6163 \, R - 2{,}9059 \, M &= 0 , \end{aligned}$$

de donde

$$\begin{aligned} R &= 8.281 \ \text{kg/m} \\ M &= 4.262 \ \text{m} \cdot \text{kg/m} . \end{aligned}$$

Y las expresiones de los esfuerzos son:

$$N_\varphi = \gamma a L \left(1 - \frac{x}{L}\right) + \frac{2\sqrt{3(1-\nu^2)}\,a}{\sqrt{a\delta}} \cdot 8.281 \, [\text{Coef. I}] + 2\,\frac{\sqrt{3(1-\nu^2)}}{\delta}\, 4.262 \, [\text{Coef. IV}] .$$

$$M_x = \frac{\sqrt{a\delta}}{\sqrt{3(1-\nu^2)}} 8.281 \, [\text{Coef. II}] + 4.262 \, [\text{Coef. V}] .$$

$$Q_x = -8.281 \, [\text{Coef. III}] - \frac{\sqrt{3(1-\nu^2)}}{\sqrt{a\delta}} 4.262 \, [\text{Coef. VI}] .$$

En el cuadro siguiente se dan los valores de los esfuerzos, y su representación gráfica, en la figura 15.

EJEMPLO 5.°

x	$\frac{x}{L}$	Coef. I	Coef. II	Coef. III	Coef. IV	Coef. V	Coef. VI	N_φ	M_x	Q_x
0	0	—1,000	0,000	—1,000	1,000	1,000	0,000	0	4.262	8.281
0,4	0,05	—0,653	—0,2455	—0,407	0,407	0,900	—0,491	4.090	1.575	5.251
0,8	0,1	—0,365	—0,321	—0,045	0,045	0,685	—0,640	12.455	— 38	2.825
1,2	0,15	—0,160	—0,299	0,140	—0,140	0,462	—0,600	20.721	— 785	1.140
1,6	0,2	—0,031	—0,2355	0,205	—0,205	0,267	—0,470	27.158	—1.031	103
2,4	0,3	0,064	—0,096	0,165	—0,160	0,033	—0,192	32.704	— 743	—630
3,2	0,4	0,054	—0,015	0,070	—0,0675	—0,040	—0,030	30.834	— 308	—465
4	0,5	0,025	0,012	0,012	—0,013	—0,035	0,025	25.696	— 38	—195
4,8	0,6	0,004	0,012	—0,0075	0,010	—0,018	0,025	19.970	34	— 34
5,6	0,7	—0,002	0,0065	—0,009	0,010	—0,004	0,012	14.634	43	29
6,4	0,8	—0,0035	0,002	—0,005	0,006	—	0	9.535	18	41
7,2	0,9	—0,0035	0,000	0	0	—	0,003	4.487	0	— 11
8	1	0,000	0	0	0	—	0	0	0	0

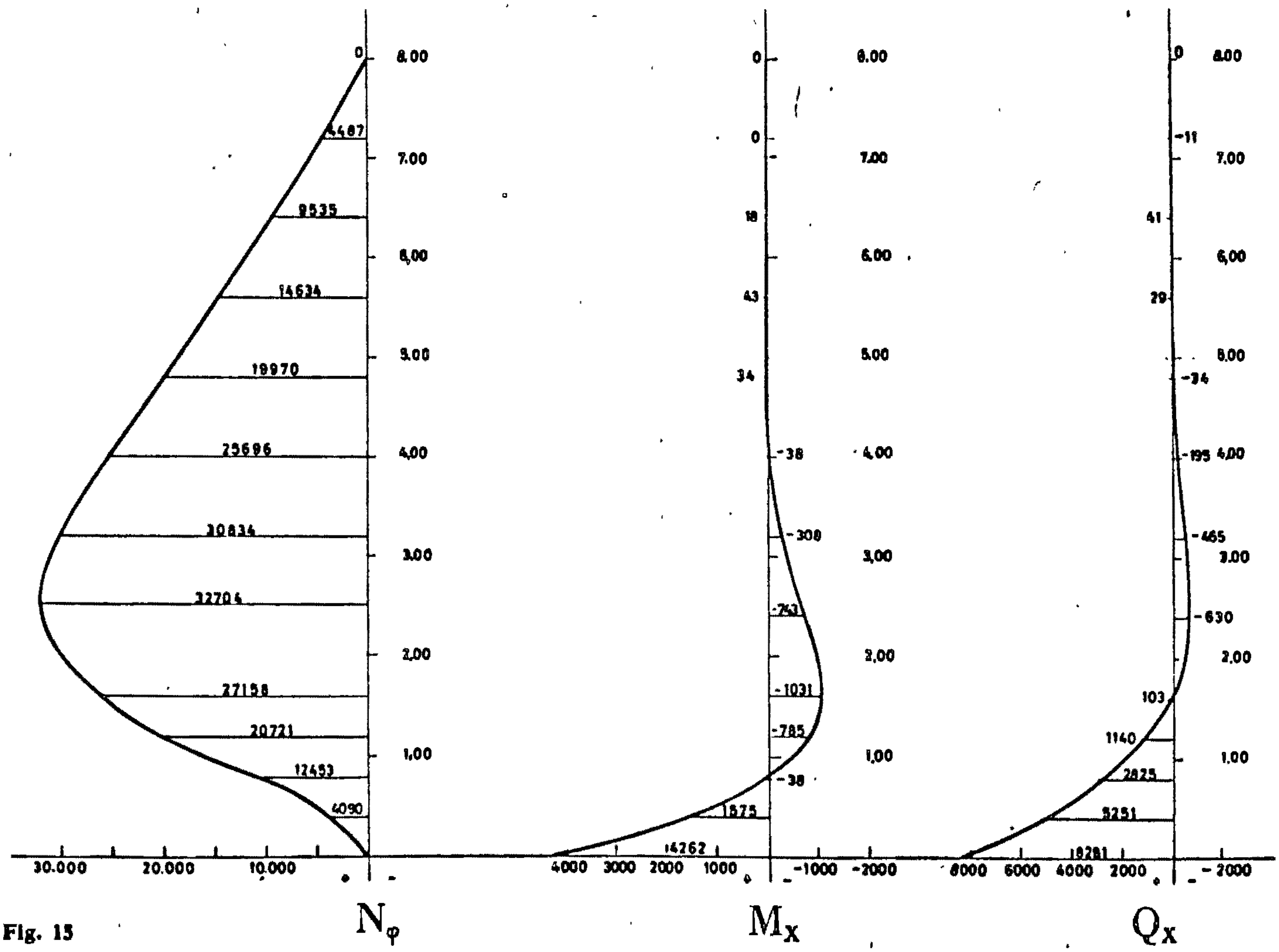

Fig. 15

Ejemplo 6

Depósito de hormigón armado empotrado en la cimentación y en el borde superior, de 2,30 m de altura, 5 m de radio medio y 20 cm de espesor de pared uniforme.

Datos.

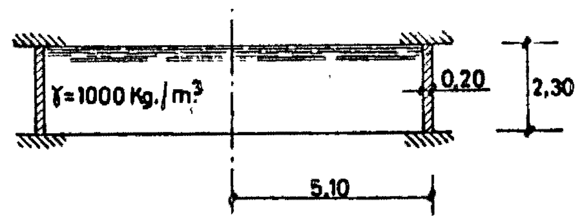

Radio medio:	$a = 5{,}00$ m
Altura:	$L = 2{,}30$ m
Espesor pared:	$\delta = 0{,}20$ m
Módulo de Poisson:	$\nu = 0{,}2$
Peso específico líquido:	$\gamma = 1.000$ kg/m³
	$\varkappa = 1{,}3027$
	$\varkappa L = 2{,}996$
	$\gamma a L = 11.500$

Solución por superposición de estados.

Se obtendrá mediante la superposición de los estados siguientes:

1.° Solución particular correspondiente a las cargas exteriores, que constituye el estado membrana.
2.° Estado correspondiente a la aplicación de un esfuerzo uniforme R_1 en el borde inferior.
3.° Estado correspondiente a la aplicación de un esfuerzo uniforme R_2 en el borde superior.
4.° Estado correspondiente a la aplicación de un momento uniforme M_1 en el borde inferior.
5.° Estado correspondiente a la aplicación de un momento uniforme M_2 en el borde superior.

Los valores numéricos de R_1, R_2, M_1 y M_2 se determinarán con las condiciones

$$[w]_{x=0} = 0$$
$$[w]_{x=L} = 0$$
$$\left[\frac{dw}{dx}\right]_{x=0} = 0$$
$$\left[\frac{dw}{dx}\right]_{x=L} = 0$$

Corrimiento en $x = 0$ de la solución particular:

$$2.300\,\frac{a^2}{E\delta}.$$

Corrimiento en $x = L$ de la solución particular: 0.

Giro en $x = 0$ de la solución particular:

$$-1.000\,\frac{a^2}{E\delta}.$$

Giro en $x = L$ de la solución particular:

$$-1.000\,\frac{a^2}{E\delta}.$$

Corrimiento en $x = 0$ debido a R_1:

$$-2{,}621 \frac{a^2}{E\delta} R_1 .$$

Corrimiento en $x = L$ debido a R_1:

$$0{,}2944 \frac{a^2}{E\delta} R_1 .$$

Giro en $x = 0$ debido a R_1:

$$16{,}977 \frac{R_1}{E\delta^2} .$$

Giro en $x = L$ debido a R_1:

$$0{,}4785 \frac{R_1}{E\delta^2} .$$

Corrimiento en $x = 0$ debido a R_2:

$$0{,}2944 \frac{a^2}{E\delta} R_2 .$$

Corrimiento en $x = L$ debido a R_2:

$$-2{,}621 \frac{a^2}{E\delta} R_2 .$$

Giro en $x = 0$ debido a R_2:

$$-0{,}4785 \frac{R_2}{E\delta^2} .$$

Giro en $x = L$ debido a R_2:

$$-16{,}977 \frac{R_2}{E\delta^2} .$$

Corrimiento en $x = 0$ debido a M_1:

$$3{,}394 \frac{a^2}{E\delta} M_1 .$$

Corrimiento en $x = L$ debido a M_1:

$$-0{,}102 \frac{a^2}{E\delta} M_1$$

Giro en $x = 0$ debido a M_1:

$$-44{,}384 \frac{M_1}{E\delta^2} .$$

Giro en $x = L$ debido a M_1:

$$3{,}745 \frac{M_1}{E\delta^2} .$$

Corrimiento en $x = 0$ debido a M_2:

$$-0{,}102 \frac{a^2}{E\delta} M_2 .$$

Corrimiento en $x = L$ debido a M_2:

$$3{,}394 \frac{a^2}{E\delta} M_2 .$$

Giro en $x = 0$ debido a M_2:

$$-3{,}745 \frac{M_2}{E\delta^2} .$$

Giro en $x = L$ debido a M_2:

$$44{,}384 \frac{M_2}{E\delta^2} .$$

El sistema de ecuaciones quedará en la forma:

$$
\begin{aligned}
2.300 - 2{,}621\ R_1 + 0{,}2944\ R_2 + 3{,}394\ M_1 - 0{,}102\ M_2 &= 0\\
0{,}2944\ R_1 - 2{,}621\ R_2 - 0{,}102\ M_1 + 3{,}394\ M_2 &= 0\\
-5.000 + 16{,}977\ R_1 - 0{,}4785\ R_2 - 44{,}384\ M_1 - 3{,}745\ M_2 &= 0\\
-5.000 + 0{,}4785\ R_1 - 16{,}977\ R_2 + 3{,}745\ M_1 + 44{,}384\ M_2 &= 0\,,
\end{aligned}
$$

de donde:

$$
\begin{aligned}
R_1 &= 1.469\ \text{kg/m} \qquad & M_1 &= 425\ \text{m}\cdot\text{kg/m}\\
R_2 &= 451\ \text{kg/m} \qquad & M_2 &= 233\ \text{m}\cdot\text{kg/m}
\end{aligned}
$$

Y las expresiones de los esfuerzos son:

$$
N_\varphi = \gamma a L\left(1 - \frac{x}{L}\right) + 2\sqrt[4]{3(1-\nu^2)}\sqrt{\frac{a}{\delta}}\,[R_1\,\text{Coef. I}_{x/L} + R_2\,\text{Coef. I}_{(1-x/L)}] + 2\sqrt{3(1-\nu^2)}\,\frac{1}{\delta}\,[M_1\,\text{Coef. IV}_{x/L} + M_2\,\text{Coef. IV}_{(1-x/L)}]\,.
$$

$$
M_x = \frac{\sqrt{a\delta}}{\sqrt[4]{3(1-\nu^2)}}\,[R_1\,\text{Coef. II}_{x/L} + R_2\,\text{Coef. II}_{(1-x/L)}] + [M_1\,\text{Coef. V}_{x/L} + M_2\,\text{Coef. V}_{(1-x/L)}]\,.
$$

$$
Q_x = -[R_1\,\text{Coef. III}_{x/L} + R_2\,\text{Coef. III}_{(1-x/L)}] + \frac{\sqrt[4]{3(1-\nu^2)}}{\sqrt{a\delta}}\,[-M_1\,\text{Coef. IV}_{x/L} + M_2\,\text{Coef. IV}_{(1-x/L)}]\,.
$$

Todos los valores de los coeficientes se obtendrán para $\varkappa L = 2{,}996$.

Los valores de los esfuerzos se dan en el cuadro siguiente, y su representación gráfica, en la figura 16.

EJEMPLO 6.°

$\frac{x}{L}$	x	Coef. I	Coef. II	Coef. III	Coef. IV	Coef. V	Coef. VI	Coef. $I_{(x/L)}$	Coef. $I_{(1-x/L)}$	Coef. $IV_{(x/L)}$	Coef. $IV_{(1-x/L)}$
0	0	−1,006	0	−1	1	1	0	−1,006	0,113	1	−0,03
0,10	0,23	−0,714	−0,2183	−0,485	0,48	0,926	−0,437	−0,714	0,104	0,48	−0,08
0,20	0,46	−0,460	−0,3075	−0,135	0,14	0,763	−0,617	−0,460	0,094	0,14	−0,13
0,30	0,69	−0,258	−0,3133	0,077	−0,07	0,573	−0,631	−0,258	0,076	−0,07	−0,17
0,40	0,92	−0,113	−0,2717	0,185	−0,18	0,393	−0,551	−0,113	0,042	−0,18	−0,20
0,50	1,15	−0,016	−0,2090	0,222	−0,21	0,246	−0,430	−0,016	−0,016	−0,21	−0,21
0,60	1,38	0,042	−0,1429	0,213	−0,20	0,136	−0,301	0,042	−0,113	−0,20	−0,18
0,70	1,61	0,076	−0,0840	0,176	−0,17	0,064	−0,185	0,076	−0,258	−0,17	−0,07
0,80	1,84	0,094	−0,0386	0,125	−0,13	0,022	−0,094	0,094	−0,460	−0,13	0,14
0,90	2,07	0,104	−0,0099	0,065	−0,08	0,004	−0,032	0,104	−0,714	−0,08	0,48
1,00	2,30	0,113	0	0	−0,03	0	0	0,113	−1,006	−0,03	1

N_φ	Coef. $II_{(x/L)}$	Coef. $II_{(1-x/L)}$	Coef. $V_{(x/L)}$	Coef. $V_{(1-x/L)}$	M_x	Coef. $III_{(x/L)}$	Coef. $III_{(1-x/L)}$	Coef. $VI_{(x/L)}$	Coef. $VI_{(1-x/L)}$	Q_x
0	0	0	1	0	425	1	0	0	0	1.469
436	— 0,2183	— 0,0099	0,926	0,004	146	0,485	0,065	0,437	— 0,032	974
1.446	— 0,3075	— 0,0386	0,773	0,022	— 31	0,135	0,125	0,617	— 0,094	568
2.385	— 0,3130	— 0,0840	0,573	0,064	— 124	— 0,077	0,176	0,631	— 0,185	259
2.898	— 0,2717	— 0,1429	0,393	0,136	— 157	— 0,185	0,213	0,551	— 0,301	38
3.004	— 0,2090	— 0,2090	0,246	0,246	— 146	— 0,222	0,222	0,430	— 0,430	— 118
2.588	— 0,1429	— 0,2717	0,136	0,393	— 106	— 0,213	0,185	0,301	— 0,551	— 230
1.858	— 0,0840	— 0,3133	0,064	0,573	— 42	— 0,176	0,077	0,185	— 0,631	— 313
1.011	— 0,0386	— 0,3075	0,022	0,763	37	— 0,125	— 0,135	0,094	— 0,617	— 380
272	— 0,0099	— 0,2183	0,004	0,926	131	— 0,065	— 0,485	0,032	— 0,437	— 429
0	0	0	0	1	233	0	— 1	0	0	— 451

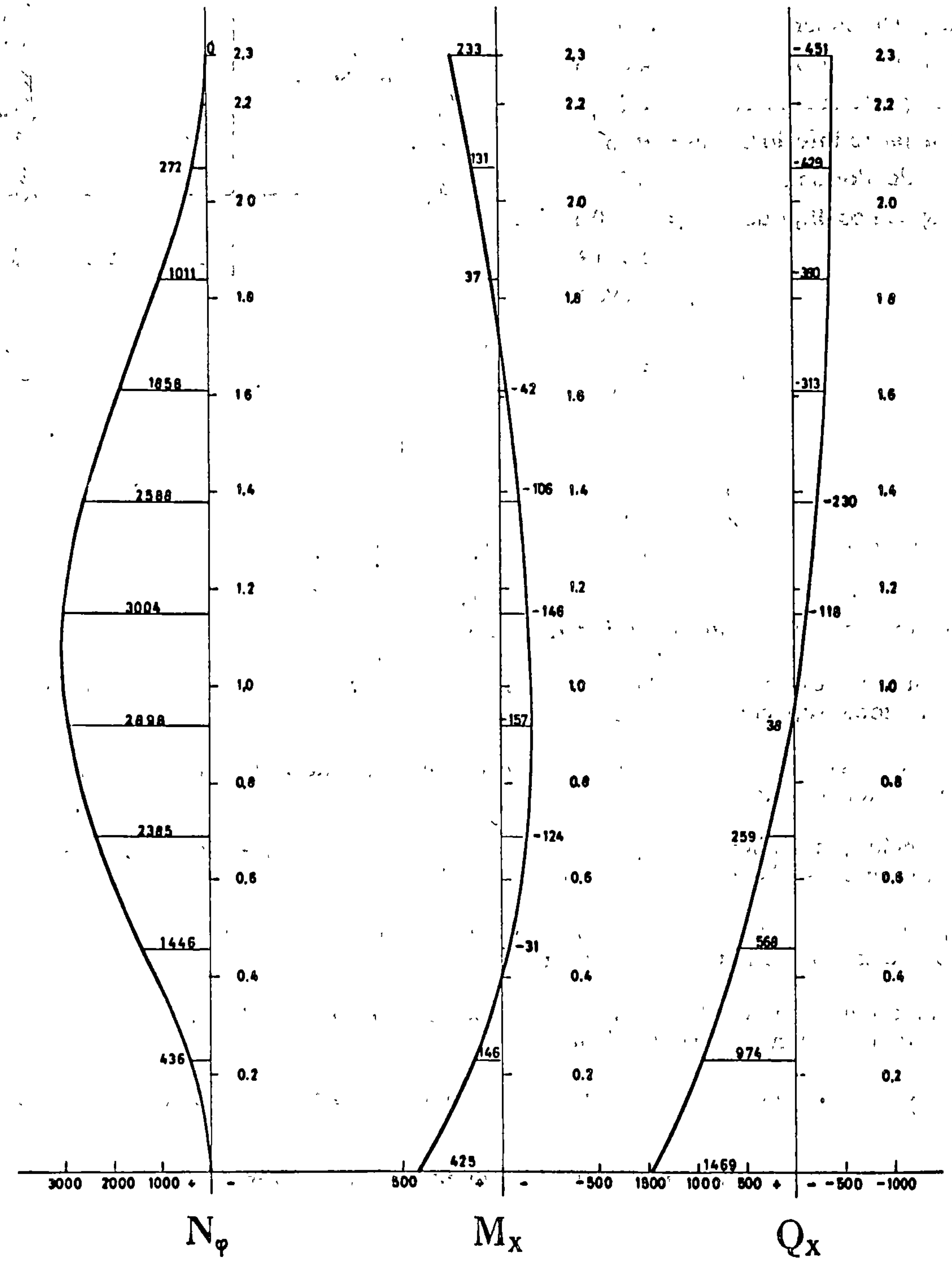

Fig. 16

Ejemplo 7

Depósito de hormigón armado, empotrado en la cimentación y libre en el borde superior, de espesor $\delta_2 = 0{,}35$ m en los 4 m inferiores y $\delta_1 = 0{,}20$ en los 4 m superiores y 6 m de radio medio.

Datos.

Radio medio parte sup.: $a_1 = 6{,}075$ m
Radio medio parte inf.: $a_2 = 6{,}000$ m
Altura parte superior: $L_1 = 4{,}00$ m
Altura parte inferior: $L_2 = 4{,}00$ m
Espesor parte superior: $\delta_1 = 0{,}20$ m
Espesor parte inferior: $\delta_2 = 0{,}35$ m
Módulo de Poisson: $\nu = 0{,}2$
Peso específico líquido: $\gamma = 1.000$ kg/cm³

$\varkappa_1 = 1{,}1819$

$\varkappa_2 = 0{,}8989$

$\varkappa_1 L_1 = 4{,}7276$

$\varkappa_2 L_2 = 3{,}5957$

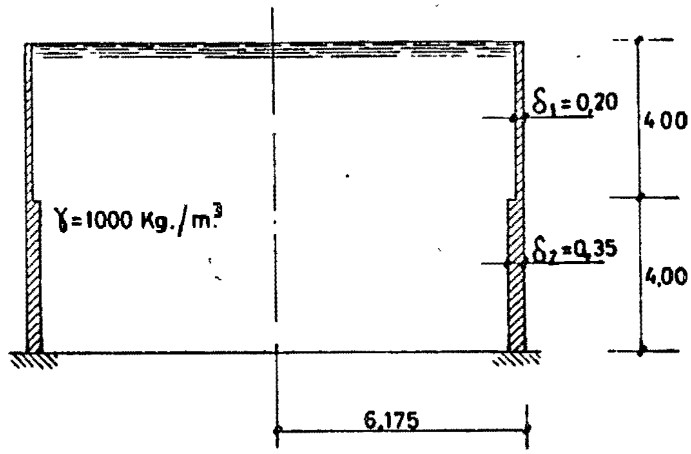

Solución por superposición de estados.

Se obtendrá mediante la superposición de los estados siguientes:

1.° Solución particular correspondiente a las cargas exteriores, que constituye el estado membrana, de la zona superior del depósito.

2.° Estado correspondiente a la aplicación de un esfuerzo uniforme R_1 en el borde inferior de la zona superior del depósito.

3.° Estado correspondiente a la aplicación de un momento uniforme M_1 en el borde inferior de la zona superior del depósito.

4.° Solución particular correspondiente a las cargas exteriores, que constituye el estado membrana, de la zona inferior del depósito.

5.° Estado correspondiente a la aplicación de un esfuerzo uniforme $-R_1$ en el borde superior de la zona inferior del depósito.

6.° Estado correspondiente a la aplicación de un momento uniforme $-M_1$ en el borde superior de la zona inferior del depósito.

7.° Estado correspondiente a la aplicación de un esfuerzo uniforme R_2 en el borde inferior del depósito.

8.° Estado correspondiente a la aplicación de un momento uniforme M_2 en el borde inferior del depósito.

Los valores numéricos de R_1, M_1, R_2 y M_2 se determinarán con las condiciones:

$$[w_2]_{x=0} = 0 ; \quad \left[\frac{dw_2}{dx}\right]_{x=0} = 0 ;$$

$$[w_1]_{x=0} = [w_2]_{x=L_2} ; \quad \left[\frac{dw_1}{dx}\right]_{x=0} = \left[\frac{dw_2}{dx}\right]_{x=L_2} .$$

Parte superior del depósito.

Corrimiento en $x = 0$ de la solución particular:

$$\frac{738.112}{E} .$$

Giro en $x = 0$ de la solución particular:

$$-\frac{184.528}{E} .$$

Corrimiento en $x = 0$ debido a R_1:

$$-436{,}1873 \frac{R_1}{E} .$$

Giro en $x = 0$ debido a R_1:

$$515{,}5298 \frac{R_1}{E} .$$

Corrimiento en $x = 0$ debido a M_1:

$$515{,}5298 \frac{M_1}{E} .$$

Giro en $x = 0$ debido a M_1:

$$-1.218{,}6093 \frac{M_1}{E} .$$

Parte inferior del depósito.

Corrimiento en $x = 0$ de la solución particular:

$$\frac{822.857}{E} .$$

Corrimiento en $x = L_2$ de la solución particular:

$$\frac{411.428{,}5}{E}$$

Giro en $x = 0$ de la solución particular:

$$\frac{102.857{,}14}{E} .$$

Giro en $x = L_2$ de la solución particular:

$$\frac{102.857{,}14}{E}$$

Corrimiento en $x = 0$ debido a $-R_1$:

$$-4{,}6229 \frac{R_1}{E}.$$

Corrimiento en $x = L_2$ debido a $-R_1$:

$$184{,}9165 \frac{R_1}{E}.$$

Giro en $x = 0$ debido a $-R_1$:

$$-8{,}0457 \frac{R_1}{E}.$$

Giro en $x = L_2$ debido a $-R_1$:

$$166{,}4359 \frac{R_1}{E}.$$

Corrimiento en $x = 0$ debido a $-M_1$:

$$8{,}1446 \frac{M_1}{E}.$$

Corrimiento en $x = L_2$ debido a $-M_1$:

$$166{,}2171 \frac{M_1}{E}.$$

Giro en $x = 0$ debido a $-M_1$:

$$-21{,}9039 \frac{M_1}{E}.$$

Giro en $x = L_2$ debido a $-M_1$:

$$299{,}7962 \frac{M_1}{E}.$$

Corrimiento en $x = 0$ debido a R_2:

$$-184{,}9165 \frac{R_2}{E}.$$

Corrimiento en $x = L_2$ debido a R_2:

$$4{,}6229 \frac{R_2}{E}.$$

Giro en $x = 0$ debido a R_2:

$$166{,}4359 \frac{R_2}{E}.$$

Giro en $x = L_2$ debido a R_2:

$$-8{,}0457 \frac{R_2}{E}.$$

Corrimiento en $x = 0$ debido a M_2:

$$166{,}2171 \frac{M_2}{E}.$$

Corrimiento en $x = L_2$ debido a M_2:

$$8{,}1446 \frac{M_2}{E}.$$

Giro en $x = 0$ debido a M_2:

$$-299{,}7962 \frac{M_2}{E}.$$

Giro en $x = L_2$ debido a M_2:

$$21{,}9039 \frac{M_2}{E}.$$

El sistema de ecuaciones queda en la forma:

$$\begin{aligned}
&-4{,}6229\,R_1 + 8{,}1446\,M_1 - 184{,}9165\,R_2 + 166{,}2171\,M_2 + 822.857{,}10 = 0\,;\\
&-8{,}0457\,R_1 - 21{,}9039\,M_1 + 166{,}4362\,R_2 - 299{,}7916\,M_2 - 102.857{,}14 = 0\,;\\
&-621{,}1038\,R_1 + 349{,}3118\,M_1 - 4{,}6229\,R_2 - 8{,}1446\,M_2 + 326.683{,}50 = 0\,;\\
&-349{,}0939\,R_1 + 1.518{,}4055\,M_1 - 8{,}0458\,R_2 + 21{,}9035\,M_2 + 81.670{,}86 = 0\,,
\end{aligned}$$

de donde:

$$\begin{aligned}
R_1 &= 424{,}9 \text{ kg/m}\\
M_1 &= 23{,}9 \text{ m}\cdot\text{kg/m}\\
R_2 &= 8.224{,}9 \text{ kg/m}\\
M_2 &= 4.209{,}7 \text{ m}\cdot\text{kg/m}
\end{aligned}$$

Y las expresiones de los esfuerzos son:

Parte superior del depósito.

$$N_\varphi = 24.300\left(1 - \frac{x}{L}\right) + 6.096{,}7677\,[\text{Coef. I}] + 404{,}9865\,[\text{Coef. IV}]\,.$$

$$M_x = 359{,}2233\,[\text{Coef. II}] + 28{,}8619\,[\text{Coef. V}]\,.$$

$$Q_x = -424{,}566\,[\text{Coef. III}] - 28{,}2024\,[\text{Coef. VI}]\,.$$

Parte inferior del depósito.

$$N_\varphi = 24.000\left(2 - \frac{x}{L}\right) + 88.715{,}83\,[\text{Coef. I}_{x/L}] - 4.579{,}81\,[\text{Coef. I}_{(1-x/L)}] + 40.821{,}82\,[\text{Coef. IV}_{x/L}] + 231{,}39\,[\text{Coef. IV}_{(1-x/L)}]\,.$$

$$M_x = 9.149{,}12\,[\text{Coef. II}_{x/L}] - 472{,}31\,[\text{Coef. II}_{(1-x/L)}] + 4.209{,}68\,[\text{Coef. V}_{x/L}] + 23{,}86\,[\text{Coef. V}_{(1-x/L)}]\,.$$

$$Q_x = -8.224{,}30\,[\text{Coef. III}_{x/L}] - 424{,}57\,[\text{Coef. III}_{(1-x/L)}] - 3.784{,}16\,[\text{Coef. VI}_{x/L}] + 21{,}45\,[\text{Coef. VI}_{(1-x/L)}]\,.$$

Los valores de los coeficientes se obtendrán para $\varkappa L = 4{,}7276$ en la parte superior y para $\varkappa L = 3{,}5957$ en la inferior.

Los valores de los esfuerzos se dan en los cuadros siguientes, y su representación gráfica, en las figuras 17 y 18.

EJEMPLO 7.° (Parte superior)

$\frac{x}{L}$	x	Coef. I	Coef. II	Coef. III	Coef. IV	Coef. V	Coef. VI	N_φ	M.	Q.
0	0	—1,000	0,000	—1,000	1,000	1,000	0,000	18.608	24	425
0,10	0,4	—0,555	—0,284	—0,272	0,272	0,839	—0,567	18.596	— 82	131
0,20	0,8	—0,226	—0,315	0,088	—0,088	0,542	—0,630	18.026	—100	—20
0,40	1,6	0,048	—0,143	0,190	—0,192	0,096	—0,288	14.795	— 49	—73
0,60	2,4	0,058	—0,020	0,069	—0,075	—0,035	—0,028	10.043	— 8	—28
0,80	3,2	0,017	0,006	0,000	0,000	—0,035	0,039	4.964	1	— 1
1,00	4,0	—0,018	0,000	0,000	0,035	0,000	0,000	—95	0	0

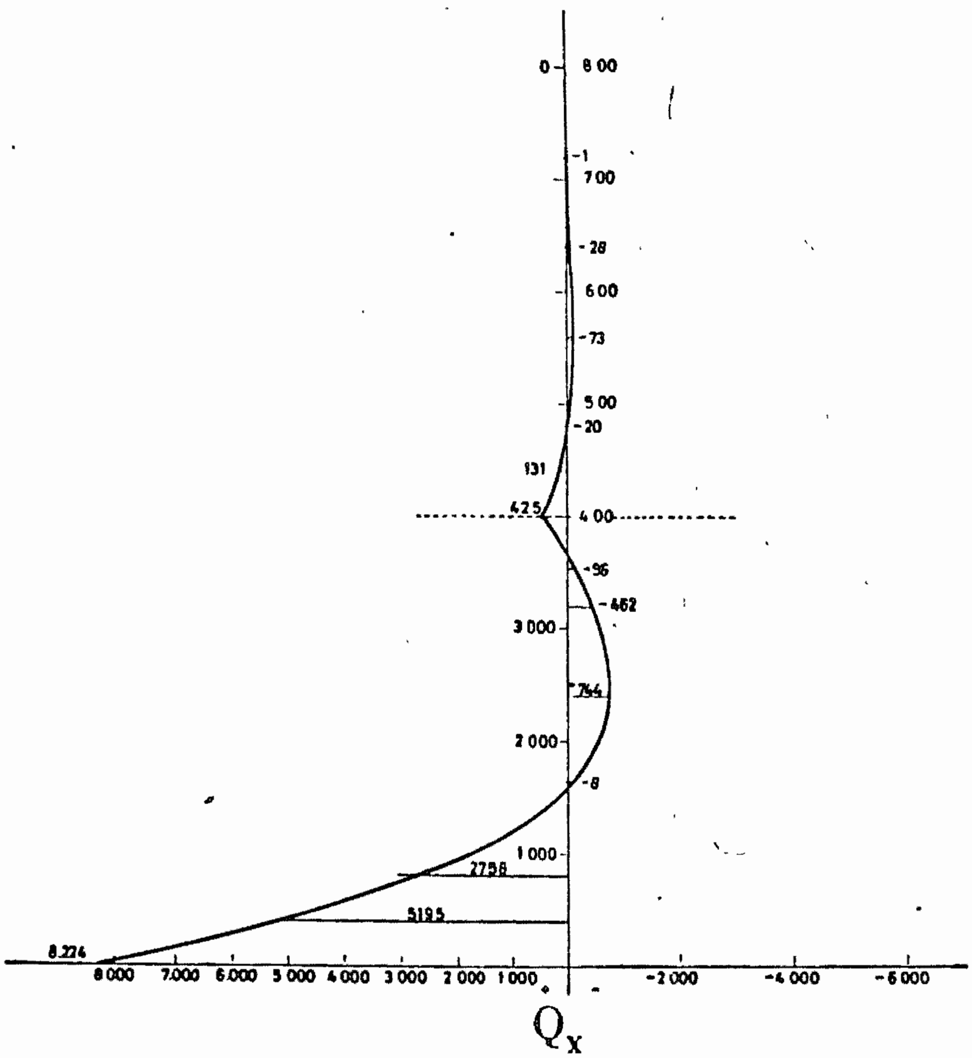

Fig. 17

EJEMPLO 7.° (Parte inferior)

$\frac{x}{L}$	x	Coef. I	Coef. II	Coef. III	Coef. IV	Coef. V	Coef. VI	N_φ	M_x	Q_x
0	0	— 1,000	0,000	— 1,000	1,000	1,000	0,000	0	4.210	8.224
0,1	0,4	— 0,653	— 0,246	— 0,407	0,406	0,899	— 0,491	4.049	1.536	5.195
0,2	0,8	— 0,366	— 0,321	— 0,044	0,041	0,687	— 0,640	12.125	— 36	2.758
0,4	1,6	— 0,030	— 0,234	0,204	— 0,212	0,270	— 0,460	26.739	— 958	— 8
0,6	2,4	0,067	— 0,096	0,157	— 0,167	0,047	— 0,170	32.815	— 563	— 744
0,8	3,2	0,058	— 0,019	0,060	— 0,058	— 0,007	— 0,007	33.263	— 35	— 462
0,9	3,6	0,042	— 0,004	0,024	— 0,004	— 0,004	0,016	33.047	84	— 96
1,0	4,0	0,025	0,000	0,000	0,048	0,000	0,000	32.988	24	425

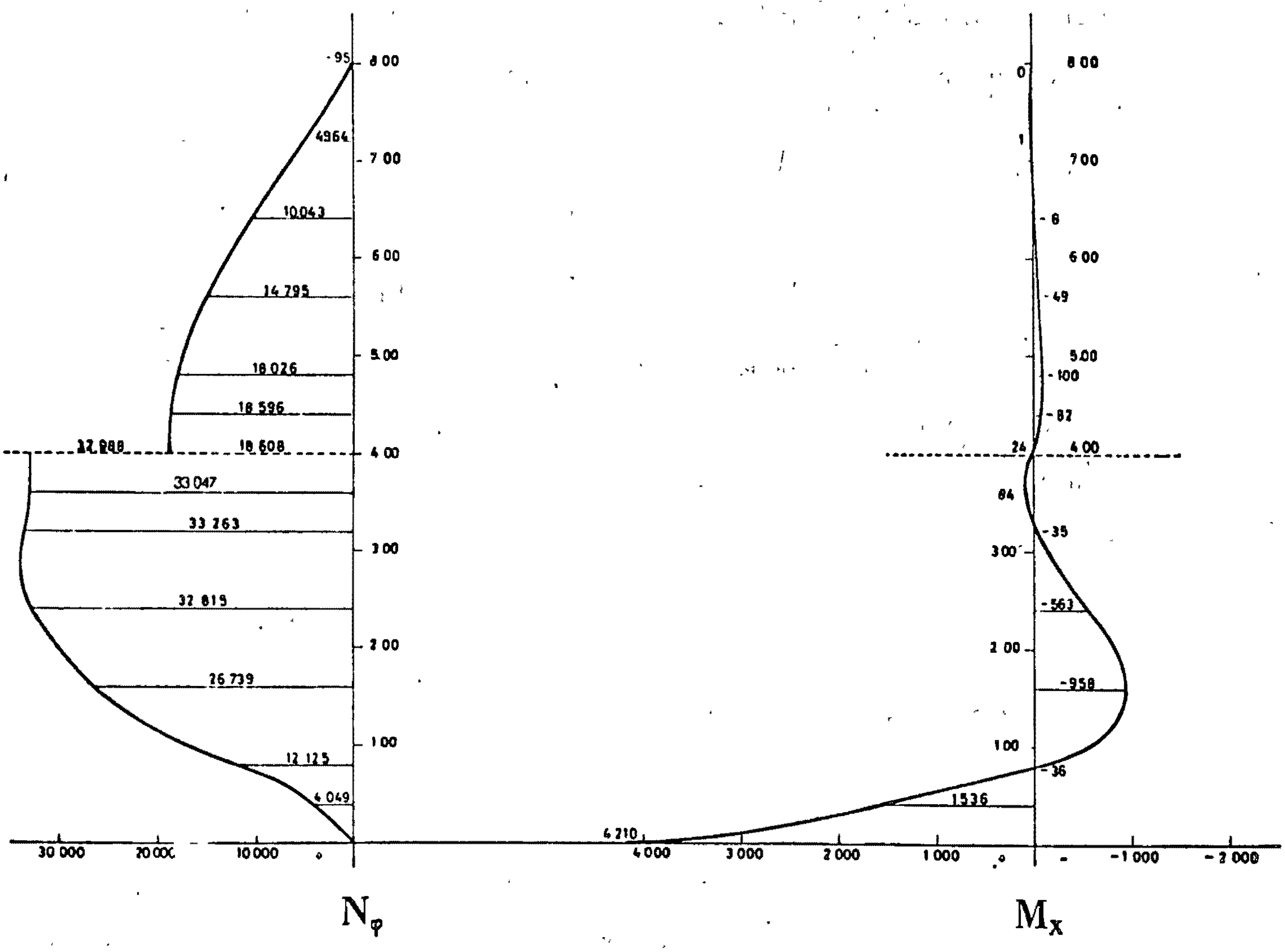

Fig. 18

4. Depósitos de espesor de pared variable

Si se supone que el espesor de la pared δ no es constante, sino una función de la coordenada x, es decir, $\delta = \delta(x)$, se plantea el problema de la integración de la ecuación diferencial de cuarto orden [III], con coeficientes, en general, variables.

La resolución de este problema presenta muchas dificultades de orden matemático, por lo que a continuación se desarrolla, a título de ejemplo, el depósito lleno, en el que el espesor es función lineal de la coordenada x. Este caso ha sido estudiado por W. Flügge y Timoshenko *.

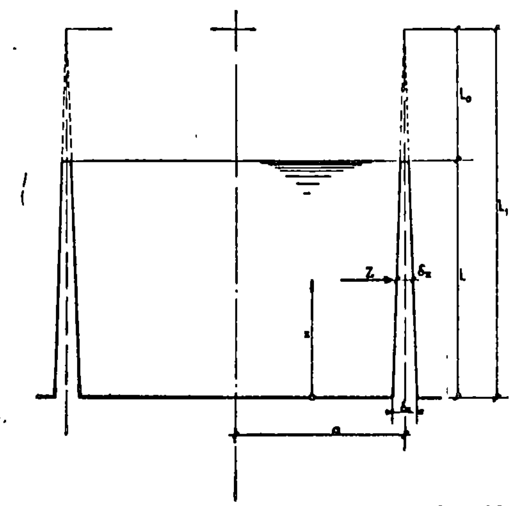

Fig. 19

De acuerdo con el origen y convenio de signos que se viene utilizando en este trabajo, se tiene:

$$\delta_x = \frac{\delta_0}{L_1}(L_1 - x) = \beta(L_1 - x) \qquad \beta = \frac{\delta_0}{L_1}$$

$$K_\beta = \frac{E\beta^3}{12(1-\nu^2)} \qquad Z = \gamma(L - x)$$

La presión de un líquido es siempre normal a la pared del depósito que lo contiene. Sin embargo, al tomar aquí el valor de esa presión como fuerza en dirección Z, no se comete inexactitud sensible, dada la pequeñez del ángulo de inclinación que se utiliza normalmente en depósitos.

Sustituyendo en la ecuación [III] se tiene:

$$K_\beta \frac{d^2}{dx^2}\left[(L_1 - x)^3 \frac{d^2 w}{dx^2}\right] + \frac{E\beta}{a^2}(L_1 - x)w - \gamma(L - x) = 0$$

Una solución particular de esta ecuación es:

$$w_p = \frac{\gamma a^2}{E\beta} \frac{L - x}{L_1 - x}$$

---

* W. FLÜGGE: *Statik und Dinamik der Schalen*, Springer Verlag, 1957; TIMOSHENKO: *Teoría de placas planas y curvas*. Editorial Acme Agency, 1947.

Los esfuerzos correspondientes a esta solución particular serán (ver fórmulas [II] y [Ib]:

$$\left.\begin{array}{l} N_\varphi = \dfrac{E\delta}{a}\, w = \gamma a (L - x) \\ \dfrac{dw_p}{dx} = -\dfrac{L_1 - L}{(L_1 - x)^2} \cdot \dfrac{\gamma a^2}{E\beta} \\ M_x = K \cdot \dfrac{d^2 w_p}{dx^2} = -\dfrac{\gamma a^2 \beta^2 (L_1 - L)}{6(1-\nu^2)} \\ Q_x = 0 \end{array}\right\} \qquad [X]$$

Aquí el valor de K no corresponde a una constante, como en el caso de depósitos de espesor de pared constante. Su valor es

$$K = K_\beta (L_1 - x)^3 = \frac{E\beta^3}{12(1-\nu^2)} (L_1 - x)^3$$

De la observación de estos esfuerzos se deduce que el momento flector M_x debido a la solución particular es constante.

Además, su valor es, en general, muy pequeño, ya que lo es β en los casos corrientes de depósitos.

Puede despreciarse este momento M_x al realizar el cálculo de un depósito de este tipo.

A la solución particular anterior, habrá que sumar la parte correspondiente a la solución general de la ecuación homogénea:

$$\frac{K_\beta}{L_1 - x} \frac{d^2}{dx^2} \left[(L_1 - x)^3 \frac{d^2 w}{dx^2} \right] + \frac{E\beta}{a^2} w = 0$$

Esta ecuación se puede poner en la forma:

$$\frac{1}{L_1 - x} \left\{ \frac{d}{dx} \left[(L_1 - x)^2 \frac{d}{dx} \left[\frac{1}{L_1 - x} \frac{d}{dx} \left((L_1 - x)^2 \frac{dw}{dx} \right) \right] \right] \right\} + \frac{E\beta}{K_\beta a^2} w = 0$$

Si utilizamos los símbolos siguientes:

$$D(w) = \frac{1}{L_1 - x} \frac{d}{dx} \left[(L_1 - x)^2 \frac{dw}{dx} \right]$$

$$\lambda^4 = \frac{E\beta}{K_\beta a^2} = \frac{12(1-\nu^2)}{\beta^2 a^2}$$

La ecuación se puede poner en la forma siguiente:

$$D\left[D(w)\right] + \lambda^4 w = 0 \qquad [XI]$$

O bien en una de las dos formas siguientes:

$$D\left[D(w)+i\lambda^2 w\right]-i\lambda^2\left[D(w)+i\lambda^2 w\right]=0$$

$$D\left[D(w)-i\lambda^2 w\right]+i\lambda^2\left[D(w)-i\lambda^2 w\right]=0$$

Luego veremos que la ecuación [XI] se satisface para las soluciones de las dos ecuaciones de segundo orden:

$$\begin{aligned} D(w)+i\lambda^2 w&=0\\ D(w)-i\lambda^2 w&=0\end{aligned} \qquad [XII]$$

Si suponemos que w_1 y w_2 sean las soluciones de la primera, w_3 y w_4 serán las de la segunda, debiéndose cumplir:

$$w_1=X_1+iX_2 \qquad w_2=X_3+iX_4$$

$$w_3=X_1-iX_2 \qquad w_4=X_3-iX_4$$

Por lo tanto, la solución general buscada de la ecuación [XI] será:

$$w = K_1X_1 + K_2X_2 + K_3X_3 + K_4X_4$$

en la que K_1, K_2, K_3 y K_4 son constantes arbitrarias y X_1, X_2, X_3 y X_4 funciones de x, determinadas como soluciones en la forma indicada anteriormente de la ecuación [XII].

Desarrollando la ecuación [XII] resulta:

$$\frac{1}{L_1-x}\frac{d}{dx}\left[(L_1-x)^2\frac{dw}{dx}\right]+i\lambda^2 w=0$$

Haciendo el cambio de función y variable

$$\xi=w\sqrt{L_1-x} \qquad \eta=2\lambda\sqrt{(L_1-x)i}$$

la ecuación anterior toma la forma:

$$\eta^2\frac{d^2\xi}{d\eta^2}+\eta\frac{d\xi}{d\eta}+(\eta^2-1)\xi=0$$

que es la conocida ecuación de Bessel, cuya solución es la serie infinita de potencias:

$$\xi=K'\frac{\eta}{2}\left[1-\frac{\eta^2}{2.4}+\frac{\eta^4}{2(4)^2 6}-\frac{\eta^6}{2(4.6)^2 8}+\cdots\cdots\right]=K'J_1(\eta)$$

en la que $J_1(\eta)$ es la función de Bessel de primera especie y orden 1.

Las funciones de Bessel de primera especie y órdenes 0 y 1, respectivamente $J_0(\eta)$ y $J_1(\eta)$, cumplen la condición:

$$J_1(\eta) = -\frac{d J_0(\eta)}{\partial \eta}$$

$$J_0(\eta) = 1 - \frac{\eta^2}{2^2} + \frac{\eta^4}{(2.4)^2} - \frac{\eta^6}{(2.4.6)^2} + \cdots$$

Como $\eta = 2\lambda\sqrt{(L_1 - x)i}$, se descompone J_0 en su parte real e imaginaria

$$J_0(\eta) = \psi_1\left(2\lambda\sqrt{L_1-x}\right) + i\,\psi_2\left(2\lambda\sqrt{L_1-x}\right)$$

siendo:

$$\psi_1\left(2\lambda\sqrt{L_1-x}\right) = 1 - \frac{\left(2\lambda\sqrt{L_1-x}\right)^4}{(2.4)^2} + \frac{\left(2\lambda\sqrt{L_1-x}\right)^8}{(2.4.6.8)^2} - \cdots\cdots$$

$$\psi_2\left(2\lambda\sqrt{L_1-x}\right) = -\frac{\left(2\lambda\sqrt{L_1-x}\right)^2}{2^2} + \frac{\left(2\lambda\sqrt{L_1-x}\right)^6}{(2.4.6)^2} - \frac{\left(2\lambda\sqrt{L_1-x}\right)^{10}}{(2.4.6.8.10)^2} - \cdots\cdots$$

Como:

$$\xi_1 = K'\,J_1(\eta) = -K'\frac{dJ_0}{d\eta} = K''\frac{dJ_0}{d\left(2\lambda\sqrt{L_1-x}\right)} \quad ; \quad K'' = -\frac{K'}{\sqrt{i}}$$

Luego

$$\xi_1 = K''\left[\frac{d\psi_1\left(2\lambda\sqrt{L_1-x}\right)}{d\left(2\lambda\sqrt{L_1-x}\right)} + i\,\frac{d\psi_2\left(2\lambda\sqrt{L_1-x}\right)}{d\left(2\lambda\sqrt{L_1-x}\right)}\right] = K''\left[\psi_1'\left(2\lambda\sqrt{L_1-x}\right) + i\,\psi_2'\left(2\lambda\sqrt{L_1-x}\right)\right]$$

La segunda solución viene dada por la función de Hankel de primera especie $H^I_1(\eta)$, verificándose

$$H^I_1(\eta) = -\frac{d H^I_0(\eta)}{d\eta}$$

siendo $H^I_1(\eta)$ la de grado 0.

$$H^I_0(\eta) = \psi_3\left(2\lambda\sqrt{L_1-x}\right) + i\,\psi_4\left(2\lambda\sqrt{L_1-x}\right)$$

$$\psi_3\left(2\lambda\sqrt{L_1-x}\right) = \frac{1}{2}\psi_1\left(2\lambda\sqrt{L_1-x}\right) - \frac{2}{\pi}\left[R_1 + \log_{nep}\frac{\beta 2\lambda\sqrt{L_1-x}}{2}\,\psi_2\left(2\lambda\sqrt{L_1-x}\right)\right]$$

$$\psi_4\left(2\lambda\sqrt{L_1-x}\right) = \frac{1}{2}\psi_2\left(2\lambda\sqrt{L_1-x}\right) + \frac{2}{\pi}\left[R_2 + \log_{nep}\frac{\beta 2\lambda\sqrt{L_1-x}}{2}\,\psi_1\left(2\lambda\sqrt{L_1-x}\right)\right]$$

de donde:

$$R_1 = \left(\frac{2\lambda\sqrt{L_1-x}}{2}\right)^2 - \frac{S(3)}{(3.2)^2}\left(\frac{2\lambda\sqrt{L_1-x}}{2}\right)^6 + \frac{S(5)}{(5.4.3.2)^2}\left(\frac{2\lambda\sqrt{L_1-x}}{2}\right)^{10} - \cdots\cdots$$

$$R_2 = \frac{S(2)}{2^2}\left(\frac{2\lambda\sqrt{L_1-x}}{2}\right)^4 - \frac{S(4)}{(4.3.2)^2}\left(\frac{2\lambda\sqrt{L_1-x}}{2}\right)^8 + \frac{S(6)}{(6.5.4.3.2)^2}\left(\frac{2\lambda\sqrt{L_1-x}}{2}\right)^{12} - \cdots\cdots$$

$$S(n) = 1 + \frac{1}{2} + \frac{1}{3} + \frac{1}{4} + \cdots\cdots + \frac{1}{n}$$

$$\log_{nep}\beta = 0{,}57722$$

y la segunda solución buscada será:

$$\xi_2 = K''' H_1^I(\eta) = -K''' \frac{dH_0^I(\eta)}{d\eta} = -\frac{K'''}{\sqrt{I}} \frac{dH_0^I(\eta)}{d(2\lambda\sqrt{L_1-x})} = K^{IV} \frac{dH_0^I(\eta)}{d(2\lambda\sqrt{L_1-x})}$$

$$\xi_2 = K^{IV}\left[\psi_3'\left(2\lambda\sqrt{L_1-x}\right) + i\,\psi_4'\left(2\lambda\sqrt{L_1-x}\right)\right]$$

La solución del corrimiento w será:

$$w = \frac{\xi}{\sqrt{L_1-x}} = \frac{1}{\sqrt{L_1-x}}\left[K_1\psi_1'\left(2\lambda\sqrt{L_1-x}\right) + K_2\psi_2'\left(2\lambda\sqrt{L_1-x}\right) + K_3\psi_3'\left(2\lambda\sqrt{L_1-x}\right) + K_4\psi_4'\left(2\lambda\sqrt{L_1-x}\right)\right]$$

Teniendo en cuenta las relaciones

$$\psi_1''(\theta) = \psi_2(\theta) - \frac{1}{\theta}\psi_1'(\theta) \qquad \psi_2''(\theta) = -\psi_1(\theta) - \frac{1}{\theta}\psi_2'(\theta)$$

$$\psi_3''(\theta) = \psi_4(\theta) - \frac{1}{\theta}\psi_3'(\theta) \qquad \psi_4''(\theta) = -\psi_3(\theta) - \frac{1}{\theta}\psi_4'(\theta)$$

$$\theta = 2\lambda\sqrt{L_1-x}$$

los esfuerzos vendrán dados por las siguientes expresiones:

$$N\varphi = \frac{E\delta}{a} w = +\frac{E\beta}{a}\sqrt{L_1-x}\left[K_1\psi_1'(\theta) + K_2\psi_2'(\theta) + K_3\psi_3'(\theta) + K_4\psi_4'(\theta)\right]$$

$$M_x = K_\beta\left(L_1-x\right)^3\frac{d^2w}{dx^2} = +\frac{K_\beta}{4}\sqrt{L_1-x}\Big[K_1\left[\theta^2\psi_2'(\theta) - 4\theta\psi_2(\theta) + 8\psi_1'(\theta)\right] - K_2\left[\theta^2\psi_1'(\theta) - 4\theta\psi_1(\theta) - 8\psi_2'(\theta)\right] +$$

$$+ K_3\left[\theta^2\psi_4'(\theta) - 4\theta\psi_4(\theta) + 8\psi_3'(\theta)\right] - K_4\left[\theta^2\psi_3'(\theta) - 4\theta\psi_3(\theta) - 8\psi_4'(\theta)\right]\Big]$$

$$Q_x = \frac{-dM_x}{dx} = -\frac{K_\beta}{2}\lambda^2\sqrt{L_1-x}\Big[K_1\left[\theta\psi_1(\theta) + 2\psi_2'(\theta)\right] + K_2\left[\theta\psi_2(\theta) - 2\psi_1'(\theta)\right] + K_3\left[\theta\psi_3(\theta) + 2\psi_4'(\theta)\right] +$$

$$+ K_4\left[\theta\psi_4(\theta) - 2\psi_3'(\theta)\right]\Big]$$

$$\frac{dw}{dx} = \frac{-1}{2(L_1-x)\sqrt{L_1-x}}\Big[K_1\left[\theta\psi_2(\theta) - 2\psi_1'(\theta)\right] - K_2\left[\theta\psi_1(\theta) + 2\psi_2'(\theta)\right] + K_3\left[\theta\psi_4(\theta) - 2\psi_3'(\theta)\right] -$$

$$- K_4\left[\theta\psi_3(\theta) + 2\psi_4'(\theta)\right]\Big]$$

En todas las fórmulas anteriores, $\vartheta = 2\lambda\sqrt{L_1 - x}$.

No hay que olvidar que la solución dada anteriormente corresponde a la solución general de la ecuación homogénea y que para obtener la solución total habrá que sumar la solución particular dada en [X].

Los valores de las funciones ψ y ψ' que intervienen en las expresiones de los esfuerzos y recorrido se pueden tomar de la tabla XIII *, si ϑ es menor de 6. Para valores de ϑ mayores de 6 se pueden utilizar en los casos prácticos, y con suficiente aproximación, los valores obtenidos en las expresiones siguientes:

$$\psi_1(\theta) \simeq \frac{1}{\sqrt{2\pi\theta}}\, e^{\frac{\theta}{\sqrt{2}}} \cos\left(\frac{\theta}{\sqrt{2}} - \frac{\pi}{8}\right) \qquad \psi_1'(\theta) \simeq \frac{1}{\sqrt{2\pi\theta}}\, e^{\frac{\theta}{\sqrt{2}}} \cos\left(\frac{\theta}{\sqrt{2}} + \frac{\pi}{8}\right)$$

$$\psi_2(\theta) \simeq \frac{-1}{\pi\theta\sqrt{2}}\, e^{\frac{\theta}{\sqrt{2}}} \operatorname{sen}\left(\frac{\theta}{\sqrt{2}} - \frac{\pi}{8}\right) \qquad \psi_2'(\theta) \simeq -\frac{1}{\pi.\theta\sqrt{2}}\, e^{\frac{\theta}{\sqrt{2}}} \operatorname{sen}\left(\frac{\theta}{\sqrt{2}} + \frac{\pi}{8}\right)$$

$$\psi_3(\theta) \simeq \sqrt{\frac{2}{\pi\theta}}\, e^{-\frac{\theta}{\sqrt{2}}} \operatorname{sen}\left(\frac{\theta}{\sqrt{2}} + \frac{\pi}{8}\right) \qquad \psi_3'(\theta) \simeq -\sqrt{\frac{2}{\pi\theta}}\, e^{-\frac{\theta}{\sqrt{2}}} \operatorname{sen}\left(\frac{\theta}{\sqrt{2}} - \frac{\pi}{8}\right)$$

$$\psi_4(\theta) \simeq -\sqrt{\frac{2}{\pi\theta}}\, e^{-\frac{\theta}{\sqrt{2}}} \cos\left(\frac{\theta}{\sqrt{2}} + \frac{\pi}{8}\right) \qquad \psi_4'(\theta) \simeq \sqrt{\frac{2}{\pi\theta}}\, e^{-\frac{\theta}{\sqrt{2}}} \cos\left(\frac{\theta}{\sqrt{2}} - \frac{\pi}{8}\right)$$

TABLA XIII

ϑ	ψ_1	ψ_2	ψ'_1	ψ'_2	ψ_3	ψ_4	ψ'_3	ψ'_4
0	1,0000	— 0,0000	— 0,0000	— 0,0000	0,5000		— 0,0000	
0,1	1,0000	— 0,0025	— 0,0001	— 0,0500	0,4946	— 1,5410	— 0,0929	6,3400
0,2	1,0000	— 0,0100	— 0,0005	— 0,1000	0,4826	— 1,1030	— 0,1419	3,1340
0,3	0,9999	— 0,0225	— 0,0017	— 0,1500	0,4667	— 0,8510	— 0,1746	2,0500
0,4	0,9996	— 0,0400	— 0,0040	— 0,2000	0,4480	— 0,6765	— 0,1970	1,4970
0,5	0,9990	— 0,0625	— 0,0078	— 0,2499	0,4275	— 0,5449	— 0,2121	1,1590
0,6	0,9980	— 0,0900	— 0,0135	— 0,2998	0,4058	— 0,4413	— 0,2216	0,9270
0,7	0,9962	— 0,1224	— 0,0214	— 0,3496	0,3834	— 0,3574	— 0,2268	0,7582
0,8	0,9936	— 0,1599	— 0,0320	— 0,3991	0,3606	— 0,2883	— 0,2286	0,6286
0,9	0,9898	— 0,2023	— 0,0455	— 0,4485	0,3377	— 0,2308	— 0,2276	0,5258
1,0	0,9844	— 0,2496	— 0,0624	— 0,4974	0,3151	— 0,1825	— 0,2243	0,4422
1,1	0,9771	— 0,3017	— 0,0831	— 0,5458	0,2929	— 0,1419	— 0,2193	0,3730
1,2	0,9676	— 0,3587	— 0,1078	— 0,5935	0,2713	— 0,1075	— 0,2129	0,3149
1,3	0,9554	— 0,4204	— 0,1370	— 0,6403	0,2504	— 0,0786	— 0,2054	0,2656
1,4	0,9401	— 0,4867	— 0,1709	— 0,6860	0,2302	— 0,0542	— 0,1971	0,2235
1,5	0,9211	— 0,5576	— 0,2100	— 0,7302	0,2110	— 0,0337	— 0,1882	0,1873
1,6	0,8979	— 0,6327	— 0,2545	— 0,7727	0,1926	— 0,0166	— 0,1788	0,1560
1,7	0,8700	— 0,7120	— 0,3048	— 0,8131	0,1752	— 0,0023	— 0,1692	0,1290
1,8	0,8367	— 0,7953	— 0,3612	— 0,8509	0,1588	0,0094	— 0,1594	0,1056
1,9	0,7975	— 0,8821	— 0,4238	— 0,1433	0,0189	0,0189	— 0,1496	0,0854
2,0	0,7517	— 0,9723	— 0,4931	— 0,9170	0,1289	0,0265	— 0,1399	0,0679
2,1	0,6987	— 1,0654	— 0,5691	— 0,9442	0,1153	0,0325	— 0,1304	0,0527
2,2	0,6377	— 1,1610	— 0,6520	— 0,9666	0,1028	0,0371	— 0,1210	0,0397
2,3	0,5680	— 1,2585	— 0,7420	— 0,9836	0,0911	0,0405	— 0,1120	0,0285
2,4	0,4890	— 1,3575	— 0,8392	— 0,9944	0,0804	0,0429	— 0,1032	0,0189
2,5	0,4000	— 1,4572	— 0,9436	— 0,9983	0,0705	0,0444	— 0,0948	0,0108
2,6	0,3001	— 1,5569	— 1,0551	— 0,9943	0,0614	0,0451	— 0,0868	0,0039
2,7	1887	— 1,6557	— 1,1738	— 0,9815	0,0531	0,0452	— 0,0791	— 0,0019
2,8	0,0651	— 1,7529	— 1,2993	— 0,9590	0,0456	0,0448	— 0,0719	— 0,0066
2,9	— 0,0714	— 1,8472	— 1,4310	— 0,9257	0,0387	0,0439	— 0,0650	— 0,0105

* Esta tabla está tomada de *Tables of Functions*, Jahnke-Emde, Berlín, 1933.

ϑ	ψ_1	ψ_2	ψ'_1	ψ'_2	ψ_3	ψ_4	ψ'_3	ψ'_4
3,0	−0,2214	−1,9376	−1,5700	−0,8805	0,0326	0,0427	−0,0586	−0,0137
3,1	−0,3855	−2,0228	−1,7140	−0,8223	0,0270	0,0412	−0,0526	−0,0162
3,2	−0,5644	−2,1016	−1,8640	−0,7499	0,0220	0,0395	−0,0470	−0,0181
3,3	−0,7584	−2,1723	−2,0180	−0,6621	0,0176	0,0376	−0,0418	−0,0195
3,4	−0,9680	−2,2334	−2,1750	−0,5577	0,0137	0,0356	−0,0369	−0,0204
3,5	−1,1940	−2,2832	−2,3360	−0,4353	0,0102	0,0335	−0,0325	−0,0210
3,6	−1,4350	−2,3199	−2,4980	−0,2937	0,0072	0,0314	−0,0284	−0,0213
3,7	−1,6930	−2,3413	−2,6610	−0,1310	0,0045	0,0293	−0,0246	−0,0213
3,8	−1,9670	−2,3454	−2,8220	0,0530	0,0022	0,0272	−0,0212	−0,0210
3,9	−2,2580	−2,3300	−2,9810	0,2600	0,0003	0,0251	−0,0181	−0,0206
4,0	−2,5630	−2,2927	−3,1350	0,4910	−0,0014	0,0230	−0,0152	−0,0200
4,1	−2,8840	−2,2309	−3,2820	0,7480	−0,0028	0,0211	−0,0127	−0,0193
4,2	−3,2190	−2,1420	−3,4200	1,0320	−0,0039	0,0192	−0,0104	−0,0185
4,3	−3,5680	−2,0240	−3.5470	1,3430	−0,0049	0,0174	−0,0083	−0,0177
4,4	−3,9280	−1,8730	−3,6590	1,6830	−0,0056	0,0156	−0,0065	−0,0168
4,5	−4,2990	−1,6860	−3,7540	2,0530	−0,0062	0,0140	−0,0049	−0,0158
4,6	−4,6708	−1,4610	−3,8280	2,4520	−0,0066	0,0125	−0,0035	−0,0148
4,7	−5,0640	−1,1950	−3,8780	2,8820	−0,0069	0,0110	−0,0023	−0,0138
4,8	−5,4530	−0,8840	−3,9010	3,3420	−0,0071	0,0097	−0,0012	−0,0129
4,9	−5,8430	−0,5250	−3,8910	3,8330	−0,0071	0,0085	−0,0003	−0,0119
5,0	−6,2300	−0,1160	−3,8450	4,3540	−0,0071	0,0073	0,0005	−0,0109
5,1	−6,6110	0,3470	−3,7590	4,9050	−0,0070	0,0063	0,0012	−0,0100
5,2	−6,9800	0,8660	−3,6270	5,4840	−0,0069	0,0053	0,0017	−0,0091
5,3	−7,3340	1,4440	−3,4450	6,0890	−0,0067	0,0045	0,0022	−0,0083
5,4	−7,6670	2,0850	−3,2060	6,7200	−0,0065	0,0037	0,0025	−0,0075
5,5	−7,9740	2,7890	−2,9070	7,3730	−0,0062	0,0029	0,0028	−0,0067
5,6	−8,2470	3,5600	−2,5410	8,0450	−0,0059	0,0023	0,0030	−0,0060
5,7	−8,4790	4,3990	−2,1020	8,7340	−0,0056	0,0017	0,0032	−0,0053
5,8	−8,6640	5,3070	−1,5860	9,4330	−0,0053	0,0012	0,0033	−0,0047
5,9	−8,7940	6,2850	−0,9840	10,1390	−0,0049	0,0008	0,0033	−0,0041
6,0	−8,8580	7,3350	−0,2930	10,8460	−0,0046	0,0004	0,0033	−0,0036
6,2	−8,7560	9,6440	−1,3840	12,2350	−0,0039	−0,0002	0,0032	−0,0026
6,4	−8,2760	12,2230	−3,4900	13,5360	−0,0033	−0,0006	0,0030	−0,0018
6,6	−7,3290	15,0470	−6,0670	14,6700	0,0027	−0,0009	0,0028	−0,0012
6,8	−5,8160	18,0740	−9,1510	15,5430	−0,0022	−0,0011	0,0025	−0,0007
7,0	−3,6330	21,2390	−12,7650	16,0410	−0,0017	−0,0012	0,0022	−0,0003
7,2	−0,6740	24,4560	−16,9180	16,0330	−0,0013	−0,0012	−0,0019	0,0000
7,4	3,1690	27,6090	−21,6000	15,3670	−0,0009	−0,0012	−0,0016	0,0003
7,6	7,9990	30,5500	−26,7770	13,8750	−0,0007	−0,0011	−0,0013	0,0004
7,8	13,9090	33,0900	−32,3800	11,3730	−0,0004	−0,0011	−0,0011	0,0005
8,0	20,9740	35,0200	−38,3100	7,6600	−0,0002	−0,0009	−0,0009	0,0006
8,2	29,2450	36,0600	−44,4200	2,5300	−0,0001	−0,0008	−0,0007	0,0006
8,4	38,7380	35,9200	−50,4900	−4,2320	0,0000	−0,0007	−0,0005	0,0006
8,6	49,4200	34,2500	−56,2800	−12,8320	0,0001	−0,0006	−0,0003	0,0005
8,8	61,2100	30,6500	−61,4500	−23,4650	0,0002	−0,0005	−0,0002	0,0005
9,0	73,9400	24,7100	−65,6000	−36,3000	0,0002	−0,0004	−0,0001	0,0005
9,2	87,3500	15,9800	−68,2500	−51,4600	0,0002	−0,0003	−0,0001	0,0004
9,4	101,1000	3,9700	−68,8200	−69,0100	0,0002	−0,0002	0,0000	0,0003
9,6	114,7000	−11,7900	−66,6700	−88,9400	0,0002	−0,0002	0,0000	0,0003
9,8	127,5400	−31,7600	−61,0700	−111,1200	0,0002	−0,0001	0,0001	0,0002
10,0	138,8400	−56,3700	−51,2000	−135,3100	0,0002	−0,0001	0,0001	0,0002

Resumen

En la presente publicación se estudia de una manera formal y de acuerdo con la teoría de láminas, aceptadas las simplificaciones usuales, el problema de un depósito cilíndrico circular destinado a contener líquidos.

El estudio se lleva hasta obtener una expresión explícita de los esfuerzos y del recorrido radial, expresión que resulta muy simple para el caso de espesor constante y algo más compleja para el espesor variable de acuerdo con una ley lineal en función de la altura.

Para el caso de espesor constante, el trabajo se completa con unas tablas y gráficos que permiten obtener cómodamente los esfuerzos en los casos más útiles, por su frecuencia o por su generalidad.

Por último, una serie de ejemplos, resueltos completamente, aclaran la utilización de tablas y gráficos.

Summary

In the present publication the problem of a circular cylindrical reservoir designated to contain liquids is studied in a formal manner, and according to the shells theory, usual simplifications being accepted.

This study reaches an explicit expression of forces and radial deformation which results a very simple one for the case of constant wall thickness and a little more complex for the wall thickness variable according to a lineal law in function of the height.

For the case of constant thickness, this work is completed with graphics and tables which permit to obtain easily stresses in the more useful cases for its frequency and for its generality.

At last a series of completely worked examples, make more clear the use of tables and graphics.

TABLA I

DEPOSITO LIBRE E. SUS DOS BORDES, SOLICITADO POR UNA FUERZA RADIAL UNIFORME, R, EN EL BORDE INFERIOR

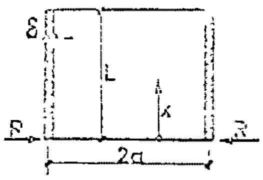

$$W=\frac{2\sqrt[4]{3(1-\nu^2)}}{E}\,\frac{a}{\delta}\,\sqrt{\frac{a}{\delta}}\,R\times\left[Coef_x\right] \qquad N_\varphi=2\sqrt[4]{3(1-\nu^2)}\,\sqrt{\frac{a}{\delta}}\,R\times\left[Coef_x\right]$$

VALORES DEL COEFICIENTE $Coef_x$

VALORES DE λL	VALORES DE X/L												
	0	0.05	0.10	0.15	0.20	0.30	0.40	0.50	0.60	0.70	0.80	0.90	1.00
0.6	-3.3374	-3.0863	-2.8353	-2.5843	-2.3334	-1.8321	-1.3314	-0.8313	-0.3318	0.1674	0.6662	1.1649	1.6636
0.8	-2.5097	-2.3196	-2.7295	-1.9397	-1.7501	-1.3720	-0.9954	-0.6202	-0.2463	0.1266	0.4989	0.8709	1.2427
1.0	-2.0189	-1.8639	-1.7088	-1.5543	-1.4003	-1.0942	-0.7910	-0.4907	-0.1928	0.1031	0.3979	0.6920	0.9858
1.2	-1.6997	-1.5650	-1.4318	-1.2990	-1.1671	-0.9067	-0.6513	-0.4007	-0.1544	0.0887	0.3297	0.5696	0.8091
1.4	-1.4795	-1.3584	-1.2879	-1.1105	-1.0006	-0.7701	-0.5473	-0.3322	-0.1237	0.0798	0.2800	0.4784	0.6764
1.6	-1.3247	-1.2104	-1.0971	-0.9850	-0.8753	-0.6645	-0.4647	-0.2761	-0.0970	0.0747	0.2416	0.4060	0.5697
1.8	-1.2148	-1.1029	-0.9923	-0.8839	-0.7787	-0.5791	-0.3956	-0.2275	-0.0726	0.0722	0.2105	0.3454	0.4793
2.0	-1.1376	-1.0245	-0.9131	-0.8040	-0.7008	-0.5074	-0.3354	-0.1836	-0.0495	0.0717	0.1844	0.2928	0.3999
2.2	-1.0845	-0.9674	-0.8527	-0.7420	-0.6368	-0.4455	-0.2817	-0.1437	-0.0276	0.0723	0.1619	0.2461	0.3288
2.4	-1.0493	-0.9261	-0.8050	-0.6909	-0.5829	-0.3909	-0.2330	-0.1068	-0.0069	0.0736	0.1420	0.2042	0.2646
2.6	-1.0270	-0.8962	-0.7691	-0.6485	-0.5365	-0.3421	-0.1883	-0.0731	0.0120	0.0750	0.1242	0.1666	0.2071
2.8	-1.0136	-0.8742	-0.7392	-0.6123	-0.4957	-0.2981	-0.1483	-0.0429	0.0286	0.0758	0.1082	0.1334	0.1565
3.0	-1.0066	-0.8575	-0.7142	-0.5805	-0.4591	-0.2582	-0.1130	[illegible]164	0.0427	0.0759	0.0937	[illegible]44	0.1130
3.2	-1.0030	-0.8442	-0.6922	-0.5518	-0.4253	-0.2221	-0.0813	0.0062	0.0537	0.0740	0.0807	0.0797	0.0767
3.4	-1.0014	-0.8328	-0.6722	-0.5252	[illegible]	[illegible]	-0.0536	0.0248	0.0618	0.0725	0.0689	0.0590	0.0475
3.6	-1.0009	-0.8225	-0.6524	-0.5001	-0.3660	-0.1595	-0.0287	0.0396	0.0670	0.0691	0.0583	0.0422	0.0243
3.8	-1.0008	-0.8126	-0.6353	-0.4760	-0.3386	-0.1325	[illegible]	0.0509	0.0696	0.0647	0.0488	0.0285	0.0080
4.0	-1.0006	-0.8029	-0.6175	-0.4526	-0.3126	-0.1079	0.0079	0.0590	0.0699	0.0595	0.0403	0.0184	-0.0038
4.2	-1.0008	-0.7932	[illegible]	-0.4302	-0.2077	-0.0956	0.0222	0.0644	[illegible]	0.0537	0.0327	0.0106	-0.0115
4.4	-1.0007	-0.7836	-0.5820	-0.4082	-0.2609	[illegible]	0.0341	0.0673	0.0682	0.0476	0.0261	0.0043	-0.0156
4.6	-1.0005	-0.7740	-0.5658	-0.3680	-0.2412	-0.0470	0.0430	0.0689	0.0611	0.0414	0.0203	0.0006	-0.0177
4.8	-1.0004	-0.7644	-0.5490	-0.3360	-0.2195	-0.0304	0.0512	0.0686	0.0562	[illegible]	0.0153	-0.0020	-0.0170
5.0	-1.0003	-0.7543	-0.5324	-0.3457	-0.1907	[illegible]	0.0571	0.0671	0.0509	0.0205	0.0110	-0.0007	-0.0167
5.5	-1.0001	-0.7311	-0.4919	-0.2374	-0.1510	0.0103	[illegible]	0.0697	0.0572	[illegible]	0.0033	-0.0031	-0.0115
6.0	-1.0000	-0.7076	-0.4530	-0.2527	-0[illegible]	[illegible]	0.0370	0.0495	[illegible]	0.0078	-0.0000	-0.0044	-0.0051
7.0	-1.0000	-0.6920	[illegible]	-0.1741	-0.0419	[illegible]	[illegible]	0.0233	0.0070	[illegible]	[illegible]	-0.0018	-0.0002
8.0	-1.0000	-0.6174	[illegible]	[illegible]	[illegible]	[illegible]	0.0407	0.0120	-0.0007	-0.0023	-0.0017	-0.0003	0.0006
9.0	-1.0000	-0.5742	[illegible]	[illegible]	0.0378	[illegible]	0.0245	0.0020	-0.0029	[illegible]	-0.0005	0.0001	0.0003
10.0	-1.0000	-0.5323	-0.1008	-0.0150	0.0560	[illegible]	0.0120	-0.0019	-0.0024	-0.0007	0.0001	0.0001	0
12.0	[illegible]	-0.4530	-0.1091	0.0378	0.0080	0.0245	-0.0007	-0.0024	-0.0005	0.0001	0.0001	0	0
14.0	-1.0000	[illegible]	[illegible]	0.0618	0.0573	0.0074	-0.0025	-0.0007	0.0001	0.0001	0	0	0
16.0	[illegible]	-0.0131	0.0050	0.0659	0.0407	-0.0007	-0.0019	0	0.0001	0	0	0	0
18.0	-1.0000	-0.2527	0.0378	0.0600	0.0245	-0.0025	-0.0005	0.0001	0	0	0	[illegible]	0
20.0	[illegible]	-0.1900	0.0600	0.0493	0.0120	[illegible]	0	0	0	0	0	0	0

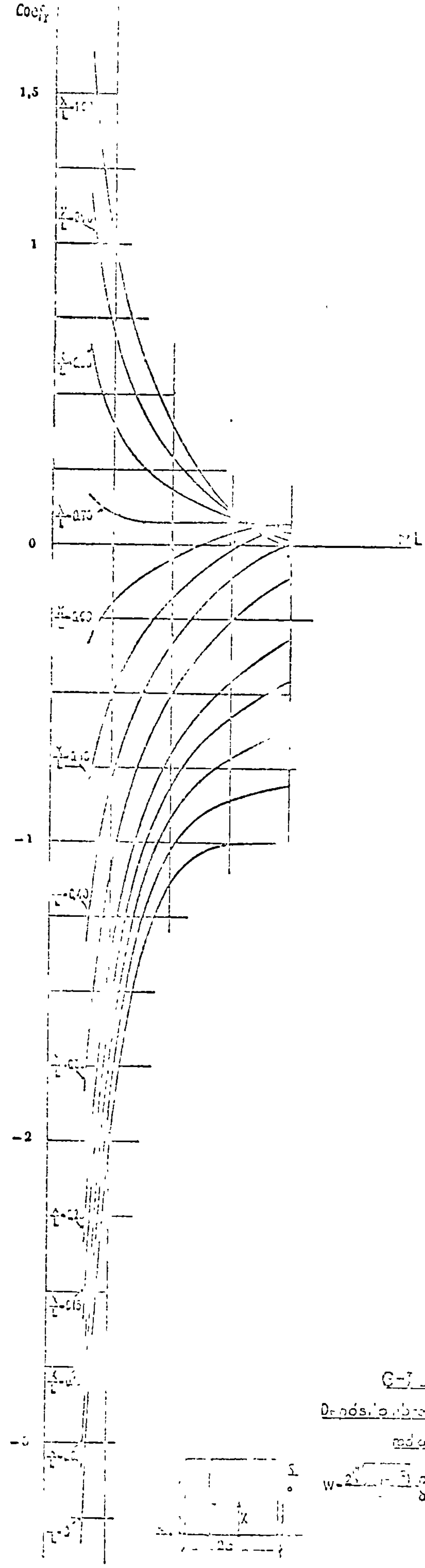

G-7 _ V[illegible] DEL COEFICIENTE $COEF_I$

De[illegible]pósito [illegible] en [illegible] dos bordes, so[illegible]ado por una [illegible]

[illegible] uniforme, R, en el borde inferior

$W = 2 [illegible] \frac{a}{\delta}\sqrt{\frac{a}{\delta}}\, R \times (Coef_I)$ $N_\varphi = 2\sqrt[4]{3(1-\nu^2)}\, [illegible]\, R \times (Coef_I)$

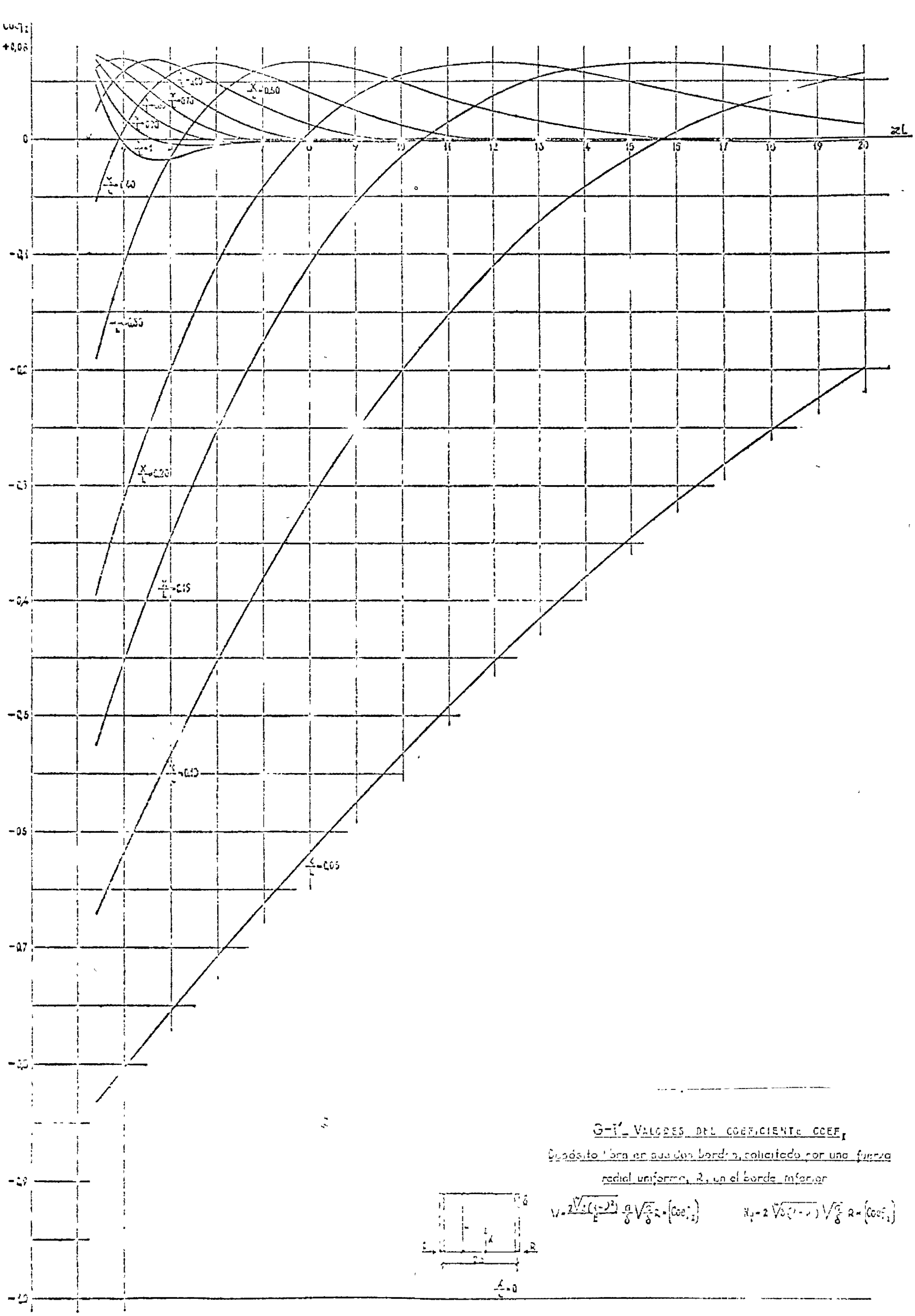

G-1'. VALORES DEL COEFICIENTE COEF$_I$

Depósito libre en sus dos bordes, solicitado por una fuerza radial uniforme, R, en el borde inferior

$V = \frac{2\sqrt[4]{3(1-\nu^2)}}{E}\,\frac{a}{\delta}\sqrt{\frac{a}{\delta}}\,R \cdot (\mathrm{Coef}_2)$ $\qquad$ $M_x = 2\sqrt[4]{3(1-\nu^2)}\,\sqrt{\frac{a}{\delta}}\,R \cdot (\mathrm{Coef}_1)$

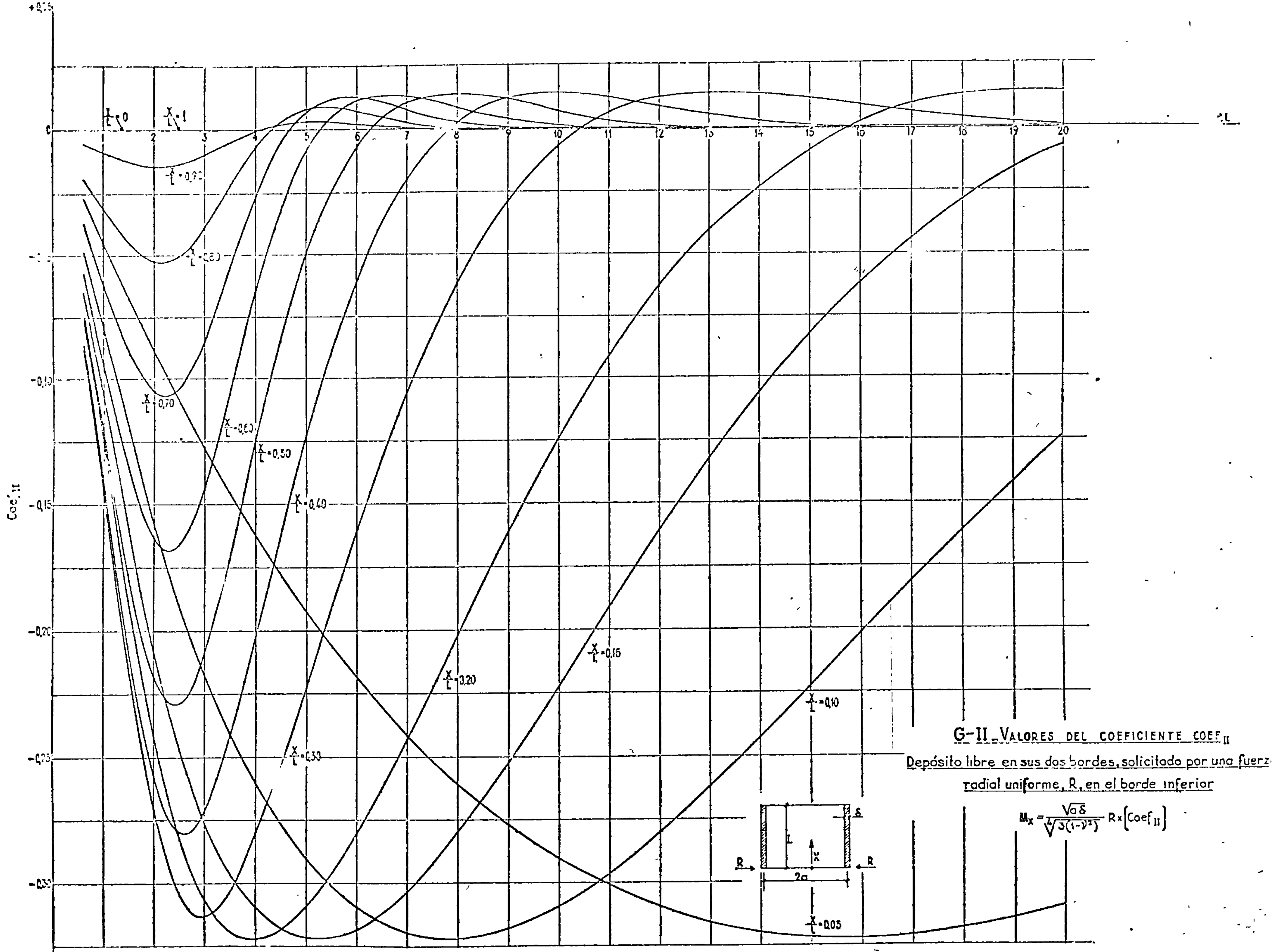

G-II _ VALORES DEL COEFICIENTE $COEF_{II}$

Depósito libre en sus dos bordes, solicitado por una fuerza radial uniforme, R, en el borde inferior

$$M_x = \frac{\sqrt{a\delta}}{\sqrt[4]{3(1-\nu^2)}} \, R \times \left[Coef_{II}\right]$$

TABLA II

DEPOSITO LIBRE EN SUS DOS BORDES, SOLICITADO POR UNA FUERZA RADIAL UNIFORME, R, EN EL BORDE INFERIOR

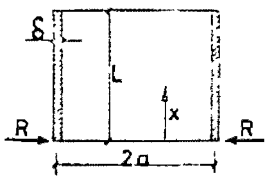

$$M_x = \frac{\sqrt{a\delta}}{\sqrt[4]{3(1-\nu^2)}} R \times \left[Coef_{II} \right]$$

VALORES DEL COEFICIENTE $Coef_{II}$

VALORES DE $a.L$	VALORES DE X/L												
	0	0.05	0.10	0.15	0.20	0.30	0.40	0.50	0.60	0.70	0.80	0.90	1.00
0.6	0	-0.0271	-0.0486	-0.0650	-0.0768	-0.0881	-0.0853	-0.0749	-0.0575	-0.0377	-0.0192	-0.0054	0
0.8	0	-0.0361	-0.0647	-0.0866	-0.1022	-0.1173	-0.1149	-0.0996	-0.0765	-0.0502	-0.0255	-0.0072	0
1.0	0	-0.0451	-0.0808	-0.1081	-0.1275	-0.1462	-0.1429	-0.1239	-0.0950	-0.0623	-0.0316	-0.0089	0
1.2	0	-0.0540	-0.0968	-0.1293	-0.1524	-0.1743	-0.1702	-0.1472	-0.1127	-0.0738	-0.0374	-0.0105	0
1.4	0	-0.0629	-0.1126	-0.1501	-0.1766	-0.2014	-0.1960	-0.1691	-0.1292	-0.0844	-0.0427	-0.0120	0
1.6	0	-0.0718	-0.1280	-0.1703	-0.1999	-0.2268	-0.2197	-0.1888	-0.1436	-0.0935	-0.0472	-0.0132	0
1.8	0	-0.0805	-0.1431	-0.1896	-0.2218	-0.2499	-0.2405	-0.2053	-0.1554	-0.1006	-0.0505	-0.0141	0
2.0	0	-0.0890	-0.1575	-0.2078	-0.2419	-0.2701	-0.2575	-0.2180	-0.1637	-0.1053	-0.0526	-0.0146	0
2.2	0	-0.0974	-0.1713	-0.2246	-0.2599	-0.2867	-0.2701	-0.2261	-0.1679	-0.1070	-0.0530	-0.0146	0
2.4	0	-0.1055	-0.1843	-0.2399	-0.2755	-0.2993	-0.2778	-0.2291	-0.1678	-0.1056	-0.0517	-0.0141	0
2.6	0	-0.1134	-0.1965	-0.2535	-0.2887	-0.3079	[illegible]	-0.2270	-0.1633	-0.1010	-0.0487	-0.0131	0
2.8	0	-0.1210	-0.2076	-0.2656	-0.2993	-0.3124	-0.2782	-0.2201	-0.1548	-0.0937	-0.0442	-0.0117	0
3.0	0	-0.1285	-0.2183	-0.2760	-0.3076	-0.3133	-0.2717	-0.2091	-0.1429	-0.0840	-0.0386	-0.0099	0
3.2	0	-0.1357	-0.2281	-0.2851	-0.3167	-0.3110	-0.2617	-0.1948	-0.1286	-0.0729	-0.0322	-0.0080	0
3.4	0	-0.1427	-0.2372	-0.2928	-0.3180	-0.3060	-0.2489	-0.1784	-0.1127	-0.0608	-0.0255	-0.0059	0
3.6	0	-0.1495	-0.2457	-0.2994	-0.3206	-0.2990	-0.2343	-0.1606	-0.0962	-0.0487	-0.0188	-0.0040	0
3.8	0	-0.1562	-0.2536	-0.3050	-0.3220	-0.2903	-0.2184	-0.1423	-0.0799	-0.0371	-0.0126	-0.0022	0
4.0	0	-0.1626	-0.2609	-0.3097	-0.3221	-0.2805	-0.2020	-0.1243	-0.0644	-0.0263	-0.0070	-0.0006	0
4.2	0	-0.1689	-0.2678	-0.3136	-0.3212	-0.2698	-0.1854	-0.1069	-0.0501	-0.0168	-0.0023	0.0007	0
4.4	0	-0.1751	-0.2742	-0.3167	-0.3194	[illegible]	-0.1690	-0.0906	-0.0373	-0.0087	0.0016	0.0017	0
4.6	0	-0.1811	-0.2802	-0.3191	-0.3168	-0.2467	-0.1530	-0.0755	-0.0260	-0.0020	0.0046	0.0025	0
4.8	0	-0.1870	-0.2857	-0.3208	-0.3134	-0.2346	-0.1376	-0.0618	-0.0165	0.0033	0.0067	0.0029	0
5.0	0	-0.1927	-0.2907	-0.3219	-0.3094	-0.2223	-0.1229	-0.0494	-0.0065	0.0072	0.0080	0.0031	0
5.5	0	-0.2063	-0.3015	-0.3218	-0.2966	-0.1913	-0.0894	-0.0244	0.0052	0.0122	0.0087	0.0029	0
6.0	0	-0.2189	-0.3099	-0.3185	-0.2807	-0.1609	-0.0612	-0.0070	0.0119	0.0125	0.0071	0.0020	0
7.0	0	-0.2416	-0.3199	-0.3035	-0.2430	-0.1057	-0.0204	0.0106	0.0130	0.0073	0.0025	0.0004	0
8.0	0	-0.2610	[illegible]	-0.2807	-0.2018	-0.0613	0.0024	0.0138	0.0082	0.0024	-0.0001	-0.0003	0
9.0	0	-0.2773	-0.3185	-0.2529	-0.1610	-0.0287	0.0121	0.0109	0.0035	0	-0.0006	-0.0002	0
10.0	0	-0.2908	-0.3096	-0.2226	-0.1231	-0.0070	0.0139	0.0065	0.0007	-0.0006	-0.0003	-0.0001	0
12.0	0	-0.3059	-0.2807	-0.1610	-0.0613	0.0121	0.0082	0.0007	-0.0006	-0.0002	0	0	0
14.0	0	-0.3199	-0.2430	-0.1057	-0.0204	0.0131	0.0023	-0.0006	-0.0002	0	0	0	0
16.0	0	-0.3223	-0.2018	-0.0613	0.0024	0.0082	-0.0002	-0.0003	0	0	0	0	0
18.0	0	-0.3165	-0.1610	-0.0287	0.0121	0.0035	-0.0006	-0.0001	0	0	0	0	0
20.0	0	-0.3096	-0.1231	-0.0070	0.0139	0.0007	-0.0003	0	0	0	0	0	0

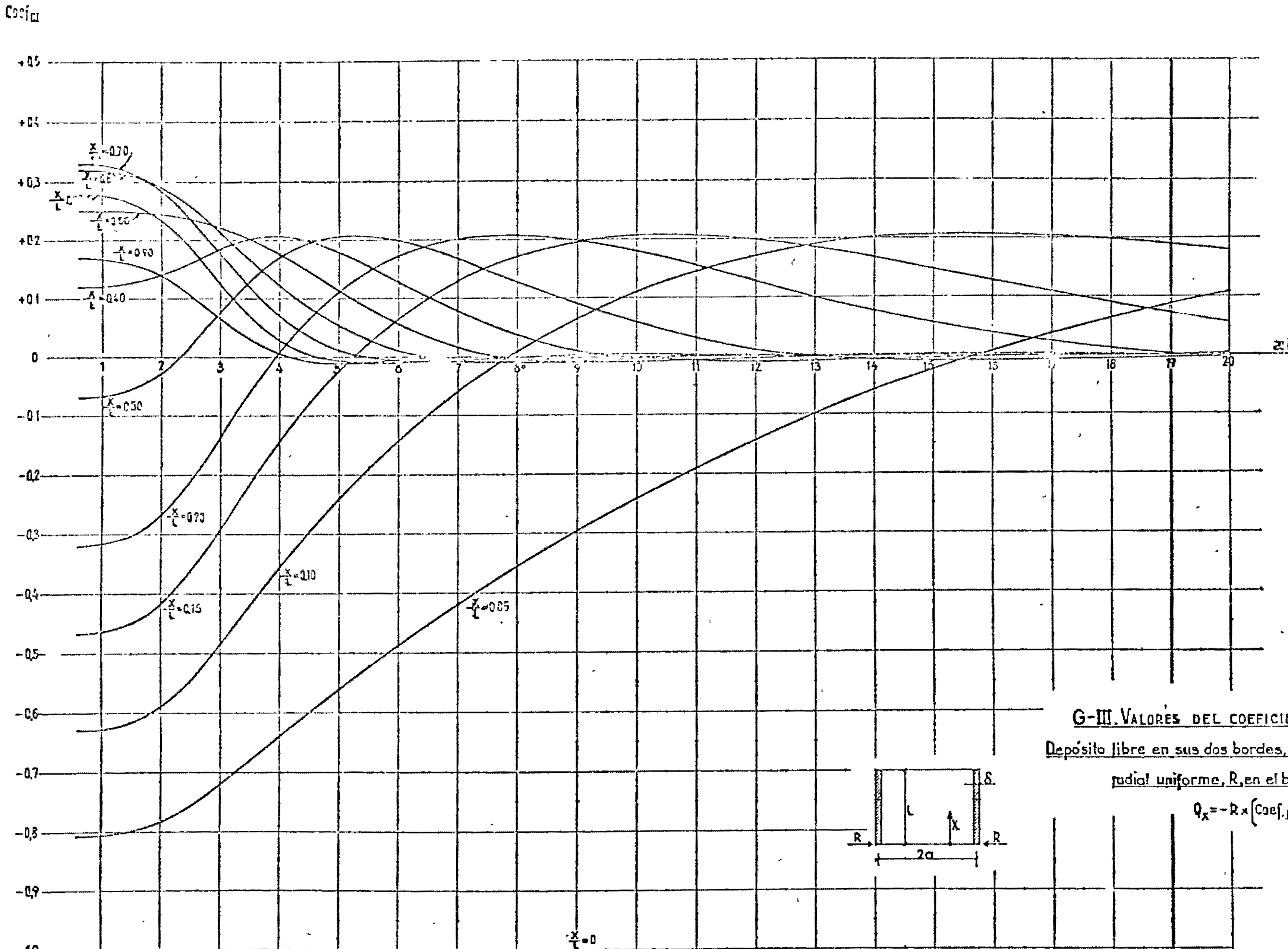

G-III. VALORES DEL COEFICIENTE COEF.III

Depósito libre en sus dos bordes, solicitado por una fuerza radial uniforme, R, en el borde inferior.

$$Q_x = -R \times (\text{Coef.}_{III})$$

TABLA III.

DEPOSITO LIBRE EN SUS DOS BORDES, SOLICITADO POR UNA FUERZA RADIAL UNIFORME, R, EN EL BORDE INFERIOR

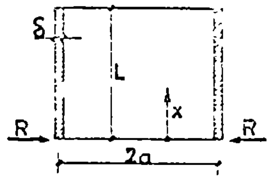

$$Q_x = -R \times \left[Coef_{III}\right]$$

VALORES DEL COEFICIENTE $Coef_{III}$

VALORES DE λ.L	VALORES DE X/L: 0	0.05	0.10	0.15	0.20	0.30	0.40	0.50	0.60	0.70	0.80	0.90	1.00
0.6	-1.0000	-0.8073	-0.6296	-0.4671	-0.3195	-0.0696	0.1202	0.2500	0.3197	0.3296	0.2796	0.1697	0
0.8	-1.0000	-0.8063	-0.6289	-0.4661	-0.3185	-0.0668	0.1206	0.2498	0.3192	0.3287	0.2787	0.1691	0
1.0	-1.0000	-0.8059	-0.6272	-0.4641	-0.3164	-0.0670	0.1215	0.2496	0.3179	0.3269	0.2768	0.1678	0
1.2	-1.0000	-0.8041	-0.6243	-0.4605	-0.3125	-0.0638	0.1231	0.2492	0.3158	0.3236	0.2734	0.1654	0
1.4	-1.0000	-0.8013	-0.6196	-0.4547	-0.3064	-0.0586	0.1256	0.2486	0.3123	0.3183	0.2679	0.1617	0
1.6	-1.0000	-0.7972	-0.6126	-0.4460	-0.2972	-0.0510	0.1293	0.2476	0.3070	0.3105	0.2598	0.1561	0
1.8	-1.0000	-0.7914	-0.6029	-0.4341	-0.2845	-0.0405	0.1344	0.2461	0.2998	0.2996	0.2486	0.1485	0
2.0	-1.0000	-0.7838	-0.5901	-0.4183	-0.2679	-0.0269	0.1410	0.2442	0.2903	0.2855	0.2341	0.1386	0
2.2	-1.0000	-0.7743	-0.5742	-0.3983	-0.2473	-0.0102	0.1488	0.2415	0.2785	0.2682	0.2164	0.1265	0
2.4	-1.0000	-0.7630	-0.5552	-0.3757	-0.2230	0.0093	0.1577	0.2381	0.2645	0.2478	0.1957	0.1125	0
2.6	-1.0000	-0.7500	-0.5337	-0.3495	-0.1957	0.0309	0.1672	0.2338	0.2486	0.2252	0.1730	0.0972	0
2.8	-1.0000	-0.7357	-0.5100	-0.3210	-0.[illegible]62	0.0538	0.1767	0.2286	0.2312	0.2010	0.1490	0.0812	0
3.0	-1.0000	-0.7205	-0.4849	-0.2910	-0.1354	0.0770	0.1857	0.2223	0.2129	0.1763	0.1249	0.0652	0
3.2	-1.0000	-0.7046	-0.4590	-0.2603	-0.1043	0.0996	0.1935	0.2150	0.1941	0.1519	0.1016	0.0501	0
3.4	-1.0000	-0.6883	-0.4328	-0.2296	-0.0737	0.1207	0.1997	0.2067	0.1753	0.1285	0.0799	0.0362	0
3.6	-1.0000	-0.6720	-0.4067	-0.1996	-0.0443	0.1399	0.2039	0.1973	0.1569	0.1068	0.0605	0.0241	0
3.8	-1.0000	-0.6557	-0.3810	-0.1705	-0.0165	0.1568	0.2060	0.1870	0.1392	0.0871	0.0436	0.0140	0
4.0	-1.0000	-0.6395	-0.3560	-0.1427	0.0095	0.1712	0.2060	0.1758	0.1223	0.0696	0.0294	0.0058	0
4.2	-1.0000	-0.6235	-0.3316	-0.1162	0.0336	0.1829	0.2039	0.1639	0.1063	0.0543	0.0178	-0.0004	0
4.4	-1.0000	-0.6078	-0.3080	-0.0910	0.0557	0.1922	0.1999	0.1516	0.0914	0.0411	0.0087	-0.0049	0
4.6	-1.0000	-0.5923	-0.2851	-0.0672	0.0760	0.1992	0.1943	0.1389	0.0755	0.0300	0.0017	-0.0078	0
4.8	-1.0000	-0.5769	-0.2628	-0.0447	0.0944	0.2040	0.1871	0.1261	0.0646	0.0207	-0.0033	-0.0095	0
5.0	-1.0000	-0.5618	-0.2413	-0.0234	0.1111	0.2066	0.1789	0.1133	0.0532	0.0131	-0.0068	-0.0103	0
5.5	-1.0000	-0.5247	-0.1902	-0.0247	0.1458	0.2067	0.1547	0.0829	0.0292	0	-0.0105	-0.0092	0
6.0	-1.0000	-0.4888	-0.1430	0.0658	0.1716	0.1986	0.1282	0.0561	0.0119	-0.0066	-0.0098	-0.0063	0
7.0	-1.0000	-0.4203	-0.0599	0.1294	0.2011	0.1675	0.0777	0.0177	0.0057	-0.0086	-0.0049	-0.0014	0
8.0	-1.0000	-0.3564	0.0093	0.1716	0.2077	0.1282	-0.0383	-0.0019	-0.0089	-0.0051	-0.0012	0.0004	0
9.0	-1.0000	-0.2968	0.0657	0.1962	0.1985	0.0895	0.0124	-0.0035	-0.0064	-0.0018	0.0002	0.0004	0
10.0	-1.0000	-0.2415	0.1108	0.2068	0.1794	0.0563	-0.0019	-0.0034	-0.0031	-0.0001	0.0004	0.0001	0
12.0	-1.0000	-0.1431	0.1716	0.1985	0.1282	0.0124	-0.0089	-0.0031	0.0001	0.0003	0.0001	0	0
14.0	-1.0000	-0.0599	0.2011	0.1675	0.0777	-0.0057	-0.0052	-0.0001	0.0003	0	0	0	0
16.0	-1.0000	0.0093	0.2077	0.1262	0.0383	-0.0089	-0.0015	0.0004	0.0001	0	0	0	0
18.0	-1.0000	0.0657	0.1985	0.0895	0.0124	-0.0064	0.0001	0.0002	0	0	0	0	0
20.0	-1.0000	0.1108	0.1794	0.0563	-0.0019	-0.0031	0.0004	0	0	0	0	0	0

TABLA IV.

DEPOSITO LIBRE EN SUS DOS BORDES, SOLICITADO POR UN MOMENTO RADIAL UNIFORME, M, EN EL BORDE INFERIOR

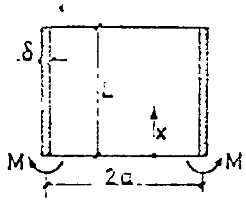

$$W = \frac{2\sqrt{3(1-\nu^2)}}{E}\,\frac{a}{\delta^2}\,M \times [Coef_{IV}] \qquad N_\varphi = 2\sqrt{3(1-\nu^2)}\,\frac{M}{\delta} \times [Coef_{IV}]$$

VALORES DEL COEFICIENTE $Coef_{IV}$

VALORES DE λ.L	VALORES DE X/L												
	0	0.05	0.10	0.15	0.20	0.30	0.40	0.50	0.60	0.70	0.80	0.90	1.00
0.6	[illegible]	7.5252	6.6812	5.3369	4.9904	3.3219	1.6512	-0.0150	-1.6775	-3.3375	-4.9960	-6.6536	-8.3111
0.8	[illegible]	4.2635	3.7756	3.2912	2.8096	1.8548	0.9100	-0.0266	-0.9568	-1.8824	-2.8053	-3.7269	-4.6460
1.0	3.1042	2.7697	2.4401	2.1154	1.7954	1.1685	0.5572	-0.0413	-0.6299	-1.2115	-1.7889	-2.3641	-2.9387
1.2	2.2324	1.9746	1.7239	1.4803	1.2433	0.7883	0.3555	-0.0509	-0.4593	-0.8497	-1.2340	-1.6154	-1.9959
1.4	1.7315	1.5116	1.3014	1.1007	0.9091	0.5515	0.2239	-0.0790	-0.3631	-0.6340	-0.8969	-1.1558	-1.4135
1.6	1.4303	1.2267	1.0359	0.8573	0.6907	0.3905	0.1290	-0.1009	-0.3069	-0.4962	-0.6754	-0.8497	-1.0226
1.8	1.2461	1.0458	0.8616	0.6930	0.5393	0.2733	0.0554	-0.1237	-0.2736	-0.4035	-0.5213	-0.6332	-0.7434
2.0	1.1341	0.9289	0.7434	0.5771	0.4290	0.1833	-0.0045	-0.1463	-0.2536	-0.3332	-0.4088	-0.4729	-0.5351
2.2	1.0681	0.8524	0.6607	0.4920	0.3453	0.1115	-0.0545	-0.1673	-0.2416	-0.2902	-0.3238	-0.3505	-0.3751
2.4	1.0310	0.8017	0.6007	0.4270	0.2791	0.0526	-0.0962	-0.1857	-0.2331	-0.2532	-0.2578	-0.2554	-0.2510
2.6	1.0119	0.7669	0.5551	0.3751	0.2248	0.0036	-0.1307	-0.2004	-0.2256	-0.2231	-0.2054	-0.1810	-0.1549
2.8	1.0034	0.7417	0.5184	0.3317	0.1789	-0.0375	-0.1584	-0.2106	-0.2175	-0.1973	-0.1631	-0.1232	-0.0819
3.0	1.0004	0.7217	0.4869	0.2938	0.1389	-0.0720	-0.1798	-0.2161	-0.2077	-0.1742	-0.1288	-0.0789	-0.0282
3.2	1.0001	0.7043	0.4585	0.2596	0.1033	-0.1010	-0.1953	-0.2171	-0.1959	-0.1528	-0.1006	-0.0457	0.0095
3.4	1.0006	0.6881	0.4318	0.2278	0.0710	-0.1252	-0.2058	-0.2138	-0.1823	-0.1327	-0.0774	-0.0215	0.0342
3.6	1.0012	0.6722	0.4060	0.1979	0.0414	-0.1453	-0.2117	-0.2071	-0.1670	-0.1137	-0.0584	-0.0045	0.0484
3.8	1.0015	0.6564	0.3808	0.1693	0.0141	-0.1618	-0.2140	-0.1975	-0.1507	-0.0958	-0.0427	0.0069	0.0548
4.0	1.0015	0.6405	0.3562	0.1421	-0.0112	-0.1753	-0.2131	-0.1858	-0.1339	-0.0792	-0.0299	0.0139	0.0555
4.2	1.0014	0.6245	0.3321	0.1160	-0.0346	-0.1860	-0.2098	-0.1727	-0.1171	-0.0639	-0.0196	0.0177	0.0523
4.4	1.0011	0.6087	0.3086	0.0911	-0.0562	-0.1944	-0.2044	-0.1586	-0.1003	[illegible]	-0.0113	0.0193	0.0468
4.6	1.0008	0.5930	0.2856	0.0674	-0.0761	-0.2006	-0.1975	-0.1445	-0.0854	-0.0380	-0.0047	0.0192	0.0400
4.8	1.0005	0.5775	0.2633	0.0450	-0.0943	-0.2048	-0.1894	-0.1303	-0.0710	-0.0274	0.0003	0.0182	0.0328
5.0	1.0003	0.5621	0.2416	0.0236	-0.1109	-0.2073	-0.1803	-0.1163	-0.0579	-0.0184	0.0040	0.0165	0.0259
5.5	1.0001	0.5248	0.1903	-0.0245	-0.1457	-0.2067	-0.1550	-0.0838	-0.0310	-0.0024	0.0088	0.0114	0.0115
6.0	1.0000	0.4888	0.1431	-0.0658	-0.1716	-0.1986	-0.1282	-0.0563	-0.0123	[illegible]	0.0094	0.0067	0.0028
7.0	1.0000	0.4203	0.0599	-0.1294	-0.2011	-0.1675	-0.0777	-0.0176	0.0059	0.0090	0.0054	0.0013	-0.0024
8.0	1.0000	0.3564	-0.0093	-0.1716	-0.2077	-0.1282	-0.0383	0.0019	0.0090	0.0053	0.0015	-0.0003	-0.0013
9.0	1.0000	0.2966	-0.0657	-0.1962	-0.1985	-0.0895	-0.0124	0.0035	0.0064	0.0016	-0.0001	-0.0004	-0.0002
10.0	1.0000	0.2415	-0.1108	-0.2069	-0.1794	-0.0563	0.0019	0.0084	0.0031	0.0001	-0.0004	-0.0002	0.0001
12.0	1.0000	0.1431	-0.1716	-0.1985	-0.1282	-0.0124	0.0039	0.0031	-0.0001	-0.0003	-0.0001	0	0
14.0	1.0000	0.0599	-0.2011	-0.1675	-0.0777	0.0057	0.0052	0.0001	-0.0003	0	0	0	0
16.0	1.0000	-0.0093	-0.2077	-0.1282	-0.0383	0.0089	0.0015	-0.0004	-0.0001	0	0	0	0
18.0	1.0000	-0.0657	-0.1985	-0.0895	-0.0124	0.0064	-0.0001	-0.0002	0	0	0	0	0
20.0	1.0000	-0.1108	-0.1794	-0.0563	0.0019	0.0031	-0.0004	0	0	0	0	0	0

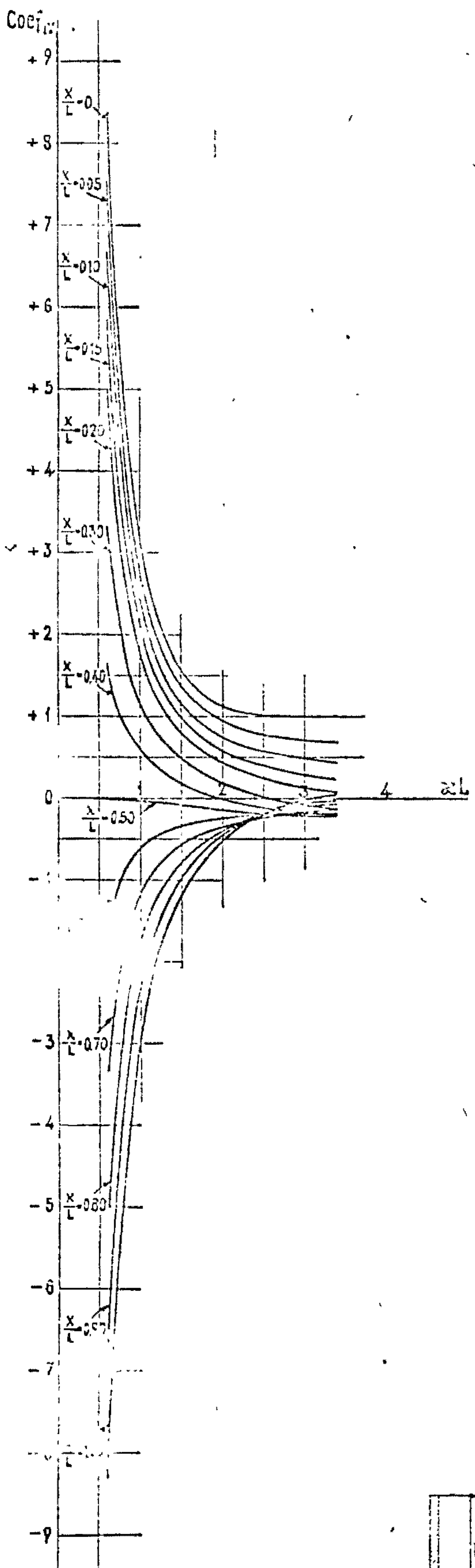

G-IV. Valores del coeficiente $COEF_{IV}$

Depósito libre en sus dos bordes, solicitado por un momento radial uniforme, M, en el borde inferior.

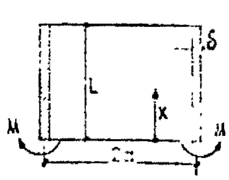

$$W = \frac{2\sqrt{3(1-\nu^2)}}{E} \cdot \frac{a}{\delta^2} M \times (Coef_{IV}) \qquad N_\varphi = 2\sqrt{3(1-\nu^2)} \frac{M}{\delta} \times (Coef_{IV})$$

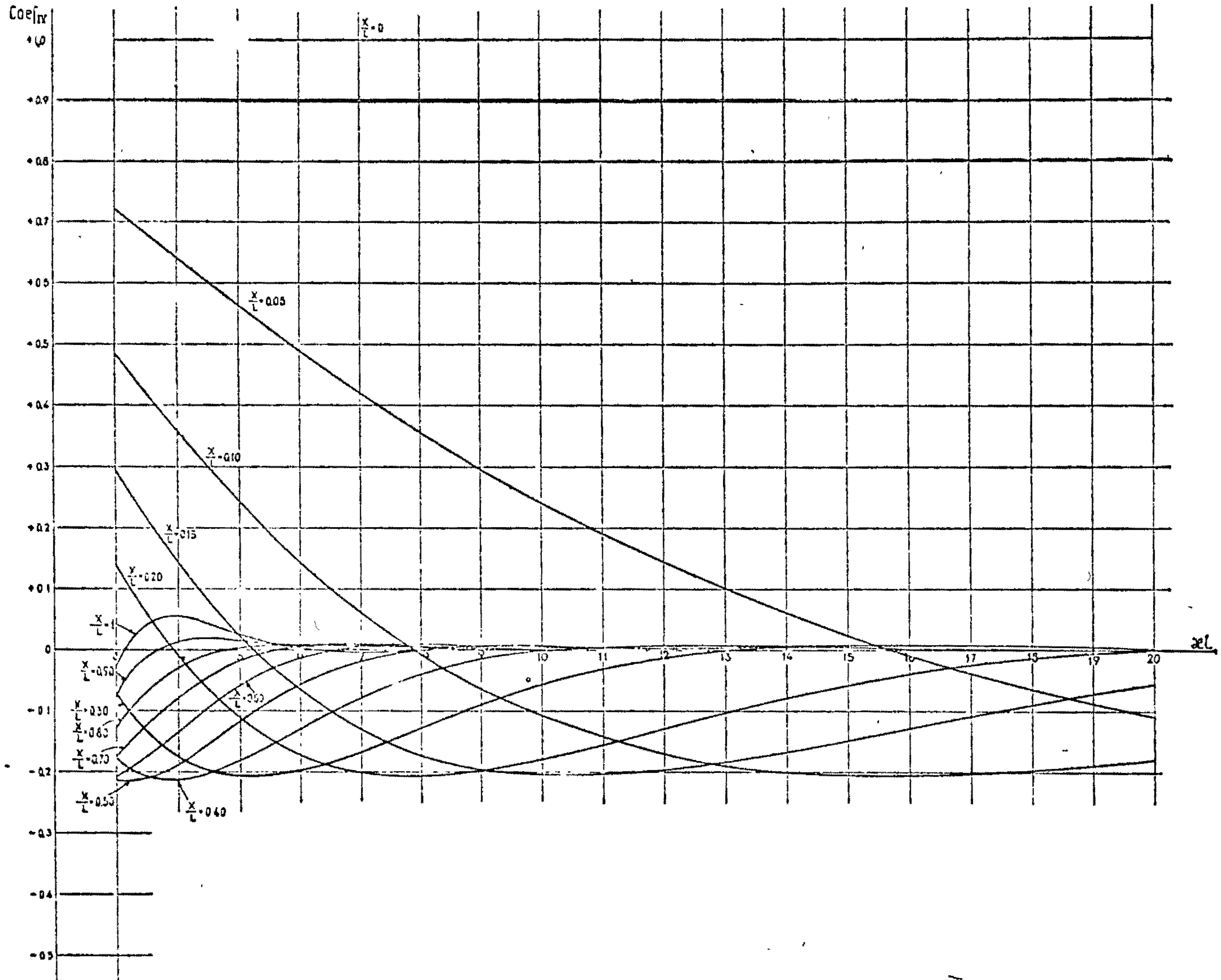

G-IV'-Valores del coeficiente $COEF_{IV}$

Deposito libre en sus dos bordes, solicitado por un momento radial uniforme, M, en el borde inferior.

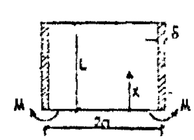

$W = \frac{2\sqrt{3(1-\nu^2)}}{E}\cdot\frac{a}{\delta^2}\cdot M\cdot(\text{Coef}_{IV})$ $\quad$ $N_\varphi = 2\sqrt{3(1-\nu^2)}\,\frac{M}{\delta}\cdot(\text{Coef}_{IV})$

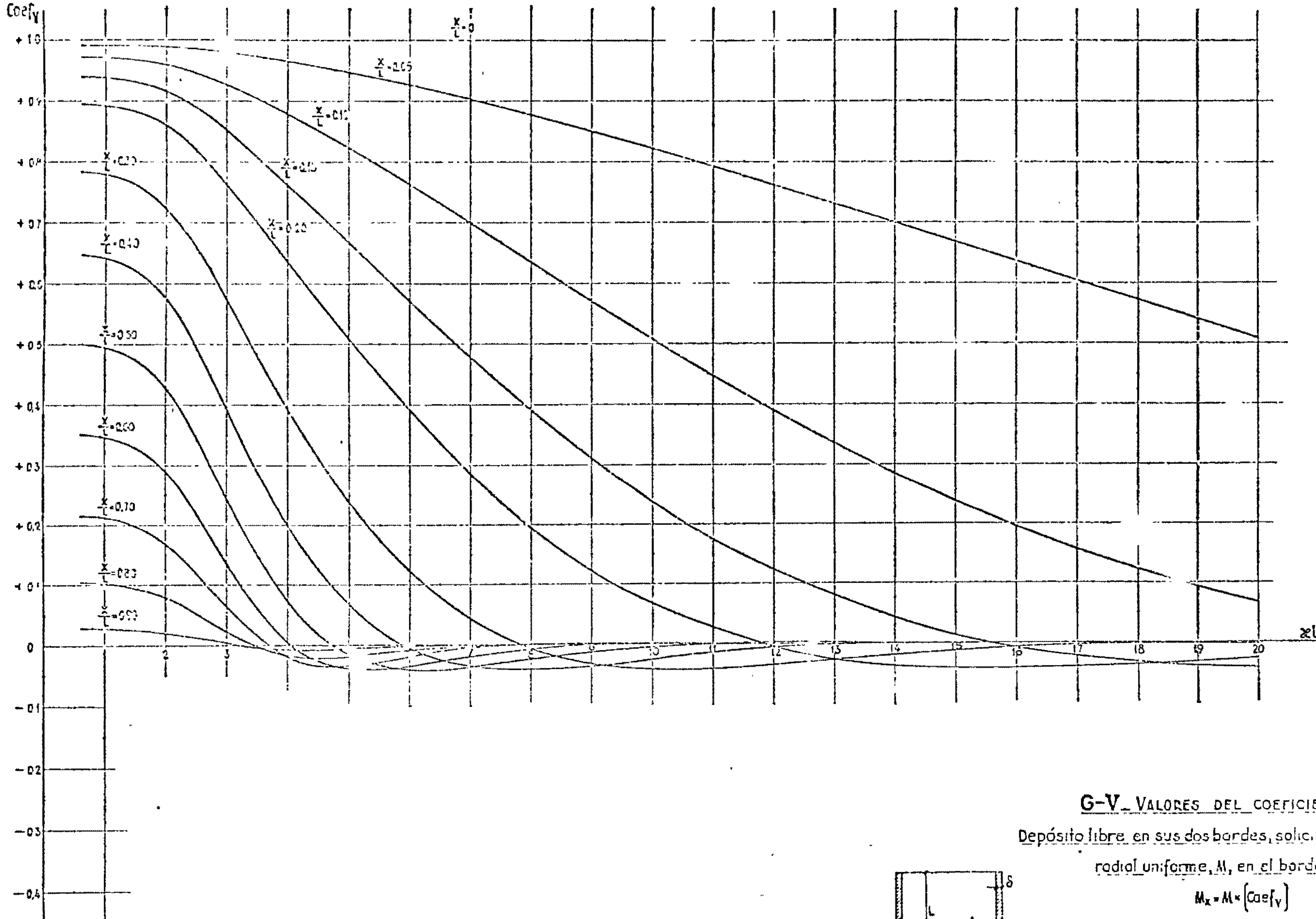

G-V. VALORES DEL COEFICIENTE COEF$_V$

Depósito libre en sus dos bordes, solicitado por un momento radial uniforme, M, en el borde inferior

$M_x = M \times (Coef_V)$

TABLA V.

DEPOSITO LIBRE EN SUS DOS BORDES, SOLICITADO POR UN MOMENTO RADIAL UNIFORME, M, EN EL BORDE INFERIOR

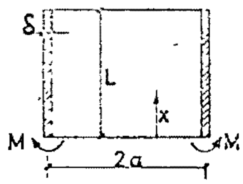

$$M_x = M \times [Coef_V]$$

VALORES DEL COEFICIENTE $Coef_V$

VALORES DE [illegible] L	VALORES DE X/L												
	0	0.05	0.10	0.15	0.20	0.30	0.40	0.50	0.60	0.70	0.80	0.90	1.00
0.6	1.0000	0.9927	0.9719	0.9390	0.8957	0.7635	0.6473	0.4993	0.3514	0.2156	0.1038	0.0279	0
0.8	1.0000	0.9927	0.9717	0.9386	0.8950	0.7823	0.6459	0.4979	0.3501	0.2147	0.1033	0.0278	0
1.0	1.0000	0.9925	0.9712	0.9377	0.8935	0.7800	0.6430	0.4948	0.3475	0.2127	0.1022	0.0275	0
1.2	1.0000	0.9923	0.9703	0.9360	0.8909	0.7757	0.6377	0.4894	[illegible]	0.2093	0.1004	0.0269	0
1.4	1.0000	0.9919	0.9689	0.9332	0.8867	0.7688	0.6291	0.4806	0.3351	0.2038	0.0973	0.0260	0
1.6	1.0000	0.9913	0.9669	0.9292	0.8805	0.7585	0.6164	0.4676	0.3238	0.1957	0.0929	0.0247	0
1.8	1.0000	0.9905	0.9640	0.9235	0.8717	0.7443	0.5988	0.4496	0.3082	0.1845	0.0868	0.0229	0
2.0	1.0000	0.9894	0.9601	0.9160	0.8602	0.7256	0.5759	0.4262	0.2880	0.1700	0.0790	0.0206	0
2.2	1.0000	0.9880	0.9553	0.9065	0.8458	0.7023	0.5475	0.3975	0.2633	0.1524	0.0694	0.0178	0
2.4	1.0000	0.9863	0.9494	0.8952	0.8286	0.6747	0.5140	0.3638	0.2347	0.1321	0.0585	0.0145	0
2.6	1.0000	0.9843	0.9426	0.8821	0.8038	0.6433	0.4764	0.3264	0.2030	0.1098	0.0466	0.0111	0
2.8	1.0000	0.9821	0.9350	0.8675	0.7863	0.6090	0.4358	0.2865	0.1697	0.0866	0.0343	0.0075	0
3.0	1.0000	0.9797	0.9267	0.8516	0.7632	0.5727	0.3936	0.2458	0.1362	0.0637	0.0223	0.0041	0
3.2	1.0000	0.9770	0.9178	0.8349	0.7385	0.5354	0.3512	0.2057	0.1040	0.0420	0.0112	0.0009	0
3.4	1.0000	0.9742	0.9084	0.8174	0.7130	0.4979	0.3096	0.1675	0.0741	0.0224	0.0014	-0.0018	0
3.6	1.0000	0.9713	0.8987	0.7994	0.6871	0.4610	0.2699	0.1321	0.0473	0.0055	-0.0063	-0.0040	0
3.8	1.0000	0.9682	0.8886	0.7811	0.6611	[illegible]	0.2325	0.1002	0.0243	-0.0083	-0.0132	-0.0056	0
4.0	1.0000	0.9650	0.8783	0.7626	0.6351	0.3901	0.1978	0.0720	0.0051	-0.0191	-0.0177	-0.0067	0
4.2	1.0000	0.9617	0.8677	0.7438	0.6093	0.3567	0.1661	0.0477	-0.0103	-0.0269	-0.0206	-0.0072	0
4.4	1.0000	0.9583	0.8569	0.7249	0.5836	0.3248	0.1371	0.0269	-0.0222	-0.0320	-0.0220	-0.0073	0
4.6	1.0000	0.9547	0.8458	0.7059	0.5582	0.2944	0.1110	0.0096	-0.0309	-0.0348	-0.0221	-0.0070	0
4.8	1.0000	0.9510	0.8345	0.6867	0.5330	0.2655	0.0876	-0.0046	-0.0368	-0.0356	-0.0212	-0.0065	0
5.0	1.0000	0.9472	0.8230	0.6675	0.5081	0.2381	0.0657	-0.0161	-0.0404	-0.0349	-0.0195	-0.0057	0
5.5	1.0000	0.9373	0.7934	0.6192	0.4476	0.1762	0.0243	-0.0345	-0.0417	-0.0289	-0.0138	-0.0035	0
6.0	1.0000	0.9267	0.7628	0.5712	0.3899	0.1234	-0.0056	-0.0422	-0.0365	-0.0204	-0.0077	-0.0015	0
7.0	1.0000	0.9036	0.6997	0.4777	0.2849	0.0439	[illegible]	-0.0388	-0.0204	-0.0061	-0.0001	0.0006	0
8.0	1.0000	0.8784	0.6354	0.3899	0.1959	-0.0056	-0.0431	-0.0258	-0.0075	0.0005	0.0017	0.0007	0
9.0	1.0000	0.8515	0.5712	0.3097	0.1234	-0.0320	-0.0366	-0.0132	-0.0005	0.0019	0.0010	0.0002	0
10.0	1.0000	0.8231	0.5083	0.2384	0.0667	-0.0423	-0.0258	-0.0046	0.0017	0.0013	0.0003	0	0
12.0	1.0000	0.7628	0.3899	0.1234	-0.0056	-0.0366	-0.0075	0.0017	0.0010	0.0001	-0.0001	0	0
14.0	1.0000	0.6997	0.2849	0.0439	-0.0369	-0.0204	0.0005	0.0013	0.0001	-0.0001	0	0	0
16.0	1.0000	0.6354	0.1959	-0.0056	-0.0431	-0.0075	0.0018	0.0003	-0.0001	0	0	0	0
18.0	1.0000	0.5712	0.1234	-0.0320	-0.0366	-0.0006	0.0010	-0.0001	0	0	0	0	0
20.0	1.0000	0.5083	0.0957	-0.0423	-0.0258	0.0017	0.0003	-0.0001	0	0	0	0	0

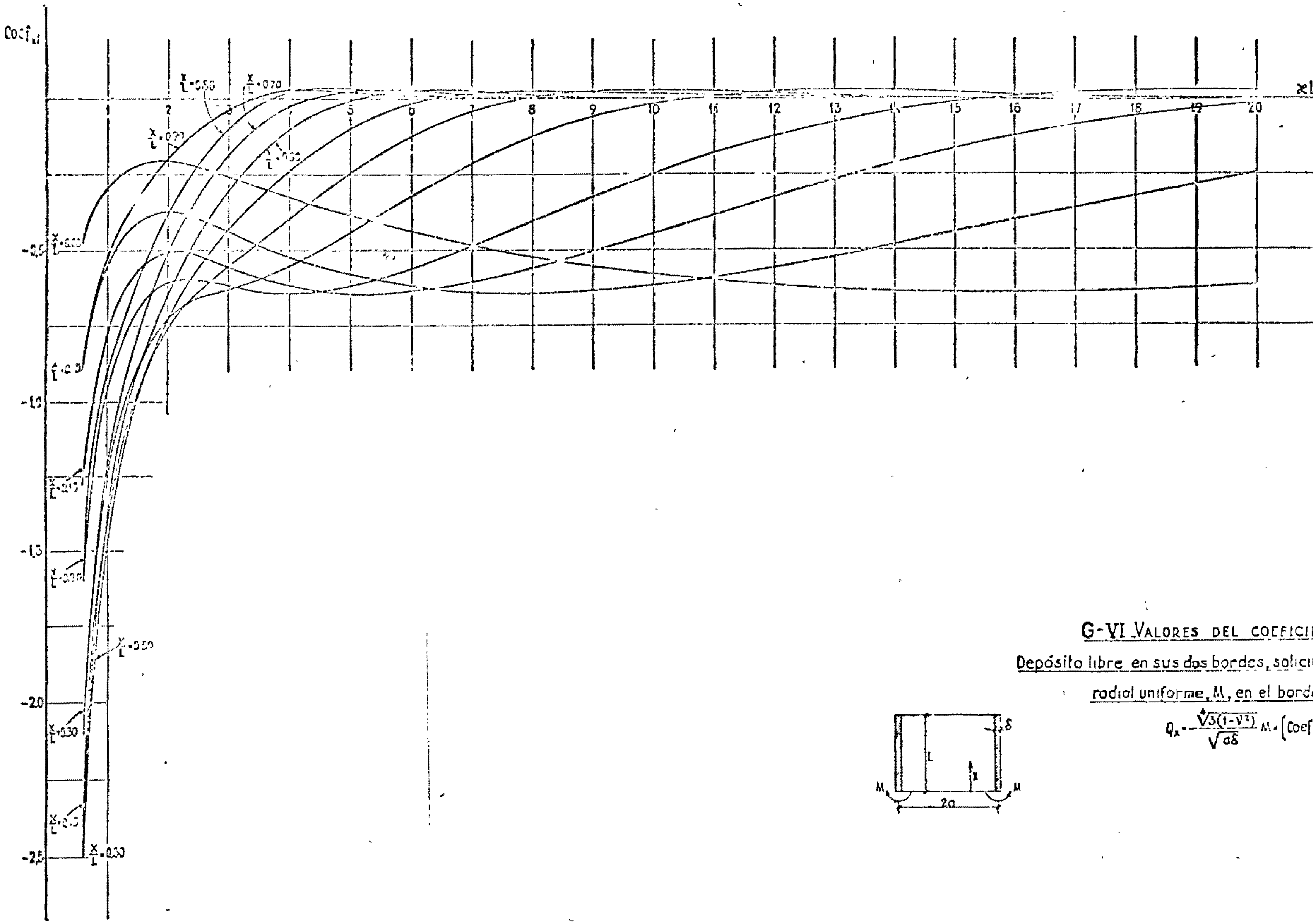

G-VI VALORES DEL COEFICIENTE COEF$_{VI}$

Depósito libre en sus dos bordes, solicitado por un momento radial uniforme, M, en el borde inferior

$$Q_x = -\frac{\sqrt[4]{3(1-\nu^2)}}{\sqrt{a\delta}}\, M \cdot \left(Coef_{VI}\right)$$

TABLA VI.

DEPOSITO LIBRE EN SUS DOS BORDES, SOLICITADO POR UN MOMENTO RADIAL UNIFORME, M, EN EL BORDE INFERIOR

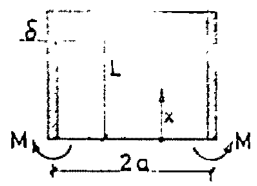

$$Q_x = -\frac{\sqrt[4]{3(1-\nu^2)}}{\sqrt{a\delta}} M \times \left[Coef_{VI}\right]$$

VALORES DEL COEFICIENTE $Coef_{VI}$.

VALORES DE 2.L	VALORES DE X/L												
	0	0.05	0.10	0.15	0.20	0.30	0.40	0.50	0.60	0.70	0.80	0.90	1.00
0.6	0	-0.4769	-0.9031	-1.2787	-1.6038	-2.1029	-2.4013	-2.4994	-2.3978	-2.0969	-1.5969	-0.8979	0
0.8		-0.3607	-0.6822	-0.9649	-1.2089	-1.5819	-1.8030	-1.8736	-1.7948	-1.5676	-1.1926	-0.6700	0
1.0	0	-0.2936	-0.5541	-0.7818	-0.9773	-1.2735	-1.4458	-1.4972	-1.4299	-1.2457	-0.9456	-0.5303	0
1.2	0	-0.2523	-0.4742	-0.6664	-0.8297	-1.0730	-1.2099	-1.2451	-1.1827	-1.0255	-0.7753	-0.4334	0
1.4	0	-0.2269	-0.4237	-0.5917	-0.7323	-0.9360	-1.0439	-1.0637	-1.0014	-0.8616	-0.6471	-0.3597	0
1.6	0	-0.2124	-0.3932	-0.5445	-0.6682	-0.8401	-0.9223	-0.9260	-0.8602	-0.7314	-0.5437	-0.2996	0
1.8	0	-0.2060	-0.3775	-0.5171	-0.6278	-0.7725	-0.8304	-0.8170	-0.7448	-0.6224	-0.4557	-0.2478	0
2.0	0	-0.2060	-0.3729	-0.5046	-0.6049	-0.7253	-0.7593	-0.7278	-0.6468	-0.5278	-0.3781	-0.2016	0
2.2	0	-0.2108	-0.3768	-0.5032	-0.5949	-0.6926	-0.7030	-0.6525	-0.5614	-0.4436	-0.3081	-0.1597	0
2.4	0	-0.2193	-0.3871	-0.5099	-0.5941	-0.6702	-0.6570	-0.5873	-0.4854	-0.3679	-0.2448	-0.1215	0
2.6	0	-0.2305	-0.4017	-0.5219	-0.5993	-0.6544	-0.6181	-0.5297	-0.4174	-0.2998	-0.1880	-0.0874	0
2.8	0	-0.2434	-0.4189	-0.5371	-0.6078	-0.6423	-0.5836	-0.4777	-0.3562	-0.2391	-0.1378	-0.0575	0
3.0	0	-0.2572	-0.4374	-0.5535	-0.6175	-0.6316	-0.5517	-0.4301	-0.3012	-0.1858	-0.0946	-0.0321	0
3.2	0	-0.2713	-0.4561	-0.5698	-0.6268	-0.6206	-0.5209	-0.3860	-0.2522	-0.1398	-0.0584	-0.0116	0
3.4	0	-0.2855	-0.4743	-0.5850	-0.6346	-0.6082	-0.4905	-0.3447	-0.2085	-0.1009	-0.0293	0.0043	0
3.6	0	-0.2993	-0.4915	-0.5986	-0.6402	-0.5939	-0.4598	-0.3060	-0.1700	-0.0686	-0.0067	0.0158	0
3.8	0	-0.3127	-0.5077	-0.6103	-0.6435	-0.5775	-0.4286	-0.2695	-0.1361	-0.0424	0.0100	0.0235	0
4.0	0	-0.3258	-0.5226	-0.6201	-0.6444	-0.5590	-0.3975	-0.2352	-0.1066	-0.0216	0.0217	0.0278	0
4.2	0	-0.3384	-0.5364	-0.6281	-0.6431	-0.5386	-0.3661	-0.2030	-0.0809	-0.0054	0.0291	0.0295	0
4.4	0	-0.3506	-0.5492	-0.6343	-0.6397	-0.5167	-0.3349	-0.1730	-0.0588	0.0068	0.0331	0.0291	0
4.6	0	-0.3626	-0.5610	-0.6390	-0.6345	-0.4936	-0.3042	-0.1451	-0.0399	0.0157	0.0344	0.0273	0
4.8	0	-0.3742	-0.5718	-0.6423	-0.6276	-0.4696	-0.2743	-0.1196	-0.0239	0.0219	0.0339	0.0245	0
5.0	0	-0.3855	-0.5818	-0.6442	-0.6194	-0.4451	-0.2454	-0.0963	-0.0106	0.0259	0.0320	0.0212	0
5.5	0	-0.4126	-0.6032	-0.6439	-0.5934	-0.3829	-0.1790	-0.0483	0.0125	0.0289	0.0242	0.0127	0
6.0	0	-0.4379	-0.6198	-0.6369	-0.5614	-0.3219	-0.1225	-0.0140	0.0242	0.0259	0.0157	0.0057	0
7.0	0	-0.4833	-0.6398	-0.6071	-0.4860	-0.2114	-0.0407	0.0212	0.0260	0.0142	0.0038	-0.0003	0
8.0	0	-0.5221	-0.6447	-0.5615	-0.4036	-0.1225	0.0048	0.0277	0.0164	0.0045	-0.0006	-0.0014	0
9.0	0	-0.5547	-0.6370	-0.5059	-0.3220	-0.0574	0.0242	0.0217	0.0070	-0.0001	-0.0012	-0.0006	0
10.0	0	-0.5816	-0.6191	-0.4451	-0.2461	-0.0141	0.0277	0.0129	0.0014	-0.0012	-0.0006	-0.0001	0
12.0	0	-0.6198	-0.5615	-0.3220	-0.1226	0.0242	0.0164	0.0014	-0.0012	-0.0004	0	0	0
14.0	0	-0.6398	[illegible]	-0.2114	-0.0407	0.0261	0.0047	-0.0012	-0.0004	0	0	0	0
16.0	0	-0.6447	-0.4036	-0.1226	0.0048	0.0164	-0.0004	-0.0007	0	0	0	0	0
18.0	0	-0.6370	-0.3220	[illegible]	0.0242	0.0070	-0.0012	-0.0001	0	0	0	0	0
20.0	0	-0.6191	-0.2461	-0.0141	0.0277	0.0014	-0.0007	0	0	0	0	0	0

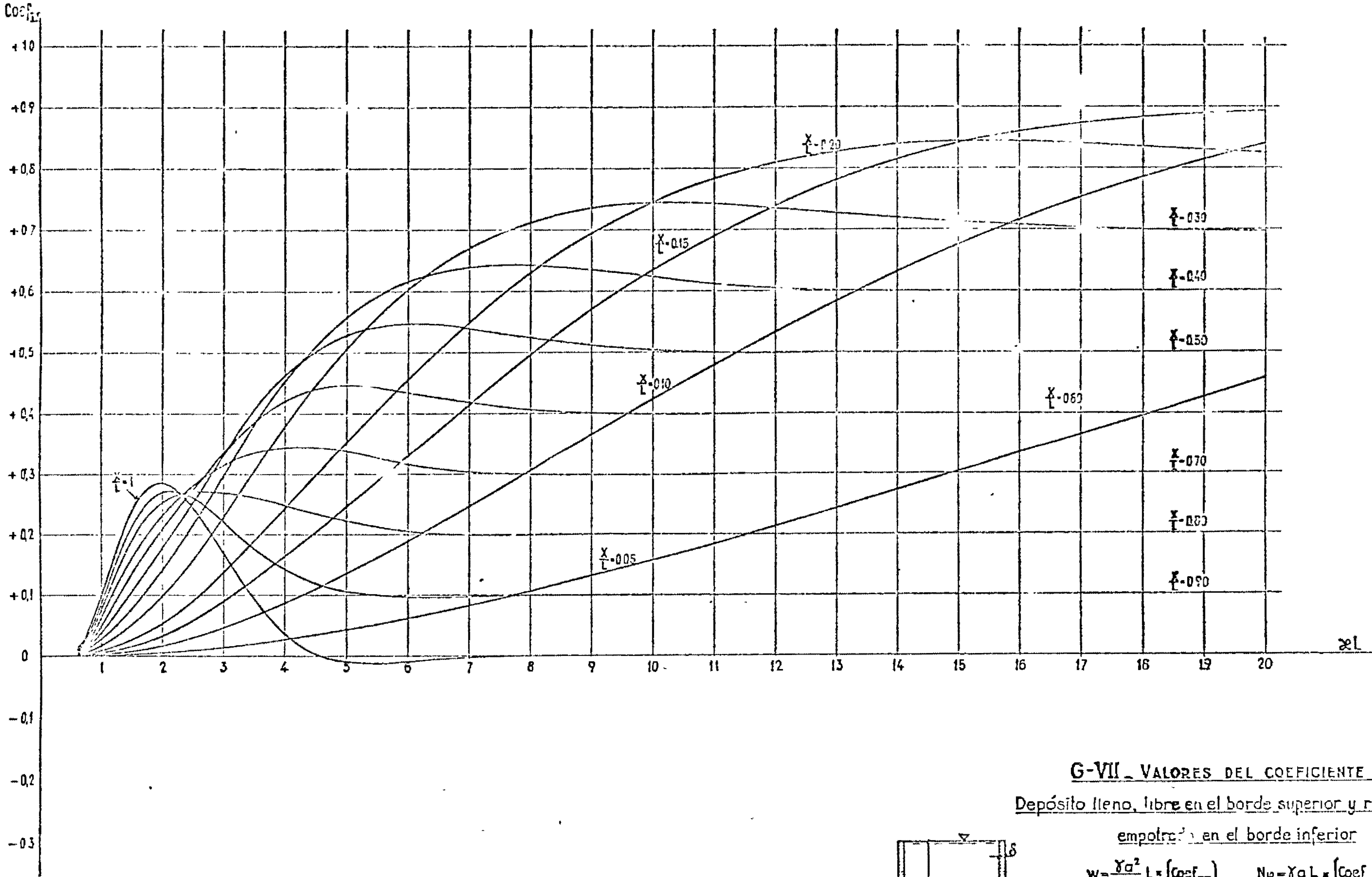

G-VII _ Valores del coeficiente Coef$_{VII}$

Depósito lleno, libre en el borde superior y rígidamente empotrado en el borde inferior

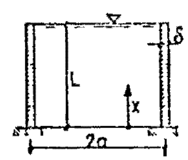

$w = \frac{\gamma a^2}{E\,\delta} L \times (\text{Coef}_{VII})$ $N_\varphi = \gamma a L \times (\text{Coef}_{VII})$

TABLA VII.

DEPOSITO LLENO, LIBRE EN EL BORDE SUPERIOR Y RIGIDAMENTE EMPOTRADO EN EL BORDE INFERIOR

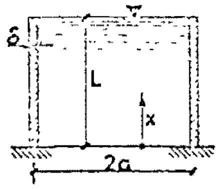

$= \frac{\gamma a^2}{E\,S} L_x \left[Coef_{VII}\right]$ $\quad N_\varphi = \gamma a L_x \left[Coef_{VII}\right]$

VALORES DEL COEFICIENTE $Coef_{VII}$

	VALORES DE X/L												
VALORES x^2/L	0	0.05	0.10	0.15	0.20	0.30	0.40	0.50	0.60	0.70	0.80	0.90	1.00
0.6	0	0.0001	0.0004	0.0009	0.0014	0.0026	0.0045	0.0064	0.0084	0.0104	0.0124	0.0145	0.0166
0.8	0	0.0003	0.0011	0.0024	0.0040	0.0082	0.0132	0.0186	0.0244	0.0302	0.0361	0.0421	0.0480
1.0	0	0.0006	0.0024	0.0052	0.0087	0.0176	0.0281	0.0395	0.0514	0.0634	0.0754	0.0875	0.0995
1.2	0	0.0011	0.0043	0.0091	0.0152	0.0303	0.0478	0.0665	0.0856	0.1047	0.1237	0.1425	0.1613
1.4	0	0.0018	0.0066	0.0138	0.0229	0.0499	0.0697	0.0954	0.1210	0.1459	0.1702	0.1941	0.2178
1.6	0	0.0025	0.0092	0.0192	0.0316	0.0607	0.0922	0.1236	0.1534	0.1814	0.2078	0.2333	0.2585
1.8	0	0.0034	0.0124	0.0255	0.0414	0.0778	0.1155	0.1508	0.1824	0.2101	0.2348	0.2579	0.2804
2.0	0	0.0044	0.0161	0.0328	0.0526	0.0970	0.1403	0.1781	0.2090	0.2332	0.2527	0.2694	0.2853
2.2	0	0.0057	0.0205	0.0414	0.0661	0.1187	0.1674	0.2066	0.2346	0.2527	0.2636	0.2706	0.2764
2.4	0	0.0072	0.0257	0.0514	0.0013	0.1431	0.1972	0.2366	0.2600	0.2696	0.2695	0.2642	0.2571
2.6	0	0.0089	0.0315	0.0623	0.0983	0.1701	0.2292	0.2680	0.2854	0.2849	0.2719	0.2523	0.2306
2.8	0	0.0108	0.0381	0.0753	0.1170	0.1990	0.2629	0.3001	0.3105	0.2987	0.2718	0.2370	0.1998
3.0	0	0.0129	0.0452	0.0887	0.1370	0.2292	0.2973	0.3322	0.3346	0.3110	0.2699	0.2199	0.1671
3.2	0	0.0152	0.0526	0.1030	0.1578	0.2601	0.3316	0.3632	0.3571	0.3215	0.2668	0.2023	0.1348
3.4	0	0.0176	0.0608	0.1178	0.1792	0.2910	0.3650	0.3924	0.3774	0.3303	0.2628	0.1852	0.1046
3.6	0	0.0201	0.0692	0.1330	0.2010	0.3214	0.3967	0.4191	0.3951	0.3371	0.2581	0.1693	0.0775
3.8	0	0.0228	0.0778	0.1486	0.2229	0.3511	0.4265	0.4430	0.4099	0.3419	0.2532	0.1550	0.0542
4.0	0	0.0256	0.0867	0.1645	0.2449	0.3799	0.4541	0.4540	0.4219	0.3448	0.2480	0.1426	0.0349
4.2	0	0.0265	0.0959	0.1806	0.2669	0.4075	0.4794	0.4819	0.4310	0.3459	0.2427	0.1321	0.0197
4.4	0	0.0315	0.1053	0.1969	0.2888	0.4340	0.5024	0.4971	0.4377	0.3456	0.2375	0.1234	0.0081
4.6	0	0.0346	0.1150	0.2134	0.3106	0.4593	0.5232	0.5096	0.4421	0.3441	0.2324	0.1164	-0.0003
4.8	0	0.0379	0.1249	0.2300	0.3322	0.4835	0.5419	0.5197	0.4445	0.3416	0.2276	0.1109	-0.0060
5.0	0	0.0413	0.1351	0.2465	0.3537	0.5065	0.5586	0.5277	0.4454	0.3383	0.2230	0.1066	-0.0095
5.5	0	0.0502	0.1614	0.2893	0.4053	0.5587	0.5923	0.5399	0.4424	0.3287	0.2132	0.1001	-0.0116
6.0	0	0.0598	0.1888	0.3319	0.4569	0.6034	0.6160	0.5438	0.4352	0.3189	0.2061	0.0976	-0.0090
7.0	0	0.0809	0.2460	0.4157	0.5498	0.6712	0.6398	0.5374	0.4166	0.3050	0.1991	0.0977	-0.0024
8.0	0	0.1042	0.3049	0.4952	0.6293	0.7133	0.6428	0.5241	0.4064	0.2991	0.1981	0.0991	0.0003
9.0	0	0.1293	0.3642	0.5684	0.6945	0.7352	0.6353	0.5120	0.4002	0.2931	0.1990	0.0999	0.0004
10.0	0	0.1560	0.4226	0.6339	0.7456	0.7430	0.6244	0.5039	0.3982	0.2938	0.1997	0.1001	0.0001
12.0	0	0.2130	0.5335	0.7400	0.8107	0.7356	0.6063	0.4003	0.3990	0.2999	0.2001	0.1000	0
14.0	0	0.2731	0.6324	0.8137	0.8384	0.7195	0.5993	0.4988	0.3999	0.3001	0.2000	0.1000	0
16.0	0	0.3348	0.7167	0.8594	0.8429	0.7070	0.5982	0.4997	0.4001	0.3000	0.2000	0.1000	0
18.0	0	0.3965	0.7855	0.8336	0.8359	0.7004	0.5990	0.5001	0.4000	0.3000	0.2000	0.1000	0
20.0	0	0.4572	0.8394	0.8926	0.8251	0.5983	0.5997	0.5001	0.4000	0.3000	0.2000	0.1000	0

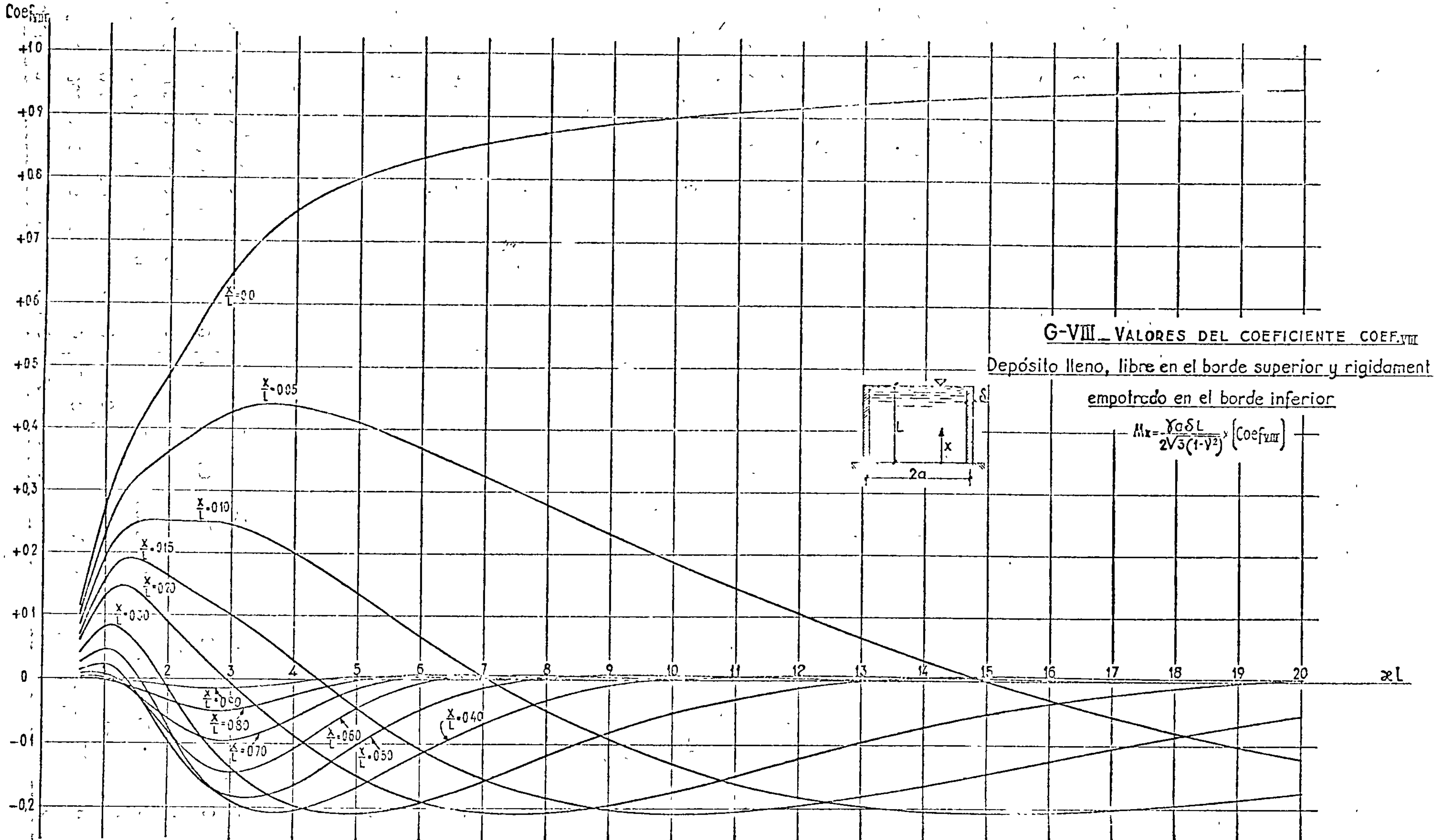
G-VIII – VALORES DEL COEFICIENTE COEF.VIII
Depósito lleno, libre en el borde superior y rigidament empotrado en el borde inferior
$M_x = \frac{\gamma a \delta L}{2\sqrt{3(1-\nu^2)}} \times (Coef_{VIII})$
$Coef_{VIII}$
+1.0
+0.9
+0.8
+0.7
+0.6
+0.5
+0.4
+0.3
+0.2
+0.1
0
-0.1
-0.2
$\varkappa L$
$\frac{x}{L}$ = 0.0
$\frac{x}{L}$ = 0.05
$\frac{x}{L}$ = 0.10
$\frac{x}{L}$ = 0.15
$\frac{x}{L}$ = 0.20
$\frac{x}{L}$ = 0.30
$\frac{x}{L}$ = 0.40
$\frac{x}{L}$ = 0.50
$\frac{x}{L}$ = 0.60
$\frac{x}{L}$ = 0.70
$\frac{x}{L}$ = 0.80
$\frac{x}{L}$ = 0.90
2a
L
x
δ

TABLA VIII

DEPOSITO LLENO LIBRE EN EL BORDE SUPERIOR Y RIGIDAMENTE EMPOTRADO EN EL BORDE INFERIOR

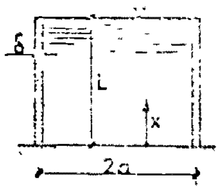

$$M_x = \frac{\gamma a \delta L}{2\sqrt{3(1-\nu^2)}} \times \left[Coef_{VIII} \right]$$

VALORES DEL COEFICIENTE $Coef_{VIII}$

VALORES DE $a^2/\delta L$	VALORES DE X/L												
	0	0.05	0.10	0.15	0.20	0.30	0.40	0.50	0.60	0.70	0.80	0.90	1.00
0.6	0.1164	0.0996	0.0844	0.0709	0.0589	0.0391	0.0243	0.0138	0.0069	0.0028	0.0007	0.0001	0
0.8	0.1949	0.1658	0.1397	0.1165	0.0960	0.0624	0.0377	0.0206	0.0095	0.0033	0.0006	-0.0001	0
1.0	0.2732	0.2290	0.1914	0.1573	0.1274	0.0793	0.0440	0.0213	0.0080	0.0011	-0.0010	-0.0006	0
1.2	0.3376	0.2792	0.2276	0.1825	0.1435	0.0819	0.0396	0.0132	-0.0007	-0.0055	-0.0047	-0.0018	0
1.4	0.3848	0.3108	0.2461	0.1901	0.1423	0.0690	0.0213	-0.0055	-0.0165	-0.0166	-0.0106	-0.0035	0
1.6	0.4210	0.3306	0.2522	0.1853	0.1290	0.0450	-0.0062	-0.0314	-0.0374	-0.0307	-0.0179	-0.0055	0
1.8	0.4535	0.3455	0.2528	0.1746	0.1096	0.0155	-0.0383	-0.0606	-0.0604	-0.0460	-0.0258	-0.0078	0
2.0	0.4864	0.3599	0.2522	0.1622	0.0885	-0.0154	-0.0711	-0.0900	-0.0831	-0.0609	-0.0333	-0.0099	0
2.2	0.5209	0.3749	0.2518	0.1499	0.0676	-0.0456	-0.1025	-0.1174	-0.1038	-0.0742	-0.0399	-0.0117	0
2.4	0.5560	0.3902	0.2516	0.1381	0.0476	-0.0737	-0.1307	-0.1412	-0.1211	-0.0848	-0.0450	-0.0130	0
2.6	0.5904	0.4048	0.2510	0.1265	0.0285	-0.0991	-0.1549	[illegible]	-0.1341	-0.0923	-0.0482	-0.0138	0
2.8	0.6227	0.4176	0.2492	0.1146	0.0103	-0.1215	-0.1745	-0.1743	-0.1424	-0.0961	-0.0495	-0.0140	0
3.0	0.6519	0.4278	0.2457	0.1021	-0.0073	-0.1409	-0.1894	-0.1829	-0.1458	-0.0964	-0.0488	-0.0136	0
3.2	0.6776	0.4351	0.2403	0.0889	-0.0243	-0.1574	-0.1998	-0.1865	-0.1446	-0.0934	-0.0463	-0.0127	0
3.4	0.6998	0.4395	0.2330	0.0749	-0.0409	-0.1711	-0.2060	-0.1856	-0.1395	-0.0876	-0.0423	-0.0113	0
3.6	0.7188	0.4413	0.2239	0.0602	-0.0570	-0.1823	-0.2085	-0.1809	-0.1313	-0.0797	-0.0373	-0.0097	0
3.8	0.7352	0.4409	0.2134	0.0451	-0.0725	-0.1913	-0.2081	-0.1733	-0.1208	-0.0704	-0.0316	-0.0079	0
4.0	0.7493	0.4387	0.2017	0.0297	-0.0875	-0.1983	-0.2051	-0.1634	-0.1080	-0.0603	-0.0256	-0.0060	0
4.2	0.7617	0.4350	0.1892	0.0142	-0.1017	-0.2035	-0.2001	-0.1521	-0.0961	-0.0500	-0.0197	-0.0042	0
4.4	0.7727	0.4301	0.1761	-0.0011	-0.1152	-0.2071	-0.1936	-0.1398	-0.0832	-0.0401	-0.0141	-0.0026	0
4.6	0.7827	0.4244	0.1626	-0.0163	-0.1278	-0.2093	-0.1858	-0.1271	-0.0706	-0.0308	-0.0091	-0.0011	0
4.8	0.7917	0.4180	0.1489	-0.0310	-0.1395	-0.2100	-0.1772	-0.1144	-0.0586	-0.0224	-0.0048	0.0001	0
5.0	0.8000	0.4111	0.1352	-0.0453	-0.1503	-0.2093	-0.1678	-0.1018	-0.0476	-0.0150	-0.0012	0.0010	0
5.5	0.8181	0.3918	0.1009	-0.0785	-0.1730	-0.2036	-0.1427	-0.0727	-0.0246	-0.0014	0.0045	0.0023	0
6.0	0.8333	0.3708	0.0676	-0.1078	-0.1897	-0.1922	-0.1169	-0.0480	-0.0086	0.0059	0.0065	0.0024	0
7.0	0.8571	0.3258	0.0056	-0.1543	-0.2071	-0.1587	-0.0695	-0.0136	0.0067	0.0084	0.0045	0.0012	0
8.0	0.8750	0.2792	-0.0484	-0.1852	-0.2070	-0.1198	-0.0332	0.0034	0.0088	0.0048	0.0014	0.0001	0
9.0	0.8889	0.2330	-0.0938	-0.2025	-0.1994	-0.0827	-0.0097	0.0080	0.0060	0.0016	-0.0001	-0.0002	0
10.0	0.9000	0.1883	-0.1307	-0.2084	-0.1737	-0.0514	0.0031	0.0082	0.0028	0	-0.0004	-0.0001	0
12.0	0.9167	0.1053	-0.1807	-0.1954	-0.1226	-0.0104	0.0089	0.0029	-0.0002	-0.0003	0	0	0
14.0	0.9286	0.0326	-0.2041	-0.1631	-0.0736	0.0062	0.0050	0	-0.0003	0	0	0	0
16.0	0.9375	-0.0283	-0.2073	-0.1240	-0.0358	0.0080	0.0014	-0.0004	-0.0001	0	0	0	0
18.0	0.9444	-0.0798	-0.1964	-0.0861	-0.0111	0.0052	-0.0002	-0.0002	0	0	0	0	0
20.0	0.9500	-0.1207	-0.1766	-0.0539	0.0025	0.0030	-0.0004	0	0	0	0	0	0

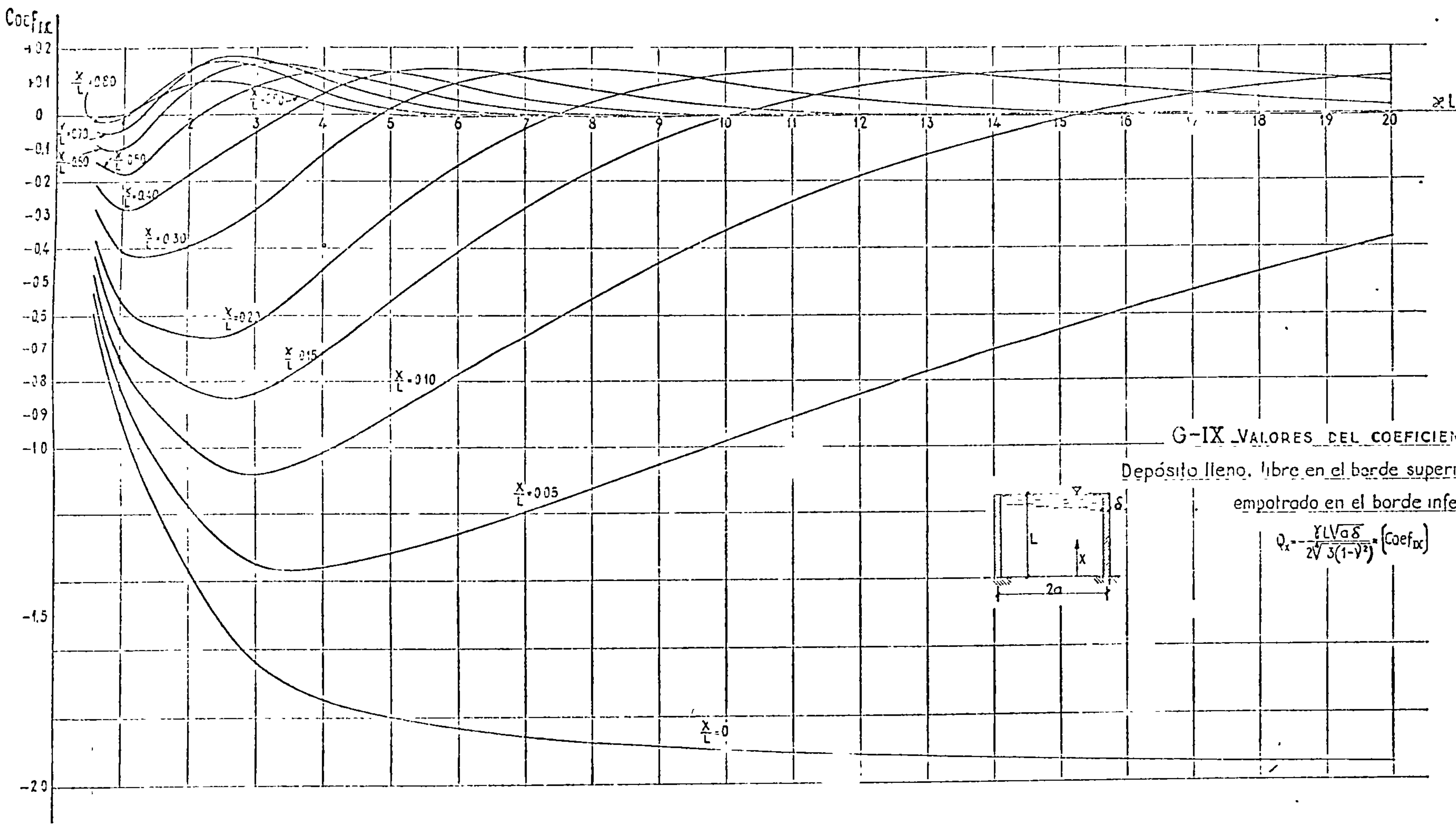

G-IX VALORES DEL COEFICIENTE COEF$_{IX}$

Depósito lleno, libre en el borde superior y rígidamente empotrado en el borde inferior

$$Q_x = -\frac{\gamma L\sqrt{a\delta}}{2\sqrt[4]{3(1-\nu^2)}} \cdot (\mathrm{Coef}_{IX})$$

TABLA IX.

DEPOSITO LLENO, LIBRE EN EL BORDE SUPERIOR Y RIGIDAMENTE EMPOTRADO EN EL BORDE INFERIOR

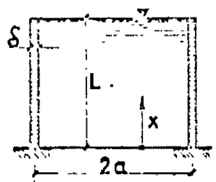

$$Q_x = -\frac{\gamma L \sqrt{a\delta}}{2\sqrt[4]{3(1-\nu^2)}} \times \left[Coef_{IX}\right]$$

VALORES DEL COEFICIENTE $Coef_{IX}$

VALORES DE $\varkappa L$	VALORES DE X/L												
	0	0.05	0.10	0.15	0.20	0.30	0.40	0.50	0.60	0.70	0.80	0.90	1.00
0.6	-0.5917	-0.5332	-0.4777	-0.4253	-0.3758	-0.2861	-0.2035	-0.1431	-0.0900	-0.0492	-0.0205	-0.0041	- 0
0.8	-0.7678	-0.6898	-0.6158	-0.5460	-0.4802	-0.3612	-0.2589	-0.1734	-0.1049	-0.0532	-0.0165	-0.0003	- 0
1.0	-0.9154	-0.8180	-0.7256	-0.6335	-0.5567	-0.4093	-0.2836	-0.1806	-0.0997	-0.0411	-0.0050	0.0087	0
1.2	-1.0321	-0.9151	-0.8044	-0.7002	-0.6026	-0.4280	-0.2814	-0.1631	-0.0733	-0.0122	0.0204	0.0245	0
1.4	-1.1263	-0.9898	-0.8609	-0.7398	-0.6268	-0.4262	-0.2603	-0.1294	-0.0337	0.0269	0.0527	0.0437	0
1.6	-1.2095	-1.0536	-0.9065	-0.7637	-0.6408	-0.4154	-0.2319	-0.0904	0.0092	0.0676	0.0853	0.0627	0
1.8	-1.2383	-1.1130	-0.9479	-0.7937	-0.6512	-0.4028	-0.2034	-0.0534	0.0534	0.0955	0.1037	0.1136	0
2.0	-1.3640	-1.1693	-0.9863	-0.8161	-0.6596	-0.3895	-0.1771	-0.0210	0.0813	0.1327	0.1354	0.0909	0
2.2	-1.4351	-1.2210	-1.0202	-0.8345	-0.6647	-0.3754	-0.1526	0.0067	0.1073	0.1537	0.1500	0.0984	0
2.4	-1.4994	-1.2660	-1.0477	-0.8468	-0.6647	-0.3587	-0.1288	0.0304	0.1266	0.1670	0.1573	0.1011	0
2.6	-1.5554	-1.3027	-1.06	-0.8518	-0.6582	-0.3383	-0.1048	0.0509	0.1402	0.1732	0.1581	0.0996	0
2.8	-1.6026	-1.3307	-1.0782	-0.8489	-0.6440	-0.3137	-0.0802	0.0689	0.1487	0.1733	0.1530	0.0943	0
3.0	-1.6414	-1.3502	-1.0811	-0.8384	-0.6240	-0.2854	-0.0549	0.0846	0.1530	0.1683	0.1433	0.0861	0
3.2	-1.6727	-1.3523	-1.0768	-0.8215	-0.5991	-0.2540	-0.0294	0.0981	0.1538	0.1593	0.1303	0.0759	0
3.4	-1.6978	-1.3684	-1.0667	-0.7993	-0.5692	-0.2207	-0.0042	0.1096	0.1517	0.1476	0.1152	0.0645	0
3.6	-1.7182	-1.3697	-1.0521	-0.7732	-0.5364	-0.1864	0.1865	0.0198	0.1190	0.1474	0.1342	0.0991	0
3.8	-1.7349	-1.3674	-1.0343	-0.7446	-0.5017	-0.1525	0.0422	0.1262	0.1414	0.1200	0.0830	0.0415	0
4.0	-1.7491	-1.3627	-1.0143	-0.7142	-0.4662	-0.1195	0.0625	0.1313	0.1340	0.1056	0.0676	0.0311	0
4.2	-1.7614	-1.3561	-0.9928	-0.6830	-0.4307	-0.0830	0.0803	0.1342	0.1256	0.0915	0.0535	0.0218	0
4.4	-1.7724	-1.3482	-0.9703	-0.6515	-0.3995	-0.0586	0.0955	0.1350	0.1165	0.0782	0.0409	0.0139	0
4.6	-1.7823	-1.3394	-0.9471	-0.6199	-0.3612	-0.0313	0.1081	0.1339	0.1070	0.0658	0.0300	0.0074	0
4.8	-1.7914	-1.3297	-0.9235	-0.5895	-0.3278	-0.0064	0.1181	0.1312	0.0972	0.0545	0.0208	0.0023	0
5.0	-1.7997	-1.3194	-0.8996	-0.5574	-0.2956	0.0152	0.1256	0.1269	0.0873	0.0442	0.0133	-0.0015	0
5.5	-1.8180	-1.2915	-0.8393	-0.4819	-0.2204	0.0626	0.1347	0.1111	0.0633	0.0237	0.0008	-0.0063	0
6.0	-1.8333	-1.2609	-0.7787	-0.4102	-0.1532	0.0958	0.1329	0.0912	0.0420	0.0095	-0.0050	-0.0059	0
7.0	-1.8571	-1.1940	-0.6597	-0.2800	-0.0431	0.1299	0.1093	0.0510	0.0117	-0.0039	-0.0059	-0.0033	0
8.0	-1.8750	-1.1230	-0.5467	-0.1595	0.0363	0.1331	0.0760	0.0207	-0.0024	-0.0056	-0.0029	-0.0005	0
9.0	-1.8889	-1.0537	-0.4470	-0.0791	0.0880	0.1100	0.0449	0.0032	-0.0053	-0.0034	-0.0007	0.0003	0
10.0	-1.9000	-0.9823	-0.3467	-0.0077	0.1193	0.0944	0.0214	-0.0043	-0.0046	-0.0012	0.0001	0.0002	0
12.0	-1.9157	-0.8423	-0.1859	0.0834	0.1333	0.0460	-0.0021	-0.0046	-0.0003	0.0002	0.0001	0	0
14.0	-1.9286	-0.7096	-0.0635	0.1258	0.1120	0.0132	-0.0057	-0.0013	0.0002	0.0001	0	0	0
16.0	-1.9375	-0.5064	0.0240	0.1334	0.0787	-0.0019	-0.0032	0.0001	0.0001	0	0	0	0
18.0	-1.9444	-0.4737	0.0820	0.1197	0.0470	-0.0058	-0.0009	0.0002	0	0	0	0	0
20.0	-1.9500	-0.3721	0.1160	0.0965	0.0227	-0.0047	0.0001	0.0001	0	0	0	0	0

G-X. Valores del coeficiente $COEF_x$

Depósito lleno, libre en el borde superior y con articulación fija en el borde inferior

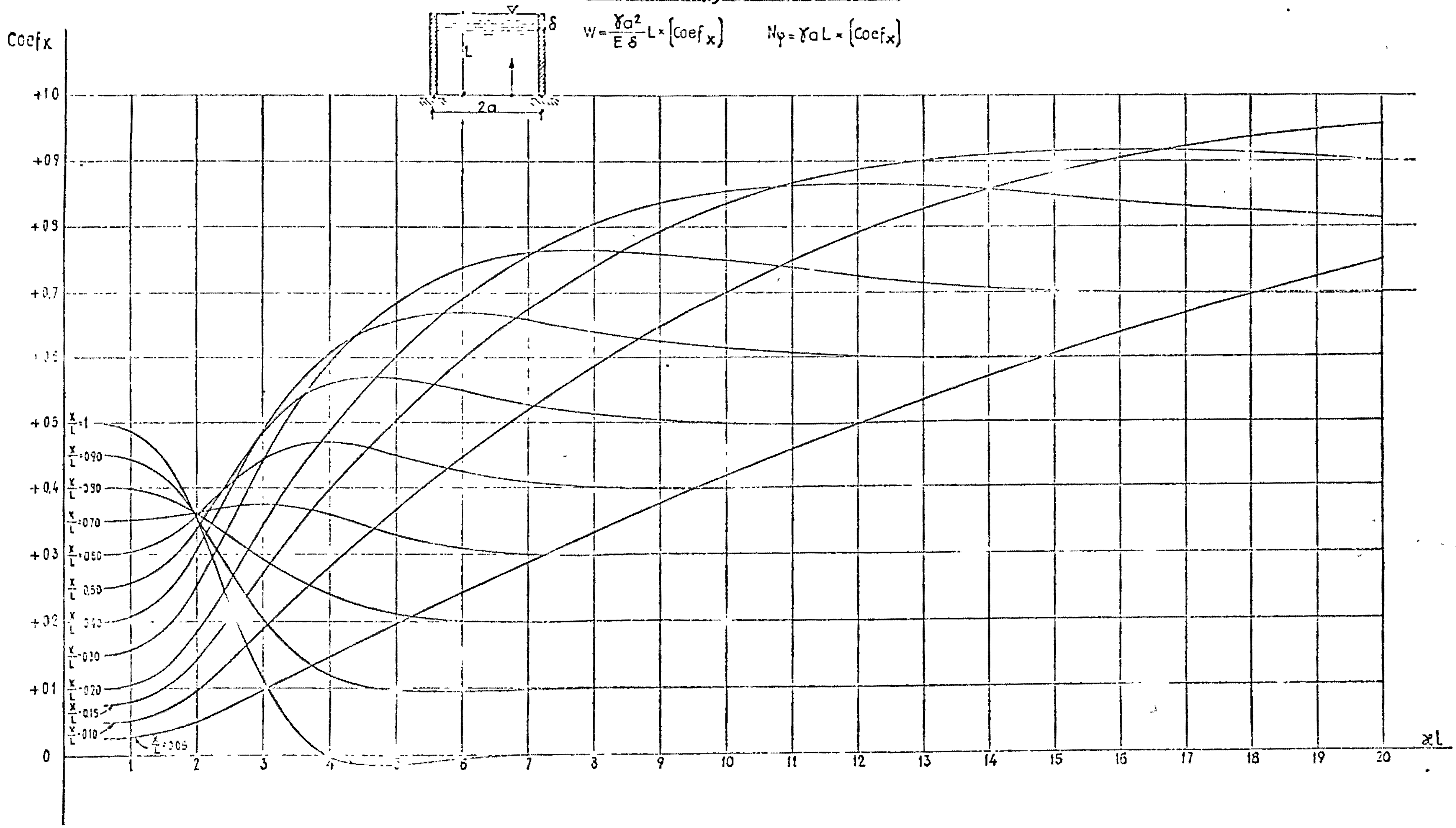

TABLA X.

DEPOSITO LLENO, LIBRE EN EL BORDE SUPERIOR Y CON ARTICULACION FIJA EN EL BORDE INFERIOR

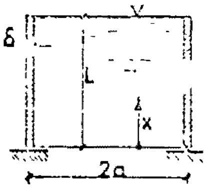

$$W=\frac{\gamma a^2}{E\delta} L \times [Coef_x] \qquad N_\varphi = \gamma a L \times [Coef_x]$$

VALORES DEL COEFICIENTE $Coef_x$

VALORES DE [illegible]	VALORES DE X/L												
	0	0.05	0.10	0.15	0.20	0.30	0.40	0.50	0.60	0.70	0.80	0.90	1.00
0.6	0	0.0252	0.0305	0.0757	0.1008	0.1511	0.2011	0.2509	0.3006	0.3501	0.3996	0.4490	0.4985
0.8	0	0.0258	0.0515	0.0771	0.1027	0.1533	0.20[illegible]	0.2529	0.3019	0.3505	0.3988	0.4470	0.4952
1.0	0	0.0269	0.0536	0.0802	0.1064	0.1580	0.2082	0.2569	0.3045	0.3511	0.3971	0.4427	0.4883
1.2	0	0.0288	0.0574	0.0855	0.1131	0.1664	0.2157	0.2641	0.3091	0.3522	0.3940	0.4352	0.4762
1.4	0	0.0316	0.0633	0.0940	0.1237	0.1795	0.2301	0.2755	0.3164	0.3539	0.3892	0.4234	0.4572
1.6	0	0.0363	0.0718	0.1062	0.1[illegible]	0.1984	0.2492	0.2916	0.3267	0.3564	0.3824	0.4065	0.4301
1.8	0	0.0421	0.0832	0.1224	0.1590	0.2233	0.2774	0.3127	0.3402	0.3594	0.3733	0.3843	0.3946
2.0	0	0.0494	0.0973	0.1425	0.1840	0.2539	0.3052	0.3384	0.3565	0.3630	0.3621	0.3574	0.3516
2.2	0	0.0579	0.1138	0.1658	0.2129	0.2892	0.3403	0.3675	0.3746	0.3667	0.3492	0.3269	0.3031
2.4	0	0.0674	0.1320	0.1915	0.2445	0.3275	0.3780	0.3982	0.3934	0.3702	0.3353	0.2946	0.2521
2.6	0	0.0774	0.1512	0.2186	0.2777	0.3669	0.4162	0.4286	0.4117	0.3730	0.3209	0.2623	0.2016
2.8	0	0.0877	0.1709	0.2461	0.3111	0.4060	0.4532	0.4577	0.4283	0.3748	0.3067	0.2316	0.1543
3.0	0	0.0980	0.1905	0.2733	0.3439	0.4435	0.4877	0.4837	0.4424	0.3754	0.2931	0.2037	0.1123
3.2	0	0.1083	0.2098	0.2999	0.3755	0.4786	0.5189	0.5062	0.4536	0.3746	0.2804	0.1794	0.0765
3.4	0	0.1184	0.2287	0.3256	0.4057	0.5110	0.5465	0.5247	0.4617	0.3724	0.2688	0.1589	0.0474
3.6	0	0.1283	0.2472	0.3504	0.4344	0.5406	0.5703	0.5395	0.4670	0.3691	0.2582	0.1421	0.0248
3.8	0	0.1381	0.2652	0.3743	0.4617	0.5676	0.5907	0.5508	0.4695	0.3647	0.2487	0.1288	0.0080
4.0	0	0.1477	0.2829	0.3976	0.4877	0.5922	0.6079	0.5590	0.4698	0.3595	0.2402	0.1184	-0.0038
4.2	0	0.1574	0.3003	0.4201	0.5125	0.6145	0.6222	0.5644	0.4682	0.3537	0.2327	0.1105	-0.0114
4.4	0	0.1669	0.3175	0.4420	0.5362	0.6347	0.6340	0.567[illegible]	0.4652	0.3476	0.2261	0.1048	-0.0150
4.6	0	0.1764	0.3345	0.4634	0.5589	0.6531	0.6436	0.5688	0.4611	0.3414	0.2203	0.1008	-0.0177
4.8	0	0.1859	0.3512	0.4842	0.5806	0.6697	0.6512	0.5685	0.4562	0.3353	0.2153	0.0980	-0.0178
5.0	0	0.1954	0.3677	0.5044	0.6014	0.6846	0.6571	0.5671	0.45[illegible]	0.3295	0.2110	0.0963	-0.0167
5.5	0	0.2190	0.4081	0.5526	0.6490	0.7153	0.6655	0.5597	0.4372	0.3168	0.2033	0.0949	-0.0116
6.0	0	0.2423	0.4470	0.5973	0.6909	0.7376	0.6670	0.5493	0.4248	0.3076	0.1991	0.0956	-0.0061
7.0	0	0.2880	0.5202	0.6759	0.7581	0.7618	0.6573	0.5263	0.4073	0.2965	0.1970	0.0982	-0.0002
8.0	0	0.3326	0.5870	0.7409	0.8059	0.7669	0.6407	0.5120	0.3993	0.2971	0.1983	0.0997	0.0008
9.0	0	0.3759	0.6473	0.7932	0.8376	0.7606	0.6245	0.5023	0.3971	0.2981	0.1995	0.1001	0.0003
10.0	0	0.4177	0.7012	0.6342	0.8563	0.7493	0.6120	0.4981	0.3976	0.2993	0.2001	0.1001	0
12.0	0	0.4970	0.7909	0.8876	0.8669	0.7245	0.5993	0.4976	0.3995	0.3001	0.2001	0.1000	0
14.0	0	0.5702	0.8581	0.9118	0.8573	0.7074	0.5971	0.4993	0.4001	0.3001	0.2000	0.1000	0
16.0	0	0.6369	0.9059	0.9169	0.8407	0.6993	0.5984	0.5000	0.4001	0.3000	0.2000	0.1000	0
18.0	0	0.6973	0.9376	0.9108	0.8245	0.6971	0.5995	0.5001	0.4000	0.3000	0.2000	0.1000	0
20.0	0	0.7512	0.9563	0.8993	0.8120	0.6976	0.6000	0.5000	0.4000	0.3000	0.2000	0.1000	0

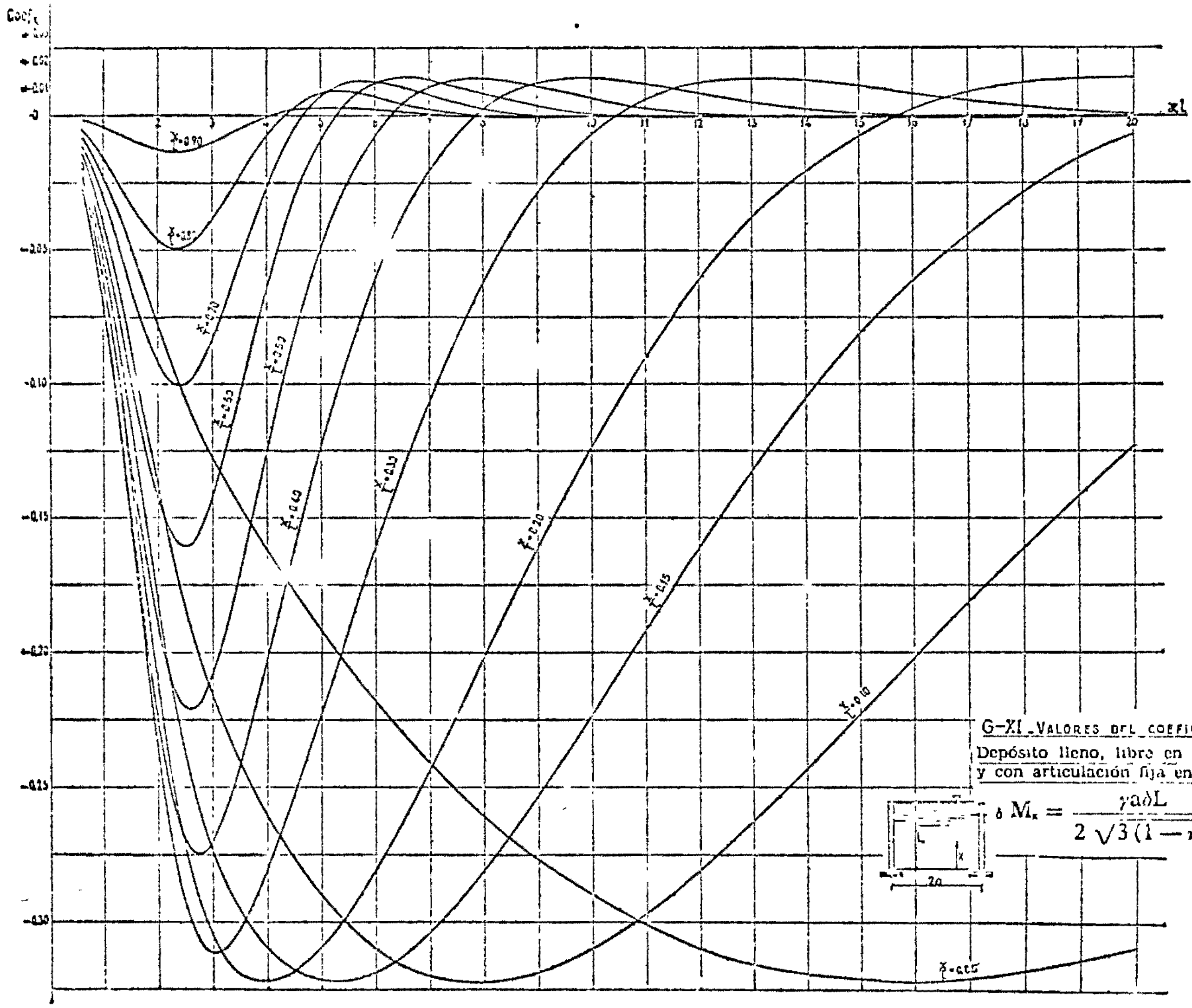

G-XI. VALORES DEL COEFICIENTE $COEF_{xl}$

Depósito lleno, libre en el borde superior y con articulación fija en el borde inferior

$$\delta M_x = \frac{\gamma a \delta L}{2\sqrt{3(1-\nu^2)}} \times [Coef_{xl}]$$

TABLA XI.

DEPOSITO LLENO, LIBRE EN EL BORDE SUPERIOR Y CON ARTICULACION FIJA EN EL BORDE INFERIOR

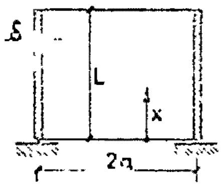

$$M_x = \frac{\gamma a \delta L}{2\sqrt{3(1-\nu^2)}} \times [\text{Coef}_{XI}]$$

VALORES DEL COEFICIENTE Coef XI

VALORES DE 2a.L	VALORES DE X/L: 0	0.05	0.10	0.15	0.20	0.30	0.40	0.50	0.60	0.70	0.80	0.90	1.00
0.6	0	−0.0081	−0.0146	−0.0195	−0.0230	−0.0264	−0.0259	−0.0224	−0.0172	−0.0113	−0.0057	−0.0016	0
0.8	0	−0.0144	−0.0258	−0.0345	−0.0407	−0.0467	−0.0458	−0.0397	−0.0305	−0.0200	−0.0101	−0.0029	0
1.0	0	−0.0223	−0.0400	−0.0535	−0.0632	−0.0724	−0.0708	−0.0614	−0.0471	−0.0308	−0.0157	−0.0044	0
1.2	0	−0.0318	−0.0570	−0.0761	−0.0897	−0.1026	−0.1002	−0.0867	−0.0664	−0.0434	−0.0220	−0.0062	0
1.4	0	−0.0425	−0.0761	−0.1014	−0.1194	−0.1361	−0.1325	−0.1143	−0.0873	−0.0570	−0.0288	−0.0081	0
1.6	0	−0.0542	−0.0967	−0.1265	−0.1509	−0.1712	−0.1659	−0.1425	−0.1084	−0.0706	−0.0356	−0.0100	0
1.8	0	−0.0662	−0.1178	−0.1560	−0.1825	−0.2057	−0.1980	−0.1690	−0.1279	[illegible]	−0.0416	−0.0116	0
2.0	0	−0.0782	−0.1385	−0.1826	−0.2126	−0.2374	−0.2264	−0.1916	−0.1439	−0.0925	−0.0462	−0.0128	0
2.2	0	−0.0898	−0.1579	−0.2071	−0.2397	−0.2643	−0.2491	−0.2084	−0.1548	−0.0987	−0.0488	−0.0134	0
2.4	0	−0.1005	−0.1756	−0.2286	−0.2626	−0.2853	−0.2647	−0.2163	−0.1599	−0.1006	−0.0492	−0.0134	0
2.6	0	−0.1104	−0.1913	−0.2469	−0.2811	−0.2998	−0.2730	−0.2210	−0.1590	−0.0983	−0.0474	−0.0127	0
2.8	0	−0.1194	−0.2050	−0.2619	−0.2952	−0.3082	−0.2744	−0.2171	−0.1527	−0.0924	−0.0436	−0.0115	0
3.0	0	−0.1276	−0.2169	−0.2742	−0.3055	−0.3113	−0.2699	−0.2077	−0.1420	−0.0835	−0.0383	−0.0099	0
3.2	0	−0.1353	−0.2274	−0.2842	−0.3128	−0.3101	−0.2600	−0.1943	−0.1282	−0.0726	−0.0321	−0.0079	0
3.4	0	−0.1425	−0.2369	−0.2924	−0.3175	−0.3056	−0.2486	−0.1781	−0.1125	−0.0608	−0.0255	−0.0059	0
3.6	0	−0.1494	−0.2455	−0.2991	−0.3204	−0.2987	−0.2341	−0.1604	−0.0961	−0.0487	−0.0188	−0.0040	0
3.8	0	−0.1560	−0.2534	−0.3046	−0.3217	−0.2901	−0.2183	−0.1422	−0.0799	[illegible]	−0.0126	−0.0022	0
4.0	0	−0.1625	−0.2607	−0.3085	−0.3218	−0.2803	−0.2018	−0.1242	−0.0644	−0.0263	−0.0070	−0.0006	0
4.2	0	−0.1688	−0.2676	−0.3134	−0.3210	−0.2696	−0.1853	−0.1069	−0.0500	−0.0166	−0.0023	0.0007	0
4.4	0	−0.1750	−0.2740	−0.3165	−0.3192	−0.2583	−0.1689	−0.0906	−0.0372	−0.0087	0.0016	0.0017	0
4.6	0	−0.1810	−0.2800	−0.3189	−0.3166	−0.2465	−0.1529	−0.0755	−0.0260	−0.0020	0.0045	0.0025	0
4.8	0	−0.1869	−0.2855	−0.3207	−0.3133	−0.2343	−0.1375	−0.0618	−0.0165	0.0033	0.0067	0.0029	0
5.0	0	−0.1926	−0.2906	−0.3218	−0.3093	−0.2222	−0.1228	−0.0494	−0.0085	0.0072	0.0080	0.0031	0
5.5	0	−0.2062	−0.3015	−0.3218	−0.2965	−0.1913	−0.0894	−0.0244	0.0052	0.0122	0.0087	0.0029	0
6.0	0	−0.2189	−0.3099	−0.3185	−0.2607	−0.1609	[illegible]	−0.0070	0.0119	0.0125	0.0071	0.0020	0
7.0	0	−0.2416	−0.3199	−0.3035	−0.2430	−0.1057	−0.0204	0.0106	0.0130	0.0073	0.0025	0.0004	0
8.0	0	−0.2610	−0.3223	−0.2807	−0.2018	−0.0613	0.0024	0.0138	0.0082	0.0024	−0.0001	−0.0003	0
9.0	0	−0.2773	−0.3185	−0.2529	−0.1610	−0.0287	0.0121	0.0109	0.0035	0	−0.0006	−0.0002	0
10.0	0	−0.2908	−0.3090	[illegible]	−0.1231	−0.0070	0.0139	0.0055	0.0007	−0.0006	−0.0003	−0.0001	0
12.0	0	−0.3090	−0.2807	[illegible]	−0.0612	0.0121	0.0082	0.0007	−0.0006	−0.0002	0	0	0
14.0	0	−0.3199	−0.2430	−0.1057	−0.0204	0.0131	0.0023	−0.0006	−0.0002	0	0	0	0
16.0	0	−0.3223	−0.2018	−0.0613	0.0024	0.0082	−0.0002	−0.0003	0	0	0	0	0
18.0	0	−0.3185	−0.1610	−0.0287	0.0121	0.0035	−0.0006	−0.0001	0	0	0	0	0
20.0	0	−0.3096	−0.1231	−0.0070	0.0139	0.0007	−0.0003	0	0	0	0	0	0

TABLA XII.

DEPOSITO LLENO, LIBRE EN EL BORDE SUPERIOR Y CON ARTICULACION FIJA E... BORDE INFERIOR

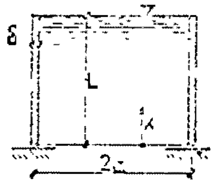

$$Q_x = -\frac{\gamma \sqrt{a \delta}\, L}{2\sqrt[4]{3(1-\nu^2)}} \times \left[Coef_{x_{II}}\right]$$

VALORES DEL COEFICIENTE $Coef_{x_{II}}$

VALORES DE λ.L	VALORES DE X/L												
	0	0.05	0.10	0.15	0.20	0.30	0.40	0.50	0.60	0.70	0.80	0.90	1.00
0.6	−0.2996	−0.2413	−0.1887	−0.1399	−0.0957	−0.0209	0.0360	0.0749	0.0958	0.0988	0.0838	0.0509	0
0.8	−0.3965	−0.3215	−0.2506	−0.1857	−0.1269	−0.0274	0.0481	0.0996	0.1272	0.1310	0.1110	0.0674	0
1.0	−0.4953	−0.3992	−0.3107	−0.2299	−0.1567	−0.0332	0.0602	0.1236	0.1575	0.1691	0.1371	0.0831	0
1.2	−0.5885	−0.4733	−0.3674	−0.2710	−0.1839	−0.0375	0.0724	0.1467	0.1859	0.1905	0.1609	0.0974	0
1.4	−0.6759	−0.5416	−0.4188	−0.3073	−0.2071	−0.0396	0.0849	0.1680	0.2111	0.2151	0.1811	0.1093	0
1.6	−0.7549	−0.6010	−0.4625	−0.3367	−0.2243	−0.0385	0.0976	0.1869	0.2318	0.2344	0.1961	0.1179	0
1.8	−0.8232	−0.6515	−0.4963	−0.3573	−0.2342	−0.0334	0.1107	0.2026	0.2468	0.2466	0.2046	0.1222	0
2.0	−0.8791	−0.6890	−0.5187	−0.3677	−0.2355	−0.0236	0.1239	0.2146	0.2552	0.2510	0.2058	0.1218	0
2.2	−0.9221	−0.7140	−0.5294	−0.3678	−0.2230	−0.0034	0.1372	0.2227	0.2568	0.2473	0.1995	0.1166	0
2.4	−0.9530	−0.7271	−0.5291	−0.3581	−0.2125	0.0089	0.1503	0.2269	0.2521	0.2362	0.1865	0.1072	0
2.6	−0.9737	−0.7303	−0.5196	−0.3403	−0.1905	0.0301	0.1628	0.2277	0.2420	0.2193	0.1634	0.0946	0
2.8	−0.9864	−0.7257	−0.5031	−0.3166	−0.1639	0.0531	0.1743	0.2255	0.2280	0.1983	0.1470	0.0801	0
3.0	−0.9935	−0.7158	−0.4817	−0.2891	−0.1345	0.0765	0.1845	0.2209	0.2115	0.1752	0.1241	0.0648	0
3.2	−0.9970	−0.7025	−0.4576	−0.2595	−0.1040	0.0993	0.1929	0.2144	0.1935	0.1514	0.1013	0.0499	0
3.4	−0.9986	−0.6873	−0.4321	−0.2293	−0.0736	0.1206	0.1994	0.2064	0.1751	0.1283	0.0798	0.0362	0
3.6	−0.9991	−0.6714	−0.4063	−0.1994	−0.0443	0.1398	0.2037	0.1971	0.1568	0.1067	0.0604	0.0241	0
3.8	−0.9992	−0.6551	−0.3807	−0.1704	−0.0165	0.1567	0.2059	0.1868	0.1391	0.0870	0.0435	0.0140	0
4.0	−0.9992	−0.6390	−0.3557	−0.1426	0.0095	0.1710	0.2058	0.1757	0.1222	0.0695	0.0293	0.0056	0
4.2	−0.9993	−0.6231	−0.3314	−0.1161	0.0336	0.1828	0.2038	0.1638	0.1062	0.0543	0.0178	−0.0004	0
4.4	−0.9993	−0.6074	−0.3078	−0.0910	0.0557	0.1921	0.1998	0.1515	0.0913	0.0411	0.0086	−0.0049	0
4.6	−0.9994	−0.5919	−0.2849	−0.0671	0.0759	0.1991	0.1941	0.1388	0.0775	0.0300	0.0017	−0.0076	0
4.8	−0.9996	−0.5767	−0.2627	−0.0446	0.0943	0.2039	0.1871	0.1260	0.0648	0.0207	−0.0033	−0.0095	0
5.0	−0.9997	−0.5616	−0.2412	−0.0234	0.1110	0.2068	0.1788	0.1133	0.0532	0.0131	−0.0066	−0.0103	0
5.5	−0.9999	−0.5247	−0.1902	0.0247	0.1458	0.2067	[illegible]	0.0829	0.0292	0	−0.0105	−0.0092	0
6.0	−1.0000	−0.4888	−0.1430	0.0658	0.1716	0.1966	0.1282	0.0561	0.0119	−0.0065	−0.0098	−0.0063	0
7.0	−1.0000	−0.4203	−0.0599	0.1294	0.2011	0.1675	0.0777	0.0177	−0.0057	−0.0080	−0.0049	−0.0014	0
8.0	−1.0000	−0.3564	0.0093	0.1716	0.2077	0.1282	0.0383	−0.0019	−0.0059	−0.0051	−0.0017	0.0004	0
9.0	−1.0000	−0.2968	0.0657	0.1962	0.1985	0.0895	0.0124	−0.0085	−0.0054	−0.0018	0.0002	0.0004	0
10.0	−1.0000	−0.2415	0.1106	0.2068	0.1794	0.0563	−0.0019	−0.0084	−0.0031	−0.0001	0.0004	0.0001	0
12.0	−1.0000	−0.1431	0.1716	0.1935	0.1282	0.0124	−0.0089	−0.0031	0.0001	0.0003	0.0001	0	0
14.0	−1.0000	−0.0599	0.2011	0.1675	[illegible]	−0.0057	−0.0052	−0.0001	0.0003	0	0	0	0
16.0	−1.0000	0.0093	0.2077	0.1282	0.0383	−0.0089	−0.0015	0.0004	0.0001	0	0	0	0
18.0	−1.0000	0.0657	0.1985	0.0895	0.0124	−0.0064	0.0001	0.0002	0	0	0	0	0
20.0	−1.0000	0.1108	0.1794	0.0563	−0.0019	−0.0031	0.0004	0	0	0	0	0	0

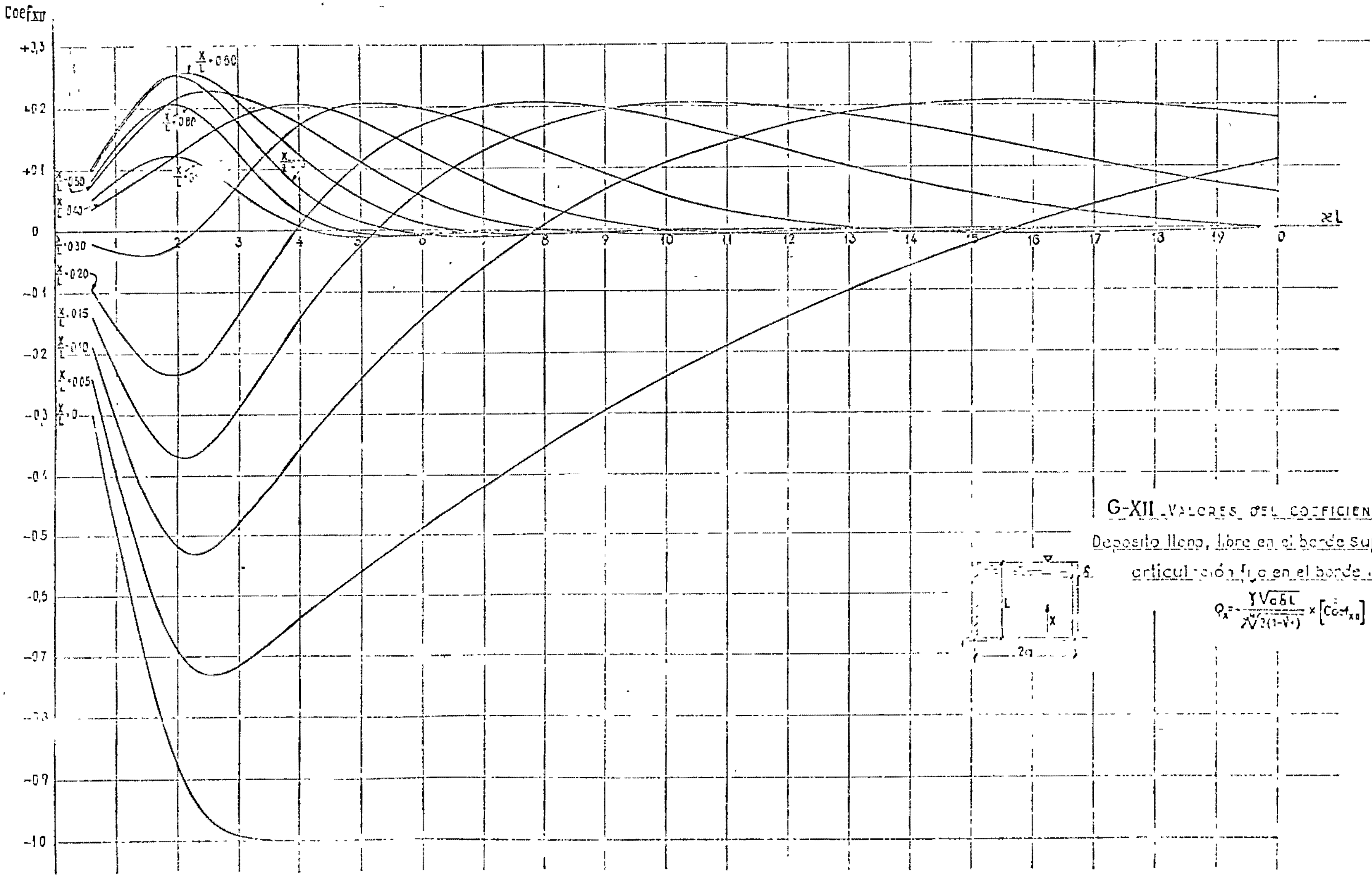

G-XII VALORES DEL COEFICIENTE $Coef_{XII}$

Deposito lleno, libre en el borde superior y con articulación fija en el borde inferior

$$Q_x = -\frac{\gamma\sqrt{a\delta L}}{\sqrt[4]{3(1-\nu^2)}} \times \left[Coef_{XII}\right]$$

"Cascarones: Teoría general de flexión"

DR. ISAIAS GARCIA TERRAZAS

Ref. A. Kalnins

Entendemos por cascarón un cuerpo tri-dimensional tal que una de sus dimensiones denominada ".espesor" es sustancialmente menor que las otras dos.

Para describir los cascarones se ha optado por el sistema coordenado sobre la "superficie de referencia del cascarón", tal que la tercera coordenada es siempre perpendicular a la sup. de referencia, mientras que las otras dos coordenadas estan contenidas en la sup. de referencia. El espesor se mide siempre en la direcciòn de la 3ª coordenada, y se hace la suposición de que el espesor permanece constante bajo cualquier condición de carga. La segunda hipotesis consiste, consiste en suponer que los puntos que originalmente coinsidian sobre una perpendicular a la superficie media, seguiran en linea recta despues de sufrir el cascarón una deformación bajo carga.

Con estas hipotesis se define que el campo de desplazamientos tiene cinco componentes; tres desplazamientos u_1, u_2 y u_3 y dos giros β_1 y β_2 que se miden en la superficie de referencia.

Con esta geometría y este campo de desplazamientos pueden definirse las deformaciones unitarias, que para este caso se han dividido en diez componentes.

Una tercera hipotesis consiste en asociar a la sup. de referencia todas las solicitaciones de carga externas así como las resultantes de esfuerzos de tal forma que las condiciones de equilibrio se establecen para un elemento diferencial de la sup. de referencia del cascarón.

Se obtienen seis ecuaciones de equilibrio; tres de equilibrio de fuerzas en las tres direcciones coordenadas del cascarón, y tres ecuaciones de equilibrio de momentos también en las direcciones de las coordenadas. De estas, la ecuación de equilibrio de momentos en la dirección normal del cascarón, resulta carente de significado debido a la primera hipotesis que reduce el orden de la ecuación diferencial que gobierna el comportamiento del cascarón. Por lo cual el problema es resuelto sin tomar en cuenta ésta consideración de equilibrio la cual es satisfecha a posteriori, esto es, conocidos M_{12}, M_{21}, N_{12}, N_{21} se encuentra m_3 que es un par aplicado tangencialmente a la sup. de referencia.

Hemos propuesto hasta ahora 25 incognita que aparecen en la teoría general de cascarones, a saber

5 - desplazamientos: u_1, u_2, u_3, β_1, y β_2

10 - deformaciones: ϵ_{11}, ϵ_{22}, γ_1, γ_2, k_{11}, k_{22}, δ_1, δ_2, γ_{13}, y γ_{23}

10 - resultantes de esfuerzos: N_{11}, N_{22}, N_{12}, N_{21}, M_{11}, M_{22}, M_{12}, M_{21}, Q_1 y Q_2

Para resolver para estas incognitas hemos propuest

2'

where we have defined

$$\varepsilon_{11} = \underset{\sim}{u}_{,1} \cdot \underset{\sim}{t}_1/\alpha_1 = u_{1,1}/\alpha_1 + \alpha_{1,2}u_2/\alpha_1\alpha_2 + u_3/R_1 \qquad (2.20a)$$

$$\varepsilon_{22} = \underset{\sim}{u}_{,2} \cdot \underset{\sim}{t}_2/\alpha_2 = u_{2,2}/\alpha_2 + \alpha_{2,1}u_1/\alpha_1\alpha_2 + u_3/R_2 \qquad (2.20b)$$

$$\gamma_1 = \underset{\sim}{u}_{,1} \cdot \underset{\sim}{t}_2/\alpha_1 = u_{2,1}/\alpha_1 - \alpha_{1,2}u_1/\alpha_1\alpha_2 \qquad (2.20c)$$

$$\gamma_2 = \underset{\sim}{u}_{,2} \cdot \underset{\sim}{t}_1/\alpha_2 = u_{1,2}/\alpha_2 - \alpha_{2,1}u_2/\alpha_1\alpha_2 \qquad (2.20d)$$

$$k_{11} = \underset{\sim}{\beta}_{,1} \cdot \underset{\sim}{t}_1/\alpha_1 = \beta_{1,1}/\alpha_1 + \alpha_{1,2}\beta_2/\alpha_1\alpha_2 \qquad (2.20e)$$

$$k_{22} = \underset{\sim}{\beta}_{,2} \cdot \underset{\sim}{t}_2/\alpha_2 = \beta_{2,2}/\alpha_2 + \alpha_{2,1}\beta_1/\alpha_1\alpha_2 \qquad (2.20f)$$

$$\delta_1 = \underset{\sim}{\beta}_{,1} \cdot \underset{\sim}{t}_2/\alpha_1 = \beta_{2,1}/\alpha_1 - \alpha_{1,2}\beta_1/\alpha_1\alpha_2 \qquad (2.20g)$$

$$\delta_2 = \underset{\sim}{\beta}_{,2} \cdot \underset{\sim}{t}_1/\alpha_2 = \beta_{1,2}/\alpha_2 - \alpha_{2,1}\beta_2/\alpha_1\alpha_2 \qquad (2.20h)$$

$$\gamma_{13} = (\underset{\sim}{u}_{,1} \cdot \underset{\sim}{t}_3 + \underset{\sim}{\beta} \cdot \alpha_1\underset{\sim}{t}_1)/\alpha_1$$

$$= u_{3,1}/\alpha_1 - u_1/R_1 + \beta_1 \qquad (2.20i)$$

$$\gamma_{23} = (\underset{\sim}{u}_{,2} \cdot \underset{\sim}{t}_3 + \underset{\sim}{\beta} \cdot \alpha_2\underset{\sim}{t}_2)/\alpha_2$$

$$= u_{3,2}/\alpha_2 - u_2/R_2 + \beta_2 \qquad (2.20j)$$

This completes the derivation of the physical components of the three-dimensional strain tensor for a shell. Clearly, Eqs. (2.19) are no longer exact for a three-dimensional medium, because the restrictive assumptions given by Eqs.(2.14) and (2.16) have been employed.

hasta ahora quince ecuaciones: cinco ecuaciones de equilibrio y diez definiciones de deformaciones unitarias en función de los desplazamientos. Es necesario para completar el planteamiento del problema otras diez ecuaciones. Estas ecuaciones restantes constituyen la ley carga-deformación y relacionan las resultantes de esfuerzos con las deformaciones unitarias.

De teoría de elasticidad conocemos las relaciones

$$e_{11} = \frac{\sigma_{11}}{E_1} - \nu_{12}\frac{\sigma_{22}}{E_2} - \nu_{13}\frac{\sigma_{33}}{E_3} + a_1 T$$

$$e_{22} = -\nu_{21}\frac{\sigma_{11}}{E_1} + \frac{\sigma_{22}}{E_2} - \nu_{23}\frac{\sigma_{33}}{E_3} + a_2 T$$

$$e_{33} = -\nu_{31}\frac{\sigma_{11}}{E_1} - \nu_{32}\frac{\sigma_{22}}{E_2} + \frac{\sigma_{33}}{E_3} + a_3 T$$

$$2\, e_{12} = \frac{\sigma_{12}}{G_{12}}$$

$$2\, e_{23} = \frac{\sigma_{23}}{G_{23}}$$

$$2\, e_{13} = \frac{\sigma_{13}}{G_{13}}$$

Puesto que hemos aceptado que el espesor permanece constante, estamos implícitamente aceptando que e_{33} es nulo lo que quiere decir que estamos tratando con un material ortotrópico en el cual $\nu_{31} = \nu_{32} = \frac{1}{E_3} = a_3 = 0$

Dadas estas restricciones es posible hacer la transformación entre los esfuerzos elásticos y las resultantes de esfuerzos consideradas en teoría de cascarones, y la transformación entre las deformaciones unitarias elásticas y las componentes de deformacion que aquí hemos definido y obtener las relaciones carga-deformación,

Para interpretar estas relaciones es necesario definir algunas constantes acontinuacion:

$$A_1 = a_1 + \nu_{12} a_2$$
$$A_2 = a_2 + \nu_{21} a_1$$
$$B_{11} = E_1 / (1 - \nu_{12}\nu_{21})$$
$$B_{12} = \nu_{12} E_1 / (1 - \nu_{12}\nu_{21}) = \nu_{12} E_2 / (1 - \nu_{12}\nu_{21})$$
$$B_{22} = E_2 / (1 - \nu_{12}\nu_{21})$$

donde a_1, a_2 son coeficientes de expansión térmica

$E_1, E_2,$ son módulos de elasticidad

ν_{12}, ν_{21} son coeficientes de Poisson

los subindices indican la dirección

$$S_{12} = \frac{1 + \frac{\xi_3}{R_1}}{1 + \frac{\xi_3}{R_2}}$$

$$S_{21} = \frac{1}{S_{12}}$$

ξ_3 = coordenada normal; R_i = radios principales de curvatura

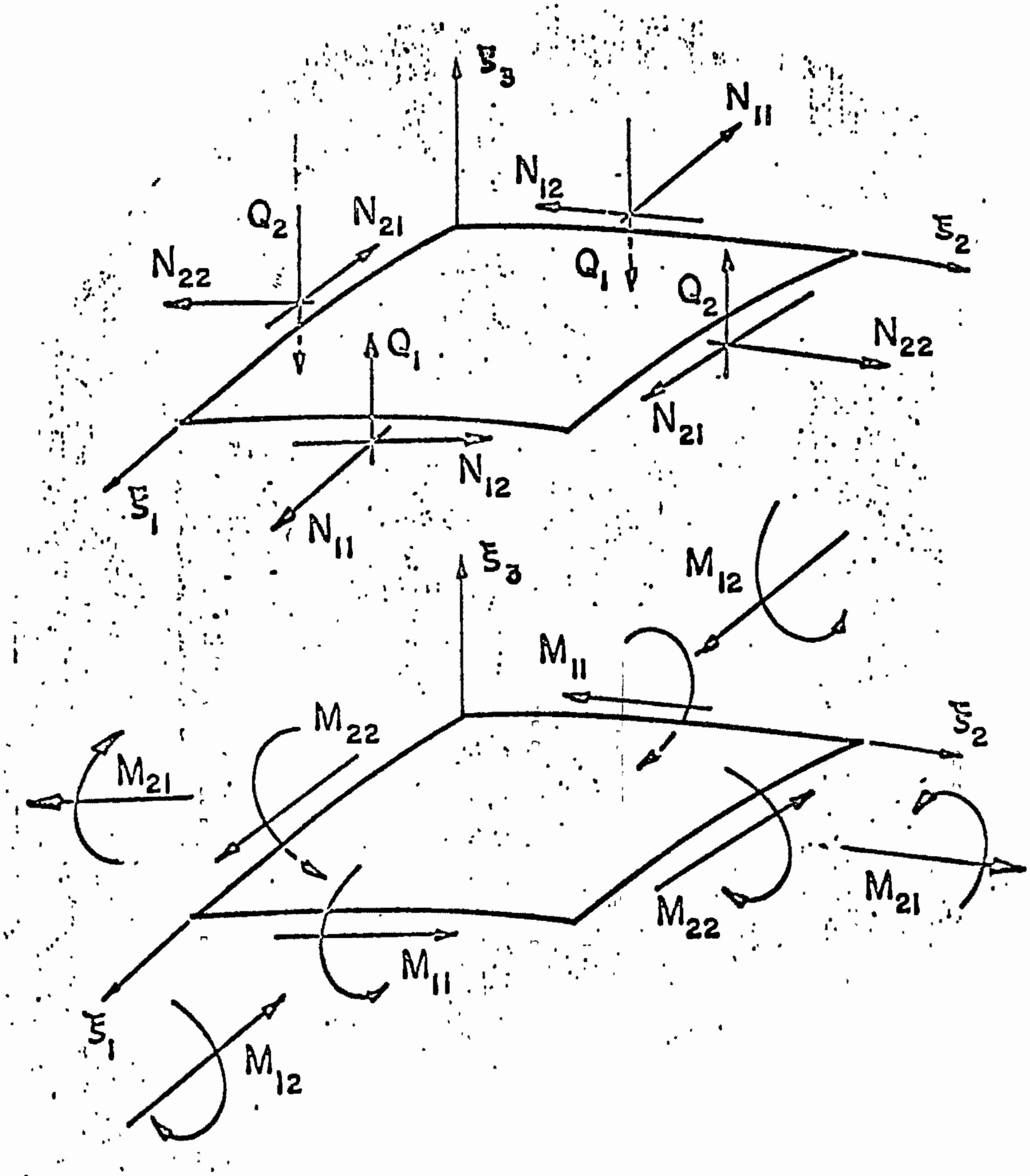

Figure 8. Stress-resultants of a Shell.

$$H_1 = \int A_1 T (1 + \xi_3/R_2)\, d\xi_3$$

$$H_2 = \int A_2 T (1 + \xi_3/R_1)\, d\xi_3$$

$$H_3 = \int A_1 T (1 + \xi_3/R_2)\, \xi_3\, d\xi_3$$

$$H_4 = \int A_2 T (1 + \xi_3/R_1)\, \xi_3\, d\xi_3$$

Otras definiciones necesarias en la descripción de la teoría son:

ξ_1, ξ_2 coordenadas en las direcciones principales

α_1, α_2 métrica del cascarón en la sup. de referencia

$\ddot{u}$ los puntos indican derivadas respecto al tiempo, en esto caso $\ddot{u} = \dfrac{d^2 u}{d t^2}$

where again the common multiplier $d\xi_1 d\xi_2$ has been cancelled and infinitesimals of third order neglected.

Substituting the stress-resultant, surface load, and displacement vectors, resolved along the unit tangent vectors $\underset{\sim}{t}_i$, into Eqs. (3.17) and (3.20), making use of Eqs. (1.19), and then setting each component of Eqs. (3.17) and (3.20) along the unit tangent vectors equal to zero, six equations of equilibrium are obtained which can be written as

$$(\alpha_2 N_{11})_{,1} + (\alpha_1 N_{21})_{,2} + \alpha_{1,2} N_{12} - \alpha_{2,1} N_{22}$$

$$+ \alpha_1\alpha_2 Q_1/R_1 + \alpha_1\alpha_2 p_1 = \alpha_1\alpha_2(b_1\ddot{u}_1 + b_2\ddot{\beta}_1) \qquad (3.21a)$$

$$(\alpha_2 N_{12})_{,1} + (\alpha_1 N_{22})_{,2} + \alpha_{2,1} N_{21} - \alpha_{1,2} N_{11}$$

$$+ \alpha_1\alpha_2 Q_2/R_2 + \alpha_1\alpha_2 p_2 = \alpha_1\alpha_2(b_1\ddot{u}_2 + b_2\ddot{\beta}_2) \qquad (3.21b)$$

$$(\alpha_2 Q_1)_{,1} + (\alpha_1 Q_2)_{,2} - \alpha_1\alpha_2(N_{11}/R_1 + N_{22}/R_2)$$

$$+ \alpha_1\alpha_2 p_3 = \alpha_1\alpha_2 b_1\ddot{u}_3 \qquad (3.21c)$$

$$(\alpha_2 M_{11})_{,1} + (\alpha_1 M_{21})_{,2} + \alpha_{1,2} M_{12} - \alpha_{2,1} M_{22}$$

$$- \alpha_1\alpha_2 Q_1 + \alpha_1\alpha_2 m_1 = \alpha_1\alpha_2(b_2\ddot{u}_1 + b_3\ddot{\beta}_1) \qquad (3.21d)$$

$$(\alpha_2 M_{12})_{,1} + (\alpha_1 M_{22})_{,2} + \alpha_{2,1} M_{21} - \alpha_{1,2} M_{11}$$

$$- \alpha_1\alpha_2 Q_2 + \alpha_1\alpha_2 m_2 = \alpha_1\alpha_2(b_2\ddot{u}_2 + b_3\ddot{\beta}_2) \qquad (3.21e)$$

$$N_{12} - N_{21} + M_{12}/R_1 - M_{21}/R_2 + m_3 = 0 \qquad (3.22)$$

The relations between the stress-resultants and the strain can now be derived by substituting the components of strain defined by Eqs. (2.19) into Eqs. (4.5) and (4.2), and the components of stress into the definitions of stress-resultants given by Eqs. (3.10). This procedure yields

$$N_{11} = C_{11}\varepsilon_{11} + C_{12}\varepsilon_{22} + E_{11}k_{11} + E_{12}k_{22} + H_1 \tag{4.7a}$$

$$N_{22} = C_{12}\varepsilon_{11} + C_{22}\varepsilon_{22} + E_{12}k_{11} + E_{22}k_{22} + H_2 \tag{4.7b}$$

$$M_{11} = E_{11}\varepsilon_{11} + E_{12}\varepsilon_{22} + D_{11}k_{11} + D_{12}k_{22} + H_3 \tag{4.7c}$$

$$M_{22} = E_{12}\varepsilon_{11} + E_{22}\varepsilon_{22} + D_{12}k_{11} + D_{22}k_{22} + H_4 \tag{4.7d}$$

$$N_{12} = F_{11}\gamma_1 + F_{12}\gamma_2 + J_{11}\delta_1 + J_{12}\delta_2 \tag{4.8a}$$

$$N_{21} = F_{12}\gamma_1 + F_{22}\gamma_2 + J_{12}\delta_1 + J_{22}\delta_2 \tag{4.8b}$$

$$M_{12} = J_{11}\gamma_1 + J_{12}\gamma_2 + K_{11}\delta_1 + K_{12}\delta_2 \tag{4.8c}$$

$$M_{21} = J_{12}\gamma_1 + J_{22}\gamma_2 + K_{12}\delta_1 + K_{22}\delta_2 \tag{4.8d}$$

$$Q_1 = L_1\gamma_{13} \tag{4.9a}$$

$$Q_2 = L_2\gamma_{23} \tag{4.9b}$$

where

$$C_{11} = \int B_{11}S_{21}d\xi_3$$

$$C_{12} = \int B_{12}d\xi_3$$

$$C_{22} = \int B_{22}S_{12}d\xi_3$$

La teoria expuesta representa el caso mas general de teoria de cascarones. Es posible simplificar esta teoria considerablemente introduciendo hipotesis adicionales a las tres hipótesis ya hechas.

La mas común de las teorías simplificadas es la teoria de Love, que contiene dos hipotesis adicionales: 1) $1/G_{13} = 1/G_{23} = 0$; 2) $\xi^3/R_i = 0$

esto equivale a suponer que las normales a la S.R del cascaron antes de cargarse permanecen normales a la S.R deformada del cascaron, y que el espesor del cascaron es lo suficientemente delgado como para despreciar el efecto de distorsión en el espesor. Si además consideramos como S.R la superficie media del cascarón encontramos que:

$$C_{11} = \frac{C_{12}}{\nu} = C_{21} = \frac{tE}{1-\nu^2}$$

$$E_{12} = E_{11} = E_{22} = 0$$

$$D_{11} = \frac{D_{12}}{\nu} = D_{22} = \frac{t^3}{12}\,\frac{E}{1-\nu^2}$$

$$F_{11} = F_{12} = F_{22} = Gt$$

$$J_{11} = J_{12} = J_{22} = 0$$

$$K_{11} = K_{12} = K_{22} = G\,t^3/12$$

$$L_1 = L_2 = \infty$$

$$\gamma_{13} = \gamma_{23} = 0$$

$$N_{12} = N_{21}$$

$$M_{12} = M_{21}$$

Por tanto

$$N_{11} = \frac{t^3 E}{1-\nu^2}\left(\epsilon_{11} + \nu\epsilon_{22}\right)$$

$$N_{22} = \frac{t^3 E}{1-\nu^2}\left(\nu\epsilon_{11} + \epsilon_{22}\right)$$

$$M_{11} = \frac{t^3 E}{12(1-\nu^2)}\left(k_{11} + \nu k_{22}\right)$$

$$M_{22} = \frac{t^3 E}{12(1-\nu^2)}\left(\nu k_{11} + k_{22}\right)$$

$$N_{12} = N_{21} = Gt\left(\gamma_1 + \gamma_2\right)$$

$$M_{12} = M_{21} = \frac{Gt^3}{12}\left(\delta_1 + \delta_2\right)$$

$$\beta_1 = \frac{u_1}{R_1} - \frac{u_{3,1}}{\alpha_1}$$

$$\beta_2 = \frac{u_2}{R_2} - \frac{u_{3,2}}{\alpha_2}$$

modificandose además $\delta_1, \delta_2, k_{11}, k_{22}$ y las ecuaciones de equilibrio

Reduciendo aun mas el orden de dificultad de la teoría se han propuesto ulteriores modificaciones como en el caso de las teorías de Fllügge y de Vlasow. que no vamos a discutir aquí.

La teoría mas simplificada de cascarones consiste en la teoría de membrana. La teoría de membrana

$$
\begin{aligned}
E_{11} &= \int B_{11}S_{21}\xi_3 d\xi_3 \\
E_{12} &= \int B_{12}\xi_3 d\xi_3 \\
E_{22} &= \int B_{22}S_{12}\xi_3 d\xi_3 \\
D_{11} &= \int B_{11}S_{21}\xi_3^2 d\xi_3 \\
D_{12} &= \int B_{12}\xi_3^2 d\xi_3 \\
D_{22} &= \int B_{22}S_{12}\xi_3^2 d\xi_3 \\
F_{11} &= \int G_{12}S_{21} d\xi_3 \\
F_{12} &= \int G_{12} d\xi_3 \\
F_{22} &= \int G_{12}S_{12} d\xi_3 \\
J_{11} &= \int G_{12}S_{21}\xi_3 d\xi_3 \\
J_{12} &= \int G_{12}\xi_3 d\xi_3 \\
J_{22} &= \int G_{12}S_{12}\xi_3 d\xi_3 \\
K_{11} &= \int G_{12}S_{21}\xi_3^2 d\xi_3 \\
K_{12} &= \int G_{12}\xi_3^2 d\xi_3 \\
K_{22} &= \int G_{12}S_{12}\xi_3^2 d\xi_3 \\
L_1 &= \int G_{13}S_{21} d\xi_3 \\
L_2 &= \int G_{23}S_{12} d\xi_3
\end{aligned}
\tag{4.10}
$$

ramo una gran variedad de recipientes a presion, tuberías, toberas, tolvas, etc, los cuales requieren de una mejor aproximación en el analisis, y que hacen indispensable intentar las teorías de mayor orden.

La dificultad para utilizar estas así llamadas teorías de cascarones de orden superior estriba en la solución del sistema de ecuaciones que engendran aun para problemas relativamente simples. De aquí que existan muy pocos casos resueltos analíticamente. Lo que se ha hecho generalmente en el pasado a sido recurrir a soluciones aproximadas de las ecs. generadas y así se ha caido o mejor dicho se han utilizado los procedimientos numéricos de diferencias finitas, elementos finitos e integración numérica.

Vamos a referirnos a este último procedimiento. Existen algunos programas para computadora escritos para resolver de esta manera un tipo muy común de cascarones que se denominan genericamente como cascarones de revolución, y que utilizan integración numérica, entre ellos estan los programa KSHEL 1 y KSHEL 2, desarrollados por el profesor Arturs Kalnins del departamento de ingeniería mecánica en la universidad de Lehigh. (Penna. U.S.A)

Establece la hipotesis de que D y C pueden variarse independientemente esto es

$$D = \frac{t^3}{12} \frac{E}{1-\nu^2} = 0$$

$$C = t \frac{E}{1-\nu^2} \neq 0$$

Evidentemente llegar a esta simplificación implica pagar un alto precio en la aproximación de la solución puesto que desaparece del cuadro todas las componentes de flexión; esto es $M_{11} = M_{12} = M_{21} = Q_1 = Q_2 = 0$. los cuales son quienes originan los esfuerzos críticos.

La teoría de membrana tiene el atractivo de ser isostática es decir puede encontrarse la solución sin recurrir a condiciones geométricas de frontera o condiciones de compatibilidad y su empleo está muy generalizado. Es necesario ser muy conciente las limitaciones que tiene esta herramienta cuando se utiliza y de sus consecuencias a fin de no incurrir en un analisis defectuoso que lleve a un diseño inadecuado.

Existen una gran variedad de cascarones en la industria para los cuales el analisis de membrana no es satisfactorio. Están incluidos en este

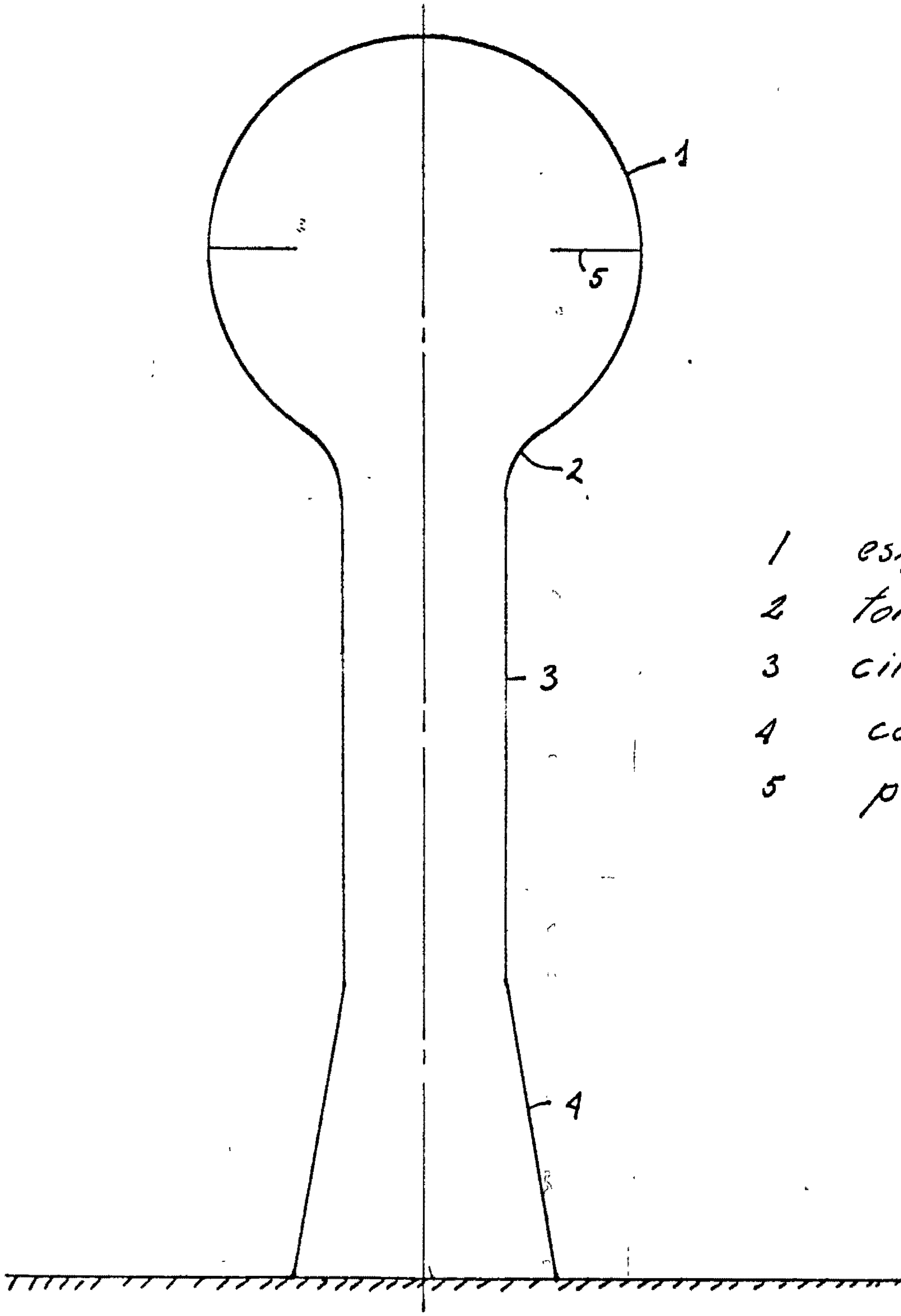

1 esfera
2 toroide
3 cilindro
4 cono
5 placa

KSHEL 1.

Es un programa escrito en lenguaje FORTRAN IV que permite el analisis de cascarones axisimétricos en sus propiedades y geometría sujetos cargas estáticas que pueden arbitrariamente variar a lo largo de la coordenada meridional y que puede tomar variaciones en las cargas en su coordenada circunferencial utilizando expansión en series de Fourier. Cualquier superficie de revolución puede ser analizada, sin embargo, dado que en la mayoría de los casos las superficies de revolución estan formadas por superficies estéricas, cilíndricas, toroidales, cónicas, elípticas y parabóli existe en el programa manera de componer el cascarón en cuestión como una sucesión de estas superficies puestas una a continuación de la otra, con lo cual se logran grandes economías de tiempo en la preparación de datos y en la ejecución del programa. A cada una de estas superficies se les llama partes, y el programa admite 20 partes las cuales pueden pertenecer al cascarón principal o formar parte de un ramal secundario. Dichos ramales pueden ser hasta tres y pueden ser abiertos o cerrados.

En cuanto al sistema de cargas a lo largo de la coordenada meridional estas pueden ser anulares concentradas, uniformemente distribuidas, o de distribucion variable.

Las condiciones de soporte o de frontera en general pueden ser cualquier combinación de las variables fundamentales de la solución esto es fuerza normal, fuerza tangencial cortante, cortante perpendicular y momento en el borde en relación a las fuerzas, y desplazamientos normal, tangencial o perpendicular a la S. R. del cascarón así como giro con respecto al bordo. Como condiciones de soporte acepta tambien resortes anulares y camas de resortes axisimétricas.

La geometría del cascarón puede variar arbitrariamente de forma de espesor y de propiedades mecánicas a lo largo de la coordenada meridional, ademas el cascarón puede estar formado por una o varias capas de diferentes materiales ortotropicos a lo largo de las coordenadas del problema.

Es por demás oubio que las particularidades del problema le dan una enorme flexibilidad y si la forma es adecuada (de revolución) el problema puede resolverse o aproximarse grandemente.

KSHEL 2

Este programa precisa del primero KSHEL 1 para generar la información básica para el problema, por tanto cuenta con casi todas las capacidades de KSHEL 1 a excepción de la asimetría circunferencial de cargas. El programa sirve para realizar analisis dinámicos y de estabilidad para cascarones presforzados (incluyendo el estado de presfuerzo nulo). En el primer caso determina la frecuencia natural mas baja de vibración y el modo. En el segundo determina el presfuerzo de pandeo. Este programa no admite un sistema de cargas externas como tal, sino un estado de esfuerzos internos, por ello es necesario correr primero KSHEL 1 para un sistema de cargas y así obtener el estado de esfuerzos, con el cual puede ~~del~~ alimentarse el programa KSHEL 2.

El tiempo de máquina requerido por este último programa puede ser substancial ya que son necesarias una serie de corridas previas de los dos programas para determinar por aproximaciones sucesivas los valores característicos

CONSTRUCTORA LOBEIRA S.A.

PARABOLOIDES HIPERBOLICOS SOBRE LA ESTRUCTURA EXISTENTE EN EL LADO SUR DEL ALMACEN DE PRODUCTO ELABORADO.

Cálculo
Dr. Porfirio Ballesteros

FEBRERO - 1968.

PARABOLOIDES HIPERBOLICOS GAMESA 1

Almacen Producto Elaborado

P. Ballesteros

PARA EL CASO DE ESTA CUBIERTA SE ESCOGIO UN PARABOLOIDE HIPERBOLICO DE CUDTRO PUNTOS CUYA SOLUCIÓN SE EXPONDRA MAS ADELANTE.

SE TIENEN ADEMAS TRES TIPOS DE PARABOLOIDE POR SUS DIFERENTES CLAROS A CUBRIR POR LO TANTO SE HARAN TRES CALCULOS POR SEPARADO.

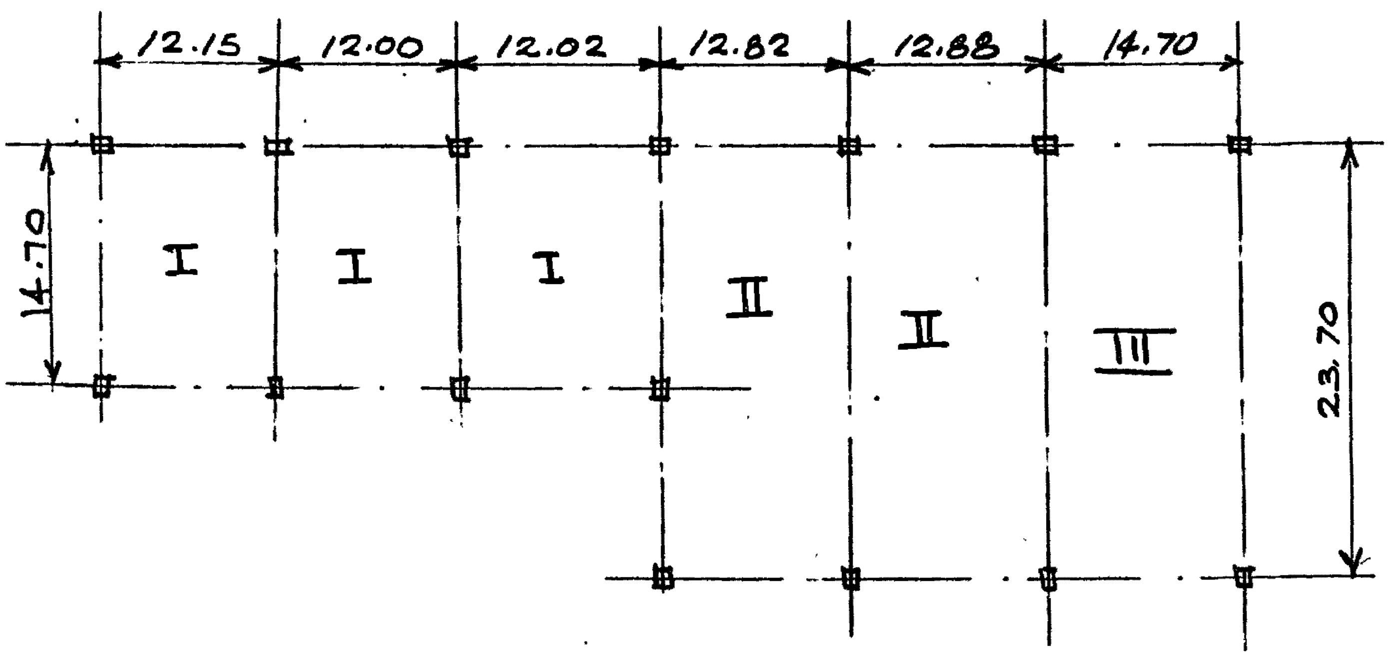

PLANTA DE LA CUBIERTA CON SUS DIFERENTES CLAROS.

P. Ballesteros

ANALISIS DE LA ESTRUCTURA:

PARA LA CUBIERTA ELEGIDA TIPO PARABOLOIDE HIPERBOLICO FIG. # 2. EL ESTADO DE ESFUERZOS EN LA MEMBRANA SERA EL SIGUIENTE:

LA ECUACION DIFERENCIAL DE TEORIA DE MEMBRANA PARA CASCARONES DE CUALQUIER FORMA REFERIDAS A UN SISTEMA DE COORDENADAS CARTESIANO ES (FIG. # 1)

$$\frac{\partial^2 F}{\partial y^2} \times \frac{\partial^2 z}{\partial x^2} + \frac{\partial^2 F}{\partial x^2} \times \frac{\partial^2 z}{\partial y^2} - 2\frac{\partial^2 F}{\partial x \partial y} \times \frac{\partial^2 z}{\partial x \partial y} =$$

$$= -Z + X\frac{\partial z}{\partial x} + Y\frac{\partial z}{\partial y} + \frac{\partial^2 z}{\partial x^2}\int_{x_0}^{x} X\,dx + \frac{\partial^2 z}{\partial y^2}\int_{y_0}^{y} Y\,dy \quad (a)$$

DONDE LAS FUERZAS DE MEMBRANA SE EXPRESAN EN TERMINOS DE LA FUNCION DE ESFUERZOS COMO SIGUE

$$\left.\begin{aligned} N'x &= N_x\frac{\cos\phi}{\cos\psi} = \frac{\partial^2 F}{\partial y^2} - \int_{x_0}^{x} X\,dx \\ N'y &= N_y\frac{\cos\psi}{\cos\phi} = \frac{\partial^2 F}{\partial x^2} - \int_{x_0}^{x} Y\,dy \\ N'xy &= N_{xy} = -\frac{\partial^2 F}{\partial x \partial y} \end{aligned}\right\} \quad (b)$$

P. Ballesteros

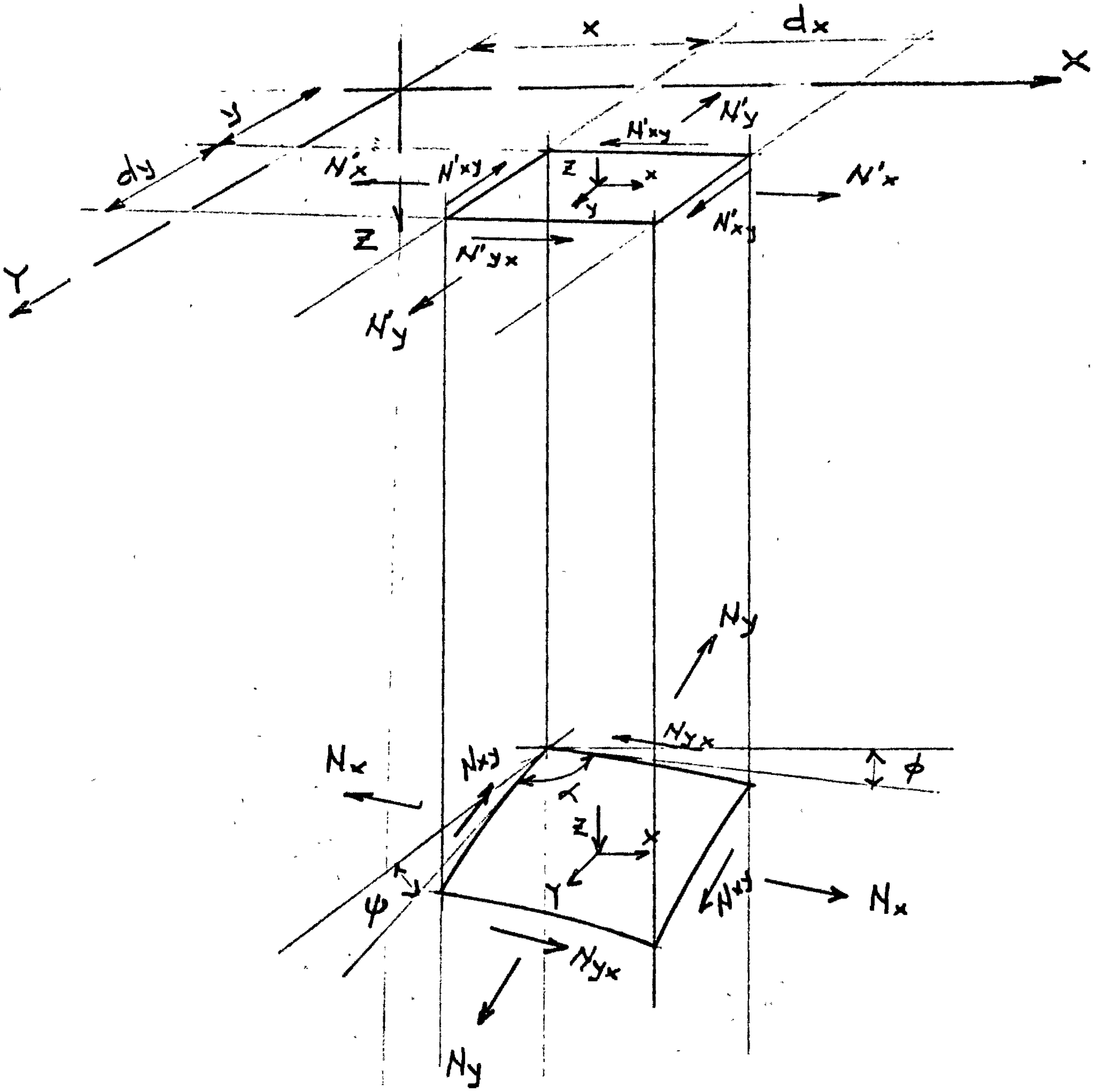

FIG. # 1 ESTADO DE ESFUERZOS.

P. Ballestero

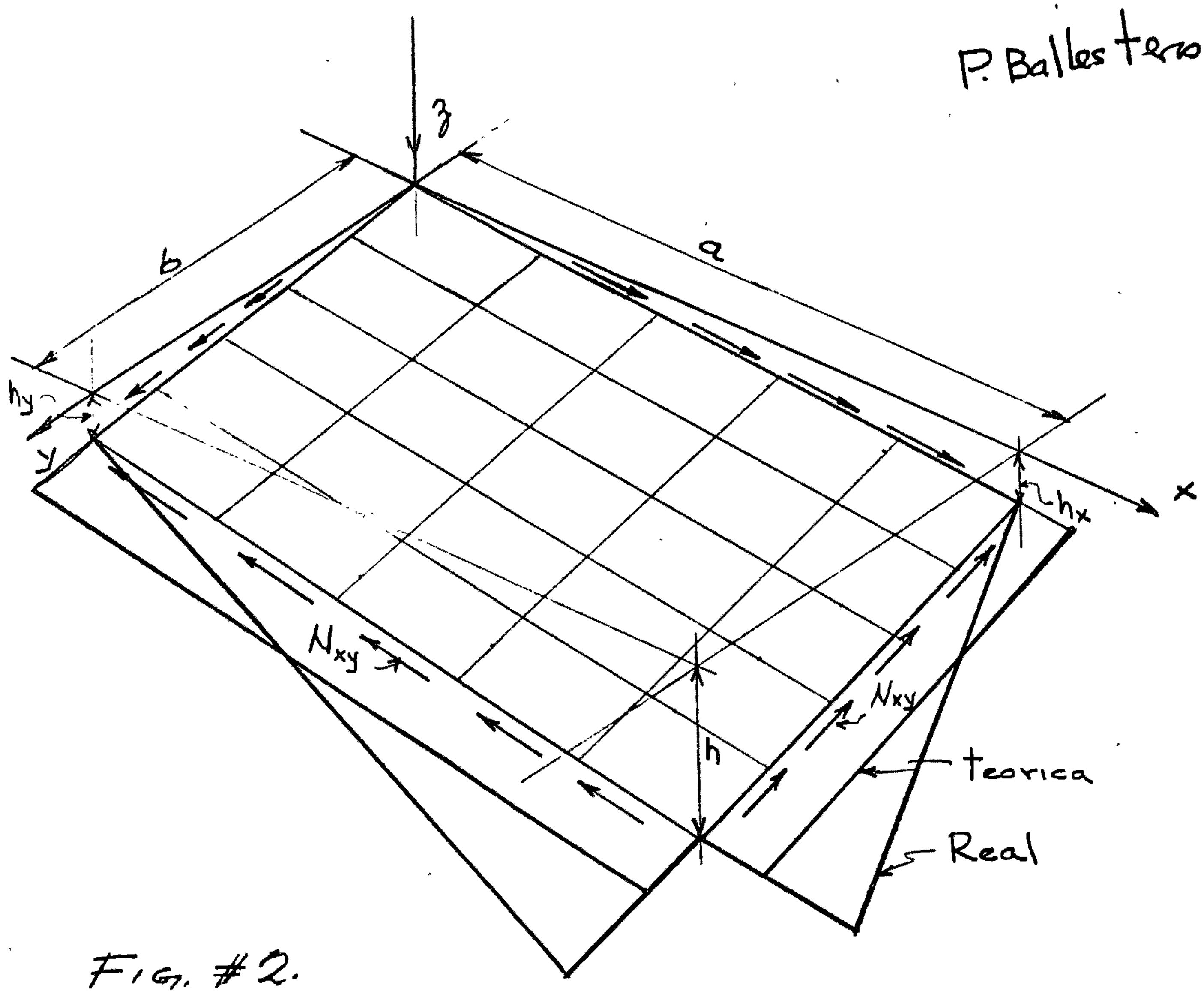

FIG. #2.

SUPERFICIE ESCOGIDA.

LA ECUACION DE LA SUPERFICIE ES:

$$z = Axy + Bx + Cy + D \qquad (1)$$

DE

$$\left.\begin{aligned} z(0,0) &= 0 \\ z(a,0) &= h_x \\ z(0,b) &= h_y \\ z(a,b) &= h \end{aligned}\right\} \qquad (2)$$

DE (1) y (2) SE OBTIENE. P. Ballesteros

$$A = \frac{h - h_x - h_y}{ab}, \quad B = \frac{h_x}{a}, \quad C = \frac{h_y}{b}, \quad D = 0 \qquad (3)$$

SUBSTITUYENDO (3) EN (1) SE OBTIENE

$$z = \frac{h - h_x - h_y}{ab} xy + \frac{h_x}{a} x + \frac{h_y}{b} y. \qquad (4)$$

SUBSTITUYENDO (4) EN LA ECUACIÓN DIFERENCIAL GENERAL DE TEORÍA DE MEMBRANA (b) PARA CASCARONES DE CUALQUIER FORMA:

$$-2 \frac{\partial^2 F}{\partial x \partial y} \cdot \frac{h - h_x - h_y}{ab} = -q$$

$$\frac{\partial^2 F}{\partial x \partial y} = \frac{q\,ab}{2(h - h_x - h_y)} = -N_{xy}.$$

$$\boxed{N_{xy} = -\frac{q\,ab}{2(h - h_x - h_y)}} \qquad (5)$$

EN NUESTRO PROBLEMA PARA LOS TRES TIPOS DE CASCARONES SE TIENE:

P. Ballesteros

CARGA VIVA = 100 kg/m².

CARGA MUERTA
(VIGAS DE BORDE E
IMPERMEABILIZANTE) = 200 kg/m².

q = 300 kg/m².

CASCARON TIPO I.

P. Ballesteros

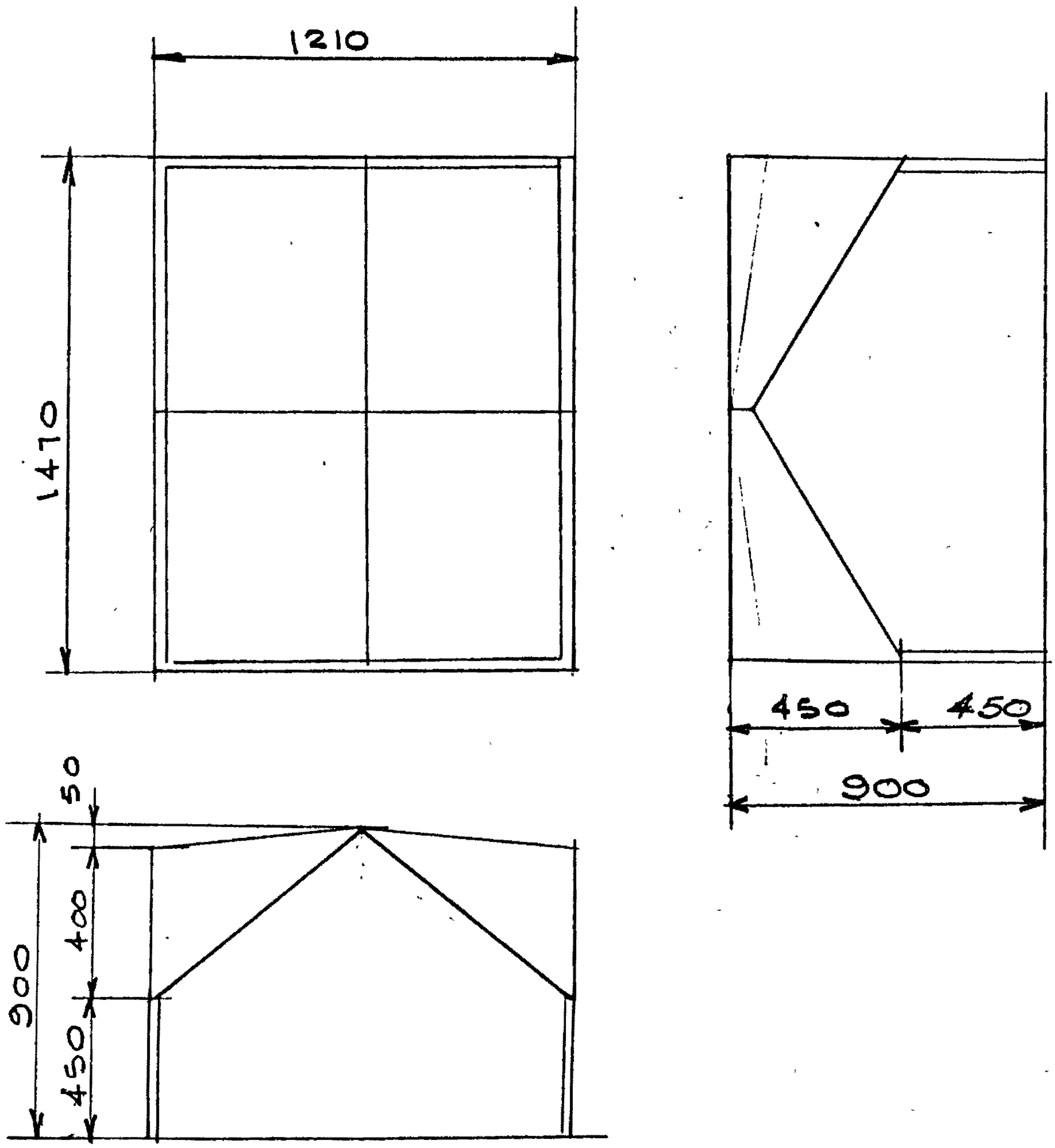

P. Ballesteros

DATOS: $q = 300\ kg/m^2$.

$h_x = 0$

$h_y = 0.50\ m.$

$h = 4.50\ m.$

$a = 7.35\ m.$

$b = 6.05\ m.$

SUBSTITUYENDO ESTOS VALORES EN (5):

$$N_{xy} = -\frac{300 \times 7.35 \times 6.05}{2(4.5 - 0.5)} = \frac{13{,}400}{8}$$

$$= 1{,}675\ kg/m.$$

$$a_s = \frac{N_{xy}}{f_s} = \frac{1{,}675}{2000} = 0.84\ cm^2/m.$$

USAR MALLA $\phi\ 5/16''$ @ 30 cms. $f_y \geq 4{,}200\ kg/cm^2$.

TENSION EN LOS TIRANTES:

$$\tfrac{1}{2} H_x = N_{xy}\, l \cos\alpha$$

$$\underline{H_x = 2 N_{xy}\, a.}$$

$$\tfrac{1}{2} H_y = N_{xy}\, l_1 \cos\beta$$

$$\underline{H_y = 2 N_{xy}\, b.}$$

P. Ballesteros

$H_x = 2 \times 1675 \times 7.35 = 24,700$ kgs.

$H_y = 2 \times 1675 \times 6.05 = 20,300$ kgs.

USANDO CABLES DE 7 m.m. ϕ con $f_y \geq 14,500$ kg/cm²

CARGA ADMISIBLE POR CABLE = 3,000 kgs.

Nº DE CABLES EN "X"

$$\frac{24,700}{3,000} = 8 \text{ CABLES.}$$

USAR 8 CABLES DE 7mm ϕ EN EJE "X"

Nº DE CABLES EN "Y"

$$\frac{20,300}{3,000} = 8 \text{ CABLES.}$$

USAR 8 CABLES DE 7mm ϕ EN EJE "Y".

ESFUERZOS EN VIGAS DE BORDE:

$(T_x)_m = N_{xy}\, a = 1,675 \times 7.35 = 12,350$ kgs.

$(T_y)_m = N_{xy}\, b = 1,675 \times 6.05 = 10,150$ kgs.

$A_s = 6$ VRS. ϕ ½".

Diseño de Columnas:

P. Ballestero

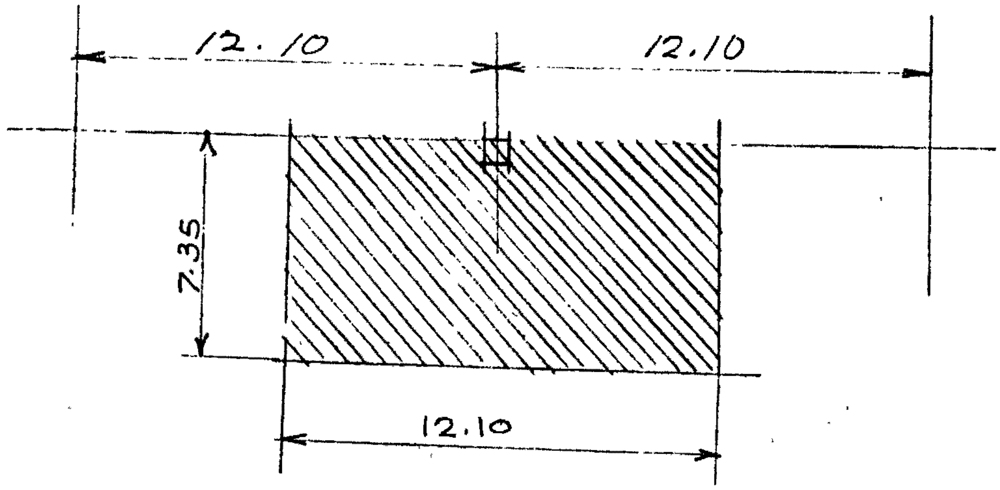

Area Tributaria $= 12.10 \times 7.35 = 89\ m^2$

$N_{col.} = 89 \times 300 = 26{,}700$ kgs.

$w\,pp_{col}$ sup $= 0.3 \times 0.4 \times 4.0 \times 2400 = 1{,}150$ kgs.

$N_{total} = 27{,}850$ Kgs.

$H_{sismica}$ = c × Peso de la Estructura

$= 0.10 \times 27{,}850 = 2{,}785$ kgs

Viento $\quad w = 70\ kg/m^2$.

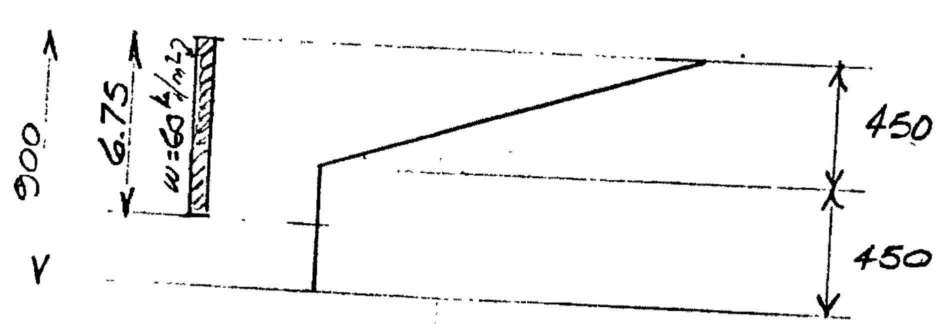

$H_{viento} = 60 \times 6.75 \times 12.0 = 4{,}870$ kgs > 2785 kgs.

P. Ballesteros

$$H_{col} = \frac{4870}{2} = 2435 \text{ kgs.}$$

$$M = 2{,}435 \times 4.5 = 10{,}900 \text{ kgs-m.}$$

SOLICITACIONES EN COLUMNAS:

$$N = 27{,}850 \text{ kgs.}$$

$$M = 10{,}900 \text{ kgs-m.}$$

$$e' = \frac{M}{N} = \frac{10900 \times 100}{27{,}850} = 39.2 \text{ cms.}$$

PROPONIENDO LA SIGUIENTE SECCIÓN Y REVISANDO:

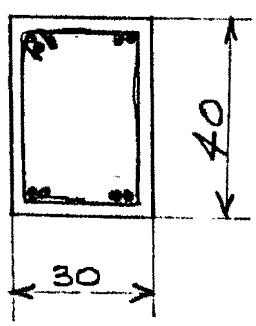

$8 \phi 3/4"$ $A_s = 22.9 \text{ cm}^2$

Est. $\phi 5/16"$ @ 30 cms.

$$p = \frac{A_s}{bd} = \frac{22.9}{30 \times 40} = 0.0191$$

$$m = \frac{f_y}{0.85 f'_c} = \frac{4200}{0.85 \times 210} = 23.5$$

$$\frac{d}{t} = \frac{35}{40} = 0.90 \qquad \frac{\ell}{t} = \frac{400}{30} = 13.5$$ Col. corta.

P. Ballesteros

$p_t\, m = 0.0191 \times 23.5 = 0.448$

$e'/t = \frac{39.2}{40} = 0.98$

$K = 0.25 \qquad K = \frac{P_u}{bt\, f'c}$

$P_u = 0.25 \times 30 \times 40 \times 210$

$P_u = 63{,}100$ Kgs.

$F.S. = \frac{P_u}{N} = \frac{63{,}100}{27{,}850} = 2.2$ ✓

SE USARA LA SECCION PROPUESTA.

CASCARON TIPO II

P. Ballestero

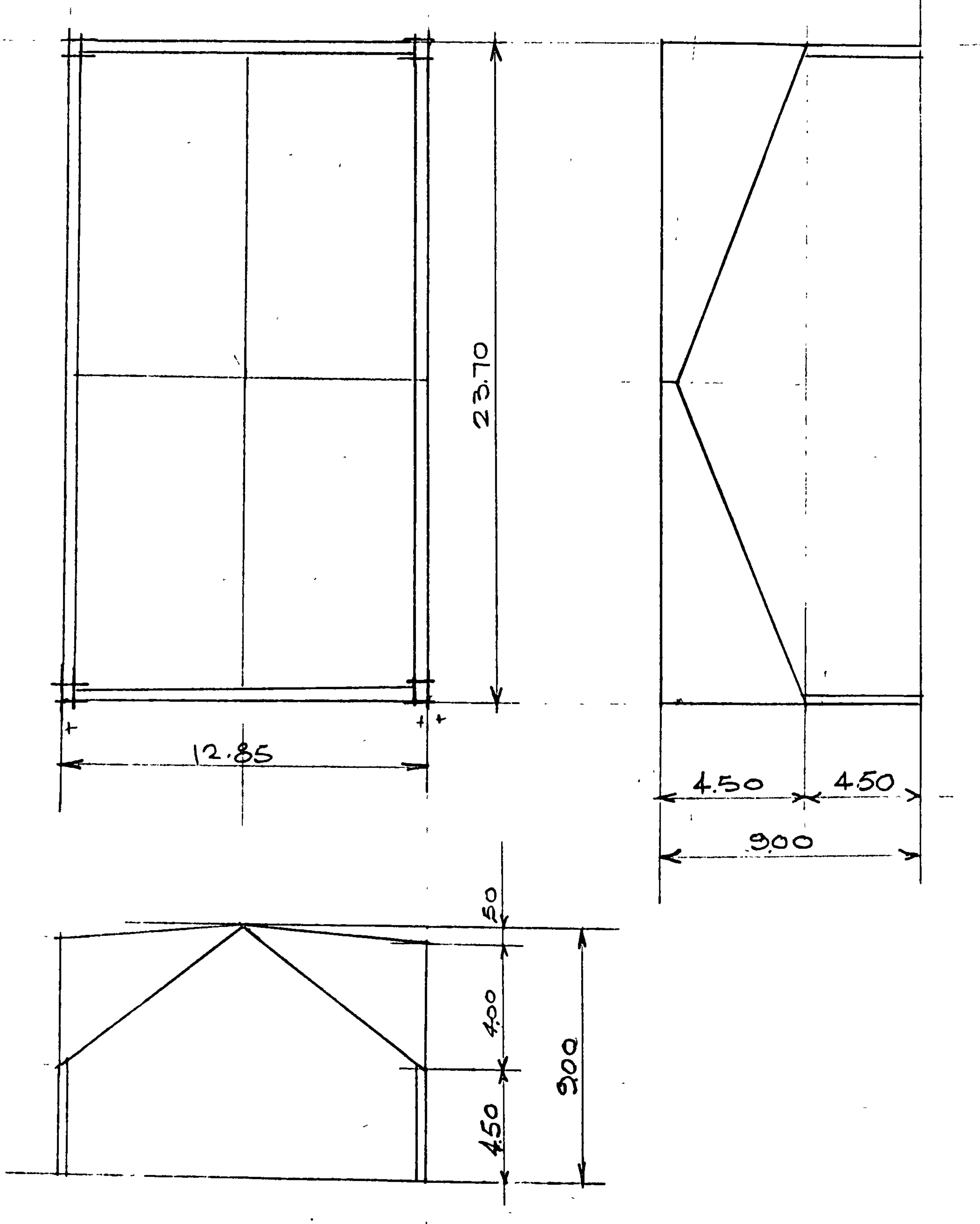

DATOS: $q = 300 \ kg/m^2$

P. Ballesteros 12

$h_x = 0 \ m.$

$h_y = 0{,}50 \ m.$

$h = 4{,}50 \ m.$

$a = 11{,}85 \ m.$

$b = 6{,}43 \ m.$

SUBSTITUYENDO ESTOS VALORES EN (5):

$$N_{xy} = -\frac{300 \times 11.85 \times 6.43}{2(4{,}5 - 0{,}5)} = \frac{22{,}800}{8}$$

$$= 2{,}850 \ kg/m.$$

$$a_s = \frac{N_{xy}}{f_s} = \frac{2{,}850}{2000} \approx 1.42 \ cm^2/m.$$

USAR MALLA ϕ 5/16" @ 30 cms. $f_y \geq 4{,}200 \ kg/cm^2$.

TENSION EN LOS TIRANTES:

$$H_x = 2 N_{xy} a$$

$$= 2 \times 2{,}850 \times 11.85 = 67{,}800 \ kgs$$

$$H_y = N_{xy} b$$

$$= 2{,}850 \times 6.48 = 18{,}400 \ kgs.$$

USANDO CABLES DE 7mm ϕ con $f_y \geq 14{,}500 \ kg/cm^2$

CARGA ADMISIBLE POR CABLE = 3000 kgs.

Nº Cables en "X" P. Ballestero

$$\frac{67,800}{3,000} = 24 \text{ cables}$$

Usar 24 cables de 7mm ϕ en eje "X"

Nº Cables en "Y"

$$\frac{18,400}{3,000} = 8 \text{ cables}$$

Usar 8 cables 7mm ϕ en eje Y.

Esfuerzos en Vigas de Borde:

$(T_x)_m = N_{xy}\, a = 2,850 \times 11.85 = 33,800$ kgs.

$(T_y)_m = N_{xy}\, b = 2,850 \times 6.43 = 18,300$ kgs.

$A_s = 6$ Vrs. ϕ 1/2".

Diseño de Columnas:

Area Tributaria $= 12.85 \times 11.85 = 152.5\ m^2$

$N_{col.} = 300 \times 152.5 = 45,800$ kgs.

w_{pp} sup. $0.35 \times 0.45 \times 2400 \times 4.00 = \underline{1500 \text{ kgs}}$ P. Ballesteros

$N_{TOTAL} = 47{,}300$ kgs.

$H_{SISMICA}$ = C × Peso de la Estructura

$= 0{,}10 \times 47{,}300 = 4{,}730$ Kgs.

Viento $w = 60$ kg/m²

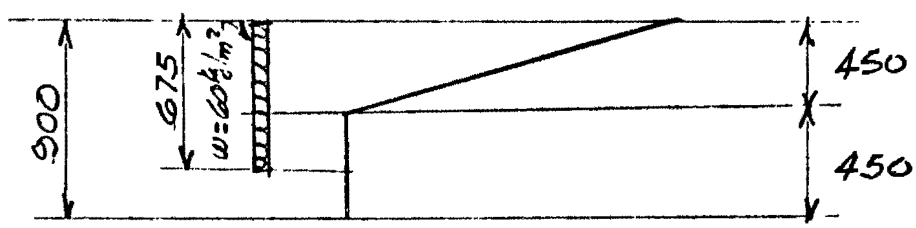

$H_{VIENTO} = 60 \times 6.75 \times 12.85 = 5{,}200$ kgs > 4730 kgs

$H_{COL.} = \frac{5{,}200}{2} = 2{,}600$ kgs.

$M = 2{,}600 \times 4.5 = 11{,}700$ kgs-m.

Solicitaciones en columnas:

$N = 47{,}300$ Kgs

$M = 11{,}700$ Kgs-m.

$e' = \frac{M}{N} = \frac{11{,}700 \times 100}{47{,}300} = 24.8$ cms.

P. Ballestero

PROPONIENDO LA SIGUIENTE SECCION Y REVISANDO:

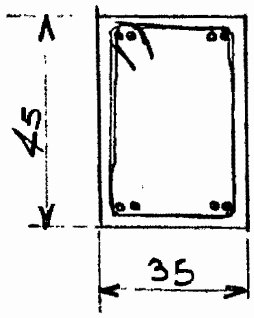

$8 \phi \, 3/4''$ $A_s = 22.9 \text{ cm}^2$

Est. $\phi \, 5/16''$ @ 30 cms.

$$p = \frac{A_s}{bd} = \frac{22.9}{35 \times 45} = 0.01475$$

$$m = \frac{f_y}{0.85 f'_c} = \frac{4200}{0.85 \times 210} = 23.5$$

$$d/t = \frac{40}{45} = 0.90 \qquad \frac{l}{t} = \frac{450}{35} = 13 \quad \text{Col. corta.}$$

$$p_t m = 0.01475 \times 23.5 = 0.347$$

$$e'/t = \frac{24.8}{45} = 0.55$$

$$K = 0.41 \qquad K = \frac{P_u}{b t f'_c}$$

$$P_u = 0.41 \times 35 \times 45 \times 210 = 135{,}500 \text{ kgs.}$$

$$F.S. = \frac{P_u}{N} = \frac{135{,}500}{47{,}300} = 2.88 \; \checkmark\checkmark$$

CASCARON TIPO III

P. Ballesteros

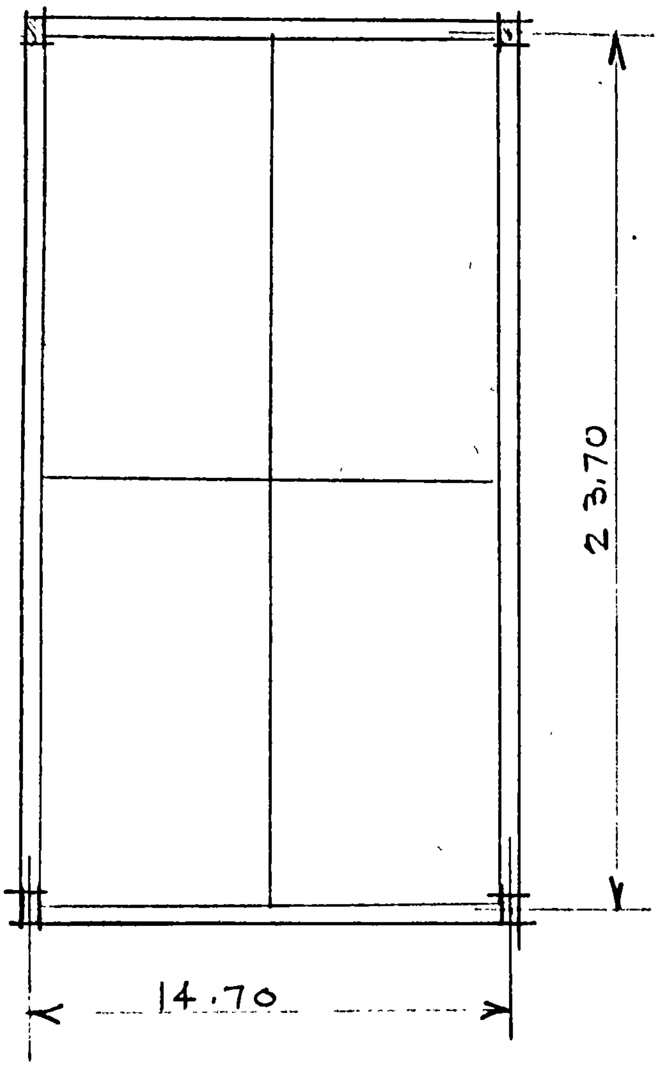

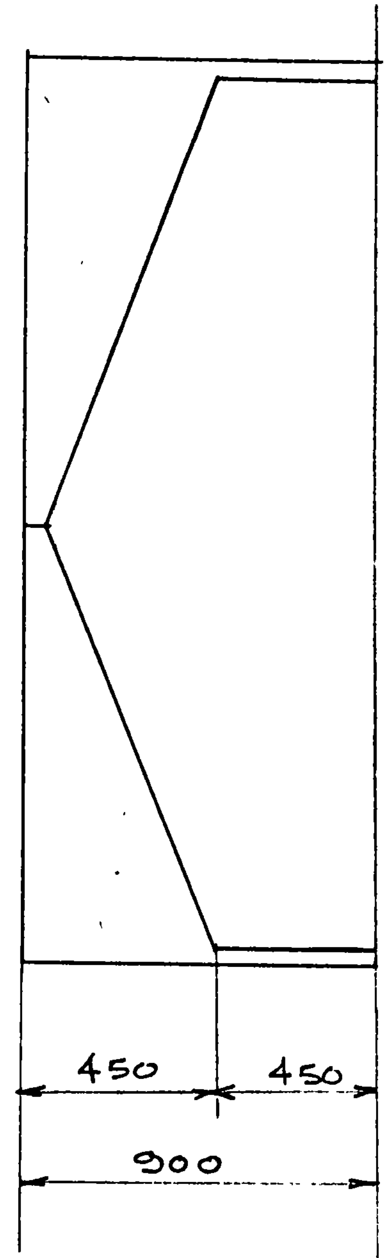

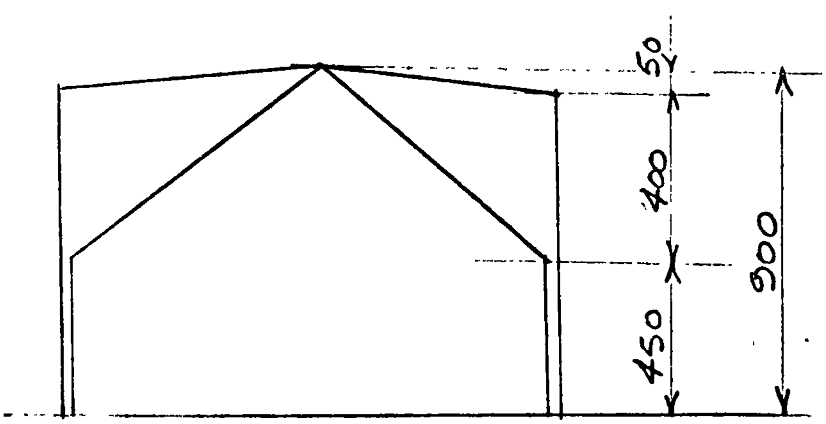

DATOS : $q = 300 \ kg/m^2$

P. Ballesteros

$h_x = 0$

$h_y = 0.50 \ m.$

$h = 4.50 \ m.$

$a = 11.85 m.$

$b = 7.35 m.$

SUBSTITUYENDO ESTOS VALORES EN (5) :

$$N_{xy} = - \frac{300 \times 11.85 \times 7.35}{2\,(4.5-0.5)} = \frac{26,200}{8}$$

$$N_{xy} = 3,280 \ Kg/m$$

$$a_s = \frac{N_{xy}}{f_s} = \frac{3,280}{2000} = 1.64 \ cm^2/m$$

USAR MALLA ϕ 5/16" @ 30 cm $f_y \geq 4200 \ kg/cm^2$

TENSIÓN EN LOS TIRANTES :

$$H_x = N_{xy}\, a$$
$$= 3,280 \times 11.85 = 38,800 \ kgs.$$

$$H_y = N_{xy}\, b$$
$$= 3,280 \times 7.35 = 24,100 \ kgs.$$

USANDO CABLES DE 7 mm ϕ CON $f_y \geq 14,500 \ kg/cm^2$.

CARGA ADMISIBLE POR CABLE = 3000 kgs.

P. Ballestero

Nº DE CABLES EN "X"

$$\frac{38,800}{3,000} = 12 \text{ CABLES}$$

USAR 12 CABLES DE 7mm ϕ EN EJE "X"

Nº DE CABLES EN "Y"

$$\frac{24,100}{3000} = 8 \text{ CABLES}$$

USAR 8 CABLES DE 7mm ϕ EN EJE Y

ESFUERZOS EN VIGAS DE BORDE:

$$(T_x)_m = N_{xy}\, a = 3,280 \times 11.85 = 38,800 \text{ kgs}$$

$$(T_y)_m = N_{xy}\, b = 3,280 \times 7.35 = 24,100 \text{ kgs.}$$

$$A_s = 6 \text{ Vrs.} \phi \tfrac{1}{2}''$$

USAR LA MISMA COLUMNA QUE PARA EL CASCARON ANTERIOR.

CARGA CRITICA DE PANDEO:

P. Ballester

DATOS: $a = 12.05\ m$

$b = 5.00\ m$

$h = 0.05\ m$

$E = 2.1 \times 10^5\ Kg/cm^2$

$\nu = 0.15$

$$(N_{xy})_{CR} = \frac{5.7\ \pi^2 D}{b^2}$$

D= RIGIDEZ FLEXIONANTE

$$= \frac{E\ h^3}{12(1-\nu^2)} = \frac{2.1 \times 10^5 \times 0.05^3}{(1-0.15)^2\ (12)} = 2.19 \times 10^6\ kg\ cm.$$

$$(N_{xy})_{CR} = \frac{5.7 \times \pi^2 \times 2.19 \times 10^6}{5.00^2}$$

$$= 49{,}800\ kg/m.$$

$$\frac{(N_{xy})_{CR}}{(N_{xy})_m} = \frac{49{,}800}{3{,}280} = 15.4$$

✓✓

DISEÑO DE CASCARON CILINDRICO PARA UNION CARBIDE MEXICANA.

FEBRERO - 1968

SECCION PROPUESTA:

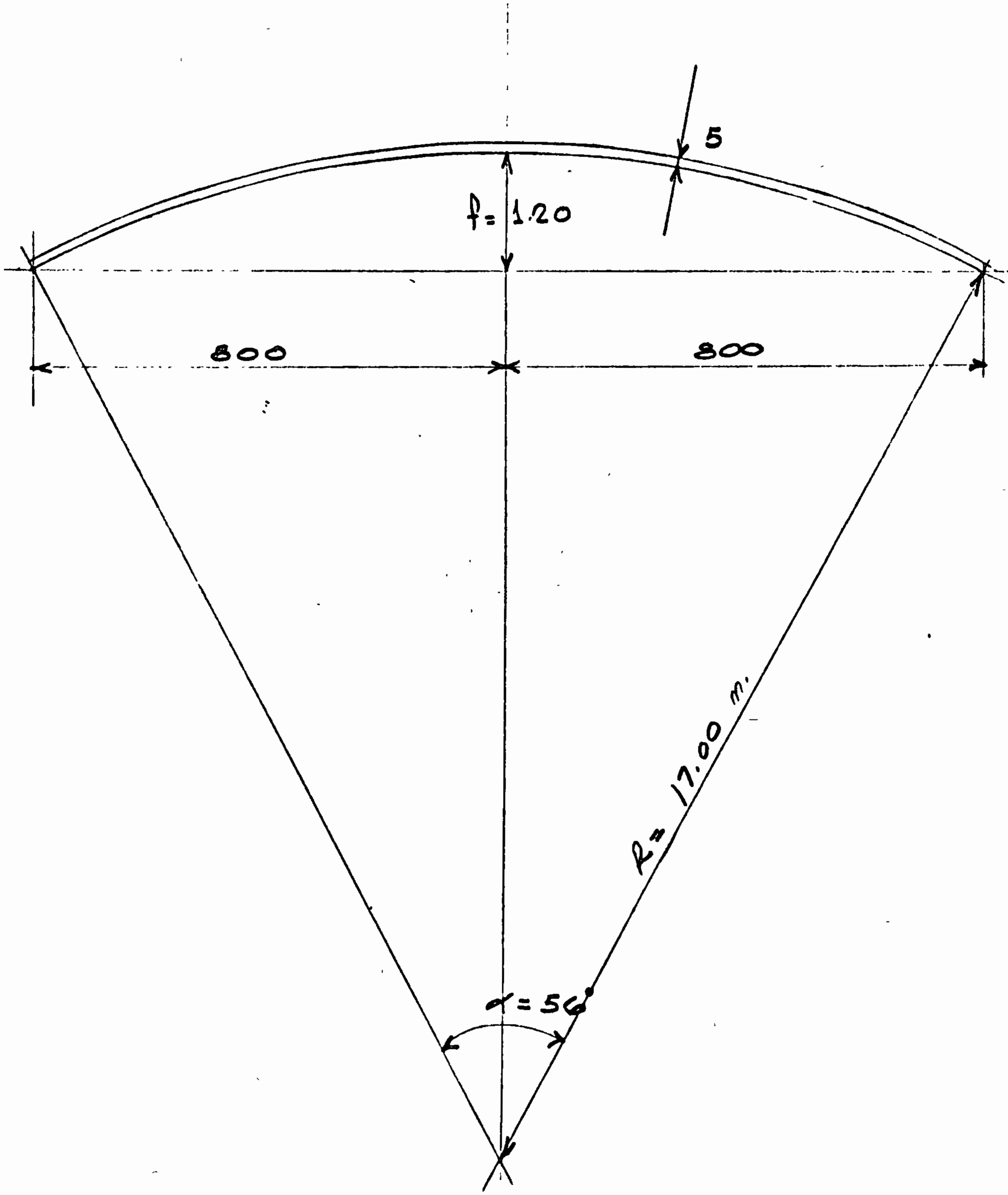

$L = 2\pi\,(17.00)\left(\frac{56}{360}\right) = 16.60$ m.

ANALISIS DE LA ESTRUCTURA

SELECCIONANDO UNA SECCION TRANSVERSAL PARABOLICA, EL ESTADO DE ESFUERZOS EN ESTE TIPO DE CASCARON SERA EL SIGUIENTE:

LA ECUACION DIFERENCIAL DE TEORIA DE MEMBRANA PARA CASCARONES DE CUALQUIER FORMA REFERIDA A UN SISTEMA DE COORDENADAS CARTESIANO ES: (FIG. 1)

$$\frac{\partial^2 F}{\partial y^2} \times \frac{\partial^2 z}{\partial x^2} + \frac{\partial^2 F}{\partial x^2} \times \frac{\partial^2 z}{\partial y^2} - 2\frac{\partial^2 F}{\partial x \partial y} \times \frac{\partial^2 z}{\partial x \partial y} =$$

$$= -Z + X\frac{\partial z}{\partial x} + Y\frac{\partial z}{\partial y} + \frac{\partial^2 z}{\partial x^2}\int_{x_0}^{x} X\,dx + \frac{\partial^2 z}{\partial y^2}\int_{y_0}^{y} Y\,dy \qquad (1)$$

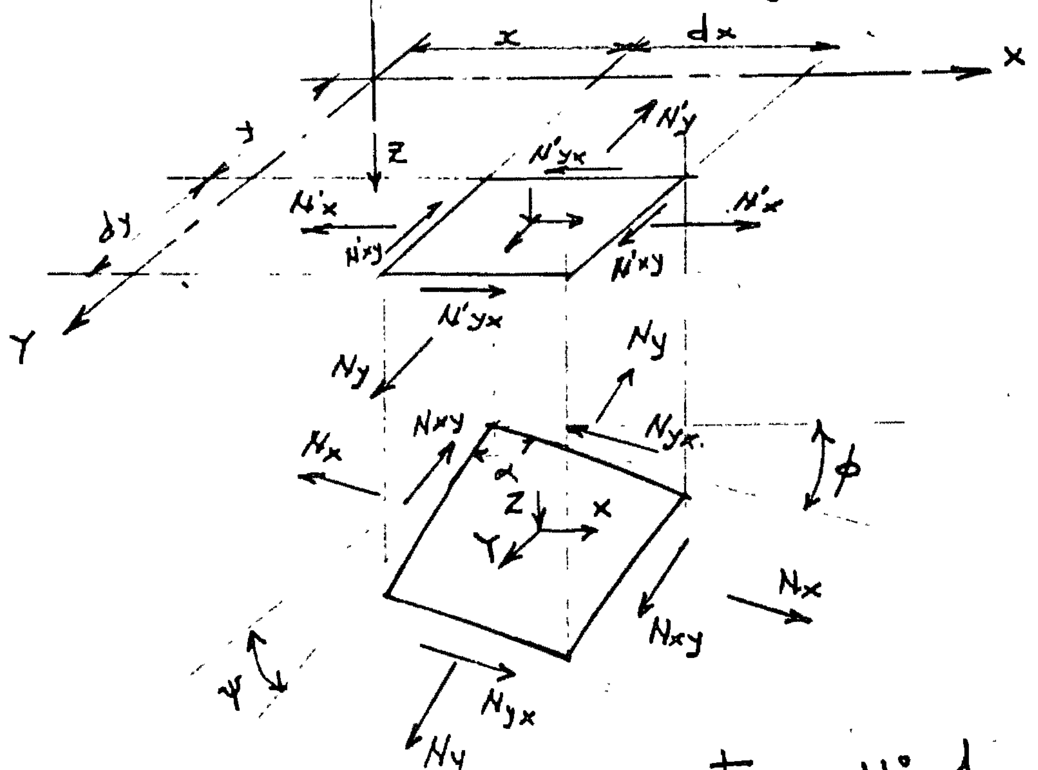

Fig. Nº 1.

DONDE LAS FUERZAS DE MEMBRANA SE EXPRESAN EN TERMINOS DE LA FUNCIÓN DE ESFUERZOS COMO SIGUE.

$$N'_x = N_x \frac{\cos\phi}{\cos\psi} = \frac{\partial^2 F}{\partial y^2} - \int_{x_0}^{x} X\,dx$$

$$N'_y = N_y \frac{\cos\psi}{\cos\phi} = \frac{\partial^2 F}{\partial x^2} - \int_{x_0}^{x} Y\,dy$$

$$N'_{xy} = N_{xy} = -\frac{\partial^2 F}{\partial x\,\partial y}$$

(2)

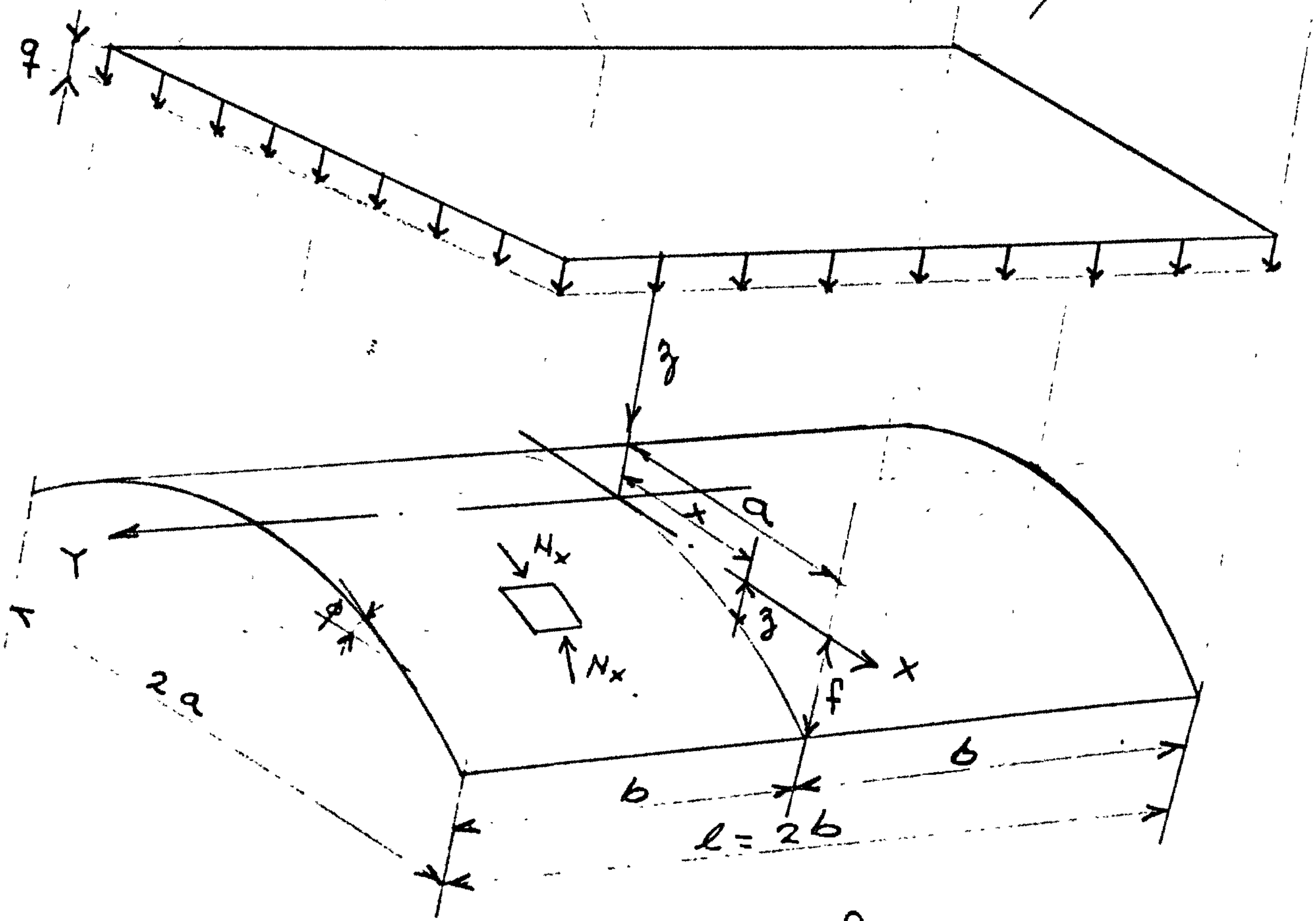

fig. # 2

LA ECUACIÓN DE LA SUPERFICIE EN ESTE CASO PARTICULAR ES

$$z = \frac{f}{a^2} x^2 \quad \text{———} \quad (3)$$

DONDE "f" ES LA FLECHA Y "a" EL SEMICLARO

LAS CARGAS EN ESTE CASO SON:

$$\left.\begin{array}{l} X = Y = 0 \\ Z = q \end{array}\right\} \quad (4)$$

$$\phi \neq 0 \quad \psi = 0$$

SUBSTITUYENDO (4) Y (3) EN (1) SE OBTIENE:

$$\frac{2f}{a^2} \times \frac{\partial^2 F}{\partial y^2} = -q \quad \text{———} \quad (5)$$

DE (5) Y (2) SE OBTIENE:

$$N'_x = -\frac{q a^2}{2f} = -\frac{q \ell^2}{8f} \quad \text{———} \quad (6)$$

DE (2) SE OBSERVA QUE

$$N_x = \frac{1}{\cos\phi} N'_x = \sqrt{1 + \left(\frac{\partial z}{\partial x}\right)^2}\; N'_x \text{———} (7)$$

SUBSTITUYENDO (3) y (6) EN (7) SE OBTIENE

$$N_x = -\sqrt{1+\frac{4f^2}{a^4}x^2} \times \frac{q\,l^2}{8f} \qquad (8)$$

$$N_{x_{max}} = -\sqrt{1+\frac{4f^2}{a^2}} \times \frac{q\,l^2}{8f}$$

$x = a.$

(-) COMPRESIÓN.
(+) TENSION.

ESTAS CONDICIONES DE BORDE DE LA ESTRUCTURA SE LOGRAN PERFECTAMENTE EN LA REALIDAD POR EL EMPLEO DE VIGAS DE BORDE LONGITUDINALES Y TIRANTES.

CARGAS:

$$\omega_{pp} = 16.6 \times 1.00 \times 0.05 \times 2400 = 1{,}990 \text{ kgs}$$

$$\omega_{imp} = 16.0 \times 1.00 \times 76 \quad 1{,}210 \text{ kgs}$$

$$\omega_{sc.} = 100 \times 1.00 \times 16 = 1{,}600 \text{ kgs}$$

$$W_{TOTAL} = 4800 \text{ kgs.}$$

$$q = \frac{4800}{16.00} = 300 \text{ kg/ml.}$$

REACCIONES:

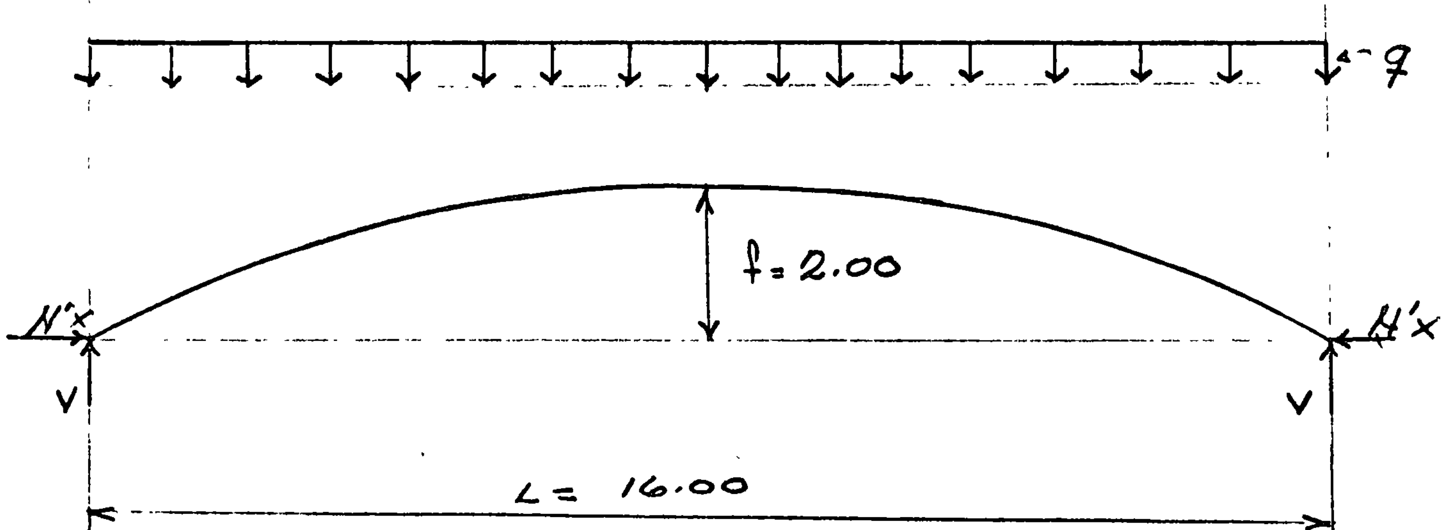

$$H'x = \frac{qL^2}{8f} = \frac{300 \times 16^2}{8 \times 2.00} = 4800 \text{ kg/m.}$$

$$V = \frac{ql}{2} = \frac{300 \times 16}{2} = 2{,}400 \text{ kg/m.}$$

$$N_{x\,max} = \sqrt{1 + \frac{4(2)^2}{(8)^2}} \left(\frac{300 \times \overline{16}^2}{8 \times 2} \right)$$

$$= 5{,}380 \ \text{kgs/m.}$$

$$N_{x\,min} = N'_{x \atop x=a} = 4{,}800 \ \text{kgs/m.}$$

$$\sigma_{comp.} = \frac{5{,}380}{100 \times 5} = 10.8 \ \text{kg/cm}^2 < 0.25 f'c \approx 50 \ \text{kg/cm}^2 \ \checkmark$$

PANDEO DEL ARCO:

$$q_{CR} = \frac{EI}{R^3} \left(\frac{4\pi^2}{\alpha^2} - 1 \right)$$

q_{CR} = CARGA DE PANDEO CRITICA.

$E = 15{,}000\sqrt{f'c} \approx 210{,}000$ kg/cm² (MODULO DE ELASTICIDAD)

$I = \frac{1}{12} bd^3 = \frac{1}{12} \times 100 \times \overline{5}^3 = 1{,}042$ cm² (MOM. DE INERCIA.)

$R = 17.00$ m (RADIO DE CURVATURA.)

$\alpha = 56^\circ$ (ANGULO CENTRAL.)

$$q_{CR} = \frac{210{,}000 \times 1042}{17.0^{-3} \times 10^6} \left(\frac{4\pi^2}{\left(\frac{56}{180}\pi\right)^2} - 1 \right)$$

$$= \frac{44{,}700}{10^6} \left(\frac{39.3}{[0.977]^2} - 1 \right) = \frac{44{,}700}{10^6} \left(\frac{39.3}{0.955} - 1 \right)$$

$$= \frac{447}{10^3} (41.2 - 1) = \frac{447}{10^3} (40.2) = 18.0 \text{ kg/cm.}$$

$$q_{CR} = 1800 \text{ kg/m.}$$

COEFICIENTE DE PANDEO:

$$C = \frac{q_{CR}}{q} = \frac{1800}{300} = 6 \quad \checkmark\checkmark$$

ACERO DE REFUERZO:

$$A_S = 0.002 \times 100 \times 5 = 1 \text{ cm}^2/\text{m}.$$

USAR VRS. ϕ 5/16" @ 30 EN AMBAS DIRECCIONES.

DISEÑO DE VIGAS LATERALES.

REACCION HORIZONTAL = 4,800 Kg/m

REACCIÓN VERTICAL = 2400 Kg/m

VIGA CENTRAL $\omega_y = 2 \times 2400 = 4{,}800$ Kg/m.

VIGA LATERAL $\omega_y = 2{,}400$ Kg/m

SE TOMARA PARA EL DISEÑO LA VIGA CENTRAL DEBIDO A FUTURAS AMPLIACIONES.

CARGA PESO PROPIO

$\omega = 0.65 \times 0.35 \times 2400 \times 1.00 = 547$ Kg/m.

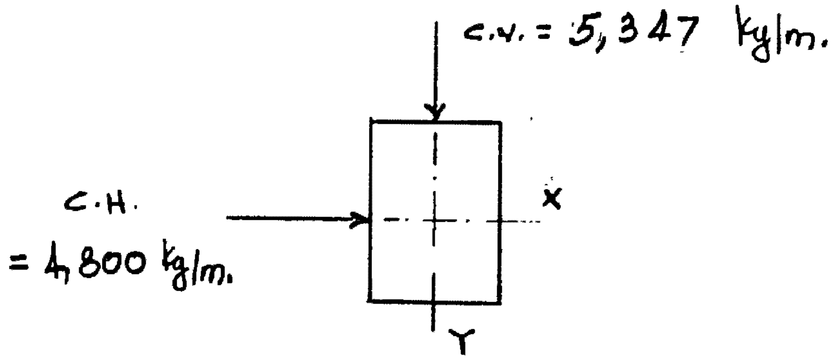

SEPARACIÓN DE TIRANTES. = 3.50 m.

CARGA POR TIRANTE = $4800 \times 3.5 = 16{,}800$ Kgs.

CARGA ADMISIBLE POR CABLE DE

7 mm ϕ $f_y = 14{,}500$ Kg/cm² = 3,000 Kgs.

$\#$ CABLES = $\dfrac{16{,}800}{3000}$ = 6 CABLES DE 7 mm ϕ.

$$M_{x\,1(-)} = \frac{1}{10}\ \omega_y\, l^2$$

$$= \frac{1}{10} \times 5347 \times \overline{7.00}^2 = 26{,}300\ \text{Kg-m.}$$

$$M_{y\,1(-)} = \frac{1}{10}\ \omega_x\, l'^2$$

$$= \frac{1}{10} \times 4{,}800 \times \overline{3.5}^2 = 5{,}900\ \text{Kg-m.}$$

$$M_{uc_x} = \frac{1}{3} \times 210 \times 35 \times \overline{60}^2$$

$$= 70 \times 35 \times 3600$$

$$= 88{,}300\ \text{Kg-m.}$$

$$F.S._x = \frac{88{,}300}{26{,}300} = 3.36 \ \checkmark\checkmark$$

$$M_{uc_y} = \frac{1}{3} \times 210 \times 65 \times \overline{30}^2$$

$$= 70 \times 65 \times 900$$

$$= 41{,}000\ \text{Kg-m.}$$

$$F.S._y = \frac{41{,}000}{5{,}900} = 6.95 \ \checkmark\checkmark$$

$$A_{sx} = \frac{M}{f_s J d} = \frac{26,300 \times 100}{2000 \times 0.85 \times 60} = 25.8 \text{ cm}^2$$

USAR 7 VRS. ϕ 7/8". ARRIBA EN LOS APOYOS.

Y 4 VRS. ϕ 7/8" ABAJO EN EL CENTRO.

$$A_{sy} = \frac{5900 \times 100}{2000 \times 0.85 \times 30} = 11.6 \text{ cm}^2$$

USAR 3 VRS. ϕ 7/8" EN LAS CARAS (AMBAS)

EN LA VIGA CENTRAL SOLO SE PROPORCIONARA REFUERZO PARA LOS EFECTOS DE w_y DEBIDO A QUE LOS COCEOS LATERALES SE ANULAN.

$$V_{max} = 1.15 \frac{w l}{2} = \frac{1.15 \times 5,347 \times 7.00}{2}$$

$$= 21,500 \text{ Kgs.}$$

$$V_c = 4.2 \times 35 \times 60 = 8,810 \text{ Kgs.}$$

$$V' = V - V_c = 21,500 - 8810 = 12,690 \text{ Kgs.}$$

$$S = \frac{4 \times 0.71 \times 1700 \times 0.85 \times 60}{12,690} = 20 \text{ cms.}$$

EST. ϕ 3/8" @20 EN LOS APOYOS (DOBLES)

Arcos de Rigidez.

Se colocaran arcos de rigidez a cada 7.00 mts.

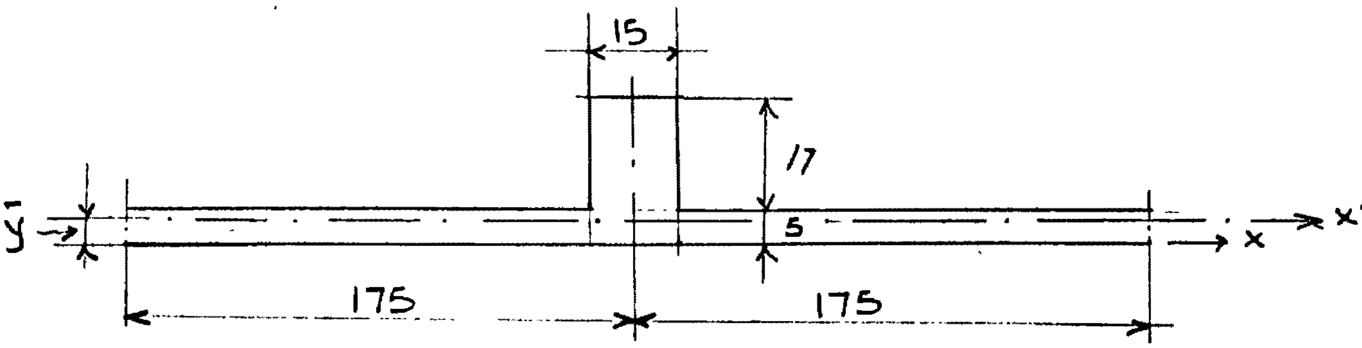

Seccion Propuesta.

Localizacion del eje centroidal:

$$\Sigma M_x = A_T \bar{y}$$

$$A_T = 15 \times 17 + 350 \times 5 = 255 + 1750$$
$$= 2005 \text{ cm}^2$$

$$M_x = (17 \times 15)(13.5) + (350 \times 5)(2.5)$$
$$= 3440 + 4380 = 7{,}820$$

$$\bar{y} = \frac{7{,}820}{2{,}005} = 3.91 \text{ cms.}$$

Determinacion de $I_{x'}$:

$$I_{x'} = \frac{1}{12}(15)\overline{17}^3 + (15 \times 17)(\overline{9.59}^2) + \frac{1}{12}(350)(\overline{5}^3) + (350 \times 5)\, 1.41$$

$$I_{x'} = 6{,}030 + 23{,}500 + 3{,}550 + 2{,}470$$

$$= 35{,}550 \text{ cm}^4$$

PANDEO :

$$q_{CR} = \frac{210{,}000 \times 35550}{17.0^3 \times 10^6}\left(\frac{4\pi^2}{\left(\frac{56}{180}\pi\right)^2} - 1\right)$$

$$= \frac{1{,}520{,}000}{10^6}\left(\frac{39.3}{0.955} - 1\right)$$

$$= \frac{152}{10^2}\left(40.2\right) = 61.0 \text{ kg/cm.}$$

$$q_{CR} = 6100 \text{ kg/m}$$

$$C = \frac{q_{CR}}{q} = \frac{6100}{300} \times \frac{1}{3.5} = 5.8$$

USAR LA SECCION INDICADA CON 4 Vrs. ϕ 5/8"
Y EST. ϕ 5/16" @ 30 cms.

REVISION DE LOS VOLADOS:

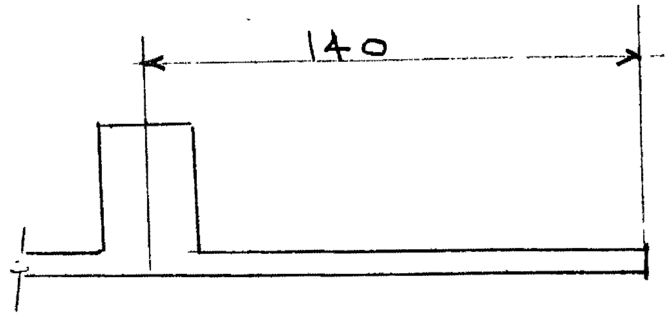

$$M_1 = \frac{q\,l^2}{2} = \frac{300 \times 1.4^2}{2} = 294 \text{ kg-m/m}$$

$$A_s = \frac{M}{f_s\, j\, d} = \frac{294 \times 1\cancel{00}}{2\cancel{000} \times 0.85 \times 3} = \frac{29.4}{6 \times 0.85}$$

$$= 5.75 \text{ cm}^2$$

con Vrs. ϕ 5/16"

$$S = \frac{100\,A_v}{A_s} = \frac{49}{5.75} = 8.5 \text{ cms.}$$

Usar 2 Vrs. ϕ 3/8" ENTRE CADA 2 DE 5/16" HASTA

l = 70 cms. DESDE AHI PROLONGAR SOLO UNA.

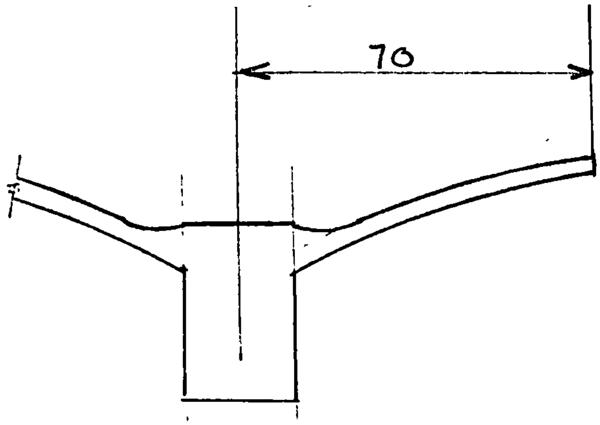

$$M_1 = \frac{q l^2}{2} = \frac{300 \times \overline{0.7}^2}{2} = 73.5 \text{ kg-m/m}$$

$$A_s = \frac{M}{f_s J d} = \frac{73.5 \times 100}{2000 \times 0.85 \times 3} = 1.44 \text{ cm}^2$$

con vrs. ϕ 5/16"

$$S = \frac{100 A_v}{A_s} = \frac{49}{1.44} = 34 \text{ cms.}$$

Pasar lamalla del cascaron unicamente.

$$M_{uc} = \frac{1}{3} f'c\, b\, d^2 = \frac{1}{3}(210)(100)(\overline{3}^2) = 630 \text{ kg/m}$$

$$F.S. = \frac{630}{294} = 2.15$$ ✓✓

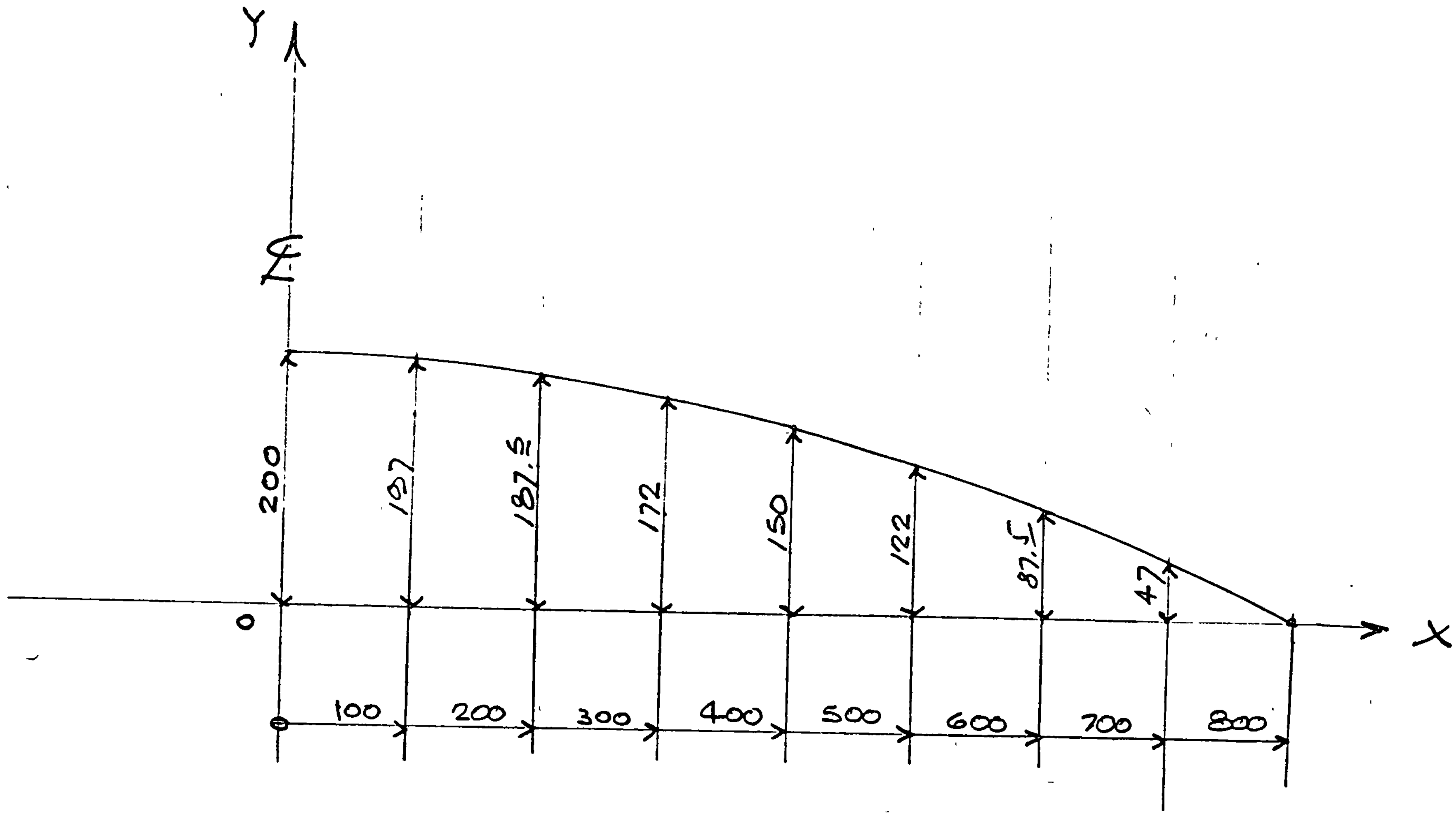

GENERATRIZ GEOMETRICA DE LA CIMBRA.

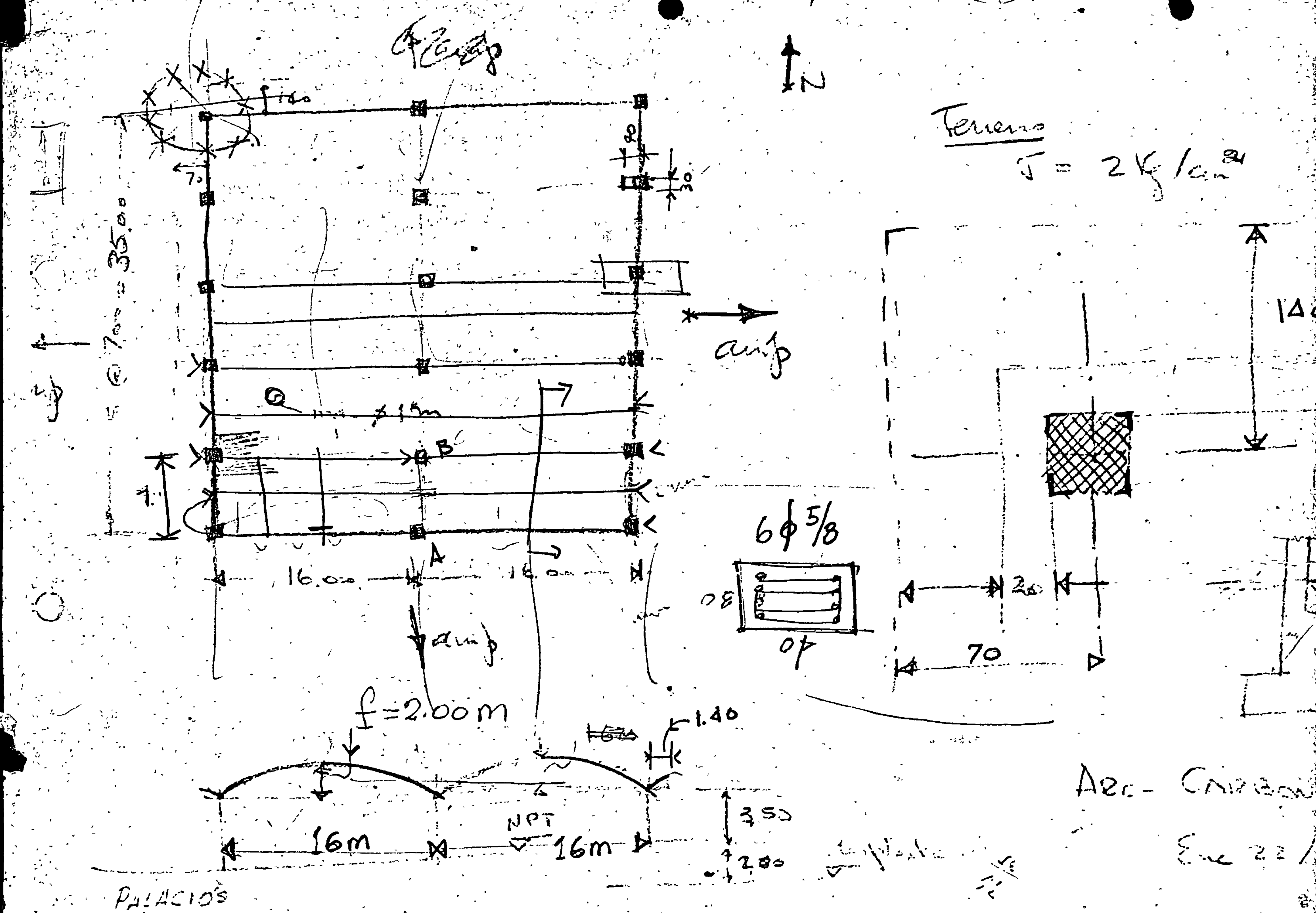

Terreno
σ = 2 Kg/cm²
16.00
f=2.00m
1.40
6φ5/8
70
16m
NPT
16m
3.50
2.00
PALACIOS